

Entwicklung und Charakterisierung funktioneller chemischer Tools für nukleäre Rezeptoren

Dissertation

zur Erlangung des Doktorgrades
der Naturwissenschaften

vorgelegt beim Fachbereich
Biochemie, Chemie und Pharmazie
der Johann Wolfgang Goethe-Universität
in Frankfurt am Main

von

Sabine Willems
aus Merzig

Frankfurt am Main (2022)

(D30)

Vom Fachbereich Biochemie, Chemie und Pharmazie
der Johann Wolfgang Goethe-Universität als Dissertation angenommen.

Dekan: Prof. Dr. Clemens Glaubitz

Gutachter: Prof. Dr. Manfred Schubert-Zsilavecz
Prof. Dr. Eugen Proschak
Prof. Dr. Verena Dirsch (Universität Wien)

Datum der Disputation: 26.10.2022

„Das gute Gelingen ist zwar nichts Kleines, fängt aber mit Kleinigkeiten an.“

„Τὸ εὖ γίνεσθαι μὲν παρὰ μικρόν, οὐ μὴν μικρόν εἶναι.“

Sokrates

Inhaltsverzeichnis

1. Einleitung.....	9
1.1 Niedermolekulare Verbindungen als funktionelle Tools	9
1.2 Nukleäre Rezeptoren	11
1.2.1 Klassifizierung.....	11
1.2.2 Struktur und Funktion.....	12
1.3 Peroxisomen-Proliferator-aktivierte Rezeptoren.....	15
1.3.1 Physiologische Funktion der PPARs.....	16
1.3.2 Bekannte PPAR-Liganden	21
1.4 Nuclear receptor related 1 protein (Nurr1)	26
1.4.1 Physiologische Funktion und therapeutisches Potenzial von Nurr1.....	27
1.4.2 Bekannte Nurr1-Liganden.....	31
2. Zielsetzung	37
3. Ergebnisse und Diskussion	39
3.1 Photohormone als lichtabhängige PPAR-Agonisten	39
3.2 Vitamin-E-Metabolite sind endogene PPAR γ -Liganden	44
3.3 Identifikation von nichtsteroidalen Antirheumatika als Nurr1-Modulatoren.....	49
3.4 Fragment-basierter Ansatz zur Entwicklung von Nurr1-Agonisten.....	54
3.5 <i>In vitro</i> Screening als Ausgangspunkt für neue Nurr1-Liganden.....	58
3.5.1 Inverse Nurr1-Agonisten mit Indol-Grundgerüst	59
3.5.2 Statine vermitteln neuroprotektive Effekte durch Nurr1 Agonismus.....	63
4. Zusammenfassung	69
5. English Summary	74
6. Literaturverzeichnis	76
7. Abkürzungsverzeichnis	115
8. Abbildungsverzeichnis	121
9. Tabellenverzeichnis	123
10. Schemenverzeichnis.....	124
11. Publikationsliste	125
12. Kooperationspartner	130
13. Curriculum Vitae	133
14. Eidesstattliche Erklärung	135
15. Danksagung	137

16. Nachdrucke der Publikationen	139
16.1 Photohormones Enable Optical Control of the Peroxisome Proliferator-Activated Receptor γ (PPAR γ).....	139
16.2 A Photohormone for Light-Dependent Control of PPAR α in Live Cells	199
16.3 Endogenous vitamin E metabolites mediate allosteric PPAR γ activation with unprecedented co-regulatory interactions	245
16.4 The orphan nuclear receptor Nurr1 is responsive to non-steroidal anti-inflammatory drugs	271
16.5 Fragment-like Chloroquinolineamines Activate the Orphan Nuclear Receptor Nurr1 and Elucidate Activation Mechanisms	289
16.6 Development and profiling of inverse agonist tools for the neuroprotective transcription factor Nurr1	315
16.7 Nurr1 modulation mediates neuroprotective effects of statins	369
16.8. Targeting nuclear receptors in neurodegeneration and neuroinflammation	393

1. Einleitung

Nukleäre Rezeptoren (NRs) sind Transkriptionsfaktoren, deren Aktivität durch die Bindung von Liganden moduliert werden kann und von denen es 48 humane Vertreter gibt^{1,2}. Für etwa ein Drittel dieser Rezeptoren sind inzwischen Arzneistoffe zugelassen³⁻⁵. Sie adressieren vor allem Steroidhormon-Rezeptoren wie den Glucocorticoid-Rezeptor oder die Estrogen-Rezeptoren (ERs), aber auch Rezeptoren mit wichtigen metabolischen Funktionen wie die Thyroidhormon-Rezeptoren (THRs) und Peroxisomen-Proliferator-aktivierten Rezeptoren (PPARs), und werden zum Teil bereits seit mehreren Jahrzehnten therapeutisch genutzt^{2,3}. Auch wenn diese Rezeptoren intensiv beforscht wurden, sind Nebenwirkungen, die aus dem gleichen primären Wirkmechanismus dieser Arzneistoffe resultieren, oft ein therapielimitierendes Problem⁶. Ein Grund dafür sind die meist breiten Expressionsmuster der NRs, die ihre wichtige Rolle in zentralen Prozessen des Körpers wie Zellwachstum und -differenzierung, Metabolismus und Homöostase unterstreichen². Außerdem erschweren strukturelle Herausforderungen die Entwicklung sicherer Arzneistoffe für nukleäre Rezeptoren. Zum einen weisen sie innerhalb der einzelnen Subfamilien zum Teil große Sequenzähnlichkeiten auf, die die Entwicklung hochselektiver Liganden erschweren^{1,7,8}. Zum anderen ist durch die lipophile Struktur der NRs die bevorzugte Bindung von ebenfalls besonders lipophilen Liganden gegeben, was jedoch die Arzneistoffentwicklung vor physikochemische und pharmakokinetische Herausforderungen stellt⁸⁻¹⁰. Zusätzlich sind einige Funktionen nukleärer Rezeptoren an den zirkadianen Rhythmus gekoppelt, wodurch eine dauerhafte Modulation nachteilig sein kann¹¹. Daher ist das Interesse, neue Liganden und Konzepte für diese Rezeptoren zu entwickeln, nach wie vor groß. So sind bei den PPARs neben dem Bedarf an neuen Therapieoptionen bei den immer häufiger werdenden komplexen metabolischen und kardiovaskulären Erkrankungen auch neue mögliche Indikationsgebiete durch Beteiligung an Entzündungsprozessen und neurodegenerativen Erkrankungen in den Fokus der Forschung gerückt¹²⁻¹⁴.

Gegenüber der genannten Gruppe gut erforschter NR sind bei etwa der Hälfte der NRs die Funktionen noch nicht umfassend verstanden^{15,16}. Bei knapp einem Drittel wurde sogar bis heute noch kein endogener Ligand identifiziert, weshalb man diese Rezeptoren auch als Waisenrezeptoren oder *Orphan*-Rezeptoren bezeichnet⁹. Dass auch sie überaus wichtige Aufgaben im Körper übernehmen und therapeutisches Potenzial besitzen, ist vor allem durch *Knockout*-Studien belegt¹⁶. Daher wäre nicht nur die Kenntnis endogener Liganden entscheidend für das Verständnis¹⁷, auch synthetische Liganden werden dringend benötigt, um die Funktionen der Waisenrezeptoren pharmakologisch charakterisieren zu können und einen möglichen therapeutischen Nutzen aus der Rezeptormodulation abzuleiten^{17,18}. Nurr1 ist ein solcher NR mit großem Potential bei neurodegenerativen Erkrankungen wie dem Morbus Parkinson (*Parkinson's disease*, PD), der Alzheimer-Demenz (AD) und der Multiplen Sklerose (MS), die im Zuge des demographischen Wandels eine immer größere Herausforderung für die Gesellschaft darstellen¹⁹⁻²¹. Diese Arbeit befasst sich in diesem Kontext mit der Identifizierung, Entwicklung und Charakterisierung neuer Liganden für die nukleären Rezeptoren der PPARs und Nurr1, um gezielte funktionelle Studien zu ermöglichen.

1.1 Niedermolekulare Verbindungen als funktionelle Tools

Niedermolekulare Verbindungen (*small molecules*), die durch direkte Interaktion mit ihrer makromolekularen Zielstruktur (Target) die Funktionen des jeweiligen Proteins modulieren können, werden – je nach Spezifität – als *tool compounds* oder auch *chemical probes* bezeichnet¹⁸. Sie werden in der

Pharmakologie und der chemischen Biologie vor allem für die mechanistische Aufklärung von Proteinfunktionen und phänotypische Untersuchungen der pharmakologischen Modulation ihres Targets verwendet und umfassen sowohl Aktivatoren (Agonisten) als auch Inhibitoren (Antagonisten bzw. inverse Agonisten)¹⁸. Deshalb ist es notwendig, dass sie bestimmte Anforderungen in Bezug auf Selektivität und Potenz je nach Art der Zielstruktur erfüllen. Dabei sind gerade zu Beginn der Erforschung eines neuen Targets bekannte *off-target*-Effekte der Substanzen zu verschmerzen, müssen allerdings bei der Beurteilung biologischer Experimente unbedingt berücksichtigt werden¹⁸. Wichtig hingegen ist, dass die direkte Interaktion mit dem Target durch orthogonale Testsysteme und Bindungsstudien zweifelsfrei belegt ist und optimalerweise Co-Kristallstrukturen eine Aufklärung des Bindemodus ermöglichen^{18,22}. Gerade für potenzielle neue Zielstrukturen zur Behandlung von Erkrankungen sind *tool compounds* von großer Bedeutung, da sie es ermöglichen, die Auswirkung einer pharmakologischen Aktivierung oder Inaktivierung ihres Targets in Krankheit und Gesundheit zu untersuchen und damit entscheidend zur präklinischen Target-Validierung beitragen²³. Die Substanzen können sowohl komplementär zu als auch anstelle von genetischen Ansätzen verwendet werden, die entweder durch genetischen *Knockout* oder *Knockdown* der Zielstruktur z. B. durch RNA-Interferenz (RNAi) den Verlust der Proteinfunktionen (*loss-of-function*) darstellen oder gezielte Überexpression bzw. gesteigerte Aktivität des Proteins (*gain-of-function*) untersuchen²⁴. Dabei sind *tool compounds* schneller und einfacher zu handhaben, ermöglichen die Anwendung in vielen unterschiedlichen Testsystemen, Zelltypen und Tiermodellen sowie Studien auf Proteinebene und sind relevanter für eine mögliche spätere Translation in eine pharmakologische Anwendung. Besonders wertvoll ist ein Set an *tool compounds* für eine Zielstruktur, die zum einen möglichst diverse chemische Strukturen aufweisen und zum anderen verschiedene Wirkungsprinzipien durch Aktivierung/Inhibition des Targets oder unterschiedliche Bindemodi abdecken, aber auch strukturell verwandte negative Kontrollen umfassen, sodass Proteinfunktionen chemogenomisch untersucht werden können^{18,22}. Die Anforderungen an physikochemische und pharmakokinetische Eigenschaften sind im Vergleich zu Arzneistoffen deutlich geringer, müssen allerdings gewisse Grundvoraussetzungen in Bezug auf Toxizität, Lipophilie und Stabilität erfüllen, um eine adäquate Verwendung in Experimenten zu gewährleisten¹⁸. Außerdem dürfen sie die Funktion des Testsystems nicht beeinträchtigen wie bspw. Substanzen, die aufgrund reaktiver Struktur motive falsch-positive Ergebnisse hervorrufen (*pan assay interference compounds*, PAINS), oder auch Substanzen, die durch ihre physikochemischen Eigenschaften wie z. B. Farbigkeit oder Eigenfluoreszenz die Resultate bestimmter Untersuchungsmethoden verfälschen^{22,25}. Dabei sind *tool compounds* nicht nur effektive Instrumente in der Forschung, sie können ebenso als wertvoller Startpunkt für die Entwicklung neuer Arzneistoffkandidaten dienen¹⁸.

Die Photopharmakologie ermöglicht über die klassische Verwendung von *tool compounds* hinaus eine gezielte räumliche und zeitliche Auflösung der Wirkung. Sie verwendet dazu Verbindungen, die mithilfe von Licht in eine andere Konfiguration gebracht werden können und dadurch die Aktivität am Target verändern^{26,27}. Dazu können verschiedene Arten von Chromophoren verwendet werden, die meist reversibel zwischen ihrer *trans*- und *cis*- Konfiguration geschaltet werden können, wie bspw. Azobenzene (Abbildung 1) oder Stilbene, oder zwischen offenen und geschlossenen Ringkonformationen wie bei Spiropyranen oder Diarylethenen^{26,27}. So wurde inzwischen mithilfe photopharmakologischer Tools die Funktion von Ionenkanälen^{28,29}, Transportern³⁰⁻³², Membranrezeptoren³³⁻³⁵ und Enzymen³⁶⁻³⁸ erfolgreich unter optische Kontrolle gebracht, aber auch photoschaltbare Lipide³⁹ entwickelt. Die Anwendung dieses Konzeptes ist bei nukleären Rezeptoren besonders interessant, da sie als ligandenaktivierte Transkriptionsfaktoren genomische Effekte durch Bindung zum Teil kurzlebiger endogener Liganden wie Hormonen und reaktiven Vitamin- und Fettsäure-Metaboliten vermitteln, aber auch nicht-genomische

Effekte von kürzerer Dauer ausüben können^{2,40}. Mit Liganden, die durch Licht innerhalb kurzer Zeit (wenige Minuten) zwischen aktivem und inaktivem Zustand umgeschaltet werden können, eröffnen sich neue Möglichkeiten funktioneller Studien, die einer physiologischen Aktivierung durch endogene Liganden deutlich näherkommen könnten. Bislang konnten für die drei Vertreter Retinsäure-Rezeptor α (RAR α)⁴¹, ER α ⁴² und Farnesoid X Rezeptor (FXR)⁴³ sogenannte Photohormone aus publizierten Liganden entwickelt werden, die zeigen, dass auch eine optische Kontrolle nukleärer Rezeptoren möglich ist. Darüber hinaus könnten solche photoschaltbaren Liganden auch therapeutisch von Bedeutung sein. Die Möglichkeit, den Arzneistoff gezielt am Wirkort zu aktivieren, könnte das Auftreten von Nebenwirkungen im restlichen Körper minimieren. Sowohl Target-vermittelte unerwünschte Effekte in anderen Geweben, aber auch *off-target*-Effekte durch unzureichende Selektivität würden so reduziert werden. Neben naheliegenden äußerlichen Anwendungen auf der Haut oder im Auge wird dabei auch an der Einbringung von Lichtquellen in den Körper geforscht, was durch Endoskopie, aber auch durch drahtlose und bio-abbaubare Optoelektronik ermöglicht werden könnte⁴⁴. Erste *in vivo* Studien zu metabolischen Erkrankungen und Krebs zeigen bereits, dass eine therapeutische Anwendung des Konzepts denkbar ist^{45–48}.

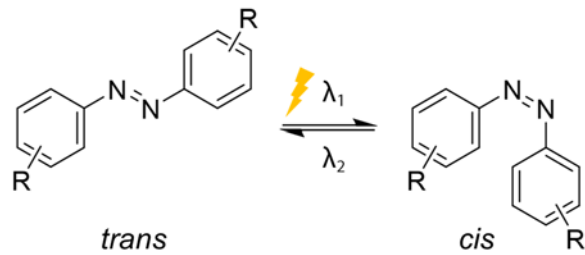


Abbildung 1: Funktionsweise photoschaltbarer Liganden am Beispiel der Azobenzene. Mit Licht unterschiedlicher Wellenlängen (λ_1 & λ_2) kann die Konfiguration reversibel von *trans* nach *cis* und umgekehrt geschaltet werden.

1.2 Nukleäre Rezeptoren

1.2.1 Klassifizierung

Die Einteilung und Nomenklatur der Familie der nukleären Rezeptoren als einer spezifischen und klar abzugrenzenden Unterkategorie von Transkriptionsfaktoren geht auf evolutionsbiologische und phylogenetische Betrachtungen der Sequenzen zurück^{49,50} (Abbildung 2). Im Jahr 1999 hat ein eigens gebildetes Komitee die Nomenklatur der nukleären Rezeptoren vereinheitlicht, um die zunehmende Zahl von Trivialnamen und Abkürzungen für diese Proteine bzw. deren Gene zu verhindern⁵⁰. Dabei ist das System so gestaltet, dass es die entsprechenden Rezeptoren aller Spezies umfasst und beliebig erweitert werden kann. Bestätigt sind derzeit 71 verschiedene Gene nukleärer Rezeptoren mit insgesamt 390 unterschiedlichen Isoformen (UniProtKB/Swiss-Prot), wovon 48 humane Gene zu beziffern sind^{15,51}. Die Bezeichnungen, beginnend mit „NR“ für *nuclear receptor*, teilen die Familie in sechs Gruppen (NR1–6) gemäß ihrer strukturellen Verwandtschaft auf. Eine siebte Gruppe (NR0) geht darauf zurück, dass es sich um Rezeptoren handelt, die einen atypischen Aufbau der Domänen aufweisen. Innerhalb der Gruppen werden die engsten Verwandten mit Großbuchstaben zu Unterfamilien zusammengefasst und in der Ebene darunter erhalten einzelne Isoformen individuelle Nummern. So wird beispielsweise PPAR γ als eine Isoform der PPAR-Unterfamilie (NR1C) in der ersten Gruppe mit NR1C3 bezeichnet⁵².

Eine weitere Möglichkeit der Klassifizierung stellt der molekulare Mechanismus der nukleären Rezeptoren dar. Dabei werden vier Typen an Rezeptoren vorwiegend hinsichtlich ihres Dimerisierungsverhaltens und der Art ihrer Erkennungssequenz (*response element*, RE) unterschieden⁹. Typ I umfasst u. a. die Steroidrezeptoren, welche hauptsächlich als Homodimere an REs mit invertierter Wiederholung (*inverted repeat*, IR) agieren und als einzige erst bei Ligandbindung zum Nukleus translozieren⁹. Typ II hingegen bildet vorwiegend Heterodimere mit einem Subtyp der Retinoid X Rezeptoren (RXR), welche REs mit direkter Wiederholung (*direct repeat*, DR) binden¹⁵ (siehe Kapitel 1.3). Hierbei lassen sich zwei

Varianten unterscheiden: die permissiven Heterodimere wie z. B. bei den PPARs (NR1C1–3) und LXRs (NR1H2 und NR1H3), welche sowohl durch Bindung eines Liganden des Dimerpartners als auch durch einen RXR-Liganden aktiviert werden können, und die nicht-permissiven Heterodimere wie z. B. bei den RARs (NR1B1–3), bei welchen die Bindung eines RXR-Liganden zur Aktivierung allein nicht ausreichend ist und somit vom Liganden des Dimerpartners abhängt^{1,15}. Bei permissiven Heterodimeren führt die gleichzeitige Bindung beider Liganden zu einem synergistischen Effekt⁵³. Rezeptoren vom Typ III bilden vorwiegend Homodimere aus, welche ebenfalls über REs mit DR aktivieren⁹. Dem Typ IV werden Rezeptoren zugeordnet, die hauptsächlich als Monomere agieren. Jedoch berücksichtigt die Einteilung nach dem molekularen Mechanismus vor allem keine Erkenntnisse zu *Orphan*-Rezeptoren, welche nicht eindeutig einer Klasse zugeordnet werden können¹, wie die Rezeptoren der NR4A-Subfamilie (siehe Kapitel 1.4)^{54–56}.

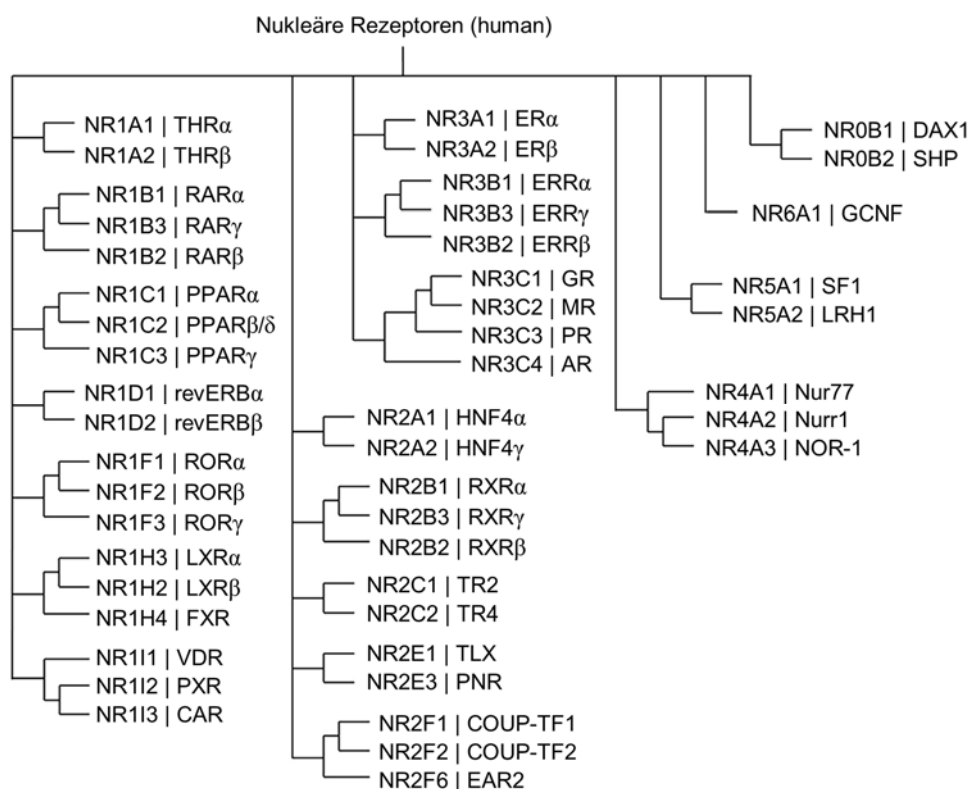


Abbildung 2: Superfamilie der 48 humanen nukleären Rezeptoren dargestellt nach ihrer phylogenetischen Klassifizierung mit zugehöriger Abkürzung⁵⁷.

1.2.2 Struktur und Funktion

Nukleäre Rezeptoren sind ligandenaktivierte Transkriptionsfaktoren, die endogene Liganden von großer Vielfalt binden, wie z. B. Hormone, Vitamine, Fettsäuren und Gallensäuren, aber auch Xenobiotika, und durch diesen Stimulus die Genexpression ihrer Zielgene modulieren können^{1,2}. Neben dieser Hauptaufgabe der direkten genomischen Regulation können NRs die Genexpression auch indirekt über die Interaktion mit anderen Transkriptionsfaktoren wie bspw. mit NFκB modulieren, wodurch sie eine antientzündliche Wirkung entfalten können^{58–61}. Außerdem können sie auch nicht-genomische Effekte ausüben, die meist durch Translokation im Zytosol stattfinden und schneller ablaufen als genomische Effekte^{40,62–65}. NRs tragen eine wichtige Rolle in zahlreichen physiologischen Prozessen wie der embryonalen Entwicklung, Zell-Proliferation, -Differenzierung, Metabolismus und Homöostase^{2,15}, und sind bei Funktionsstörungen auch beteiligt an der Entstehung und dem Fortschreiten von bspw. Krebs, Entzündungsprozessen, metabolischen Erkrankungen wie Diabetes und neurodegenerativen

Erkrankungen^{9,66}. Trotz dieser enormen Bandbreite an Funktionen verbindet die Klasse der NRs aber ihr typischer struktureller Aufbau, der hochkonserviert ist und sich in vier unterschiedliche Domänen einteilen lässt (Abbildung 3)².

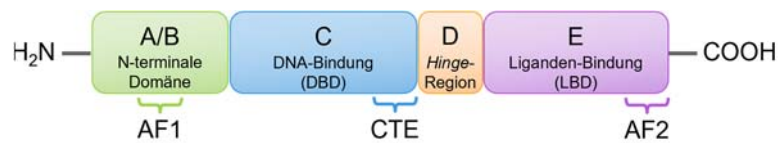


Abbildung 3: Allgemeiner struktureller Aufbau nukleärer Rezeptoren.

Die N-terminale A/B-Domäne ist der variabelste Bereich und beinhaltet die Aktivierungsfunktion 1 (AF1), welche vor allem zur konstitutiven Aktivierung des Rezeptors beiträgt und zell- und promotor-spezifische Aktivität zeigt^{1,2}. Dabei ist diese Domäne auch das Ziel von zahlreichen posttranslationalen Modifikationen wie Phosphorylierungen und Ubiquitinierungen, welche die Aktivität des Rezeptors ligandenunabhängig modulieren können^{1,67}. Daran schließt sich die C-Domäne an, auch DNA-Bindedomäne (DBD) genannt, welche besonders konserviert ist und für die Erkennung spezifischer DNA-Sequenzen, der sog. *Response-Elemente* (RE), in der Promotorregion der Zielgene verantwortlich ist (Abbildung 4)^{1,68}. Die Erkennungssequenz für NRs besteht zu meist aus der Basenfolge AGGTCA, welche bei der Erkennung durch Dimere auf verschiedene Weise angeordnet wiederholt im RE auftreten, mit direkter Wiederholung (*direct repeat*, DR), mit invertierter Wiederholung (*inverted repeat*, IR) oder auswärtsgedrehter Wiederholung (*everted repeat*, ER)⁶⁹⁻⁷¹. Dabei befindet sich eine Halb-

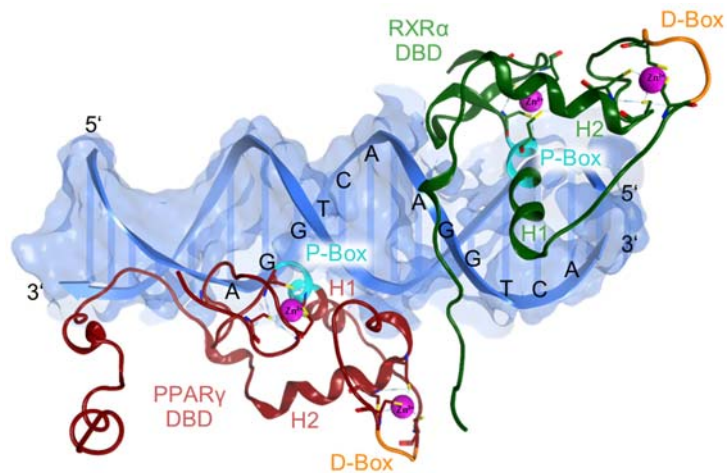


Abbildung 4: DNA-Bindung des PPAR γ -RXR α -Heterodimers (PDB: 3DZY⁷⁶). Gezeigt sind die DBDs der beiden Rezeptoren, PPAR γ in rot und RXR α in grün, gebunden an das PPRE Response-Element mit DR1-Wiederholung. Die spezifische Interaktion mit der DNA erfolgt über die P-Box (türkis). Jeweils zwei Zinkfinger-motive koordinieren Zn²⁺ (magenta) über je vier konservierte Cysteine, die D-Box (orange) ist an der Dimerisierung beteiligt.

seite bei den palindromischen IR- und ER-Erkennungssequenzen auf dem gegenüberliegenden DNA-Strang^{56,69,72}. Strukturell charakteristisch sind zwei α -Helices der DBD, welche senkrecht zueinander angeordnet sind und zwei Zinkfinger-motive aufweisen. Für die spezifische Erkennung der DNA ist ein Bereich verantwortlich, der als P-Box (P steht für proximal) bezeichnet wird und die ersten fünf Aminosäuren der N-terminalen Helix umfasst, welche in einer großen Furche des Doppelstrangs direkt mit den Nukleobasen interagieren^{1,68,73}. Fixiert durch das C-terminale Zinkfinger-motiv ist der Bereich der sog. D-Box, welcher einhergehend mit Konformationsänderungen bei der DNA-Bindung eine wichtige Rolle bei der Dimerisierung der DBDs spielt, dabei aber nicht selbst mit der DNA interagiert^{68,73,74}. Dem zweiten Zinkfinger-motiv folgt eine C-terminale Verlängerung (*C-terminal extension*, CTE), die zum einen die Kontaktstelle der Dimere vervollständigt und den korrekten Abstand der Wiederholungen der REs vorgibt, aber bei Monomer-Aktivität auch dafür verantwortlich ist, durch direkte Interaktion mit der angrenzenden kleinen Furche des Doppelstrangs die DNA-Bindung zu stabilisieren^{68,71,75}.

Nach einem variablen und konformationell flexiblen Überbrückungsbereich (*Hinge-Region*, D-Domäne), welcher an der Interaktion mit Co-Regulatoren beteiligt ist und Sequenzen zur

Kernlokalisierung (*nuclear localization signal*, NLS) enthält, folgt C-terminal die Ligandenbindedomäne (LBD, E-Domäne) des Rezeptors^{1,77}. Neben der Bindung von (endogenen) Liganden, die zur Modulation der Rezeptoraktivität führt, ist diese multifunktionale Domäne außerdem maßgeblich verantwortlich für die Interaktion mit Co-Regulatoren sowie für die Homo- und Heterodimerisierung mit anderen NRs^{1,77}. Dabei ist die kanonische Struktur der LBD meist aus zwölf α -Helices und einem Abschnitt aus β -Faltblättern aufgebaut, deren kompakte Anordnung in drei Schichten als antiparalleles α -helikales Sandwich beschrieben wird und in deren unterer Hälfte sich in den meisten Fällen die hydrophobe Ligandenbindetasche befindet^{1,8,68} (Abbildung 5). Die Tasche ist in Volumen und Form hochvariabel und kann sich bei Ligandbindung großen Konformationsänderungen unterziehen, wobei die Bandbreite

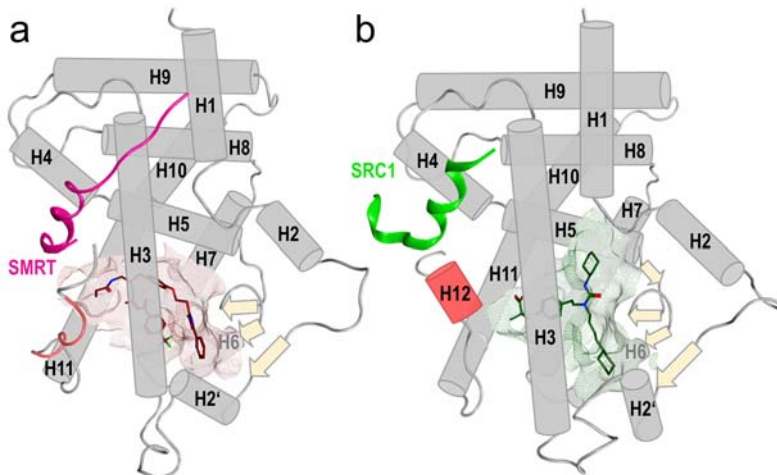


Abbildung 5: Modell der ligandenabhängigen Aktivierung und Inaktivierung durch Konformationsänderung der LBD am Beispiel von PPAR α . Bereich der H12 (AF2) in rot. (a) PPAR α im Komplex mit dem Antagonist GW6471 und Co-Repressor SMRT (magenta, PDB: 1KKQ⁷⁹). (b) PPAR α im Komplex mit dem Agonist GW7647 (1) und Co-Aktivator SRC1 (grün, PDB: 7BQ3⁸⁰).

von fast nicht vorhandener Tasche (blockiert durch hydrophobe Aminosäurereste) bis hin zu großen leeren Volumina von $> 1500 \text{ \AA}^3$ reicht^{17,75,78}. In der C-terminalen Helix, meist Helix 12 (H12), enthält die LBD die ligandenabhängige Aktivierungsfunktion 2 (AF2)⁷⁸. Spezifität bei der Ligandbindung entsteht überwiegend durch die Geometrie der Liganden und durch Wasserstoffbrückenbindungen der Liganden mit wenigen hydrophilen Aminosäureresten^{8,68}.

Die ligandabhängige Regulation von NRs schließt mechanistisch die Bindung und Freisetzung von Co-Regulatoren als essenzielle Komponente der Aktivität von NRs ein. Klassischerweise werden die Co-Regulatoren in Co-Aktivatoren und Co-Repressoren eingeteilt, deren Interaktion mit dem jeweiligen NR von dessen Aktivierung abhängt^{81,82}. Im inaktiven Zustand des Rezeptors, in apo-Form oder Antagonist-gebunden, weist der AF2-Bereich der LBD meist eine große Flexibilität auf und ist nicht an den Kern der LBD gebunden (Abbildung 5a). Somit liegt eine hydrophobe Oberfläche zwischen H3 und H4 frei, welche Co-Repressoren über spezifische α -helikale Motive bindet, die sog. CoRNR-Box mit einer (L/I)XX(I/V)I-Sequenz (L = Leucin, I = Isoleucin, V = Valin, X = beliebige Aminosäure). Die bekanntesten Co-Repressoren sind der Nukleäre Co-Repressor 1⁸³ (NCoR1) und der dämpfende Mediator der Retinoid- und Thyroidhormonrezeptoren⁸⁴ (*silencing mediator of retinoid and thyroid hormone receptors*, SMRT, auch NCoR2 genannt), welche epigenetische Regulatoren wie Histon-Deacetylasen (HDACs) und -Demethylasen rekrutieren und aktivieren, sodass sich ein multifaktorieller Co-Repressor-Komplex ausbildet, welcher vor allem durch Chromatin-Modifikationen die Transkription verhindert⁸¹. Durch Bindung eines Agonisten ändert sich die Konformation der H12 (Abbildung 5b), sodass sie den Eingang der Bindetasche verschließt („Mausefalle“-Modell) bzw. sich durch Interaktion mit dem Liganden eine stabilisierte Konformation ausbildet (Modell dynamischer Stabilisation)⁹. Im Zuge dessen ändert sich auch die hydrophobe Proteinoberfläche der LBD, Co-Repressoren lösen sich von der LBD und Co-Aktivatoren wie bspw. die Steroidrezeptor-Co-Aktivatoren⁸⁵⁻⁸⁷ (SRCs) oder der PPAR γ -Co-Aktivator 1 α ⁸⁸ (PGC-1 α) binden an die veränderte hydrophobe Furche über eine α -Helix mit dem Konsensus-Motiv LXXLL^{81,89,90}. Dabei ist der Abstand zwischen zwei konservierten geladenen Seitenketten (sog.

charge clamp), meist einem Glutaminsäure-Rest in H12 und einem Lysin-Rest in H3, entscheidend, um Co-Aktivatoren zu koordinieren und trägt im aktiven Zustand meist 18–20 Å⁹¹. Co-Aktivatoren besitzen zum einen selbst intrinsische Enzymaktivität als Histon-Acetyltransferasen (HAT) oder -Methyltransferasen und rekrutieren zum anderen wiederum weitere Co-Faktoren, um die Transkriptionsmaschinerie zu starten^{81,82}.

Es häufen sich jedoch Erkenntnisse, die von der klassischen Einteilung der Co-Regulatoren abweichen^{82,92,93}. So wurde für die Rezeptoren VDR (NR1I1), ER α (NR3A1), RAR α (NR1B1) und THR α (NR1A1) gezeigt, dass die vermeintlichen Co-Repressoren NCoR1 und SMRT zellspezifisch auch für die ligandenabhängige Aktivierung der Rezeptoren benötigt werden und mit Co-Aktivator-Komplexen assoziieren^{94–98}. Passend dazu sind Beobachtungen, dass HDACs in Einzelfällen auch eine aktive Genexpression unterstützen, was man sich als eine Art *Reset* des Chromatins bei wiederholter Transkription erklärt^{99–101}. Umgekehrt wurden auch repressive Funktionen von SRC Co-Aktivatoren berichtet, sowie die Assoziation von SRC1 an einen Antagonist-gebundenen NR^{102–104}. Weiterhin scheint sich die Funktion und Zusammensetzung der Co-Regulator-Komplexe im Gehirn, wo epigenetische Mechanismen eine wichtige Rolle bei der neuronalen Entwicklung und kognitiven Prozessen spielen, zum Teil von denen in nichtneuronalen Geweben zu unterscheiden¹⁰⁵. Ein Beispiel für einen Co-Regulator mit erwiesener dualer Funktion als Co-Aktivator und Co-Repressor^{106,107} ist das Nukleäre-Rezeptoren-interagierende Protein 1¹⁰⁸ (NRIP1). Erklärungen dafür liefert die Struktur des Proteins, welches neun LXXLL-Motive in der Proteinsequenz aufweist, aber auch vier autonome Repressions-Domänen, welche HDACs rekrutieren können. Auch werden veränderte Konformationen durch post-translationale Modifikationen für die dualen Eigenschaften des Proteins verantwortlich gemacht. Dabei funktioniert NRIP1 vermutlich als Adapter-Protein ohne eigene intrinsische Enzymaktivität¹⁰⁶.

1.3 Peroxisomen-Proliferator-aktivierte Rezeptoren

Im Jahr 1990 wurde PPAR α (NR1C1) als erster von drei Vertretern einer neuen Subfamilie nukleärer Rezeptoren durch die Induktion von hepatischer Peroxisomen-Proliferation in Nagetieren identifiziert¹⁰⁹. Hiervon leitet sich auch der Name der NR-Subfamilie ab, obwohl die PPARs beim Menschen keinen Einfluss auf Peroxisomen haben¹¹⁰. Wenig später wurden die zwei übrigen Subtypen PPAR β/δ (NR1C2; auch NUC1¹¹¹, FAAR¹¹²) und PPAR γ (NR1C3) charakterisiert¹¹³. Da man aufgrund der geringen Homologie zwischen dem als PPAR β identifizierten Amphibien-Rezeptor und dem PPAR δ bei Säugtieren¹¹⁴ zunächst von vier unterschiedlichen Subtypen der PPARs ausging, kam es zur Doppelbezeichnung der orthologen Rezeptoren verschiedener Spezies⁵². Nachfolgend wird nur noch die inzwischen etablierte Bezeichnung PPAR δ verwendet. Jeder der drei PPAR-Subtypen wird von einem eigenen Gen kodiert, welche auf unterschiedlichen Chromosomen lokalisiert sind und sich vor allem in der Länge der A/B-Domäne unterscheiden⁵². Bei PPAR γ sind drei relevante Isoformen bekannt, die sich aus insgesamt sieben unterschiedlichen Splicevarianten ergeben¹¹⁵. PPAR γ 1 und - γ 3, - γ 5 und - γ 7 sind auf Proteinebene identisch, ebenso wie PPAR γ 4 und - γ 6, welche ein um acht Aminosäuren längeres Protein am N-Terminus ergeben^{115,116}. PPAR γ 2 ist die längste Isoform beim Menschen und am N-Terminus um 28 Aminosäuren länger^{115,117}. Somit ergeben sich zum Teil unterschiedliche Bezifferungen der einzelnen Aminosäuren und die Isoformen unterscheiden sich in ihrer Gewebeverteilung, die Sequenzen der LBDs sind jedoch identisch^{115,118}. Strukturell entsprechen die PPARs dem in Kapitel 1.2.2 beschriebenen klassischen Aufbau nukleärer Rezeptoren⁵². Sie bilden permissive Heterodimere mit einem Subtyp der

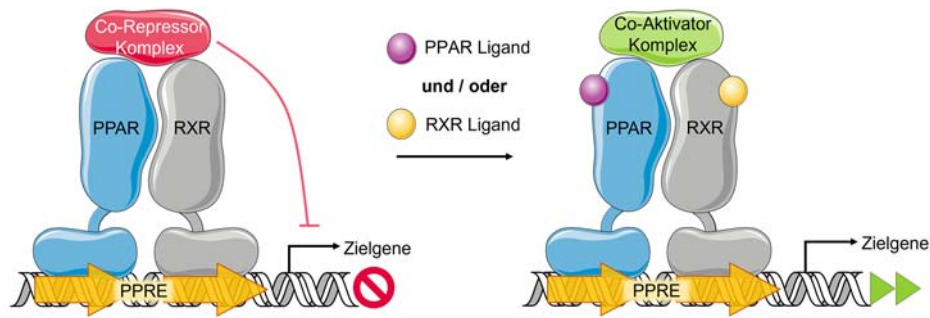


Abbildung 6: Molekularer Mechanismus der PPARs.

RXRs, die sowohl durch PPAR-Liganden als auch durch RXR-Liganden aktiviert werden können (Abbildung 6)^{119,120}. Dabei führt die gleichzeitige Bindung von Liganden beider Rezeptoren zu einer synergistischen Aktivierung^{119,120}. Die Erkennungssequenz ist ein spezifisches PPAR-Response-Element (PPRE), welches als *direct repeat* mit einer Nukleinbase Abstand (DR1) angeordnet ist und die Konsensus-Sequenz AGGNCANAGGTCA aufweist (N steht für eine beliebige Base)^{119,121,122}. Dabei ist die erste Halbseite des PPRE, welche den PPAR-Subtypen bindet, häufig keine exakte Wiederholung der zweiten Halbseite und variiert meist in der Nukleinbase der 4. Position^{119,121,122}. Die in 5'-Richtung vorangehende Sequenz ist verantwortlich für die Selektivität der verschiedenen PPAR-Subtypen^{122,123}. Analog zum klassischen Mechanismus der Rezeptoraktivierung durch Ligandbindung (siehe Kapitel 1.2.2) kommt es durch Konformationsänderung zum Austausch der Co-Repressoren, meist NCoR1 oder SMRT, aber auch NRIP1, durch Co-Aktivatoren wie dem CREB-bindenden Protein (CBP), dem 300-kDA-Protein (p300), PGC-1 α , dem PPAR-interagierenden Protein (PRIP, auch Nukleärer-Rezeptor-Co-Aktivator 6 (NCoA6)), den SRCs und den Multiprotein-Komplexen des Thyroidhormon-Rezeptor-assoziierten Proteins (TRAP) bzw. des Vitamin-D-Rezeptor-interagierenden Proteins (DRIP)¹²⁰. Die PPARs weisen aber auch eine geringe Basalaktivität auf, die bei PPAR α am stärksten ausgeprägt ist und aus der verhältnismäßig stabilen Position der H12 im ligandenungebundenen Zustand sowie der Phosphorylierung der A/B-Domäne resultiert^{91,124}. Insgesamt zählen die PPARs zu den am besten beforschten nukleären Rezeptoren. Sie sind wichtige Regulatoren im Glucose- und Lipidmetabolismus und synthetische Agonisten von PPAR α (Fibrate) und PPAR γ (Glitazone) wurden bereits therapeutisch angewendet, bevor ihr Wirkmechanismus überhaupt aufgeklärt werden konnte^{125,126}. PPAR δ -Agonisten hingegen befinden sich derzeit in klinischer Prüfung und haben bislang keine Zulassung erhalten. Während Fibrate und Glitazone in der Therapie von Dyslipidämien und Diabetes mellitus Typ 2 heute eine eher untergeordnete Rolle spielen, rücken neben neuen potenziellen Indikationsgebieten für PPAR-Agonisten auch neue Konzepte zur selektiven Aktivierung der PPARs, wie die sog. selektiven PPAR Modulatoren (sPPARMs), unter Vermeidung der klassenspezifischen Nebenwirkungen in den Fokus der aktuellen Wirkstoffforschung¹⁴.

1.3.1 Physiologische Funktion der PPARs

Als Lipidsensoren haben die PPARs ihre Hauptaufgabe in der Regulation des Nährstoffhaushaltes, die sie auf Grund unterschiedlicher Expressionsmuster zum Teil in ähnlicher, aber auch in komplementärer Art und Weise erfüllen¹²⁷. Im Folgenden werden die physiologischen Funktionen der einzelnen Subtypen näher beschrieben (Abbildung 7).

PPAR α ist der in der Leber dominierende PPAR-Subtyp, wird aber auch im braunen Fettgewebe, Herz, Skelettmuskel, der Niere und der Darmmukosa exprimiert, welche allesamt Gewebe mit hohem Energieverbrauch und somit hoher mitochondrialer und peroxisomaler β -Oxidation darstellen^{52,128}. So

reguliert PPAR α in der Leber zahlreiche Gene, die den katabolen Fettsäure-Stoffwechsel fördern, indem es zur Aktivierung von Fettsäuren sowie deren β -Oxidation und mikrosomalen ω -Oxidation kommt¹²⁹. Auch sind sie für die Gluconeogenese und Synthese von Ketonkörpern verantwortlich, und kontrollieren die Zusammensetzung der Lipoproteine durch Regulation der Fettsäure-Aufnahme und des intrazellulären Transports in Hepatozyten¹²⁹. In Einklang damit steht, dass PPAR α in Situationen von Stress und Hunger in der Leber durch erhöhte Glucocorticoid-Spiegel induziert wird, um eine Umwandlung und Nutzung von Lipiden als Energiequelle zu fördern. Damit unterliegt PPAR α auch dem Tag-Nacht-Rhythmus^{120,128,130}. Berichte über Polymorphismen im humanen PPAR α -Gen unterstreichen die zentrale Rolle des Rezeptors im Lipidmetabolismus¹³¹. Durch die Aktivierung von PPAR α mit Fibraten kommt es vor allem zu einer signifikanten Senkung der Triglycerid-Spiegel im Blut und gleichzeitig zu einer Steigerung der atheroprotektiven Lipoproteine hoher Dichte (*high density lipoprotein*, HDL)^{131,132}. Da die Effektivität der Fibrate in der Reduktion der Lipoproteine niedriger Dichte (*low density lipoprotein*, LDL) jedoch eher moderat ist, werden sie nur noch zur Behandlung von Hypertriglyceridämien eingesetzt, bei Hypercholesterinämien und Dyslipidämien sind Statine die erste Wahl^{132,133}. Zusätzlich zum positiven Effekt auf das Lipidprofil vermittelt PPAR α auch zahlreiche antientzündliche Effekte, die zum Teil über die Repression proinflammatorischer Transkriptionsfaktoren wie NF κ B reguliert werden^{120,132,134}. Durch die Expression des Rezeptors in glatten Muskelzellen des vaskulären Endothels sorgt eine gesteigerte PPAR α -Aktivität für vasoprotektive Effekte bei Atherosklerose, indem unter anderem die Rekrutierung von Monozyten unterdrückt wird, proinflammatorische Zytokine sowie das Adhäsionsmolekül VCAM1 herunterreguliert werden und es zu einem gesteigerten Cholesterolefflux der Makrophagen in atherosklerotischen Plaques kommt^{131,132,135}. Somit ist das Wirkprofil von PPAR α -Agonisten insgesamt protektiv für kardiovaskuläre Erkrankungen, wobei vor allem Patienten mit Diabetes mellitus Typ 2 und dem Metabolischen Syndrom profitieren^{132,135}. Eine generelle Prävention von kardiovaskulären Ereignissen durch PPAR α -Agonisten ist bislang jedoch nicht hinreichend belegt, was der geringen Potenz und Selektivität der zugelassenen Fibrate geschuldet sein könnte^{132,135,136}.

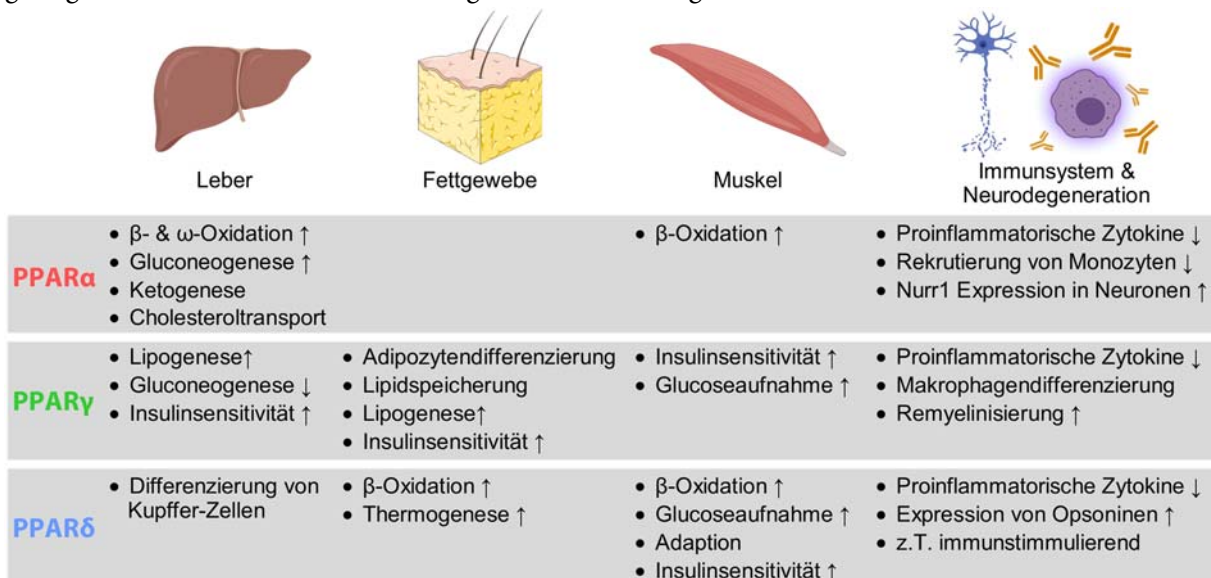


Abbildung 7: Physiologische Funktionen der drei PPAR-Subtypen. Regulation des Energiemetabolismus in Leber, Fettgewebe und Muskel, sowie Auswirkungen auf Entzündungsprozesse im Allgemeinen und Neurodegeneration im ZNS.

Die PPAR α -Expression im Gehirn ist auf keine spezifischen Regionen beschränkt und, wie auch PPAR δ , weitverbreitet. Dabei überwiegt die Expression aller PPARs vor allem in Neuronen im Vergleich zu geringer Expression in Astrozyten und Mikroglia¹³⁷. Obwohl die Funktion von PPAR α im zentralen

Nervensystem (ZNS) noch nicht gänzlich verstanden ist, deuten zahlreiche Studien darauf hin, dass eine Aktivierung des Rezeptors durch antiinflammatorische und antioxidative Wirkungen, aber auch durch veränderten Zellmetabolismus, positive Effekte auf neurodegenerative Erkrankungen wie AD und PD hat¹³⁸⁻¹⁴⁰. Von Relevanz ist auch, dass PPAR α -Aktivität die Expression des neuroprotektiven Transkriptionsfaktors Nurr1 (siehe Kapitel 1.4.1) in dopaminergen Neuronen steigert¹⁴¹. Somit ergeben sich neben dem erprobten Indikationsgebiet der Hyperlipidämien neue interessante therapeutische Optionen für PPAR α -Liganden.

PPAR γ wird vor allem im weißen und braunen Fettgewebe exprimiert, zeigt aber ein insgesamt breites Expressionsmuster, das außerdem Darm, Leber, Herz, Niere, Gefäß- und Immunzellen umfasst^{52,128}. Die Expression im Skelettmuskel ist hingegen eher gering^{117,128}. Dabei ist PPAR γ 1 die insgesamt dominierende Isoform, PPAR γ 2 kommt basal nur im Fettgewebe vor und kann bei übermäßiger Energiezufuhr in Leber und Skelettmuskel induziert werden^{117,142,143}. Die Expression von PPAR γ 3 und - γ 4 betrifft hauptsächlich Makrophagen und das Fettgewebe, während PPAR γ 3 zusätzlich im Darmepithel zu finden ist^{116,143,144}. Die Beobachtung, dass PPAR γ bei Hunger und Insulin-Mangel herunterreguliert wird und vor allem fettreiche Ernährung die Expression des Rezeptors induziert, deutet bereits auf eine zentrale Rolle im Lipid- und Glukose-Metabolismus hin^{117,128,145}.

PPAR γ ist der essenzielle Regulator bei der Adipozytendifferenzierung aus Präadipozyten im weißen und braunen Fettgewebe und maßgeblich für deren Erhaltung und Funktion verantwortlich^{52,146-149}. So fördert eine Aktivierung des Rezeptors die Lipidspeicherung in Adipozyten des weißen Fettgewebes durch die Expression von Fettsäuretransportern wie der Fettsäure-Translokase (FAT bzw. CD36 in Makrophagen)¹⁵⁰, dem Fettsäure-Transport-Protein (FATP)¹⁵¹, der Lipoproteinlipase (LPL)¹⁵² und dem Fettsäure-Bindungs-Protein 4 (FABP4)^{153,154}, wodurch freie Fettsäuren aus der Peripherie aufgenommen werden^{120,155}. Außerdem wird durch PPAR γ -Aktivität in Adipozyten Lipogenese induziert^{149,156}. Fettsäuren unterschiedlicher Genese werden durch Veresterung mit Glycerol zur vermehrten Triglycerid-Synthese verwendet¹⁵⁷, und anschließend in Lipidtropfen gespeichert, an deren Bildung PPAR γ über die Regulation von bspw. Perilipinen (PLINs) beteiligt ist^{120,128,158,159}. Neben zahlreichen adipogenen Wirkungen unterstreichen auch lipolytische Effekte die Bedeutung von PPAR γ in der Lipidhomöostase^{160,161}. Darüber hinaus greift PPAR γ entscheidend in den Glucosestoffwechsel ein und ist somit über die Verknüpfung des Kohlehydrat- und Fettsäure-Metabolismus für eine gesteigerte Glukoseverwertung und verbesserte Insulinsensitivität verantwortlich, und reguliert vielfältige Gene, die an der Glukosehomöostase beteiligt sind^{52,162,163}. PPAR γ steuert außerdem die Expression von Adiponektin¹⁶⁴ und *Angiopoietin-like protein 4* (ANGPTL4)^{165,166}, sogenannte Adipokine, welche Zytokine des Fettgewebes darstellen¹⁶⁷. Dadurch kommt es zum einen zur vermehrten β -Oxidation von Fettsäuren und zum anderen zur Lipolyse durch Hemmung der LPL, aber durch Hemmung der Glukoneogenese auch zu einem Einfluss auf die Blutglukosespiegel, was insgesamt zu einer Verbesserung der Insulinsensitivität führt^{166,168-170}. Zusätzlich induziert PPAR γ die Expression von Glukosetransportern wie GLUT4^{171,172}, wodurch es insulinvermittelt zu einer gesteigerten Aufnahme von Glukose kommt, und hemmt die Glukoneogenese in der Leber über eine Inhibition der zentralen Enzyme Phosphoenolpyruvat-Carboxykinase (PEPCK) und Glukose-6-Phosphatase (G6Pase)^{173,174}. Diese insulinsensitivierenden Effekte von PPAR γ werden mit der Aktivierung durch die Wirkstoffklasse der Glitazone (siehe Kapitel 1.3.2) therapeutisch bereits seit den 1980er Jahren zur Behandlung von Diabetes mellitus Typ 2 genutzt und führen zu einer signifikanten Senkung der Blutzuckerspiegel sowie reduzierten Lipid- und Insulinlevels^{163,175}. Die Glitazone haben jedoch aufgrund eines ungünstigen Nebenwirkungsprofils, vor allem wegen Ödembildung,

Gewichtszunahme und einem erhöhten Risiko für Herzinsuffizienz und Knochenbrüche, in der Anwendung erheblich an Bedeutung verloren^{176,177}.

Neben seiner zentralen Rolle im Metabolismus werden PPAR γ zahlreiche antientzündliche und immunmodulierende Effekte zugeschrieben¹⁷⁸. So hemmt die ligandenabhängige Aktivierung von PPAR γ durch eine Blockade des Transkriptionsfaktors NF κ B in Makrophagen die Expression proinflammatorischer Zytokine wie dem Tumornekrosefaktor α (TNF α), der Interleukine (IL) 1 β und 6 sowie der induzierbaren Stickstoffmonoxid-Synthase (iNOS, Abbildung 8)^{179,180}. Außerdem spielt PPAR γ eine wichtige Rolle bei der Differenzierung von Monozyten zu Makrophagen^{150,181}. Nach der Aktivierung von Monozyten, die selbst nur wenig PPAR γ exprimieren, ist der Rezeptor, induziert von IL-4, an der Verschiebung der Differenzierung von proinflammatorischen M1-Makrophagen hin zum vermehrt antiinflammatorischen M2-Phänotyp beteiligt und fördert somit die sog. alternative Aktivierung¹⁸¹⁻¹⁸⁴. Zusätzlich exprimieren Makrophagen durch PPAR γ -Aktivität verstärkt CD36 auf der Zelloberfläche, wodurch oxidiertes LDL aus der Peripherie aufgenommen und metabolisiert wird¹⁸⁵. In ähnlicher

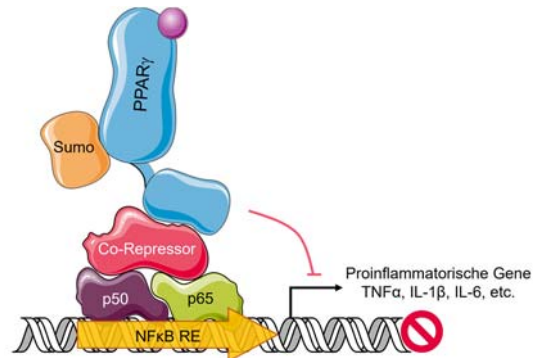


Abbildung 8: Mechanismus der PPAR γ -vermittelten Transrepression proinflammatorischer Gene über NF κ B (p65/p50).

Weise reguliert PPAR γ den Lipidmetabolismus in dendritischen Zellen, greift aber auch in Prozesse wie die Aktivierung und Differenzierung der Zellen, Migration und Antigen-Prozessierung ein^{178,186}. Durch eine verringerte Sekretion von IL-12 und veränderte Expression kostimulierender Moleküle wie CD80 und CD86 wird zusätzlich die T-Zell-Antwort beeinflusst¹⁸⁶. Obwohl bereits in Tiermodellen positive Effekte bei Atherosklerose und Autoimmunerkrankungen wie der rheumatoiden Arthritis und chronisch entzündlichen Darmerkrankungen gezeigt werden konnten, muss der therapeutische Nutzen der antientzündlichen PPAR γ -Wirkung noch näher untersucht werden^{127,178}.

Obwohl PPAR γ der PPAR-Subtyp mit der geringsten Expression im ZNS ist, wo er vor allem in Neuronen vorkommt, ist die Evidenz für neuroprotektive Effekte bei AD, PD und MS durch PPAR γ -Aktivierung am stärksten^{66,137}. Hierfür ist vor allem eine PPAR γ -vermittelte Reduktion der Neuroinflammation verantwortlich¹⁸⁷. In zahlreichen Tiermodellen der AD reduzierte PPAR γ -Aktivierung außerdem kognitive Defizite^{188,189} und verringerte β -Amyloid-Ablagerungen¹⁹⁰⁻¹⁹², was zum einen durch Induktion des insulinabbauenden Enzyms (*Insulin-degrading enzyme*, IDE) und zum anderen durch Reduktion der β -Sekretase (*β -site amyloid precursor protein cleaving enzyme*, BACE1) zu erklären ist¹⁹³⁻¹⁹⁵. In Modellen der PD konnte durch PPAR γ -Aktivierung der Verlust dopaminerger Neurone verringert werden, eine Aktivierung der Mikroglia wurde unterdrückt und motorische Beeinträchtigungen verbessert¹⁹⁶⁻²⁰⁰. Kohortenstudien deuten darauf hin, dass die Einnahme von Glitazonen das Risiko für AD²⁰¹⁻²⁰³ und PD²⁰⁴ senken kann. Im Krankheitsgeschehen von MS kommt zusätzlich zur antientzündlichen Wirkung die immunmodulierende Rolle von PPAR γ zum Tragen. Zu beachten ist dabei auch, dass PPAR γ in Makrophagen von MS-Patienten signifikant herunterreguliert ist²⁰⁵ und somit die fehlende Expression von CD36 eine Beseitigung der Myelinreste durch Phagozytose erschwert und gleichzeitig Neuroinflammation begünstigt wird²⁰⁶. PPAR γ -Aktivierung fördert außerdem die Differenzierung von Oligodendrozyten-Vorläuferzellen²⁰⁷, die eine tragende Rolle bei der Remyelinisierung spielen, und schützt die noch vorhandenen Oligodendrozyten vor inflammatorischer Schädigung²⁰⁸. Auch im Modell der experimentellen autoimmunen Enzephalomyelitis (EAE), dem gängigsten Tiermodell der

MS, verbesserten PPAR γ -Agonisten den Krankheitsverlauf^{209–212}. Obwohl erste klinische Studien vielversprechende Ergebnisse für die Wirksamkeit von Pioglitazon (2), nicht jedoch Rosiglitazon (3)^{213,214}, bei AD^{215,216} und vor allem MS^{217–219} zeigten, sind größer angelegte Studien, weitere mechanistische Analysen und neue PPAR γ -Agonisten mit höherer Bioverfügbarkeit im ZNS notwendig, um einen therapeutischen Nutzen bei neurodegenerativen Erkrankungen zu belegen.

PPAR δ wird im Körper ubiquitär exprimiert, wobei er die höchste basale Expression im Skelettmuskel und Gastrointestinaltrakt zeigt^{220,221}. Des Weiteren wird der Rezeptor besonders bei Zelldifferenzierungsprozessen induziert, wohingegen während der Zellproliferation geringere Level auftreten^{112,128}. Außer im Gehirn sind die Expressionslevels dieses PPAR-Subtyps insgesamt jedoch meist niedriger als bei PPAR α und PPAR γ ^{137,220}. Aufgrund der unspezifischen Expression und bislang fehlender zugelassener Arzneistoffe für PPAR δ ist die Evidenz der pleiotropen metabolischen Funktionen für diesen Subtypen geringer, das Forschungsinteresse hat aber mit der Entdeckung der Schlüsselfunktionen im Energiehaushalt des Muskels stark zugenommen^{143,222}. So bewirkt eine Überexpression von PPAR δ im Skelettmuskel einen gesteigerten oxidativen Metabolismus von Fettsäuren, vermehrte Aufnahme von Glukose in die Zellen sowie erhöhte mitochondriale Biogenese, vermittelt über die Aktivierung der AMP-aktivierten Proteinkinase (AMPK)²²³. Dadurch wird außerdem die Lactatdehydrogenase B (LDHB) verstärkt induziert, wodurch die Akkumulation von Lactat verringert wird und die mitochondriale Oxidation von Pyruvat steigt²²³. Zusätzlich nimmt die Bildung von oxidativen Muskelfasern zu, ein Effekt, der sonst durch wiederholte Beanspruchung der Muskeln auftritt, und es kommt zu einer allgemeinen Abnahme des Körperfettanteils und gesteigerter Insulinsensitivität^{224–226}. Der Phänotyp der PPAR δ -Überexpression wurde auch als „Marathon-Mäuse“ bezeichnet, da die Tiere eine signifikant höhere Ausdauer zeigten^{222,227}. Auch im Fettgewebe fördert PPAR δ den Fettsäure-Abbau und induziert Gene, die Fettsäure-Oxidation und Thermogenese steigern wie die Carnitin-Acyltransferase 1 (CPT1) und das Thermogenin (*uncoupling protein*, UCP1)¹⁴³. Therapeutisch impliziert dies eine mögliche Anwendung von PPAR δ -selektiven Agonisten bei Adipositas und Dyslipidämien^{228–230}, wofür erste klinische Studien bereits eine Wirksamkeit belegen konnten, aber auch bei degenerativen Muskel-erkrankungen²³¹. Des Weiteren ist auch PPAR δ an der Glukose-Verwertung und dem Lipoprotein-metabolismus in der Leber beteiligt, wobei Transkriptom-Analysen gezeigt haben, dass sich die Zielgene von PPAR α und PPAR δ hier nur wenig überschneiden²³². Außerdem fördert PPAR δ die alternative Aktivierung der Kupffer-Zellen (Makrophagen der Leber), sodass eine Aktivierung des Rezeptors anti-entzündliche Effekte in der Leber vermittelt²³³. Ein zusätzlicher antientzündlicher Mechanismus von PPAR δ in Makrophagen wird ligandeninduziert über die Freisetzung des Co-Repressors BCL6 vermittelt, wodurch es zu einer Unterdrückung von NF κ B-regulierten proinflammatorischen Zytokinen kommt^{234,235}. Außerdem fördert PPAR δ die Phagozytose apoptotischer Zellen durch Makrophagen über die Expression von Opsoninen, wodurch der Rezeptor indirekt die Bildung von Autoantikörpern vorbeugt und damit eine protektive Rolle bei der Entwicklung von Autoimmunerkrankungen spielen könnte²³⁶. Erste Tierversuche deuten außerdem darauf hin, dass PPAR δ -Agonisten vor allem durch antientzündliche Effekte im EAE-Modell^{237,238} und in verschiedenen PD-Modellen^{239–242} therapeutisches Potenzial bei neurodegenerativen Erkrankungen aufweisen. Insgesamt wird die Rolle von PPAR δ im Entzündungsgeschehen jedoch noch kontrovers diskutiert und bedarf weiterer Untersuchungen, da in einigen Studien auch immunstimulierende Effekte auf eine Aktivierung des Rezeptors zurückzuführen waren^{243–245}.

1.3.2 Bekannte PPAR-Liganden

Die LBDs der PPAR-Subtypen untereinander weisen eine Sequenzhomologie von 60–70 % auf, sodass sich auch Unterschiede bei den Aminosäuren feststellen lassen, welche an der Ausbildung der Ligandenbindetasche beteiligt sind^{163,246}. Die Volumina der jeweiligen Bindetaschen sind mit etwa 1200–1400 Å³ vergleichbar in ihrer Größe und innerhalb der Familie nukleärer Rezeptoren relativ groß^{17,247}. Dabei ist das Volumen von PPAR δ innerhalb der Subfamilie am kleinsten und nimmt über PPAR α zu PPAR γ hin zu^{52,246}. Die Ligandbindung der PPARs wird durch starke hydrophile Interaktionen der kanonischen Aktivierungs-Tetrade an Aminosäuren bestimmt, bestehend aus Tyrosin in H12 (α : Tyr464, γ : Tyr473, δ : Tyr437), Histidin in H11 (α : His440, γ : His449, δ : His413), Histidin in H5 (γ : His323, δ : His287) und Serin in H3 (α : Ser280, γ : Ser289), die mit der sauren Kopfgruppe des jeweiligen Liganden wechselwirken (Abbildung 9)^{246–248}. Bei PPAR α befindet sich anstelle des Histidins in Helix 5 jedoch ein Tyrosin (Tyr314), welches weiter in die Bindetasche hineinragt²⁴⁶. Bei PPAR δ ist anstelle des Serins in Helix 3 ein Threonin-Rest (Thr253) vorzufinden, der zusammen mit dem sperrigen Met417 in Helix 11 für einen schmalen Interaktionsbereich der Bindetasche nahe Helix 12 verantwortlich ist^{246,249,250}. Somit sind strukturell subtypenselektive Liganden möglich, deren Entwicklung jedoch nicht trivial ist. Abgeleitet von Fettsäuren als endogenen PPAR-Liganden sind synthetische Liganden in der Regel als Fettsäuremimetika zu verstehen¹⁰. Sie liegen daher meist als Carboxylate vor, welche bei PPAR α und PPAR γ vorwiegend in α -Position mit teils sperrigen Resten, wie bspw. bei den Glitazaren, substituiert sind, während bei PPAR δ in der Regel α -unsubstituierte Phenoxyessigsäure-Derivate vorzufinden sind^{246,251,252}. Bei den Glitazonen als selektiven PPAR γ -Liganden ist die Carbonsäure bioisoster durch ein Thiazolidindion-Strukturmotiv ersetzt^{251,253}. Die Bindetasche der PPARs wird häufig als Y- oder auch T-förmig bezeichnet, an deren Fuß die beschriebenen hydrophilen Interaktionen nahe Helix 12 stattfinden^{249,251}. Dabei ist vor allem die direkte Interaktion mit dem Tyrosinrest in Helix 12 für eine volle PPAR-Aktivierung entscheidend und stabilisiert die AF2 in der aktiven Konformation^{247,254,255}. Der restliche voluminöse Teil der Bindetasche ist überwiegend von hydrophoben Aminosäuren geprägt, weist eine hohe Flexibilität auf und unterscheidet sich deutlicher zwischen den Subtypen^{52,247}. So ist die Bindetasche bei PPAR α insgesamt lipophiler als bei PPAR γ und PPAR δ ²⁴⁶. Im Allgemeinen sind die hydrophoben Wechselwirkungen mit dem Liganden eher unspezifisch, was die große strukturelle Diversität der Liganden erklärt²⁵¹. Eine Besonderheit der PPARs, die sich aus der ungewöhnlichen Größe und Flexibilität der Bindetasche ergibt, ist die Möglichkeit, einen Liganden in unterschiedlichen Bindemodi innerhalb der orthosterischen Bindestelle zu koordinieren, aber auch zwei gleiche oder unterschiedliche endogene wie synthetische Liganden parallel zu binden^{80,249,256,257}.

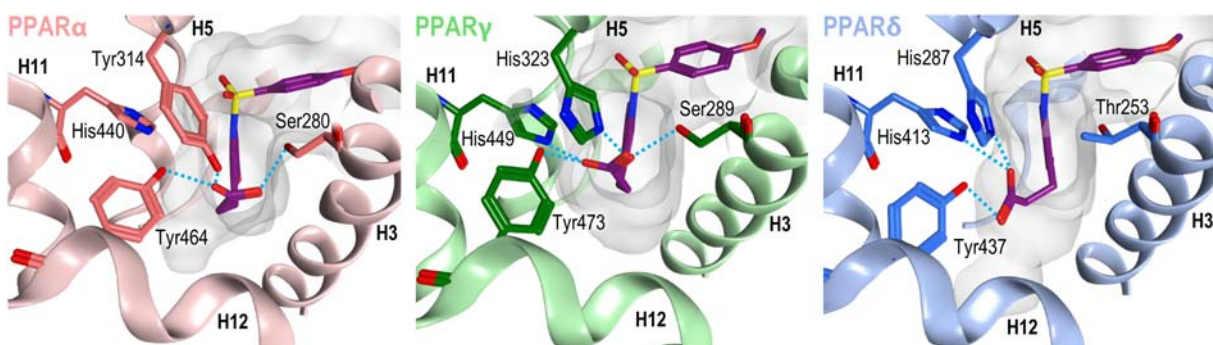


Abbildung 9: Vergleich der Liganden-Protein-Interaktion mit der kanonischen Aktivierungs-Tetrade der drei PPAR-Subtypen. Gezeigt ist jeweils die Co-Kristallstruktur des pan-PPAR-Agonisten Indeglitazar (violett) mit PPAR α (PDB: 3ET1), PPAR γ (PDB: 3ET3) und PPAR δ (PDB: 3ET2)²⁵⁸.

Als Regulatoren des Glucose- und Lipidstoffwechsels binden die PPARs physiologisch vor allem ungesättigte, aber auch gesättigte Fettsäuren wie die Ölsäure (C18:1), Linolsäure (C18:2), Arachidonsäure (C20:4) und Palmitinsäure (C16:0) mit meist moderater Affinität im mikromolaren Bereich^{127,249}. Diese recht unspezifischen Interaktionen aller drei Subtypen deuten auf eine allgemein modulierende Rolle der Rezeptoren im Lipidstoffwechsel hin, stellen die physiologische Relevanz aufgrund geringer intrazellulärer Konzentrationen der entsprechenden Fettsäuren jedoch zum Teil in Frage²⁵⁹. Es gibt aber auch spezifischere endogene Liganden, die überwiegend zu den Eicosanoiden gehören, welche Metabolite der Arachidonsäure mit überwiegend proinflammatorischen Eigenschaften sind^{260,261}. Im Folgenden werden einige spezifische endogene und synthetische Liganden der einzelnen PPAR-Subtypen näher betrachtet.

Zu den endogenen **PPAR α** -Liganden zählt zum Beispiel der Arachidonsäure-Metabolit Leukotrien B₄ (**4**, LTB₄, Abbildung 10)^{262–264}. PPAR α -Aktivierung fördert den Abbau des Entzündungsmediators im Sinne eines negativen Feedback-Mechanismus, sodass die LTB₄-induzierte Entzündungsreaktion begrenzt wird²⁶². Außerdem konnten zwei Analoga des endogenen Cannabinoids Anandamid als PPAR α -selektive Liganden identifiziert werden²⁶⁵. Zum einen Palmitoylethanolamid (**5**, Abbildung 10) mit einem EC₅₀-Wert von 3,1 μ M, das ebenso antiinflammatorische Eigenschaften von PPAR α aktiviert²⁶⁶. Zum anderen wird PPAR α durch Oleoylethanolamid (**6**, Abbildung 10) aktiviert, welches mit einem EC₅₀-Wert von 0,12 μ M eine deutlich höhere Affinität als die meisten endogenen PPAR-Liganden aufweist und einen Einfluss auf Sättigungsgefühl und Körpergewicht hat²⁶⁷. Zu den synthetischen PPAR α -Liganden gehört die Arzneistoffklasse der Fibrate, welche als Lipidsenker vor allem zur Senkung der Triglyceride bereits seit den 1960er Jahren eingesetzt werden, deren Wirkmechanismus allerdings erst später aufgeklärt wurde¹²⁵. Mit Ausnahme von Bezafibrat, einem moderaten pan-PPAR-Agonist, sind die Fibrate selektive PPAR α -Aktivatoren mit Aktivitäten im mikromolaren Bereich, die die 2-Methyl-2-phenoxy-propansäure als gemeinsames Strukturmotiv aufweisen und wie der bekannteste Vertreter Fenofibrat (**7**, Abbildung 10) zum Teil als Prodrugs eingesetzt werden^{163,268,269}. Heutzutage haben die Fibrate jedoch aufgrund ihres Langzeitnutzens in Bezug auf kardiovaskuläre Ereignisse an Bedeutung verloren und sind in der therapeutischen Anwendung den Statinen unterlegen^{136,270}. Die Entwicklung von Pemafibrat (**8**, Abbildung 10) zeigt allerdings, dass PPAR α immer noch eine relevante Zielstruktur zur Behandlung von Dyslipidämien im Zusammenhang des metabolischen Syndroms darstellt und durch das Konzept der neuen selektiven PPAR α -Modulatoren (sPPAR α M) eine Alternative mit

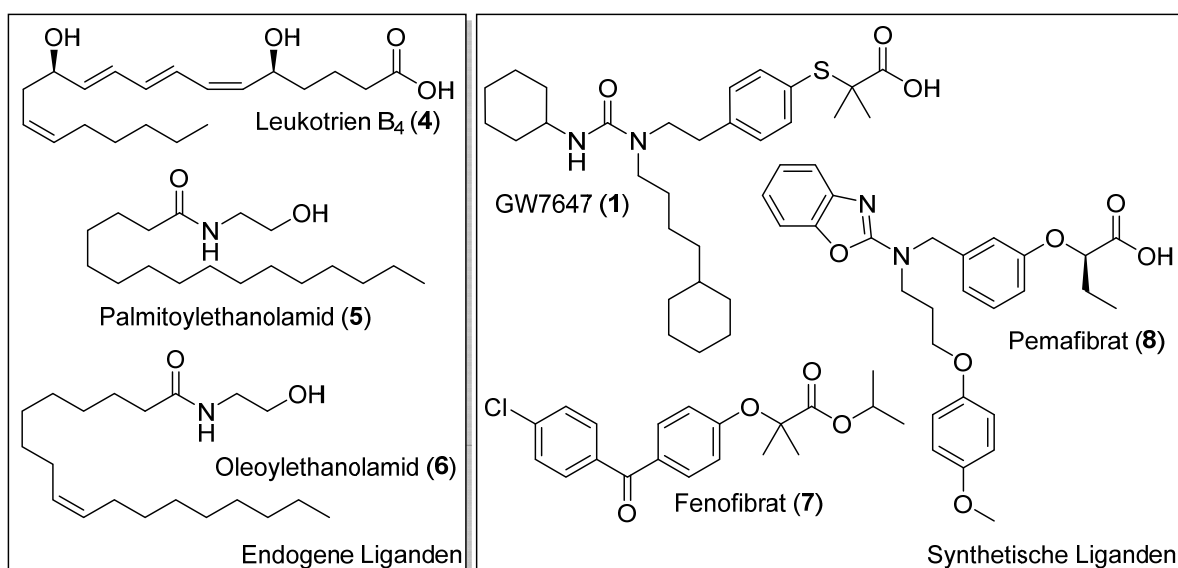


Abbildung 10: PPAR α -selektive Liganden

verbessertem Nutzen-Risiko-Profil bestehen könnte^{271,272}. **8** adressiert dabei neben der klassischen Fettsäure-Bindestelle gezielter die Y-förmige Bindetasche mit einem EC₅₀-Wert von 1 nM und zeichnet sich durch eine hohe Subtypenselektivität (> 1000-fach) aus^{271,273}. Ein weiterer wichtiger PPAR α -selektiver Ligand ist GW7647 (**1**, Abbildung 10), welcher sich durch einen Thioether in der Kopfgruppe sowie eine substituierte Harnstoff-Struktur auszeichnet und sich als Referenzagonist für PPAR α etabliert hat²⁷⁴.

Als erster möglicher endogener PPAR γ -Ligand wurde der Arachidonsäure-Metabolit 15-deoxy- $\Delta^{12,14}$ -Prostaglandin J₂ (**9**, 15d-PGJ₂, Abbildung 11) entdeckt, der mit EC₅₀-Werten und Bindungsaffinitäten im unteren mikromolaren Bereich beschrieben wird^{275,276}. Es konnte gezeigt werden, dass **9** eine kovalente Bindung mit dem Cys285-Rest des Rezeptors eingeht, welche entscheidend für dessen Aktivierung ist²⁷⁷⁻²⁷⁹. Die physiologische Bedeutung ist jedoch wie auch bei weiteren Fettsäure-Metaboliten als potenziellen endogenen PPAR γ -Liganden umstritten, nicht zuletzt, da sich die Gewebekonzentrationen im Bereich unter 100 nM bewegen^{259,280,281}. Mehrere Studien haben jedoch eine mit den Thiazolidindion-basierten Agonisten vergleichbare Wirkung von **9** beobachtet, in denen der natürliche Lipidmediator neben adipogenen und antientzündlichen Effekten auch neuroprotektive Wirkungen durch PPAR γ -Aktivierung zeigte^{212,275,276,282-284}. Außerdem wurden Nitrofettsäuren, insbesondere Derivate der Linolsäure, als potente PPAR γ -Agonisten mit Bindungsaffinitäten von 0,41–0,60 μ M postuliert^{285,286}. Vor allem die 12-NO₂-Linolsäure (**10**, Abbildung 11) zeigt mit einem EC₅₀-Wert von 0,045 μ M eine physiologisch relevante Aktivität am Rezeptor²⁸⁶ und deutet darauf hin, dass NO-vermittelte Signalwege in Form von Nitrofettsäuren durch PPAR γ reguliert werden und so antientzündliche Effekte ausüben könnten²⁸⁵. Kürzlich konnte TETRAC (**11**, Abbildung 11), ein Metabolit des Thyroidhormons L-Thyroxin, als weiterer potenzieller endogener PPAR γ -Ligand mit einem EC₅₀-Wert von 0,10 μ M und einer Bindungsaffinität von 0,11 μ M charakterisiert werden²⁸⁷. Dabei ist vor allem die Effizienz (vergleichbar mit **3**) am Heterodimer mit RXR α bemerkenswert, was auf eine physiologische Rolle als metabolischem Gegenspieler zum Thyroidhormon-Rezeptor (THR) auf genomischer Ebene hindeutet²⁸⁷.

Mit der Arzneistoffklasse der Glitazone wurden Anfang der 1980er Jahre die ersten synthetischen selektiven PPAR γ -Agonisten mit zunächst unbekanntem Wirkmechanismus entwickelt, welche als sog. Insulin-Sensitizer zu einer Senkung des Blutzuckerspiegels bei Diabetes mellitus Typ 2 führen^{126,288}. Die Thiazolidindion-Struktur ist charakteristisch für diese Wirkstoffklasse und interagiert mit der gleichen kanonischen Bindestelle wie die Carboxylfunktion endogener Fettsäuren^{126,251}. Rosiglitazon (**3**) und Pioglitazon (**2**) sind die zwei Vertreter, die in Deutschland eine Zulassung erhalten haben und als orale Antidiabetika eingesetzt wurden (Abbildung 11). Das Nebenwirkungsprofil ist bei beiden Substanzen jedoch ungünstig, da gerade bei dieser Indikation eine erhöhte Gewichtszunahme unvorteilhaft ist, aber auch schwerwiegende Nebenwirkungen wie vermehrte Knochenbrüche und ein erhöhtes Blasenkrebsrisiko bekannt sind^{176,289}. Aktuell ist nur Pioglitazon (**2**) in Ausnahmefällen noch verschreibungsfähig, Rosiglitazon (**3**) ist aufgrund von zusätzlich erhöhten kardiovaskulären Risiken seit November 2010 nicht mehr verkehrsfähig²⁹⁰⁻²⁹². Beide Substanzen werden aber nach wie vor als potente Referenzagonisten für PPAR γ genutzt, da sie sich durch eine hohe Subtypen-Selektivität auszeichnen und mit **3** (EC₅₀ 0,043 μ M) und **2** (EC₅₀ 0,58 μ M) zwei umfassend charakterisierte Agonisten mit unterschiedlicher Aktivierungseffizienz zur Verfügung stehen^{163,293}.

Da sich einige der Glitazon-bedingten Nebenwirkungen auf die volle Aktivierung des Rezeptors zurückführen lassen, hat sich die Entwicklung neuer PPAR γ -Liganden hin zu Partialagonisten und selektiven PPAR γ -Modulatoren (sPPAR γ M) entwickelt, welche durch veränderte Co-Regulator-Interaktionsprofile, gewebespezifische Effekte, Inhibierung der Phosphorylierung an Ser245 (PPAR γ 1, bzw. Ser273

bei PPAR γ 2) oder unterschiedlichen Bindemodus bestimmte Gene gezielter aktivieren können²⁹⁴⁻²⁹⁹. Somit sollen die unerwünschten adipogenen Effekte, Gewichtszunahme, Ödembildung und ein erhöhtes Herzinsuffizienz-Risiko verringert werden, um die positiven Wirkungen auf die Glucose- und Lipid-Homöostase besser nutzen zu können²⁹⁴. Ein Beispiel für einen sPPAR γ M ist MRL24 (**12**, Abbildung 11), welcher mit einem EC₅₀-Wert von 2 nM und einer Aktivierungseffizienz von 36 % (vs. **3**) einen hochpotenten und selektiven Partialagonisten darstellt^{300,301}. Neben erfolgreichen *Proof-of-Concept*-Studien in Tiermodellen³⁰⁰ zeigte eine Untersuchung des Bindemodus, dass es zu einer Stabilisierung der Helix 3 sowie zur Koordination der β -Faltblattstruktur über die Säurefunktion des Liganden kommt, während Helix 12 flexibel bleibt, was in der verminderten Aktivierungseffizienz resultiert^{256,302}. Eine Phase-2-Studie mit dem analogen MK-0533 zur Behandlung von Diabetes mellitus Typ 2 im Vergleich zu Pioglitazon (**2**) wurde jedoch aufgrund mangelnder Wirksamkeit frühzeitig beendet³⁰³. Mit INT-131 und MBX-102 sind weitere sPPAR γ M in klinischer Prüfung zur Behandlung von Diabetes mellitus Typ 2, aber auch bei anderen Indikationsgebieten wie Gicht und MS und demonstrieren somit die vielfältigen Strategien zur therapeutischen Nutzung neuer PPAR γ -Modulatoren³⁰⁴⁻³⁰⁸. Die Entwicklung dualer PPAR α/γ -Agonisten, der Stoffklasse der Glitazare, als vielversprechende Therapieoption bei Patienten mit Diabetes mellitus Typ 2 und erhöhtem kardiovaskulärem Risiko war bislang aufgrund ihres ungünstigen Nebenwirkungsprofils nicht erfolgreich, lediglich Saroglitazar konnte bisher eine Zulassung in Indien erhalten¹³¹. PPAR γ -Antagonisten spielen therapeutisch bislang keine Rolle, werden aber in Bezug auf positive Effekte bei Adipositas und Krebserkrankungen untersucht^{296,309,310}. Vor allem aber sind sie hilfreiche *tool compounds* zur Charakterisierung neuer PPAR γ -Modulatoren und zur Validierung der Zielstruktur in neuen Indikationsgebieten. GW9662 (**13**, Abbildung 11) ist der meistgenutzte Vertreter, der mit einem IC₅₀-Wert von 0,076 μ M die Aktivierung des Rezeptors effektiv inhibiert und irreversibel eine kovalente Bindung mit Cys285 eingeht, wodurch die orthosterische Bindetasche blockiert wird³¹¹.

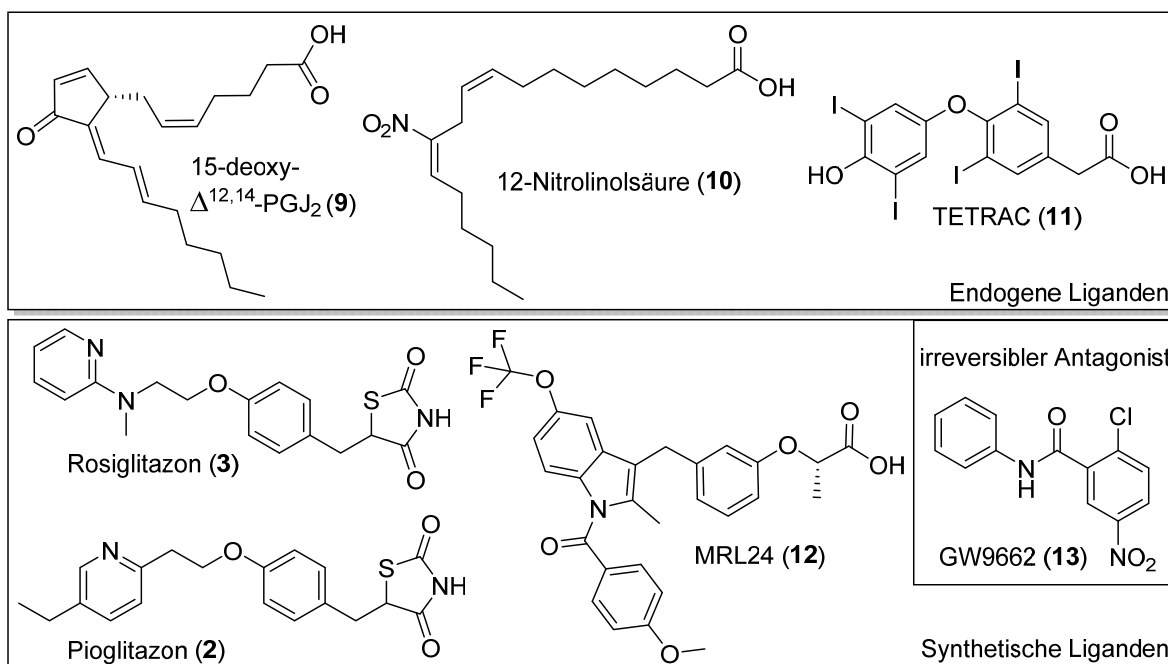


Abbildung 11: PPAR γ -selektive Liganden

Auch für **PPAR δ** wurde mit dem Linolsäure-Metaboliten (S)-13-Hydroxy-9,11-octadecadiensäure (13-S-HODE, **14**, Abbildung 12) ein Fettsäuremetabolit als endogener Ligand identifiziert, der eine Bindungsaffinität von 10,8 μM aufweist³¹². Durch Bindung des Liganden wird die Aktivierung des Rezeptors jedoch inhibiert sowie dessen Expression herunterreguliert, wodurch Apoptose in Krebszellen induziert wird³¹². Diese spezifische Aktivität an PPAR δ unterscheidet sich damit von der moderaten PPAR γ -Aktivierung durch 13-S-HODE (**14**), vor allem aber durch das Isomer 9-S-HODE¹⁸⁵. Außerdem weist der Arachidonsäure-Metabolit 15-Hydroxyeicosatetraensäure (15-HETE, **15**, Abbildung 12) eine Präferenz für PPAR δ auf, da dieser den Rezeptor mit hoher Effizienz aktiviert und eine direkte Interaktion mit der LBD zeigt³¹³. Synthetische PPAR δ -Liganden sind Fettsäuremimetika mit einer 2-Phenoxyessigsäurestruktur wie bei dem Agonisten L165,041 (**16**, Abbildung 12), der sich durch eine hohe Bindungsaffinität ($K_i = 6 \text{ nM}$), einen EC_{50} -Wert von 0,53 μM und eine 10-fache Selektivität gegenüber PPAR α und PPAR γ auszeichnet^{163,314}. **16** wird häufig als Referenzsubstanz bei *in vitro* Versuchen verwendet, erreichte aber nie die klinische Prüfung aufgrund der moderaten Subtypen-Selektivität. Besonders potent ($\text{EC}_{50} 0,0012 \mu\text{M}$) und Subtypen-selektiv (~ 1000 -fach) ist der PPAR δ -Agonist GW501516 (**17**, Abbildung 12)^{315,316}, der bereits in klinischen Studien zur Behandlung von Dyslipidämien, Adipositas und kardiovaskulären Erkrankungen untersucht wurde, bis Tierversuche Kanzerogenität in mehreren Organen zeigten³¹⁷⁻³¹⁹. Seit Studien **17** eine deutliche leistungssteigernde Wirkung bei Mäusen durch veränderten Energiestoffwechsel attestierten, wird die Substanz trotz bekannter Risiken unter dem Namen Endurobol als illegales Dopingmittel im Sport verwendet^{320,321}. Mit Seladelpar (**18**, Abbildung 12) wird derzeit ein selektiver PPAR δ -Agonist mit dem gleichen 2-(4-Mercapto-2-methylphenoxy)essigsäure-Grundgerüst wie **17** in klinischen Studien zur primären biliären Cholangitis (PBC) bereits in Phase 3, sowie bei primärer sklerosierender Cholangitis (PSC), nicht-alkoholischer Steatohepatitis (NASH) und Dyslipidämien in Phase-2-Studien geprüft^{228,322,323}. Dabei adressiert **18** durch die Ethoxy-Seitenkette in *R*-Konfiguration die Y-förmige Bindetasche und zeichnet sich durch hohe Potenz ($\text{EC}_{50} 0,0019 \mu\text{M}$) und Subtypen-Selektivität (> 500 -fach) aus^{250,324}. Der potente duale PPAR α/δ -Ligand Elafibranor musste kürzlich einen Rückschlag erleiden, als die Phase-3-Studie zur Behandlung von NASH aufgrund mangelnder Effektivität vorzeitig beendet wurde^{319,325}. Derzeit wird die Substanz ebenfalls noch in einer Phase-3-Studie bei PBC untersucht³²⁶.

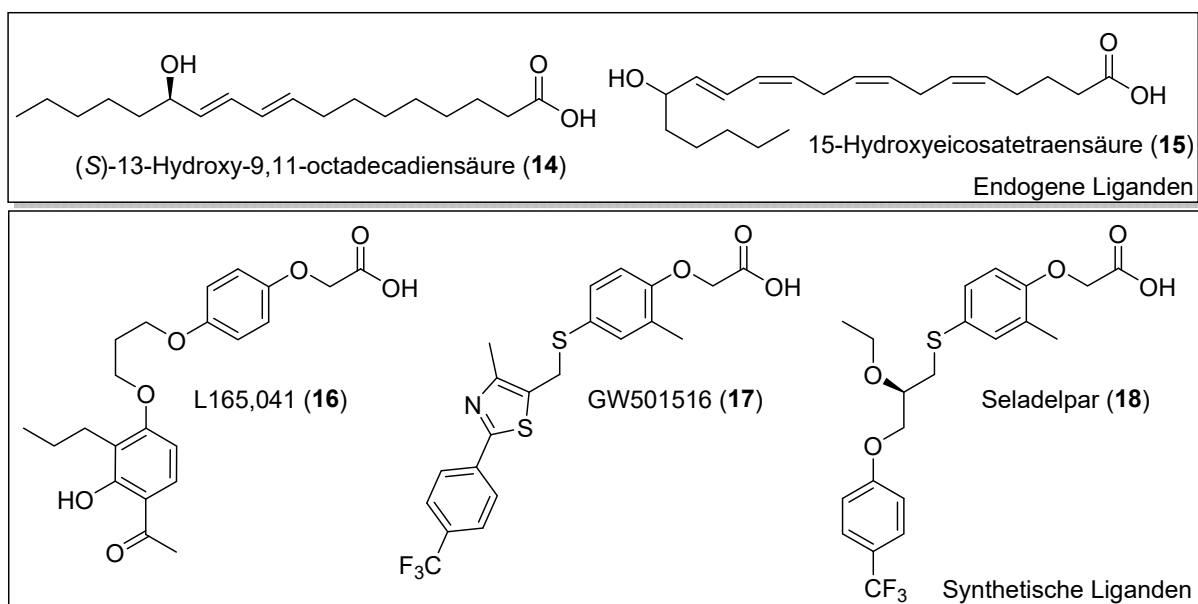


Abbildung 12: PPAR δ -selektive Liganden

1.4 Nuclear receptor related 1 protein (Nurr1)

Der Transkriptionsfaktor *nuclear receptor related 1 protein*³²⁷ (Nurr1, NR4A2) wurde als eng verwandtes Protein zum Nervenwachstumsfaktor-induzierten Gen B^{328,329} (NGFI-B, Nur77, NR4A1) erstmals Anfang der 1990er Jahre identifiziert und ist auch unter den Bezeichnungen nukleärer Rezeptor der T-Zellen (NOT)³³⁰, transkriptionell induzierbarer nukleärer Rezeptor (TINUR)³³¹, regenerierender nukleärer Rezeptor der Leber (RNR-1)³³² und hippocampaler Zinkfinger 3 (HZF-3)³³³ bekannt¹⁶. Zusammen mit dem Neuronen-abgeleiteten *Orphan*-Rezeptor 1 (NOR-1, NR4A3) bilden diese drei nukleären Rezeptoren die NR4A-Subfamilie, welche unter anderem für die Entwicklung und Erhaltung von Neuronen essenziell ist^{9,16,49}. Strukturell entsprechen sie dem klassischen Aufbau nukleärer Rezeptoren wie in Kapitel 1.2.2 beschrieben. Mechanistisch unterscheiden sie sich jedoch von diesen. Sie können sowohl als Monomere und Homodimere die Transkription ihrer Zielgene aktivieren^{55,334,335}, Nur77 und Nurr1 zusätzlich auch als permissive RXR-Heterodimere^{54,336} (Abbildung 13). Dabei binden sie direkt an spezifische Response-Elemente entsprechend der vorliegenden Konstitution. Monomere binden an die NGFI-B-Erkennungssequenz (NBRE) mit dem verlängerten Motiv AAAGGTCA^{334,335}. Homodimere erkennen das sogenannte Nur-Response-Element (NurRE), bei welchem die zwei Halbsseiten mit auswärtsgedrehter Wiederholung angeordnet sind (TGATATTTACCTCC-AAATGCCA) und welches zuerst in der Promotorregion des Proopiomelanocortin(POMC)-Gens identifiziert wurde^{55,337}. Die Heterodimere binden entsprechend anderer RXR-Heterodimere an Erkennungssequenzen mit direkter Wiederholung, welche in diesem Fall einen Abstand von fünf Nukleinbasen aufweisen (DR5; GGTTCACCGAAAGGTCA)^{54,55,336}.

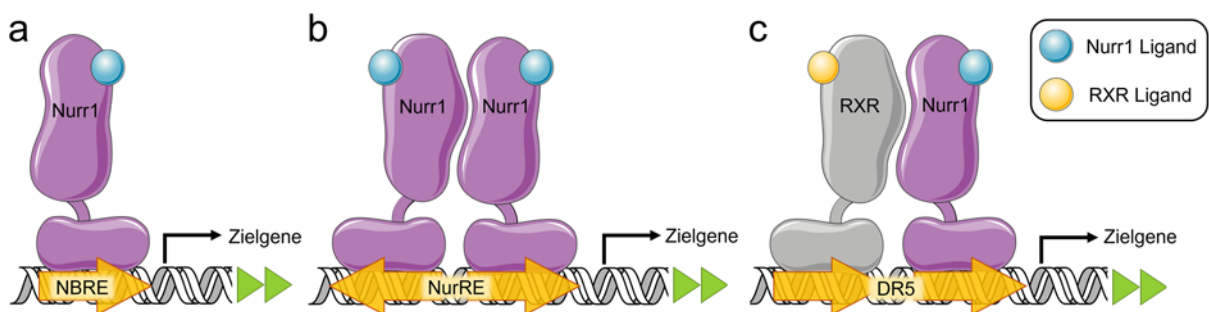


Abbildung 13: Aktivität der NR4A-Rezeptoren als Monomer oder Dimer am Beispiel von Nurr1. Die Rezeptoren Nur77, Nurr1, und NOR-1 sind konstitutiv aktiv und können direkt an spezifische Erkennungssequenzen der DNA als a) Monomer, b) Homodimer oder als c) Heterodimer mit RXR (nicht NOR-1³³⁶) binden. Dabei ist die Bindung eines Liganden nicht zwingend notwendig zur Aktivierung der Transkription.

Eine weitere Besonderheit der NR4A-Subfamilie stellt die hohe konstitutive Aktivität der Rezeptoren dar³³⁸⁻³⁴¹. Ursprünglich wurden Nurr1 und die beiden verwandten Vertreter daher als liganden-unabhängige Transkriptionsfaktoren angesehen^{338,341-343}. Eine Erklärung dafür lieferte die erste Kristallstruktur (PDB: 1OVL) der NR4A-Familie aus dem Jahr 2003, in der die apo-Form der Nurr1-LBD in einer autoaktivierten Konformation mit stabilisierter und an den Kern der LBD gebundener H12 vorliegt, welche an ligandengebundene nukleäre Rezeptoren erinnert (Abbildung 14, vgl. Kapitel 1.2.2 Abbildung 5)^{8,338}. Außerdem ist die kanonische Ligandenbindetasche innerhalb des LBD-Kerns aufgrund dicht gepackter, sperriger, hydrophober Aminosäuren blockiert (Abbildung 14a), welche bei den drei Mitgliedern der NR4A-Subfamilie sowie dem *Drosophila*-Ortholog DHR38 konserviert sind^{338,343,344}. Daher wurden die NR4A-Rezeptoren lange zu den *Orphan*-Rezeptoren gezählt¹⁶. Doch zumindest für Nurr1 ist diese Bezeichnung inzwischen nicht mehr zutreffend, da ungesättigte Fettsäuren als endogene Liganden identifiziert werden konnten, obwohl die physiologische Relevanz dieser Entdeckungen

noch ungeklärt ist (siehe Kapitel 1.4.2)^{9,345-347}. Auch die hochkonservierte Co-Regulator-Bindestelle klassischer NRs unterscheidet sich erheblich bei den NR4A-Rezeptoren^{338,344}. Der sonst hydrophobe Bereich zwischen Helix 3, Helix 4/5 und Helix 12, der für die Bindung des Erkennungsmotivs LXXLL verantwortlich ist^{90,251}, ist bei den NR4A-Rezeptoren eine geladene hydrophile Oberfläche, bei der die Möglichkeit zu hydrophoben Interaktionen mit den Leucin-Resten eines klassischen Co-Aktivators fehlt^{338,344}. Außerdem ist die spezifische Anordnung des Lysin-Restes in Helix 3 und des Glutaminsäure-Restes in Helix 12, welche typischerweise die α -Helix des Co-Regulators stabilisieren („charge clamp“), bei den NR4A-Rezeptoren in umgedrehter Anordnung vorzufinden: Glutaminsäure in Helix 3, Lysin in Helix 12 (Abbildung 14b)^{251,338,341}. Zusätzlich erschwert bei Nurr1 die starke ionische Wechselwirkung dieses Lysin-Restes (Lys590) mit einem Glutaminsäure-Rest aus Helix 4 (Glu440), welche zum Teil für die konstitutive Aktivität des Rezeptors verantwortlich gemacht wird, die Interaktion mit einem Co-Regulator³³⁸. So ist es nicht verwunderlich, dass bisher keine direkte Interaktion der LBD mit einem der klassischen Co-Aktivatoren wie SRC-1, -2 und -3, PGC-1 α und CBP gezeigt werden konnte^{338,341,344,348}. Allerdings konnte eine hydrophobe Furche zwischen Helix 11 und 12 als potenzielle Co-Regulator-Bindestelle ausfindig gemacht werden, die zwei Peptidsequenzen der Co-Repressoren SMRT und NCoR1 bindet (Abbildung 14b)^{343,349}. Außerdem ist die SUMO-E3-Ligase PIAS γ als starker Co-Repressor der Nurr1-Transaktivierung beschrieben, wobei der Mechanismus bisher ungeklärt ist³⁵⁰. Diese Erkenntnisse deuten bereits darauf hin, dass sich die Regulationsmechanismen und das Co-Regulator-Netzwerk bei den NR4A-Rezeptoren von klassischen nukleären Rezeptoren unterscheiden^{348,351}. Um hier detailliertere Einblicke zu ermöglichen, aber auch das therapeutische Potenzial des neuroprotektiven Transkriptionsfaktors Nurr1 besser untersuchen zu können, fehlt es allerdings an selektiven Modulatoren, die durch direkte Interaktion mit der LBD die intrinsische Aktivität des Rezeptors zum einen hemmen, aber auch weiter steigern können.

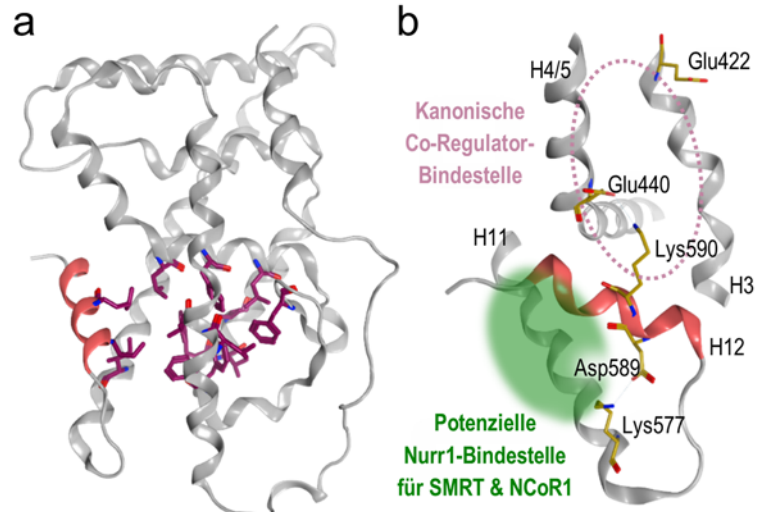


Abbildung 14: Besonderheiten der LBD bei den NR4A-Rezeptoren am Beispiel von Nurr1 (PDB: 1OVL³³⁸). a) Die kanonische Bindetasche ist durch sperrige hydrophobe Seitenketten blockiert³³⁸. b) Helix 12 wird durch zwei starke ionische Wechselwirkungen in der aktiven Konformation stabilisiert. Der Bereich der kanonischen Co-Regulator-Bindestelle ist besonders hydrophil (violett), hingegen kommt der hydrophobe Bereich zwischen H11 und H12 (grün) für Co-Regulator-Interaktionen in Frage.

Restes in Helix 12, welche typischerweise die α -Helix des Co-Regulators stabilisieren („charge clamp“), bei den NR4A-Rezeptoren in umgedrehter Anordnung vorzufinden: Glutaminsäure in Helix 3, Lysin in Helix 12 (Abbildung 14b)^{251,338,341}. Zusätzlich erschwert bei Nurr1 die starke ionische Wechselwirkung dieses Lysin-Restes (Lys590) mit einem Glutaminsäure-Rest aus Helix 4 (Glu440), welche zum Teil für die konstitutive Aktivität des Rezeptors verantwortlich gemacht wird, die Interaktion mit einem Co-Regulator³³⁸. So ist es nicht verwunderlich, dass bisher keine direkte Interaktion der LBD mit einem der klassischen Co-Aktivatoren wie SRC-1, -2 und -3, PGC-1 α und CBP gezeigt werden konnte^{338,341,344,348}. Allerdings konnte eine hydrophobe Furche zwischen Helix 11 und 12 als potenzielle Co-Regulator-Bindestelle ausfindig gemacht werden, die zwei Peptidsequenzen der Co-Repressoren SMRT und NCoR1 bindet (Abbildung 14b)^{343,349}. Außerdem ist die SUMO-E3-Ligase PIAS γ als starker Co-Repressor der Nurr1-Transaktivierung beschrieben, wobei der Mechanismus bisher ungeklärt ist³⁵⁰. Diese Erkenntnisse deuten bereits darauf hin, dass sich die Regulationsmechanismen und das Co-Regulator-Netzwerk bei den NR4A-Rezeptoren von klassischen nukleären Rezeptoren unterscheiden^{348,351}. Um hier detailliertere Einblicke zu ermöglichen, aber auch das therapeutische Potenzial des neuroprotektiven Transkriptionsfaktors Nurr1 besser untersuchen zu können, fehlt es allerdings an selektiven Modulatoren, die durch direkte Interaktion mit der LBD die intrinsische Aktivität des Rezeptors zum einen hemmen, aber auch weiter steigern können.

1.4.1 Physiologische Funktion und therapeutisches Potenzial von Nurr1

Nurr1 wird hauptsächlich im ZNS exprimiert, mit besonderer Häufigkeit in mesenzephalen dopaminergen Neuronen der Area tegmentalis ventralis, der Substantia nigra pars compacta sowie in den paraventriculären Thalamuskernen^{327,352-354}. Als wichtiger Regulator bei der Entwicklung und Erhaltung dopaminergener Neuronen wird Nurr1 im Mittelhirn vom frühen pränatalen Stadium bis zum Erwachsenenalter exprimiert^{353,354}. Auch in Astrozyten und Mikroglia sowie in weiteren Zellen des Immunsystems wie Makrophagen wird Nurr1 zum Teil konstitutiv exprimiert, aber auch induziert, um antientzündliche Effekte auszuüben^{59,355,356}. Außerdem kann Nurr1 in glatten Muskelzellen und Endothelzellen

induziert werden und zeigt zusammen mit Nur77 positive Effekte bei Atherosklerose, indem die Proliferation und Entzündungsreaktion glatter Muskelzellen reduziert und die Bildung von Gefäßläsionen gehemmt wird^{356,357}. In der Leber wird Nurr1 über cAMP induziert und ist zusammen mit den anderen NR4A-Rezeptoren an der Glukose-Verwertung sowie der Homöostase im Cholesterin- und Fettsäurestoffwechsel beteiligt^{332,358}. Daher wird Nurr1 als ein potenzieller Faktor bei metabolischen Erkrankungen³⁵⁸, der entzündlichen Arthritis³⁵⁹, der Aufmerksamkeitsdefizit-Hyperaktivitätsstörung³⁶⁰ und bei verschiedenen Krebserkrankungen³⁵⁵ angesehen. Eine besonders wichtige Rolle wird Nurr1 aber vor allem bei der Pathogenese von neurodegenerativen Erkrankungen wie Parkinson, Alzheimer und Multipler Sklerose zugeschrieben^{19,20,361,362}.

Deutlich wird dies nicht zuletzt durch die von Nurr1 regulierten Gene (Abbildung 15), die wesentliche Faktoren der Dopamin-Neurotransmission und -Homöostase sind, wie Tyrosinhydroxylase (TH), Dopamintransporter (DAT), vesikulärer Monoamintransporter 2 (VMAT2, SLC18A2) und DOPA-Decarboxylase (DDC)^{353,363-365}. In dopaminergen Neuronen wurden weitere Zielgene entdeckt, darunter das *Delta-like-Protein 1* (DLK1), die Protein-Tyrosin-Phosphatase vom Rezeptor-Typ U (PTPRU) und das *Kelch-like-Protein 1* (KLHL1), die an neuronalen Prozessen wie axonalem Wachstum und terminaler Differenzierung beteiligt sind³⁶⁶. Außerdem die Rezeptor-Tyrosinkinase Ret, welche für die Signaltransduktion neurotropher Faktoren wie GDNF entscheidend und somit an der Erhaltung dopaminergener Neurone beteiligt ist³⁶⁷. Als Nurr1-reguliert sind weiterhin der Rezeptor Neuropilin-1³⁶⁸, die GTP-Cyclohydrolase³⁶⁹, das vasoaktive intestinale Peptid (VIP)³⁷⁰, und die Topoisomerase II β ³⁷¹ zu nennen. Auch durch die Regulation der Expression mitochondrialer Gene wie der Superoxid-Dismutase 1

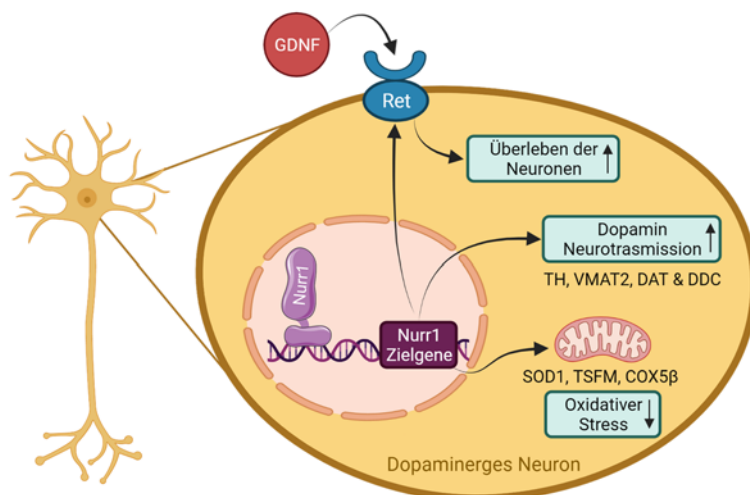


Abbildung 15: Molekulare Funktionen von Nurr1 in dopaminergen Neuronen.

(SOD1) und des mitochondrialen Elongationsfaktors Ts (TSFM) sowie wichtiger Gene für die oxidative Phosphorylierung wie der Cytochrom-c-Oxidase 5 β (COX5 β) scheint Nurr1 in Neuronen essentiell für die Aufrechterhaltung der Atmungskette zu sein und vor oxidativem Stress zu schützen³⁷². Darüber hinaus wurden in Osteoblasten Osteopontin und Osteocalcin als Zielgene identifiziert, was auf eine Rolle von Nurr1 bei der Regulierung der Knochenhomöostase hindeutet^{373,374}.

Die wichtige regulatorische Funktion von Nurr1 bei der Entwicklung dopaminergener Neuronen wurde in ersten *Knockout*-Studien Ende der 1990er Jahre deutlich^{353,375}. Homozygoten *Nurr1-Knockout*-Mäusen fehlte gänzlich die Fähigkeit ventrale mesenzephal dopaminerge Neuronen auszubilden^{353,375}. Außerdem war eine veränderte Genexpression im dorsalen motorischen Nucleus des Hirnstamms zu erkennen, sodass es zu Atemstörungen und auffälliger Hypoaktivität der Tiere kam, welche innerhalb von zwei Tagen nach der Geburt starben^{16,353,367,375,376}. Somit müssen Untersuchungen zur Rolle von Nurr1 in verschiedenen Erkrankungen auf komplexere Modelle mit konditionalem, gewebespezifischen *Knockout*^{372,377}, heterozygote *Knockout*-Tiere^{378,379} oder *Knockdown*-Methoden in späteren Entwicklungsstadien zurückgreifen^{59,380,381}. So zeigte die Deletion von Nurr1 in adulten dopaminergen Neuronen

eine fortschreitende Pathologie mit Verringerung der Marker dopaminerger Neuronen im ventralen Mittelhirn und Striatum, reduziertem striatalen Dopamin und einem beeinträchtigten motorischen Verhalten, was frühe Merkmale des Phänotyps von PD widerspiegelt^{19,372}. Die herausragende Bedeutung des Rezeptors für die pränatale Entwicklung, aber auch adulte Erhaltung von dopaminergen Neuronen brachte den Funktionsverlust von Nurr1 schon früh mit der Pathogenese von PD in Verbindung und förderte das Interesse an Nurr1 als potenzieller Zielstruktur für die Behandlung von PD^{19,353,372}.

Auch genetische Assoziationen und *post-mortem* Analysen von PD-Patienten sowie zahlreiche Studien zu Nurr1 in PD-Modellen *in vitro* und *in vivo* untermauern die Rolle des Rezeptors bei PD zusätzlich. Einige Fälle von familiärer PD weisen Punktmutationen (*single nucleotide polymorphisms*, SNPs) im Nurr1-Gen auf^{16,19} und vor allem der Polymorphismus rs35479735 im Intron 6, welcher das Spleißen beeinflussen kann, korreliert stark mit einem erhöhten Risiko für sporadische und familiäre PD³⁸². In Gehirnen von PD-Patienten zeigte sich außerdem eine signifikante Abnahme der Nurr1-Expression in nigralen Neuronen mit α -Synuclein-Einschlüssen, was mit dem Verlust von TH⁺-Neuronen korrelierte³⁸³. Eine Tatsache, die vergleichbar in nigralen dopaminergen Neuronen von Ratten mit erhöhtem α -Synuclein-Spiegel³⁷⁷ und in Mäusen des 1-Methyl-4-phenyl-1,2,3,6-tetrahydropyridin (MPTP)-Modells³⁸⁴ durch verminderte Nurr1-Konzentrationen nachgewiesen wurde. Im Gegensatz dazu schützte die Überexpression von Nurr1 dopaminerge Neuronen vor verschiedenen toxischen Einflüssen *in vitro* und *in vivo*, was sich auch in einer verstärkten Expression neuroprotektiver Gene, verbessertem Überleben der Neuronen und reduzierter Neuroinflammation zeigte^{377,379,384–386}. Obwohl die Ursachen der meisten Formen von PD nach wie vor nur unzureichend geklärt sind, wird die Krankheit im Allgemeinen mit einer Entzündungskomponente in Verbindung gebracht, die sich u. a. durch aktivierte Mikroglia und erhöhte Konzentrationen an Entzündungsmediatoren im Serum oder Liquor manifestiert und die Progression der Erkrankung beeinflusst^{59,387}. Auch an diesem Aspekt von PD ist Nurr1 beteiligt, da der Rezeptor in Mikroglia und Astrozyten als negativer Regulator von NF κ B-regulierten Entzündungsgenen durch Stabilisierung des CoREST-Co-Repressor-Komplexes wirkt (Abbildung 16) und dadurch die Expression von neuro-

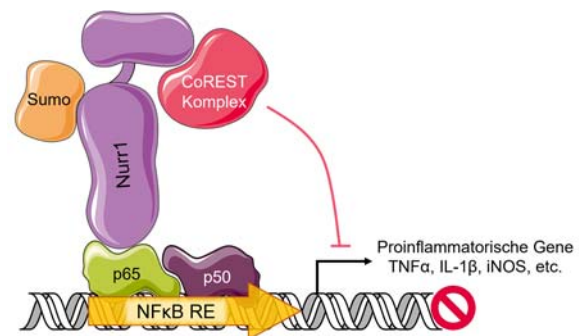


Abbildung 16: Modell der Nurr1/CoREST-vermittelten Transrepression proinflammatorischer Gene über NF κ B (p65/p50).

toxischen Mediatoren wie TNF α , IL-1 β und iNOS in der Substantia nigra von mit Lipopolysacchariden (LPS) behandelten Mäusen begrenzte⁵⁹. Im Gegensatz dazu ist die Interaktion von Nurr1 mit dem Co-Aktivator Foxa2 in dopaminergen Neuronen des Mittelhirns zu sehen, welche die Nurr1-CoREST-Interaktion abschwächt und die Expression von Genen des Dopamin-Phänotyps induziert³⁸⁸.

Erste Studien mit Nurr1-Liganden und -Modulatoren sowie Nurr1-RXR-Heterodimer-selektiven RXR-Agonisten haben die Aktivierung des Rezeptors bereits vorläufig als einen möglichen vielversprechenden Ansatz zur Behandlung von Neuroinflammation und PD *in vitro* und *in vivo* validiert. Sie lassen sich bislang aufgrund mangelnder Potenz und Selektivität der Substanzen (siehe Kapitel 1.4.2) jedoch nur begrenzt auf eine mögliche humane Anwendung übertragen. Sowohl der Nurr1-Agonist Amodiaquin (AQ, **19**) als auch die potenziellen endogenen Liganden PGA1 (**20**), PGE1 (**21**) und 5,6-Dihydroxyindol (**22**) haben *in vitro* und *in vivo* Nurr1-abhängige dopaminerge Gene (TH, VMAT2, DAT und DDC) induziert^{347,389,390}. Außerdem konnte AQ (**19**) *in vitro* die Expression von

proinflammatorischen Zytokinen (IL-1 β , IL-6, TNF α und iNOS) verringern³⁸⁹ und PGA1 (**20**) und PGE1 (**21**) bewirkten neuroprotektive Effekte gegenüber LPS- und MPTP-Stimulation³⁴⁷. Darüber hinaus zeigten AQ (**19**) und SA00025 (**23**) neuroprotektive Wirkungen und verbesserte Symptomatik im 6-OHDA-induzierten Parkinson-Modell in Ratten^{389,391} und die Prostaglandine A1 (**20**) und E1 (**21**) konnten die motorischen Defizite bei MPTP-behandelten Mäusen mildern³⁴⁷. Obwohl diese Untersuchungen auf ein großes therapeutisches Potenzial für Nurr1-Agonisten bei PD hindeuten, fehlt es an potenten und selektiven Nurr1-Liganden, um dieses Konzept zu validieren. Denn die wenigen bisherigen Studien haben nur geringe Aussagekraft, die neben der geringen Potenz der Substanzen zum einen der Verwendung von endogenen Liganden (**20-22**) geschuldet ist, die bekannt sind für ihre pleiotropen Effekte, und zum anderen der mangelnden Selektivität des synthetischen Agonisten AQ (**19**) sowie dem ungeklärten Mechanismus der Nurr1-Aktivierung durch SA00025 (**23**).

Auch bei der Pathogenese der Alzheimer-Demenz (AD) scheint Nurr1 eine Rolle zu spielen²⁰. *Post-mortem* Analysen von AD-Patienten zeigten eine signifikante Abnahme der Nurr1-Expression in Neuronen der Substantia nigra, welche Ablagerungen von Neurofibrillen aufwiesen, was analog zu PD mit dem Verlust von TH⁺-Neuronen korrelierte³⁸³. In Übereinstimmung damit waren in einem transgenen Mausmodell mit mutiertem humanen Amyloid-Vorläuferprotein (APP), welches den frühen Gedächtnisverlust der AD simuliert, die Nurr1-mRNA-Spiegel im Hippocampus reduziert^{392,393}. Eine weitere Studie untersuchte die Nurr1-Expression im zeitlichen Verlauf der Erkrankung von 5XFAD-Mäusen und zeigte, dass es in frühen Stadien zu einer verstärkten Expression von Nurr1 bei A β -Akkumulationen im frontalen Kortex und Subiculum kommt, und erst in späteren Stadien ein Verlust Nurr1-exprimierender Zellen zu erkennen ist³⁹⁴. Zwei *in vitro* Modelle zeigten allerdings auch herunterregulierte Nurr1-Protein- und mRNA-Spiegel in primären Rattenneuronen und in einer humanen neuronal differenzierten mesenchymalen Zelllinie, die jeweils mit β -Amyloid (A β 42) behandelt wurden³⁹⁵. All diese Beobachtungen legen nahe, dass die Nurr1-Expression im Zusammenhang mit AD beeinträchtigt ist, lassen jedoch keine direkte Aussage zur Kausalität zu. Moon et al. konnten als erste im Jahr 2019 zeigen, dass ein Nurr1-*Knockdown* im Subiculum von 5XFAD-Mäusen die Symptome der AD verstärkte, während eine Nurr1-Überexpression sowie die Aktivierung mit dem Agonisten AQ (**19**) zu einer Verbesserung der AD-Pathologie führte, indem es zu verringerten A β -Akkumulationen, reduzierter Neurodegeneration und verbesserten kognitiven Funktionen kam³⁸⁰. Außerdem sind die allgemein neuroprotektiven und antientzündlichen Wirkungen von Nurr1 im Zusammenhang mit der AD von Bedeutung und lassen vermuten, dass eine Aktivierung des Rezeptors vorteilhaft wäre. Dennoch basieren die Studien, die ein therapeutisches Potenzial der Nurr1-Modulation zur Behandlung der AD andeuten, überwiegend auf *Knockout*- und Überexpressions-Experimenten, während die pharmakologische Regulation des Rezeptors aufgrund fehlender potenter und selektiver Liganden nur unzureichend untersucht ist²⁰.

Im Kontext der neurologischen Autoimmunerkrankung MS ist die Evidenz zur Beteiligung von Nurr1 zum Teil kontrovers. Sieben von acht Untersuchungen zur Genexpression von Nurr1 in verschiedenen Blutkompartimenten (Vollblut, mononukleäre Zellen des peripheren Blutes, CD14⁺-Monozyten und CD4⁺-T-Zellen) von Patienten mit schubförmig remittierender MS zeigten eine reduzierte Nurr1-Expression im Vergleich zu gesunden Kontrollgruppen³⁶². Diese Beobachtungen sind insofern gut nachvollziehbar, als überschießende Entzündungsreaktionen charakteristisch für die Erkrankung sind, und die antientzündliche Rolle von Nurr1 möglicherweise unterdrückt wird³⁶². Eine Studie, die zusätzlich auch Patienten mit sekundär progressiver MS einschloss, stellte hingegen eine erhöhte Expression von Nurr1 in CD3⁺-T-Zellen fest^{362,396}. Ähnlich verhalten sich die Ergebnisse im EAE-Maus-Modell, bei

denen drei von vier Studien eine protektive Wirkung von Nurr1 verzeichneten³⁶². So zeigten heterozygote Nurr1-*Knockout*-Mäuse einen früheren Krankheitsbeginn der EAE mit vermehrter Infiltration von Entzündungszellen im Rückenmark³⁷⁸. Eine präventive Behandlung mit dem Nurr1-Aktivator IP7e (**24**) führte zu protektiven Effekten bei EAE-Mäusen und reduzierte die Infiltration von T-Zellen und Makrophagen ins Rückenmark, indem die NFκB-vermittelte Entzündung unterdrückt wurde³⁹⁷. Eine therapeutische Behandlung mit IP7e (**24**) nach der Induktion von EAE zeigte jedoch keine Effekte³⁹⁷. Auch eine Überexpression von Nurr1 in dendritischen Zellen des Knochenmarks, die EAE-Mäusen systemisch appliziert wurden, war in der Lage, die Progression der EAE durch vermehrte Differenzierung von T_{Reg}-Zellen und damit verminderte Neuroinflammation zu verlangsamen³⁹⁸. Im Gegensatz dazu führte ein systemischer *Knockdown* von Nurr1 in Mäusen zu einer verringerten EAE-Symptomatik, was auf einen Einfluss von Nurr1 bei der Th17-Differenzierung zurückgeführt wurde, indem es zu Veränderungen in der IL-21- und IL23R-Expression kam³⁸¹. Insgesamt deuten auch die Untersuchungen zur Rolle von Nurr1 bei MS darauf hin, dass eine Aktivierung des Rezeptors von Nutzen sein könnte. Weitere Studien sind aber dringend notwendig, um Nurr1 als potenzielle Zielstruktur zur Behandlung der Multiplen Sklerose zu validieren.

1.4.2 Bekannte Nurr1-Liganden

Obwohl Nurr1 lange als ligandenunabhängiger Transkriptionsfaktor^{17,338} galt und die kanonische Ligandenbindestelle nukleärer Rezeptoren nicht aufweist, wurden einige niedermolekulare Verbindungen identifiziert, die in der Lage sind, die Aktivität von Nurr1 direkt zu regulieren. Strukturanalysen, mechanistische Untersuchungen, Hinweise auf endogene Liganden und einige Tiermodelle legen außerdem nahe, dass Nurr1 ein vielversprechendes Target zur Behandlung neurodegenerativer Erkrankungen darstellt. Die verfügbaren direkten Nurr1-Modulatoren sind jedoch bei Weitem unzureichend, um als chemische Tools eine Validierung des therapeutischen Potenzials von Nurr1 zu ermöglichen.

Im Jahr 2015 wurden die alten Antimalariamittel³⁹⁹ Amodiaquin (AQ, **19**) und Chloroquin (CQ, **25**) als erste direkte Liganden der Nurr1-LBD beschrieben (Abbildung 17)³⁸⁹. Sie sind zusammen mit dem nichtsteroidalen Antirheumatikum (NSAR) Glafenin aus einem Arzneistoffscreening hervorgegan-

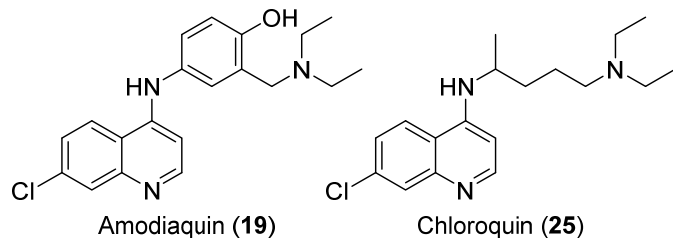


Abbildung 17: Synthetische Nurr1 Agonisten AQ und CQ.

gen, in dem die Aktivität des Nurr1-Vollängenrezeptors an einem Reporterkonstrukt, welches vier Wiederholungen des NBRE-*Response*-Elements enthielt, in einer humanen Neuroblastom-Zelllinie (SK-N-BE(2)C) bestimmt wurde³⁸⁹. AQ (**19**) und CQ (**25**) aktivierten das Monomer-*Response*-Element ungefähr 3-fach, während Glafenin einen schwächeren Effekt zeigte (1,5-fach) und nicht weiter untersucht wurde³⁸⁹. Versuche an zwei unterschiedlichen Gal4-Nurr1-Hybrid-Konstrukten, die entweder die Nurr1-DBD oder -LBD enthielten, deuteten an, dass die Aktivität auf eine direkte Interaktion mit der Nurr1-LBD zurückzuführen ist³⁸⁹. Hier zeigten AQ (**19**) und CQ (**25**) 15- bzw. 10-fache Aktivierungen mit EC₅₀ Werten von etwa 20 μM und 50 μM³⁸⁹. Basierend auf 2D ¹H-¹⁵N-*Heteronuclear Single Quantum Coherence*(HSQC)-NMR-Daten konnte die Bindestelle im Nurr1-Protein näher lokalisiert und durch Mutations-Studien untermauert werden³⁸⁹. Die durch AQ-Bindung beeinflussten Aminosäuren befinden sich vor allem im unteren Teil der Helix 3 (Aminosäuren 402–409) und im Bereich von Helix 6 und der β-Faltblatt-Struktur, vereinzelt aber auch in Helix 11 und 12 (siehe Abbildung 22a)³⁸⁹. Fraglich bleibt jedoch, ob es sich bei dieser Bindestelle um eine Tasche nahe der orthosterischen Bindestelle nukleärer

Rezeptoren im unteren Drittel der LBD und innerhalb der LBD handelt⁴⁰⁰, oder ob die Bindungsstelle an der Oberfläche der LBD lokalisiert ist³⁸⁹, wie es beim verwandten Rezeptor Nur77 mehrfach beobachtet wurde (siehe Abbildung 22c)^{64,401,402}. Bislang gibt es jedoch keine Co-Kristallstruktur der Nurr1-LBD im Komplex mit AQ (19) oder CQ (25), sodass der eindeutige Bindemodus dieser Substanzklasse nicht bekannt ist. Die Bedeutung der beiden Substanzen zur Prophylaxe und Behandlung von Malaria ist heute aufgrund von Erregerresistenzen und schlechtem Nutzen-Risiko-Verhältnis gering³⁹⁹. Dennoch findet vor allem CQ (25) aktuell Einsatz bei rheumatischen Erkrankungen wie dem Systemischen Lupus Erythematodes, aber auch Wirkungen bei weiteren Infektionskrankheiten sind bekannt^{403,404}. Neben der geringen Potenz an Nurr1 im zweistelligen mikromolaren Bereich erschweren jedoch mangelnde Selektivität, zahlreiche unspezifische Effekte sowie Wirkungen auf andere Proteine und Signalwege^{400,405–409} und z. T. schwere Nebenwirkungen *in vivo*^{404,410–413} den Einsatz als Modell-Substanzen für Nurr1. Zusätzlich ist ihr Einsatz in zellfreien fluoreszenzbasierten Testsystemen aufgrund der ungünstigen photophysikalischen Eigenschaften kritisch zu beurteilen⁴¹⁴.

Erste Hinweise auf potenzielle endogene Nurr1-Liganden lieferte ein massenspektrometrischer Metabolomik-Ansatz, bei dem Interaktionen verschiedener ungesättigter Fettsäuren und Prostaglandine aus dem Gewebe von Mäuse-Gehirnen mit der rekombinanten Nurr1-LBD untersucht wurden³⁴⁵. Daraus konnte die ungesättigte Fettsäure Docosahexaensäure (DHA, 26) als

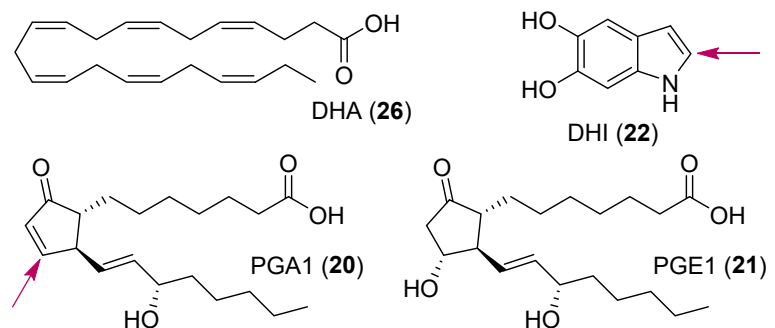


Abbildung 18: Potenzielle endogene Nurr1-Liganden. Der jeweilige Anknüpfungspunkt bei einer kovalenten Bindung an Cys556 der Nurr1-LBD ist mit einem Pfeil markiert.

direkter Nurr1-Ligand bestätigt werden (Abbildung 18)³⁴⁶. Zwei Vollängen-Reporterassays unter Verwendung eines NBRE-Reporterkonstrukts in HEK293T-Zellen und dopaminergen MN9D-Mauszellen zeigten eine dosisabhängige Unterdrückung der Nurr1-Aktivität um $\sim 25\%$ bei $50\ \mu\text{M}$ DHA (26)³⁴⁶. NMR-basierte Strukturanalysen lokalisierten die Bindestelle für DHA (26) innerhalb der LBD, potenziell überlappend mit der AQ-Bindestelle, dort wo die kanonische Bindetasche zu erwarten ist³⁴⁶. Hier sind vor allem Aminosäuren der Helices 3 und 11 an der Interaktion beteiligt, aber auch Konformationsänderungen durch Interaktion mit Helix 5, 7 und 12 sind zu erkennen (Abbildung 22a)³⁴⁶. Orthogonal bestätigt wurde die Nurr1-DHA-Bindung durch verstärkte Rekrutierung des PIASy Co-Regulator-Peptides in einem zellfreien TR-FRET-Assay-System^{346,415}. Außerdem konnte direkte Bindung der ungesättigten Fettsäuren Arachidonsäure, Linolsäure und Ölsäure in gleicher Weise über NMR-Strukturanalyse gezeigt werden und deren Titration in einem Tryptophan-Fluoreszenz-Bindungsassay deutete K_D -Werte zwischen 50 und $100\ \mu\text{M}$ an⁴¹⁶. Weitere Strukturanalysen durch NMR-Experimente, Wasserstoff-Deuterium-Austausch-Massenspektrometrie und molekulardynamische Simulationen legen nahe, dass die mutmaßliche kanonische Ligandenbindungstasche in der Lage ist ihre Konformation derart zu erweitern, dass die Bindung ungesättigter Fettsäuren ermöglicht wird^{416,417}. Im Falle von DHA (26), welche ein molekulares Volumen von $355\ \text{\AA}^3$ aufweist⁴¹⁸, müsste sich die blockierte Nurr1-Bindestasche mit einem Volumen von $30\ \text{\AA}^3$ in apo-Form (PDB: 1OVL) um mehr als das 10-fache ausdehnen, was Simulationen mit einem Volumen von bis zu $\sim 500\ \text{\AA}^3$ der Nurr1-Bindestasche bestätigen^{17,416,417}.

Dem gegenüber stehen die Untersuchungen von Rajan et al. aus dem Jahr 2020, die die Prostaglandine A1 (**20**) und E1 (**21**) als aktivierende natürliche Nurr1-Liganden beschreiben (Abbildung 18)³⁴⁷. PGA1 (**20**) und PGE1 (**21**) aktivierten Nurr1 in zwei verschiedenen Reporterassays, einem Gal4-Nurr1- und einem NBRE-Nurr1-Vollängenassay, durchgeführt in humanen Neuroblastom Zellen (SK-N-BE(2)C) und zwei verschiedenen dopaminergen Zelllinien aus Maus (MN9D) und Ratte (N27-A) mit EC₅₀-Werten von ~ 5 μ M und ~ 3 μ M³⁴⁷. Die Aktivierungseffizienz lag dabei je nach Zelllinie und Assay-Format im Bereich von ca. 6- bis 12-facher Aktivierung für PGA1 (**20**) und 10- bis 25-facher Aktivierung für PGE1 (**21**)³⁴⁷. Für letzteres ist jedoch eine Beteiligung des G-Protein-gekoppelten Prostaglandin-E2-Rezeptors (EP2) an den Nurr1 aktivierenden Effekten nachgewiesen worden³⁴⁷. Beide Prostaglandine binden dabei in eine nicht-kanonische Bindetasche mit hoher Lösemittelexposition zwischen den Helices 4/5, 11 und 12 der Nurr1-LBD, ähnlich wie bereits bei Nur77 beobachtet (Abbildung 22b, c)^{61,401}. Die Co-Kristallstruktur der Nurr1-LBD im Komplex mit PGA1 (PDB: 5Y41)⁴¹⁹ zeigt, dass PGA1 (**20**) kovalent an Cys566 in Form eines Michael-Addukts gebunden vorliegt und eine Auswärtsverschiebung der Helix 12 von 21° induziert. Die hydrophobe Seitenkette ragt tief in den entstandenen hydrophoben Tunnel, der aus den Aminosäure-Resten von Phe443, Leu444 (Helix 4/5), Leu570, Ile573 (Helix 11), Ile588, Leu591 und Phe592 (Helix 12) gebildet wird (Abbildung 19). Die Carbonsäure-Kette scheint flexibler zu sein, wenn man die beiden Monomere der asymmetrischen Einheit miteinander vergleicht, und wird über Wasserstoffbrückenbindungen mit Arg515 und His516 (Helix 8–9 Loop) sowie mit einem Wassermolekül über Arg563 (Helix 11) stabilisiert (Komplex B). Die Hydroxygruppe der Seitenkette bildet Wasserstoffbrückenbindungen mit dem *Backbone* von Glu440 und Leu444 (Helix 4/5) aus. Bei PGE1 (**21**) hingegen führten die Kristallisationsbedingungen im sauren Bereich (pH 5,5) zur Konversion in das entsprechende Anhydrid PGA1 (**20**). Zusätzlich steht eine vergleichbare Co-Kristallstruktur der Nurr1-LBD im Komplex mit PGA2 (PDB: 5YD6)⁴²⁰ der gleichen Autoren zur Verfügung⁴²¹.

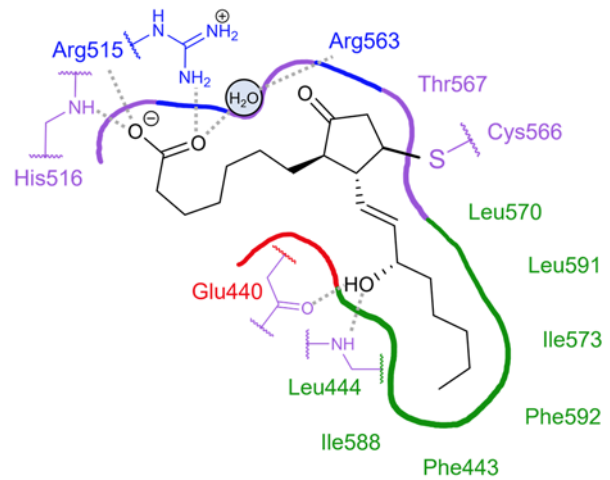


Abbildung 19: Zweidimensionale Darstellung der kovalenten Koordination von PGA1 (**20**) an die Nurr1-LBD (PDB: 5Y41)³⁴⁷. Gezeigt ist der lipophile Tunnel (grün) und der polare Bereich (violett) im oberen Teil mit großer Lösemittelexposition, mit basischen (blau) und sauren Seitenketten (rot).

Ein weiterer potenzieller endogener Nurr1-Ligand ist der Dopamin-Metabolit 5,6-Dihydroxyindol (DHI, **22**, Abbildung 18), welcher ebenfalls kovalent gebunden an Cys566 vorliegt (vgl. Abbildung 22b) und vermutlich aus der reversiblen Reaktion des Thiolats (Cys566) mit dem auto-oxidierten 5,6-Indolchinon hervorgegangen ist³⁹⁰. Die Auswärtsbewegung von Helix 12 fällt mit etwa 10° geringer aus als bei der Bindung der Prostaglandine an Nurr1 und ermöglicht so die Ausbildung einer überwiegend hydrophilen Bindetasche in der gleichen nicht-kanonischen Region zwischen den Helices 4/5, 11 und 12³⁹⁰. Zusätzlich zur kovalenten Bindung wird DHI (**22**) durch eine Wasserstoffbrückenbindung mit der Glu445-Seitenkette (Helix 4/5), Kation- π -Wechselwirkungen mit Arg515 (Helix 8–9 Loop) und Arg563 (Helix 11) sowie schwache Interaktionen der beiden Hydroxygruppen des Liganden mit dem Guanidin-Rest von Arg515 stabilisiert (Abbildung 20). Mittels Oberflächenplasmonenresonanzspektroskopie (SPR) wurden Interaktionen mit dem Liganden ab einer Konzentration von 0,25 μ M nachgewiesen und Konzentrationen im niedrigen mikromolaren Bereich (2,5 μ M) zeigten bereits eine gesättigte Bindung³⁹⁰. *In vitro* stimulierte DHI (**22**) die Nurr1-Aktivität in einem Gal4-Nurr1-Hybrid-Reporter-

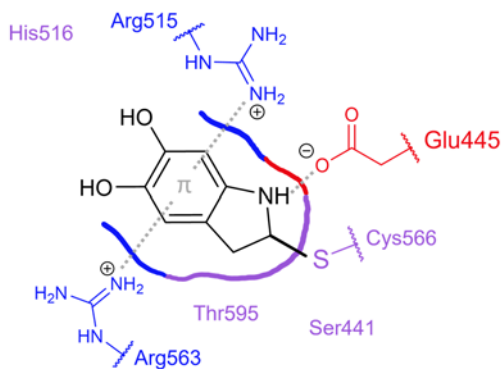


Abbildung 20: Zweidimensionale Darstellung der kovalenten Bindung von DHI (22) an die Nurr1-LBD (PDB: 6DDA³⁹⁰). Kation- π Interaktionen mit den basischen Seitenketten (blau) von Arg515 und Arg563 und eine Wasserstoffbrückenbindung mit dem sauren (rot) Glu445 Rest stabilisieren die Bindung von DHI in der polaren Bindestelle (violett) zusätzlich.

Computersimulationen deuten darauf hin, dass nicht-kovalente Bindung in der gleichen Ligandenbindetasche möglich ist und durch eine zusätzliche Halogenbindung mit His516 stabilisiert werden kann⁴²². Die Untersuchungen zu DHI (22) und davon abgeleiteten Derivaten als Nurr1-Liganden sind erst im Laufe dieser Arbeit veröffentlicht worden.

Die physiologische Relevanz der beschriebenen potenziellen endogenen Nurr1-Liganden (Abbildung 18) ist zunächst fraglich, da alle genannten Studien eine Modulation der Rezeptoraktivität erst im μM -Bereich zeigen^{346,347,390}. Dies gilt allerdings auch für andere bekannte endogene Liganden nukleärer Rezeptoren wie 15-d-PGJ_2 (9, PPAR γ), Oxysterol (LXR α) und DHA (26, RXR), die ihre Rezeptoren in vergleichbaren Reporterassays im μM -Konzentrationsbereich aktivierten^{275,276,423,424}. Auch die K_D -Werte von DHA (26) für Nurr1 und RXR α sind mit $30\ \mu\text{M}$ und $33\ \mu\text{M}$ nahezu identisch³⁴⁶. Im murinen und menschlichen Gehirn konnten größere Mengen der ungesättigten Fettsäure DHA (26) nachgewiesen werden und deren Akkumulation ist wichtig für die Entwicklung des Gehirns⁴²⁵. Auch wenn Neuronen selbst nicht in der Lage sind, essenzielle Fettsäuren zu produzieren, konnte gezeigt werden, dass Astrozyten DHA (26) und Arachidonsäure aus Vorstufen herstellen und freisetzen können und diese dann den Neuronen zur Verfügung stehen⁴²⁶. Somit ist eine physiologische Funktion der DHA-Bindung von Nurr1 denkbar³⁴⁶. Die Prostaglandine PGA1 (20) und PGE1 (21) sind Lipidmediatoren mit einer reaktiven Cyclopentenon-Struktur, die sich vor allem durch antientzündliche Eigenschaften auszeichnen⁴²⁷. Als kovalente Liganden könnten sie einen mechanistischen Vorteil haben, sodass auch geringere Konzentrationen ausreichen, um durch akkumulierte aktivierende Protein-Modifikationen eine verlängerte Wirkung zu erzielen⁴²⁸. Im Striatum und Mesencephalon von Mäusen sind mit $15\text{--}70\ \text{nM}$ nennenswerte Konzentrationen in den betreffenden Hirnarealen beobachtet worden, sodass die PGA1-vermittelte Aktivierung von Nurr1 physiologische Relevanz bei den neuroprotektiven Effekten dieser Lipidmediatoren haben könnte^{347,429–431}. Gerade Untersuchungen von ungesättigten Fettsäuren und deren Stoffwechsel-Produkten sind im zellulären System jedoch kritisch zu betrachten, da sie unter anderem als essenzieller Bestandteil der Zellmembran von den Zellen anderweitig verstoffwechselt und verwendet werden können und somit potenziell nicht mehr intrazellulär als Liganden zur Verfügung stehen^{425,432}.

Reaktive Dopamin-Chinone wie DHI (22) entstehen unter anderem aus zytoplasmatischem Dopamin unter Bedingungen von oxidativem Stress als Folge von dysreguliertem Dopamin-Metabolismus im Zusammenhang mit dem Krankheitsgeschehen von Parkinson^{433–435}. Dabei konnten im Zytoplasma

assay in humanen Choriokarzinom-JGE3-Zellen nur um das 1,6-fache bei $100\ \mu\text{M}$ ³⁹⁰. Ein EC_{50} -Wert konnte aufgrund von Toxizität nicht bestimmt werden³⁹⁰. Zusätzlich erschweren die reaktiven Eigenschaften von DHI (22) wie die Neigung zur Auto-Oxidation und Polymerisation den Einsatz als Nurr1-Modell-Substanz^{390,422}. Weiterführende Untersuchungen zu 5,6-substituierten Indolen brachten das 5-Chlorindol mit verbesserten Eigenschaften und reduzierter Toxizität hervor⁴²². Seine Nurr1-Bindungsaffinität wurde über Thermophoresis (*microscale thermophoresis*, MST) mit einem K_D -Wert von $15,0 \pm 1,2\ \mu\text{M}$ bestimmt⁴²². In zwei verschiedenen Nurr1-Reporterassays (Gal4-Nurr1 und NBRE-Nurr1-Volllänge) zeigte 5-Chlorindol eine ca. 2-fache Aktivierung bei $10\ \mu\text{M}$ in dopaminergen MN9D-Maus-Zellen⁴²².

Dopamin-Konzentrationen im hohen nanomolaren bis mikromolaren Bereich nachgewiesen werden⁴³⁶⁻⁴³⁸. Dass die kovalente Proteinmodifikation von Nurr1 durch den auto-oxidierten Dopamin-Metaboliten DHI (**22**) zu einem stimulierenden Effekt führt, ist jedoch ungewöhnlich und spricht für die neuroprotektive Wirkung des Rezeptors, da diese Modifikationen die normale Funktion von Parkinson-assoziierten Proteinen wie SOD2, TH, DAT, α -Synuclein und Parkin beeinträchtigen und Proteinakkumulationen fördern können⁴³⁹⁻⁴⁴³.

Zusätzlich zu diesen wenigen orthogonal validierten direkten Nurr1-Modulatoren sind weitere Substanzen beschrieben, wie bspw. SA00025 (**23**) und IP7e (**24**, Abbildung 21), die die Nurr1-Aktivität beeinflussen, für die eine Bestätigung der direkten Bindung an die LBD aber fehlt^{66,400}. Eine weitere Möglichkeit, die neuroprotektiven Effekte von Nurr1 zu aktivieren, besteht über RXR-Agonisten, die selektiv das permissive RXR-Nurr1-Heterodimer aktivieren können. Hier konnten bereits mehrere vielversprechende Kandidaten entwickelt werden, welche zum Teil schon erfolgreich in Tiermodellen untersucht wurden (zusammengefasst in⁶⁶).

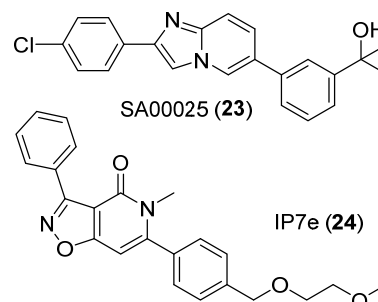


Abbildung 21: Weitere Nurr1-Modulatoren

Nach aktuellem Stand der Forschung lassen sich zwei unterschiedliche Bindestellen in der Nurr1-LBD vermuten, wovon jedoch nur die nicht-kanonische Bindestelle im Bereich von Helix 4/5, 11 und 12 über Co-Kristallstrukturen mit drei verschiedenen kovalent gebundenen Liganden bestätigt ist (Abbildung 22a,b)^{347,390,420}. Eine Co-Kristallstruktur eines in der mutmaßlichen kanonischen Bindestelle gebundenen Liganden, wie für AQ (**19**) und ungesättigte Fettsäuren postuliert^{346,389,400,416}, fehlt derzeit, sodass strukturbasiertes Liganden-Design noch nicht zielführend ist. Außerdem bleibt neben der offenen Frage verschiedener Bindestellen unklar, wie die Liganden auf die molekulare Funktion des Rezeptors einwirken und welche Interaktionen für die Regulation der konstitutiven Aktivität verantwortlich sind. So erscheint eine Auswärtsbewegung der Helix 12, die eine weitere Aktivierung des Rezeptors bewirkt^{347,390}, widersprüchlich, wenn man den Vergleich zum klassischen Mechanismus der Aktivierung von NRs durch Ligandbindung zieht⁹. Die Interaktion zwischen Glu440 und Lys590, welche die Helix 12 in ihrer auto-aktivierten Konformation stabilisiert, geht im Fall der PGA1(**20**)-Bindung verloren, wird jedoch durch die Bindung von DHI (**22**) verstärkt^{338,347,390,444}. Aufgrund der Schwierigkeiten, die diese endogenen Liganden in zellulären Testsystemen mit sich bringen, wie hohe Lipophilie und Toxizität, sind bis heute die Antimalariamittel AQ (**19**) und CQ (**25**) trotz geringer Potenz und mangelnder Selektivität die einzigen validen Kontroll-Substanzen für Nurr1.

Eine weitere Herausforderung in der Entwicklung von Nurr1-Modulatoren stellt die Subtypen-Selektivität innerhalb der NR4A-Familie dar. Zwar beträgt die Sequenz-Ähnlichkeit der Nurr1-LBD nur 66,4 % im Vergleich zu Nur77 und 65,3 % gegenüber NOR-1, was vergleichbar ist mit den PPAR-LBDs untereinander, aber der Bereich der mutmaßlichen kanonischen Bindestelle ist hochkonserviert^{51,163,445}. Dennoch ist nur in wenigen Fällen bei der Charakterisierung neuer Nurr1-Liganden untersucht worden, ob ebenfalls eine Aktivität an den verwandten Rezeptoren Nur77 und NOR-1 vorhanden ist^{339,347,446,447}. Gerade weil bekannt ist, dass sich die Aktivität und Expression von Nurr1 und Nur77 gegenseitig beeinflussen⁴⁴⁸⁻⁴⁵⁰, sollten zukünftig bei der Charakterisierung neuer NR4A-Liganden die anderen Subtypen Beachtung finden^{51,445}. Beispielsweise wurde für den Nur77-Liganden Cytosporon B^{400,402} und dessen Derivat PDNPA⁶¹ sowie für die potenziellen endogenen NR4A-Liganden PGA1 (**20**) und PGA2^{347,451} bereits nachgewiesen, dass eine direkte Bindung bei zumindest zwei der drei NR4A-Rezeptoren zu

beobachten ist^{347,451}. Daher wäre es für eine gezielte Entwicklung von selektiven NR4A-Liganden von großem Vorteil, Co-Kristallstrukturen aller drei Subtypen mit möglichst dem gleichen Liganden zu erhalten. Denn die ersten Erfolge der letzten Jahre mit ligandengebundenen Nurr1-Kristallstrukturen^{347,390,420} im Vergleich zu den zahlreicheren Nur77-Strukturen deuten darauf hin, dass die besondere Art, Liganden außerhalb der kanonischen Bindestelle zu binden, die Rezeptoren der NR4A-Unterfamilie eint und auch für Nurr1 und NOR-1 Ligandenbindestellen an der Oberfläche der LBD mit großer Lösemittelexposition denkbar sind (Abbildung 22c)^{64,401,402}. Im Fall von NOR-1 ist es bislang jedoch noch nicht, gelungen eine Kristallstruktur zu lösen, weder in apo-Form noch ligandengebunden.

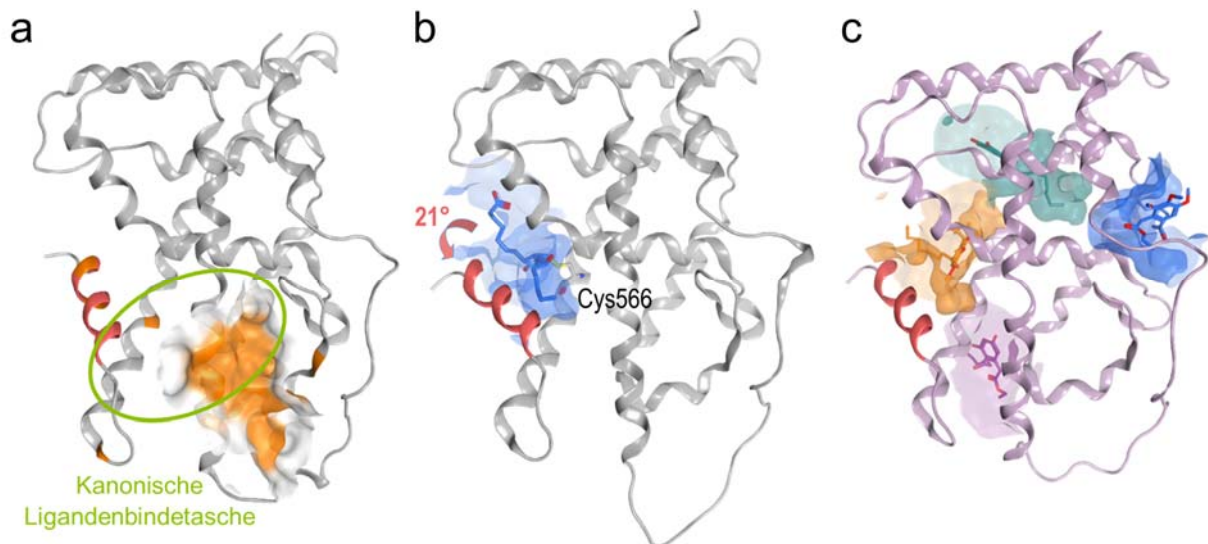


Abbildung 22: Ligandenbindung an die Nurr1-LBD. a) Mutmaßliche Bindestelle von AQ (19, orange) und DHA (26, grün) in der Nurr1-LBD verortet anhand von NMR-Bindungsstudien^{346,389,416} (apo, PDB: 1OVL³³⁸). b) Die Co-Kristallstruktur der Nurr1-LBD in Komplex mit PGA1 (20, blau, PDB: 5Y41) zeigt eine kovalente Bindung an Cys566 in einer Bindestasche zwischen den Helices 4/5, 11 und 12, die durch eine Auswärtsbewegung der Helix 12 von 21° gebildet wurde. c) Ligandenbindungsstellen in der Nur77-LBD zum Vergleich. Alle identifizierten Ligandenbindungsstellen befinden sich an der Proteinoberfläche. Cytosporon B (violett) ist an der Dimerschnittstelle gebunden, THPN (petrol, PDB: 4JGV⁶⁴) bindet zwischen den Helices 5 und 7 und TMPA (PDB: 3V3Q⁴⁰¹) befindet sich an zwei Bindungsstellen, eine (orange), die der kovalenten Bindungsstelle hinter H12 (b) ähnelt, und eine (blau) in einem Hohlraum zwischen den Helices 1, 5 und 8. Die Bindungsstellen wurden auf die Co-Kristallstruktur von Nur77 im Komplex mit dem Agonisten Cytosporon B (PDB: 6KZ5⁴⁰²) in MOE2020.09 abgebildet.

Es gibt zahlreiche Erkenntnisse, die auf ein therapeutisches Potenzial von Nurr1 bei neurodegenerativen Erkrankungen hindeuten, insbesondere bei AD und PD, aber auch bei MS. Nurr1 zeigt neuroprotektive Effekte vor allem in dopaminergen Neuronen und kann außerdem neuroinflammatorischen Prozessen in Astrozyten und Gliazellen entgegenwirken. Der Nurr1-Knockout in Tiermodellen von PD, AD und MS hat zu einer Verschlimmerung der Krankheit geführt, während die Überexpression des Rezeptors mehrere positive Effekte gezeigt hat. Doch außer einigen wenigen Studien mit schwachen und nicht-selektiven Nurr1-Modulatoren stammen die vielversprechenden Beobachtungen zu Nurr1 als potenziellem therapeutischem Target hauptsächlich aus *Knockout*- bzw. Überexpressions-Studien. Um die Nurr1-Modulation als neues therapeutisches Konzept zu validieren, mangelt es daher an geeigneten chemischen Tools zur spezifischen pharmakologischen Kontrolle der Nurr1-Aktivität. Die Entwicklung von Nurr1-Modulatoren stellt jedoch eine große Herausforderung dar, da die strukturellen Kenntnisse über die Ligandenbindungsstellen begrenzt sind und das Wissen über molekulare Mechanismen und Interaktionspartner unvollständig ist. Trotz der jüngsten Erkenntnisse zu einer direkten Interaktion der Nurr1-LBD mit *small molecules* und der Entdeckung potenzieller endogener Liganden stehen noch keine ausreichend potenten und selektiven synthetischen Nurr1-Agonisten und inversen Agonisten zur Verfügung, um therapeutische Effekte der Nurr1-Modulation zuverlässig zu ermitteln.

2. Zielsetzung

Ziel der vorliegenden Arbeit war es, mittels verschiedener pharmazeutisch-chemischer Techniken und Strategien, neue chemische Tools für zwei wichtige nukleäre Rezeptoren – PPAR und Nurr1 – zu entwickeln und mit deren Hilfe verbessertes mechanistisches Verständnis über diese Transkriptionsfaktoren zu gewinnen. Wie zuvor dargestellt gehören die PPARs zu den mit am besten erforschten nukleären Rezeptoren, deren Liganden zum Teil bereits als Arzneistoffe zugelassen sind bzw. waren¹⁴. Allerdings ergaben sich bei ihrer Anwendung vielfach Probleme, die u. a. auf den Wirkmechanismus der vollen Rezeptoraktivierung durch orthosterische Agonisten zurückzuführen sind^{14,294}. Eine weitere Herausforderung auch bei hochselektiven und potenten Liganden ist die zeitlich definierte pharmakologische Kontrolle der Rezeptoraktivität, welche aufgrund der verzögerten genomischen Effekte zum Teil auch bei guten pharmakokinetischen Eigenschaften nicht erreicht wird^{2,14}. Um das therapeutische Potenzial der PPARs besser ausschöpfen zu können, bedarf es daher neuer *tool compounds*, die gezieltere funktionelle Studien ermöglichen, um daraus neue Konzepte der Rezeptormodulation abzuleiten.

Mit dem Ansatz der Photopharmakologie (siehe Kapitel 1.1) sollten in diesem Kontext neue PPAR-Liganden entwickelt werden, die mit der Fähigkeit der reversiblen Aktivierung und Inaktivierung durch Licht eine gezielte zeitliche und räumliche Kontrolle der Wirkung ermöglichen^{26,27}. Dabei sollte auf bekannte PPAR-Liganden zurückgegriffen werden, die mit Hilfe computergestützten Designs zu photoschaltbareren selektiven Agonisten optimiert werden sollten. Zusätzlich sollte ein neues Testsystem mit zeitlicher und räumlicher Auflösung der Rezeptoraktivierung entwickelt werden, um das Potenzial der neuen *tool compounds* in diesem Kontext zu demonstrieren. Die Ergebnisse der hieraus entstandenen Publikationen^{452,453} (Kapitel 16.1 und 16.2) sind in Kapitel 3.1 zusammengefasst.

Neben der Verwendung dezidierter chemischer Tools kann gerade auch die Kenntnis endogener Liganden nukleärer Rezeptoren Aufschluss über den Nutzen und die Möglichkeiten ihrer pharmakologischen Modulation geben²⁵⁹. Im Falle von PPAR γ wurden Vitamin-E-Metabolite als mögliche natürliche Liganden identifiziert. Deren molekularer Wirkmechanismus sollte daher umfassend charakterisiert und deren Auswirkungen auf die Genexpression humaner Hepatozyten untersucht werden. Die Ergebnisse dieser Studie sind in Kapitel 3.2 dargestellt und die zugehörige Publikation⁴⁵⁴ ist in Kapitel 16.3 zu finden.

Der zweite Schwerpunkt dieser Arbeit lag auf der Identifizierung, Entwicklung und Charakterisierung neuer *tool compounds* für den neuroprotektiven Transkriptionsfaktor Nurr1. Wie in Kapitel 1.4.1 erläutert wird diesem nukleären Rezeptor großes Potenzial als Target zur Behandlung neurodegenerativer Erkrankungen wie PD, AD und MS zugeschrieben⁶⁶. Eine umfassende Literaturrecherche (zusammengefasst in Kapitel 1.4, nachzulesen in Kapitel 16.8) zeigte jedoch, dass sich bisherige Untersuchungen vor allem auf *Knockout*-Studien und Überexpressions-Experimente von Nurr1 in Tiermodellen stützen, da es an validierten Nurr1-Liganden mangelt. Wie in Kapitel 1.4.2 dargelegt ist es in den letzten Jahren gelungen potenzielle endogene Nurr1-Liganden zu identifizieren^{346,347,390,416}, doch die zur Verfügung stehenden synthetischen Liganden beschränkten sich zu Beginn dieser Arbeit auf lediglich zwei unselektive und nur moderat potente Agonisten: die Antimalariawirkstoffe AQ (19) und CQ (25)^{389,400}. Um den molekularen Mechanismus von Nurr1-Liganden zu studieren und das Konzept einer pharmakologischen Nurr1-Modulation zur Behandlung neurodegenerativer Erkrankungen validieren zu können, fehlt es daher an potenten und selektiven synthetischen *tool compounds*. Es sollten deshalb verschiedene

Strategien zur Identifikation und Entwicklung neuer Nurr1-Liganden verfolgt werden, um den Strukturraum schnell und chemisch divers erweitern zu können.

Der erste Ansatz wurde inspiriert von den ersten ligandengebundenen Co-Kristallstrukturen der Nurr1-LBD mit den Prostaglandinen A1⁴¹⁹ und A2⁴²⁰. Die potenziellen endogenen Liganden liegen darin an einer ungewöhnlichen Bindestelle nahe Helix 12 kovalent gebunden vor³⁴⁷. Der Hypothese folgend, dass Arzneistoffe, die mit Prostaglandin-Bindungsstellen in anderen Proteinen, nämlich den an ihrer Biogenese beteiligten Enzymen, interagieren, aufgrund struktureller Ähnlichkeit auch an Nurr1 binden könnten, sollten nichtsteroidale Antirheumatika in einem ersten *in vitro* Screening auf ihre Nurr1-modulatorische Aktivität untersucht werden. Die identifizierten Nurr1-Modulatoren sollten anschließend näher charakterisiert und ihr molekularer Einfluss auf die Interaktion mit Co-Regulatoren und das Dimerisierungsverhalten von Nurr1 analysiert werden. Die Ergebnisse der hieraus entstandenen Publikation⁴⁴⁴ (Kapitel 16.4) sind in Kapitel 3.3 dargestellt.

Aus den strukturellen Gemeinsamkeiten der validierten Nurr1-Agonisten AQ (19) und CQ (25)³⁸⁹ – nämlich vor allem dem in beiden Verbindungen enthaltenen 7-Chlorochinolin-4-amin – entstand der zweite Ansatz, in dem Fragment-basiert neue Agonisten identifiziert, optimiert und charakterisiert werden sollten. Anschließend sollten die so erhaltenen hinsichtlich ihrer Aktivität an Nurr1 optimierten Fragmente über eine Rekombination mit bekannten Strukturmotiven weiterentwickelt werden. Die Ergebnisse dieser Untersuchungen sind in Kapitel 3.4 dargestellt und die daraus hervorgegangene Veröffentlichung⁴⁵⁵ ist in Kapitel 16.5 nachzulesen.

Als dritter Ansatz wurde im Sinne eines *Fragment-Screenings* eine Substanzbibliothek von 480 Fragmenten zugelassener Arzneistoffe auf seine Aktivität im zellulären Nurr1-Testsystem untersucht, um chemisch möglichst diverse Struktur motive als Ausgangspunkt für die Entwicklung von neuen Nurr1-Liganden zu erhalten⁴⁵⁶. Die Verwendung dieser speziellen Substanzkollektion bot sich dabei für zwei verschiedene Vorgehensweisen an, um potenzielle Treffer weiterzuentwickeln. Zum einen eignen sich die Arzneistoff-Fragmente aufgrund ihres geringen Molekulargewichts und ihrer vorteilhaften physikochemischen Eigenschaften für einen klassisch medizinal-chemischen Ansatz, indem durch geeignete Erweiterungen, dem sog. *fragment-growing*, und systematische Strukturoptimierung neue Liganden generiert werden^{457,458}. Zum anderen bieten die zugehörigen Arzneistoffe, von denen sich die potenziellen Treffer ableiten, eine gute Möglichkeit zur Identifikation neuer Substanzklassen, deren Wirkungen bereits vielfach klinisch untersucht wurden und die daher meist gute physikochemische und pharmakokinetische Eigenschaften (*drug-likeness*) mit sich bringen⁴⁵⁹. Die Ergebnisse des Screenings sind in Kapitel 3.5 zusammengefasst und als Teil des Preprints⁴⁶⁰ in Kapitel 16.7 nachzulesen.

Eine systematische Optimierungsstrategie wurde anschließend anhand eines invers agonistischen Treffers aus dem Screening angewendet, um potente und selektive inverse Nurr1 Agonisten zu entwickeln und charakterisieren. Die daraus entstandenen Liganden sollten anschließend für mechanistische Studien der reduzierten Rezeptoraktivität dienen. Kapitel 3.5.1 fasst die Ergebnisse der hieraus entstandenen Publikation⁴⁶¹ (Kapitel 16.6) zusammen. Die zweite Strategie führte von einem agonistischen Treffer aus dem Screening zur Identifikation eines Nurr1-Agonismus der Arzneistoffklasse der Statine. Diese Erkenntnisse sollten anhand von zwei Vertretern grundlegend mechanistisch charakterisiert werden und auf eine potenzielle klinische Relevanz mittels *Knockdown*-Experimenten und Genexpressionsanalyse in humanen Astrozyten untersucht werden. Die Ergebnisse dieser Studie sind in Kapitel 3.5.2 dargestellt und das zugehörige Preprint⁴⁶⁰ in Kapitel 16.7 nachzulesen.

3. Ergebnisse und Diskussion

3.1 Photohormone als lichtabhängige PPAR-Agonisten

Zur Entwicklung photoschaltbarer PPAR-Liganden wurden zunächst Leitstrukturen aus dem großen Schatz der publizierten PPAR-Agonisten (DrugBank, PDB, ChEMBL, IUPHAR) ausgewählt und mittels computergestütztem Design auf ihre Eignung als potenzielle Photohormone analysiert. Da die meisten PPAR-Liganden eine fettsäuremimetische Struktur aufweisen, besitzen sie einen lipophilen Bereich, der sich für die Substitution durch ein Azobenzen-Motiv eignet. Bei diesem als „Azologisierung“ bezeichneten Ansatz wird bevorzugt eine Diaryleinheit mit zweiatomigem Linker (z. B. Stilben, Diarylamid) der Leitstruktur durch eine Azogruppe ersetzt. Dies verleiht dem Molekül somit photoschaltbare Eigenschaften mit guter Stabilität über mehrere Lichtschaltzyklen, weshalb sich diese Substanzklasse in der Photopharmakologie, auch wegen ihrer guten synthetischen Zugänglichkeit, etabliert hat⁴⁶². Für das computergestützte Design besonders geeignet waren PPAR-Liganden, die aufgrund verfügbarer Co-Kristallstrukturen mit der jeweiligen PPAR-LBD ein valides strukturbasiertes Design ermöglichten, welches mittels molekularen Dockings mit der Software *Molecular Operating Environment* (MOE) durchgeführt wurde. So wurden vier unterschiedliche Chemotypen als Leitstrukturen ausgewählt (Abbildung 23): die PPAR γ -Agonisten MDG548⁴⁶³ (**27**), GW1929⁴⁶⁴ (**28**) und Rosiglitazon²⁹³ (**3**) sowie der pan-PPAR-Agonist GL479^{465,466} (**29**). Bei **27** wurde das Benzylphenylether-Motiv durch ein unsubstituiertes Azobenzen ausgetauscht (**30**) und aufgrund der strukturellen Verwandtschaft eine Co-Kristallstruktur von **3** mit der PPAR γ -LBD (PDB: 5YCP²⁴⁸) zur Analyse verwendet. Dabei zeigte der vorhergesagte Bindemodus für *trans*-**30** eine gute Übereinstimmung mit der gedockten Leitstruktur **27** und dem kristallisierten Liganden **3**, was Potenzial für die PPAR γ -Modulation des Azologs andeutete. Die Analyse der Co-Kristallstruktur von **28** mit der PPAR γ -LBD (PDB: 6D8X⁴⁶⁷) zeigte, dass das Benzophenon-Motiv in einer engen lipophilen Tasche der LBD gebunden ist, die nur wenig Platz und Flexibilität für strukturelle Veränderungen bietet. Docking-Studien der Azologa von **28** bestätigten dies, da ein Azobenzen statt des Benzophenons keine plausiblen Bindungsmodi lieferte. Die Azogruppe anstelle des Aminoethoxy-Linkers (**31**) hingegen zeigte eine vielversprechende Übereinstimmung mit dem kristallisierten Liganden **28** sowohl in *trans*- als auch in *cis*-Konfiguration. Beim dritten PPAR γ -Agonisten **3** wurde in gleicher Weise der Aminoethoxy-Linker substituiert (**32**), sodass alle drei potenziellen Photohormone plausible Bindungsmodi im Docking zeigten und eine Interaktion mit der kanonischen Aktivierungstriade eingingen. Der pan-PPAR-Agonist **29** enthielt bereits ein Azobenzen im lipophilen Bereich des Moleküls und zudem standen Co-Kristallstrukturen mit den Subtypen PPAR α und - γ zur Verfügung⁴⁶⁸, wodurch **29** einen guten Startpunkt zur Optimierung photoschaltbarer PPAR-Liganden darstellte.

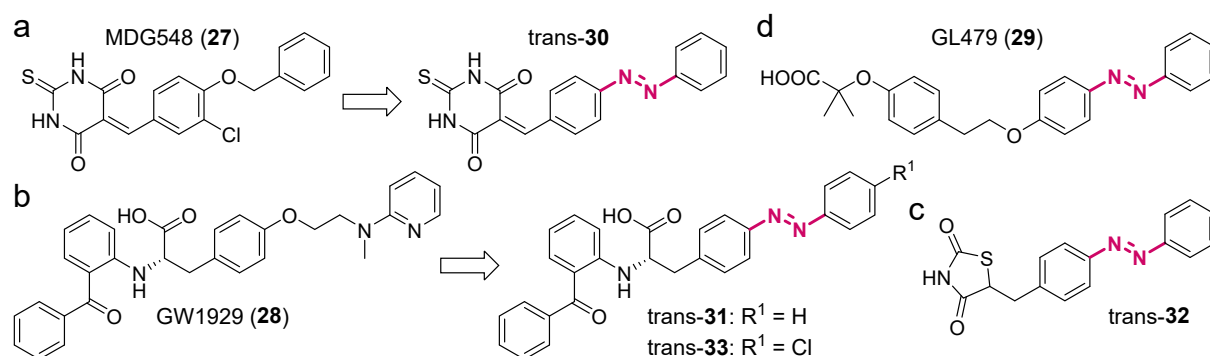


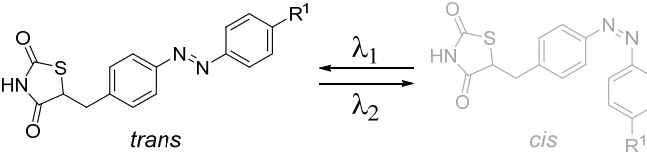
Abbildung 23: Leitstrukturen der photoschaltbaren PPAR-Agonisten. (a–c) Entwicklung aus den bekannten PPAR γ -Agonisten MDG548⁴⁶³ (a), GW1929⁴⁶⁴ (b) und Rosiglitazon²⁹³ (c) durch Austausch der Linker-Region gegen eine Azogruppe (rot). (d) Der pan-PPAR-Agonist GL479^{465,466} enthielt bereits ein Azobenzen-Strukturmotiv.

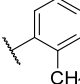
Die beiden Projekte, die aus diesen ersten Untersuchungen hervorgegangen sind, wurden in konstruktiver Zusammenarbeit mit der Arbeitsgruppe von Prof. Dr. Dirk Trauner (Universität New York) durchgeführt, wobei Dr. Johannes Morstein und Konstantin Hinnah maßgeblich für die Synthesen der hier gezeigten Photohormone und deren photo-physikalische Charakterisierung verantwortlich waren, welche daher nicht Gegenstand dieses Kapitels sind (siehe Kapitel 16.1 und 16.2).

Zur *in vitro* Charakterisierung der Photohormone wurden einheitliche Gal4-PPAR-Reporterassays in HEK293T-Zellen eingesetzt. Diese verwenden jeweils ein Rezeptorkonstrukt aufgebaut aus der LBD einer der drei humanen PPAR-Subtypen fusioniert mit der Gal4-DBD aus der Hefe⁴⁶⁹ sowie ein Gal4-abhängiges *Firefly*-Luciferase-Reporter-Plasmid und ein konstitutiv exprimierendes *Renilla*-Luciferase-Konstrukt zur Normalisierung und Toxizitätskontrolle. Um beide Isomere getrennt zu charakterisieren, wurden die Experimente mit den *trans*-Isomeren weitestgehend unter Lichtausschluss durchgeführt. Für die Testung der *cis*-Isomere wurden die Substanzen im Inkubationsmedium vorab für 3 min mit einer LED-Lampe ($\lambda = 365$ nm) beleuchtet, um das jeweilige energetisch begünstigte *trans*-Isomer möglichst vollständig in das entsprechende *cis*-Isomer zu überführen. Die betreffenden Zellplatten wurden während der Inkubationszeit über Nacht (14–16 h) im Brutschrank mit einem sog. CellDISCO-System⁴⁶ betrieben, welches mit Lichtimpulsen ($\lambda = 370$ nm) von 75 ms alle 15 s für eine Aufrechterhaltung der *cis*-Konfiguration sorgte.

Die erste Untersuchung der Photohormon-Leitstrukturen **29–32** auf ihre PPAR-Aktivität zeigte, dass *trans*-**30** an allen drei PPAR-Subtypen inaktiv war, sodass es nicht weiterverfolgt wurde. Die Azologa **31** und **32** der potenteren PPAR γ -Agonisten **28** und **3** aktivierten PPAR γ mit Potenzen im unteren mikromolaren Bereich (*trans*-**31**: EC₅₀ 1,0 ± 0,1 μ M, 30 ± 2 % rel. max. Aktivierung; **32** in Tabelle 1) und waren selektiv über die verwandten Subtypen PPAR α und - δ . Der pan-PPAR-Agonist **29** zeigte eine ausgeglichene Aktivität an allen drei PPAR-Subtypen im unteren mikromolaren Bereich in Übereinstimmung mit der Literatur^{465,466}, wobei die relative Aktivierungseffizienz an PPAR δ am höchsten war (Tabelle 2). Alle drei aktiven Photohormone zeigten in ihrer *cis*-Konfiguration vergleichbare Aktivitäten mit dem *trans*-Isomer, doch bei **31** waren die Dosis-Wirkungskurven des *cis*- und *trans*-Isomers nahezu identisch, was durch die schlechteren photophysikalischen Eigenschaften zu erklären war. Nach 5 min Bestrahlung ($\lambda = 365$ nm) waren im NMR nur 33 % der Substanz als *cis*-Isomer zu detektieren (**32**: 96 %; siehe Kapitel 16.1). Auch das zweite Derivat **33** verhielt sich ähnlich und konnte keine gesteigerte Potenz und Präferenz für eines der Isomere erzielen, sodass dieser Chemotyp für weitere Optimierungen wenig aussichtsreich erschien und nicht weiterverfolgt wurde. Somit stand mit **32** ein subtypenselektives PPAR γ -Photohormon zur Verfügung, das in seiner Präferenz für eines der Isomere optimiert werden sollte. Zur Entwicklung photoschaltbarer und subtypenselektiver PPAR α - und - δ -Agonisten wurde **29** als Leitstruktur verwendet, um ein Set an photopharmakologischen Tools für alle drei PPAR-Subtypen zu ermöglichen.

Tabelle 1: Untersuchung der *para*-Position des terminalen Phenylrings am Rosiglitazon-Azolog **32**. Die Aktivitäten wurden im Gal4-PPAR γ -Reporterassay in HEK293T-Zellen bestimmt. *cis*-Isomere wurden vorab beleuchtet ($\lambda = 365$ nm, 3 min) und mit einem CellDISCO-System⁴⁶ in *cis*-Konfiguration gehalten. Alle Werte sind MW ± S.E.M.; $n \geq 2$. Die max. rel. Aktivierung bezieht sich auf Pioglitazon (2, 1 μ M).



ID	R ¹	PPAR γ - EC ₅₀ [μ M] (max. rel. Aktivierung [%])	
		<i>trans</i>	<i>cis</i>
32	H	2,2 ± 0,2 (21 ± 1)	6,3 ± 1,4 (38 ± 5)
34	Cl	2,9 ± 0,2 (25 ± 1)	7,0 ± 1,0 (49 ± 4)
35	CF ₃	2,2 ± 0,7 (33 ± 5)	6,5 ± 1,5 (52 ± 11)
36		2,8 ± 1,3 (12 ± 2)	6,4 ± 0,4 (39 ± 2)

Das Docking der beiden Isomere von **32** zeigte (Abbildung 24a), dass der terminale Phenylring in *trans*-Konfiguration (magenta) durch die lineare Struktur des Moleküls einen Hohlraum ausfüllt, der nur wenig Platz für Substituenten bietet. Das *cis*-Isomer (violett) hingegen ragt, ähnlich dem kristallisierten Liganden **3**, in den zweiten lipophilen Arm der PPAR γ -Bindetasche hinein, was Potenzial zur terminalen Verlängerung in *para*-Position andeutete, um einen Vorzug für die *cis*-Konfiguration zu erreichen. Basierend auf diesen Beobachtungen wurden potenziell *cis*-präferenzielle Derivate mit einem Chlor- (**34**) oder Trifluormethyl-Rest (**35**) in *para*-Position sowie einem sperrigen *ortho*-Tolyl-Rest (**36**) designt, um dadurch die Bindung des jeweiligen *trans*-Isomers zu verhindern. Während die Potenzen der Isomere durch die Substituenten weitgehend unverändert blieben (Tabelle 1), steigerten **34** und **35** die Aktivierungseffizienz des *cis*-Isomers deutlich, wobei sich bei **35** auch die Effizienz des *trans*-Isomers erhöhte. **36** hingegen konnte die Effizienz des *trans*-Isomers deutlich senken auf nur noch 12 %, sodass mit der hohen Aktivierungseffizienz des *cis*-Isomers von 39 % ein mehr als 3-facher Unterschied zwischen beiden Konfigurationen erzielt wurde. Eine Untersuchung der Bindungsaffinitäten mittels isothermer Titrations-Kalorimetrie (ITC) bestätigte, dass das dunkeladaptierte *trans*-**36** nicht an die rekombinante PPAR γ -LBD binden kann, das lichtaktivierte *cis*-**36** hingegen mit einem K_D -Wert von 9,3 μ M bindet (Abbildung 24b). Um diese Erkenntnisse auch am endogenen Rezeptor zu überprüfen, wurde ein natives zelluläres Testsystem etabliert, bei dem humane Hepatozyten (HepG2-Zellen) nur mit einem Reporter-Plasmid unter Kontrolle des nativen PPRE und dem *Renilla*-Luciferase-Kontroll-Plasmid transfiziert wurden. Dabei konnte das Photohormon *cis*-**36** den PPRE-Reporter 2,4 \pm 0,1-fach mit einem EC_{50} -Wert von 0,9 \pm 0,2 μ M aktivieren (Abbildung 24c). Doch auch *trans*-**36** zeigte trotz fehlender Bindungsaffinität eine moderate Aktivierung des PPRE bei 10 μ M, was möglicherweise auf eine Isomerisierung im zellulären System ohne Licht zurückzuführen sein könnte. Mit **36** ist es somit gelungen, aus dem bekannten PPAR γ -Agonisten Rosiglitazon (**3**) durch computergestützte Optimierung einen photoschaltbaren PPAR γ -Liganden zu entwickeln, der erst durch Licht zum PPAR γ -aktiven *cis*-Isomer aktiviert wird, während das *trans*-Isomer nur geringe Aktivität am Rezeptor aufweist.

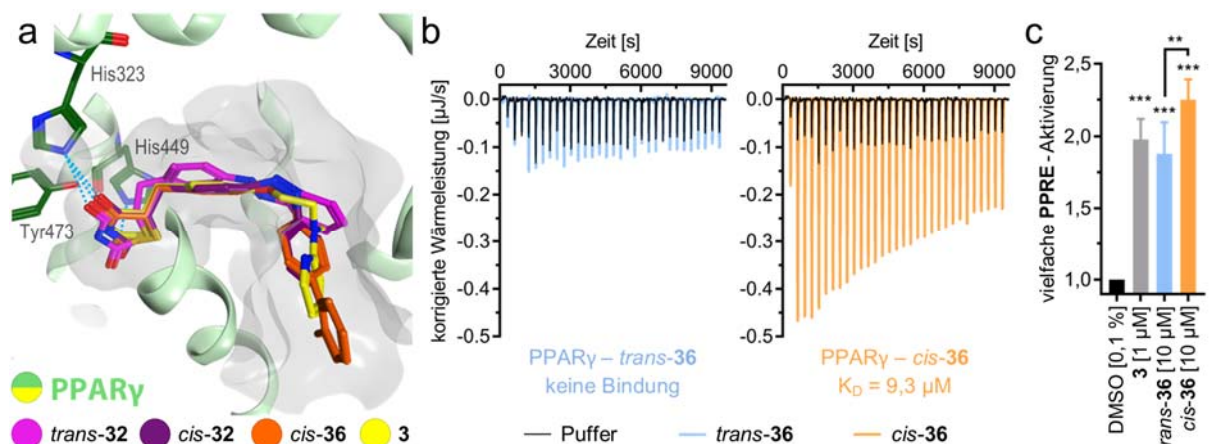


Abbildung 24: Design und Charakterisierung des lichtaktivierbaren Rosiglitazon-Derivates **36**. (a) Docking beider Isomere der Leitstruktur **32** zeigt Potential für ein *cis*-bevorzugtes Derivat durch Verlängerung in *para*-Position. Der sperrige *o*-Tolyl-Rest in *cis*-**36** ragt vorteilhaft in den lipophilen Tunnel. Das Docking wurde in MOE durchgeführt mit der Co-Kristallstruktur von PPAR γ mit **3** (PDB: 5YCP²⁴⁸). (b) ITC-Experiment von *trans*-**36** (dunkel, 300 μ M) und *cis*-**36** (beleuchtet mit $\lambda = 365$ nm für 5 min, 300 μ M) mit dem rekombinanten PPAR γ -LBD-Protein (64 μ M) zeigt alleinige Bindung des *cis*-Isomers. Titration des Puffers zur Kontrolle. (c) *cis*-**36** aktivierte das humane PPRE ohne die Überexpression von PPAR γ und Heterodimer-Partner RXR in HepG2-Zellen. **3** diente als Referenzagonist für PPAR γ -Aktivierung. Gezeigt sind MW \pm SD; n = 6; **p < 0,01 und ***p < 0,001 (t-Test).

Die Analyse des Dockings für **29**, welches mit der vorhandenen Co-Kristallstruktur von **29** in PPAR α (PDB: 4CI4⁴⁶⁸) und der Co-Kristallstruktur eines verwandten GW501516³¹⁵(**17**)-Analogons in PPAR δ (PDB: 5Y7X⁴⁷⁰) durchgeführt wurde, zeigte drei vielversprechende Optimierungsmöglichkeiten. Als

erste Strukturvariation wurden verschiedene Längen des Alkoxy-Linkers zwischen den aromatischen Systemen virtuell und *in vitro* untersucht. Dabei zeigte nur das Kürzen um ein Kohlenstoffatom vielversprechende Dockingergebnisse, da das verkürzte *cis*-Isomer weniger Kollisionen aufwies als *cis*-**29**. Im zellulären Assay konnte jedoch für keines der verkürzten Isomere eine Steigerung der Potenz beobachtet werden, weshalb die ursprüngliche Kettenlänge von **29** beibehalten wurde.

Als weitere Modifikation für eine bevorzugte *trans*-Konfiguration deuteten sich Substituenten am terminalen Phenylring an, die so die Bindung des *cis*-Isomers weiter zu erschweren und in der *trans*-Konfiguration eine zusätzliche kleine Ausbuchtung in beiden Rezeptor-Bindestaschen auszufüllen schienen (Abbildung 25a, c). Neben einem Chlor- und Isopropyl-Rest erwies sich der Methyl-Rest (**37**) in *para*-Position am vielversprechendsten, da eine moderate *trans*-Präferenz bestätigt werden konnte und zusätzlich die Selektivität über PPAR γ gesteigert wurde (Tabelle 2). Insgesamt konnte jedoch keine deutliche Optimierung durch diese Substituenten in *para*-Position erzielt werden. Als dritte Variation ergab die Dockingstudie, dass Substituenten in *ortho*-Position des zentralen Phenylrings einen zusätzlichen lipophilen Hohlraum in den Bindestellen von PPAR α und - δ adressieren würden, um so die Affinität zu erhöhen (Abbildung 25b, d). Besonders die Einführung eines Methyl-Rests (**38**) erbrachte eine beachtliche Steigerung der Affinität an PPAR α und zugleich eine erhebliche Verbesserung der *trans*-Präferenz (Tabelle 2). Die Auswirkungen auf die Aktivität an PPAR δ waren ähnlich, jedoch weniger stark ausgeprägt. Auch ein Chloratom an dieser Position (**39**) konnte die Aktivität an PPAR α und - δ deutlich steigern, was allerdings mit dem Verlust der *trans*-Präferenz einherging. Zusätzlich wurde ein Trifluormethyl-Substituent in *ortho*-Position (**40**) untersucht, der sich als potenteste Modifikation für PPAR δ -Aktivierung herausstellte, an PPAR α jedoch, trotz ebenfalls hoher Affinität, eine deutlich geringere *trans*-Präferenz aufwies als **38** und außerdem die geringste Selektivität über PPAR γ zeigte. Schließlich wurde die bevorzugte Modifikation aus **37** mit den drei verschiedenen Substituenten in *ortho*-Position kombiniert und brachte mit **41** einen dualen PPAR α / δ -Agonisten mit ausgeglichen hoher Potenz und Aktivierungseffizienz an beiden Rezeptoren sowie guter *trans*-Präferenz hervor, die sich vor allem im Unterschied der Aktivierungseffizienzen bemerkbar machte (Tabelle 2).

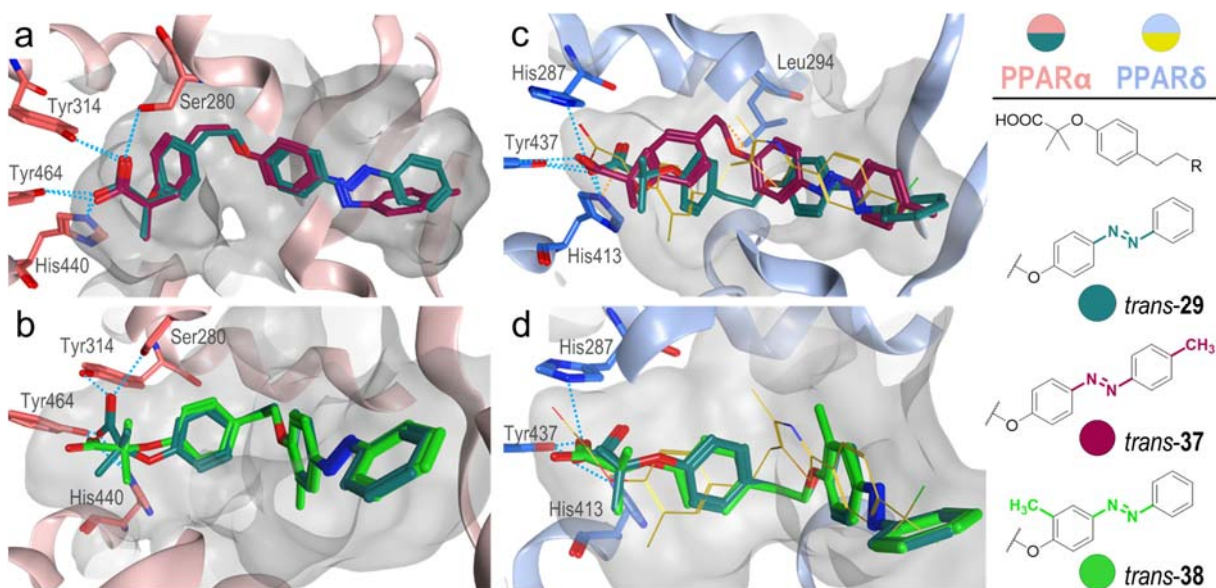


Abbildung 25: Dockinganalyse zu **29** zeigt Optimierungsmöglichkeiten für photoschaltbare PPAR α - und - δ Liganden. Die Leitstruktur *trans*-**29** (petrol) ist in allen Modellen zum Vergleich gezeigt. (a, b) PPAR α -Bindungsstelle (rosa) aus der Co-Kristallstruktur mit **29** (PDB: 4CI4⁴⁶⁸) und (c, d) PPAR δ -Tasche (hellblau) mit der gedockten Leitstruktur **29** zum Vergleich (PDB: 5Y7X⁴⁷⁰). Die terminale Verlängerung mit einer *p*-Methylgruppe ermöglicht verbesserte Bindungsmodi von *trans*-**37** (bordeaux, a und c). Die Einführung eines *o*-Methyl-Rests in **38** (grün, b und d) füllt einen zusätzlichen lipophilen Hohlraum aus.

Tabelle 2: Optimierung des pan-PPAR-Agonisten **29** zu photoschaltbaren PPAR α - und - δ -Agonisten. Die Aktivitäten wurden in einheitlichen Gal4-PPAR-Reporterassays in HEK293T-Zellen bestimmt. *cis*-Isomere wurden vorab beleuchtet ($\lambda = 365$ nm, 3 min) und mit einem CellDISCO-System⁴⁶ in *cis*-Konfiguration gehalten. Alle Werte sind MW \pm S.E.M.; $n \geq 3$. Die max. relative Aktivierung bezieht sich auf GW7647 (**1**, PPAR α), Pioglitazon (**2**, PPAR γ) und L165,041 (**16**, PPAR δ) bei 1 μ M.

ID	R ¹	R ²	Konf.	EC ₅₀ [μ M] (max. rel. Aktivierung [%])		
				PPAR α	PPAR γ	PPAR δ
29	H	H	<i>trans</i>	1,09 \pm 0,02 (31 \pm 1)	2,7 \pm 0,2 (25 \pm 1)	2,2 \pm 0,1 (61 \pm 2)
			<i>cis</i>	0,8 \pm 0,2 (29 \pm 2)	6,0 \pm 0,6 (28 \pm 2)	6 \pm 1 (34 \pm 6)
37	CH ₃	H	<i>trans</i>	0,66 \pm 0,07 (24 \pm 1)	EC ₅₀ > 10 μ M (tox. \geq 6 μ M)	1,42 \pm 0,09 (33 \pm 1)
			<i>cis</i>	1,1 \pm 0,2 (22 \pm 3)	EC ₅₀ > 10 μ M	3,8 \pm 0,8 (31 \pm 5)
38	H	CH ₃	<i>trans</i>	0,0070 \pm 0,0006 (38 \pm 1)	1,2 \pm 0,1 (20 \pm 1)	0,54 \pm 0,04 (45 \pm 1)
			<i>cis</i>	0,24 \pm 0,02 (43 \pm 1)	1,7 \pm 0,8 (24 \pm 1)	3,0 \pm 0,5 (41 \pm 4)
39	H	Cl	<i>trans</i>	0,029 \pm 0,004 (49 \pm 2)	0,82 \pm 0,07 (14 \pm 1)	0,24 \pm 0,02 (46 \pm 1)
			<i>cis</i>	0,040 \pm 0,003 (45 \pm 1)	0,92 \pm 0,08 (22 \pm 1)	0,35 \pm 0,06 (44 \pm 2)
40	H	CF ₃	<i>trans</i>	0,009 \pm 0,002 (46 \pm 2)	0,6 \pm 0,1 (34 \pm 2)	0,14 \pm 0,01 (45 \pm 2)
			<i>cis</i>	0,071 \pm 0,007 (42 \pm 1)	0,77 \pm 0,07 (32 \pm 1)	0,31 \pm 0,03 (37 \pm 2)
41	CH ₃	Cl	<i>trans</i>	0,04 \pm 0,01 (76 \pm 8)	4,5 \pm 0,2 (68 \pm 2)	0,12 \pm 0,02 (65 \pm 4)
			<i>cis</i>	0,29 \pm 0,05 (41 \pm 4)	4,8 \pm 0,4 (42 \pm 2)	0,38 \pm 0,03 (35 \pm 2)

Das Potenzial der neuen photopharmakologischen *tool compounds* **38** und **41** für PPAR α und - δ , welche zudem günstige photophysikalische Eigenschaften aufwiesen, sollte in einem neuen Testsystem unter Beweis gestellt werden. Um eine zugleich räumliche und zeitliche Auflösung zu ermöglichen, wurden HEK293T-Zellen mit mCherry oder dem grün fluoreszierenden Protein (eGFP) als Gal4-abhängigen Fluoreszenz-Reportern und dem jeweiligen Gal4-PPAR-Rezeptor-Plasmid transfiziert, sodass die reversible Aktivierung der Photohormone in intakten lebenden Zellen untersucht werden konnte. So wurde ein Zeitverlauf der PPAR α -Aktivierung 8 h nach Inkubation mit **38** durch stündliche Messungen der mCherry-Fluoreszenz-Intensität aufgenommen (Abbildung 26a). Für das dunkeladaptierte *trans*-**38** zeigte sich dabei ein stetiger Anstieg der Fluoreszenz-Intensität (blaue Kurve), während das Umschalten zum *cis*-Isomer nach 8 h zu einem Stagnieren der Fluoreszenz-Intensität auf einem niedrigeren Plateau führte (grüne Kurve). Im umgekehrten Fall (8 h *cis*-**38**, anschließend *trans*-**38**, rote Kurve) zeigte sich ein verspäteter Anstieg des mCherry-Signals, welches sich nach 36 h dem Niveau des vollständig dunkeladaptierten *trans*-**38** angleichen konnte. Für **41** ergab sich auf PPAR δ ein vergleichbares Bild. Eine räumliche Auflösung der Photohormon-Aktivität wurde mittels Fluoreszenz-Mikroskopie der lebenden Zellen durchgeführt. Diese wurden zuvor mit der Kombination aus mCherry-Reporter/Gal4-PPAR α oder eGFP-Reporter/Gal4-PPAR δ transfiziert, nach 5 h gepoolt und im Anschluss mit einem der Photohormone für 40 h behandelt. *Trans*-**38** induzierte die mCherry-Expression bereits bei einer Konzentration von 10 nM deutlich, während *cis*-**38** nur einen geringen Effekt zeigte (Abbildung 26b). Bei höheren Konzentrationen (300 nM) war die mCherry-Expression beider Isomere schließlich vergleichbar und zeigte nur eine geringe PPAR δ -Aktivierung durch erhöhte eGFP-Expression, wodurch die hohe Potenz, Subtypenselektivität und *trans*-Präferenz von **38** zusätzlich bestätigt wurden.

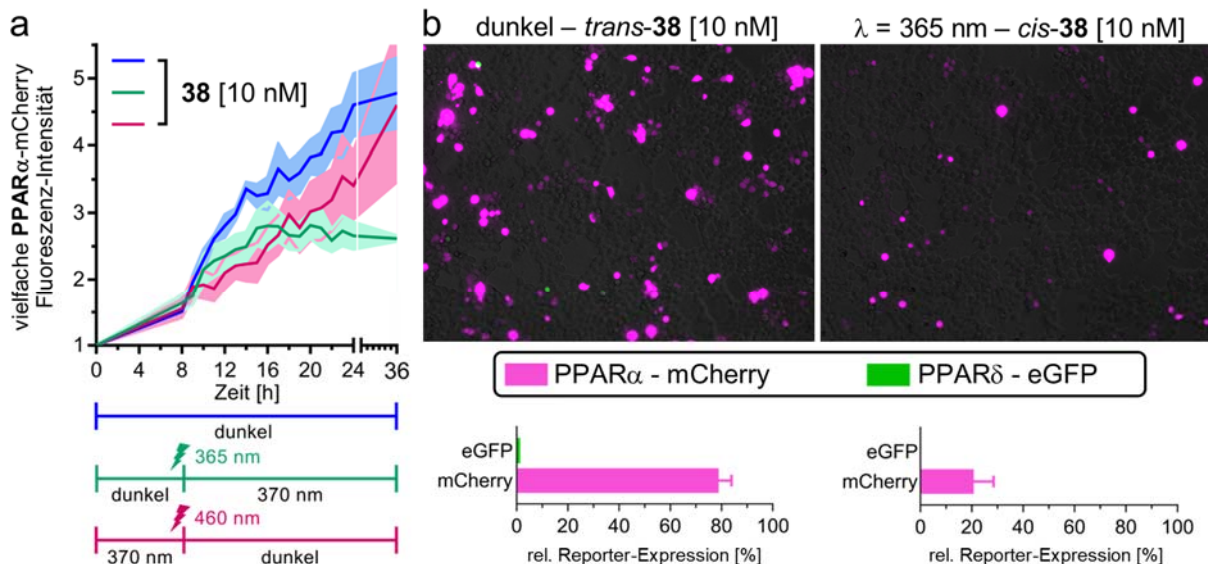


Abbildung 26: Spatiotemporale Kontrolle von PPAR α durch **38** in lebenden HEK293T-Zellen. (a) Zeit-abhängige PPAR α -Aktivierung durch **38** mithilfe eines mCherry-Fluoreszenz-Reporters. *trans-38* wurde dunkeladaptiert verwendet (blau). Das Umschalten zwischen dem *cis*- und *trans*-Isomer erfolgte nach 8 h durch Beleuchtung mit $\lambda = 365$ nm (grün) oder $\lambda = 460$ nm (rot) für 3 min und anschließender Aufrechterhaltung des *cis*-Zustands mit dem CellDISCO-System⁴⁶. Die vielfache Fluoreszenz-Intensität bezieht sich auf 0,1 % DMSO. Gezeigt sind die MW \pm S.E.M.; $n = 3$. (b) Fluoreszenz-Mikroskopie zeigte PPAR α -vermittelte mCherry-Induktion durch *trans-38* (dunkel) und *cis-38* ($\lambda = 365$ nm). Die PPAR δ -abhängige eGFP-Fluoreszenz war vernachlässigbar. Die rel. Reporter-Expression bezieht sich auf GW7647 (PPAR α) bzw. L165,041 (PPAR δ) bei 1 μ M; MW \pm S.E.M.; $n = 2$.

Somit konnte durch computergestützte Optimierung des pan-PPAR-Agonisten **29** ein hochpotenter und selektiver PPAR α -Agonist (**38**) entwickelt werden, der durch Licht von seiner aktiven *trans*-Konfiguration in das entsprechende *cis*-Isomer gebracht werden kann, welches 35-fach geringere Aktivität am Rezeptor aufweist. Durch die selektive optische Kontrolle von PPAR α und - γ ermöglichen **38** und **36** als wertvolle photopharmakologische Tools Untersuchungen der Rezeptoraktivierung mit spatiotemporaler Auflösung, die durch konstitutiv aktive Modulatoren nicht möglich wären.

3.2 Vitamin-E-Metabolite sind endogene PPAR γ -Liganden

Unter dem Begriff Vitamin E werden acht verschiedene Strukturen zusammengefasst, nämlich jeweils vier (α - δ) Tocopherole und Tocotrienole, die sich in ihrer Methylierung am Chromanolmotiv unterscheiden (Abbildung 27a)⁴⁷¹. Die antioxidativen Wirkungen von Vitamin E sind hinreichend bekannt⁴⁷¹, doch auch antientzündliche Effekte und positive Effekte bei der nicht-alkoholischen Fettlebererkrankung (NAFLD) und AD wurden beschrieben⁴⁷²⁻⁴⁷⁶. Für diese Aktivitäten werden oxidative Metabolite wie die 13'-Hydroxylat- und 13'-Carboxylat-Tocopherole verantwortlich gemacht, obwohl die zugrundeliegenden Mechanismen weitestgehend unbekannt sind^{471,477,478}. Die fettsäuremimetische Struktur der Vitamin-E-Metabolite deutete auf eine Beteiligung von Lipidsensoren wie den nukleären Rezeptoren hin und sollte anhand von den α - und δ -Tocopherol(**42** & **43**)-Metaboliten **44-47** sowie dem Vitamin-E-Mimetikum Garcinolsäure (**48**) untersucht werden (Abbildung 27a). **48** ist ein Naturstoff, der aus den Samen der bitteren Kolanuss (*Garcinia kola*) isoliert wurde⁴⁷³ und als das Carboxylat des δ -Tocotrienols die Metabolite der zweiten Gruppe von Vitamin-E-Vitaminen vertritt. Ein Aktivitätsscreening über 16 verschiedene nukleäre Rezeptoren in einheitlichen Gal4-Hybrid-Reporterassays zeigte vor allem Aktivitäten der 13'-Carboxylate **46** und **47** sowie der Garcinolsäure (**48**) an den PPARs (Abbildung 27b), neben moderaten Aktivitäten an den RARs, FXR und CAR. Dabei war die Aktivierungseffizienz von **46** und **48** bemerkenswert und überstieg sogar die potenten synthetischen PPAR-Referenzagonisten. Die nähere Charakterisierung ergab einen starken Agonismus von **48** im Gal4-PPAR γ -Reporterassay

mit einem EC₅₀-Wert von 1,7 ± 0,1 µM und 168 ± 4 % maximaler Aktivierung (bezogen auf **2**, 1 µM). Bei Co-Inkubation mit dem irreversiblen PPARγ-Antagonisten GW9662 (**13**) wurde die Reporterinduktion durch **48** blockiert, was auf eine direkte Interaktion mit PPARγ hindeutete (Abbildung 27c). Außerdem wurde die Wechselwirkung mit dem orthosterischen Agonisten Pioglitazon (**2**) untersucht. Die Titration von **48** in Gegenwart von **2** zeigte einen erstaunlichen additiven Effekt beider Substanzen mit einer ~ 250 %igen Aktivierungseffizienz in Bezug auf **2** (Abbildung 27c). Dabei blieb der EC₅₀-Wert von **48** unverändert und das obere Plateau erreichte etwa das 1,5-fache der alleinigen PPARγ-Aktivierung durch **48**. Diese kooperative Aktivität beider Liganden konnte auch in einem nativen Reporterassay beobachtet werden, bei dem durch Bindung des endogenen PPARγ in HepG2-Zellen das humane PPRE aktiviert wird (Abbildung 27d). Am PPRE zeigte **48** eine vergleichbare Aktivität mit einem EC₅₀-Wert von 1,1 µM und 1,7-facher maximaler Aktivierung. In diesem System verschob die Anwesenheit von **2** den EC₅₀-Wert von **48** leicht auf 4,8 µM, führte aber ebenfalls zu einer beachtlichen additiven 3,5-fachen PPRE-Aktivierung. Diese Beobachtungen lassen vermuten, dass **48** die PPARγ-LBD gleichzeitig mit dem orthosterischen Agonisten **2** an verschiedenen Bindestellen bindet. Mittels ITC konnte die direkte Interaktion von **48** mit dem Target zusätzlich bestätigt (K_D = 13,2 µM) und durch ein stöchiometrisches Verhältnis von 2:1 (**48**:PPARγ) die These einer zweiten Bindestelle weiter gestützt werden.

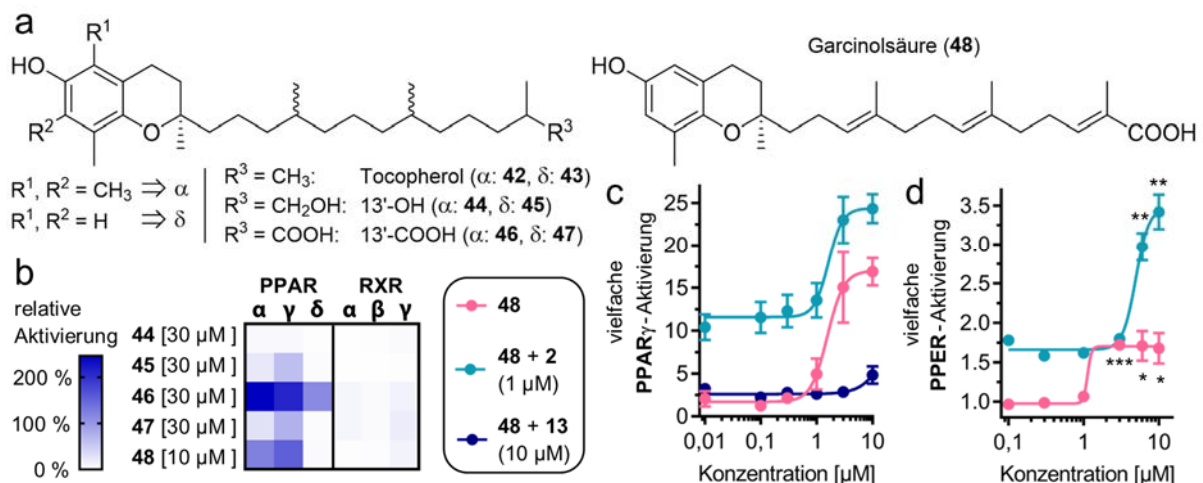


Abbildung 27: Vitamin-E-Metabolite modulieren PPARs. (a) Chemische Strukturen der Vitamin-E-Metabolite (**44-47**) und Garcinolsäure (**48**). (b) Aktivitätsscreening in einheitlichen Gal4-Reporterassays in HEK293T-Zellen. Die relative Aktivierung bezieht sich auf GW7647 (**1**, PPARα), Pioglitazon (**2**, PPARγ), L165,041 (**16**, PPARδ) und Bexaroten (RXRs) bei 1 µM; n ≥ 3. (c) Dosis-Wirkungskurven von **48** (rosa) sowie **48** in Gegenwart von Agonist **2** (1 µM, petrol) und Antagonist **13** (10 µM, blau) bestimmt in einem Gal4-PPARγ-Reporterassay. Gezeigt sind MW ± S.E.M.; n ≥ 3. (d) Dosis-Wirkungskurven von **48** (rosa) und **48** in Gegenwart von **2** (1 µM, petrol) auf dem nativen humanen PPRE in HepG2-Zellen ohne Rezeptorüberexpression. Gezeigt sind MW ± S.E.M.; n = 4. *p < 0,05, **p < 0,01, ***p < 0,001; t-Test vs. 0,1 % DMSO (**48**) oder vs. 1 µM **2** (**48** + **2**).

Um zu analysieren, wie sich die ungewöhnliche PPARγ-Modulation durch **48** auf das Co-Regulator-Netzwerk des Rezeptors auswirkt, wurde die Interaktion der PPARγ-LBD mit 29 Co-Regulator-Peptiden in einem zellfreien Testsystem mit zeitlich aufgelöstem Fluoreszenz-Resonanz-Energietransfer (*time-resolved fluorescence resonance energy transfer*, TR-FRET) untersucht. Dazu wurde die PPARγ-LBD mit Terbium-Kryptat (Tb³⁺) gelabelt als FRET-Donor verwendet. Fluoreszenz-gekoppelte Peptide mit Interaktionsmotiven bekannter Co-Regulatoren dienten entsprechend als FRET-Akzeptoren. Dabei zeigte **48** ein erstaunliches Rekrutierungsprofil, was sich deutlich von dem von **2** unterschied (Abbildung 28a). Die nähere Betrachtung von sechs modulierten Co-Faktor-Interaktionen bestätigte vollständig gegensätzliche Effekte von **48** und **2** auf die PPARγ-Co-Regulator Interaktionen. Während der Agonist **2**, wie zu erwarten, Co-Aktivatoren wie CBP, PGC-1α, NCoA6 und DRIP-2 rekrutierte und den

Co-Repressor SMRT verdrängt, wurden durch **48** die gleichen Co-Aktivatoren von der PPAR γ -LBD verdrängt und die Co-Repressoren NCoR1 und SMRT rekrutiert (Abbildung 28b,c). Dabei waren die EC₅₀/IC₅₀-Werte von **48** mit 3–22 μ M im Einklang mit den übrigen Aktivitätsdaten. Auch in Gegenwart von **2** dominierten die Effekte von **48** die Interaktionen, lediglich die Grundlinien wurden verschoben. Dass die Interaktion mit den SRC Co-Aktivatoren von beiden Liganden kaum beeinflusst wurde, ist nicht weiter verwunderlich, da viele Untersuchungen bereits eine untergeordnete Rolle bei den PPARs bestätigten¹²⁰. Somit kann möglicherweise auch die Inaktivität von **48** an PPAR γ im Selektivitätsscreening von Bartolini et al. erklärt werden, die zur Kontrolle des PXR-selektiven Effektes ein Alpha-Screen-Testsystem mit SRC1 als Co-Faktor verwendeten⁴⁷⁹. Insgesamt deutet der Einfluss von **48** auf das Co-Regulator-Netzwerk durch die Rekrutierung von Co-Repressoren, trotz der aktivierenden Effekte in beiden zellulären Systemen, auf ein invers agonistisches Profil des Liganden hin.

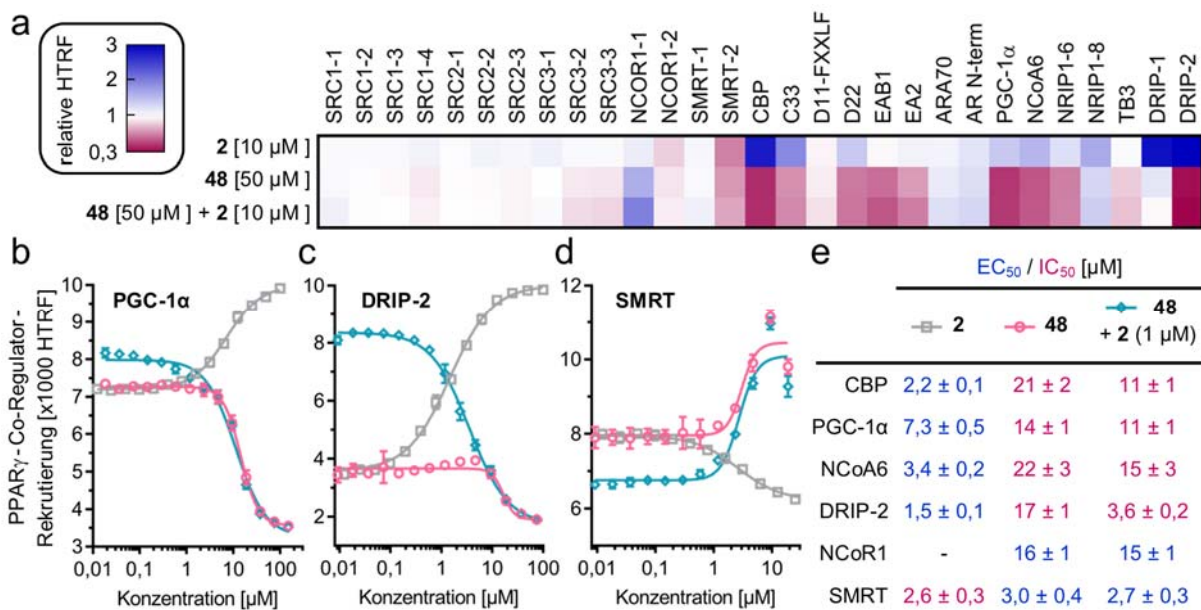


Abbildung 28: Einfluss von Garcinolsäure (**48**) und Pioglitazon (**2**) auf die Co-Regulator-Rekrutierung von PPAR γ . Die Interaktionen wurden in einem zellfreien TR-FRET-System mit Tb³⁺-gekoppelter PPAR γ -LBD als FRET-Donor und Fluoreszeingelabelten Co-Regulator-Peptiden als FRET-Akzeptoren untersucht. (a) Screening der Interaktion mit 29 Co-Regulator-Peptiden. Gezeigt sind die MW der relativen HTRF-Werte bezogen auf 1 % DMSO; N = 4. (b–d) Dosisabhängige Effekte von **2** (grau), **48** (rosa) und **48** + **2** (1 μ M, petrol) auf die Rekrutierung von PGC-1 α (b), DRIP-2 (c) und SMRT (d). (e) Zugehörige EC₅₀/IC₅₀-Werte, sowie weitere Interaktionen mit CBP, NCoA6 und NCoR1. (b–e) Gezeigt sind die dimensionslosen HTRF-Signale; MW \pm SD; N = 3.

In Zusammenarbeit mit Dr. Apirat Chaikuad konnte die Co-Kristallstruktur der PPAR γ -LBD im Komplex mit **48** (PDB: 7AWD) gelöst werden, die eine strukturelle Erklärung für das ungewöhnliche Modulationsprofil des Liganden liefert. Um die Konformation des Proteins besser bewerten und vergleichen zu können, wurde der Komplex ohne einen Co-Regulator generiert und eine analoge Kristallstruktur des orthosterischen Agonisten Rosiglitazon (**3**, PDB: 7AWC) ebenfalls ohne Co-Regulator angefertigt. Der PPAR γ :**48** Komplex bestätigte, wie bereits das ITC-Experiment vermuten ließ, dass zwei Moleküle des Liganden gleichzeitig innerhalb der LBD gebunden sind (Abbildung 29a). Ein Molekül **48** (orange) bindet in der orthosterischen Bindestelle und geht mit der Säurefunktion die typischen Interaktionen wie **3** mit der kanonischen Aktivierungstetrade der LBD ein (Abbildung 29b), wodurch die AF2 der Helix 12 in der gleichen aktiven Konformation fixiert wird. Die allosterische Bindestelle des zweiten Moleküls **48** (rosa) wird zwischen Helix 3 und 4, dem β -Faltblatt-Bereich und dem Ω -Loop mit großer Lösemittelexposition ausgebildet, wobei der Ligand über mehrere Wasserstoffbrückenbindungen stabilisiert wird. Der Vergleich zum PPAR γ :**3** Kristall zeigte, dass durch eine Bewegung des Arg288 um 3,8 Å

zum einen die direkte Interaktion mit der Säurefunktion des allosterisch gebundenen **48** möglich wird und zum anderen das Chromanolmotiv des orthosterisch gebundenen **48** den hydrophoben Bereich nahe Helix 3 ausfüllen kann (Abbildung 29c). Im Gegensatz dazu ragt der lipophile Schwanz des orthosterischen Liganden **3** (gelb) in den Bereich der allosterischen Bindestelle. Die Ergebnisse einer Dockingstudie von **3** in der orthosterischen Bindestelle von **48** (PDB: 7AWD) deuten jedoch darauf hin, dass beide Liganden auch gleichzeitig die PPAR γ -LBD binden könnten, wodurch sich die kooperative Aktivität eines synthetischen Agonisten mit **48** im zellulären System erklären ließe.

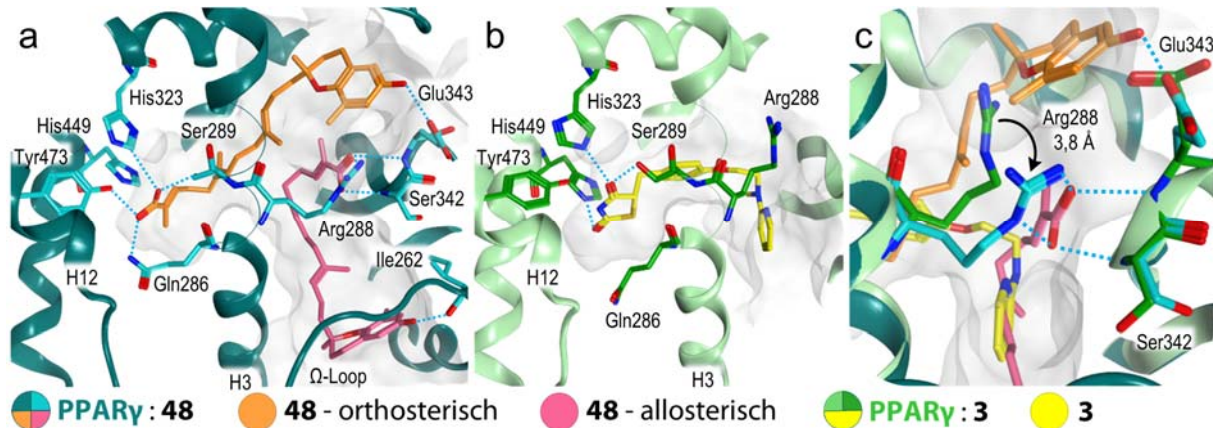


Abbildung 29: Co-Kristallstrukturen der PPAR γ -LBD im Komplex mit Garcinolsäure (**48**) und Rosiglitazon (**3**). (a) Der PPAR γ :**48** Komplex (PDB: 7AWD) zeigt die gleichzeitige Bindung von zwei Molekülen **48**: orthosterisch (orange) und allosterisch (rosa). (b) Der PPAR γ :**3** Komplex (PDB: 7AWC) weist eine ähnliche Anordnung der sauren Kopfgruppe von **3** (gelb) im Vergleich zu **48** (orange) innerhalb der orthosterischen Bindungsstelle auf. (c) Die Überlagerung der **48**- und **3**-gebundenen Komplexe zeigt eine Konformationsänderung des Arg288, das sich dreht, um mit dem Carbonsäurerest des allosterisch gebundenen **48** zu interagieren.

Um die Auswirkung der beachtlichen mechanistischen Unterschiede in der PPAR γ -Modulation durch **48** und **2** im zellulären Kontext zu studieren, wurde die Genexpression von humanen Hepatozyten (HepG2) 8 h nach der Behandlung mit einem der Agonisten, der Kombination beider und der gleichzeitigen Inkubation von **48** mit dem irreversiblen Antagonisten **13** untersucht (Abbildung 30). Dafür wurde die gesamte mRNA aus den Zellen extrahiert und mittels RNA-Sequencing (durch die Firma Novogene) analysiert. Bemerkenswert war dabei besonders der quantitative Unterschied signifikant regulierter Gene mit 5578 Genen bei **48** und 439 Genen bei **2** (Abbildung 30a,b). Mit 158 ähnlich in der Expression veränderten Genen beeinflusste **48** in etwa ein Drittel der von **2** regulierten Gene, wodurch PPAR γ als Target, aber auch eine differenzierte PPAR γ -Modulation durch beide Substanzen bestätigt wurde. So induzierte **2** selektiv nur Gene, die mit dem PPAR-Signalweg zusammenhängen und vor allem an Lipidspeicherung (PLINs), Gluconeogenese und Fettsäureoxidation beteiligt sind. **48** veränderte darüber hinaus auch die Expression von Fettsäuretransportern, induzierte Gene der Lipogenese, sowie den Wachstumsfaktor 3-Phosphoinositid-abhängige Proteinkinase 1 (PDPK1), welche ebenfalls mit PPAR-Aktivität assoziiert werden^{120,480,481}. Durch die gleichzeitige Inkubation mit **13** wurden insgesamt 51 % der signifikanten Effekte von **48** aufgehoben, wodurch die Regulation dieser 2817 Gene als PPAR γ -vermittelt angenommen werden kann (Abbildung 30b). Darunter befanden sich zusätzlich wichtige Gene des Insulin-Signalweges, des Glucose-Stoffwechsels und der oxidativen Phosphorylierung, welche nicht von **2** reguliert wurden und somit **48**-spezifische PPAR γ -Modulation darstellen. Die anderen 49 % der durch **48** regulierten Gene, die zusammen mit **13** noch signifikant waren, zeigten aber auch, dass weitere Targets und Signalwege an der Aktivität des Vitamin-E-Metaboliten beteiligt sind, obwohl auch spezifische Effekte durch die ausschließliche allosterische PPAR γ -Bindung von **48** trotz Anwesenheit des Antagonisten **13** denkbar wären²⁵⁶. Erstaunlich war, dass durch die gleichzeitige Inkubation der

Zellen mit **48** und **2** deutlich weniger Gene reguliert wurden als durch **48** allein (740 vs. 5578 Gene, Abbildung 30b), was für eine gegenseitige Beeinflussung der beiden Wirkungsweisen auf die PPAR γ -Modulation spricht. Auch eine Analyse der Anreicherung von Pfaden nach der Kyoto-Enzyklopädie der Gene und Genome (KEGG)^{482,483} veranschaulichte die großen Unterschiede zwischen den Genexpressionsprofilen durch **48** und **2** (Abbildung 30c). Dabei zeigte **2** nur eine selektive und hochsignifikante Induktion des PPAR-Signalwegs, während Auswirkungen auf den Kohlenhydrat- und Lipidmetabolismus gering waren. Im Gegensatz dazu beeinflusste **48** deutlich mehr KEGG-Pfade mit Bezug zu PPAR γ -Aktivität signifikant wie die Thermogenese, oxidative Phosphorylierung und den Insulin-Signalweg. Auch die signifikante Regulation von Genen, die mit neurodegenerativen Erkrankungen wie AD, PD oder Chorea Huntington in Verbindung gebracht werden, deutet auf ein therapeutisches Potenzial der allosterischen PPAR γ -Modulation hin. Allerdings war unter der Behandlung mit **48** allein der PPAR-Signalweg nicht signifikant angereichert, obwohl 27 zugehörige Gene reguliert wurden.

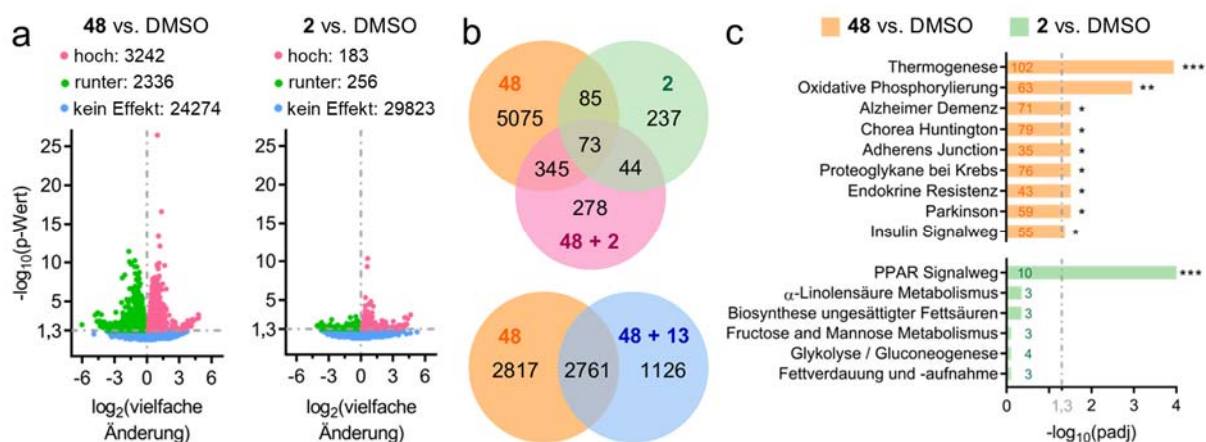


Abbildung 30: Einfluss von **48** auf die Genexpression in HepG2-Zellen. Die Zellen wurden mit **48** (10 μ M), **2** (1 μ M), **48** (10 μ M) + **2** (1 μ M), oder **48** (10 μ M) + **13** (10 μ M) behandelt; n = 4. (a) Gesamtverteilung der differenziell exprimierten Gene für **48** bzw. **2** vs. DMSO. Vulkan-Diagramme zeigen den \log_2 der vielfachen Änderung in den Genexpressionslevels (x-Achse) vs. statistische Signifikanz ($-\log_{10}$ (p-Wert); y-Achse). (b) Venn-Diagramme für die unterschiedlichen Genexpressionen (vs. DMSO). (c) Anreicherung von KEGG-Pfaden zeigt den Einfluss von **48** bzw. **2** auf verschiedene Signalwege. Gezeigt sind die statistischen Signifikanzniveaus ($-\log_{10}(\text{padj})$) der regulierten KEGG-Pfade. Die Zahlen beziehen sich auf die Anzahl der differenziell exprimierten Gene, die mit dem Pfad verbunden sind. * $p < 0,05$, ** $p < 0,01$, *** $p < 0,001$.

Insgesamt trägt die Entdeckung und Charakterisierung von **48** als einem natürlichen PPAR γ -Liganden²⁸⁷ zu einem umfassenderen Bild der komplexen Modulation des Rezeptors bei. So lieferte die Co-Kristallstruktur mit ihrer eindeutig aktiven Konformation ein strukturelles Fundament für die allosterische Bindung eines PPAR γ -Agonisten²⁵⁶ und bestätigte außerdem, dass ein allosterischer Ligand die Aktivität eines orthosterischen Agonisten steigern kann^{484,485}. Des Weiteren deuten die Ergebnisse darauf hin, dass die klassischen Co-Repressoren NCoR1 und SMRT die agonistische Aktivität von **48** an PPAR γ vermitteln. Daher sind mit dem additiven Effekt der allosterischen Bindung und dem ungewöhnlichen Einfluss auf die Co-Regulator-Rekrutierung zwei potenzielle neue Aktivierungsmechanismen von PPAR γ identifiziert, die das differenzierte Genexpressionsprofil von **48** erklären können. Obwohl bislang keine endogenen Gewebespiegel und pharmakokinetischen Untersuchungen zu **48** vorliegen, lässt die Detektion von **46** und **48** im Plasma^{472,486,487} sowie die Tatsache, dass der hepatische Stoffwechsel von Vitamin E eine hohe Verfügbarkeit der oxidativen Metabolite in der Leber bewirkt⁴⁸⁸, eine pharmakologische Relevanz der Erkenntnisse vermuten. Durch selektives Adressieren der allosterischen Bindestelle könnte der Einfluss auf das Co-Regulator-Netzwerk und die transkriptionellen Effekte gezielter untersucht werden, um mögliche therapeutische Anwendungen daraus abzuleiten.

3.3 Identifikation von nichtsteroidalen Antirheumatika als Nurr1-Modulatoren

Da sich validierte Nurr1-Liganden zu Beginn dieser Arbeit auf die synthetischen Agonisten AQ (**19**) und CQ (**25**) sowie die Fettsäure DHA (**26**) beschränkten^{346,389}, war die Veröffentlichung der ersten ligandengebundenen Nurr1-Co-Kristallstrukturen mit den Prostaglandinen A1⁴¹⁹ (**20**) und A2⁴²⁰ ein vielversprechender Anhaltspunkt für die Suche nach neuen Nurr1-Modulatoren. Als Entzündungsmediatoren mit vornehmlich antientzündlichen Effekten gehen PGA1 und PGA2 aus der Arachidonsäure und weiteren mehrfach ungesättigten Fettsäuren mittels Umwandlung durch die Cyclooxygenasen (COX) 1 oder 2 hervor^{489,490}. Basierend auf diesen Erkenntnissen sollten synthetische COX-Inhibitoren, auch bekannt als nichtsteroidale Antirheumatika (NSARs), auf ihre Nurr1-modulatorischen Aktivitäten untersucht werden.

Dazu wurde ein zelluläres Testsystem in humanen HEK293T-Zellen etabliert, welches analog zu den zuvor beschriebenen Gal4-Reporterassays ein Rezeptor-Konstrukt aus der humanen Nurr1-LBD fusioniert mit der Gal4-DBD der Hefe verwendet. Hierbei zeigte sich bereits die hohe konstitutive Aktivität des Rezeptors ohne weitere Aktivierung durch einen Agonisten im Vergleich zu den Gal4-basierten Testsystemen anderer NRs wie bspw. der PPARs. Um stabile Testergebnisse zu ermöglichen, wurden die transfizierten Plasmid-Mengen an Rezeptor- und *Firefly*-Konstrukt deutlich reduziert. Validiert wurde das Testsystem mit den publizierten Agonisten AQ (**19**) und CQ (**25**) und lieferte vergleichbare EC₅₀-Werte³⁸⁹ im mikromolaren Bereich mit $36 \pm 4 \mu\text{M}$ (**19**) und $47 \pm 5 \mu\text{M}$ (**25**) sowie einer Effizienz von 3,6 (**19**)- bzw. 2,0 (**25**)-facher Aktivierung. Die hohe konstitutive Aktivität des Rezeptors erklärt zum einen die moderate Aktivierungseffizienz der bekannten Agonisten, ermöglicht zum anderen aber auch eine bidirektionale Rezeptor-Modulation. Um unspezifische zelluläre Effekte sowohl auf die Luciferasen als auch auf die Transkription im Allgemeinen ausschließen zu können, wurde ein Kontrollexperiment entwickelt, das die Transkription ebenfalls ligandenunabhängig induziert und dafür ein Gal4-VP16-Konstrukt (ein Protein aus dem *Herpes-simplex-Virus*) anstelle des Rezeptor-Konstruktes im gleichen System verwendet^{491,492}. Zusätzlich sind für die verwandten Rezeptoren Nur77 und NOR-1 in gleicher Weise Testsysteme etabliert worden, die die gleichen Rezeptorplasmid-Mengen verwenden, um einen direkten Vergleich innerhalb der NR4A-Familie zu ermöglichen.

Mithilfe dieser Reporterassays wurden insgesamt 39 strukturell diverse NSARs, die alle Untergruppen dieser Arzneistoffklasse abdeckten, auf ihre Aktivität an den NR4A-Rezeptoren bei zwei Konzentrationen (10 & 30 μM) untersucht (Abbildung 31). Dieses erste Screening brachte sowohl aktivierende (> 1,5-fache Aktivierung) als auch inhibierende Substanzen (< 0,8 verbleibende Aktivität) hervor, was auf eine mögliche bidirektionale Modulation von Nurr1 hindeutete. Im Anschluss wurden die aktiven NSARs im VP16-Kontrollassay untersucht und bei validierter NR4A-vermittelter Aktivität umfassend charakterisiert. Von den vier agonistischen Kandidaten Meclofenaminsäure (**49**), Clonixin, Nabumeton und Tiaprofensäure konnte nur **49** als Agonist an allen drei NR4A-Subtypen im Gal4-Hybridsystem bestätigt werden (Abbildung 32), die anderen Substanzen zeigten unspezifische Aktivität an VP16. Bei den anfänglichen neun invers agonistischen Kandidaten war das Bild etwas differenzierter. Meloxicam (**50**), Oxaprozin (**51**) und Parecoxib (**52**) zeigten an allen drei Rezeptoren signifikante Inhibition, während Valdecoxib (**53**) lediglich Nurr1 inhibierte (Abbildung 32), Lornoxicam und Mofezolac hingegen die beiden verwandten Rezeptoren Nur77 und NOR-1. Die restlichen inhibierenden Effekte von **53**, Aceclofenac (**54**), Celecoxib und Lumiracoxib stellten sich als unspezifisch heraus und sind vermutlich zum Teil auf eine Inhibition der *Firefly*-Luciferase zurückzuführen. Nach näherer Untersuchung zeigte **54** jedoch eine schwache, aber signifikante Aktivierung von Nurr1 bei niedrigeren Konzentrationen

(Abbildung 32). Auch die Referenzsubstanzen **19** und **25** aktivierten die beiden verwandten NR4A-Subtypen Nur77 und NOR-1, im Falle von **19** sogar effizienter als Nurr1, was bisher nicht bekannt war.

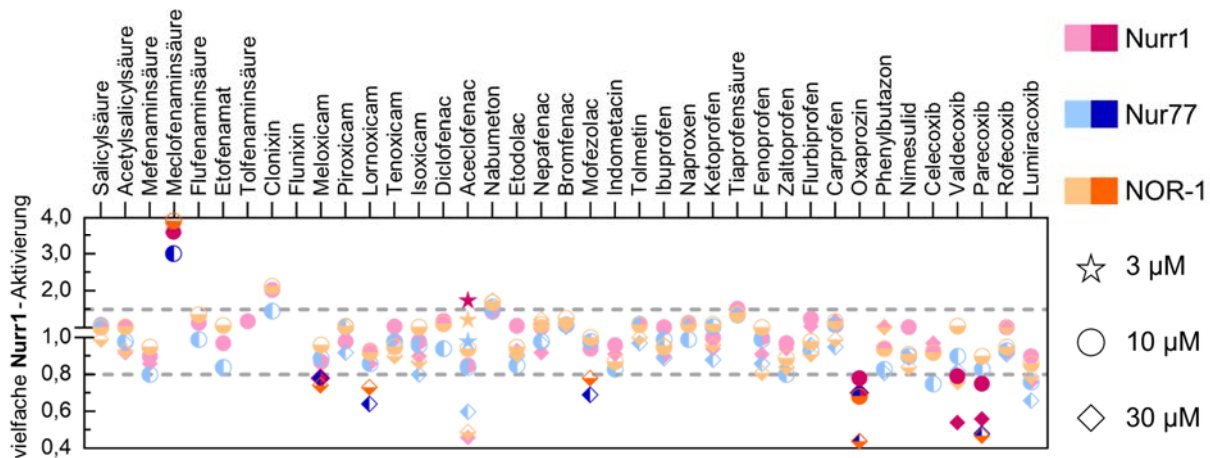


Abbildung 31: Screening von strukturell diversen NSARs auf ihre Aktivität an NR4A-Rezeptoren in einheitlichen Gal4-Hybrid-Reportergerneassays. Gezeigt sind die MW der vielfachen Aktivierung (vs. 0,1 % DMSO); $n \geq 2$. Agonisten $> 1,5$ -fache Aktivierung, inverse Agonisten $< 0,8$ -fache Aktivierung. Aktive Substanzen aus dem ersten Screening wurden nur weiter untersucht, wenn sich keine Aktivität im Gal4-VP16-Kontrollassay ($n \geq 4$) zeigte. Mit dunklen Farben markierte Aktivitäten zeigen validierte NR4A-vermittelte Effekte. Dargestellt sind nur Aktivitäten bei nicht-toxischen Konzentrationen (Kreis/Raute).

Zusammengenommen deutete dieses NSAR-Screening darauf hin, dass es eine große Herausforderung sein wird, neue Liganden für die NR4A-Rezeptoren zu entwickeln, die selektiv nur einen der drei Rezeptoren modulieren. Doch **53** und **54**, die ausschließlich die Nurr1-Aktivität modulierten, und Lornoxicam und Mofezolac, die trotz naher struktureller Verwandtschaft zu den pan-NR4A inversen Agonisten **50** und **51** nur zwei der drei Subtypen inhibierten, könnten auf eine Möglichkeit der Subtypenselektivität hinweisen. Außerhalb der NR4A-Familie zeigten die Liganden Selektivität über andere NRs, die dafür bekannt sind durch Fettsäuremimetika aktiviert zu werden wie die PPARs, RXR und RAR¹⁰. Nur der inverse Agonist **51** wies eine signifikante Aktivierung an RXR auf, die bereits vorher beschrieben wurde⁴⁹³. Als *tool compound* für weitere mechanistische Studien wurde zum einen der

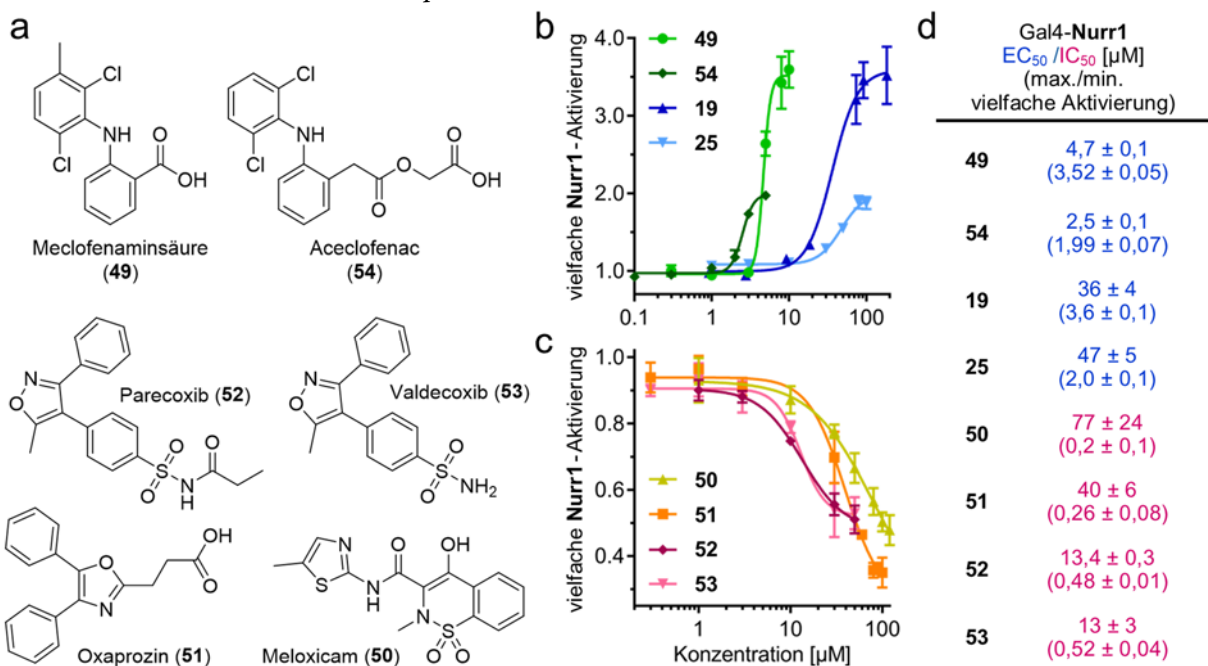


Abbildung 32: Bidirektionale Modulation von Nurr1 durch NSARs. (a) Chemische Strukturen der neuen Nurr1-Modulatoren. (b, c) Dosis-Wirkungskurven der validierten NSARs als Nurr1-Agonisten (b) und inverse Nurr1-Agonisten (c) im zellulären Gal4-Nurr1-Reportergerneassay und zugehörige Aktivitäten (d). **19** und **25** zum Vergleich. Alle Werte sind MW ± S.E.M., $n \geq 3$.

Agonist **49** aufgrund seiner hohen Aktivierungseffizienz für eine weitere Charakterisierung ausgewählt. Zum anderen dienten die inversen Agonisten **51** und **52** aufgrund ihrer strukturellen Diversität als Vertreter mit starker repressiver Effizienz (**51**) und höherer Potenz (**52**) für weitere Untersuchungen.

Um eine direkte Modulation der Nurr1-Aktivität durch Interaktion mit der LBD orthogonal zu bestätigen, wurde in Zusammenarbeit mit Dr. W. Kilu/Dr. J. Heering die Rekrutierung von Co-Regulatoren im zellfreien System untersucht. Bisherige Studien deuteten jedoch darauf hin, dass sich die Regulationsmechanismen von Nurr1 von denen anderer NRs deutlich unterscheiden (siehe Kapitel 1.4). Daher wurde zunächst ein Screening mit 29 verschiedenen Co-Regulator-Peptiden in einem TR-FRET-Testsystem durchgeführt (Abbildung 33), um einer-

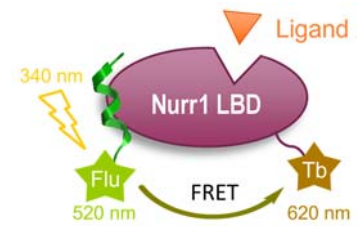


Abbildung 33: Schematische Darstellung des Nurr1-Co-Regulator-Rekrutierungsassays.

seits neue Co-Regulatoren zu identifizieren und andererseits den Einfluss von Liganden auf diese Interaktionen zu untersuchen. In Übereinstimmung mit früheren Studien wurde je ein Motiv der Co-Repressoren NCoR1 und SMRT in Abwesenheit von Liganden rekrutiert^{343,349}. Außerdem konnten NCoA6 und NRIP1 als neue Nurr1-Co-Regulatoren identifiziert werden. In diesem ersten Screening verdrängten **49** und **51** alle vier Peptide von der Nurr1-LBD, wohingegen der inverse Agonist **52**, und die Agonisten **19** und **25** die Interaktionen nur wenig beeinflussten. Die klassischen Co-Aktivatoren wie die SRCs, CBP, PGC-1 α und DRIP zeigten auch ligandenabhängig keine direkte Interaktion mit der Nurr1-LBD. Eine umfassende Evaluation der Dosis-Wirkungs-Beziehungen bestätigte, dass **49** und **51** alle vier Co-Regulator-Peptide effektiv verdrängten (Abbildung 34). **52** konnte dosisabhängig nur die Rekrutierung von NCoR1 und SMRT reduzieren, während NCoA6 und NRIP1 kaum verdrängt wurden. Die beiden Agonisten **19** und **25** erwiesen sich aufgrund ihrer photophysikalischen Eigenschaften⁴¹⁴ als ungeeignet für dieses Testsystem, da sie bei steigenden Konzentrationen die Donor-Fluoreszenz beeinträchtigten und dadurch die Ergebnisse verfälschten. Ein veränderter Aufbau des Systems zeigte jedoch exemplarisch für NCoR1, dass **19** und **25** die Rekrutierung des Co-Repressors verstärken. Um hierbei Quenching-Effekte zu minimieren, wurden die Liganden-Konzentrationen sowie die Menge an Tb³⁺-gekoppeltem Peptid konstant gehalten und die sGFP-gelabelte Nurr1-LBD in ihrer Konzentration variiert.

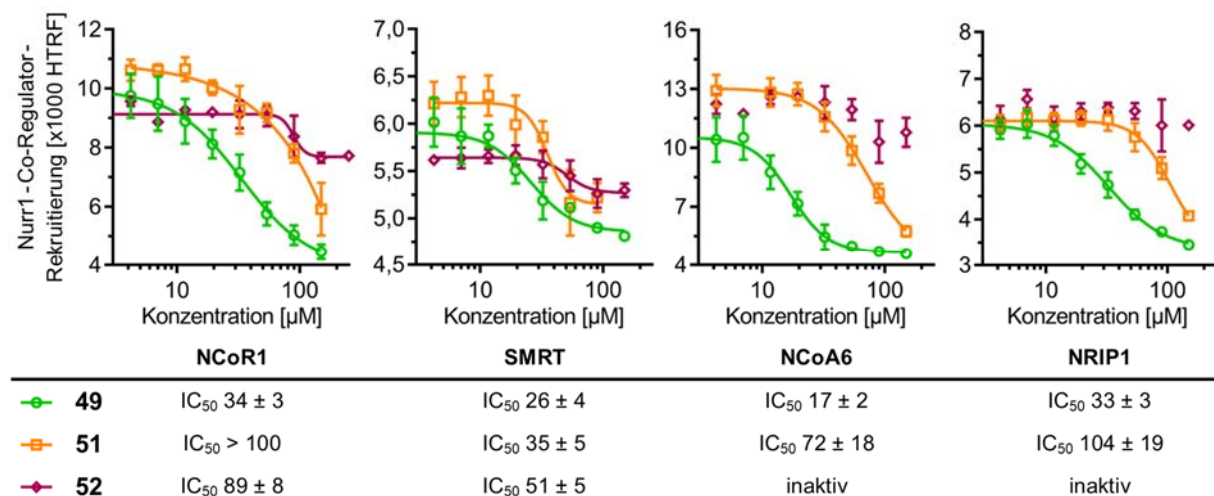


Abbildung 34: Dosis-Wirkungskurven der Nurr1-Modulatoren **49**, **51** und **52** zeigen die Verdrängung der Co-Regulatoren NCoR1, SMRT, NCoA6 und NRIP1 von der Nurr1-LBD. Die Interaktionen wurden in einem zellfreien TR-FRET-System mit Tb³⁺-gekoppelter Nurr1-LBD als FRET-Donor und Fluoreszeim-gelabelten Co-Regulator-Peptiden als FRET-Akzeptoren untersucht. Gezeigt sind die dimensionslosen HTRF-Signale und zugehörige IC₅₀-Werte [μ M]; MW \pm S.E.M.; N = 3.

Da alle drei untersuchten NSARs ein ähnliches Verhalten bei der Verdrängung der Co-Regulatoren von der Nurr1-LBD zeigten, **49** jedoch im Gal4-Reporterassay einen gegenteiligen Effekt aufwies, wurde im nächsten Schritt das Dimerisierungsverhalten des Rezeptors betrachtet. Dazu wurden weitere zelluläre (HEK293T) Reporterassays etabliert, die die physiologische Situation genauer wiedergeben, indem der Volllängenrezeptor Nurr1 überexprimiert wird und entsprechend den drei möglichen Dimerisierungs-Mechanismen (siehe Kapitel 1.4) jeweils ein *Firefly*-Reporter-Konstrukt unter Kontrolle der *Response*-Elemente für das Monomer (NBRE), das Nurr1-Homodimer (NurRE) oder das RXR-Nurr1-Heterodimer (DR5) mit einfacher Wiederholung verwendet wird (Klonierung der Konstrukte erfolgte durch Dr. Jan Heering). Für letzteres wurde außerdem der Volllängenrezeptor RXR α als Heterodimerpartner überexprimiert. Auch diese Systeme wurden mit den Agonisten **19** und **25** validiert, wobei **19** die Rezeptoraktivität stark induzierte (50–100-fach) und **25** deutlich geringere Effizienz (2–3-fach) aufwies. **51** und **52** zeigten an allen drei *Response*-Elementen deutlichen inversen Agonismus in guter Übereinstimmung mit den Ergebnissen aus dem Gal4-Assay, sodass dieser Wirkmechanismus bestätigt werden konnte (Tabelle 3). **49** hingegen war inaktiv am Nurr1-Monomer und reduzierte die Aktivität beider Dimere dosisabhängig, wodurch sich ein komplexes Profil der Nurr1-Modulation ergab.

Tabelle 3: Zusammengefasste Aktivitäten der NSARs in zellulären Nurr1-Reporterassays. **19** und **25** zum Vergleich. EC₅₀- und IC₅₀-Werte sind MW \pm S.E.M.; n \geq 3. Max./min. vielfache Aktivierung bezieht sich auf mit DMSO (0,1 %) behandelte Zellen.

Testsystem	EC ₅₀ / IC ₅₀ [μ M] (max./min. vielfache Aktivierung)				
	MFS (49)	Oxaprozoin (51)	Parecoxib (52)	AQ (19)	CQ (25)
Gal4-Nurr1	4,7 \pm 0,1 (3,52 \pm 0,05)	40 \pm 6 (0,26 \pm 0,08)	13,4 \pm 0,3 (0,48 \pm 0,01)	36 \pm 4 (3,6 \pm 0,1)	47 \pm 5 (2,0 \pm 0,1)
Nurr1-Monomer (NBRE)	inaktiv	12 \pm 2 (0,20 \pm 0,05)	15 \pm 3 (0,41 \pm 0,05)	92 \pm 1 (62 \pm 2)	38 \pm 7 (2,2 \pm 0,2)
Nurr1-Homodimer (NurRE)	5,2 \pm 0,1 (0,70 \pm 0,01)	17 \pm 3 (0,27 \pm 0,05)	21 \pm 6 (0,4 \pm 0,1)	87 \pm 2 (109 \pm 5)	54 \pm 7 (3,1 \pm 0,2)
Nurr1-RXRα-Heterodimer (DR5)	10,7 \pm 0,1 (0,79 \pm 0,01)	12 \pm 2 (0,27 \pm 0,05)	20 \pm 8 (0,5 \pm 0,1)	97 \pm 3 (59 \pm 4)	57 \pm 8 (2,6 \pm 0,2)

In Zusammenarbeit mit Dr. W. Kilo/Dr. J. Heering wurden auch zellfreie Experimente zur Dimerisierung des Rezeptors durchgeführt, die ein ähnliches Profil zeigten. Im TR-FRET-System wurde bei konstanten Konzentrationen an Tb³⁺-gekoppelter Nurr1-LBD entweder sGFP-Nurr1-LBD oder sGFP-RXR α hinzutitriert. In Abwesenheit eines Liganden zeigte Nurr1 stabile Dimerisierung in beiden Systemen, wobei die Affinität der Homodimerbildung etwa 600-mal höher war als die der Heterodimerisierung. Agonist **19** förderte nur die Nurr1-Homodimerisierung, während **25** die Bildung beider Dimere steigerte. Durch die NSARs wurde die Dimerbildung hingegen beeinträchtigt, wobei **49** die stärksten Effekte zeigte und die Homodimerisierung des Rezeptors vollständig unterdrückte (Abbildung 35a). Der Einfluss von **51** auf die Heterodimerisierung mit RXR α ist durch den gleichzeitigen inversen Agonismus an Nurr1 und den Agonismus an RXR jedoch schwierig zu bewerten. Der starke Einfluss von **49** auf die Dimerisierung auf Proteinebene konnte durch weitere zelluläre Experimente untermauert werden. Im Gal4-Nurr1-Assay bewirkte die Co-Transfektion von zunehmenden Mengen an Gal4-RXR α eine signifikante Reduktion der Reporteraktivierung, sogar in Gegenwart des RXR-Agonisten Bexaroten, wohingegen eine Veränderung der Gal4-Nurr1-Menge allein keinen signifikanten Effekt auf die Aktivität von **49** zeigte (Abbildung 35b). Zusammengefasst zeigten diese Analysen, dass das Dimerisierungsverhalten von Nurr1 eine entscheidende Rolle für seine ligandenabhängige Modulation spielt. Obwohl im Volllängenassay am Monomer (NBRE) für **49** keine Aktivität zu erkennen war, deuteten diese

mechanistischen Studien auf eine Monomerpräferenz des Liganden hin. Möglicherweise sind hier weitere, ggf. noch nicht identifizierte Co-Regulatoren und die spezifische zelluläre Ausstattung von Bedeutung, die die Diskrepanz zwischen den verschiedenen zellulären Systemen erklären. Allerdings erscheint durch gezielte Verschiebung der Dimer-Equilibria eine genselektive Nurr1-Modulation denkbar.

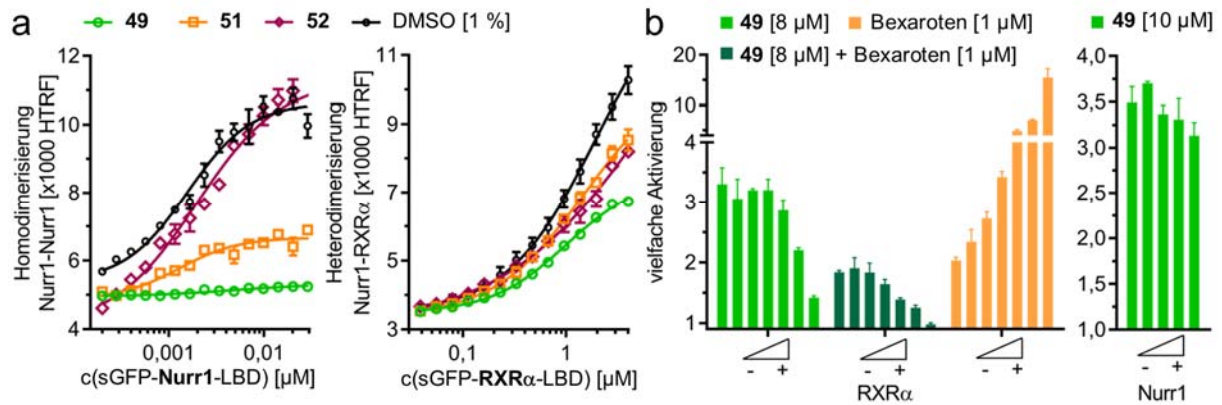


Abbildung 35: Einfluss der NSARs auf das Dimerisierungsverhalten von Nurr1. (a) Nurr1-Homodimerisierung und -Heterodimerisierung mit RXRα wurden im zellfreien TR-FRET-System in Abwesenheit von Liganden (DMSO) und in Gegenwart von NSARs (100 μM) untersucht. Gezeigt sind die MW ± S.E.M. der dimensionslosen HTRF-Signale, N = 3. (b) Co-Transfektion steigender Mengen (0,125–6 ng/well; 0 ng/well zum Vergleich) Gal4-RXRα im Gal4-Nurr1 (6 ng/well) -Reporterassay reduzierte die Aktivierungseffizienz von 49 (vs. DMSO) und 49 + Bexaroten (vs. Bexaroten). Veränderte Mengen (0,22–18 ng/well) an Gal4-Nurr1 beeinträchtigten die Aktivierungseffizienz von 49 nicht. Die Werte sind MW ± S.E.M.; n ≥ 3.

Die neuen ligandengebundenen Kristallstrukturen des Rezeptors^{347,390} im Vergleich zu den Studien der AQ-Bindestelle³⁸⁹ deuten darauf hin, dass es zwei potenzielle Bindestellen in der Nurr1-LBD gibt (siehe Kapitel 1.4.2). Daher wurden die neuen *tool compounds* auf eine mögliche gleichzeitige Modulation des Rezeptors zusammen mit dem bekannten Agonisten 19 untersucht. Im Gal4-Nurr1-Reporterassay wurde dafür bei konstanter aktiver Konzentration eines Liganden (> EC₉₀) der jeweils andere hinzutitriert. Für 49 und 19 zeigten sich in beiden Richtungen synergistische Effekte, die in Dosis-Wirkungskurven mit deutlich erhöhtem Plateau im Vergleich zur Inkubation mit nur einem der Liganden resultierten (Abbildung 36a,b). Der Kurvenverlauf wurde dabei fast ausschließlich auf der y-Achse nach oben verschoben, während sich die EC₅₀-Werte kaum veränderten. Auch das gleichzeitige Titrieren beider Substanzen im Verhältnis 1:10, entsprechend ihres etwa 10-fachen Unterschiedes in der Potenz, zeigte den additiven Effekt in der maximalen Aktivierung (Abbildung 36c). Auf allen drei *Response*-Elementen in den Nurr1-Vollängenassays konnten 49 und 52 außerdem die Effizienz des Agonisten 19 reduzieren, sodass das Plateau der Dosis-Wirkungs-Kurve von 19 deutlich niedriger lag und auch hohe Konzentrationen des Agonisten 19 die inversen Agonisten nicht verdrängen konnten.

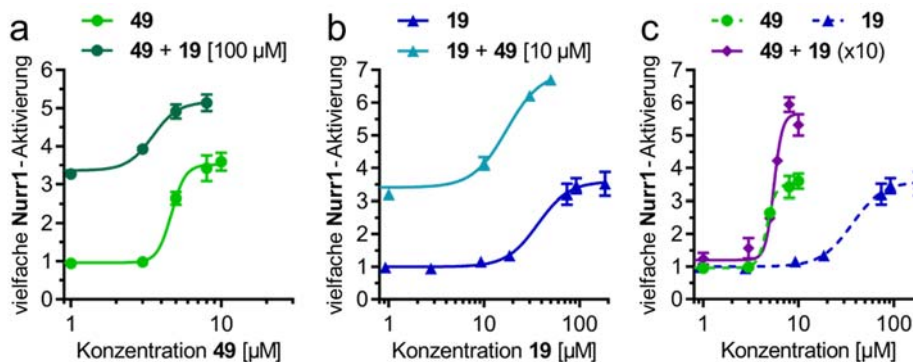


Abbildung 36: Gleichzeitige Modulation der Nurr1-Aktivität durch 49 und 19 im zellulären Gal4-Nurr1-Reporterassay deutete auf unterschiedliche Bindestelle hin, nicht auf Konkurrenz. Kreuztitrationskurven sowie gleichzeitige Titration im Verhältnis 1:10 (49:19). Die Daten sind MW ± S.E.M. der Reporteraktivierung vs. 0,1 % DMSO; n ≥ 3.

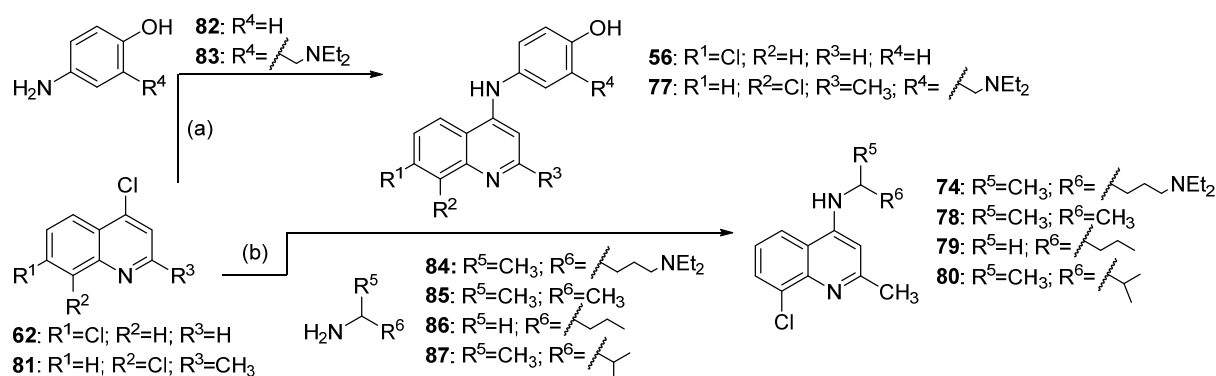
Insgesamt deuteten diese Ergebnisse also darauf hin, dass die NSARs und AQ (**19**) nicht um die gleiche Bindestelle konkurrieren und somit die These von zwei potenziellen Bindestellen innerhalb der Nurr1-LBD gestützt wird. Ob die NSARs allerdings die gleiche Bindetasche nahe Helix 12 adressieren wie die Prostaglandine, bleibt noch fraglich, würde aber das differenzierte Bild des inversen Agonismus durch einen direkten Einfluss auf die Position der Helix 12 unterstreichen. Mit den NSARs als den ersten inversen Nurr1-Agonisten konnte somit gezeigt werden, dass die hohe konstitutive Aktivität des Rezeptors bidirektional moduliert werden kann und Rekrutierung von Co-Regulatoren sowie auch Rezeptordimerisierung einen entscheidenden Einfluss auf die Interaktion mit Liganden haben.

3.4 Fragment-basierter Ansatz zur Entwicklung von Nurr1-Agonisten

Als zweiter Ansatz zur Entwicklung neuer Nurr1-Modulatoren wurde eine Fragment-basierte Strategie verfolgt, die auf den strukturellen Gemeinsamkeiten der bekannten Nurr1-Agonisten AQ (**19**), CQ (**25**) und Glafenin aufbaut³⁸⁹. Alle drei Substanzen teilen als gemeinsames Grundgerüst eine 7-Chloro-chinolin-4-amin-Struktur, die daher als vielversprechender und durch die Aktivität von **19** und **25** validierter Startpunkt für die Entwicklung neuer Nurr1-Agonisten erschien⁴⁰⁰. Dies ist insbesondere von Bedeutung, da **19** und **25** aufgrund unspezifischer Effekte nicht für eine verlässliche Anwendung zur Targetvalidierung *in vitro* und *in vivo* dienen können^{400,404–414}.

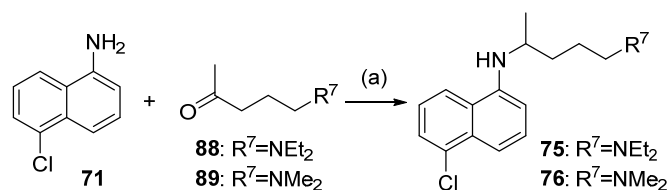
Für die Fragment-basierte Entwicklung neuer aus **19** und **25** abgeleiteter Nurr1-Agonisten diente wiederum der zelluläre Gal4-Nurr1-Reporterassay in HEK293T-Zellen als primäres Testsystem, um direkte Aussagen über die Art der Nurr1-Aktivierung neuer Liganden treffen zu können. Alle Aktivitäten wurden zusätzlich im Gal4-VP16-Kontrollexperiment validiert. Der dritte Nurr1-Agonist Glafenin aus der Originalpublikation³⁸⁹ konnte aufgrund von Toxizität nicht vollständig charakterisiert werden.

Die Chinolin-Derivate **56**, **74** und **77–80** wurden durch nukleophile aromatische Substitution des entsprechenden Dichlorochinolins **62** und **81** mit den jeweiligen Aminen **82–87** nach einer publizierten Synthese zu **56**⁴⁹⁴ mit geeigneten Änderungen erhalten (Schema 1).



Schema 1: Synthesen der Chinolin-Derivate **56**, **74** und **77–80**.

(a) KI, Ethanol, 2 N HCl, 90 °C, 14–20 h, 51–98 %; (b) Ethanol, Mikrowelle, 140 °C, 36–48 h, 4–54 %.



Schema 2: Synthesen der Naphthalin-Derivate **75** und **76**.

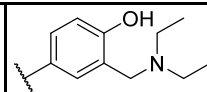
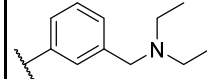
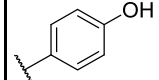
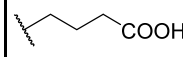
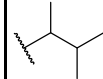
(a) Essigsäure, 1,2-Dichlorethan, Raumtemperatur, 30 min; dann NaB(OAc)₃H, 1,2-Dichlorethan, 50 °C, 24 h, 25–45 %.

Die Erweiterung des Naphthalin-Fragments **71** zu den CQ-Analoga **75** und **76** erfolgte durch reduktive Aminierung von **71** mit den entsprechenden Ketonen **88** und **89** (Schema 2). Die restlichen Derivate dieser Untersuchung waren kommerziell erhältlich.

Zunächst wurden die Strukturelemente von **19** einzeln hinsichtlich ihrer Aktivität an Nurr1 evaluiert (Tabelle 4). Ein Fehlen der phenolischen Hydroxylgruppe in **55** reduzierte die Potenz, während ein Entfernen der basischen Seitenkette in **56** zum kompletten Aktivitätsverlust führte. Das 7-Chlorochinolin-4-amin (**57**) als gemeinsames Grundgerüst dieser Substanzklasse hingegen war allein ausreichend, um den Rezeptor mit moderater Potenz im hohen mikromolaren Bereich zu aktivieren. Um das Optimierungspotenzial dieses Fragmentes abzustecken, wurden vier weitere Substitutionen der Seitenkette getestet. Der Austausch zur Buttersäure (**58**) führte zur Aktivitätsumkehr und brachte einen inversen Agonisten mit moderater Potenz hervor.

Tabelle 4: SAR der Seitenkette im AQ/CQ-Chemotyp. **19** zum Vergleich.

Die Aktivität wurde im Gal4-Nurr1-Reporterassay bestimmt. EC_{50}/IC_{50} -Werte sind $MW \pm S.E.M.$; $n \geq 3$. Max./min. vielfache Aktivierung bezieht sich auf 0,1% DMSO. ^a Inaktiv: kein signifikanter Effekt der Reporteraktivität (verglichen mit Gal4-VP16 bei der angegebenen höchsten nicht-toxischen Konzentration).

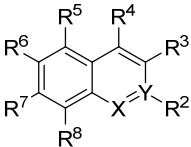
ID	R ¹	Art der Aktivierung	EC_{50}/IC_{50} [μ M] (max./min. vielfache Aktivierung)
19		Agonist	36 ± 4 ($3,6 \pm 0,1$)
55		Agonist	116 ± 4 ($3,1 \pm 0,2$)
56		inaktiv (30μ M) ^a	
57	-H	Agonist	259 ± 70 ($2,5 \pm 0,4$)
58		Inverser Agonist	132 ± 1 ($0,59 \pm 0,00$)
59		Agonist	$1,8 \pm 0,3$ ($1,47 \pm 0,03$)

Die lipophile Isopentyl-Seitenkette (**59**) ergab einen Agonisten mit beachtlicher Potenz ($EC_{50} = 1,8 \mu$ M), jedoch geringer Aktivierungseffizienz. Größere lipophile Gruppen wie ein 4-Methylcyclohexyl-Rest und ein Benzyl-Rest zeigten hingegen keine Aktivität an Nurr1. Diese erste grobe Evaluation der Struktur-Wirkungs-Beziehung (SAR) des Chemotyps zeigte, dass die Modifikation der Seitenkette einen erheblichen Einfluss auf die Aktivität an Nurr1 hat, ließ aber noch keine klare Präferenz für bestimmte Motive erkennen, da zum einen die basische Seitenkette essenziell erschien, aber mit einer lipophilen Erweiterung des Grundgerüsts ebenfalls eine Nurr1-Aktivierung erreicht wurde. Dass das Chinolingrundgerüst (**57**) jedoch für eine Aktivierung des Rezeptors ausreichend ist und für die Aktivität der Agonisten **19** und **25** hauptverantwortlich zu sein scheint, motivierte zur Optimierung dieser Teilstruktur in einem Fragment-basierten Ansatz.

Dazu wurde als Erstes der Einfluss des Substitutionsmusters am Chinolingerüst untersucht (Tabelle 5). Das Fehlen der 4-Amino-Funktion in **60** führte abermals zu einer Umkehr der Aktivität und brachte mit einer verbleibenden Rezeptoraktivität von 29 % einen effizienten inversen Agonisten hervor. Durch die fehlende 7-Chlor-Substitution in **61** ging die Nurr1-Modulation dagegen vollständig verloren. Auch ein Austausch der Aminofunktion in 4-Position durch ein Chloratom (**62**) führte zu einem inaktiven Fragment, was zusätzlich die Relevanz beider Substituenten unterstrich. Eine systematische Variation des Substitutionsmusters zeigte, dass beim Verschieben der Amino-Funktion nur die 5-Position (**65**) toleriert wurde und eine erhebliche 14-fache Steigerung der Potenz bewirkte. Auch das Verschieben der Chlor-Substitution in 6 (**66**)- oder 8 (**67**)-Position steigerte die Potenz im Vergleich zum Ausgangsfragment **57**. Die Kombination der bevorzugten Modifikationen in **68** und **69** wurde jedoch nicht toleriert und das Chloratom in **67** schien eine besonders wichtige Rolle zu spielen, da der Austausch zur sperrigen Trifluormethyl-Gruppe sowie zum kleineren Fluoratom nicht toleriert wurde. Das zusätzliche Einführen einer Methylgruppe in 2-Position (**70**) brachte eine 8-fache Steigerung der Potenz im Vergleich zum Ausgangsfragment **57**. Außerdem bewirkte die Modifikation des Grundgerüsts zum Naphthalin (**71**)

mit gleichem Substitutionsmuster wie **67** nochmals eine deutliche Verbesserung der Aktivität an Nurr1 sowohl in Bezug auf Potenz als auch Aktivierungseffizienz, sodass ein agonistisches Fragment mit beachtlicher Aktivität im unteren mikromolaren Bereich erhalten wurde. Ein Isochinolin-Grundgerüst mit gleichem Substitutionsmuster (**72**) zeigte dagegen keine Nurr1-modulatorische Aktivität mehr. Als letzter Optimierungsschritt wurden die bevorzugten Substituenten des Chinolin-Fragmentes aus **67** und **70** in einem Molekül (**73**) vereint, was nochmals eine Steigerung der Potenz hervorbrachte, während die Aktivierungseffizienz etwas reduziert wurde. Diese systematische Analyse der SAR des gemeinsamen Strukturmotivs bekannter Nurr1-Liganden zeigte großes Potenzial zur Optimierung des Fragmentes durch kleine Änderungen im Substitutionsmuster und brachte mit **71** und **73** zwei Analoga hervor, die sogar die wesentlich größeren Ausgangssubstanzen **19** und **25** in ihrer Aktivität übertreffen.

Tabelle 5: SAR der Substituenten am Chlorochinolinamin-Grundgerüst und Optimierung der Nurr1-Aktivität. **57** zum Vergleich.



Die Aktivität wurde im Gal4-Nurr1-Reporterassay bestimmt. EC₅₀/IC₅₀-Werte sind MW ± S.E.M.; n ≥ 3. Max./min. vielfache Aktivierung bezieht sich auf mit DMSO (0,1 %) behandelte Zellen. ^a Inaktiv: kein signifikanter Effekt der Reporteraktivität (≥ 1,5-fache Akt. oder verglichen mit Gal4-VP16 bei der angegebenen höchsten nicht-toxischen Konzentration).

ID	R ²	R ³	R ⁴	R ⁵	R ⁶	R ⁷	R ⁸	X	Y	Art der Aktivierung	EC ₅₀ /IC ₅₀ [µM]
											(max./min. vielfache Aktivierung)
57	H	H	NH ₂	H	H	Cl	H	N	C	Agonist	259 ± 70 (2,5 ± 0,4)
60	H	H	H	H	H	Cl	H	N	C	Inverser Agonist	89 ± 14 (0,29 ± 0,08)
61	H	H	NH ₂	H	H	H	H	N	C		inaktiv (300 µM) ^a
62	H	H	Cl	H	H	Cl	H	N	C		inaktiv (300 µM) ^a
63	NH ₂	H	H	H	H	Cl	H	N	C		inaktiv (100 µM) ^a
64	H	NH ₂	H	H	H	Cl	H	N	C		inaktiv (300 µM) ^a
65	H	H	H	NH ₂	H	Cl	H	N	C	Agonist	19 ± 4 (3,4 ± 0,3)
66	H	H	NH ₂	H	Cl	H	H	N	C	Agonist	117 ± 24 (2,8 ± 0,3)
67	H	H	NH ₂	H	H	H	Cl	N	C	Agonist	49 ± 5 (2,6 ± 0,1)
68	H	H	H	NH ₂	Cl	H	H	N	C		inaktiv (100 µM) ^a
69	H	H	H	NH ₂	H	H	Cl	N	C		inaktiv (100 µM) ^a
70	CH ₃	H	NH ₂	H	H	Cl	H	N	C	Agonist	33 ± 5 (2,3 ± 0,2)
71	H	H	NH ₂	H	H	H	Cl	C	C	Agonist	7,3 ± 0,5 (5,3 ± 0,2)
72	H	H	NH ₂	H	H	H	Cl	C	N		inaktiv (200 µM) ^a
73	CH ₃	H	NH ₂	H	H	H	Cl	N	C	Agonist	17 ± 6 (1,71 ± 0,11)

Die optimierten Fragmente boten sich für eine Rekombination mit den Seitenketten der Leitstrukturen **19** und **25** an, um dadurch möglicherweise weiter optimierte Nurr1-Agonisten zu erhalten. Jedoch war die aliphatische CQ-Seitenkette an beiden Fragmenten (**74** und **75**) nicht in der Lage die Nurr1-Aktivität zu erhalten. Auch ein Verkürzen der CQ-Seitenkette zum Dimethyl-Analog **76**, um sterische Probleme auszuschließen, war nicht zielführend. Da bei beiden Naphthalin-Derivaten (**75** und **76**) Toxizität die vollständige Charakterisierung verhinderte, wurde die Kombination mit der aromatischen Seitenkette von AQ nur für das Chinolin-Fragment in **77** untersucht. Jedoch zeigte auch diese Verbindung keine Aktivität an Nurr1. Inspiriert von **59** wurden zusätzlich noch verschiedene kleine lipophile Reste als Erweiterung des Chinolin-Fragmentes **73** getestet. Mit diesen Derivaten (**78–80**) konnte die Aktivität am Rezeptor wieder zurückerlangt werden, doch eine weitere Steigerung der Potenz wurde nicht erreicht, sodass sich die Rekombination der optimierten Fragmente mit bekannten Strukturmotiven für die Seitenkette nicht als additiv erwies.

Somit gingen aus Fragment-basierten SAR-Untersuchungen die Fragmente **71** und **73** als vielversprechendste und potenteste Nurr1 Agonisten hervor, die anschließend hinsichtlich ihrer Aktivität und ihres Wirkmechanismus näher charakterisiert wurden. In Kooperation mit Dr. W. Kilu/Dr. J. Heering wurde im zellfreien System der Einfluss der beiden Liganden auf die Co-Regulator-Rekrutierung und Homodimerisierung der Nurr1-LBD untersucht. Da bereits die Leitstrukturen **19** und **25** durch ihre photo-physikalischen Eigenschaften im TR-FRET-System problematisch zu beurteilen waren (siehe Kapitel 3.3), wurde hier das Setting gewählt, bei dem die Konzentration des Liganden und des Tb³⁺-gekoppelten Peptids als FRET-Donor konstant bleibt, während die sGFP-gelabelte Nurr1-LBD als FRET-Akzeptor titriert wird. So wurde die Rekrutierung der beiden Co-Repressoren NCoR1 und SMRT durch die Anwesenheit der Fragmente **71** und **73** deutlich gefördert und die Bildung des Nurr1-Homodimers gesteigert (Abbildung 37), was den agonistischen Charakter dieser Liganden im Vergleich zu den NSARs als inversen Agonisten bestätigte.

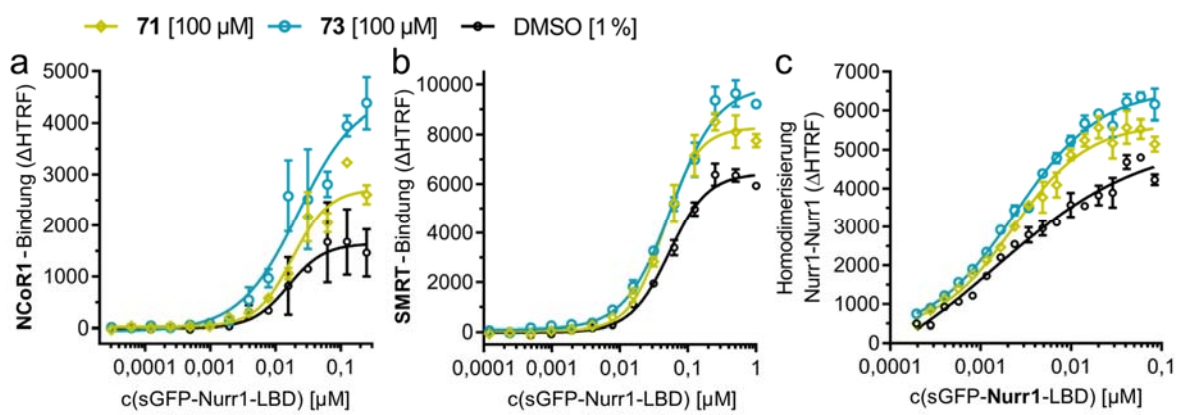


Abbildung 37: Effekte der Fragmente **71** und **73** im zellfreien TR-FRET-System. (a, b) Rekrutierung der Tb³⁺-gekoppelten Co-Repressoren NCoR1 (a) und SMRT (b) zur sGFP-gelabelten Nurr1-LBD. (c) Homodimerisierung der Tb³⁺- und sGFP-gelabelten Nurr1-LBD. Gezeigt sind die dimensionslosen Δ HTRF-Werte in Bezug auf die interne DMSO (1 %) Kontrolle; MW \pm SD; N = 3.

Darüber hinaus aktivierten beide Fragmente den Volllängenrezeptor Nurr1 im weniger artifiziellen Testsystem in HEK293T-Zellen an allen drei nativen *Response*-Elementen (NBRE, NurRE und DR5) für das Nurr1-Monomer, -Homodimer und -RXR-Heterodimer (Abbildung 38a). Dabei waren die Aktivitäten in guter Übereinstimmung mit den Daten aus dem Gal4-Nurr1-Reportergenassay und zeigten höhere Potenzen für **71** im unteren mikromolaren Bereich, während **73** insgesamt höhere Effizienzen aufwies. Vor allem das Homodimer-*Response*-Element NurRE wurde von beiden Fragmenten mit der höchsten Effizienz aktiviert, was die Beobachtungen zur Homodimerisierung im zellfreien System widerspiegelt. Auch in einem orthogonalen nativen zellulären System konnten die neuen agonistischen Tools überzeugen. Dafür wurden humane Astrozyten der T98G-Zelllinie mit den Fragmenten **71** und **73** für 8 h behandelt. Anschließend wurde die mRNA der Zellen extrahiert, in cDNA transkribiert und mittels quantitativer Echtzeit-Polymerase-Kettenreaktion (*quantitative real time polymerase chain reaction*, qRT-PCR) die Expression der Nurr1-abhängigen Gene VMAT2 und TH bestimmt. **71** und **73** zeigten dabei dosisabhängig eine starke Induktion der dopaminergen Gene (Abbildung 38b), was das Nurr1-agonistische Profil der Fragmente nochmals unterstrich.

Insgesamt haben die neuen Nurr1 Agonisten **71** und **73** gegenüber den Leitstrukturen AQ (**19**) und CQ (**25**) an Potenz gewonnen und überzeugen vor allem durch ihren Fragment-Charakter mit geringerem Molekulargewicht und niedriger Lipophilie. Auch nachteilige zelluläre Effekte auf die Transkriptionsaktivität konnten mit **73** reduziert werden, während **71** gegenteilige (potenziell zytotoxische) Effekte auf das Kontrollgen bewirkte, wodurch die effektive Aktivierungseffizienz dieses Liganden vermutlich etwas

geringer ist. Beide Fragmente zeigten ein gutes Profil als neue agonistische Tools für Nurr1 und können gleichzeitig als attraktiver Startpunkt für die Entwicklung neuer Nurr1 Liganden dienen.

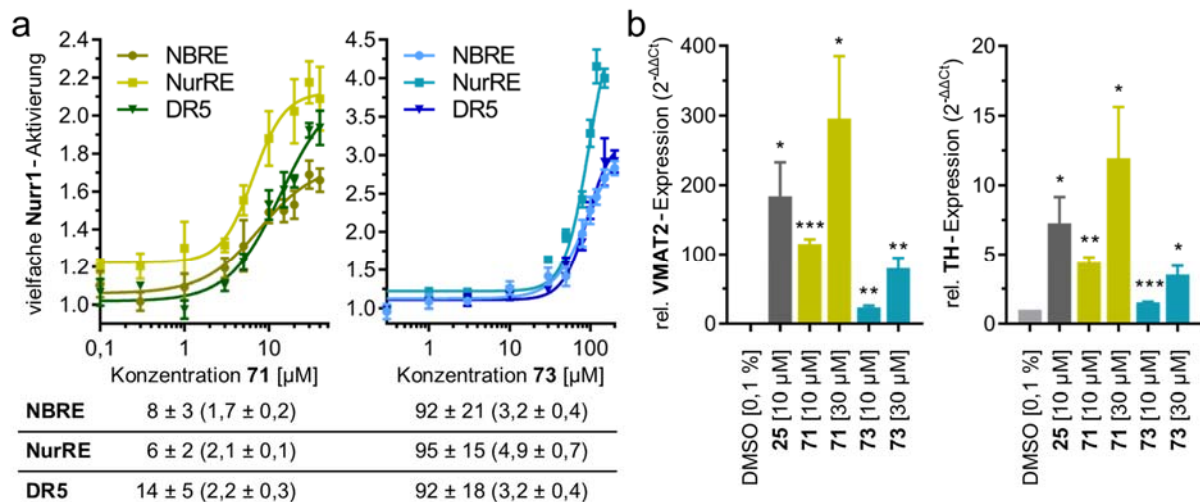


Abbildung 38: Nurr1-Agonismus von 71 und 73 in zellulären Settings. (a) Aktivität am Vollängenrezeptor Nurr1 als Monomer (NBRE), Homodimer (NurRE), und RXR-Heterodimer (DR5). Zugehörige EC_{50} -Werte [µM] und maximale vielfache Aktivierungen (vs. 0,1 % DMSO) sind in der Tabelle unterhalb dargestellt. Alle Werte sind $MW \pm S.E.M.$, $n \geq 3$. (b) Effekte auf die mRNA-Expression der Nurr1-abhängigen Gene VMAT2 und TH in T98G-Zellen. 25 zum Vergleich. Die gezeigten Werte sind $MW \pm S.E.M.$; $n = 4$. mRNA-Level wurden über qRT-PCR bestimmt und durch die $2^{-\Delta\Delta C_t}$ -Methode in Bezug auf das Referenzgen GAPDH und unbehandelte Zellen (0,1 % DMSO) analysiert. * $p < 0,05$, ** $p < 0,01$, *** $p < 0,001$ vs. 0,1 % DMSO (t-Test).

3.5 In vitro Screening als Ausgangspunkt für neue Nurr1-Liganden

Als dritter Ansatz zur Identifikation und Entwicklung neuer Nurr1-Liganden wurde ein breit angelegtes Screening einer Fragment-Bibliothek im zellulären Gal4-Nurr1-Reporterassay durchgeführt. Die Kollektion der 480 getesteten Fragmente bestand dabei aus bekannten Strukturmotiven von zugelassenen Arzneistoffen und stammte von Prestwick. Eine computergestützte Analyse der Fragment-Strukturen im Vergleich zur Drugbank⁴⁹⁵, welche Arzneistoffe in Zulassung und klinischer Forschung enthält, zeigte, dass die Fragmente, trotz der geringen Molekulargewichte im Bereich von 80 bis 300 g/mol, die große chemische Diversität der Drugbank in Bezug auf die Anzahl an Ringsystemen, Wasserstoffbrücken-Donor- und -Akzeptor-Funktionen sowie Lipophilie und polarer Oberfläche gut abbilden konnten. Die hohe strukturelle Vielfalt konnte zusätzlich durch eine Analyse der zugrunde liegenden *Murcko Scaffolds*⁴⁹⁶ belegt werden (Abbildung 39a). Aufgrund des Fragment-Charakters der getesteten Substanzen wurden die Fragmente bei einer Konzentration von 100 µM auf ihre Nurr1-modulatorische Aktivität in Ein-Punkt-Messungen mit zwei biologischen Replikaten im Gal4-Nurr1-Reporterassay getestet (Abbildung 39b). 24 Fragmente mit einer Reporter-Aktivierung von $\geq 1,50$ oder -Repression auf $\leq 0,60$ der Aktivität wurden als primäre Treffer bewertet und weiter auf ihre Nurr1-modulatorische Aktivität überprüft. Dabei stellten sich die Effekte von 17 Substanzen als unspezifisch oder toxisitätsbedingt heraus und sieben Substanzen (90-96), welche kein gemeinsames bevorzugtes Grundgerüst aufwiesen, konnten als Nurr1-Modulatoren im Gal4-Testsystem validiert werden (Abbildung 39c). Dazu diente der Vergleich mit der Aktivität im Gal4-VP16-Kontrollsystem als Entscheidungskriterium für signifikante Nurr1-vermittelte Effekte auf die Reporteraktivität. Um die verwandten Arzneistoffe zu identifizieren, von denen die jeweiligen Fragmente abgeleitet waren, wurde eine computergestützte Struktursuche in KNIME innerhalb der Drugbank⁴⁹⁵ durchgeführt. Nur Fluvastatin (97) und die Antibiotika Sulfadoxin sowie Sulfadimethoxin der zugrunde liegenden Fragmente 91 und 96 zeigten ebenfalls Aktivität an Nurr1. Aus diesem Screening sind zwei Projekte hervorgegangen, die im Folgenden

vorgestellt werden. Zum einen wurde der inverse Nurr1-Agonismus von Fragment **95** näher analysiert und optimiert (Kapitel 3.5.1), zum anderen die Arzneistoffklasse der Statine als neue Nurr1-Agonisten identifiziert und die mögliche klinische Relevanz dieser Aktivität untersucht (Kapitel 3.5.2).

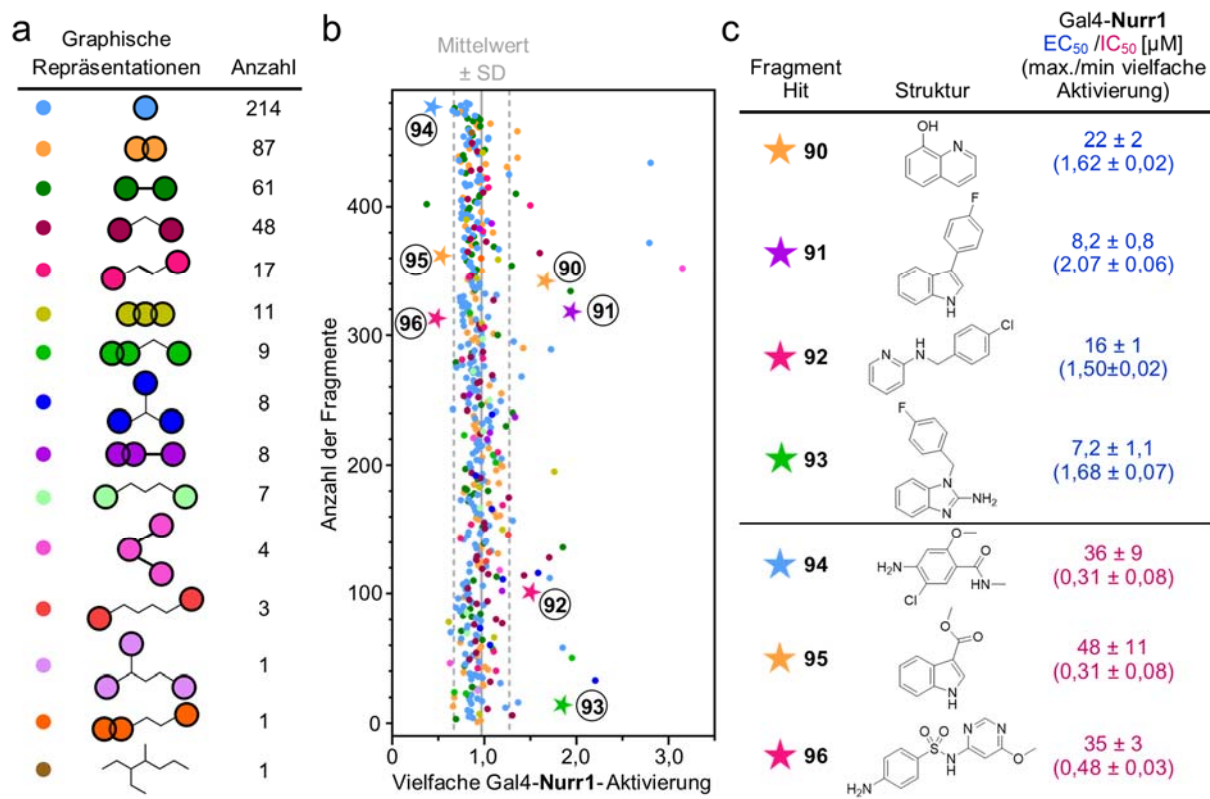


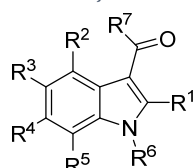
Abbildung 39: Arzneistoff-Fragment-Screening zur Identifikation neuer Nurr1-Modulatoren. (a) Graphische Repräsentationen der Strukturen in der untersuchten Bibliothek nach Murcko Scaffolds⁴⁹⁶ und deren Häufigkeiten. (b) Primäre Screening-Ergebnisse zeigen die Aktivität der Fragmente bei 100 µM in einem zellulären Gal4-Nurr1-Reporterassay. Gezeigt sind die MW der Reporteraktivität vs. 0,4 % DMSO; n = 2. Die Farben korrelieren mit dem strukturellen Aufbau der Fragmente in (a). Sterne markieren Fragmente, die im Gal4-VP16-Kontrollexperiment validiert werden konnten. Die grauen Linien zeigen MW ± SD des gesamten Screenings an. (c) Zugehörige Aktivitäten der validierten Fragmente. Die gezeigten Werte sind MW ± S.E.M.; n ≥ 3.

3.5.1 Inverse Nurr1-Agonisten mit Indol-Grundgerüst

Da die 5-HT₃-Rezeptor-Antagonisten Dolasetron und Ondansetron als Arzneistoff-Analoga des Screeninghits Indol-3-carbonsäure-methylester (**95**) keine Aktivität an Nurr1 zeigten, bot sich das Indol-Derivat als günstiger Startpunkt für eine klassisch systematische Analyse der SAR des inversen Agonismus an Nurr1 an. Durch die geringe Größe des Fragments bestanden optimale Voraussetzungen zur strukturellen Erweiterung des Grundgerüsts. Dieses Projekt wurde in Zusammenarbeit mit Daniel Zaienne durchgeführt, der maßgeblich für die Synthesen verantwortlich war, welche daher nicht Gegenstand dieses Kapitels sind (siehe Kapitel 16.6). Im ersten Schritt wurden die freien Positionen des stickstoffhaltigen Zweiringsystems in **95** systematisch durch Substitution mit je entweder einer Methylgruppe oder einem Chloratom untersucht, um die günstigsten Positionen zur Erweiterung des Grundgerüsts zu identifizieren (Tabelle 6). Beide Erweiterungen wurden in 2-Position (**98** und **99**) toleriert, zeigten jedoch nur wenig Änderung der Aktivität. In 4-Position führte die Methyl-Gruppe (**100**) zu einem kompletten Verlust der Nurr1-repressiven Aktivität, während auch die Einführung des Chlorsubstituenten (**101**) nicht begünstigt war und die Repressions-Effizienz stark reduzierte. Die Einführung von Substituenten in 5-Position (**102** und **103**) führte hingegen zu einer zweifachen Verbesserung der Potenz im Vergleich zum Ausgangsfragment **95**, wobei der Chlorsubstituent in **103** zusätzlich auch die

Repressions-Effizienz steigern konnte. In 6-Position wurden beide Substituenten (**104** und **105**) toleriert, wobei für den Chlorsubstituenten (**105**) eine Potenzsteigerung, aber auch ein Verlust an Repressions-Effizienz zu verzeichnen war. Die 7-Position tolerierte ebenfalls die Einführung einer Methylgruppe (**106**) und bevorzugte ein Chloratom (**107**), wodurch die Potenz zweifach gesteigert und die gute Repressions-Effizienz der Leitstruktur erhalten werden konnte. Somit erschienen die 5- und 7-Position als die Vielversprechendsten zur Erweiterung des Indolgerüsts und wurden durch Einführung einer Methoxy-Funktion in beiden Positionen weiter untersucht (Tabelle 6). Während die Methoxy-Gruppe in 5-Position (**108**) eine vergleichbare Aktivität wie das Chlor-Derivat **103** zeigte, wurde die Methoxy-Erweiterung in 7-Position (**109**) nicht toleriert und die Aktivität am Rezeptor gänzlich verloren.

Tabelle 6: Systematische Untersuchung von Substitutionen am Indol-Grundgerüst. Leitstruktur **95** zum Vergleich.



Die Aktivität wurde im Gal4-Nurr1-Reporterassay bestimmt. EC_{50}/IC_{50} -Werte sind $MW \pm S.E.M.$; $n \geq 3$. Maximale/minimale verbleibende Aktivierung bezieht sich auf mit DMSO (0,1 %) behandelte Zellen. ^a Inaktiv: kein signifikanter Effekt auf die Reporteraktivität ($\leq 0,8$ -fache Akt. bei der angegebenen höchsten nicht-toxischen Konzentration). Ph = Phenylrest, Bn = Benzylrest, tBu = tertiär Butylrest.

ID	R ¹	R ²	R ³	R ⁴	R ⁵	R ⁶	R ⁷	EC_{50}/IC_{50} [μ M] (max./min. vielfache Aktivierung)
★ 95	H	H	H	H	H	H	OCH ₃	48 ± 11 (0,31 ± 0,08)
98	CH ₃	H	H	H	H	H	OCH ₃	53 ± 20 (0,29 ± 0,18)
99	Cl	H	H	H	H	H	OCH ₃	34 ± 10 (0,39 ± 0,09)
100	H	CH ₃	H	H	H	H	OCH ₃	inaktiv (100 μ M) ^a
101	H	Cl	H	H	H	H	OCH ₃	55 ± 7 (0,72 ± 0,03)
102	H	H	CH ₃	H	H	H	OCH ₃	20 ± 4 (0,61 ± 0,03)
103	H	H	Cl	H	H	H	OCH ₃	24 ± 5 (0,18 ± 0,06)
104	H	H	H	CH ₃	H	H	OCH ₃	57 ± 7 (0,49 ± 0,05)
105	H	H	H	Cl	H	H	OCH ₃	8,9 ± 0,1 (0,73 ± 0,01)
106	H	H	H	H	CH ₃	H	OCH ₃	35 ± 6 (0,46 ± 0,07)
107	H	H	H	H	Cl	H	OCH ₃	19 ± 9 (0,30 ± 0,15)
108	H	H	OCH ₃	H	H	H	OCH ₃	23 ± 3 (0,28 ± 0,04)
109	H	H	H	H	OCH ₃	H	OCH ₃	inaktiv (100 μ M) ^a
110	H	H	Br	H	H	H	OCH ₃	15 ± 3 (0,16 ± 0,07)
111	H	H	Ph	H	H	H	OCH ₃	2,5 ± 0,5 (0,56 ± 0,02)
112	H	H	Bn	H	H	H	OCH ₃	inaktiv (150 μ M) ^a
113	H	H	H	H	H	CH ₃	OCH ₃	21 ± 2 (0,31 ± 0,04)
114	H	H	H	H	H	CH ₂ CH ₃	OCH ₃	31 ± 2 (0,73 ± 0,02)
115	H	H	H	H	H	Ph	OCH ₃	81 ± 3 (1,90 ± 0,08)
116	H	H	H	H	H	Bn	OCH ₃	inaktiv (30 μ M) ^a
117	H	H	H	H	H	H	OCH ₂ CH ₃	inaktiv (30 μ M) ^a
118	H	H	H	H	H	H	OtBu	inaktiv (30 μ M) ^a
119	H	H	H	H	H	H	OPh	11 ± 1 (1,93 ± 0,02)
120	H	H	Ph	H	H	CH ₃	OCH ₃	2,3 ± 0,7 (0,58 ± 0,04)
121	H	H	Ph	H	H	CH ₃	NHCH ₃	14 ± 3 (0,08 ± 0,05)
122	H	H	2-furyl	H	H	CH ₃	OCH ₃	1,5 ± 0,5 (0,36 ± 0,06)
123	H	H	3-furyl	H	H	CH ₃	OCH ₃	8 ± 2 (0,01 ± 0,01)
124	H	H	2-thiophenyl	H	H	CH ₃	OCH ₃	4 ± 1 (0,39 ± 0,05)
125	H	H	3-thiophenyl	H	H	CH ₃	OCH ₃	2,5 ± 0,7 (0,53 ± 0,04)
126	H	H	4-pyridyl	H	H	CH ₃	OCH ₃	9 ± 4 (0,1 ± 0,2)
127	H	H	3-pyridyl	H	H	CH ₃	OCH ₃	3,8 ± 0,6 (0,06 ± 0,05)

Daher wurden anschließend weitere Modifikationen in 5-Position untersucht (Tabelle 6). Die Einführung eines Brom-Substituenten (**110**) verbesserte die Potenz nochmals leicht im Vergleich zum Chlor-Derivat **103**, während die Erweiterung mit einem Phenyl-Rest (**111**) die Potenz um das 10-fache steigern konnte. Die Verlängerung des Linkers zum Benzyl-Rest (**112**) in 5-Position hingegen wurde nicht toleriert, was auf die Präferenz eines starren Biarylsystems hindeutete.

Des Weiteren wurden Substituenten am Stickstoff im Indol-Gerüst untersucht (Tabelle 6), wobei eine zweifache Steigerung der Potenz durch Einführung einer Methyl-Funktion (**113**) im Vergleich zum unsubstituierten Ausgangsfragment **95** beobachtet wurde. Die Verlängerung zum Ethyl-Analog (**114**) hingegen war nicht bevorzugt. Ein Phenyl-Rest in 1-Position (**115**) kehrte sogar die Aktivität am Rezeptor um und führte zu schwacher Aktivierung von Nurr1, wohingegen auch hier die Verlängerung des Linkers zum Benzyl-Derivat **116** nicht toleriert wurde. Außerdem wurde die Rolle des metabolisch instabilen Methylesters in 3-Position des Fragments **95** näher analysiert (Tabelle 6). Der Austausch zur freien Carbonsäure, sowie zum Aldehyd und dem Methyl- bzw. Ethylketon führte jedoch zu inaktiven Derivaten. Auch die Expansion zum Ethyl- (**117**) und *tert*-Butyl-Ester (**118**) wurde nicht toleriert. Wie auch im N-Phenyl-Derivat **115**, bewirkte die Einführung eines Phenyl-Restes (**119**) als Erweiterung des Esters eine Umkehr zu agonistischer Aktivität an Nurr1 und erinnert an das Substitutionsmuster des Chinolins im Agonisten **19**. Nach der systematischen Untersuchung aller Strukturelemente und Positionen des inversen Nurr1-Agonisten **95** wurden die bevorzugten Modifikationen des Phenyl-Restes in 5-Position (**111**) und der N-Methyl-Substitution (**113**) in Derivat **120** kombiniert (Tabelle 6), was jedoch keine weitere Steigerung der Potenz brachte, in der Aktivität dem Analog **111** aber gleichwertig war. **120** diente daher als neuer Ausgangspunkt für weitere Optimierungsversuche, wobei wiederum versucht wurde, den metabolisch instabilen Methylester zu ersetzen. Doch auch der Austausch des Ester-Motivs gegen Carbonsäureamide in 3-Position war nicht zielführend. Das Methylamid **121** wurde zwar toleriert, führte aber trotz hoher Repressions-Effizienz zu einer 10-fach verringerten Potenz. Ein zweifach substituiertes Dimethylamid-Derivat sowie der größere Ethylamid-Substituent führten hingegen zu vollständigem Aktivitätsverlust an Nurr1. Somit konnte kein adäquater Ersatz für den Methylester gefunden werden. Abschließend wurde durch das Einführen von aromatischen Heterozyklen (**122–127**) anstelle des bevorzugten Phenyl-Restes in 5-Position versucht **120** weiter zu optimieren (Tabelle 6). Die Furan-Derivate **122** und **123** sowie die Thiophen-Analoga **124** und **125** zeigten vergleichbare Potenzen im unteren mikromolaren Bereich mit verbesserter Repressions-Effizienz gegenüber **120**. Ebenso wurde das Einführen von Pyridin-Substituenten in **126** und **127** gut toleriert und zeigte mit dem 3-Pyridyl-Derivat **127** eine sehr hohe Repressions-Effizienz mit lediglich 6 % verbleibender Rezeptoraktivität. Ein Versuch, die zuvor beobachteten günstigen Modifikationen durch den 7-Chlor-Substituenten in **107** und den unsubstituierten Stickstoff im Indolgrundgerüst (**111**) mit dem bevorzugten Pyridin-Derivat **127** zu kombinieren, erreichte keine weitere Steigerung der Aktivität.

Somit gingen **120** und **127** als zwei potente inverse Nurr1-Agonisten mit unterschiedlicher Effizienz aus dieser umfangreichen SAR-Studie hervor, die die NSARs als erste Vertreter dieser Klasse an Nurr1-Liganden in ihrer Potenz etwa um den Faktor 10 überstiegen. Wie schon bei den NSARs, zeigte sich innerhalb der NR4A-Familie keine Selektivität gegenüber den verwandten Rezeptoren Nur77 und NOR-1 im Gal4-Hybrid-Reportergenassay, jedoch war für beide Substanzen die Repressions-Effizienz an Nurr1 am stärksten ausgeprägt. Außerhalb der NR4A-Subfamilie zeigten **120** und **127** keine Aktivität an weiteren NRs. In Kooperation mit Dr. Jan Heering wurde auch für diese Substanzklasse der molekulare Wirkmechanismus anhand von **127** im zellfreien TR-FRET-System näher untersucht. Der inverse

Agonist verdrängte die Co-Repressoren NCoR1 und SMRT von der Nurr1-LBD (Abbildung 40a, b), war jedoch nicht in der Lage, die Rekrutierung des Co-Aktivators NCoA6 zu beeinflussen. Auch der Einfluss auf das Dimerisierungsverhalten des Rezeptors unterschied sich bei **127** von den NSARs. Während die Homodimerisierung dosisabhängig unterdrückt wurde (Abbildung 40c), zeigte sich kein Effekt auf die Bildung des Heterodimers mit der RXR α -LBD. Auch die Beobachtungen im zellulären Testsystem des Vollängenrezeptors Nurr1 sprechen für eine Monomerpräferenz dieser Substanzklasse, da sowohl **127** als auch **120** bis 50 μ M keinerlei Aktivität am Homodimer (NurRE)- und Heterodimer (DR5)-Response-Element zeigten. Die Nurr1-Aktivität am Monomer Response-Element (NBRE) wurde jedoch von beiden Substanzen mit moderater Effizienz und IC₅₀-Werten im unteren mikromolaren Bereich reduziert (Abbildung 40d). Somit ergaben sich einige mechanistische Unterschiede zu den NSARs als inversen Nurr1-Agonisten, die ein differenziertes Bild der Co-Regulator-Interaktion und der Modulation der Monomer-Oligomer-Equilibria zeigen, wodurch die Entwicklung genselektiver Liganden möglich erscheint. Allerdings bedarf es für das umfassende Verständnis der inversen Nurr1-Agonisten noch eines besseren Verständnisses der molekularen Aktivierungsmechanismen von Nurr1.

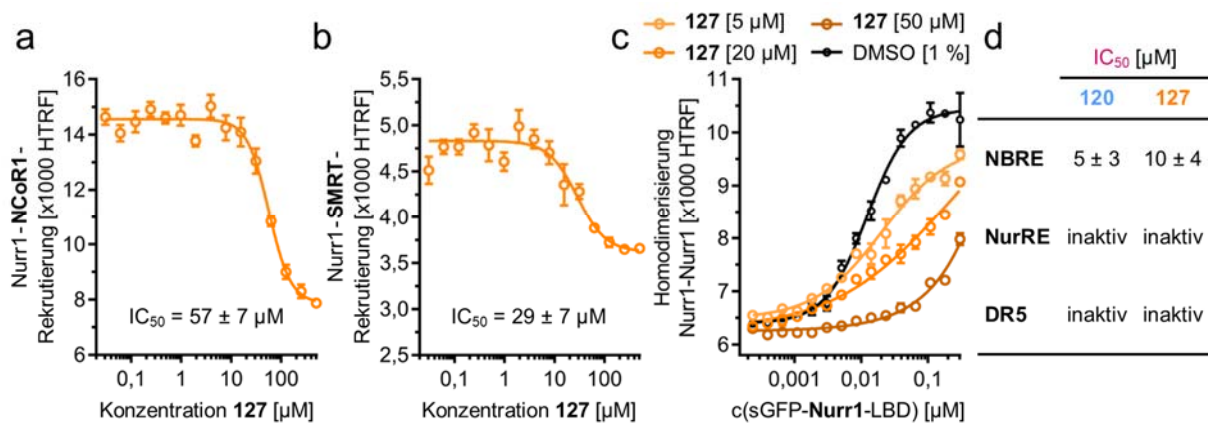


Abbildung 40: Charakterisierung von **127** und **120** in zellfreien und zellulären Systemen. (a–c) **127** verdrängte die Tb³⁺-gekoppelten Co-Repressoren NCoR1 (a) und SMRT (b) von der sGFP-gelabelten Nurr1-LBD und konnte die Homodimerisierung (c) der Tb³⁺- und sGFP-gelabelten Nurr1-LBD dosisabhängig verhindern. Gezeigt sind die dimensionslosen HTRF-Werte als MW \pm S.E.M.; N = 3. (d) Eine Aktivität von **120** und **127** am Vollängenrezeptor Nurr1 in HEK293T-Zellen konnte nur für das Monomer-Response-Element (NBRE) festgestellt werden, nicht jedoch für das Homodimer (NurRE) und Heterodimer (DR5). IC₅₀-Werte [μ M] sind MW \pm S.E.M.; n \geq 3.

Kreuztitrationen von **127** mit AQ (**19**) im Gal4-Nurr1-Reporterassay deuteten ähnlich wie bei den NSARs (siehe Kapitel 3.3) darauf hin, dass die inversen Agonisten mit Indol-Grundgerüst mit einer anderen Bindestelle interagieren als AQ (**19**), da die Dosis-Wirkungskurven nur auf der y-Achse verschoben und gestaucht wurden, jedoch kein kompetitiver Effekt der beiden Liganden zu erkennen war. Abschließend wurde die Wirkung der neuen inversen Nurr1-Agonisten in einem nativen zellulären System validiert, wofür humane Astrozyten (T98G) für 8 h mit **120** und **127** inkubiert und anschließend der Einfluss auf die Expression Nurr1-abhängiger dopaminergischer Gene mittels qRT-PCR untersucht wurden. Beide Substanzen bewirkten eine signifikante Reduktion der mRNA-Expression von DDC, TH und VMAT2 im Vergleich zu unbehandelten Zellen, wodurch der inverse Agonismus an Nurr1 auf zellulärer Ebene bestätigt werden konnte (Abbildung 41a). Die zuvor im Gal4-Nurr1-Testsystem beobachteten Unterschiede in der Repressions-Effizienz beider Substanzen waren allerdings nicht erkennbar, was durch die zytotoxischen Effekten von **127** bedingt sein könnte, die sich auch durch einen Einfluss auf das Referenzgen GAPDH zeigten. Des Weiteren wurde die Freisetzung des proinflammatorischen Zytokins IL-6 von T98G-Zellen 24 h nach der Inkubation mit **120** mittels *Enzyme-linked Immunosorbent Assay* (ELISA) aus dem Medium der Zellen bestimmt. Dabei steigerte der inverse Agonist

dosisabhängig die IL-6-Level und ähnelte damit in seiner Wirkung dem Effekt des siRNA-vermittelten *Knockdowns* von Nurr1 (si-Nurr1) auf die IL-6-Ausschüttung (Abbildung 41b, c), was eine mögliche Beteiligung von Nurr1 an neuroinflammatorischen Prozessen unterstreicht (siehe Kapitel 3.5.2).

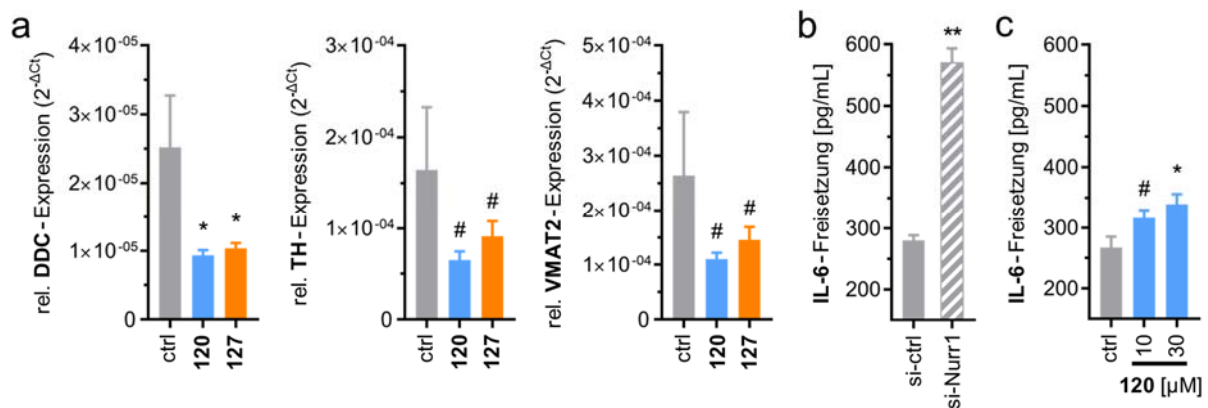


Abbildung 41: Biologische Effekte von 120 und 127. (a) Effekte von 120 und 127 (je 30 µM) auf die mRNA-Expression der Nurr1-abhängigen Gene DDC, TH und VMAT2 in T98G-Zellen vs. 0,1 % DMSO (ctrl). Die gezeigten Werte sind MW ± S.E.M.; n = 4. mRNA-Level wurden mittels qRT-PCR bestimmt und durch die 2^{-ΔCt}-Methode in Bezug auf das Referenzgen GAPDH analysiert. (b) T98G setzten nach Behandlung mit LPS (1 µg/mL) IL-6 frei, was durch si-Nurr1 (vs. Kontroll-siRNA, si-ctrl) deutlich gesteigert wurde. Die Werte sind MW ± S.E.M. der IL-6-Level; n = 3. (c) In gleicher Weise förderte 120 signifikant die Freisetzung von IL-6 in LPS-behandelten T98G-Zellen. Die Werte sind MW ± S.E.M.; n = 4. # p < 0,1, * p < 0,05, ** p < 0,01 vs. 0,1 % DMSO (t-Test).

Somit erweisen sich die aus einem Fragment Screening entwickelten, neuen, inversen Nurr1 Agonisten als hilfreiche *tool compounds*, um eine reduzierte Aktivität des konstitutiv aktiven Rezeptors zu untersuchen, wobei sich besonders 120 für zelluläre Studien eignet.

3.5.2 Statine vermitteln neuroprotektive Effekte durch Nurr1 Agonismus

Anders als bei den Indol-basierten inversen Agonisten (Kapitel 3.5.1) zeigte der Arzneistoff Fluvastatin (97), von dem sich der agonistische Treffer 91 im Fragment-Screening ableitet, ebenfalls Aktivität im Gal4-Nurr1-Reportergenassay, sogar mit gesteigerter Potenz (Abbildung 42a,b). Aufgrund dieser vielversprechenden Beobachtung wurden die übrigen Vertreter der Arzneistoffklasse der Statine, die als Lipidsenker vielfach klinisch angewendet werden, auf ihre Nurr1-modulatorische Aktivität untersucht, um zu sehen, ob es sich hierbei um einen Klasseneffekt handelt. Die strukturell verwandten synthetischen Statine der zweiten Generation 128–130 zeigten ebenfalls agonistische Aktivität an Nurr1 mit großen Unterschieden in der Potenz und insgesamt geringerer Aktivierungseffizienz. Pitavastatin (128) war dabei das potenteste Statin mit einem EC₅₀-Wert von 0,12 µM, während Rosuvastatin (130) die geringste Potenz zeigte (EC₅₀ 23 µM). Die Statine der ersten Generation Lovastatin (131) und Simvastatin (132) waren in Potenz und Effizienz mit Fluvastatin (97) vergleichbar, nur Pravastatin (133) zeigte als einziger Vertreter dieser Arzneistoffklasse keine Aktivität an Nurr1. Wie bereits bei der Aktivitätsumkehr durch den Phenylester in 119 der Indol-basierten Klasse von inversen Nurr1-Agonisten beobachtet wurde, weisen auch die Nurr1-Agonisten 97 und 128 strukturelle Verwandtschaft zum bekannten Liganden 19 auf, wie ein *Alignment* der Strukturen veranschaulicht (Abbildung 42c). Auch die synthetischen Statine 129 und 130 teilen ein ähnliches Grundgerüst des zentralen stickstoffhaltigen Heterozyklus mit *para*-Fluor-substituiertem Phenylring in gleicher Orientierung. Die Statine 131–133 sind dagegen als natürlich vorkommende Monacoline extrahiert oder von diesen abgeleitet und weisen daher keine aromatischen Ringsysteme auf. Da bei 131 und 132 die charakteristische Carbonsäure-Seitenkette in einer geschlossenen Lactonform vorliegt, scheint eine direkte Interaktion

der Säurefunktion mit Nurr1 für die Aktivierung nicht entscheidend zu sein, sondern andere Molekülmerkmale von Bedeutung. Dafür spricht auch, dass das offenkettige Statin **133** als einziger Vertreter keinerlei Aktivität an Nurr1 aufwies.

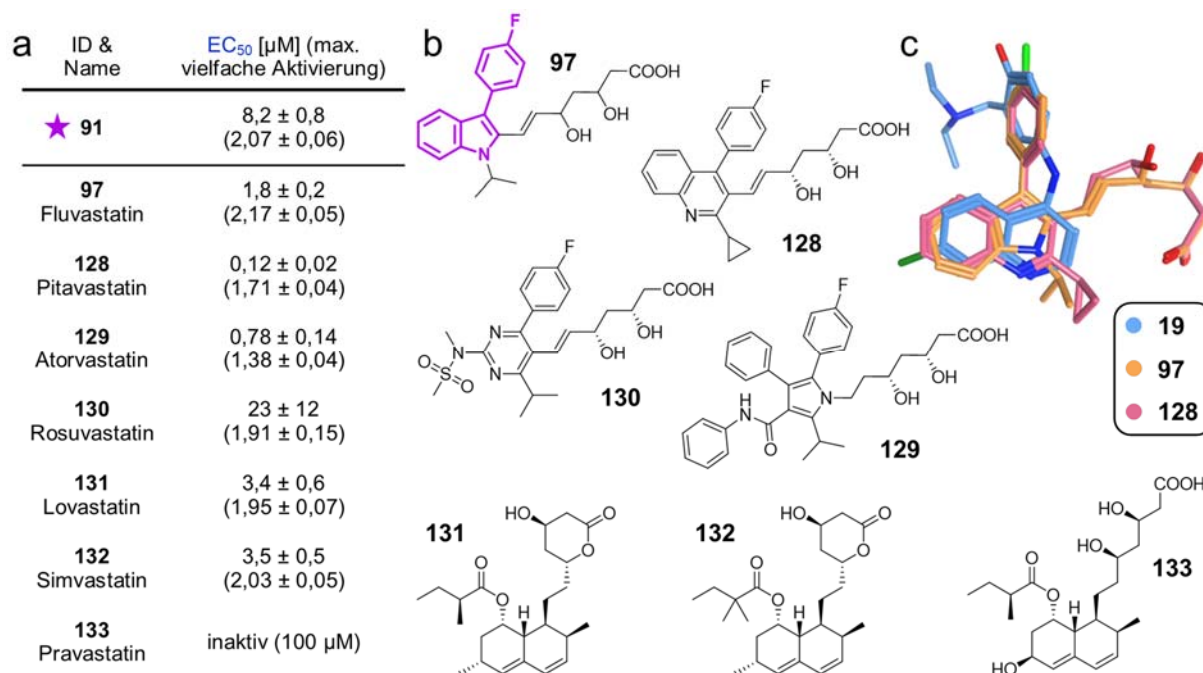


Abbildung 42: Identifikation von Statinen als Nurr1-Modulatoren. (a) Aktivitäten der Statine im Gal4-Nurr1-Reporterassay, Screeninghit **91** zum Vergleich. EC₅₀-Werte sind MW ± S.E.M.; n ≥ 3. Max. vielfache Aktivierung bezieht sich auf 0,1 % DMSO. (b) Chemische Strukturen der zugelassenen Statine. Fragment **91** ist im davon abgeleiteten Fluvastatin (**97**) gekennzeichnet. (c) Das Alignment von Fluvastatin (**97**) und Pitavastatin (**128**) mit AQ (**19**) zeigt gemeinsame strukturelle Merkmale.

Um die Aktivität der Statine an Nurr1 näher zu charakterisieren, wurden die beiden effizientesten Substanzen, **97** und **132**, als Vertreter aus beiden Gruppen dieser Arzneistoffklasse für tiefgreifende mechanistische Studien ausgewählt. Ein wichtiger Vorteil für Untersuchungen im TR-FRET-System ergab sich dabei auch aufgrund des fehlenden Chromophors in Statinen der ersten Generation. Alle vier zuvor untersuchten Interaktionen der Nurr1-LBD mit Peptiden der Co-Regulatoren NCoR1, SMRT, NCoA6 und NRIP1 (vgl. Kapitel 3.3) wurden durch beide Statine im zellfreien System dosisabhängig blockiert (Abbildung 43a–d). In Kooperation mit Dr. W. Kilu/Dr. J. Heering wurde auch der Einfluss auf das Dimerisierungsverhalten des Rezeptors im TR-FRET-Setting untersucht (Abbildung 43e,g) und zeigte, dass **132** die Homodimerisierung fast vollständig unterdrückte, während **97** einen schwächeren Effekt zeigte. Anders als bei den NSARs **49** und **51** beobachtet, zeigten die Statine allerdings keinen Effekt auf die Heterodimerisierung mit der RXRα-LBD. Die Effekte von **132** auf das Co-Regulator-Interaktionsprofil und die Homodimerisierung von Nurr1 waren insgesamt stärker ausgeprägt und zeigten höhere Potenz (Abbildung 43g). Obwohl das Profil im zellfreien System den inversen Agonisten (Kapitel 3.3 und 3.5.1) ähnelte, konnte **132** in den nativen Reporterassays den Vollängenrezeptor Nurr1 an allen drei *Response*-Elementen mit Potenzen im unteren mikromolaren bis nanomolaren Bereich aktivieren (Abbildung 43f,g) und eignete sich damit gut als Nurr1-agonistische Modells substanz für weitere zelluläre Untersuchungen.

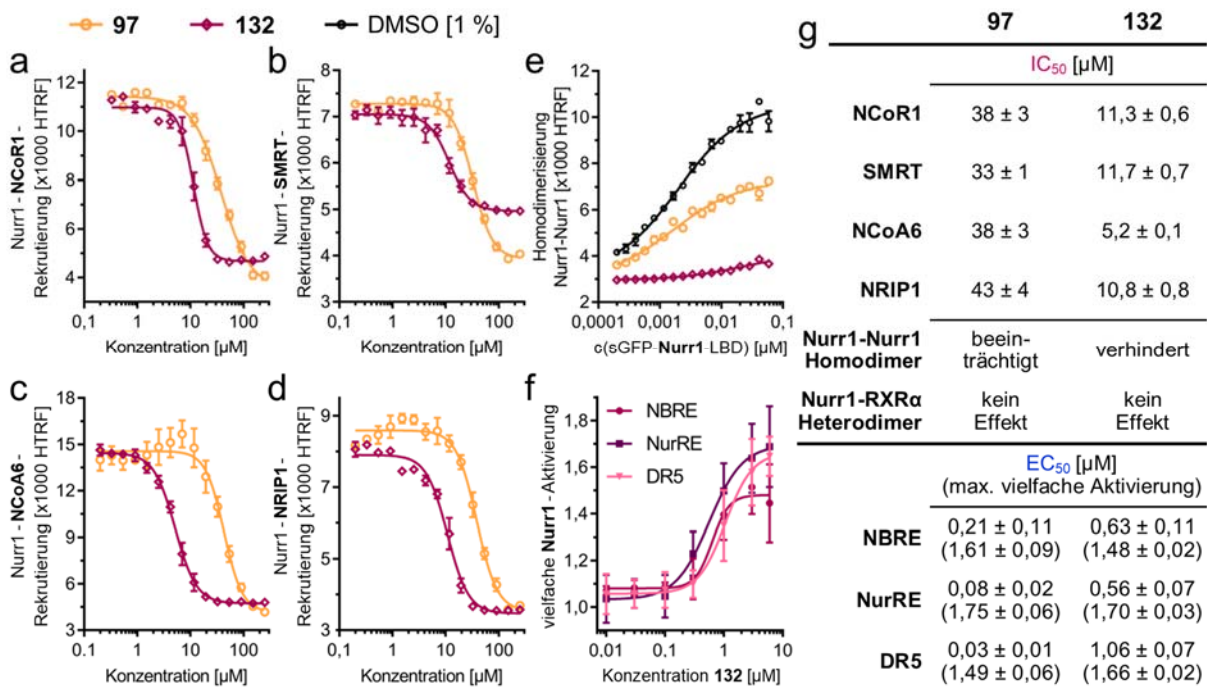


Abbildung 43: Charakterisierung von **97** und **132** in zellfreien und zellulären Systemen. (a–d) **97** und **132** verdrängten die Fluoreszein-gelabelten Co-Regulatoren NCoR1 (a), SMRT (b), NCoA6 (c) und NRIP1 (d) von der Tb³⁺-gekoppelten Nurr1-LBD. (e) Die Homodimerisierung der Tb³⁺- und sGFP-gelabelten Nurr1-LBD wurde von **132** verhindert und von **97** beeinträchtigt. (a–e) Dargestellt sind die dimensionslosen HTRF-Werte als MW ± S.E.M.; N = 3. (f) **132** aktivierte den Volllängenrezeptor Nurr1 in zellulären Reporterassays (HEK293T) für das Monomer (NBRE), das Homodimer (NurRE) und das RXR-Heterodimer (DR5). Die Werte sind MW ± S.E.M., n ≥ 3. (g) Zusammengefasste Aktivitäten im TR-FRET-Setting (oben) und den Volllängen-Reporterassays (unten); EC₅₀-Werte als MW ± S.E.M.; max. vielfache Aktivierung bezogen auf 0,1 % DMSO; n ≥ 3.

Um eine mögliche klinische Relevanz der Nurr1-Aktivierung durch Statine vorläufig bewerten zu können, wurde zunächst in humanen Astrozyten (T98G) ihr Effekt auf eine LPS-induzierte Neuroinflammation anhand der Freisetzung von IL-6 mittels ELISA untersucht. Die Tatsache, dass sowohl **97** als auch **132** die Freisetzung von IL-6 signifikant senken konnten und **133** als einziges inaktives Statin an Nurr1 keinen Effekt zeigte, deutete darauf hin, dass diese Reduktion der inflammatorischen Antwort Nurr1-vermittelt stattfindet (Abbildung 44a). Durch *Knockdown* des Rezeptors, der mittels Transfektion von T89G-Zellen mit Nurr1-gerichteter siRNA (si-Nurr1) erzielt wurde (Kontroll-siRNA zum Vergleich, si-ctrl), konnte diese Vermutung für **132** im gleichen Versuchsaufbau weiter bestätigt werden (Abbildung 44b). Die *Knockdown*-Effizienz wurde anhand der relativen Nurr1-mRNA-Expression mittels qRT-PCR über die 2^{-ΔCt}-Methode mit GAPDH als Referenzgen bestimmt und zeigte eine 63 %ige Reduktion des Rezeptorgens im Vergleich zu Zellen, die mit si-ctrl behandelt wurden. Der Nurr1-*Knockdown* steigerte die Freisetzung von IL-6 erheblich, Simvastatin (**132**) bewirkte jedoch kaum eine Reduktion der IL-6-Freisetzung in mit si-Nurr1 behandelten Zellen.

Basierend auf diesen sehr vielversprechenden Beobachtungen wurden die möglichen Nurr1-vermittelten antineuroinflammatorischen und neuroprotektiven Effekte durch differenzielle Genexpressionsanalyse in Astrozyten näher untersucht. Dazu wurden ebenfalls T98G-Zellen mit si-Nurr1 und si-ctrl transfiziert und nach 24 h entweder mit oder ohne LPS als Entzündungsstimulus für 12 h mit DMSO (0,1 %) inkubiert. Die gesamte mRNA wurde anschließend aus den Zellen extrahiert und mittels RNA-Sequencing (durch die Firma Novogene) analysiert. Dabei bestätigte sich die Vermutung, dass allein der Nurr1-*Knockdown* in Astrozyten Neuroinflammation induzierte. Er veränderte in beiden Fällen (+/- LPS) signifikant die Expression von knapp 8000 Genen (Abbildung 44c,d). Die veränderte

Expression von 5868 Genen war hierbei unabhängig von der Inkubation mit LPS nur auf den *Knockdown* des Rezeptors zurückzuführen und bei jeweils knapp 2000 Genen zeigten sich Unterschiede im Kontext der LPS-induzierten Neuroinflammation (Abbildung 44d). So wurden zahlreiche Interferone und Chemokine, Zytokinrezeptoren, Gene des JAK-STAT-Signalweges und der TNF-Superfamilie teils deutlich durch den Nurr1-*Knockdown* induziert. Außerdem zeigte eine Analyse der KEGG-Pfade^{482,483}, dass vor allem Gene, die mit PD und AD assoziiert werden, sowie an oxidativer Phosphorylierung, Apoptose und dem p53-Signalweg beteiligt sind, verändert exprimiert wurden (Abbildung 44e).

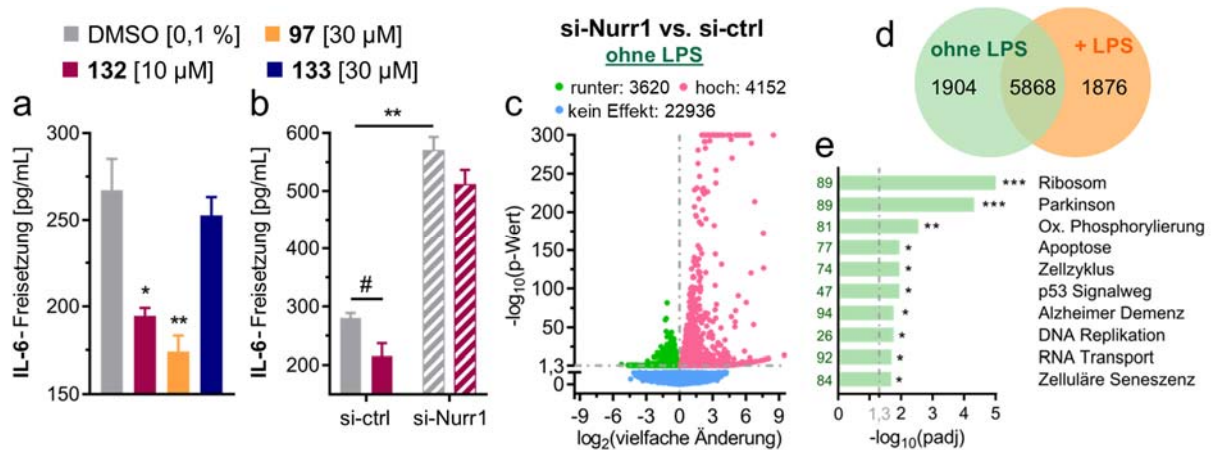


Abbildung 44: Beteiligung von Nurr1 an Neuroinflammation. (a) Mit LPS (1 µg/mL) behandelte T98G-Zellen setzen nach Behandlung mit **97** und **132** signifikant weniger IL-6 frei. **133** diente als Negativkontrolle und zeigte keinen Einfluss auf die IL-6-Freisetzung. Die Werte sind MW ± S.E.M., n = 4. (b) Der Effekt von **132** auf die IL-6-Freisetzung von LPS-behandelten T98G-Zellen ist mit si-Nurr1 nicht mehr signifikant. Die Werte sind MW ± S.E.M., n = 3. (c–e) Differenzielle Genexpressionsanalyse in T98G behandelt mit si-Nurr1 oder si-ctrl; n = 3 (c) Vulkan-Diagramm zeigt den log₂ der vielfachen Änderung in den Genexpressionslevels (x-Achse) vs. statistische Signifikanz (–log₁₀ (p-Wert); y-Achse) ohne LPS. (d) Venn-Diagramm der gleichen Analyse für Zellen, die ohne oder mit LPS behandelt wurden. (e) Anreicherung von KEGG-Pfaden zeigt die Beteiligung von Nurr1 an neurodegenerativen Erkrankungen und Neuroinflammation. Gezeigt sind die statistischen Signifikanzniveaus (–log₁₀(padj)) der regulierten KEGG-Pfade. Die Zahlen beziehen sich auf die Anzahl der differenziell regulierten Gene, die mit dem Pfad verbunden sind. #p < 0,1, *p < 0,05, **p < 0,01, ***p < 0,001 (a,b,e).

Um die möglichen Nurr1-vermittelten neuroprotektiven Effekte von **132** näher zu untersuchen, wurden T98G in gleicher Weise für 12 h mit **132** (10 µM) behandelt und dessen Effekte auf die Genexpression mit denen des Nurr1-*Knockdown* verglichen (Abbildung 45). Dabei wurden 405 durch den *Knockdown* herunterregulierte Gene durch **132** induziert und 363 durch den *Knockdown* induzierte Gene von **132** signifikant herunterreguliert (Abbildung 45a). Unter diesen fiel besonders die Häufung von Genen auf, die mit der Regulation metabolischer Pfade assoziiert werden (Abbildung 45b). So wurden Gene, die an der Glukose-Verwertung (PGM1, SLC2A6) und Energiegewinnung (ACSS2) beteiligt sind, entgegengesetzt reguliert. Interessanterweise induzierte der Cholesterinsenker **132** auch Gene der Cholesterolsynthese (z. B. MVD, TM7SF2, MVK, DHCR7, LSS), die durch den Nurr1-*Knockdown* herunterreguliert wurden. Außerdem zeigte **132** ein antientzündliches und antiapoptotisches Genexpressionsprofil, indem **132** beispielsweise den NFκB-Inhibitor α (NFKBIA) induzierte und die Expression der NFκB-induzierenden Kinase MAP3K14 sowie des Interferon-alpha-induzierbaren Proteins 27 (IFI27) herunterregulierte (Abbildung 45c). Der Nurr1-*Knockdown* hingegen zeigte die gegenteilige Wirkung, was auf zytoprotektive Effekte der Nurr1-Aktivierung durch **132** hindeutet.

Auch in Nurr1-defizienten Zellen (si-Nurr1) wurde der Einfluss von **132** auf die Genexpression untersucht. Somit konnte die Regulation von 1948 Genen (1058 induziert, 890 herunterreguliert) durch **132** als Nurr1-vermittelt angenommen werden, da diese Effekte mit **132** in Nurr1-defizienten Zellen nicht

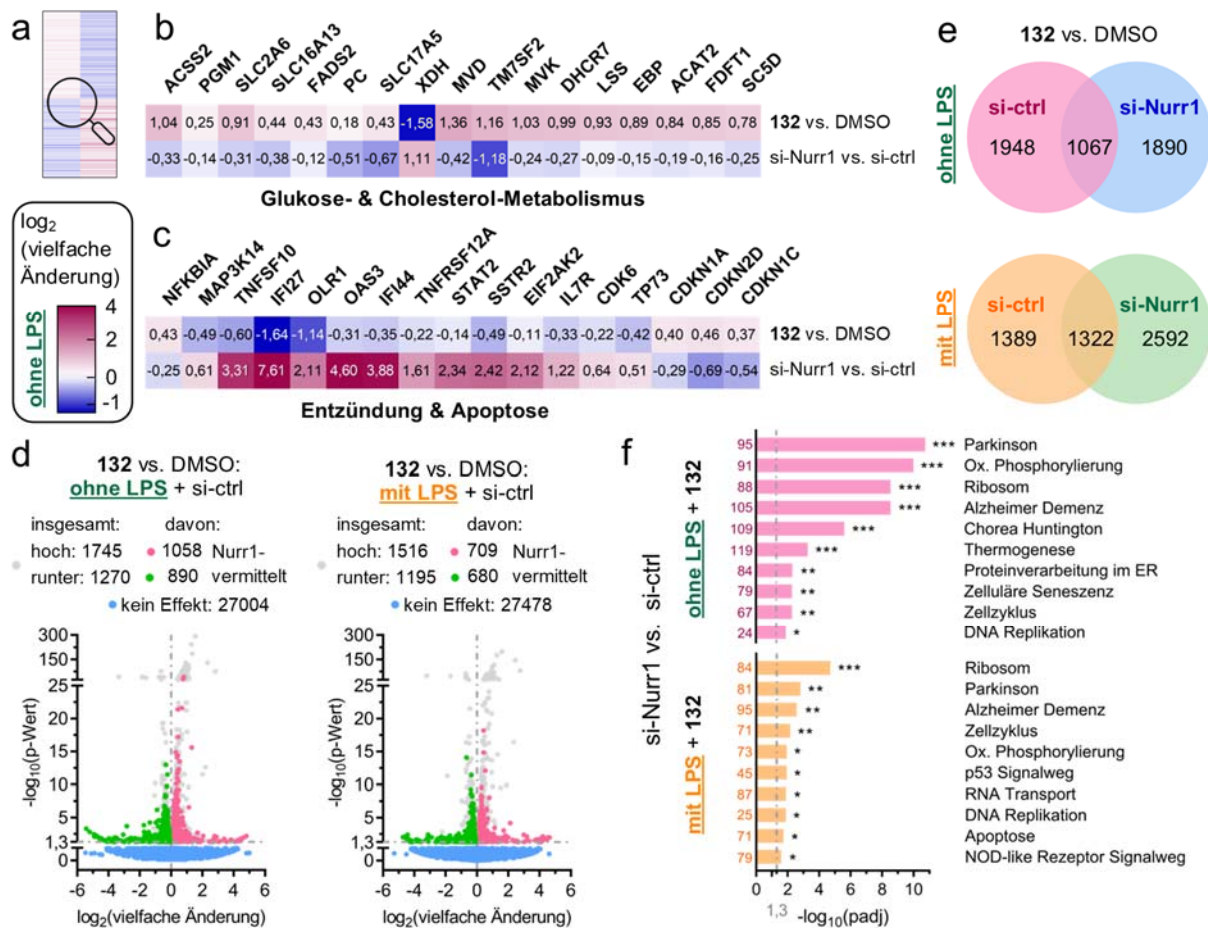


Abbildung 45: Simvastatin (132) beeinflusste die Genexpression von Astrozyten (T98G) in Abhängigkeit von Nurr1. (a–c) Die Heatmaps zeigen gegenteilige signifikante Effekte ($p < 0,05$) von 132 (vs. DMSO, in Gegenwart von si-ctrl) und si-Nurr1-vermitteltem Knockdown (vs. si-ctrl, in Gegenwart von DMSO) als \log_2 der vielfachen Änderung; $n = 3$. Insgesamt wurden 768 Gene entgegengesetzt reguliert (a), wobei besonders Gene des Glukose- und Cholesterol-Stoffwechsels (b) betroffen waren, sowie Gene, die in Entzündungs- und Apoptose-Prozesse eingreifen (c). (d–f) Nurr1-vermittelte Effekte von 132 wurden zusätzlich durch gleichzeitige Behandlung der Zellen mit 132 (vs. DMSO) und si-Nurr1 oder si-ctrl analysiert; $n = 3$. (d) Vulkan-Diagramme zeigen den \log_2 der vielfachen Änderung in den Genexpressionslevels (x-Achse) vs. statistische Signifikanz ($-\log_{10}(p\text{-Wert})$; y-Achse) mit si-ctrl und +/- LPS. Effekte von 132, die auch mit si-Nurr1 signifikant waren, sind grau dargestellt. (e) Venn-Diagramme der gleichen Analysen zeigen den Anteil der Nurr1-vermittelten Effekte von 132. (f) Die Nurr1-vermittelte Auswirkung von 132 auf die Regulation von KEGG-Pfaden ist anhand der statistischen Signifikanzniveaus ($-\log_{10}(padj)$) gezeigt. Die Zahlen beziehen sich auf die Anzahl der differenziell regulierten Gene, die mit dem Pfad verbunden sind. * $p < 0,05$, ** $p < 0,01$, *** $p < 0,001$.

signifikant waren (Abbildung 45d,e). 1067 weitere Gene, die sowohl in Zellen mit si-Nurr1 als auch mit si-ctrl von 132 beeinflusst wurden, deuten auf die Beteiligung anderer Signalwege hin. Die gleichen Untersuchungen wurden außerdem in LPS-behandelten Zellen durchgeführt, um den Nurr1-vermittelten Einfluss von 132 auf neuroinflammatorische Prozesse zu analysieren. Hierbei war die Zahl der durch 132 Nurr1-vermittelt regulierten Gene mit 1389 (709 induziert, 680 herunterreguliert) etwas geringer (Abbildung 45d,e). Eine Analyse der KEGG-Pfade^{482,483} der mit si-ctrl im Vergleich zu si-Nurr1 behandelten Zellen zeigte, dass 132 Nurr1-vermittelte Effekte auf Gene hatte, die mit PD, AD, oxidativer Phosphorylierung, Zellzyklus und DNA-Replikation zusammenhängen (Abbildung 45f). Bei LPS-behandelten Zellen waren zusätzlich Effekte auf Apoptose und p53-Signalwege zu erkennen. Eine genauere Untersuchung dieser Effekte ergab mehrere neuroprotektive Wirkungen, darunter bspw. eine Induktion der Hexokinasen, welche zu einer verbesserten Glucoseverwertung im Gerhin beitragen könnten^{497–499}. Außerdem zeigte 132 Nurr1-vermittelte Effekte auf Neurotransmitter-Rezeptoren und -Transporter sowie auf Entzündungsgene. So wurde bspw. in beiden Fällen der GABA-Rezeptor A3

(GABRA3) herunterreguliert und interzelluläre Adhäsionsmoleküle (ICAMs) sowie NFKBIA induziert. Insgesamt bestätigte die differenzielle Genexpressionsanalyse, dass Nurr1 an den neuroprotektiven Wirkungen von **132** mit metabolischen, antientzündlichen und antiapoptotischen Komponenten beteiligt ist.

Dass Statine als 3-Hydroxy-3-Methylglutaryl-Coenzym-A(HMG-CoA)-Reduktase-Inhibitoren über einen verbesserten Cholesterol Haushalt neuroprotektive Wirkungen erzielen, ist nicht verwunderlich. Doch deuten zahlreiche Untersuchungen von Statinen im Kontext neurodegenerativer Erkrankungen darauf hin, dass Cholesterol-abhängige Mechanismen diese Wirkung nicht alleine erklären können⁵⁰⁰⁻⁵⁰². Da für die lipophilen Statine in Laktonform (**131** und **132**) bereits gezeigt wurde⁵⁰³, dass sie die Blut-Hirn-Schranke überwinden können, und für Statine in der freien Säure-Form aktive Transport-Mechanismen vermutet werden⁵⁰⁴, ist die Aktivierung von Nurr1 durch Statine im ZNS potenziell klinisch relevant. Vor allem **132** konnte im Kontext neurodegenerativer Erkrankungen *in vitro* und *in vivo* überzeugen und führte zu einer Reduktion proinflammatorischer Moleküle und einer verringerten Aktivierung der Mikroglia, zeigte antioxidative Effekte, verhinderte die Aggregation von α -Synuclein und schützte vor dem Untergang dopaminerger Neurone^{501,505}. Bemerkenswert ist auch, dass eine Studie allen Statinen außer **133** eine protektive Wirkung gegen PD zuschreibt⁵⁰⁶, da **133** auch das einzige Statin ist, das keine Aktivität an Nurr1 zeigte. Die zahlreichen vielversprechenden Untersuchungen zum möglichen therapeutischen Nutzen der Statine bei neurodegenerativen Erkrankungen motivierten bereits mehrere klinische Studien mit **132** zur Behandlung von PD, AD und MS. So deutete eine retrospektive Beobachtungsstudie bei PD-Patienten im Frühstadium, die über vier Jahre ein Statin einnahmen, auf eine verlangsamte Progression der Erkrankung hin und zeigte geringere motorische Beeinträchtigungen im Vergleich zu Patienten ohne Statin-Therapie⁵⁰⁵. Die vorläufigen Ergebnisse einer zweijährigen Phase-2-Interventionsstudie zur Behandlung von moderater PD mit **132** (PD-STAT)⁵⁰⁷ konnten noch keinen signifikanten Einfluss auf das Fortschreiten der Erkrankungen feststellen⁵⁰⁸, weshalb weitere Studien zur Klärung dieser Diskrepanz benötigt werden. Eindeutig waren hingegen die Ergebnisse der Phase-2-Studie MS-STAT, die über zwei Jahre die tägliche Einnahme von **132** (80 mg) bei sekundär progredienter MS untersuchte. Sie zeigten eine signifikante Reduktion der Hirnatrophie und verbesserte Funktion des Frontallappens im Vergleich zu Placebo mit zusätzlich gesteigerter körperlicher Lebensqualität^{502,509}. Diese bemerkenswerten Erkenntnisse unterstützten die Fortführung der Untersuchungen in einer Phase-3-Studie⁵¹⁰ trotz bislang ungeklärten molekularen Mechanismus der Neuroprotektion. Die Aktivierung von Nurr1 scheint daher, neben anderen bekannten Mechanismen⁵¹¹⁻⁵¹⁵ möglicherweise maßgeblich an der neuroprotektiven und antineuroinflammatorischen Wirkung der Statine beteiligt zu sein.

Somit sind aus dem Fragment-Screening zwei entscheidende Fortschritte zur Identifikation, Entwicklung und Charakterisierung neuer Nurr1-Liganden hervorgegangen. Auf einem klassisch medizinisch-chemischen Weg gelang es, neue inverse Nurr1-Agonisten als wertvolle *tool compounds* zu entwickeln und die Entdeckung des Nurr1 Agonismus von Statinen liefert eine potenziell klinisch relevante Erklärung der neuroprotektiven Wirkung dieser Arzneistoffklasse.

4. Zusammenfassung

Nukleäre Rezeptoren (NRs) sind eine Familie von 48 ligandenaktivierten Transkriptionsfaktoren, die an der Regulation unzähliger (patho-)physiologischer Prozesse im Körper beteiligt sind, wie Zell-Proliferation, -Differenzierung, Metabolismus und Entzündungen, wodurch sie interessante therapeutische Zielstrukturen darstellen^{1,2,15}. Etwa die Hälfte der NRs ist inzwischen gut erforscht, ihre Funktionen und endogenen Liganden weitestgehend bekannt und synthetische Liganden dieser NRs zum Teil als Arzneistoffe zugelassen^{3-5,9}. Hierzu zählen die Peroxisomen-Proliferator-aktivierten Rezeptoren (PPARs) α , γ und δ , die als Lipidsensoren vor allem metabolische Funktionen im Glukose- und Lipidstoffwechsel haben, denen aber auch eine Beteiligung an Entzündungsprozessen und neurodegenerativen Erkrankungen zugeschrieben wird¹²⁻¹⁴. Mit den Fibraten (PPAR α) zur Behandlung von Dyslipidämien und Glitazonen (PPAR γ) bei Diabetes mellitus Typ 2 haben bereits mehrere PPAR-Agonisten eine Arzneistoffzulassung erhalten^{14,125,126}. Sie sind in ihrer Wirksamkeit jedoch anderen Therapieoptionen unterlegen und ihre Anwendung ist zusätzlich aufgrund von Nebenwirkungen, die sich aus dem primären Wirkmechanismus dieser Substanzklassen ableiten lassen, begrenzt^{6,14}. Daher ist der Bedarf an neuen Konzepten zur selektiven Modulation der PPARs unter Vermeidung der klassenspezifischen Nebenwirkungen groß und neben neuen potenziellen Indikationsgebieten für PPAR-Liganden in den Fokus der aktuellen Forschung gerückt¹⁴. Demgegenüber steht die andere Hälfte der NRs, deren Funktionen noch nicht umfassend verstanden sind und deren endogene Liganden meist noch nicht identifiziert werden konnten, weshalb sie auch Waisenrezeptoren genannt werden^{9,15,16}. Nurr1 ist ein solcher NR, dem großes therapeutisches Potential bei neurodegenerativen Erkrankungen wie dem Morbus Parkinson, der Alzheimer-Demenz und der Multiplen Sklerose zugeschrieben wird¹⁹⁻²¹. Als konstitutiv aktiver NR wird Nurr1 hauptsächlich im ZNS, und dort vor allem in dopaminergen Neuronen, exprimiert, wo er nach aktuellen Erkenntnissen neuroprotektive und antientzündliche Effekte vermittelt¹⁹. Die Funktionen des Rezeptors sind bislang allerdings überwiegend durch *Knockout*-Studien untersucht worden, da geeignete chemische Tools zur spezifischen pharmakologischen Kontrolle der Nurr1-Aktivität fehlen. Die strukturellen Kenntnisse über die Ligandenbindungsstellen innerhalb der Nurr1-Ligandenbindedomäne (LBD) sind begrenzt und das Wissen über molekulare Mechanismen und Interaktionspartner ist unvollständig, was die Entwicklung von Nurr1-Liganden erschwert. Trotz der jüngsten Entdeckungen potenzieller endogener Liganden^{347,390,416} und der Erkenntnisse zu einer direkten Interaktion der Nurr1-LBD mit kleinen, wirkstoffartigen Molekülen^{389,400,422}, mangelt es daher an ausreichend potenten und selektiven synthetischen Nurr1-Agonisten und inversen Agonisten, um die Nurr1-Modulation als neues therapeutisches Konzept zu validieren. Ziel dieser Arbeit war daher die Identifikation, Entwicklung und Charakterisierung neuer *tool compounds* für die PPARs und Nurr1.

Das Konzept der Photopharmakologie eröffnet neue Möglichkeiten in der zeitlichen und räumlichen Auflösung und Präzision der biologischen Effekte von wirkstoffartigen Molekülen^{26,27}. Dieses Prinzip erschien für die Anwendung auf die PPARs sehr attraktiv, um neue Wege in der Modulation dieser NRs zu beschreiten. Zwei Projekte dieser Arbeit befassten sich daher mit der Anwendung dieses Prinzips auf PPAR-Liganden. Mit Hilfe computergestützten Designs wurden photoschaltbare PPAR-Agonisten, sog. Photohormone, entwickelt, die die Möglichkeit zur zeitlichen und räumlichen Kontrolle der Rezeptoraktivität mit sich bringen. Durch das Einführen eines Azobenzens in den lipophilen Teil bekannter PPAR-Agonisten erhielten die Moleküle die Eigenschaft durch Licht verschiedener Wellenlängen reversibel von dem energetisch begünstigten *trans*-Isomer in das entsprechende *cis*-Isomer umwandelbar zu sein. Die auf diese Weise erhaltenen Photohormone wurden anschließend durch geeignete aus Docking-

Studien abgeleitete Modifikationen in Bezug auf die Selektivität für einen der drei PPAR-Subtypen und die präferierte Aktivität einer der beiden Konfigurationen optimiert. Als Leitstruktur für PPAR γ diente dabei der potente Arzneistoff Rosiglitazon²⁹³ (**3**). Für PPAR α und - δ wurde der pan-PPAR-Agonist GL479⁴⁶⁶ (**29**) als Startpunkt verwendet, welcher bereits über eine Azogruppe verfügte (Abbildung 46). Durch die terminale Erweiterung des Rosiglitazon-Azologs (**32**) in *p*-Position konnte aus drei Derivaten ein selektiver PPAR γ -Agonist (**36**) erhalten werden, dessen *cis*-Isomer den Rezeptor *in vitro* 3-fach effizienter aktivierte als das entsprechende *trans*-Isomer und somit durch Licht aktiviert werden konnte. Die Potenzen waren dabei vergleichbar und lagen im unteren mikromolaren Bereich (Abbildung 46). Mittels isothermer Titrationskalorimetrie (ITC) konnte bestätigt werden, dass nur das *cis*-Isomer die PPAR γ -LBD bindet, während *trans*-**36** keine Bindungsaffinität aufwies. Die dennoch im zellulären System beobachtete Aktivität lässt sich daher möglicherweise auf verstärkte Isomerisierung zurückführen.

Aus dem molekularen Docking von **29** in geeigneten Kristallstrukturen der PPAR α - und - δ -LBDs ergaben sich drei verschiedene Optimierungsansätze, die anhand von zehn Derivaten *in vitro* analysiert wurden. Aus diesen Untersuchungen ging durch gezielte strukturelle Modifikationen ein hochpotenter und selektiver PPAR α -Agonist (**38**) hervor, der in seiner *trans*-Konfiguration 35-mal potenter war als das entsprechende *cis*-Isomer. Außerdem wurde ein dualer PPAR α - und - δ -Agonist (**41**) mit ausgeglichenen Aktivierungseffizienzen und Potenzen an beiden Rezeptoren erhalten, dessen *trans*-Präferenz sich vor allem im Unterschied der Aktivierungseffizienzen zeigte (Abbildung 46). Das Potenzial der photoschaltbaren Liganden, wurde in einem neuen Testsystem unter Beweis gestellt, indem im zellulären Assay Fluoreszenzreporter statt der Luciferase-Reporter verwendet wurden und somit die Rezeptoraktivität in lebenden Zellen im zeitlichen Verlauf bestimmt werden konnte. Das ermöglichte eine spatio-temporale Auflösung der PPAR-Aktivierung, die durch konstitutiv aktive Modulatoren nicht möglich wäre und somit den Nutzen der neuen Liganden als wertvolle photopharmakologische Tools belegte.

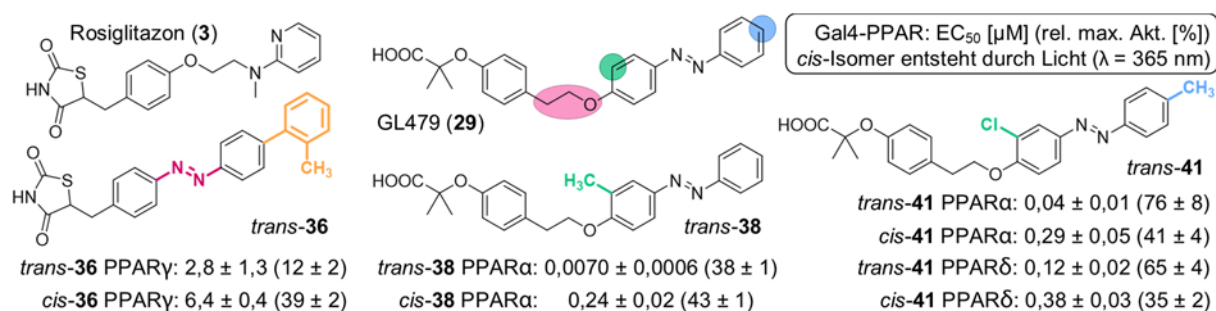


Abbildung 46: Optimierung der Leitstrukturen **3** und **29** zu photoschaltbaren PPAR-Agonisten. Die Aktivitäten wurden in Gal4-PPAR-Reporterassays bestimmt. EC₅₀-Werte sind MW ± S.E.M.; n ≥ 3. Rel. max. Aktivierung vs. 1 μM **1** (α), **2** (γ) und **16** (δ).

Neben der Photopharmakologie als neuem Modulations-Konzept für NRs ist auch die Identifikation und Charakterisierung endogener Liganden für die Entwicklung neuartiger *tool compounds* von großer Relevanz, da sie Aufschluss über den Nutzen und die Möglichkeiten einer pharmakologischen Rezeptor-modulation geben können²⁵⁹. Mit der Entdeckung der PPAR γ -Aktivierung durch oxidierte Vitamin-E-Metaboliten und den verwandten Naturstoff Garcinolsäure (**48**) konnte ein neuer Aktivierungsmechanismus aufgedeckt und anhand von **48** näher analysiert werden. *In vitro* führte die gleichzeitige Inkubation mit **48** und dem orthosterischen Agonisten Pioglitazon (**2**) zu einer additiven PPAR γ -Aktivierung und deutete auf die Bindung verschiedener Bindestellen hin. Eine Analyse des PPAR γ -Co-Regulator-Interaktionsprofils in Gegenwart der beiden Agonisten im zellfreien System zeigte erstaunliche Effekte, indem durch den Agonisten **48** die Co-Repressoren NCoR1 und SMRT rekrutiert und die Co-Aktivatoren CBP, PGC-1 α , NCoA6 und DRIP-2 verdrängt wurden, während **2** sich genau

gegensätzlich verhielt. Das Lösen einer Co-Kristallstruktur der PPAR γ -LBD im Komplex mit **48** lieferte eine Erklärung für dieses ungewöhnliche Verhalten. Die PPAR γ -LBD zeigte dabei eine typisch aktive Konformation wie im Komplex mit dem Agonisten **3**, wobei ein Molekül **48** in der orthosterischen Bindetasche mit seiner Säurefunktion die kanonische Aktivierungstetrad koordinierte. Zusätzlich war allerdings noch ein zweites Molekül **48** in einer allosterischen Bindetasche vorzufinden, welche den ausgedehnten lipophilen Raum im Anschluss an die klassische orthosterische Tasche ausfüllte. Eine Genexpressionsanalyse in humanen Hepatozyten zeigte, dass sich dieser besondere Aktivierungsmechanismus von **48** auch in der Modulation der PPAR γ -regulierten Genexpression widerspiegelte und erheblich differenzierter war als das Profil von **2**. Möglicherweise lässt sich aus dem selektiven Adressieren dieser allosterischen Bindestelle zukünftig eine therapeutische Anwendung ableiten, die das Potenzial der PPAR γ Aktivierung besser ausschöpft als es bisherige orthosterische PPAR γ -Agonisten tun. Mit der Entwicklung von Photohormonen für PPARs und der umfassenden molekularen Charakterisierung der PPAR γ -Modulation durch das Vitamin-E-Mimetikum **48** hat die vorliegende Arbeit somit wichtige neue Erkenntnisse und chemische Tools für diese vermeintlich umfassend studierte Familie nukleärer Rezeptoren hervorgebracht, die neue Wege zu selektiver PPAR-Modulation eröffnen.

Aufgrund der wenigen bekannten Nurr1-Liganden, die als Anhaltspunkte zu Beginn dieser Arbeit zur Verfügung standen, sollten verschiedene Strategien zur Identifikation und Entwicklung neuer *tool compounds* verfolgt werden, um den Strukturraum schnell und divers erweitern zu können. Der erste Ansatz wurde inspiriert von den ersten ligandengebundenen Co-Kristallstrukturen der Nurr1-LBD im Komplex mit den Prostaglandinen A1⁴¹⁹ und A2⁴²⁰. Die potenziell endogenen Nurr1-Liganden sind Entzündungsmediatoren, die aus mehrfach ungesättigten Fettsäuren mittels Umwandlung durch die Cyclooxygenasen (COX) 1 und 2 hervorgehen^{489,490}. Daher entstand die Hypothese, dass synthetische COX-Inhibitoren, auch bekannt als nichtsteroidale Antirheumatika (NSARs), Nurr1 modulieren könnten. *In vitro* Untersuchungen (Gal4-Testsystem) bestätigten diese Vermutung und aufgrund der hohen konstitutiven Nurr1-Aktivität konnte eine bidirektionale Modulation beobachtet werden. Aus 39 strukturell diversen NSARs wurden zwei aktivierende (Meclofenaminsäure (**49**) und Aceclofenac (**54**)) und vier inhibierende (Meloxicam (**50**), Oxaprozin (**51**), Parecoxib (**52**) und Valdecoxib (**53**)) Substanzen identifiziert, wovon die potentesten und effizientesten Vertreter (**49**, **51** und **52**) verwendet wurden, um Co-Regulator-Interaktionen und Dimerisierungsverhalten von Nurr1 zu studieren (Abbildung 47). Neben zwei bekannten Interaktionen^{343,349} mit den Co-Repressoren NCoR1 und SMRT, konnten NCoA6 und NRIP1 als weitere Co-Regulatoren von Nurr1 identifiziert werden. Überraschenderweise zeigten **49**, **51** und **52** im zellfreien System ein ähnliches Profil, indem alle vier Co-Regulatoren von der Nurr1-LBD verdrängt wurden. Diese Diskrepanz wurde am Vollängenrezeptor Nurr1 anhand der drei nativen *Response*-Elemente (REs) entsprechend den Aktivitäten als Monomer, Homodimer und RXR-Heterodimer näher analysiert. Damit konnten **51** und **52** als inverse Nurr1-Agonisten an allen drei REs bestätigt werden. **49** hingegen zeigte ein differenzierteres Aktivitätsprofil, da kein Effekt am Nurr1-Monomer zu erkennen war, während die Aktivität beider Dimere dosisabhängig reduziert wurde. Trotz der fehlenden Aktivität am Monomer-RE deuteten weitere Untersuchungen auf eine Monomerpräferenz von **49** hin. Durch die gleichzeitige Inkubation mit einem der NSARs und dem publizierten Nurr1-Agonisten Amodiaquin (AQ, **19**) in den verschiedenen Nurr1-Reporterassays konnte schließlich die These von zwei unabhängigen Bindestellen innerhalb der Nurr1-LBD gestützt werden. Mit den NSARs als den ersten inversen Nurr1-Agonisten konnte somit gezeigt werden, dass die hohe konstitutive Nurr1-Aktivität bidirektional moduliert werden kann, und dass sowohl das Co-Regulator-Rekrutierungsprofil als auch das Dimerisierungsverhalten an der Vermittlung von Ligand-Effekten entscheidend beteiligt sind.

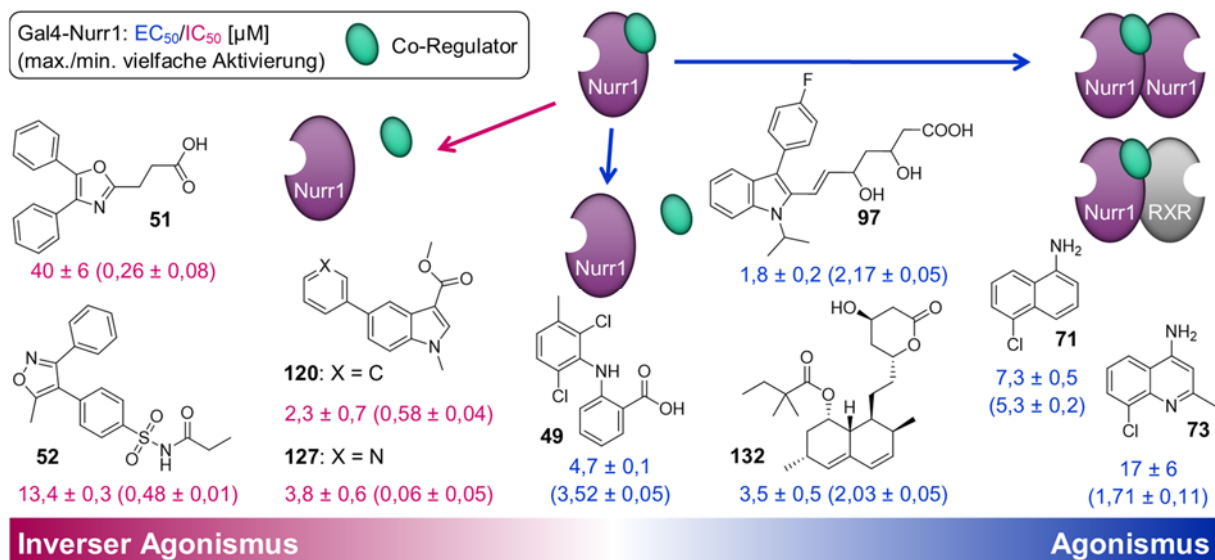


Abbildung 47: Modell der Nurr1-Modulation durch niedermolekulare Liganden. Die Aktivitäten wurden im Gal4-Nurr1-Reportergenassay bestimmt. EC_{50}/IC_{50} -Werte sind $MW \pm S.E.M.$; $n \geq 3$. Max./min. vielfache Akt. vs. DMSO (0,1 %).

Der zweite Ansatz zur Identifikation neuer Nurr1-Liganden beruhte auf den synthetischen Liganden AQ (19) und Chloroquin (25)^{389,400}. Bekannt als alte Antimalariawirkstoffe, sind beide Substanzen moderate Nurr1-Agonisten (EC_{50} Nurr1: 36 μ M (19), 47 μ M (25))⁴⁴⁴ mit zahlreichen unspezifischen Effekten^{400,404–414}, die den Einsatz als *tool compounds* für Nurr1 erschweren. Eine Evaluation der einzelnen Strukturmerkmale dieses Chemotyps zeigte, dass das gemeinsame 7-Chlorochinolin-4-amin (57) Grundgerüst von 19 und 25 ausreichend ist, um Nurr1 zu aktivieren (EC_{50} Nurr1: 259 μ M). Daraufhin wurde 57 in einem Fragment-basierten Ansatz durch systematische Veränderungen im Substitutionsmuster und Zweiringsystem in seinem Nurr1-Agonismus optimiert. Die beiden potentesten Fragmente 71 und 73 zeigten dabei eine 35- bzw. 15-fach gesteigerte Potenz im Vergleich zum Startfragment 57 und übertrafen damit sogar 19 und 25 (Abbildung 47). Der agonistische Charakter bestätigte sich durch eine vermehrte Rekrutierung der Co-Regulatoren NCoR1 und SMRT und gesteigerte Bildung des Nurr1-Homodimers im zellfreien System. Außerdem aktivierten beide Fragmente den Volllängenrezeptor Nurr1 an allen drei nativen REs und induzierten deutlich die Genexpression Nurr1-abhängiger dopaminergischer Gene in humanen Astrozyten. Die Nurr1-Agonisten 71 und 73 zeigten damit ein geeignetes Profil, um als neue Tools für Nurr1 zu dienen, und sind gleichzeitig durch ihren Fragment-Charakter attraktive Startpunkte für die Entwicklung neuer Nurr1-Liganden.

Die dritte Strategie der Suche nach Nurr1-Liganden umfasste ein breitangelegtes *in vitro* Screening (Gal4-Assay), bei dem eine Bibliothek von 480 Arzneistoff-Fragmenten auf ihre Nurr1-modulatorische Aktivität getestet wurde. Aus 24 primären Treffern (Reporteraktivität $\geq 1,50$ oder $\leq 0,60$) konnten sieben Fragmente (90–96; vier aktivierende, drei inhibierende) als Nurr1-Modulatoren im Gal4-Testsystem validiert werden. Aus den Ergebnissen des Screenings gingen anschließend zwei Projekte hervor, wobei zum einen inverse Nurr1-Agonisten mit Indol-Grundgerüst aus Fragment 95 entwickelt und charakterisiert wurden, und zum anderen die Arzneistoffklasse der Statine als neue Nurr1-Agonisten identifiziert und diese Aktivität auf ihre mögliche biologische Relevanz hin untersucht werden konnte.

Der Indol-3-carbonsäure-methylester (95) bot sich aufgrund seiner geringen Größe als günstiger Startpunkt für eine klassisch systematische Analyse der SAR des inversen Agonismus an Nurr1 an. Durch schrittweise Substitution aller freien Positionen am Indol-Grundgerüst wurden anhand von 28 Derivaten die 1- und 5-Position als vielversprechend für strukturelle Erweiterungen identifiziert. Dabei zeigte sich anschließend eine Präferenz für starre Biarylsysteme für die Erweiterung in 5-Position und ein N-Methyl-Substituent konnte die Potenz zusätzlich um das 2-Fache steigern. Die Suche nach einem

adäquaten Ersatz für den metabolisch labilen Methylester anhand von zehn weiteren Derivaten war jedoch nicht erfolgreich. Mit **120** und **127** gingen zwei potente inverse Nurr1-Agonisten aus dieser umfangreichen SAR-Studie hervor, die die NSARs etwa um den Faktor 10 in ihrer Potenz überstiegen (Abbildung 47). Auch die Indol-basierten inversen Agonisten scheinen eine andere Bindestelle zu adressieren als die Liganden vom AQ-Chemotyp, was Kreuztitrationsexperimente im Gal4-Assay andeuteten. Der inverse Agonismus von **127** wurde durch Verdrängung der Co-Repressoren NCoR1 und SMRT von der Nurr1-LBD im zellfreien System charakterisiert, während kein Einfluss auf NCoA6 zu erkennen war. Außerdem wurde die Bildung des Homodimers durch **127** dosisabhängig verhindert. Erstaunlich war jedoch, dass **120** und **127**, im Unterschied zu den NSARs, nur die Aktivität des Monomers im Nurr1-Vollängenassay reduzieren konnten. Am Homo- und Heterodimer-RE zeigte sich keine Aktivität. Durch reduzierte Expression Nurr1-abhängiger Gene in humanen Astrozyten und gesteigerte Freisetzung von Interleukin (IL) 6 nach LPS-Stimulation von Astrozyten konnten die inversen Nurr1-Agonisten **120** und **127** zusätzlich als hilfreiche *tool compounds* für *in vitro* Studien validiert werden.

Der agonistische Screeninghit 3-(4-Fluorophenyl)-1*H*-indol (**91**), welcher sich von dem Arzneistoff Fluvastatin (**97**) ableitet, inspirierte dazu alle sieben zugelassenen Statine auf ihre Aktivität an Nurr1 im Gal4-Testsystem zu untersuchen. Dabei wiesen sechs Statine einen Nurr1-Agonismus mit teils beachtlichen Potenzen im unteren mikromolaren bis nanomolaren Bereich auf. Nur Pravastatin (**133**) zeigte keine Aktivität an Nurr1 *in vitro*. Anhand der beiden effizientesten Vertreter, **97** und Simvastatin (**132**), wurde der Einfluss der Statine auf das Co-Regulator-Interaktionsprofil und Dimerisierungsverhalten von Nurr1 analysiert (Abbildung 47). Im zellfreien System verdrängten beide Statine die Co-Regulatoren NCoR1, SMRT, NCoA6 und NRIP1 von der Nurr1-LBD und unterdrückten die Homodimerisierung, wobei **132** jeweils größere Effekte zeigte als **97**. Im Unterschied zu den zuvor dargestellten inversen Agonisten, die vergleichbare Einflüsse auf die Co-Regulator-Interaktionen aufwiesen, aktivierten **97** und **132** jedoch den Vollängenrezeptor Nurr1 an allen drei nativen REs, wodurch abermals eine neue Variante der Nurr1-Modulation beobachtet werden konnte. Da zahlreiche Untersuchungen *in vitro* und *in vivo* den Statinen, und besonders **132**, bereits neuroprotektive Effekte bescheinigen konnten⁵⁰⁵⁻⁵¹⁰, Cholesterin-abhängige Mechanismen diese Wirkungen aber nicht alleine erklären können⁵⁰⁰⁻⁵⁰², wurden die biologischen Effekte und eine mögliche Relevanz des Nurr1-Agonismus durch **132** näher untersucht. In humanen Astrozyten konnte mittels Nurr1-*Knockdown* (siRNA-vermittelt), welcher nach LPS-Stimulation eine erhebliche Steigerung der IL-6-Freisetzung bewirkte, die Reduktion des IL-6-Spiegels durch **132** als Nurr1-vermittelt angenommen werden. Basierend darauf wurde eine umfassende Genexpressionsanalyse in der gleichen Zelllinie durchgeführt. Dabei bestätigte sich die Vermutung, dass allein der Nurr1-*Knockdown* in Astrozyten Neuroinflammation induzierte. Außerdem zeigte sich, dass **132**, neben Wirkungen auf andere Signalwege, auch zahlreiche neuroprotektive Effekte in Abhängigkeit von Nurr1 vermitteln konnte. Zum einen fiel die Regulation von Genen auf, die an Glukose-Verwertung und Energiegewinnung beteiligt sind. Zum anderen zeigte sich ein antientzündliches und antiapoptisches Genexpressionsprofil durch **132**, sowie ein Einfluss auf Gene der Zellzyklus-Kontrolle. Somit scheint der Nurr1-Agonismus der Statine, neben anderen bekannten Mechanismen⁵¹¹⁻⁵¹⁵, möglicherweise maßgeblich für die neuroprotektiven und antineuroinflammatorischen Wirkungen verantwortlich zu sein.

Mit der Entwicklung und Charakterisierung von Liganden für den neuroprotektiven Transkriptionsfaktor Nurr1 hat die vorliegende Arbeit daher wichtige chemisch diverse Tools und neue Erkenntnisse zum molekularen Mechanismus der Nurr1-Modulation hervorgebracht, die entscheidend zur Validierung dieses vielversprechenden Targets bei neurodegenerativen Erkrankungen beitragen können.

5. English Summary

Nuclear receptors (NRs) are ligand-activated transcription factors involved in the regulation of numerous (patho)physiological processes, such as cell differentiation, metabolism, and inflammation, thus representing attractive therapeutic targets^{1,2,15}. Among them, the peroxisome proliferator-activated receptors (PPARs) α , γ , and δ belong to the well-studied NRs. As lipid sensors, they mainly exert metabolic functions in glucose and lipid metabolism and synthetic PPAR agonists (PPAR α : fibrates, PPAR γ : glitazones) have received drug approval¹⁴. However, their therapeutic application is limited due to lower efficacy compared to alternative options and undesirable side effects caused by their primary mode of action^{6,14}. New concepts to selectively modulate the PPARs while avoiding the class-specific side effects are therefore urgently needed¹⁴.

For the second half of the NR family, the so-called orphan receptors, roles and functions are not comprehensively studied, yet^{9,15,16}. Among them, Nurr1 is considered to have great therapeutic potential in neurodegenerative diseases such as Parkinson's disease, Alzheimer's disease, and multiple sclerosis¹⁹⁻²¹. The constitutively active NR is mainly expressed in the central nervous system – especially in dopaminergic neurons – where it seems to mediate neuroprotective and anti-inflammatory effects¹⁹. Despite recent findings of potential endogenous ligands^{347,390,416} and evidence for a direct interaction of the Nurr1 ligand-binding domain (LBD) with small, drug-like molecules^{389,400,422}, there is a lack of suitable chemical tools to validate Nurr1 modulation as a novel therapeutic approach. Accordingly, the aim of this thesis was to identify, develop, and characterize new tool compounds for the PPARs and Nurr1.

The concept of photopharmacology opens new possibilities in the temporal and spatial control of biological effects of drug-like molecules^{26,27}, which made it attractive for application to PPARs. Computer-aided design was used to develop azobenzene-based photoswitchable PPAR agonists from the PPAR γ agonist rosiglitazone²⁹³ (**3**) and the pan-PPAR agonist GL479⁴⁶⁶ (**29**), which were subsequently optimized for subtype selectivity and preferred activity of either configuration. The rosiglitazone azolog **36** was obtained by terminal extension as a *cis*-preferential PPAR γ selective agonist that could be activated by light. Based on **29**, targeted structural modifications resulted firstly in **38** as a highly potent and selective PPAR α agonist, whose *trans* configuration exhibited 35-fold higher potency than the *cis*-counterpart. Secondly, a dual *trans*-preferential PPAR α - and - δ -agonist (**41**) with balanced activation efficiencies and potencies at both receptors was developed. In a dedicated fluorescent reporter gene assay, these new photopharmacological tools allowed for the control of PPAR activity in living cells over time.

In addition to photopharmacology as a new strategy in the field of NRs, the identification and characterization of endogenous ligands is also of great relevance²⁵⁹. The discovery of PPAR γ activation by the vitamin E metabolite garcinoic acid (**48**) revealed a new activation mechanism with a distinct co-regulator interaction profile. A co-crystal structure of the PPAR γ LBD in complex with **48** demonstrated that **48** addresses the orthosteric as well as an allosteric binding site. Gene expression analysis in human hepatocytes showed that the special PPAR activation mechanism of **48** was also reflected in differential modulation of PPAR γ -regulated gene expression, potentially suggesting therapeutic implications for selectively addressing this allosteric binding site.

Nurr1 appears to hold great therapeutic potential but there is a lack of Nurr1 ligands as tools. The search for new Nurr1 modulators by various strategies was hence a major topic of this thesis. The first approach to Nurr1 ligand discovery was inspired by the prostaglandins A1⁴¹⁹ and A2⁴²⁰ as potential endogenous

Nurr1 ligands, which are inflammatory mediators generated by cyclooxygenase (COX) 1 and 2 activity^{489,490}. Therefore, it was hypothesized that synthetic COX inhibitors, also known as nonsteroidal anti-inflammatory drugs (NSAIDs), might modulate Nurr1, and screening of 39 structurally diverse NSAIDs for Nurr1 activity confirmed this assumption. Meclofenamic acid (**49**) was discovered as a differential Nurr1 modulator, oxaprozin (**51**) and parecoxib (**52**) emerged as the first-in-class inverse Nurr1 agonists demonstrating that the high constitutive Nurr1 activity can be modulated bidirectionally. Further studies with NSAIDs as tools showed that both the co-regulator recruitment profile and dimerization equilibria of Nurr1 are critically involved in mediating ligand effects.

The second approach to Nurr1 modulators was based on the old antimalarials amodiaquine (**19**) and chloroquine (**25**), which have been reported as weak Nurr1 agonists^{389,400} (EC_{50} Nurr1: 36 μ M (**19**), 47 μ M (**25**))⁴⁴⁴ but are inappropriate as tool compounds for Nurr1 due to numerous nonspecific effects^{400,404-414}. Evaluation of the individual structural features of this chemotype showed that the shared 7-chloroquinoline-4-amine (**57**) scaffold of **19** and **25** is sufficient to activate Nurr1 (EC_{50} Nurr1: 259 μ M). Structural modifications of the scaffold resulted in **71** and **73** as potent Nurr1 agonists (EC_{50} Nurr1: 7.3 μ M (**71**), 17 μ M (**73**)), even exceeding the lead structures **19** and **25** in potency. Nurr1 agonism by both tools has been confirmed in several orthogonal systems. **71** and **73** hence are useful Nurr1 agonist tools and attractive leads for the development of Nurr1 ligands but also enabled important insights in Nurr1 activation mechanisms.

The third strategy in the search for Nurr1 ligands involved a broad *in vitro* screening in which 480 drug fragments were assayed for their Nurr1 modulatory activity. From this, indole-3-carboxylic acid methyl ester (**95**) emerged as an inverse agonist hit and, because of its low molecular weight, presented as attractive starting point for systematic structure-activity relationship and optimization. By successive substitution of every free position on the indole scaffold, the 1- and 5-positions were identified as promising for structural extensions. Further optimizations resulted in the rigid biaryl systems **120** and **127** as potent inverse Nurr1 agonists that exceed NSAIDs in potency by a factor of 10. Both caused a co-regulator interaction profile similar to the NSAIDs, but interestingly revealed differences in their activity on the three Nurr1 response elements. Evaluation of **120** and **127** in human astrocytes showed biological effects mimicking Nurr1 knockdown thus validating the inverse agonists as useful tool compounds for *in vitro* studies.

In addition to the inverse agonists, the fluvastatin (**97**) fragment 3-(4-fluorophenyl)-1*H*-indole (**91**) emerged as a Nurr1 agonist from the screening. Of the seven approved statins subsequently studied, six showed Nurr1 agonism in the Gal4 assay with considerable potencies (EC_{50} 0.12–23 μ M). The mechanistic evaluation of the two most efficient representatives, **97** and simvastatin (**132**), revealed another variety of Nurr1 activation in terms of effects on the co-regulator interaction profile and dimerization equilibria. Moreover, in-depth analysis of the effects of **132** or siRNA-mediated Nurr1 knockdown in astrocytes demonstrated anti-inflammatory and anti-apoptotic effects on gene expression as well as a regulation of metabolic pathways as Nurr1 mediated neuroprotective effects⁵⁰⁵⁻⁵¹⁰ of **132**. These findings provide improved understanding of the attractive therapeutic potential of statins in neurodegeneration.

Using various strategies and techniques, this thesis has yielded diverse chemical tools for the nuclear receptors PPAR and Nurr1 and with their help elucidated the molecular mechanisms of PPAR and Nurr1 modulation. The results importantly contribute to the validation of the transcription factors as promising therapeutic targets especially in neurodegenerative diseases.

6. Literaturverzeichnis

- (1) Aranda, A.; Pascual, A. Nuclear Hormone Receptors and Gene Expression. *Physiol. Rev.* **2001**, *81* (3), 1269–1304.
- (2) Gronemeyer, H.; Gustafsson, J.-A.; Laudet, V. Principles for Modulation of the Nuclear Receptor Superfamily. *Nat. Rev. Drug Discov.* **2004**, *3* (11), 950–964.
- (3) Imming, P.; Sinning, C.; Meyer, A. Drugs, Their Targets and the Nature and Number of Drug Targets. *Nat. Rev. Drug Discov.* **2006**, *5* (10), 821–834.
- (4) Querfeld, C.; Nagelli, L. V.; Rosen, S. T.; Kuzel, T. M.; Guitart, J. Bexarotene in the Treatment of Cutaneous T-Cell Lymphoma. *Expert Opin. Pharmacother.* **2006**, *7* (7), 907–915.
- (5) Markham, A.; Keam, S. J. Obeticholic Acid: First Global Approval. *Drugs* **2016**, *76*, 1221–1226.
- (6) Moore, J. T.; Collins, J. L.; Pearce, K. H. The Nuclear Receptor Superfamily and Drug Discovery. *ChemMedChem* **2006**, *1* (5), 504–523.
- (7) de Lera, A. R.; Bourguet, W.; Altucci, L.; Gronemeyer, H. Design of Selective Nuclear Receptor Modulators: RAR and RXR as a Case Study. *Nat. Rev. Drug Discov.* **2007**, *6* (10), 811–820.
- (8) Wurtz, J.-M.; Bourguet, W.; Renaud, J.-P.; Vivat, V.; Chambon, P.; Moras, D.; Gronemeyer, H. A Canonical Structure for the Ligand-Binding Domain of Nuclear Receptors. *Nat. Struct. Biol.* **1996**, *3* (1), 87–94.
- (9) Weikum, E. R.; Liu, X.; Ortlund, E. A. The Nuclear Receptor Superfamily: A Structural Perspective. *Protein Sci.* **2018**, *27* (11), 1876–1892.
- (10) Proschak, E.; Heitel, P.; Kalinowsky, L.; Merk, D. Opportunities and Challenges for Fatty Acid Mimetics in Drug Discovery. *J. Med. Chem.* **2017**, *60* (13), 5235–5266.
- (11) Zhao, X.; Cho, H.; Yu, R. T.; Atkins, A. R.; Downes, M.; Evans, R. M. Nuclear Receptors Rock around the Clock. *EMBO Rep.* **2014**, *15* (5), 518–528.
- (12) Montaigne, D.; Butruille, L.; Staels, B. PPAR Control of Metabolism and Cardiovascular Functions. *Nat. Rev. Cardiol.* **2021**, *18* (12), 809–823.
- (13) Benedetti, E.; Cristiano, L.; Antonosante, A.; D'Angelo, M.; D'Angelo, B.; Selli, S.; Castelli, V.; Ippoliti, R.; Giordano, A.; Cimini, A. PPARs in Neurodegenerative and Neuroinflammatory Pathways. *Curr. Alzheimer Res.* **2018**, *15* (4), 336–344.
- (14) Cheng, H. S.; Tan, W. R.; Low, Z. S.; Marvalim, C.; Lee, J. Y. H.; Tan, N. S. Exploration and Development of PPAR Modulators in Health and Disease: An Update of Clinical Evidence. *Int. J. Mol. Sci.* **2019**, *20* (20), 5055.
- (15) Evans, R. M.; Mangelsdorf, D. J. Nuclear Receptors, RXR, and the Big Bang. *Cell* **2014**, *157* (1), 255–266.
- (16) Benoit, G.; Cooney, A.; Giguere, V.; Ingraham, H.; Lazar, M.; Muscat, G.; Perlmann, T.; Renaud, J.-P.; Schwabe, J.; Sladek, F.; Tsai, M.-J.; Laudet, V. International Union of Pharmacology. LXVI. Orphan Nuclear Receptors. *Pharmacol. Rev.* **2006**, *58* (4), 798–836.
- (17) Gallastegui, N.; Mackinnon, J. A. G.; Fletterick, R. J.; Estébanez-Perpiñá, E. Advances in Our

- Structural Understanding of Orphan Nuclear Receptors. *Trends Biochem. Sci.* **2015**, *40* (1), 25–35.
- (18) Arrowsmith, C. H.; Audia, J. E.; Austin, C.; Baell, J.; Bennett, J.; Blagg, J.; Bountra, C.; Brennan, P. E.; Brown, P. J.; Bunnage, M. E.; Buser-Doepner, C.; Campbell, R. M.; Carter, A. J.; Cohen, P.; Copeland, R. A.; Cravatt, B.; Dahlin, J. L.; Dhanak, D.; Edwards, A. M.; et al. The Promise and Peril of Chemical Probes. *Nat. Chem. Biol.* **2015**, *11* (8), 536–541.
- (19) Decressac, M.; Volakakis, N.; Björklund, A.; Perlmann, T. NURR1 in Parkinson Disease - From Pathogenesis to Therapeutic Potential. *Nat. Rev. Neurol.* **2013**, *9* (11), 629–636.
- (20) Jeon, S. G.; Yoo, A.; Chun, D. W.; Hong, S. B.; Chung, H.; Kim, J.-I.; Moon, M. The Critical Role of Nurr1 as a Mediator and Therapeutic Target in Alzheimer's Disease-Related Pathogenesis. *Aging Dis.* **2020**, *11* (3), 705.
- (21) Jakaria, M.; Haque, M. E.; Cho, D.-Y.; Azam, S.; Kim, I.-S.; Choi, D.-K. Molecular Insights into NR4A2(Nurr1): An Emerging Target for Neuroprotective Therapy Against Neuroinflammation and Neuronal Cell Death. *Mol. Neurobiol.* **2019**, *56* (8), 5799–5814.
- (22) Jones, L. H.; Bunnage, M. E. Applications of Chemogenomic Library Screening in Drug Discovery. *Nat. Rev. Drug Discov.* **2017**, *16* (4), 285–296.
- (23) Bunnage, M. E.; Chekler, E. L. P.; Jones, L. H. Target Validation Using Chemical Probes. *Nat. Chem. Biol.* **2013**, *9* (4), 195–199.
- (24) Weiss, W. A.; Taylor, S. S.; Shokat, K. M. Recognizing and Exploiting Differences between RNAi and Small-Molecule Inhibitors. *Nat. Chem. Biol.* **2007**, *3* (12), 739–744.
- (25) Baell, J. B.; Holloway, G. A. New Substructure Filters for Removal of Pan Assay Interference Compounds (PAINS) from Screening Libraries and for Their Exclusion in Bioassays. *J. Med. Chem.* **2010**, *53* (7), 2719–2740.
- (26) Szymański, W.; Beierle, J. M.; Kistemaker, H. A. V.; Velema, W. A.; Feringa, B. L. Reversible Photocontrol of Biological Systems by the Incorporation of Molecular Photoswitches. *Chem. Rev.* **2013**, *113* (8), 6114–6178.
- (27) Hüll, K.; Morstein, J.; Trauner, D. In Vivo Photopharmacology. *Chem. Rev.* **2018**, *118* (21), 10710–10747.
- (28) Banghart, M.; Borges, K.; Isacoff, E.; Trauner, D.; Kramer, R. H. Light-Activated Ion Channels for Remote Control of Neuronal Firing. *Nat. Neurosci.* **2004**, *7* (12), 1381–1386.
- (29) Broichhagen, J.; Schönberger, M.; Cork, S. C.; Frank, J. A.; Marchetti, P.; Bugliani, M.; Shapiro, A. M. J.; Trapp, S.; Rutter, G. A.; Hodson, D. J.; Trauner, D. Optical Control of Insulin Release Using a Photoswitchable Sulfonylurea. *Nat. Commun.* **2014**, *5*, 5116.
- (30) Quandt, G.; Höfner, G.; Pabel, J.; Dine, J.; Eder, M.; Wanner, K. T. First Photoswitchable Neurotransmitter Transporter Inhibitor: Light-Induced Control of γ -Aminobutyric Acid Transporter 1 (GAT1) Activity in Mouse Brain. *J. Med. Chem.* **2014**, *57* (15), 6809–6821.
- (31) Cheng, B.; Shchepakin, D.; Kavanaugh, M. P.; Trauner, D. Photoswitchable Inhibitor of a Glutamate Transporter. *ACS Chem. Neurosci.* **2017**, *8* (8), 1668–1672.
- (32) Cheng, B.; Morstein, J.; Ladefoged, L. K.; Maesen, J. B.; Schiøtt, B.; Sinning, S.; Trauner, D. A

- Photoswitchable Inhibitor of the Human Serotonin Transporter. *ACS Chem. Neurosci.* **2020**, *11* (9), 1231–1237.
- (33) Broichhagen, J.; Damijonaitis, A.; Levitz, J.; Sokol, K. R.; Leippe, P.; Konrad, D.; Isacoff, E. Y.; Trauner, D. Orthogonal Optical Control of a G Protein-Coupled Receptor with a SNAP-Tethered Photochromic Ligand. *ACS Cent. Sci.* **2015**, *1* (7), 383–393.
- (34) Morstein, J.; Dacheux, M. A.; Norman, D. D.; Shemet, A.; Donthamsetti, P. C.; Citir, M.; Frank, J. A.; Schultz, C.; Isacoff, E. Y.; Parrill, A. L.; Tigyi, G. J.; Trauner, D. Optical Control of Lysophosphatidic Acid Signaling. *J. Am. Chem. Soc.* **2020**, *142* (24), 10612–10616.
- (35) Prischich, D.; Gomila, A. M. J.; Milla-Navarro, S.; Sangüesa, G.; Diez-Alarcia, R.; Preda, B.; Matera, C.; Batlle, M.; Ramírez, L.; Giralt, E.; Hernando, J.; Guasch, E.; Meana, J. J.; de la Villa, P.; Gorostiza, P. Adrenergic Modulation With Photochromic Ligands. *Angew. Chemie Int. Ed.* **2021**, *60* (7), 3625–3631.
- (36) Velema, W. A.; van der Berg, J. P.; Hansen, M. J.; Szymanski, W.; Driessen, A. J. M.; Feringa, B. L. Optical Control of Antibacterial Activity. *Nat. Chem.* **2013**, *5* (11), 924–928.
- (37) Tsai, Y.-H.; Essig, S.; James, J. R.; Lang, K.; Chin, J. W. Selective, Rapid and Optically Switchable Regulation of Protein Function in Live Mammalian Cells. *Nat. Chem.* **2015**, *7* (7), 554–561.
- (38) Kol, M.; Williams, B.; Toombs-Ruane, H.; Franquelim, H. G.; Korneev, S.; Schroeer, C.; Schwille, P.; Trauner, D.; Holthuis, J. C.; Frank, J. A. Optical Manipulation of Sphingolipid Biosynthesis Using Photoswitchable Ceramides. *Elife* **2019**, *8*, e43230.
- (39) Morstein, J.; Impastato, A. C.; Trauner, D. Photoswitchable Lipids. *ChemBioChem* **2021**, *22* (1), 73–83.
- (40) Unsworth, A. J.; Flora, G. D.; Gibbins, J. M. Non-Genomic Effects of Nuclear Receptors: Insights from the Anucleate Platelet. *Cardiovasc. Res.* **2018**, *114* (5), 645–655.
- (41) Morstein, J.; Awale, M.; Reymond, J.-L.; Trauner, D. Mapping the Azolog Space Enables the Optical Control of New Biological Targets. *ACS Cent. Sci.* **2019**, *5* (4), 607–618.
- (42) Tsuchiya, K.; Umeno, T.; Tsuji, G.; Yokoo, H.; Tanaka, M.; Fukuhara, K.; Demizu, Y.; Misawa, T. Development of Photoswitchable Estrogen Receptor Ligands. *Chem. Pharm. Bull.* **2020**, *68* (4), 398–402.
- (43) Morstein, J.; Trads, J. B.; Hinnah, K.; Willems, S.; Barber, D. M.; Trauner, M.; Merk, D.; Trauner, D. Optical Control of the Nuclear Bile Acid Receptor FXR with a Photohormone. *Chem. Sci.* **2020**, *11* (2), 429–434.
- (44) Morstein, J.; Trauner, D. New Players in Phototherapy: Photopharmacology and Bio-Integrated Optoelectronics. *Curr. Opin. Chem. Biol.* **2019**, *50*, 145–151.
- (45) Mehta, Z. B.; Johnston, N. R.; Nguyen-Tu, M.-S.; Broichhagen, J.; Schultz, P.; Larner, D. P.; Leclerc, I.; Trauner, D.; Rutter, G. A.; Hodson, D. J. Remote Control of Glucose Homeostasis in Vivo Using Photopharmacology. *Sci. Rep.* **2017**, *7*, 291.
- (46) Borowiak, M.; Nahaboo, W.; Reynders, M.; Nekolla, K.; Jalinot, P.; Hasserodt, J.; Rehberg, M.; Delattre, M.; Zahler, S.; Vollmar, A.; Trauner, D.; Thorn-Seshold, O. Photoswitchable Inhibitors of Microtubule Dynamics Optically Control Mitosis and Cell Death. *Cell* **2015**, *162* (2), 403–411.

- (47) Babii, O.; Afonin, S.; Garmanchuk, L. V.; Nikulina, V. V.; Nikolaienko, T. V.; Storozhuk, O. V.; Shelest, D. V.; Dasyukevich, O. I.; Ostapchenko, L. I.; Iurchenko, V.; Zozulya, S.; Ulrich, A. S.; Komarov, I. V. Direct Photocontrol of Peptidomimetics: An Alternative to Oxygen-Dependent Photodynamic Cancer Therapy. *Angew. Chemie Int. Ed.* **2016**, *55* (18), 5493–5496.
- (48) Gutzeit, V. A.; Acosta-Ruiz, A.; Munguba, H.; Häfner, S.; Landra-Willm, A.; Mathes, B.; Mony, J.; Yarotski, D.; Börjesson, K.; Liston, C.; Sandoz, G.; Levitz, J.; Broichhagen, J. A Fine-Tuned Azobenzene for Enhanced Photopharmacology in Vivo. *Cell Chem. Biol.* **2021**, *28* (11), 1648–1663.e16.
- (49) Laudet, V. Evolution of the Nuclear Receptor Superfamily: Early Diversification from an Ancestral Orphan Receptor. *J. Mol. Endocrinol.* **1997**, *19* (3), 207–226.
- (50) Nuclear Receptors Nomenclature Committee. A Unified Nomenclature System for the Nuclear Receptor Superfamily. *Cell* **1999**, *97* (2), 161–163.
- (51) The UniProt Consortium. UniProt: The Universal Protein Knowledgebase in 2021. *Nucleic Acids Res.* **2021**, *49* (D1), D480–D489.
- (52) Michalik, L.; Auwerx, J.; Berger, J. P.; Chatterjee, V. K.; Glass, C. K.; Gonzalez, F. J.; Grimaldi, P. A.; Kadowaki, T.; Lazar, M. A.; O’Rahilly, S.; Palmer, C. N. A.; Plutzky, J.; Reddy, J. K.; Spiegelman, B. M.; Staels, B.; Wahli, W. International Union of Pharmacology. LXI. Peroxisome Proliferator-Activated Receptors. *Pharmacol. Rev.* **2006**, *58* (4), 726–741.
- (53) Shulman, A. I.; Larson, C.; Mangelsdorf, D. J.; Ranganathan, R. Structural Determinants of Allosteric Ligand Activation in RXR Heterodimers. *Cell* **2004**, *116* (3), 417–429.
- (54) Perlmann, T.; Jansson, L. A Novel Pathway for Vitamin A Signaling Mediated by RXR Heterodimerization with NGFI-B and NURR1. *Genes Dev.* **1995**, *9*, 769–782.
- (55) Maira, M.; Martens, C.; Philips, A.; Drouin, J. Heterodimerization between Members of the Nur Subfamily of Orphan Nuclear Receptors as a Novel Mechanism for Gene Activation. *Mol. Cell. Biol.* **1999**, *19* (11), 7549–7557.
- (56) Jiang, L.; Dai, S.; Li, J.; Liang, X.; Qu, L.; Chen, X.; Guo, M.; Chen, Z.; Chen, L.; Wei, H.; Chen, Y. Structural Basis of Binding of Homodimers of the Nuclear Receptor NR4A2 to Selective Nur-Responsive DNA Elements. *J. Biol. Chem.* **2019**, *294* (51), 19795–19803.
- (57) Robinson-Rechavi, M.; Garcia, H. E.; Laudet, V. The Nuclear Receptor Superfamily. *J. Cell Sci.* **2003**, *116* (4), 585–586.
- (58) Glass, C. K.; Saijo, K. Nuclear Receptor Transrepression Pathways That Regulate Inflammation in Macrophages and T Cells. *Nat. Rev. Immunol.* **2010**, *10* (5), 365–376.
- (59) Saijo, K.; Winner, B.; Carson, C. T.; Collier, J. G.; Boyer, L.; Rosenfeld, M. G.; Gage, F. H.; Glass, C. K. A Nurr1/CoREST Pathway in Microglia and Astrocytes Protects Dopaminergic Neurons from Inflammation-Induced Death. *Cell* **2009**, *137* (1), 47–59.
- (60) Perissi, V.; Jepsen, K.; Glass, C. K.; Rosenfeld, M. G. Deconstructing Repression: Evolving Models of Co-Repressor Action. *Nat. Rev. Genet.* **2010**, *11* (2), 109–123.
- (61) Li, L.; Liu, Y.; Chen, H.; Li, F.; Wu, J.; Zhang, H.; He, J.; Xing, Y.; Chen, Y.; Wang, W.; Tian, X.; Li, A.; Zhang, Q.; Huang, P.; Han, J.; Lin, T.; Wu, Q. Impeding the Interaction between Nur77 and P38 Reduces LPS-Induced Inflammation. *Nat. Chem. Biol.* **2015**, *11* (5), 339–346.

- (62) Lösel, R.; Wehling, M. Nongenomic Actions of Steroid Hormones. *Nat. Rev. Mol. Cell Biol.* **2003**, *4* (1), 46–55.
- (63) Ordóñez-Morán, P.; Muñoz, A. Nuclear Receptors: Genomic and Non-Genomic Effects Converge. *Cell Cycle* **2009**, *8* (11), 1675–1680.
- (64) Wang, W.; Wang, Y.; Chen, H.; Xing, Y.; Li, F.; Zhang, Q.; Zhou, B.; Zhang, H.; Zhang, J.; Bian, X.; Li, L.; Liu, Y.; Zhao, B.; Chen, Y.; Wu, R.; Li, A.; Yao, L.; Chen, P.; Zhang, Y.; et al. Orphan Nuclear Receptor TR3 Acts in Autophagic Cell Death via Mitochondrial Signaling Pathway. *Nat. Chem. Biol.* **2014**, *10* (2), 133–140.
- (65) Hu, M.; Luo, Q.; Alitongbieke, G.; Chong, S.; Xu, C.; Xie, L.; Chen, X.; Zhang, D.; Zhou, Y.; Wang, Z.; Ye, X.; Cai, L.; Zhang, F.; Chen, H.; Jiang, F.; Fang, H.; Yang, S.; Liu, J.; Diaz-Meco, M. T.; et al. Celastrol-Induced Nur77 Interaction with TRAF2 Alleviates Inflammation by Promoting Mitochondrial Ubiquitination and Autophagy. *Mol. Cell* **2017**, *66* (1), 141–153.e6.
- (66) Willems, S.; Zaienne, D.; Merk, D. Targeting Nuclear Receptors in Neurodegeneration and Neuroinflammation. *J. Med. Chem.* **2021**, *64* (14), 9592–9638.
- (67) Anbalagan, M.; Huderson, B.; Murphy, L.; Rowan, B. G. Post-Translational Modifications of Nuclear Receptors and Human Disease. *Nucl. Recept. Signal.* **2012**, *10* (1), nrs.10001.
- (68) Bain, D. L.; Heneghan, A. F.; Connaghan-Jones, K. D.; Miura, M. T. Nuclear Receptor Structure: Implications for Function. *Annu. Rev. Physiol.* **2007**, *69*, 201–220.
- (69) Laudet, V.; Gronemeyer, H. DNA Recognition by Nuclear Receptors. In *The Nuclear Receptor FactsBook*; Academic Press, 2002; pp 22–36.
- (70) Khorasanizadeh, S.; Rastinejad, F. Nuclear-Receptor Interactions on DNA-Response Elements. *Trends Biochem. Sci.* **2001**, *26* (6), 384–390.
- (71) Helsen, C.; Kerkhofs, S.; Clinckemalie, L.; Spans, L.; Laurent, M.; Boonen, S.; Vanderschueren, D.; Claessens, F. Structural Basis for Nuclear Hormone Receptor DNA Binding. *Mol. Cell. Endocrinol.* **2012**, *348* (2), 411–417.
- (72) Maletta, M.; Orlov, I.; Roblin, P.; Beck, Y.; Moras, D.; Billas, I. M. L.; Klaholz, B. P. The Palindromic DNA-Bound USP/EcR Nuclear Receptor Adopts an Asymmetric Organization with Allosteric Domain Positioning. *Nat. Commun.* **2014**, *5*, 4139.
- (73) Negishi, M.; Kobayashi, K.; Sakuma, T.; Sueyoshi, T. Nuclear Receptor Phosphorylation in Xenobiotic Signal Transduction. *J. Biol. Chem.* **2020**, *295* (45), 15210–15225.
- (74) Baumann, H.; Paulsen, K.; Kovacs, H.; Berglund, H.; Wright, A. P. H.; Gustafsson, J. A.; Haerd, T. Refined Solution Structure of the Glucocorticoid Receptor DNA-Binding Domain. *Biochemistry* **1993**, *32* (49), 13463–13471.
- (75) Rastinejad, F.; Huang, P.; Chandra, V.; Khorasanizadeh, S. Understanding Nuclear Receptor Form and Function Using Structural Biology. *J. Mol. Endocrinol.* **2013**, *51* (3), T1–T21.
- (76) Chandra, V.; Huang, P.; Hamuro, Y.; Raghuram, S.; Wang, Y.; Burriss, T. P.; Rastinejad, F. Structure of the Intact PPAR- γ -RXR- α Nuclear Receptor Complex on DNA. *Nature* **2008**, *456*, 350–356.
- (77) De Bosscher, K.; Desmet, S. J.; Clarisse, D.; Estébanez-Perpiña, E.; Brunsveld, L. Nuclear Receptor

- Crosstalk — Defining the Mechanisms for Therapeutic Innovation. *Nat. Rev. Endocrinol.* **2020**, *16* (7), 363–377.
- (78) Li, Y.; Lambert, M. H.; Xu, H. E. Activation of Nuclear Receptors: A Perspective from Structural Genomics. *Structure* **2003**, *11* (7), 741–746.
- (79) Xu, H. E.; Stanley, T. B.; Montana, V. G.; Lambert, M. H.; Shearer, B. G.; Cobb, J. E.; McKee, D. D.; Galardi, C. M.; Plunket, K. D.; Nolte, R. T.; Parks, D. J.; Moore, J. T.; Kliewer, S. A.; Willson, T. M.; Stimmel, J. B. Structural Basis for Antagonist-Mediated Recruitment of Nuclear Co-Repressors by PPAR α . *Nature* **2002**, *415*, 813–817.
- (80) Kamata, S.; Oyama, T.; Saito, K.; Honda, A.; Yamamoto, Y.; Suda, K.; Ishikawa, R.; Itoh, T.; Watanabe, Y.; Shibata, T.; Uchida, K.; Suematsu, M.; Ishii, I. PPAR α Ligand-Binding Domain Structures with Endogenous Fatty Acids and Fibrates. *iScience* **2020**, *23* (11), 101727.
- (81) Savkur, R. S.; Bramlett, K. S.; Clawson, D.; Burris, T. P. Pharmacology of Nuclear Receptor–Coregulator Recognition. In *Vitamins and Hormones*; 2004; Vol. 68, pp 145–183.
- (82) Millard, C. J.; Watson, P. J.; Fairall, L.; Schwabe, J. W. R. An Evolving Understanding of Nuclear Receptor Coregulator Proteins. *J. Mol. Endocrinol.* **2013**, *51* (3), T23–T36.
- (83) Perissi, V.; Staszewski, L. M.; McInerney, E. M.; Kurokawa, R.; Kronen, A.; Rose, D. W.; Lambert, M. H.; Milburn, M. V.; Glass, C. K.; Rosenfeld, M. G. Molecular Determinants of Nuclear Receptor–Corepressor Interaction. *Genes Dev.* **1999**, *13*, 3198–3208.
- (84) Chen, J. D.; Evans, R. M. A Transcriptional Co-Repressor That Interacts with Nuclear Hormone Receptors. *Nature* **1995**, *377*, 454–457.
- (85) Oñate, S. A.; Tsai, S. Y.; Tsai, M.-J.; O’Malley, B. W. Sequence and Characterization of a Coactivator for the Steroid Hormone Receptor Superfamily. *Science* **1995**, *270* (5240), 1354–1357.
- (86) Takeshita, A.; Yen, P. M.; Misiti, S.; Cardona, G. R.; Liu, Y.; Chin, W. W. Molecular Cloning and Properties of a Full-Length Putative Thyroid Hormone Receptor Coactivator. *Endocrinology* **1996**, *137* (8), 3594–3597.
- (87) Anzick, S. L.; Kononen, J.; Walker, R. L.; Azorsa, D. O.; Tanner, M. M.; Guan, X.-Y.; Sauter, G.; Kallioniemi, O.-P.; Trent, J. M.; Meltzer, P. S. AIB1, a Steroid Receptor Coactivator Amplified in Breast and Ovarian Cancer. *Science* **1997**, *277* (5328), 965–968.
- (88) Puigserver, P.; Wu, Z.; Park, C. W.; Graves, R.; Wright, M.; Spiegelman, B. M. A Cold-Inducible Coactivator of Nuclear Receptors Linked to Adaptive Thermogenesis. *Cell* **1998**, *92* (6), 829–839.
- (89) Heery, D. M.; Kalkhoven, E.; Hoare, S.; Parker, M. G. A Signature Motif in Transcriptional Co-Activators Mediates Binding to Nuclear Receptors. *Nature* **1997**, *387*, 733–736.
- (90) Darimont, B. D.; Wagner, R. L.; Apriletti, J. W.; Stallcup, M. R.; Kushner, P. J.; Baxter, J. D.; Fletterick, R. J.; Yamamoto, K. R. Structure and Specificity of Nuclear Receptor–Coactivator Interactions. *Genes Dev.* **1998**, *12*, 3343–3356.
- (91) Molnár, F.; Matilainen, M.; Carlberg, C. Structural Determinants of the Agonist-Independent Association of Human Peroxisome Proliferator-Activated Receptors with Coactivators. *J. Biol. Chem.* **2005**, *280* (28), 26543–26556.

- (92) Baymaz, H. I.; Karemaker, I. D.; Vermeulen, M. Perspective on Unraveling the Versatility of “co-Repressor” Complexes. *Biochim. Biophys. Acta - Gene Regul. Mech.* **2015**, *1849* (8), 1051–1056.
- (93) White, J. H.; Fernandes, I.; Mader, S.; Yang, X.-J. Corepressor Recruitment by Agonist-Bound Nuclear Receptors. *Vitam. Horm.* **2004**, *68*, 123–143.
- (94) Meyer, M. B.; Pike, J. W. Corepressors (NCoR and SMRT) as Well as Coactivators Are Recruited to Positively Regulated 1 α ,25-Dihydroxyvitamin D₃-Responsive Genes. *J. Steroid Biochem. Mol. Biol.* **2013**, *136*, 120–124.
- (95) Peterson, T. J.; Karmakar, S.; Pace, M. C.; Gao, T.; Smith, C. L. The Silencing Mediator of Retinoic Acid and Thyroid Hormone Receptor (SMRT) Corepressor Is Required for Full Estrogen Receptor α Transcriptional Activity. *Mol. Cell. Biol.* **2007**, *27* (17), 5933–5948.
- (96) Jepsen, K.; Hermanson, O.; Onami, T. M.; Gleiberman, A. S.; Lunyak, V.; McEvelly, R. J.; Kurokawa, R.; Kumar, V.; Liu, F.; Seto, E.; Hedrick, S. M.; Mandel, G.; Glass, C. K.; Rose, D. W.; Rosenfeld, M. G. Combinatorial Roles of the Nuclear Receptor Corepressor in Transcription and Development. *Cell* **2000**, *102* (6), 753–763.
- (97) Berghagen, H.; Ragnhildstveit, E.; Krogsrud, K.; Thuestad, G.; Apriletti, J.; Saatcioglu, F. Corepressor SMRT Functions as a Coactivator for Thyroid Hormone Receptor T3R α from a Negative Hormone Response Element. *J. Biol. Chem.* **2002**, *277* (51), 49517–49522.
- (98) Tagami, T.; Madison, L. D.; Nagaya, T.; Jameson, J. L. Nuclear Receptor Corepressors Activate Rather than Suppress Basal Transcription of Genes That Are Negatively Regulated by Thyroid Hormone. *Mol. Cell. Biol.* **1997**, *17* (5), 2642–2648.
- (99) Wang, Z.; Zang, C.; Cui, K.; Schones, D. E.; Barski, A.; Peng, W.; Zhao, K. Genome-Wide Mapping of HATs and HDACs Reveals Distinct Functions in Active and Inactive Genes. *Cell* **2009**, *138* (5), 1019–1031.
- (100) van Oevelen, C.; Bowman, C.; Pellegrino, J.; Asp, P.; Cheng, J.; Parisi, F.; Micsinai, M.; Kluger, Y.; Chu, A.; Blais, A.; David, G.; Dynlacht, B. D. The Mammalian Sin3 Proteins Are Required for Muscle Development and Sarcomere Specification. *Mol. Cell. Biol.* **2010**, *30* (24), 5686–5697.
- (101) Cheng, J.; Blum, R.; Bowman, C.; Hu, D.; Shilatifard, A.; Shen, S.; Dynlacht, B. D. A Role for H3K4 Monomethylation in Gene Repression and Partitioning of Chromatin Readers. *Mol. Cell* **2014**, *53* (6), 979–992.
- (102) Rogatsky, I.; Zarembler, K. A.; Yamamoto, K. R. Factor Recruitment and TIF2/GRIP1 Corepressor Activity at a Collagenase-3 Response Element That Mediates Regulation by Phorbol Esters and Hormones. *EMBO J.* **2001**, *20* (21), 6071–6083.
- (103) Yu, C.; York, B.; Wang, S.; Feng, Q.; Xu, J.; O’Malley, B. W. An Essential Function of the SRC-3 Coactivator in Suppression of Cytokine mRNA Translation and Inflammatory Response. *Mol. Cell* **2007**, *25* (5), 765–778.
- (104) Jang, J. Y.; Kim, H.-J.; Han, B. W. Structural Basis for the Regulation of PPAR γ Activity by Imatinib. *Molecules* **2019**, *24* (19), 3562.
- (105) Schoch, H.; Abel, T. Transcriptional Co-Repressors and Memory Storage. *Neuropharmacology* **2014**, *80*, 53–60.
- (106) Nautiyal, J.; Christian, M.; Parker, M. G. Distinct Functions for RIP140 in Development,

- Inflammation, and Metabolism. *Trends Endocrinol. Metab.* **2013**, *24* (9), 451–459.
- (107) Nautiyal, J. Transcriptional Coregulator RIP140: An Essential Regulator of Physiology. *J. Mol. Endocrinol.* **2017**, *58* (3), R147–R158.
- (108) Cavailles, V.; Dauvois, S.; L’Horset, F.; Lopez, G.; Hoare, S.; Kushner, P. J.; Parker, M. G. Nuclear Factor RIP140 Modulates Transcriptional Activation by the Estrogen Receptor. *EMBO J.* **1995**, *14* (15), 3741–3751.
- (109) Issemann, I.; Green, S. Activation of a Member of the Steroid Hormone Receptor Superfamily by Peroxisome Proliferators. *Nature* **1990**, *347*, 645–650.
- (110) Vamecq, J.; Latruffe, N. Medical Significance of Peroxisome Proliferator-Activated Receptors. *Lancet* **1999**, *354* (9173), 141–148.
- (111) Schmidt, A.; Endo, N.; Rutledge, S. J.; Vogel, R.; Shinar, D.; Rodan, G. A. Identification of a New Member of the Steroid Hormone Receptor Superfamily That Is Activated by a Peroxisome Proliferator and Fatty Acids. *Mol. Endocrinol.* **1992**, *6* (10), 1634–1641.
- (112) Amri, E.-Z.; Bonino, F.; Ailhaud, G.; Abumrad, N. A.; Grimaldi, P. A. Cloning of a Protein That Mediates Transcriptional Effects of Fatty Acids in Preadipocytes: Homology to Peroxisome Proliferator-Activated Receptors. *J. Biol. Chem.* **1995**, *270* (5), 2367–2371.
- (113) Dreyer, C.; Krey, G.; Keller, H.; Givel, F.; Helftenbein, G.; Wahli, W. Control of the Peroxisomal β -Oxidation Pathway by a Novel Family of Nuclear Hormone Receptors. *Cell* **1992**, *68* (5), 879–887.
- (114) Kliewer, S. A.; Forman, B. M.; Blumberg, B.; Ong, E. S.; Borgmeyer, U.; Mangelsdorf, D. J.; Umesono, K.; Evans, R. M. Differential Expression and Activation of a Family of Murine Peroxisome Proliferator-Activated Receptors. *Proc. Natl. Acad. Sci.* **1994**, *91* (15), 7355–7359.
- (115) Chen, Y.; Jimenez, A. R.; Medh, J. D. Identification and Regulation of Novel PPAR- γ Splice Variants in Human THP-1 Macrophages. *Biochim. Biophys. Acta - Gene Struct. Expr.* **2006**, *1759* (1–2), 32–43.
- (116) Fajas, L.; Fruchart, J.-C.; Auwerx, J. PPAR γ 3 MRNA: A Distinct PPAR γ MRNA Subtype Transcribed from an Independent Promoter. *FEBS Lett.* **1998**, *438* (1–2), 55–60.
- (117) Fajas, L.; Auboeuf, D.; Raspé, E.; Schoonjans, K.; Lefebvre, A.-M.; Saladin, R.; Najib, J.; Laville, M.; Fruchart, J.-C.; Deeb, S.; Vidal-Puig, A.; Flier, J.; Briggs, M. R.; Staels, B.; Vidal, H.; Auwerx, J. The Organization, Promoter Analysis, and Expression of the Human PPAR γ Gene. *J. Biol. Chem.* **1997**, *272* (30), 18779–18789.
- (118) Usuda, D.; Kanda, T. Peroxisome Proliferator-Activated Receptors for Hypertension. *World J. Cardiol.* **2014**, *6* (8), 744–754.
- (119) Kliewer, S. A.; Umesono, K.; Noonan, D. J.; Heyman, R. A.; Evans, R. M. Convergence of 9-Cis Retinoic Acid and Peroxisome Proliferator Signalling Pathways through Heterodimer Formation of Their Receptors. *Nature* **1992**, *358*, 771–774.
- (120) Feige, J. N.; Gelman, L.; Michalik, L.; Desvergne, B.; Wahli, W. From Molecular Action to Physiological Outputs: Peroxisome Proliferator-Activated Receptors Are Nuclear Receptors at the Crossroads of Key Cellular Functions. *Prog. Lipid Res.* **2006**, *45* (2), 120–159.

- (121) Palmer, C. N. A.; Hsu, M.-H.; Griffin, K. J.; Johnson, E. F. Novel Sequence Determinants in Peroxisome Proliferator Signaling. *J. Biol. Chem.* **1995**, *270* (27), 16114–16121.
- (122) IJpenberg, A.; Jeannin, E.; Wahli, W.; Desvergne, B. Polarity and Specific Sequence Requirements of Peroxisome Proliferator-Activated Receptor (PPAR)/Retinoid X Receptor Heterodimer Binding to DNA. *J. Biol. Chem.* **1997**, *272* (32), 20108–20117.
- (123) Juge-Aubry, C.; Pernin, A.; Favez, T.; Burger, A. G.; Wahli, W.; Meier, C. A.; Desvergne, B. DNA Binding Properties of Peroxisome Proliferator-Activated Receptor Subtypes on Various Natural Peroxisome Proliferator Response Elements. *J. Biol. Chem.* **1997**, *272* (40), 25252–25259.
- (124) Werman, A.; Hollenberg, A.; Solanes, G.; Bjørnbæk, C.; Vidal-Puig, A. J.; Flier, J. S. Ligand-Independent Activation Domain in the N Terminus of Peroxisome Proliferator-Activated Receptor γ (PPAR γ). *J. Biol. Chem.* **1997**, *272* (32), 20230–20235.
- (125) Green, S.; Wahli, W. Peroxisome Proliferator-Activated Receptors: Finding the Orphan a Home. *Mol. Cell. Endocrinol.* **1994**, *100* (1–2), 149–153.
- (126) Willson, T. M.; Cobb, J. E.; Cowan, D. J.; Wiethe, R. W.; Correa, I. D.; Prakash, S. R.; Beck, K. D.; Moore, L. B.; Kliewer, S. A.; Lehmann, J. M. The Structure–Activity Relationship between Peroxisome Proliferator-Activated Receptor γ Agonism and the Antihyperglycemic Activity of Thiazolidinediones. *J. Med. Chem.* **1996**, *39* (3), 665–668.
- (127) Wahli, W.; Michalik, L. PPARs at the Crossroads of Lipid Signaling and Inflammation. *Trends Endocrinol. Metab.* **2012**, *23* (7), 351–363.
- (128) Desvergne, B.; Wahli, W. Peroxisome Proliferator-Activated Receptors: Nuclear Control of Metabolism. *Endocr. Rev.* **1999**, *20* (5), 649–688.
- (129) Mandard, S.; Müller, M.; Kersten, S. Peroxisome Proliferator-Activated Receptor α Target Genes. *Cell. Mol. Life Sci.* **2004**, *61*, 393–416.
- (130) Lemberger, T.; Saladin, R.; Vázquez, M.; Assimacopoulos, F.; Staels, B.; Desvergne, B.; Wahli, W.; Auwerx, J. Expression of the Peroxisome Proliferator-Activated Receptor α Gene Is Stimulated by Stress and Follows a Diurnal Rhythm. *J. Biol. Chem.* **1996**, *271* (3), 1764–1769.
- (131) Han, L.; Shen, W. J.; Bittner, S.; Kraemer, F. B.; Azhar, S. PPARs: Regulators of Metabolism and as Therapeutic Targets in Cardiovascular Disease. Part I: PPAR- α . *Future Cardiol.* **2017**, *13* (3), 259–278.
- (132) Bougarne, N.; Weyers, B.; Desmet, S. J.; Deckers, J.; Ray, D. W.; Staels, B.; De Bosscher, K. Molecular Actions of PPAR α in Lipid Metabolism and Inflammation. *Endocr. Rev.* **2018**, *39* (5), 760–802.
- (133) Tokuno, A.; Hirano, T.; Hayashi, T.; Mori, Y.; Yamamoto, T.; Nagashima, M.; Shiraishi, Y.; Ito, Y.; Adachi, M. The Effects of Statin and Fibrate on Lowering Small Dense LDL- Cholesterol in Hyperlipidemic Patients with Type 2 Diabetes. *J. Atheroscler. Thromb.* **2007**, *14* (3), 128–132.
- (134) Pawlak, M.; Lefebvre, P.; Staels, B. Molecular Mechanism of PPAR α Action and Its Impact on Lipid Metabolism, Inflammation and Fibrosis in Non-Alcoholic Fatty Liver Disease. *J. Hepatol.* **2015**, *62* (3), 720–733.
- (135) Lefebvre, P.; Chinetti, G.; Fruchart, J.-C.; Staels, B. Sorting out the Roles of PPAR α in Energy Metabolism and Vascular Homeostasis. *J. Clin. Invest.* **2006**, *116* (3), 571–580.

- (136) Jakob, T.; Nordmann, A. J.; Schandelmaier, S.; Ferreira-González, I.; Briel, M. Fibrates for Primary Prevention of Cardiovascular Disease Events. *Cochrane Database Syst. Rev.* **2016**, No. 11, CD009753.
- (137) Warden, A.; Truitt, J.; Merriman, M.; Ponomareva, O.; Jameson, K.; Ferguson, L. B.; Mayfield, R. D.; Harris, R. A. Localization of PPAR Isotypes in the Adult Mouse and Human Brain. *Sci. Rep.* **2016**, *6*, 27618.
- (138) Wójtowicz, S.; Strosznajder, A. K.; Jeżyna, M.; Strosznajder, J. B. The Novel Role of PPAR Alpha in the Brain: Promising Target in Therapy of Alzheimer's Disease and Other Neurodegenerative Disorders. *Neurochem. Res.* **2020**, *45*, 972–988.
- (139) Uppalapati, D.; Das, N. R.; Gangwal, R. P.; Damre, M. V.; Sangamwar, A. T.; Sharma, S. S. Neuroprotective Potential of Peroxisome Proliferator Activated Receptor- α Agonist in Cognitive Impairment in Parkinson's Disease: Behavioral, Biochemical, and PBPB Profile. *PPAR Res.* **2014**, *2014*, 753587.
- (140) Barbiero, J. K.; Santiago, R.; Tonin, F. S.; Boschen, S.; da Silva, L. M.; de Paula Werner, M. F.; da Cunha, C.; Lima, M. M. S.; Vital, M. A. B. F. PPAR- α Agonist Fenofibrate Protects against the Damaging Effects of MPTP in a Rat Model of Parkinson's Disease. *Prog. Neuro-Psychopharmacology Biol. Psychiatry* **2014**, *53*, 35–44.
- (141) Gottschalk, C. G.; Roy, A.; Jana, M.; Kundu, M.; Pahan, K. Activation of Peroxisome Proliferator-Activated Receptor- α Increases the Expression of Nuclear Receptor Related 1 Protein (Nurr1) in Dopaminergic Neurons. *Mol. Neurobiol.* **2019**, *56* (11), 7872–7887.
- (142) Mukherjee, R.; Jow, L.; Croston, G. E.; Paterniti, J. R. Identification, Characterization, and Tissue Distribution of Human Peroxisome Proliferator-Activated Receptor (PPAR) Isoforms PPAR γ 2 versus PPAR γ 1 and Activation with Retinoid X Receptor Agonists and Antagonists. *J. Biol. Chem.* **1997**, *272* (12), 8071–8076.
- (143) Han, L.; Shen, W.-J.; Bittner, S.; Kraemer, F. B.; Azhar, S. PPARs: Regulators of Metabolism and as Therapeutic Targets in Cardiovascular Disease. Part II: PPAR- β/δ and PPAR- γ . *Future Cardiol.* **2017**, *13* (3), 279–296.
- (144) Ricote, M.; Huang, J.; Fajas, L.; Li, A.; Welch, J.; Najib, J.; Witztum, J. L.; Auwerx, J.; Palinski, W.; Glass, C. K. Expression of the Peroxisome Proliferator-Activated Receptor γ (PPAR γ) in Human Atherosclerosis and Regulation in Macrophages by Colony Stimulating Factors and Oxidized Low Density Lipoprotein. *Proc. Natl. Acad. Sci.* **1998**, *95* (13), 7614–7619.
- (145) Vidal-Puig, A.; Jimenez-Liñan, M.; Lowell, B. B.; Hamann, A.; Hu, E.; Spiegelman, B.; Flier, J. S.; Moller, D. E. Regulation of PPAR Gamma Gene Expression by Nutrition and Obesity in Rodents. *J. Clin. Invest.* **1996**, *97* (11), 2553–2561.
- (146) Tontonoz, P.; Hu, E.; Spiegelman, B. M. Stimulation of Adipogenesis in Fibroblasts by PPAR γ 2, a Lipid-Activated Transcription Factor. *Cell* **1994**, *79* (7), 1147–1156.
- (147) Imai, T.; Takakuwa, R.; Marchand, S.; Dentz, E.; Bornert, J.-M.; Messaddeq, N.; Wendling, O.; Mark, M.; Desvergne, B.; Wahli, W.; Chambon, P.; Metzger, D. Peroxisome Proliferator-Activated Receptor γ Is Required in Mature White and Brown Adipocytes for Their Survival in the Mouse. *Proc. Natl. Acad. Sci.* **2004**, *101* (13), 4543–4547.
- (148) Rosen, E. D.; Sarraf, P.; Troy, A. E.; Bradwin, G.; Moore, K.; Milstone, D. S.; Spiegelman, B. M.;

- Mortensen, R. M. PPAR γ Is Required for the Differentiation of Adipose Tissue In Vivo and In Vitro. *Mol. Cell* **1999**, 4 (4), 611–617.
- (149) Rosen, E. D.; Walkey, C. J.; Puigserver, P.; Spiegelman, B. M. Transcriptional Regulation of Adipogenesis. *Genes Dev.* **2000**, 14 (11), 1293–1307.
- (150) Tontonoz, P.; Nagy, L.; Alvarez, J. G. A.; Thomazy, V. A.; Evans, R. M. PPAR γ Promotes Monocyte/Macrophage Differentiation and Uptake of Oxidized LDL. *Cell* **1998**, 93 (2), 241–252.
- (151) Frohnert, B. I.; Hui, T. Y.; Bernlohr, D. A. Identification of a Functional Peroxisome Proliferator-Responsive Element in the Murine Fatty Acid Transport Protein Gene. *J. Biol. Chem.* **1999**, 274 (7), 3970–3977.
- (152) Schoonjans, K.; Peinado-Onsurbe, J.; Lefebvre, A. M.; Heyman, R. A.; Briggs, M.; Deeb, S.; Staels, B.; Auwerx, J. PPAR α and PPAR γ Activators Direct a Distinct Tissue-Specific Transcriptional Response via a PPRE in the Lipoprotein Lipase Gene. *EMBO J.* **1996**, 15 (19), 5336–5348.
- (153) Tontonoz, P.; Hu, E.; Graves, R. A.; Budavari, A. I.; Spiegelman, B. M. mPPAR Gamma 2: Tissue-Specific Regulator of an Adipocyte Enhancer. *Genes Dev.* **1994**, 8, 1224–1234.
- (154) Haunerland, N. H.; Spener, F. Fatty Acid-Binding Proteins – Insights from Genetic Manipulations. *Prog. Lipid Res.* **2004**, 43 (4), 328–349.
- (155) Lehrke, M.; Lazar, M. A. The Many Faces of PPAR γ . *Cell* **2005**, 123 (6), 993–999.
- (156) Schadinger, S. E.; Bucher, N. L. R.; Schreiber, B. M.; Farmer, S. R. PPAR γ 2 Regulates Lipogenesis and Lipid Accumulation in Steatotic Hepatocytes. *Am. J. Physiol. Metab.* **2005**, 288 (6), E1195–E1205.
- (157) Guan, H.-P.; Li, Y.; Jensen, M. V.; Newgard, C. B.; Steppan, C. M.; Lazar, M. A. A Futile Metabolic Cycle Activated in Adipocytes by Antidiabetic Agents. *Nat. Med.* **2002**, 8 (10), 1122–1128.
- (158) Dalen, K. T.; Schoonjans, K.; Ulven, S. M.; Weedon-Fekjaer, M. S.; Bentzen, T. G.; Kontnikova, H.; Auwerx, J.; Nebb, H. I. Adipose Tissue Expression of the Lipid Droplet-Associating Proteins S3-12 and Perilipin Is Controlled by Peroxisome Proliferator-Activated Receptor- γ . *Diabetes* **2004**, 53 (5), 1243–1252.
- (159) Itabe, H.; Yamaguchi, T.; Nimura, S.; Sasabe, N. Perilipins: A Diversity of Intracellular Lipid Droplet Proteins. *Lipids Health Dis.* **2017**, 16, 83.
- (160) Festuccia, W. T.; Laplante, M.; Berthiaume, M.; G elinas, Y.; Deshaies, Y. PPAR γ Agonism Increases Rat Adipose Tissue Lipolysis, Expression of Glyceride Lipases, and the Response of Lipolysis to Hormonal Control. *Diabetologia* **2006**, 49 (10), 2427–2436.
- (161) Rodriguez-Cuenca, S.; Carobbio, S.; Velagapudi, V. R.; Barbarroja, N.; Moreno-Navarrete, J. M.; Tinahones, F. J.; Fernandez-Real, J. M.; Ore i c, M.; Vidal-Puig, A. Peroxisome Proliferator-Activated Receptor γ -Dependent Regulation of Lipolytic Nodes and Metabolic Flexibility. *Mol. Cell. Biol.* **2012**, 32 (8), 1555–1565.
- (162) Martin, G.; Schoonjans, K.; Staels, B.; Auwerx, J. PPAR γ Activators Improve Glucose Homeostasis by Stimulating Fatty Acid Uptake in the Adipocytes. *Atherosclerosis* **1998**, 137 (Suppl. 1), S75–S80.

- (163) Willson, T. M.; Brown, P. J.; Sternbach, D. D.; Henke, B. R. The PPARs: From Orphan Receptors to Drug Discovery. *J. Med. Chem.* **2000**, *43* (4), 527–550.
- (164) Maeda, N.; Takahashi, M.; Funahashi, T.; Kihara, S.; Nishizawa, H.; Kishida, K.; Nagaretani, H.; Matsuda, M.; Komuro, R.; Ouchi, N.; Kuriyama, H.; Hotta, K.; Nakamura, T.; Shimomura, I.; Matsuzawa, Y. PPAR γ Ligands Increase Expression and Plasma Concentrations of Adiponectin, an Adipose-Derived Protein. *Diabetes* **2001**, *50* (9), 2094–2099.
- (165) Yoon, J. C.; Chickering, T. W.; Rosen, E. D.; Dussault, B.; Qin, Y.; Soukas, A.; Friedman, J. M.; Holmes, W. E.; Spiegelman, B. M. Peroxisome Proliferator-Activated Receptor γ Target Gene Encoding a Novel Angiopoietin-Related Protein Associated with Adipose Differentiation. *Mol. Cell. Biol.* **2000**, *20* (14), 5343–5349.
- (166) La Paglia, L.; Listì, A.; Caruso, S.; Amodeo, V.; Passiglia, F.; Bazan, V.; Fanale, D. Potential Role of ANGPTL4 in the Cross Talk between Metabolism and Cancer through PPAR Signaling Pathway. *PPAR Res.* **2017**, *2017*, 8187235.
- (167) Berg, A. H.; Combs, T. P.; Scherer, P. E. ACRP30/Adiponectin: An Adipokine Regulating Glucose and Lipid Metabolism. *Trends Endocrinol. Metab.* **2002**, *13* (2), 84–89.
- (168) Xu, A.; Lam, M. C.; Chan, K. W.; Wang, Y.; Zhang, J.; Hoo, R. L. C.; Xu, J. Y.; Chen, B.; Chow, W.-S.; Tso, A. W. K.; Lam, K. S. L. Angiopoietin-like Protein 4 Decreases Blood Glucose and Improves Glucose Tolerance but Induces Hyperlipidemia and Hepatic Steatosis in Mice. *Proc. Natl. Acad. Sci.* **2005**, *102* (17), 6086–6091.
- (169) Fruebis, J.; Tsao, T.-S.; Javorschi, S.; Ebbets-Reed, D.; Erickson, M. R. S.; Yen, F. T.; Bihain, B. E.; Lodish, H. F. Proteolytic Cleavage Product of 30-KDa Adipocyte Complement-Related Protein Increases Fatty Acid Oxidation in Muscle and Causes Weight Loss in Mice. *Proc. Natl. Acad. Sci.* **2001**, *98* (4), 2005–2010.
- (170) Wang, Z. V.; Scherer, P. E. Adiponectin, the Past Two Decades. *J. Mol. Cell Biol.* **2016**, *8* (2), 93–100.
- (171) Armoni, M.; Kritz, N.; Harel, C.; Bar-Yoseph, F.; Chen, H.; Quon, M. J.; Karnieli, E. Peroxisome Proliferator-Activated Receptor- γ Represses GLUT4 Promoter Activity in Primary Adipocytes, and Rosiglitazone Alleviates This Effect. *J. Biol. Chem.* **2003**, *278* (33), 30614–30623.
- (172) Wu, Z.; Xie, Y.; Morrison, R. F.; Bucher, N. L. R.; Farmer, S. R. PPAR γ Induces the Insulin-Dependent Glucose Transporter GLUT4 in the Absence of C/EBP α during the Conversion of 3T3 Fibroblasts into Adipocytes. *J. Clin. Invest.* **1998**, *101* (1), 22–32.
- (173) Way, J. M.; Harrington, W. W.; Brown, K. K.; Gottschalk, W. K.; Sundseth, S. S.; Mansfield, T. A.; Ramachandran, R. K.; Willson, T. M.; Kliewer, S. A. Comprehensive Messenger Ribonucleic Acid Profiling Reveals That Peroxisome Proliferator-Activated Receptor γ Activation Has Coordinate Effects on Gene Expression in Multiple Insulin-Sensitive Tissues. *Endocrinology* **2001**, *142* (3), 1269–1277.
- (174) Kim, H.; Ahn, Y. Role of Peroxisome Proliferator-Activated Receptor- γ in the Glucose-Sensing Apparatus of Liver and β -Cells. *Diabetes* **2004**, *53* (Suppl. 1), S60–S65.
- (175) Grossman, S. L.; Lessem, J. Mechanisms and Clinical Effects of Thiazolidinediones. *Expert Opin. Investig. Drugs* **1997**, *6* (8), 1025–1040.

- (176) Kahn, B. B.; McGraw, T. E. Rosiglitazone, PPAR γ , and Type 2 Diabetes. *N. Engl. J. Med.* **2010**, *363* (27), 2667–2669.
- (177) Ahmadian, M.; Suh, J. M.; Hah, N.; Liddle, C.; Atkins, A. R.; Downes, M.; Evans, R. M. PPAR γ Signaling and Metabolism: The Good, the Bad and the Future. *Nat. Med.* **2013**, *19* (5), 557–566.
- (178) Széles, L.; Töröcsik, D.; Nagy, L. PPAR γ in Immunity and Inflammation: Cell Types and Diseases. *Biochim. Biophys. Acta - Mol. Cell Biol. Lipids* **2007**, *1771* (8), 1014–1030.
- (179) Pascual, G.; Fong, A. L.; Ogawa, S.; Gamliel, A.; Li, A. C.; Perissi, V.; Rose, D. W.; Willson, T. M.; Rosenfeld, M. G.; Glass, C. K. A SUMOylation-Dependent Pathway Mediates Transrepression of Inflammatory Response Genes by PPAR- γ . *Nature* **2005**, *437*, 759–763.
- (180) Jiang, C.; Ting, A. T.; Seed, B. PPAR- γ Agonists Inhibit Production of Monocyte Inflammatory Cytokines. *Nature* **1998**, *391*, 82–86.
- (181) Bouhrel, M. A.; Derudas, B.; Rigamonti, E.; Dièvert, R.; Brozek, J.; Haulon, S.; Zawadzki, C.; Jude, B.; Torpier, G.; Marx, N.; Staels, B.; Chinetti-Gbaguidi, G. PPAR γ Activation Primes Human Monocytes into Alternative M2 Macrophages with Anti-Inflammatory Properties. *Cell Metab.* **2007**, *6* (2), 137–143.
- (182) Odegaard, J. I.; Ricardo-Gonzalez, R. R.; Goforth, M. H.; Morel, C. R.; Subramanian, V.; Mukundan, L.; Eagle, A. R.; Vats, D.; Brombacher, F.; Ferrante, A. W.; Chawla, A. Macrophage-Specific PPAR γ Controls Alternative Activation and Improves Insulin Resistance. *Nature* **2007**, *447*, 1116–1120.
- (183) Huang, J. T.; Welch, J. S.; Ricote, M.; Binder, C. J.; Willson, T. M.; Kelly, C.; Witztum, J. L.; Funk, C. D.; Conrad, D.; Glass, C. K. Interleukin-4-Dependent Production of PPAR- γ Ligands in Macrophages by 12/15-Lipoxygenase. *Nature* **1999**, *400*, 378–382.
- (184) Chinetti, G.; Griglio, S.; Antonucci, M.; Torra, I. P.; Delerive, P.; Majd, Z.; Fruchart, J.-C.; Chapman, J.; Najib, J.; Staels, B. Activation of Proliferator-Activated Receptors α and γ Induces Apoptosis of Human Monocyte-Derived Macrophages. *J. Biol. Chem.* **1998**, *273* (40), 25573–25580.
- (185) Nagy, L.; Tontonoz, P.; Alvarez, J. G. A.; Chen, H.; Evans, R. M. Oxidized LDL Regulates Macrophage Gene Expression through Ligand Activation of PPAR γ . *Cell* **1998**, *93* (2), 229–240.
- (186) Szatmari, I.; Rajnavolgyi, E.; Nagy, L. PPAR γ , a Lipid-Activated Transcription Factor as a Regulator of Dendritic Cell Function. *Ann. N. Y. Acad. Sci.* **2006**, *1088* (1), 207–218.
- (187) Kapadia, R.; Yi, J.-H.; Vemuganti, R. Mechanisms of Anti-Inflammatory and Neuroprotective Actions of PPAR-Gamma Agonists. *Front. Biosci. (Landmark Ed)* **2008**, *13* (5), 1813–1826.
- (188) Fernandez-Martos, C. M.; Atkinson, R. A. K.; Chuah, M. I.; King, A. E.; Vickers, J. C. Combination Treatment with Leptin and Pioglitazone in a Mouse Model of Alzheimer's Disease. *Alzheimer's Dement. Transl. Res. Clin. Interv.* **2017**, *3* (1), 92–106.
- (189) Chen, J.; Li, S.; Sun, W.; Li, J. Anti-Diabetes Drug Pioglitazone Ameliorates Synaptic Defects in AD Transgenic Mice by Inhibiting Cyclin-Dependent Kinase5 Activity. *PLoS One* **2015**, *10* (4), e0123864.
- (190) Yang, S.; Chen, Z.; Cao, M.; Li, R.; Wang, Z.; Zhang, M. Pioglitazone Ameliorates A β 42 Deposition in Rats with Diet-Induced Insulin Resistance Associated with AKT/GSK3 β

- Activation. *Mol. Med. Rep.* **2017**, *15* (5), 2588–2594.
- (191) Chang, K. L.; Wong, L. R.; Pee, H. N.; Yang, S.; Ho, P. C.-L. Reverting Metabolic Dysfunction in Cortex and Cerebellum of APP/PS1 Mice, a Model for Alzheimer's Disease by Pioglitazone, a Peroxisome Proliferator-Activated Receptor Gamma (PPAR γ) Agonist. *Mol. Neurobiol.* **2019**, *56* (11), 7267–7283.
- (192) Yu, Y.; Li, X.; Blanchard, J.; Li, Y.; Iqbal, K.; Liu, F.; Gong, C.-X. Insulin Sensitizers Improve Learning and Attenuate Tau Hyperphosphorylation and Neuroinflammation in 3xTg-AD Mice. *J. Neural Transm.* **2015**, *122* (4), 593–606.
- (193) Du, J.; Zhang, L.; Liu, S.; Zhang, C.; Huang, X.; Li, J.; Zhao, N.; Wang, Z. PPAR γ Transcriptionally Regulates the Expression of Insulin-Degrading Enzyme in Primary Neurons. *Biochem. Biophys. Res. Commun.* **2009**, *383* (4), 485–490.
- (194) Quan, Q.; Qian, Y.; Li, X.; Li, M. Pioglitazone Reduces β Amyloid Levels via Inhibition of PPAR γ Phosphorylation in a Neuronal Model of Alzheimer's Disease. *Front. Aging Neurosci.* **2019**, *11*, 178.
- (195) Sastre, M.; Dewachter, I.; Rossner, S.; Bogdanovic, N.; Rosen, E.; Borghgraef, P.; Evert, B. O.; Dumitrescu-Ozimek, L.; Thal, D. R.; Landreth, G.; Walter, J.; Klockgether, T.; van Leuven, F.; Heneka, M. T. Nonsteroidal Anti-Inflammatory Drugs Repress β -Secretase Gene Promoter Activity by the Activation of PPAR γ . *Proc. Natl. Acad. Sci.* **2006**, *103* (2), 443–448.
- (196) Breidert, T.; Callebert, J.; Heneka, M. T.; Landreth, G.; Launay, J. M.; Hirsch, E. C. Protective Action of the Peroxisome Proliferator-Activated Receptor- γ Agonist Pioglitazone in a Mouse Model of Parkinson's Disease. *J. Neurochem.* **2002**, *82* (3), 615–624.
- (197) Quinn, L. P.; Crook, B.; Hows, M. E.; Vidgeon-Hart, M.; Chapman, H.; Upton, N.; Medhurst, A. D.; Virley, D. J. The PPAR γ Agonist Pioglitazone Is Effective in the MPTP Mouse Model of Parkinson's Disease through Inhibition of Monoamine Oxidase B. *Br. J. Pharmacol.* **2008**, *154* (1), 226–233.
- (198) Swanson, C. R.; Joers, V.; Bondarenko, V.; Brunner, K.; Simmons, H. A.; Ziegler, T. E.; Kemnitz, J. W.; Johnson, J. A.; Emborg, M. E. The PPAR- γ Agonist Pioglitazone Modulates Inflammation and Induces Neuroprotection in Parkinsonian Monkeys. *J. Neuroinflammation* **2011**, *8*, 91.
- (199) Machado, M. M. F.; Bassani, T. B.; C oppola-Segovia, V.; Moura, E. L. R.; Zanata, S. M.; Andreatini, R.; Vital, M. A. B. F. PPAR- γ Agonist Pioglitazone Reduces Microglial Proliferation and NF-KB Activation in the Substantia Nigra in the 6-Hydroxydopamine Model of Parkinson's Disease. *Pharmacol. Reports* **2019**, *71* (4), 556–564.
- (200) Lee, E. Y.; Lee, J. E.; Park, J. H.; Shin, I. C.; Koh, H. C. Rosiglitazone, a PPAR- γ Agonist, Protects against Striatal Dopaminergic Neurodegeneration Induced by 6-OHDA Lesions in the Substantia Nigra of Rats. *Toxicol. Lett.* **2012**, *213* (3), 332–344.
- (201) Lu, C.-H.; Yang, C.-Y.; Li, C.-Y.; Hsieh, C.; Ou, H.-T. Lower Risk of Dementia with Pioglitazone, Compared with Other Second-Line Treatments, in Metformin-Based Dual Therapy: A Population-Based Longitudinal Study. *Diabetologia* **2018**, *61* (3), 562–573.
- (202) Heneka, M. T.; Fink, A.; Doblhammer, G. Effect of Pioglitazone Medication on the Incidence of Dementia. *Ann. Neurol.* **2015**, *78* (2), 284–294.

- (203) Chou, P.-S.; Ho, B.-L.; Yang, Y.-H. Effects of Pioglitazone on the Incidence of Dementia in Patients with Diabetes. *J. Diabetes Complications* **2017**, *31* (6), 1053–1057.
- (204) Brauer, R.; Bhaskaran, K.; Chaturvedi, N.; Dexter, D. T.; Smeeth, L.; Douglas, I. Glitazone Treatment and Incidence of Parkinson's Disease among People with Diabetes: A Retrospective Cohort Study. *PLOS Med.* **2015**, *12* (7), e1001854.
- (205) Wouters, E.; Grajchen, E.; Jorissen, W.; Dierckx, T.; Wetzels, S.; Loix, M.; Tulleners, M. P.; Staels, B.; Stinissen, P.; Haidar, M.; Bogie, J. F. J.; Hendriks, J. J. A. Altered PPAR γ Expression Promotes Myelin-Induced Foam Cell Formation in Macrophages in Multiple Sclerosis. *Int. J. Mol. Sci.* **2020**, *21* (23), 9329.
- (206) Grajchen, E.; Wouters, E.; van de Haterd, B.; Haidar, M.; Hardonnière, K.; Dierckx, T.; Van Broeckhoven, J.; Erens, C.; Hendrix, S.; Kerdine-Römer, S.; Hendriks, J. J. A.; Bogie, J. F. J. CD36-Mediated Uptake of Myelin Debris by Macrophages and Microglia Reduces Neuroinflammation. *J. Neuroinflammation* **2020**, *17*, 224.
- (207) Bernardo, A.; Giammarco, M. L.; De Nuccio, C.; Ajmone-Cat, M. A.; Visentin, S.; De Simone, R.; Minghetti, L. Docosaheptaenoic Acid Promotes Oligodendrocyte Differentiation via PPAR- γ Signalling and Prevents Tumor Necrosis Factor- α -Dependent Maturation Arrest. *Biochim. Biophys. Acta - Mol. Cell Biol. Lipids* **2017**, *1862* (9), 1013–1023.
- (208) De Nuccio, C.; Bernardo, A.; Cruciani, C.; De Simone, R.; Visentin, S.; Minghetti, L. Peroxisome Proliferator Activated Receptor- γ Agonists Protect Oligodendrocyte Progenitors against Tumor Necrosis Factor-Alpha-Induced Damage: Effects on Mitochondrial Functions and Differentiation. *Exp. Neurol.* **2015**, *271*, 506–514.
- (209) Feinstein, D. L.; Galea, E.; Gavriilyuk, V.; Brosnan, C. F.; Whitacre, C. C.; Dumitrescu-Ozimek, L.; Landreth, G. E.; Pershadsingh, H. A.; Weinberg, G.; Heneka, M. T. Peroxisome Proliferator-Activated Receptor- γ Agonists Prevent Experimental Autoimmune Encephalomyelitis. *Ann. Neurol.* **2002**, *51* (6), 694–702.
- (210) Klotz, L.; Burgdorf, S.; Dani, I.; Saijo, K.; Flossdorf, J.; Hucke, S.; Alferink, J.; Novak, N.; Beyer, M.; Mayer, G.; Langhans, B.; Klockgether, T.; Waisman, A.; Eberl, G.; Schultze, J.; Famulok, M.; Kolanus, W.; Glass, C.; Kurts, C.; et al. The Nuclear Receptor PPAR γ Selectively Inhibits Th17 Differentiation in a T Cell-Intrinsic Fashion and Suppresses CNS Autoimmunity. *J. Exp. Med.* **2009**, *206* (10), 2079–2089.
- (211) Chedrawe, M. A. J.; Holman, S. P.; Lamport, A.-C.; Akay, T.; Robertson, G. S. Pioglitazone Is Superior to Quetiapine, Clozapine and Tamoxifen at Alleviating Experimental Autoimmune Encephalomyelitis in Mice. *J. Neuroimmunol.* **2018**, *321*, 72–82.
- (212) Diab, A.; Deng, C.; Smith, J. D.; Hussain, R. Z.; Phanavanh, B.; Lovett-Racke, A. E.; Drew, P. D.; Racke, M. K. Peroxisome Proliferator-Activated Receptor- γ Agonist 15-Deoxy- $\Delta^{12,14,14}$ -Prostaglandin J₂ Ameliorates Experimental Autoimmune Encephalomyelitis. *J. Immunol.* **2002**, *168* (5), 2508–2515.
- (213) Harrington, C.; Sawchak, S.; Chiang, C.; Davies, J.; Donovan, C.; Saunders, A. M.; Irizarry, M.; Jeter, B.; Zvartau-Hind, M.; van Dyck, C. H.; Gold, M. Rosiglitazone Does Not Improve Cognition or Global Function When Used as Adjunctive Therapy to AChE Inhibitors in Mild-to-Moderate Alzheimer's Disease: Two Phase 3 Studies. *Curr. Alzheimer Res.* **2011**, *8* (5), 592–606.

- (214) Gold, M.; Alderton, C.; Zvartau-Hind, M.; Egginton, S.; Saunders, A. M.; Irizarry, M.; Craft, S.; Landreth, G.; Linnamägi, Ü.; Sawchak, S. Rosiglitazone Monotherapy in Mild-to-Moderate Alzheimer's Disease: Results from a Randomized, Double-Blind, Placebo-Controlled Phase III Study. *Dement. Geriatr. Cogn. Disord.* **2010**, *30* (2), 131–146.
- (215) Cheng, H.; Shang, Y.; Jiang, L.; Shi, T.-L.; Wang, L. The Peroxisome Proliferators Activated Receptor-Gamma Agonists as Therapeutics for the Treatment of Alzheimer's Disease and Mild-to-Moderate Alzheimer's Disease: A Meta-Analysis. *Int. J. Neurosci.* **2016**, *126* (4), 299–307.
- (216) Liu, J.; Wang, L.; Jia, J. Peroxisome Proliferator-Activated Receptor-Gamma Agonists for Alzheimer's Disease and Amnesic Mild Cognitive Impairment: A Systematic Review and Meta-Analysis. *Drugs Aging* **2015**, *32* (1), 57–65.
- (217) Kaiser, C. C.; Shukla, D. K.; Stebbins, G. T.; Skias, D. D.; Jeffery, D. R.; Stefoski, D.; Katsamakias, G.; Feinstein, D. L. A Pilot Test of Pioglitazone as an Add-on in Patients with Relapsing Remitting Multiple Sclerosis. *J. Neuroimmunol.* **2009**, *211* (1–2), 124–130.
- (218) Shukla, D. K.; Kaiser, C. C.; Stebbins, G. T.; Feinstein, D. L. Effects of Pioglitazone on Diffusion Tensor Imaging Indices in Multiple Sclerosis Patients. *Neurosci. Lett.* **2010**, *472* (3), 153–156.
- (219) Negrotto, L.; Farez, M. F.; Correale, J. Immunologic Effects of Metformin and Pioglitazone Treatment on Metabolic Syndrome and Multiple Sclerosis. *JAMA Neurol.* **2016**, *73* (5), 520–528.
- (220) Braissant, O.; Fougelle, F.; Scotto, C.; Dauça, M.; Wahli, W. Differential Expression of Peroxisome Proliferator-Activated Receptors (PPARs): Tissue Distribution of PPAR-Alpha, -Beta, and -Gamma in the Adult Rat. *Endocrinology* **1996**, *137* (1), 354–366.
- (221) Higashiyama, H.; Billin, A. N.; Okamoto, Y.; Kinoshita, M.; Asano, S. Expression Profiling of Peroxisome Proliferator-Activated Receptor-Delta (PPAR-Delta) in Mouse Tissues Using Tissue Microarray. *Histochem. Cell Biol.* **2007**, *127* (5), 485–494.
- (222) Giordano Attianese, G. M. P.; Desvergne, B. Integrative and Systemic Approaches for Evaluating PPAR β/δ (PPARD) Function. *Nucl. Recept. Signal.* **2015**, *13* (1), nrs.13001.
- (223) Gan, Z.; Burkart-Hartman, E. M.; Han, D. H.; Finck, B.; Leone, T. C.; Smith, E. Y.; Ayala, J. E.; Holloszy, J.; Kelly, D. P. The Nuclear Receptor PPAR β/δ Programs Muscle Glucose Metabolism in Cooperation with AMPK and MEF2. *Genes Dev.* **2011**, *25*, 2619–2630.
- (224) Luquet, S.; Lopez-Soriano, J.; Holst, D.; Fredenrich, A.; Melki, J.; Rassoulzadegan, M.; Grimaldi, P. A. Peroxisome Proliferator-Activated Receptor δ Controls Muscle Development and Oxidative Capability. *FASEB J.* **2003**, *17* (15), 2299–2301.
- (225) Lee, C. H.; Olson, P.; Hevener, A.; Mehl, I.; Chong, L. W.; Olefsky, J. M.; Gonzalez, F. J.; Ham, J.; Kang, H.; Peters, J. M.; Evans, R. M. PPAR δ Regulates Glucose Metabolism and Insulin Sensitivity. *Proc. Natl. Acad. Sci.* **2006**, *103* (9), 3444–3449.
- (226) Fan, W.; Waizenegger, W.; Lin, C. S.; Sorrentino, V.; He, M.-X.; Wall, C. E.; Li, H.; Liddle, C.; Yu, R. T.; Atkins, A. R.; Auwerx, J.; Downes, M.; Evans, R. M. PPAR δ Promotes Running Endurance by Preserving Glucose. *Cell Metab.* **2017**, *25* (5), 1186–1193.e4.
- (227) Wang, Y.-X.; Zhang, C.-L.; Yu, R. T.; Cho, H. K.; Nelson, M. C.; Bayuga-Ocampo, C. R.; Ham, J.; Kang, H.; Evans, R. M. Regulation of Muscle Fiber Type and Running Endurance by PPAR δ . *PLoS Biol.* **2004**, *2* (10), e294.

- (228) Bays, H. E.; Schwartz, S.; Littlejohn, T.; Kerzner, B.; Krauss, R. M.; Karpf, D. B.; Choi, Y.-J.; Wang, X.; Naim, S.; Roberts, B. K. MBX-8025, A Novel Peroxisome Proliferator Receptor- δ Agonist: Lipid and Other Metabolic Effects in Dyslipidemic Overweight Patients Treated with and without Atorvastatin. *J. Clin. Endocrinol. Metab.* **2011**, *96* (9), 2889–2897.
- (229) Ooi, E. M. M.; Watts, G. F.; Sprecher, D. L.; Chan, D. C.; Barrett, P. H. R. Mechanism of Action of a Peroxisome Proliferator-Activated Receptor (PPAR)- δ Agonist on Lipoprotein Metabolism in Dyslipidemic Subjects with Central Obesity. *J. Clin. Endocrinol. Metab.* **2011**, *96* (10), E1568–E1576.
- (230) Olson, E. J.; Pearce, G. L.; Jones, N. P.; Sprecher, D. L. Lipid Effects of Peroxisome Proliferator-Activated Receptor- δ Agonist GW501516 in Subjects with Low High-Density Lipoprotein Cholesterol: Characteristics of Metabolic Syndrome. *Arterioscler. Thromb. Vasc. Biol.* **2012**, *32* (9), 2289–2294.
- (231) Miura, P.; Chakkalakal, J. V.; Boudreault, L.; Bélanger, G.; Hébert, R. L.; Renaud, J. M.; Jasmin, B. J. Pharmacological Activation of PPAR β/δ Stimulates Utrophin A Expression in Skeletal Muscle Fibers and Restores Sarcolemmal Integrity in Mature Mdx Mice. *Hum. Mol. Genet.* **2009**, *18* (23), 4640–4649.
- (232) Sanderson, L. M.; Boekschoten, M. V.; Desvergne, B.; Müller, M.; Kersten, S. Transcriptional Profiling Reveals Divergent Roles of PPAR α and PPAR β/δ in Regulation of Gene Expression in Mouse Liver. *Physiol. Genomics* **2010**, *41* (1), 42–52.
- (233) Odegaard, J. I.; Ricardo-Gonzalez, R. R.; Red Eagle, A.; Vats, D.; Morel, C. R.; Goforth, M. H.; Subramanian, V.; Mukundan, L.; Ferrante, A. W.; Chawla, A. Alternative M2 Activation of Kupffer Cells by PPAR δ Ameliorates Obesity-Induced Insulin Resistance. *Cell Metab.* **2008**, *7* (6), 496–507.
- (234) Takata, Y.; Liu, J.; Yin, F.; Collins, A. R.; Lyon, C. J.; Lee, C. H.; Atkins, A. R.; Downes, M.; Barish, G. D.; Evans, R. M.; Hsueh, W. A.; Tangirala, R. K. PPAR δ -Mediated Antiinflammatory Mechanisms Inhibit Angiotensin II-Accelerated Atherosclerosis. *Proc. Natl. Acad. Sci.* **2008**, *105* (11), 4277–4282.
- (235) Lee, C. H.; Chawla, A.; Urbiztondo, N.; Liao, D.; Boisvert, W. A.; Evans, R. M. Transcriptional Repression of Atherogenic Inflammation: Modulation by PPAR δ . *Science* **2003**, *302* (5644), 453–457.
- (236) Mukundan, L.; Odegaard, J. I.; Morel, C. R.; Heredia, J. E.; Mwangi, J. W.; Ricardo-Gonzalez, R. R.; Goh, Y. P. S.; Eagle, A. R.; Dunn, S. E.; Awakuni, J. U. H.; Nguyen, K. D.; Steinman, L.; Michie, S. A.; Chawla, A. PPAR- δ Senses and Orchestrates Clearance of Apoptotic Cells to Promote Tolerance. *Nat. Med.* **2009**, *15* (11), 1266–1272.
- (237) Kanakasabai, S.; Chearwae, W.; Walline, C. C.; Iams, W.; Adams, S. M.; Bright, J. J. Peroxisome Proliferator-Activated Receptor δ Agonists Inhibit T Helper Type 1 (Th1) and Th17 Responses in Experimental Allergic Encephalomyelitis. *Immunology* **2010**, *130* (4), 572–588.
- (238) Polak, P. E.; Kalinin, S.; Dello Russo, C.; Gavrilyuk, V.; Sharp, A.; Peters, J. M.; Richardson, J.; Willson, T. M.; Weinberg, G.; Feinstein, D. L. Protective Effects of a Peroxisome Proliferator-Activated Receptor- β/δ Agonist in Experimental Autoimmune Encephalomyelitis. *J. Neuroimmunol.* **2005**, *168* (1–2), 65–75.

- (239) Das, N. R.; Gangwal, R. P.; Damre, M. V.; Sangamwar, A. T.; Sharma, S. S. A PPAR- β/δ Agonist Is Neuroprotective and Decreases Cognitive Impairment in a Rodent Model of Parkinson's Disease. *Curr. Neurovasc. Res.* **2014**, *11* (2), 114–124.
- (240) Martin, H. L.; Mounsey, R. B.; Sathe, K.; Mustafa, S.; Nelson, M. C.; Evans, R. M.; Teismann, P. A Peroxisome Proliferator-Activated Receptor- δ Agonist Provides Neuroprotection in the 1-Methyl-4-Phenyl-1,2,3,6-Tetrahydropyridine Model of Parkinson's Disease. *Neuroscience* **2013**, *240*, 191–203.
- (241) Chen, L.; Xue, L.; Zheng, J.; Tian, X.; Zhang, Y.; Tong, Q. PPAR β/δ Agonist Alleviates NLRP3 Inflammasome-Mediated Neuroinflammation in the MPTP Mouse Model of Parkinson's Disease. *Behav. Brain Res.* **2019**, *356*, 483–489.
- (242) Tong, Q.; Wu, L.; Gao, Q.; Ou, Z.; Zhu, D.; Zhang, Y. PPAR β/δ Agonist Provides Neuroprotection by Suppression of IRE1 α -Caspase-12-Mediated Endoplasmic Reticulum Stress Pathway in the Rotenone Rat Model of Parkinson's Disease. *Mol. Neurobiol.* **2016**, *53* (8), 3822–3831.
- (243) Adhikary, T.; Wortmann, A.; Schumann, T.; Finkernagel, F.; Lieber, S.; Roth, K.; Toth, P. M.; Diederich, W. E.; Nist, A.; Stiewe, T.; Kleinesudeik, L.; Reinartz, S.; Müller-Brüsselbach, S.; Müller, R. The Transcriptional PPAR β/δ Network in Human Macrophages Defines a Unique Agonist-Induced Activation State. *Nucleic Acids Res.* **2015**, *43* (10), 5033–5051.
- (244) Romanowska, M.; Reilly, L.; Palmer, C. N. A.; Gustafsson, M. C. U.; Foerster, J. Activation of PPAR β/δ Causes a Psoriasis-Like Skin Disease In Vivo. *PLoS One* **2010**, *5* (3), e9701.
- (245) Bishop-Bailey, D.; Bystrom, J. Emerging Roles of Peroxisome Proliferator-Activated Receptor- β/δ in Inflammation. *Pharmacol. Ther.* **2009**, *124* (2), 141–150.
- (246) Xu, H. E.; Lambert, M. H.; Montana, V. G.; Plunket, K. D.; Moore, L. B.; Collins, J. L.; Oplinger, J. A.; Kliewer, S. A.; Gampe, R. T.; McKee, D. D.; Moore, J. T.; Willson, T. M. Structural Determinants of Ligand Binding Selectivity between the Peroxisome Proliferator-Activated Receptors. *Proc. Natl. Acad. Sci.* **2001**, *98* (24), 13919–13924.
- (247) Zoete, V.; Grosdidier, A.; Michielin, O. Peroxisome Proliferator-Activated Receptor Structures: Ligand Specificity, Molecular Switch and Interactions with Regulators. *Biochim. Biophys. Acta - Mol. Cell Biol. Lipids* **2007**, *1771* (8), 915–925.
- (248) Jang, J. Y.; Bae, H.; Lee, Y. J.; Choi, Y. Il; Kim, H.-J.; Park, S. B.; Suh, S. W.; Kim, S. W.; Han, B. W. Structural Basis for the Enhanced Anti-Diabetic Efficacy of Lobeglitazone on PPAR γ . *Sci. Rep.* **2018**, *8*, 31.
- (249) Xu, H. E.; Lambert, M. H.; Montana, V. G.; Parks, D. J.; Blanchard, S. G.; Brown, P. J.; Sternbach, D. D.; Lehmann, J. M.; Wisely, G. B.; Willson, T. M.; Kliewer, S. A.; Milburn, M. V. Molecular Recognition of Fatty Acids by Peroxisome Proliferator-Activated Receptors. *Mol. Cell* **1999**, *3* (3), 397–403.
- (250) Wu, C. C.; Baiga, T. J.; Downes, M.; La Clair, J. J.; Atkins, A. R.; Richard, S. B.; Fan, W.; Stockley-Noel, T. A.; Bowman, M. E.; Noel, J. P.; Evans, R. M. Structural Basis for Specific Ligation of the Peroxisome Proliferator-Activated Receptor δ . *Proc. Natl. Acad. Sci.* **2017**, *114* (13), E2563–E2570.
- (251) Nolte, R. T.; Wisely, G. B.; Westin, S.; Cobb, J. E.; Lambert, M. H.; Kurokawa, R.; Rosenfeld, M.

- G.; Willson, T. M.; Glass, C. K.; Milburn, M. V. Ligand Binding and Co-Activator Assembly of the Peroxisome Proliferator-Activated Receptor- γ . *Nature* **1998**, *395*, 137–143.
- (252) Miyachi, H. Design, Synthesis, and Structure-Activity Relationship Study of Peroxisome Proliferator-Activated Receptor (PPAR) δ -Selective Ligands. *Curr. Med. Chem.* **2007**, *14* (22), 2335–2343.
- (253) Buckle, D. R.; Cantello, B. C. C.; Cawthorne, M. A.; Coyle, P. J.; Dean, D. K.; Faller, A.; Haigh, D.; Hindley, R. M.; Jecfott, L. J.; Lister, C. A.; Pinto, I. L.; Rami, H. K.; Smith, D. G.; Smith, S. A. Non Thiazolidinedione Antihyperglycaemic Agents. 2: α -Carbon Substituted β -Phenylpropanoic Acids. *Bioorg. Med. Chem. Lett.* **1996**, *6* (17), 2127–2130.
- (254) Sime, M.; Allan, A. C.; Chapman, P.; Fieldhouse, C.; Giblin, G. M. P.; Healy, M. P.; Lambert, M. H.; Leesnitzer, L. M.; Lewis, A.; Merrihew, R. V.; Rutter, R. A.; Sasse, R.; Shearer, B. G.; Wilson, T. M.; Xu, R. X.; Virley, D. J. Discovery of GSK1997132B a Novel Centrally Penetrant Benzimidazole PPAR γ Partial Agonist. *Bioorg. Med. Chem. Lett.* **2011**, *21* (18), 5568–5572.
- (255) Motani, A.; Wang, Z.; Weiszmann, J.; McGee, L. R.; Lee, G.; Liu, Q.; Staunton, J.; Fang, Z.; Fuentes, H.; Lindstrom, M.; Liu, J.; Biermann, D. H. T.; Jaen, J.; Walker, N. P. C.; Learned, R. M.; Chen, J.-L.; Li, Y. INT131: A Selective Modulator of PPAR γ . *J. Mol. Biol.* **2009**, *386* (5), 1301–1311.
- (256) Hughes, T. S.; Giri, P. K.; de Vera, I. M. S.; Marciano, D. P.; Kuruvilla, D. S.; Shin, Y.; Blayo, A.-L.; Kamenecka, T. M.; Burris, T. P.; Griffin, P. R.; Kojetin, D. J. An Alternate Binding Site for PPAR γ Ligands. *Nat. Commun.* **2014**, *5*, 3571.
- (257) Shang, J.; Brust, R.; Mosure, S. A.; Bass, J.; Munoz-Tello, P.; Lin, H.; Hughes, T. S.; Tang, M.; Ge, Q.; Kamenecka, T. M.; Kojetin, D. J. Cooperative Cobinding of Synthetic and Natural Ligands to the Nuclear Receptor PPAR γ . *Elife* **2018**, *7*, e43320.
- (258) Artis, D. R.; Lin, J. J.; Zhang, C.; Wang, W.; Mehra, U.; Perreault, M.; Erbe, D.; Krupka, H. I.; England, B. P.; Arnold, J.; Plotnikov, A. N.; Marimuthu, A.; Nguyen, H.; Will, S.; Signaevsky, M.; Kral, J.; Cantwell, J.; Settachatgull, C.; Yan, D. S.; et al. Scaffold-Based Discovery of Indeglitazar, a PPAR Pan-Active Anti-Diabetic Agent. *Proc. Natl. Acad. Sci.* **2009**, *106* (1), 262–267.
- (259) Subramani, P. A.; Reddy, M. C.; Narala, V. R. The Need for Physiologically Relevant Peroxisome Proliferator-Activated Receptor-Gamma (PPAR- γ) Ligands. *Endocrine, Metab. Immune Disord. - Drug Targets* **2013**, *13* (2), 175–183.
- (260) Forman, B. M.; Chen, J.; Evans, R. M. Hypolipidemic Drugs, Polyunsaturated Fatty Acids, and Eicosanoids Are Ligands for Peroxisome Proliferator-Activated Receptors α and δ . *Proc. Natl. Acad. Sci.* **1997**, *94* (9), 4312–4317.
- (261) Kliewer, S. A.; Sundseth, S. S.; Jones, S. A.; Brown, P. J.; Wisely, G. B.; Koble, C. S.; Devchand, P.; Wahli, W.; Willson, T. M.; Lenhard, J. M.; Lehmann, J. M. Fatty Acids and Eicosanoids Regulate Gene Expression through Direct Interactions with Peroxisome Proliferator-Activated Receptors α and γ . *Proc. Natl. Acad. Sci.* **1997**, *94* (9), 4318–4323.
- (262) Devchand, P. R.; Keller, H.; Peters, J. M.; Vazquez, M.; Gonzalez, F. J.; Wahli, W. The PPAR α -Leukotriene B₄ Pathway to Inflammation Control. *Nature* **1996**, *384*, 39–43.
- (263) Lin, Q.; Ruuska, S. E.; Shaw, N. S.; Dong, D.; Noy, N. Ligand Selectivity of the Peroxisome Proliferator-Activated Receptor α . *Biochemistry* **1999**, *38* (1), 185–190.

- (264) Krey, G.; Braissant, O.; L'Horset, F.; Kalkhoven, E.; Perroud, M.; Parker, M. G.; Wahli, W. Fatty Acids, Eicosanoids, and Hypolipidemic Agents Identified as Ligands of Peroxisome Proliferator-Activated Receptors by Coactivator-Dependent Receptor Ligand Assay. *Mol. Endocrinol.* **1997**, *11* (6), 779–791.
- (265) Lo Verme, J.; La Rana, G.; Russo, R.; Calignano, A.; Piomelli, D. The Search for the Palmitoylethanolamide Receptor. *Life Sci.* **2005**, *77* (14), 1685–1698.
- (266) Lo Verme, J.; Fu, J.; Astarita, G.; La Rana, G.; Russo, R.; Calignano, A.; Piomelli, D. The Nuclear Receptor Peroxisome Proliferator-Activated Receptor- α Mediates the Anti-Inflammatory Actions of Palmitoylethanolamide. *Mol. Pharmacol.* **2005**, *67* (1), 15–19.
- (267) Fu, J.; Gaetani, S.; Oveisi, F.; Lo Verme, J.; Serrano, A.; Rodríguez de Fonseca, F.; Rosengarth, A.; Luecke, H.; Di Giacomo, B.; Tarzia, G.; Piomelli, D. Oleyethanolamide Regulates Feeding and Body Weight through Activation of the Nuclear Receptor PPAR- α . *Nature* **2003**, *425*, 90–93.
- (268) Giampietro, L.; Ammazalorso, A.; Amoroso, R.; De Filippis, B. Development of Fibrates as Important Scaffolds in Medicinal Chemistry. *ChemMedChem* **2019**, *14* (11), 1051–1066.
- (269) Kane, S. P. Fenofibrate, ClinCalc DrugStats Database, Version 2021.10. ClinCalc: <https://clincalc.com/DrugStats/Drugs/Fenofibrate> (accessed Mar 3, 2022).
- (270) Abourbih, S.; Filion, K. B.; Joseph, L.; Schiffrin, E. L.; Rinfret, S.; Poirier, P.; Pilote, L.; Genest, J.; Eisenberg, M. J. Effect of Fibrates on Lipid Profiles and Cardiovascular Outcomes: A Systematic Review. *Am. J. Med.* **2009**, *122* (10), 962.e1-962.e8.
- (271) Yamashita, S.; Masuda, D.; Matsuzawa, Y. Pemaifibrate, a New Selective PPAR α Modulator: Drug Concept and Its Clinical Applications for Dyslipidemia and Metabolic Diseases. *Curr. Atheroscler. Rep.* **2020**, *22*, 5.
- (272) Araki, E.; Yamashita, S.; Arai, H.; Yokote, K.; Satoh, J.; Inoguchi, T.; Nakamura, J.; Maegawa, H.; Yoshioka, N.; Tanizawa, Y.; Watada, H.; Suganami, H.; Ishibashi, S. Effects of Pemaifibrate, a Novel Selective PPAR α Modulator, on Lipid and Glucose Metabolism in Patients With Type 2 Diabetes and Hypertriglyceridemia: A Randomized, Double-Blind, Placebo-Controlled, Phase 3 Trial. *Diabetes Care* **2018**, *41* (3), 538–546.
- (273) Yamazaki, Y.; Abe, K.; Toma, T.; Nishikawa, M.; Ozawa, H.; Okuda, A.; Araki, T.; Oda, S.; Inoue, K.; Shibuya, K.; Staels, B.; Fruchart, J.-C. Design and Synthesis of Highly Potent and Selective Human Peroxisome Proliferator-Activated Receptor α Agonists. *Bioorg. Med. Chem. Lett.* **2007**, *17* (16), 4689–4693.
- (274) Brown, P. J.; Stuart, L. W.; Hurley, K. P.; Lewis, M. C.; Winegar, D. A.; Wilson, J. G.; Wilkison, W. O.; Ittoop, O. R.; Willson, T. M. Identification of a Subtype Selective Human PPAR α Agonist through Parallel-Array Synthesis. *Bioorg. Med. Chem. Lett.* **2001**, *11* (9), 1225–1227.
- (275) Kliewer, S. A.; Lenhard, J. M.; Willson, T. M.; Patel, I.; Morris, D. C.; Lehmann, J. M. A Prostaglandin J_2 Metabolite Binds Peroxisome Proliferator-Activated Receptor γ and Promotes Adipocyte Differentiation. *Cell* **1995**, *83* (5), 813–819.
- (276) Forman, B. M.; Tontonoz, P.; Chen, J.; Brun, R. P.; Spiegelman, B. M.; Evans, R. M. 15-Deoxy- $\Delta^{12,14}$ -Prostaglandin J_2 Is a Ligand for the Adipocyte Determination Factor PPAR γ . *Cell* **1995**, *83* (5), 803–812.

- (277) Soares, A. F.; Nosjean, O.; Cozzone, D.; D’Orazio, D.; Becchi, M.; Guichardant, M.; Ferry, G.; Boutin, J. A.; Lagarde, M.; G elo en, A. Covalent Binding of 15-Deoxy-Delta^{12,14}-Prostaglandin J₂ to PPAR γ . *Biochem. Biophys. Res. Commun.* **2005**, 337 (2), 521–525.
- (278) Shiraki, T.; Kodama, T. S.; Shiki, S.; Nakagawa, T.; Jingami, H. Spectroscopic Analyses of the Binding Kinetics of 15d-PGJ₂ to the PPAR γ Ligand-Binding Domain by Multi-Wavelength Global Fitting. *Biochem. J.* **2006**, 393 (3), 749–755.
- (279) Waku, T.; Shiraki, T.; Oyama, T.; Fujimoto, Y.; Maebara, K.; Kamiya, N.; Jingami, H.; Morikawa, K. Structural Insight into PPAR γ Activation Through Covalent Modification with Endogenous Fatty Acids. *J. Mol. Biol.* **2009**, 385 (1), 188–199.
- (280) Villacorta, L.; Schopfer, F. J.; Zhang, J.; Freeman, B. A.; Chen, Y. E. PPAR γ and Its Ligands: Therapeutic Implications in Cardiovascular Disease. *Clin. Sci.* **2009**, 116 (3), 205–218.
- (281) Powell, W. S. 15-Deoxy- $\Delta^{12,14}$ -PGJ₂: Endogenous PPAR γ Ligand or Minor Eicosanoid Degradation Product? *J. Clin. Invest.* **2003**, 112 (6), 828–830.
- (282) Combs, C. K.; Johnson, D. E.; Karlo, J. C.; Cannady, S. B.; Landreth, G. E. Inflammatory Mechanisms in Alzheimer’s Disease: Inhibition of β -Amyloid-Stimulated Proinflammatory Responses and Neurotoxicity by PPAR γ Agonists. *J. Neurosci.* **2000**, 20 (2), 558–567.
- (283) Storer, P. D.; Xu, J.; Chavis, J.; Drew, P. D. Peroxisome Proliferator-Activated Receptor-Gamma Agonists Inhibit the Activation of Microglia and Astrocytes: Implications for Multiple Sclerosis. *J. Neuroimmunol.* **2005**, 161 (1–2), 113–122.
- (284) Tzamelis, I.; Fang, H.; Ollero, M.; Shi, H.; Hamm, J. K.; Kievit, P.; Hollenberg, A. N.; Flier, J. S. Regulated Production of a Peroxisome Proliferator-Activated Receptor- γ Ligand during an Early Phase of Adipocyte Differentiation in 3T3-L1 Adipocytes. *J. Biol. Chem.* **2004**, 279 (34), 36093–36102.
- (285) Schopfer, F. J.; Lin, Y.; Baker, P. R. S.; Cui, T.; Garcia-Barrio, M.; Zhang, J.; Chen, K.; Chen, Y. E.; Freeman, B. A. Nitrolinoleic Acid: An Endogenous Peroxisome Proliferator-Activated Receptor γ Ligand. *Proc. Natl. Acad. Sci.* **2005**, 102 (7), 2340–2345.
- (286) Alexander, R. L.; Wright, M. W.; Gorczynski, M. J.; Smitherman, P. K.; Akiyama, T. E.; Wood, H. B.; Berger, J. P.; King, S. B.; Morrow, C. S. Differential Potencies of Naturally Occurring Regioisomers of Nitrolinoleic Acid in PPAR γ Activation. *Biochemistry* **2009**, 48 (2), 492–498.
- (287) Gellrich, L.; Heitel, P.; Heering, J.; Kilo, W.; Pollinger, J.; Goebel, T.; Kahnt, A.; Arifi, S.; Pogoda, W.; Paulke, A.; Steinhilber, D.; Proschak, E.; Wurglics, M.; Schubert-Zsilavecz, M.; Chaikuad, A.; Knapp, S.; Bischoff, I.; F urst, R.; Merk, D. L-Thyroxin and the Nonclassical Thyroid Hormone TETRAC Are Potent Activators of PPAR γ . *J. Med. Chem.* **2020**, 63 (13), 6727–6740.
- (288) Sohda, T.; Mizuna, K.; Imamiya, E.; Sugiyama, Y.; Fujita, T.; Kawamatsu, Y. Studies on Antidiabetic Agents. II. Synthesis of 5-[4-(1-Methylcyclohexylmethoxy)-Benzyl] Thiazolidine-2,4-Dione (ADD-3878) and Its Derivatives. *Chem. Pharm. Bull.* **1982**, 30 (10), 3580–3600.
- (289) European Medicines Agency. European Medicines Agency recommends new contra-indications and warnings for pioglitazone to reduce small increased risk of bladder cancer. Press release 21/07/2011: <https://www.ema.europa.eu/en/news/european-medicines-agency-recommends-new-contra-indications-warnings-pioglitazone-reduce-small> (accessed Mar 3, 2022).

- (290) Nissen, S. E.; Wolski, K. Effect of Rosiglitazone on the Risk of Myocardial Infarction and Death from Cardiovascular Causes. *N. Engl. J. Med.* **2007**, *356* (24), 2457–2471.
- (291) Nissen, S. E.; Wolski, K. Rosiglitazone Revisited: An Updated Meta-Analysis of Risk for Myocardial Infarction and Cardiovascular Mortality. *Arch. Intern. Med.* **2010**, *170* (14), 1191–1201.
- (292) Biermann, D. Rosiglitazon: Marktrücknahme Zum 1. November. *PZ - Pharm. Zeitung* **2010**, *39*.
- (293) Lehmann, J. M.; Moore, L. B.; Smith-Oliver, T. A.; Wilkison, W. O.; Willson, T. M.; Kliewer, S. A. An Antidiabetic Thiazolidinedione Is a High Affinity Ligand for Peroxisome Proliferator-Activated Receptor γ (PPAR γ). *J. Biol. Chem.* **1995**, *270* (22), 12953–12956.
- (294) Higgins, L. S.; DePaoli, A. M. Selective Peroxisome Proliferator-Activated Receptor γ (PPAR γ) Modulation as a Strategy for Safer Therapeutic PPAR γ Activation. *Am. J. Clin. Nutr.* **2010**, *91* (1), 267S–272S.
- (295) Jang, J. Y.; Koh, M.; Bae, H.; An, D. R.; Im, H. N.; Kim, H. S.; Yoon, J. Y.; Yoon, H.-J.; Han, B. W.; Park, S. B.; Suh, S. W. Structural Basis for Differential Activities of Enantiomeric PPAR γ Agonists: Binding of S35 to the Alternate Site. *Biochim. Biophys. Acta - Proteins Proteomics* **2017**, *1865* (6), 674–681.
- (296) Brust, R.; Shang, J.; Fuhrmann, J.; Mosure, S. A.; Bass, J.; Cano, A.; Heidari, Z.; Chrisman, I. M.; Nemetchek, M. D.; Blayo, A.-L.; Griffin, P. R.; Kamenecka, T. M.; Hughes, T. S.; Kojetin, D. J. A Structural Mechanism for Directing Corepressor-Selective Inverse Agonism of PPAR γ . *Nat. Commun.* **2018**, *9*, 4687.
- (297) Bae, H.; Jang, J. Y.; Choi, S.-S.; Lee, J.-J.; Kim, H.; Jo, A.; Lee, K.-J.; Choi, J. H.; Suh, S. W.; Park, S. B. Mechanistic Elucidation Guided by Covalent Inhibitors for the Development of Anti-Diabetic PPAR γ Ligands. *Chem. Sci.* **2016**, *7*, 5523–5529.
- (298) Choi, J. H.; Banks, A. S.; Kamenecka, T. M.; Busby, S. A.; Chalmers, M. J.; Kumar, N.; Kuruvilla, D. S.; Shin, Y.; He, Y.; Bruning, J. B.; Marciano, D. P.; Cameron, M. D.; Laznik, D.; Jurczak, M. J.; Schürer, S. C.; Vidović, D.; Shulman, G. I.; Spiegelman, B. M.; Griffin, P. R. Antidiabetic Actions of a Non-Agonist PPAR γ Ligand Blocking Cdk5-Mediated Phosphorylation. *Nature* **2011**, *477*, 477–481.
- (299) Xie, X.; Chen, W.; Zhang, N.; Yuan, M.; Xu, C.; Zheng, Z.; Li, H.; Wang, L. Selective Tissue Distribution Mediates Tissue-Dependent PPAR γ Activation and Insulin Sensitization by INT131, a Selective PPAR γ Modulator. *Front. Pharmacol.* **2017**, *8*, 317.
- (300) Acton III, J. J.; Black, R. M.; Jones, A. B.; Moller, D. E.; Colwell, L.; Doebber, T. W.; MacNaul, K. L.; Berger, J.; Wood, H. B. Benzoyl 2-Methyl Indoles as Selective PPAR γ Modulators. *Bioorg. Med. Chem. Lett.* **2005**, *15* (2), 357–362.
- (301) Acton III, J. J.; Akiyama, T. E.; Chang, C. H.; Colwell, L.; Debenham, S.; Doebber, T.; Einstein, M.; Liu, K.; McCann, M. E.; Moller, D. E.; Muise, E. S.; Tan, Y.; Thompson, J. R.; Wong, K. K.; Wu, M.; Xu, L.; Meinke, P. T.; Berger, J. P.; Wood, H. B. Discovery of (2R)-2-(3-{3-[(4-Methoxyphenyl)Carbonyl]-2-Methyl-6-(Trifluoromethoxy)-1H-Indol-1-yl}phenoxy)Butanoic Acid (MK-0533): A Novel Selective Peroxisome Proliferator-Activated Receptor γ Modulator for the Treatment of Type 2 Diabetes Mellitus With . *J. Med. Chem.* **2009**, *52* (13), 3846–3854.
- (302) Bruning, J. B.; Chalmers, M. J.; Prasad, S.; Busby, S. A.; Kamenecka, T. M.; He, Y.; Nettles, K. W.;

- Griffin, P. R. Partial Agonists Activate PPAR γ Using a Helix 12 Independent Mechanism. *Structure* **2007**, *15* (10), 1258–1271.
- (303) ClinicalTrials.gov Identifier: NCT00543959. Efficacy and Tolerability of MK0533 in Patients With Type 2 Diabetes (0533-005) <https://clinicaltrials.gov/ct2/show/NCT00543959> (accessed Mar 3, 2022).
- (304) Gregoire, F. M.; Zhang, F.; Clarke, H. J.; Gustafson, T. A.; Sears, D. D.; Favelyukis, S.; Lenhard, J.; Rentzeperis, D.; Clemens, L. E.; Mu, Y.; Lavan, B. E. MBX-102/JNJ39659100, a Novel Peroxisome Proliferator-Activated Receptor-Ligand with Weak Transactivation Activity Retains Antidiabetic Properties in the Absence of Weight Gain and Edema. *Mol. Endocrinol.* **2009**, *23* (7), 975–988.
- (305) Poiley, J.; Steinberg, A. S.; Choi, Y.-J.; Davis, C. S.; Martin, R. L.; McWherter, C. A.; Boudes, P. F. A Randomized, Double-Blind, Active- and Placebo-Controlled Efficacy and Safety Study of Arhalofenate for Reducing Flare in Patients With Gout. *Arthritis Rheumatol.* **2016**, *68* (8), 2027–2034.
- (306) Wang, G.; Zuo, T.; Li, R. The Mechanism of Arhalofenate in Alleviating Hyperuricemia - Activating PPAR γ Thereby Reducing Caspase-1 Activity. *Drug Dev. Res.* **2020**, *81* (7), 859–866.
- (307) DePaoli, A. M.; Higgins, L. S.; Henry, R. R.; Mantzoros, C.; Dunn, F. L. Can a Selective PPAR γ Modulator Improve Glycemic Control in Patients With Type 2 Diabetes With Fewer Side Effects Compared With Pioglitazone? *Diabetes Care* **2014**, *37* (7), 1918–1923.
- (308) ClinicalTrials.gov Identifier: NCT02638038. This is a Randomized Study Comparing Two Doses of INT131 (3 mg and 1 mg) Administered Orally (PO) Daily (QD) Versus Placebo 1 Tablet PO QD in Subjects With Treatment-naïve RRMS for ≤ 3 Years <https://clinicaltrials.gov/ct2/show/NCT02638038> (accessed Mar 3, 2022).
- (309) Burton, J. D.; Goldenberg, D. M.; Blumenthal, R. D. Potential of Peroxisome Proliferator-Activated Receptor Gamma Antagonist Compounds as Therapeutic Agents for a Wide Range of Cancer Types. *PPAR Res.* **2008**, *2008*, 494161.
- (310) Nakano, R.; Kurosaki, E.; Yoshida, S.; Yokono, M.; Shimaya, A.; Maruyama, T.; Shibasaki, M. Antagonism of Peroxisome Proliferator-Activated Receptor γ Prevents High-Fat Diet-Induced Obesity in Vivo. *Biochem. Pharmacol.* **2006**, *72* (1), 42–52.
- (311) Leesnitzer, L. M.; Parks, D. J.; Bledsoe, R. K.; Cobb, J. E.; Collins, J. L.; Consler, T. G.; Davis, R. G.; Hull-Ryde, E. A.; Lenhard, J. M.; Patel, L.; Plunket, K. D.; Shenk, J. L.; Stimmel, J. B.; Therapontos, C.; Willson, T. M.; Blanchard, S. G. Functional Consequences of Cysteine Modification in the Ligand Binding Sites of Peroxisome Proliferator Activated Receptors by GW9662. *Biochemistry* **2002**, *41* (21), 6640–6650.
- (312) Shureiqi, I.; Jiang, W.; Zuo, X.; Wu, Y.; Stimmel, J. B.; Leesnitzer, L. M.; Morris, J. S.; Fan, H.-Z.; Fischer, S. M.; Lippman, S. M. The 15-Lipoxygenase-1 Product 13-S-Hydroxyoctadecadienoic Acid down-Regulates PPAR- δ to Induce Apoptosis in Colorectal Cancer Cells. *Proc. Natl. Acad. Sci.* **2003**, *100* (17), 9968–9973.
- (313) Naruhn, S.; Meissner, W.; Adhikary, T.; Kaddatz, K.; Klein, T.; Watzer, B.; Müller-Brüsselbach, S.; Müller, R. 15-Hydroxyeicosatetraenoic Acid Is a Preferential Peroxisome Proliferator-Activated Receptor β/δ Agonist. *Mol. Pharmacol.* **2010**, *77* (2), 171–184.

- (314) Berger, J.; Leibowitz, M. D.; Doebber, T. W.; Elbrecht, A.; Zhang, B.; Zhou, G.; Biswas, C.; Cullinan, C. A.; Hayes, N. S.; Li, Y.; Tanen, M.; Ventre, J.; Wu, M. S.; Berger, G. D.; Mosley, R.; Marquis, R.; Santini, C.; Sahoo, S. P.; Tolman, R. L.; et al. Novel Peroxisome Proliferator-Activated Receptor (PPAR) γ and PPAR δ Ligands Produce Distinct Biological Effects. *J. Biol. Chem.* **1999**, *274* (10), 6718–6725.
- (315) Oliver, W. R.; Shenk, J. L.; Snaith, M. R.; Russell, C. S.; Plunket, K. D.; Bodkin, N. L.; Lewis, M. C.; Winegar, D. A.; Sznajdman, M. L.; Lambert, M. H.; Xu, H. E.; Sternbach, D. D.; Kliewer, S. A.; Hansen, B. C.; Willson, T. M. A Selective Peroxisome Proliferator-Activated Receptor δ Agonist Promotes Reverse Cholesterol Transport. *Proc. Natl. Acad. Sci.* **2001**, *98* (9), 5306–5311.
- (316) Sznajdman, M. L.; Haffner, C. D.; Maloney, P. R.; Fivush, A.; Chao, E.; Goreham, D.; Sierra, M. L.; LeGrumelec, C.; Xu, H. E.; Montana, V. G.; Lambert, M. H.; Willson, T. M.; Oliver, W. R.; Sternbach, D. D. Novel Selective Small Molecule Agonists for Peroxisome Proliferator-Activated Receptor δ (PPAR δ)—Synthesis and Biological Activity. *Bioorg. Med. Chem. Lett.* **2003**, *13* (9), 1517–1521.
- (317) Barish, G. D.; Narkar, V. A.; Evans, R. M. PPAR δ : A Dagger in the Heart of the Metabolic Syndrome. *J. Clin. Invest.* **2006**, *116* (3), 590–597.
- (318) Billin, A. N. PPAR- β/δ Agonists for Type 2 Diabetes and Dyslipidemia: An Adopted Orphan Still Looking for a Home. *Expert Opin. Investig. Drugs* **2008**, *17* (10), 1465–1471.
- (319) Sahebkar, A.; Chew, G. T.; Watts, G. F. New Peroxisome Proliferator-Activated Receptor Agonists: Potential Treatments for Atherogenic Dyslipidemia and Non-Alcoholic Fatty Liver Disease. *Expert Opin. Pharmacother.* **2014**, *15* (4), 493–503.
- (320) Narkar, V. A.; Downes, M.; Yu, R. T.; Emblar, E.; Wang, Y.-X.; Banayo, E.; Mihaylova, M. M.; Nelson, M. C.; Zou, Y.; Juguilon, H.; Kang, H.; Shaw, R. J.; Evans, R. M. AMPK and PPAR δ Agonists Are Exercise Mimetics. *Cell* **2008**, *134* (3), 405–415.
- (321) Thevis, M.; Geyer, H.; Thomas, A.; Schänzer, W. Trafficking of Drug Candidates Relevant for Sports Drug Testing: Detection of Non-Approved Therapeutics Categorized as Anabolic and Gene Doping Agents in Products Distributed via the Internet. *Drug Test. Anal.* **2011**, *3* (5), 331–336.
- (322) Hirschfield, G.; Kowdley, K. V.; Shiffman, M. L.; Lawitz, E. J.; Guevara, L. L. De; Silveria, M. G.; Corpechot, C.; Swain, M. G.; Yimam, K. K.; Younes, Z.; Zuckerman, E.; Corpechot, C.; Harrison, S. A.; Nevens, F.; Thorburn, D.; Bowlus, C. L.; Jones, D.; Kremer, A. E.; Pares, A.; et al. ENHANCE: Safety and efficacy of seladelpar in patients with primary biliary cholangitis (PBC) - A phase 3 international, randomized, placebo-controlled study. The Liver Meeting Digital Experience AASLD 2020. <https://aasld.confex.com/aasld/2020/meetingapp.cgi/Paper/24463> (accessed Mar 3, 2022).
- (323) Harrison, S. A.; Gunn, N. T.; Khazanchi, A.; Guy, C. D.; Brunt, E. M.; Moussa, S.; Baum, S. J.; Frias, J. P.; Trotter, J. F.; Lazas, D.; Kohli, A.; Vander Veen, B.; Younes, Z. H.; Moore, A. C.; Huffman, J. L.; Poulos, J.; Boudes, P.; Rossi, S.; Choi, Y.-J.; et al. A 52-week multi-center double-blind randomized phase 2 study of seladelpar, a potent and selective peroxisome proliferator-activated receptor delta (PPAR-delta) agonist, in patients with nonalcoholic steatohepatitis (NASH). The Liver Meeting Digital Experience AASLD 2020. https://www.natap.org/2020/AASLD/AASLD_159.htm (accessed Mar 3, 2022).

- (324) Zhang, R.; Wang, A.; DeAngelis, A.; Pelton, P.; Xu, J.; Zhu, P.; Zhou, L.; Demarest, K.; Murray, W. V.; Kuo, G.-H. Discovery of Para-Alkylthiophenoxyacetic Acids as a Novel Series of Potent and Selective PPAR δ Agonists. *Bioorg. Med. Chem. Lett.* **2007**, *17* (14), 3855–3859.
- (325) ClinicalTrials.gov Identifier: NCT02704403. Phase 3 Study to Evaluate the Efficacy and Safety of Elafibranor Versus Placebo in Patients With Nonalcoholic Steatohepatitis (NASH) (RESOLVE-IT) <https://clinicaltrials.gov/ct2/show/NCT02704403> (accessed Mar 3, 2022).
- (326) ClinicalTrials.gov Identifier: NCT04526665. Study of Elafibranor in Patients With Primary Biliary Cholangitis (PBC) (ELATIVE) <https://clinicaltrials.gov/ct2/show/NCT04526665> (accessed Mar 3, 2022).
- (327) Law, S. W.; Conneely, O. M.; DeMayo, F. J.; O'Malley, B. W. Identification of a New Brain-Specific Transcription Factor, NURR1. *Mol. Endocrinol.* **1992**, *6* (12), 2129–2135.
- (328) Milbrandt, J. Nerve Growth Factor Induces a Gene Homologous to the Glucocorticoid Receptor Gene. *Neuron* **1988**, *1* (3), 183–188.
- (329) Hazel, T. G.; Nathans, D.; Lau, L. F. A Gene Inducible by Serum Growth Factors Encodes a Member of the Steroid and Thyroid Hormone Receptor Superfamily. *Proc. Natl. Acad. Sci.* **1988**, *85* (22), 8444–8448.
- (330) Mages, H. W.; Rilke, O.; Bravo, R.; Senger, G.; Kroczeck, R. A. NOT, a Human Immediate-Early Response Gene Closely Related to the Steroid/Thyroid Hormone Receptor NAK1/TR3. *Mol. Endocrinol.* **1994**, *8* (11), 1583–1591.
- (331) Okabe, T.; Takayanagi, R.; Imasaki, K.; Haji, M.; Nawata, H.; Watanabe, T. CDNA Cloning of a NGFI-B/Nur77-Related Transcription Factor from an Apoptotic Human T Cell Line. *J. Immunol.* **1995**, *154* (8), 3871–3879.
- (332) Scarce, L. M.; Laz, T. M.; Hazel, T. G.; Lau, L. F.; Taub, R. RNR-1, a Nuclear Receptor in the NGFI-B/Nur77 Family That Is Rapidly Induced in Regenerating Liver. *J. Biol. Chem.* **1993**, *268* (12), 8855–8861.
- (333) de Ortiz, S. P.; Cannon, M. M.; Jamieson, G. A. Expression of Nuclear Hormone Receptors within the Rat Hippocampus: Identification of Novel Orphan Receptors. *Mol. Brain Res.* **1994**, *23* (3), 278–283.
- (334) Paulsen, R. E.; Granås, K.; Johnsen, H.; Rolseth, V.; Sterri, S. Three Related Brain Nuclear Receptors, NGFI-B, Nurr1, and NOR-1, as Transcriptional Activators. *J. Mol. Neurosci.* **1995**, *6*, 249–255.
- (335) Wilson, T. E.; Fahrner, T. J.; Johnston, M.; Milbrandt, J. Identification of the DNA Binding Site for NGFI-B by Genetic Selection in Yeast. *Science* **1991**, *252* (5010), 1296–1300.
- (336) Zetterström, R. H.; Solomin, L.; Mitsiadis, T.; Olson, L.; Perlmann, T. Retinoid X Receptor Heterodimerization and Developmental Expression Distinguish the Orphan Nuclear Receptors NGFI-B, Nurr1, and Nor1. *Mol. Endocrinol.* **1996**, *10* (12), 1656–1666.
- (337) Murphy, E. P.; Conneely, O. M. Neuroendocrine Regulation of the Hypothalamic Pituitary Adrenal Axis by the Nurr1/Nur77 Subfamily of Nuclear Receptors. *Mol. Endocrinol.* **1997**, *11* (1), 39–47.
- (338) Wang, Z.; Benoit, G.; Liu, J.; Prasad, S.; Aarnisalo, P.; Liu, X.; Xu, H.; Walker, N. P. C.; Perlmann,

- T. Structure and Function of Nurr1 Identifies a Class of Ligand-Independent Nuclear Receptors. *Nature* **2003**, 423, 555–560.
- (339) Wansa, K. D. S. A.; Harris, J. M.; Yan, G.; Ordentlich, P.; Muscat, G. E. O. The AF-1 Domain of the Orphan Nuclear Receptor NOR-1 Mediates Trans-Activation, Coactivator Recruitment, and Activation by the Purine Anti-Metabolite 6-Mercaptopurine. *J. Biol. Chem.* **2003**, 278 (27), 24776–24790.
- (340) Wansa, K. D. S. A.; Harris, J. M.; Muscat, G. E. O. The Activation Function-1 Domain of Nur77/NR4A1 Mediates Trans-Activation, Cell Specificity, and Coactivator Recruitment. *J. Biol. Chem.* **2002**, 277 (36), 33001–33011.
- (341) Castro, D. S.; Arvidsson, M.; Bolin, M. B.; Perlmann, T. Activity of the Nurr1 Carboxyl-Terminal Domain Depends on Cell Type and Integrity of the Activation Function 2. *J. Biol. Chem.* **1999**, 274 (52), 37483–37490.
- (342) Escriva, H.; Safi, R.; Hänni, C.; Langlois, M.-C.; Saumitou-Laprade, P.; Stehelin, D.; Capron, A.; Pierce, R.; Laudet, V. Ligand Binding Was Acquired during Evolution of Nuclear Receptors. *Proc. Natl. Acad. Sci.* **1997**, 94 (13), 6803–6808.
- (343) Flaig, R.; Greschik, H.; Peluso-Iltis, C.; Moras, D. Structural Basis for the Cell-Specific Activities of the NGFI-B and the Nurr1 Ligand-Binding Domain. *J. Biol. Chem.* **2005**, 280 (19), 19250–19258.
- (344) Baker, K. D.; Shewchuk, L. M.; Kozlova, T.; Makishima, M.; Hassell, A.; Wisely, B.; Caravella, J. A.; Lambert, M. H.; Reinking, J. L.; Krause, H.; Thummel, C. S.; Willson, T. M.; Mangelsdorf, D. J. The *Drosophila* Orphan Nuclear Receptor DHR38 Mediates an Atypical Ecdysteroid Signaling Pathway. *Cell* **2003**, 113 (6), 731–742.
- (345) McFedries, A. K. Characterization of Protein-Metabolite and Protein-Substrate Interactions of Disease Genes, Harvard University, 2014.
- (346) de Vera, I. M. S.; Giri, P. K.; Munoz-Tello, P.; Brust, R.; Fuhrmann, J.; Matta-Camacho, E.; Shang, J.; Campbell, S.; Wilson, H. D.; Granados, J.; Gardner, W. J.; Creamer, T. P.; Solt, L. A.; Kojetin, D. J. Identification of a Binding Site for Unsaturated Fatty Acids in the Orphan Nuclear Receptor Nurr1. *ACS Chem. Biol.* **2016**, 11 (7), 1795–1799.
- (347) Rajan, S.; Jang, Y.; Kim, C.-H.; Kim, W.; Toh, H. T.; Jeon, J.; Song, B.; Serra, A.; Lescar, J.; Yoo, J. Y.; Beldar, S.; Ye, H.; Kang, C.; Liu, X.-W.; Feitosa, M.; Kim, Y.; Hwang, D.; Goh, G.; Lim, K.-L.; et al. PGE1 and PGA1 Bind to Nurr1 and Activate Its Transcriptional Function. *Nat. Chem. Biol.* **2020**, 16 (8), 876–886.
- (348) Maira, M.; Martens, C.; Batsché, E.; Gauthier, Y.; Drouin, J. Dimer-Specific Potentiation of NGFI-B (Nur77) Transcriptional Activity by the Protein Kinase A Pathway and AF-1-Dependent Coactivator Recruitment. *Mol. Cell. Biol.* **2003**, 23 (3), 763–776.
- (349) Codina, A.; Benoit, G.; Gooch, J. T.; Neuhaus, D.; Perlmann, T.; Schwabe, J. W. R. Identification of a Novel Co-Regulator Interaction Surface on the Ligand Binding Domain of Nurr1 Using NMR Footprinting. *J. Biol. Chem.* **2004**, 279 (51), 53338–53345.
- (350) Galleguillos, D.; Vecchiola, A.; Fuentealba, J. A.; Ojeda, V.; Alvarez, K.; Gómez, A.; Andrés, M. E. PIAS γ Represses the Transcriptional Activation Induced by the Nuclear Receptor Nurr1. *J. Biol. Chem.* **2004**, 279 (3), 2005–2011.

- (351) Lammi, J.; Perlmann, T.; Aarnisalo, P. Corepressor Interaction Differentiates the Permissive and Non-Permissive Retinoid X Receptor Heterodimers. *Arch. Biochem. Biophys.* **2008**, *472* (2), 105–114.
- (352) Xiao, Q.; Castillo, S. .; Nikodem, V. . Distribution of Messenger RNAs for the Orphan Nuclear Receptors Nurr1 and Nur77 (NGFI-B) in Adult Rat Brain Using in Situ Hybridization. *Neuroscience* **1996**, *75* (1), 221–230.
- (353) Zetterström, R. H.; Solomin, L.; Jansson, L.; Hoffer, B. J.; Olson, L.; Perlmann, T. Dopamine Neuron Agenesis in Nurr1-Deficient Mice. *Science* **1997**, *276* (5310), 248–250.
- (354) Zetterström, R. H.; Williams, R.; Perlmann, T.; Olson, L. Cellular Expression of the Immediate Early Transcription Factors Nurr1 and NGFI-B Suggests a Gene Regulatory Role in Several Brain Regions Including the Nigrostriatal Dopamine System. *Mol. Brain Res.* **1996**, *41* (1–2), 111–120.
- (355) Safe, S.; Jin, U.-H.; Morpurgo, B.; Abudayyeh, A.; Singh, M.; Tjalkens, R. B. Nuclear Receptor 4A (NR4A) Family – Orphans No More. *J. Steroid Biochem. Mol. Biol.* **2016**, *157*, 48–60.
- (356) Hamers, A. A. J.; Hanna, R. N.; Nowyhed, H.; Hedrick, C. C.; de Vries, C. J. M. NR4A Nuclear Receptors in Immunity and Atherosclerosis. *Curr. Opin. Lipidol.* **2013**, *24* (5), 381–385.
- (357) Bonta, P. I.; Pols, T. W. H.; van Tiel, C. M.; Vos, M.; Arkenbout, E. K.; Rohlena, J.; Koch, K. T.; de Maat, M. P. M.; Tanck, M. W. T.; de Winter, R. J.; Pannekoek, H.; Biessen, E. A. L.; Bot, I.; de Vries, C. J. M. Nuclear Receptor Nurr1 Is Expressed in and Is Associated with Human Restenosis and Inhibits Vascular Lesion Formation in Mice Involving Inhibition of Smooth Muscle Cell Proliferation and Inflammation. *Circulation* **2010**, *121* (18), 2023–2032.
- (358) Pearen, M. A.; Muscat, G. E. O. Minireview: Nuclear Hormone Receptor 4A Signaling: Implications for Metabolic Disease. *Mol. Endocrinol.* **2010**, *24* (10), 1891–1903.
- (359) McCoy, J. M.; Walkenhorst, D. E.; McCauley, K. S.; Elaasar, H.; Everett, J. R.; Mix, K. S. Orphan Nuclear Receptor NR4A2 Induces Transcription of the Immunomodulatory Peptide Hormone Prolactin. *J. Inflamm.* **2015**, *12*, 13.
- (360) Montarolo, F.; Martire, S.; Perga, S.; Spadaro, M.; Brescia, I.; Allegra, S.; De Francia, S.; Bertolotto, A. NURR1 Deficiency Is Associated to ADHD-like Phenotypes in Mice. *Transl. Psychiatry* **2019**, *9*, 207.
- (361) Dong, J.; Li, S.; Mo, J.-L.; Cai, H.-B.; Le, W.-D. Nurr1-Based Therapies for Parkinson’s Disease. *CNS Neurosci. Ther.* **2016**, *22* (5), 351–359.
- (362) Montarolo, F.; Martire, S.; Perga, S.; Bertolotto, A. NURR1 Impairment in Multiple Sclerosis. *Int. J. Mol. Sci.* **2019**, *20* (19), 4858.
- (363) Wallén, Å.; Zetterström, R. H.; Solomin, L.; Arvidsson, M.; Olson, L.; Perlmann, T. Fate of Mesencephalic AHD2-Expressing Dopamine Progenitor Cells in Nurr1 Mutant Mice. *Exp. Cell Res.* **1999**, *253* (2), 737–746.
- (364) Smits, S. M.; Ponnio, T.; Conneely, O. M.; Burbach, J. P. H.; Smidt, M. P. Involvement of Nurr1 in Specifying the Neurotransmitter Identity of Ventral Midbrain Dopaminergic Neurons. *Eur. J. Neurosci.* **2003**, *18* (7), 1731–1738.
- (365) Hermanson, E.; Joseph, B.; Castro, D.; Lindqvist, E.; Aarnisalo, P.; Wallén, Å.; Benoit, G.; Hengerer, B.; Olson, L.; Perlmann, T. Nurr1 Regulates Dopamine Synthesis and Storage in

- MN9D Dopamine Cells. *Exp. Cell Res.* **2003**, 288 (2), 324–334.
- (366) Jacobs, F. M. J.; van der Linden, A. J. A.; Wang, Y.; von Oerthel, L.; Sul, H. S.; Burbach, J. P. H.; Smidt, M. P. Identification of Dlk1, Ptpru and Klhl1 as Novel Nurr1 Target Genes in Meso-Diencephalic Dopamine Neurons. *Development* **2009**, 136 (14), 2363–2373.
- (367) Wallén, Å.; Castro, D. S.; Zetterström, R. H.; Karlén, M.; Olson, L.; Ericson, J.; Perlmann, T. Orphan Nuclear Receptor Nurr1 Is Essential for Ret Expression in Midbrain Dopamine Neurons and in the Brain Stem. *Mol. Cell. Neurosci.* **2001**, 18 (6), 649–663.
- (368) Hermanson, E.; Borgius, L.; Bergsland, M.; Joodmardi, E.; Perlmann, T. Neuropilin1 Is a Direct Downstream Target of Nurr1 in the Developing Brain Stem. *J. Neurochem.* **2006**, 97 (5), 1403–1411.
- (369) Gil, M.; McKinney, C.; Lee, M. K.; Eells, J. B.; Phyllaier, M. A.; Nikodem, V. M. Regulation of GTP Cyclohydrolase I Expression by Orphan Receptor Nurr1 in Cell Culture and in Vivo. *J. Neurochem.* **2007**, 101 (1), 142–150.
- (370) Luo, Y.; Henricksen, L. A.; Giuliano, R. E.; Prifti, L.; Callahan, L. M.; Federoff, H. J. VIP Is a Transcriptional Target of Nurr1 in Dopaminergic Cells. *Exp. Neurol.* **2007**, 203 (1), 221–232.
- (371) Heng, X.; Jin, G.; Zhang, X.; Yang, D.; Zhu, M.; Fu, S.; Li, X.; Le, W. Nurr1 Regulates Top II β and Functions in Axon Genesis of Mesencephalic Dopaminergic Neurons. *Mol. Neurodegener.* **2012**, 7, 4.
- (372) Kadkhodaei, B.; Alvarsson, A.; Schintu, N.; Ramsköld, D.; Volakakis, N.; Joodmardi, E.; Yoshitake, T.; Kehr, J.; Decressac, M.; Björklund, A.; Sandberg, R.; Svenningsson, P.; Perlmann, T. Transcription Factor Nurr1 Maintains Fiber Integrity and Nuclear-Encoded Mitochondrial Gene Expression in Dopamine Neurons. *Proc. Natl. Acad. Sci.* **2013**, 110 (6), 2360–2365.
- (373) Lammi, J.; Hupponen, J.; Aarnisalo, P. Regulation of the Osteopontin Gene by the Orphan Nuclear Receptor NURR1 in Osteoblasts. *Mol. Endocrinol.* **2004**, 18 (6), 1546–1557.
- (374) Pirih, F. Q.; Tang, A.; Ozkurt, I. C.; Nervina, J. M.; Tetradis, S. Nuclear Orphan Receptor Nurr1 Directly Transactivates the Osteocalcin Gene in Osteoblasts. *J. Biol. Chem.* **2004**, 279 (51), 53167–53174.
- (375) Castillo, S. O.; Baffi, J. S.; Palkovits, M.; Goldstein, D. S.; Kopin, I. J.; Witta, J.; Magnuson, M. A.; Nikodem, V. M. Dopamine Biosynthesis Is Selectively Abolished in Substantia Nigra/Ventral Tegmental Area but Not in Hypothalamic Neurons in Mice with Targeted Disruption of the Nurr1 Gene. *Mol. Cell. Neurosci.* **1998**, 11 (1–2), 36–46.
- (376) Nsegbe, E.; Wallén-Mackenzie, Å.; Dauger, S.; Roux, J.-C.; Shvarev, Y.; Lagercrantz, H.; Perlmann, T.; Herlenius, E. Congenital Hypoventilation and Impaired Hypoxic Response in Nurr1 Mutant Mice. *J. Physiol.* **2004**, 556 (1), 43–59.
- (377) Decressac, M.; Kadkhodaei, B.; Mattsson, B.; Laguna, A.; Perlmann, T.; Björklund, A. α -Synuclein-Induced Down-Regulation of Nurr1 Disrupts GDNF Signaling in Nigral Dopamine Neurons. *Sci. Transl. Med.* **2012**, 4 (163), 163ra156.
- (378) Montarolo, F.; Perga, S.; Martire, S.; Bertolotto, A. Nurr1 Reduction Influences the Onset of Chronic EAE in Mice. *Inflamm. Res.* **2015**, 64 (11), 841–844.
- (379) Volakakis, N.; Kadkhodaei, B.; Joodmardi, E.; Wallis, K.; Panman, L.; Silvaggi, J.; Spiegelman, B.

- M.; Perlmann, T. NR4A Orphan Nuclear Receptors as Mediators of CREB-Dependent Neuroprotection. *Proc. Natl. Acad. Sci.* **2010**, *107* (27), 12317–12322.
- (380) Moon, M.; Jung, E. S.; Jeon, S. G.; Cha, M.-Y.; Jang, Y.; Kim, W.; Lopes, C.; Mook-Jung, I.; Kim, K.-S. Nurr1 (NR4A2) Regulates Alzheimer's Disease-Related Pathogenesis and Cognitive Function in the 5XFAD Mouse Model. *Aging Cell* **2019**, *18* (1), e12866.
- (381) Raveney, B. J. E.; Oki, S.; Yamamura, T. Nuclear Receptor NR4A2 Orchestrates Th17 Cell-Mediated Autoimmune Inflammation via IL-21 Signalling. *PLoS One* **2013**, *8* (2), e56595.
- (382) Liu, H.; Liu, H.; Li, T.; Cui, J.; Fu, Y.; Ren, J.; Sun, X.; Jiang, P.; Yu, S.; Li, C. NR4A2 Genetic Variation and Parkinson's Disease: Evidence from a Systematic Review and Meta-Analysis. *Neurosci. Lett.* **2017**, *650*, 25–32.
- (383) Chu, Y.; Le, W.; Kompoliti, K.; Jankovic, J.; Mufson, E. J.; Kordower, J. H. Nurr1 in Parkinson's Disease and Related Disorders. *J. Comp. Neurol.* **2006**, *494* (3), 495–514.
- (384) Liu, W.; Gao, Y.; Chang, N. Nurr1 Overexpression Exerts Neuroprotective and Anti-Inflammatory Roles via down-Regulating CCL2 Expression in Both in Vivo and in Vitro Parkinson's Disease Models. *Biochem. Biophys. Res. Commun.* **2017**, *482* (4), 1312–1319.
- (385) Volakakis, N.; Tiklova, K.; Decressac, M.; Papatthanou, M.; Mattsson, B.; Gillberg, L.; Nobre, A.; Björklund, A.; Perlmann, T. Nurr1 and Retinoid X Receptor Ligands Stimulate Ret Signaling in Dopamine Neurons and Can Alleviate α -Synuclein Disrupted Gene Expression. *J. Neurosci.* **2015**, *35* (42), 14370–14385.
- (386) Wang, X.; Zhuang, W.; Fu, W.; Wang, X.; Lv, E.; Li, F.; Zhou, S.; Rausch, W.-D.; Wang, X. The Lentiviral-Mediated Nurr1 Genetic Engineering Mesenchymal Stem Cells Protect Dopaminergic Neurons in a Rat Model of Parkinson's Disease. *Am. J. Transl. Res.* **2018**, *10* (6), 1583–1599.
- (387) Pajares, M.; Rojo, A. I.; Manda, G.; Boscá, L.; Cuadrado, A. Inflammation in Parkinson's Disease: Mechanisms and Therapeutic Implications. *Cells* **2020**, *9* (7), 1687.
- (388) Yi, S.-H.; He, X.-B.; Rhee, Y.-H.; Park, C.-H.; Takizawa, T.; Nakashima, K.; Lee, S.-H. Foxa2 Acts as a Co-Activator Potentiating Expression of the Nurr1-Induced DA Phenotype via Epigenetic Regulation. *Development* **2014**, *141* (4), 761–772.
- (389) Kim, C.-H.; Han, B.-S.; Moon, J.; Kim, D.-J.; Shin, J.; Rajan, S.; Nguyen, Q. T.; Sohn, M.; Kim, W.-G.; Han, M.; Jeong, I.; Kim, K.-S.; Lee, E.-H.; Tu, Y.; Naffin-Olivos, J. L.; Park, C.-H.; Ringe, D.; Yoon, H. S.; Petsko, G. A.; et al. Nuclear Receptor Nurr1 Agonists Enhance Its Dual Functions and Improve Behavioral Deficits in an Animal Model of Parkinson's Disease. *Proc. Natl. Acad. Sci.* **2015**, *112* (28), 8756–8761.
- (390) Bruning, J. M.; Wang, Y.; Oltrabella, F.; Tian, B.; Kholodar, S. A.; Liu, H.; Bhattacharya, P.; Guo, S.; Holton, J. M.; Fletterick, R. J.; Jacobson, M. P.; England, P. M. Covalent Modification and Regulation of the Nuclear Receptor Nurr1 by a Dopamine Metabolite. *Cell Chem. Biol.* **2019**, *26* (5), 674–685.e6.
- (391) Smith, G. A.; Rocha, E. M.; Rooney, T.; Barneoud, P.; McLean, J. R.; Beagan, J.; Osborn, T.; Coimbra, M.; Luo, Y.; Hallett, P. J.; Isacson, O. A Nurr1 Agonist Causes Neuroprotection in a Parkinson's Disease Lesion Model Primed with the Toll-Like Receptor 3 DsRNA Inflammatory Stimulant Poly(I:C). *PLoS One* **2015**, *10* (3), e0121072.

- (392) España, J.; Valero, J.; Miñano-Molina, A. J.; Masgrau, R.; Martín, E.; Guardia-Laguarta, C.; Lleó, A.; Giménez-Llort, L.; Rodríguez-Alvarez, J.; Saura, C. A. β -Amyloid Disrupts Activity-Dependent Gene Transcription Required for Memory through the CREB Coactivator CRTCC1. *J. Neurosci.* **2010**, *30* (28), 9402–9410.
- (393) Parra-Damas, A.; Valero, J.; Chen, M.; España, J.; Martín, E.; Ferrer, I.; Rodríguez-Alvarez, J.; Saura, C. A. Crtc1 Activates a Transcriptional Program Deregulated at Early Alzheimer's Disease-Related Stages. *J. Neurosci.* **2014**, *34* (17), 5776–5787.
- (394) Moon, M.; Jeong, I.; Kim, C.-H.; Kim, J.; Lee, P. K. J.; Mook-Jung, I.; Leblanc, P.; Kim, K.-S. Correlation between Orphan Nuclear Receptor Nurr1 Expression and Amyloid Deposition in 5XFAD Mice, an Animal Model of Alzheimer's Disease. *J. Neurochem.* **2015**, *132* (2), 254–262.
- (395) Terzioglu-Usak, S.; Negis, Y.; Karabulut, D. S.; Zaim, M.; Isik, S. Cellular Model of Alzheimer's Disease: A β 1-42 Peptide Induces Amyloid Deposition and a Decrease in Topo Isomerase II β and Nurr1 Expression. *Curr. Alzheimer Res.* **2017**, *14* (6), 636–644.
- (396) Satoh, J.; Nakanishi, M.; Koike, F.; Onoue, H.; Aranami, T.; Yamamoto, T.; Kawai, M.; Kikuchi, S.; Nomura, K.; Yokoyama, K.; Ota, K.; Saito, T.; Ohta, M.; Miyake, S.; Kanda, T.; Fukazawa, T.; Yamamura, T. T Cell Gene Expression Profiling Identifies Distinct Subgroups of Japanese Multiple Sclerosis Patients. *J. Neuroimmunol.* **2006**, *174* (1–2), 108–118.
- (397) Montarolo, F.; Raffaele, C.; Perga, S.; Martire, S.; Finardi, A.; Furlan, R.; Hintermann, S.; Bertolotto, A. Effects of Isoxazolo-Pyridinone 7e, a Potent Activator of the Nurr1 Signaling Pathway, on Experimental Autoimmune Encephalomyelitis in Mice. *PLoS One* **2014**, *9* (9), e108791.
- (398) Saini, A.; Mahajan, S.; Gupta, P. Nuclear Receptor Expression Atlas in BMDCs: Nr4a2 Restricts Immunogenicity of BMDCs and Impedes EAE. *Eur. J. Immunol.* **2016**, *46* (8), 1842–1853.
- (399) Egan, T. J. Quinoline Antimalarials. *Expert Opin. Ther. Pat.* **2001**, *11* (2), 185–209.
- (400) Munoz-Tello, P.; Lin, H.; Khan, P.; de Vera, I. M. S.; Kamenecka, T. M.; Kojetin, D. J. Assessment of NR4A Ligands That Directly Bind and Modulate the Orphan Nuclear Receptor Nurr1. *J. Med. Chem.* **2020**, *63* (24), 15639–15654.
- (401) Zhan, Y.; Chen, Y.; Zhang, Q.; Zhuang, J.; Tian, M.; Chen, H.; Zhang, L.; Zhang, H.; He, J.; Wang, W.; Wu, R.; Wang, Y.; Shi, C.; Yang, K.; Li, A.; Xin, Y.; Li, T. Y.; Yang, J. Y.; Zheng, Z.; et al. The Orphan Nuclear Receptor Nur77 Regulates LKB1 Localization and Activates AMPK. *Nat. Chem. Biol.* **2012**, *8* (11), 897–904.
- (402) Yang, P.-B.; Hou, P.-P.; Liu, F.-Y.; Hong, W.-B.; Chen, H.-Z.; Sun, X.-Y.; Li, P.; Zhang, Y.; Ju, C.-Y.; Luo, L.-J.; Wu, S.; Zhou, J.-X.; Wang, Z.-J.; He, J.-P.; Li, L.; Zhao, T.-J.; Deng, X.; Lin, T.; Wu, Q. Blocking PPAR γ Interaction Facilitates Nur77 Interdiction of Fatty Acid Uptake and Suppresses Breast Cancer Progression. *Proc. Natl. Acad. Sci.* **2020**, *117* (44), 27412–27422.
- (403) Wei, Z.-X.; Tang, T.-T.; Jiang, S.-P. The Antiviral Mechanisms, Effects, Safety and Adverse Effects of Chloroquine. *Eur. Rev. Med. Pharmacol. Sci.* **2020**, *24* (12), 7164–7172.
- (404) Plantone, D.; Koudriavtseva, T. Current and Future Use of Chloroquine and Hydroxychloroquine in Infectious, Immune, Neoplastic, and Neurological Diseases: A Mini-Review. *Clin. Drug Investig.* **2018**, *38* (8), 653–671.

- (405) Lee, S. G.; Alpert, T. D.; Jez, J. M. Crystal Structure of Phosphoethanolamine Methyltransferase from *Plasmodium Falciparum* in Complex with Amodiaquine. *Bioorg. Med. Chem. Lett.* **2012**, *22* (15), 4990–4993.
- (406) Ren, S.; Zeng, J.; Mei, Y.; Zhang, J. Z. H.; Yan, S. F.; Fei, J.; Chen, L. Discovery and Characterization of Novel, Potent, and Selective Cytochrome P450 2J2 Inhibitors. *Drug Metab. Dispos.* **2013**, *41* (1), 60–71.
- (407) Gordon, D. E.; Jang, G. M.; Bouhaddou, M.; Xu, J.; Obernier, K.; White, K. M.; O’Meara, M. J.; Rezelj, V. V.; Guo, J. Z.; Swaney, D. L.; Tummino, T. A.; Hüttenhain, R.; Kaake, R. M.; Richards, A. L.; Tutuncuoglu, B.; Foussard, H.; Batra, J.; Haas, K.; Modak, M.; et al. A SARS-CoV-2 Protein Interaction Map Reveals Targets for Drug Repurposing. *Nature* **2020**, *583*, 459–468.
- (408) Tang, Y.; Wu, Q.; Beland, F. A.; Chen, S.; Fang, J.-L. Apoptosis Contributes to the Cytotoxicity Induced by Amodiaquine and Its Major Metabolite N-Desethylamodiaquine in Hepatic Cells. *Toxicol. Vitro.* **2020**, *62*, 104669.
- (409) Kim, T. H.; Kim, H. K.; Hwang, E. S. Novel Anti-Adipogenic Activity of Anti-Malarial Amodiaquine through Suppression of PPAR γ Activity. *Arch. Pharm. Res.* **2017**, *40* (11), 1336–1343.
- (410) White, N. J. Cardiotoxicity of Antimalarial Drugs. *Lancet Infect. Dis.* **2007**, *7* (8), 549–558.
- (411) Neftel, K. A.; Woodtly, W.; Schmid, M.; Frick, P. G.; Fehr, J. Amodiaquine Induced Agranulocytosis and Liver Damage. *BMJ (Clin Res Ed)* **1986**, *292*, 721–723.
- (412) Hatton, C. S. R.; Bunch, C.; Peto, T. E. A.; Pasvol, G.; Russell, S. J.; Singer, C. R. J.; Edwards, G.; Winstanley, P. Frequency of Severe Neutropenia Associated with Amodiaquine Prophylaxis against Malaria. *Lancet* **1986**, *327* (8478), 411–414.
- (413) Costedoat-Chalumeau, N.; Dunogué, B.; Leroux, G.; Morel, N.; Jallouli, M.; Le Guern, V.; Piette, J.-C.; Brézin, A. P.; Melles, R. B.; Marmor, M. F. A Critical Review of the Effects of Hydroxychloroquine and Chloroquine on the Eye. *Clin. Rev. Allergy Immunol.* **2015**, *49*, 317–326.
- (414) Viola, G.; Salvador, A.; Ceconet, L.; Basso, G.; Vedaldi, D.; Dall’Acqua, F.; Aloisi, G. G.; Amelia, M.; Barbafina, A.; Latterini, L.; Elisei, F. Photophysical Properties and Photobiological Behavior of Amodiaquine, Primaquine and Chloroquine. *Photochem. Photobiol.* **2007**, *83* (6), 1415–1427.
- (415) Arredondo, C.; Orellana, M.; Vecchiola, A.; Pereira, L. A.; Galdames, L.; Andrés, M. E. PIASy Enhanced SUMO-2 Modification of Nurr1 Activation-Function-1 Domain Limits Nurr1 Transcriptional Synergy. *PLoS One* **2013**, *8* (1), e55035.
- (416) de Vera, I. M. S.; Munoz-Tello, P.; Zheng, J.; Dharmarajan, V.; Marciano, D. P.; Matta-Camacho, E.; Giri, P. K.; Shang, J.; Hughes, T. S.; Rance, M.; Griffin, P. R.; Kojetin, D. J. Defining a Canonical Ligand-Binding Pocket in the Orphan Nuclear Receptor Nurr1. *Structure* **2019**, *27* (1), 66–77.e5.
- (417) Windshügel, B. Structural Insights into Ligand-Binding Pocket Formation in Nurr1 by Molecular Dynamics Simulations. *J. Biomol. Struct. Dyn.* **2019**, *37* (17), 4651–4657.
- (418) Hashimoto, M.; Hossain, S.; Mamun, A. Al; Matsuzaki, K.; Arai, H. Docosahexaenoic Acid: One Molecule Diverse Functions. *Crit. Rev. Biotechnol.* **2017**, *37* (5), 579–597.
- (419) Rajan, S.; Lescar, J.; Yoon, H. S. Co-Crystal Structure and Function of Nurr1 Bound to the

- Cyclopentenone Prostaglandin A₁. *PDB ID: 5Y41*. <http://www.rcsb.org/structure/5Y41>. December 26, **2018**.
- (420) Rajan, S.; Toh, H. T.; Lim, K. H.; Yoon, H. S. Structure of Nurr1 Bound to Cyclopentenone Prostaglandin A₂ and Its Mechanism of Action in Ameliorating Dopaminergic Neurodegeneration in *Drosophila*. *PDB ID: 5YD6*. <http://www.rcsb.org/structure/5YD6>. March 27, **2019**.
- (421) Yoon, H. S.; Rajan, S.; Toh, H. T.; Liu, X.; Yao, H. Co-Crystals of Nurr1-LBD in Complex with a Cyclopentenone Prostaglandin and Modulators of Nurr1. WO2018/056905A1. *Nanyang Technol. Univ.* **2018**.
- (422) Kholodar, S. A.; Lang, G.; Cortopassi, W. A.; Iizuka, Y.; Brah, H. S.; Jacobson, M. P.; England, P. M. Analogs of the Dopamine Metabolite 5,6-Dihydroxyindole Bind Directly to and Activate the Nuclear Receptor Nurr1. *ACS Chem. Biol.* **2021**, *16* (7), 1159–1163.
- (423) Janowski, B. A.; Willy, P. J.; Devi, T. R.; Falck, J. R.; Mangelsdorf, D. J. An Oxysterol Signalling Pathway Mediated by the Nuclear Receptor LXR α . *Nature* **1996**, *383*, 728–731.
- (424) de Urquiza, A. M.; Liu, S.; Sjöberg, M.; Zetterström, R. H.; Griffiths, W.; Sjövall, J.; Perlmann, T. Docosahexaenoic Acid, a Ligand for the Retinoid X Receptor in Mouse Brain. *Science* **2000**, *290* (5499), 2140–2144.
- (425) Neuringer, M.; Anderson, G. J.; Connor, W. E. The Essentiality of N-3 Fatty Acids for the Development and Function of the Retina and Brain. *Annu. Rev. Nutr.* **1988**, *8*, 517–541.
- (426) Moore, S. A.; Yoder, E.; Murphy, S.; Dutton, G. R.; Spector, A. A. Astrocytes, Not Neurons, Produce Docosahexaenoic Acid (22:6 ω -3) and Arachidonic Acid (20:4 ω -6). *J. Neurochem.* **1991**, *56* (2), 518–524.
- (427) Code, C.; Ebbesen, M. F.; Sood, R.; Kinnunen, P. K. J. Activation of Phospholipase A₂ by Prostaglandin in Vitro. *Prostaglandins Other Lipid Mediat.* **2021**, *152*, 106500.
- (428) Higdon, A.; Diers, A. R.; Oh, J. Y.; Landar, A.; Darley-Usmar, V. M. Cell Signalling by Reactive Lipid Species: New Concepts and Molecular Mechanisms. *Biochem. J.* **2012**, *442* (3), 453–464.
- (429) Zhang, H.-L.; Huang, Z. H.; Zhu, Y.; Liang, Z.-Q.; Han, R.; Wang, X.-X.; Chase, T. N.; Qin, Z.-H. Neuroprotective Effects of Prostaglandin A₁ in Animal Models of Focal Ischemia. *Brain Res.* **2005**, *1039* (1–2), 203–206.
- (430) Wang, X.; Qin, Z.-H.; Leng, Y.; Wang, Y.; Jin, X.; Chase, T. N.; Bennett, M. C. Prostaglandin A₁ Inhibits Rotenone-Induced Apoptosis in SH-SY5Y Cells. *J. Neurochem.* **2002**, *83* (5), 1094–1102.
- (431) Qin, Z.-H.; Wang, Y.; Chen, R.-W.; Wang, X.; Ren, M.; Chuang, D.-M.; Chase, T. N. Prostaglandin A₁ Protects Striatal Neurons against Excitotoxic Injury in Rat Striatum. *J. Pharmacol. Exp. Ther.* **2001**, *297* (1), 78–87.
- (432) Spector, A. A. Essentiality of Fatty Acids. *Lipids* **1999**, *34*, S1–S3.
- (433) Burbulla, L. F.; Song, P.; Mazzulli, J. R.; Zampese, E.; Wong, Y. C.; Jeon, S.; Santos, D. P.; Blanz, J.; Obermaier, C. D.; Strojny, C.; Savas, J. N.; Kiskinis, E.; Zhuang, X.; Krüger, R.; Surmeier, D. J.; Krainc, D. Dopamine Oxidation Mediates Mitochondrial and Lysosomal Dysfunction in Parkinson's Disease. *Science* **2017**, *357* (6357), 1255–1261.

- (434) Hastings, T. G. The Role of Dopamine Oxidation in Mitochondrial Dysfunction: Implications for Parkinson's Disease. *J. Bioenerg. Biomembr.* **2009**, *41*, 469–472.
- (435) Lotharius, J.; Brundin, P. Pathogenesis of Parkinson's Disease: Dopamine, Vesicles and α -Synuclein. *Nat. Rev. Neurosci.* **2002**, *3* (12), 932–942.
- (436) Olefirowicz, T. M.; Ewing, A. G. Dopamine Concentration in the Cytoplasmic Compartment of Single Neurons Determined by Capillary Electrophoresis. *J. Neurosci. Methods* **1990**, *34* (1–3), 11–15.
- (437) Mosharov, E. V.; Staal, R. G. W.; Bové, J.; Prou, D.; Hananiya, A.; Markov, D.; Poulsen, N.; Larsen, K. E.; Moore, C. M. H.; Troyer, M. D.; Edwards, R. H.; Przedborski, S.; Sulzer, D. α -Synuclein Overexpression Increases Cytosolic Catecholamine Concentration. *J. Neurosci.* **2006**, *26* (36), 9304–9311.
- (438) Mosharov, E. V.; Larsen, K. E.; Kanter, E.; Phillips, K. A.; Wilson, K.; Schmitz, Y.; Krantz, D. E.; Kobayashi, K.; Edwards, R. H.; Sulzer, D. Interplay between Cytosolic Dopamine, Calcium, and α -Synuclein Causes Selective Death of Substantia Nigra Neurons. *Neuron* **2009**, *62* (2), 218–229.
- (439) Belluzzi, E.; Bisaglia, M.; Lazzarini, E.; Tabares, L. C.; Beltramini, M.; Bubacco, L. Human SOD2 Modification by Dopamine Quinones Affects Enzymatic Activity by Promoting Its Aggregation: Possible Implications for Parkinson's Disease. *PLoS One* **2012**, *7* (6), e38026.
- (440) Kuhn, D. M.; Arthur, R. E.; Thomas, D. M.; Elferink, L. A. Tyrosine Hydroxylase Is Inactivated by Catechol-Quinones and Converted to a Redox-Cycling Quinoprotein. *J. Neurochem.* **1999**, *73* (3), 1309–1317.
- (441) Whitehead, R. E.; Ferrer, J. V.; Javitch, J. A.; Justice, J. B. Reaction of Oxidized Dopamine with Endogenous Cysteine Residues in the Human Dopamine Transporter. *J. Neurochem.* **2001**, *76* (4), 1242–1251.
- (442) Bisaglia, M.; Mammi, S.; Bubacco, L. Kinetic and Structural Analysis of the Early Oxidation Products of Dopamine: Analysis of the Interactions with α -Synuclein. *J. Biol. Chem.* **2007**, *282* (21), 15597–15605.
- (443) LaVoie, M. J.; Ostaszewski, B. L.; Weihofen, A.; Schlossmacher, M. G.; Selkoe, D. J. Dopamine Covalently Modifies and Functionally Inactivates Parkin. *Nat. Med.* **2005**, *11* (11), 1214–1221.
- (444) Willems, S.; Kilu, W.; Ni, X.; Chaikuad, A.; Knapp, S.; Heering, J.; Merk, D. The Orphan Nuclear Receptor Nurr1 Is Responsive to Non-Steroidal Anti-Inflammatory Drugs. *Commun. Chem.* **2020**, *3*, 85.
- (445) Camacho, C.; Coulouris, G.; Avagyan, V.; Ma, N.; Papadopoulos, J.; Bealer, K.; Madden, T. L. BLAST+: Architecture and Applications. *BMC Bioinformatics* **2009**, *10*, 421.
- (446) Inamoto, T.; Papineni, S.; Chintharlapalli, S.; Cho, S.-D.; Safe, S.; Kamat, A. M. 1,1-Bis(3'-Indolyl)-1-(*p*-Chlorophenyl)Methane Activates the Orphan Nuclear Receptor Nurr1 and Inhibits Bladder Cancer Growth. *Mol. Cancer Ther.* **2008**, *7* (12), 3825–3833.
- (447) Ordentlich, P.; Yan, Y.; Zhou, S.; Heyman, R. A. Identification of the Antineoplastic Agent 6-Mercaptopurine as an Activator of the Orphan Nuclear Hormone Receptor Nurr1. *J. Biol. Chem.* **2003**, *278* (27), 24791–24799.
- (448) Wei, X.; Gao, H.; Zou, J.; Liu, X.; Chen, D.; Liao, J.; Xu, Y.; Ma, L.; Tang, B.; Zhang, Z.; Cai, X.;

- Jin, K.; Xia, Y.; Wang, Q. Contra-Directional Coupling of Nur77 and Nurr1 in Neurodegeneration: A Novel Mechanism for Memantine-Induced Anti-Inflammation and Anti-Mitochondrial Impairment. *Mol. Neurobiol.* **2016**, *53*, 5876–5892.
- (449) Rouillard, C.; Baillargeon, J.; Paquet, B.; St-Hilaire, M.; Maheux, J.; Lévesque, C.; Darlix, N.; Majeur, S.; Lévesque, D. Genetic Disruption of the Nuclear Receptor Nur77 (Nr4a1) in Rat Reduces Dopamine Cell Loss and L-Dopa-Induced Dyskinesia in Experimental Parkinson's Disease. *Exp. Neurol.* **2018**, *304*, 143–153.
- (450) Popichak, K. A.; Hammond, S. L.; Moreno, J. A.; Afzali, M. F.; Backos, D. S.; Slayden, R. D.; Safe, S.; Tjalkens, R. B. Compensatory Expression of Nur77 and Nurr1 Regulates NF-KB-Dependent Inflammatory Signaling in Astrocytes. *Mol. Pharmacol.* **2018**, *94* (4), 1174–1186.
- (451) Kagaya, S.; Ohkura, N.; Tsukada, T.; Miyagawa, M.; Sugita, Y.; Tsujimoto, G.; Matsumoto, K.; Saito, H.; Hashida, R. Prostaglandin A2 Acts as a Transactivator for NOR1 (NR4A3) within the Nuclear Receptor Superfamily. *Biol. Pharm. Bull.* **2005**, *28* (9), 1603–1607.
- (452) Hinnah, K.; Willems, S.; Morstein, J.; Heering, J.; Hartrampf, F. W. W.; Broichhagen, J.; Leippe, P.; Merk, D.; Trauner, D. Photohormones Enable Optical Control of the Peroxisome Proliferator-Activated Receptor γ (PPAR γ). *J. Med. Chem.* **2020**, *63* (19), 10908–10920.
- (453) Willems, S.; Morstein, J.; Hinnah, K.; Trauner, D.; Merk, D. A Photohormone for Light-Dependent Control of PPAR α in Live Cells. *J. Med. Chem.* **2021**, *64* (14), 10393–10402.
- (454) Willems, S.; Gellrich, L.; Chaikuad, A.; Kluge, S.; Werz, O.; Heering, J.; Knapp, S.; Lorkowski, S.; Schubert-Zsilavecz, M.; Merk, D. Endogenous Vitamin E Metabolites Mediate Allosteric PPAR γ Activation with Unprecedented Co-Regulatory Interactions. *Cell Chem. Biol.* **2021**, *28* (10), 1489-1500.e8.
- (455) Willems, S.; Ohrndorf, J.; Kilu, W.; Heering, J.; Merk, D. Fragment-like Chloroquinolineamines Activate the Orphan Nuclear Receptor Nurr1 and Elucidate Activation Mechanisms. *J. Med. Chem.* **2021**, *64* (5), 2659–2668.
- (456) MacArron, R.; Banks, M. N.; Bojanic, D.; Burns, D. J.; Cirovic, D. A.; Garyantes, T.; Green, D. V. S.; Hertzberg, R. P.; Janzen, W. P.; Paslay, J. W.; Schopfer, U.; Sittampalam, G. S. Impact of High-Throughput Screening in Biomedical Research. *Nat. Rev. Drug Discov.* **2011**, *10* (3), 188–195.
- (457) Jhoti, H.; Williams, G.; Rees, D. C.; Murray, C. W. The “rule of Three” for Fragment-Based Drug Discovery: Where Are We Now? *Nat. Rev. Drug Discov.* **2013**, *12* (8), 644.
- (458) Baker, M. Fragment-Based Lead Discovery Grows Up. *Nat. Rev. Drug Discov.* **2013**, *12* (1), 5–7.
- (459) Wermuth, C. G. Selective Optimization of Side Activities: The SOSA Approach. *Drug Discov. Today* **2006**, *11* (3–4), 160–164.
- (460) Willems, S.; Kilu, W.; Faudone, G.; Heering, J.; Merk, D. Nurr1 Modulation Mediates Neuroprotective Effects of Statins. *bioRxiv* **2021**, 2021.09.15.460433.
- (461) Zaienne, D.; Willems, S.; Schierle, S.; Heering, J.; Merk, D. Development and Profiling of Inverse Agonist Tools for the Neuroprotective Transcription Factor Nurr1. *J. Med. Chem.* **2021**, *64* (20), 15126–15140.
- (462) Broichhagen, J.; Frank, J. A.; Trauner, D. A Roadmap to Success in Photopharmacology. *Acc. Chem. Res.* **2015**, *48* (7), 1947–1960.

- (463) Nevin, D. K.; Peters, M. B.; Carta, G.; Fayne, D.; Lloyd, D. G. Integrated Virtual Screening for the Identification of Novel and Selective Peroxisome Proliferator-Activated Receptor (PPAR) Scaffolds. *J. Med. Chem.* **2012**, *55* (11), 4978–4989.
- (464) Henke, B. R.; Blanchard, S. G.; Brackeen, M. F.; Brown, K. K.; Cobb, J. E.; Collins, J. L.; Harrington, W. W.; Hashim, M. A.; Hull-Ryde, E. A.; Kaldor, I.; Kliewer, S. A.; Lake, D. H.; Leesnitzer, L. M.; Lehmann, J. M.; Lenhard, J. M.; Orband-Miller, L. A.; Miller, J. F.; Mook, R. A.; Noble, S. A.; et al. *N*-(2-Benzoylphenyl)-*L*-Tyrosine PPAR γ Agonists. 1. Discovery of a Novel Series of Potent Antihyperglycemic and Antihyperlipidemic Agents. *J. Med. Chem.* **1998**, *41* (25), 5020–5036.
- (465) Giampietro, L.; D'Angelo, A.; Giancristofaro, A.; Ammazalorso, A.; De Filippis, B.; Fantacuzzi, M.; Linciano, P.; Maccallini, C.; Amoroso, R. Synthesis and Structure-Activity Relationships of Fibrate-Based Analogues inside PPARs. *Bioorg. Med. Chem. Lett.* **2012**, *22* (24), 7662–7666.
- (466) Giampietro, L.; Laghezza, A.; Cerchia, C.; Florio, R.; Recinella, L.; Capone, F.; Ammazalorso, A.; Bruno, I.; De Filippis, B.; Fantacuzzi, M.; Ferrante, C.; Maccallini, C.; Tortorella, P.; Verginelli, F.; Brunetti, L.; Cama, A.; Amoroso, R.; Loiodice, F.; Lavecchia, A. Novel Phenylidiazanyl Fibrate Analogues as PPAR $\alpha/\gamma/\delta$ Pan-Agonists for the Amelioration of Metabolic Syndrome. *ACS Med. Chem. Lett.* **2019**, *10* (4), 545–551.
- (467) Chrisman, I. M.; Mou, T. C.; Sprang, S. R.; Hughes, T. S. PPAR Gamma LBD Complexed with the Agonist GW1929. *PDB: 6D8X*. <https://www.rcsb.org/structure/6D8X>. May 1, **2019**.
- (468) dos Santos, J. C.; Bernardes, A.; Giampietro, L.; Ammazalorso, A.; De Filippis, B.; Amoroso, R.; Polikarpov, I. Different Binding and Recognition Modes of GL479, a Dual Agonist of Peroxisome Proliferator-Activated Receptor α/γ . *J. Struct. Biol.* **2015**, *191* (3), 332–340.
- (469) Rau, O.; Wurglics, M.; Paulke, A.; Zitzkowski, J.; Meindl, N.; Bock, A.; Dingermann, T.; Abdel-Tawab, M.; Schubert-Zsilavecz, M. Carnosic Acid and Carnosol, Phenolic Diterpene Compounds of the Labiate Herbs Rosemary and Sage, Are Activators of the Human Peroxisome Proliferator-Activated Receptor Gamma. *Planta Med.* **2006**, *72* (10), 881–887.
- (470) Kim, H. L.; Chin, J. W.; Cho, S. J.; Song, J. Y.; Yoon, H. S.; Bae, J. H. Design, Synthesis, and the X-Ray Co-Crystal Structure of Highly Potent, Selective, and Orally Bioavailable, Novel Peroxisome Proliferator-Activated Receptor Delta Agonists. *PDB ID: 5Y7X*. <https://www.rcsb.org/structure/5Y7X>. August 1, 2018.
- (471) Birringer, M.; Lorkowski, S. Vitamin E: Regulatory Role of Metabolites. *IUBMB Life* **2019**, *71* (4), 479–486.
- (472) Pein, H.; Ville, A.; Pace, S.; Temml, V.; Garscha, U.; Raasch, M.; Alsabil, K.; Viault, G.; Dinh, C.-P.; Guilet, D.; Troisi, F.; Neukirch, K.; König, S.; Bilancia, R.; Waltenberger, B.; Stuppner, H.; Wallert, M.; Lorkowski, S.; Weinigel, C.; et al. Endogenous Metabolites of Vitamin E Limit Inflammation by Targeting 5-Lipoxygenase. *Nat. Commun.* **2018**, *9*, 3834.
- (473) Wallert, M.; Bauer, J.; Kluge, S.; Schmölz, L.; Chen, Y.-C.; Ziegler, M.; Searle, A. K.; Maxones, A.; Schubert, M.; Thürmer, M.; Pein, H.; Koeberle, A.; Werz, O.; Birringer, M.; Peter, K.; Lorkowski, S. The Vitamin E Derivative Garcinoic Acid from *Garcinia Kola* Nut Seeds Attenuates the Inflammatory Response. *Redox Biol.* **2019**, *24*, 101166.
- (474) Lavine, J. E.; Schwimmer, J. B.; Van Natta, M. L.; Molleston, J. P.; Murray, K. F.; Rosenthal, P.;

- Abrams, S. H.; Scheimann, A. O.; Sanyal, A. J.; Chalasani, N.; Tonascia, J.; Ünalp, A.; Clark, J. M.; Brunt, E. M.; Kleiner, D. E.; Hoofnagle, J. H.; Robuck, P. R. Effect of Vitamin E or Metformin for Treatment of Nonalcoholic Fatty Liver Disease in Children and Adolescents. *JAMA* **2011**, *305* (16), 1659–1668.
- (475) Sanyal, A. J.; Chalasani, N.; Kowdley, K. V.; McCullough, A.; Diehl, A. M.; Bass, N. M.; Neuschwander-Tetri, B. A.; Lavine, J. E.; Tonascia, J.; Ünalp, A.; Van Natta, M.; Clark, J.; Brunt, E. M.; Kleiner, D. E.; Hoofnagle, J. H.; Robuck, P. R. Pioglitazone, Vitamin E, or Placebo for Nonalcoholic Steatohepatitis. *N. Engl. J. Med.* **2010**, *362* (18), 1675–1685.
- (476) Dysken, M. W.; Sano, M.; Asthana, S.; Vertrees, J. E.; Pallaki, M.; Llorente, M.; Love, S.; Schellenberg, G. D.; McCarten, J. R.; Malphurs, J.; Prieto, S.; Chen, P.; Loreck, D. J.; Trapp, G.; Bakshi, R. S.; Mintzer, J. E.; Heidebrink, J. L.; Vidal-Cardona, A.; Arroyo, L. M.; et al. Effect of Vitamin E and Memantine on Functional Decline in Alzheimer Disease: The TEAM-AD VA Cooperative Randomized Trial. *JAMA* **2014**, *311* (1), 33–44.
- (477) Zhao, Y.; Lee, M.-J.; Cheung, C.; Ju, J.-H.; Chen, Y.-K.; Liu, B.; Hu, L.-Q.; Yang, C. S. Analysis of Multiple Metabolites of Tocopherols and Tocotrienols in Mice and Humans. *J. Agric. Food Chem.* **2010**, *58* (8), 4844–4852.
- (478) Schmözl, L.; Birringer, M.; Lorkowski, S.; Wallert, M. Complexity of Vitamin E Metabolism. *World J. Biol. Chem.* **2016**, *7* (1), 14–43.
- (479) Bartolini, D.; De Franco, F.; Torquato, P.; Marinelli, R.; Cerra, B.; Ronchetti, R.; Schon, A.; Fallarino, F.; De Luca, A.; Bellezza, G.; Ferri, I.; Sidoni, A.; Walton, W. G.; Pellock, S. J.; Redinbo, M. R.; Mani, S.; Pellicciari, R.; Gioiello, A.; Galli, F. Garcinoic Acid Is a Natural and Selective Agonist of Pregnane X Receptor. *J. Med. Chem.* **2020**, *63* (7), 3701–3712.
- (480) Yin, Y.; Yuan, H.; Wang, C.; Pattabiraman, N.; Rao, M.; Pestell, R. G.; Glazer, R. I. 3-Phosphoinositide-Dependent Protein Kinase-1 Activates the Peroxisome Proliferator-Activated Receptor- γ and Promotes Adipocyte Differentiation. *Mol. Endocrinol.* **2006**, *20* (2), 268–278.
- (481) KEGG Pathways. PPAR signaling pathway - Homo sapiens (entry hsa03320) <https://www.kegg.jp/entry/pathway+hsa03320> (accessed Feb 15, 2022).
- (482) Kanehisa, M.; Furumichi, M.; Tanabe, M.; Sato, Y.; Morishima, K. KEGG: New Perspectives on Genomes, Pathways, Diseases and Drugs. *Nucleic Acids Res.* **2017**, *45* (D1), D353–D361.
- (483) Ogata, H.; Goto, S.; Sato, K.; Fujibuchi, W.; Bono, H.; Kanehisa, M. KEGG: Kyoto Encyclopedia of Genes and Genomes. *Nucleic Acids Res.* **1999**, *27* (1), 29–34.
- (484) Hurtado, O.; Ballesteros, I.; Cuartero, M. I.; Moraga, A.; Pradillo, J. M.; Ramírez-Franco, J.; Bartolomé-Martín, D.; Pascual, D.; Torres, M.; Sánchez-Prieto, J.; Salom, J. B.; Lizasoain, I.; Moro, M. A. Daidzein Has Neuroprotective Effects through Ligand-Binding-Independent PPAR γ Activation. *Neurochem. Int.* **2012**, *61* (1), 119–127.
- (485) Lea, M. A.; Sura, M.; Desbordes, C. Inhibition of Cell Proliferation by Potential Peroxisome Proliferator-Activated Receptor (PPAR) Gamma Agonists and Antagonists. *Anticancer Res.* **2004**, *24* (5A), 2765–2772.
- (486) Marinelli, R.; Torquato, P.; Bartolini, D.; Mas-Bargues, C.; Bellezza, G.; Gioiello, A.; Borrás, C.; De Luca, A.; Fallarino, F.; Sebastiani, B.; Mani, S.; Sidoni, A.; Viña, J.; Leri, M.; Bucciantini, M.; Nardiello, P.; Casamenti, F.; Galli, F. Garcinoic Acid Prevents β -Amyloid (A β) Deposition in the

- Mouse Brain. *J. Biol. Chem.* **2020**, 295 (33), 11866–11876.
- (487) Wallert, M.; Mosig, S.; Rennert, K.; Funke, H.; Ristow, M.; Pellegrino, R. M.; Cruciani, G.; Galli, F.; Lorkowski, S.; Birringer, M. Long-Chain Metabolites of α -Tocopherol Occur in Human Serum and Inhibit Macrophage Foam Cell Formation in Vitro. *Free Radic. Biol. Med.* **2014**, 68, 43–51.
- (488) Bardowell, S. A.; Duan, F.; Manor, D.; Swanson, J. E.; Parker, R. S. Disruption of Mouse Cytochrome P450 4f14 (Cyp4f14 Gene) Causes Severe Perturbations in Vitamin E Metabolism. *J. Biol. Chem.* **2012**, 287 (31), 26077–26086.
- (489) Rossi, A.; Elia, G.; Santoro, M. G. Inhibition of Nuclear Factor KB by Prostaglandin A₁: An Effect Associated with Heat Shock Transcription Factor Activation. *Proc. Natl. Acad. Sci.* **1997**, 94 (2), 746–750.
- (490) Milne, G. L.; Musiek, E. S.; Morrow, J. D. The Cyclopentenone (A2/J2) Isoprostanes—Unique, Highly Reactive Products of Arachidonate Peroxidation. *Antioxid. Redox Signal.* **2005**, 7 (1–2), 210–220.
- (491) Sadowski, I.; Ma, J.; Triezenberg, S.; Ptashne, M. GAL4-VP16 Is an Unusually Potent Transcriptional Activator. *Nature* **1988**, 335, 563–564.
- (492) Budzyński, M. A.; Puustinen, M. C.; Joutsen, J.; Sistonen, L. Uncoupling Stress-Inducible Phosphorylation of Heat Shock Factor 1 from Its Activation. *Mol. Cell. Biol.* **2015**, 35 (14), 2530–2540.
- (493) Kramer, J. S.; Woltersdorf, S.; Dufлот, T.; Hiesinger, K.; Lillich, F. F.; Knöll, F.; Wittmann, S. K.; Klingler, F.-M.; Brunst, S.; Chaikuad, A.; Morisseau, C.; Hammock, B. D.; Buccellati, C.; Sala, A.; Rovati, G. E.; Leuillier, M.; Fraineau, S.; Rondeaux, J.; Hernandez-Olmos, V.; et al. Discovery of the First in Vivo Active Inhibitors of the Soluble Epoxide Hydrolase Phosphatase Domain. *J. Med. Chem.* **2019**, 62 (18), 8443–8460.
- (494) Apelt, J.; Ligneau, X.; Pertz, H. H.; Arrang, J.; Ganellin, C. R.; Schwartz, J.-C.; Schunack, W.; Stark, H. Development of a New Class of Nonimidazole Histamine H₃ Receptor Ligands with Combined Inhibitory Histamine N-Methyltransferase Activity. *J. Med. Chem.* **2002**, 45 (5), 1128–1141.
- (495) Wishart, D. S.; Feunang, Y. D.; Guo, A. C.; Lo, E. J.; Marcu, A.; Grant, J. R.; Sajed, T.; Johnson, D.; Li, C.; Sayeeda, Z.; Assempour, N.; Iynkkaran, I.; Liu, Y.; MacIejewski, A.; Gale, N.; Wilson, A.; Chin, L.; Cummings, R.; Le, D.; et al. DrugBank 5.0: A Major Update to the DrugBank Database for 2018. *Nucleic Acids Res.* **2018**, 46 (D1), D1074–D1082.
- (496) Bemis, G. W.; Murcko, M. A. The Properties of Known Drugs. 1. Molecular Frameworks. *J. Med. Chem.* **1996**, 39 (15), 2887–2893.
- (497) Cisternas, P.; Salazar, P.; Silva-Álvarez, C.; Barros, L. F.; Inestrosa, N. C. Activation of Wnt Signaling in Cortical Neurons Enhances Glucose Utilization through Glycolysis. *J. Biol. Chem.* **2016**, 291 (50), 25950–25964.
- (498) Haenig, C.; Atias, N.; Taylor, A. K.; Mazza, A.; Schaefer, M. H.; Russ, J.; Riechers, S.-P.; Jain, S.; Coughlin, M.; Fontaine, J.-F.; Freibaum, B. D.; Brusendorf, L.; Zenkner, M.; Porras, P.; Stroedicke, M.; Schnoegl, S.; Arnsburg, K.; Boeddrich, A.; Pigazzini, L.; et al. Interactome Mapping Provides a Network of Neurodegenerative Disease Proteins and Uncovers Widespread

Protein Aggregation in Affected Brains. *Cell Rep.* **2020**, *32* (7), 108050.

- (499) Winkler, E. A.; Nishida, Y.; Sagare, A. P.; Rege, S. V.; Bell, R. D.; Perlmutter, D.; Sengillo, J. D.; Hillman, S.; Kong, P.; Nelson, A. R.; Sullivan, J. S.; Zhao, Z.; Meiselman, H. J.; Wenby, R. B.; Soto, J.; Abel, E. D.; Makshanoff, J.; Zuniga, E.; De Vivo, D. C.; et al. GLUT1 Reductions Exacerbate Alzheimer's Disease Vasculo-Neuronal Dysfunction and Degeneration. *Nat. Neurosci.* **2015**, *18* (4), 521–530.
- (500) Torrandell-Haro, G.; Branigan, G. L.; Vitali, F.; Geifman, N.; Zissimopoulos, J. M.; Brinton, R. D. Statin Therapy and Risk of Alzheimer's and Age-related Neurodegenerative Diseases. *Alzheimer's Dement. Transl. Res. Clin. Interv.* **2020**, *6* (1), e12108.
- (501) Carroll, C. B.; Wyse, R. K. H. Simvastatin as a Potential Disease-Modifying Therapy for Patients with Parkinson's Disease: Rationale for Clinical Trial, and Current Progress. *J. Parkinsons. Dis.* **2017**, *7* (4), 545–568.
- (502) Chataway, J.; Schuerer, N.; Alsanousi, A.; Chan, D.; MacManus, D.; Hunter, K.; Anderson, V.; Bangham, C. R. M.; Clegg, S.; Nielsen, C.; Fox, N. C.; Wilkie, D.; Nicholas, J. M.; Calder, V. L.; Greenwood, J.; Frost, C.; Nicholas, R. Effect of High-Dose Simvastatin on Brain Atrophy and Disability in Secondary Progressive Multiple Sclerosis (MS-STAT): A Randomised, Placebo-Controlled, Phase 2 Trial. *Lancet* **2014**, *383* (9936), 2213–2221.
- (503) Johnson-Anuna, L. N.; Eckert, G. P.; Keller, J. H.; Igbavboa, U.; Franke, C.; Fechner, T.; Schubert-Zsilavecz, M.; Karas, M.; Müller, W. E.; Wood, W. G. Chronic Administration of Statins Alters Multiple Gene Expression Patterns in Mouse Cerebral Cortex. *J. Pharmacol. Exp. Ther.* **2005**, *312* (2), 786–793.
- (504) Fracassi, A.; Marangoni, M.; Rosso, P.; Pallottini, V.; Fioramonti, M.; Siteni, S.; Segatto, M. Statins and the Brain: More than Lipid Lowering Agents? *Curr. Neuropharmacol.* **2019**, *17* (1), 59–83.
- (505) Palermo, G.; Giannoni, S.; Giuntini, M.; Belli, E.; Frosini, D.; Siciliano, G.; Ceravolo, R. Statins in Parkinson's Disease: Influence on Motor Progression. *J. Parkinsons. Dis.* **2021**, *11* (4), 1651–1662.
- (506) Wahner, A. D.; Bronstein, J. M.; Bordelon, Y. M.; Ritz, B. Statin Use and the Risk of Parkinson Disease. *Neurology* **2008**, *70* (16, Part 2), 1418–1422.
- (507) Carroll, C. B.; Webb, D.; Stevens, K. N.; Vickery, J.; Eyre, V.; Ball, S.; Wyse, R.; Webber, M.; Foggo, A.; Zajicek, J.; Whone, A.; Creanor, S. Simvastatin as a Neuroprotective Treatment for Parkinson's Disease (PD STAT): Protocol for a Double-Blind, Randomised, Placebo-Controlled Futility Study. *BMJ Open* **2019**, *9*, e029740.
- (508) Stott, S. R. W.; Wyse, R. K.; Brundin, P. Drug Repurposing for Parkinson's Disease: The International Linked Clinical Trials Experience. *Front. Neurosci.* **2021**, *15*, 653377.
- (509) Chan, D.; Binks, S.; Nicholas, J. M.; Frost, C.; Cardoso, M. J.; Ourselin, S.; Wilkie, D.; Nicholas, R.; Chataway, J. Effect of High-Dose Simvastatin on Cognitive, Neuropsychiatric, and Health-Related Quality-of-Life Measures in Secondary Progressive Multiple Sclerosis: Secondary Analyses from the MS-STAT Randomised, Placebo-Controlled Trial. *Lancet Neurol.* **2017**, *16* (8), 591–600.
- (510) ClinicalTrials.gov Identifier: NCT03387670. Multiple Sclerosis-Simvastatin Trial 2 (MS-STAT2) <https://clinicaltrials.gov/ct2/show/NCT03387670> (accessed Jan 3, 2022).

- (511) Yan, J.; Liu, A.; Fan, H.; Qiao, L.; Wu, J.; Shen, M.; Lai, X.; Huang, J. Simvastatin Improves Behavioral Disorders and Hippocampal Inflammatory Reaction by NMDA-Mediated Anti-Inflammatory Function in MPTP-Treated Mice. *Cell. Mol. Neurobiol.* **2020**, *40* (10), 1155–1164.
- (512) Ghosh, A.; Roy, A.; Matras, J.; Brahmachari, S.; Gendelman, H. E.; Pahan, K. Simvastatin Inhibits the Activation of p21^{ras} and Prevents the Loss of Dopaminergic Neurons in a Mouse Model of Parkinson's Disease. *J. Neurosci.* **2009**, *29* (43), 13543–13556.
- (513) Xu, Y.-Q.; Long, L.; Yan, J.-Q.; Wei, L.; Pan, M.-Q.; Gao, H.-M.; Zhou, P.; Liu, M.; Zhu, C.-S.; Tang, B.-S.; Wang, Q. Simvastatin Induces Neuroprotection in 6-OHDA-Lesioned PC12 via the PI3K/AKT/Caspase 3 Pathway and Anti-Inflammatory Responses. *CNS Neurosci. Ther.* **2013**, *19* (3), 170–177.
- (514) Huang, W.; Li, Z.; Zhao, L.; Zhao, W. Simvastatin Ameliorate Memory Deficits and Inflammation in Clinical and Mouse Model of Alzheimer's Disease via Modulating the Expression of MiR-106b. *Biomed. Pharmacother.* **2017**, *92*, 46–57.
- (515) van der Most, P. J.; Dolga, A. M.; Nijholt, I. M.; Luiten, P. G. M.; Eisel, U. L. M. Statins: Mechanisms of Neuroprotection. *Prog. Neurobiol.* **2009**, *88* (1), 64–75.

7. Abkürzungsverzeichnis

13'COOH	13'-Carboxylat-Tocopherol	BCL6	B-Zell-Lymphom 6 Protein (engl. <i>B-cell lymphoma 6 protein</i>)
13'OH	13'-Hydroxylat-Tocopherol	Bn	Benzylrest
13-S-HODE	(S)-13-Hydroxy-9,11-octadecadiensäure	bspw.	beispielsweise
15d-PGJ₂	15-Deoxy- $\Delta^{12,14}$ -prostaglandin J ₂	bzw.	beziehungsweise
15-HETE	15-Hydroxyeicosatetraensäure	C	Cytosin
5-HT	5-Hydroxytryptamin, = Serotonin	ca.	circa
6-OHDA	6-Hydroxydopamin	cAMP	cyclisches Adenosinmonophosphat
A	Adenin	CAR	Konstitutiver Androstan-Rezeptor
ACAT2	Acetyl-Coenzym-A-Acetyltransferase 2	CBP	CREB bindendes Protein
ACSS2	kurz-kettige Acyl-Coenzym-A-Synthetase 2 (engl. <i>Acyl-Coenzyme A Synthetase short-chain family member 2</i>)	CD	Unterscheidungsgruppen immunphänotypischer Oberflächenmerkmale von Zellen (engl. <i>cluster of differentiation</i>)
AD	Alzheimer-Demenz (engl. <i>Alzheimer's disease</i>)	CDK6	Cyclin-abhängige Kinase 6 (engl. <i>cyclin-dependent kinase 6</i>)
AF	Aktivierungsfunktion	CDKN	Inhibitor Cyclin-abhängiger Kinasen (engl. <i>cyclin-dependent kinase inhibitor</i>)
AMP	Adenosin-5'-monophosphat	cDNA	komplementäre DNA
AMPK	AMP-aktivierte Proteinkinase	ChEMBL	engl. <i>Chemical database of the European Molecular Biology Laboratory</i>
ANGPTL4	Angiopoetin-ähnliches Protein 4 (engl. <i>Angiopoetin-like protein 4</i>)	CoREST	Co-Repressor-Komplex
AQ	Amodiaquin	COX	Cyclooxygenase
Arg	Arginin	CPT1	Carnitin-Acyltransferase 1
Asp	Asparaginsäure	CQ	Chloroquin
Aβ	β -Amyloid	CREB	cAMP-Response-Element-bindendes Protein
BACE1	β -Sekretase (engl. <i>β-site amyloid precursor protein cleaving enzyme</i>)		

CTE	C-terminale Verlängerung (engl. <i>C-terminal extension</i>)	ELISA	engl. <i>Enzyme-linked Immunosorbent Assay</i>
ctrl	Kontrolle	EP2	Prostaglandin-E2-Rezeptor
Cys	Cystein	ER	auswärtsgedrehte Wiederholung (engl. <i>everted repeat</i>)
DAT	Dopamintransporter	ERs	Estrogen-Rezeptoren (ER α und ER β)
DBD	DNA-Bindedomäne	FABP4	Fettsäure-Bindungs-Protein 4
DDC	DOPA-Decarboxylase	FADS2	Fettsäure-Desaturase 2 (engl. <i>Fatty acid desaturase 2</i>)
DHA	Docosahexaensäure (engl. <i>docosahexaenoic acid</i>)	FAT	Fettsäure-Translokase
DHCR7	7-Dehydrocholesterol- Reduktase	FATP	Fettsäure-Transport-Protein
DHI	5,6-Dihydroxyindol	FDFT1	Farnesyl-diphosphat Farnesyl- transferase 1
DLK1	<i>Delta-like</i> Protein 1	Flu	Fluoreszein
DMSO	Dimethylsulfoxid	FXR	Farnesoid X Rezeptor
DNA	Desoxyribonukleinsäure (engl. <i>deoxyribonucleic acid</i>)	G	Guanin
DOPA	Levodopa	G6Pase	Glucose-6-Phosphatase
DR	direkte Wiederholung (engl. <i>direct repeat</i>)	GABRA3	GABA-Rezeptor A3
DRIP	Vitamin-D-Rezeptor-interagie- rendes Proteins	GAPDH	Glyzerylaldehyd-3-phosphat- Dehydrogenase
EAE	Experimentelle autoimmune Enzephalomyelitis	GDNF	von Gliazellen stammender neurotropher Faktor (engl. <i>Glial cell-derived neurotrophic factor</i>)
EBP	Cholestenol delta-Isomerase (engl. <i>Emopamil binding protein</i>)	Gln	Glutamin
EC₅₀	mittlere effektive Konzentration (engl. <i>half maximal effective concentration</i>)	Glu	Glutaminsäure
eGFP	grün-fluoreszierendes Protein (engl. <i>enhanced green flu- orescent protein</i>)	GLUT	Glukosetransporter
EIF2AK2	Eukaryotische Translations- Initiations-Faktor-2-alpha- Kinase 2, = Proteinkinase R	GTP	Guanosintriphosphat
		H	Helix
		HAT	Histon-Acetyltransferase
		HDAC	Histon-Deacetylase
		HDL	Lipoprotein hoher Dichte (engl. <i>high density lipoprotein</i>)

His	Histidin	KEGG	Kyoto-Enzyklopädie der Gene und Genome
HMG-CoA	3-Hydroxy-3-Methylglutaryl-Coenzym-A	KLHL1	<i>Kelch-like</i> Protein 1
HSQC	engl. <i>Heteronuclear Single Quantum Coherence</i>	KNIME	engl. <i>Konstanz Information Miner</i>
HTRF	Homogener zeitaufgelöster Fluoreszenz-Resonanz-Energietransfer (engl. <i>homogeneous time-resolved fluorescence resonance energy transfer</i>)	Konf.	Konfiguration
HZF-3	hippocampaler Zinkfinger 3	LBD	Ligandenbindedomäne
IC₅₀	mittlere inhibitorische Konzentration (engl. <i>half maximal inhibitory concentration</i>)	LDHB	Lactatdehydrogenase B
ICAM	interzelluläres Adhäsionsmolekül	LDL	Lipoprotein niedriger Dichte (engl. <i>low density lipoprotein</i>)
IDE	Insulin-abbauendes Enzym (engl. <i>Insulin-degrading enzyme</i>)	LED	Leuchtdiode (engl. <i>light-emitting diode</i>)
IFI27	Interferon-alpha-induzierbares Protein 27	Leu	Leucin
IL	Interleukin	LPL	Lipoproteinlipase
Ile	Isoleucin	LPS	Lipopolysaccharide
iNOS	induzierbare Stickstoffmonoxid-Synthase	LSS	Lanosterol-Synthase
IR	invertierte Wiederholung (engl. <i>inverted repeat</i>)	LTB4	Leukotrien B4
ITC	isothermer Titrationskalorimetrie	LXR	Leber X Rezeptor
IUPHAR	engl. <i>The International Union of Basic and Clinical Pharmacology</i>	Lys	Lysin
JAK	Januskinase	MAP3K14	NFκB-induzierende Kinase
K_D	Dissoziationskonstante	max.	maximal
		Met	Methionin
		min.	minimal
		MOE	engl. <i>Molecular Operating Environment</i>
		MPTP	1-Methyl-4-phenyl-1,2,3,6-tetrahydropyridin
		mRNA	Boten-RNA (engl. <i>messenger RNA</i>)
		MS	Multiple Sklerose
		MST	Thermophorese (engl. <i>microscale thermophoresis</i>)

MVD	Mevalonat-Diphosphat-Decarboxylase	Nurr1	Nuklären-Rezeptoren-verwandtes Protein 1 (engl. <i>nuclear receptor related 1 protein</i>)
MVK	Mevalonat-Kinase		
MW	Mittelwert	NurRE	Nur-Response-Element
n	biologische Replikate	OAS3	2'-5'-Oligoadenylat Synthetase 3
N	technische Replikate	OLR1	engl. <i>oxidized LDL receptor 1</i>
NAFLD	nicht-alkoholischer Fettlebererkrankung (engl. <i>non-alcoholic fatty liver disease</i>)	p	Signifikanzniveau
NASH	nicht-alkoholische Steatohepatitis	p300	300 kDA Protein, = eine Histon-Acetyltransferase
NBRE	NGFI-B-Response-Element	p53	Tumorsuppressorprotein
NCoA6	Nukleärer Rezeptor Co-Aktivator 6, = PRIP	padj	angepasstes Signifikanzniveau (engl. <i>adjusted p value</i>)
NCoR1	Nukleärer Co-Repressor 1	PAINS	engl. <i>pan assay interference compounds</i>
NFKBIA	NFκB Inhibitor α	PBC	primäre biliäre Cholangitis
NFκB	engl. <i>nuclear factor 'kappa-light-chain-enhancer' of activated B-cells</i>	PC	Pyruvatcarboxylase
NGFI-B	Nervenwachstumsfaktor-induziertes Gen B, = Nur77	PD	Morbus Parkinson (engl. <i>Parkinson's disease</i>)
NLS	Sequenzen zur Kernlokalisierung (engl. <i>nuclear localization signal</i>)	PDB	Proteindatenbank (engl. <i>Protein Data Bank</i>)
NMR	Kernresonanzspektroskopie	PDPK1	3-Phosphoinositid-abhängige Proteinkinase 1
NOR-1	Neuronen-abgeleiteter Orphan-Rezeptor 1	PEPCK	Phosphoenolpyruvate-Carboxykinase
NOT	nukleärer Rezeptor der T-Zellen	PG	Prostaglandin
NR	nukleärer Rezeptor	PGC-1α	PPARγ-Co-Aktivator 1α
NRIP1	Nukleäre-Rezeptoren-interagierendes Protein 1	PGM1	Phosphoglucomutase 1
NSAR	Nichtsteroidales Antirheumatikum	Ph	Phenylrest
		Phe	Phenylalanin
		PIASy	SUMO-E3-Ligase (engl. <i>protein inhibitor of activated STATy</i>)
		PLIN	Perilipin

POMC	Proopiomelanocortin	si-Nurr1	Nurr1-siRNA
PPAR	Peroxisomen-Proliferator-aktivierter Rezeptor	siRNA	engl. <i>Small interfering RNA</i>
PPRE	PPAR- <i>Response</i> -Element	SLCs	Membran-Transportproteine (engl. <i>solute carrier</i>)
PRIP	PPAR-interagierendes Protein, = NCoA6	SMRT	=NCoR2, dämpfender Mediator der Retinoid- und Thyroidhormonrezeptoren (engl. <i>silencing mediator of retinoid and thyroid hormone receptor</i>)
PSC	primäre sklerosierende Cholangitis	SNP	Punktmutation (engl. <i>single nucleotide polymorphism</i>)
PTPRU	Protein-Tyrosin-Phosphatase vom Rezeptor-Typ U	SOD	Superoxid-Dismutase
qRT-PCR	quantitative Echtzeit-Polymerase-Kettenreaktion (engl. <i>quantitative real time polymerase chain reaction</i>)	sog.	sogenannt
RAR	Retinsäure-Rezeptor	sPPARM	selektiver PPAR-Modulator
RE	Erkennungssequenz (engl. <i>response element</i>)	SPR	Oberflächenplasmonenresonanzspektroskopie (engl. <i>surface plasmon resonance spectroscopy</i>)
Ret	Rezeptor-Tyrosinkinase Ret	SRC	Steroidrezeptor-Co-Aktivator
RNA	Ribonukleinsäure	SSTR2	Somatostatin-Rezeptor 2
RNAi	RNA-Interferenz	STAT	engl. <i>Signal Transducers and Activators of Transcription</i>
RNR-1	regenerierender nukleärer Rezeptor der Leber	SUMO	= eine posttranslationale Modifikation (engl. <i>Small Ubiquitin-Related Modifier</i>)
RXR	Retinoid X Rezeptor	T	Thymin
S.E.M.	Standardfehler (engl. <i>standard error of the mean</i>)	Tb	Terbium
SAR	Struktur-Wirkungs-Beziehung (engl. <i>structure-activity relationship</i>)	TETRAC	Tetraiodthyroacetat
SC5D	Sterol-C5-desaturase	TH	Tyrosinhydroxylase
SD	Standardabweichung (engl. <i>standard deviation</i>)	Th	T-Helfer-Zelle
Ser	Serin	THR	Thyroidhormon-Rezeptor
sGFP	engl. <i>superfolder GFP</i>	Thr	Threonin
si-ctrl	Kontroll-siRNA (engl. <i>non-targeting siRNA</i>)		

TINUR	transkriptionell induzierbarer nukleärer Rezeptor	u. a.	unter anderem
TM7SF2	Delta(14)-Sterol-Reduktase (engl. <i>transmembrane 7 superfamily member 2</i>)	UCP1	Thermogenin (engl. <i>uncoupling protein 1</i>)
TNFRSF12A	TNF-Rezeptor-Superfamilien-Mitglied 12A	VCAM1	vaskulärer Zelladhäsionsmolekül 1 (engl. <i>vascular cell adhesion molecule 1</i>)
TNFSF10	TNF-Superfamilien-Mitglied 10	VDR	Vitamin-D-Rezeptor
TNFα	Tumornekrosefaktor α	vgl.	vergleiche
tox.	toxisch	VIP	vasoaktives intestinales Peptid
TP73	Tumorprotein p73	VMAT2	vesikulärer Monoamintransporter 2, = SLC18A2
TRAP	Thyroidhormon-Rezeptor-assoziiertes Protein	VP16	<i>Herpes-simplex-Virus</i> -Protein vmw65
TR-FRET	zeitlich aufgelöster Fluoreszenz-Resonanz-Energietransfer (engl. <i>time-resolved fluorescence resonance energy transfer</i>)	vs.	versus
TSMF	mitochondrialer Elongationsfaktor T	XDH	Xanthin-Dehydrogenase
Tyr	Tyrosin	z. B.	zum Beispiel
		z. T.	zum Teil
		ZNS	zentrales Nervensystem
		λ	Wellenlänge

8. Abbildungsverzeichnis

Abbildung 1: Funktionsweise photoschaltbarer Liganden am Beispiel der Azobenzene	11
Abbildung 2: Superfamilie der 48 humanen nukleären Rezeptoren dargestellt nach ihrer phylogenetischen Klassifizierung mit zugehöriger Abkürzung	12
Abbildung 3: Allgemeiner struktureller Aufbau nukleärer Rezeptoren	13
Abbildung 4: DNA-Bindung des PPAR γ -RXR α -Heterodimers (PDB: 3DZY)	13
Abbildung 5: Modell der ligandenabhängigen Aktivierung und Inaktivierung durch Konformationsänderung der LBD am Beispiel von PPAR α	14
Abbildung 6: Molekularer Mechanismus der PPARs	16
Abbildung 7: Physiologische Funktionen der drei PPAR-Subtypen	17
Abbildung 8: Mechanismus der PPAR γ -vermittelten Transrepression proinflammatorischer Gene über NF κ B (p65/p50)	19
Abbildung 9: Vergleich der Liganden-Protein-Interaktion mit der kanonischen Aktivierungs-Tetrad der drei PPAR-Subtypen	21
Abbildung 10: PPAR α -selektive Liganden	22
Abbildung 11: PPAR γ -selektive Liganden	24
Abbildung 12: PPAR δ -selektive Liganden	25
Abbildung 13: Aktivität der NR4A-Rezeptoren als Monomer oder Dimer am Beispiel von Nurr1	26
Abbildung 14: Besonderheiten der LBD bei den NR4A-Rezeptoren am Beispiel von Nurr1 (PDB: 1OVL)	27
Abbildung 15: Molekulare Funktionen von Nurr1 in dopaminergen Neuronen	28
Abbildung 16: Modell der Nurr1/CoREST-vermittelten Transrepression proinflammatorischer Gene über NF κ B (p65/p50)	29
Abbildung 17: Synthetische Nurr1 Agonisten AQ und CQ	31
Abbildung 18: Potenzielle endogene Nurr1-Liganden	32
Abbildung 19: Zweidimensionale Darstellung der kovalenten Koordination von PGA1 (20) an die Nurr1-LBD (PDB: 5Y41)	33
Abbildung 20: Zweidimensionale Darstellung der kovalenten Bindung von DHI (22) an die Nurr1-LBD (PDB: 6DDA)	34
Abbildung 21: Weitere Nurr1-Modulatoren	35
Abbildung 22: Ligandenbindung an die Nurr1-LBD	36
Abbildung 23: Leitstrukturen der photoschaltbaren PPAR-Agonisten	39
Abbildung 24: Design und Charakterisierung des lichtaktivierbaren Rosiglitazon-Derivates 36	41
Abbildung 25: Dockinganalyse zu 29 zeigt Optimierungsmöglichkeiten für photoschaltbare PPAR α - und - δ Liganden	42
Abbildung 26: Spatiotemporale Kontrolle von PPAR α durch 38 in lebenden HEK293T-Zellen	44
Abbildung 27: Vitamin-E-Metabolite modulieren PPARs	45
Abbildung 28: Einfluss von Garcinolsäure (48) und Pioglitazon (2) auf die Co-Regulator-Rekrutierung von PPAR γ	46
Abbildung 29: Co-Kristallstrukturen der PPAR γ -LBD im Komplex mit Garcinolsäure (48) und Rosiglitazon (3)	47
Abbildung 30: Einfluss von 48 auf die Genexpression in HepG2-Zellen	48

Abbildung 31: Screening von strukturell diversen NSARs auf ihre Aktivität an NR4A-Rezeptoren in einheitlichen Gal4-Hybrid-Reporterassays	50
Abbildung 32: Bidirektionale Modulation von Nurr1 durch NSARs	50
Abbildung 33: Schematische Darstellung des Nurr1-Co-Regulator-Rekrutierungsassays	51
Abbildung 34: Dosis-Wirkungskurven der Nurr1-Modulatoren 49 , 51 und 52 zeigen die Verdrängung der Co-Regulatoren NCoR1, SMRT, NCoA6 und NRIP1 von der Nurr1-LBD	51
Abbildung 35: Einfluss der NSARs auf das Dimerisierungsverhalten von Nurr1	53
Abbildung 36: Gleichzeitige Modulation der Nurr1-Aktivität durch 49 und 19 im zellulären Gal4-Nurr1-Reporterassay deutete auf unterschiedliche Bindestelle hin, nicht auf Konkurrenz	53
Abbildung 37: Effekte der Fragmente 71 und 73 im zellfreien TR-FRET-System	57
Abbildung 38: Nurr1-Agonismus von 71 und 73 in zellulären Settings	58
Abbildung 39: Arzneistoff-Fragment-Screening zur Identifikation neuer Nurr1-Modulatoren	59
Abbildung 40: Charakterisierung von 127 und 120 in zellfreien und zellulären Systemen	62
Abbildung 41: Biologische Effekte von 120 und 127	63
Abbildung 42: Identifikation von Statinen als Nurr1-Modulatoren	64
Abbildung 43: Charakterisierung von 97 und 132 in zellfreien und zellulären Systemen	65
Abbildung 44: Beteiligung von Nurr1 an Neuroinflammation	66
Abbildung 45: Simvastatin (132) beeinflusste die Genexpression von Astrozyten (T98G) in Abhängigkeit von Nurr1	67
Abbildung 46: Optimierung der Leitstrukturen 3 und 29 zu photoschaltbaren PPAR-Agonisten	70
Abbildung 47: Modell der Nurr1-Modulation durch niedermolekulare Liganden	72

9. Tabellenverzeichnis

Tabelle 1: Untersuchung der <i>para</i> -Position des terminalen Phenylrings am Rosiglitazon-Azolog 32 ..	40
Tabelle 2: Optimierung des pan-PPAR-Agonisten 29 zu photoschaltbaren PPAR α - und - δ -Agonisten	43
Tabelle 3: Zusammengefasste Aktivitäten der NSARs in zellulären Nurr1-Reporterassays	52
Tabelle 4: SAR der Seitenkette im AQ/CQ-Chemotyp	55
Tabelle 5: SAR der Substituenten am Chlorochinolinamin-Grundgerüst und Optimierung der Nurr1-Aktivität	56
Tabelle 6: Systematische Untersuchung von Substitutionen am Indol-Grundgerüst	60

10. Schemenverzeichnis

Schema 1: Synthesen der Chinolin-Derivate 56, 74 und 77–80	54
Schema 2: Synthesen der Naphthalin-Derivate 75 und 76	54

11. Publikationsliste

Dieser Arbeit zugrundeliegende Publikationen:

- **Willems, S.**; Kilu, W.; Ni, X.; Chaikuad, A.; Knapp, S.; Heering, J.; Merk, D. The Orphan Nuclear Receptor Nurr1 Is Responsive to Non-Steroidal Anti-Inflammatory Drugs. *Commun. Chem.* **2020**, *3*, 85. <https://doi.org/10.1038/s42004-020-0331-0>

Eigener Beitrag: Etablierung der zellulären Gal4-Reporterassays für die NR4A-Rezeptoren, sowie Charakterisierung aller Substanzen in diesen Systemen und Selektivitäts-Testung. Etablierung und Durchführung der Nurr1-Vollängen-Experimente. Computerbasierte Untersuchung der potenziellen Bindestelle in der Nurr1-LBD. HTRF-basierte Nurr1-Peptid-Rekrutierungsassays für die Substanzen Chloroquin und Parecoxib. Konzeption und Verfassen des Manuskripts.

Etablierung und Durchführung der HTRF basierten Nurr1-Peptid-Rekrutierungsassays für die Substanzen Amodiaquin, Oxaprozin und Meclofenaminsäure, sowie der Nurr1-Dimerisierungsassays und Nurr1-NCoR1-Bindungsassays durch W. K. und J. H. Klonieren der Gal4-NR4A-Rezeptor Plasmide sowie der Nurr1-Vollängen-Reporter-Konstrukte durch J. H. Durchführung von Gal4-Reporterassays und computerbasierte Untersuchung der potenziellen Bindestelle in der Nurr1-LBD in Zusammenarbeit mit D. M. Generieren des rekombinanten Nurr1-LBD Proteins durch X. N., A. C. und S. K. Konzeption und Verfassen des Manuskripts in Zusammenarbeit mit D. M. Leitung der Studie durch D. M.

- Hinnah, K.[‡]; **Willems, S.[‡]**; Morstein, J.; Heering, J.; Hartrampf, F. W. W.; Broichhagen, J.; Leippe, P.; Merk, D.; Trauner, D. Photohormones Enable Optical Control of the Peroxisome Proliferator-Activated Receptor γ (PPAR γ). *J. Med. Chem.* **2020**, *63* (19), 10908–10920. <https://doi.org/10.1021/acs.jmedchem.0c00654>

Eigener Beitrag: Computergestütztes Design der Photohormone sowie deren Charakterisierung in zellulären PPAR-Gal4-Reporterassays. Etablierung und Durchführung des zellulären nativen PPAR γ -Reporterassays in humanen Hepatozyten. Durchführung und Auswertung der ITC-Experimente. Verfassen des Manuskripts.

[‡] Hier liegt eine geteilte Erstautorenschaft zwischen K. H. und S. W. vor.

Synthese und photophysikalische Charakterisierung der Photohormone durch K. H. und J. M. Expression des PPAR γ -LBD-Proteins für ITC-Experimente durch J. H. Etablierung der Synthesen durch F. W. W. H., J. B. und P. L. Computergestütztes Design der Photohormone in Zusammenarbeit mit D. M. Verfassen des Manuskripts zusammen mit K. H., J. M., D. M. und D. T. Konzeption und Leitung der Studie durch D. M. und D. T.

- **Willems, S.**; Ohrndorf, J.; Kilu, W.; Heering, J.; Merk, D. Fragment-like Chloroquinoline-amines Activate the Orphan Nuclear Receptor Nurr1 and Elucidate Activation Mechanisms. *J. Med. Chem.* **2021**, *64* (5), 2659–2668. <https://doi.org/10.1021/acs.jmedchem.0c01779>

Eigener Beitrag: Charakterisierung der Substanzen **1–33** in einem zellulären Nurr1-Gal4-Reporterassay, sowie Synthese der neuen Verbindungen, Durchführung der Nurr1-Vollängen-Experimente, Quantifizierung der Nurr1-regulierten mRNA-Expression und Toxizitätsmessung. Verfassen des Manuskripts.

Synthese der neuen Verbindungen in Zusammenarbeit mit J. O. Durchführung der HTRF-basierenden Nurr1-Peptid-Bindungsassays, sowie der Nurr1-Dimerisierungsassays durch W. K. und J. H. Verfassen des Manuskripts zusammen mit D. M. Konzeption und Leitung der Studie durch D. M.

- **Willems, S.;** Gellrich, L.; Chaikuad, A.; Kluge, S.; Werz, O.; Heering, J.; Knapp, S.; Lorkowski, S.; Schubert-Zsilavec, M.; Merk, D. Endogenous Vitamin E Metabolites Mediate Allosteric PPAR γ Activation with Unprecedented Co-Regulatory Interactions. *Cell Chem. Biol.* **2021**, *28* (10), 1489-1500. <https://doi.org/10.1016/j.chembiol.2021.04.019>

Eigener Beitrag: Etablierung des zellulären nativen PPAR γ -Reporterassays in humanen Hepatozyten. Planung, Durchführung und Auswertung aller HTRF-basierten PPAR γ -Peptid-Rekrutierungsassays. Docking verwandter PPAR γ -Liganden. Generieren der mRNA-Proben sowie Analyse und Darstellung der RNAseq-Daten. Verfassen des Manuskripts.

Aktivitätsscreening und Charakterisierung der Vitamin-E-Metabolite in zellulären Gal4-Reporterassays, sowie Durchführung der ITC-Experimente durch L. G. und D. M. Lösen der Kristallstrukturen durch A. C. und S. Kn. Zurverfügungstellen der Vitamin-E-Metabolite durch S. Kl. und S. L. Etablierung der HTRF-basierten PPAR γ -Peptid-Rekrutierungsassays, sowie Expression des gelabelten PPAR γ -LBD Proteins für die HTRF-Assays und des PPAR γ -LBD-Proteins für ITC-Experimente durch J. H. Analyse der RNAseq-Daten zusammen mit D. M. Konzeption der Studie durch O. W., S. L., M. S.-Z., und D. M. Verfassen des Manuskripts in Zusammenarbeit mit D. M. Leitung der Studie durch D. M.

- **Willems, S.†;** Morstein, J. †; Hinnah, K.; Trauner, D.; Merk, D. A Photohormone for Light-dependent Control of PPAR α in Live Cells. *J. Med. Chem.* **2021**, *64* (14), 10393–10402. <https://doi.org/10.1021/acs.jmedchem.1c00810>

Eigener Beitrag: Computergestütztes Design der Photohormone sowie deren Charakterisierung in zellulären PPAR-Gal4-Reporterassays. Etablierung, Durchführung und Auswertung des zellulären Fluoreszenz-Reporterassays und bildgebende Analyse. Konzeption und Verfassen des Manuskripts.

† Hier liegt eine geteilte Erstautorenschaft zwischen S.W. und J.M. vor.

Synthese und photophysikalische Charakterisierung der Photohormone durch J. M. und K. H. Computergestütztes Design der Photohormone, sowie Konzeption und Verfassen des Manuskripts in Zusammenarbeit mit D. M. Leitung der Studie durch D. T. und D. M.

- **Willems, S.†;** Zaienne, D.†; Merk, D. Targeting nuclear receptors in neurodegeneration and neuroinflammation. *J. Med. Chem.* **2021**, *64* (14), 9592–9638. <https://doi.org/10.1021/acs.jmedchem.1c00186>

Eigener Beitrag: Literaturrecherche und Verfassen des Manuskripts, Kapitel zu Nur77 und Nurr1.

† Hier liegt eine geteilte Erstautorenschaft zwischen S.W. und D.Z. vor.

Literaturrecherche und Verfassen des Manuskripts zusammen mit D. Z. (RXR, NOR-1) und D. M. (PPAR, revERB, LXR, VDR, TLX, ER). Konzeption und Leitung der Studie durch D. M.

- Zaienne, D.[‡]; **Willems, S.**[‡]; Schierle, S.; Heering, J.; Merk, D. Development and profiling of inverse agonist tools for the neuroprotective transcription factor Nurr1. *J. Med. Chem.* **2021**, 64 (20), 15126-15140. <https://doi.org/10.1021/acs.jmedchem.1c01077>

Eigener Beitrag: Charakterisierung der synthetisierten Substanzen **1–30** in einem zellulären Nurr1-Gal4-Reporterassay, sowie Durchführung der Nurr1-Vollängen-Experimente, des Nurr1-*Knockdown* in humanen Astrozyten, der IL-6-Freisetzung mittels ELISA und der Quantifizierung der Nurr1-regulierten mRNA-Expression. Computergestützte Analyse der Konversion zum Nurr1-Agonismus. Verfassen des Manuskripts.

[‡] Hier liegt eine geteilte Erstautorenschaft zwischen D. Z. und S. W. vor.

Synthese der neuen Verbindungen durch D. Z. und S. S. Charakterisierung der synthetisierten Substanzen **31–42** in einem zellulären Nurr1-Gal4-Reporterassay, sowie Toxizitätsmessung, Selektivitätsscreening und Kreuztitrationen durch D. Z. Durchführung der HTRF-basierten zellfreien Assays durch J. H. Verfassen des Manuskripts zusammen mit D. Z. und D. M. Konzeption und Leitung der Studie durch D. M.

- **Willems, S.**; Kilu, W.; Faudone, G.; Heering, J.; Merk, D. Nurr1 modulation mediates neuroprotective effects of statins. *bioRxiv* **2021**. 2021.09.15.460433. <https://doi.org/10.1101/2021.09.15.460433>

Eigener Beitrag: Durchführung des Drug-Fragment-Screenings und Charakterisierung daraus abgeleiteter Arzneistoffe in einem zellulären Nurr1-Gal4-Reporterassay. Durchführung der Nurr1-Vollängen-Experimente, des Nurr1-*Knockdown* in humanen Astrozyten, der IL-6-Freisetzung mittels ELISA und Generieren der mRNA-Proben. Durchführung der HTRF-basierten Nurr1-Peptid-Rekrutierungsassays. Computergestützte Analyse der Screening-Datenbank. Analyse und Darstellung der RNAseq-Daten. Konzeption und Verfassen des Manuskripts.

Durchführung des Drug-Fragment-Screenings in Zusammenarbeit mit G. F. Durchführung der HTRF-basierten Nurr1-Dimerisierungsassays durch W. K. und J. H. Analyse der RNAseq-Daten, sowie Konzeption und Verfassen des Manuskriptes zusammen mit D. M. Leitung der Studie durch D. M.

Weitere peer-reviewed Publikationen:

- Schierle, S.; Flauaus, C.; Heitel, P.; **Willems, S.**; Schmidt, J.; Kaiser, A.; Weizel, L.; Goebel, T.; Kahnt, A. S.; Geisslinger, G.; Steinhilber, D.; Wurglics, M.; Rovati, G. E.; Schmidtko, A.; Proschak, E.; Merk, D. Boosting Anti-Inflammatory Potency of Zafirlukast by Designed Polypharmacology. *J. Med. Chem.* **2018**, *61* (13), 5758–5764. <https://doi.org/10.1021/acs.jmedchem.8b00458>

Eigener Beitrag: Etablierung der Synthesen zu den Vorstufen **11**, **14–17**, **21** und **24**.

- Morstein, J.; Trads, J. B.; Hinnah, K.; **Willems, S.**; Barber, D. M.; Trauner, M.; Merk, D.; Trauner, D. Optical Control of the Nuclear Bile Acid Receptor FXR with a Photohormone. *Chem. Sci.* **2020**, *11*, 429–434. <https://doi.org/10.1039/c9sc02911g>

Eigener Beitrag: Molekulares Docking von *trans*- und *cis*-**AzoGW** in die FXR-LBD. Durchführung der Reporterassays für das Selektivitätsscreening und der ITC-Experimente.

- Schierle, S.; Neumann, S.; Heitel, P.; **Willems, S.**; Kaiser, A.; Pollinger, J.; Merk, D. Design and Structural Optimization of Dual FXR/PPAR δ Activators. *J. Med. Chem.* **2020**, *63* (15), 8369–8379. <https://doi.org/10.1021/acs.jmedchem.0c00618>

Eigener Beitrag: Computergestütztes Design der dualen Leitstruktur **5** und molekulares Docking der Substanzen **21** und **25** zur Untersuchung des Bindemodus in den FXR- und PPAR δ -LBDs.

- Meijer, I.; **Willems, S.**; Ni, X.; Heering, J.; Chaikuad, A.; Merk, D. Chemical Starting Matter for HNF4 α Ligand Discovery and Chemogenomics. *Int. J. Mol. Sci.* **2020**, *21* (21), 7895. <https://doi.org/10.3390/ijms21217895>

Eigener Beitrag: Durchführung der ITC-Experimente für die Substanzen **6** und **10**. Quantifizierung der HNF4 α -regulierten mRNA aus humanen Hepatozyten durch qRT-PCR.

- Helmstädter, M.; Vietor, J.; Sommer, J.; Schierle, S.; **Willems, S.**; Kaiser, A.; Schmidt, J.; Merk, D. A New FXR Ligand Chemotype with Agonist/Antagonist Switch. *ACS Med. Chem. Lett.* **2021**, *12* (2), 267–274. <https://doi.org/10.1021/acsmchemlett.0c00647>

Eigener Beitrag: Molekulares Docking zur Untersuchung des Bindemodus der Substanzen **14** und **18** in der FXR-LBD.

- Faudone, G.; Bischoff-Kont, I.; Rachor, L.; **Willems, S.**; Zhubi, R.; Kaiser, A.; Chaikuad, A.; Knapp, S.; Fürst, R.; Heering, J.; Merk, D. Propranolol Activates the Orphan Nuclear Receptor TLX to Counteract Proliferation and Migration of Glioblastoma Cells. *J. Med. Chem.* **2021**, *64* (12), 8727–8738. <https://doi.org/10.1021/acs.jmedchem.1c00733>

Eigener Beitrag: Durchführung des Fragment Screenings in Zusammenarbeit mit G. F.

- Lillich, F.; **Willems, S.**; Ni, X.; Borkowsky, C.; Kilu, W.; Brodsky, M.; Kramer, J.; Brunst, S.; Hernandez-Olmos, V.; Heering, J.; Schierle, S.; Kestner, R.; Mayser, F.; Helmstädter, M.; Göbel, T.; Weizel, L.; Namgaladze, D.; Kaiser, A.; Steinhilber, D.; Pfeilschifter, W.; Kahnt, A.; Proschak, A.; Chaikuad, A.; Knapp, S.; Merk, D.; Proschak, E. Structure-Based Design of Dual Partial Peroxisome Proliferator Activated Receptor γ Agonists/Soluble Epoxide Hydrolase Inhibitors. *J. Med. Chem.* **2021**, *64* (23), 17259–17276. <https://doi.org/10.1021/acs.jmedchem.1c01331>

Eigener Beitrag: Charakterisierung der Substanzen in einem zellulären PPAR γ -Gal4-Reporter-genassay.

- **Willems, S.**[‡]; Müller, M.[‡]; Ohrndorf, J.; Heering, J.; Proschak, E.; Merk, D. Scaffold hopping from amodiaquine to novel Nurr1 agonist chemotypes via microscale analogue libraries. *ChemMedChem* **2022**, e202200026. <https://doi.org/10.1002/cmdc.202200026>

Eigener Beitrag: Computergestütztes Design der Substanz-Bibliotheken **A** und **B**. Durchführung der Synthesen im Mikromaßstab und der Synthese von Substanz **4**. Charakterisierung der generierten Substanz-Bibliotheken **A** und **B** in einem zellulären Nurr1-Gal4-Reporter-genassay, sowie der daraus abgeleiteten Verbindungen **3j**, **4** und **4e**. Verfassen des Manuskripts.

[‡] Hier liegt eine geteilte Erstautorenschaft zwischen S. W. und M. M. vor.

Sonstige Publikationen:

- **Willems, S.**; Merk, D. Innovative Pharmacological Strategies in Osteoporosis Treatment. *Pharmakon* **2019**, *7* (4), 287–294.

12. Kooperationspartner

Sofern nicht anders durch Quellenangabe oder Danksagung angegeben, wurde die vorgelegte Arbeit von mir unter der Aufsicht meiner Betreuer während meines Promotionsstudiums erstellt. Alle Beiträge von Kollegen sind explizit in dieser Dissertation gekennzeichnet.

Für die Erstellung einiger Abbildungen wurde Material von <https://smart.servier.com/> genutzt und bearbeitet. Die Nutzung dieses Materials geschah mit erteilter Genehmigung: "Servier Medical Art by Servier is licensed under a Creative Commons Attribution 3.0 Unported License. To view a copy of this license, visit <http://creativecommons.org/licenses/by/3.0/>".

Für die Erstellung einiger Abbildungen wurde Material von <https://app.biorender.com/> genutzt. Die Nutzung dieses Materials geschah mit erteilter Genehmigung: „The Figure was exported under a paid subscription. Created with BioRender.com”

Für die Erstellung der Abbildungen von Kristallstrukturanalysen wurde die Software Molecular Operating Environment (MOE 2020.09) der Chemical Computing Group (Montreal, Kanada) genutzt.

Nachfolgend aufgelistetes Material/Ergebnisse/Daten wurde im Zuge kollaborativer Forschung erhalten:

Photohormone als licht-abhängige PPAR-Agonisten

- Synthese und photophysikalische Charakterisierung der Substanzen **29–41**: Dr. Johannes Morstein und Konstantin Hinnah, AK Prof. Trauner, Department of Chemistry, New York University, New York, USA.
- ITC Experimente: rekombinante PPAR γ -LBD bereitgestellt durch Dr. Jan Heering, Fraunhofer-Institut für Translationale Medizin und Pharmakologie ITMP, Frankfurt.
- Bestimmung der metabolischen Stabilität: Astrid Kaiser, AK Prof. Schubert-Zsilavecz, Institut für Pharmazeutische Chemie, Goethe-Universität Frankfurt.
- Fluoreszenz-Mikroskopie: Anleitung und Bereitstellung durch Dr. Eric Kowarz, AK Prof. Marschalek, Institut für Pharmazeutische Biologie, Goethe-Universität Frankfurt.

Vitamine E Metabolite sind endogene PPAR γ -Liganden

- Substanzen **44–48**: zur Verfügung gestellt von Dr. Stefan Kluge und Prof. Dr. Stefan Lorkowski, Institut für Ernährungswissenschaften, Friedrich-Schiller-Universität Jena.
- Gal4-Reporterassays: Durchführung und Auswertung durch Dr. Leonie Gellrich, AK Prof. Schubert-Zsilavecz, und Prof. Dr. Daniel Merk, Institut für Pharmazeutische Chemie, Goethe-Universität Frankfurt.
- ITC-Experimente: Durchführung und Auswertung durch Dr. Leonie Gellrich, AK Prof. Schubert-Zsilavecz, Institut für Pharmazeutische Chemie, Goethe-Universität Frankfurt; rekombinante PPAR γ -LBD bereitgestellt durch Dr. Jan Heering, Fraunhofer-Institut für Translationale Medizin und Pharmakologie ITMP, Frankfurt.
- TR-FRET Experimente: rekombinante gelabelte PPAR γ -LBD bereitgestellt durch Dr. Jan Heering, Fraunhofer-Institut für Translationale Medizin und Pharmakologie ITMP, Frankfurt. Eigener Beitrag: Durchführung der PPAR γ -Peptid-Rekrutierungsassays.

- Lösen der Kristallstrukturen der PPAR γ -LBD im Komplex mit **3** und **48**: Dr. Apirat Chaikuad, AK Prof. Knapp, Institut für Pharmazeutische Chemie, Goethe-Universität Frankfurt.
- Genexpressionsanalyse: RNA Sequencing wurde von der Firma Novogene (Cambridge, England) durchgeführt. Eigener Beitrag: Generieren der mRNA Proben sowie Analyse und Darstellung der Daten.

Identifikation von nichtsteroidalen Antirheumatika als Nurr1-Modulatoren

- TR-FRET Experimente: Etablierung und Durchführung der Nurr1-Peptid-Rekrutierungsassays für die Substanzen **19**, **49**, und **51**, sowie der Nurr1-Dimerisierungsassays und Nurr1-NCoR1 Bindungsassays; Bereitstellung der rekombinanten gelabelten Nurr1-LBD durch Dr. Whitney Kilu, AK Prof. Proschak, Institut für Pharmazeutische Chemie, Goethe-Universität Frankfurt, und Dr. Jan Heering, Fraunhofer-Institut für Translationale Medizin und Pharmakologie ITMP, Frankfurt. Eigener Beitrag: Durchführung der Nurr1-Peptid-Rekrutierungsassays für die Substanzen **25** und **52**, und Erstellung der Abbildungen.
- Klonieren der Plasmide pFA-CMV-hNurr1-LBD, pFA-CMV-hNur77-LBD, pFA-CMV-hNOR1-LBD, pFRLuc-NBRE, pFR-Luc-NurRE, und pFRLuc-DR5 durch Dr. Jan Heering, Fraunhofer-Institut für Translationale Medizin und Pharmakologie ITMP, Frankfurt.

Fragment-basierter Ansatz zu Entwicklung von Nurr1-Agonisten

- Synthese der Substanzen **74–80**: Julia Ohrndorf, AK Prof. Schubert-Zsilavec, Institut für Pharmazeutische Chemie, Goethe-Universität Frankfurt. Eigener Beitrag: Erstellung der Syntheschemen.
- Bestimmung der Reinheit: Astrid Kaiser und Julia Ohrndorf, AK Prof. Schubert-Zsilavec, Institut für Pharmazeutische Chemie, Goethe-Universität Frankfurt.
- TR-FRET Experimente: Dr. Whitney Kilu, AK Prof. Proschak, Institut für Pharmazeutische Chemie, Goethe-Universität Frankfurt, und Dr. Jan Heering, Fraunhofer-Institut für Translationale Medizin und Pharmakologie ITMP, Frankfurt.

Inverse Nurr1 Agonisten mit Indol-Grundgerüst

- Synthese der Substanzen **98–127**: Daniel Zaienne, unterstützt durch Dr. Simone Schierle, AK Prof. Schubert-Zsilavec, Institut für Pharmazeutische Chemie, Goethe-Universität Frankfurt.
- Bestimmung der Reinheit: Astrid Kaiser und Julia Ohrndorf, AK Prof. Schubert-Zsilavec, Institut für Pharmazeutische Chemie, Goethe-Universität Frankfurt.
- Gal4-Reportergenassays: Charakterisierung der Substanzen **120–127** in einem zellulären Gal4-Nurr1-Reportergenassay, Toxizitätsmessung und Selektivitätsscreening der Substanzen **120** und **127**, sowie Kreuztitrationen von **19** und **127** durch Daniel Zaienne, AK Prof. Schubert-Zsilavec, Institut für Pharmazeutische Chemie, Goethe-Universität Frankfurt. Eigener Beitrag: Charakterisierung der Substanzen **95** und **98–119** in einem zellulären Gal4-Nurr1 Reportergenassay und Betreuung der Masterarbeit von Daniel Zaienne.
- TR-FRET Experimente: Dr. Jan Heering, Fraunhofer-Institut für Translationale Medizin und Pharmakologie ITMP, Frankfurt.

Statine vermitteln neuroprotektive Effekte durch Nurr1 Agonismus

- Drug Fragment Screening in einem Gal4-Nurr1 Reporterassay: in Zusammenarbeit mit Giuseppe Faudone, AK Prof. Schubert-Zsilavec, Institut für Pharmazeutische Chemie, Goethe-Universität Frankfurt.
- TR-FRET Experimente: Durchführung der Nurr1-Dimerisierungsassays und Bereitstellen der rekombinanten gelabelten Nurr1-LBD durch Dr. Whitney Kilu, AK Prof. Proschak, Institut für Pharmazeutische Chemie, Goethe-Universität Frankfurt, und Dr. Jan Heering, Fraunhofer-Institut für Translationale Medizin und Pharmakologie ITMP, Frankfurt. Eigener Beitrag: Durchführung der Nurr1-Peptid-Rekrutierungsassays.
- Genexpressionsanalyse: RNA Sequencing wurde von der Firma Novogene (Cambridge, England) durchgeführt. Eigener Beitrag: Generieren der mRNA Proben sowie Analyse und Darstellung der Daten.

Die folgenden Teile der Dissertation wurden zuvor veröffentlicht:

- Abbildung 2, 6, 8, 13, 16, 22: bearbeitet nach [66], Genehmigung erteilt durch American Chemical Society (2021).
- Abbildung 24: bearbeitet nach [452], Genehmigung erteilt durch American Chemical Society (2020).
- Abbildung 25 und 26: bearbeitet nach [453], Genehmigung erteilt durch American Chemical Society (2021).
- Abbildung 27, 28, 30: bearbeitet nach [454], Genehmigung erteilt durch Elsevier Ltd. (2021).
- Abbildung 35: bearbeitet nach [444], keine Genehmigung notwendig.
- Schema 1 und 2, Abbildung 38: bearbeitet nach [455], Genehmigung erteilt durch American Chemical Society (2021).
- Abbildung 39 und 44: bearbeitet nach [460], keine Genehmigung notwendig.
- Abbildung 40 und 41: bearbeitet nach [461], Genehmigung erteilt durch American Chemical Society (2021).

Die Rechte zum Nachdruck aller Originalpublikationen wurden eingeholt: [444] und [460] keine Genehmigung notwendig; [452] Copyright (2020) American Chemical Society; [455], [66], [453] und [461] Copyright (2021) American Chemical Society; [454] Copyright (2021) Elsevier Ltd.

13. Curriculum Vitae

Persönliche Angaben

Name	Sabine Willems
Adresse	[REDACTED] [REDACTED]
Geburtstag	22.06.1994
Geburtsort	Merzig
Staatsangehörigkeit	deutsch



Werdegang

seit 02/2018	Wissenschaftliche Mitarbeiterin im Arbeitskreis von Prof. Dr. M. Schubert-Zsilavec am Institut für Pharmazeutische Chemie der Goethe-Universität Frankfurt
13.12.2017	Approbation als Apothekerin (Gesamtnote: 1,98)
30.11.2017	3. Teil der pharmazeutischen Prüfung (Note: 2,50)
05/2017 bis 10/2017	Zweite Hälfte des Praktischen Jahres in der „Apotheke des Klinikums der Universität München“
11/2016 bis 04/2017	Erste Hälfte des Praktischen Jahres in der „Arnsburg Apotheke“ in Frankfurt am Main
12.10.2016	2. Teil der pharmazeutischen Prüfung (Note: 1,80)
22.08.2014	1. Teil der pharmazeutischen Prüfung (Note: 1,75)
10/2012 bis 10/2016	Studium der Pharmazie an der Goethe-Universität Frankfurt
22.03.2012	Allgemeine Hochschulreife (Abitur: 1,4)
08/2003 bis 03/2012	Friedrich-Wilhelm-Gymnasium in Trier
08/2000 bis 07/2003	Grundschule St. Johann in Konz

Tagungsbesuche

09/2019	Annual Meeting of the German Pharmaceutical Society – DPhG, Heidelberg. <i>Poster: The orphan nuclear receptor Nurr1 is responsive to non-steroidal anti-inflammatory drugs.</i>
03/2019	Annual Meeting on Frontiers in Medicinal Chemistry, Würzburg. <i>Poster: A fragment approach to orphan nuclear receptor Nurr1 ligand discovery.</i>
03/2019	EUFEPS Annual Meeting, Frankfurt am Main. <i>Poster: A fragment approach to orphan nuclear receptor Nurr1 ligand discovery.</i>

Lehrerfahrung

seit 02/2018	Betreuung des Praktikums „Allgemeine und analytische Chemie der anorganischen Arznei-, Hilfs- und Schadstoffe (unter Einbeziehung von Arzneibuchmethoden)“ und Lehrbeteiligung am zugehörigen Seminar „Stöchiometrie“ für Studierende im 1. Semester Pharmazie an der Goethe-Universität Frankfurt
10/2015 bis 07/2016	Betreuung des Tutoriums „Stöchiometrie“ für Studierende im 1. Semester Pharmazie an der Goethe-Universität Frankfurt

Zertifikate

Zertifikat über die „Fortbildungsveranstaltung gemäß §15 GenTSV zur Sicherheit in der Gentechnik“

Zertifikat für „Hochschuldidaktik“ des Interdisziplinären Kollegs Hochschullehre der Goethe-Universität Frankfurt

Sprachkenntnisse

Deutsch	Muttersprache
Englisch	fließend
	Graecum, Latinum

Akademische Lehrer

Prof. Dr. Jennifer Dressman

Prof. Dr. Gunter Eckert

Prof. Dr. Robert Fürst

Prof. Dr. Michael Karas

Prof. Dr. Jochen Klein

Prof. Dr. Rolf Marschalek

Prof. Dr. Eugen Proschak

Prof. Dr. Dr. Achim Schmidtke

Prof. Dr. Dieter Steinhilber

Prof. Dr. Daniel Merk

Prof. Dr. Manfred Schubert-Zsilavec

14. Eidesstattliche Erklärung

Erklärung

Ich erkläre hiermit, dass ich mich bisher keiner Doktorprüfung im Mathematisch-Naturwissenschaftlichen Bereich unterzogen habe.

Frankfurt am Main, den

Sabine Willems

Eidesstattliche Versicherung

Ich erkläre hiermit, dass ich die vorgelegte Dissertation über

Entwicklung und Charakterisierung

funktioneller chemischer Tools

für nukleäre Rezeptoren

selbständig angefertigt und mich anderer Hilfsmittel als der in ihr abgegebenen nicht bedient habe, insbesondere, dass alle Entlehnungen aus anderen Schriften mit Angabe der betreffenden Schrift gekennzeichnet sind.

Ich versichere, die Grundsätze der guten wissenschaftlichen Praxis beachtet und nicht die Hilfe einer kommerziellen Promotionsvermittlung in Anspruch genommen zu haben.

Frankfurt am Main, den

Sabine Willems

15. Danksagung

An erster Stelle möchte ich Prof. Dr. Daniel Merk meinen herzlichen Dank für die großartige Unterstützung und Betreuung meiner Arbeit aussprechen. Danke für deinen unverbesserlichen Optimismus und unermüdlichen Tatendrang, wodurch du mir zahlreiche spannende Projekte ermöglicht hast. Deine ansteckende Begeisterung und deine kreativen Ideen haben wesentlich zum Gelingen dieser Arbeit beigetragen. Danke, dass du immer an mich geglaubt hast!

Mein besonderer Dank gilt ebenfalls meinem Doktorvater Prof. Dr. Manfred Schubert-Zsilavec für seine fachliche und menschliche Unterstützung und die Möglichkeit in seinem Arbeitskreis zu promovieren. Außerdem danke ich ihm für die vielen schönen Arbeitsgruppen-Seminare in Aigen, Zürich und dem Montafon. Es hat mich sehr gefreut, dass wir die Begeisterung für die Musik bei zahlreichen Konzerten des Collegium Musicum teilen konnten.

Außerdem möchte ich mich bei Prof. Dr. Eugen Proschak und seinem Arbeitskreis für die wertvolle Zusammenarbeit bedanken. Insbesondere durch die Kooperation mit Dr. Jan Heering und Dr. Whitney Kilu konnten einige meiner Projekte an Komplexität und Verständnis gewinnen. Dr. Jan Heering möchte ich außerdem für das entgegengebrachte Vertrauen und seine fachliche Unterstützung danken.

Danke auch an Prof. Dr. Stefan Knapp und seine Mitarbeiter Dr. Apirat Chaikwad und Xiaomin Ni für die hilfreiche Unterstützung meiner Projekte.

Des Weiteren möchte ich mich bei Prof. Dr. Dirk Trauner von der Universität New York und seinen Mitarbeitern Dr. Johannes Morstein und Konstantin Hinnah bedanken für die überaus konstruktive und unkomplizierte Kooperation über den Atlantik hinweg.

Ferner danke ich Prof. Dr. Dieter Steinhilber und seiner Arbeitsgruppe für die Unterstützung und Möglichkeit Geräte und Ressourcen zu nutzen.

Ein großes Dankeschön an Etienne Dehò und Laura Isigkeit für die kritischen Korrekturen dieser Arbeit!

Außerdem möchte ich meinen Kollegen im Arbeitskreis von Prof. Dr. Manfred Schubert-Zsilavec für die letzten vier Jahre danken.

Besonders danke ich Dr. Julius Pollinger und Dr. Leonie Gellrich für die herzliche Aufnahme im Arbeitskreis und die schöne Zeit im gemeinsamen Labor.

Danke auch an Jan Vietor und Espen Schallmeyer für die gute Stimmung im Labor.

Danke an Laura Isigkeit, dass du immer für ein kreatives Kaffeepäuschen zu gewinnen warst :)

Daniel Zaienne danke ich für die gute Zusammenarbeit und Julia Ohrndorf für die synthetische Unterstützung.

Danke auch an Astrid Kaiser, Dr. Mario Wurglics, Alisa Lang, Silvia Arifi, Minh Sai, Gustave Adouvi und Marcel Müller.

Meinen Freunden danke ich für die Unterstützung und den (musikalischen) Ausgleich zum Promotionsalltag.

Vor allem danke an Valeska Pichler – wer weiß welche Wege wir gegangen wären, wenn die Münze damals anders entschieden hätte ;P

Und danke auch an Dr. Domagoj Šegregur, dass wir vom ersten Tag des Studiums bis zum Ende der Promotion diesen Weg in Frankfurt gemeinsam gegangen sind.

Zum Schluss ein Dank von Herzen an meine Mama! Danke, für deine unglaubliche Unterstützung und dafür, dass du immer einen guten Rat und ein offenes Ohr für mich hast, und dass du mich darin bestärkt hast meinen Weg zielstrebig zu gehen.

In liebevollem Gedenken an Guy Bausch.

16. Nachdrucke der Publikationen

16.1 Photohormones Enable Optical Control of the Peroxisome Proliferator-Activated Receptor γ (PPAR γ)

Hinnah, K.[‡]; **Willems, S.**[‡]; Morstein, J.; Heering, J.; Hartrampf, F. W. W.; Broichhagen, J.; Leippe, P.; Merk, D.; Trauner, D. Photohormones Enable Optical Control of the Peroxisome Proliferator-Activated Receptor γ (PPAR γ). *J. Med. Chem.* **2020**, *63* (19), 10908–10920.

[‡] *Hier liegt eine geteilte Erstautorenschaft zwischen K. H. und S. W. vor.*

Reprinted with permission from Hinnah, K.[‡]; Willems, S.[‡]; Morstein, J.; Heering, J.; Hartrampf, F. W. W.; Broichhagen, J.; Leippe, P.; Merk, D.; Trauner, D. *J. Med. Chem.* **2020**, *63* (19), 10908–10920. Copyright (2020) American Chemical Society.

Photohormones Enable Optical Control of the Peroxisome Proliferator-Activated Receptor γ (PPAR γ)Konstantin Hinnah,¹ Sabine Willems,¹ Johannes Morstein, Jan Heering, Felix W. W. Hartrampf, Johannes Broichhagen, Philipp Leippe, Daniel Merk,* and Dirk Trauner*Cite This: *J. Med. Chem.* 2020, 63, 10908–10920

Read Online

ACCESS |



Metrics & More

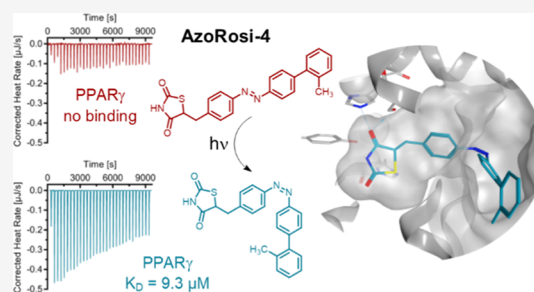


Article Recommendations



Supporting Information

ABSTRACT: Photopharmacology aims at the optical control of protein activity using synthetic photoswitches. This approach has been recently expanded to nuclear hormone receptors with the introduction of “photohormones” for the retinoic acid receptor, farnesoid X receptor, and estrogen receptor. Herein, we report the development and profiling of photoswitchable agonists for peroxisome proliferator-activated receptor γ (PPAR γ). Based on known PPAR γ ligands (MDG548, GW1929, and rosiglitazone), we have designed and synthesized azobenzene derivatives, termed **AzoGW1929** and **AzoRosi**, which were confirmed to be active in cell-based assays. Subsequent computer-aided optimization of **AzoRosi** resulted in the photohormone **AzoRosi-4**, which bound and activated PPAR γ preferentially in its light-activated *cis*-configuration.



INTRODUCTION

Nuclear hormone receptors (NHRs) are ligand-inducible transcription factors that interact with specific DNA response elements to elicit a transcriptional response of their target genes.^{1,2} They control a wide variety of biological processes, ranging from cell proliferation and differentiation to metabolism, homeostasis, and morphogenesis.³ This receptor class is modulated by a broad spectrum of endogenous molecules, including thyroid and steroid hormones, bile acids and fatty acids, retinoids, and vitamin D.⁴

Peroxisome proliferator-activated receptors (PPARs) belong to the class I subfamily of NHRs and comprise three isoforms (PPAR α , PPAR δ , and PPAR γ), which exhibit different tissue localizations.^{5,6} PPARs form a heterodimer with the retinoid X receptor (RXR), and upon ligand binding, they regulate transcription levels of genes involved, e.g., in metabolic balance and inflammatory processes.⁷ The PPAR γ subtype is mainly expressed in adipose tissue and also found in the liver, heart, brain, and macrophages. It controls insulin secretion, lipid, and glucose metabolism, and is considered the master regulator of adipogenesis.⁸ PPAR γ is linked to diverse pathological conditions, such as diabetes, cardiovascular disorders, Alzheimer's and Parkinson's disease, multiple sclerosis, stroke, and cancer.^{9–14}

In photopharmacology, photoswitchable small molecules are used to control biological processes with light.^{15–18} This approach has proven to be especially successful with lipophilic or amphiphilic molecules that can control GPCRs, ion channels, enzymes, or biophysical aspects of lipids.^{19–26} Amphiphilic agonists of NHRs could therefore be ideally

suited for this approach. This was first exemplified with a photoswitchable retinoic acid derivative targeting the retinoic acid receptor α (RAR α).²⁷ Subsequently, we developed a photohormone for the bile acid receptor farnesoid X receptor (FXR) that allows for the optical control of gene regulation in liver cells. In addition, a photoswitchable estrogen receptor (ER) agonist was recently reported by Tsuchiya.^{28,29} Here, we disclose the development of photohormones for PPAR γ , extending the reach of photopharmacology to another important member of the NHR superfamily.

RESULTS AND DISCUSSION

In our search for photoswitchable PPAR γ modulators, we screened various drug databases (DrugBank, PDB, ChEMBL, IUPHAR) for known PPAR γ modulators to identify promising chemotypes that could be modified with an azobenzene photoswitch. Molecules containing lipophilic segments that can be substituted with an azobenzene (“azologization”) are particularly amenable to this approach.^{27,30} Most PPAR γ agonists share the common structure of fatty acid mimetics³¹ that are comprised of a polar, usually acidic, headgroup that engages in hydrogen bonding with the ligand-dependent activation function (AF-2), an aliphatic linker, and a bulky

Received: April 30, 2020

Published: September 4, 2020



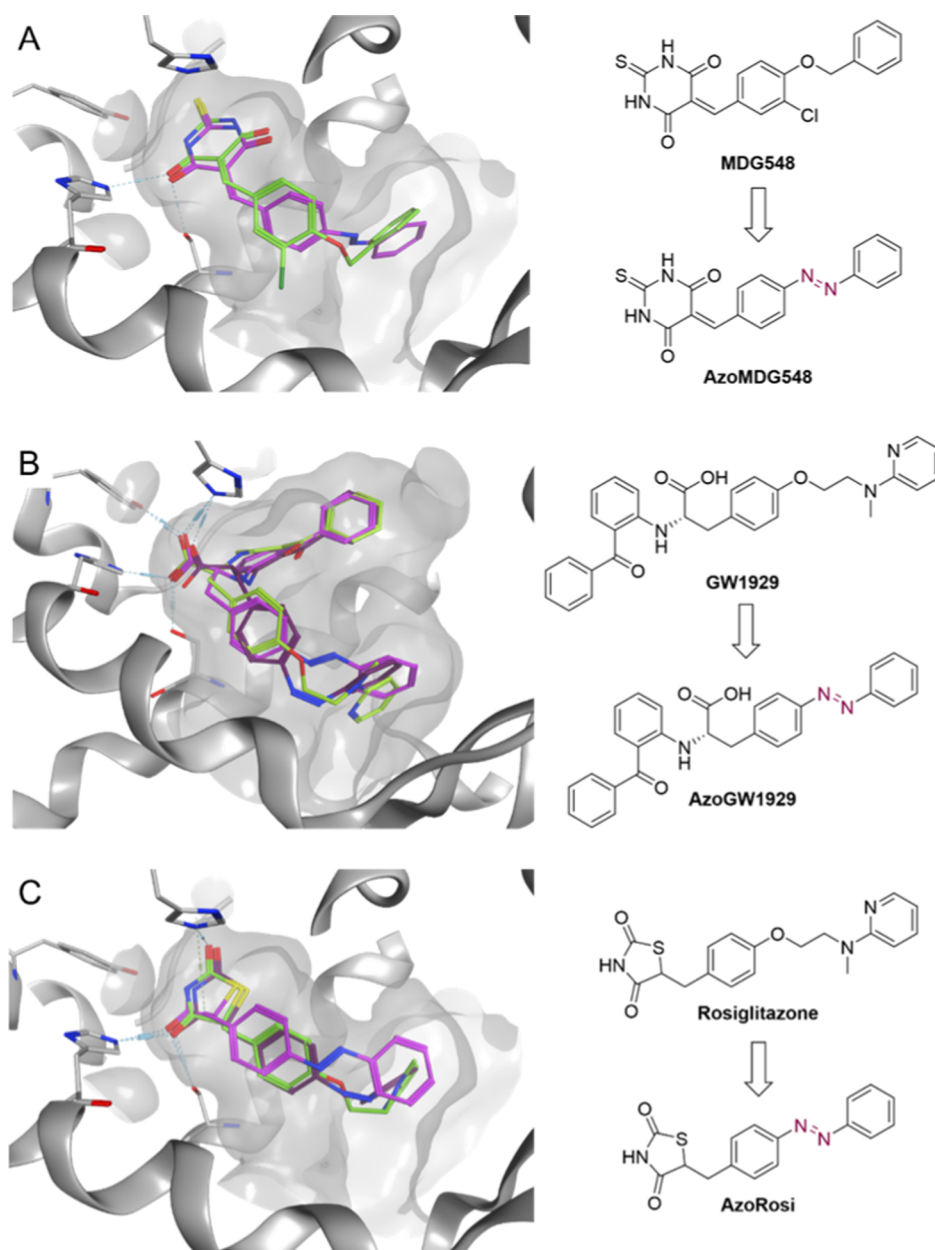
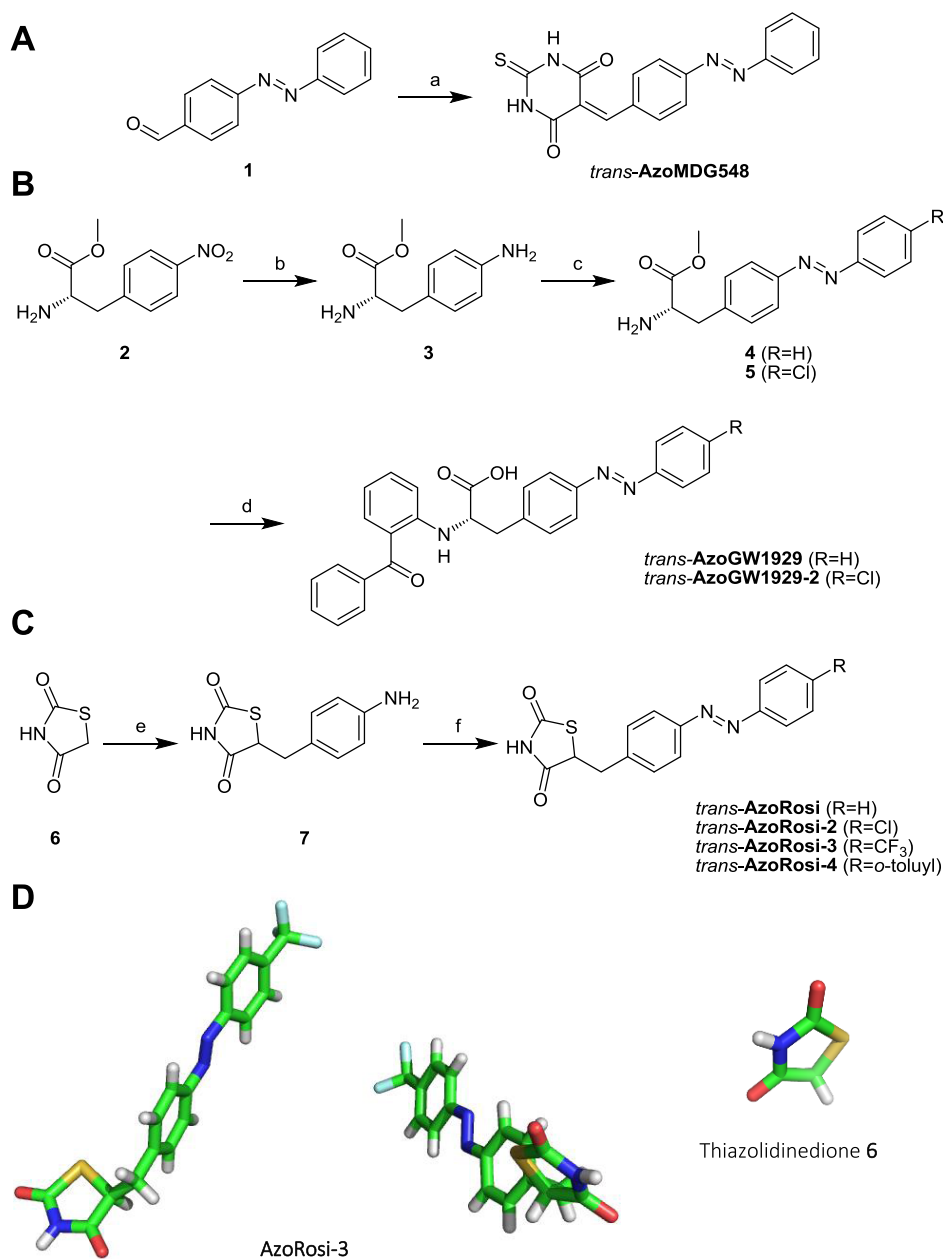


Figure 1. Molecular docking guides the design of photohormones for PPAR γ . Docking was performed in MOE³⁸ using X-ray crystal structures of PPAR γ complexed with the template ligands rosiglitazone (A, C, green, PDB ID: 5YCP³⁶) and GW1929 (B, green, PDB ID: 6D8X³⁷). (A) Incorporation of an azo group in MDG548 (green) to AzoMDG548 (magenta) allowed minimal changes to the structure. (B) In AzoGW1929 (magenta), the azo group replaces the aminoethoxy linker of GW1929. (C) Azologization of rosiglitazone by replacement of the aminoethoxy linker region (AzoRosi, magenta) resulted in favorable predicted binding modes of both (*cis*-/*trans*-) isomers.

aromatic tail that contributes to their function and potency (effector module).³² Based on this structural information, we envisioned that optical control over PPAR γ could be achieved by the incorporation of an azobenzene photoswitch into the hydrophobic tail—a strategy that has been very successful for a number of bioactive lipids. Photoisomerization of the tail should lead to a steric clash in the ligand binding site that significantly decreases the affinity of one isomer to the receptor. Initial hits were further assessed based on previous SAR studies, crystal structure data, and molecular docking.^{33–37} Based on these considerations, we selected three chemotypes (MDG548, GW1929, and rosiglitazone) as leads to develop PPAR γ -targeting photohormones (Figure 1).

The potential of the lead azolog scaffolds to act as photoswitchable PPAR γ ligands was studied by molecular docking. The X-ray complex structures of the PPAR γ ligand binding domain with bound rosiglitazone (PDB ID: 5YCP³⁶) or GW1929 (PDB ID: 6D8X³⁷) served as templates. Structures were prepared and docking was performed in the molecular operating environment (MOE). For each azolog, *cis*- and *trans*-isomer were individually docked and the resulting predicted binding modes were evaluated considering participation in the canonical H-bond network with the PPAR γ activation triad His323, His449, and Tyr473, additional direct contacts to the binding site, absence or presence of clashes, and similarity to the binding mode of the cocrystallized ligands. The design of candidate derivatives of AzoGW1929 and

Scheme 1. Synthesis of Photohormones for PPAR γ ^a

^aReagents and conditions: (A) (a) Thiobarbituric acid, EtOH, 80 °C, 2 h (46%); (B) (b) Pd/C, MeOH, rt, 16 h (quant.) (c) (i) Aniline/4-chloroaniline, oxone, CH₂Cl₂, H₂O, rt, 16 h, (ii) 3, MeOH, rt, 16 h (70% R = H, 34% R = Cl), (d) (i) (2-Bromophenyl)(phenyl)methanone, Cs₂CO₃, Pd(OAc)₂, BINAP, toluene, 110 °C, 3 h (ii) LiOH, H₂O, ACN, rt, 3 h (56% R = H, 31% R = Cl over 2 Steps); (C) (e) (i) 4-Nitrobenzaldehyde, piperidine, AcOH, EtOH, μ w 150 °C, 20 min (ii) Hantzsch ester, SiO₂, toluene, 110 °C, 20 h (iii) Pd/C, MeOH, rt, 16 h (24% over 3 Steps) (f) (i) Aniline/4-chloroaniline/4-trifluoromethylaniline/2'-methyl-[1,1'-biphenyl]-4-amine 9, oxone, CH₂Cl₂, H₂O, rt, 16 h (ii) 7, MeOH, rt, 16 h (72% R = H, 71% R = Cl, 57% R = CF₃, 49% R = *o*-toluyl) (D) Crystal structure of thiazolidinedione 6 and *trans*-AzoRosi-3.

AzoRosi was similarly supported by molecular docking to computationally assess their potential to act as optimized photohormones.

AzoMDG548 (Figure 1A) was derived from the PPAR γ agonist MDG548 (EC₅₀ = 215 nM)³⁵ featuring a benzyl phenyl ether moiety, which is a common motif for azologization.²⁷ The predicted binding mode of *trans*-AzoMDG548 aligned well with the docked pose of MDG548 and with rosiglitazone suggesting the potential of the azolog for PPAR γ modulation. AzoGW1929 was derived from the potent (EC₅₀ = 1.47 nM) and selective PPAR γ

agonist GW1929³⁹ (Figure 1B). Crystallographic data of the parent compound bound to PPAR γ showed that the benzophenone motif is bound in a lipophilic subpocket deep inside the ligand binding domain (LBD) (PDB ID: 6D8X), providing little space and flexibility for structural variation. Therefore, we reasoned that the aliphatic linker was more suitable for azologization. Docking studies on GW1929-derived azologs agreed with this hypothesis since predicted binding modes for analogues bearing the azo group in the benzophenone region did not align with the cocrystallized ligand but partly placed the designed structure outside the

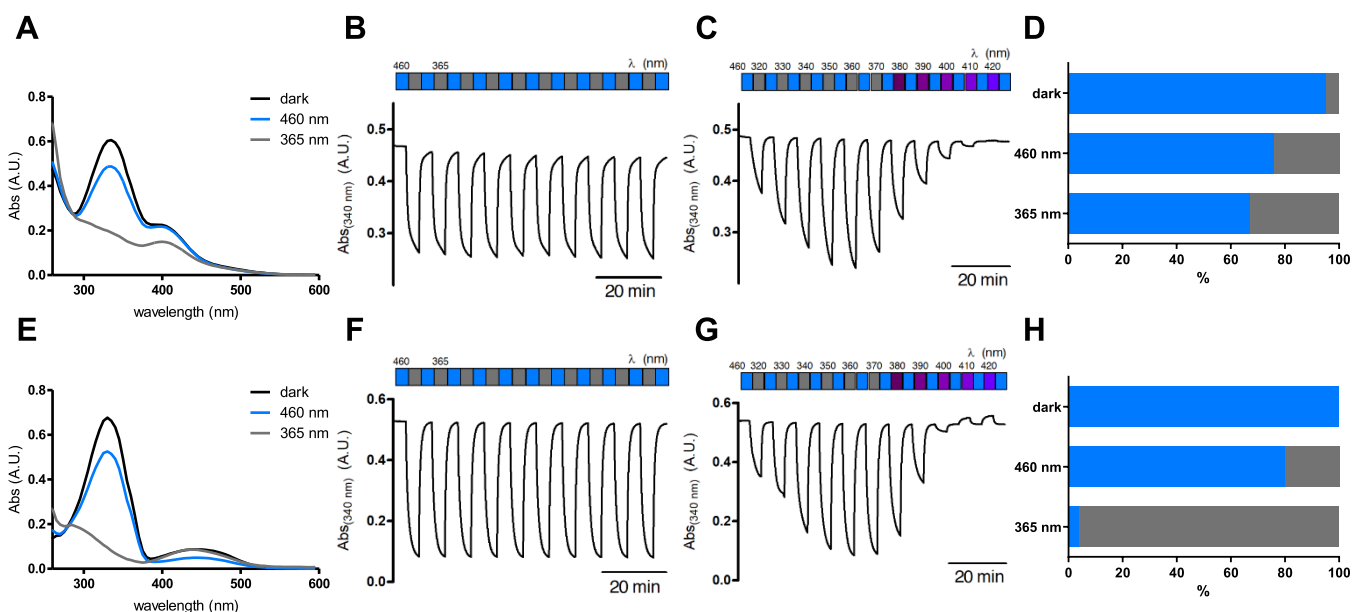


Figure 2. Photophysical evaluation. The UV–vis spectra of **AzoGW1929** (A) and **AzoRosi** (E) (25 μM in DMSO) in the dark-adapted (*trans*, black), 365 nm-adapted (*cis*, gray), and 460 nm-adapted (*trans*, blue) photostationary states. Reversible cycling of **AzoGW1929** (B) and **AzoRosi** (F) (25 μM in DMSO) with alternating illumination at 365 and 460 nm. Reversible cycling between photoisomers of **AzoGW1929** (C) and **AzoRosi** (G) (25 μM in DMSO) with alternating illumination at varying wavelengths between 320 and 420 nm and 460 nm. Photostationary states of **AzoGW1929** (D) in $\text{MeOD-}d_4$ and **AzoRosi** (H) in CDCl_3 of the dark-adapted state and after irradiation with 460 and 365 nm for 5 min.

canonical binding pocket. In contrast, the predicted binding modes of **AzoGW1929**, where the azo motif replaces the aminoethoxy linker, aligned well with the cocrystallized ligand GW1929. Favorable poses were observed for both the *cis*- and *trans*-configuration of **AzoGW1929**, however. The preferred absolute configuration of GW1929 was retained in our azolog design, and the (*S*)-enantiomer of **AzoGW1929** was prepared through an enantioselective synthesis.³² The clinically approved PPAR γ agonist rosiglitazone⁴⁰ served as a template for our third azolog design. Multiple SAR studies demonstrate the importance of the thiazolidinedione headgroup and methylene linker of rosiglitazone ($\text{EC}_{50} = 43 \text{ nM}$)^{41,42} for potency. Therefore, we proposed to incorporate the azobenzene photoswitch into the hydrophobic tail of rosiglitazone (Figure 1C). Docking of the azolog, termed **AzoRosi**, to a rosiglitazone-bound PPAR γ crystal structure (PDB ID: SYCP) resulted in favorable binding modes for both *cis*- and *trans*-**AzoRosi** that aligned with the crystal bound template ligand and revealed participation in the canonical H-bond network with the activation triad (His323, His449, Tyr473).

The synthesis of **AzoMDG548** was achieved by the coupling of 4-phenylazobenzaldehyde **1** to thiobarbituric acid via Knoevenagel-type condensation under reflux in ethanol (Scheme 1A). The synthesis route for **AzoGW1929** and derivative **AzoGW1929-2** started from (*S*)-4-nitrophenylalanine methyl ester hydrochloride **2**, which was reduced to the corresponding amino compound using palladium on charcoal and hydrogen (Scheme 1B). Baeyer–Mills coupling of methyl (*S*)-2-amino-3-(4-aminophenyl)propanoate **3** with the corresponding aniline (unsubstituted aniline for **AzoGW1929** or 4-chloroaniline for **AzoGW1929-2**) and subsequent Buchwald–Hartwig cross-coupling to the free amine of the amino acid afforded the methyl ester derivatives of the corresponding photohormones. Cleavage of the methyl esters with lithium hydroxide yielded **AzoGW1929** and **AzoGW1929-2**. Photo-

switchable derivatives of rosiglitazone (**AzoRosi**, **AzoRosi-2-4**) were obtained in four steps (Scheme 1C), starting with the coupling of *para*-nitrobenzaldehyde to thiazolidinedione **6** in a Knoevenagel-type reaction. Two subsequent reduction steps with Hantzsch ester and palladium on charcoal under a hydrogen atmosphere gave 5-(4-aminobenzyl)thiazolidine-2,4-dione **7**. The final step comprised Baeyer–Mills coupling with the corresponding (*para*-substituted) anilines to afford **AzoRosi** and derivatives **AzoRosi-2** to **AzoRosi-4**. The required aniline **9** for **AzoRosi-4** was synthesized in a Suzuki reaction from *para*-aminoboronic acid **8** and 2-bromotoluene (Scheme S1). The X-ray structure of the thiazolidinedione **6** and of *trans*-**AzoRosi-3** is shown in Scheme 1D.

The photophysical properties and photostationary states (PSS) of **AzoGW1929** and **AzoRosi** were determined by UV–vis and ¹H NMR spectroscopy (Figure 2). The absorption spectra after illumination with $\lambda = 460 \text{ nm}$ (*trans*, blue) and $\lambda = 365 \text{ nm}$ (*cis*, gray) demonstrated wavelength-dependent switching as expected for “classical” unsubstituted azobenzenes. **AzoGW1929** showed an additional local absorption maximum at 400 nm, which is likely caused by additional absorption of the benzophenone moiety. Photoswitching was repeated over multiple cycles indicating good photostability of these photohormones. Photostationary states could further be titrated using different wavelengths of light (“color-dosing”). Half-life times of the thermally unstable *cis*-isomer were determined in dimethyl sulfoxide (DMSO) at room temperature (Figure S1) and are $t_{1/2} = 37.0 \text{ h}$ (**AzoGW1929**) and $t_{1/2} = 64.1 \text{ h}$ (**AzoRosi**). The PSS after illumination with the optimal wavelengths for photoisomerization ($\lambda = 365 \text{ nm}$ and $\lambda = 460 \text{ nm}$, respectively) are as follows: 95% *trans*-**AzoGW1929** (dark), 76% *trans*-**AzoGW1929** (460 nm), 67% *trans*-**AzoGW1929** (365 nm), and 100% *trans*-**AzoRosi** (dark), 80% *trans*-**AzoRosi** (460 nm) and 4% *trans*-**AzoRosi** (365 nm). These data revealed slow switching kinetics for

AzoGW1929, whereas illumination with 365 nm allows for effective isomerization of **AzoRosi**.

The biological evaluation of the photohormones for modulation of PPAR γ was performed using hybrid Gal4 reporter gene assays in HEK293T cells. These test systems rely on chimeric transcription factors composed of the respective human nuclear receptor ligand binding domain and the DNA binding domain of the yeast protein Gal4. Gal4-responsive firefly luciferase was employed as a reporter gene, and a constitutively expressed *Renilla* luciferase served for normalization and to monitor test compound toxicity. Pioglitazone (1 μ M) served as a reference agonist on every plate to calculate the relative activation efficacy of the test compounds. To individually characterize both isomers of the photohormones, the assays were conducted with the *trans*-photohormones in the dark and with the preilluminated *cis*-isomers using a Cell Disco.⁴³

Profiling of the three first-generation photohormones **AzoMDG548**, **AzoGW1929**, and **AzoRosi** revealed no activity for *trans*-**AzoMDG548** on PPAR γ up to 10 μ M concentration, while *trans*-**AzoGW1929** and *trans*-**AzoRosi** were confirmed as PPAR γ modulators with promising potencies and activation efficacies (Table 1). Preliminary evaluation of the *cis*-

Table 1. PPAR Modulatory Activity of Photohormones **AzoMDG548**, **AzoGW1929**, and **AzoRosi** in a Gal4 Hybrid Reporter Gene Assay^a

ID	PPAR γ modulation	PPAR α modulation	PPAR δ modulation
<i>trans</i> - AzoMDG548	inactive	inactive	inactive
<i>trans</i> - AzoGW1929	EC ₅₀ = 1.0 \pm 0.1 μ M (30 \pm 2% max. rel. act.)	inactive	inactive
<i>trans</i> - AzoRosi	EC ₅₀ = 2.2 \pm 0.2 μ M (21 \pm 1% max. rel. act.)	8% activation at 10 μ M	inactive

^aMaximum relative activation (max. rel. act.) refers to the activity of 1 μ M pioglitazone. Data are the mean \pm standard deviation (SD). Each sample was tested in technical duplicates in at least two independent biological repeats. Inactive: no statistically significant activity at 10 μ M.

counterparts revealed similar activity on PPAR γ as for the *trans*-isomers, which aligned with our observations in the docking studies. Except for the weak activity of **AzoRosi** on PPAR α at 10 μ M, all three photohormones were selective for PPAR γ over the closely related PPAR α and PPAR δ subtypes. Due to the lack of activity of **AzoMDG548**, we did not further characterize this compound and focused our further study on the other two lead compounds.

Encouraged by the favorable PPAR γ modulatory activity and promising photophysical characteristics of **AzoGW1929** and **AzoRosi**, we selected both photohormones for further structural refinement. Analysis of the predicted binding mode of **AzoGW1929** in the PPAR γ ligand binding site indicated the occupation of the subpocket accommodating the azobenzene motif with little space for further derivatization. However, we observed the potential for a chlorine substituent in position 4 of the azobenzene moiety to generate a preference for the *trans*-configuration since docking simulation of **AzoGW1929-2** in the GW1929-bound structure (PDB ID: 6D8X) revealed favorable binding for the *trans*-isomer but no reasonable pose for the *cis*-counterpart (Figure 3A). The docking pose of **AzoRosi** suggested an opportunity for structural refinement,

too. As discussed above, the benzylthiazolidinedione motif has been characterized as essential for activity, prompting us to focus on the azobenzene part for optimization. In the docked *trans*-configuration of **AzoRosi**, the azobenzene was bound in a cavity with little space available for substituents. However, **AzoRosi** analogues bearing bulky substituents in position 4 of the azobenzene motif were observed to bind favorably to PPAR γ in *cis*-configuration, with the extra substituents protruding into an unoccupied pocket of the Y-shaped PPAR γ ligand binding site (Figure 3B). This optimization potential seemed particularly attractive as it suggested preference for the *cis*-configurations of **AzoRosi** descendants. The effect was observed in the molecular docking of **AzoRosi-2** bearing a chlorine atom in position 4 of the azobenzene motif, and even more pronounced for the trifluoromethyl analogue **AzoRosi-3**. **AzoRosi-4** was designed as a maximally *cis*-favoring structure according to our results in the molecular docking. The *cis*-isomer of **AzoRosi-4** formed a favorable binding mode to the PPAR γ ligand binding site (Figures 3B and 5A) with H-bond interactions to the canonical activation triad of PPAR γ (His323, His449, Tyr473). The extended and lipophilic biphenyl azobenzene protruded to a hydrophobic tunnel in the Y-shaped PPAR γ pocket formed by Ile281 and the backbones of Gly284 and Cys285 from helix 3 as well as Ile341 and Met348 from the β sheet near helix 6. In contrast, the extended linear structure of *trans*-**AzoRosi-4** could not be reasonably placed in the angled PPAR γ ligand binding site.

The second-generation azologs **AzoGW1929-2** and **AzoRosi-2** to **AzoRosi-4** were prepared as described in Scheme 1. Their photophysical properties are depicted in Figures 4 and S1. The spectra of **AzoGW1929-2** showed photophysical properties similar to the unsubstituted parent azolog **AzoGW1929**. Photophysical evaluation of **AzoRosi-2** to **AzoRosi-4** also showed that these analogues behaved similar to their predecessor **AzoRosi**, with respect to absorption spectra for both isomers, switching kinetics, thermal stability of the *cis*-isomer, and PSS (99% *trans*-**AzoRosi-4** (dark), 83% *trans*-**AzoRosi-4** (460 nm), and 23% *trans*-**AzoRosi-4** (365 nm)).

Biological evaluation of **AzoGW1929-2** for PPAR γ modulation revealed neither improved potency nor a clear preference for either isomer (Table 2). This chemotype, therefore, seems to hold little promise for continued refinement and was not further pursued. **AzoRosi-2**, which bears a chlorine substituent on the azobenzene, was almost equally active as *trans*-**AzoRosi** in its *trans*-configuration and showed enhanced PPAR γ activation in its *cis*-configuration (Table 2). This agrees with our hypothesis that the extension of **AzoRosi** in position 4 of the azobenzene would promote preferential PPAR γ agonism of the *cis*-isomer. Accordingly, the *cis*-isomer of the trifluoromethyl derivative **AzoRosi-3** was more active than *trans*-**AzoRosi-3**. However, the maximum activation efficacy of dark-adapted *trans*-**AzoRosi-3** was also higher than that of its parent azolog *trans*-**AzoRosi**. By contrast, the *o*-toluyl derivative **AzoRosi-4** was less active in its *trans*-configuration than *trans*-**AzoRosi** (12 vs 21% maximum activation), while the *cis*-isomer of **AzoRosi-4** increased its PPAR γ agonism approximately threefold with 39% maximum relative activation efficacy (Table 2). Therefore, **AzoRosi-4** is a photohormone for PPAR γ that can be activated with light. This relative dark inactivity and gain in potency upon irradiation is a desirable functional feature in photopharmacology.

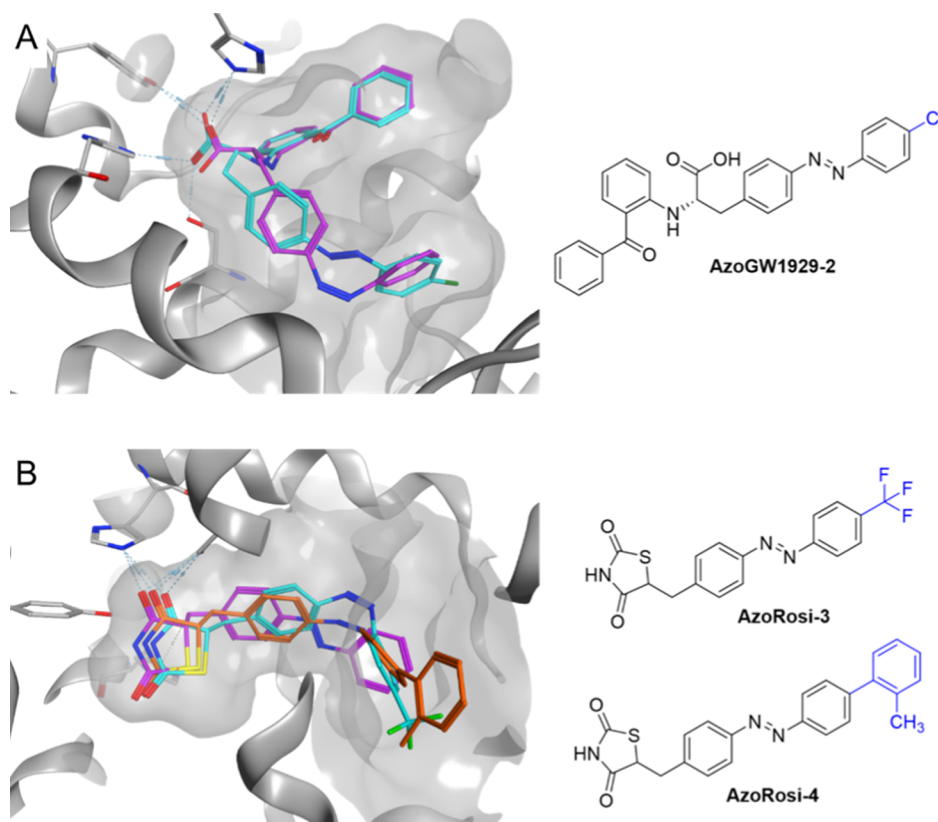


Figure 3. Molecular docking study to design optimized **AzoGW1929** (A, magenta) and **AzoRosi** (B, magenta) derivatives. Docking was performed in MOE using X-ray crystal structures of PPAR γ complexed with the template ligands GW1929 (A, PDB ID: 6D8X) and rosiglitazone (B, PDB ID: SYCP). (A) Docking simulations suggested that the introduction of a chlorine substituent in position 4 of the azobenzene residue in **AzoGW1929-2** (cyan) would promote the preferential binding of the *trans*-isomer. (B) *cis*-**AzoRosi-3** (cyan) and *cis*-**AzoRosi-4** (orange) favorably extended to a tunnel in the PPAR γ ligand binding site that is not occupied by the template ligand rosiglitazone or by **AzoRosi**.

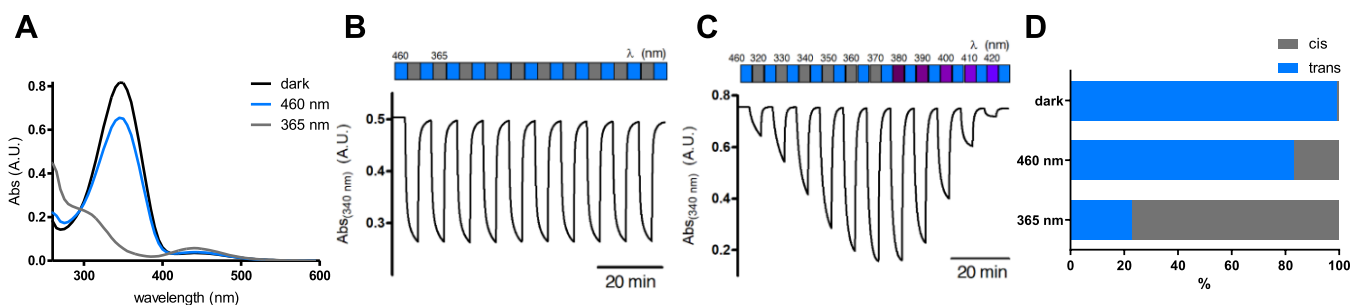


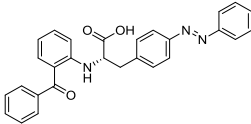
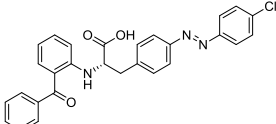
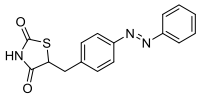
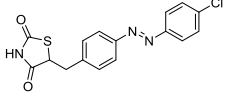
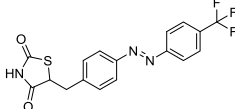
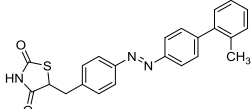
Figure 4. (A) Photophysical evaluation of **AzoRosi-4** (25 μ M in DMSO) in the dark-adapted (*trans*, black), 365 nm-adapted (*cis*, gray), and 460 nm-adapted (*trans*, blue) photostationary states. Reversible cycling of **AzoRosi-4** (25 μ M in DMSO) with alternating illumination at 365 and 460 nm (B) or with alternating illumination at varying wavelengths between 320 and 420 nm (C). (D) Photostationary states of **AzoRosi-4** in CDCl₃ of the dark-adapted state and after irradiation with 460 and 365 nm.

Next, we determined the binding affinity of **AzoRosi-4** for both photoisomers by isothermal titration calorimetry (ITC, Figure 5B). The light-activated *cis*-isomer is bound to the recombinant PPAR γ ligand binding domain with a K_D value of 9.3 μ M. Under identical conditions, no binding of dark-adapted *trans*-**AzoRosi-4** was detectable in ITC, corroborating the predicted binding of *cis*-**AzoRosi-4** (Figure 5A) and the anticipated clashes of the *trans*-isomer with the PPAR γ ligand binding site.

Next, we probed *cis*-**AzoRosi-4** for the ability to activate endogenous PPAR γ in a cellular setting. Given the complex regulation of transcriptional control by various transcription factors and potential compensatory effects on the expression

levels of PPAR γ target genes, we aimed to analyze target engagement in native liver cells with a reliable luminescent readout. For this, we transiently transfected PPAR γ expressing HepG2 cells with a reporter construct comprising the human full-length PPAR response element (PPRE) to control the expression of a firefly luciferase reporter gene. PPAR γ and its heterodimer partner RXR were not overexpressed to enable the observation of endogenous cellular PPAR γ activation. The light-activated photohormone *cis*-**AzoRosi-4** activated the PPRE reporter with an EC_{50} value of $0.9 \pm 0.2 \mu$ M and 2.4 ± 0.1 -fold maximum activation efficacy. Interestingly, despite the absence of binding affinity for *trans*-**AzoRosi-4** in the ITC,

Table 2. Light-dependent PPAR γ Modulatory Activity of Photohormones AzoGW1929, AzoGW1929-2, AzoRosi, and AzoRosi-2-4 in a Gal4 Hybrid Reporter Gene Assay^a

ID	structure	PPAR γ modulation	
		<i>trans</i>	<i>cis</i>
AzoGW1929		EC ₅₀ = 1.0±0.1 μ M (30±2% max. rel. act.)	EC ₅₀ = 1.30±0.01 μ M (27.2±0.1% max. rel. act.)
AzoGW1929-2		EC ₅₀ = 1.6±0.1 μ M (20±1% max. rel. act.)	EC ₅₀ = 5.0±0.4 μ M (35±2% max. rel. act.)
AzoRosi		EC ₅₀ = 2.2±0.2 μ M (21±1% max. rel. act.)	EC ₅₀ = 6.3±1.4 μ M (38±5% max. rel. act.)
AzoRosi-2		EC ₅₀ = 2.9±0.2 μ M (25±1% max. rel. act.)	EC ₅₀ = 7.0±1.0 μ M (49±4% max. rel. act.)
AzoRosi-3		EC ₅₀ = 2.2±0.7 μ M (33±5% max. rel. act.)	EC ₅₀ = 6.5±1.5 μ M (52±11% max. rel. act.)
AzoRosi-4		EC ₅₀ = 2.8±1.3 μ M (12±2% max. rel. act.)	EC ₅₀ = 6.4±0.4 μ M (39±2% max. rel. act.)

^aMaximum relative activation (max. rel. act.) refers to the activity of 1 μ M Pioglitazone. Data are the mean \pm SD. Each sample was tested in technical duplicates in at least two independent biological repeats.

some PPRE activation was observed in the cellular setting by the *trans*-isomer at 10 μ M (Figure 5C).

Conclusions and Outlook. We report on the computer-aided development of photohormones for the nuclear hormone receptor PPAR γ . Supported by docking simulations, we identified PPAR γ ligand chemotypes that allow for azologization and confirmed PPAR γ modulation for two out of three basic photohormones. Subsequent structure-guided optimization resulted in second-generation photoswitchable analogues of rosiglitazone that exhibit stronger PPAR γ activation in their *cis*-configuration. Among the seven PPAR γ -modulating photohormones developed in this study, **AzoRosi-4** was designed to have low biological activity in its native *trans*-configuration but markedly activated PPAR γ upon light-activation to the *cis*-isomer. This successful computer-aided development of **AzoRosi-4** demonstrates that structure-guided designs of azologs are feasible for proteins with highly flexible binding regions, such as PPAR γ . With its attractive activity profile and its favorable photophysical characteristics, **AzoRosi-4** emerges as a first-in-class photohormone for PPAR γ enabling new types of *in vitro* studies with light-dosing of PPAR γ activation. This photohormone could become a useful tool for the study of PPAR γ biology, including spatiotemporal aspects of its regulation that cannot be studied with constitutively active modulators or caged compounds. These properties are particularly useful in the context of drug discovery, as adverse effect profiles have recently limited clinical use or development of PPAR γ agonists. A photohormone may, for example, be light-activated in certain tissues to activate PPAR γ for beneficial effects, while other organs

where the nuclear receptor mediates adverse activities, such as in the brain⁴⁴ or bone,⁴⁵ can be spared. Photohormones that can be locally activated at their desired site of action potentially exhibit an improved pharmacological profile and could ultimately pave the way for novel drugs for the treatment of metabolic disorders (including diabetes mellitus and obesity). Our study underscores that photopharmacology is a promising approach for the precision control of nuclear hormone receptors, as we expanded the scope of photohormones to PPAR γ . Photohormones will allow the study of NHR biology with unprecedented resolution in space and time and could potentially be useful for new forms of photodynamic therapy.^{46,47}

EXPERIMENTAL SECTION

General Information. All reagents and solvents were purchased from commercial sources (Sigma-Aldrich, TCI America, Strem Chemicals, Thermo Fischer Scientific, etc.) and were used without further purification. Reactions were monitored by TLC on precoated, Merck Silica gel 60 F₂₅₄ glass-backed plates, and the chromatograms were visualized by UV irradiation at $\lambda = 254$ nm. Flash silica gel chromatography was performed using silica gel (SiO₂, particle size 40–63 μ m) purchased from SiliCycle. NMR spectra were measured on a Bruker Avance III HD 400 (equipped with CryoProbe). Multiplicities in the following experimental procedures are abbreviated as follows: s = singlet, d = doublet, t = triplet, q = quartet, m = multiplet. Proton chemical shifts are expressed in parts per million (ppm, δ scale) and are referenced to the residual proton in the NMR solvent (CDCl₃: $\delta = 7.26$; DMSO-*d*₆: $\delta = 2.50$; MeOD-*d*₄: $\delta = 3.31$). Carbon chemical shifts are expressed in ppm (δ scale) and are referenced to the carbon resonance of the NMR solvent (CDCl₃: $\delta = 77.2$; DMSO-*d*₆: $\delta = 39.5$; MeOD-*d*₄: $\delta = 49.0$). *Note:* Due to the

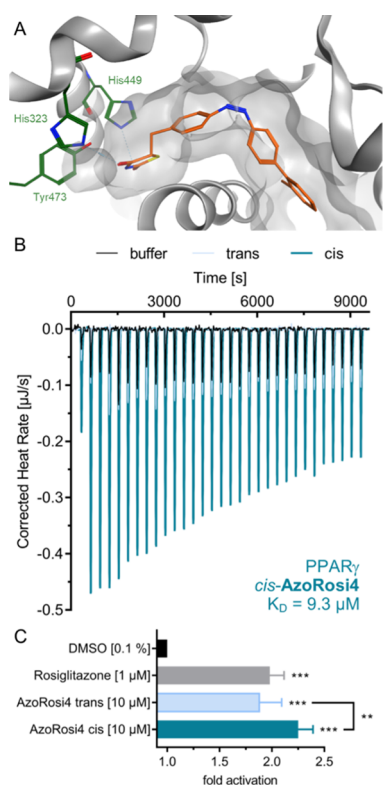


Figure 5. (A) Molecular docking of *cis*-AzoRosi-4 to the PPAR γ ligand binding site (PDB ID: 5YCP). (B) Isothermal titration calorimetry experiment of *trans*-AzoRosi-4 (dark-adapted, 300 μ M) and *cis*-AzoRosi-4 (irradiated with $\lambda=365$ nm for 5 min, 300 μ M) to recombinant PPAR γ ligand binding domain protein revealed exclusive binding of *cis*-AzoRosi-4. Buffer as control. $K_D = 9.3$ μ M. Colors are specified in the figure. Individual titrations are shown in Figure S3 (Supporting Information). (C) *cis*-AzoRosi-4 robustly activated the human PPAR response element (PPRE) in the absence of receptor overexpression in HepG2 cells. Rosiglitazone served as a reference agonist for PPAR γ activation. Data are the mean \pm SD. Each sample was tested in technical duplicates in six independent biological repeats; ** $p < 0.01$ and *** $p < 0.001$ (t -test).

trans/cis isomerization of compounds containing an azobenzene functionality, more signals were observed in the ^1H NMR and ^{13}C NMR spectra than expected for the pure *trans*-isomer. Only signals for the major *trans*-isomer are reported.

The purity of the compounds was measured on an Agilent Technologies 1260 II Infinity connected to an Agilent Technologies 6120 Quadrupole mass spectrometer with ESI ionization source. Elution was performed using a gradient from 25:75 to 100:0% MeCN/H $_2$ O with 0.1% formic acid over 5 min, and the whole UV–vis spectrum was recorded. The purity of all final compounds was $\geq 90\%$ for AzoGW1929 and AzoGW1929-2, and $\geq 95\%$ for AzoRosi, AzoRosi-2, AzoRosi-3, and AzoRosi-4, as determined by high-performance liquid chromatography/UV–vis (HPLC-UV/Vis). UV–vis spectra were recorded using a Varian Cary 50 Bio UV–Visible Spectrophotometer with BRAND Ultra-Micro UV-Cuvettes (10 mm light path). Further absorption measurements were performed on a FLUOstar Omega plate reader (BMG Labtech). The LED light sources were obtained from Amazon ($\lambda = 365$ nm and $\lambda = 460$ nm, $P = 1.5$ W) and LEDSupply (LuxStrip II LED bar, $\lambda = 660$ nm), respectively. Illumination for the reversible *trans* \leftrightarrow *cis* and action spectra was provided by an OptoSource Illuminator (CAIRN-Research) supplied by an OptoScan Power Supply (CAIRN-Research) and connected to an OptoScan Monochromator (CAIRN-Research).⁴³ The Cell Disco System is in-house made.

Hybrid Reporter Gene Assays for PPAR α , PPAR γ , and PPAR δ . The Gal4-fusion receptor plasmids pFA-CMV-hPPAR α -LBD, pFA-CMV-hPPAR γ -LBD, and pFA-CMV-hPPAR δ -LBD coding for the hinge region and ligand binding domain of the canonical isoform of the respective nuclear receptor have been reported previously.⁴⁸ pFR-Luc (Stratagene) was used as the reporter plasmid and pRL-SV40 (Promega) for normalization of transfection efficiency and cell growth. The HEK293T cells were obtained from DSMZ (German Collection of Microorganisms and Cell Culture GmbH) and tested for mycoplasma contamination.

PPRE Reporter Gene Assay in PPAR γ Expressing HepG2 Cells. The reporter plasmid PPPE1-pGL3 coding for the firefly luciferase reporter gene under the control of the human full-length PPAR response element (PPRE) has been described previously.⁴⁹ pRL-SV40 (Promega) was used for normalization of transfection efficiency and cell growth. The HepG2 cells were obtained from DSMZ (German Collection of Microorganisms and Cell Culture GmbH) and tested for mycoplasma contamination.

(E)-5-(4-(Phenyldiazenyl)benzylidene)-2-thioxodihydropyrimidine-4,6(1H,5H)-dione (AzoMDG548). Thiobarbituric acid (10.3 mg, 71.0 μ mol, 1.00 equiv) was suspended in anhydrous EtOH (1.5 mL), and 4-phenylazobenzaldehyde **1** (15.0 mg, 71.0 μ mol, 1.00 equiv) in EtOH (1 mL) was slowly added. After stirring at 80 $^\circ\text{C}$ for 2 h, the resulting solid was filtered off, washed with EtOH, and dried under vacuum. The product was obtained as a dark-red solid (11.0 mg, 32.7 μ mol, 46%). ^1H NMR (400 MHz, DMSO- d_6) δ 12.51 (s, 1H), 12.40 (s, 1H), 8.35 (s, 1H), 8.30 (s, 1H), 8.28 (s, 1H), 7.95–7.93 (m, 4H), 7.64–7.62 (m, 3H). ^{13}C NMR (101 MHz, DMSO- d_6) δ 178.6, 161.5, 159.4, 153.7, 153.3, 152.0, 135.5, 134.4 (2C), 132.2, 129.6 (2C), 122.9 (2C), 121.9 (2C), 120.3. HRMS: m/z calcd for C $_{17}$ H $_{13}$ N $_4$ O $_2$ S $^+$ ($[\text{M} + \text{H}]^+$): 337.0754, found: 337.0755.

Methyl (S)-2-Amino-3-(4-aminophenyl)propanoate (3). An oven-dried round bottom flask was charged with methyl (S)-2-amino-3-(4-nitrophenyl)propanoate **2** (1.00 g, 3.84 mmol, 1.00 equiv). The reaction vessel was evacuated and purged with nitrogen three times. Palladium on charcoal (81.7 mg, 76.8 μ mol, 0.20 equiv) was added, and the headspace was thoroughly purged with nitrogen before degassed MeOH (25 mL) was added. The nitrogen atmosphere was replaced by hydrogen, and the suspension was saturated with hydrogen by sparging. The reaction mixture was stirred at room temperature for 16 h. The headspace was purged with nitrogen, and the reaction mixture was filtered through a pad of silica with CH $_2$ Cl $_2$. The filtrate was concentrated, yielding the product as a off-white solid (751 mg, 3.97 mmol, quant.). ^1H NMR (400 MHz, MeOD- d_4) δ 6.98 (d, $J = 8.5$ Hz, 2H), 6.72 (d, $J = 8.5$ Hz, 2H), 4.21 (dd, $J = 7.4$, 5.8 Hz, 1H), 3.81 (s, 3H), 3.16–3.00 (m, 2H). ^{13}C NMR (101 MHz, MeOD- d_4) δ 170.7, 148.5, 131.1 (2C), 124.0, 117.0 (2C), 55.5, 53.5, 36.8. HRMS: m/z calcd for C $_{10}$ H $_{15}$ N $_2$ O $_2$ $^+$ ($[\text{M} + \text{H}]^+$): 195.1128, found: 195.1130.

Methyl (S,E)-2-Amino-3-(4-(phenyldiazenyl)phenyl)propanoate (4) and Methyl (S,E)-2-Amino-3-(4-(4-chlorophenyldiazenyl)phenyl)propanoate (5). Aniline/4-chloroaniline (288/394 mg, 3.10 mmol, 3.00 equiv) was dissolved in CH $_2$ Cl $_2$ (15 mL), and oxone (3.80 g, 6.12 mmol, 6.00 equiv) in water (15 mL) was added to the solution. The suspension was vigorously stirred at room temperature for 16 h during which the reaction mixture turned green. The two phases were separated, and the organic phase was washed with 1 M HCl, sat. aq. NaHCO $_3$, and water. The organic phase was dried over Na $_2$ SO $_4$ before methyl (S)-2-amino-3-(4-aminophenyl)propanoate **3** (200 mg, 1.03 mmol, 1.00 equiv) and glacial acetic acid (2 mL) were added. The solution was concentrated under reduced pressure to remove CH $_2$ Cl $_2$ and finally stirred at room temperature overnight. Acetic acid was removed by azeotropic distillation with toluene (three times). Flash column chromatography with CH $_2$ Cl $_2$ /MeOH (1:0 to 9:1) yielded the corresponding product as a yellow oil. **4** (203 mg, 71.7 μ mol, 70%): ^1H NMR (400 MHz, MeOD- d_4) δ 7.89 (t, $J = 7.3$ Hz, 4H), 7.54 (q, $J = 9.2$, 7.8 Hz, 3H), 7.41 (d, $J = 8.3$ Hz, 2H), 3.96 (t, $J = 6.7$ Hz, 1H), 3.73 (s, 3H), 3.18 (dd, $J = 13.7$, 6.3 Hz, 1H), 3.09 (dd, $J = 13.7$, 7.1 Hz, 1H). ^{13}C NMR (101 MHz, MeOD- d_4) δ 174.6, 154.0, 153.1, 141.2, 132.3, 131.3

(2C), 130.3 (2C), 124.1 (2C), 123.8 (2C), 56.2, 52.8, 40.4. HRMS: m/z calcd for $C_{16}H_{18}N_3O_3^+$ ($[M + H]^+$): 284.1394, found: 284.1388. **5** (110 mg, 34.7 μ mol, 34%): 1H NMR (400 MHz, MeOD- d_4) δ 7.88 (dd, $J = 11.9, 8.6$ Hz, 4H), 7.56 (d, $J = 8.7$ Hz, 2H), 7.40 (d, $J = 8.3$ Hz, 2H), 3.79 (t, $J = 6.7$ Hz, 1H), 3.69 (s, 3H), 3.15–2.99 (m, 2H). ^{13}C NMR (101 MHz, MeOD- d_4) δ 176.1, 152.8, 152.5, 142.6, 138.0, 131.3 (2C), 130.5 (2C), 125.2 (2C), 124.1 (2C), 56.6, 52.4, 41.6. HRMS: m/z calcd for $C_{16}H_{17}ClN_3O_2^+$ ($[M + H]^+$): 318.1004, found: 318.0991.

(S,E)-2-((2-Benzoylphenyl)amino)-3-(4-(phenyldiazenyl)phenyl)propanoic Acid (AzoGW1929) and **(S,E)-2-((2-Benzoylphenyl)amino)-3-(4-((4-chlorophenyl)diazenyl)phenyl)propanoic Acid (AzoGW1929-2)**. An oven-dried microwave vessel was charged with methyl (S,E)-2-amino-3-(4-(phenyldiazenyl)phenyl)propanoate 4/methyl (S,E)-2-amino-3-(4-((4-chlorophenyl)diazenyl)phenyl)propanoate 5 (50.0 mg, 176.4 μ mol/157.4 μ mol, 1.20 equiv), (2-bromophenyl)(phenyl)methanone (34.3 mg, 132.2 μ mol, 1.00 equiv), CS_2CO_3 (111 mg, 341 μ mol, 2.60 equiv), $Pd(OAc)_2$ (2.9 mg, 13 μ mol, 10 mol %), and (\pm)-BINAP (12.3 mg, 19.7 μ mol, 0.15 equiv) in toluene (2 mL). The reaction mixture was stirred at 110 °C for 3 h under a nitrogen atmosphere. Subsequently, the reaction was quenched with water, diluted with EtOAc, and filtered through a pad of silica. The filtrate was concentrated, and the residue was purified by flash column chromatography (hexane/EtOAc 1/0 to 1/1) to give the product as a viscous orange oil. Methyl (S,E)-2-((2-benzoylphenyl)amino)-3-(4-(phenyldiazenyl)phenyl)propanoate/methyl (S,E)-2-((2-benzoylphenyl)amino)-3-(4-((4-chlorophenyl)diazenyl)phenyl)propanoate (39.2/21.7 mg, 84.6/43.6 μ mol, 1.00 equiv) was dissolved in acetonitrile (0.5 mL) and an aqueous solution of LiOH (5.1 mg/2.6 mg, 0.21 mmol/0.11 mmol, 2.5 equiv in 0.5 mL H_2O) was added. The mixture was stirred at 0 °C for 30 min and then acidified to pH = 2 with 1 M HCl. The aqueous phase was extracted with CH_2Cl_2 three times, and the combined organic layers were dried over Na_2SO_4 and concentrated to give the desired product as a red solid. **AzoGW1929** (37.0 mg, 82.3 μ mol, 97%): 1H NMR (400 MHz, $CDCl_3$) δ 7.87 (ddd, $J = 10.7, 7.6, 1.7$ Hz, 4H), 7.60 (dt, $J = 6.9, 1.4$ Hz, 2H), 7.53–7.43 (m, 9H), 7.39 (t, $J = 7.8$ Hz, 1H), 6.73–6.63 (m, 2H), 4.48 (dd, $J = 7.8, 5.3$ Hz, 1H), 3.45 (dd, $J = 13.9, 5.2$ Hz, 1H), 3.29 (dd, $J = 13.8, 8.0$ Hz, 1H). ^{13}C NMR (101 MHz, $CDCl_3$) δ 199.6, 174.5, 152.8, 151.9, 149.9, 140.1, 139.4, 135.7, 135.2, 131.3, 131.1, 130.3, 129.4 (2C), 129.3, 129.2 (2C), 128.3, 123.4 (2C), 123.0 (2C), 119.0, 116.1, 112.3, 57.9, 38.6, 29.9. HRMS: m/z calcd for $C_{28}H_{23}N_3NaO_3^+$ ($[M + Na]^+$): 472.1632, found: 472.1652. **AzoGW1929-2** (19.5 mg, 40.3 μ mol, 93%): 1H NMR (400 MHz, $CDCl_3$) δ 8.88 (s, 1H), 7.84 (dd, $J = 8.5, 2.8$ Hz, 4H), 7.61–7.57 (m, 2H), 7.53–7.42 (m, 8H), 7.39 (t, $J = 7.8$ Hz, 1H), 6.70 (d, $J = 8.5$ Hz, 1H), 6.66 (t, $J = 7.5$ Hz, 1H), 4.49 (dd, $J = 7.9, 5.2$ Hz, 1H), 3.44 (dd, $J = 13.9, 5.1$ Hz, 1H), 3.28 (dd, $J = 13.9, 7.8$ Hz, 1H). ^{13}C NMR (101 MHz, $CDCl_3$) δ 199.6, 174.3, 151.7, 151.1, 149.9, 140.1, 139.8, 137.0, 135.7, 135.2, 131.3, 130.3, 129.5 (2C), 129.3 (2C), 128.3, 124.2 (2C), 123.4 (2C), 119.0, 116.1, 112.3, 57.8, 38.6, 29.9, 14.3. HRMS: m/z calcd for $C_{28}H_{22}ClN_3NaO_3^+$ ($[M + Na]^+$): 506.1242, found: 506.1257.

(E)-5-(4-(Phenyldiazenyl)benzyl)thiazolidine-2,4-dione (AzoRosi), **(E)-5-(4-((4-Chlorophenyl)diazenyl)benzyl)thiazolidine-2,4-dione (AzoRosi-2)**, **(E)-5-(4-((4-(Trifluoromethyl)phenyl)diazenyl)benzyl)thiazolidine-2,4-dione (AzoRosi-3)** and **(E)-5-(4-((2'-Methyl-[1,1'-biphenyl]-4-yl)diazenyl)benzyl)thiazolidine-2,4-dione (AzoRosi-4)**. Aniline/4-Chloroaniline/4-(trifluoromethyl)aniline/2'-methyl-[1,1'-biphenyl]-4-amine (31.4/43.0/54.4/61.8 mg, 337 μ mol, 3.00 equiv) was dissolved in CH_2Cl_2 (2 mL) and oxone (415 mg, 675 μ mol, 6.00 equiv) in water (2 mL) was added to the solution. The suspension was vigorously stirred at room temperature for 16 h, during which the mixture turned green. The two phases were separated, and the organic phase was washed with 1 M HCl, sat. aq. $NaHCO_3$, and water. The organic phase was dried over Na_2SO_4 before 5-(4-aminobenzyl)thiazolidine-2,4-dione **7** (25.0 mg, 113 μ mol, 1.00 equiv) was synthesized according to the literature procedures⁴¹ and glacial acetic acid (250 μ L) was added. The solution was concentrated under reduced pressure to remove CH_2Cl_2 and finally stirred at room

temperature overnight. The acetic acid was removed by azeotropic distillation with toluene (three times) and removed under reduced pressure three times. Flash column chromatography with $CH_2Cl_2/MeOH$ (1:0 to 9:1) yielded the corresponding product as a yellow solid. **AzoRosi** (25.2 mg, 80.9 μ mol, 72%): 1H NMR (400 MHz, $CDCl_3$) δ 7.90 (t, $J = 8.0$ Hz, 4H), 7.52 (q, $J = 10.1, 9.2$ Hz, 3H), 7.40 (d, $J = 8.2$ Hz, 2H), 4.60 (dd, $J = 9.5, 4.0$ Hz, 1H), 3.61 (dd, $J = 14.1, 3.9$ Hz, 1H), 3.26 (dd, $J = 14.1, 9.5$ Hz, 1H). ^{13}C NMR (101 MHz, $CDCl_3$) δ 173.9, 170.0, 152.7, 152.2, 138.8, 131.3, 130.2 (2C), 129.3 (2C), 123.4 (2C), 123.0 (2C), 53.1, 38.5. HRMS: m/z calcd for ($[M + H]^+$): 312.0801, found: 312.0788. **AzoRosi-2** (27.7 mg, 80.1 μ mol, 71%): 1H NMR (400 MHz, $CDCl_3$) δ 7.87 (dd, $J = 8.3, 6.0$ Hz, 4H), 7.49 (d, $J = 8.7$ Hz, 2H), 7.39 (d, $J = 8.3$ Hz, 2H), 4.59 (dd, $J = 9.4, 4.0$ Hz, 1H), 3.60 (dd, $J = 14.1, 3.9$ Hz, 1H), 3.26 (dd, $J = 14.1, 9.5$ Hz, 1H). ^{13}C NMR (101 MHz, $CDCl_3$) δ 173.5, 169.6, 152.1, 151.1, 139.1, 137.3, 130.3 (2C), 129.5 (2C), 124.3 (2C), 123.5 (2C), 53.0, 38.5. HRMS: m/z calcd for ($[M + H]^+$): 346.0412, found: 346.0401. **AzoRosi-3** (24.3 mg, 64.1 μ mol, 57%): 1H NMR (400 MHz, $CDCl_3$) δ 7.99 (d, $J = 8.3$ Hz, 2H), 7.92 (d, $J = 8.0$ Hz, 2H), 7.78 (d, $J = 8.3$ Hz, 2H), 7.41 (d, $J = 8.1$ Hz, 2H), 4.60 (dd, $J = 9.4, 3.8$ Hz, 1H), 3.61 (dd, $J = 14.1, 4.0$ Hz, 1H), 3.28 (dd, $J = 14.1, 9.4$ Hz, 1H). ^{13}C NMR (101 MHz, $CDCl_3$) δ 173.7, 169.8, 154.5, 152.0, 139.7, 132.5 (q, $J = 32.5$ Hz, 2C), 130.3 (2C), 126.5 (q, $J = 3.8$ Hz, 2C), 124.0 (q, $J = 27.4$ Hz, 2C), 123.8, 123.2, 53.0, 38.5. ^{19}F NMR (377 MHz, $CDCl_3$) δ 0.29, 0.17. HRMS: m/z calcd for ($[M + H]^+$): 360.0675, found: 380.0662. **AzoRosi-4** (21.9 mg, 54.5 μ mol, 49%): 1H NMR (400 MHz, $CDCl_3$) δ 7.97 (d, $J = 8.3$ Hz, 2H), 7.91 (d, $J = 8.2$ Hz, 2H), 7.49 (d, $J = 8.2$ Hz, 2H), 7.41 (d, $J = 8.2$ Hz, 2H), 7.30 (m, 4H), 4.60 (dd, $J = 9.5, 3.9$ Hz, 1H), 3.62 (dd, $J = 14.1, 3.8$ Hz, 1H), 3.26 (dd, $J = 14.0, 9.6$ Hz, 1H), 2.32 (s, 3H). ^{13}C NMR (101 MHz, $CDCl_3$) δ 173.7, 169.8, 152.3, 151.5, 145.2, 141.1, 138.7, 135.5, 130.7 (2C), 130.2 (2C), 129.8 (2C), 127.9, 126.1, 123.5 (2C), 122.8 (2C), 53.1, 38.6, 20.6. HRMS: m/z calcd for ($[M + H]^+$): 402.1271, found: 402.1261.

2'-Methyl-[1,1'-biphenyl]-4-amine (9). An oven-dried miniature reflux equipment was charged with (4-aminophenyl)boronic acid **8** (192 mg, 1.40 mmol, 1.20 equiv), 2-bromotoluene (200 mg, 1.18 mmol, 1.00 equiv), and $Pd(PPh_3)_4$ (67.6 mg, 58.5 μ mol, 5 mol %) in DMF (5 mL). Potassium carbonate (1.10 g, 7.96 mmol, 6.74 equiv) in H_2O (6 mL) was added and the mixture was heated to 85 °C and stirred for 16 h under a nitrogen atmosphere. The reaction mixture was cooled to room temperature and extracted with CH_2Cl_2 three times. The combined organic layers were dried over Na_2SO_4 , concentrated under reduced pressure, and purified by flash column chromatography (hexane/EtOAc 1/0 to 1/3), yielding the product as a yellow viscous oil (118 mg, 641 μ mol, 55%). 1H NMR (400 MHz, $CDCl_3$) δ 7.24–7.21 (m, 4H), 7.14 (d, $J = 8.4$ Hz, 2H), 6.77 (d, $J = 8.3$ Hz, 2H), 4.09 (s, 2H), 2.29 (s, 3H). ^{13}C NMR (101 MHz, $CDCl_3$) δ 145.3, 142.1, 135.6, 132.4, 130.4, 130.3 (2C), 130.0, 126.8, 125.9, 114.9 (2C), 20.7. HRMS: m/z calcd for $C_{13}H_{14}N^+$ ($[M + H]^+$): 184.1121, found: 184.1118.

Crystallography. The X-ray intensity data of thiazolidinedione **6** were measured on an Oxford Diffraction Xcalibur 3 system equipped with a graphite monochromator and a sealed-tube Mo $K\alpha$ X-ray tube ($\lambda = 0.71073$ Å). The frames were integrated with the Agilent CrysAlis PRO software package.⁵⁰ Data were corrected for absorption effects using the Multi-Scan method (ABSPACK embedded in the Agilent CrysAlis PRO software package). The structure was solved with SIR97⁵¹ and refined with SHELXL.⁵² All C-bound hydrogen atoms have been calculated in ideal geometry riding on their parent atoms, while the N-bound hydrogen atoms have been refined freely. The figures have been drawn at the 50% ellipsoid probability level.⁵³ Crystallographic data for thiazolidinedione **6** are available free of charge from the Cambridge Crystallographic Data Center via http://www.ccdc.cam.ac.uk/data_request/cif (accession ref CCDC 1997329). The X-ray intensity data of **AzoRosi-3** were measured on a Bruker D8 Venture TXS system equipped with a multilayer mirror monochromator and a Mo $K\alpha$ rotating anode X-ray tube ($\lambda = 0.71073$ Å). The frames were integrated with the Bruker SAINT software package.⁵⁴ Data were corrected for absorption effects using

the Multi-Scan method (SADABS).⁵⁵ The structure was solved with SIR97 and refined with SHELXL. All hydrogen atoms have been calculated in ideal geometry riding on their parent atoms. The figures have been drawn at the 50% ellipsoid probability level. There are two formula units in the asymmetric unit. Crystallographic data for AzoRosi-3 are available free of charge from the Cambridge Crystallographic Data Center via http://www.ccdc.cam.ac.uk/data_request/cif (accession ref CCDC 1997328).

Computational Methods. General: Calculations were performed in Molecular Operating Environment (MOE, version 2018.0101, Chemical Computing Group Inc. Montreal, QC, Canada) using default settings for each tool/function unless stated otherwise. Amber10:EHT was used as the default force field for all calculations. Molecular docking: docking was performed using X-ray structures of the PPAR γ ligand binding domain (LBD) complexed with different ligands, each serving for a different photohormone series based on structural similarity of the bound ligand and the photohormone. For GW1929 azologs, docking was performed using the X-ray structure of the PPAR γ LBD in complex with the parent compound GW1929 (PDB ID: 6D8X). For azologs of rosiglitazone and MDG548, the structure of the PPAR γ LBD in complex with rosiglitazone was used for molecular docking (PDB ID: 5YCP). Protonation states of the complexes were adjusted using the MOE QuickPrep tool. Redocking of the crystallized ligands resulted in binding poses with RMSD 0.5994 relative to the crystallized binding mode for GW1929 and RMSD 0.1871 for rosiglitazone, respectively. The compounds were prepared using the MOE Wash tool: protonation state dominant at pH 7; coordinates rebuild 3D; and preserved existing chirality. Docking was performed using the following settings in the MOE Dock tool: receptor: receptor + solvent; site: ligand atoms; placement: triangle matcher; score: London dG; poses: 100; refinement: rigid receptor; refinement score: GBVI/WSA dG; poses: 10. The highest ranked binding mode with the carboxylate or thiazolidinedione participating in the H-bond network with the canonical activation triad was used. The respective cocrystallized template ligands GW1929 and rosiglitazone and the parent compound MDG548 are colored in green, the respective azologs AzoMDG548, AzoGW1929, and AzoRosi are colored in magenta. The second-generation azologs AzoGW1929-2 and AzoRosi-3 are colored cyan, whereas AzoRosi-4 is colored orange.

Photophysical Characterization and Photostationary States (PSS). UV–vis spectra were recorded using a Varian Cary 50 Bio UV–Visible Spectrophotometer with BRAND Ultra-Micro UV-Cuvettes (10 mm light path). Switching was achieved using $\lambda = 365$ nm or $\lambda = 460$ nm LED light sources. The LEDs were pointed directly into the top of the sample cuvette. An initial spectrum of all photohormones (25 μ M in DMSO) was recorded (dark-adapted state, black) and then again following illumination at $\lambda = 365$ nm for 2 min (*cis*-adapted state, gray). A third spectrum was recorded after irradiation at $\lambda = 460$ nm for 2 min (*trans*-adapted state, blue). To obtain the reversible *trans* \leftrightarrow *cis* spectrum, absorption at $\lambda_{\text{Abs}} = 340$ nm was constantly measured while alternating illumination at $\lambda = 365$ nm or $\lambda = 460$ nm for the indicated times allowed for rapid isomerization of the photohormones (25 μ M in DMSO). Therefore, a mercury lamp with a power of 75 watts connected to a monochromator was directly pointed into the top of the sample cuvette, providing irradiation via an optic fiber cable with the two distinct wavelengths $\lambda = 365$ and 460 nm for 4 min each (absorption was read at $\lambda_{\text{Abs}} = 340$ nm). For the color-dosing experiment, the same experimental setup comprising the mercury lamp, monochromator, and optic fiber cable was used. The monochromator allowed for the illumination of the photohormones (25 μ M in DMSO) with the indicated wavelengths for 4 min each ($\lambda_{\text{Abs}} = 340$ nm). Determination of the half-life was achieved by the illumination of the photohormones (25 μ M in DMSO) with $\lambda = 365$ nm for 5 min to yield the corresponding *cis*-isomers. Then, the sample has been excluded from light and absorption was read at room temperature every minute for 2 days. Fitting of the experimental data provided for the half-life time, assuming a one-phase decay. The photostationary states were determined by ^1H NMR. Therefore, 1 mg of the

corresponding photohormone was dissolved in deuterated solvent (CDCl_3 or $\text{MeOD-}d_4$), and a ^1H spectrum was recorded before (dark-adapted) and after illumination with $\lambda = 365$ nm (*cis*-adapted) and $\lambda = 460$ nm (*trans*-adapted) for 5 min. The integration of characteristic product peaks and normalization yielded the PSS.

In Vitro Pharmacological Characterization. Hybrid Reporter Gene Assay. The HEK293T cells were cultured in Dulbecco's modified Eagle's medium (DMEM), high glucose with 10% fetal calf serum (FCS), sodium pyruvate (1 mM), penicillin (100 U/mL), and streptomycin (100 μ g/mL) at 37 $^\circ\text{C}$ and 5% CO_2 . Twenty-four hours before transfection, the cells were seeded in 96-well plates (3×10^4 cells/well). Before transfection, the medium was changed to Opti-MEM without supplements. Transient transfection was carried out using Lipofectamine LTX reagent (Invitrogen) according to the manufacturer's protocol with pFR-Luc (Stratagene), pRL-SV40 (Promega), and the corresponding Gal4-fusion nuclear receptor plasmid. Five hours after transfection, the medium was changed to Opti-MEM supplemented with penicillin (100 U/mL), streptomycin (100 μ g/mL), and additionally containing 0.1% dimethyl sulfoxide (DMSO) and the respective test compound or 0.1% DMSO alone as an untreated control. Each concentration was tested in duplicates, and each experiment was repeated independently at least two times. After overnight (14–16 h) incubation, the cells were assayed for luciferase activity using the Dual-Glo Luciferase Assay System (Promega) according to the manufacturer's protocol. Luminescence was measured with a Tecan Spark luminometer (Tecan Deutschland GmbH, Germany). Normalization of transfection efficiency and cell growth was done by the division of firefly luciferase data by *Renilla* luciferase data and multiplying the value by 1000, resulting in relative light units (RLU). Fold activation was obtained by dividing the mean RLU of the test compound by the mean RLU of the untreated control. Maximum relative activation refers to fold reporter activity divided by the fold activation of respective reference agonist (at a concentration of 1 μ M) treated cells. All hybrid assays were validated with the respective reference agonists (PPAR α : GW7647; PPAR γ : pioglitazone; PPAR δ : L165041), which yielded EC_{50} values in agreement with the literature. Characterization of the respective *cis*-counterparts was performed in the same way with the preirradiated compounds (irradiation for 3 min at $\lambda = 365$ nm right before incubation). To maintain the compound in the *cis*-adapted state, the Cell Disco System was used during incubation with 75 ms light pulses ($\lambda = 370$ nm) every 15 s.

PPRE Reporter Assay in HepG2. The HepG2 cells were cultured in Dulbecco's modified Eagle's medium (DMEM), high glucose with 10% fetal calf serum (FCS), sodium pyruvate (1 mM), penicillin (100 U/mL), and streptomycin (100 μ g/mL) at 37 $^\circ\text{C}$ and 5% CO_2 . Twenty-four hours before transfection, the cells were seeded in 96-well plates (1.25×10^4 cells/well) precoated with collagen G solution. Before transfection, the medium was changed to Opti-MEM without supplements. Transient transfection was carried out using the Lipofectamine 3000 reagent (Invitrogen) according to the manufacturer's protocol with PPRE1-pGL3⁴⁹ and pRL-SV40 (Promega). Five hours after transfection, the medium was changed to Opti-MEM supplemented with penicillin (100 U/mL), streptomycin (100 μ g/mL), and additionally containing 0.1% DMSO and the respective test compound or 0.1% DMSO alone as an untreated control. Each concentration was tested in duplicates, and each experiment was repeated independently at least three times. After overnight (14–16 h) incubation, the cells were assayed for luciferase activity using the Dual-Glo Luciferase Assay System (Promega) according to the manufacturer's protocol. Luminescence was measured with a Tecan Spark luminometer (Tecan Deutschland GmbH). Normalization of transfection efficiency and cell growth was done by the division of firefly luciferase data by *Renilla* luciferase data and multiplying the value by 1000, resulting in relative light units (RLU). Fold activation was obtained by dividing the mean RLU of the test compound by the mean RLU of the untreated control. The PPRE reporter gene assay was validated with rosiglitazone as PPAR γ reference agonist, which yielded an EC_{50} value in agreement with the literature. Characterization of *cis*-AzoRosi-4 was performed in the same way with the

preirradiated compound (irradiation for 3 min at $\lambda = 365$ nm right before incubation). To maintain the compound in the *cis*-adapted state, the Cell Disco System was used during incubation with 75 ms light pulses ($\lambda = 370$ nm) every 15 s.

Production of a Recombinant PPAR γ LBD Protein. *Cloning of PPAR γ LBD.* A cDNA sequence optimized for codon usage in *Escherichia coli* K12 and coding for an N-terminal His₁₀-tag followed in frame by a tobacco etch virus (TEV) cleavage site and the PPAR γ LBD (aa 234–505) was cloned into the backbone of pET29b for expression under the control of the T7 promoter.

Protein Expression. *E. coli* BL21 DE3 was transformed with the described expression plasmid and the plasmid pGro7 for coexpression of GroEL/ES (chaperone plasmid set; TaKaRa Bio, Inc.). Cultures in the Luria-Bertani (LB) medium containing 35 μ g/mL kanamycin and 34 μ g/mL chloramphenicol were grown at 37 °C and 180 rpm. When OD₆₀₀ reached 0.6–0.7, the temperature was lowered to 18 °C and the expression of GroEL/ES was induced by the addition of 1 g/L L-arabinose. Thirty minutes later, the expression of PPAR γ LBD was induced by the addition of 0.5 mM IPTG and the cultures were supplemented with ~200 μ L Antifoam Y-30 (Sigma-Aldrich) per liter. After 14–18 h, the cells were harvested by centrifugation (20 min, 6000g, 4 °C).

Purification. A cell pellet from 2 L of culture was thawed and resuspended in a total volume of 50 mL of lysis buffer (400 mM NaCl, 25 mM Tris (pH 7.8), 20 mM β -mercaptoethanol, 10% w/v glycerol) supplemented with 25 mM imidazole, 2 mM MgSO₄, 750 Kunitz DNase I, 250 Kunitz RNase A, a spatula tip of lysozyme, and one tablet of Roche complete ethylenediaminetetraacetic acid (EDTA)-free protease inhibitor cocktail. After incubation for 30 min on wet ice, the slurry was diluted with three volumes of IMAC buffer A (400 mM NaCl, 25 mM NaPi (pH 7.8), 20 mM β -mercaptoethanol, 10% w/v glycerol) supplemented with 25 mM imidazole and cell lysis was enforced by passage through a homogenizer at a combined pressure of 1000 psi. The suspension was supplemented with 1 mM ATP and incubated for another 30 min on wet ice. The cell debris was removed by centrifugation (20 min, 16 500g, 4 °C), and the supernatant was loaded at a flow rate of 3 mL/min onto a prepacked 5 mL HisTrap FF column (Ge Healthcare) pre-equilibrated in 95% IMAC buffer A and 5% IMAC buffer B (IMAC buffer A containing 500 mM imidazole). To remove unbound proteins, the column was washed with 15 column volumes of the same buffer at 5 mL/min. PPAR γ LBD was eluted by a linear gradient of 20–60% IMAC buffer B and supplemented with His₆-tagged TEV protease (molar ratio of 1:25) for the digestion of the His-tag during overnight dialysis against a volume of IMAC buffer A sufficient to reduce imidazole to 10–15 mM. The mixture was run through a gravity-flow column packed with 10 mL Ni Sepharose 6 Fast Flow (Ge Healthcare), and the flow-through was concentrated under 2 bar pressure from nitrogen gas in an Amicon-stirred cell equipped with a 10.000 MWCO membrane. Then, 5 mL of concentrate was separated on a HiLoad 16/600 Superdex 75 pg gel filtration column (Ge Healthcare) equilibrated and run in assay buffer (150 mM KF, 25 mM N-(2-hydroxyethyl)piperazine-*N'*-ethanesulfonic acid (HEPES) pH 7.5, 10% w/v glycerol, 5 mM dithiothreitol (DTT)) at 1 mL/min. The protein used for isothermal titration experiments was taken from the middle of the peak corresponding to monomeric PPAR γ LBD.

Isothermal Titration Calorimetry (ITC). ITC was conducted on a TA Instruments Affinity ITC (TA Instruments, New Castle, Delaware) using recombinant PPAR γ LBD protein dissolved in buffer at pH 7.5 containing 25 mM HEPES, 150 mM KF, 5 mM DTT, 10% w/v glycerol, and 1% DMSO. AzoRosi-4 was dissolved to a final concentration of 300 μ M in the same buffer, placed into the ITC syringe, and titrated to 172 μ L of PPAR γ LBD protein (64 μ M). Characterization of *cis*-AzoRosi-4 was performed in the same way with the preirradiated compound (irradiation for 5 min at $\lambda = 365$ nm right before titration). The titration was performed at a temperature of 25 °C with a stirring rate of 75 rpm and 31 injections. The first injection had a reduced volume of 1.0 μ L, followed by 30 injections of 2.5 μ L. An interval of 300 s was maintained between injections. ITC raw data were analyzed using the NanoAnalyze software package

(version 3.7.5). An independent binding model was used to fit the reaction enthalpy (ΔH), binding affinity constant (K_D), and stoichiometry (n). Free energy change (ΔG) was calculated from the equation $\Delta G = -RT \ln K$, and the entropy (ΔS) was calculated from $\Delta G = \Delta H - T\Delta S$.

■ ASSOCIATED CONTENT

Supporting Information

The Supporting Information is available free of charge at <https://pubs.acs.org/doi/10.1021/acs.jmedchem.0c00654>.

Molecular formula strings (CSV)

NMR spectra and HPLC analysis, further photophysical characterization, crystallography, and ITC data (PDF)

Docking AzoGW1929 (PDB)

Docking AzoGW1929-2 (PDB)

Docking AzoRosi-3&4 (PDB)

Docking AzoRosi_4 (PDB)

Docking AzoRosi_trans&cis (PDB)

Docking MDG548_AzoMDG548 (PDB)

■ AUTHOR INFORMATION

Corresponding Authors

Daniel Merk – Institute of Pharmaceutical Chemistry, Goethe-University Frankfurt, 60438 Frankfurt, Germany;

✉ orcid.org/0000-0002-5359-8128; Email: merk@pharmchem.uni-frankfurt

Dirk Trauner – Department of Chemistry, New York University, New York, New York 10003, United States; Department of Chemistry and Center for Integrated Protein Science (CIPSM), Ludwig-Maximilians-University Munich, 81377 Munich, Germany; ✉ orcid.org/0000-0002-6782-6056; Email: dirktrauner@nyu.edu

Authors

Konstantin Hinnah – Department of Chemistry, New York University, New York, New York 10003, United States

Sabine Willems – Institute of Pharmaceutical Chemistry, Goethe-University Frankfurt, 60438 Frankfurt, Germany

Johannes Morstein – Department of Chemistry, New York University, New York, New York 10003, United States;

✉ orcid.org/0000-0002-6940-288X

Jan Heering – Fraunhofer Institute for Molecular Biology and Applied Ecology IME, Branch for Translational Medicine and Pharmacology TMP, 60596 Frankfurt, Germany

Felix W. W. Hartrampf – Department of Chemistry and Center for Integrated Protein Science (CIPSM), Ludwig-Maximilians-University Munich, 81377 Munich, Germany

Johannes Broichhagen – Department of Chemistry and Center for Integrated Protein Science (CIPSM), Ludwig-Maximilians-University Munich, 81377 Munich, Germany; ✉ orcid.org/0000-0003-3084-6595

Philipp Leippe – Department of Chemistry and Center for Integrated Protein Science (CIPSM), Ludwig-Maximilians-University Munich, 81377 Munich, Germany

Complete contact information is available at: <https://pubs.acs.org/doi/10.1021/acs.jmedchem.0c00654>

Author Contributions

[†]K.H. and S.W. contributed equally to this work

Notes

The authors declare no competing financial interest.

ACKNOWLEDGMENTS

J. M. and K. H. thank the German Academic Scholarship Foundation for a fellowship, and J. M. thanks the New York University for a MacCracken fellowship and a Margaret and Herman Sokol fellowship. D.M. is grateful for financial support by the Aventis Foundation. We thank Dr. Lisa Suwandhi and Dr. Siegfried Ussar from Helmholtz Zentrum München for experimental support in the initial stages of the project and Dr. Peter Mayer from LMU for X-ray crystallography data. We thank Boehringer Ingelheim for generous financial support. This work was supported by the National Institutes of Health (Grant R01NS108151-01).

ABBREVIATIONS USED

NHR, nuclear hormone receptor; RXR, retinoic X receptor; FXR, farnesoid X receptor; ER, estrogen receptor; ChEMBL, chemical database of the European Molecular Biology Laboratory; IUPHAR, International Union of Basic and Clinical Pharmacology; AF-2, activation function 2; LBD, ligand binding domain; PSS, photostationary state; PPRE, PPAR response element

REFERENCES

- (1) Aranda, A.; Pascual, A. Nuclear Hormone Receptors and Gene Expression. *Physiol. Rev.* **2001**, *81*, 1269–1304.
- (2) Mangelsdorf, D. J.; Thummel, C.; Beato, M.; Herrlich, P.; Schütz, G.; Umesono, K.; Blumberg, B.; Kastner, P.; Mark, M.; Chambon, P.; Evans, R. M. The Nuclear Receptor Superfamily: The Second Decade. *Cell* **1995**, *83*, 835–839.
- (3) Evans, R. M.; Mangelsdorf, D. J. Nuclear Receptors, RXR, and the Big Bang. *Cell* **2014**, *157*, 255–266.
- (4) Gronemeyer, H.; Gustafsson, J.-Å.; Laudet, V. Principles for Modulation of the Nuclear Receptor Superfamily. *Nat. Rev. Drug Discovery* **2004**, *3*, 950–964.
- (5) Ehrmann, J.; Vavrusova, N.; Collan, Y.; Kolar, Z. Peroxisome Proliferator-Activated Receptors (PPARs) in Health and Disease. *Biomed. Pap.* **2002**, *146*, 11–14.
- (6) Nolte, R. T.; Wisely, G. B.; Westin, S.; Cobb, J. E.; Lambert, M. H.; Kurokawa, R.; Rosenfeld, M. G.; Willson, T. M.; Glass, C. K.; Milburn, M. V. Ligand Binding and Co-Activator Assembly of the Peroxisome Proliferator-Activated Receptor- γ . *Nature* **1998**, *395*, 137–143.
- (7) Katsouri, L.; Blondrath, K.; Sastre, M. Peroxisome Proliferator-Activated Receptor- γ Cofactors in Neurodegeneration. *IUBMB Life* **2012**, *64*, 958–964.
- (8) Villapol, S. Roles of Peroxisome Proliferator-Activated Receptor Gamma on Brain and Peripheral Inflammation. *Cell. Mol. Neurobiol.* **2018**, *38*, 121–132.
- (9) Chen, Y.-C.; Wu, J.-S.; Tsai, H.-D.; Huang, C.-Y.; Chen, J.-J.; Sun, G. Y.; Lin, T.-N. Peroxisome Proliferator-Activated Receptor Gamma (PPAR- γ) and Neurodegenerative Disorders. *Mol. Neurobiol.* **2012**, *46*, 114–124.
- (10) Cho, N.; Momose, Y. Peroxisome Proliferator-Activated Receptor γ Agonists as Insulin Sensitizers: From the Discovery to Recent Progress. *Curr. Top. Med. Chem.* **2008**, *8*, 1483–1507.
- (11) Kvandová, M.; Majzúnová, M.; Dvořáková, I. The Role of PPAR γ in Cardiovascular Diseases. *Physiol. Res.* **2016**, *65*, S343–S363.
- (12) Vella, V.; Nicolosi, M. L.; Giuliano, S.; Bellomo, M.; Belfiore, A.; Malaguarnera, R. PPAR- γ Agonists As Antineoplastic Agents in Cancers with Dysregulated IGF Axis. *Front. Endocrinol.* **2017**, *8*, No. 31.
- (13) Koeffler, H. P. Peroxisome Proliferator-Activated Receptor and Cancers. *Clin. Cancer Res.* **2003**, *9*, 1–9.
- (14) Dhiman, V. K.; Bolt, M. J.; White, K. P. Nuclear Receptors in Cancer — Uncovering New and Evolving Roles through Genomic Analysis. *Nat. Rev. Genet.* **2018**, *19*, 160–174.
- (15) Broichhagen, J.; Frank, J. A.; Trauner, D. A Roadmap to Success in Photopharmacology. *Acc. Chem. Res.* **2015**, *48*, 1947–1960.
- (16) Szymanski, W.; Beierle, J. M.; Kistemaker, H. A. V.; Velema, W. A.; Feringa, B. L. Reversible Photocontrol of Biological Systems by the Incorporation of Molecular Photoswitches. *Chem. Rev.* **2013**, *113*, 6114–6178.
- (17) Hüll, K.; Morstein, J.; Trauner, D. *In Vivo* Photopharmacology. *Chem. Rev.* **2018**, *118*, 10710–10747.
- (18) Beharry, A. A.; Wong, L.; Tropepe, V.; Woolley, G. A. Fluorescence Imaging of Azobenzene Photoswitching In Vivo. *Angew. Chem., Int. Ed.* **2011**, *50*, 1325–1327.
- (19) Morstein, J.; Hill, R. Z.; Novak, A. J. E.; Feng, S.; Norman, D. D.; Donthamsetti, P. C.; Frank, J. A.; Harayama, T.; Williams, B. M.; Parrill, A. L.; Tigyi, G. J.; Riezman, H.; Isacoff, E. Y.; Bautista, D. M.; Trauner, D. Optical Control of Sphingosine-1-Phosphate Formation and Function. *Nat. Chem. Biol.* **2019**, *15*, 623–631.
- (20) Frank, J. A.; Yushchenko, D. A.; Hodson, D. J.; Lipstein, N.; Nagpal, J.; Rutter, G. A.; Rhee, J.-S.; Gottschalk, A.; Brose, N.; Schultz, C.; Trauner, D. Photoswitchable Diacylglycerols Enable Optical Control of Protein Kinase C. *Nat. Chem. Biol.* **2016**, *12*, 755–762.
- (21) Frank, J. A.; Yushchenko, D. A.; Fine, N. H. F.; Duca, M.; Citir, M.; Broichhagen, J.; Hodson, D. J.; Schultz, C.; Trauner, D. Optical Control of GPR40 Signalling in Pancreatic β -Cells. *Chem. Sci.* **2017**, *8*, 7604–7610.
- (22) Frank, J. A.; Moroni, M.; Moshourab, R.; Sumser, M.; Lewin, G. R.; Trauner, D. Photoswitchable Fatty Acids Enable Optical Control of TRPV1. *Nat. Commun.* **2015**, *6*, No. 7118.
- (23) Frank, J. A.; Franquelim, H. G.; Schwillle, P.; Trauner, D. Optical Control of Lipid Rafts with Photoswitchable Ceramides. *J. Am. Chem. Soc.* **2016**, *138*, 12981–12986.
- (24) Kol, M.; Williams, B.; Toombs-Ruane, H.; Franquelim, H. G.; Korneev, S.; Schroeder, C.; Schwillle, P.; Trauner, D.; Holthuis, J. C. M.; Frank, J. A. Optical manipulation of sphingolipid biosynthesis using photoswitchable ceramides. *eLife* **2019**, *8*, No. e43230.
- (25) Leinders-Zufall, T.; Storch, U.; Blyemehl, K.; Mederos, y.; Schnitzler, M.; Frank, J. A.; Konrad, D. B.; Trauner, D.; Gudenmann, T.; Zufall, F. PhoDAGs Enable Optical Control of Diacylglycerol-Sensitive Transient Receptor Potential Channels. *Cell Chem. Biol.* **2018**, *25*, 215–223.e3.
- (26) Lichtenegger, M.; Tiapko, O.; Svobodova, B.; Stockner, T.; Glasnov, T. N.; Schreimbayer, W.; Platzer, D.; Cruz, G. G.; de la Krenn, S.; Schober, R.; Shrestha, N.; Schindl, R.; Romanin, C.; Groschner, K. An Optically Controlled Probe Identifies Lipid-Gating Fenestrations within the TRPC3 Channel. *Nat. Chem. Biol.* **2018**, *14*, 396–404.
- (27) Morstein, J.; Awale, M.; Reymond, J.-L.; Trauner, D. Mapping the Azolog Space Enables the Optical Control of New Biological Targets. *ACS Cent. Sci.* **2019**, *5*, 607–618.
- (28) Morstein, J.; Trads, J. B.; Hinnah, K.; Willems, S.; Barber, D. M.; Trauner, M.; Merk, D.; Trauner, D. Optical Control of the Nuclear Bile Acid Receptor FXR with a Photohormone. *Chem. Sci.* **2020**, *11*, 429–434.
- (29) Tsuchiya, K.; Umeno, T.; Tsuji, G.; Yokoo, H.; Tanaka, M.; Fukuhara, K.; Demizu, Y.; Misawa, T. Development of Photoswitchable Estrogen Receptor Ligands. *Chem. Pharm. Bull.* **2020**, *68*, 398–402.
- (30) Schoenberger, M.; Damijonaitis, A.; Zhang, Z.; Nagel, D.; Trauner, D. Development of a New Photochromic Ion Channel Blocker via Azologization of Fmocaine. *ACS Chem. Neurosci.* **2014**, *5*, 514–518.
- (31) Proschak, E.; Heitel, P.; Kalinowsky, L.; Merk, D. Opportunities and Challenges for Fatty Acid Mimetics in Drug Discovery. *J. Med. Chem.* **2017**, *60*, S235–S266.
- (32) Pirat, C.; Farce, A.; Lebègue, N.; Renault, N.; Furman, C.; Millet, R.; Yous, S.; Specia, S.; Berthelot, P.; Desreumaux, P.; Chavatte, P. Targeting Peroxisome Proliferator-Activated Receptors (PPARs): Development of Modulators. *J. Med. Chem.* **2012**, *55*, 4027–4061.

- (33) Frkic, R. L.; He, Y.; Rodriguez, B. B.; Chang, M. R.; Kuruvilla, D.; Ciesla, A.; Abell, A. D.; Kamenecka, T. M.; Griffin, P. R.; Bruning, J. B. Structure–Activity Relationship of 2,4-Dichloro-*N*-(3,5-Dichloro-4-(Quinolin-3-Yloxy)Phenyl)Benzenesulfonamide (INT131) Analogs for PPAR γ -Targeted Antidiabetics. *J. Med. Chem.* **2017**, *60*, 4584–4593.
- (34) Giampietro, L.; D'Angelo, A.; Giancristofaro, A.; Ammazalorso, A.; De Filippis, B.; Fantacuzzi, M.; Linciano, P.; Maccallini, C.; Amoroso, R. Synthesis and Structure–Activity Relationships of Fibrate-Based Analogues inside PPARs. *Bioorg. Med. Chem. Lett.* **2012**, *22*, 7662–7666.
- (35) Nevin, D. K.; Peters, M. B.; Carta, G.; Fayne, D.; Lloyd, D. G. Integrated Virtual Screening for the Identification of Novel and Selective Peroxisome Proliferator-Activated Receptor (PPAR) Scaffolds. *J. Med. Chem.* **2012**, *55*, 4978–4989.
- (36) Jang, J. Y.; Bae, H.; Lee, Y. J.; Choi, Y. L.; Kim, H. J.; Park, S. B.; Suh, S. W.; Kim, S. W.; Han, B. W. Structural Basis for the Enhanced Anti-Diabetic Efficacy of Lobeglitazone on PPAR Gamma. *Sci. Rep.* **2018**, *8*, No. 31.
- (37) PPAR Gamma LBD Complexed with the Agonist GW1929 (PDB 6D8X) DOI: 10.2210/Pdb6D8X/Pdb.
- (38) *Molecular Operating Environment (MOE)*, Version 2018.0101; Chemical Computing Group Inc: Montreal, QC, Canada.
- (39) Henke, B. R.; Blanchard, S. G.; Brackeen, M. F.; Brown, K. K.; Cobb, J. E.; Collins, J. L.; Harrington, W. W.; Hashim, M. A.; Hull-Ryde, E. A.; Kaldor, I.; Kliewer, S. A.; Lake, D. H.; Leesnitzer, L. M.; Lehmann, J. M.; Lenhard, J. M.; Orband-Miller, L. A.; Miller, J. F.; Mook, R. A.; Noble, S. A.; Oliver, W.; Parks, D. J.; Plunket, K. D.; Szewczyk, J. R.; Willson, T. M. *N*-(2-Benzoylphenyl)-*l*-Tyrosine PPAR γ Agonists. 1. Discovery of a Novel Series of Potent Antihyperglycemic and Antihyperlipidemic Agents. *J. Med. Chem.* **1998**, *41*, 5020–5036.
- (40) Lehmann, J. M.; Moore, L. B.; Smith-Oliver, T. A.; Wilkison, W. O.; Willson, T. M.; Kliewer, S. A. An Antidiabetic Thiazolidinedione Is a High Affinity Ligand for Peroxisome Proliferator-Activated Receptor γ (PPAR γ). *J. Biol. Chem.* **1995**, *270*, 12953–12956.
- (41) Zidar, N.; Tomašić, T.; Šink, R.; Rupnik, V.; Kovač, A.; Turk, S.; Patin, D.; Blanot, D.; Contreras Martel, C.; Dessen, A.; Müller Premru, M.; Zega, A.; Gobec, S.; Peterlin Mašič, L.; Kikelj, D. Discovery of Novel 5-Benzylidenerhodanine and 5-Benzylidene-thiazolidine-2,4-Dione Inhibitors of MurD Ligase. *J. Med. Chem.* **2010**, *53*, 6584–6594.
- (42) Liu, C.; Feng, T.; Zhu, N.; Liu, P.; Han, X.; Chen, M.; Wang, X.; Li, N.; Li, Y.; Xu, Y.; Si, S. Identification of a Novel Selective Agonist of PPAR γ with No Promotion of Adipogenesis and Less Inhibition of Osteoblastogenesis. *Sci. Rep.* **2015**, *5*, No. 9530.
- (43) Borowiak, M.; Nahaboo, W.; Reynders, M.; Nekolla, K.; Jalinot, P.; Hasserodt, J.; Rehberg, M.; Delattre, M.; Zahler, S.; Vollmar, A.; Trauner, D.; Thorn-Seshold, O. Photoswitchable Inhibitors of Microtubule Dynamics Optically Control Mitosis and Cell Death. *Cell* **2015**, *162*, 403–411.
- (44) Diabetes Drug Affects the Brain. *Nature* **2011**, *473*, 9.
- (45) Cao, J.; Ou, G.; Yang, N.; Ding, K.; Kream, B. E.; Hamrick, M. W.; Isales, C. M.; Shi, X. M. Impact of Targeted PPAR γ Disruption on Bone Remodeling. *Mol. Cell. Endocrinol.* **2015**, *410*, 27–34.
- (46) Lerch, M. M.; Hansen, M. J.; van Dam, G. M.; Szymanski, W.; Feringa, B. L. Emerging Targets in Photopharmacology. *Angew. Chem., Int. Ed.* **2016**, *55*, 10978–10999.
- (47) Morstein, J.; Trauner, D. New Players in Phototherapy: Photopharmacology and Bio-Integrated Optoelectronics. *Curr. Opin. Chem. Biol.* **2019**, *50*, 145–151.
- (48) Rau, O.; Wurglics, M.; Paulke, A.; Zitzkowski, J.; Meindl, N.; Bock, A.; Dingermann, T.; Abdel-Tawab, M.; Schubert-Zsilavecz, M. Carnosic Acid and Carnosol, Phenolic Diterpene Compounds of the Labiate Herbs Rosemary and Sage, Are Activators of the Human Peroxisome Proliferator-Activated Receptor Gamma. *Planta Med.* **2006**, *72*, 881–887.
- (49) Pollinger, J.; Gellrich, L.; Schierle, S.; Kilu, W.; Schmidt, J.; Kalinowsky, L.; Ohrndorf, J.; Kaiser, A.; Heering, J.; Proschak, E.; Merk, D. Tuning Nuclear Receptor Selectivity of Wy14,643 towards Selective Retinoid X Receptor Modulation. *J. Med. Chem.* **2019**, *62*, 2112–2126.
- (50) Agilent. *CrysAlis PRO*. Agilent Technologies Ltd.: Yarnton, Oxfordshire, England, 2014.
- (51) Altomare, A.; Burla, M. C.; Camalli, M.; Casciaro, G. L.; Giacovazzo, C.; Guagliardi, A.; Moliterni, A. G. G.; Polidori, G.; Spagna, R. SIR97: A New Tool for Crystal Structure Determination and Refinement. *J. Appl. Crystallogr.* **1999**, *32*, 115–119.
- (52) Sheldrick, G. M. SHELXT – Integrated Space-Group and Crystal-Structure Determination. *Acta Crystallogr., Sect. A: Found. Adv.* **2015**, *71*, 3–8.
- (53) Farrugia, L. J. WinGX and ORTEP for Windows: An Update. *J. Appl. Crystallogr.* **2012**, *45*, 849–854.
- (54) Bruker. *SAINTE*. Bruker AXS Inc.: Madison, Wisconsin, USA, 2012.
- (55) Sheldrick, G. M. *SADABS*. University of Göttingen: Germany, 1996.

Supporting Information

Photohormones Enable Optical Control of the Peroxisome Proliferator-Activated Receptor Gamma (PPAR γ)

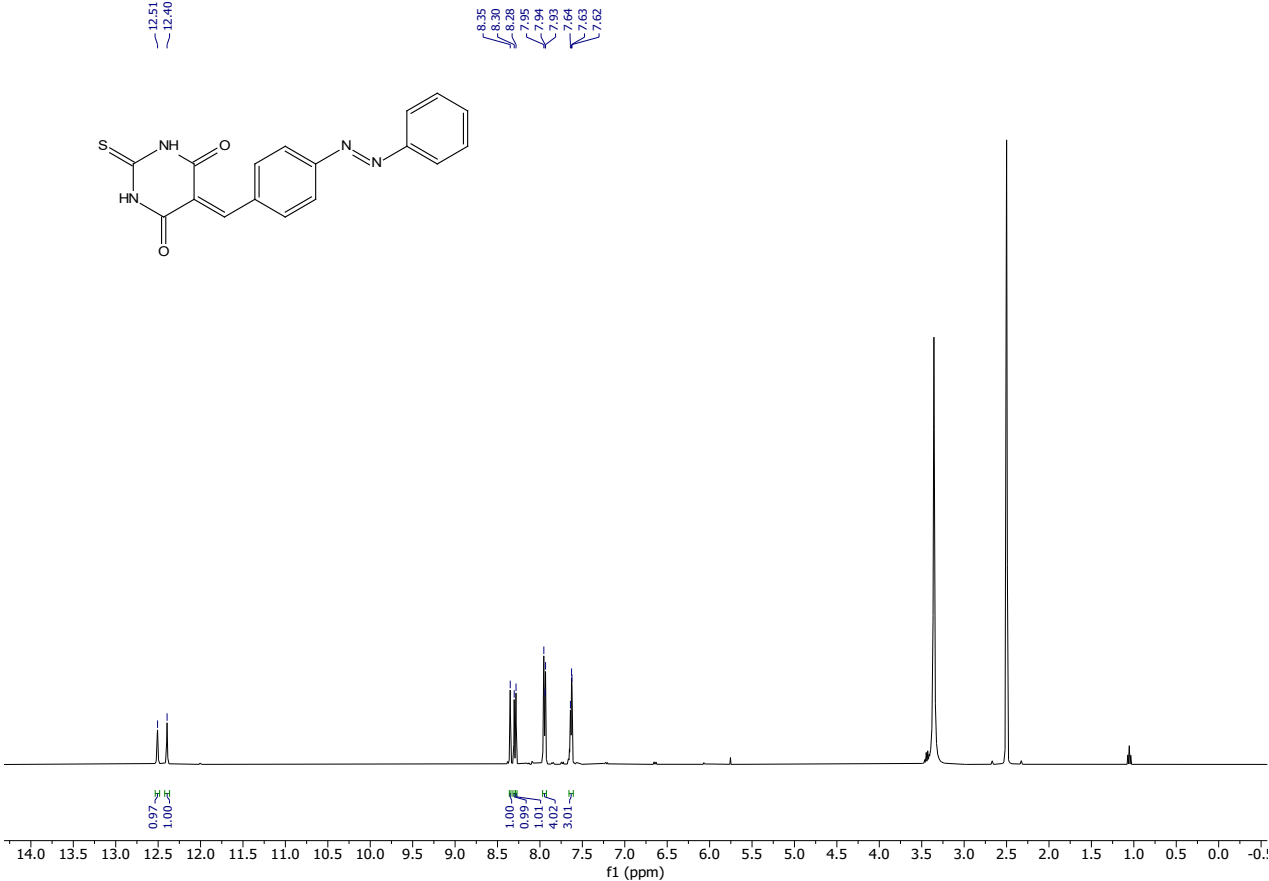
Konstantin Hinnah, Sabine Willems, Johannes Morstein, Jan Heering, Felix W. W.
Hartrampf, Johannes Broichhagen, Philipp Leippe, Daniel Merk, Dirk Trauner

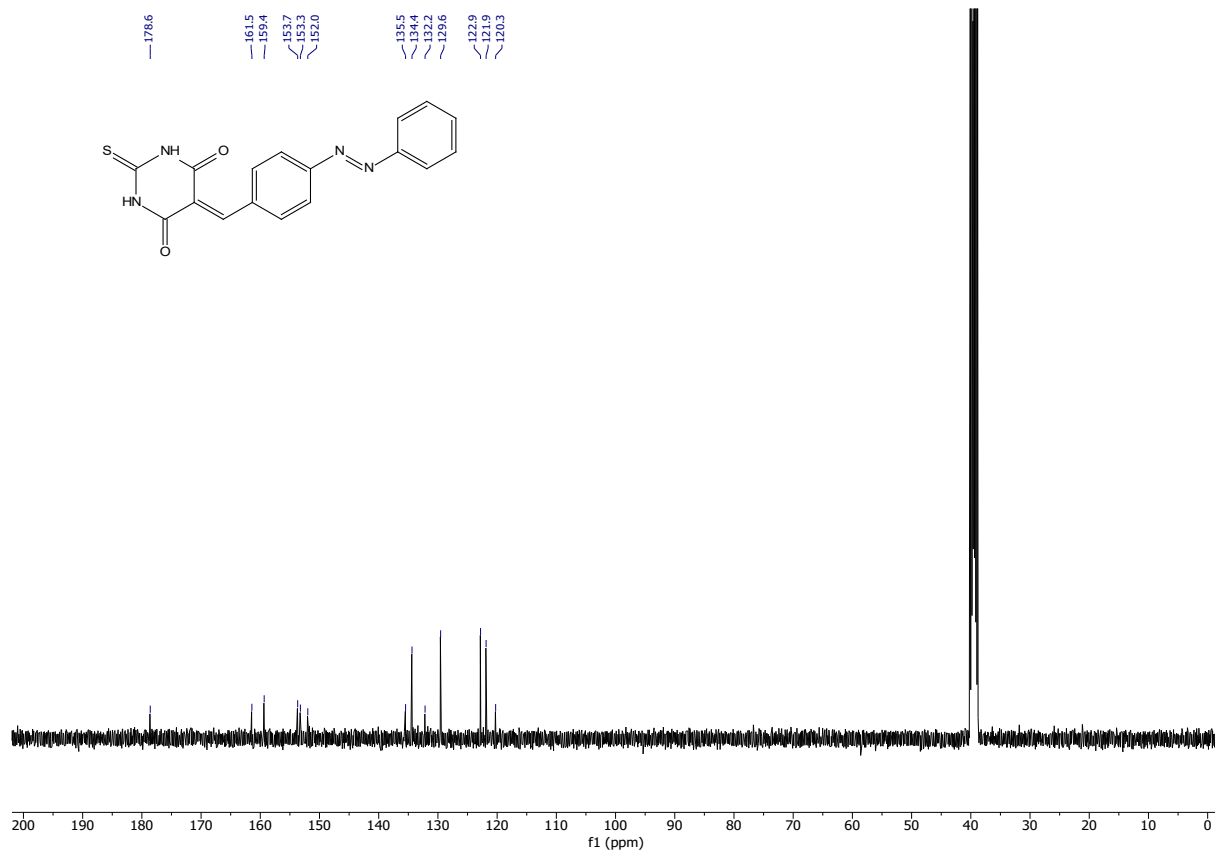
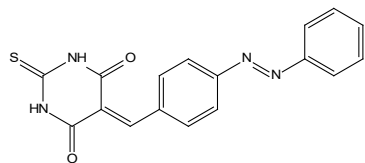
Table of Contents

NMR-Spectra and HPLC.....	2
AzoMDG548	2
Methyl (S)-2-amino-3-(4-aminophenyl)propanoate 3	4
Methyl (S,E)-2-amino-3-(4-(phenyldiazenyl)phenyl)propanoate 4	6
Methyl (S,E)-2-amino-3-(4-((4-chlorophenyl)diazenyl)phenyl)propanoate 5	8
AzoGW1929	10
AzoGW1929-2	15
2'-methyl-[1,1'-biphenyl]-4-amine 9	20
AzoRosi	22
AzoRosi-2	27
AzoRosi-3	32
AzoRosi-4	37
Photophysical Characterization and Photostationary States (PSS).....	42
Crystallography	44
Isothermal titration calorimetry (ITC)	46

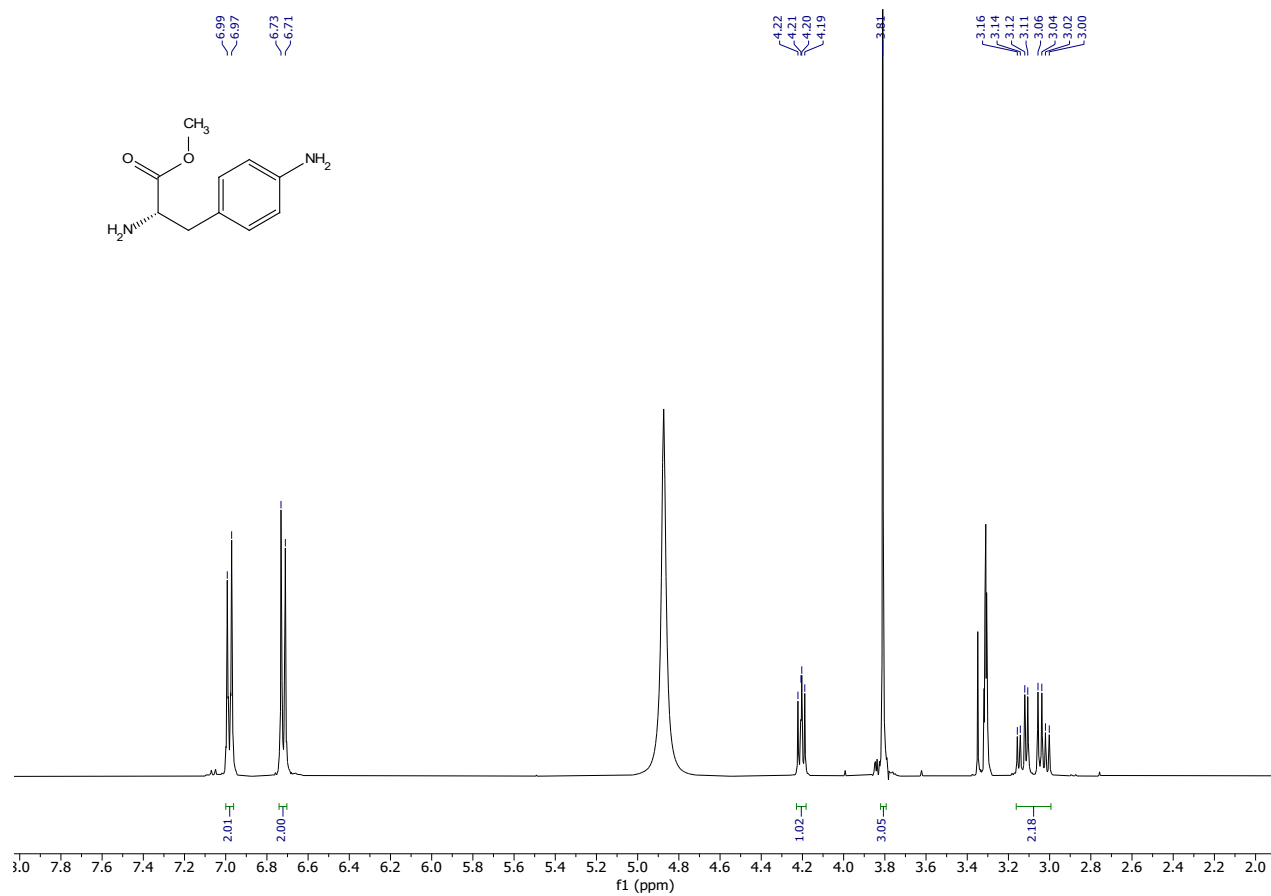
NMR-Spectra and HPLC

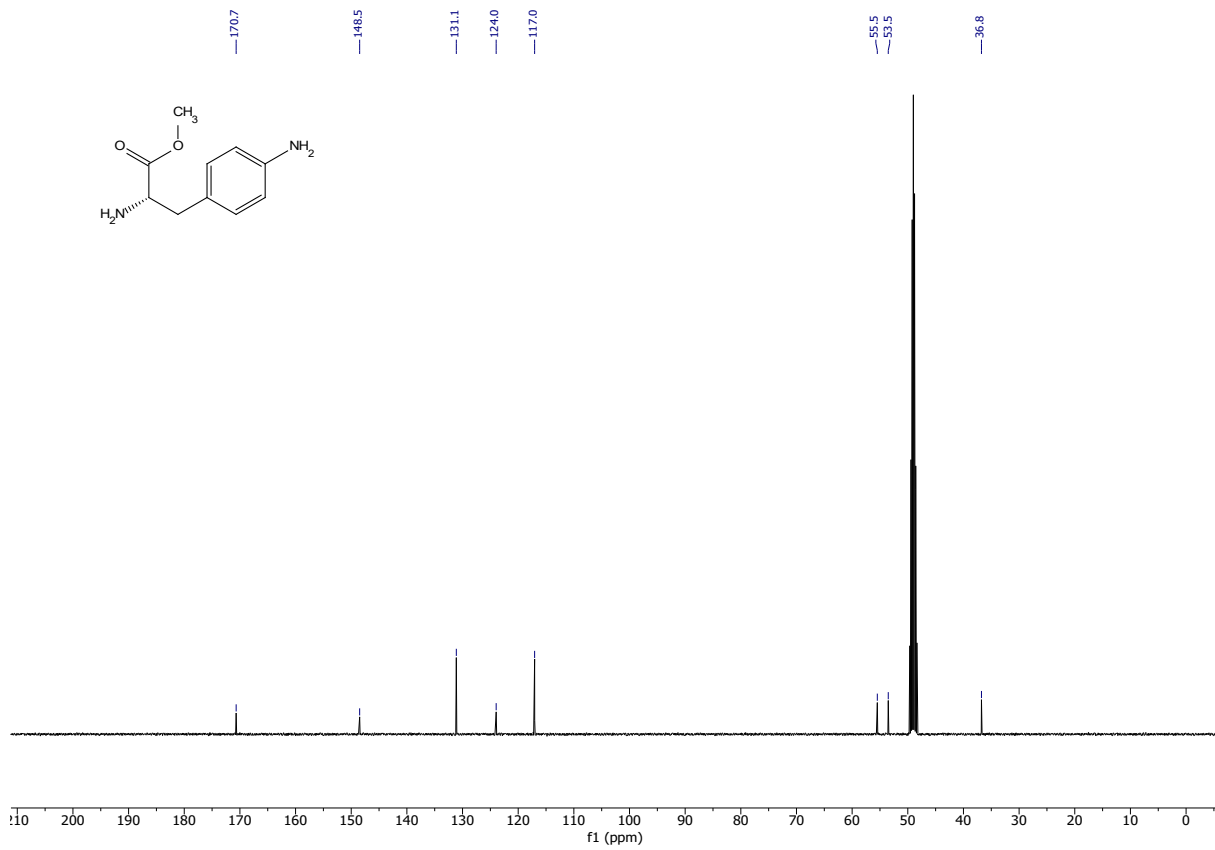
AzoMDG548





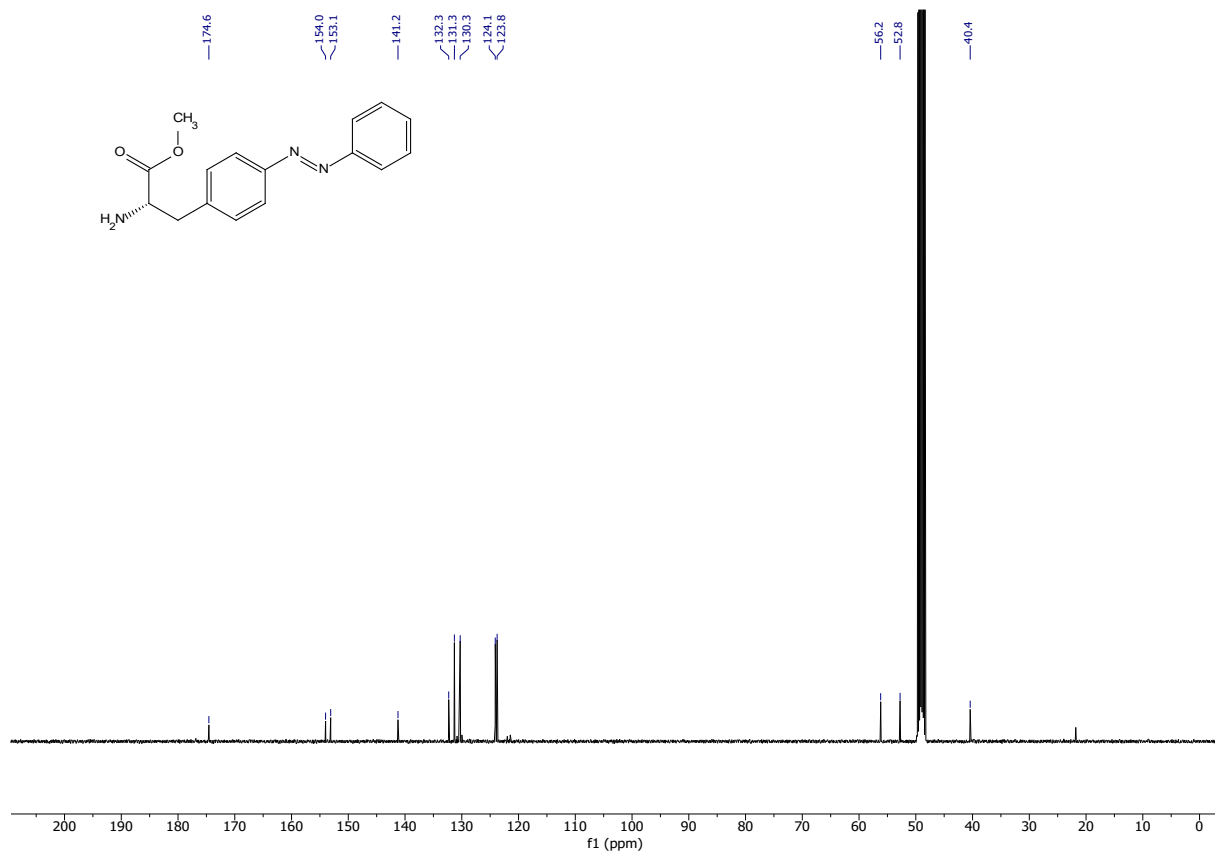
Methyl (S)-2-amino-3-(4-aminophenyl)propanoate 3





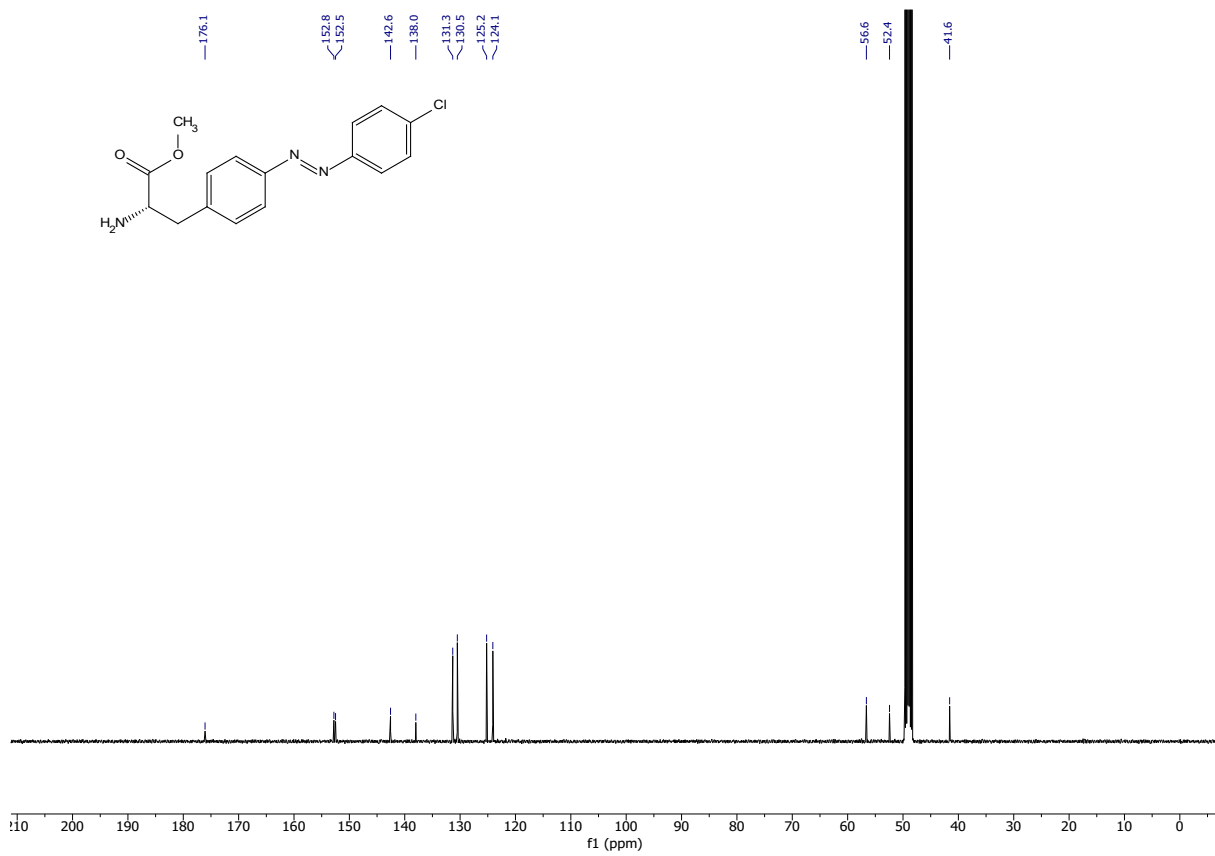
Methyl (S,E)-2-amino-3-(4-(phenyldiazenyl)phenyl)propanoate 4



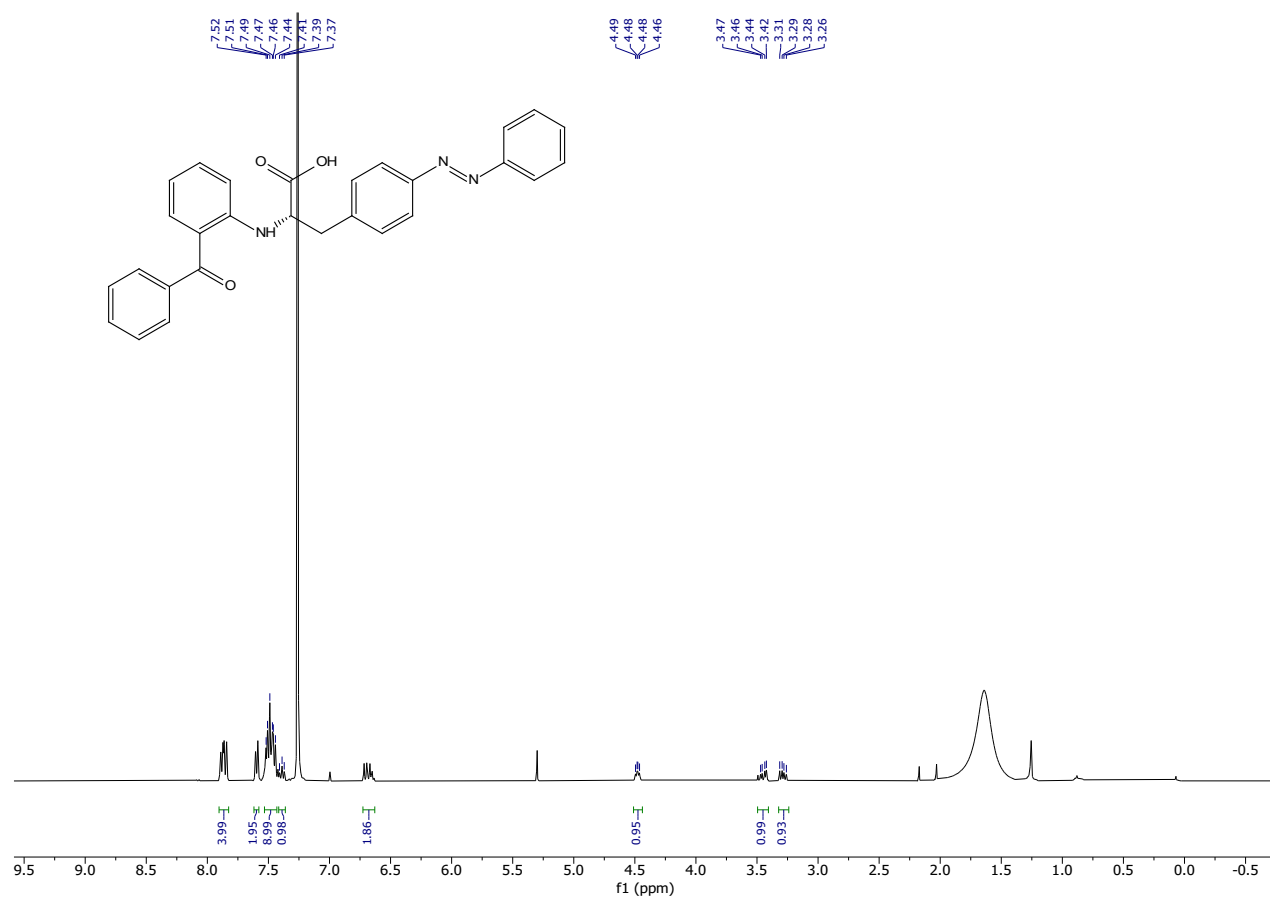


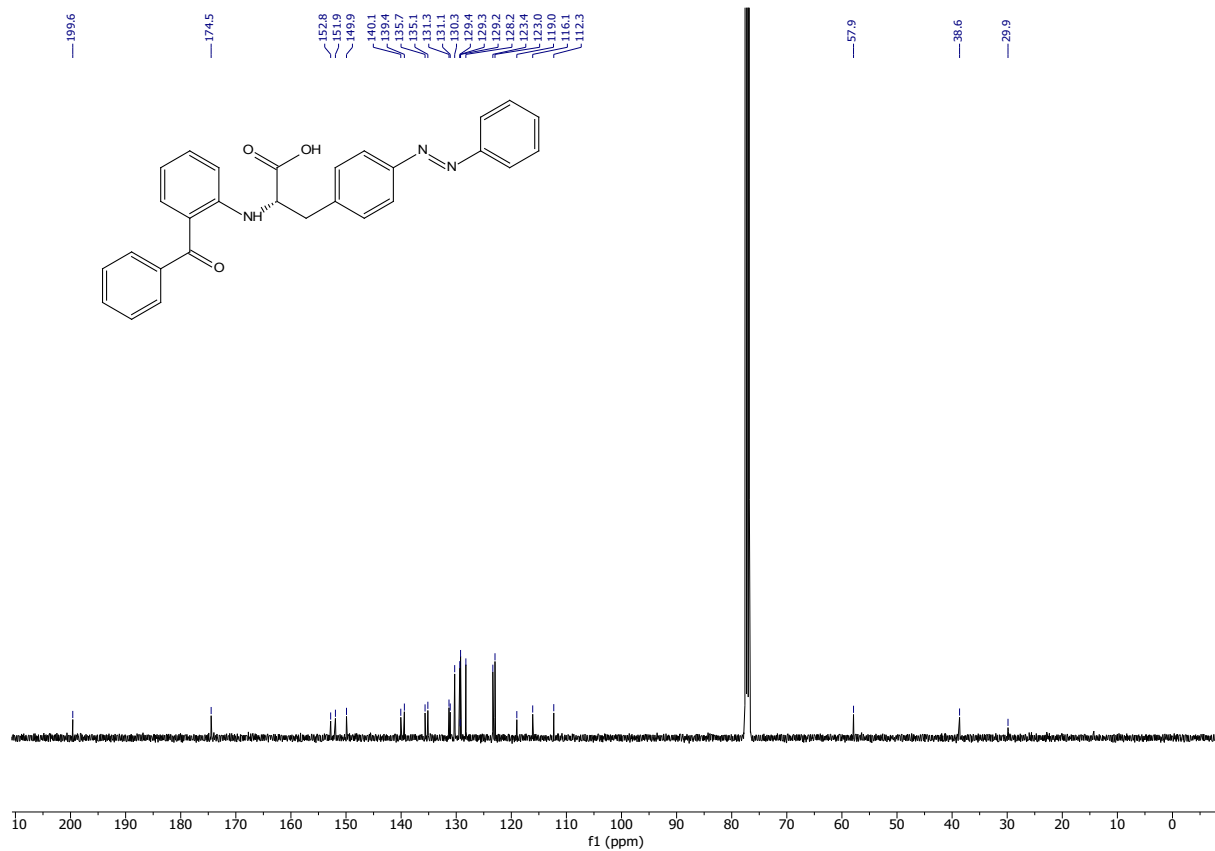
Methyl (S,E)-2-amino-3-(4-((4-chlorophenyl)diazenyl)phenyl)propanoate 5





AzoGW1929

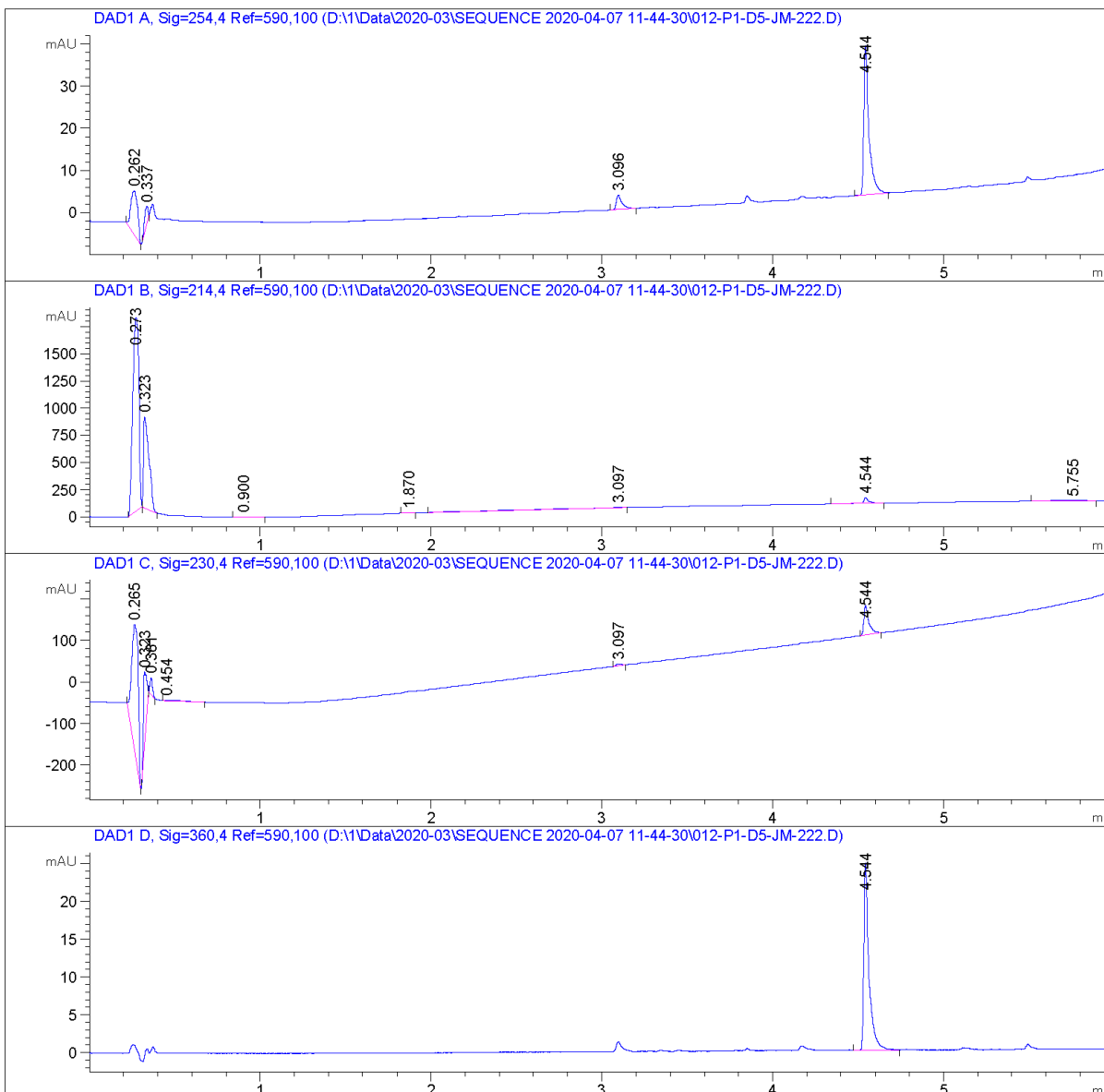


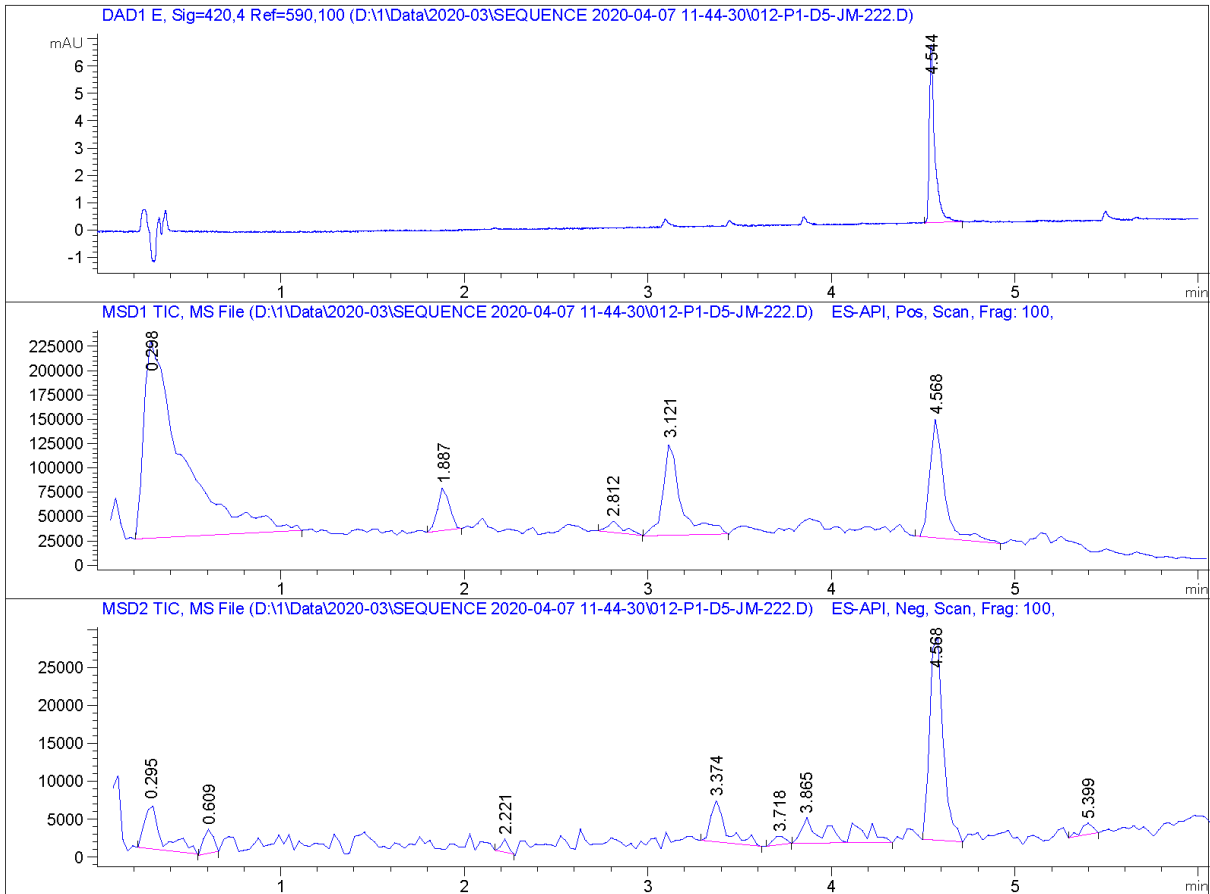


```

=====
Acq. Operator   : SYSTEM                      Seq. Line : 12
Acq. Instrument : LCMS                      Location  : P1-D5
Injection Date  : 4/7/2020 1:14:25 PM       Inj       : 1
                                                Inj Volume: 5.000 µl

Method         : D:\1\Data\2020-03\SEQUENCE 2020-04-07 11-44-30\AZO 25% to100%B over5 min
                uvvis 1 mlmin.M (Sequence Method)
Last changed   : 4/18/2018 2:31:20 PM by SYSTEM
Method Info    : FULL uv spectrum recording; eq 1 min with prerun macro; inject; 25 to 100%
                B over 5 min, flush at 100% B for 1 min, no postrun, FULL uv spectrum
                recording
  
```





=====
 Area Percent Report
 =====

Sorted By : Signal
 Multiplier : 1.0000
 Dilution : 1.0000
 Use Multiplier & Dilution Factor with ISTDs

Signal 1: DAD1 A, Sig=254,4 Ref=590,100

Peak #	RetTime [min]	Type	Width [min]	Area [mAU*s]	Height [mAU]	Area %
1	0.262	BB	0.0375	27.90848	10.33663	24.2471
2	0.337	BB	0.0265	6.50088	4.10729	5.6480
3	3.096	BB	0.0334	7.96568	3.44863	6.9206
4	4.544	BB	0.0294	72.72526	35.46495	63.1842

Totals : 115.10031 53.35750

Signal 2: DAD1 B, Sig=214,4 Ref=590,100

Peak #	RetTime [min]	Type	Width [min]	Area [mAU*s]	Height [mAU]	Area %
1	0.273	BB	0.0401	4365.83691	1782.35706	67.7716
2	0.323	BB	0.0292	1848.05823	837.58618	28.6877
3	0.900	BB	0.0573	5.10932	1.08727	0.0793
4	1.870	BB	0.0352	9.78878	4.19642	0.1520
5	3.097	BB	0.2220	68.55415	3.69350	1.0642
6	4.544	BB	0.0297	103.65650	49.92537	1.6091
7	5.755	BB	0.1409	40.98670	3.46874	0.6362

Totals : 6441.99059 2682.31454

Signal 3: DAD1 C, Sig=230,4 Ref=590,100

Peak #	RetTime [min]	Type	Width [min]	Area [mAU*s]	Height [mAU]	Area %
1	0.265	BB	0.0431	805.95990	302.01370	65.6306
2	0.323	BB	0.0177	225.54097	178.56525	18.3662
3	0.361	BB	0.0159	38.53959	39.49973	3.1383
4	0.454	BB	0.1148	10.02569	1.07524	0.8164
5	3.097	BB	0.0279	9.13874	4.98535	0.7442
6	4.544	BB	0.0285	138.81964	70.32796	11.3043

Totals : 1228.02452 596.46723

Signal 4: DAD1 D, Sig=360,4 Ref=590,100

Peak #	RetTime [min]	Type	Width [min]	Area [mAU*s]	Height [mAU]	Area %
1	4.544	BB	0.0299	51.72208	24.77613	100.0000

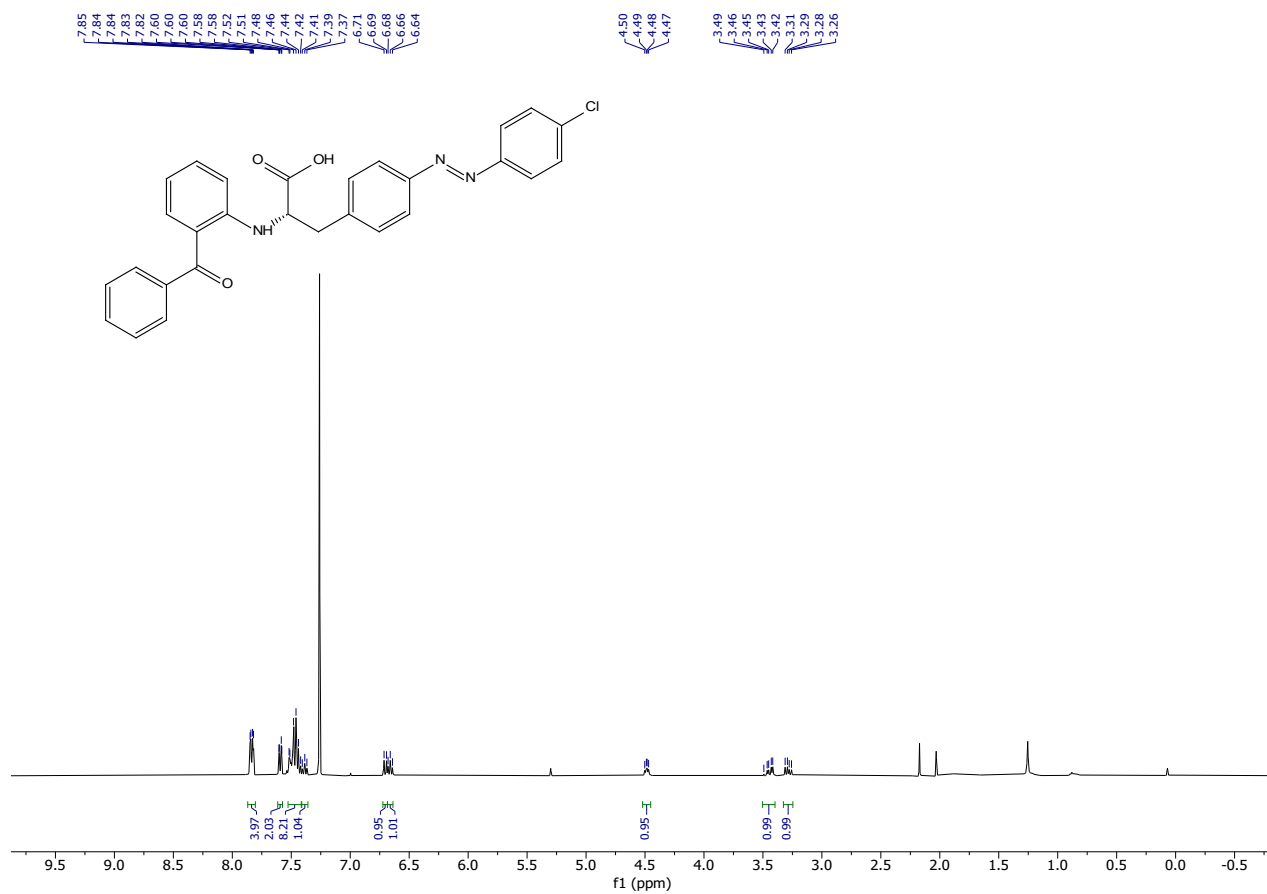
Totals : 51.72208 24.77613

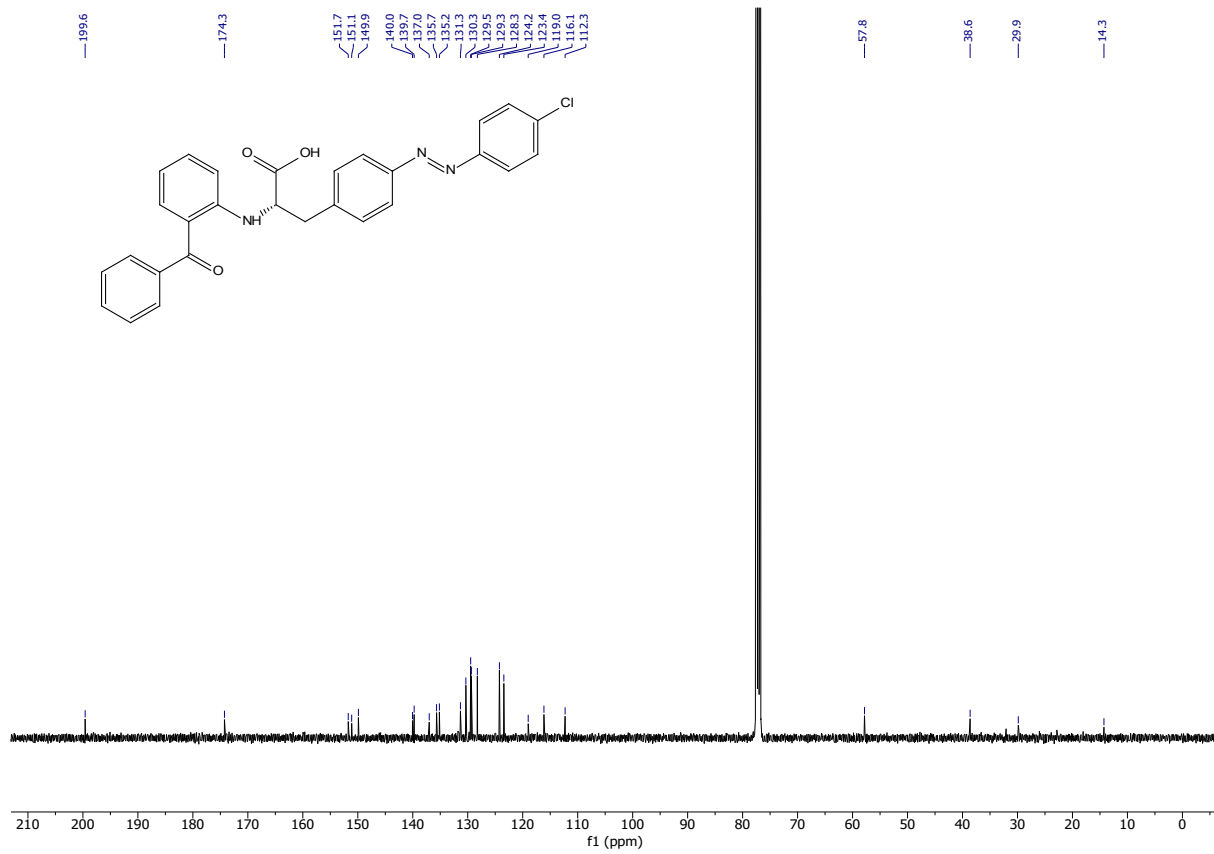
Signal 5: DAD1 E, Sig=420,4 Ref=590,100

Peak #	RetTime [min]	Type	Width [min]	Area [mAU*s]	Height [mAU]	Area %
1	4.544	BB	0.0298	13.55693	6.50382	100.0000

Totals : 13.55693 6.50382

AzoGW1929-2

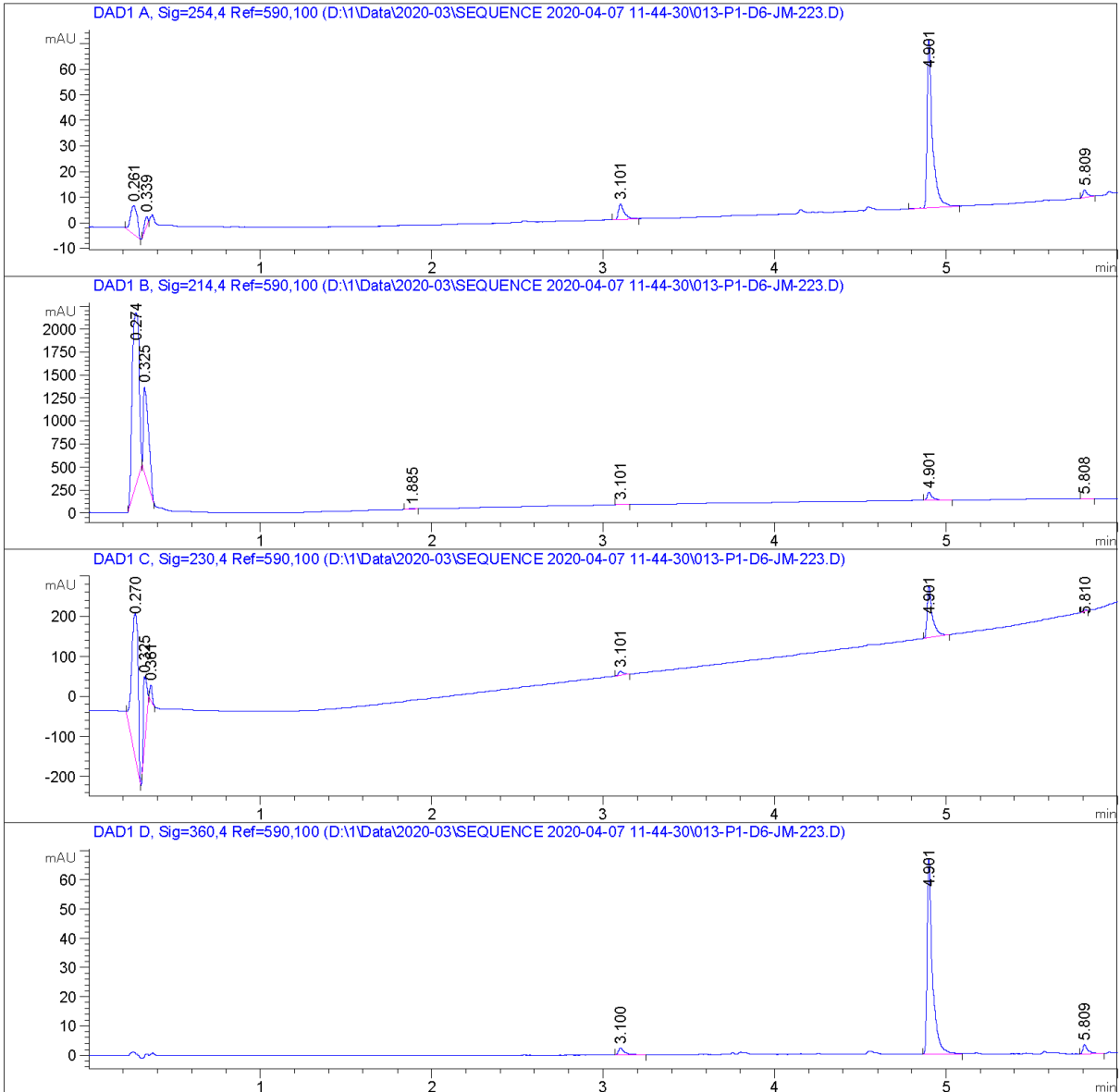


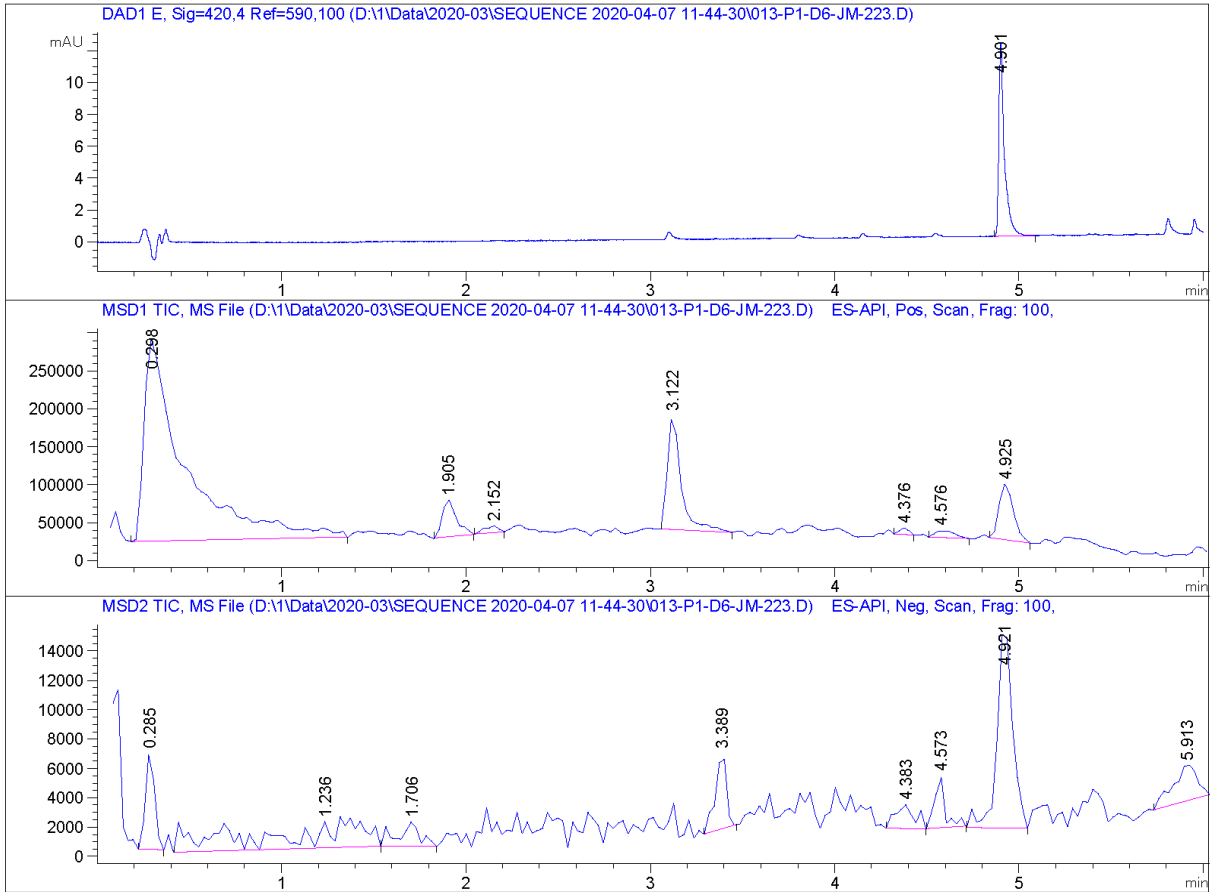



```

=====
Acq. Operator   : SYSTEM                      Seq. Line : 13
Acq. Instrument : LCMS                      Location  : P1-D6
Injection Date  : 4/7/2020 1:22:21 PM       Inj       : 1
                                           Inj Volume: 5.000 µl

Method          : D:\1\Data\2020-03\SEQUENCE 2020-04-07 11-44-30\AZO 25% to100%B over5 min
                  uvvis 1 m1min.M (Sequence Method)
Last changed    : 4/18/2018 2:31:20 PM by SYSTEM
Method Info     : FULL uv spectrum recording; eq 1 min with prerun macro; inject; 25 to 100%
                  B over 5 min, flush at 100% B for 1 min, no postrun, FULL uv spectrum
                  recording
  
```





=====
 Area Percent Report
 =====

Sorted By : Signal
 Multiplier : 1.0000
 Dilution : 1.0000
 Use Multiplier & Dilution Factor with ISTDs

Signal 1: DAD1 A, Sig=254,4 Ref=590,100

Peak #	RetTime [min]	Type	Width [min]	Area [mAU*s]	Height [mAU]	Area %
1	0.261	BB	0.0385	30.35172	11.08144	15.5292
2	0.339	BB	0.0273	6.07196	3.77485	3.1067
3	3.101	BB	0.0335	14.16368	6.12669	7.2467
4	4.901	BB	0.0309	139.56461	65.50099	71.4070
5	5.809	BB	0.0262	5.29757	2.98812	2.7105
Totals :				195.44954	89.47209	

Signal 2: DAD1 B, Sig=214,4 Ref=590,100

Peak #	RetTime [min]	Type	Width [min]	Area [mAU*s]	Height [mAU]	Area %
1	0.274	BB	0.0462	5281.47070	1881.68628	70.2185
2	0.325	BB	0.0340	2025.44312	925.29602	26.9288
3	1.885	BB	0.0358	10.01634	4.35787	0.1332
4	3.101	BB	0.0294	13.50913	6.72264	0.1796
5	4.901	BB	0.0306	184.27742	87.51632	2.4500
6	5.808	BB	0.0260	6.76451	3.94204	0.0899

Totals : 7521.48122 2909.52116

Signal 3: DAD1 C, Sig=230,4 Ref=590,100

Peak #	RetTime [min]	Type	Width [min]	Area [mAU*s]	Height [mAU]	Area %
1	0.270	BB	0.0418	911.26532	356.31747	62.1523
2	0.325	BB	0.0187	228.41936	174.83612	15.5792
3	0.361	BB	0.0150	35.27077	37.44576	2.4056
4	3.101	BB	0.0298	18.66773	9.35178	1.2732
5	4.901	BB	0.0297	266.89438	128.89406	18.2034
6	5.810	BB	0.0199	5.66301	4.58458	0.3862

Totals : 1466.18057 711.42977

Signal 4: DAD1 D, Sig=360,4 Ref=590,100

Peak #	RetTime [min]	Type	Width [min]	Area [mAU*s]	Height [mAU]	Area %
1	3.100	BB	0.0347	5.69685	2.36090	3.7284
2	4.901	BB	0.0302	140.89314	66.51421	92.2089
3	5.809	BB	0.0290	6.20779	3.07748	4.0628

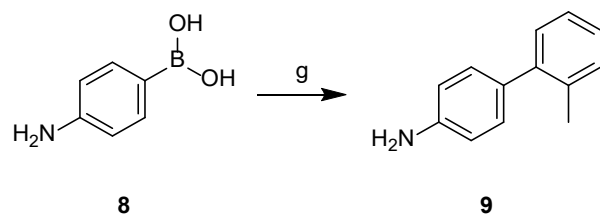
Totals : 152.79778 71.95258

Signal 5: DAD1 E, Sig=420,4 Ref=590,100

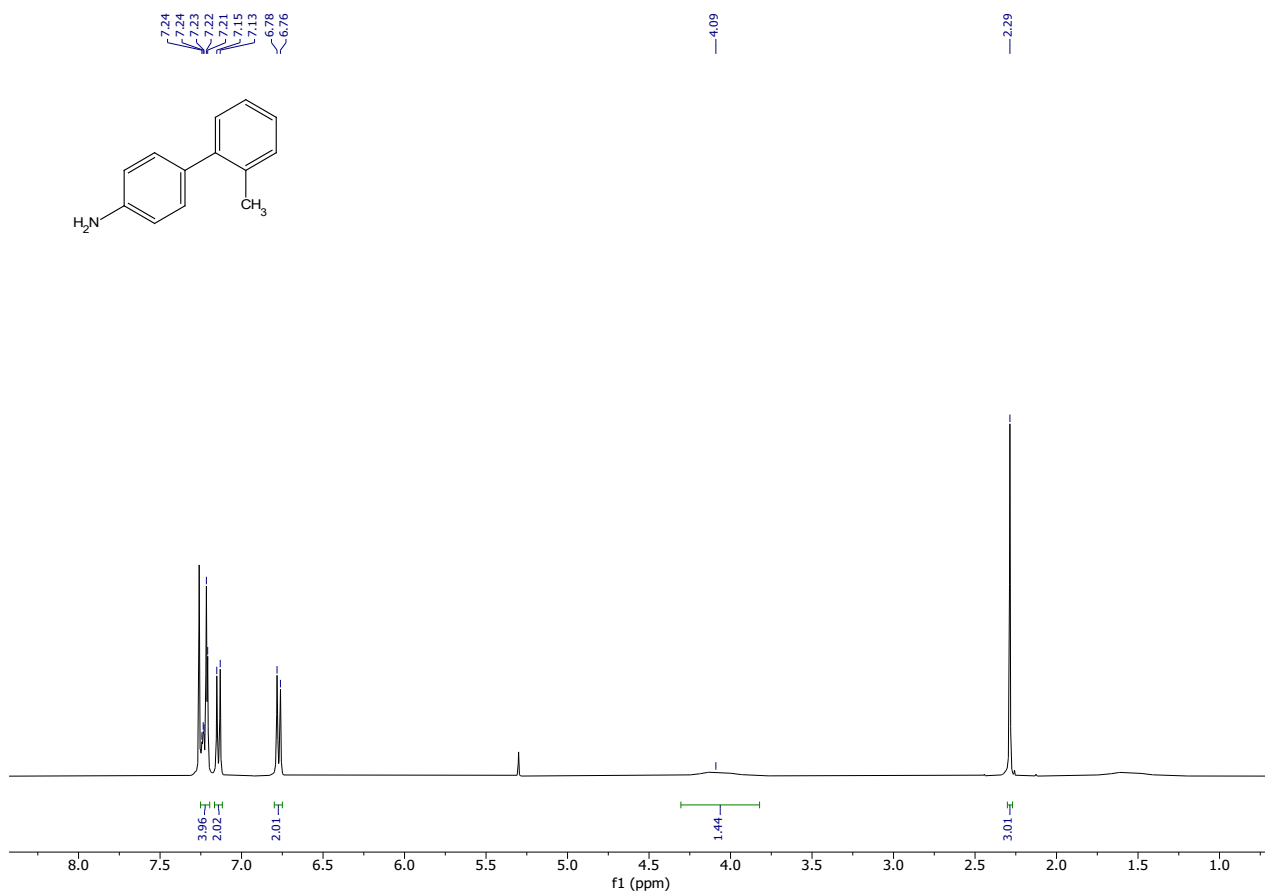
Peak #	RetTime [min]	Type	Width [min]	Area [mAU*s]	Height [mAU]	Area %
1	4.901	BB	0.0308	25.72222	12.08782	100.0000

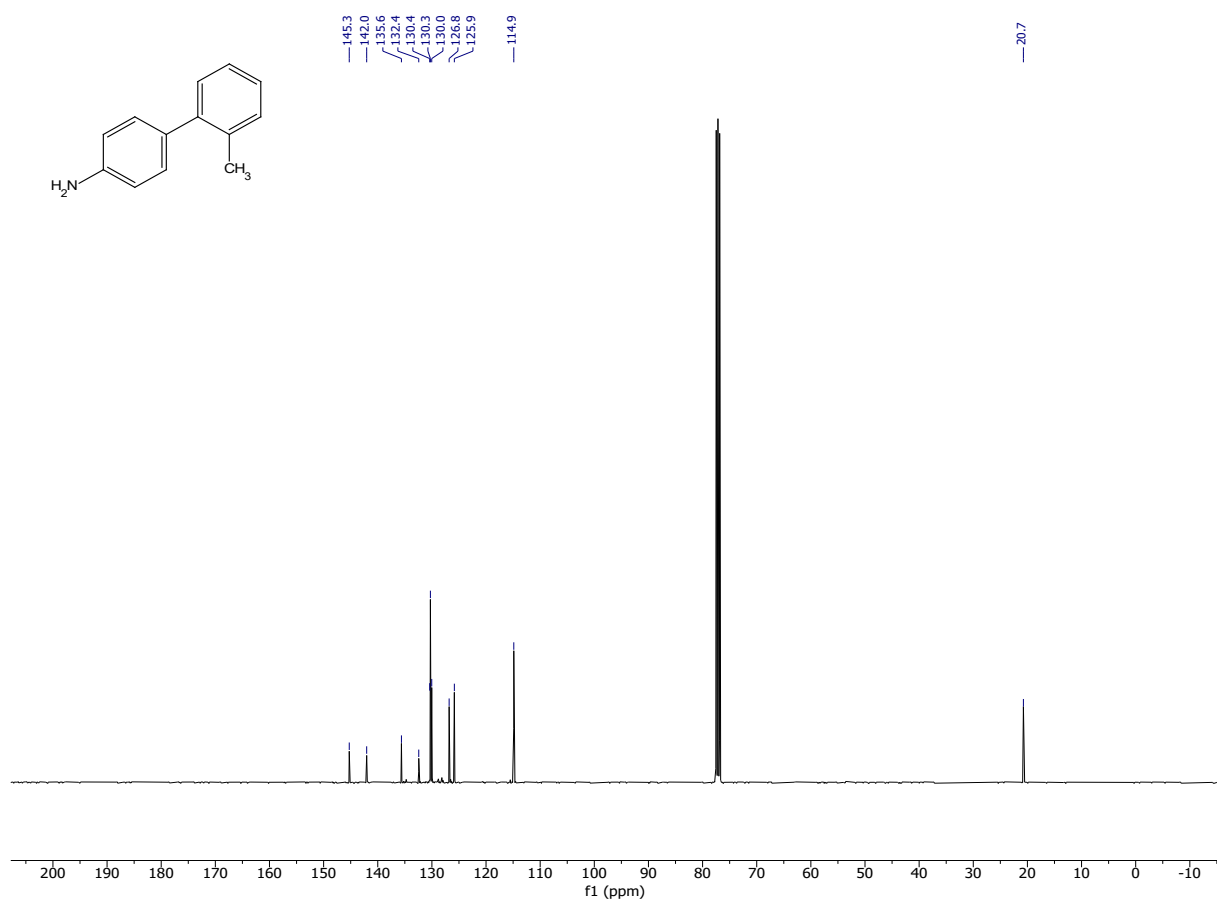
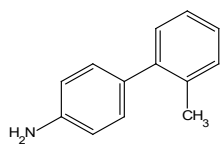
Totals : 25.72222 12.08782

2'-methyl-[1,1'-biphenyl]-4-amine **9**

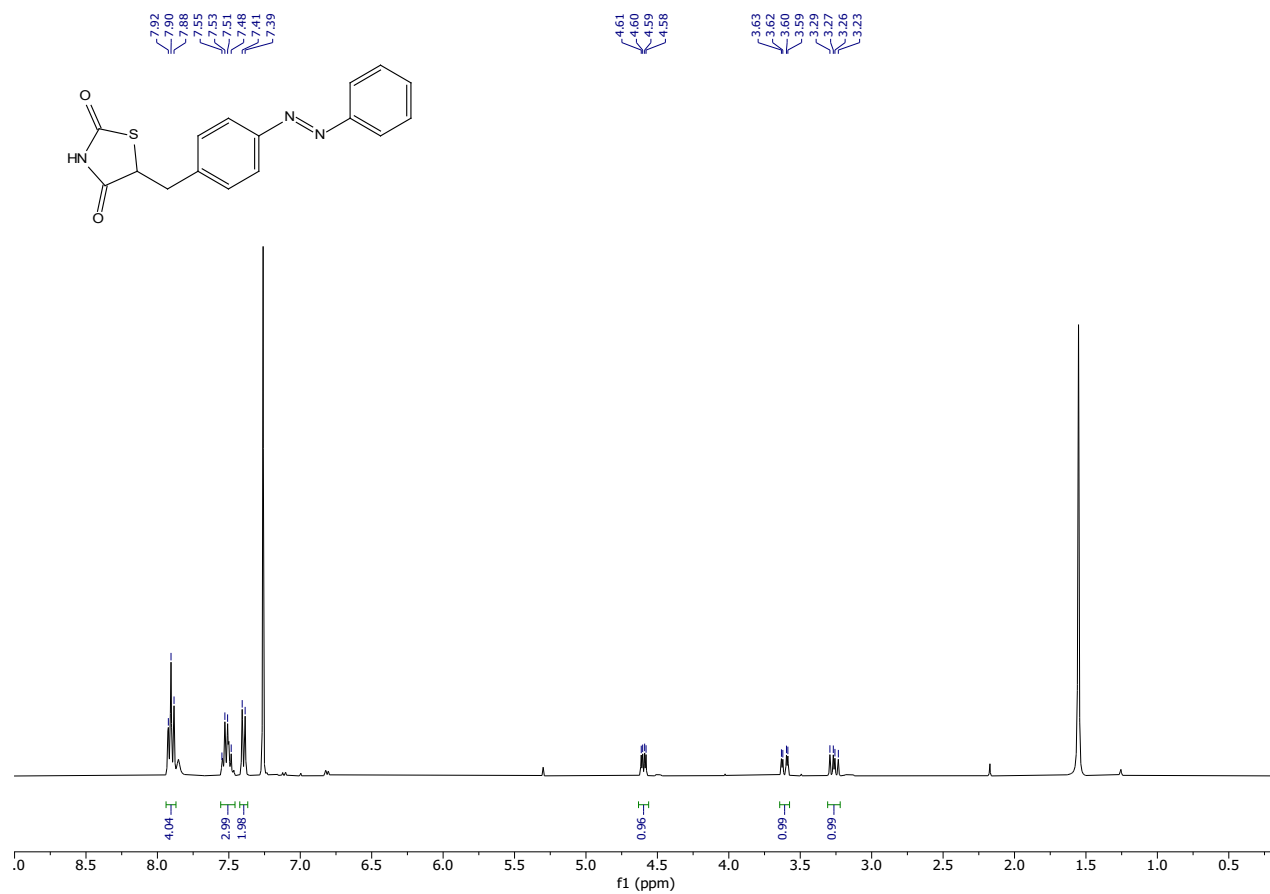


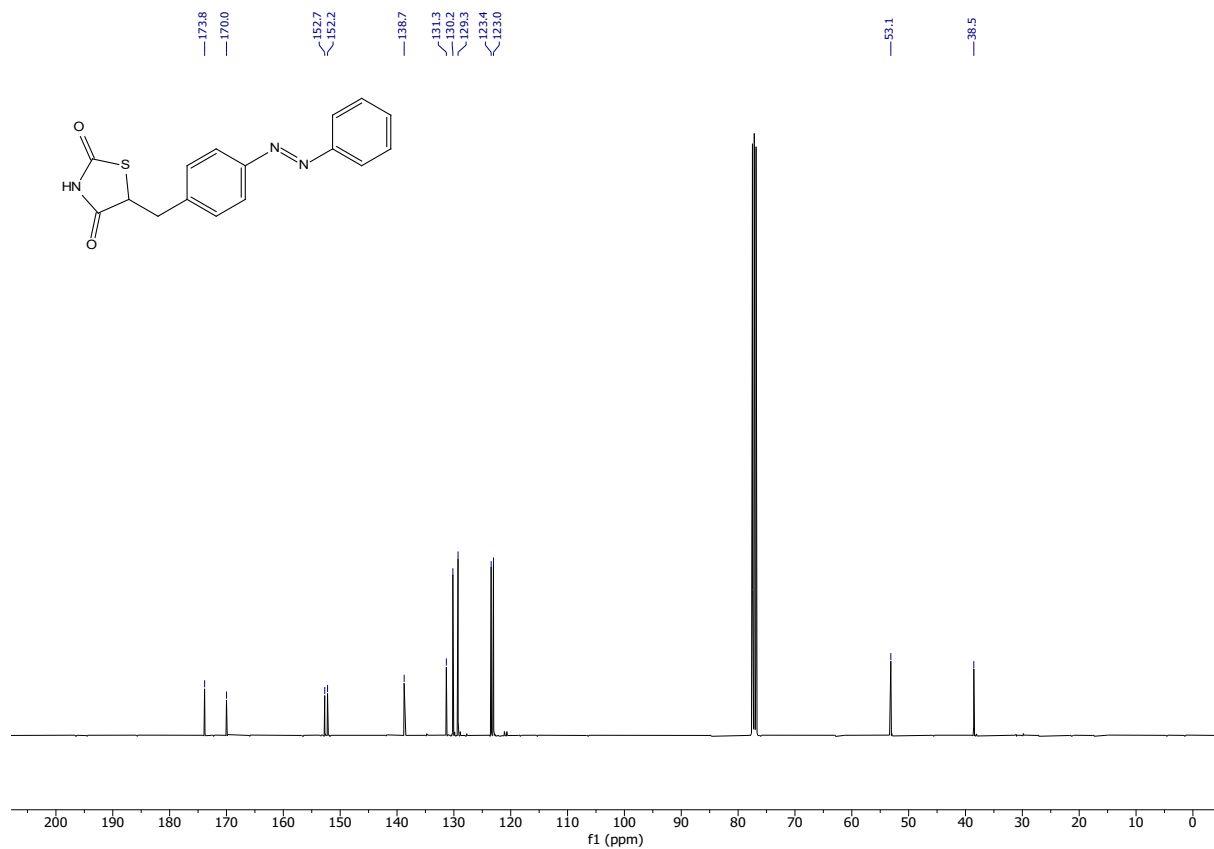
Scheme S1 g) 2-bromotoluene, Pd(PPh₃)₄, K₂CO₃, H₂O, DMF, 85 °C, 16 h (55 %).





AzoRosi



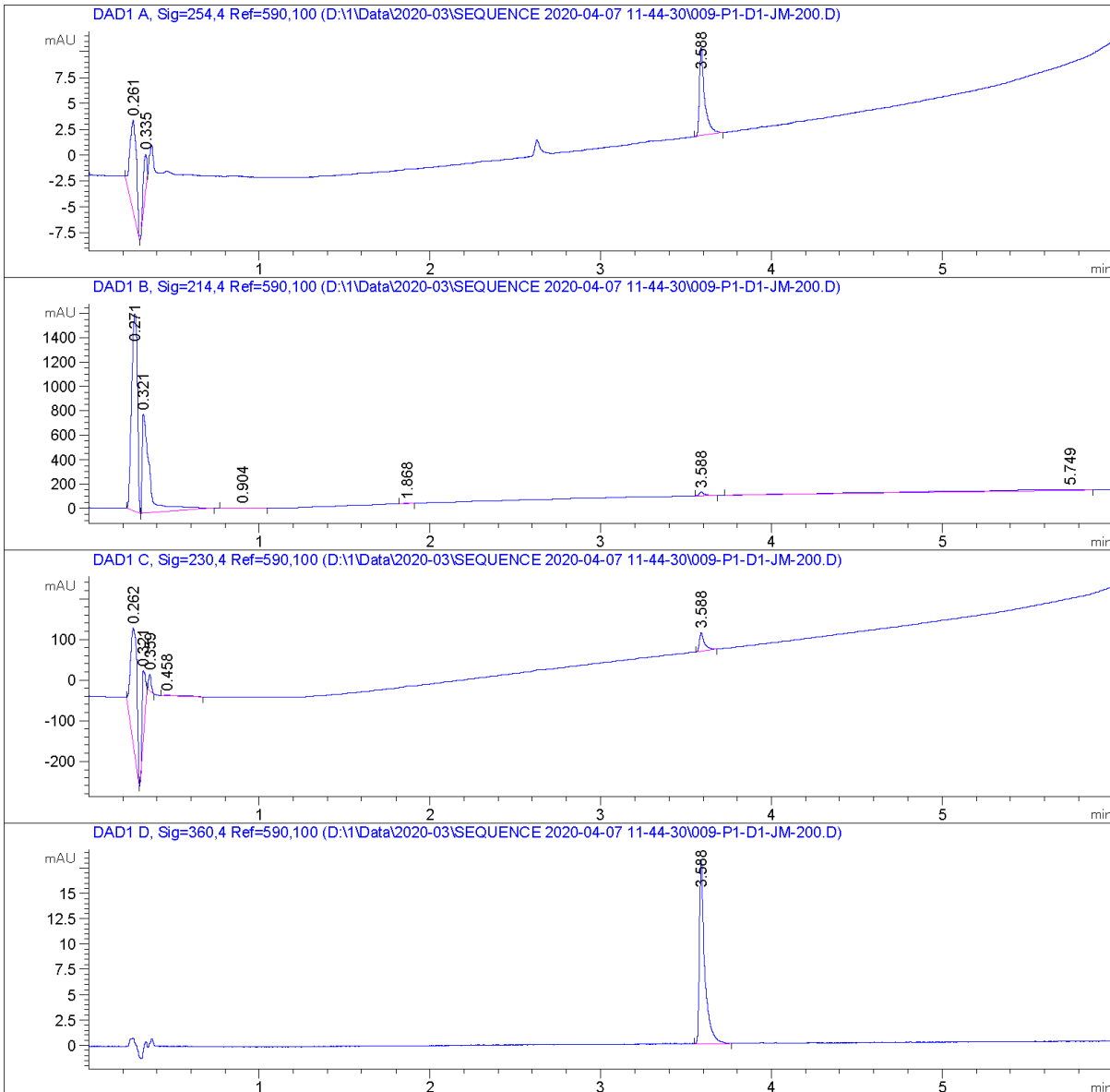


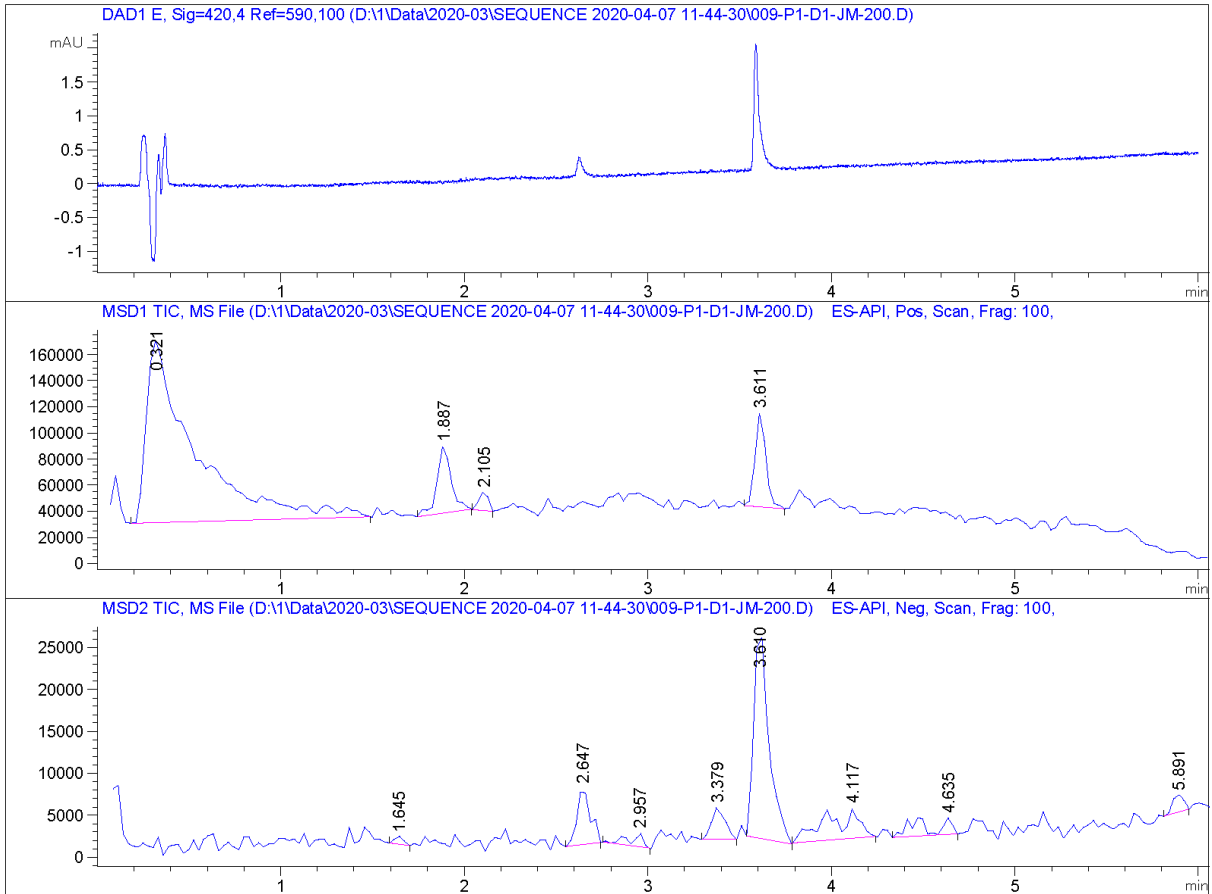
```

=====
Acq. Operator   : SYSTEM                               Seq. Line :    9
Acq. Instrument : LCMS                               Location  : P1-D1
Injection Date  : 4/7/2020 12:50:41 PM                Inj       :    1
                                                    Inj Volume: 5.000 µl

Method          : D:\1\Data\2020-03\SEQUENCE 2020-04-07 11-44-30\AZO 25% to100%B over5 min
                uvvis 1 mlmin.M (Sequence Method)
Last changed    : 4/18/2018 2:31:20 PM by SYSTEM
Method Info     : FULL uv spectrum recording; eq 1 min with prerun macro; inject; 25 to 100%
                B over 5 min, flush at 100% B for 1 min, no postrun, FULL uv spectrum
                recording
=====

```





=====
 Area Percent Report
 =====

Sorted By : Signal
 Multiplier : 1.0000
 Dilution : 1.0000
 Use Multiplier & Dilution Factor with ISTDs

Signal 1: DAD1 A, Sig=254,4 Ref=590,100

Peak #	RetTime [min]	Type	Width [min]	Area [mAU*s]	Height [mAU]	Area %
1	0.261	BB	0.0354	23.37692	8.82044	49.4039
2	0.335	BB	0.0272	5.97125	3.72908	12.6194
3	3.588	BB	0.0302	17.96977	8.48414	37.9767

Totals : 47.31795 21.03366

Signal 2: DAD1 B, Sig=214,4 Ref=590,100

Peak #	RetTime [min]	Type	Width [min]	Area [mAU*s]	Height [mAU]	Area %
1	0.271	BB	0.0375	3814.06641	1620.68970	55.0159
2	0.321	BB	0.0395	2516.03198	814.41064	36.2924
3	0.904	BB	0.0651	6.54737	1.25098	0.0944
4	1.868	BB	0.0334	10.25311	4.45158	0.1479
5	3.588	BB	0.0294	66.52601	32.49927	0.9596
6	5.749	BB	1.0335	519.24066	5.87013	7.4898

Totals : 6932.66554 2479.17230

Signal 3: DAD1 C, Sig=230,4 Ref=590,100

Peak #	RetTime [min]	Type	Width [min]	Area [mAU*s]	Height [mAU]	Area %
1	0.262	BB	0.0422	752.18109	281.60706	67.2772
2	0.321	BB	0.0177	219.80719	174.09190	19.6602
3	0.359	BB	0.0160	39.76826	40.27479	3.5570
4	0.458	BB	0.1122	13.59028	1.48641	1.2156
5	3.588	BB	0.0291	92.68646	45.77426	8.2901

Totals : 1118.03329 543.23441

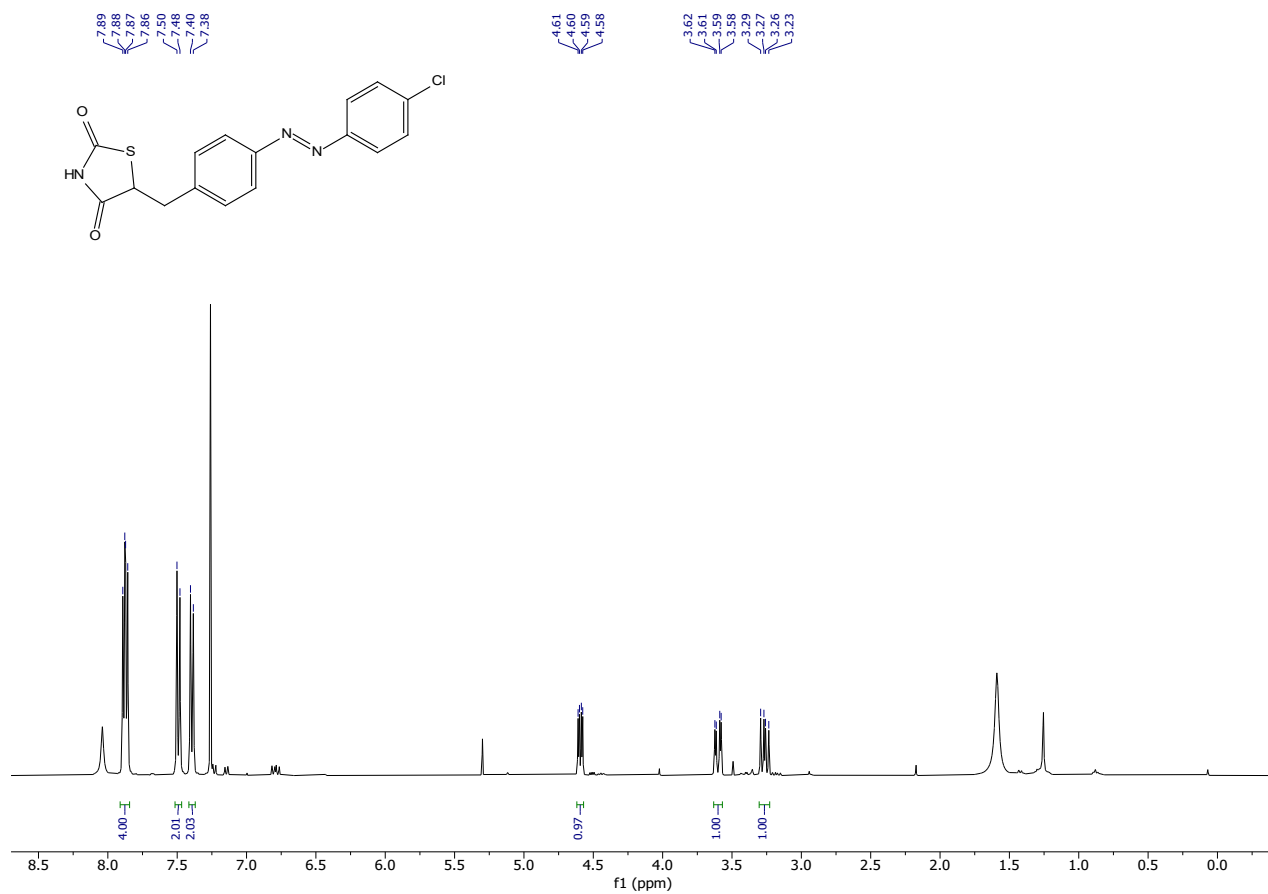
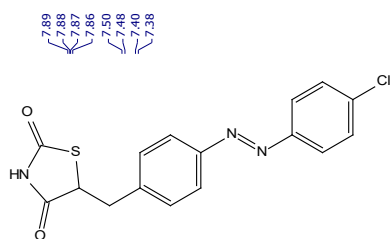
Signal 4: DAD1 D, Sig=360,4 Ref=590,100

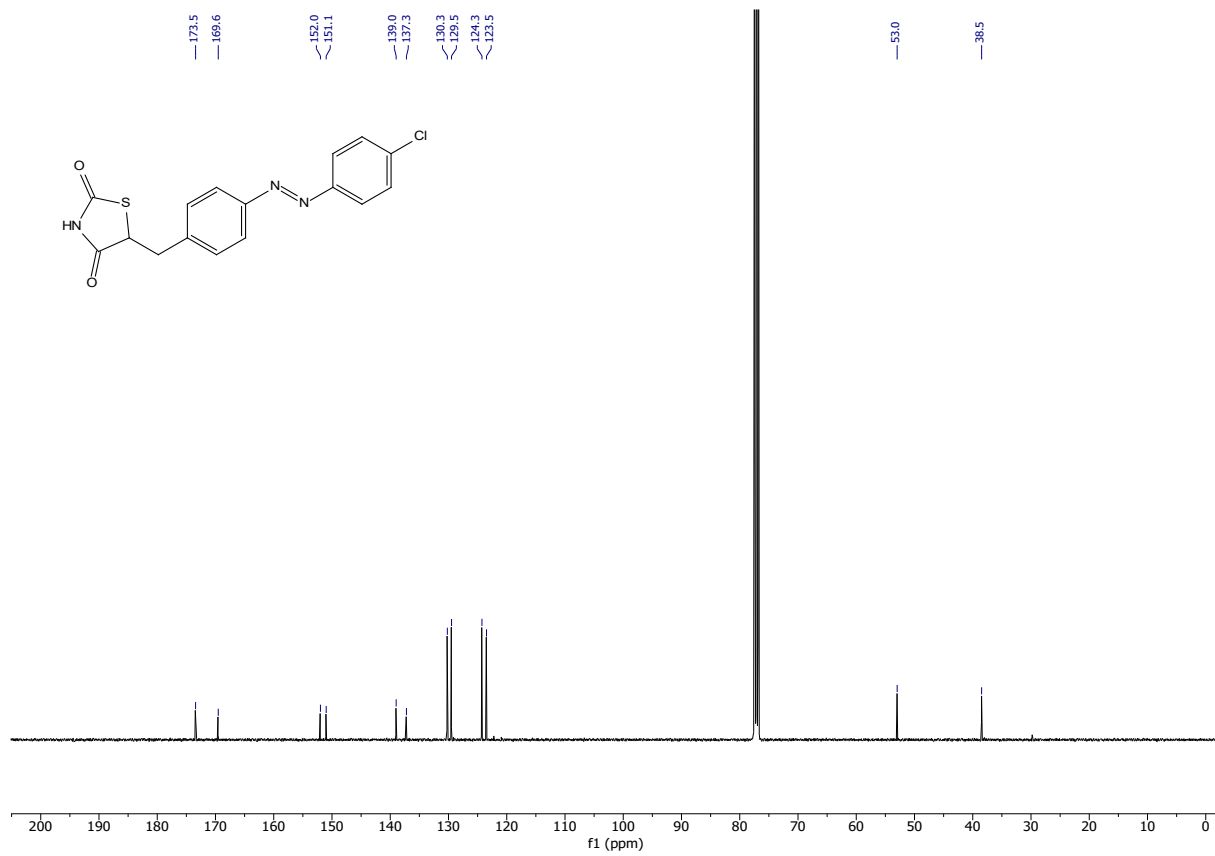
Peak #	RetTime [min]	Type	Width [min]	Area [mAU*s]	Height [mAU]	Area %
1	3.588	BB	0.0305	39.05832	18.20165	100.0000

Totals : 39.05832 18.20165

Signal 5: DAD1 E, Sig=420,4 Ref=590,100

AzoRosi-2





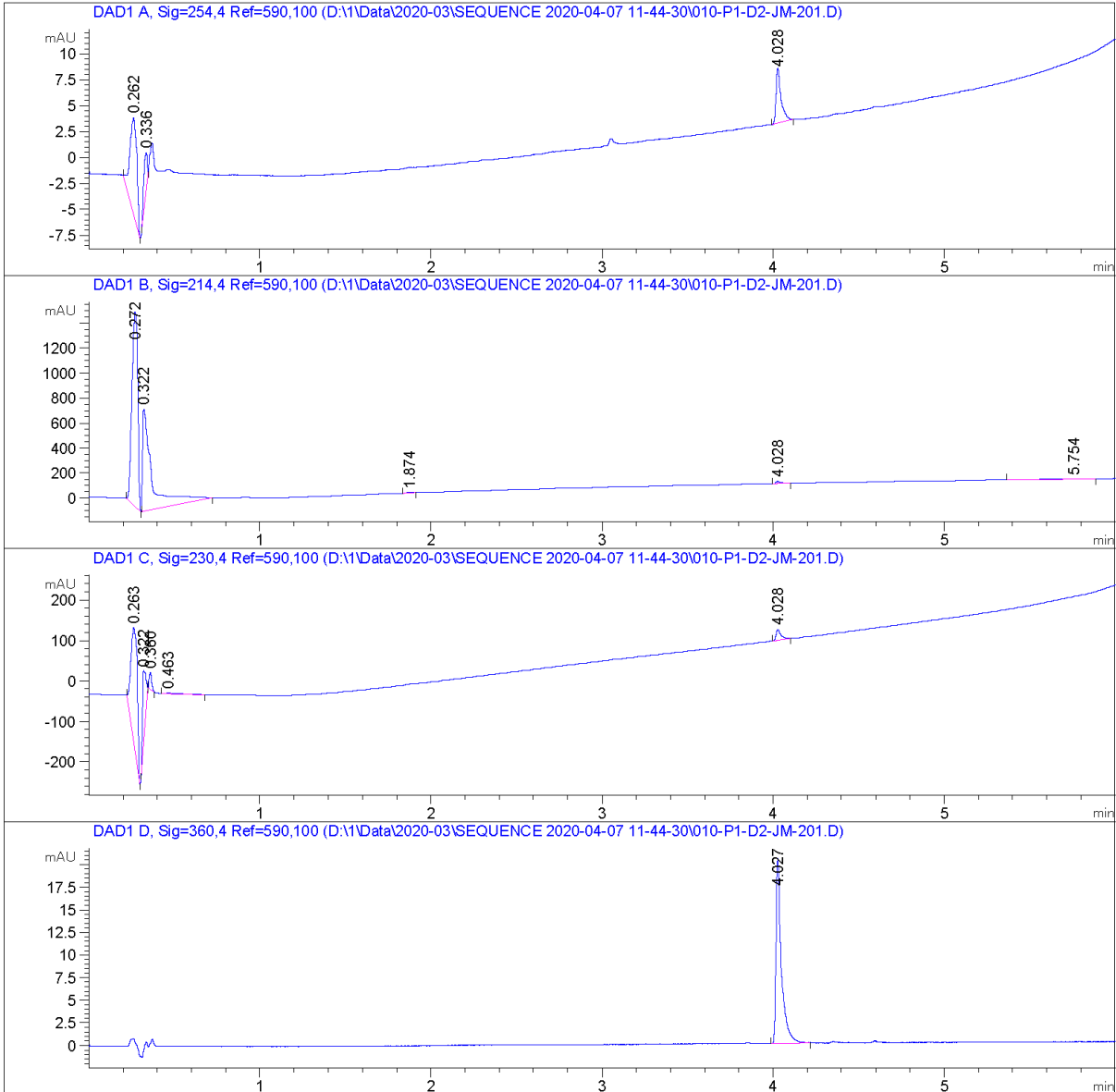
```

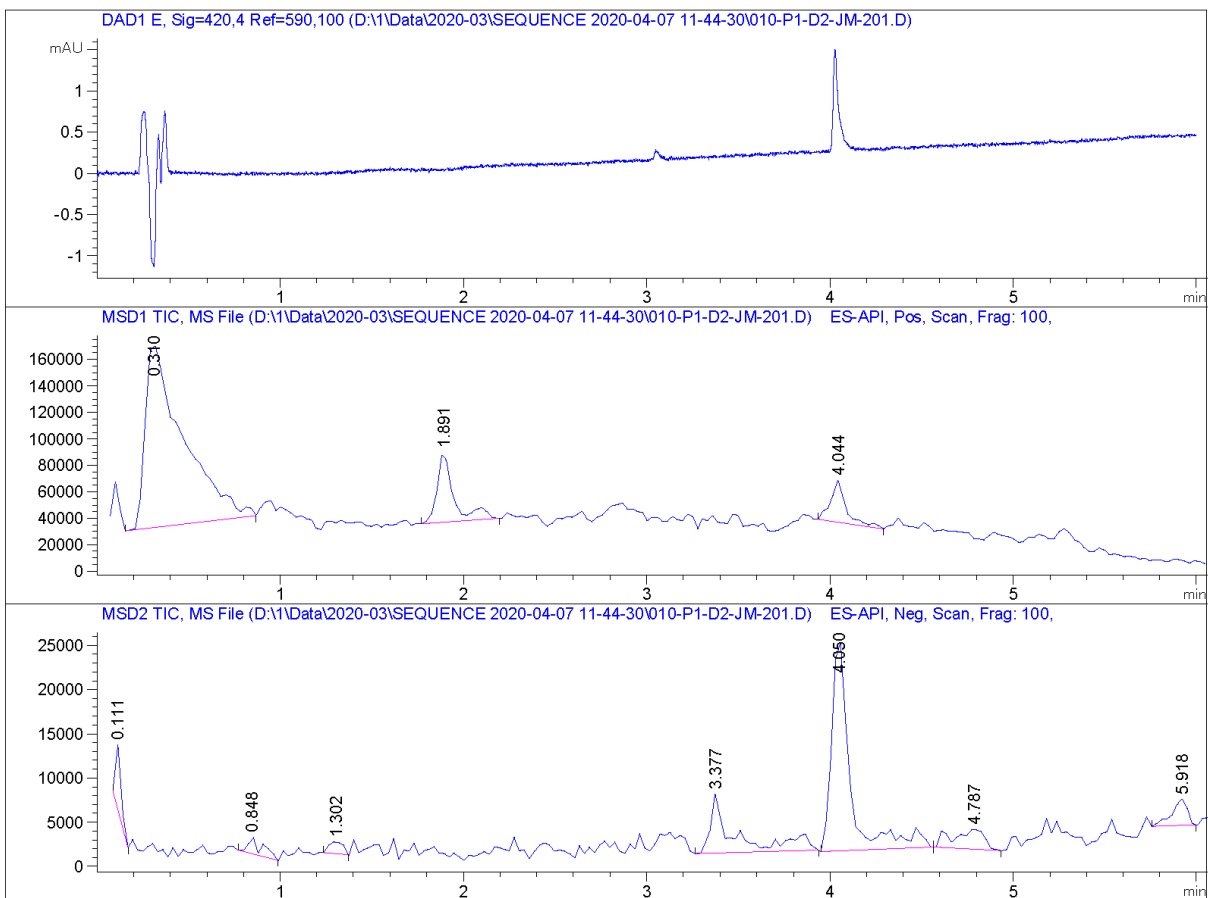
=====
Acq. Operator   : SYSTEM                               Seq. Line : 10
Acq. Instrument : LCMS                               Location  : P1-D2
Injection Date  : 4/7/2020 12:58:36 PM                Inj       : 1
                                                    Inj Volume: 5.000 µl

Method          : D:\1\Data\2020-03\SEQUENCE 2020-04-07 11-44-30\10-P1-D2-JM-201.D
                : uvvis 1 mlmin.M (Sequence Method)

Last changed    : 4/18/2018 2:31:20 PM by SYSTEM

Method Info     : FULL uv spectrum recording; eq 1 min with prerun macro; inject; 25 to 100%
                : B over 5 min, flush at 100% B for 1 min, no postrun, FULL uv spectrum
                : recording
  
```





=====
 Area Percent Report
 =====

Sorted By : Signal
 Multiplier : 1.0000
 Dilution : 1.0000
 Use Multiplier & Dilution Factor with ISTDs

Signal 1: DAD1 A, Sig=254,4 Ref=590,100

Peak #	RetTime [min]	Type	Width [min]	Area [mAU*s]	Height [mAU]	Area %
1	0.262	BB	0.0385	25.82895	9.27723	60.7570
2	0.336	BB	0.0272	5.89526	3.67283	13.8673
3	4.028	BB	0.0291	10.78769	5.32349	25.3757

Totals : 42.51190 18.27355

Signal 2: DAD1 B, Sig=214,4 Ref=590,100

Peak #	RetTime [min]	Type	Width [min]	Area [mAU*s]	Height [mAU]	Area %
1	0.272	BB	0.0389	3655.89795	1554.87585	52.5946
2	0.322	BB	0.0489	3175.53784	815.24115	45.6840
3	1.874	BB	0.0338	10.25463	4.55460	0.1475
4	4.028	BB	0.0281	34.25156	17.31449	0.4928
5	5.754	BB	0.2143	75.15277	4.14849	1.0812

Totals : 6951.09475 2396.13458

Signal 3: DAD1 C, Sig=230,4 Ref=590,100

Peak #	RetTime [min]	Type	Width [min]	Area [mAU*s]	Height [mAU]	Area %
1	0.263	BB	0.0424	749.61902	282.66257	69.7345
2	0.322	BB	0.0180	217.63289	169.42757	20.2456
3	0.360	BB	0.0156	41.53300	41.68375	3.8637
4	0.463	BB	0.1078	14.36261	1.63725	1.3361
5	4.028	BB	0.0284	51.81408	26.45210	4.8201

Totals : 1074.96160 521.86323

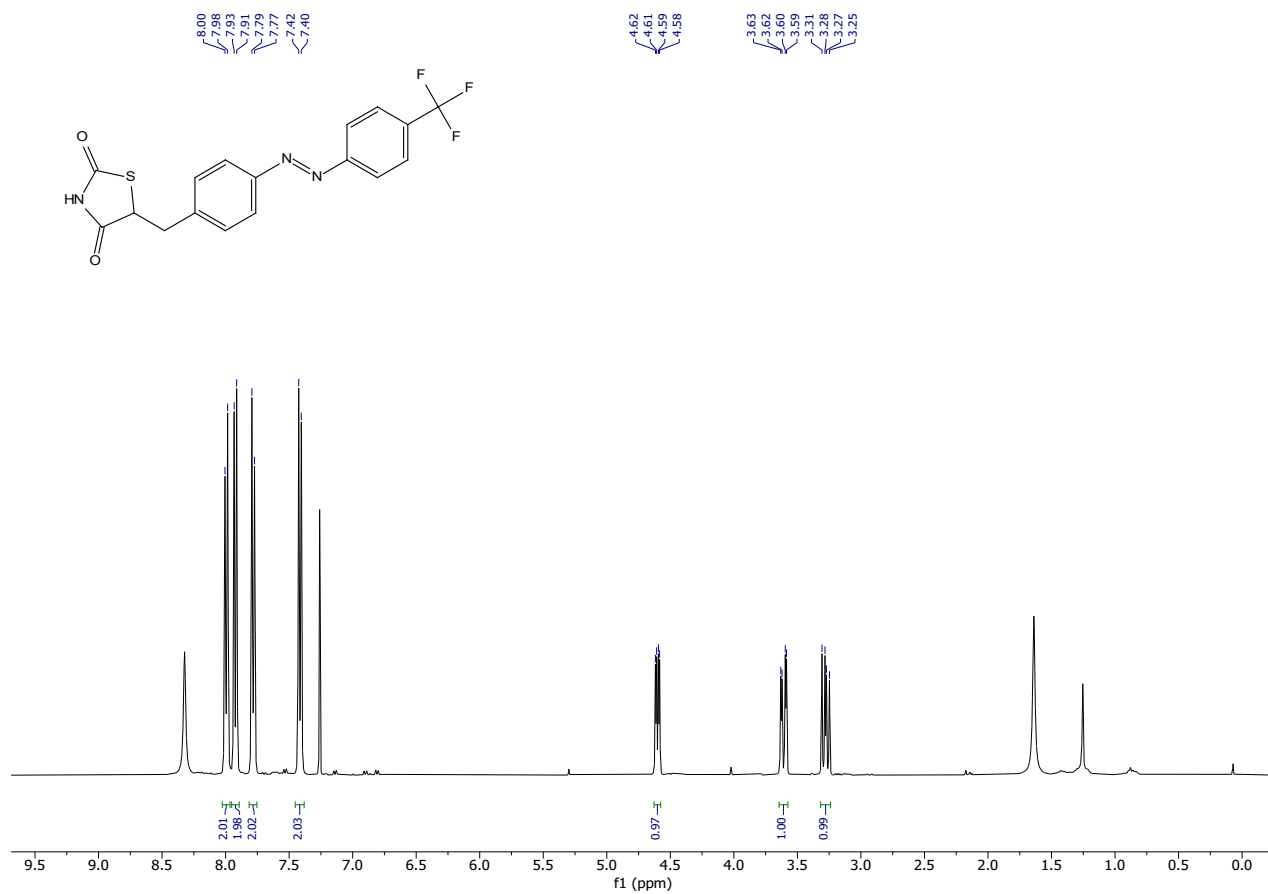
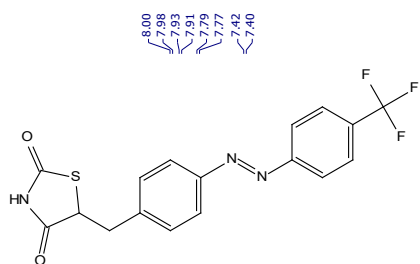
Signal 4: DAD1 D, Sig=360,4 Ref=590,100

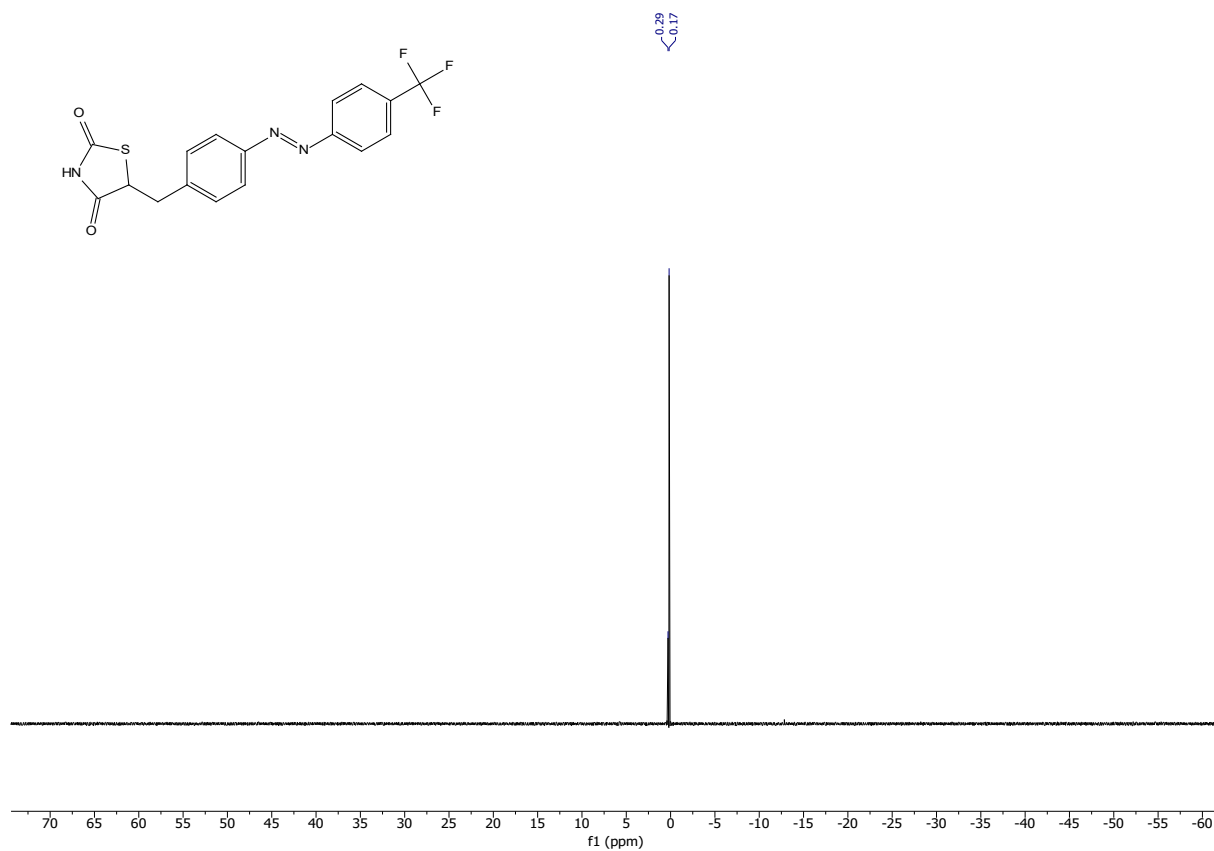
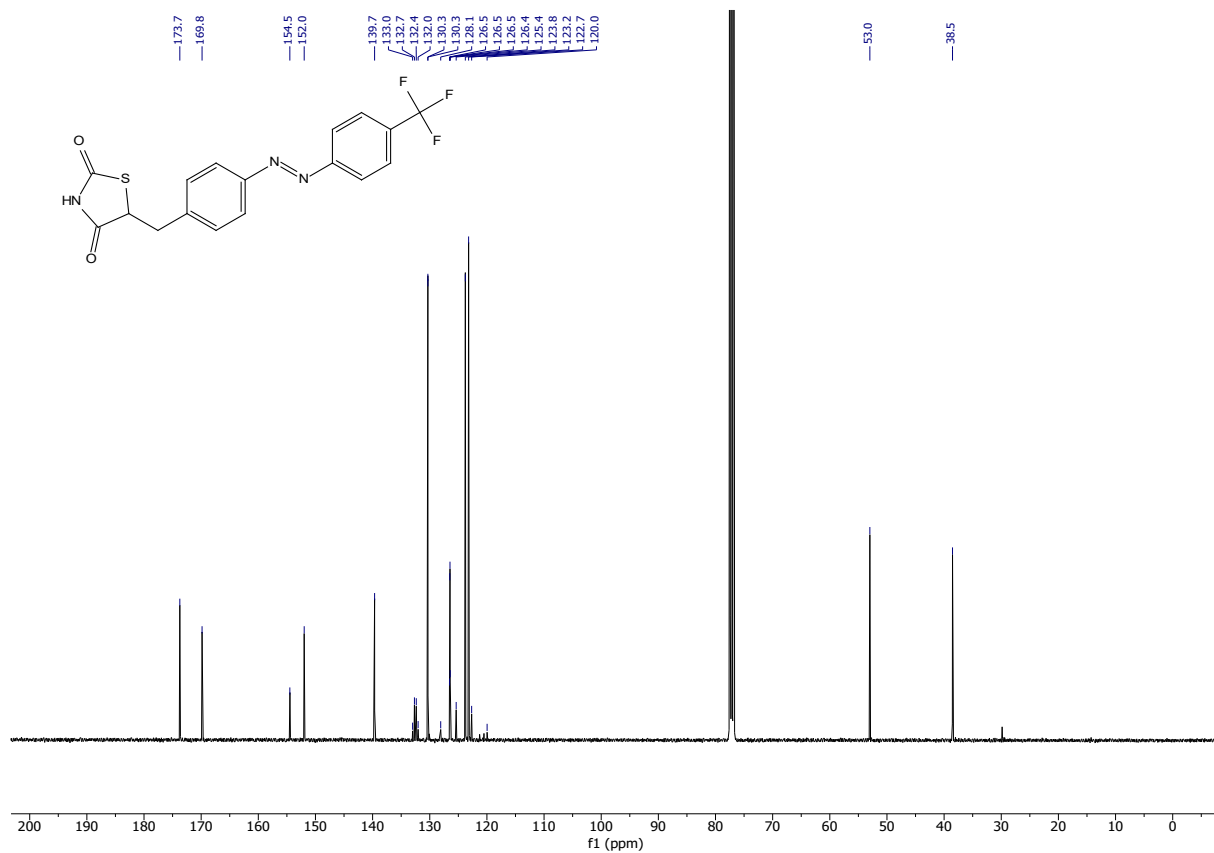
Peak #	RetTime [min]	Type	Width [min]	Area [mAU*s]	Height [mAU]	Area %
1	4.027	BB	0.0307	44.24614	20.46470	100.0000

Totals : 44.24614 20.46470

Signal 5: DAD1 E, Sig=420,4 Ref=590,100

AzoRosi-3





```

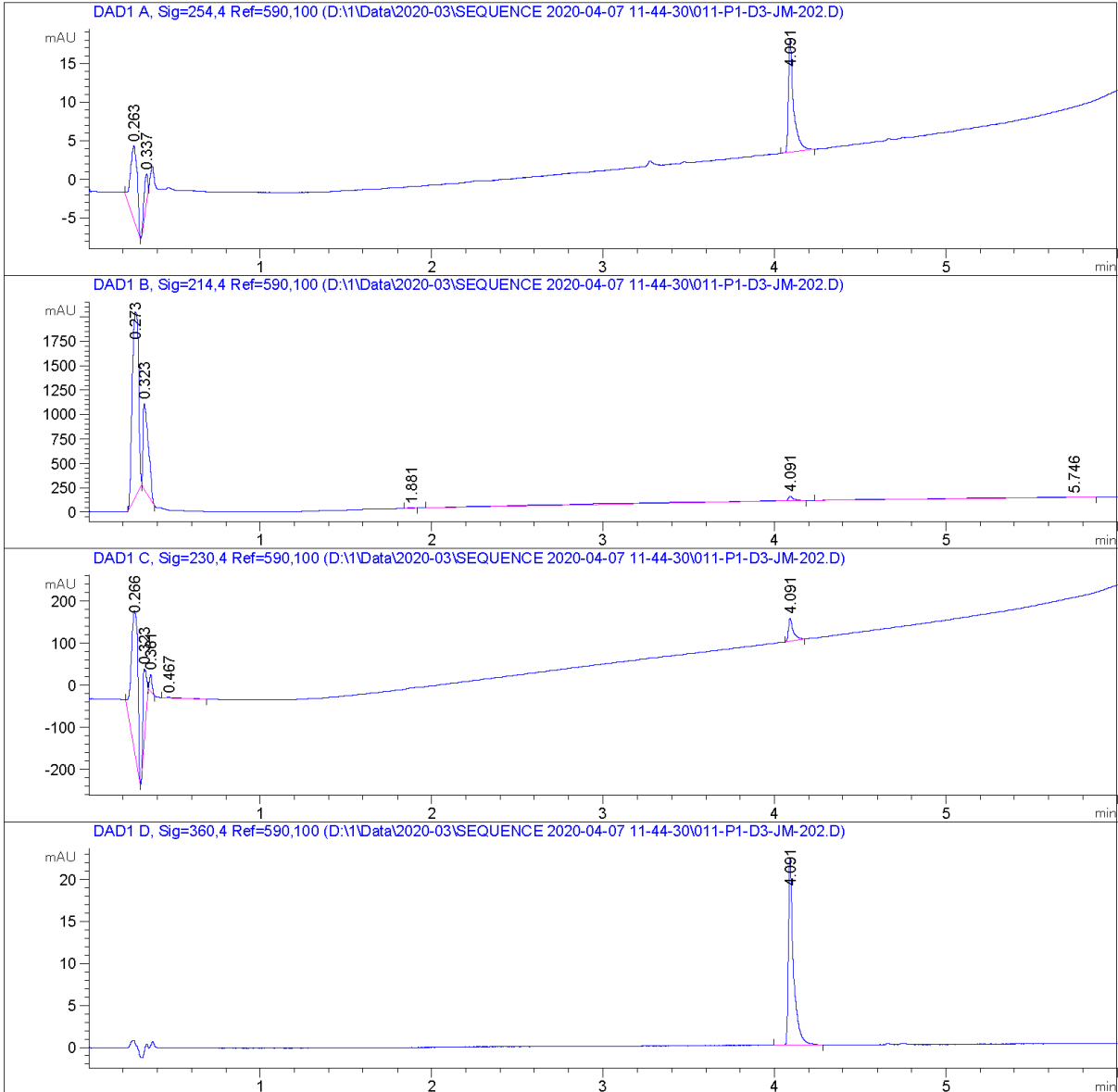
=====
Acq. Operator   : SYSTEM                      Seq. Line :   11
Acq. Instrument : LCMS                      Location  : P1-D3
Injection Date  : 4/7/2020 1:06:31 PM       Inj       :    1
                                           Inj Volume: 5.000 µl

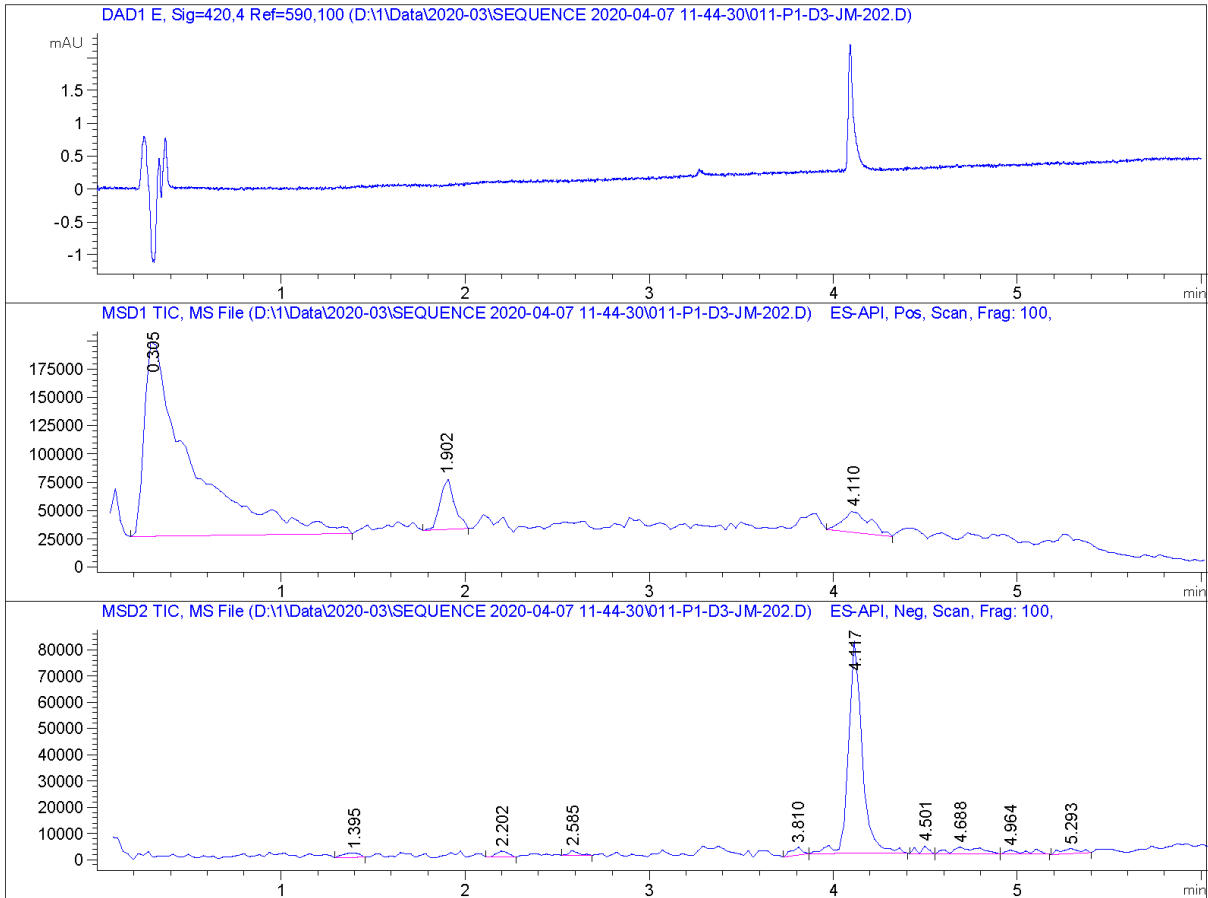
Method          : D:\1\Data\2020-03\SEQUENCE 2020-04-07 11-44-30\011-P1-D3-JM-202.D
                : uvvis 1 ml/min.M (Sequence Method)

Last changed    : 4/18/2018 2:31:20 PM by SYSTEM

Method Info     : FULL uv spectrum recording; eq 1 min with prerun macro; inject; 25 to 100%
                : B over 5 min, flush at 100% B for 1 min, no postrun, FULL uv spectrum
                : recording

```





=====
 Area Percent Report
 =====

Sorted By : Signal
 Multiplier : 1.0000
 Dilution : 1.0000
 Use Multiplier & Dilution Factor with ISTDs

Signal 1: DAD1 A, Sig=254,4 Ref=590,100

Peak #	RetTime [min]	Type	Width [min]	Area [mAU*s]	Height [mAU]	Area %
1	0.263	BB	0.0381	25.51149	9.43239	41.3674
2	0.337	BB	0.0273	5.84364	3.62553	9.4756
3	4.091	BB	0.0296	30.31535	14.65060	49.1570

Totals : 61.67049 27.70852

Signal 2: DAD1 B, Sig=214,4 Ref=590,100

Peak #	RetTime [min]	Type	Width [min]	Area [mAU*s]	Height [mAU]	Area %
1	0.273	BB	0.0429	4863.40820	1898.63660	63.4639
2	0.323	BB	0.0327	1900.50647	878.64752	24.8002
3	1.881	BB	0.0345	9.54535	4.36023	0.1246
4	4.091	BB	0.1565	583.50250	45.07872	7.6143
5	5.746	BB	0.6802	306.30579	5.26560	3.9971

Totals : 7663.26832 2831.98867

Signal 3: DAD1 C, Sig=230,4 Ref=590,100

Peak #	RetTime [min]	Type	Width [min]	Area [mAU*s]	Height [mAU]	Area %
1	0.266	BB	0.0432	866.26727	329.47742	69.8498
2	0.323	BB	0.0179	220.52608	173.05574	17.7817
3	0.361	BB	0.0157	37.51884	39.21706	3.0253
4	0.467	BB	0.1084	11.00784	1.26665	0.8876
5	4.091	BB	0.0280	104.86537	54.32415	8.4556

Totals : 1240.18540 597.34102

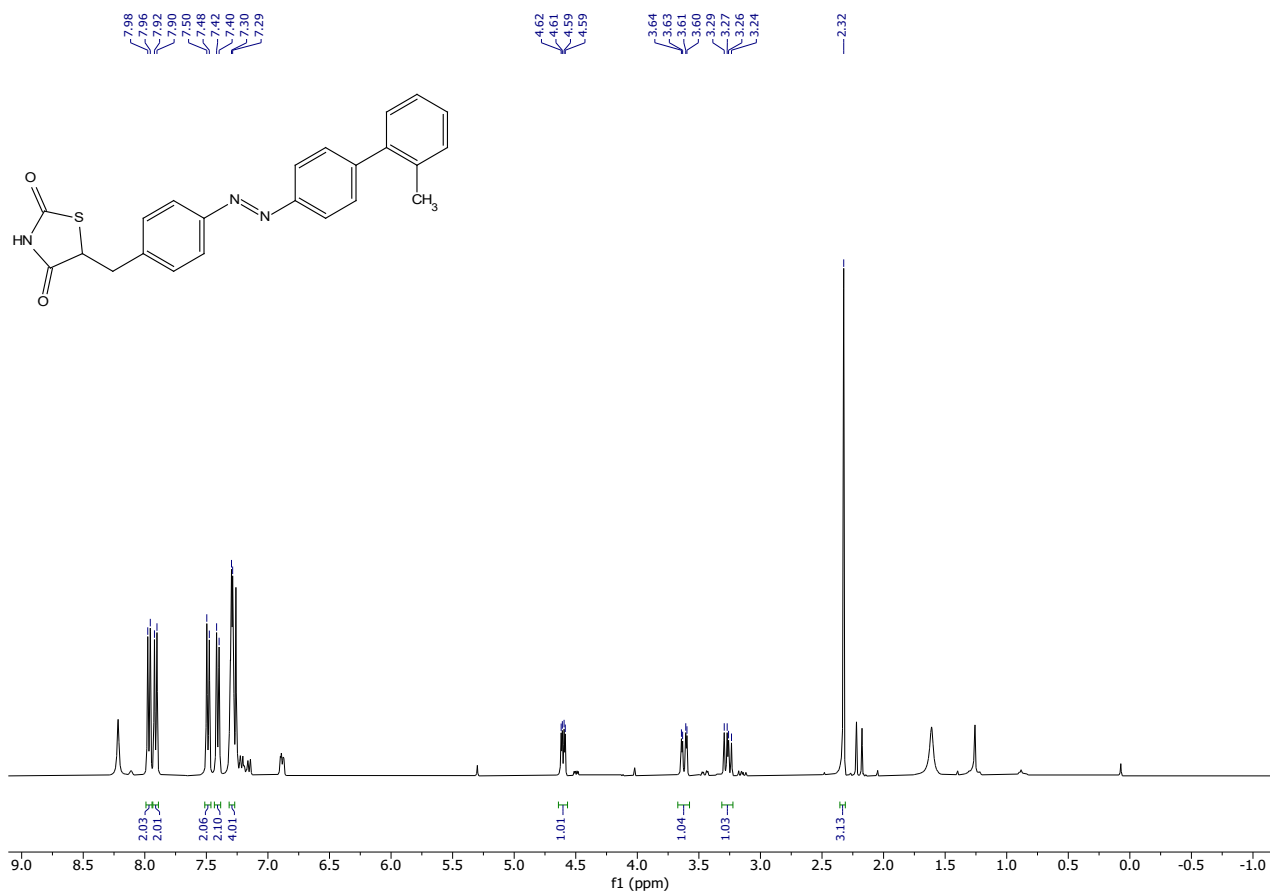
Signal 4: DAD1 D, Sig=360,4 Ref=590,100

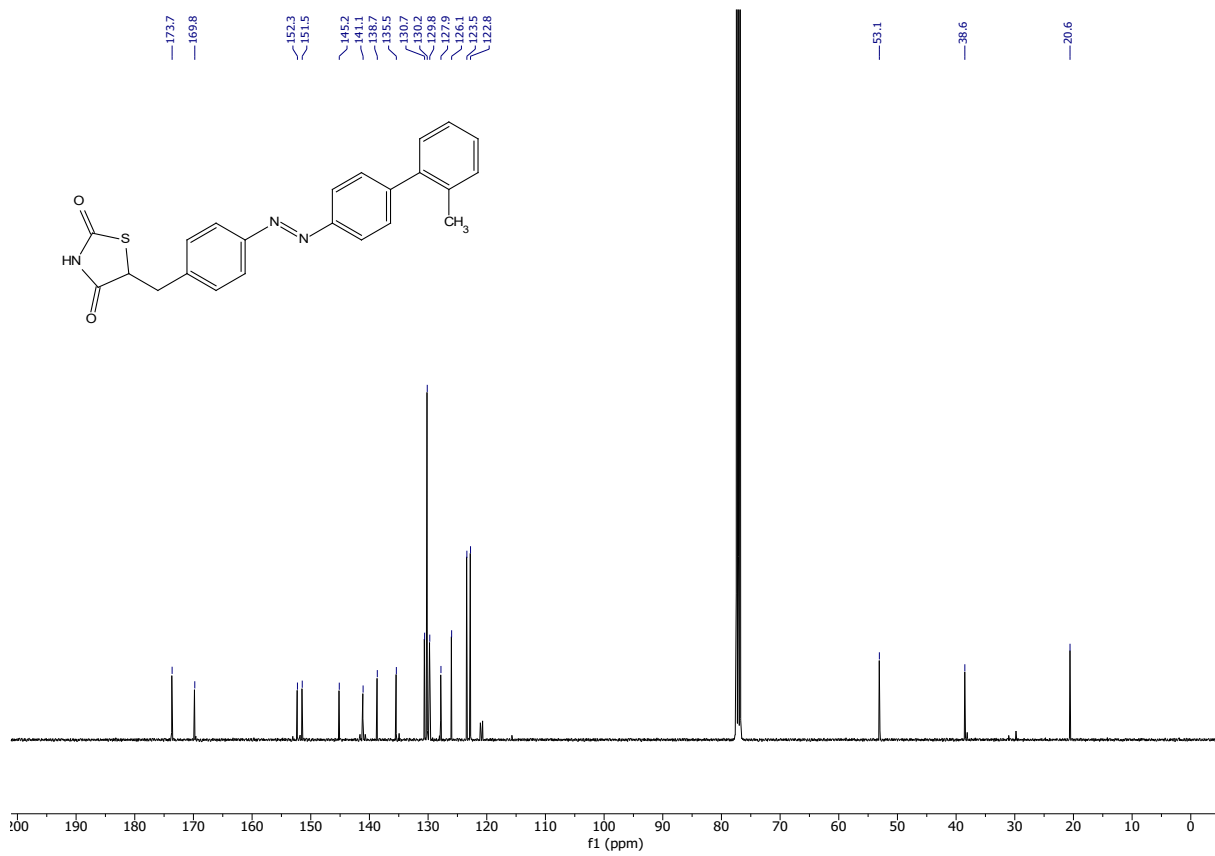
Peak #	RetTime [min]	Type	Width [min]	Area [mAU*s]	Height [mAU]	Area %
1	4.091	BB	0.0294	45.68192	22.28056	100.0000

Totals : 45.68192 22.28056

Signal 5: DAD1 E, Sig=420,4 Ref=590,100

AzoRosi-4

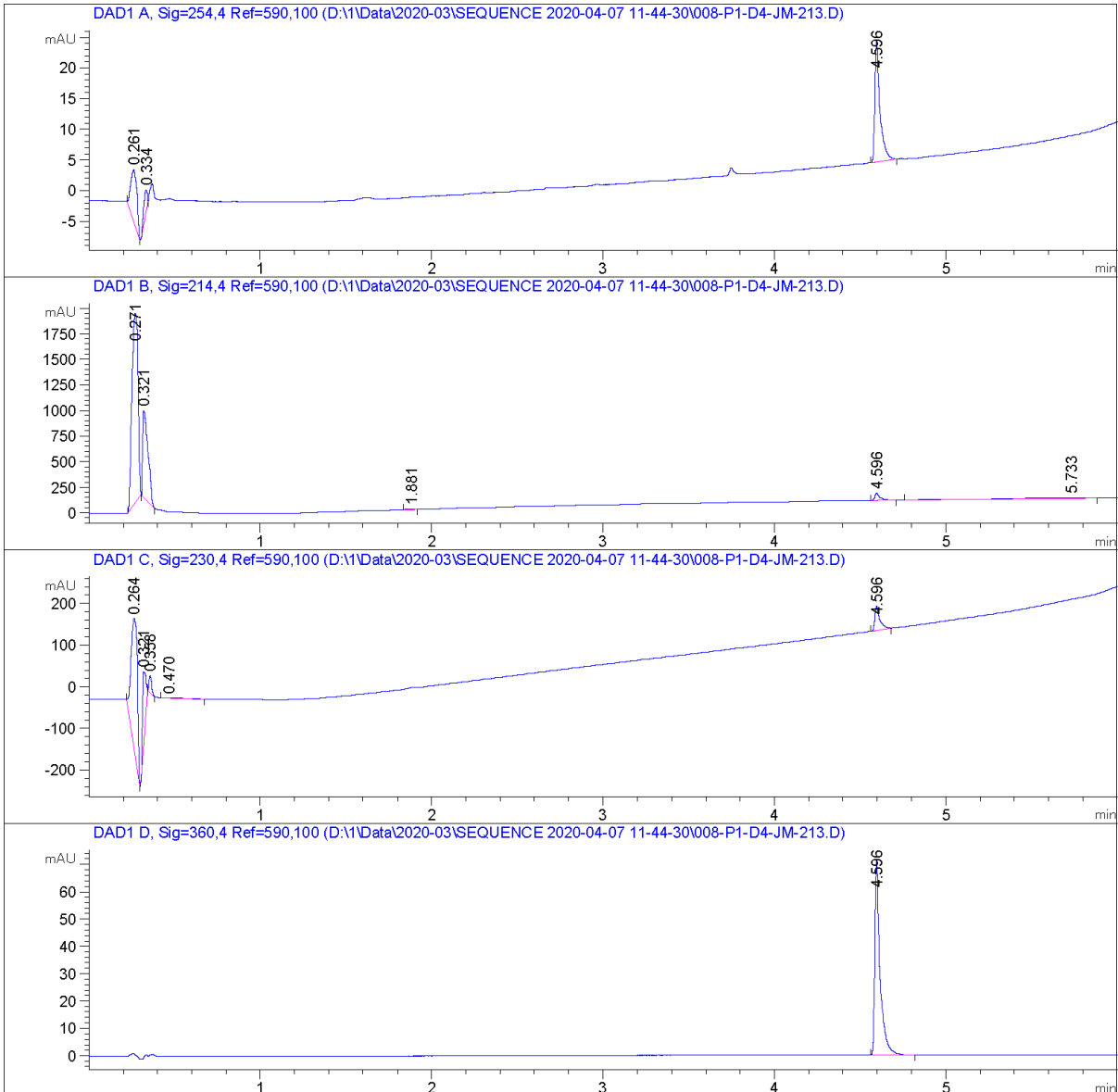


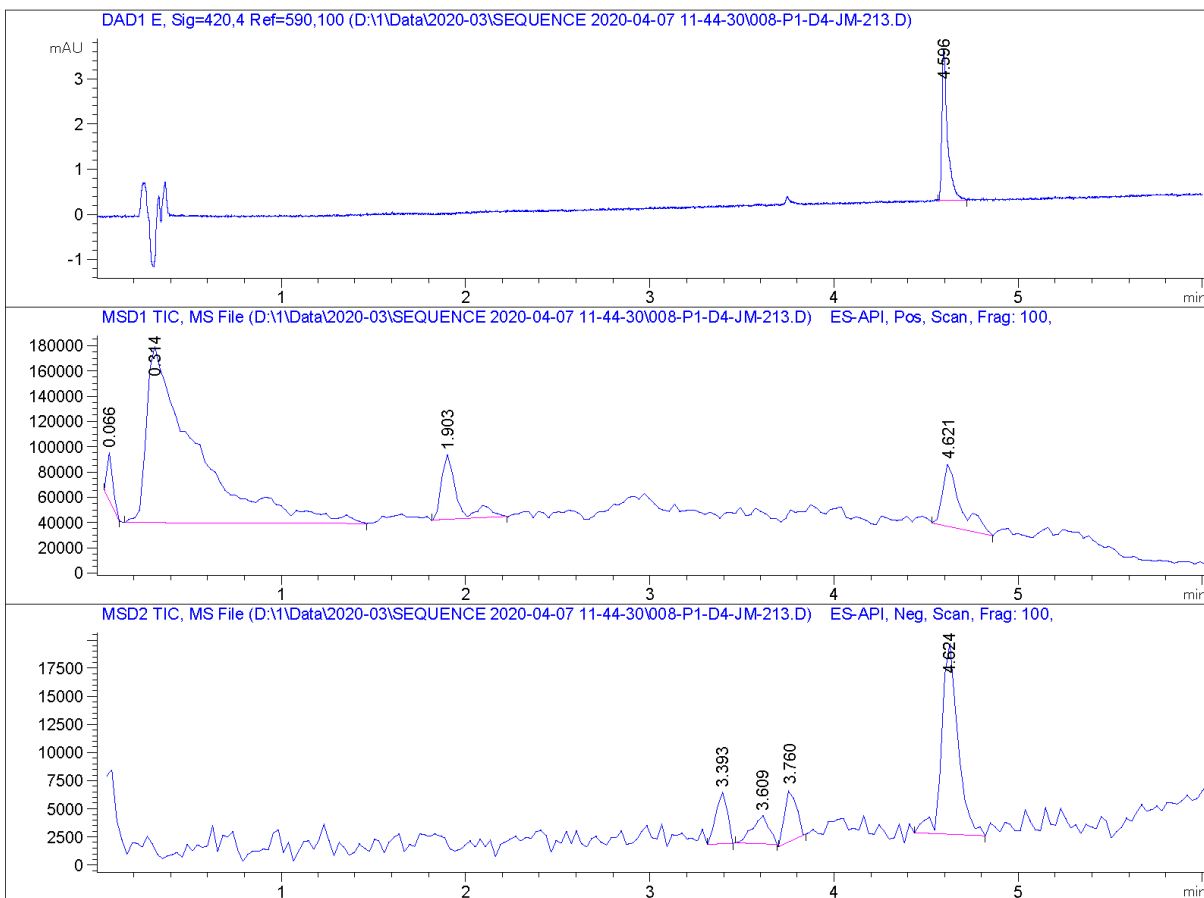


```

=====
Acq. Operator   : SYSTEM                               Seq. Line :    8
Acq. Instrument : LCMS                               Location  : P1-D4
Injection Date  : 4/7/2020 12:42:48 PM              Inj       :    1
                                                    Inj Volume: 5.000 µl

Method          : D:\1\Data\2020-03\SEQUENCE 2020-04-07 11-44-30\AZO 25% to100%B over5 min
                uvvis 1 mlmin.M (Sequence Method)
Last changed    : 4/18/2018 2:31:20 PM by SYSTEM
Method Info     : FULL uv spectrum recording; eq 1 min with prerun macro; inject; 25 to 100%
                B over 5 min, flush at 100% B for 1 min, no postrun, FULL uv spectrum
                recording
  
```





=====
 Area Percent Report
 =====

Sorted By : Signal
 Multiplier : 1.0000
 Dilution : 1.0000
 Use Multiplier & Dilution Factor with ISTDs

Signal 1: DAD1 A, Sig=254,4 Ref=590,100

Peak #	RetTime [min]	Type	Width [min]	Area [mAU*s]	Height [mAU]	Area %
1	0.261	BB	0.0338	21.03139	8.36906	31.0741
2	0.334	BB	0.0269	5.63250	3.57943	8.3221
3	4.596	BB	0.0296	41.01757	19.83499	60.6038

Totals : 67.68147 31.78348

Signal 2: DAD1 B, Sig=214,4 Ref=590,100

Peak #	RetTime [min]	Type	Width [min]	Area [mAU*s]	Height [mAU]	Area %
1	0.271	BB	0.0424	4597.81152	1853.67236	67.7838
2	0.321	BB	0.0323	1839.37866	849.63068	27.1173
3	1.881	BB	0.0362	10.31890	4.50889	0.1521
4	4.596	BB	0.0297	145.21613	70.08344	2.1409
5	5.733	BB	0.3946	190.32539	5.64810	2.8059

Totals : 6783.05061 2783.54346

Signal 3: DAD1 C, Sig=230,4 Ref=590,100

Peak #	RetTime [min]	Type	Width [min]	Area [mAU*s]	Height [mAU]	Area %
1	0.264	BB	0.0431	806.65173	312.26050	67.8114
2	0.321	BB	0.0185	214.92200	166.82777	18.0675
3	0.358	BB	0.0154	38.83908	39.66283	3.2650
4	0.470	BB	0.1117	14.47311	1.59019	1.2167
5	4.596	BB	0.0286	114.66630	57.88530	9.6395

Totals : 1189.55222 578.22659

Signal 4: DAD1 D, Sig=360,4 Ref=590,100

Peak #	RetTime [min]	Type	Width [min]	Area [mAU*s]	Height [mAU]	Area %
1	4.596	BB	0.0302	150.97096	71.44523	100.0000

Totals : 150.97096 71.44523

Signal 5: DAD1 E, Sig=420,4 Ref=590,100

Peak #	RetTime [min]	Type	Width [min]	Area [mAU*s]	Height [mAU]	Area %
1	4.596	BB	0.0303	7.12706	3.35655	100.0000

Totals : 7.12706 3.35655

Photophysical Characterization and Photostationary States (PSS)

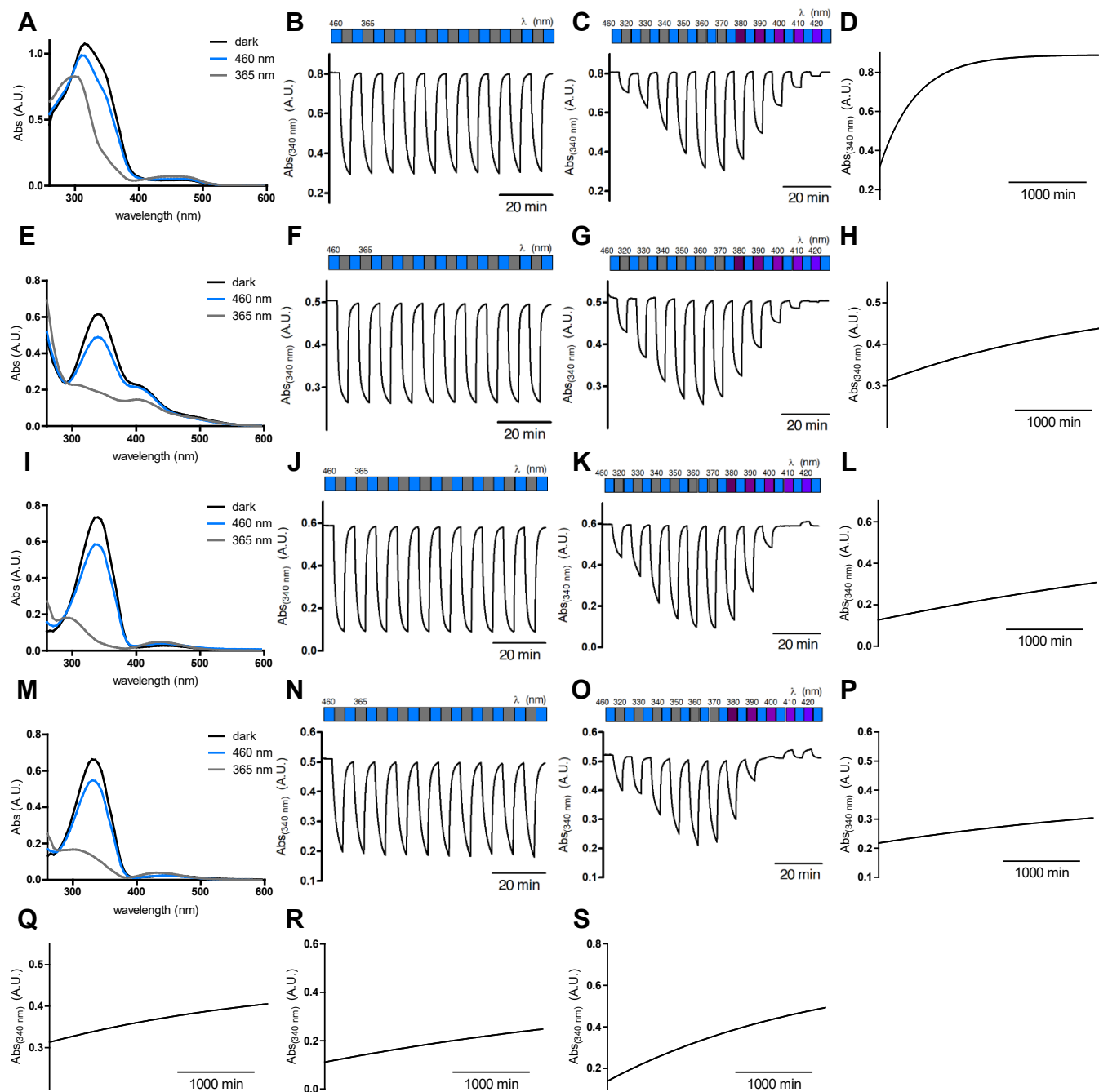


Figure S1 Photophysical evaluation of PPAR γ photohormones **AzoMDG548** (A-D), **AzoGW1929-2** (E-H), **AzoRosi-2** (I-L), **AzoRosi-3** (M-P), **AzoGW1929** (Q), **AzoRosi** (R) and **AzoRosi-4** (S). The UV-Vis spectra of the photohormones (25 μ M in DMSO) in the dark-adapted (*trans*, black), 365 nm-adapted (*cis*, gray) and 460 nm-adapted (*trans*, blue) photostationary states (A,E,I,M).

Reversible cycling of the photohormones (25 μM in DMSO) between photoisomers with alternating illumination at the two distinct wavelengths 365 nm and 460 nm (B,F,J,N). Reversible cycling between photoisomers of the photohormones (25 μM in DMSO) with alternating illumination at varying wavelengths between 320 nm and 420 nm (C,G,K,O). Natural thermal relaxation rates of the *cis*-isomers of the photohormones (25 μM in DMSO) at room temperature in the dark (D,H,L,P,Q,R,S).

Crystallography

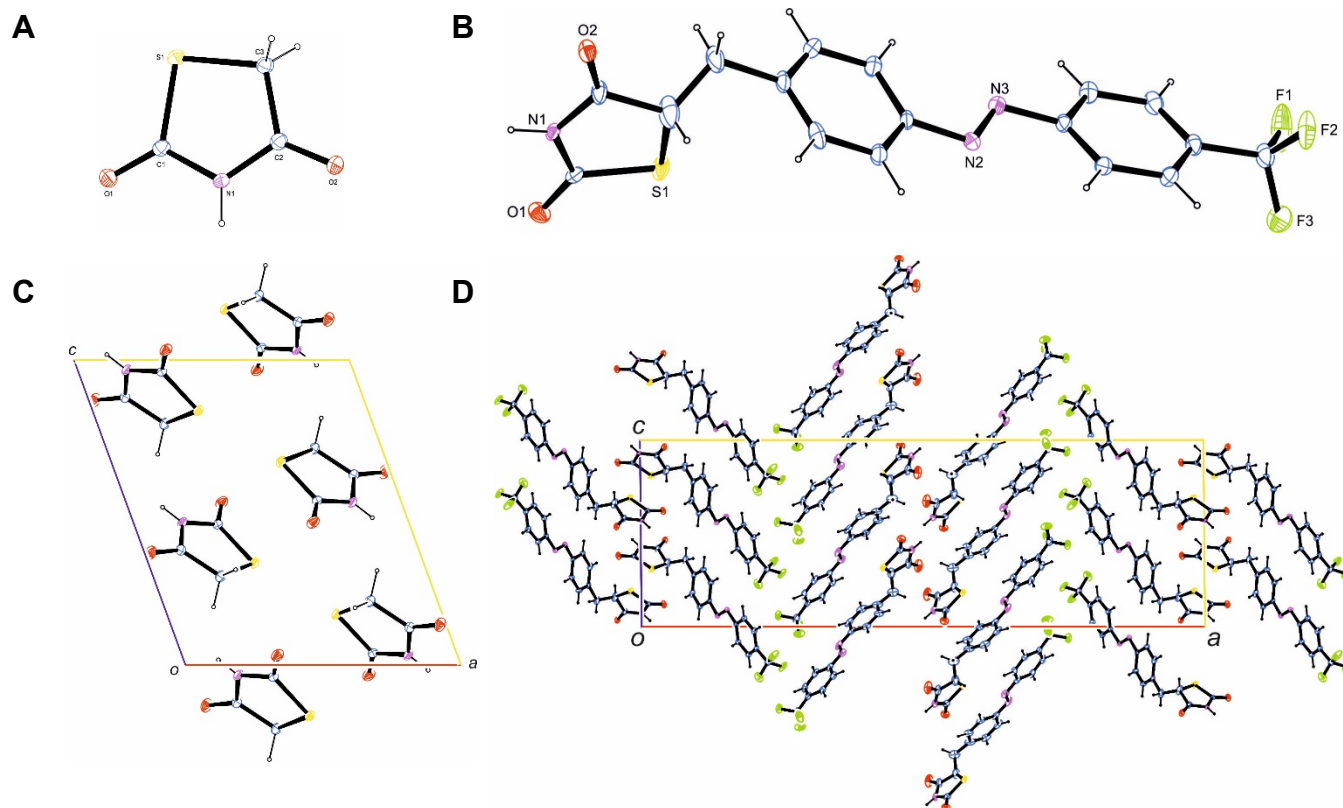


Figure S2 (A) Structure of thiazolidinedione **6** drawn at the 50% ellipsoid probability level. (B) Structure of *trans*-AzoRosi-3 drawn at the 50% ellipsoid probability level. (C) Cell of thiazolidinedione **6**. (D) Cell of *trans*-AzoRosi-3.

Table S1 Crystallographic data for thiazolidinedione **6** and *trans*-**AzoRosi-3**.

	Thiazolidinedione 6	<i>trans</i> - AzoRosi-3
net formula	C ₃ H ₃ NO ₂ S	C ₁₇ H ₁₂ F ₃ N ₃ O ₂ S
<i>M_r</i> /g mol ⁻¹	117.127	379.36
crystal size/mm	0.466 × 0.264 × 0.162	0.100 × 0.090 × 0.060
<i>T</i> /K	173(2)	100(2)
radiation	MoKα	MoKα
diffractometer	'Oxford XCalibur'	'Bruker D8 Venture TXS'
crystal system	monoclinic	monoclinic
space group	<i>P</i> 2 ₁ / <i>c</i>	' <i>P</i> 21/ <i>c</i> '
<i>a</i> /Å	8.6725(6)	41.211(2)
<i>b</i> /Å	5.3541(3)	5.7604(3)
<i>c</i> /Å	10.2330(8)	13.6180(7)
α/°	90	90
β/°	110.081(8)	90.4930(10)
γ/°	90	90
<i>V</i> /Å ³	446.27(5)	3232.7(3)
<i>Z</i>	4	8
calc. density/g cm ⁻³	1.74332(20)	1.559
μ/mm ⁻¹	0.585	0.251
absorption correction	'multi-scan'	multi-scan
transmission factor range	0.97519–1.00000	0.8803–0.9585
refls. measured	2322	38444
<i>R</i> _{int}	0.0223	0.0587
mean σ(<i>I</i>)/ <i>I</i>	0.0257	0.0525
θ range	4.24–26.37	2.966–26.47
observed refls.	820	4920
<i>x</i> , <i>y</i> (weighting scheme)	0.0292, 0.1830	0.0585, 15.7648
hydrogen refinement	H(C) constr, H(N) refall	constr
refls in refinement	916	6598
parameters	68	469
restraints	0	0
<i>R</i> (<i>F</i> _{obs})	0.0260	0.0847
<i>R</i> _w (<i>F</i> ²)	0.0670	0.2055
<i>S</i>	1.093	1.020
shift/error _{max}	0.001	0.001
max electron density/e Å ⁻³	0.335	1.890
min electron density/e Å ⁻³	-0.258	-0.870

Isothermal titration calorimetry (ITC)

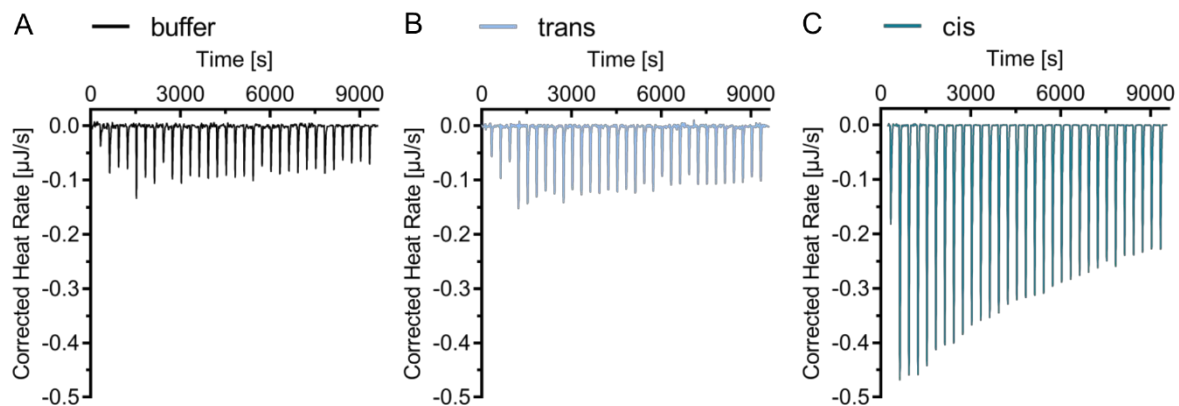


Figure S3 Isothermal titration calorimetry experiments show exclusive binding of *cis*-AzoRosi4 to recombinant PPAR γ LBD protein.

16.2 A Photohormone for Light-Dependent Control of PPAR α in Live Cells

Willems, S.[‡]; Morstein, J.[‡]; Hinnah, K.; Trauner, D.; Merk, D. A Photohormone for Light-dependent Control of PPAR α in Live Cells. *J. Med. Chem.* **2021**, *64* (14), 10393–10402.

[‡] *Hier liegt eine geteilte Erstautorenschaft zwischen S. W. und J. M. vor.*

Reprinted with permission from Willems, S.[‡]; Morstein, J.[‡]; Hinnah, K.; Trauner, D.; Merk, D. *J. Med. Chem.* **2021**, *64* (14), 10393–10402. Copyright (2021) American Chemical Society.

A Photohormone for Light-Dependent Control of PPAR α in Live Cells

Sabine Willems,[§] Johannes Morstein,[§] Konstantin Hinnah, Dirk Trauner,^{*} and Daniel Merk^{*}

Cite This: *J. Med. Chem.* 2021, 64, 10393–10402

Read Online

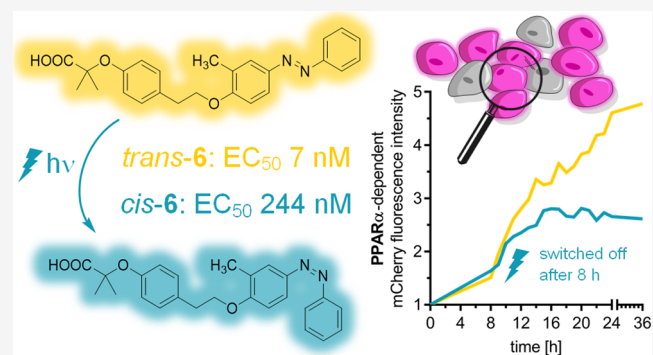
ACCESS |

Metrics & More

Article Recommendations

Supporting Information

ABSTRACT: Photopharmacology enables the optical control of several biochemical processes using small-molecule photoswitches that exhibit different bioactivities in their *cis*- and *trans*-conformations. Such tool compounds allow for high spatiotemporal control of biological signaling, and the approach also holds promise for the development of drug molecules that can be locally activated to reduce target-mediated adverse effects. Herein, we present the expansion of the photopharmacological arsenal to two new members of the peroxisome proliferator-activated receptor (PPAR) family, PPAR α and PPAR δ . We have developed a set of highly potent PPAR α and PPAR δ targeting photohormones derived from the weak pan-PPAR agonist GL479 that can be deactivated by light. The photohormone **6** selectively activated PPAR α in its *trans*-conformation with high selectivity over the related PPAR subtypes and was used in live cells to switch PPAR α activity on and off in a light- and time-dependent fashion.



INTRODUCTION

Photopharmacology utilizes photoswitchable small molecules as tools to obtain optical control of biological activity and modulate cellular processes with unprecedented spatiotemporal resolution.^{1–4} While this approach has been successfully established to control ion channels,^{5,6} membrane receptors,^{7–9} transporters,^{10–13} and enzymes,^{14–16} nuclear receptors (NRs) are fairly new to this proceeding. Upon binding of mainly amphiphilic ligands, NRs interact with specific DNA response elements to regulate the transcription of their target genes.^{17,18} The success of photoswitchable lipids¹⁹ suggests that fatty acid mimetic²⁰ NR ligands could also be suitable for photopharmacology. This could indeed be demonstrated with a few classes of NRs, including retinoic acid receptor α (RAR α), which can be optically controlled by a photoswitchable retinoic acid derivative.²¹ Subsequently, we have developed dedicated photohormones for the bile acid-activated transcription factor farnesoid X receptor (FXR)²² and the fatty acid-sensing peroxisome proliferator-activated receptor γ (PPAR γ),²³ and Tsuchiya et al. have reported a photoswitchable estrogen receptor (ER) agonist.²⁴ Still, in light of their value as chemical tools for pharmacology, the collection of available photoswitchable ligands for transcription factors is scarce.

The NRs' function governs multiple physiological processes, comprising embryonal development, cell proliferation, differentiation, metabolism, and homeostasis.²⁵ NR modulation by a wide variety of endogenous ligands, including thyroid and steroid hormones, bile acids, fatty acids, and vitamins causes intermediate (minutes) to prolonged (hours–days) actions.^{17,26}

The PPARs, belonging to the subfamily I of NRs (NR1C), comprise three isoforms PPAR α , PPAR δ , and PPAR γ , which are fatty acid- and lipid-activated transcription factors essentially involved in metabolic balance and inflammatory processes.²⁷ The PPAR α subtype is mainly expressed in tissues with high β -oxidation rates, such as the liver, brown adipose tissue, heart, and kidney, and is considered the master regulator of fatty acid catabolism, gluconeogenesis, and ketone body synthesis in a nutrition-dependent manner.^{27,28} Comparably, PPAR δ is involved in fatty acid uptake and oxidation, blood glucose homeostasis, and thermogenesis. It is ubiquitously expressed with main functions in skeletal muscles and brown adipose tissue.^{27,29,30} Both PPAR α and PPAR δ are closely linked to metabolic disorders, such as diabetes, cardiovascular disorders, nonalcoholic fatty liver disease (NAFLD), dyslipidemia, and obesity.^{30–32}

Here, we report the development of potent photoswitchable ligands for PPAR α and PPAR δ , extending the reach of photopharmacology to the remaining members of the important PPAR subfamily of nuclear receptors. Using a novel cellular test system embedding fluorescent reporter genes, we demonstrate a

Received: May 4, 2021

Published: July 2, 2021

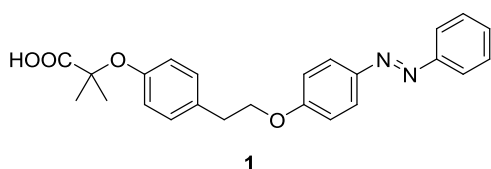


photoswitchable, time-resolved control of PPAR activation with these new photohormones in living cells.

RESULTS AND DISCUSSION

Owing to their superior photophysical properties, stability over multiple light-switching cycles, compatibility with various scaffolds, and ease of synthesis, azobenzenes have emerged as the most widely used compound class in photopharmacology.² Additionally, the photoswitching of azobenzenes employed in amphiphilic molecules is ideally suited to achieve reversible photoswitchable properties.³³ Based on these considerations, we employed GL479^{34,35} (**1**, Chart 1) as a lead compound, since it

Chart 1. Lead Compound pan-PPAR Agonist GL479 (**1**)

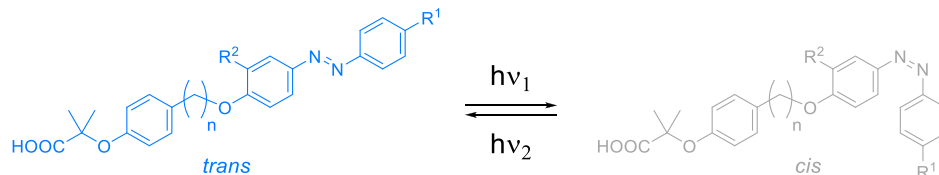


already contains an azobenzene linker but has not been previously investigated in a light-dependent fashion and was exclusively studied in the dark-adapted *trans*-form. GL479 (**1**) is a moderately potent pan-PPAR agonist with balanced potencies

on all PPARs but with a slight functional preference (higher efficacy) for the PPAR δ subtype (Table 1). Using light of wavelength $\lambda = 365$ nm for photoswitching, we also probed PPAR activation by the *cis*-isomer of **1**, which exhibited similar activity on all subtypes except a slight *trans*-preference for PPAR δ .

Co-crystal structures of the PPAR α (PDB ID: 4CI4) and PPAR γ (PDB ID: 4CI5)³⁶ ligand binding domains (LBDs) in complex with **1** were available for structure-based optimization. To obtain structural insights for PPAR δ , we employed molecular docking using a high-resolution PPAR δ co-crystal structure with a close analogue of the PPAR δ selective agonist GW501516³⁷ (PDB ID: 5Y7X)^{38,39} as a template. Initially, we studied the chain length of the alkoxy linker between the aromatic systems for potential optimization of the scaffold (Figure S1). Shortening by one carbon (**2**) appeared to be well-tolerated, while the further shortened diphenylether failed to span the ample binding pocket. As a result, the methyl propionate side chain was not properly placed in the lipophilic subpocket of PPAR α formed by Phe273, Val444, Leu456, and Leu460, but its methyl decoration clashed with His440. The extended chain of the phenoxypropyl analogue of **1**, in contrast, was too long causing a twisted conformation and a clash with Ser280. The phenoxyethyl (**1**) and phenoxyethyl (**2**) linkers were hence favored according to the docking studies.

Table 1. PPAR Modulatory Activity of GL479 (**1**) and Derivatives 2–11^a



#	R ¹	R ²	n	conf.	EC ₅₀ [μ M] (max. rel. act. [%])		
					PPAR α	PPAR γ	PPAR δ
1 (GL479)	-H	-H	2	<i>trans</i>	1.09 \pm 0.02 (31 \pm 1)	2.67 \pm 0.16 (25 \pm 1)	2.2 \pm 0.1 (61 \pm 2)
				<i>cis</i>	0.8 \pm 0.2 (29 \pm 2)	6.0 \pm 0.6 (28 \pm 2)	6 \pm 1 (34 \pm 6)
2	-H	-H	1	<i>trans</i>	3.7 \pm 0.3 (40 \pm 3)	5.40 \pm 0.07 (23 \pm 1)	2.8 \pm 0.3 (40 \pm 3)
				<i>cis</i>	3.5 \pm 0.7 (28 \pm 3)	6.6 \pm 0.3 (22 \pm 1)	4.1 \pm 0.2 (26 \pm 1)
3	-CH ₃	-H	2	<i>trans</i>	0.66 \pm 0.07 (24 \pm 1)	EC ₅₀ > 10 μ M (toxic \geq 6 μ M)	1.42 \pm 0.09 (33 \pm 1)
				<i>cis</i>	1.1 \pm 0.2 (22 \pm 3)	EC ₅₀ > 10 μ M	3.8 \pm 0.8 (31 \pm 5)
4	-Cl	-H	2	<i>trans</i>	0.79 \pm 0.09 (26 \pm 1)	3.2 \pm 1.3 (14 \pm 1)	8 \pm 2 (39 \pm 6)
				<i>cis</i>	1.1 \pm 0.2 (24 \pm 2)	EC ₅₀ > 10 μ M	8.1 \pm 0.4 (28 \pm 1)
5	-CH(CH ₃) ₂	-H	2	<i>trans</i>	0.47 \pm 0.01 (25 \pm 1)	2.1 \pm 0.2 (54 \pm 3)	1.77 \pm 0.07 (40 \pm 1)
				<i>cis</i>	0.28 \pm 0.05 (19 \pm 2)	2.6 \pm 0.2 (17 \pm 1)	3.4 \pm 0.2 (22 \pm 1)
6	-H	-CH ₃	2	<i>trans</i>	0.0070 \pm 0.0006 (38 \pm 1)	1.2 \pm 0.1 (20 \pm 1)	0.54 \pm 0.04 (45 \pm 1)
				<i>cis</i>	0.24 \pm 0.02 (43 \pm 1)	1.7 \pm 0.8 (24 \pm 1)	3.0 \pm 0.5 (41 \pm 4)
7	-H	-Cl	2	<i>trans</i>	0.029 \pm 0.004 (49 \pm 2)	0.82 \pm 0.07 (14 \pm 1)	0.24 \pm 0.02 (46 \pm 1)
				<i>cis</i>	0.040 \pm 0.003 (45 \pm 1)	0.92 \pm 0.08 (22 \pm 1)	0.35 \pm 0.06 (44 \pm 2)
8	-H	-CF ₃	2	<i>trans</i>	0.009 \pm 0.002 (46 \pm 2)	0.6 \pm 0.1 (34 \pm 2)	0.14 \pm 0.01 (45 \pm 2)
				<i>cis</i>	0.071 \pm 0.007 (42 \pm 1)	0.77 \pm 0.07 (32 \pm 1)	0.31 \pm 0.03 (37 \pm 2)
9	-CH ₃	-CH ₃	2	<i>trans</i>	0.036 \pm 0.006 (34 \pm 2)	2.3 \pm 0.1 (77 \pm 2)	0.12 \pm 0.01 (47 \pm 1)
				<i>cis</i>	0.64 \pm 0.08 (26 \pm 2)	1.2 \pm 0.3 (23 \pm 2)	0.8 \pm 0.1 (32 \pm 1)
10	-CH ₃	-CF ₃	2	<i>trans</i>	0.07 \pm 0.01 (87 \pm 5)	1.2 \pm 0.2 (65 \pm 5)	0.113 \pm 0.004 (43 \pm 1)
				<i>cis</i>	0.19 \pm 0.01 (41 \pm 1)	1.3 \pm 0.2 (33 \pm 2)	0.41 \pm 0.09 (40 \pm 6)
11	-CH ₃	-Cl	2	<i>trans</i>	0.04 \pm 0.01 (76 \pm 8)	4.5 \pm 0.2 (68 \pm 2)	0.12 \pm 0.02 (65 \pm 4)
				<i>cis</i>	0.29 \pm 0.05 (41 \pm 4)	4.8 \pm 0.4 (42 \pm 2)	0.38 \pm 0.03 (35 \pm 2)

^aActivities were determined in uniform Gal4 hybrid reporter gene assays in HEK293T cells. Maximum relative activation (max. rel. act.) refers to the activity of the respective reference agonist (PPAR α : GW7647; PPAR γ : pioglitazone; PPAR δ : L165,041; each at 1 μ M). Data are the mean \pm standard deviation (SD), $n \geq 3$.

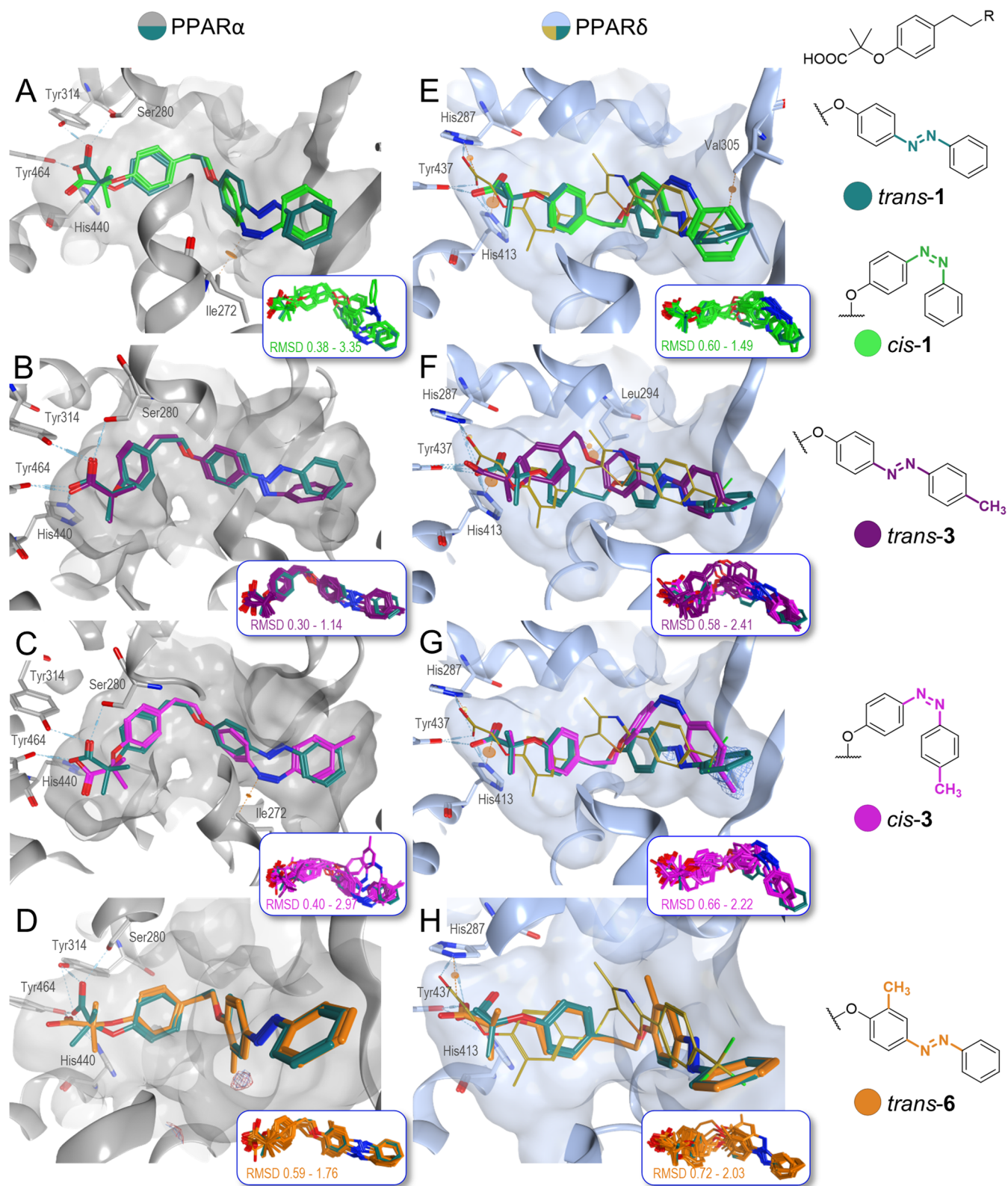
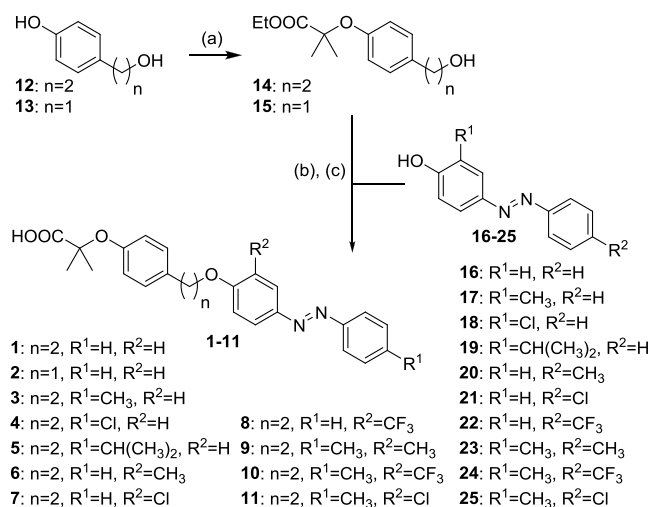


Figure 1. Molecular docking of 1, 3, and 6 to reveal optimization potential. *Trans*-1 (teal) is shown in all models for comparison. (A–D) PPAR α binding site (gray) from the co-crystal structure with lead 1 (teal, PDB ID: 4CI4³⁶) and (E–H) PPAR δ pocket (light blue) with the docked lead structure 1 for comparison (PDB ID: 5Y7X³⁸). The insets show overlays of the top 10 binding poses for each structure with their respective root-mean-square deviation (RMSD) range to the pose shown in the binding site. Docking of *cis*-1 (green, A and E) suggested that binding of the *cis*-counterpart is not favored. Terminal elongation with a *p*-methyl group enables improved binding modes of 3 in *trans*- (purple, B and F) and *cis*-states (magenta, G). An *o*-methyl residue introduced in 6 (orange, D and H) extends into a lipophilic cavity. Also see Figures S1 and S2.

In line with the activities observed *in vitro*, docking of **1** in *trans*- and *cis*-states revealed slightly unfavorable binding modes for the *cis*-counterpart with clashes of the azo linker (Figure 1A) and the terminal phenyl ring (Figure 1E). No clashes were observed for the shortened analogue *cis*-2, and several sound binding poses were predicted (Figure S1). These computational observations suggested **1** as a preferable lead for the development of *trans*-selective analogues and that *trans*-binding might be optimized by extension in the *para*-position of the terminal ring to hinder *cis*-binding (Figure 1C,G). Introduction of a methyl group in the *para*-position was well-tolerated by PPAR α as *trans*-3 and the co-crystallized ligand aligned well (Figure 1B). However, molecular docking of the extended *trans*-3 to the PPAR δ ligand binding site revealed its *cis*-counterpart *cis*-3 as the two top-ranked poses (Figures 1F,G and S2A). This observation together with high-energy barriers for *cis/trans*-isomerization of 43–52 kcal/mol in the forcefield used for the calculations (Amber10:EHT, Figure S3A,B) suggested less preference of PPAR δ for *trans*-binding. Further structural analysis indicated that introduction of methyl, chlorine, or trifluoromethyl modifications in the *ortho*-position of the central phenyl ring would address unoccupied space in the binding sites of PPAR α and PPAR δ to enhance affinity (Figure 1D,H). Especially in PPAR α , introduction of a methyl group in the *ortho*-position (**6**) seemed favorable as the moiety extended toward a lipophilic subpocket (Figures 1D and S2B).

Following these computational observations, we studied analogues **2–11** for improved optical control of PPAR α and PPAR δ (Scheme 1). All photohormone candidates **1–11** were

Scheme 1. Synthesis of **1–11**^a



^aReagents and conditions: (a) ethyl 2-bromo-2-methylpropanoate, K₂CO₃, DMF, reflux, 4 h, 47–80%; (b) azobenzenes **16–25**, PPh₃, DEAD, THF, room temperature (rt), 16 h; and (c) NaOH, EtOH, rt, 16 h, 20–93% over two steps.

obtained from the respective esters **14** and **15** following an S_N2 reaction of the phenols **12** and **13** with ethyl 2-bromo-2-methylpropanoate and K₂CO₃ in dimethylformamide (DMF) as previously reported.³⁴ The Mitsunobu reaction of **14** and **15** with the commercially available azobenzenes **16–25** using triphenylphosphine and diethyl azodicarboxylate (DEAD) in tetrahydrofuran (THF) and subsequent saponification of the obtained esters under basic conditions gave the desired carboxylic acids **1–11** (Scheme 1).

The biological evaluation of the photoswitchable ligands for PPAR modulation was performed in uniform hybrid Gal4 reporter gene assays in HEK293T cells. These test systems utilize chimeric constructs composed of the respective human nuclear receptor LBD and the DNA-binding domain of the Gal4 protein derived from yeast. Gal4-responsive firefly luciferase was used as a reporter gene, and constitutively expressed *Renilla* luciferase served for normalization and to monitor test compound toxicity. GW7647, Pioglitazone, and L165,041 (each at 1 μM) served as reference agonists for the three PPAR isoforms α, γ, and δ, respectively, to obtain the relative activation efficacy of the test compounds. To characterize both isomers of **1–11** individually, all assays were conducted with the *trans*-isomers in the dark and with the preilluminated *cis*-isomers (λ = 365 nm) using a Cell DISCO^{40,41} system during incubation. The biological activity of **1–11** is shown in Table 1.

Profiling of the lead compound GL479 (**1**) revealed agonism on all three PPAR isoforms with low micromolar EC₅₀ values in consistence with the previously reported data for PPAR α and γ.^{34,35} The *trans*-**1** and *cis*-**1** isomers exhibited comparable activity, except for a weak preference for *trans*-**1** on PPAR δ . Aiming to improve upon the potency, subtype-selectivity, and *trans*-preference of this new photohormone chemotype, we systematically varied the structural features of **1** suggested by molecular docking to hold optimization potential. Chain shortening by one carbon in *cis/trans*-**2** slightly reduced potency, thereby not evolving as a preferred modification and was not further pursued. Extension in the *para*-position of the terminal phenyl motif of **1** with methyl- (**3**) and chloro- (**4**) substituents hardly affected potency but slightly improved the desired *trans*-preference on PPAR α . The isopropyl analogue **5**, in contrast, was slightly more active on PPAR α than **1** with a preference for the *cis*-conformation. Additionally, the *para*-modifications (**3–5**) moderately improved selectivity over PPAR γ . Overall, **3–5** failed to provide a marked structural optimization. Hence, we focused our attention on the *ortho*-position of the central phenyl motif (**6–8**). As suggested by molecular docking, introduction of a methyl group (**6**) provided a remarkable improvement in PPAR α agonism, which was accompanied by a pronounced preference for *trans*-**6**. This modification was also favored by PPAR δ in terms of potency and *trans*-preference despite a smaller impact. Activity on PPAR γ was not affected, resulting in strongly improved selectivity over this PPAR subtype. A chlorine atom in the *ortho*-position (**7**) increased potency on PPAR α and PPAR δ as well, but *trans*-preference was lost. Trifluoromethyl analogue **8** was also very potent on PPAR α and exhibited a 10-fold preference for the *trans*-state but was not superior to **6**. On PPAR δ , trifluoromethyl substitution (**8**) evolved as the most favored modification in terms of potency. In an attempt to fuse the terminal (**3–5**) and central modifications (**6–8**) of the GL479 scaffold, we first combined methyl groups in both positions (**9**), resulting in a potent dual PPAR α /δ agonist with pronounced *trans*-preference but moderate activation efficiency. The combination of the terminal methyl motif with a trifluoromethyl group on the central ring (**10**) markedly improved activation efficiency with a slight loss in potency on PPAR α and less *trans*-preference while a chlorine atom on the central ring (**11**) resulted in balanced high potency on PPAR α /δ with strong activation efficiency and higher *trans*-preference. Additionally, **11** was selective for PPAR α /δ over PPAR γ . Overall, the computer-aided structural refinement of GL479 (**1**) as a photohormone yielded the highly potent and selective photoswitchable PPAR α agonist **6** (Figure

2A,B) and the dual PPAR α / δ photohormone **11**, which was equally equipped with favorable potency and selectivity (Figure

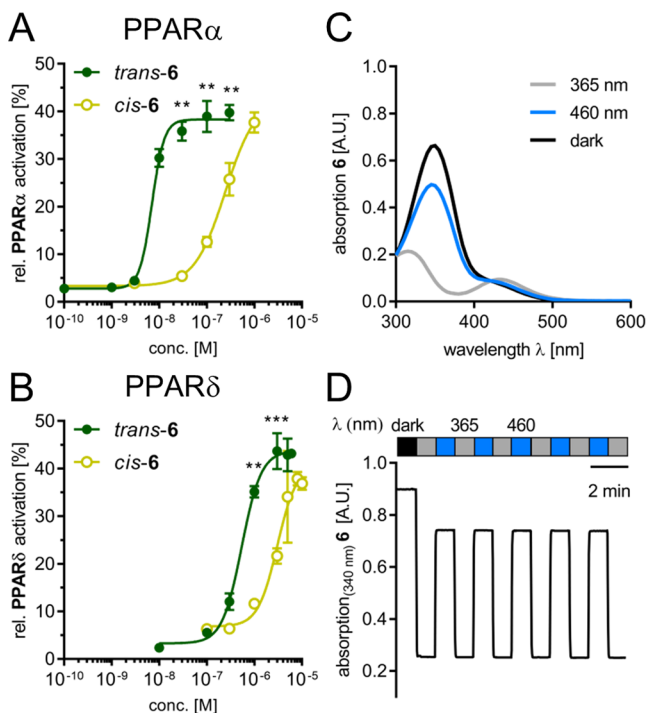


Figure 2. Characterization of photohormone **6**. Dose–response curves in cellular Gal4-PPAR α (A) or Gal4-PPAR δ (B) hybrid reporter gene assays in HEK293T cells. *Cis-6* was preilluminated ($\lambda = 365$ nm, 3 min) and maintained in *cis*-state with a Cell DISCO system.^{40,41} Relative activation refers to 1 μ M GW7647 (PPAR α) or L165,041 (PPAR δ). Data are the mean \pm SD, $n \geq 3$. ** $p < 0.01$ and *** $p < 0.001$ (*t*-test vs *cis-6*). Photophysical characteristics of **6**: UV–vis absorption scans (C, 50 μ M in dimethyl sulfoxide (DMSO)) in dark-adapted (*trans*, black), 460 nm adapted (*trans*, blue), and 365 nm adapted (*cis*, gray) photostationary states. (D) Reversible cycling (50 μ M in DMSO) with alternating illumination at 365 and 460 nm.

S4A,B). The PPAR α selective photohormone **6** additionally revealed high stability against microsomal degradation with an in vitro half-life of 103 ± 20 min (Figure S5), suggesting favorable metabolic stability and potential for in vivo applications.

Photophysical characterization of the new photohormones **6** and **11** by UV–vis spectroscopy upon illumination with $\lambda = 460$ nm (*trans*, blue) and $\lambda = 365$ nm (*cis*, gray) confirmed wavelength-dependent switching (Figures 2C and S4C), and repeated photoswitching over multiple cycles demonstrated high photostability (Figures 2D and S4D; 1 in Figure S3C,D).

Intrigued by the favorable activity profile and photophysical properties of the photohormones **6** and **11**, we studied their applicability as tools in a cellular setting. To reflect spatiotemporal control as a key feature of photopharmacology, we established a new cellular assay to observe time-resolved nuclear receptor activation and reversible activity of photohormones in intact living cells over a long time period.

For this, we used Gal4-responsive fluorescent mCherry or enhanced green fluorescent protein (eGFP) expression constructs as reporter genes in HEK293T cells. After transient transfection with the reporter and Gal4-PPAR α , cells were treated with photohormone **6** (Figure 3A). Light ($\lambda = 460$ and 365 nm) was used for switching between *cis*- and *trans*-conformations, and a Cell DISCO system^{40,41} (75 ms light

pulses every 15 s) served to maintain the *cis*-conformation while using a minimal nontoxic light dose. mCherry fluorescence was measured every hour starting 8 h after addition of **6** (10 nM). When cells were treated with *trans-6*, a constant increase in mCherry fluorescence was observed between 8 and 24 h after incubation (Figure 3A, blue curve). When cells were initially treated with *cis-6* for 8 h before switching to the *trans*-counterpart, the mCherry signal was markedly delayed (Figure 3A, red curve). By contrast, when cells were initially treated with *trans-6* before switching to the *cis*-form after 8 h, the mCherry signal initially increased similar to pure *trans-6* treatment for 2 h and then reached a low plateau with no further increase (Figure 3A, green curve). Similar observations were made with photohormone **11** on Gal4-PPAR δ (Figure S6A). Hence, photohormones **6** and **11** enable spatiotemporal control of the transcription factors PPAR α and PPAR δ .

Next, we studied selective and dual optical control of PPAR α and PPAR δ in a similar setting (Figure 3B). HEK293T cells were transiently transfected with Gal4-responsive mCherry and Gal4-PPAR α or Gal4-responsive eGFP and Gal4-PPAR δ . The cells were then pooled 5 h after transfection and treated with DMSO (0.1%), *cis*-/*trans-6*, or *cis*-/*trans-11*, and the fluorescence of mCherry and eGFP was determined after 40 h using a fluorescence microscope (Figures 3B, S6B, and S7). DMSO-treated cells revealed almost no mCherry or eGFP fluorescence. *Trans-6* at 10 nM markedly induced mCherry expression while *cis-6* had almost no effect, demonstrating optical control of PPAR α activity. At a higher concentration (300 nM), the mCherry signals were similar for *cis*- and *trans-6*, and slight eGFP fluorescence indicated weak PPAR δ activation. Hence, the photohormone **6** allows for strong, selective, and light-dependent PPAR α activation at a low 10 nM concentration, qualifying **6** as an attractive tool for photopharmacology.

CONCLUSIONS

Photohormones have evolved as a new attractive type of tool compounds that enable light-dependent modulation of transcription factors to achieve spatiotemporal control of transcriptional activity. As shown by our live-cell fluorescence reporter gene assay, this allows for photoswitching between transcriptionally active and inactive states, hence presenting photohormones as valuable in vitro tools for functional studies. In the field of nuclear receptors, temporal control appears particularly relevant since these (hormone) receptors are endogenously activated by short-lived molecules such as hormones and reactive metabolites. Hence, nuclear receptors are shortly stimulated under physiological conditions, which can be unmatched mimicked with photohormones. The importance of time in nuclear receptor modulation is further highlighted by their involvement in the circadian clock. Beyond this, optical control of nuclear receptor activity may also gain therapeutic relevance as it opens an avenue to local activation and inactivation, for example, with wirelessly powered and biodegradable optoelectronics to convert photohormones between active and inactive conformations in certain tissues.⁴² This may enable reduction of target-mediated adverse effects that cannot be avoided by conventional structural optimization to improve selectivity. Photohormones, in contrast, can be on-site activated or deactivated to spare tissues in which the target of interest mediates side effects. In vivo studies have shown that such optical control has therapeutic potential in metabolic diseases⁴³ and cancer.^{40,44}

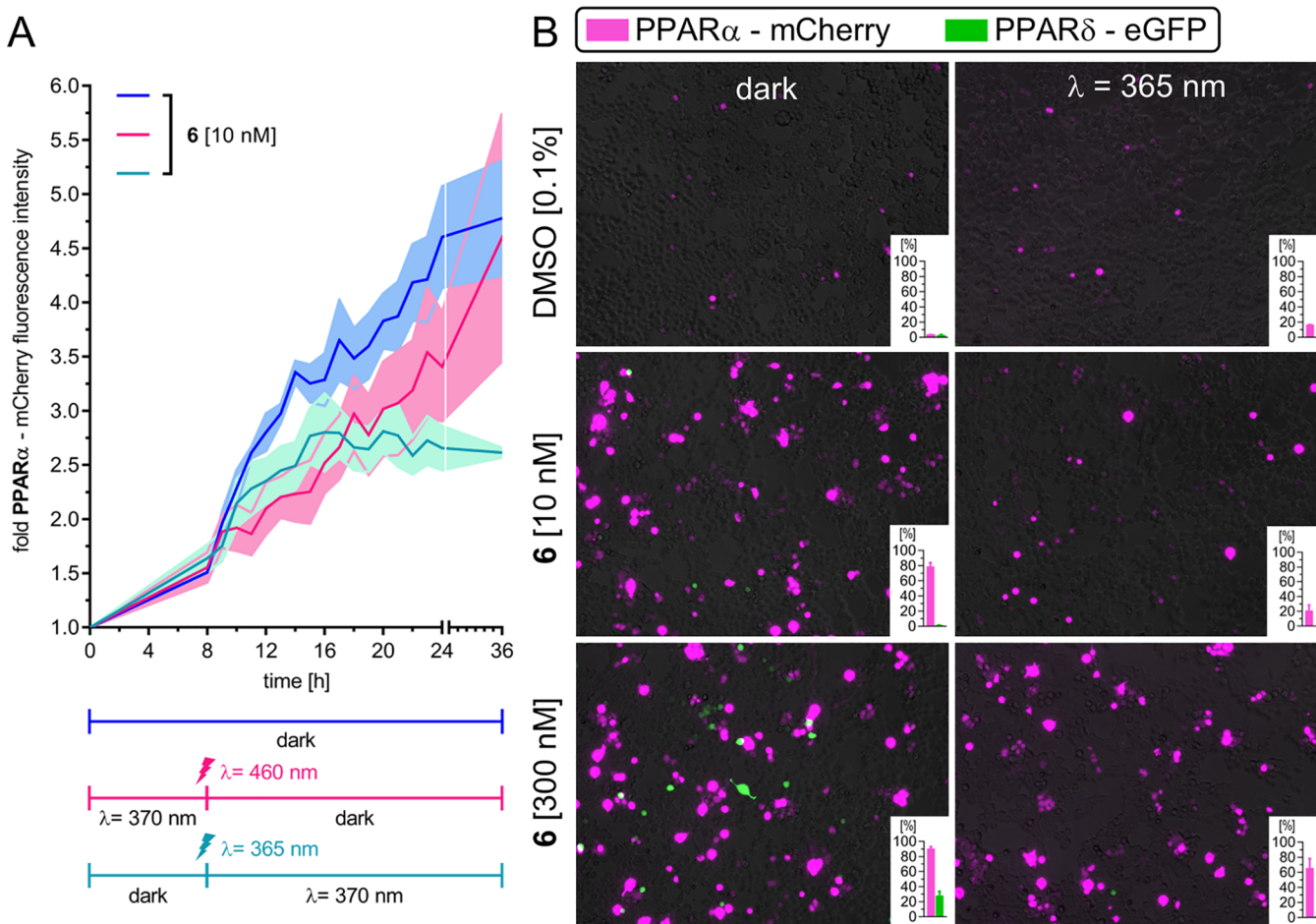


Figure 3. Spatiotemporal control of PPAR α by **6**. (A) Time-dependent PPAR α activation by **6** using an mCherry fluorescence reporter in live HEK293T cells. *Trans*-**6** was maintained in the dark (blue). Switching between the *cis*- and *trans*-isomers after 8 h was performed by illumination with $\lambda = 460$ nm (red) or $\lambda = 365$ nm (green) for 3 min, with subsequent maintenance of the *cis*-state using the Cell DISCO system.^{40,41} Fold fluorescence intensity refers to 0.1% DMSO. Lines, mean; shadows, standard error of the mean (SEM); $n = 3$. (B) Live-cell imaging of PPAR α -dependent mCherry reporter induction by *trans*-**6** (dark) and *cis*-**6** ($\lambda = 365$ nm). The PPAR δ -dependent eGFP fluorescence is negligible. The insets show mean \pm SEM relative reporter expression compared to GW7647 (PPAR α) or L165,041 (PPAR δ), $n = 2$.

Following these considerations, we have developed a highly potent and selective PPAR α photophormone from the weak pan-PPAR agonist GL479 (**1**) in a structure-guided fashion. The resulting analogue **6** not only exceeds the template compound **1** in terms of potency (factor > 150) and selectivity on PPAR α but is also equipped with the ability to be switched off by light-induced isomerization to its *cis*-conformer, which is less active on the intended target by a factor of 35. By enabling selective optical control of PPAR α , the photophormone **6** valuably expands the photopharmacology toolbox for nuclear receptors, enabling unprecedented in vitro and in cellulo experiments.

EXPERIMENTAL SECTION

Chemistry. General. All reagents and solvents were purchased from commercial sources (Sigma-Aldrich, TCI Europe N.V., Strem Chemicals, etc.) and used without further purification unless otherwise noted. Reactions were monitored by TLC on precoated, Merck silica gel 60 F_{254} glass-backed plates. Flash silica gel chromatography was performed using silica gel (SiO₂, particle size 40–63 μ m) purchased from Merck. All NMR spectra were measured on a Bruker Avance III HD 400 spectrometer (equipped with a CryoProbe). Multiplicities in the following experimental procedures are abbreviated as follows: s = singlet, d = doublet, t = triplet, q = quartet, quint = quintet, sext = sextet, hept = heptet, br = broad, and m = multiplet. Proton chemical shifts are expressed in parts per million (ppm, δ scale) and are referenced to the

residual protium in the NMR solvent (CDCl₃; $\delta = 7.26$; DMSO-*d*₆; $\delta = 2.50$; THF-*d*₈; $\delta = 1.72$). Carbon chemical shifts are expressed in ppm (δ scale) and are referenced to the carbon resonance of the NMR solvent (CDCl₃; $\delta = 77.16$; DMSO-*d*₆; $\delta = 39.52$; THF-*d*₈; $\delta = 25.31$). High-resolution mass spectra (HRMS) were obtained with an Agilent 6224 accurate mass time-of-flight (TOF) liquid chromatography/mass spectrometry (LC/MS) system using either an electrospray ionization (ESI) or atmospheric pressure chemical ionization (APCI) ion source. All reported data refer to the positive ionization mode. The compound purity was analyzed by high-performance liquid chromatography-ultraviolet (HPLC-UV) detection, and all compounds used for biological characterization had a purity $\geq 95\%$.

Synthesis and Analytical Characterization of **6 and **11** and Their Precursor **14**.** (*E*)-2-Methyl-2-(4-(2-(2-methyl-4-(phenyldiazenyl)phenoxy)ethyl)phenoxy)propanoic acid (**6**). Ethyl 2-(4-(2-hydroxyethyl)phenoxy)-2-methylpropanoate⁴⁵ (**14**, 20.0 mg, 79.3 mmol, 1.00 equiv), (*E*)-2-methyl-4-(phenyldiazenyl)phenol (**20**, 21.9 mg, 103 mmol, 1.30 equiv), and triphenylphosphine (27.0 mg, 103 mmol, 1.30 equiv) were dissolved in anhydrous THF (0.5 mL). DEAD (44.6 mg, 103 mmol, 1.30 equiv, 40% solution in toluene) was added dropwise at 0 °C. The mixture was stirred at rt overnight. The solvent was removed under reduced pressure. The crude was dissolved in EtOH, and 1M NaOH was added. The reaction was stirred at rt for 16 h. The solvent was removed under reduced pressure, and water was added and acidified with 1 M HCl. The mixture was extracted with CH₂Cl₂, dried over Na₂SO₄, filtered, and concentrated under reduced pressure.

The crude product was purified using flash column chromatography (CH_2Cl_2 to 20% MeOH in CH_2Cl_2) to yield **6** (28.2 mg, 67.4 μmol , 85%) as an orange solid. $^1\text{H NMR}$ (400 MHz, $\text{THF}-d_8$): δ = 7.84 (d, J = 7.3 Hz, 2H), 7.74 (s, 2H), 7.46 (t, J = 7.4 Hz, 2H), 7.40 (d, J = 7.1 Hz, 1H), 7.19 (d, J = 8.5 Hz, 2H), 7.05–6.99 (m, 1H), 6.84 (d, J = 8.5 Hz, 2H), 4.30–4.19 (m, 2H), 3.06 (t, J = 6.9 Hz, 2H), 2.25 (s, 3H), 1.52 (s, 6H). $^{13}\text{C NMR}$ (100 MHz, $\text{THF}-d_8$): δ = 175.6, 160.8, 155.7, 153.9, 147.4, 132.6, 131.0, 130.5, 129.8, 128.1, 124.8, 124.6, 123.3, 120.1, 111.5, 79.5, 70.1, 35.8, 25.9, 16.6. HRMS: m/z calcd for $\text{C}_{25}\text{H}_{27}\text{N}_2\text{O}_4^+$ ($[\text{M} + \text{H}]^+$): 419.1965; found, 419.1963.

(*E*)-2-(4-(2-(2-Chloro-4-(*p*-tolylidiazanyl)phenoxy)ethyl)phenoxy)-2-methylpropanoic acid (**11**). Ethyl 2-(4-(2-hydroxyethyl)phenoxy)-2-methylpropanoate (**14**, 21.9 mg, 87.0 μmol , 1.00 equiv), (*E*)-2-chloro-4-(*p*-tolylidiazanyl)phenol (**25**, 30.0 mg, 113 μmol , 1.30 equiv), and triphenylphosphine (29.6 mg, 113 μmol , 1.30 equiv) were dissolved in anhydrous THF (0.5 mL). DEAD (49.1 mg, 113 μmol , 1.30 equiv, 40% solution in toluene) was added dropwise at 0 °C. The mixture was stirred at rt overnight. The solvent was removed under reduced pressure. The crude was dissolved in EtOH, and 1 M NaOH was added. The reaction was stirred at rt for 16 h. The solvent was removed under reduced pressure, and water was added and acidified with 1 M HCl. The mixture was extracted with CH_2Cl_2 , dried over Na_2SO_4 , filtered, and concentrated under reduced pressure. The crude product was purified using flash column chromatography (CH_2Cl_2 to 20% MeOH in CH_2Cl_2) to yield **11** (17.6 mg, 38.9 μmol , 45%) as an orange solid. $^1\text{H NMR}$ (400 MHz, $\text{DMSO}-d_6$): δ = 7.94–7.85 (m, 2H), 7.78 (d, J = 8.3 Hz, 2H), 7.39 (dd, J = 8.6, 3.8 Hz, 3H), 7.27 (d, J = 8.7 Hz, 2H), 6.78 (d, J = 8.6 Hz, 2H), 4.34 (t, J = 6.9 Hz, 2H), 3.11–3.01 (m, 2H), 2.40 (s, 3H), 1.49 (s, 6H). $^{13}\text{C NMR}$ (101 MHz, $\text{DMSO}-d_6$): δ = 175.1, 156.0, 153.9, 149.9, 145.9, 141.6, 130.9, 130.0, 129.9, 124.9, 122.5, 122.5, 122.1, 118.4, 113.8, 78.3, 69.8, 33.9, 25.0, 21.0. HRMS: m/z calcd for $\text{C}_{25}\text{H}_{26}\text{ClN}_2\text{O}_4^+$ ($[\text{M} + \text{H}]^+$): 453.1576; found, 453.1573.

Ethyl 2-(4-(2-hydroxyethyl)phenoxy)-2-methylpropanoate (**14**). 4-(Hydroxyethyl)phenol (**12**, 200 mg, 1.45 mmol, 1.00 equiv) and K_2CO_3 (2.00 g, 14.5 mmol, 10.0 equiv) were dissolved in DMF (4.5 mL). Ethyl 2-bromo-2-methylpropanoate (875 mg, 4.48 mmol, 3.10 equiv) was added, and the mixture was stirred for 4 h under reflux. Water was added, phases were separated, and the aqueous layer was extracted with EtOAc, washed with brine, dried over Na_2SO_4 , filtered, and concentrated under reduced pressure. The crude product was purified using flash column chromatography (hexanes/EtOAc (8:2)) to yield **14** (292 mg, 1.16 mmol, 80%) as a colorless liquid. $^1\text{H NMR}$ (400 MHz, CDCl_3): δ = 7.13–7.05 (m, 2H), 6.83–6.76 (m, 2H), 4.24 (q, J = 7.1 Hz, 2H), 3.82 (t, J = 6.5 Hz, 2H), 2.80 (t, J = 6.6 Hz, 2H), 1.58 (s, 6H), 1.25 (d, J = 7.1 Hz, 3H). $^{13}\text{C NMR}$ (100 MHz, CDCl_3): δ = 174.5, 154.2, 132.1, 129.8, 119.6, 79.2, 63.9, 61.5, 38.5, 25.5, 14.2. HRMS: m/z calcd for $\text{C}_{14}\text{H}_{19}\text{O}_3^+$ ($[\text{M} - \text{H}_2\text{O}]^+$): 235.1329; found, 235.1335.

Photophysical Characterization. UV–vis spectra were recorded using a Varian Cary 50 Bio UV–visible spectrophotometer with BRAND Ultra-Micro UV-Cuvettes (10 mm light path). Switching was achieved using λ = 365 or 460 nm light-emitting diode (LED) light sources. The LEDs were pointed directly into the top of the sample cuvette. An initial spectrum of all photohormones (50 μM in DMSO) was recorded (dark-adapted state, black) and then again following illumination at λ = 365 nm for 1 min (*cis*-adapted state, gray). A third spectrum was recorded after irradiation at λ = 460 nm for 1 min (*trans*-adapted state, blue). To obtain the reversible *trans* \leftrightarrow *cis* spectrum, absorption at $\lambda_{\text{abs}} = 340$ nm was constantly measured, while alternating illumination at λ = 365 or 460 nm for the indicated times allowed for rapid isomerization of the photohormones (50 μM in DMSO). A mercury lamp with a power of 75 watts connected to a monochromator was directly pointed into the top of the sample cuvette, providing irradiation via an optic fiber cable with the two distinct wavelengths λ = 365 and 460 nm for 1 min each (absorption was read at $\lambda_{\text{abs}} = 340$ nm).

Computational Methods. *General.* Calculations were performed in Molecular Operating Environment (MOE, version 2020.09, Chemical Computing Group ULC, Montreal, QC, Canada) using

default settings for each tool/function unless stated otherwise. Amber10:EHT was used as the default forcefield for all calculations.

Molecular Docking. Docking was performed using the X-ray structures of the PPAR α LBD complexed with GL479 (PDB ID: 4CI4³⁶) and the PPAR δ LBD complexed with GW501516 derivative (PDB ID: 5Y7X³⁸). Protonation states of the complexes were adjusted using the MOE QuickPrep tool. The compounds were prepared using the Energy minimize tool and MOE Wash tool: protonation state dominant at pH 7.0. Docking was performed using the following settings in the MOE Dock tool: receptor: receptor + solvent; site: ligand atoms; placement: Triangle matcher; score: London dG; poses: 100; refinement: induced fit; refinement score: GBVI/WSA dG; poses: 10. As a pharmacophore query, the carboxylate oxygen of the respective crystallized ligand was set as an anionic H-bond acceptor feature with a 1.0 radius and one H-bond acceptor projection feature with a radius of 1.4 from the same atom. All 10 superimposed binding poses are shown as insets. The RMSD values between docked poses were calculated with the mol_rmsd SVL script in MOE and are displayed as min–max ranges. Redocking of the crystallized ligand GL479 (**1**) in PPAR α (PDB ID: 4CI4³⁶) resulted in an RMSD value of 0.1565 (range 0.1565–1.1580, mean 0.6668).

Torsion Profile. The minimized energies (in kcal/mol) of the associated lowest-energy structure were calculated for the conversion from *trans*- to *cis*-state of **1** and vice versa using the MOE torsion profile tool in bidirectional mode with both nitrogen atoms selected from the azo ($\text{N}=\text{N}$) double bond.

In Vitro Pharmacological Characterization. *Hybrid Reporter Gene Assays. Plasmids.* The Gal4-fusion receptor plasmids pFA-CMV-hPPAR α -LBD, pFA-CMV-hPPAR γ -LBD, and pFA-CMV-hPPAR δ -LBD coding for the hinge region and the ligand binding domain of the canonical isoform of the respective nuclear receptor have been reported previously.⁴⁶ pFR-Luc (Stratagene, La Jolla, CA) was used as the reporter plasmid and pRL-SV40 (Promega, Madison, WI) for normalization of transfection efficiency and cell growth.

Procedure. HEK293T cells were cultured in Dulbecco's modified Eagle's medium (DMEM), high glucose with 10% fetal calf serum (FCS), sodium pyruvate (1 mM), penicillin (100 U/mL), and streptomycin (100 $\mu\text{g}/\text{mL}$) at 37 °C and 5% CO_2 . Twenty-four hours before transfection, the cells were seeded in transparent 96-well plates (3×10^4 cells/well). Before transfection, the medium was changed to Opti-MEM without supplements. Transient transfection was carried out using Lipofectamine LTX reagent (Invitrogen, Carlsbad, CA) according to the manufacturer's protocol with pFR-Luc (Stratagene), pRL-SV40 (Promega), and the corresponding Gal4-fusion nuclear receptor plasmid. Five hours after transfection, the medium was changed to Opti-MEM supplemented with penicillin (100 U/mL) and streptomycin (100 $\mu\text{g}/\text{mL}$) and additionally containing 0.1% dimethyl sulfoxide (DMSO) and the respective test compound or 0.1% DMSO alone as the untreated control. Each concentration was tested in duplicate, and each experiment was repeated independently at least three times. After incubation overnight (14–16 h), the cells were assayed for luciferase activity using the Dual-Glo Luciferase Assay System (Promega) according to the manufacturer's protocol. Luminescence was measured with a Tecan Spark 10M luminometer (Tecan Deutschland GmbH, Crailsheim, Germany). Normalization of transfection efficiency and cell growth was done by dividing the firefly luciferase data by *Renilla* luciferase data and multiplying the value by 1000, resulting in relative light units (RLUs). Fold activation was obtained by dividing the mean RLU of the test compound by the mean RLU of the untreated control. Max. relative activation refers to the max fold activation by a test compound divided by the fold activation of the respective reference agonist (at a concentration of 1 μM). All hybrid assays were validated with the respective reference agonists (PPAR α : GW7647; PPAR γ : pioglitazone; PPAR δ : L165,041), which yielded EC₅₀ values in agreement with the literature. Characterization of the respective *cis*-counterparts was performed in the same way with preirradiated compounds (irradiation for 3 min at λ = 365 nm before incubation). To maintain the compound in the *cis*-adapted state, the Cell DISCO system was used during incubation with 75 ms light pulses (λ = 370 nm) every 15 s. For dose–response curve fitting and

calculation of EC_{50} values, the equation “[Agonist] vs response–variable slope (four parameters)” was performed with mean relative activations \pm SD using GraphPad Prism (version 7.00, GraphPad Software, La Jolla, CA).

Microsomal Stability Assay. The solubilized test compound **6** or 7-ethoxycoumarin as a reference (5 μ L, final concentration 10 μ M) was preincubated at 37 °C in 432 μ L of phosphate buffer (0.1 M, pH 7.4) together with 50 μ L of an NADPH regenerating system (30 mM glucose-6-phosphate, 4 U/mL glucose-6-phosphate dehydrogenase, 10 mM NADP, 30 mM $MgCl_2$). After 5 min, the reaction was started by the addition of 13 μ L of the microsome mix from the liver of Sprague–Dawley rats (Invitrogen; 20 mg protein/mL in 0.1 M phosphate buffer) in a shaking water bath at 37 °C. The reaction was stopped by adding 500 μ L of ice-cold methanol at 0, 15, 30, and 60 min. The samples were centrifuged at 5000g for 5 min at 4 °C, and the test compound was quantified from the supernatants using HPLC-UV detection. The composition of the mobile phase was adapted to the test compound in a range of MeOH 40–90% and water (0.1% formic acid) 10–60%; flow-rate: 1 mL/min; stationary phase: Purospher STAR, RP18, 5 μ m, 125 \times 4; precolumn: Purospher STAR, RP18, 5 μ m, 4 \times 4; detection wavelength: 254 and 280 nm; and injection volume: 50 μ L. Control samples were performed to check the test compound’s stability in the reaction mixture: the first control was without NADPH, which is needed for the enzymatic activity of the microsomes, the second control was with inactivated microsomes (incubated for 20 min at 90 °C), and the third control was without the test compound (to determine the baseline). The amounts of the test compound were quantified by an external calibration curve. Data are expressed as the mean \pm SEM of the remaining compound from three independent experiments. In vitro half-life was calculated by a logarithmic linear transformation of the remaining amounts of nonmetabolized test compound versus time in GraphPad Prism 7 as described previously.^{47,48}

Fluorescence Reporter Gene Assay. *Plasmids.* The Gal4-responsive fluorescence reporter mCherry was expressed from plasmid pUAS-mCherry-NLS (Addgene, entry 87695, Watertown, MA, U.S.A.).⁴⁹ The Gal4-fusion receptor plasmid pFA-CMV-hPPAR α -LBD and pFA-CMV-hPPAR δ -LBD coding for the hinge region and the ligand binding domain of the canonical isoform of the respective nuclear receptor have been reported previously.⁴⁶

Procedure. HEK293T cells were cultured in DMEM, high glucose with 10% FCS, sodium pyruvate (1 mM), penicillin (100 U/mL), and streptomycin (100 μ g/mL) at 37 °C and 5% CO_2 . Twenty-four hours before transfection, the cells were seeded in black cell culture 96-well microplates with μ Clear flat bottom (3 \times 10⁴ cells/well; Greiner Bio-One GmbH, Frickenhausen, Germany). Before transfection, the medium was changed to Opti-MEM without supplements. Transient transfection was carried out using Lipofectamine LTX reagent (Invitrogen) according to the manufacturer’s protocol with pUAS-mCherry-NLS (Addgene, entry 87695) and the corresponding Gal4-fusion nuclear receptor plasmid. Five hours after transfection, the medium was changed to Opti-MEM supplemented with penicillin (100 U/mL) and streptomycin (100 μ g/mL) and additionally containing 0.1% DMSO and the respective test compound or 0.1% DMSO alone as the untreated control. Each concentration was tested in duplicate, and each experiment was repeated independently three times. After incubation for 8 h, the living cells were assayed for fluorescence reporter intensity every hour until 24 h and at 36 h. The fluorescence intensity (FI) was measured after excitation at 585/10 nm with the emission wavelength of 610/10 nm in bottom reading mode with a Tecan Spark luminometer (Tecan Deutschland GmbH). Fold FI was obtained by dividing the mean FI of the test compound by the mean FI of the untreated control. Hybrid fluorescence assay performance was monitored with the respective reference agonists at a concentration of 1 μ M (PPAR α : GW7647; PPAR δ : L165,041). Characterization of the respective *cis*-counterparts was performed in the same way with preirradiated compounds (irradiation for 3 min at λ = 365 nm before incubation). To maintain the compound in the *cis*-adapted state, the Cell DISCO system was used during incubation with 75 ms light pulses (λ = 370 nm) every 15 s. For two of the three study arms,

photoswitching of the test compounds was conducted after 8 h of incubation with irradiation for 3 min at λ = 365 or 460 nm, respectively.

Fluorescence Cell Imaging. *Plasmids.* The Gal4-responsive fluorescence reporters mCherry and eGFP were expressed from the plasmids pUAS-mCherry-NLS (Addgene, entry 87695)⁴⁹ and pGRE-GFP (Addgene, entry 12516),⁵⁰ respectively. The Gal4-fusion receptor plasmid pFA-CMV-hPPAR α -LBD and pFA-CMV-hPPAR δ -LBD coding for the hinge region and the ligand binding domain of the canonical isoform of the respective nuclear receptor have been reported previously.⁴⁶

Procedure. HEK293T cells were cultured in DMEM, high glucose with 10% FCS, sodium pyruvate (1 mM), penicillin (100 U/mL), and streptomycin (100 μ g/mL) at 37 °C and 5% CO_2 . Twenty-four hours before transfection, cells were seeded in 24-well plates (1.5 \times 10⁵ cells/well). Before transfection, the medium was changed to Opti-MEM without supplements. Transient transfection was carried out using Lipofectamine LTX reagent (Invitrogen) according to the manufacturer’s protocol with the combination of pUAS-mCherry-NLS (Addgene, entry 87695) and pFA-CMV-hPPAR α -LBD or pGRE-GFP (Addgene, entry 12516) and pFA-CMV-hPPAR δ -LBD. Five hours after transfection, the cells transfected with pUAS-mCherry-NLS and pFA-CMV-hPPAR α -LBD or pGRE-GFP and pFA-CMV-hPPAR δ -LBD were trypsinized and pooled in a 50 mL tube, centrifuged, and resuspended in Opti-MEM supplemented with penicillin (100 U/mL) and streptomycin (100 μ g/mL). The transfected cells were then reseeded in 96-well plates already containing Opti-MEM with supplements and 0.1% DMSO and the respective test compound or 0.1% DMSO alone as the untreated control. Each concentration was performed in duplicate, and each experiment was repeated independently two times. Characterization of the respective *cis*-counterparts was performed in the same way with preirradiated compounds (irradiation for 3 min at λ = 365 nm before incubation). To maintain the compound in the *cis*-adapted state, the Cell DISCO system was used during incubation with 75 ms light pulses (λ = 370 nm) every 15 s.

Imaging. For the analysis of fluorescence reporter gene expression, images were acquired 40 h after incubation with the test compounds using a Zeiss Axio Observer Z1 (Carl Zeiss AG, Oberkochen, Germany) microscope equipped with a 10 \times objective lens. The filter sets had the following wavelengths/bandwidths: mCherry, excitation 545/40 nm ET bandpass; beam splitter T570 LPXR; and emission 620/60 nm ET bandpass; and eGFP, excitation 470/40 nm ET bandpass; beam splitter T495 LPXR; and emission 525/50 nm ET bandpass. Image analysis was performed with ImageJ software (version 1.53e). Integrated densities were measured from representative images in separated stacks (mCherry and eGFP channel) as RGB color images for the whole area, and relative integrated densities refer to mean integrated densities divided by the mean integrated density of the respective reference agonist (at a concentration of 1 μ M; PPAR α : GW7647; PPAR δ : L165,041).

■ ASSOCIATED CONTENT

Supporting Information

The Supporting Information is available free of charge at <https://pubs.acs.org/doi/10.1021/acs.jmedchem.1c00810>.

Supporting Information containing Figures S1–S7, Table S1, synthesis and analytical characterization of **1–11** and their precursors, HPLC traces, and NMR spectra (PDF)

Molecular formula strings containing molecular structures of **1–11** in *trans* and *cis* conformations and associated activity data (csv)

■ AUTHOR INFORMATION

Corresponding Authors

Dirk Trauner – Department of Chemistry, New York University, New York, New York 10003, United States;

orcid.org/0000-0002-6782-6056; Email: dirktrauner@nyu.edu

Nyuu Merk – Institute of Pharmaceutical Chemistry, Goethe University Frankfurt, 60438 Frankfurt, Germany;

orcid.org/0000-0002-5359-8128; Email: merk@pharmchem.uni-frankfurt.de

Authors

Sabine Willems – Institute of Pharmaceutical Chemistry, Goethe University Frankfurt, 60438 Frankfurt, Germany

Johannes Morstein – Department of Chemistry, New York University, New York, New York 10003, United States

Konstantin Hinnah – Department of Chemistry, New York University, New York, New York 10003, United States

Complete contact information is available at:

<https://pubs.acs.org/10.1021/acs.jmedchem.1c00810>

Author Contributions

[§]S.W. and J.M. contributed equally to this study.

Notes

The authors declare no competing financial interest.

ACKNOWLEDGMENTS

pUAS-mCherry-NLS was a gift from Robert Campbell (Addgene plasmid no. 87695; <http://n2t.net/addgene:87695>; RRID:Addgene_87695). pGRE-GFP was a gift from Bert Vogelstein (Addgene plasmid no. 12516; <http://n2t.net/addgene:12516>; RRID:Addgene_12516). J.M. and K.H. thank the German Academic Scholarship Foundation for a fellowship. J.M. thanks the New York University for a Margaret and Herman Sokol fellowship and the NCI for an F99/K00 award (1F99CA253758-01). D.M. thanks the Aventis Foundation for financial support.

ABBREVIATIONS USED

DEAD, diethyl azodicarboxylate; eGFP, enhanced green fluorescent protein; ER, estrogen receptor; FI, fluorescence intensity; FXR, farnesoid X receptor; LBD, ligand binding domain; NAFLD, nonalcoholic fatty liver disease; NR, nuclear receptor; PPAR, peroxisome proliferator-activated receptor; RAR, retinoic acid receptor; RLU, relative light units; rt, room temperature

REFERENCES

- (1) Szymański, W.; Beierle, J. M.; Kistemaker, H. A. V.; Velema, W. A.; Feringa, B. L. Reversible Photocontrol of Biological Systems by the Incorporation of Molecular Photoswitches. *Chem. Rev.* **2013**, *113*, 6114–6178.
- (2) Broichhagen, J.; Frank, J. A.; Trauner, D. A Roadmap to Success in Photopharmacology. *Acc. Chem. Res.* **2015**, *48*, 1947–1960.
- (3) Hüll, K.; Morstein, J.; Trauner, D. In Vivo Photopharmacology. *Chem. Rev.* **2018**, *118*, 10710–10747.
- (4) Fuchter, M. J. On the Promise of Photopharmacology Using Photoswitches: A Medicinal Chemist's Perspective. *J. Med. Chem.* **2020**, *63*, 11436–11447.
- (5) Banghart, M.; Borges, K.; Isacoff, E.; Trauner, D.; Kramer, R. H. Light-Activated Ion Channels for Remote Control of Neuronal Firing. *Nat. Neurosci.* **2004**, *7*, 1381–1386.
- (6) Broichhagen, J.; Schönberger, M.; Cork, S. C.; Frank, J. A.; Marchetti, P.; Bugliani, M.; Shapiro, A. M. J.; Trapp, S.; Rutter, G. A.; Hodson, D. J.; Trauner, D. Optical Control of Insulin Release Using a Photoswitchable Sulfonyleurea. *Nat. Commun.* **2014**, *5*, No. 5116.
- (7) Broichhagen, J.; Damijonaitis, A.; Levitz, J.; Sokol, K. R.; Leippe, P.; Konrad, D.; Isacoff, E. Y.; Trauner, D. Orthogonal Optical Control

of a G Protein-Coupled Receptor with a SNAP-Tethered Photochromic Ligand. *ACS Cent. Sci.* **2015**, *1*, 383–393.

- (8) Morstein, J.; Dacheux, M. A.; Norman, D. D.; Shemet, A.; Donthamsetti, P. C.; Citir, M.; Frank, J. A.; Schultz, C.; Isacoff, E. Y.; Parrill, A. L.; Tigyi, G. J.; Trauner, D. Optical Control of Lysophosphatidic Acid Signaling. *J. Am. Chem. Soc.* **2020**, *142*, 10612–10616.
- (9) Prischich, D.; Gomila, A. M. J.; Milla-Navarro, S.; Sangüesa, G.; Diez-Alarcia, R.; Preda, B.; Matera, C.; Batlle, M.; Ramírez, L.; Giralt, E.; Hernando, J.; Guasch, E.; Meana, J. J.; de la Villa, P.; Gorostiza, P. Adrenergic Modulation With Photochromic Ligands. *Angew. Chem., Int. Ed.* **2021**, *60*, 3625–3631.
- (10) Quandt, G.; Höfner, G.; Pabel, J.; Dine, J.; Eder, M.; Wanner, K. T. First Photoswitchable Neurotransmitter Transporter Inhibitor: Light-Induced Control of γ -Aminobutyric Acid Transporter 1 (GAT1) Activity in Mouse Brain. *J. Med. Chem.* **2014**, *57*, 6809–6821.
- (11) Cheng, B.; Morstein, J.; Ladefoged, L. K.; Maesen, J. B.; Schiøtt, B.; Sinning, S.; Trauner, D. A Photoswitchable Inhibitor of the Human Serotonin Transporter. *ACS Chem. Neurosci.* **2020**, *11*, 1231–1237.
- (12) Cheng, B.; Shchepakina, D.; Kavanaugh, M. P.; Trauner, D. Photoswitchable Inhibitor of a Glutamate Transporter. *ACS Chem. Neurosci.* **2017**, *8*, 1668–1672.
- (13) Bonardi, F.; London, G.; Nouwen, N.; Feringa, B. L.; Driessen, A. J. M. Light-Induced Control of Protein Translocation by the SecYEG Complex. *Angew. Chem., Int. Ed.* **2010**, *49*, 7234–7238.
- (14) Velema, W. A.; Van Der Berg, J. P.; Hansen, M. J.; Szymanski, W.; Driessen, A. J. M.; Feringa, B. L. Optical Control of Antibacterial Activity. *Nat. Chem.* **2013**, *5*, 924–928.
- (15) Tsai, Y.-H.; Essig, S.; James, J. R.; Lang, K.; Chin, J. W. Selective, Rapid and Optically Switchable Regulation of Protein Function in Live Mammalian Cells. *Nat. Chem.* **2015**, *7*, 554–561.
- (16) Kol, M.; Williams, B.; Toombs-Ruane, H.; Franquelim, H. G.; Korneev, S.; Schroerer, C.; Schwill, P.; Trauner, D.; Holthuis, J. C.; Frank, J. A. Optical Manipulation of Sphingolipid Biosynthesis Using Photoswitchable Ceramides. *eLife* **2019**, *8*, No. e43230.
- (17) Gronemeyer, H.; Gustafsson, J. Å.; Laudet, V. Principles for Modulation of the Nuclear Receptor Superfamily. *Nat. Rev. Drug Discovery* **2004**, *3*, 950–964.
- (18) Aranda, A.; Pascual, A. Nuclear Hormone Receptors and Gene Expression. *Physiol. Rev.* **2001**, *81*, 1269–1304.
- (19) Morstein, J.; Impastato, A. C.; Trauner, D. Photoswitchable Lipids. *ChemBioChem* **2021**, *22*, 73–83.
- (20) Proschak, E.; Heitel, P.; Kalinowsky, L.; Merk, D. Opportunities and Challenges for Fatty Acid Mimetics in Drug Discovery. *J. Med. Chem.* **2017**, *60*, 5235–5266.
- (21) Morstein, J.; Awale, M.; Raymond, J. L.; Trauner, D. Mapping the Azolog Space Enables the Optical Control of New Biological Targets. *ACS Cent. Sci.* **2019**, *5*, 607–618.
- (22) Morstein, J.; Trads, J. B.; Hinnah, K.; Willems, S.; Barber, D. M.; Trauner, M.; Merk, D.; Trauner, D. Optical Control of the Nuclear Bile Acid Receptor FXR with a Photohormone. *Chem. Sci.* **2020**, *11*, 429–434.
- (23) Hinnah, K.; Willems, S.; Morstein, J.; Heering, J.; Hartrampf, F. W. W.; Broichhagen, J.; Leippe, P.; Merk, D.; Trauner, D. Photohormones Enable Optical Control of the Peroxisome Proliferator-Activated Receptor γ (PPAR γ). *J. Med. Chem.* **2020**, *63*, 10908–10920.
- (24) Tsuchiya, K.; Umeno, T.; Tsuji, G.; Yokoo, H.; Tanaka, M.; Fukuhara, K.; Demizu, Y.; Misawa, T. Development of Photoswitchable Estrogen Receptor Ligands. *Chem. Pharm. Bull.* **2020**, *68*, 398–402.
- (25) Evans, R. M.; Mangelsdorf, D. J. Nuclear Receptors, RXR, and the Big Bang. *Cell* **2014**, *157*, 255–266.
- (26) Unsworth, A. J.; Flora, G. D.; Gibbins, J. M. Non-Genomic Effects of Nuclear Receptors: Insights from the Anucleate Platelet. *Cardiovasc. Res.* **2018**, *114*, 645–655.
- (27) Michalik, L.; Auwerx, J.; Berger, J. P.; Chatterjee, V. K.; Glass, C. K.; Gonzalez, F. J.; Grimaldi, P. A.; Kadowaki, T.; Lazar, M. A.; O'Rahilly, S.; Palmer, C. N. A.; Plutzky, J.; Reddy, J. K.; Spiegelman, B. M.; Staels, B.; Wahli, W. International Union of Pharmacology. LXI.

Peroxisome Proliferator-Activated Receptors. *Pharmacol. Rev.* **2006**, *58*, 726–741.

(28) Pawlak, M.; Lefebvre, P.; Staels, B. Molecular Mechanism of PPAR α Action and Its Impact on Lipid Metabolism, Inflammation and Fibrosis in Non-Alcoholic Fatty Liver Disease. *J. Hepatol.* **2015**, *62*, 720–733.

(29) Tanaka, T.; Yamamoto, J.; Iwasaki, S.; Asaba, H.; Hamura, H.; Ikeda, Y.; Watanabe, M.; Magoori, K.; Ioka, R. X.; Tachibana, K.; Watanabe, Y.; Uchiyama, Y.; Sumi, K.; Iguchi, H.; Ito, S.; Doi, T.; Hamakubo, T.; Naito, M.; Auwerx, J.; Yanagisawa, M.; Kodama, T.; Sakai, J. Activation of Peroxisome Proliferator-Activated Receptor δ Induces Fatty Acid β -Oxidation in Skeletal Muscle and Attenuates Metabolic Syndrome. *Proc. Natl. Acad. Sci. U.S.A.* **2003**, *100*, 15924–15929.

(30) Liu, Y.; Colby, J.; Zuo, X.; Jaoude, J.; Wei, D.; Shureiqi, I. The Role of PPAR- δ in Metabolism, Inflammation, and Cancer: Many Characters of a Critical Transcription Factor. *Int. J. Mol. Sci.* **2018**, *19*, No. 3339.

(31) Ratziu, V.; Harrison, S. A.; Francque, S.; Bedossa, P.; Lehert, P.; Serfaty, L.; Romero-Gomez, M.; Boursier, J.; Abdelmalek, M.; Caldwell, S.; Drenth, J.; Anstee, Q. M.; Hum, D.; Hanf, R.; Roudot, A.; Megnier, S.; Staels, B.; Sanyal, A.; et al. Elafibranor, an Agonist of the Peroxisome Proliferator-Activated Receptor- α and - δ , Induces Resolution of Nonalcoholic Steatohepatitis Without Fibrosis Worsening. *Gastroenterology* **2016**, *150*, 1147–1159.e5.

(32) Bougarne, N.; Weyers, B.; Desmet, S. J.; Deckers, J.; Ray, D. W.; Staels, B.; De Bosscher, K. Molecular Actions of PPAR α in Lipid Metabolism and Inflammation. *Endocr. Rev.* **2018**, *39*, 760–802.

(33) Beharry, A. A.; Woolley, G. A. Azobenzene Photoswitches for Biomolecules. *Chem. Soc. Rev.* **2011**, *40*, 4422–4437.

(34) Giampietro, L.; D'Angelo, A.; Giancristofaro, A.; Ammazalorso, A.; De Filippis, B.; Fantacuzzi, M.; Linciano, P.; MacCallini, C.; Amoroso, R. Synthesis and Structure-Activity Relationships of Fibrate-Based Analogues inside PPARs. *Bioorg. Med. Chem. Lett.* **2012**, *22*, 7662–7666.

(35) Giampietro, L.; Laghezza, A.; Cerchia, C.; Florio, R.; Recinella, L.; Capone, F.; Ammazalorso, A.; Bruno, I.; De Filippis, B.; Fantacuzzi, M.; Ferrante, C.; MacCallini, C.; Tortorella, P.; Verginelli, F.; Brunetti, L.; Cama, A.; Amoroso, R.; Loidice, F.; Lavecchia, A. Novel Phenylidiazanyl Fibrate Analogues as PPAR $\alpha/\gamma/\delta$ Pan-Agonists for the Amelioration of Metabolic Syndrome. *ACS Med. Chem. Lett.* **2019**, *10*, 545–551.

(36) dos Santos, J. C.; Bernardes, A.; Giampietro, L.; Ammazalorso, A.; De Filippis, B.; Amoroso, R.; Polikarpov, I. Different Binding and Recognition Modes of GL479, a Dual Agonist of Peroxisome Proliferator-Activated Receptor α/γ . *J. Struct. Biol.* **2015**, *191*, 332–340.

(37) Oliver, W. R.; Shenk, J. L.; Snaith, M. R.; Russell, C. S.; Plunket, K. D.; Bodkin, N. L.; Lewis, M. C.; Winegar, D. A.; Sznajdman, M. L.; Lambert, M. H.; Xu, H. E.; Sternbach, D. D.; Kliewer, S. A.; Hansen, B. C.; Willson, T. M. A Selective Peroxisome Proliferator-Activated Receptor δ Agonist Promotes Reverse Cholesterol Transport. *Proc. Natl. Acad. Sci. U.S.A.* **2001**, *98*, 5306–5311.

(38) Kim, H. L.; Chin, J. W.; Cho, S. J.; Song, J. Y.; Yoon, H. S.; Bae, J. H. Design, synthesis, and the X-ray co-crystal structure of Highly Potent, Selective, and Orally Bioavailable, Novel Peroxisome Proliferator-Activated Receptor delta Agonists. 2018, PDB ID 5Y7X, DOI: [10.2210/pdb5Y7X/pdb](https://doi.org/10.2210/pdb5Y7X/pdb).

(39) Wu, C. C.; Baiga, T. J.; Downes, M.; La Clair, J. J.; Atkins, A. R.; Richard, S. B.; Fan, W.; Stockley-Noel, T. A.; Bowman, M. E.; Noel, J. P.; Evans, R. M. Structural Basis for Specific Ligation of the Peroxisome Proliferator-Activated Receptor δ . *Proc. Natl. Acad. Sci. U.S.A.* **2017**, *114*, E2563–E2570.

(40) Borowiak, M.; Nahaboo, W.; Reynders, M.; Nekolla, K.; Jalinot, P.; Hasserodt, J.; Rehberg, M.; Delattre, M.; Zahler, S.; Vollmar, A.; Trauner, D.; Thorn-Seshold, O. Photoswitchable Inhibitors of Microtubule Dynamics Optically Control Mitosis and Cell Death. *Cell* **2015**, *162*, 403–411.

(41) Morstein, J.; Trauner, D. Photopharmacological Control of Lipid Function. In *Methods in Enzymology*; Academic Press Inc., 2020; Vol. 638, pp 219–232.

(42) Morstein, J.; Trauner, D. New Players in Phototherapy: Photopharmacology and Bio-Integrated Optoelectronics. *Curr. Opin. Chem. Biol.* **2019**, *50*, 145–151.

(43) Mehta, Z. B.; Johnston, N. R.; Nguyen-Tu, M.-S.; Broichhagen, J.; Schultz, P.; Larner, D. P.; Leclerc, I.; Trauner, D.; Rutter, G. A.; Hodson, D. J. Remote Control of Glucose Homeostasis in Vivo Using Photopharmacology. *Sci. Rep.* **2017**, *7*, No. 291.

(44) Babii, O.; Afonin, S.; Garmanchuk, L. V.; Nikulina, V. V.; Nikolaienko, T. V.; Storozhuk, O. V.; Shelest, D. V.; Dasyukevich, O. I.; Ostapchenko, L. I.; Iurchenko, V.; Zozulya, S.; Ulrich, A. S.; Komarov, I. V. Direct Photocontrol of Peptidomimetics: An Alternative to Oxygen-Dependent Photodynamic Cancer Therapy. *Angew. Chem., Int. Ed.* **2016**, *55*, 5493–5496.

(45) Giampietro, L.; D'Angelo, A.; Giancristofaro, A.; Ammazalorso, A.; De Filippis, B.; Fantacuzzi, M.; Linciano, P.; Maccallini, C.; Amoroso, R. Synthesis and Structure-Activity Relationships of Fibrate-Based Analogues inside PPARs. *Bioorg. Med. Chem. Lett.* **2012**, *22*, 7662–7666.

(46) Rau, O.; Wurglics, M.; Paulke, A.; Zitzkowski, J.; Meindl, N.; Bock, A.; Dingermann, T.; Abdel-Tawab, M.; Schubert-Zsilavecz, M. Carnosic Acid and Carnosol, Phenolic Diterpene Compounds of the Labiate Herbs Rosemary and Sage, Are Activators of the Human Peroxisome Proliferator-Activated Receptor Gamma. *Planta Med.* **2006**, *72*, 881–887.

(47) Obach, R. S. Prediction of Human Clearance of Twenty-Nine Drugs from Hepatic Microsomal Intrinsic Clearance Data: An Examination of In Vitro Half-Life Approach and Nonspecific Binding to Microsomes. *Drug Metab. Dispos.* **1999**, *27*, 1350–1359.

(48) Brian Houston, J. Utility of in Vitro Drug Metabolism Data in Predicting in Vivo Metabolic Clearance. *Biochem. Pharmacol.* **1994**, *47*, 1469–1479.

(49) Zhang, W.; Lohman, A. W.; Zhuravlova, Y.; Lu, X.; Wiens, M. D.; Hoi, H.; Yaganoglu, S.; Mohr, M. A.; Kitova, E. N.; Klassen, J. S.; Pantazis, P.; Thompson, R. J.; Campbell, R. E. Optogenetic Control with a Photocleavable Protein, Phocl. *Nat. Methods* **2017**, *14*, 391–394.

(50) Da Costa, L. T.; Jen, J.; He, T. C.; Chan, T. A.; Kinzler, K. W.; Vogelstein, B. Converting Cancer Genes into Killer Genes. *Proc. Natl. Acad. Sci. U.S.A.* **1996**, *93*, 4192–4196.

- Supporting Information -

A Photohormone for Light-dependent Control of PPAR α in Live Cells

Sabine Willems^{1‡}, Johannes Morstein^{2‡}, Konstantin Hinnah², Dirk Trauner^{2*} and Daniel Merk^{1*}

¹ Institute of Pharmaceutical Chemistry, Goethe University Frankfurt, Max-von-Laue-Str. 9, 60438 Frankfurt, Germany

² Department of Chemistry, New York University, New York, New York 10003, United States

‡ S.W. and J.M. contributed equally to this work

* Correspondence: dirktrauner@nyu.edu (D.T.), merk@pharmchem.uni-frankfurt.de (D.M.)

Table of contents

Supporting Figures and Tables	S2
Experimental Section	S8
HPLC traces of 1-11	S17
NMR spectra of 1-11	S23
References	S34

Supporting Figures and Tables

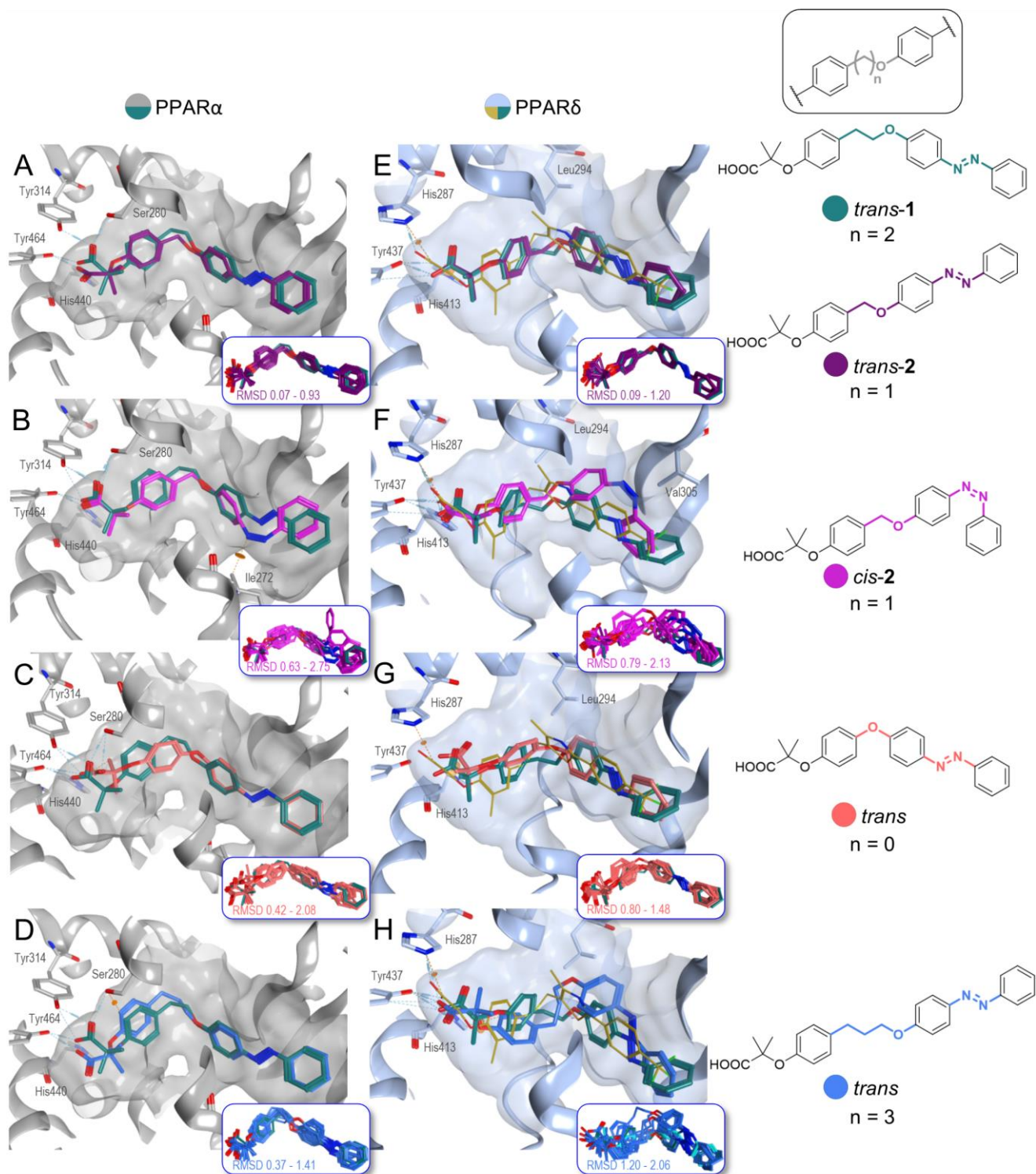


Figure S1. Molecular docking of **1** and derivatives with altered chain length. *Trans*-1 (teal) is shown in all models for comparison. (A - D) PPAR α binding site (grey) from co-crystal structure with lead **1** (teal, PDB ID: 4CI4¹), (E - H) PPAR δ pocket (light blue) with docked lead structure **1** for comparison (PDB ID: 5Y7X²). The inserts show overlays of the top 10 binding poses for each structure with their respective RMSD range to the pose shown in the binding site.

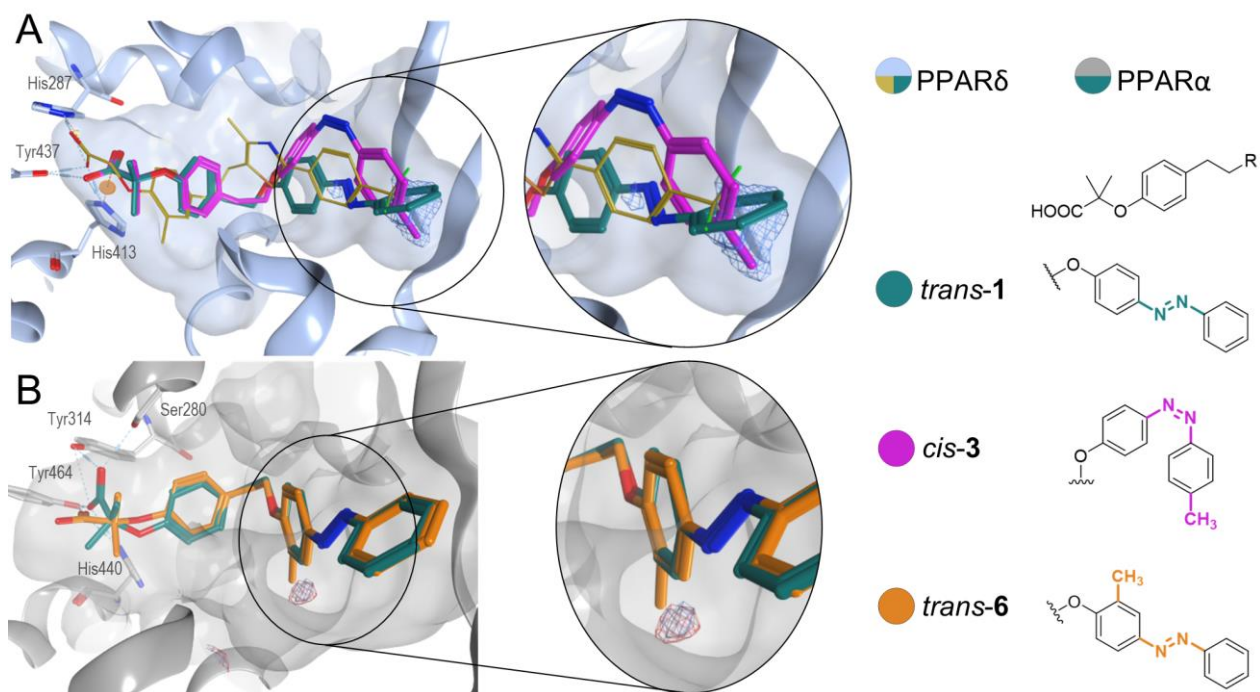


Figure S2. Molecular docking of *cis-3* and *trans-6* in detail. *Trans-1* (teal) is shown in both models for comparison. (A) PPAR δ pocket (light blue) with docked lead structure 1 (teal, PDB ID: 5Y7X²), (B) PPAR α binding site (grey) from co-crystal structure with lead 1 (PDB ID: 4CI4¹). (A) Extension in *para*-position of the terminal ring in *cis-3* suggested a slight *cis*-preference for PPAR δ . Interaction potential is shown for methyl-group (blue). (B) The methyl-group of *trans-6* in *ortho*-position of the central phenyl ring extends towards a lipophilic sub-pocket of PPAR α suggesting enhanced affinity by addressing the unoccupied space. Interaction potential is shown for methyl-group (blue) and chlorine-atom (red).

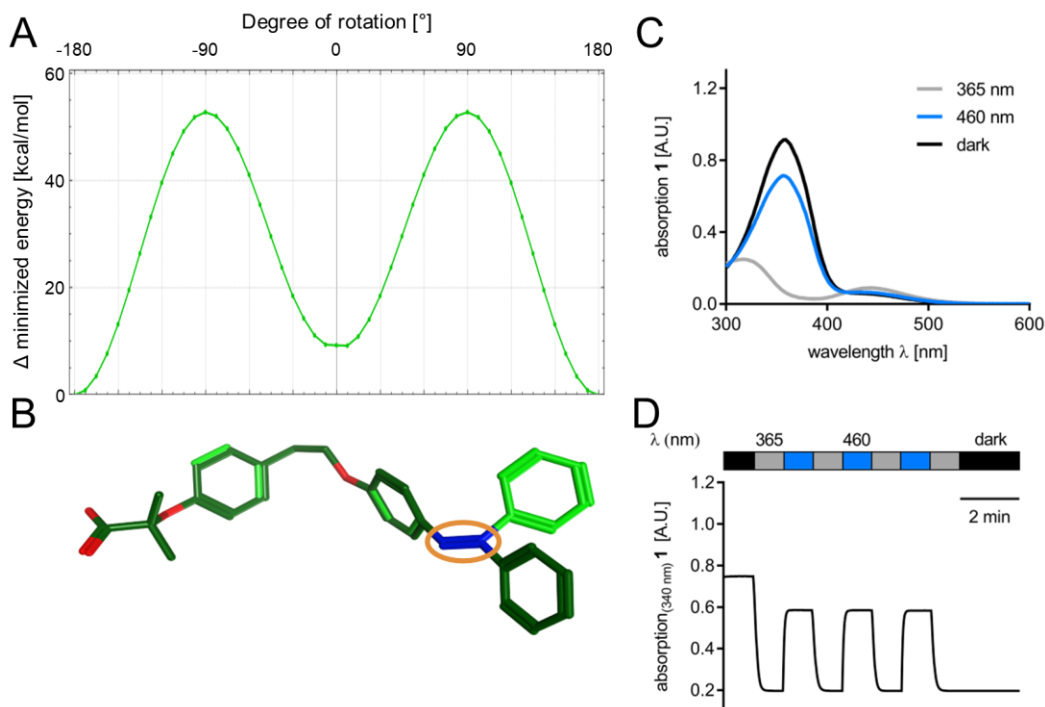


Figure S3. Characterization of lead GL479 (**1**). Torsion profile of **1**: (A) Energy minimized calculation for the rotation of the N=N (azo) double bond in MOE using the Amber10:EHT forcefield revealed a local energy minimum of *cis*-**1** at ~ 9 kcal/mol compared to *trans*, and a high energy barrier of ~ 52 kcal/mol for conversion from *trans*- to *cis*-state, and ~ 43 kcal/mol vice versa. (B) Molecular representation of *trans*-**1** (dark green) and *cis*-**1** (light green), N=N double bond is indicated in orange. Photophysical characteristics of **1**: (C) UV-vis absorption scans (50 μ M in DMSO) in dark-adapted (*trans*, black), 460 nm-adapted (*trans*, blue), and 365 nm-adapted (*cis*, grey) photostationary states. (D) Reversible cycling (50 μ M in DMSO) with alternating illumination at 365 nm and 460 nm.

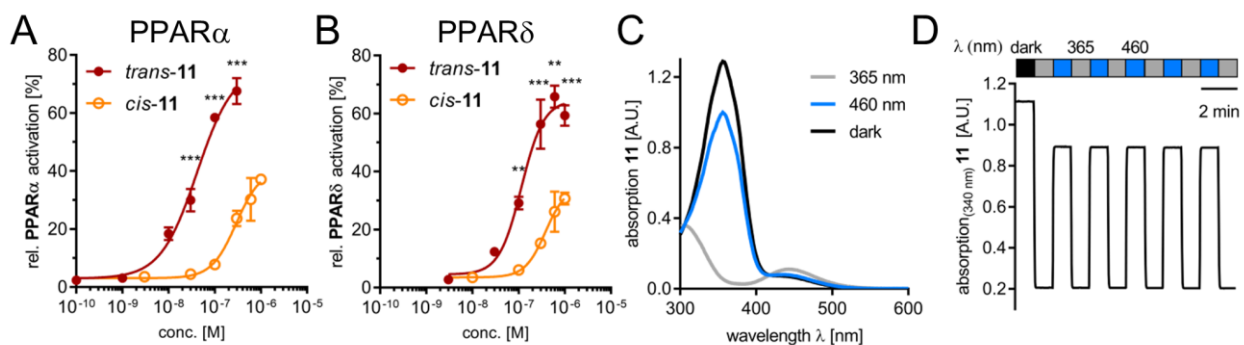


Figure S4. Characterization of photohormone **11**. Dose-response curves in cellular Gal4-PPAR α (A) or Gal4-PPAR δ (B) hybrid reporter gene assays in HEK293T cells. *Cis*-**11** was pre-illuminated ($\lambda = 365$ nm, 3 min) and maintained in *cis*-state with the CellDISCO. Relative activation refers 1 μ M GW7647 (PPAR α) or L165,041 (PPAR δ). Data are the mean \pm SD; $n \geq 3$. ** $p < 0.01$, *** $p < 0.001$ (t-test vs *cis*-**11**). Photophysical characteristics of **11**: UV-vis absorption scans (C, 50 μ M in DMSO) in dark-adapted (*trans*, black), 460 nm-adapted (*trans*, blue), and 365 nm-adapted (*cis*, grey) photostationary states. (D) Reversible cycling (50 μ M in DMSO) with alternating illumination at 365 nm and 460 nm.

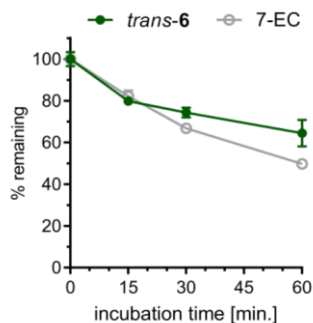


Figure S5. Microsomal stability assay. The PPAR α selective photohormone **6** revealed favorable stability against degradation by rat liver microsomes with a half-life of 103 \pm 20 minutes and 65% parent compound remaining after 60 min. incubation. 7-Ethoxycoumarin (7-EC) as control. Data are mean \pm S.E.M. % remaining compound; n=3.

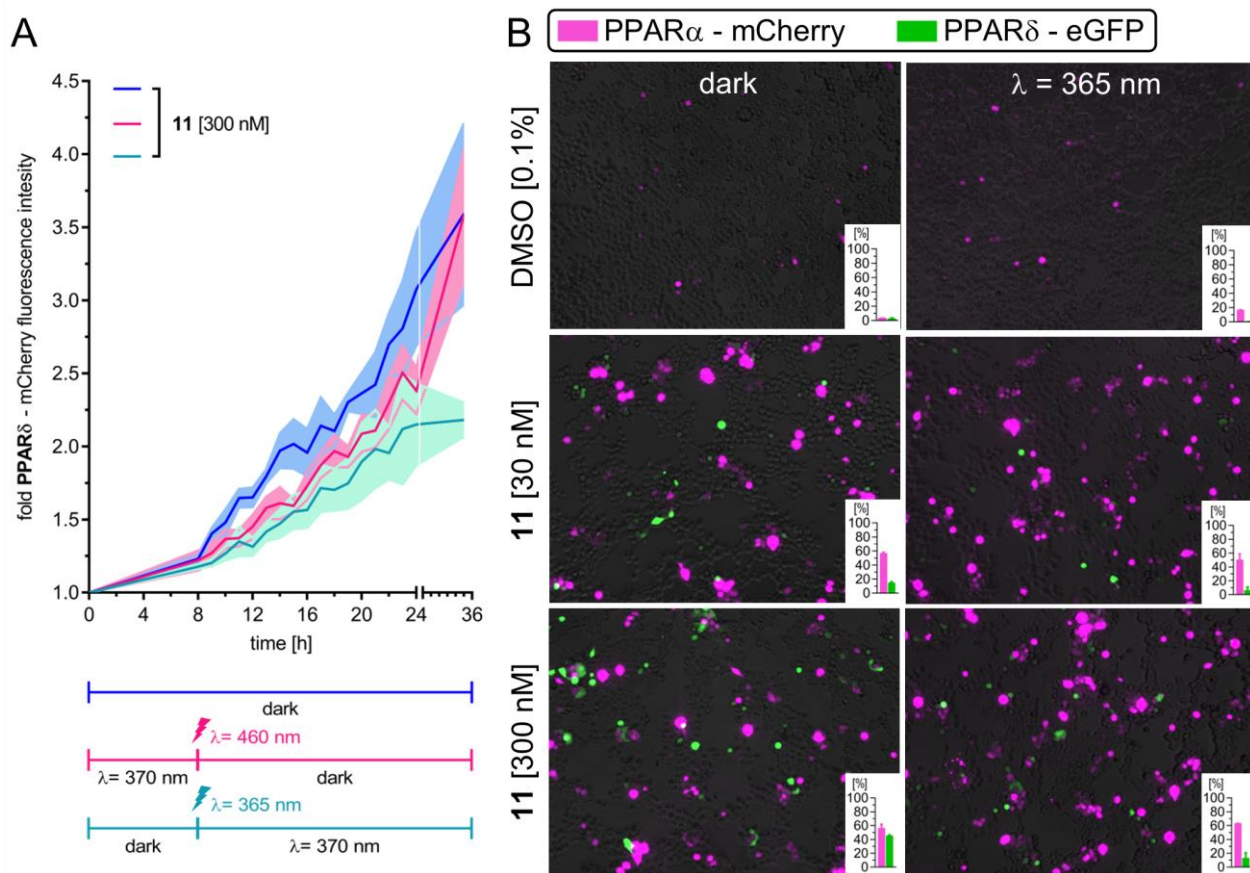


Figure S6. Spatiotemporal control of PPAR δ by **11**. (A) Time dependent PPAR δ activation by **11** using an mCherry fluorescence reporter in live HEK293T cells. *Trans*-**11** was maintained in the dark (blue). Switching between the *cis*-/*trans*-isomers after 8 h was performed by illumination with $\lambda = 460$ nm (red) or $\lambda = 365$ nm (green) for 3 min and subsequent maintenance of the *cis*-state using the CellDISCO. Fold fluorescence intensity refers to 0.1 % DMSO. Lines: mean, shadows: S.E.M.; n=3. (B) Live cell imaging of PPAR α -dependent mCherry and PPAR δ -dependent eGFP reporter induction by *trans*-**11** (dark adapted) and *cis*-**11** ($\lambda = 365$ nm). Inserts show mean \pm S.E.M. relative reporter expression compared to GW7647 (PPAR α) or L165,041 (PPAR δ), n=2.

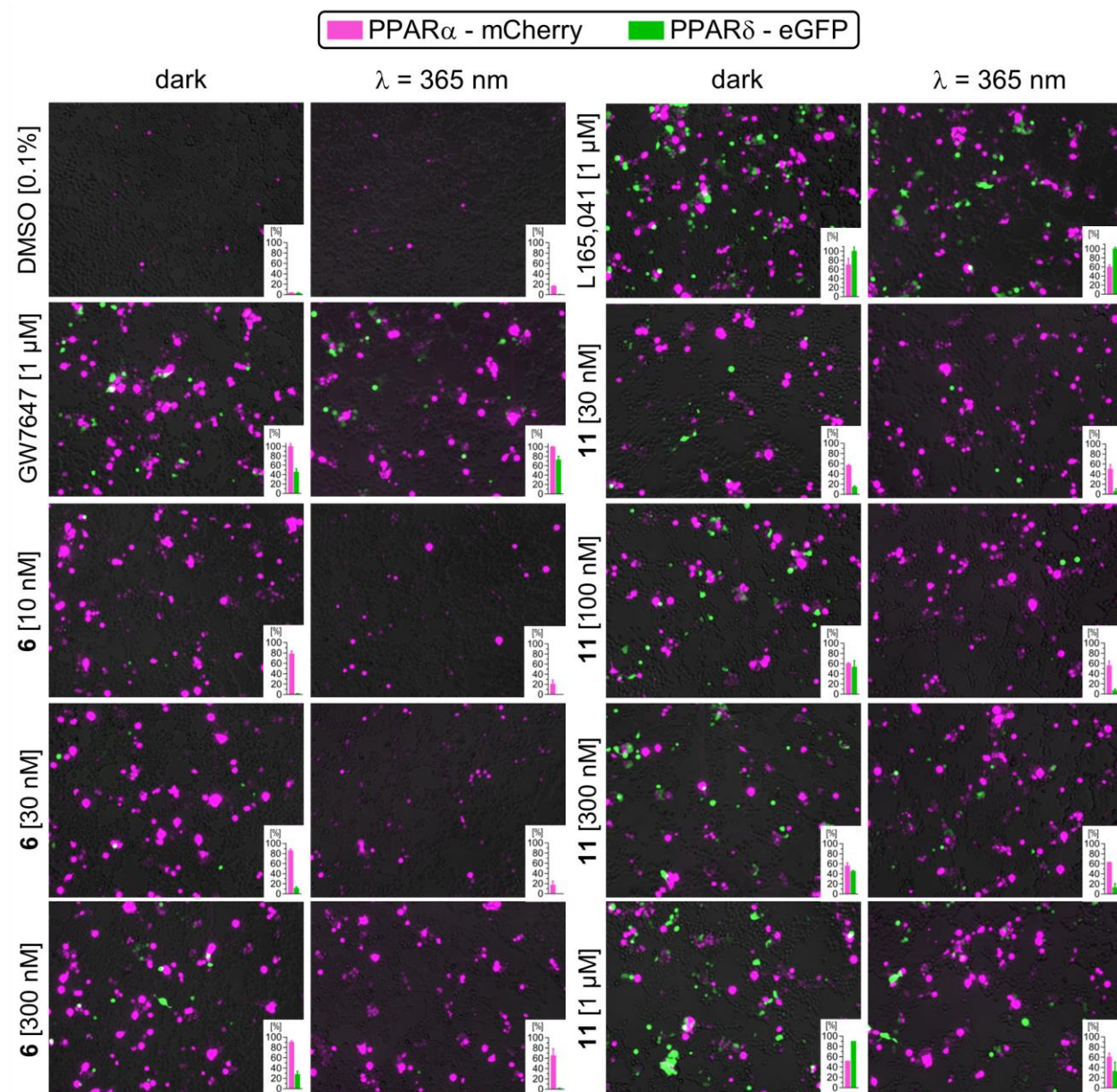


Figure 7. Overview of the live cell imaging of PPAR α -dependent mCherry and PPAR δ -dependent eGFP reporter induction by **6** and **11** in *trans*- (dark adapted) and *cis*-state (illuminated with $\lambda = 365$ nm). PPAR δ -dependent eGFP fluorescence by **6** is negligible. Inserts show mean \pm SEM of relative integrated densities referring to the maximum effect of the respective reference agonist at 1 μ M (PPAR α : GW7647; PPAR δ : L165,041), n=2.

Table S1. Overview of compound numbering for GL479 derivatives **1 - 11** and precursors

#	R ¹	R ²	n	ester	azobenzene
1	-H	-H	2	14	16
2	-H	-H	1	15	16
3	-CH ₃	-H	2	14	17
4	-Cl	-H	2	14	18
5	-CH(CH ₃) ₂	-H	2	14	19
6	-H	-CH ₃	2	14	20
7	-H	-Cl	2	14	21
8	-H	-CF ₃	2	14	22
9	-CH ₃	-CH ₃	2	14	23
10	-CH ₃	-CF ₃	2	14	24
11	-CH ₃	-Cl	2	14	25

Experimental Section

Chemistry

General. All reagents and solvents were purchased from commercial sources (Sigma-Aldrich, TCI Europe N.V., Strem Chemicals, etc.) and were used without further purification unless otherwise noted. Reactions were monitored by TLC on pre-coated, Merck Silica gel 60 F₂₅₄ glass backed plates. Flash silica gel chromatography was performed using silica gel (SiO₂, particle size 40-63 μm) purchased from Merck. All NMR spectra were measured on a BRUKER Avance III HD 400 (equipped with a CryoProbeTM). Multiplicities in the following experimental procedures are abbreviated as follows: s = singlet, d = doublet, t = triplet, q = quartet, quint = quintet, sext = sextet, hept = heptet, br = broad, m = multiplet. Proton chemical shifts are expressed in parts per million (ppm, δ scale) and are referenced to the residual protium in the NMR solvent (CDCl₃: δ = 7.26; DMSO-*d*₆: δ = 2.50; THF-*d*₈: δ = 1.72). Carbon chemical shifts are expressed in ppm (δ scale) and are referenced to the carbon resonance of the NMR solvent (CDCl₃: δ = 77.16; DMSO-*d*₆: δ = 39.52; THF-*d*₈: δ = 25.31). High-resolution mass spectra (HRMS) were obtained with an Agilent 6224 Accurate Mass time-of-flight (TOF) LC/MS system using either an electrospray ionization (ESI) or atmospheric pressure chemical ionization (APCI) ion source. All reported data refers to positive ionization mode.

Synthesis and analytical characterization data of 1-11 and their precursors.

(*E*)-2-Methyl-2-(4-(2-(4-(phenyldiazenyl)phenoxy)ethyl)phenoxy)propanoic acid (**1**). Ethyl 2-(4-(2-hydroxyethyl)phenoxy)-2-methylpropanoate³ (**14**, 50.0 mg, 0.198 mmol, 1.00 equiv.), 4-hydroxyazobenzene (**16**, 51.1 mg, 0.258 mmol, 1.30 equiv.) and triphenylphosphine (67.6 mg, 0.258 mmol, 1.30 equiv.) were dissolved in anhydrous THF (1.25 mL). DEAD (112 mg, 0.258 mmol, 1.30 equiv., 40 % solution in toluene) was added dropwise at 0 °C. The mixture was stirred at rt overnight. The solvent was removed under reduced pressure. The crude was dissolved in EtOH and 1M NaOH was added. The reaction was stirred at rt for 16 h. Solvent was removed under reduced pressure, water was added and acidified with 1M HCl. The mixture was extracted with CH₂Cl₂, dried over Na₂SO₄, filtered, and concentrated under reduced pressure. The crude product was purified using flash column chromatography (CH₂Cl₂ to 20% MeOH in CH₂Cl₂) to yield **1** (47.2 mg, 117 μmol, 59%) as an orange solid. ¹H NMR (400 MHz, CDCl₃): δ = 7.85 (dd, *J* = 12.2, 8.7 Hz, 4H), 7.55 (dt, *J* = 14.9, 6.9 Hz, 3H), 7.14 (dd, *J* = 8.8, 3.2 Hz, 4H), 6.76 (d, *J* = 8.5 Hz, 2H), 4.25 (t, *J* = 7.0 Hz, 2H), 2.98 (t, *J* = 6.9 Hz, 2H), 1.40 (s, 6H). ¹³C NMR (100 MHz, CDCl₃): δ = 175.0, 161.3, 155.0, 152.0, 146.1, 130.8, 129.4, 129.2, 124.6, 122.2, 119.3, 117.8, 115.1, 79.4, 68.9, 34.0, 25.8. HRMS: *m/z* calc. for C₂₄H₂₅N₂O₄⁺ ([M+H]⁺): 405.1809, found: 405.1803.

(*E*)-2-Methyl-2-(4-((4-(phenyldiazenyl)phenoxy)methyl)phenoxy)propanoic acid (**2**). Ethyl 2-(4-(hydroxymethyl)phenoxy)-2-methylpropanoate³ (**15**, 30.0 mg, 0.126 mmol, 1.00 equiv.), 4-hydroxyazobenzene (**16**, 32.4 mg, 0.164 mmol, 1.30 equiv.) and triphenylphosphine (42.9 mg, 0.164 mmol, 1.30 equiv.) were dissolved in anhydrous THF (0.80 mL). DEAD (71.3 mg, 0.164 mmol, 1.30 equiv., 40 % solution in toluene) was added dropwise at 0 °C. The mixture was stirred at rt overnight. The solvent was removed under reduced pressure. The crude was dissolved in EtOH and 1M NaOH was added. The reaction was stirred at rt for 16 h. Solvent was removed under reduced pressure, water was added and acidified with 1M HCl. The mixture was extracted with CH₂Cl₂, dried over Na₂SO₄, filtered, and concentrated under reduced pressure. The crude

product was purified using flash column chromatography (CH₂Cl₂ to 20% MeOH in CH₂Cl₂) to yield **2** (18.8 mg, 48 μmol, 38%) as an orange solid. ¹H NMR (400 MHz, DMSO-*d*₆): δ = 7.91 – 7.81 (m, 4H), 7.62 – 7.48 (m, 3H), 7.32 (d, *J* = 8.5 Hz, 2H), 7.23 – 7.16 (m, 2H), 6.90 – 6.82 (m, 2H), 5.09 (s, 2H), 1.46 (s, 6H). ¹³C NMR (100 MHz, CDCl₃): δ = 174.3, 161.7, 156.6, 152.5, 146.6, 131.3, 129.8, 129.6, 128.5, 125.0, 122.7, 118.4, 115.8, 79.9, 70.1, 26.1. HRMS: *m/z* calc. for C₂₃H₂₃N₂O₄⁺ ([M+H]⁺): 391.1652, found: 391.1647.

(*E*)-2-Methyl-2-(4-(2-(4-(*p*-tolylidiazanyl)phenoxy)ethyl)phenoxy)propanoic acid (**3**). Ethyl 2-(4-(2-hydroxyethyl)phenoxy)-2-methylpropanoate³ (**14**, 10.0 mg, 39.7 mmol, 1.00 equiv.), (*E*)-4-(*p*-tolylidiazanyl)phenol (**17**, 10.9 mg, 51.5 mmol, 1.30 equiv.) and triphenylphosphine (13.5 mg, 51.5 mmol, 1.30 equiv.) were dissolved in anhydrous THF (0.5 mL). DEAD (22.4 mg, 51.5 mmol, 1.30 equiv., 40 % solution in toluene) was added dropwise at 0 °C. The mixture was stirred at rt overnight. The solvent was removed under reduced pressure. The crude was dissolved in EtOH and 1M NaOH was added. The reaction was stirred at rt for 16 h. Solvent was removed under reduced pressure, water was added and acidified with 1M HCl. The mixture was extracted with CH₂Cl₂, dried over Na₂SO₄, filtered, and concentrated under reduced pressure. The crude product was purified using flash column chromatography (CH₂Cl₂ to 20% MeOH in CH₂Cl₂) to yield **3** (10.6 mg, 25.3 μmol, 64%) as an orange solid. ¹H NMR (400 MHz, THF-*d*₈): δ = 7.86 (d, *J* = 8.9 Hz, 2H), 7.76 (d, *J* = 8.2 Hz, 2H), 7.29 (d, *J* = 8.0 Hz, 2H), 7.18 (d, *J* = 8.5 Hz, 2H), 7.07 – 7.01 (m, 2H), 6.84 (d, *J* = 8.5 Hz, 2H), 4.22 (t, *J* = 7.1 Hz, 2H), 3.03 (t, *J* = 7.1 Hz, 2H), 1.53 (s, 6H). ¹³C NMR (100 MHz, THF-*d*₈): δ = 175.6, 162.5, 155.7, 151.9, 147.9, 141.6, 132.3, 130.4, 130.4, 125.3, 123.4, 120.1, 115.5, 79.5, 70.1, 35.7, 30.7, 21.4. HRMS: *m/z* calc. for C₂₅H₂₇N₂O₄⁺ ([M+H]⁺): 419.1965, found: 419.1960.

(*E*)-2-(4-(2-(4-((4-Chlorophenyl)diazanyl)phenoxy)ethyl)phenoxy)-2-methylpropanoic acid (**4**). Ethyl 2-(4-(2-hydroxyethyl)phenoxy)-2-methylpropanoate³ (**14**, 9.4 mg, 37 mmol, 1.00 equiv.), (*E*)-4-((4-chlorophenyl)diazanyl)phenol (**18**, 11 mg, 49 mmol, 1.30 equiv.) and triphenylphosphine (13

mg, 49 mmol, 1.30 equiv.) were dissolved in anhydrous THF (0.5 mL). DEAD (21 mg, 49 mmol, 1.30 equiv., 40 % solution in toluene) was added dropwise at 0 °C. The mixture was stirred at rt overnight. The solvent was removed under reduced pressure. The crude was dissolved in EtOH and 1M NaOH was added. The reaction was stirred at rt for 16 h. Solvent was removed under reduced pressure, water was added and acidified with 1M HCl. The mixture was extracted with CH₂Cl₂, dried over Na₂SO₄, filtered, and concentrated under reduced pressure. The crude product was purified using flash column chromatography (CH₂Cl₂ to 20% MeOH in CH₂Cl₂) to yield **4** (3.2 mg, 7.3 μmol, 20%) as an orange solid. ¹H NMR (400 MHz, CDCl₃): δ = 7.88 (d, *J* = 8.7 Hz, 2H), 7.82 (d, *J* = 8.5 Hz, 2H), 7.46 (d, *J* = 8.5 Hz, 2H), 7.21 (d, *J* = 8.2 Hz, 2H), 6.99 (d, *J* = 8.7 Hz, 2H), 6.90 (d, *J* = 8.3 Hz, 2H), 4.23 (t, *J* = 6.9 Hz, 2H), 3.09 (t, *J* = 6.9 Hz, 2H), 1.58 (s, 6H). ¹³C NMR (100 MHz, CDCl₃): δ = 176.8, 161.5, 152.8, 151.1, 146.8, 136.2, 133.1, 129.9, 129.2, 124.9, 123.8, 121.0, 114.8, 80.0, 69.0, 34.9, 25.0. HRMS: *m/z* calc. for C₂₄H₂₄ClN₂O₄⁺ ([M+H]⁺): 439.1419, found: 439.1416.

(*E*)-2-(4-(2-(4-((4-Isopropylphenyl)diazenyl)phenoxy)ethyl)phenoxy)-2-methylpropanoic acid (**5**). Ethyl 2-(4-(2-hydroxyethyl)phenoxy)-2-methylpropanoate³ (**14**, 9.4 mg, 37 mmol, 1.00 equiv.), (*E*)-4-((4-isopropylphenyl)diazenyl)phenol (**19**, 12 mg, 49 mmol, 1.30 equiv.) and triphenylphosphine (13 mg, 49 mmol, 1.30 equiv.) were dissolved in anhydrous THF (0.5 mL). DEAD (21 mg, 49 mmol, 1.30 equiv., 40 % solution in toluene) was added dropwise at 0 °C. The mixture was stirred at rt overnight. The solvent was removed under reduced pressure. The crude was dissolved in EtOH and 1M NaOH was added. The reaction was stirred at rt for 16 h. Solvent was removed under reduced pressure, water was added and acidified with 1M HCl. The mixture was extracted with CH₂Cl₂, dried over Na₂SO₄, filtered, and concentrated under reduced pressure. The crude product was purified using flash column chromatography (CH₂Cl₂ to 20% MeOH in CH₂Cl₂) to yield **5** (10.0 mg, 22.4 μmol, 61%) as an orange solid. ¹H NMR (400 MHz, CDCl₃): δ = 7.87 (d, *J* = 8.8 Hz, 2H), 7.81 (d, *J* = 8.3 Hz, 2H), 7.35 (d, *J* = 8.3 Hz, 2H), 7.19 (d, *J* = 8.3 Hz, 2H), 6.98 (d, *J* = 8.8 Hz, 2H), 6.89 (d, *J* = 8.3 Hz, 2H), 4.22 (t, *J* = 7.0 Hz, 2H), 3.08 (t, *J* = 6.9 Hz, 2H), 2.98 (quint, *J* = 6.7 Hz,

1H), 1.60 (s, 6H), 1.29 (d, $J = 6.9$ Hz, 6H). ^{13}C NMR (100 MHz, CDCl_3): $\delta = 177.3, 161.2, 153.3, 151.8, 151.2, 147.2, 132.8, 130.0, 127.2, 124.7, 122.7, 120.7, 114.9, 69.1, 35.1, 34.2, 25.2, 24.0, 20.9$. HRMS: m/z calc. for $\text{C}_{27}\text{H}_{29}\text{N}_2\text{O}_3^+$ ($[\text{M}-\text{H}_2\text{O}]^+$): 429.2173, found: 429.2152.

(*E*)-2-Methyl-2-(4-(2-(2-methyl-4-(phenyldiazenyl)phenoxy)ethyl)phenoxy)propanoic acid (**6**). Ethyl 2-(4-(2-hydroxyethyl)phenoxy)-2-methylpropanoate³ (**14**, 20.0 mg, 79.3 mmol, 1.00 equiv.), (*E*)-2-methyl-4-(phenyldiazenyl)phenol (**20**, 21.9 mg, 103 mmol, 1.30 equiv.) and triphenylphosphine (27.0 mg, 103 mmol, 1.30 equiv.) were dissolved in anhydrous THF (0.5 mL). DEAD (44.6 mg, 103 mmol, 1.30 equiv., 40 % solution in toluene) was added dropwise at 0 °C. The mixture was stirred at rt overnight. The solvent was removed under reduced pressure. The crude was dissolved in EtOH and 1M NaOH was added. The reaction was stirred at rt for 16 h. Solvent was removed under reduced pressure, water was added and acidified with 1M HCl. The mixture was extracted with CH_2Cl_2 , dried over Na_2SO_4 , filtered, and concentrated under reduced pressure. The crude product was purified using flash column chromatography (CH_2Cl_2 to 20% MeOH in CH_2Cl_2) to yield **6** (28.2 mg, 67.4 μmol , 85%) as an orange solid. ^1H NMR (400 MHz, $\text{THF}-d_8$): $\delta = 7.84$ (d, $J = 7.3$ Hz, 2H), 7.74 (s, 2H), 7.46 (t, $J = 7.4$ Hz, 2H), 7.40 (d, $J = 7.1$ Hz, 1H), 7.19 (d, $J = 8.5$ Hz, 2H), 7.05 – 6.99 (m, 1H), 6.84 (d, $J = 8.5$ Hz, 2H), 4.30 – 4.19 (m, 2H), 3.06 (t, $J = 6.9$ Hz, 2H), 2.25 (s, 3H), 1.52 (s, 6H). ^{13}C NMR (100 MHz, $\text{THF}-d_8$): $\delta = 175.6, 160.8, 155.7, 153.9, 147.4, 132.6, 131.0, 130.5, 129.8, 128.1, 124.8, 124.6, 123.3, 120.1, 111.5, 79.5, 70.1, 35.8, 25.9, 16.6$. HRMS: m/z calc. for $\text{C}_{25}\text{H}_{27}\text{N}_2\text{O}_4^+$ ($[\text{M}+\text{H}]^+$): 419.1965, found: 419.1963.

(*E*)-2-(4-(2-(2-Chloro-4-(phenyldiazenyl)phenoxy)ethyl)phenoxy)-2-methylpropanoic acid (**7**). Ethyl 2-(4-(2-hydroxyethyl)phenoxy)-2-methylpropanoate³ (**14**, 9.4 mg, 37 mmol, 1.00 equiv.), (*E*)-2-chloro-4-(phenyldiazenyl)phenol (**21**, 11 mg, 49 mmol, 1.30 equiv.) and triphenylphosphine (13 mg, 49 mmol, 1.30 equiv.) were dissolved in anhydrous THF (0.5 mL). DEAD (21 mg, 49 mmol, 1.30 equiv., 40 % solution in toluene) was added dropwise at 0 °C. The mixture was stirred at rt overnight. The solvent was removed under reduced pressure. The crude was dissolved in EtOH

and 1M NaOH was added. The reaction was stirred at rt for 16 h. Solvent was removed under reduced pressure, water was added and acidified with 1M HCl. The mixture was extracted with CH₂Cl₂, dried over Na₂SO₄, filtered, and concentrated under reduced pressure. The crude product was purified using flash column chromatography (CH₂Cl₂ to 20% MeOH in CH₂Cl₂) to yield **7** (15.2 mg, 34.6 μmol, 93%) as an orange solid. ¹H NMR (400 MHz, CDCl₃): δ = 8.00 (d, *J* = 2.1 Hz, 1H), 7.87 (d, *J* = 7.5 Hz, 2H), 7.83 (dd, *J* = 8.7, 2.2 Hz, 1H), 7.49 (dt, *J* = 13.1, 6.9 Hz, 3H), 7.26 (d, *J* = 8.3 Hz, 2H), 7.00 (d, *J* = 8.8 Hz, 1H), 6.91 (d, *J* = 8.4 Hz, 2H), 4.28 (t, *J* = 6.8 Hz, 2H), 3.15 (t, *J* = 6.7 Hz, 2H), 1.60 (s, 6H). ¹³C NMR (100 MHz, CDCl₃) δ 177.7, 156.6, 153.1, 152.6, 146.9, 133.0, 131.0, 130.3, 129.2, 124.9, 124.0, 123.3, 122.9, 121.0, 112.6, 80.0, 70.2, 35.0, 25.2. HRMS: *m/z* calc. for C₂₄H₂₄ClN₂O₄⁺ ([M+H]⁺): 439.1419, found: 439.1404.

(*E*)-2-Methyl-2-(4-(2-(4-(phenyldiazenyl)-2-(trifluoromethyl)phenoxy)ethyl)phenoxy)propanoic acid (**8**). Ethyl 2-(4-(2-hydroxyethyl)phenoxy)-2-methylpropanoate³ (**14**, 21.9 mg, 87.0 mmol, 1.00 equiv.), (*E*)-4-(phenyldiazenyl)-2-(trifluoromethyl)phenol (**22**, 31.6 mg, 113 mmol, 1.30 equiv.) and triphenylphosphine (29.6 mg, 113 mmol, 1.30 equiv.) were dissolved in anhydrous THF (0.5 mL). DEAD (49.1 mg, 113 mmol, 1.30 equiv., 40 % solution in toluene) was added dropwise at 0 °C. The mixture was stirred at rt overnight. The solvent was removed under reduced pressure. The crude was dissolved in EtOH and 1M NaOH was added. The reaction was stirred at rt for 16 h. Solvent was removed under reduced pressure, water was added and acidified with 1M HCl. The mixture was extracted with CH₂Cl₂, dried over Na₂SO₄, filtered, and concentrated under reduced pressure. The crude product was purified using flash column chromatography (CH₂Cl₂ to 20% MeOH in CH₂Cl₂) to yield **8** (20.1 mg, 42.5 μmol, 49%) as an orange solid. ¹H NMR (400 MHz, CDCl₃): δ = 8.20 (d, *J* = 2.2 Hz, 1H), 8.06 (dd, *J* = 8.8, 2.3 Hz, 1H), 7.92 – 7.85 (m, 2H), 7.55 – 7.43 (m, 3H), 7.23 (d, *J* = 8.5 Hz, 2H), 7.06 (d, *J* = 8.9 Hz, 1H), 6.91 (d, *J* = 8.5 Hz, 2H), 4.31 (t, *J* = 6.6 Hz, 2H), 3.13 (t, *J* = 6.6 Hz, 2H), 1.59 (s, 7H). ¹³C NMR (100 MHz, CDCl₃): δ = 177.3, 158.8, 153.0, 152.5, 145.8, 133.1, 131.1, 130.2, 129.3, 128.3, 122.9, 122.3 (q), 122.2 (q), 122.1 (q), 122.1

(q), 121.1, 120.1 (q), 119.8 (q), 119.5 (q), 119.1 (q), 112.9, 80.1, 70.1, 35.0, 25.1. HRMS: m/z calc. for $C_{25}H_{24}F_3N_2O_4^+$ ($[M+H]^+$): 473.1683, found: 473.1673.

(*E*)-2-Methyl-2-(4-(2-(2-methyl-4-(*p*-tolylidiazanyl)phenoxy)ethyl)phenoxy)propanoic acid (**9**). Ethyl 2-(4-(2-hydroxyethyl)phenoxy)-2-methylpropanoate³ (**14**, 9.4 mg, 37 mmol, 1.00 equiv.), (*E*)-2-methyl-4-(*p*-tolylidiazanyl)phenol (**23**, 11 mg, 49 mmol, 1.30 equiv.) and triphenylphosphine (13 mg, 49 mmol, 1.30 equiv.) were dissolved in anhydrous THF (0.5 mL). DEAD (21 mg, 49 mmol, 1.30 equiv., 40 % solution in toluene) was added dropwise at 0 °C. The mixture was stirred at rt overnight. The solvent was removed under reduced pressure. The crude was dissolved in EtOH and 1M NaOH was added. The reaction was stirred at rt for 16 h. Solvent was removed under reduced pressure, water was added and acidified with 1M HCl. The mixture was extracted with CH_2Cl_2 , dried over Na_2SO_4 , filtered, and concentrated under reduced pressure. The crude product was purified using flash column chromatography (CH_2Cl_2 to 20% MeOH in CH_2Cl_2) to yield **9** (4.1 mg, 9.5 μ mol, 26%) as an orange solid. ¹H NMR (400 MHz, $CDCl_3$): δ = 7.82 – 7.71 (m, 4H), 7.29 (d, J = 8.2 Hz, 2H), 7.22 (d, J = 8.3 Hz, 2H), 6.90 (t, J = 8.6 Hz, 3H), 4.23 (t, J = 6.6 Hz, 2H), 3.10 (t, J = 6.6 Hz, 2H), 2.42 (s, 3H), 2.25 (s, 3H), 1.59 (s, 6H). ¹³C NMR (100 MHz, $CDCl_3$): δ = 176.2, 159.5, 152.9, 151.0, 146.7, 140.8, 133.7, 130.2, 129.8, 127.7, 123.9, 123.8, 122.6, 121.1, 110.7, 80.1, 69.0, 35.2, 25.1, 21.6, 16.6. HRMS: m/z calc. for $C_{26}H_{29}N_2O_4^+$ ($[M+H]^+$): 433.2122, found: 433.2136.

(*E*)-2-Methyl-2-(4-(2-(4-(*p*-tolylidiazanyl)-2-(trifluoromethyl)phenoxy)ethyl)phenoxy)propanoic acid (**10**). Ethyl 2-(4-(2-hydroxyethyl)phenoxy)-2-methylpropanoate³ (**14**, 21.9 mg, 87.0 mmol, 1.00 equiv.), (*E*)-4-(*p*-tolylidiazanyl)-2-(trifluoromethyl)phenol (**24**, 27.8 mg, 113 mmol, 1.30 equiv.) and triphenylphosphine (29.6 mg, 113 mmol, 1.30 equiv.) were dissolved in anhydrous THF (0.5 mL). DEAD (49.1 mg, 113 mmol, 1.30 equiv., 40 % solution in toluene) was added dropwise at 0 °C. The mixture was stirred at rt overnight. The solvent was removed under reduced pressure. The crude was dissolved in EtOH and 1M NaOH was added. The reaction was stirred at rt for 16h.

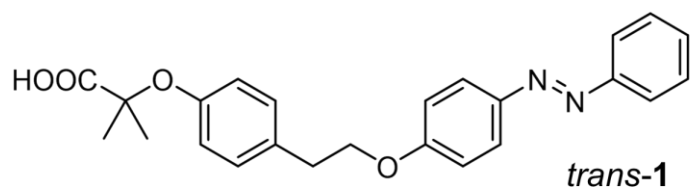
Solvent was removed under reduced pressure, water was added and acidified with 1M HCl. The mixture was extracted with CH₂Cl₂, dried over Na₂SO₄, filtered, and concentrated under reduced pressure. The crude product was purified using flash column chromatography (CH₂Cl₂ to 20% MeOH in CH₂Cl₂) to yield **10** (23.7 mg, 48.7 μmol, 56%) as an orange solid. ¹H NMR (400 MHz, CDCl₃): δ = 8.18 (d, *J* = 2.3 Hz, 1H), 8.06 – 8.02 (m, 1H), 7.83 – 7.77 (m, 2H), 7.30 (d, *J* = 8.1 Hz, 2H), 7.24 (s, 1H), 7.05 (d, *J* = 8.9 Hz, 1H), 6.91 (d, *J* = 8.5 Hz, 2H), 4.30 (t, *J* = 6.6 Hz, 2H), 3.12 (t, *J* = 6.6 Hz, 2H), 2.43 (s, 3H), 1.59 (s, 6H). ¹³C NMR (100 MHz, CDCl₃): δ = 177.4, 158.5, 153.0, 150.6, 145.9, 141.8, 133.1, 130.2, 129.9, 128.1, 122.9, 122.1 (q), 122.1 (q), 122.0 (q), 122.0 (q), 121.1, 120.0 (q), 119.7 (q), 119.4 (q), 119.1 (q), 112.9, 80.0, 70.1, 35.0, 25.1, 21.7. HRMS: *m/z* calc. for C₂₆H₂₆F₃N₂O₄⁺ ([M+H]⁺): 487.1839, found: 487.1852.

(*E*)-2-(4-(2-(2-Chloro-4-(*p*-tolylidiazanyl)phenoxy)ethyl)phenoxy)-2-methylpropanoic acid (**11**). Ethyl 2-(4-(2-hydroxyethyl)phenoxy)-2-methylpropanoate³ (**14**, 21.9 mg, 87.0 mmol, 1.00 equiv.), (*E*)-2-chloro-4-(*p*-tolylidiazanyl)phenol (**25**, 30.0 mg, 113 mmol, 1.30 equiv.) and triphenylphosphine (29.6 mg, 113 mmol, 1.30 equiv.) were dissolved in anhydrous THF (0.5 mL). DEAD (49.1 mg, 113 mmol, 1.30 equiv., 40 % solution in toluene) was added dropwise at 0 °C. The mixture was stirred at rt overnight. The solvent was removed under reduced pressure. The crude was dissolved in EtOH and 1M NaOH was added. The reaction was stirred at rt for 16 h. Solvent was removed under reduced pressure, water was added and acidified with 1M HCl. The mixture was extracted with CH₂Cl₂, dried over Na₂SO₄, filtered, and concentrated under reduced pressure. The crude product was purified using flash column chromatography (CH₂Cl₂ to 20% MeOH in CH₂Cl₂) to yield **11** (17.6 mg, 38.9 μmol, 45%) as an orange solid. ¹H NMR (400 MHz, DMSO-*d*₆): δ = 7.94 – 7.85 (m, 2H), 7.78 (d, *J* = 8.3 Hz, 2H), 7.39 (dd, *J* = 8.6, 3.8 Hz, 3H), 7.27 (d, *J* = 8.7 Hz, 2H), 6.78 (d, *J* = 8.6 Hz, 2H), 4.34 (t, *J* = 6.9 Hz, 2H), 3.11 – 3.01 (m, 2H), 2.40 (s, 3H), 1.49 (s, 6H). ¹³C NMR (101 MHz, DMSO): δ = 175.1, 156.0, 153.9, 149.9, 145.9, 141.6, 130.9, 130.0, 129.9, 124.9, 122.5, 122.5, 122.1, 118.4, 113.8, 78.3, 69.8, 33.9, 25.0, 21.0. HRMS: *m/z* calc. for C₂₅H₂₆ClN₂O₄⁺ ([M+H]⁺): 453.1576, found: 453.1573.

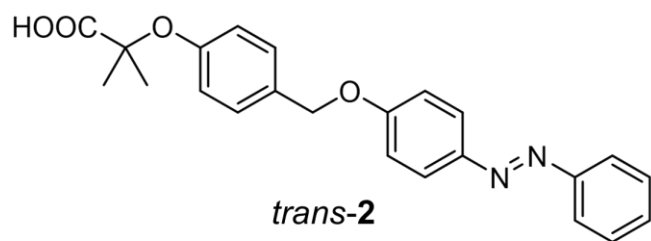
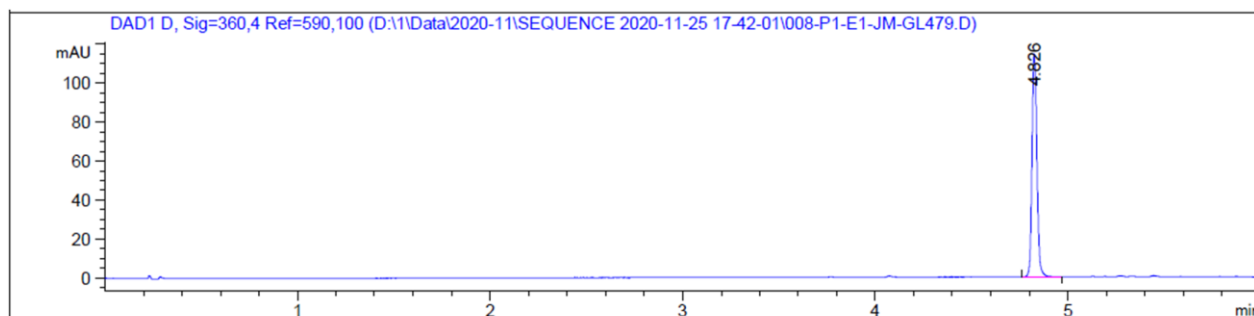
Ethyl 2-(4-(2-hydroxyethyl)phenoxy)-2-methylpropanoate³ (**14**). 4-(Hydroxyethyl)phenol (**12**, 200 mg, 1.45 mmol, 1.00 equiv.) and K₂CO₃ (2.00 g, 14.5 mmol, 10.0 equiv.) were dissolved in DMF (4.5 mL). Ethyl 2-bromo-2-methylpropanoate (875 mg, 4.48 mmol, 3.10 equiv.) was added and the mixture was stirred for 4 h under reflux. Water was added, phases were separated, the aqueous layer was extracted with EtOAc, washed with brine, dried over Na₂SO₄, filtered, and concentrated under reduced pressure. The crude product was purified using flash column chromatography (hexanes:EtOAc (8:2)) to yield **14** (292 mg, 1.16 mmol, 80%) as a colorless liquid. ¹H NMR (400 MHz, CDCl₃): δ = 7.13 – 7.05 (m, 2H), 6.83 – 6.76 (m, 2H), 4.24 (q, *J* = 7.1 Hz, 2H), 3.82 (t, *J* = 6.5 Hz, 2H), 2.80 (t, *J* = 6.6 Hz, 2H), 1.58 (s, 6H), 1.25 (d, *J* = 7.1 Hz, 3H). ¹³C NMR (100 MHz, CDCl₃): δ = 174.5, 154.2, 132.1, 129.8, 119.6, 79.2, 63.9, 61.5, 38.5, 25.5, 14.2. HRMS: *m/z* calc. for C₁₄H₁₉O₃⁺ ([M-H₂O]⁺): 235.1329, found: 235.1335.

Ethyl 2-(4-(hydroxymethyl)phenoxy)-2-methylpropanoate (**15**). 4-(Hydroxymethyl)phenol (**13**, 180 mg, 1.45 mmol, 1.00 equiv.) and K₂CO₃ (2.00 g, 14.5 mmol, 10.0 equiv.) were dissolved in DMF (4.5 mL). Ethyl 2-bromo-2-methylpropanoate (875 mg, 4.48 mmol, 3.10 equiv.) was added and the mixture was stirred for 4 h under reflux. Water was added, phases were separated, the aqueous layer was extracted with EtOAc, washed with brine, dried over Na₂SO₄, filtered, and concentrated under reduced pressure. The crude product was purified using flash column chromatography (hexanes:EtOAc (8:2)) to yield **15** (162 mg, 0.680 mmol, 47%) as a colorless liquid. ¹H NMR (400 MHz, CDCl₃): δ = 7.23 (d, *J* = 8.3 Hz, 2H), 6.86 – 6.79 (m, 2H), 4.61 (d, *J* = 1.5 Hz, 2H), 4.23 (q, *J* = 7.1 Hz, 2H), 1.59 (s, 6H), 1.25 (t, *J* = 7.1 Hz, 3H). ¹³C NMR (100 MHz, CDCl₃): δ = 174.4, 155.1, 134.7, 128.3, 119.3, 79.3, 65.1, 61.6, 25.5, 14.2. HRMS: *m/z* calc. for C₁₃H₁₇O₃⁺ ([M-H₂O]⁺): 221.1172, found: 221.1173.

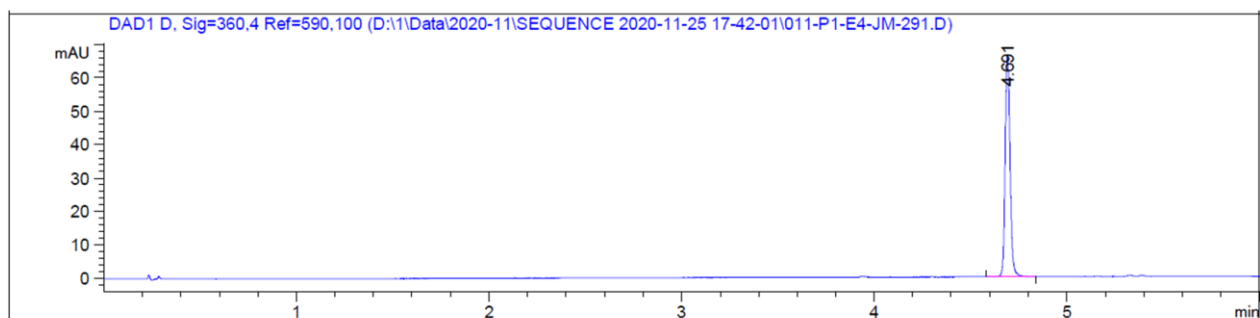
HPLC Traces

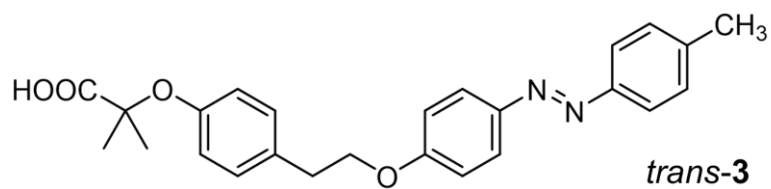


Detection wavelength $\lambda = 360$ nm

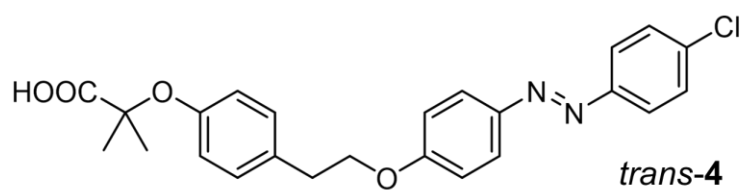
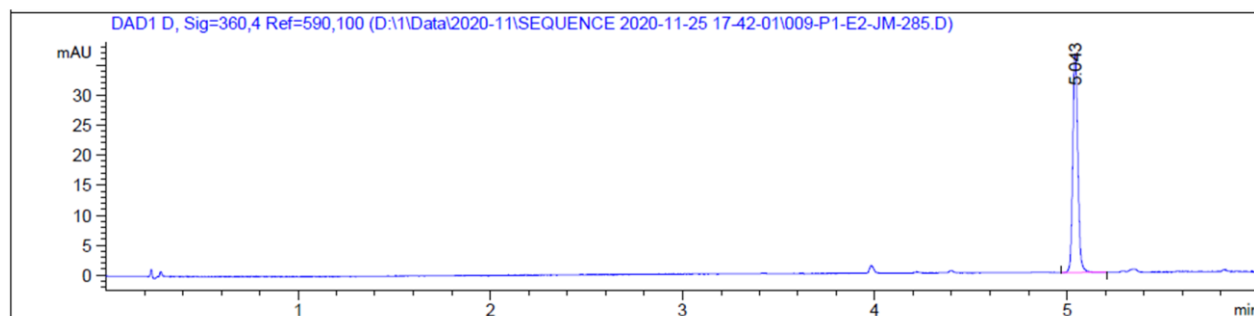


Detection wavelength $\lambda = 360$ nm

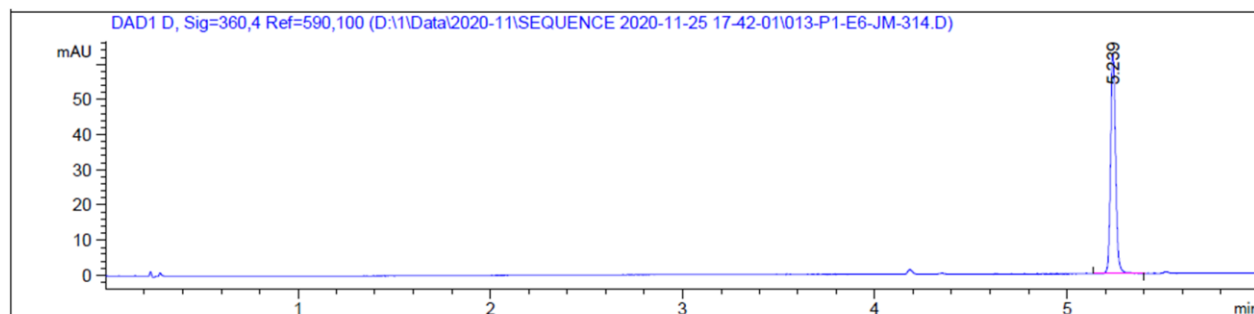


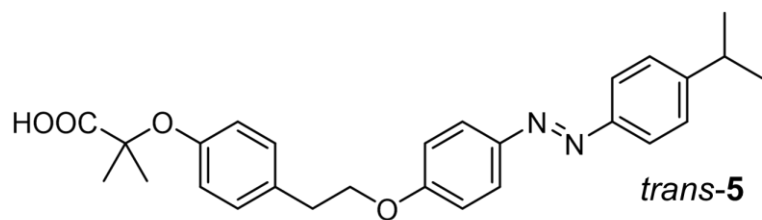


Detection wavelength $\lambda = 360$ nm

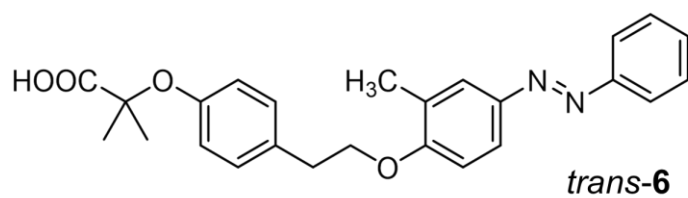
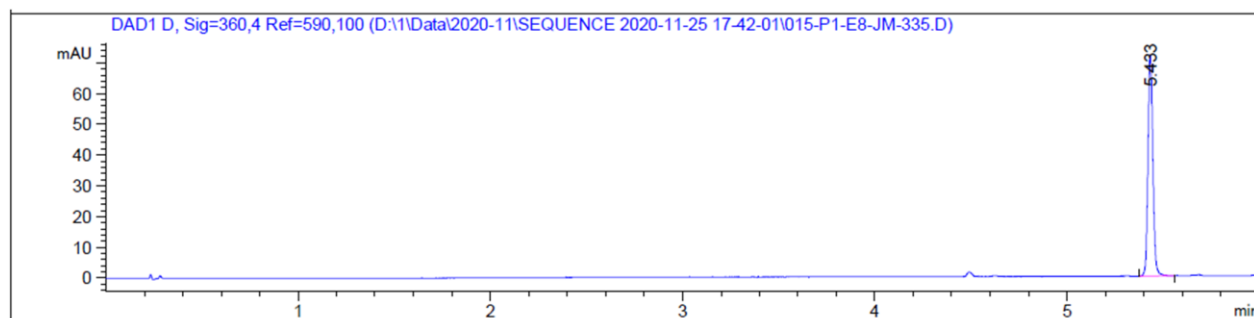


Detection wavelength $\lambda = 360$ nm

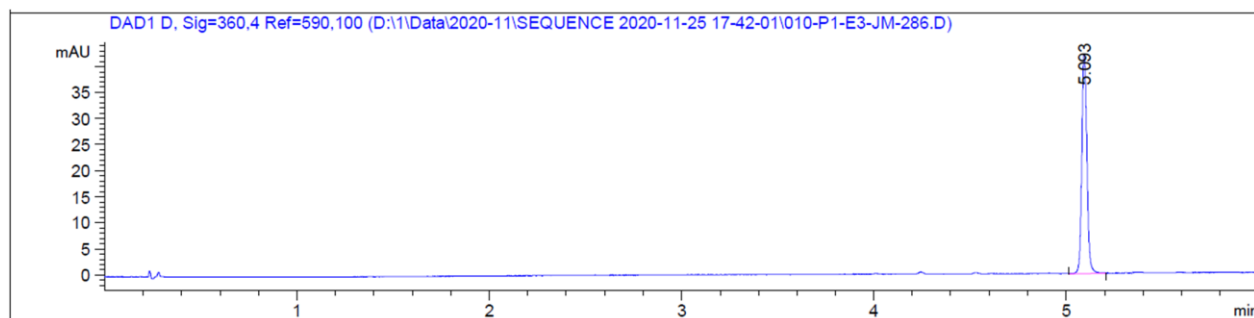


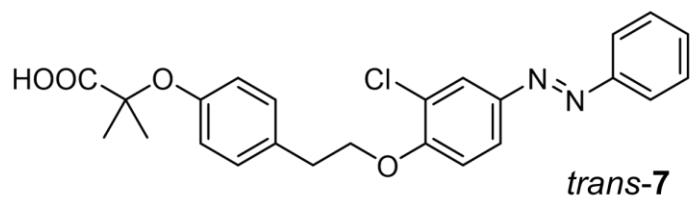


Detection wavelength $\lambda = 360$ nm

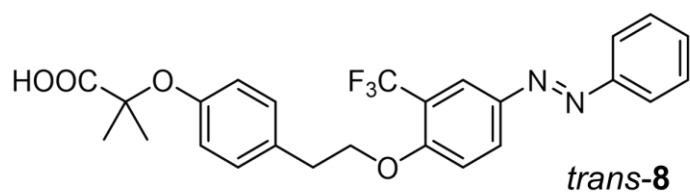
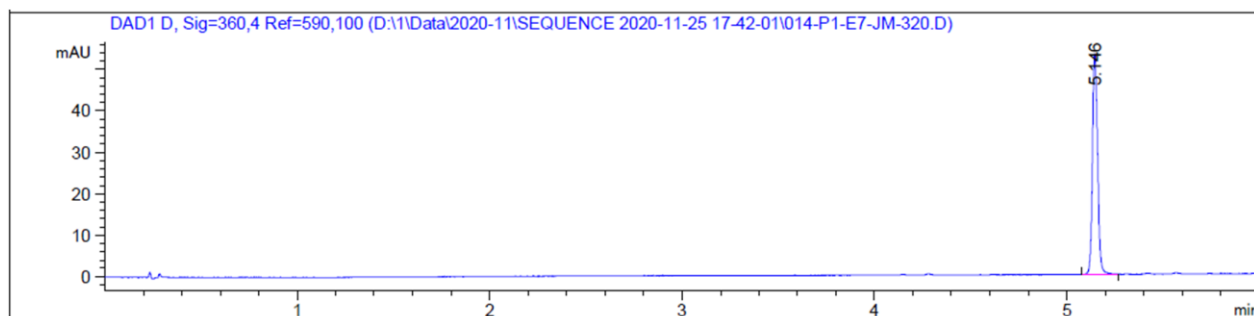


Detection wavelength $\lambda = 360$ nm

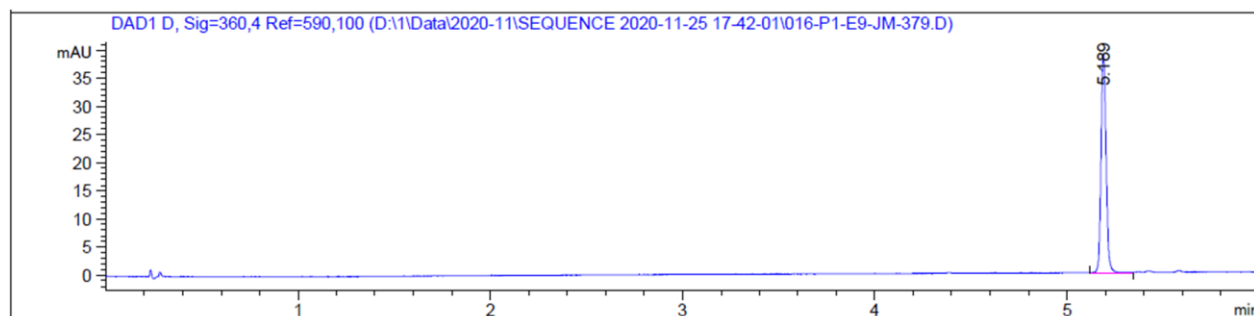


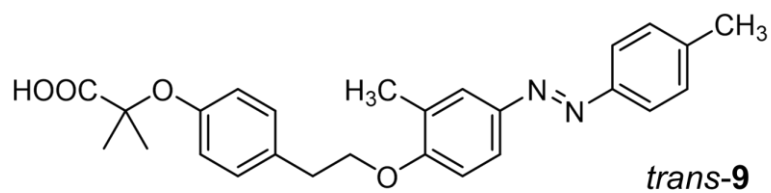


Detection wavelength $\lambda = 360$ nm

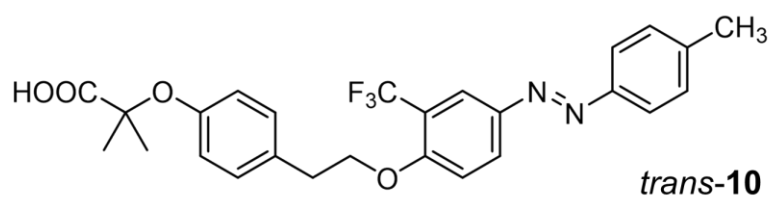
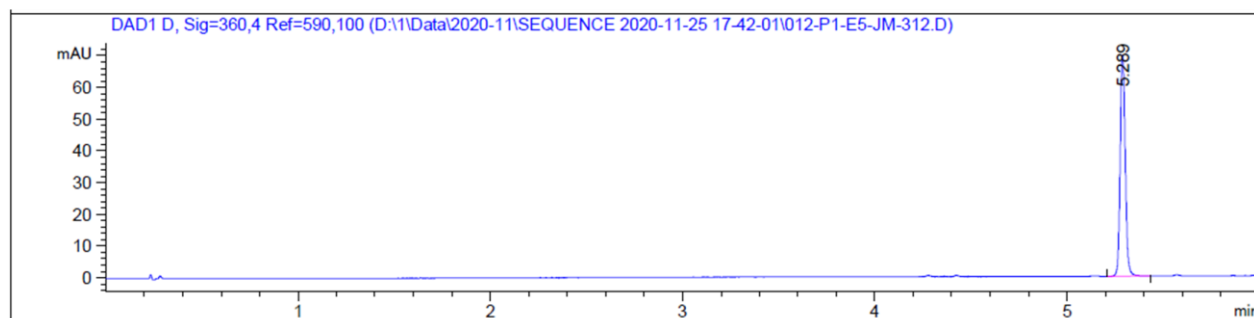


Detection wavelength $\lambda = 360$ nm

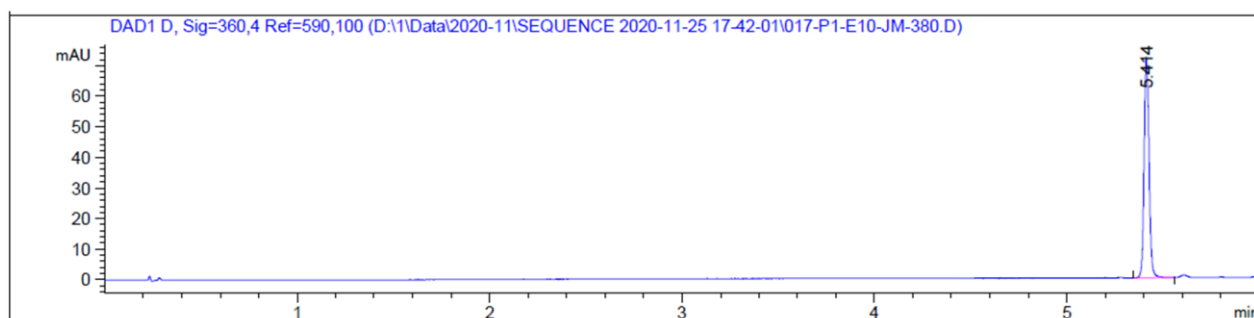


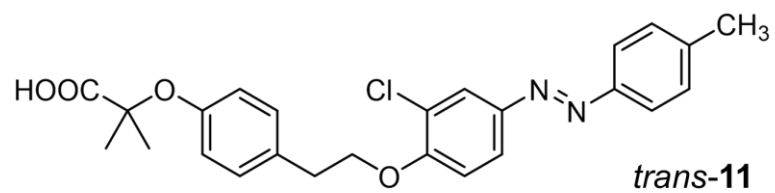


Detection wavelength $\lambda = 360$ nm

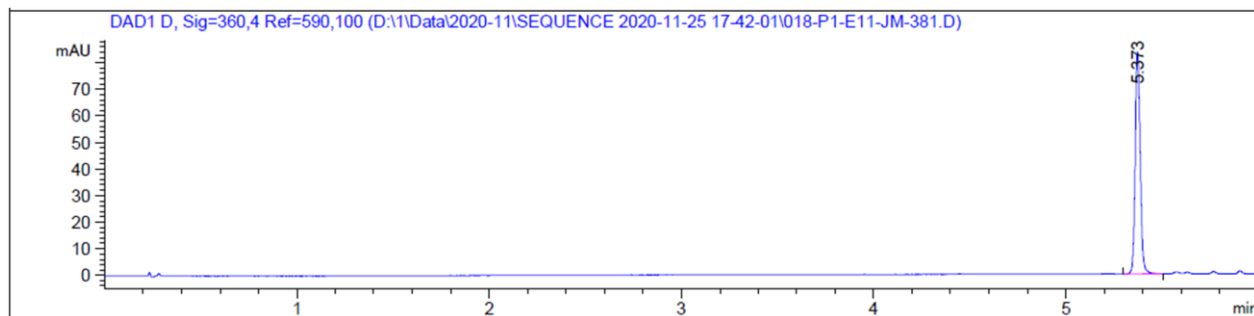


Detection wavelength $\lambda = 360$ nm



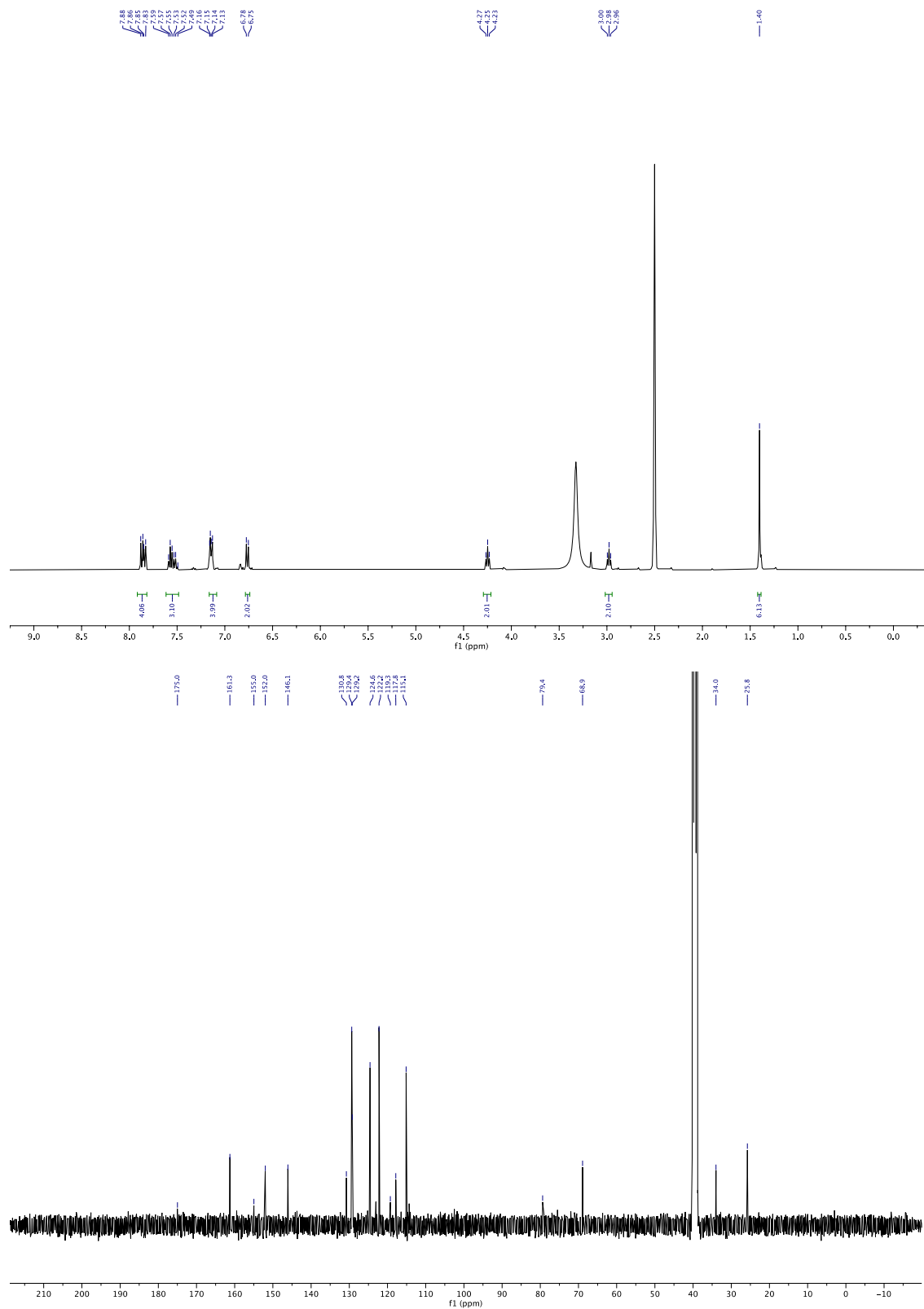


Detection wavelength $\lambda = 360$ nm

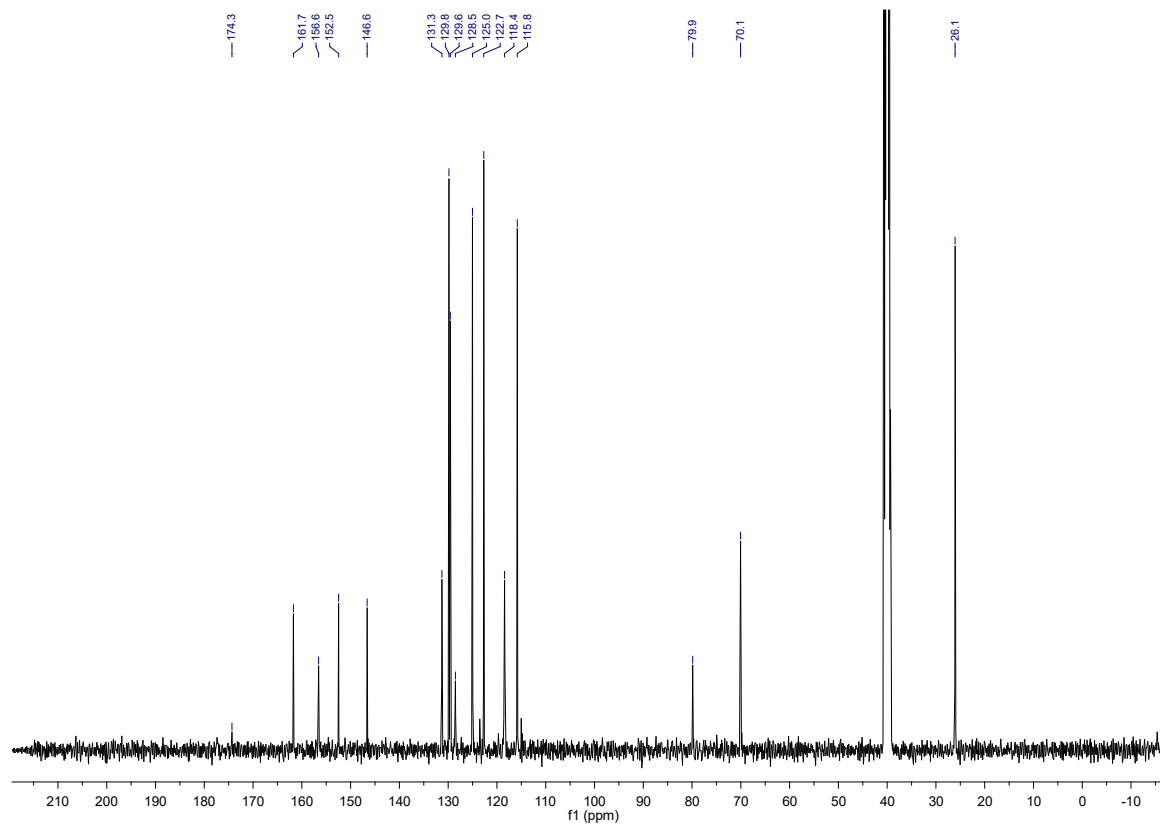
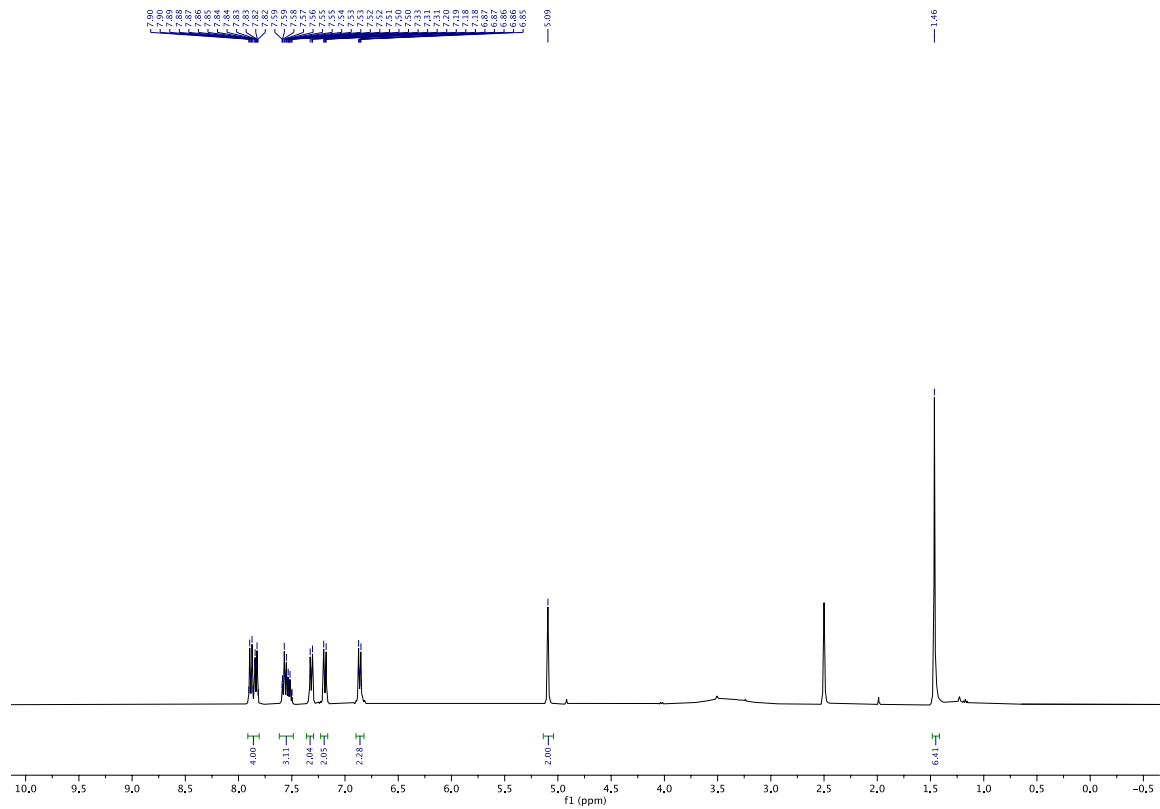


¹H and ¹³C NMR Spectra

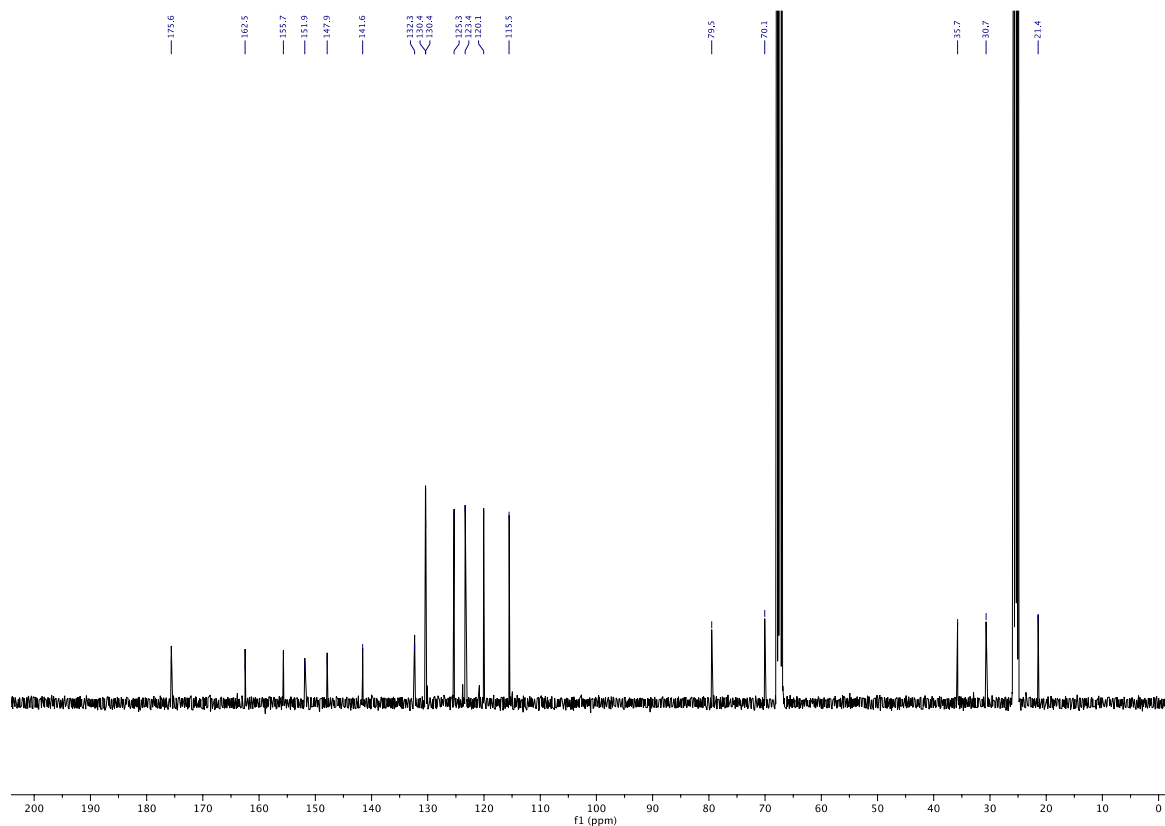
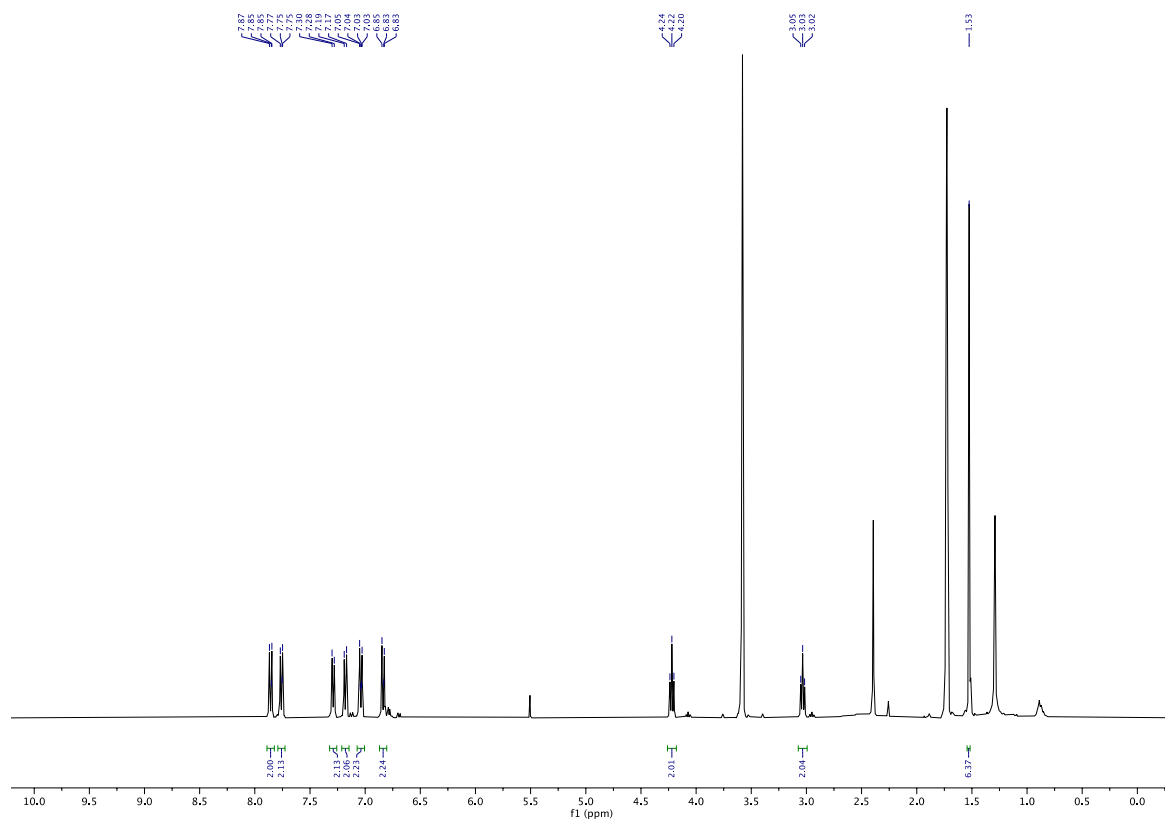
Compound 1



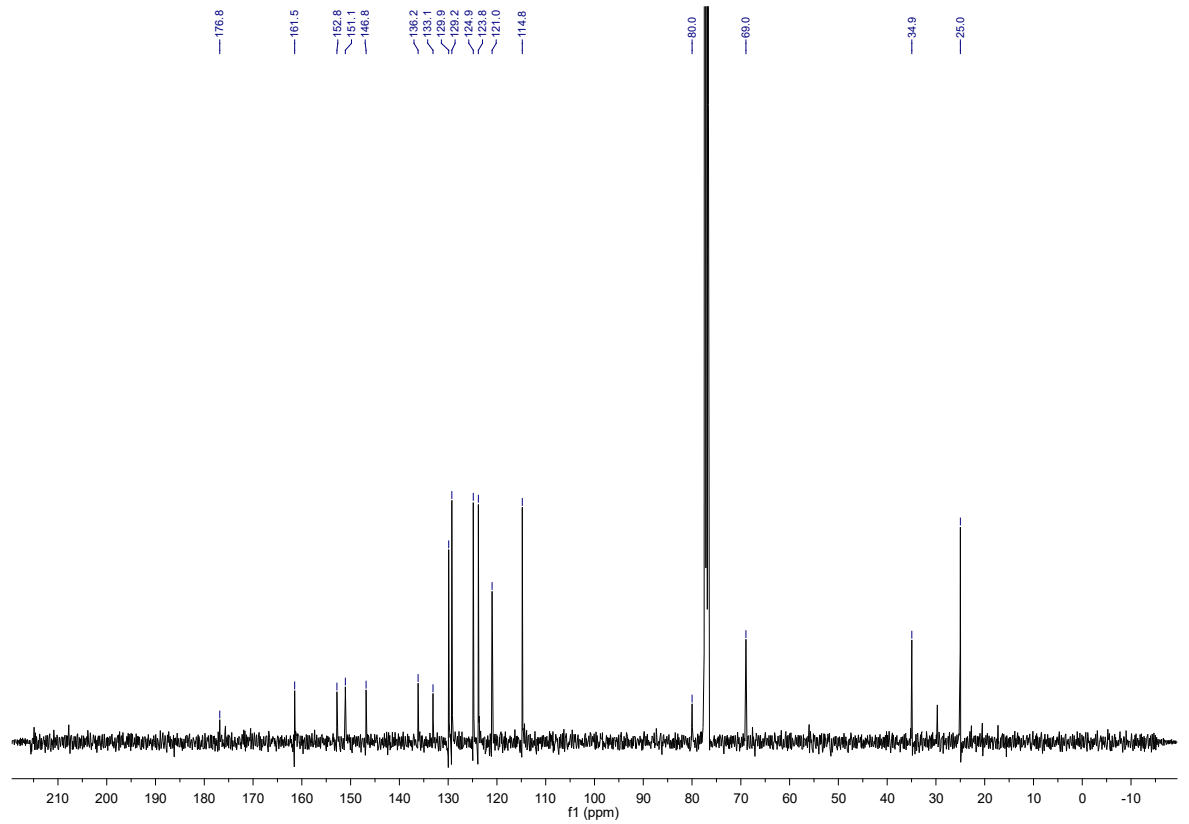
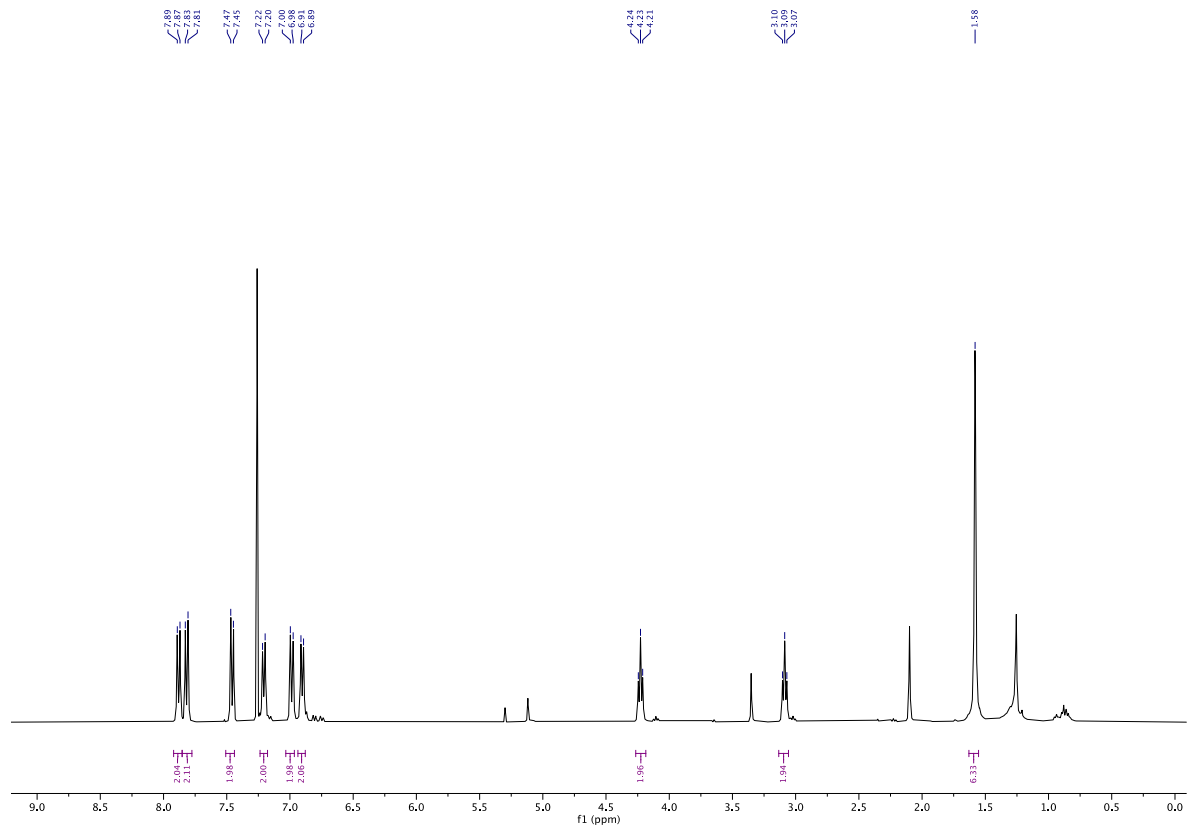
Compound 2



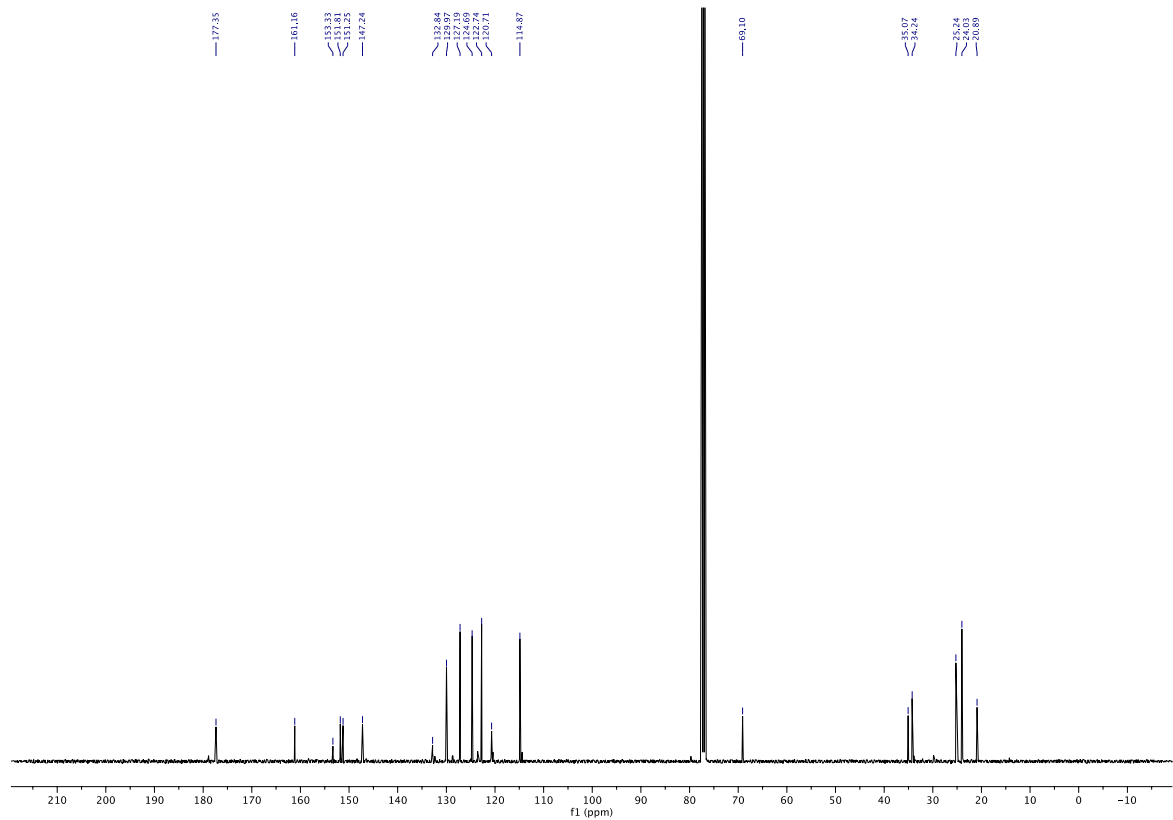
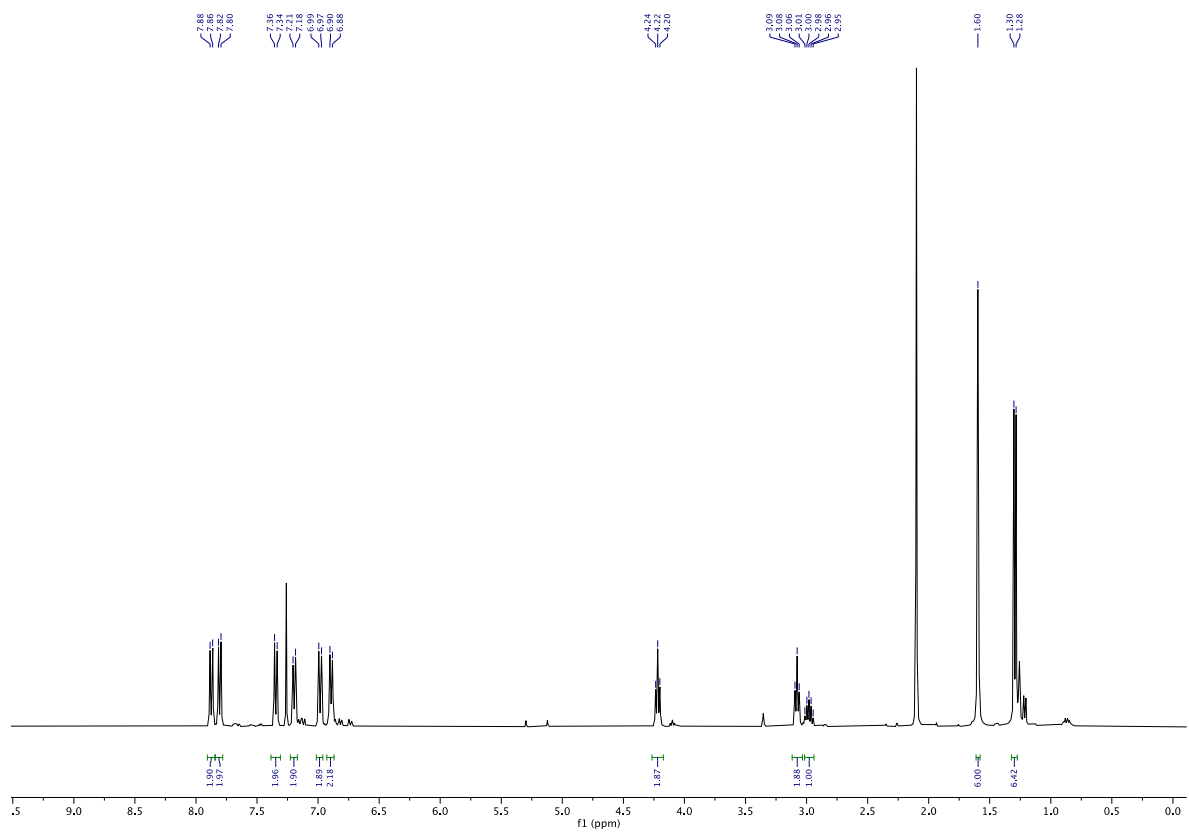
Compound 3



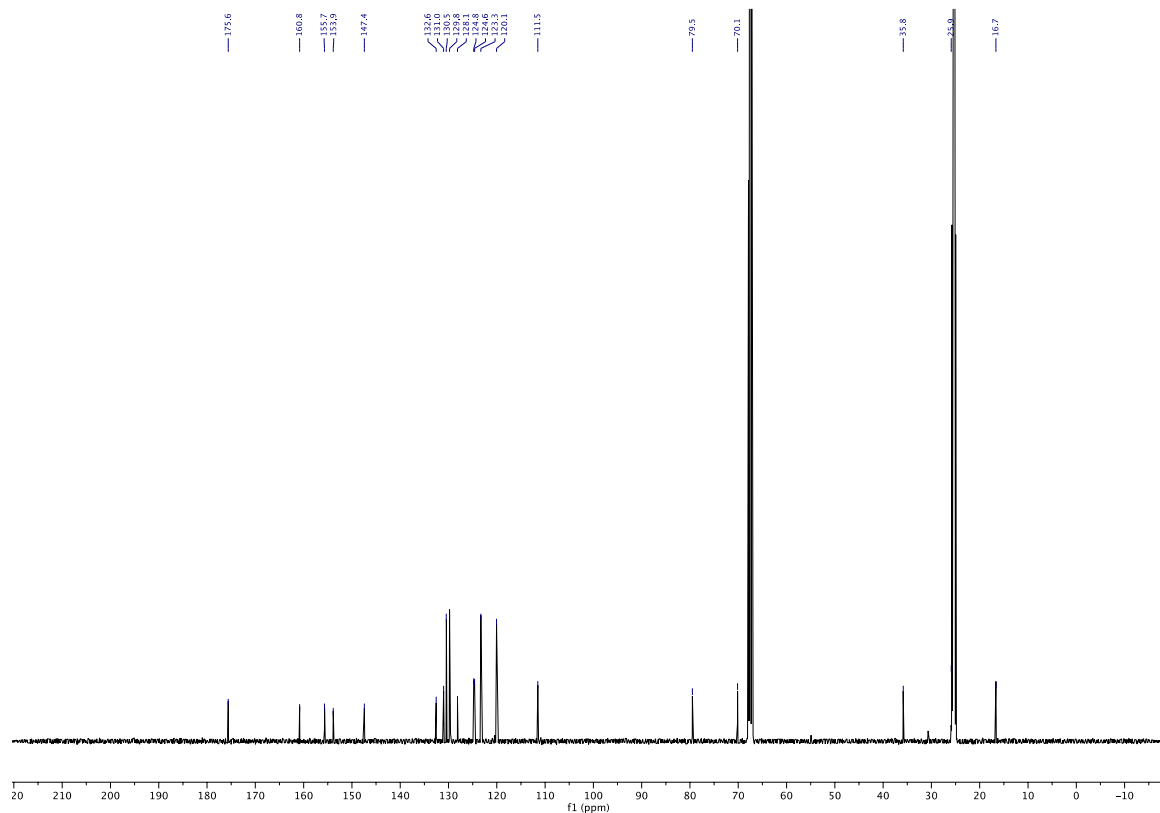
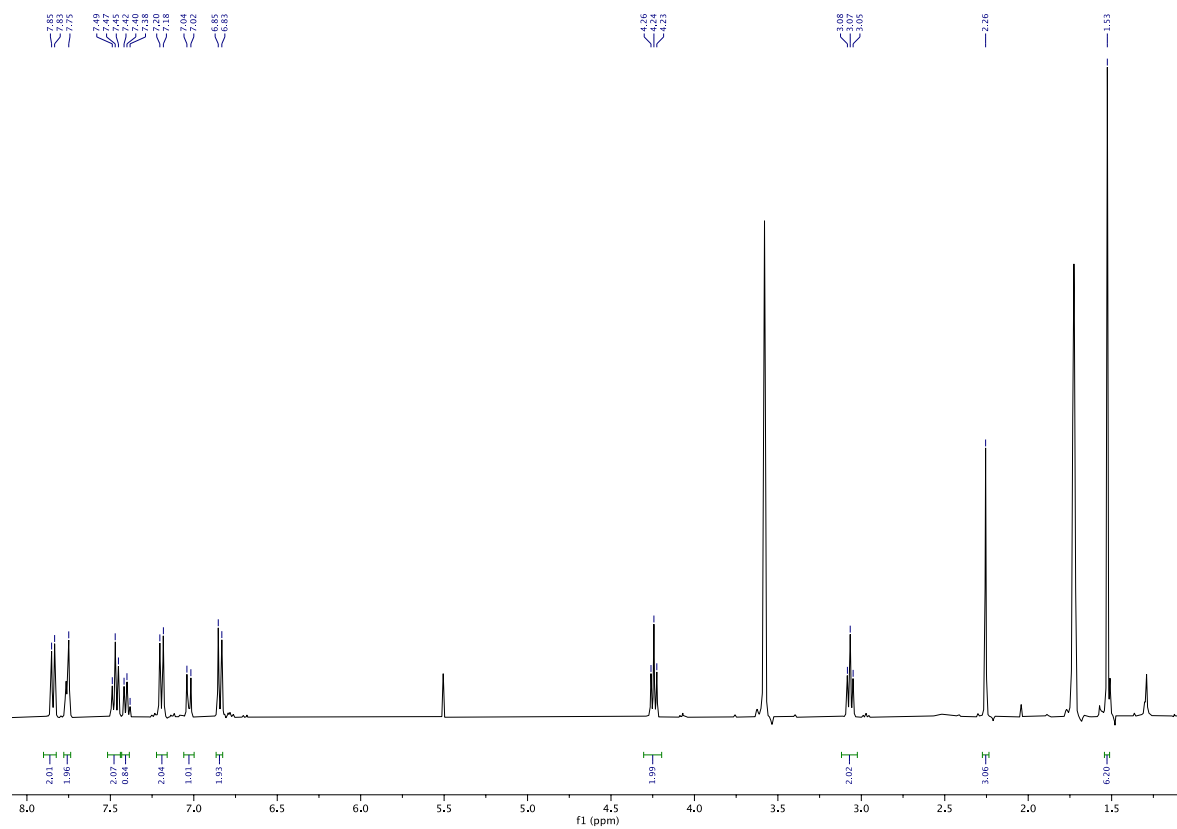
Compound 4



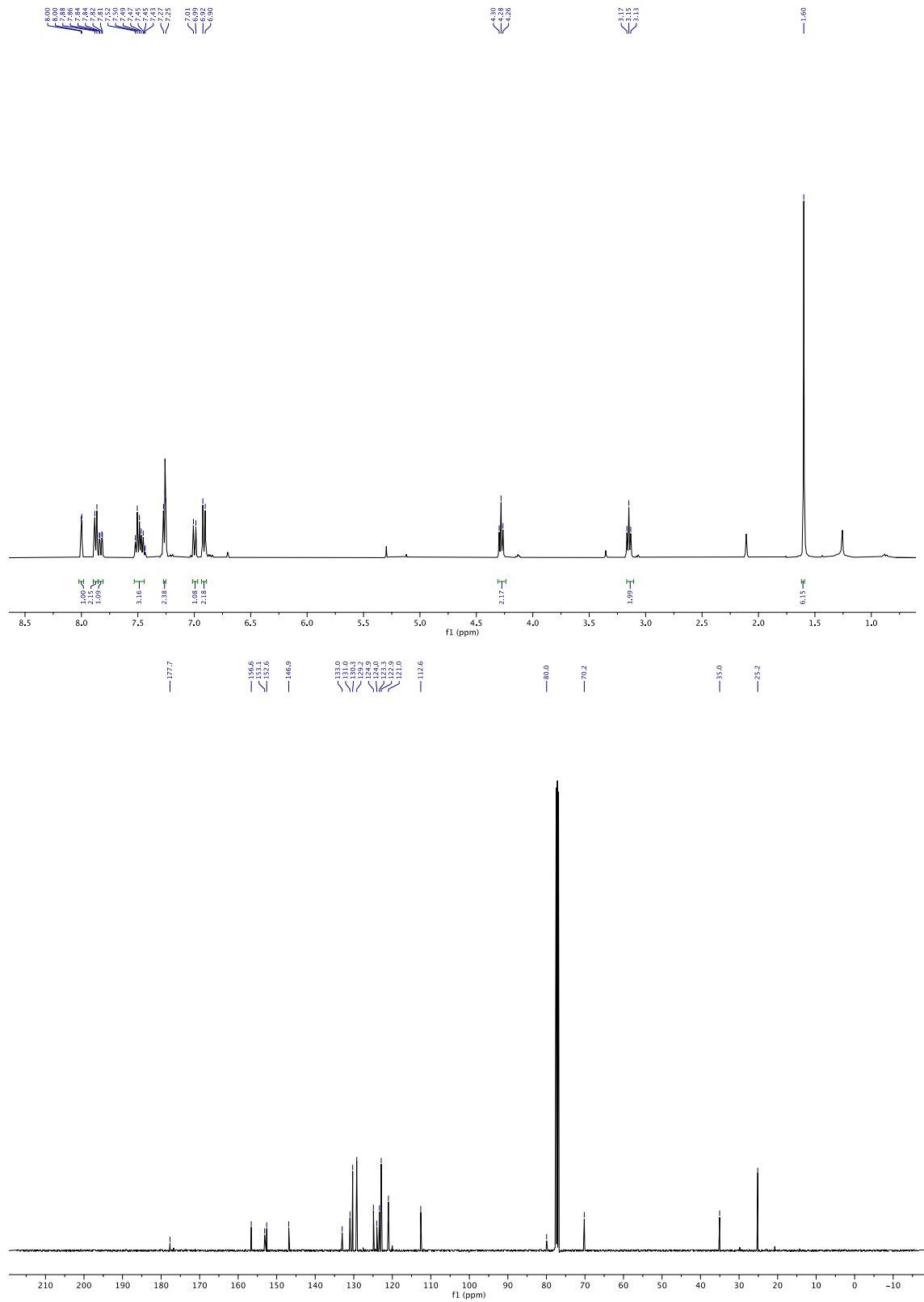
Compound 5



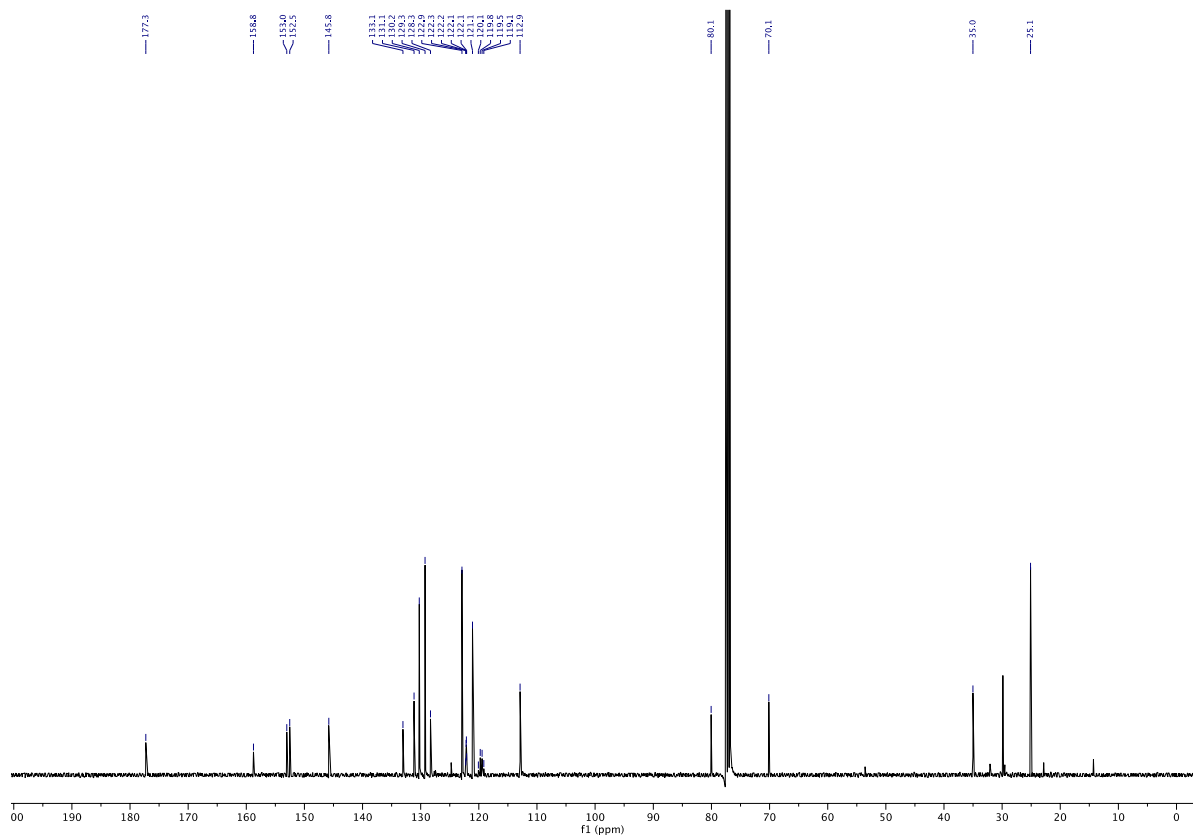
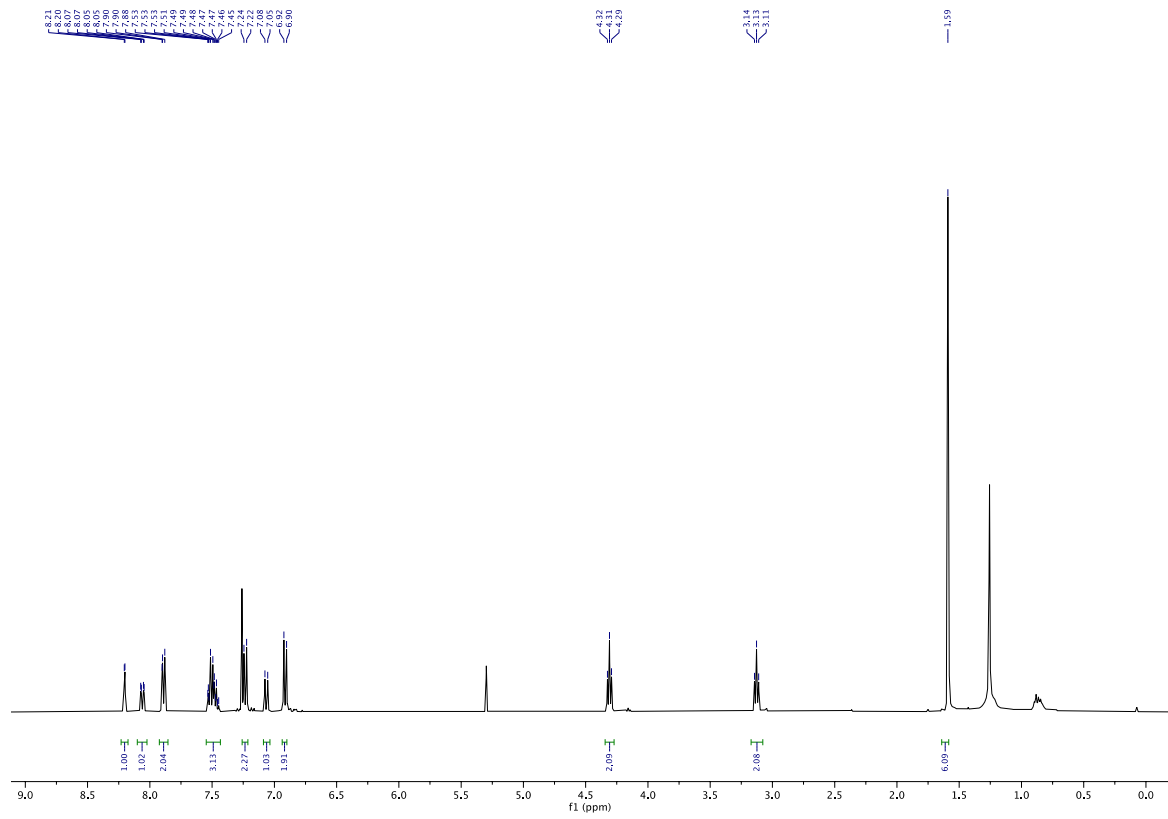
Compound 6



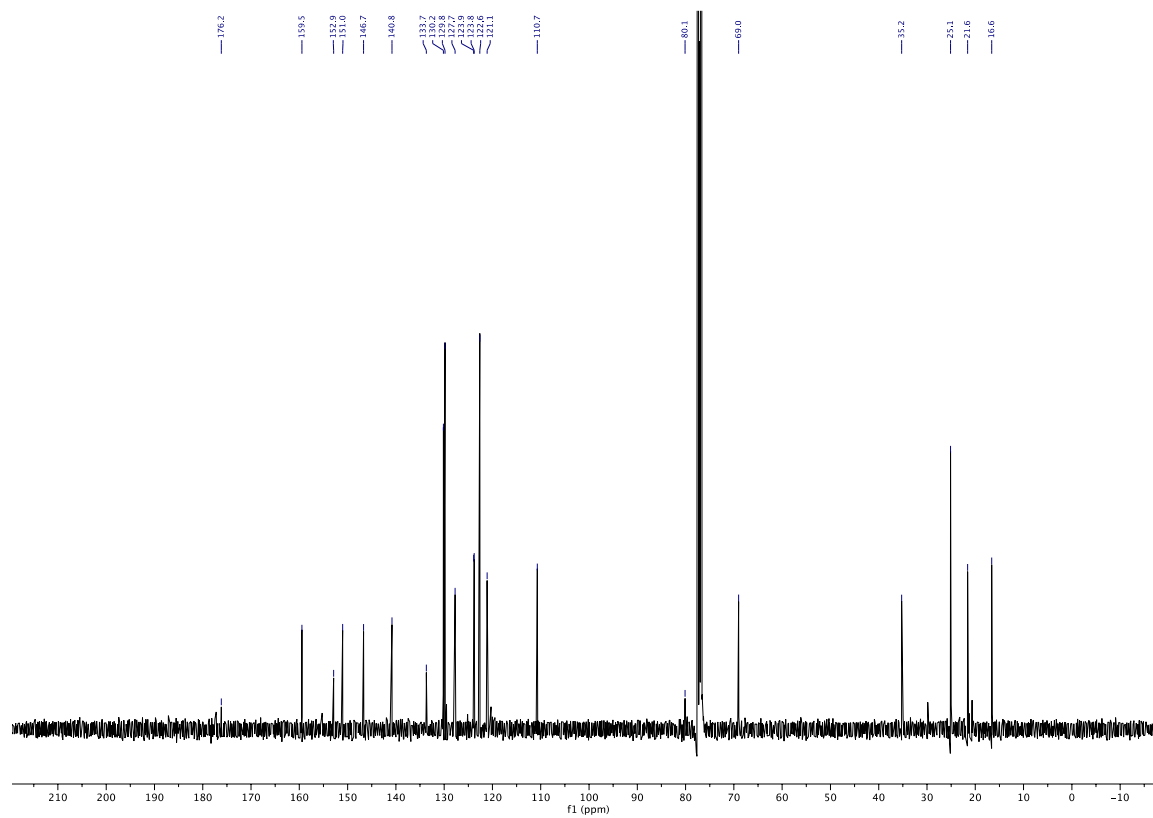
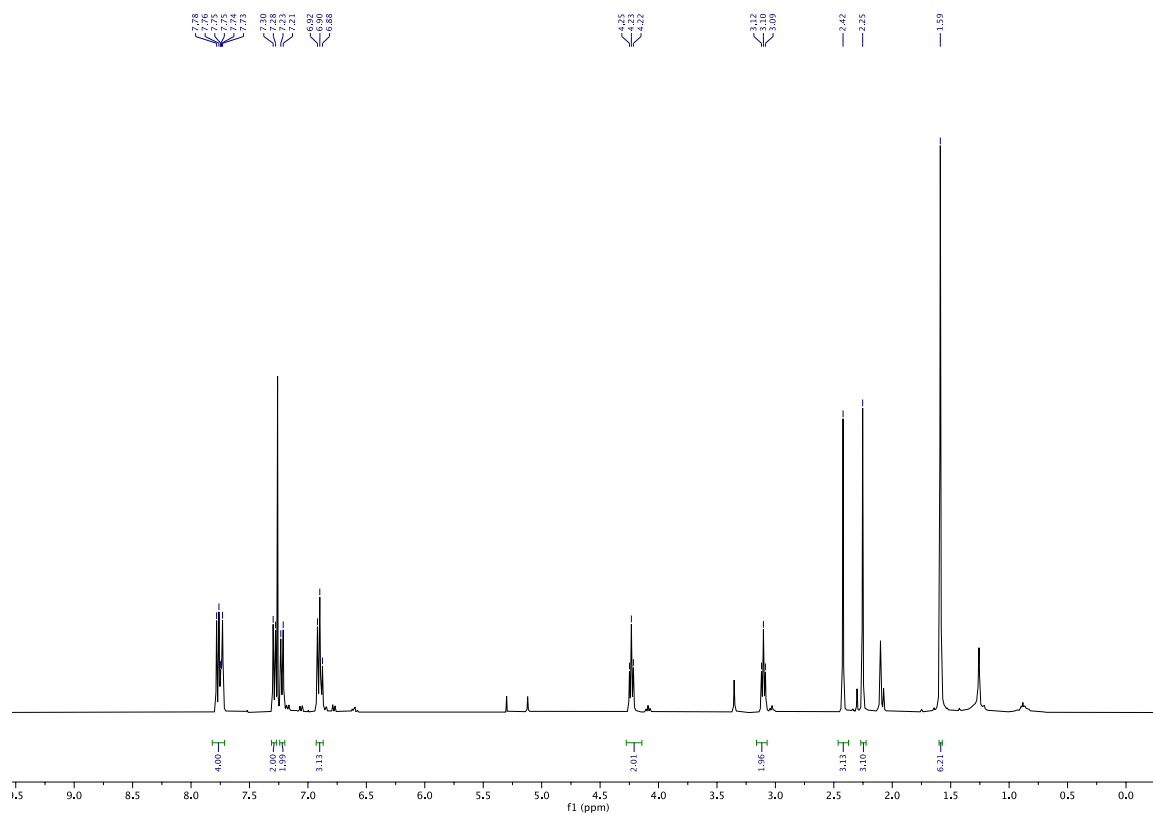
Compound 7



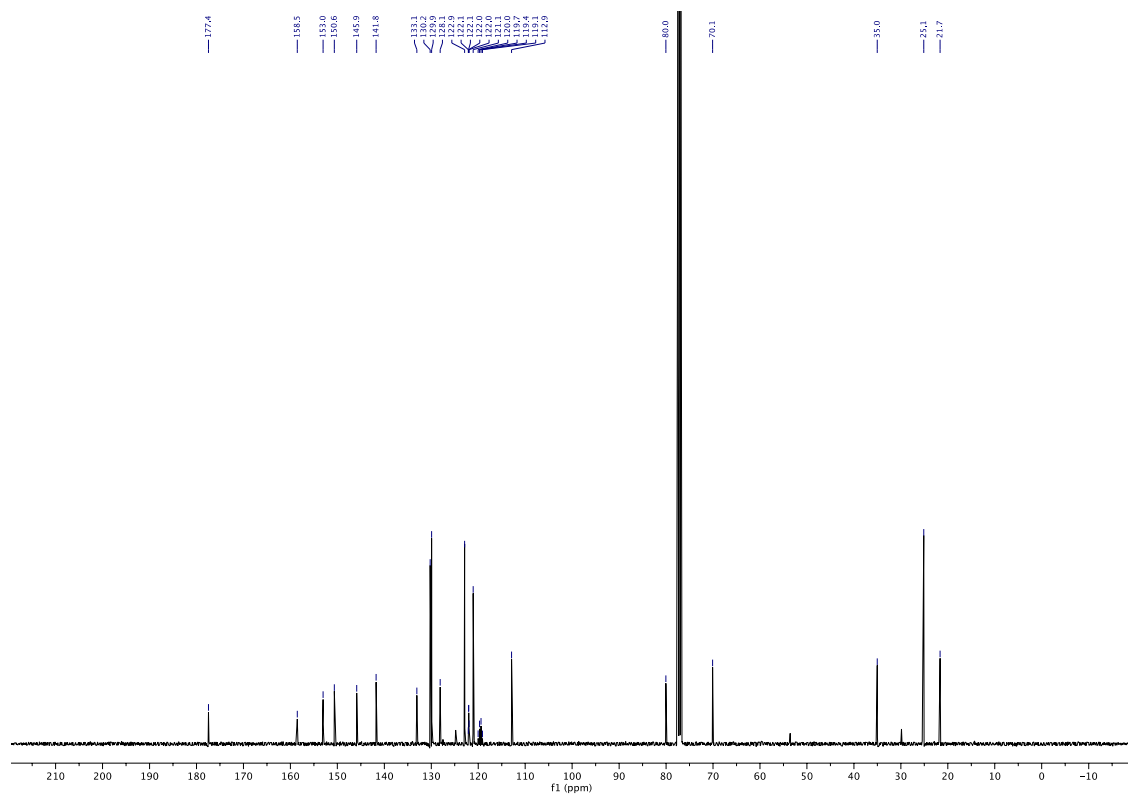
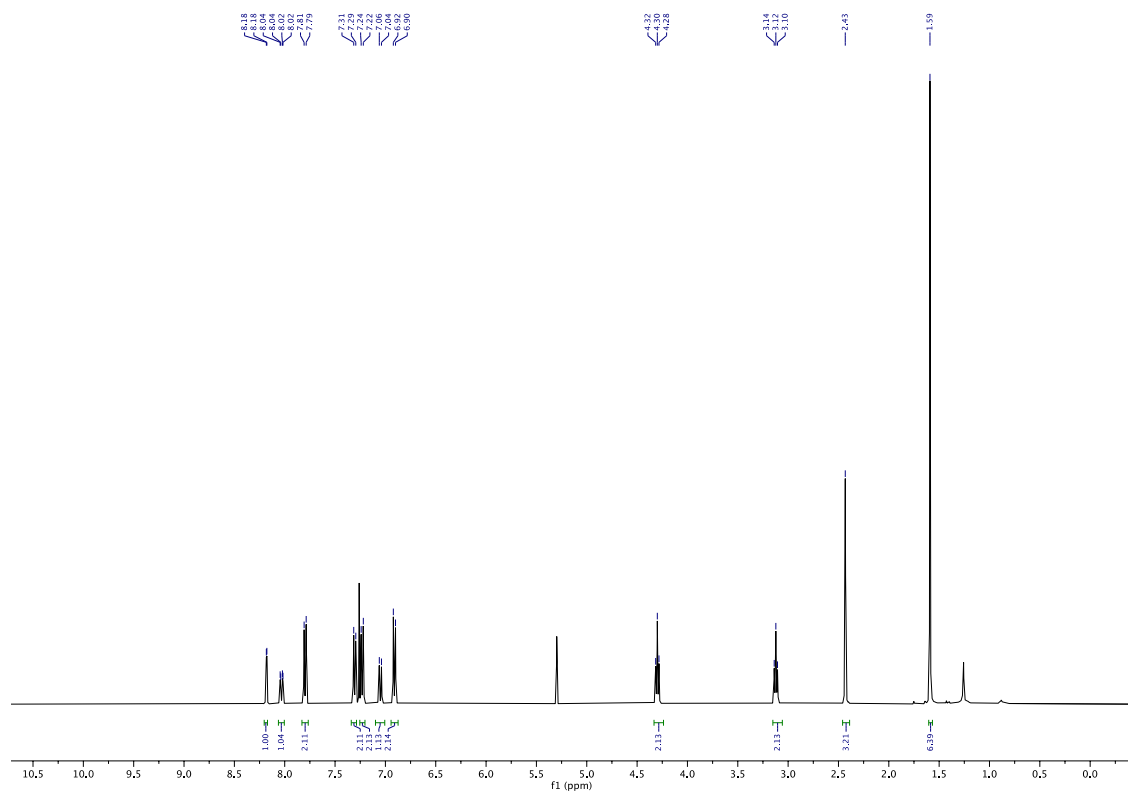
Compound 8



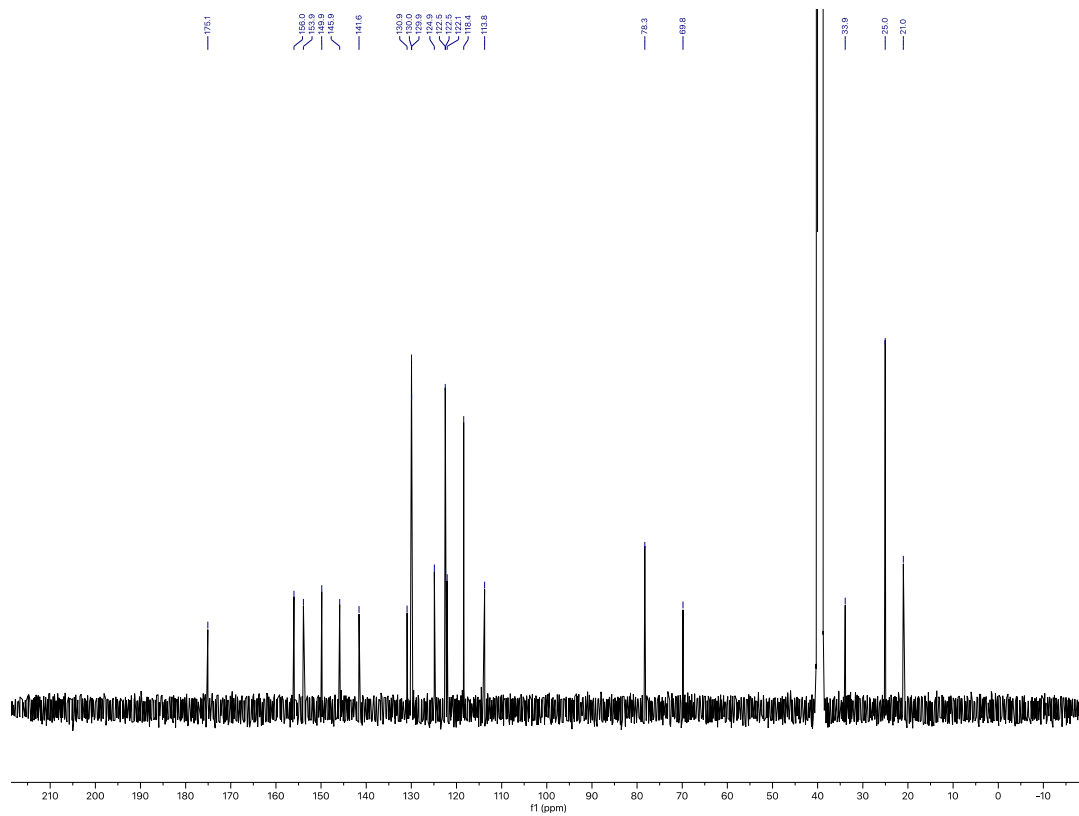
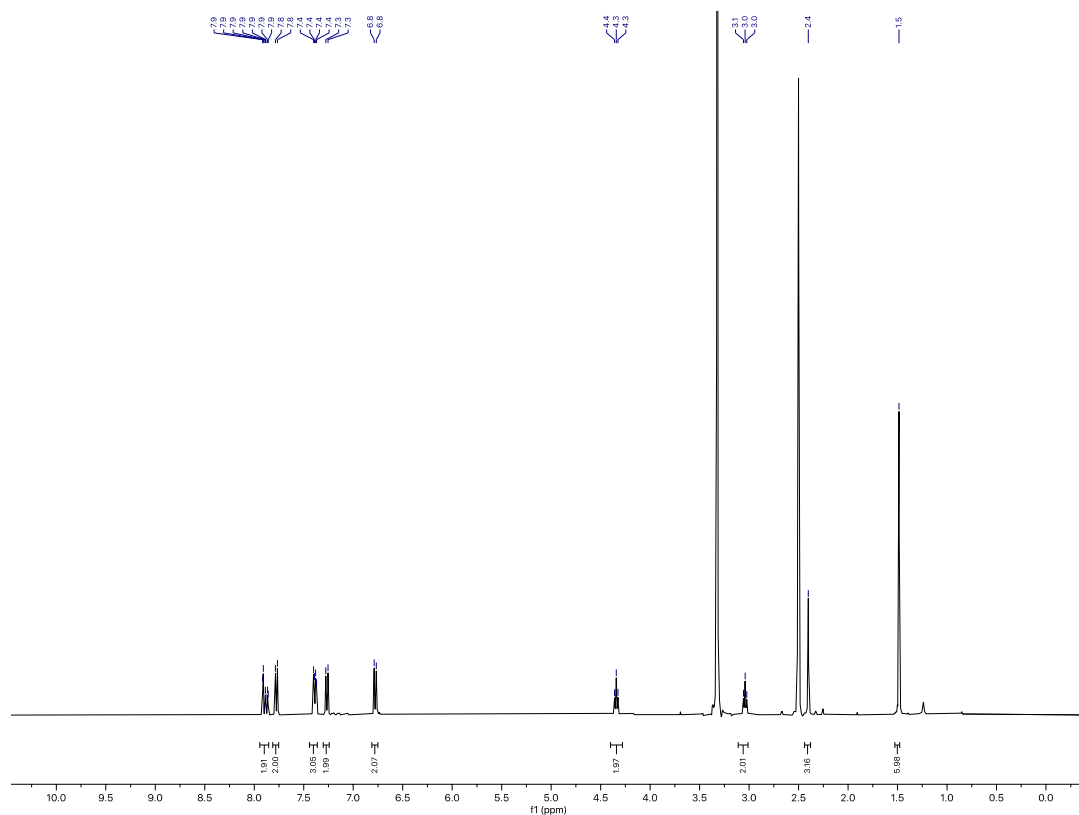
Compound 9



Compound 10



Compound 11



References

- (1) dos Santos, J. C.; Bernardes, A.; Giampietro, L.; Ammazalorso, A.; De Filippis, B.; Amoroso, R.; Polikarpov, I. Different Binding and Recognition Modes of GL479, a Dual Agonist of Peroxisome Proliferator-Activated Receptor α/γ . *J. Struct. Biol.* **2015**, *191* (3), 332–340. <https://doi.org/10.1016/j.jsb.2015.07.006>.
- (2) Kim, H. L.; Chin, J. W.; Cho, S. J.; Song, J. Y.; Yoon, H. S.; Bae, J. H. Design, synthesis, and the X-ray co-crystal structure of Highly Potent, Selective, and Orally Bioavailable, Novel Peroxisome Proliferator-Activated Receptor delta Agonists <https://www.rcsb.org/structure/5Y7X>. <https://doi.org/10.2210/pdb5Y7X/pdb>.
- (3) Giampietro, L.; D'Angelo, A.; Giancristofaro, A.; Ammazalorso, A.; De Filippis, B.; Fantacuzzi, M.; Linciano, P.; MacCallini, C.; Amoroso, R. Synthesis and Structure-Activity Relationships of Fibrate-Based Analogues inside PPARs. *Bioorganic Med. Chem. Lett.* **2012**, *22* (24), 7662–7666. <https://doi.org/10.1016/j.bmcl.2012.09.111>.

16.3 Endogenous vitamin E metabolites mediate allosteric PPAR γ activation with unprecedented co-regulatory interactions

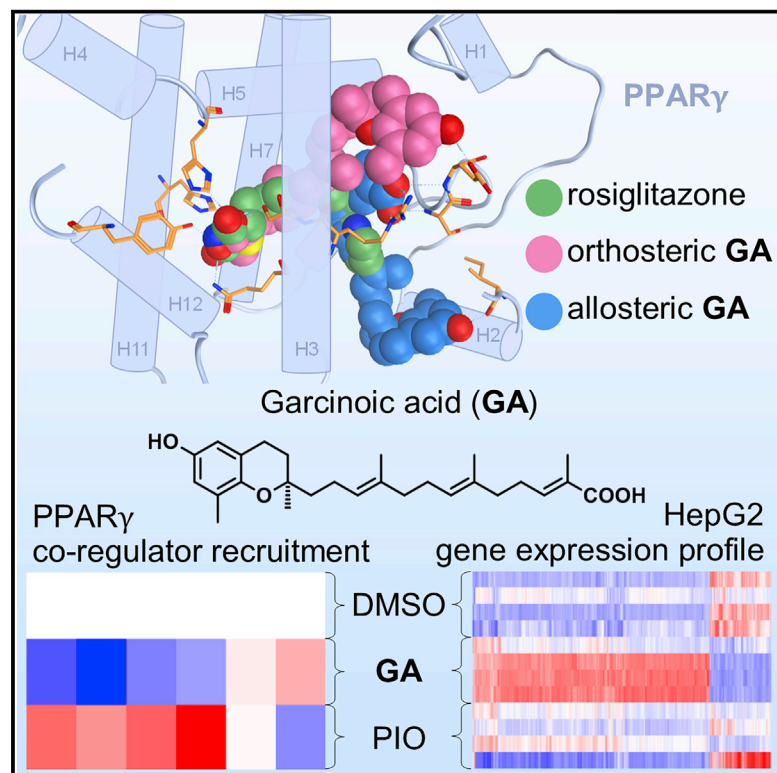
Willems, S.; Gellrich, L.; Chaikuad, A.; Kluge, S.; Werz, O.; Heering, J.; Knapp, S.; Lorkowski, S.; Schubert-Zsilavecz, M.; Merk, D. Endogenous Vitamin E Metabolites Mediate Allosteric PPAR γ Activation with Unprecedented Co-Regulatory Interactions. *Cell Chem. Biol.* **2021**, 28, 1–12.

Reprinted with permission from Willems, S.; Gellrich, L.; Chaikuad, A.; Kluge, S.; Werz, O.; Heering, J.; Knapp, S.; Lorkowski, S.; Schubert-Zsilavecz, M.; Merk, D. *Cell Chem. Biol.* **2021**, 28 (10), 1489–1500.e8. Copyright (2021) Elsevier Ltd.

Cell Chemical Biology

Endogenous vitamin E metabolites mediate allosteric PPAR γ activation with unprecedented co-regulatory interactions

Graphical abstract



Authors

Sabine Willems, Leonie Gellrich, Apirat Chaikuad, ..., Stefan Lorkowski, Manfred Schubert-Zsilavecz, Daniel Merk

Correspondence

merk@pharmchem.uni-frankfurt.de

In brief

Garcinoic acid (GA) structurally mimics tocopherol carboxylates that are endogenously formed metabolites of vitamin E. Willems et al. characterize GA as a ligand of the transcription factor PPAR γ with distinctive binding and modulatory properties pointing to an involvement of PPAR γ modulation in the pharmacological actions of vitamin E.

Highlights

- Garcinoic acid and tocopherol carboxylates are natural PPAR γ ligands
- Garcinoic acid binds to the orthosteric and an allosteric PPAR γ ligand binding site
- Garcinoic acid and pioglitazone induce different PPAR γ -co-regulator interactions
- Garcinoic acid and pioglitazone have different effects on gene expression profiles



Article

Endogenous vitamin E metabolites mediate allosteric PPAR γ activation with unprecedented co-regulatory interactions

Sabine Willems,¹ Leonie Gellrich,¹ Apirat Chaikuad,^{1,2} Stefan Kluge,^{3,4} Oliver Werz,⁵ Jan Heering,⁶ Stefan Knapp,^{1,2} Stefan Lorkowski,^{3,4} Manfred Schubert-Zsilavecz,¹ and Daniel Merk^{1,7,*}

¹Institute of Pharmaceutical Chemistry, Goethe University Frankfurt, Frankfurt 60438, Germany

²Structural Genomics Consortium, BMLS, Goethe University Frankfurt, Frankfurt 60438, Germany

³Chair of Nutritional Biochemistry and Physiology, Institute of Nutrition, Friedrich-Schiller-University Jena, Jena 07743, Germany

⁴Competence Cluster for Nutrition and Cardiovascular Health (nutriCARD) Halle-Jena-Leipzig, University of Jena, Jena 07743, Germany

⁵Chair of Pharmaceutical/Medicinal Chemistry, Institute of Pharmacy, Friedrich-Schiller-University Jena, Jena 07743, Germany

⁶Fraunhofer Institute for Translational Medicine and Pharmacology ITMP, Frankfurt 60596, Germany

⁷Lead contact

*Correspondence: merk@pharmchem.uni-frankfurt.de

<https://doi.org/10.1016/j.chembiol.2021.04.019>

SUMMARY

Vitamin E exhibits pharmacological effects beyond established antioxidant activity suggesting involvement of unidentified mechanisms. Here, we characterize endogenously formed tocopherol carboxylates and the vitamin E mimetic garcinoic acid (GA) as activators of the peroxisome proliferator-activated receptor gamma (PPAR γ). Co-stimulation of PPAR γ with GA and the orthosteric agonist pioglitazone resulted in additive transcriptional activity. In line with this, the PPAR γ -GA complex adopted a fully active conformation and interestingly contained two bound GA molecules with one at an allosteric site. A co-regulator interaction scan demonstrated an unanticipated co-factor recruitment profile for GA-bound PPAR γ compared with canonical PPAR γ agonists and gene expression analysis revealed different effects of GA and pioglitazone on PPAR signaling in hepatocytes. These observations reveal allosteric mechanisms of PPAR γ modulation as an alternative avenue to PPAR γ targeting and suggest contributions of PPAR γ activation by α -13-tocopherolcarboxylate to the pharmacological effects of vitamin E.

INTRODUCTION

Vitamin E exhibits pharmacological effects, for example, in non-alcoholic fatty liver disease (NAFLD) (Lavine et al., 2011; Sanyal et al., 2010) or Alzheimer's disease (AD) (Dysken et al., 2014) far beyond its established antioxidant activity (Birringer and Lorkowski, 2019); however, the mechanisms and protein targets mediating these effects remained elusive. Four saturated tocopherols and four unsaturated tocotrienols have been classified as constituents of vitamin E (Birringer and Lorkowski, 2019), yet only α -tocopherol has been demonstrated to have vitamin activity (Azzi, 2019). This class of organic compounds can undergo metabolic processing mainly by side chain oxidation at the ω -position leading to a number of fatty acid-like species, which could potentially be the active metabolites of vitamin E (Birringer and Lorkowski, 2019; Schmölz, 2016; Zhao et al., 2010). Recent studies have reported direct interactions of such vitamin E metabolites with 5-lipoxygenase (5-LO) (Pein et al., 2018) and anti-inflammatory effects of the vitamin E mimetic garcinoic acid (GA) involving changes in cytokine, cyclooxygenase (COX)-2, and inducible nitric oxide synthase

(iNOS) expression (Wallert et al., 2019). Nevertheless, the mechanistic details of these activities remain elusive. Here, we identify endogenously formed tocopherol carboxylates and GA as potent activators of the peroxisome proliferator-activated receptor gamma (PPAR γ) with remarkable activation efficacy. The co-crystal structure of the PPAR γ -GA complex revealed surprisingly the binding of two GA molecules at orthosteric and allosteric sites inducing a fully active conformation of the receptor. Consistent with the observation of allosteric binding, GA and the orthosteric agonist pioglitazone cooperatively stimulated PPAR γ , resulting in additive transcriptional activity. A co-regulator interaction scan demonstrated an unanticipated co-factor recruitment profile for GA-bound PPAR γ compared with that of canonical agonists and differential gene expression analysis of human hepatocytes (HepG2) after GA or pioglitazone treatment revealed distinct effects on PPAR signaling. Such mechanisms may open alternative avenues for PPAR γ modulation through allosteric regulation. Our findings of PPAR γ activation by GA and α -13-tocopherolcarboxylate suggest therefore a potential contribution of this pathway for example in NAFLD.



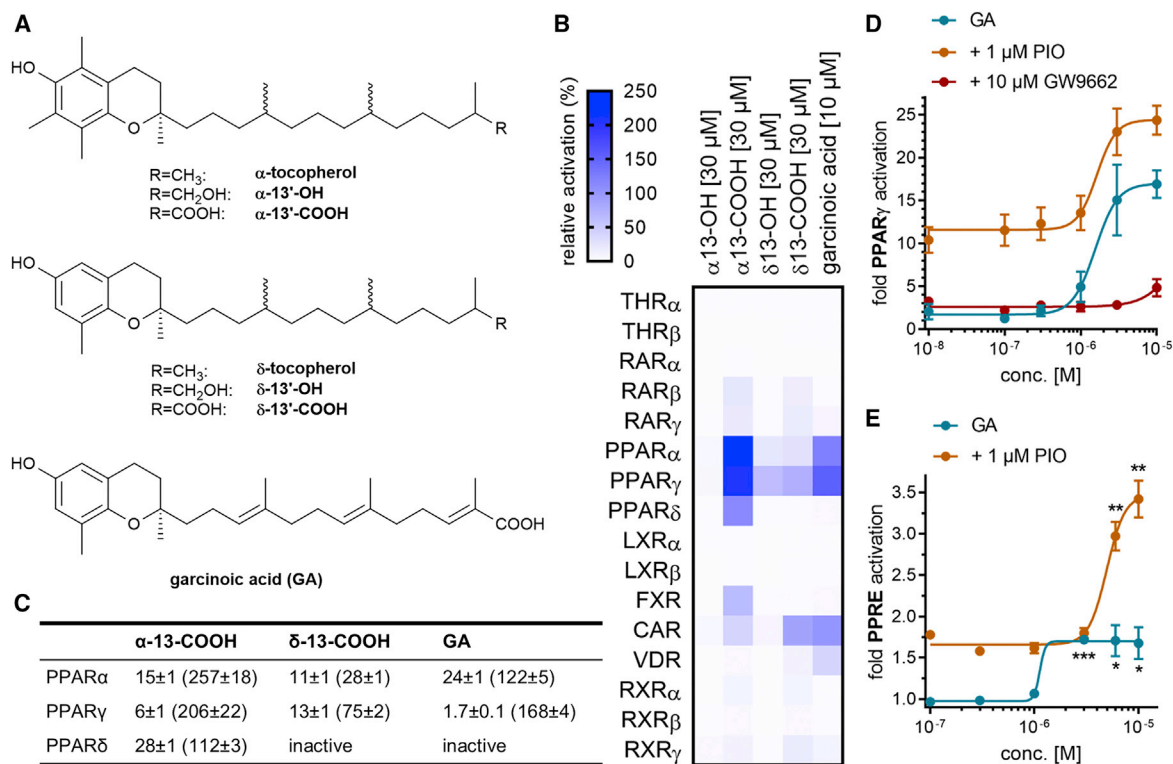


Figure 1. Tocopherol carboxylates and garcinoic acid modulate nuclear receptors

(A) Chemical structures of vitamin E metabolites and garcinoic acid (GA).

(B) Activity screening of tocopherol metabolites and GA on lipid-sensing nuclear receptors. Heatmap shows mean relative activation compared with reference agonists (see the STAR Methods for details).

(C) Biological activity of vitamin E metabolites and GA on PPARs in uniform Gal4 hybrid reporter gene assays. Half-maximal effective concentration (EC₅₀) values are shown in μM and are the mean ± SD, n ≥ 3. Maximum relative activation (% in parentheses) refers to the activity of reference agonists GW7647 (PPARα), pioglitazone (PPARγ), and L165,041 (PPARδ) at 1 μM.

(D) Concentration-response curves of GA (teal), GA in the presence of 10 μM of the irreversible PPARγ antagonist GW9662 (red), and GA in the presence of 1 μM pioglitazone (PIO) (orange) in a hybrid Gal4-PPARγ reporter gene assay. Data are the mean ± SEM, n = 4.

(E) Dose-response curves of GA (teal) and GA in presence of 1 μM PIO (orange) on a native human PPRE reporter without receptor overexpression. Data are the mean ± SEM, n = 4. *p < 0.05, **p < 0.01, ***p < 0.001; t test versus 0.1% DMSO (GA) or versus 1 μM PIO (GA + PIO).

RESULTS

Vitamin E metabolites and GA activate nuclear receptors

The natural constituents of vitamin E are endogenously metabolized to 13'-hydroxylated species and further oxidation of which generates tocopherol 13'-carboxylates (Figure 1A) (Schmölz, 2016). The natural product GA strongly resembles these oxidized metabolites and is commonly used as vitamin E mimetic. GA and the tocopherol 13'-carboxylate metabolites comprise typical lipid structures with a polar acidic head and a highly lipophilic tail, suggesting a role as endogenous lipid mediators. To examine the potential activities of vitamin E constituents and GA on nuclear receptors, we profiled α- and δ-tocopherol and their 13'-hydroxylated metabolites, tocopherol 13'-carboxylates, as well as GA on lipid-sensing transcription factors using uniform Gal4 hybrid reporter gene assays (Figure 1B). Albeit no detectable activity of tocopherols, considerably promiscuous effects of tocopherol-13'-carboxylates and GA on several nuclear receptors were observed. These compounds activated retinoic acid receptors (RARs), peroxisome proliferator-activated recep-

tors (PPARs), farnesoid X receptor (FXR), and constitutive androstane receptor (CAR). This observation was consistent with the recent report on the activation of pregnane X receptor (PXR) by GA (Bartolini et al., 2020). The activity profile of GA highly resembled that of the tocopherol 13'-carboxylates, while 13'-hydroxytocopherols were less active. By comparison, the agonist effects of GA and the tocopherol 13'-carboxylates on PPARs were the most pronounced.

Further characterization on the three PPAR subtypes revealed considerable potencies of the tocopherol 13'-carboxylates and GA (Figure 1C). While tocopherols and α-13'-OH were inactive on PPARs at 10 μM concentration, δ-13'-OH weakly activated PPARα (half-maximal effective concentration (EC₅₀) 15 ± 3 μM, 22% ± 2% efficacy) and PPARγ (EC₅₀ 13 ± 2 μM, 62% ± 7% efficacy). α-13'-COOH activated all three PPARs in a dose-dependent manner, exhibiting low micromolar potency and remarkable activation efficacy that surpassed potent synthetic agonists (PPARα, GW7647; PPARγ, pioglitazone; PPARδ, L165,041). On PPARγ, α-13'-COOH exhibited strong agonist effects with an EC₅₀ value of ~6 μM and ~206% activation efficacy relative to that of pioglitazone. The δ-13'-COOH analog showed similar

EC₅₀ values but weaker activation efficacy and did not activate PPAR δ . GA shared the activity profile of the tocopherol 13'-carboxylates, exhibiting strong PPAR γ agonism with an EC₅₀ value of 1.7 μ M and 168% efficacy of pioglitazone. The irreversible PPAR γ antagonist GW9662 fully blocked PPAR γ activation by GA (Figure 1D), suggesting direct binding of GA to the receptor as confirmed also by isothermal titration calorimetry (ITC) with low micromolar affinity (Figure S1). Interestingly, ITC revealed a stoichiometry of 2:1 for GA binding to PPAR γ , suggesting potentially two concurrent binding modes of the compound.

GA and pioglitazone act cooperatively on PPAR γ

We next probed an interference of GA and orthosteric PPAR γ agonists. Interestingly, GA and pioglitazone together led to an additive PPAR γ activation strongly exceeding the efficacy of the individual compounds (Figure 1D). When GA was titrated in the presence of 1 μ M pioglitazone, PPAR γ activation reached ~250% of pioglitazone, an ~1.5-fold increase compared with GA alone. Interestingly, no change of the EC₅₀ of GA was observed when the drug was present, suggesting therefore potential simultaneous binding of these two compounds at different binding sites.

We also observed PPAR γ agonism of GA and collaborative activity with pioglitazone on a native human PPAR response element (PPRE)-dependent reporter in HepG2 cells (Figure 1E). Of note, PPAR γ and its obligate heterodimer partner retinoid X receptor (RXR) were not overexpressed in this setting, indicating modulation of endogenous cellular PPAR γ . GA activated the PPRE with an EC₅₀ value of 1.1 μ M and 1.7-fold efficacy. The presence of 1 μ M pioglitazone slightly shifted the EC₅₀ value of GA to 4.8 μ M and resulted in a remarkable 3.5-fold PPRE activation.

GA shows a double binding mode to PPAR γ

To provide structural insights into this interesting PPAR γ modulatory profile, we solved the crystal structure of the PPAR γ ligand binding domain (LBD) in complex with GA (Figure 2). We observed two molecules of GA bound to PPAR γ (Figures 2A–2C), which was consistent with the ITC results and the unusual cellular activities. One GA molecule occupied the canonical orthosteric binding site where its carboxylic moiety bound within the same pocket utilized by rosiglitazone and engaged the canonical H-bond network with Tyr473 (Figures 2B and 2D). This direct interaction with Tyr473 provided an explanation for the high PPAR γ activation efficacy of GA since this residue is part of the activation function in helix 12. It strongly contributes to stabilizing PPAR γ in active conformation and is also observed for glitazone-type PPAR γ ligands and other agonists (Hanke et al., 2020; Jang et al., 2018).

The presence of the second molecule of GA at a different pocket formed between helices 3 and 4 and the β sheet connecting helices 6 and 7 was rather intriguing (Figures 2C and 2E). In contrast to the orthosteric site of nuclear receptors, this allosteric binding site is solvent accessible. The binding of GA at this site was assisted by Arg288 from helix 3, which engaged a bidentate salt bridge to the GA carboxylic acid group, and hydrophobic contacts between nonpolar residues and the lipophilic tail of the ligand at the solvent-exposed region (Figures 2C and 2E). Such allosteric binding with both concurrent binding modes enabling overall stabilization of the PPAR γ LBD likely provides a basis for the high activation efficacy and ago-positive activity of GA.

For direct structural comparison, we determined the structure of the PPAR γ -rosiglitazone complex and compared it with the PPAR γ -GA complex. In the absence of a co-activator peptide, both structures superimposed well without major conformational differences (Figure 2A). Helices H3 and H12, as well as the Ω loop involved in transcriptional activation, did not differ in their positions nor orientations. Nevertheless, closer inspection revealed slight alterations of some residues lining the pockets. For instance, slight conformational changes were observed for His449 and Tyr473 in the orthosteric binding site (Figure 2D). Such differences could likely be due to an adaptation of helix H12 to the different ligands. Another rearrangement was noted for Arg288, which underwent a 3.8-Å positional shift enabling its side chain to form the salt bridge contact with the allosteric GA molecule (Figure 2E). Structural superimposition further showed that, although the polar head groups of GA and rosiglitazone shared the similar pocket, the pyridineamine motif of rosiglitazone and the chromanol tail of GA protruded into different cavities. A kink at the middle part of rosiglitazone descended the pyridineamine toward the part of the allosteric pocket used for accommodation of the polar head of GA bound at the allosteric site, whereas a linear binding mode of GA enabled binding of the chromanol moiety at the vast hydrophobic space adjacent to helix 3. Based on the observation of cooperativity between synthetic agonists and GA toward activation of PPAR γ , we predicted that both ligands might be accommodated within the receptor at the same time. Molecular docking indeed revealed that this scenario might be possible. Structural modeling suggested that rosiglitazone bound to the canonical orthosteric site with its pyridineamine group linearly extended to the cavity adjacent to helix 3, leaving the allosteric site for the binding of GA (Figure 2F). For their shared chromanol motif, we also compared binding of GA and troglitazone to PPAR γ . Docking of troglitazone to the orthosteric GA site and superimposition of the PPAR γ -GA and PPAR γ -troglitazone complexes, however, revealed slightly different binding sites and different interactions for the chromanol scaffolds of GA and troglitazone (Figures S2A and S2B).

The allosteric binding of GA to PPAR γ aligns with previous NMR-based observations (Hughes et al., 2014) that have located an alternative PPAR γ ligand binding site opposite to the orthosteric pocket in proximity of helix H3 (Figure 2G). Moreover, *in vitro* studies (Hurtado et al., 2012; Lea et al., 2004) have suggested that ligand binding outside the orthosteric pocket can contribute to activation of PPAR γ in cooperation with an orthosteric ligand, likely due to stabilization of the PPAR γ LBD by allosteric ligands. The dual binding mode of GA to PPAR γ provided further evidence and a structural basis for such allosteric cooperativity toward PPAR γ modulation. The allosteric binding of GA partly overlaps with the previously characterized alternative region (Hughes et al., 2014) but extends further toward the orthosteric site and toward helix H2 (Figure 2H).

GA and pioglitazone induce opposing co-regulator interactions

PPAR γ activity is strongly regulated by ligand-dependent interactions with co-activators and co-repressors (Michalik et al., 2006; Mouchiroud et al., 2014). To evaluate whether PPAR γ modulation by GA involves specific effects on this regulatory protein-protein interaction network, we screened a collection

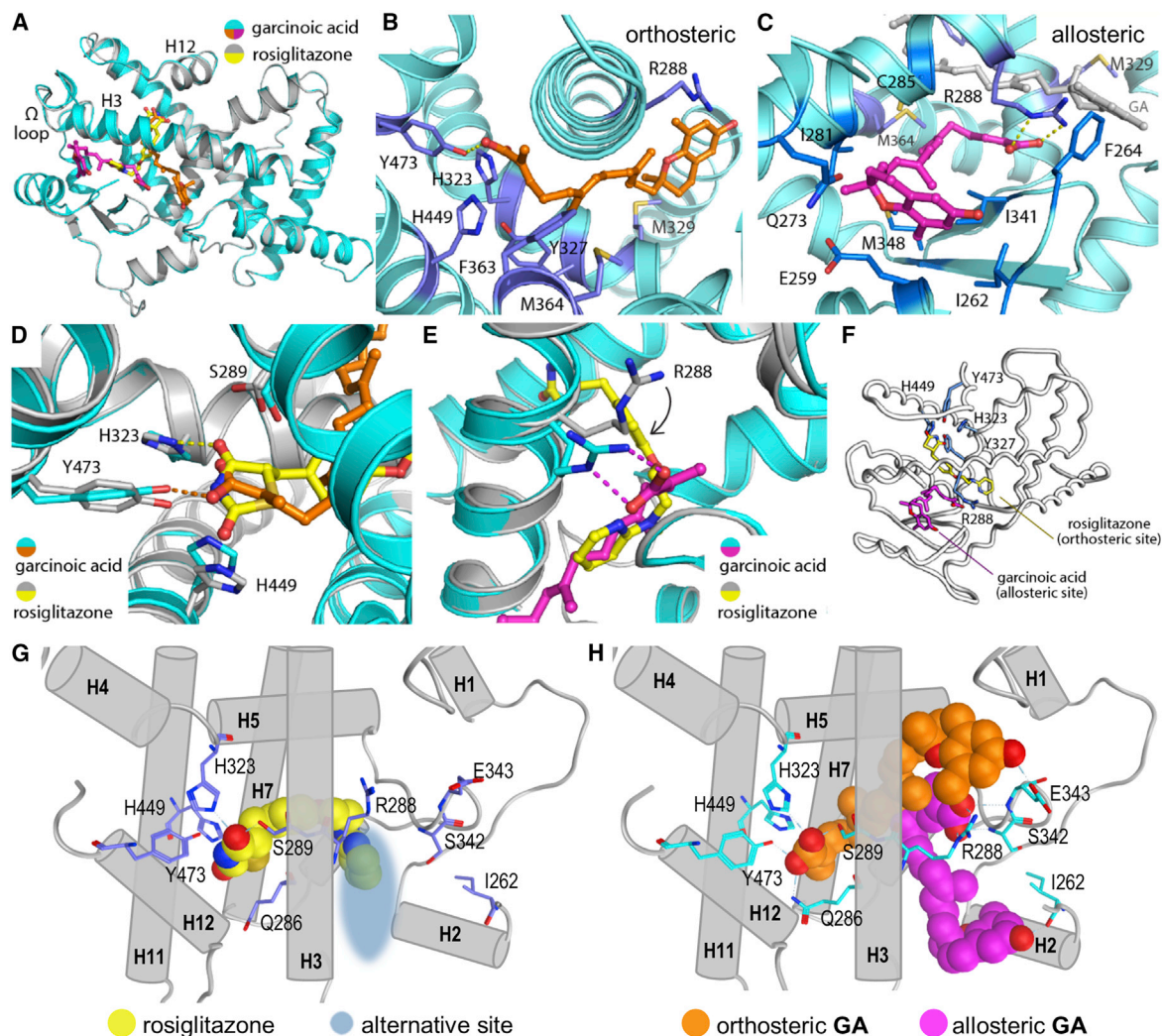


Figure 2. X-ray co-crystal structures of the PPAR γ LBD complexed with GA and rosiglitazone

(A) Superimposition of the PPAR γ :GA (PDB: 7AWD) and PPAR γ :rosiglitazone (yellow, PDB: 7AWC) complexes. Two binding modes of GA were observed: orthosteric (orange) and allosteric (magenta).

(B and C) Detailed binding of GA within the receptor at the canonical orthosteric binding site (B) and allosteric binding site (C).

(D) Structural comparison reveals similar accommodation of the acidic motifs of GA (orange) and rosiglitazone (yellow) within the orthosteric binding site.

(E) Superimposition of GA- and rosiglitazone-bound complexes demonstrates conformational alteration of R288, which rotates to interact with the carboxylic acid moiety of allosterically bound GA.

(F) Modeling of potential simultaneous binding of rosiglitazone at the orthosteric site and GA at the allosteric site calculated using Molecular Operating Environment.

(G and H) Schematic illustration of the rosiglitazone-bound (G) and GA-bound (H) PPAR γ LBD. (G) The canonical orthosteric binding site of rosiglitazone (yellow) spans between helices 3, 5, 7, 11, and 12. The shaded light blue circle indicates an alternative binding site lining H3 opposite the orthosteric site as described previously (Hughes et al., 2014). (H) The orthosteric binding of GA (orange) resembles that of rosiglitazone, albeit with a marked extension toward helix H1. This allows allosteric binding of the second GA molecule (magenta), which spans between helices H2 and H5 partially occupying the alternative site and a cavity of the orthosteric pocket.

See also Figure S2 and Table S1.

of 29 fluorescein-labeled canonical nuclear receptor co-regulator interaction motifs for binding to the Tb³⁺-cryptate-labeled PPAR γ LBD upon addition of GA in the absence or presence of pioglitazone in homogeneous time-resolved fluorescence resonance energy transfer (HTRF) assays (Figure 3A). Interestingly, we observed that the recruitment profile for GA was remarkably different from that of pioglitazone. While pioglitazone enhanced the recruitment of CREB-binding protein (CBP),

PPAR γ co-activator 1- α (PGC-1 α), vitamin D receptor interacting protein (DRIP), and nuclear receptor co-activator 6 (NCoA6, also termed PRIP, RAP250) as well as steroid receptor co-activator (SRC) to some extent, GA exhibited the opposite effect by displacing these co-activators from PPAR γ . In reverse, GA was observed to promote the recruitment of nuclear receptor co-repressors 1 (NCoR1) and 2 (NCoR2, also termed silencing mediator for retinoid or thyroid hormone receptors, SMRT),

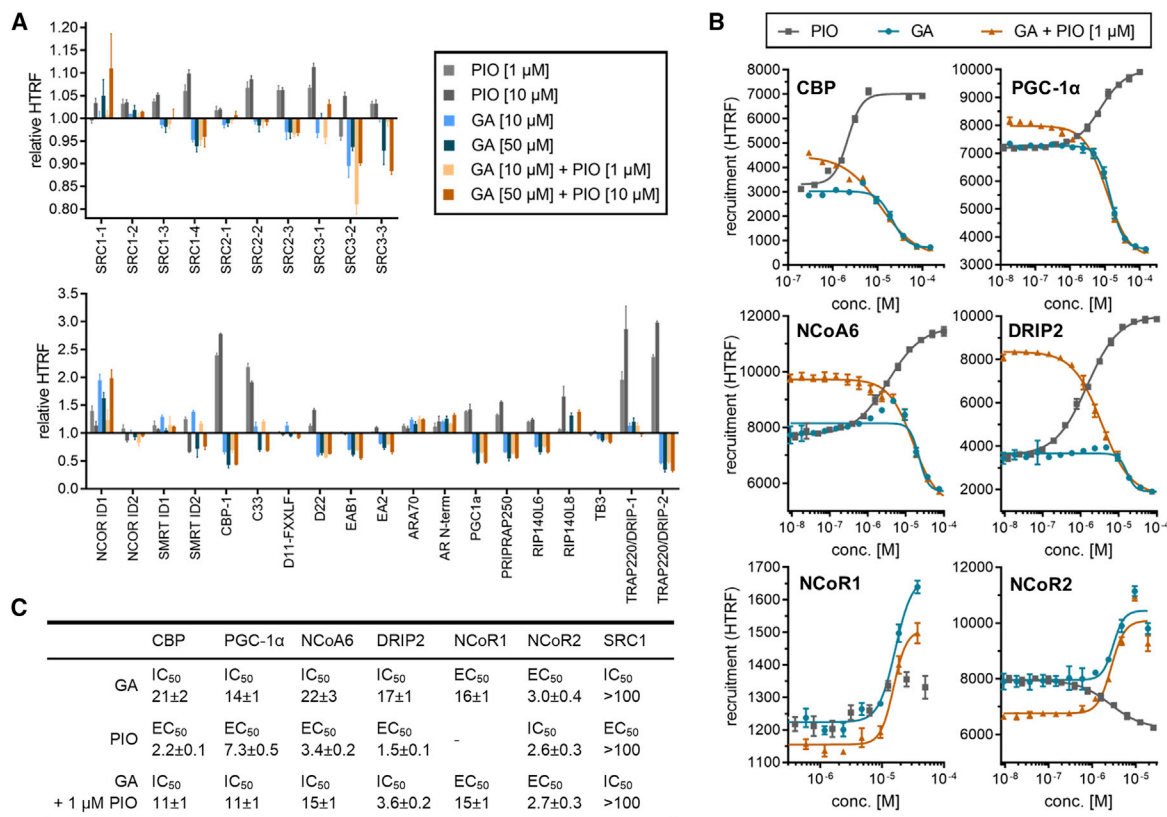


Figure 3. Effects of PIO, GA, and GA + PIO on co-regulator recruitment to PPAR_γ in homogeneous time-resolved fluorescence resonance energy transfer (HTRF)-based settings

Tb³⁺-cryptate-labeled PPAR_γ LBD served as FRET donor, fluorescein-labeled co-regulator peptides were used as FRET acceptors.

(A) Interaction scan for PIO-, GA-, and GA + PIO-induced changes in the PPAR_γ recruitment profile. Two concentrations were tested for each compound. Data are the mean ± SD relative HTRF compared with 1% DMSO, N = 4.

(B) Dose-dependent effects of PIO, GA and GA + PIO on the recruitment of the interactors CBP, PGC-1α, NCoA6, DRIP2, NCoR1, and NCoR2 (SMRT). Data are the mean ± SD, N = 3.

(C) Corresponding EC₅₀ and half-maximal inhibitory concentration (IC₅₀) values of PIO, GA, and GA + 1 μM PIO on co-regulator recruitment to PPAR_γ.

which was in contrast to pioglitazone that displaced NCoR2 from PPAR_γ. Surprisingly, when both ligands were combined, GA dominated and counteracted all pioglitazone-induced effects on co-regulator binding.

From the primary co-regulator screen, six interactors emerged as potential targets of GA-mediated PPAR_γ modulation. We next profiled the concentration-dependent effects of GA on their recruitment in the absence or presence of pioglitazone (Figures 3B and 3C). The results further confirmed that GA robustly displaced the co-activator motifs CBP, PGC-1α, NCoA6, and DRIP from PPAR_γ in a dose-dependent fashion with half-maximal inhibitory concentration (IC₅₀) values of ~14–22 μM. In addition, the positive effect of GA on the recruitment of the co-repressors NCoR1 and NCoR2 was confirmed with EC₅₀ values of 16 and 3 μM, respectively. The addition of 1 μM pioglitazone promoted the binding of the co-activators (CBP, PGC-1α, NCoA6, and DRIP) observable in a higher baseline, yet did not counteract the displacement effects of GA. Similarly, the addition of pioglitazone displaced NCoR2 from PPAR_γ, resulting in a lower baseline; however, this effect was fully conquered by GA.

GA and pioglitazone induce different gene expression patterns

Intrigued by the opposing effects of GA and pioglitazone on PPAR_γ co-regulator interactions, we probed whether this distinguished behavior on the molecular level would translate into different effects on gene expression. We treated PPAR_γ-expressing human hepatocytes (HepG2) with GA (10 μM), pioglitazone (1 μM), GA (10 μM) + pioglitazone (1 μM), or GA (10 μM) + GW9662 (10 μM) and determined differential gene expression by mRNA sequencing (Figure 4). GA (5,578 genes regulated, p < 0.05) had a more pronounced impact on the HepG2 gene expression profile than pioglitazone (439 genes regulated), likely attributable to its lower selectivity compared with the synthetic drug (Figure 4A). Nevertheless, 158 common genes were affected by pioglitazone and by GA treatment (Figure 4B), corroborating the modulation of a common target. However, the fact that GA did not alter expression of two-thirds of genes that were regulated by the selective PPAR_γ agonist pioglitazone suggested differential PPAR_γ modulation by both compounds. Indeed, clustering of the genetic effects (Figure 4C) illustrated markedly different gene expression patterns for GA- and pioglitazone-treated cells.

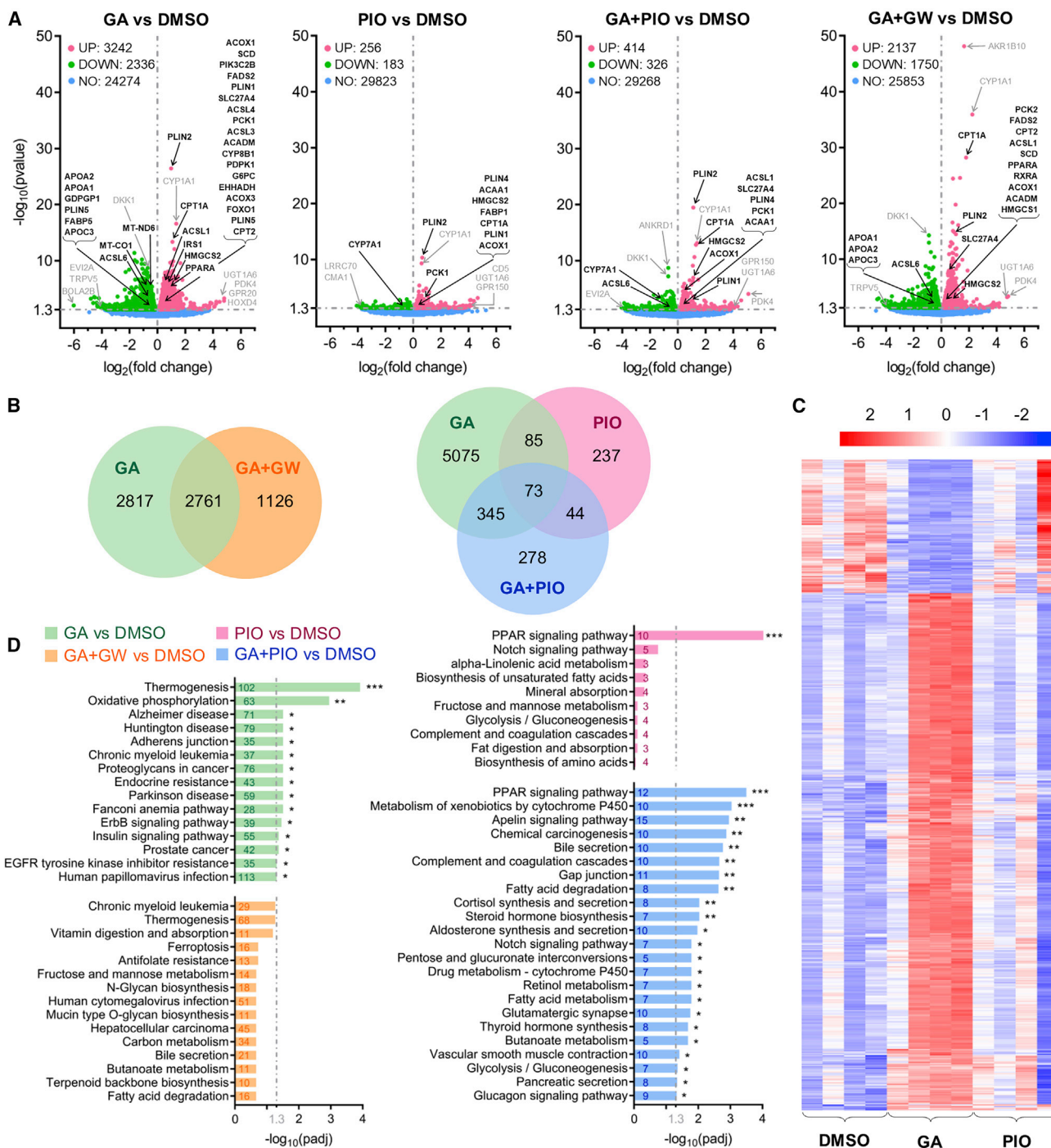


Figure 4. Differential gene expression in human hepatocytes (HepG2) after treatment with PPAR γ ligands

HepG2 cells were treated with GA (10 μM), PIO (1 μM), GA (10 μM) + PIO (1 μM), or GA (10 μM) + GW9662 (10 μM); n = 4.

(A) Overall distribution of differentially expressed genes for the different treatments versus DMSO. Volcano plots show \log_2 fold change in gene expression level (x axis) versus statistical significance level ($-\log_{10}(p\text{ value})$; y axis). Genes associated with PPAR signaling according to KEGG are marked in black, further details are shown in Table 1. Other genes with strong or highly significant regulation in gray.

(B) Co-expression Venn diagrams for differential gene expression (versus DMSO) of the different treatments.

(C) Cluster analysis of differential gene expression with the different treatments.

(D) KEGG pathway enrichment analysis illustrating differential regulation of signaling pathways by the different treatments. Bar plots show statistical significance level ($-\log_{10}(\text{padj})$) of regulated KEGG pathways, numbers refer to the count of differentially expressed genes concerning the pathway. See also Table S2.

Table 1. Effects of different PPAR γ ligands on gene expression in HepG2 cells

Gene name	GA versus DMSO	PIO versus DMSO	GA + PIO versus DMSO	GA + GW versus DMSO
PLIN2	0.978 (< 0.001)	0.649 (< 0.001)	1.114 (< 0.001)	0.927 (< 0.001)
CPT1A	1.075 (< 0.001)	0.342 (0.042)	1.301 (< 0.001)	1.785 (< 0.001)
ACSL1	0.578 (< 0.001)		0.498 (0.002)	0.377 (0.005)
HMGCS2	1.070 (< 0.001)	0.604 (0.021)	1.113 (< 0.001)	0.725 (0.002)
PPARA	0.792 (< 0.001)			0.572 (0.008)
ACOX1	0.291 (< 0.001)	0.150 (0.049)	0.373 (< 0.001)	0.208 (0.016)
SCD	0.413 (< 0.001)			0.418 (0.005)
ACSL6	-0.580 (< 0.001)		-0.472 (0.023)	-0.583 (0.001)
FADS2	0.287 (0.001)			0.330 (0.001)
HMGCS1	0.394 (0.001)			0.282 (0.031)
PLIN1	0.899 (0.002)	0.622 (0.045)	0.971 (0.001)	
SLC27A4	0.323 (0.002)		0.305 (0.005)	0.510 (< 0.001)
ACSL4	0.471 (0.003)			
RXRA	0.233 (0.004)			0.255 (0.011)
PCK1	0.667 (0.004)	0.775 (0.001)	0.594 (0.022)	
APOA2	-0.457 (0.006)			-0.369 (0.013)
ACSL3	0.369 (0.006)			
APOA1	-0.453 (0.007)			-0.406 (0.008)
ACADM	0.325 (0.010)			0.347 (0.020)
CYP8B1	0.364 (0.011)			
PDPK1	0.289 (0.011)			
EHHADH	0.342 (0.019)			
ACOX3	0.233 (0.030)			
PLIN5	-0.410 (0.034)			
CPT2	0.272 (0.040)			0.411 (0.004)
FABP5	-0.291 (0.041)			
APOC3	-0.531 (0.047)			-0.390 (0.028)
ACAA1		0.237 (0.006)	0.210 (0.026)	
PCK2				0.333 (0.001)
PLIN4		0.419 (0.006)	0.387 (0.016)	
CYP7A1		-0.635 (0.043)	-1.092 (0.001)	
FABP1		0.357 (0.025)		
IRS1	0.688 (< 0.001)			
G6PC	0.544 (0.013)			
GDPGP1	-0.603 (0.017)			
FOXO1	0.420 (0.033)			
PIK3C2B	0.495 (< 0.001)			
PIK3C2A	0.459 (0.003)			
PIK3CA	0.482 (0.003)			
PIK3C3	0.350 (0.013)			
PIK3AP1	0.317 (0.048)			
NDUFS2	0.298 (0.003)			
NDUFAF3	-0.506 (0.004)			
NDUFC1	-0.392 (0.007)			
NDUFV3	-0.312 (0.010)			
NDUFA8	-0.303 (0.026)			
NDUFB10	-0.318 (0.028)			
NDUFS8	-0.284 (0.028)			
NDUFA6	-0.306 (0.031)			

(Continued on next page)

Table 1. Continued

Gene name	GA versus DMSO	PIO versus DMSO	GA + PIO versus DMSO	GA + GW versus DMSO
NDUFA11	−0.385 (0.031)			
NDUFB1	−0.355 (0.033)			
NDUFA2	−0.345 (0.042)			
COX6B1	−0.477 (0.004)			
COA6	−0.327 (0.023)			
COA3	−0.314 (0.023)			
COX7C	−0.282 (0.037)			
COX5B	−0.353 (0.043)			
COX10	0.220 (0.045)			

HepG2 cells were treated with GA (10 μ M), PIO (1 μ M), GA (10 μ M) + PIO (1 μ M), or GA (10 μ M) + GW9662 (10 μ M); n = 4. Data are shown as log₂fold change in gene expression with p values in parentheses. The upper part shows all statistically significant (p < 0.05 versus DMSO) effects on genes associated with PPAR signaling according to KEGG. The lower part shows selected statistically significant (p < 0.05 versus DMSO) effects on genes involved in insulin signaling, glucose metabolism, and oxidative phosphorylation that were selectively regulated by GA treatment. See also [Table S2](#).

Combined GA and pioglitazone treatment, interestingly, induced less changes in the HepG2 gene expression profile (740 genes regulated) than GA alone. The combination of both compounds, hence, did not cause the sum of their effects, suggesting interference of their modes of action.

The covalent PPAR γ antagonist GW9662 (10 μ M) partly blocked the effects of GA on gene expression ([Figure 4A](#)), demonstrating the PPAR-mediated effects of GA. Nonetheless, 2,761 (49%) of genes altered upon GA treatment were also regulated in the presence of GW9662 ([Figure 4B](#)), illustrating that further macromolecular targets and signaling pathways are involved in the activities of GA.

Closer inspection of differential gene expression revealed pronounced modulation of several PPAR γ -regulated genes for GA and pioglitazone treatment, but with obvious differences ([Figure 4A](#); [Tables 1](#) and [S2](#)). The thiazolidinedione mainly induced genes involved in lipid storage (PLINs), gluconeogenesis (PCK1), and fatty acid oxidation (ACAA1, ACOX, and CPT1A). GA similarly promoted gluconeogenesis (PCK1) and induced even more genes of fatty acid oxidation (ACOX1, ACOX3, ACADM, CPT1A, CPT2, and EHHADH), yet differentially modulated lipid storage genes with PLIN1 and PLIN2 upregulation but PLIN5 downregulation. In addition, GA affected fatty acid transport genes (ACSLs, SLC27A4), promoted lipogenesis (SCD, FADS2), and induced the cell survival factor PDPK1, all of which are associated with PPAR signaling. Moreover, GA regulated key genes of insulin signaling (FOXO1, IRS1, PIK3s), glucose metabolism (G6PC, GDPGP1), and oxidative phosphorylation (cytochrome c oxidases, NADH dehydrogenases) that were not affected by pioglitazone. The PPAR γ antagonist GW9662 efficiently blocked effects of GA on lipid storage (PLIN1, PLIN5), gluconeogenesis (PCK1), fatty acid transport (ACSLs), cell survival (PDPK1), insulin signaling (FOXO1, IRS1, PIK3s), glucose metabolism (G6PC, GDPGP1), and oxidative phosphorylation (cytochrome c oxidases, NADH dehydrogenases) suggesting the involvement of PPAR γ in their modulation by GA. Overall, GA caused significant (p < 0.05) changes in the expression of 2,191 protein-coding genes ([Table S2](#)) that were reversed by the PPAR γ antagonist GW9662 and not altered upon pioglitazone treatment, suggesting them as potential spe-

cific PPAR γ -mediated effects of GA. Among them, the orphan G protein-coupled receptor 20 (GPR20), the transcription factor encoding homeobox D4 (HOXD4), and the solute carrier neutral and basic amino acid transport protein (SLC3A1) revealed the strongest selective induction by GA (log₂fold change > 4).

When applied together, GA and pioglitazone exhibited different effects on PPAR γ -regulated genes compared with the individual compounds aligning with their opposing effects on PPAR γ co-regulator interactions. Combined GA and pioglitazone treatment amplified several effects of pioglitazone on PPAR γ -regulated genes such as CPT1A (log₂fold increase 1.3 versus 0.3), PLIN1 (1.0 versus 0.6), and PLIN2 (1.1 versus 0.6). In addition, this combination induced PPAR γ -regulated genes that were not upregulated by pioglitazone alone (e.g., ACSL1, ACSL6, SLC27A4) and it failed to regulate genes that were affected by GA alone (e.g., SCD, FADS2, EHHADH, CPT2, PDPK1).

Remarkable differences between GA and pioglitazone treatment were also evident in Kyoto Encyclopedia of Genes and Genomes (KEGG) ([Kanehisa et al., 2017](#); [Ogata et al., 1999](#)) pathway enrichment analysis ([Figure 4D](#)). Although pioglitazone selectively and significantly upregulated PPAR signaling, only weak tendencies toward effects on lipid and carbohydrate metabolism were detected. GA affected several more KEGG pathways, including strong enrichment of thermogenesis, oxidative phosphorylation, fatty acid metabolism, and insulin signaling, all of which are linked to PPAR activation. Interestingly, however, the PPAR signaling pathway was not significantly affected by GA treatment. All effects of GA on KEGG pathways were abolished by the PPAR γ antagonist GW9662, demonstrating PPAR γ -mediated activity of GA. As observed for individual PPAR γ -regulated genes, combined GA and pioglitazone treatment had a weaker effect on PPAR signaling than pioglitazone but induced several pathways associated with PPAR activation, such as glycolysis, gluconeogenesis, fatty acid metabolism, and CYP metabolism, which were not upregulated for individual GA or pioglitazone treatment.

DISCUSSION

It has been proposed that vitamin E, in analogy to the lipophilic vitamins A and D, has to undergo metabolic activation to act

on specific regulatory enzymes and receptors (Schubert et al., 2018). Recent reports on 5-LO-mediated (Pein et al., 2018) and PXR-mediated (Bartolini et al., 2020) activities of vitamin E metabolites, together with our findings, strongly support this hypothesis and suggest rather promiscuous activities for vitamin E metabolites. Among various nuclear receptors, α -13'-COOH exhibited the most promiscuous activity profile while δ -13'-COOH was slightly more selective for PPAR modulation. The natural vitamin E mimetic GA revealed PPAR agonism representative for the vitamin E metabolites and thus was profiled in depth for its mode of action. Co-crystal structure analysis demonstrated the binding of two GA molecules within the PPAR γ LBD: one in the canonical orthosteric site and the other in an allosteric pocket. This structural finding was consistent with the GA-mediated PPAR γ modulation in the presence of the orthosteric reference agonist pioglitazone observed in two cellular settings. Detectable ability of GA to further enhance the activity of pioglitazone-activated PPAR γ suggested therefore simultaneous modulation. These observations provide a structural basis supporting previous reports that have located an alternate binding site within PPAR γ (Hughes et al., 2014) and proposed cooperative activity of ligands binding outside the canonical binding pocket with orthosteric agonists (Hurtado et al., 2012; Lea et al., 2004).

Although exhibiting activation effects in reporter gene assays similar to synthetic agonists, GA caused remarkably different effects on co-regulator recruitment to PPAR γ in comparison with known ligands, such as pioglitazone. While pioglitazone induced robust co-activator (CBP, PGC-1 α , NCoA6, and DRIP) recruitment to PPAR γ , GA strongly favored binding of the bona fide co-repressors NCoR1 and NCoR2. Therein, GA was also able to counteract pioglitazone. At first glance, this might suggest that GA acts as an inverse PPAR γ agonist that stabilizes an inactive repressed state of the nuclear receptor. However, the PPAR γ -GA co-crystal complex adopts an active conformation with helix 12 tightly bound to the core of the LBD, which strongly contradicts inverse agonism (Heidari et al., 2019). Moreover, GA robustly activated native human PPAR γ and the Gal4-PPAR γ hybrid in cellular settings with higher efficacy than the orthosteric agonist pioglitazone.

The observation of GA inducing an active conformation and activating transcriptional activity of PPAR γ but favoring NCoR1 and NCoR2 binding has important implications on molecular understanding of the nuclear receptor's activation mechanisms. Previous studies (Heidari et al., 2019) have demonstrated that both the active and the inactive conformation of PPAR γ are dynamic and mainly differ in the positions of helices H12 and H3, and the Ω loop. Structural comparison between the GA- and pioglitazone-PPAR γ complexes revealed no major differences in these regions. The activation helices (H12) of both structures were highly aligned and there was also no difference observed in H3 despite direct contacts of allosterically bound GA to this helix. Our findings, furthermore, suggest that GA can also bind to the allosteric site of PPAR γ with an orthosterically bound agonist such as glitazones, providing an explanation for the synergistic activity observed in cellular settings.

Thus, our results show that PPAR γ can recruit NCoR1 and NCoR2 also in a conformation involving active arrangements of helix 12, helix 3, and the Ω loop, suggesting a PPAR γ co-acti-

vator role of NCoR1 and NCoR2. Several bona fide NCoRs have been previously associated with increased transcriptional activation (Baymaz et al., 2015; White et al., 2004), demonstrating that a clear separation in co-activator and co-repressor is not possible in many cases. This is further exemplified by the kinase inhibitor imatinib, which was recently identified as a PPAR γ antagonist but crystallized with PPAR γ in complex with the co-activator SRC1 (PDB: 6KTN) (Jang et al., 2019). Imatinib occupies parts of the orthosteric and allosteric GA binding sites but lacks contact to the activation tetrad (Figures S2C and S2D). Moreover, a recent study revealed that NCoR recruitment to PPAR δ alone is not sufficient for full transcriptional repression (Legrand et al., 2019). Despite testing only a subset of potential co-regulators in the PPAR γ activation network, we propose that the agonist activity of GA is not mediated by canonical co-activators, but merely involves contributions by NCoRs, as has been described for other ligand-activated transcription factors. Both NCoR1 (Lima et al., 2018) and PPARs (Jamwal et al., 2020) are crucially involved in the transcriptional control of mitochondrial homeostasis and oxidative metabolism, and PPAR-NCoR interactions have, for example, been ascribed an important role in nutrient-dependent signaling in liver (Kang and Fan, 2020).

The mechanistically different modes of PPAR γ modulation by GA and pioglitazone translated into remarkably different effects in cellular settings. While differential gene expression analysis of HepG2 cells after GA or pioglitazone treatment revealed induction of PPAR γ -regulated genes by both compounds, pronounced differences were observable. Pioglitazone exclusively induced canonical PPAR signaling and mainly upregulated genes involved in lipid storage, gluconeogenesis, and fatty acid oxidation. GA affected the expression levels of significantly more genes than pioglitazone, including PPAR γ -dependent and -independent effects. Compared with pioglitazone, GA caused additional effects on fatty acid transport, cell survival, insulin signaling, glucose metabolism, and oxidative phosphorylation pathways, which were blocked by the covalent PPAR γ antagonist GW9662 and hence were likely PPAR γ -mediated. Especially GA-induced upregulation of oxidative metabolism was intriguing as it aligned with the observed GA-dependent recruitment of NCoR1 to PPAR γ . In line with opposing effects of GA and pioglitazone on several co-regulators, combined treatment with both compounds abrogated some PPAR γ -dependent effects of the individual compounds, while other PPAR γ -dependent genes remained upregulated. Allosteric PPAR γ regulation by GA, hence, cannot be simply described by ago-positive activity, as observed in reporter gene assays but involves additive and antagonistic components regarding orthosteric activation as obvious from differential co-regulator recruitment and gene expression profiles. Selective targeting of the allosteric binding site may enable further elucidation of the complex co-regulatory network and transcriptional effects of allosteric PPAR γ modulation.

In addition to these mechanistic findings on PPAR γ modulation, our observations also have considerable importance regarding the profound yet elusive pharmacological activities of vitamin E (Dysken et al., 2014; Lavine et al., 2011; Sanyal et al., 2010). PPARs have a longstanding history as drug targets in type 2 diabetes and other metabolic diseases (Lamers et al.,

2012), providing a link between PPAR modulation by oxidized vitamin E metabolites and the recommendation status of vitamin E as a major treatment option in NAFLD (Chalasanani et al., 2018). Remarkably, such recommendation also exists for the PPAR γ agonist pioglitazone by some societies (Chalasanani et al., 2018). Pharmacokinetic profiles and endogenous tissue levels of GA and naturally formed tocopherol carboxylates to estimate pharmacological relevance of PPAR γ -mediated effects have not been precisely determined yet. However, both GA and α -13'-COOH have been detected in plasma (Marinelli et al., 2020; Pein et al., 2018; Wallert et al., 2014), indicating also considerable exposure in the liver. Moreover, α -13'-COOH was characterized as a major vitamin E metabolite in humans (Pein et al., 2018) and, since vitamin E mainly undergoes hepatic metabolism (Bardowell et al., 2012), α -13'-COOH and other oxidized metabolites likely have high abundance and a profound relevance in the liver. In addition, in the context of AD, GA was found to decrease brain β -amyloid in experimental AD in mice (Marinelli et al., 2020). Such effects have also been demonstrated for PPAR activation in concert with other factors (Galimberti and Scarpini, 2017).

Allosteric modulation of PPAR γ by GA and oxidized vitamin E metabolites adds another dimension to the already complex picture of natural PPAR γ ligands (Gellrich et al., 2020). Through such an allosteric mechanism, vitamin E metabolites might potentiate activities of natural orthosteric PPAR γ ligands and thereby importantly contribute to PPAR signaling. Moreover, allosteric binding of GA, together with its remarkable PPAR γ activation efficacy despite an NCoR favoring co-regulator recruitment profile, calls into question common understanding of PPAR γ and suggests that more factors are involved in its complex regulatory network. Targeting this allosteric PPAR regulation with next-generation PPAR ligands might enable a more specific modulation and open therapeutic avenues.

SIGNIFICANCE

Vitamin E exhibits profound pharmacological activities, for example, in Alzheimer's disease and NAFLD, and even holds therapeutic recommendation to treat the latter pathology. However, mechanistic understanding and knowledge of macromolecular targets mediating the effects of vitamin E are lacking. Our findings characterize vitamin E metabolites as modulators of the ligand-activated transcription factor PPAR γ whose beneficial effects on metabolic balance are well defined, providing a link to the effects of vitamin E in NAFLD. Moreover, PPAR γ activation has been associated with neuroprotective actions suggesting a link to Alzheimer's disease, too. Vice versa, our observations are of considerable importance for molecular understanding of PPAR γ . The discovery of allosteric binding of the vitamin E mimetic garcinoic acid provides a structural basis for an alternative mode of PPAR γ modulation. This is highlighted by remarkably different effects of garcinoic acid and the orthosteric agonist pioglitazone on co-regulatory interactions of PPAR γ with, for example, an ability of garcinoic acid to recruit NCoR1 and NCoR2 to PPAR γ . These unprecedented co-regulatory interactions of PPAR γ align with the markedly distinct effects of garcinoic acid and pioglitazone on PPAR-regulated gene expression profiles in HepG2 cells. In

contrast to strong induction of PPAR signaling by pioglitazone, garcinoic acid mainly affected thermogenesis and oxidative phosphorylation pathways. These findings imply alternative PPAR γ modulation by garcinoic acid and suggest a possibility of gene-selective PPAR γ regulation by ligands. Hence, our findings not only characterize garcinoic acid and tocopherol carboxylates as PPAR γ modulators but also open an alternative avenue for therapeutic targeting of this important transcription factor.

STAR★METHODS

Detailed methods are provided in the online version of this paper and include the following:

- KEY RESOURCES TABLE
- RESOURCE AVAILABILITY
 - Lead contact
 - Materials availability
 - Data and code availability
- EXPERIMENTAL MODEL AND SUBJECT DETAILS
 - Cell lines
- METHOD DETAILS
 - Chemicals and compounds
 - Hybrid reporter gene assays
 - PPRE reporter assay in PPAR γ expressing HepG2 cells
 - Production of recombinant PPAR γ LBD protein for ITC
 - Isothermal titration calorimetry (ITC)
 - Production of recombinant PPAR γ fusion protein
 - PPAR γ co-regulator recruitment assays
 - PPAR γ LBD expression, purification and crystallization
 - Differential gene expression analysis
 - Computational methods
- QUANTIFICATION AND STATISTICAL ANALYSIS
 - Reporter gene assays
 - Co-regulator recruitment assays
 - Differential gene expression experiment

SUPPLEMENTAL INFORMATION

Supplemental information can be found online at <https://doi.org/10.1016/j.chembiol.2021.04.019>.

ACKNOWLEDGMENTS

This research was financially supported by the Aventis Foundation (Life Science Bridge Award to D.M.), the Deutsche Forschungsgemeinschaft (DFG) (SFB 1278 PolyTarget to O.W. and S.L.; SFB 1127 ChemBioSys to O.W.), the Free State of Thuringia, the European Social Fund (2019 FGR 0095 to S.L. and O.W.). S. Knapp and A.C. acknowledge support by the SGC, a registered charity (no. 1097737) that receives funds from; AbbVie, Bayer AG, Boehringer Ingelheim, Canada Foundation for Innovation, Eshelman Institute for Innovation, Genentech, Genome Canada, EU/EFPIA, Innovative Medicines Initiative 2 Joint Undertaking (EUBOPEN grant 875510), Janssen, Merck KGaA, Pfizer, São Paulo Research Foundation-FAPESP, Takeda and Wellcome, and support by the German translational Cancer Network DKTK and the Frankfurt Cancer Institute (FCI). The authors thank staff at Swiss Light Source for their assistance during crystallographic data collection. The authors dedicate this paper to Professor Ernst Mutschler on the occasion of his 90th birthday.

AUTHOR CONTRIBUTIONS

S.W., L.G., and D.M. performed the experiments. A.C. and S. Knapp generated and solved the co-crystal structures. S. Kluge and S.L. contributed the vitamin E metabolites. J.H. contributed the HTRF system, labeled PPAR γ LBD protein for HTRF assays, and PPAR γ LBD protein for ITC. O.W., S.L., M.S.-Z., and D.M. conceived the study. D.M. designed and supervised the study. S.W. and D.M. analyzed the data, generated the figures, and wrote the manuscript. All authors read the manuscript and provided feedback.

DECLARATION OF INTERESTS

O.W. is an inventor of the patent WO/2017/032881 on tocotrienole derivatives related to 5-LOX. The authors declare no other competing interests.

Received: November 16, 2020

Revised: March 29, 2021

Accepted: April 23, 2021

Published: May 13, 2021

REFERENCES

Anders, S., Pyl, P.T., and Huber, W. (2015). HTSeq—a Python framework to work with high-throughput sequencing data. *Bioinformatics* *31*, 166–169.

Azzi, A. (2019). Tocopherols, tocotrienols and tocomonoenols: are similar molecules but only one vitamin E. *Redox Biol.* *26*, 101259.

Bardowell, S.A., Duan, F., Manor, D., Swanson, J.E., and Parker, R.S. (2012). Disruption of mouse cytochrome P450 4f14 (*Cyp4f14* gene) causes severe perturbations in vitamin E metabolism. *J. Biol. Chem.* *287*, 26077–26086.

Bartolini, D., De Franco, F., Torquato, P., Marinelli, R., Cerra, B., Ronchetti, R., Schon, A., Fallarino, F., De Luca, A., Bellezza, G., et al. (2020). Garcinoic acid is a natural and selective agonist of pregnane X receptor. *J. Med. Chem.* *63*, 3701–3712.

Baymaz, H.I., Karemaker, I.D., and Vermeulen, M. (2015). Perspective on unraveling the versatility of “co-repressor” complexes. *Biochim. Biophys. Acta* *1849*, 1051–1056.

Birringner, M., and Lorkowski, S. (2019). Vitamin E: regulatory role of metabolites. *IUBMB Life* *71*, 479–486.

Birringner, M., Lington, D., Vertuani, S., Manfredini, S., Scharlau, D., Glej, M., and Ristow, M. (2010). Proapoptotic effects of long-chain vitamin E metabolites in HepG2 cells are mediated by oxidative stress. *Free Radic. Biol. Med.* *49*, 1315–1322.

Chalasan, N., Younossi, Z., Lavine, J.E., Charlton, M., Cusi, K., Rinella, M., Harrison, S.A., Brunt, E.M., and Sanyal, A.J. (2018). The diagnosis and management of nonalcoholic fatty liver disease: practice guidance from the American Association for the Study of Liver Diseases. *Hepatology* *67*, 328–357.

Chen, S., Zhou, Y., Chen, Y., and Gu, J. (2018). fastp: an ultra-fast all-in-one FASTQ preprocessor. *Bioinformatics* *34*, i884–i890.

Dobin, A., Davis, C.A., Schlesinger, F., Drenkow, J., Zaleski, C., Jha, S., Batut, P., Chaisson, M., and Gingeras, T.R. (2013). STAR: ultrafast universal RNA-seq aligner. *Bioinformatics* *29*, 15–21.

Dysken, M.W., Sano, M., Asthana, S., Vertrees, J.E., Pallaki, M., Llorente, M., Love, S., Schellenberg, G.D., McCarten, J.R., Malphurs, J., et al. (2014). Effect of vitamin E and memantine on functional decline in Alzheimer disease: the TEAM-AD VA cooperative randomized trial. *JAMA* *311*, 33–44.

Emsley, P., Lohkamp, B., Scott, W.G., and Cowtan, K. (2010). Features and development of Coot. *Acta Crystallogr. Sect. D Biol. Crystallogr.* *66*, 486–501.

Evans, P.R., and Murshudov, G.N. (2013). How good are my data and what is the resolution? *Acta Crystallogr. D Biol. Crystallogr.* *69*, 1204–1214.

Flesch, D., Cheung, S.-Y., Schmidt, J., Gabler, M., Heitel, P., Kramer, J.S., Kaiser, A., Hartmann, M., Lindner, M., Lüddens-Dämgen, K., et al. (2017). Non-acidic farnesoid X receptor modulators. *J. Med. Chem.* *60*, 7199–7205.

Galimberti, D., and Scarpini, E. (2017). Pioglitazone for the treatment of Alzheimer’s disease. *Expert Opin. Investig. Drugs* *26*, 97–101.

Gellrich, L., Heitel, P., Heering, J., Kilu, W., Pollinger, J., Goebel, T., Kahnt, A., Arifi, S., Pogoda, W., Paulke, A., et al. (2020). I-Thyroxin and the nonclassical thyroid hormone TETRAC are potent activators of PPAR γ . *J. Med. Chem.* *63*, 6727–6740.

Hanke, T., Cheung, S.Y., Kilu, W., Heering, J., Ni, X., Planz, V., Schierle, S., Faudone, G., Friedrich, M., Wanior, M., et al. (2020). A selective modulator of peroxisome proliferator-activated receptor γ with an unprecedented binding mode. *J. Med. Chem.* *63*, 4555–4561.

Heidari, Z., Chrisman, I.M., Nemetchek, M.D., Novick, S.J., Blayo, A.L., Patton, T., Mendes, D.E., Diaz, P., Kamenecka, T.M., Griffin, P.R., et al. (2019). Definition of functionally and structurally distinct repressive states in the nuclear receptor PPAR γ . *Nat. Commun.* *10*, 5825.

Heitel, P., Achenbach, J., Moser, D., Proschak, E., and Merk, D. (2017). DrugBank screening revealed alitretinoin and bexarotene as liver X receptor modulators. *Bioorg. Med. Chem. Lett.* *27*, 1193–1198.

Hinnah, K., Willems, S., Morstein, J., Heering, J., Hartrampf, F.W.W., Broichhagen, J., Leippe, P., Merk, D., and Trauner, D. (2020). Photohormones enable optical control of the peroxisome proliferator-activated receptor γ (PPAR γ). *J. Med. Chem.* *63*, 10908–10920.

Hughes, T.S., Giri, P.K., De Vera, I.M.S., Marciano, D.P., Kuruvilla, D.S., Shin, Y., Blayo, A.L., Kamenecka, T.M., Burris, T.P., Griffin, P.R., et al. (2014). An alternate binding site for PPAR γ ligands. *Nat. Commun.* *5*, 3571.

Hurtado, O., Ballesteros, I., Cuartero, M.I., Moraga, A., Pradillo, J.M., Ramirez-Franco, J., Bartolomé-Martín, D., Pascual, D., Torres, M., Sánchez-Prieto, J., et al. (2012). Daidzein has neuroprotective effects through ligand-binding-independent PPAR γ activation. *Neurochem. Int.* *61*, 119–127.

Jamwal, S., Blackburn, J.K., and Elsworth, J.D. (2020). PPAR γ /PGC1 α signaling as a potential therapeutic target for mitochondrial biogenesis in neurodegenerative disorders. *Pharmacol. Ther.* *219*–107705.

Jang, J.Y., Bae, H., Lee, Y.J., Choi, Y.I., Kim, H.-J., Park, S.B., Suh, S.W., Kim, S.W., and Han, B.W. (2018). Structural basis for the enhanced anti-diabetic efficacy of lobeglitazone on PPAR γ . *Sci. Rep.* *8*, 31.

Jang, J.Y., Kim, H.J., and Han, B.W. (2019). Structural basis for the regulation of PPAR γ activity by imatinib. *Molecules* *24*, 3562.

Kabsch, W. (2010). XDS. *Acta Crystallogr. D Biol. Crystallogr.* *66*, 125–132.

Kanehisa, M., Furumichi, M., Tanabe, M., Sato, Y., and Morishima, K. (2017). KEGG: new perspectives on genomes, pathways, diseases and drugs. *Nucleic Acids Res.* *45*, D353–D361.

Kang, Z., and Fan, R. (2020). PPAR α and NCOR/SMRT corepressor network in liver metabolic regulation. *FASEB J.* *34*, 8796–8809.

Lamers, C., Schubert-Zsilavecz, M., and Merk, D. (2012). Therapeutic modulators of peroxisome proliferator-activated receptors (PPAR): a patent review (2008–present). *Expert Opin. Ther. Pat.* *22*, 803–841.

Lavine, J.E., Schwimmer, J.B., Van Natta, M.L., Molleston, J.P., Murray, K.F., Rosenthal, P., Abrams, S.H., Scheimann, A.O., Sanyal, A.J., Chalasan, N., et al. (2011). Effect of vitamin E or metformin for treatment of nonalcoholic fatty liver disease in children and adolescents the tonic randomized controlled trial. *JAMA* *305*, 1659–1668.

Lea, M., Sura, M., and Desbordes, C. (2004). Inhibition of cell proliferation by potential peroxisome proliferator-activated receptor (PPAR) gamma agonists and antagonists. *Anticancer Res.* *24*, 2765–2772.

Legrand, N., Bretscher, C.L., Zielke, S., Wilke, B., Daude, M., Fritz, B., Diederich, W.E., and Adhikary, T. (2019). PPAR β/δ recruits NCOR and regulates transcription reinitiation of ANGPTL4. *Nucleic Acids Res.* *47*, 9573–9591.

Lima, T.I., Valentim, R.R., Araújo, H.N., Oliveira, A.G., Favero, B.C., Menezes, E.S., Araújo, R., and Silveira, L.R. (2018). Role of NCoR1 in mitochondrial function and energy metabolism. *Cell Biol. Int.* *42*, 734–741.

Love, M.I., Huber, W., and Anders, S. (2014). Moderated estimation of fold change and dispersion for RNA-seq data with DESeq2. *Genome Biol.* *15*, 550.

Marinelli, R., Torquato, P., Bartolini, D., Mas-Bargues, C., Bellezza, G., Gioiello, A., Borras, C., De Luca, A., Fallarino, F., Sebastiani, B., et al. (2020). Garcinoic acid prevents β -amyloid (A β) deposition in the mouse brain. *J. Biol. Chem.* *295*, 11866–11876.

- Mazzini, F., Betti, M., Netscher, T., Galli, F., and Salvadori, P. (2009). Configuration of the vitamin E analogue garcinoic acid extracted from *garcinia kola* seeds. *Chirality* 21, 519–524.
- McCoy, A.J., Grosse-Kunstleve, R.W., Adams, P.D., Winn, M.D., Storoni, L.C., and Read, R.J. (2007). Phaser crystallographic software. *J. Appl. Crystallogr.* 40, 658–674.
- Michalik, L., Auwerx, J., Berger, J.P., Chatterjee, V.K., Glass, C.K., Gonzalez, F.J., Grimaldi, P.A., Kadowaki, T., Lazar, M.A., O’Rahilly, S., et al. (2006). International Union of Pharmacology. LXI. Peroxisome proliferator-activated receptors. *Pharmacol. Rev.* 58, 726–741.
- Mouchiroud, L., Eichner, L.J., Shaw, R.J., and Auwerx, J. (2014). Transcriptional coregulators: fine-tuning metabolism. *Cell Metab.* 20, 26–40.
- Ogata, H., Goto, S., Sato, K., Fujibuchi, W., Bono, H., and Kanehisa, M. (1999). KEGG: Kyoto Encyclopedia of Genes and Genomes. *Nucleic Acids Res.* 27, 29–34.
- Pein, H., Ville, A., Pace, S., Temml, V., Garscha, U., Raasch, M., Alsabil, K., Viault, G., Dinh, C.P., Guilet, D., et al. (2018). Endogenous metabolites of vitamin E limit inflammation by targeting 5-lipoxygenase. *Nat. Commun.* 9, 3834.
- Pollinger, J., Gellrich, L., Schierle, S., Kilu, W., Schmidt, J., Kalinowsky, L., Ohmdorf, J., Kaiser, A., Heering, J., Proschak, E., et al. (2019). Tuning nuclear receptor selectivity of Wy14,643 towards selective retinoid X receptor modulation. *J. Med. Chem.* 62, 2112–2126.
- Rau, O., Wurglics, M., Paulke, A., Zitzkowski, J., Meindl, N., Bock, A., Dingermann, T., Abdel-Tawab, M., and Schubert-Zsilavecz, M. (2006). Carnosic acid and carnosol, phenolic diterpene compounds of the labiate herbs rosemary and sage, are activators of the human peroxisome proliferator-activated receptor gamma. *Planta Med.* 72, 881–887.
- Sanyal, A.J., Chalasani, N., Kowdley, K.V., McCullough, A., Diehl, A.M., Bass, N.M., Neuschwander-Tetri, B.A., Lavine, J.E., Tonascia, J., Unalp, A., et al. (2010). Pioglitazone, vitamin E, or placebo for nonalcoholic steatohepatitis. *N. Engl. J. Med.* 362, 1675–1685.
- Schmidt, J., Klingler, F.-M., Proschak, E., Steinhilber, D., Schubert-Zsilavecz, M., and Merk, D. (2015). NSAIDs ibuprofen, indometacin, and diclofenac do not interact with farnesoid X receptor. *Sci. Rep.* 5, 14782.
- Schmölz, L. (2016). Complexity of vitamin E metabolism. *World J. Biol. Chem.* 7, 14.
- Schubert, M., Kluge, S., Schmölz, L., Wallert, M., Galli, F., Birringer, M., and Lorkowski, S. (2018). Long-chain metabolites of vitamin E: metabolic activation as a general concept for lipid-soluble vitamins? *Antioxidants* 7, 10.
- Shang, J., Brust, R., Griffin, P.R., Kamenecka, T.M., and Kojetin, D.J. (2019). Quantitative structural assessment of graded receptor agonism. *Proc. Natl. Acad. Sci. U S A* 116, 22179–22188.
- Skubák, P., Murshudov, G.N., and Pannu, N.S. (2004). Direct incorporation of experimental phase information in model refinement. *Acta Crystallogr. Sect. D Biol. Crystallogr.* 60, 2196–2201.
- Trapnell, C., Roberts, A., Goff, L., Pertea, G., Kim, D., Kelley, D.R., Pimentel, H., Salzberg, S.L., Rinn, J.L., and Pachter, L. (2012). Differential gene and transcript expression analysis of RNA-seq experiments with TopHat and Cufflinks. *Nat. Protoc.* 7, 562–578.
- Wallert, M., Mosig, S., Rennert, K., Funke, H., Ristow, M., Pellegrino, R.M., Cruciani, G., Galli, F., Lorkowski, S., and Birringer, M. (2014). Long-chain metabolites of α -tocopherol occur in human serum and inhibit macrophage foam cell formation in vitro. *Free Radic. Biol. Med.* 68, 43–51.
- Wallert, M., Bauer, J., Kluge, S., Schmölz, L., Chen, Y.C., Ziegler, M., Searle, A.K., Maxones, A., Schubert, M., Thürmer, M., et al. (2019). The vitamin E derivative garcinoic acid from *Garcinia kola* nut seeds attenuates the inflammatory response. *Redox Biol.* 24, 101166.
- White, J.H., Fernandes, I., Mader, S., and Yang, X.J. (2004). Corepressor recruitment by agonist-bound nuclear receptors. *Vitam. Horm.* 68, 123–143.
- Willems, S., Kilu, W., Ni, X., Chaikuad, A., Knapp, S., Heering, J., and Merk, D. (2020). The orphan nuclear receptor Nurr1 is responsive to non-steroidal anti-inflammatory drugs. *Commun. Chem.* 3, 85.
- Yu, G., Wang, L.G., Han, Y., and He, Q.Y. (2012). ClusterProfiler: an R package for comparing biological themes among gene clusters. *Omi. A. J. Integr. Biol.* 16, 284–287.
- Zhao, Y., Lee, M.J., Cheung, C., Ju, J.H., Chen, Y.K., Liu, B., Hu, L.Q., and Yang, C.S. (2010). Analysis of multiple metabolites of tocopherols and tocotrienols in mice and humans. *J. Agric. Food Chem.* 58, 4844–4852.

STAR★METHODS

KEY RESOURCES TABLE

REAGENT or RESOURCE	SOURCE	IDENTIFIER
Bacterial and virus strains		
<i>E. coli</i> BL21 T7 Express (High efficiency)	New England Biolabs	Cat#C2566
Chemicals, peptides, and recombinant proteins		
Garcinoic acid (GA)	(Wallert et al., 2019)	Isolation from <i>Garcinia kola</i> seeds
α -13'-carboxytocopherol	(Birringer et al., 2010; Mazzini et al., 2009)	Semisynthesis from GA
α -13'-hydroxytocopherol	(Birringer et al., 2010; Mazzini et al., 2009)	Semisynthesis from GA
δ -13'-carboxytocopherol	(Birringer et al., 2010; Mazzini et al., 2009)	Semisynthesis from GA
δ -13'-hydroxytocopherol	(Birringer et al., 2010; Mazzini et al., 2009)	Semisynthesis from GA
Pioglitazone	Sigma-Aldrich	Cat#CDS021593; CAS: 111025-46-8
Rosiglitazone	TCI	Cat#R0106; CAS: 122320-73-4
GW9662	Sigma-Aldrich	Cat#M6191; CAS: 22978-25-2
Recombinant PPAR γ LBD protein (aa 234-505) for ITC	(Hinnah et al., 2020)	N/A
Recombinant PPAR γ LBD protein (aa 203-477) for crystallization	(Gellrich et al., 2020)	N/A
Biotinylated recombinant PPAR γ LBD (aa 234-505) fusion protein	(Gellrich et al., 2020)	N/A
Streptavidin-Tb cryptate	Cisbio Bioassays	Cat#610SATLB
SRC 1-1: Fluorescein-KYSQTSKHLVQLLTTTAEQQL-OH	Life Technologies	Cat#PV4576
SRC 1-2: Fluorescein-LTARHKILHRLQEGSPSD-OH	Life Technologies	Cat#PV4578
SRC 1-3: Fluorescein-ESKDHQLLRYLLDKDEKDL-OH	Life Technologies	Cat#PV4580
SRC 1-4: Fluorescein-GPQTPQAQKSLQLLQTE-OH	Life Technologies	Cat#PV4582
SRC 2-1: Fluorescein-DSKGQTKLLQLLTTKSDQM-OH	Life Technologies	Cat#PV4584
SRC 2-2: Fluorescein-LKEKHILHRLQDSSSPV-OH	Life Technologies	Cat#PV4586
SRC 2-3: Fluorescein-KKKENALLRYLLDKDDTKD-OH	Life Technologies	Cat#PV4588
SRC 3-1: Fluorescein-ESKGHKLLQLLTCSSDDR-OH	Life Technologies	Cat#PV4590
SRC 3-2: Fluorescein-LQEKHRILHKLQNGNSPA-OH	Life Technologies	Cat#PV4592
SRC 3-3: Fluorescein-KKENALLRYLLDRDDPSD-OH	Life Technologies	Cat#PV4594
NCOR ID1: Fluorescein-RTHRLITLADHICQIITQDFARN-OH	Life Technologies	Cat#PV4622
NCOR ID2: Fluorescein-DPASNLGLEIIRKALMGSFDDK-OH	Life Technologies	Cat#PV4624
SMRT ID1: Fluorescein-GHQRVVTLAQHISEVITQDYTRH-OH	Life Technologies	Cat#PV4620
SMRT ID2: Fluorescein -HASTNMGLEAIIRKALMGKYDQW-OH	Life Technologies	Cat#PV4423

(Continued on next page)

Continued

REAGENT or RESOURCE	SOURCE	IDENTIFIER
CBP-1: Fluorescein-AASKHKQLSELLRGGSGSS-OH	Life Technologies	Cat#PV4596
C33: Fluorescein-HVEMHPLLMLLMESQWGA-OH	Life Technologies	Cat#PV4606
D11-FXRLF: Fluorescein-VESGSSRFMQLFMANDLLT-OH	Life Technologies	Cat#PV4382
D22: Fluorescein-LPYEGSLLLKLLRAPVEEV-OH	Life Technologies	Cat#PV4386
EAB1: Fluorescein-SSNHQSSRLIELLSR-OH	Life Technologies	Cat#PV4608
EA2: Fluorescein-SSKGLWRMLAEPVSR-OH	Life Technologies	Cat#PV4610
ARA70: Fluorescein-SRETSEKFKLLFQSYNVND-OH	Life Technologies	Cat#PV4618
AR N-term: Fluorescein-SKTYRGAFQNLQSVREVI-OH	Life Technologies	Cat#PV4616
PGC1a: Fluorescein-EAEEPSLLKLLLAPANTQ-OH	Life Technologies	Cat#PV4421
PRIPRAP250: Fluorescein-VLTSPLLVNLQSDISAG-OH	Life Technologies	Cat#PV4604
RIP140L6: Fluorescein-SHQKVTLQLLLGHKNEEN-OH	Life Technologies	Cat#PV4600
RIP140L8: Fluorescein-SFSKNGLLSRLLRQNDQSY-OH	Life Technologies	Cat#PV4602
TB3: Fluorescein-SSVASREWWVRELSR-OH	Life Technologies	Cat#PV4614
TRAP220/DRIP-1: Fluorescein-KVSNPILTSLLQITGNGG-OH	Life Technologies	Cat#PV4598
TRAP220/DRIP-2: Fluorescein-NTKNHPMLMNLKDNPAQD-OH	Life Technologies	Cat#PV4549

Critical commercial assays

Dual-Glo® Luciferase Assay System	Promega	Cat#E2940
E.Z.N.A.® Total RNA Kit I	Omega Bio-Tek Inc.	R6834-02
NEBNext® Ultra™ RNA Library Prep Kit for Illumina®	New England Biolabs	Cat#E7530L
AMPure XP system	Beckman Coulter	Cat#A63882
PE Cluster Kit cBot-HS	Illumina	Cat#PE-401

Deposited data

PPAR γ -GA crystal structure	This paper	PDB: 7AWD
PPAR γ -rosiglitazone crystal structure	This paper	PDB: 7AWC
Differential gene expression data	This paper	ArrayExpress: E-MTAB-10328
Human reference genome NCBI build 38, GRCh38	Genome Reference Consortium	http://www.ncbi.nlm.nih.gov/projects/genome/assembly/grc/human/
KEGG database resource	(Kanehisa et al., 2017; Ogata et al., 1999)	https://www.genome.jp/kegg/

Experimental models: cell lines

Human: HEK293T cells	DSMZ	ACC 635
Human: HepG2 cells	DSMZ	ACC 180

Recombinant DNA

Plasmid: pFA-CMV-hPPAR α -LBD	(Rau et al., 2006)	N/A
Plasmid: pFA-CMV-hPPAR γ -LBD	(Rau et al., 2006)	N/A

(Continued on next page)

Continued

REAGENT or RESOURCE	SOURCE	IDENTIFIER
Plasmid: pFA-CMV-hPPAR δ -LBD	(Rau et al., 2006)	N/A
Plasmid: pFA-CMV-hTHR α -LBD	(Gellrich et al., 2020)	N/A
Plasmid: pFA-CMV-hTHR β -LBD	(Gellrich et al., 2020)	N/A
Plasmid: pFA-CMV-hRAR α -LBD	(Flesch et al., 2017)	N/A
Plasmid: pFA-CMV-hRAR β -LBD	(Flesch et al., 2017)	N/A
Plasmid: pFA-CMV-hRAR γ -LBD	(Flesch et al., 2017)	N/A
Plasmid: pFA-CMV-hLXR α -LBD	(Heitel et al., 2017)	N/A
Plasmid: pFA-CMV-hLXR β -LBD	(Heitel et al., 2017)	N/A
Plasmid: pFA-CMV-hRXR α -LBD	(Flesch et al., 2017)	N/A
Plasmid: pFA-CMV-hRXR β -LBD	(Flesch et al., 2017)	N/A
Plasmid: pFA-CMV-hRXR γ -LBD	(Flesch et al., 2017)	N/A
Plasmid: pFA-CMV-hFXR-LBD	(Schmidt et al., 2015)	N/A
Plasmid: pFA-CMV-hCAR-LBD	(Flesch et al., 2017)	N/A
Plasmid: pFA-CMV-hVDR-LBD	(Flesch et al., 2017)	N/A
Plasmid: pFR-Luc	Stratagene	Cat#219050
Plasmid: pRL-SV40	Promega	Cat#E2231
Plasmid: PPRE1-pGL3	(Pollinger et al., 2019)	N/A

Software and algorithms

GraphPad Prism version 7.00	GraphPad Software	https://www.graphpad.com/scientific-software/prism/
NanoAnalyze version 3.7.5	TA Instruments	https://www.tainstruments.com/support/software-downloads-support/downloads/
XDS	(Kabsch, 2010)	http://xds.mpimf-heidelberg.mpg.de/
AIMLESS from CCP4 Suite	(Evans and Murshudov, 2013)	http://www.ccp4.ac.uk/
Phaser	(McCoy et al., 2007)	https://www.phaser.cimr.cam.ac.uk/index.php/Phaser_Crystallographic_Software
Coot	(Emsley et al., 2010)	https://www2.mrc-lmb.cam.ac.uk/personal/pemsley/coot/
REFMAC5	(Skubák et al., 2004)	https://www2.mrc-lmb.cam.ac.uk/groups/murshudov/content/refmac/refmac.html
Fastp	(Chen et al., 2018)	https://github.com/OpenGene/fastp
STAR v2.5	(Dobin et al., 2013)	https://github.com/alexdobin/STAR/releases
HTseq v0.6.1	(Anders et al., 2015)	https://htseq.readthedocs.io/en/master/
Cufflink	(Trapnell et al., 2012)	http://cole-trapnell-lab.github.io/cufflinks/
TopHat	(Trapnell et al., 2012)	http://ccb.jhu.edu/software/tophat/index.shtml
DESeq2 R package v2_1.6.3	(Love et al., 2014)	http://www.bioconductor.org/packages/release/bioc/html/DESeq2.html
clusterProfiler R package v3.8.1	(Yu et al., 2012)	https://bioconductor.org/packages/release/bioc/html/clusterProfiler.html
MOE version 2018.0101	Chemical Computing Group	https://www.chemcomp.com/Products.htm

RESOURCE AVAILABILITY

Lead contact

Further information and requests for resources and reagents should be directed to and will be fulfilled by the lead contact, Daniel Merk (merk@pharmchem.uni-frankfurt.de).

Materials availability

This study did not generate new unique reagents.

Data and code availability

Coordinates of the co-crystal structures solved and analyzed in this study are available at the wwPDB with the accession codes 7AWD (PPAR γ -GA) and 7AWC (PPAR γ -rosiglitazone). Differential gene expression data are available at ArrayExpress with the accession code E-MTAB-10328.

EXPERIMENTAL MODEL AND SUBJECT DETAILS

Cell lines

HEK293T cells (German Collection of Microorganisms and Cell Culture GmbH, DSMZ) and HepG2 cells (DSMZ) were cultured in Dulbecco's modified Eagle's medium (DMEM), high glucose supplemented with 10% fetal calf serum (FCS), sodium pyruvate (1 mM), penicillin (100 U/mL), and streptomycin (100 μ g/mL) at 37°C and 5% CO₂.

METHOD DETAILS

Chemicals and compounds

GA was isolated as described previously (Wallert et al., 2019). In brief, *Garcinia kola* seeds were mashed and extracted three times with methanol (1 L/kg). The solvent was evaporated and the residue was dissolved in a mixture of methanol and chloroform (95:5). The mixture was dried over sodium sulfate, and the solvents were evaporated under reduced pressure. Garcinoic acid (purity > 95%) was isolated from the crude extract by column chromatography using chloroform/methanol and hexane/acetone as solvent systems. The 13'-carboxytocopherols (α -13'-COOH and δ -13'-COOH) and the 13'-hydroxytocopherols (α -13'-OH and δ -13'-OH) were obtained from GA by semi-synthesis as reported previously (Birringer et al., 2010; Mazzini et al., 2009). In brief, GA was hydrogenated using Adam's catalyst to obtain δ -13'-COOH. SnCl₂-mediated methylation of δ -13'-COOH with paraformaldehyde gave α -13'-COOH. Reduction of α -13'-COOH and δ -13'-COOH with LiAlH₄ produced the corresponding alcohols α -13'-OH and δ -13'-OH.

Hybrid reporter gene assays

The plasmids pFA-CMV-hPPAR α -LBD, pFA-CMV-hPPAR γ -LBD, pFA-CMV-hPPAR δ -LBD, pFA-CMV-hTHR α -LBD, pFA-CMV-hTHR β -LBD, pFA-CMV-hRAR α -LBD, pFA-CMV-hRAR β -LBD, pFA-CMV-hRAR γ -LBD, pFA-CMV-hLXR α -LBD, pFA-CMV-hLXR β -LBD, pFA-CMV-hRXR α -LBD, pFA-CMV-hRXR β -LBD, pFA-CMV-hRXR γ -LBD, pFA-CMV-hFXR-LBD, pFA-CMV-hCAR-LBD and pFA-CMV-hVDR-LBD coding for the hinge region and ligand binding domain of the canonical isoform of the respective nuclear receptor were used to express the Gal4 hybrid receptors and have been described previously (Flesch et al., 2017; Gellrich et al., 2020; Heitel et al., 2017; Rau et al., 2006; Schmidt et al., 2015). pFR-Luc (Stratagene, La Jolla, CA, USA) served as Gal4 responsive reporter and pRL-SV40 (Promega, Madison, WI, USA) was used as internal control in the hybrid reporter gene assays. HEK293T cells (German Collection of Microorganisms and Cell Culture GmbH, DSMZ) were cultured in Dulbecco's modified Eagle's medium (DMEM), high glucose supplemented with 10% fetal calf serum (FCS), sodium pyruvate (1 mM), penicillin (100 U/mL), and streptomycin (100 μ g/mL) at 37°C and 5% CO₂ and seeded in 96-well plates (3 \times 10⁴ cells/well) twenty-four hours prior to transfection. Before transfection, medium was changed to Opti-MEM without supplements and transient transfection with above mentioned plasmids (pFR-Luc, pRL-SV40 and one pFA-CMV-NR-LBD clone) was carried out with Lipofectamine LTX reagent (Invitrogen, Carlsbad, CA, USA) according to the manufacturer's protocol. Five hours after transfection, medium was changed to Opti-MEM supplemented with penicillin (100 U/mL) and streptomycin (100 μ g/mL) additionally containing 0.1% dimethyl sulfoxide (DMSO) and the respective test compound or 0.1% DMSO alone as untreated control. Each concentration was tested in duplicates and each experiment was repeated independently at least three times. Following overnight (14–16 h) incubation, cells were assayed for luciferase activity using the Dual-Glo[®] Luciferase Assay System (Promega) according to the manufacturer's protocol. Luminescence was measured with a Tecan Spark luminometer (Tecan Deutschland GmbH, Germany). Normalization of transfection efficiency and cell growth was done by division of firefly luciferase data by Renilla luciferase data and multiplying the value by 1000 resulting in relative light units (RLU). Fold activation was obtained by dividing the mean RLU of test compound by the mean RLU of the untreated control. Max. relative activation refers to fold reporter activity divided by the fold activation of respective reference agonist (PPAR α : 1 μ M GW7647; PPAR γ : 1 μ M pioglitazone; PPAR δ : 1 μ M L165,041; THR α / β : 0.1 μ M triiodothyronine; RAR α / β / γ : 1 μ M tretinoin; LXR α / β : 1 μ M T0901317; RXR α / β / γ : 1 μ M bexarotene; FXR: 1 μ M GW4064; CAR: 1 μ M CITCO; VDR: 1 μ M calcitriol) treated cells. All hybrid assays were validated with the respective reference agonists which yielded EC₅₀ values in agreement with the literature.

PPRE reporter assay in PPAR γ expressing HepG2 cells

The reporter plasmid PPRE1-pGL3 coding for a firefly luciferase reporter gene under control of the human full length PPAR response element (PPRE) has been described previously (Pollinger et al., 2019). pRL-SV40 (Promega) was used for normalization of transfection efficiency and cell growth. HepG2 cells (DSMZ) were cultured in DMEM, high glucose supplemented with 10% fetal calf serum (FCS), sodium pyruvate (1 mM), penicillin (100 U/mL), and streptomycin (100 μ g/mL) at 37°C and 5% CO₂ and seeded twenty-four hours prior to transfection in 96-well plates (1.25 \times 10⁴ cells/well) pre-coated with Collagen G solution. Before transfection, medium was changed to Opti-MEM without supplements and transient transfection was carried out using Lipofectamine 3000 reagent (Invitrogen) according to the manufacturer's protocol with PPRE1-pGL3 and pRL-SV40 (Promega). Five hours after transfection, medium was changed to Opti-MEM supplemented with penicillin (100 U/mL) and streptomycin (100 μ g/mL), additionally containing 0.1%

DMSO and the respective test compound or 0.1% DMSO alone as untreated control. Each concentration was tested in duplicates and each experiment was repeated independently four times. After overnight (14–16 h) incubation the cells were assayed for luciferase activity as described above. The PPRE reporter gene assay was validated with rosiglitazone as PPAR γ reference agonist which yielded an EC₅₀ value in agreement with the literature.

Production of recombinant PPAR γ LBD protein for ITC

As described previously (Hinnah et al., 2020), a cDNA sequence optimized for codon usage in *E. coli* K12 and coding for an N-terminal His₁₀-Tag followed in frame by a TEV cleavage site and the PPAR γ isoform 2 LBD (aa 234–505) was cloned into the backbone of pET29b for expression under the control of the T7 promoter. *E. coli* BL21 T7 express were transformed with the described expression plasmid and the plasmid pGro7 for co-expression of GroEL/ES (chaperone plasmid set; TaKaRa Bio, Inc.). Cultures in LB medium containing 35 μ g/mL kanamycin and 34 μ g/mL chloramphenicol were grown at 37°C and 180 rpm. When OD₆₀₀ reached 0.6–0.7 the temperature was lowered to 18°C and expression of GroEL/ES was induced by addition of 1 g/L L-arabinose. 30 minutes later expression of PPAR γ LBD was induced by the addition of 0.5 mM IPTG and the cultures were supplemented with ~200 μ L Antifoam Y-30 (Sigma-Aldrich) per liter. After 14–18 h the cells were harvested by centrifugation (20 min, 6000xg, 4°C). A cell pellet from 2 L of culture was thawed and resuspended in a total volume of 50 mL of lysis buffer (400 mM NaCl, 25 mM Tris pH 7.8, 20 mM β -mercaptoethanol, 10% w/v glycerol) supplemented with 25 mM imidazole, 2 mM MgSO₄, 750 Kunitz DNase I, 250 Kunitz RNase A, a spatula tip of lysozyme and one tablet of Roche complete EDTA-free protease inhibitor cocktail. After incubation for 30 minutes on wet ice the slurry was diluted with three volumes of IMAC buffer A (400 mM NaCl, 25 mM NaP_i pH 7.8, 20 mM β -mercaptoethanol, 10% w/v glycerol) supplemented with 25 mM imidazole and cell lysis was enforced by passage through a homogenizer at a combined pressure of 1000 psi. The suspension was supplemented with 1 mM ATP and incubated for another 30 min on wet ice. Cell debris was removed by centrifugation (20 min, 16500xg, 4°C) and the supernatant was loaded at a flowrate of 3 mL/min onto a prepacked 5 mL HisTrap FF column (Ge Healthcare) preequilibrated in 95% IMAC buffer A and 5% IMAC buffer B (IMAC buffer A containing 500 mM imidazole). To remove unbound proteins, the column was washed with 15 column volumes of the same buffer at 5 mL/min. PPAR γ LBD was eluted by a linear gradient of 20–60% IMAC buffer B and supplemented with His7-tagged TEV protease (molar ratio of 1:25) for digestion of the His-tag during overnight dialysis against a volume of IMAC buffer A sufficient to reduce imidazole to 10–15 mM. The mixture was run gravity flow through a column packed with 10 mL Ni Sepharose 6 Fast Flow (GE Healthcare) and the flow through was concentrated under 2 bar pressure from nitrogen gas in an amicon stirring cell equipped with a 10,000 MWCO membrane. 5 mL concentrate were separated on a HiLoad 16/600 Superdex 75 pg gel filtration column (GE Healthcare) equilibrated and run in assay buffer (150 mM KF, 25 mM HEPES pH 7.5, 10% w/v glycerol, 5 mM DTT) at 1 mL/min. The protein used for isothermal titration experiments was taken from the middle of the peak corresponding to monomeric PPAR γ LBD.

Isothermal titration calorimetry (ITC)

ITC was conducted on a TA Instruments Affinity ITC (TA Instruments, New Castle, Delaware, USA) using recombinant PPAR γ LBD protein dissolved in buffer at pH 7.5 containing 25 mM HEPES, 150 mM KF, 5 mM DTT, 10% w/v glycerol and 1% DMSO. Garcinoic acid was dissolved to a final concentration of 300 μ M in the same buffer, placed into the ITC syringe and titrated to 172 μ L of PPAR γ LBD protein (64 μ M). The titration was performed at a temperature of 25°C with a stirring rate of 75 rpm and 31 injections. The first injection had a reduced volume of 1.0 μ L, followed by 30 injections of 2.5 μ L. An interval of 300 s was maintained between injections. ITC raw data were analyzed using NanoAnalyze software package (version 3.7.5). An independent binding model was used to fit the reaction enthalpy (ΔH), binding affinity constant (KD), and stoichiometry (n). Free energy change (ΔG) was calculated from the equation $\Delta G = -RT \ln K$ and the entropy (ΔS) was calculated from $\Delta G = \Delta H - T\Delta S$.

Production of recombinant PPAR γ fusion protein

For generation of site-specifically biotin-labeled PPAR γ LBD, the before described pET29b plasmid was modified as described previously (Gellrich et al., 2020). A DNA sequence coding for Avi-Tag [GLNDIFEAKIEWHE] followed by an in frame BamHI restriction site was introduced between [TEV site] and the PPAR γ LBD encoding sequence. From this construct, a fusion protein is expressed with N-terminal His₁₀-Tag followed by a cleavage site for TEV protease, an Avi-Tag, and PPAR γ LBD (aa 234–505; isoform 2). *E. coli* BL21 T7 express were transformed with the described expression plasmid and the plasmid pGro7 for co-expression of GroEL/ES (chaperone plasmid set; TaKaRa Bio, Inc.) and selected overnight at 37°C on LB (Luria Broth) agar containing 34 μ g/ml Chloramphenicol and 35 μ g/ml Kanamycin. Liquid LB was inoculated and the culture grown at 37°C with constant shaking at 180 rpm until optical density at 600 nm (OD₆₀₀) reached 0.7. At this time point, expression of the chaperone GroEL/ES from pGro7 was induced with 1 g/L L(+)-Arabinose, temperature was reduced to 20°C, and shaking to 120 rpm. 20 to 30 minutes later OD₆₀₀ reached ~1 and expression of the target protein was induced by addition of 0.5 mM IPTG. The expression cultures were incubated overnight, harvested at 6000 rpm at 4°C and pellets were stored at -80°C or processed right away. Pellets corresponding to 2 L of culture were resuspended in 50 mL buffer A (400 mM NaCl, 20 mM NaP_i pH 7.8, 10% w/v Glycerol and 20 mM β -mercaptoethanol) supplemented with 20 mM imidazole. Cells were kept on ice and disrupted in presence of 1 mM ATP, 750 Kunitz DNase I and 250 Kunitz RNase A (AppliChem, Darmstadt, Germany), 2–5 mM MgSO₄, and 1x EDTA-free cOmplete™ protease inhibitor cocktail (F. Hoffmann-La Roche AG, Basel, Switzerland) by addition of lysozyme and 10 passages through an Invensys APV-1000 homogenizer (APV Systems, Silkeborg, Denmark). Cell debris was removed by centrifugation at 16500 x g for 20 minutes at 4°C. Initial purification was achieved by immobilized metal chromatography (IMAC) using columns packed with Ni Sepharose 6 Fast Flow resin on an ÄKTApurifier FPLC system (GE Healthcare, Chicago, IL,

USA). After washing with buffer supplemented with 25 mM imidazole the protein was eluted with 300 mM imidazole. The elution from IMAC was supplemented with His-tagged TEV protease (molar ratio approx. 1:50), and His-tagged *E. coli* biotin ligase BirA (molar ratio approx. 1:10) for site-specific biotinylation of the Lys residue in the Avi-tag in a dialysis setting against buffer A supplemented with 0.5 mM biotin, 0.5 mM ATP, and 5 mM MgCl₂. After overnight incubation at 4°C, the concentration of biotin was reduced to approx. below 1 μM by repeated dialysis against buffer A. The mixture was then supplemented with 10 mM imidazole and passed gravity flow through a column packed with the same resin as used for positive IMAC in order to remove TEV, birA, and unprocessed PPAR_γ. The flow through containing the TEV processed PPAR_γ protein was then subjected to a column packed with 5 mL monomeric avidin Ultra-Link™ resin (Pierce Biotechnology Inc., Rockford, IL, USA). Unlabeled protein was removed by washing for 10 column volumes with buffer A before biotin labeled protein was eluted using buffer A supplemented with 2 mM biotin. The product was then concentrated and subjected to SEC using a 10/30 Superdex75™ column equilibrated and run in high glycerol HTRF buffer (25 mM HEPES pH 7.5, 150 mM KF, 10% w/v glycerol, 5 mM DTT). After the final purification step by SEC, proteins were aliquoted, flash frozen in liquid nitrogen, and stored at -80°C. Proteins were not concentrated thereafter in order to prevent aggregation and assay artefacts.

PPAR_γ co-regulator recruitment assays

Recruitment of co-regulator peptides to the PPAR_γ LBD was studied in a homogeneous time-resolved fluorescence resonance energy transfer (HT-FRET) assay system. Terbium cryptate as streptavidin conjugate (Tb-SA; Cisbio Bioassays, Codolet, France) was used as FRET donor for stable coupling to biotinylated recombinant PPAR_γ LBD protein. 29 co-regulator peptides (Willems et al., 2020) fused to fluorescein as FRET acceptor were purchased from ThermoFisher Scientific (Life Technologies GmbH, Darmstadt, Germany). Assay solutions were prepared in HTRF assay buffer supplemented with 0.1% w/v CHAPS and contained recombinant biotinylated PPAR_γ LBD (final concentration 3 nM), Tb-SA (3 nM) and the respective fluorescein-labeled co-regulator peptide (100 nM) as well as 1% DMSO with test compounds or DMSO alone as negative control. All HTRF experiments were carried out in 384 well format using white flat bottom polystyrol microtiter plates (Greiner Bio-One, Frickenhausen, Germany). Each sample was tested in three (dose-response) or four (primary screen) technical replicates. After 2 h incubation at RT, fluorescence intensities (FI) after excitation at 340 nm were recorded at 520 nm for fluorescein acceptor fluorescence and 620 nm for Tb-SA donor fluorescence on a SPARK plate reader (Tecan Deutschland GmbH). FI_{520nm} was divided by FI_{620nm} and multiplied with 10,000 to give a dimensionless HTRF signal. Dose-response experiments with varying concentrations of the test compounds garcinic acid and pioglitazone were conducted in the same manner and setting. The co-regulator peptides in this experiment were the following: steroid receptor co-activator (SRC) 1-1, Fluorescein-KYSQTSKHLVQLLTTTAEQQL-OH; SRC 1-2, Fluorescein-LTARHKILHRLQLQEGSPSD-OH; SRC 1-3, Fluorescein-ESKD HQLLRYLDDKDEKDL-OH; SRC 1-4, Fluorescein-GPQTPQAQKSLQQLLQTE-OH; SRC 2-1, Fluorescein-DSKGQTKLLQLLTTKSDQ M-OH; SRC 2-2, Fluorescein-LKEKHILHRLQLQDSSSPV-OH; SRC 2-3, Fluorescein-KKKENALLRYLLDKDDTKD-OH; SRC 3-1, Fluorescein-ESKGHKLLQLLTCSSDDR-OH; SRC 3-2, Fluorescein-LQEKHRLHKLQNGNSPA-OH; SRC 3-3, Fluorescein-KKENALLR YLLDRDDPSD-OH; nuclear receptor co-repressor (NCOR) ID1, Fluorescein-RTHRLITLADHICQIITQDFARN-OH; NCOR ID2, Fluorescein-DPASNLGLEDIIRKALMGSFDDK-OH; silencing mediator for retinoid and thyroid hormone receptor (SMRT) ID1, Fluorescein-GHQRVTLAQHISEVITQDYTRH-OH; SMRT ID2, Fluorescein - HASTNMGLEAIRKALMGKYDQW-OH; CREB-binding protein 1 (CBP-1), Fluorescein-AASKHKQLSELLRGGSGSS-OH; C33, Fluorescein-HVEMHPLLMGLLMESQWGA-OH; D11-FXXLF, Fluorescein-VESGSSRFMQLFMANDLLT-OH; D22, Fluorescein-LPYEGSLLKLLRAPVEEV-OH; EAB1, Fluorescein-SSNHQSSRLIELLSR-OH; EA2, Fluorescein-SSKGVLRWMLAEPVSR-OH; androgen receptor-associated protein 70 (ARA70), Fluorescein-SRETS EKFKLLFQSYNVND-OH; N-terminal sequence of androgen receptor (AR N-term), Fluorescein-SKTYRGAFQNLQFQSVREVI-OH; peroxisome proliferator-activated receptor gamma co-activator 1-alpha (PGC1a), Fluorescein-EAEEPSLLKLLAPANTQ-OH; nuclear receptor co-activator 6 (NCoA6, also termed PRIPRAP250), Fluorescein-VTLTSPLLVNLQSDISAG-OH; nuclear receptor interacting protein 1 (NRIP1, also termed RIP140, interaction motif L6), Fluorescein-SHQKVTLQLLGHKNEEN-OH; RIP140L8, Fluorescein-SFSKNGLLSRLLRQNQDSY-OH; TB3, Fluorescein-SSVASREWWVRELSR-OH; thyroid hormone receptor associated protein (TRAP) TRAP220/DRIP-1, Fluorescein-KVSNPILTSLLQITGNGG-OH; TRAP220/DRIP-2, Fluorescein-NTKNHPMLMNLKDNPAQD-OH.

PPAR_γ LBD expression, purification and crystallization

The PPAR_γ LBD (aa. 203-477) was expressed as described previously (Gellrich et al., 2020). The protein initially purified by Ni²⁺-affinity chromatography was treated with TEV to remove the histidine tag. The cleaved protein was passed through reverse Ni²⁺-affinity chromatography and further purified by size exclusion chromatography. The pure protein at 12 mg/mL in 20 mM Tris, pH 8, 200 mM NaCl and 0.5 mM TCEP was mixed with the ligands at 10- and 5-fold molar excess for GA and rosiglitazone, respectively. Crystallization was performed using sitting drop vapor diffusion method at 20°C and the solution containing 1.2-1.4 M ammonium sulfate, 0.1 M Tris, pH 7.5-8.0. Diffraction data were collected at Swiss Light Source, X06SA, and were processed and scaled with XDS (Kabsch, 2010) and AIMLESS (Evans and Murshudov, 2013), respectively. Initial structure solution was obtained by molecular replacement using Phaser (McCoy et al., 2007) and the published coordinates of PPAR_γ (PDB: 6TSG (Gellrich et al., 2020)). Iterative cycles of manual model rebuilding alternated with refinement were performed in Coot (Emsley et al., 2010) and REFMAC5 (Skubák et al., 2004), respectively. Data collection and refinement statistics are summarized in Table S1.

Differential gene expression analysis

Sample preparation. HepG2 cells (DSMZ) were cultured in DMEM, high glucose supplemented with 10% fetal calf serum (FCS), sodium pyruvate (1 mM), penicillin (100 U/mL), and streptomycin (100 μg/mL) at 37°C and 5% CO₂ and seeded in 6-well plates (1.0 × 10⁶

cells/well) for gene expression analysis. 24 h after seeding, medium was changed to minimal essential medium (MEM) supplemented with 1% charcoal-stripped FCS, penicillin (100 U/mL) and streptomycin (100 µg/mL). After further 24 h, medium was changed again to MEM supplemented as described above now additionally containing 0.1% DMSO and the test compounds (10 µM GA, 10 µM GA + 10 µM GW9662, 1 µM pioglitazone, or 10 µM GA + 1 µM pioglitazone) or 0.1% DMSO alone as control. Each treatment condition was set up in four independent biological repeats ($n = 4$). After 8 h incubation, cells were harvested, washed twice with cold phosphate buffered saline (PBS) and then directly used for RNA extraction by the E.Z.N.A.® Total RNA Kit I (R6834-02, Omega Bio-Tek Inc., Norcross, GA, USA). *mRNA sequencing*. A total amount of 1 µg RNA per sample was used as input material for the RNA sample preparations. Sequencing libraries were generated using NEBNext® Ultra™ RNA Library Prep Kit for Illumina® (New England Biolabs (NEB), Ipswich, MA, U.S.A.) following manufacturer's recommendations and index codes were added to attribute sequences to each sample. Briefly, mRNA was purified from total RNA using poly-T oligo-attached magnetic beads. Fragmentation was carried out using divalent cations under elevated temperature in NEBNext First Strand Synthesis Reaction Buffer (5X). First strand cDNA was synthesized using random hexamer primer and M-MuLV Reverse Transcriptase (RNase H-). Second strand cDNA synthesis was subsequently performed using DNA Polymerase I and RNase H. Remaining overhangs were converted into blunt ends via exonuclease/polymerase activities. After adenylation of 3' ends of DNA fragments, NEBNext Adaptor with hairpin loop structure were ligated to prepare for hybridization. In order to select cDNA fragments of preferentially 150~200 bp in length, the library fragments were purified with AMPure XP system (Beckman Coulter, Beverly, USA). Then 3 µL USER Enzyme (NEB, USA) was used with size-selected, adaptorligated cDNA at 37°C for 15 min followed by 5 min at 95°C before PCR. Then PCR was performed with Phusion High-Fidelity DNA polymerase, Universal PCR primers and Index (X) Primer. At last, PCR products were purified (AMPure XP system) and library quality was assessed on the Agilent Bioanalyzer 2100 system. The clustering of the index-coded samples was performed on a cBot Cluster Generation System using PE Cluster Kit cBot-HS (Illumina) according to the manufacturer's instructions. After cluster generation, the library preparations were sequenced on an Illumina NovaSeq 6000 platform and paired-end reads were generated. *Data analysis*. Raw data (raw reads) of FASTQ format were firstly processed through fastp (Chen et al., 2018). In this step, clean data (clean reads) were obtained by removing reads containing adapter and poly-N sequences and reads with low quality from raw data. At the same time, Q20, Q30 and GC content of the clean data were calculated. All the downstream analyses were based on the clean data with high quality. Downstream analysis was performed using a combination of programs including STAR (Dobin et al., 2013), HTseq (Anders et al., 2015), Cufflink (Trapnell et al., 2012) and wrapped scripts. Alignments were parsed using TopHat program (Trapnell et al., 2012) and differential expressions were determined through DESeq2 (Love et al., 2014). KEGG enrichment analysis was implemented by the ClusterProfiler. Reference genome and gene model annotation files were downloaded from genome website browser (NCBI/UCSC/Ensembl) directly. Indexes of the reference genome were built using STAR and paired-end clean reads were aligned to the reference genome using STAR (v2.5). STAR used the method of Maximal Mappable Prefix (MMP) which can generate a precise mapping result for junction reads. HTSeq v0.6.1 was used to count the read numbers mapped of each gene. Reads per kilobase of exon model per million mapped reads (RPKM, considering the effect of sequencing depth and gene length for the reads count at the same time) of each gene was calculated based on the length of the gene and reads count mapped to this gene. Differential expression analysis between two conditions/groups (four biological replicates per condition) was performed using the DESeq2 R package (2_1.6.3). DESeq2 provides statistical routines for determining differential expression in digital gene expression data using a model based on the negative binomial distribution. The resulting p values were adjusted using the Benjamini and Hochberg's approach for controlling the False Discovery Rate (FDR). Genes with an adjusted p value < 0.05 found by DESeq2 were assigned as differentially expressed. Venn diagrams were prepared using the function vennDiagram in R based on the gene list for different group. We used clusterProfiler R package (Yu et al., 2012) to test the statistical enrichment of differential expression genes in KEGG pathways using the KEGG database resource (<http://www.genome.jp/kegg/>) (Kanehisa et al., 2017; Ogata et al., 1999). Correlations between individual samples were determined using the cor.test function in R with options set alternative = "greater" and method = "Spearman". To identify the correlation between difference, different samples were clustered by expression level RPKM using hierarchical clustering distance method with the function heatmap, SOM (Self-organization mapping) and kmeans using silhouette coefficient to adapt the optimal classification with default parameter in R.

Computational methods

General. Calculations were performed in Molecular Operating Environment (MOE, version 2018.0101, Chemical Computing Group Inc. Montreal, QC, Canada) using default settings for each tool/function unless stated otherwise. Amber10:EHT was used as the default force field for all calculations. *Molecular docking of rosiglitazone and troglitazone*. Docking was performed using the X-ray structure of PPAR γ LBD complexed with GA (PDB: 7AWD). Protonation states of the complex were adjusted using the MOE QuickPrep tool. The compound was prepared using the MOE Wash tool: protonation state enumerate at pH 7.4; coordinates rebuild 3D. Docking was performed using the following settings in the MOE Dock tool: receptor: receptor + solvent + allosteric bound GA; site: ligand atoms (of orthosteric bound GA); placement: pharmacophore; score: London dG; poses: 100; refinement: induced fit; refinement score: GBVI/WSA dG; poses: 10. As pharmacophore query the carbonyl oxygen of orthosteric bound GA was set as acceptor feature with 1.5 radius. The highest ranked binding mode was used. Alignment and superimposition of PPAR γ :GA (PDB: 7AWD) with PPAR γ :rosiglitazone (PDB: 7AWC) or PPAR γ :troglitazone (PDB: 6DGO (Shang et al., 2019), chain A) was performed after protonation states of the complexes were adjusted using the MOE QuickPrep tool.

QUANTIFICATION AND STATISTICAL ANALYSIS

Reporter gene assays

Gal4-NR and PPRE reporter gene assays were performed in at least three biologically independent experiments in technical duplicates. Statistical significance of Gal4-NR or PPRE activation by test compounds versus DMSO was evaluated by two-sided student's t test. Effects with $p < 0.05$ were considered as statistically significant and only compound/target pairs with statistically significant effect were considered as active. GraphPad Prism 7 was used to fit dose-response curves by non-linear regression ([Agonist] vs. response – Variable slope (four parameters)) and to calculate EC_{50} values.

Co-regulator recruitment assays

The co-regulator interaction screen was performed in four technical repeats, the dose-response curves were recorded with three technical replicates. GraphPad Prism 7 was used to fit dose-response curves by non-linear regression ([Agonist] or [Inhibitor] vs. response – Variable slope (four parameters)) and to calculate EC_{50} or IC_{50} values.

Differential gene expression experiment

For the differential gene expression experiment, HepG2 cells were treated with the test compounds or DMSO (0.1%) in four biologically independent repeats. Differential expression analysis between groups was performed using the DESeq2 R package (2_1.6.3) using a model based on the negative binomial distribution. The resulting p values were adjusted using the Benjamini and Hochberg's approach for controlling the False Discovery Rate (FDR). Genes with an adjusted p value < 0.05 found by DESeq2 were assigned as differentially expressed. Venn diagrams were prepared using the function `vennDiagram` in R based on the gene list for different group. The `clusterProfiler` R package was used to test the statistical enrichment of differential expression genes in KEGG pathways using the KEGG database resource (<http://www.genome.jp/kegg/>) (Kanehisa et al., 2017; Ogata et al., 1999). Correlations between individual samples were determined using the `cor.test` function in R with options set `alternative = "greater"` and `method = "Spearman"`. To identify the correlation between difference, different samples were clustered by expression level RPKM using hierarchical clustering distance method with the functions `heatmap`, `SOM` (Self-organization mapping) and `kmeans` using silhouette coefficient to adapt the optimal classification with default parameter in R.

Cell Chemical Biology, Volume 28

Supplemental information

**Endogenous vitamin E metabolites mediate
allosteric PPAR γ activation with unprecedented
co-regulatory interactions**

Sabine Willems, Leonie Gellrich, Apirat Chaikuad, Stefan Kluge, Oliver Werz, Jan Heering, Stefan Knapp, Stefan Lorkowski, Manfred Schubert-Zsilavecz, and Daniel Merk

Supplemental Items

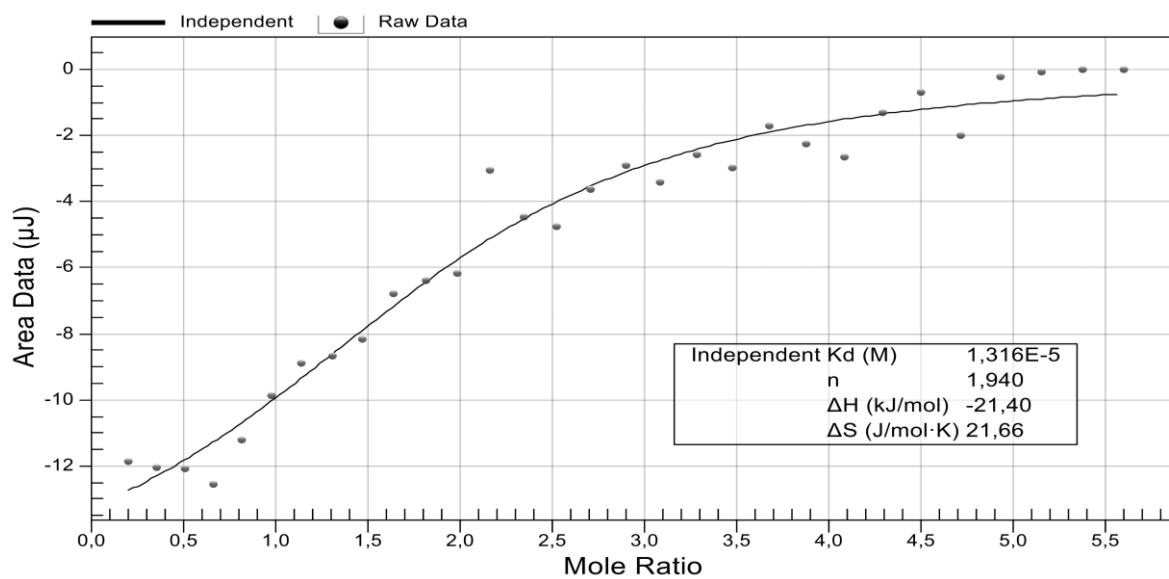


Figure S1. Binding of garcinoic acid (GA) to PPAR γ . Isothermal titration calorimetry of GA to the recombinant PPAR γ LBD. GA binds to PPAR γ with an affinity of approx. 10 μM and a ligand:protein stoichiometry (n) of approx. 2:1. See STAR Methods.

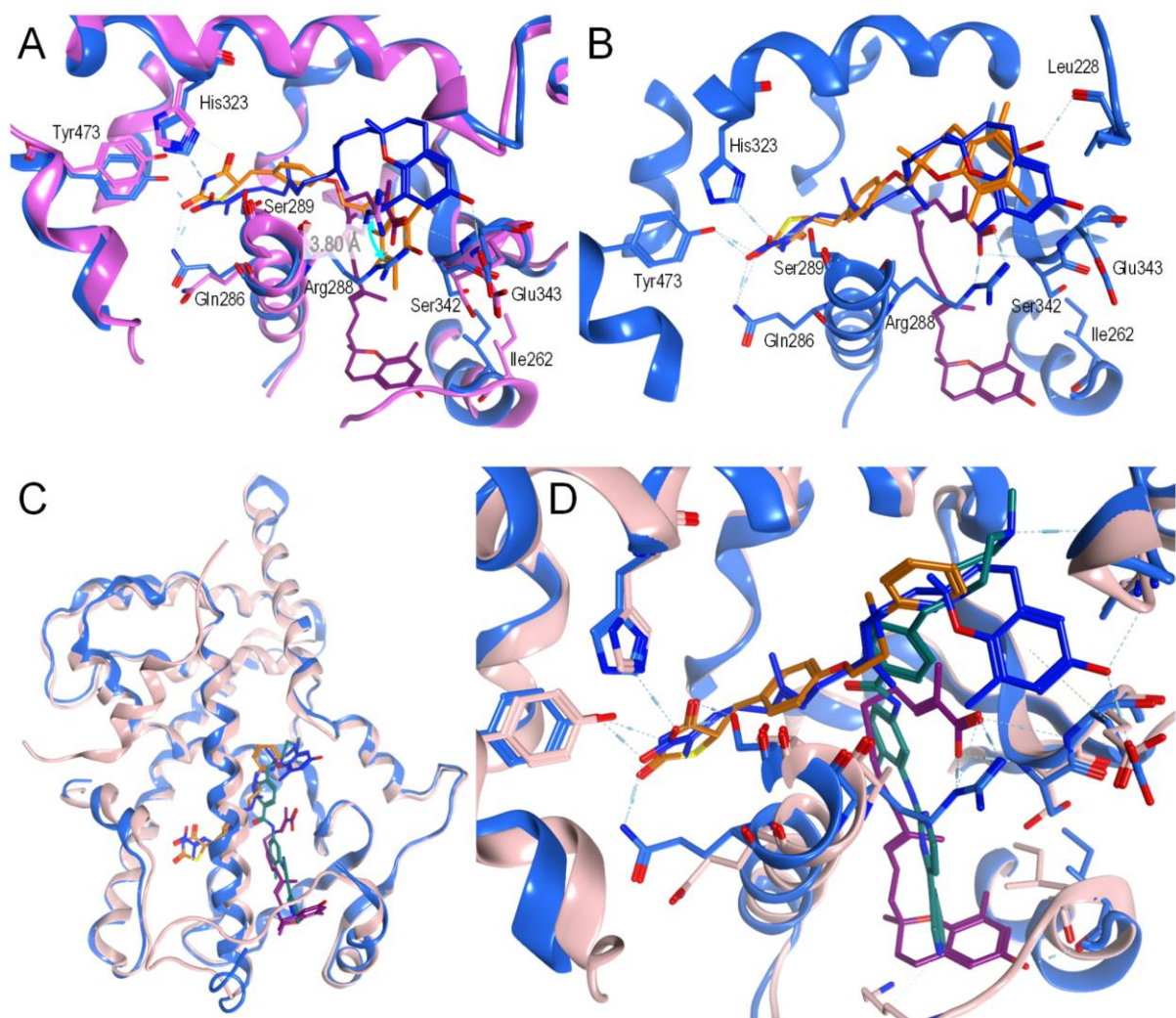


Figure S2. Comparison of GA binding to PPAR γ with other ligands. (A,B) Comparison of the PPAR γ :troglitazone and PPAR γ :GA:GA complexes. (A) Superimposition of PPAR γ :troglitazone (protein pink, ligand orange, PDB: 6DGO (Shang et al., 2019)) and PPAR γ :GA:GA (protein blue, ligands blue and violet, PDB: 7AWD) shows similar conformations of the PPAR γ LBD but a 3.8 Å shift of Arg288 to allow pocket formation for GA binding. The chromanol motifs of troglitazone (orange) and orthosteric GA (blue) are bound to different binding site regions. (B) The chromanol motifs of troglitazone (orange) and orthosteric GA (blue) are also not aligned when troglitazone is docked to the orthosteric pocket of the PPAR γ :GA:GA complex (blue, PDB: 7AWD) and form different interactions. (C,D) Superimposition of PPAR γ :imatinib:SRC1 (protein beige, ligand teal, PDB: 6KTN (Jang et al., 2019)) with the PPAR γ :GA:GA complex (blue, PDB: 7AWD) and docked rosiglitazone (orange) illustrates orthosteric and allosteric sites. (C) The overall conformation of PPAR γ bound to GA or imatinib only differs in the Ω -loop and slightly in the position of H12. (D) Binding site view. See also Figure 2.

Table S1. Data collection and refinement statistics for PPAR γ -GA and PPAR γ -rosiglitazone structures (see also Figure 2).

Complex	PPAR γ -garcinoic acid	PPAR γ -rosiglitazone
PDB codes	7AWD	7AWC
<i>Data Collection</i>		
Resolution ^a (Å)	46.22-1.93 (2.00-1.93)	46.33-1.74 (1.80-1.74)
Spacegroup	<i>P</i> 4 ₃ 2 ₁ 2	<i>P</i> 4 ₃ 2 ₁ 2
Cell dimensions	a=b=65.4, c=156.5 Å $\alpha=\beta=\gamma=90.0^\circ$	a=b=65.5, c=157.0 Å $\alpha=\beta=\gamma=90.0^\circ$
No. unique reflections	26,357 (2,529)	36,073 (3,461)
Completeness (%)	99.8 (100.0)	100.0 (100.0)
I/ σ	17.2 (2.2)	24.7 (2.2)
R _{merge} (%)	0.051 (0.910)	0.034 (0.930)
CC (1/2)	0.999 (0.819)	1.000 (0.829)
Redundancy	8.1 (8.4)	9.2 (9.5)
<i>Refinement</i>		
No. atoms in refinement (P/L/O) ^b	2,178/ 62/ 151	2,203/ 25/ 225
B factor (P/L/O) ^b (Å ²)	50/ 81/ 53	43/ 35/ 49
R _{fact} (%)	18.9	17.4
R _{free} (%)	23.0	20.4
rms deviation bond (Å)	0.014	0.016
rms deviation angle (°)	1.4	1.5
<i>Molprobit Ramachandran</i>		
Favour (%)	97.01	99.25
Disallowed (%)	0	0

^a Value in brackets indicates high resolution shell statistics.

^b P/L/O indicates protein, ligand, and others.

16.4 The orphan nuclear receptor Nurr1 is responsive to non-steroidal anti-inflammatory drugs

Willems, S.; Kilu, W.; Ni, X.; Chaikuad, A.; Knapp, S.; Heering, J.; Merk, D. The Orphan Nuclear Receptor Nurr1 Is Responsive to Non-Steroidal Anti-Inflammatory Drugs. *Commun. Chem.* **2020**, *3*, 85.

Dieser Artikel ist lizenziert durch eine Creative Commons Attribution 4.0 International License. Eine Kopie dieser Lizenz ist unter <http://creativecommons.org/licenses/by/4.0/> verfügbar. Es wurden keine Änderungen vorgenommen.

The orphan nuclear receptor Nurr1 is responsive to non-steroidal anti-inflammatory drugs

Sabine Willems¹, Whitney Kilu¹, Xiaomin Ni^{1,2}, Apirat Chaikuad^{1,2}, Stefan Knapp^{1,2}, Jan Heering³ & Daniel Merk¹✉

Nuclear receptor related 1 (Nurr1) is an orphan ligand-activated transcription factor and considered as neuroprotective transcriptional regulator with great potential as therapeutic target for neurodegenerative diseases. However, the collection of available Nurr1 modulators and mechanistic understanding of Nurr1 are limited. Here, we report the discovery of several structurally diverse non-steroidal anti-inflammatory drugs as inverse Nurr1 agonists demonstrating that Nurr1 activity can be regulated bidirectionally. As chemical tools, these ligands enable unraveling the co-regulatory network of Nurr1 and the mode of action distinguishing agonists from inverse agonists. In addition to its ability to dimerize, we observe an ability of Nurr1 to recruit several canonical nuclear receptor co-regulators in a ligand-dependent fashion. Distinct dimerization states and co-regulator interaction patterns arise as discriminating factors of Nurr1 agonists and inverse agonists. Our results contribute a valuable collection of Nurr1 modulators and relevant mechanistic insights for future Nurr1 target validation and drug discovery.

¹Institute of Pharmaceutical Chemistry, Goethe University Frankfurt, Max-von-Laue-Str. 9, 60438 Frankfurt, Germany. ²Structural Genomics Consortium, BMLS, Goethe-University Frankfurt, Max-von-Laue-Str. 15, 60438 Frankfurt, Germany. ³Fraunhofer Institute for Molecular Biology and Applied Ecology IME, Branch for Translational Medicine and Pharmacology TMP, Theodor-Stern-Kai 7, 60596 Frankfurt, Germany. ✉email: merk@pharmchem.uni-frankfurt.de

Nuclear receptor related 1 (Nurr1, NR4A2), a member of the nerve growth factor-induced β subfamily of orphan nuclear receptors^{1,2}, is a neuroprotective transcription factor mainly found in dopaminergic neurons. Levels of Nurr1 are diminished in Parkinson's disease (PD) patients and midbrain dopaminergic neuron development is Nurr1 dependent. Moreover, Nurr1 knock-out in mice in mature dopamine neurons resembled the progressive pathology seen in early stage of PD³ suggesting therefore Nurr1 as promising target in PD treatment.

Nurr1 was originally considered as a ligand-independent nuclear receptor (NR) due to its closed ligand-free conformation and its high constitutive activity¹. However, recent reports indicate that Nurr1 activity can be modulated with small-molecule ligands. Despite the lack of a canonical binding site in the apo structure of the Nurr1 ligand-binding domain (LBD), dynamic NMR, hydrogen deuterium exchange, and mutagenesis studies have defined two potentially overlapping ligand-binding regions within the Nurr1 LBD for unsaturated fatty acids (UFAs) and amodiaquine type ligands^{4–6}. These putative, highly solvent accessible binding sites⁵ are located on the LBD surface around helix 3, which is distant from helix 12 that often has a canonical activation function in other nuclear receptors. In addition, X-ray structures of the Nurr1 LBD in complexes with prostaglandin A1 (PGA1, PDB-ID: 5Y41⁷), prostaglandin A2 (PGA2, PDB-ID: 5YD6⁸), and 5,6-dihydroindole (DHI, PDB-ID: 6DDA⁹) have been reported recently, in which the ligands are covalently bound in an induced pocket between helices 5 and 12 that is not present in the apo structure.

Some recent studies have reported a number of Nurr1 ligands, demonstrating the potential of modulation of the receptor activity by small molecules. UFAs such as docosahexaenoic acid (DHA), arachidonic acid, linoleic acid, and oleic acid were identified as the first natural Nurr1 ligands^{4,5,10}. Neutral antagonistic effects of DHA and other UFA metabolites without intrinsic activity have been suggested^{4,5,10}, however, their cellular effects on Nurr1 activity and potential biological relevance remain elusive. Conversely, the prostaglandins E1 and A1 have recently been reported as naturally occurring Nurr1 activators and found to exhibit Nurr1-dependent neuroprotective effects⁷. A series of isoxazopyridinones has been described as synthetic Nurr1 activators, albeit with weak activation efficacies not exceeding 2-fold activation¹¹. Recently, the antimalarials amodiaquine (AQ) and chloroquine (CQ) with chloroquinoline scaffold were also discovered as Nurr1 modulators with a slightly higher efficacy (~3-fold activation) but markedly lower potency⁶. While the putative neutral Nurr1 antagonism of UFAs requires further characterization, the prostaglandins E1 and A1 as well as all synthetic Nurr1 ligands activate the nuclear receptor and further promote its already high basal transcriptional inducer activity. The limited efficacies of these Nurr1 activators coupled with the lack of inverse Nurr1 agonists that suppress the receptor's intrinsic activity prompt further efforts in the search for potent Nurr1 ligands that can be used as a tool for biological studies of the receptor's roles in health and disease.

Here we report the discovery of several structurally diverse cyclooxygenase (COX) inhibitors as Nurr1 modulators with distinct activity profiles. The tricyclic compounds oxaprozol, valdecoxib, and parecoxib, as well as meloxicam markedly diminish constitutive Nurr1 activity and thereby act as inverse Nurr1 agonists. Meclofenamic acid (MFA) is characterized as selective Nurr1 modulator with agonist and inverse agonist properties. Together with the previously reported Nurr1 agonists AQ and CQ, these Nurr1 ligands serve as chemical tools to study the receptor's mode of action. Both classes of binders with converse effects demonstrate that Nurr1 activity can be modulated by small-molecule ligands in a bidirectional fashion. The use of

Nurr1 agonists and inverse agonists in cofactor recruitment assays reveals potential interactions between Nurr1 and several nuclear receptor co-regulators, including NCoR-1, NCoR-2, NRIP1, and NCoA6, in a ligand-concentration-dependent manner. Moreover, the Nurr1 modulators interestingly affect heterodimerization between Nurr1 and RXR α as well as Nurr1 homodimerization with distinctive profiles. Cross-titration additionally demonstrates that Nurr1 can be modulated simultaneously by the different types of binders suggesting distinct binding sites. These results contribute to our understanding of Nurr1 biology, and may open new avenues for pharmacological Nurr1 modulation.

Results

Nurr1 reveals binding site close to the activation function. The recently published co-crystal structures of the Nurr1 LBD bound to prostaglandin A1 (PGA1; PDB-ID: 5Y41⁷) and the dopamine metabolite DHI (PDB-ID: 6DDA⁹) reveal a ligand-binding site differing from typical nuclear receptor LBDs (Fig. 1). While most nuclear receptors accommodate ligands inside the three-layer sandwich LBD structure between helices 2, 3, 5, 6, 7, 11, and 12, this pocket is located between helices 5 and 12 in Nurr1 and it is closer to the LBD surface. In comparison to the Nurr1 apo structure (PDB-ID: 1OVL¹), the binding of PGA1 and DHI requires an outward movement of helix 12 by ~10–21° from its closed position, essential for activation, to create the ligand-binding pocket. Such movement upon ligand binding affects and may weaken the salt bridge between Lys590 (H12) and Glu440 (H5) observed in the ligand-free state, suggesting that this region in proximity to helix 5 and 12 might provide a handle to modulate transcriptional inducer activity of Nurr1. In parallel, a different binding site has been postulated for the Nurr1 activator AQ, and is located at the Nurr1 LBD surface between helices 3 and 6⁶. Mutagenesis experiments support this assumption indicating that Nurr1 has two, potentially independent, ligand-binding pockets that enable modulation by small-molecule ligands.

Cyclooxygenase inhibitors modulate NR4A receptors in vitro.

Inspired by the processed COX metabolite PGA1 as Nurr1 ligand⁷, we hypothesized that COX inhibitors might bind to Nurr1, prompting us to screen a comprehensive collection of drug-approved COX-1 and COX-2 inhibitors for Nurr1 modulation. To capture also selectivity or promiscuity among the closely related NR4A receptors nerve growth factor-induced β (Nur77, NR4A1) and neuron-derived orphan receptor 1 (NOR1, NR4A3), we included all three NR4A receptors in this primary screen. For this, we employed cellular hybrid reporter gene assays based on chimeric receptors composed of the human NR4A receptor LBD and the DNA binding domain of Gal4 from yeast. A Gal4-sensitive firefly luciferase reporter construct served as reporter gene and constitutively expressed renilla luciferase (SV40 promoter) was employed to normalize for transfection efficiency and to monitor test compound toxicity. In agreement with their natural behavior¹, the chimeric Gal4-NR4A receptors revealed strong ligand-independent, intrinsic transcriptional inducer activity in this setting. AQ and CQ in conformity with literature⁶ activated Gal4-Nurr1 with EC₅₀ values in an intermediate micromolar range and up to 3.6-fold activation efficacy. To exclude non-specific effects in this cellular test system, control experiments were performed for all compounds affecting NR4A receptor activity, in which the potent ligand-independent transcriptional inducer Gal4-VP16¹² replaced Gal4-NR in the assay setup. Only compounds affecting NR4A-dependent but not

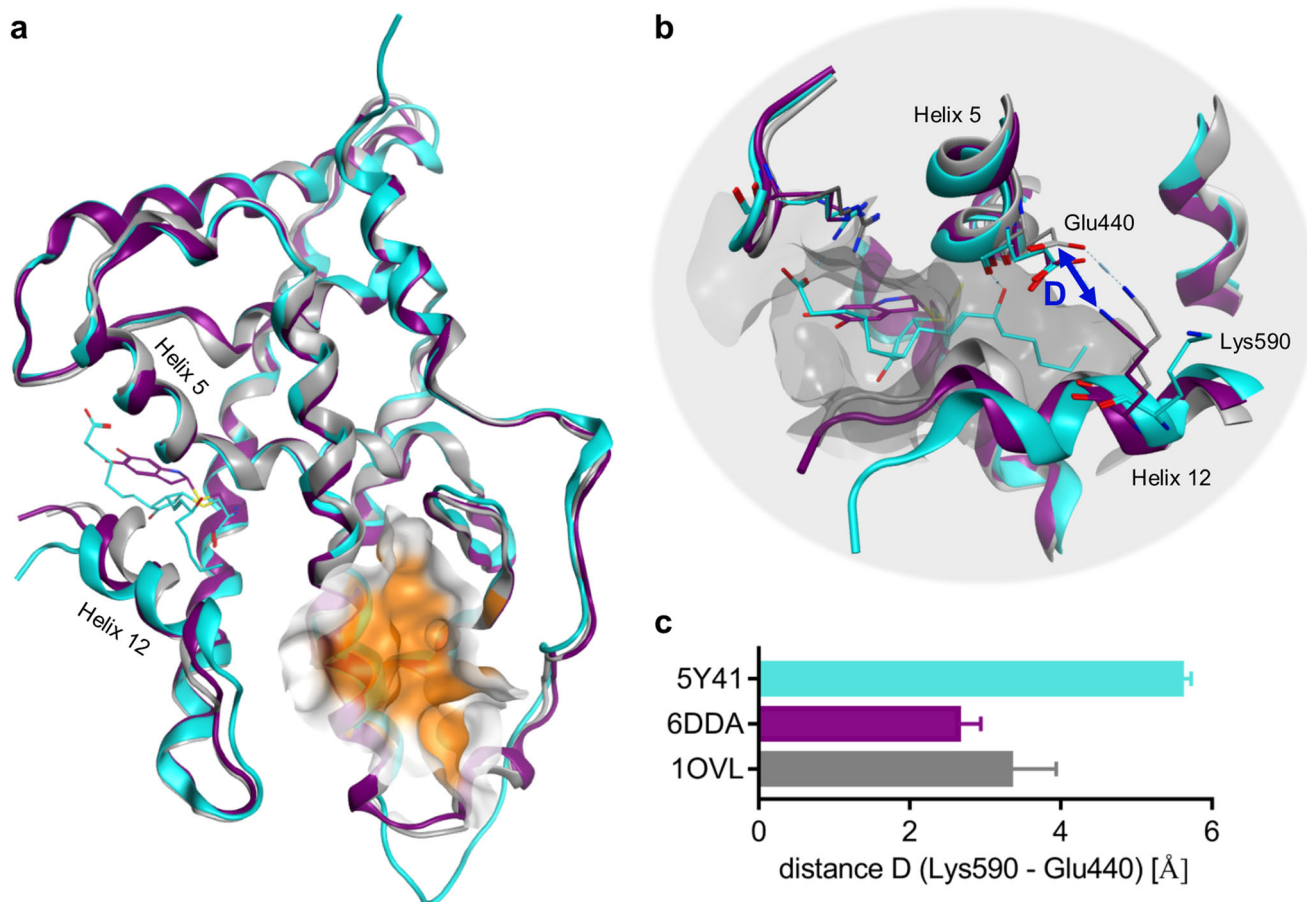


Fig. 1 Structural differences in apo and ligand-bound Nurr1 LBD. **a** Superposition of the Nurr1 LBD in apo state (PDB: 1OVL¹, gray), Nurr1 LBD bound to prostaglandin A1 (PGA1; PDB: 5Y41⁷, cyan) and to dopamine metabolite 5,6-dihydroindole (DHI; PDB: 6DDA⁹, purple). The proposed binding region for amodiaquine type ligands⁶ is highlighted in orange. **b** In apo state, helix 12 forms several contacts with helix 5, including a prominent salt-bridge interaction between Lys590 and Glu440 likely stabilizing a transcriptionally active conformation of the activation function. Ligand binding causes an outward swing of helix 12 for creating the binding pocket, which interferes helix 5 and 12 interaction as demonstrated for example by different Lys590–Glu440 distances in different structures (shown in **c**). **c** Distances (D) between Lys590 (NH_3^+) and Glu440 (CO_2^-) measured in the different Nurr1 LBD X-ray structures. Compared with the apo state (1OVL, gray), the DHI bound structure (6DDA, purple) revealed a diminished distance, while the distance was increased in the PGA1 bound structure (5Y41, cyan). Bars represent the mean \pm SD distances measured in the subunits of the respective structures.

VP16-dependent reporter activity were further considered as NR4A modulators.

Thirty-nine non-steroidal anti-inflammatory drugs (NSAIDs) covering all chemotypes of drug-approved COX inhibitors were initially screened in the Gal4-NR4A reporter gene assays at concentrations of 10 and 30 μM for NR4A modulatory activity (Fig. 2a). Meclofenamic acid, clonixin, and tiaprofenic acid enhanced Nurr1-dependent reporter activity (>1.5 -fold activation) indicating Nurr1 agonism. Control experiments on Gal4-VP16 revealed non-specific activity of clonixin and tiaprofenic acid whereas the activity of meclofenamic acid was clearly Nurr1 mediated (Fig. 3e). Full dose–response characterization of meclofenamic acid resulted in an EC_{50} value of $4.7 \pm 0.1 \mu\text{M}$ and 3.52 ± 0.05 -fold maximum activation on Gal4-Nurr1 (Fig. 3a, Table 1). For aceclofenac, the primary screen indicated Nurr1 repressor activity, however, full characterization conversely revealed this compound as a potent Nurr1 agonist ($\text{EC}_{50} = 2.5 \pm 0.1 \mu\text{M}$, 1.99 ± 0.07 -fold max. activation), suggesting that the repressive effect at high concentration is likely due to inhibition of firefly luciferase. Nurr1 repression (<0.80 -fold activation) was observed for oxaprozin, valdecoxib, and parecoxib at 10 or 30 μM . Control experiments on Gal4-VP16 indicated no non-specific reporter suppression (Fig. 3e, Supplementary Fig. 1b) and

dose–response characterization confirmed inverse agonism for all three compounds (Fig. 3a, Supplementary Fig. 1c). Oxaprozin was the strongest Nurr1 repressor and diminished Nurr1 activity to 0.26 ± 0.08 -fold minimum activation with an IC_{50} value of $40 \pm 6 \mu\text{M}$. Meloxicam demonstrated also strong repressor efficacy with a higher IC_{50} value while valdecoxib and parecoxib were less effective but had slightly lower IC_{50} values on Nurr1.

Neither the Nurr1 modulators discovered in our screening nor the previously known ligands AQ and CQ were selective for Nurr1 over the related NR4A receptors. AQ (100 μM) revealed even stronger activation efficacy on Nur77 and NOR1 while CQ (100 μM) and MFA (10 μM) as well as inverse agonists parecoxib (30 μM) and oxaprozin (50 μM) caused similar modulation of all three NR4A receptors (Fig. 2c, Supplementary Table 1). Generally, the activity of NSAIDs was similar on all three NR4As with few exceptions (Fig. 2a, Supplementary Table 1). Lornoxicam and mofezolac demonstrated inverse agonism on Nur77 and NOR1 (Supplementary Fig. 2) without affecting Nurr1 activity. Considering also the structural similarity of mofezolac and oxaprozin, this suggests that selectivity amongst NR4As is achievable despite their close similarity.

To profile also the selectivity of Nurr1 modulators MFA, parecoxib and oxaprozin (Fig. 2d; aceclofenac, meloxicam, and

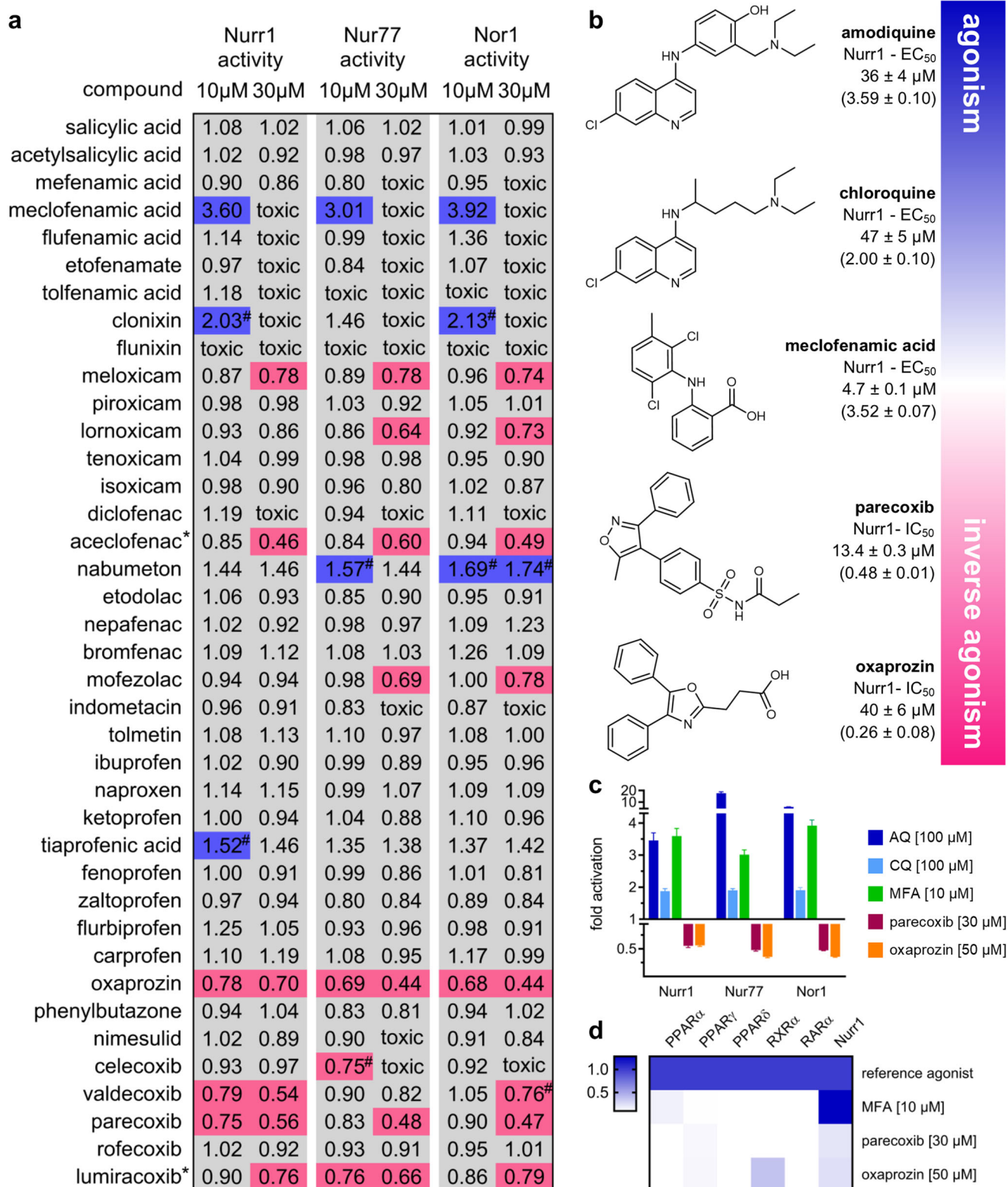


Fig. 2 Bidirectional modulation of Nurr1 activity by drug-approved COX inhibitors. **a** Screening of structurally diverse COX inhibitors for NR4A modulation in uniform Gal4-hybrid reporter gene assays. Heatmap shows mean fold activation; $n \geq 2$; agonists > 1.5-fold activation (blue), inverse agonists < 0.8-fold activation (magenta); all compounds displaying NR4A modulation in the primary screen were validated on Gal4-VP16 ($n \geq 4$) and only compounds not affecting Gal4-VP16 activity were further considered. Activities marked with # were not significant compared with VP16 control. Compounds marked with * were found to inhibit firefly luciferase. **b** Molecular structures and activities of Nurr1 modulators. AQ and CQ were reported as Nurr1 ligands previously⁶. EC₅₀ and IC₅₀ values were determined in the Gal4-Nurr1 hybrid reporter gene assay and are the mean ± SD; $n \geq 3$. Dose-response curves and control experiments on Gal4-VP16 hybrid receptor are shown in Fig. 3. **c** Activity profiles of Nurr1 modulators on the NR4A family receptors; mean fold activation ± S.E.M.; $n \geq 3$. **d** Selectivity profiles of MFA, parecoxib and oxaprozin on lipid-activated transcription factors outside the NR4A family. Heatmap shows mean rel. activation which refers to reference agonists at 1 μ M for PPARs (α : GW7647; γ : rosiglitazone; δ : L165,041), RXR α (bexarotene), RAR α (tretinoin) and 100 μ M for Nurr1 (AQ); $n \geq 4$.

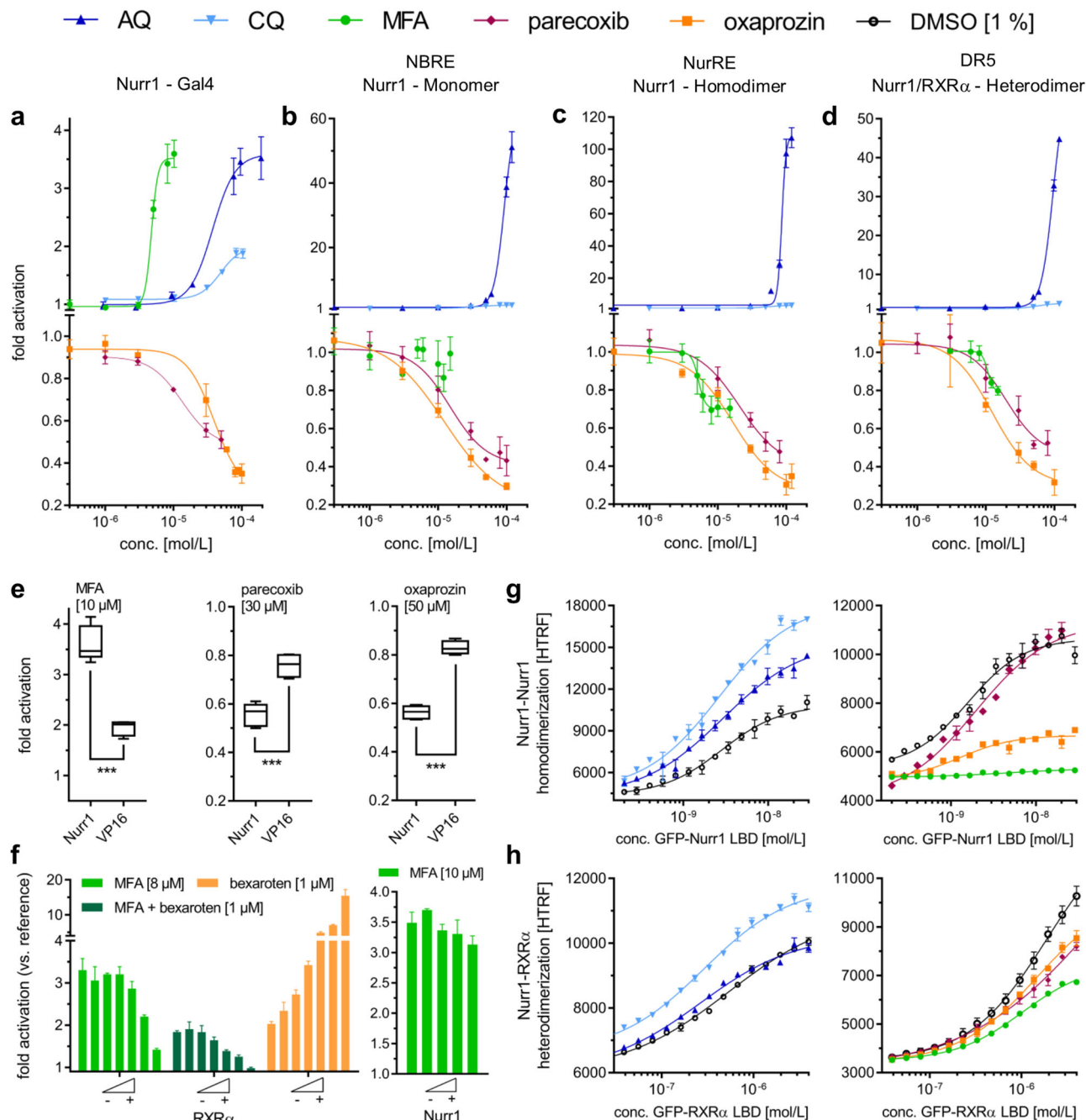


Fig. 3 Cellular and cell-free profiling of Nurr1 modulation by small-molecule ligands. **a** Gal4-hybrid reporter gene assay demonstrated Nurr1 activation by AQ, CQ, and MFA as well as inverse Nurr1 agonism for parecoxib and oxaprozin. **b–d** Nurr1 full-length reporter gene assays with the human Nurr1 response elements NBRE (Nurr1 monomer, **b**), NurRE (Nurr1 homodimer, **c**), and DR5 (Nurr1:RXR heterodimer, **d**) confirmed agonism of AQ and CQ (see also Supplementary Fig. 3) as well as inverse agonism of parecoxib and oxaprozin while MFA revealed a selective modulatory profile. All cellular experiments were performed in transiently transfected HEK293T cells. Results are the mean \pm S.E.M.; $n \geq 3$. **e** Control experiments employing a Gal4-VP16 hybrid receptor confirmed Nurr1 mediated activity of MFA, parecoxib, and oxaprozin. Boxplots show: center line, median; box limits, upper and lower quartiles; whiskers, min/max; $n \geq 4$. **f** With co-transfection of increasing amounts of Gal4-RXR α in the Gal4-Nurr1 reporter gene assay, activation efficacy of MFA (relative to DMSO) and MFA/bexarotene (relative to bexarotene) dropped pointing to monomer preference of MFA. Variations in the amount of Gal4-Nurr1 did not affect efficacy of MFA. Results are the mean \pm S.E.M.; $n \geq 3$. **g** Nurr1 formed homodimers with high affinity in absence of ligands (DMSO). Nurr1 activators AQ and CQ promoted homodimerization. The inverse agonists parecoxib and oxaprozin diminished Nurr1 dimer formation and MFA entirely prevented homodimerization. Data are the mean \pm S.E.M.; $N \geq 3$. **h** Nurr1 robustly heterodimerized with RXR α in apo state (DMSO). The Nurr1 activator CQ promoted dimerization between Nurr1 and RXR α whereas AQ was indifferent, and parecoxib, oxaprozin, and MFA had the opposite effect. Data are the mean \pm S.E.M.; $N \geq 3$.

Table 1 Summarized activities of Nurr1 modulators in cellular and cell-free experiments.

	AQ	CQ	MFA	Parecoxib	Oxaprozin
Gal4-Nurr1	EC ₅₀ 36 ± 4 (3.6 ± 0.1)	EC ₅₀ 47 ± 5 (2.0 ± 0.1)	EC ₅₀ 4.7 ± 0.1 (3.52 ± 0.05)	IC ₅₀ 13.4 ± 0.3 (0.48 ± 0.01)	IC ₅₀ 40 ± 6 (0.26 ± 0.08)
NBRE: Nurr1 monomer	EC ₅₀ 92 ± 1 (62 ± 2)	EC ₅₀ 38 ± 7 (2.2 ± 0.2)	Inactive	IC ₅₀ 15 ± 3 (0.41 ± 0.05)	IC ₅₀ 12 ± 2 (0.20 ± 0.05)
NurRE: Nurr1 homodimer	EC ₅₀ 87 ± 2 (109 ± 5)	EC ₅₀ 54 ± 7 (3.1 ± 0.2)	IC ₅₀ 5.2 ± 0.1 (0.70 ± 0.01)	IC ₅₀ 21 ± 6 (0.4 ± 0.1)	IC ₅₀ 17 ± 3 (0.27 ± 0.05)
DR5: Nurr1-RXRα heterodimer	EC ₅₀ 97 ± 3 (59 ± 4)	EC ₅₀ 57 ± 8 (2.6 ± 0.2)	IC ₅₀ 10.7 ± 0.1 (0.79 ± 0.01)	IC ₅₀ 20 ± 8 (0.5 ± 0.1)	IC ₅₀ 12 ± 2 (0.27 ± 0.05)
Homodimerization	Promotes dimerization	Promotes dimerization	Decreases dimerization	Inactive	Decreases dimerization
Heterodimerization	Inactive	Promotes dimerization	Decreases dimerization	Decreases dimerization	Decreases dimerization
NCoR-1 affinity	Enhances affinity	Enhances affinity	Decreases affinity	Decreases affinity	Inactive
NCoR ID1 recruitment	Inactive	EC ₅₀ > 100	IC ₅₀ 34 ± 3	IC ₅₀ 89 ± 8	IC ₅₀ > 100
SMRT ID2 recruitment	Inactive	EC ₅₀ > 100	EC ₅₀ 26 ± 4	IC ₅₀ 51 ± 5	IC ₅₀ 35 ± 5
PRIPRAP250 recruitment	Inactive	EC ₅₀ > 100	IC ₅₀ 17 ± 2	Inactive	IC ₅₀ 72 ± 18
RIP140L6 recruitment	Inactive	EC ₅₀ 61 ± 18	IC ₅₀ 33 ± 3	Inactive	IC ₅₀ 104 ± 19

All EC₅₀/IC₅₀ values are shown in μM. Values in parentheses are maximum/minimum activation. All values are the mean ± SD.

valdecoxib in Supplementary Fig. 1d) outside the NR4A family, we studied their activity on other lipid- and fatty acid mimetic¹³-activated nuclear receptors (peroxisome proliferator-activated receptors, PPAR; retinoid X receptor α, RXRα; retinoic acid receptor α, RARα) which confirmed selectivity except weak RXR agonism of oxaprozin which has been described previously¹⁴.

AQ, CQ, MFA, parecoxib, and oxaprozin displayed distinctive activity profiles of Nurr1 modulation ranging from agonism to inverse agonism, and therefore, emerged as a valuable set of tool compounds to assess Nurr1 modulation by chemical ligands.

Modulation of Nurr1 depends on the DNA response element.

While the Gal4-hybrid reporter gene assay system is very reliable and provides a uniform setting for screening, it is also artificial. Physiologically, nuclear receptors have the ability to dimerize as a key regulatory interaction. They can act as monomers, homodimers or heterodimers with retinoid X receptor (RXR) the latter of which has also been suggested for Nurr1¹⁵. Understanding of Nurr1 modulation by ligands, thus, must also take ligand effects in more physiological settings into consideration where reporter activity is controlled by the native human full-length Nurr1 protein as monomer, homodimer, or RXR heterodimer. To study the effects of AQ, CQ, MFA, parecoxib, and oxaprozin on the activity of full-length human Nurr1 in cellular settings, we employed reporter constructs bearing a single repeat of the human DNA response elements for the Nurr1 monomer (NGFI-B response element, NBRE), the Nurr1 homodimer (Nur-response element, NurRE), or the Nurr1:RXR heterodimer (direct repeats spaced by 5 nucleotides, DR5) to control reporter gene expression. Nurr1 (and for DR5 also RXRα) was overexpressed by co-transfection of a CMV-dependent expression plasmid. These cellular assay settings revealed further differences for the individual Nurr1 modulators (Fig. 3b–d, Table 1). AQ robustly induced reporter activity on all response elements confirming Nurr1 agonism. CQ activated all Nurr1 reporters as well (Supplementary Fig. 3), but with markedly lower efficacy compared with AQ. Parecoxib and oxaprozin exhibited strong inverse agonism on NBRE, NurRE, and DR5 response elements, validating their inverse agonist activity, as well. MFA, however, revealed a more complex activity profile on the human Nurr1 response elements. On the monomer response element (NBRE), MFA was inactive while it suppressed activity of either Nurr1 dimer on NurRE and DR5 suggesting a selective Nurr1 modulatory profile.

Nurr1 ligands modulate Nurr1 dimerization. The observation of opposed effects of MFA on Nurr1 monomers and dimers suggested crucial involvement of Nurr1 dimerization in mediating responses to ligands. Therefore, we studied association of the LBDs of Nurr1 and RXR in time-resolved fluorescence resonance energy transfer (TR-FRET) based settings using GFP-labeled RXRα or Nurr1 LBDs and Tb-labeled Nurr1 LBD, from which the results demonstrated robust homodimeric (Fig. 3g) and heterodimeric binding (Fig. 3h) between the proteins in absence of a ligand. Consistent with our observations from the cellular settings, addition of Nurr1 ligands affected homo- and heterodimerization of Nurr1 in a distinctive fashion. The Nurr1 agonist AQ promoted formation of homodimers whereas the less effective agonist CQ enhanced homo- and heterodimerization. The inverse agonists parecoxib and oxaprozin, in contrast, diminished dimerization. Since oxaprozin also exhibits RXR agonism, its effects on heterodimerization must be interpreted with care, however. The Nurr1 modulator MFA exhibited the strongest effect on Nurr1 homodimerization and fully prevented formation of a Nurr1:Nurr1 dimer whereas heterodimerization was decreased in presence of MFA but not entirely disrupted.

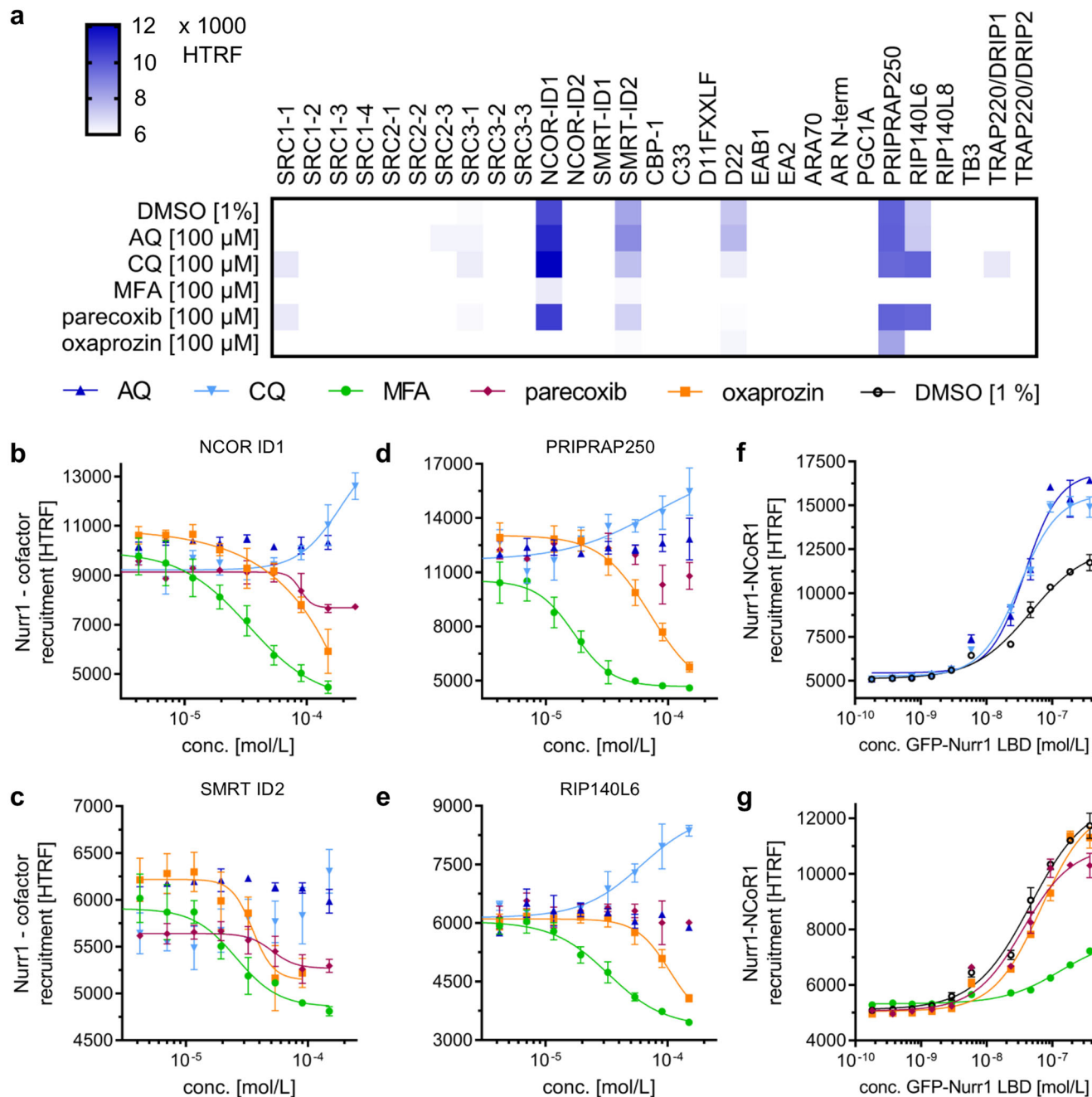


Fig. 4 Interaction pattern of the Nurr1 LBD with co-regulators. All interactions were studied in cell-free homogenous time-resolved fluorescence resonance energy transfer (HTRF)-based settings. Tb-labeled Nurr1 LBD as FRET donor and Fluorescein-labeled co-regulator peptides as FRET acceptors were used in (a–e). Tb-labeled NCoR-1 as FRET donor and GFP-labeled Nurr1 LBD as FRET acceptor were used in (f, g). **a** Twenty-nine peptides were screened for recruitment to Nurr1 in presence of 1% DMSO-control or ligands AQ, CQ, MFA, parecoxib, and oxaprozin at 100 μM. Heatmap of co-regulator recruitment screening shows the mean dimensionless HTRF signal, $N = 4$. **b–e** Dose-response curves of Nurr1 modulators in affecting recruitment of co-regulators NCoR-1 (**b**), SMRT (**c**), PRIPRAP250 (**d**), and RIP140 (**e**). Data are the mean \pm S.E.M.; $N = 3$. **f, g** Binding curves for the Nurr1-NCoR-1 interaction in presence of 1% DMSO and AQ-type ligands (**f**) or NSAID-type ligands (**g**). Concentration of all ligands in (**f**) and (**g**) was fixed at 100 μM. Data are the mean \pm S.E.M.; $N = 3$.

These observations further supported our hypothesis that the selective Nurr1 modulatory effects of MFA are mediated by changes in the dimerization state of the nuclear receptor. To observe this activity in another cellular setting, we studied how co-transfection of Gal4-RXR α affected MFA-mediated activation of Gal4-Nurr1 (Fig. 3f). In accordance with our previous results, increasing amounts of Gal4-RXR α resulted in a loss of activity of MFA while varying amounts of Gal4-Nurr1 had no effect.

Changes in the dimerization state of Nurr1, thus, emerge as key mechanism of Nurr1 modulation by small-molecule ligands. Therein, agonists (AQ, CQ) promote dimerization while inverse agonists (parecoxib, oxaprozin) diminish Nurr1 dimer formation.

Nurr1 recruits canonical nuclear receptor co-regulators. In addition to dimerization, nuclear receptor activity depends on interactions with various co-regulators. To capture also the

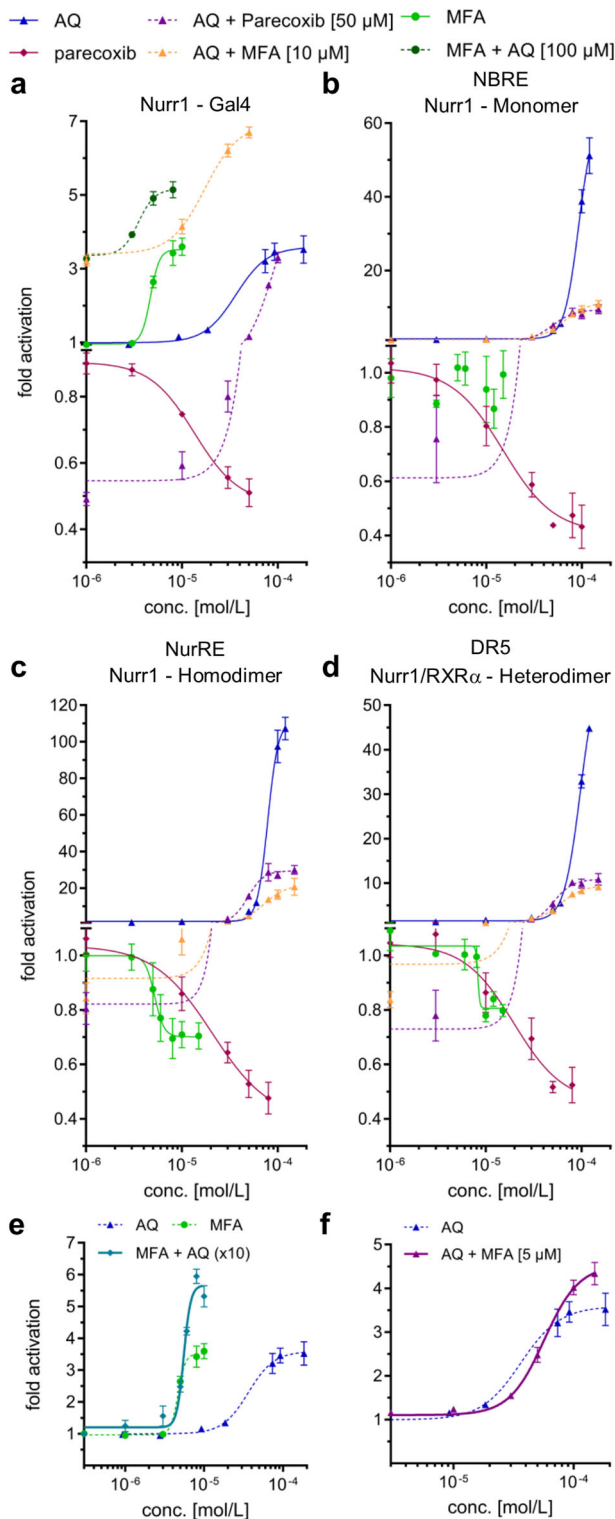


Fig. 5 Simultaneous modulation of Nurr1 by AQ and NSAIDs in cellular reporter gene assays. **a–d** Cross-titration curves of MFA or parecoxib and AQ on Gal4-Nurr1 (**a**) and on full-length human Nurr1 on the human Nurr1 response elements NBRE (**b**), NurRE (**c**), and DR5 (**d**). **e** Simultaneous titration of MFA and AQ (ratio 1:10) on Gal4-Nurr1. **f** Cross-titration experiment of AQ with lower fixed concentration of MFA (5 μ M) in the Gal4-Nurr1 assay. All data are the mean \pm S.E.M.; $n \geq 3$.

molecular mechanisms by which the Nurr1 co-regulator network responds to small-molecule ligands, we studied co-regulator binding to Nurr1 by TR-FRET in cell-free setting. We used a Tb-cryptate-labeled Nurr1 LBD and twenty nine Fluorescein-labeled co-regulator peptides (Fig. 4a). In absence of ligands, the Nurr1 LBD robustly recruited interaction motifs of nuclear receptor co-repressors 1 (NCoR-1) and 2 (NCoR-2, also termed silencing mediator for retinoid and thyroid hormone receptors, SMRT), nuclear receptor interacting protein 1 (NRIP1, also termed receptor interacting protein 140, RIP140), and nuclear receptor co-activator 6 (NCoA6, also termed TRBP, PRIP, RAP250). In agreement with earlier reports¹⁶, no strong direct association of the Nurr1 LBD with the canonical steroid receptor co-activators (SRC) was observed.

Nurr1 co-regulator interactions are responsive to ligands. We then determined the effects of Nurr1 modulators AQ, CQ, MFA, parecoxib, and oxaprozin (all at 100 μ M) on the recruitment of all twenty nine co-regulators to the Nurr1 LBD. While no pronounced effects were detected for AQ and CQ in this primary screen, MFA, parecoxib, and oxaprozin markedly altered the Nurr1 recruitment ability for NCoR-1, SMRT, PRIPRAP, and RIP140. In addition, the peptide D22 was recruited by Nurr1 in a ligand-dependent fashion but not further considered due to its artificial origin¹⁷. Full dose–response characterization further confirmed distinctive ligand effects on co-regulator recruitment. MFA, characterized as Nurr1 modulator in the cellular settings, displaced NCoR-1, SMRT, PRIPRAP, and RIP140 from the Nurr1 LBD in a dose-dependent fashion with similar potencies (IC₅₀ of 17–33 μ M) (Table 1, Fig. 4b–e). The co-regulator recruitment profile of the inverse Nurr1 agonist oxaprozin resembled that of MFA despite lower potency of oxaprozin. Parecoxib, in contrast, only displaced NCoR-1 and SMRT from Nurr1 efficiently and merely tended to decrease the Nurr1–PRIPRAP and Nurr1–RIP140 interactions. The Nurr1 agonist CQ revealed a tendency to promote recruitment of NCoR-1, SMRT, PRIPRAP, and RIP140 while no effect was observed for AQ. However, due to the photophysical characteristics of AQ and CQ¹⁸, and potential interference with the HTRF assay system through absorbance and quenching effects, these results for AQ and CQ must be interpreted with care. Thus, we employed a different setting and evaluated the affinity of Nurr1 for NCoR-1 binding in presence of the various ligands (Fig. 4f, g). Since ligand concentration was fixed in this setting, interference with the HTRF system is less prone to generate potential artifacts. Titration of GFP-labeled Nurr1 LBD against Tb-labeled NCoR-1 revealed markedly reduced affinity of Nurr1 for NCoR-1 recruitment in presence of MFA (100 μ M) while AQ (100 μ M) and CQ (100 μ M) promoted the Nurr1–NCoR-1 interaction.

Thus, in addition to differential control of the Nurr1 dimerization state, ligands modulate Nurr1 activity by regulating cofactor recruitment. Agonists (CQ and potentially AQ) enhance recruitment of co-regulators such as NCoR-1, SMRT, PRIPRAP, and RIP140 while inverse agonists (parecoxib, oxaprozin) promote displacement of these co-factors.

NSAIDs and amodiaquine simultaneously modulate Nurr1. The PGA1 bound Nurr1 LBD X-ray structure (PDB-ID: 5Y41⁷) together with the mutagenesis and NMR-based analysis⁶ of the putative binding site for AQ on Nurr1 suggest the existence of two independent ligand-binding pockets within the Nurr1 LBD (Fig. 1a) potentially allowing simultaneous modulation by small-molecule ligands. To test this hypothesis in vitro, we first treated

cells in the Gal4-Nurr1 reporter gene assay setting with either Nurr1 activator AQ or MFA at a fixed active concentration ($\geq EC_{90}$) and then monitored the activation upon cross-titrating the other respective agonist into the assay vice versa (Fig. 5a). Both compounds revealed additive effects and together (50 μ M AQ and 10 μ M MFA) achieved a strong Nurr1 activation, which clearly exceeded their individual activation efficacies (Fig. 5a, e, f). The EC_{50} values of both compounds were not markedly affected by the presence of the other respective Nurr1 activator, suggesting that they interact with the receptor independently. Next, we performed a similar experiment but titrated both Nurr1 ligands in a fixed ratio of MFA/AQ 1:10 corresponding to their \sim 10-fold difference in potency, and observed a sigmoidal dose–response that reached considerably higher maximum activation efficacy than the individual compounds contradicting competitive behavior (Fig. 5e). Enhanced activation efficacy of Gal4-Nurr1 was also observed in cross-titration of AQ with lower fixed concentration (5 μ M) of MFA (Fig. 5f). Furthermore, when we combined AQ with the inverse agonist parecoxib in cross-titration experiments (Fig. 5a), we found that the AQ dose–response curve was shifted to lower efficacy in presence of parecoxib. Together, these results strongly support our hypothesis of different binding sites for AQ and NSAIDs within the Nurr1 LBD.

We then expanded the cross-titration experiments to the more physiological settings of the full-length Nurr1 reporters (Fig. 5b–d) which agreed with our previous observations. On all three Nurr1 response elements, MFA (10 μ M) and parecoxib (50 μ M) prevented the full unfolding of AQ's agonistic potential even at high AQ concentrations suggesting simultaneous binding of either NSAID with AQ since with competitive antagonism, high AQ concentrations would displace the competitor and reach maximum efficacy.

Discussion

The orphan nuclear receptor Nurr1 has been characterized as a neuroprotective and anti-neuroinflammatory transcription factor¹⁹. Evidence from animal models and human points to relevance of Nurr1 in PD^{3,19,20}, Alzheimer's disease^{21,22}, and multiple sclerosis^{23–25} indicating a potential of the orphan nuclear receptor as therapeutic target in neurodegenerative diseases. However, the collection of Nurr1 modulators and knowledge on the receptor's molecular mode of action are limited advocating mechanistic studies on Nurr1 function and the search for new Nurr1 modulators as initial tool compounds for functional studies.

To assist validation of Nurr1 as future therapeutic target, there is a need for Nurr1 ligands as template for drug discovery and as chemical tools for biological studies to improve our knowledge on this orphan nuclear receptor. We have screened for alternative and additional Nurr1 modulators with higher potencies and distinct activity profiles, and employed them as *in vitro* tools for mode of action studies. Based on the recently published X-ray complex structure of the Nurr1 LBD bound to PGA1⁷, which arises from cyclooxygenase activity, we hypothesized that COX inhibitors might potentially bind to Nurr1. We discovered the six NSAIDs MFA, aceclofenac, oxaprozin, valdecoxib, parecoxib, and meloxicam acting as Nurr1 modulators in cellular setting. Together with the previously reported⁶ AQ-type Nurr1 ligands, the NSAID-type Nurr1 modulators discovered in our screening provide a valuable collection of initial tool compounds to evaluate Nurr1 activity covering activators and inverse agonists. These Nurr1 ligands demonstrate that the receptor's constitutive transcriptional inducer activity can be modulated by small molecules in a bidirectional fashion. Thereby, Nurr1 resembles other

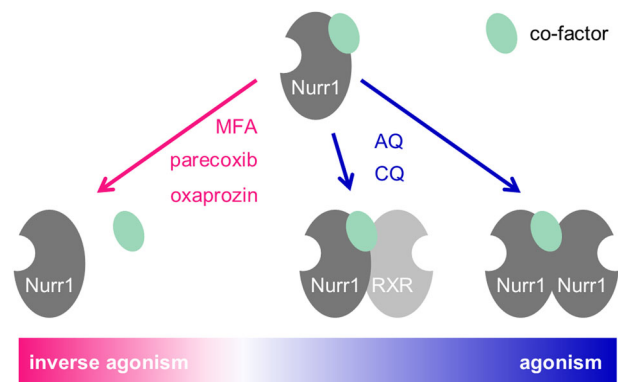


Fig. 6 Model of Nurr1 responses to modulation by small-molecule ligands. Agonists promote dimerization of Nurr1 as a homodimer or as a heterodimer with RXR and additionally stabilize interaction of the Nurr1 LBD with co-regulators. Inverse agonists favor monomeric Nurr1 and decrease Nurr1 co-regulator interactions.

nuclear receptors such as the RAR-related orphan receptors (RORs) which comprise high intrinsic activity and possess agonistic and inverse agonistic ligands². Moreover, the simultaneous Nurr1 modulation by NSAIDs (MFA, parecoxib) and AQ observed in cross-titration experiments suggests potentially the existence of two ligand-binding pockets in Nurr1, both of which can control the receptor activity.

The Gal4-hybrid reporter gene assay employed for our primary screening is a robust test system but does not fully capture the physiological behavior of nuclear receptors in terms of dimerization. Jiang *et al.*²⁶ recently demonstrated that Nurr1 monomers, Nurr1 homodimers, and Nurr1:RXR heterodimers address distinct response elements on DNA. To transfer our findings to endogenous conditions with different Nurr1 DNA response elements and dimerization states, we profiled the entire set of initial Nurr1 tool compounds (AQ, CQ, MFA, parecoxib, oxaprozin) in reporter gene assays involving the human Nurr1 response elements NBRE, NurRE, and DR5 as well as the full-length human Nurr1 protein as monomer, homodimer, or heterodimer. Dose–response experiments on NBRE-, NurRE-, and DR5-dependent reporter expression confirmed agonism of AQ and CQ as well as inverse agonism of parecoxib and oxaprozin on Nurr1 monomers (NBRE), homodimers (NurRE), and heterodimers (DR5). MFA, however, exhibited a less consistent activity profile with agonism on Gal4-Nurr1, inverse agonism on Nurr1 dimers (NurRE, DR5) and no activity on full-length Nurr1 monomers (NBRE). This observation suggests promising potential for (gene-)selective modulation of Nurr1 but also demonstrates limitations of the Gal4-hybrid assay setting to study Nurr1 modulation since it was not predictive of MFA's mode of activity on full-length human Nurr1.

In order to observe the molecular modes by which agonists and inverse agonists differentially modulate Nurr1, we studied the dimerization behavior of the Nurr1 LBD and its interaction with co-regulators in presence and absence of ligands. We observed high affinity of Nurr1 to homodimerize and to form heterodimers with RXR. These interactions were markedly affected by Nurr1 modulators and enable distinction between agonism and inverse agonism with agonists promoting dimer formation and inverse agonists decreasing dimerization. MFA was most effective in countering Nurr1 dimer formation regarding both, homo- and heterodimer which suggests that MFA shifts the binding equilibrium of Nurr1 to a fully monomeric state. This is in line with different behavior of the compound in cellular settings involving monomers (Gal4-assay, NBRE) or dimers (NurRE, DR5) and

provides preliminary explanation why the observed activities of MFA differed in different cellular settings. In addition, the ligand-induced Nurr1 dimerization state appears to affect Nurr1 activation efficacy since AQ which primarily promoted Nurr1 homodimerization in cell-free setting concomitantly exhibited the strongest activation efficacy on the human Nurr1 homodimer response element (NurRE, >100-fold max. activation).

We then assessed how ligands modulate the interaction between Nurr1 and co-regulators, and screened a library of twenty nine known nuclear receptor co-regulator fragments for their recruitment to Nurr1. We observed robust binding of NCoR-1, NCoR-2, NCoA6, and NR1P1 to the Nurr1 LBD and discovered that these interactions are responsive to Nurr1 ligands. The Nurr1 agonist CQ revealed a trend to enhanced recruitment of co-regulators and both AQ and CQ increased the affinity between the Nurr1 LBD and NCoR-1 while inverse agonists parecoxib and oxaprozin displaced co-regulator interaction motifs from the Nurr1 LBD. Different effects of Nurr1 modulators on co-regulator recruitment to the Nurr1 LBD therefore arise as further contributing factor to discriminate Nurr1 agonism and inverse agonism. In addition, different effects of AQ and CQ on co-regulator recruitment by Nurr1—beyond their distinctive modulation of Nurr1 dimerization—provide a basis for their different Nurr1 activation efficacies. Using a limited coverage of potential interactors, our results indicated strongly a similar ability of Nurr1 to other nuclear receptors for interactions with a number of co-regulators and we postulate that further biologically-relevant co-regulators might involve in Nurr1 regulation.

Based on our findings in orthogonal cellular and cell-free assay systems, we conclude that bidirectional modulation of Nurr1 by small-molecule ligands results from two contributions. Agonists promote dimerization of Nurr1 as a homodimer or as a heterodimer with RXR and additionally stabilize interaction of the Nurr1 LBD with co-regulators. Inverse agonists favor monomeric Nurr1 and decrease Nurr1 co-regulator interactions (Fig. 6). These changes in protein–protein interactions of Nurr1 result in differential cellular effects on reporter/gene expression. Therein, MFA exhibited a profile between agonism and inverse agonism on different Nurr1 response elements and since these DNA motifs are found in the promoter regions of different genes, gene selective modulation of Nurr1 activity seems possible with ligands that either favor monomeric or dimeric states. These considerations give our observation of ligand-dependent preference of Nurr1 for monomeric or dimeric forms considerable relevance.

Overall our studies have demonstrated that Nurr1 activity can be modulated by small-molecule ligands in a bidirectional fashion and we report first-in-class inverse Nurr1 agonists that counter the receptor's high constitutive transcriptional inducer activity. The opposite activities of Nurr1 agonists and inverse agonists are rationalized by their distinct effects on Nurr1's interaction profile with co-regulators and dimerization state. Moreover, our results point to the existence of two binding sites within the Nurr1 LBD that can accommodate ligands, of which the binding can modulate Nurr1 activity both independently and simultaneously. This is demonstrated by pairs of modulators involving AQ and MFA or parecoxib, which achieve different Nurr1 activation efficacy when they are applied together compared with their individual effects, offering potentially another avenue for the design of selective Nurr1 modulators or agonists with enhanced efficacy. These results markedly contribute to molecular understanding of Nurr1's activity and advocate the development of several types of potent Nurr1 modulator tool compounds that address the different binding sites and distinct receptor responses to enable in depth functional validation of Nurr1 as future drug target.

Methods

Reporter gene assays. *Plasmids:* The Gal4-fusion receptor plasmids pFA-CMV-hNur77-LBD, pFA-CMV-hNURR1-LBD, and pFA-CMV-hNOR1-LBD coding for the hinge region and LBD of the canonical isoforms of the human nuclear receptors Nur77 (uniprot entry: hNUR77-P22736, residues 358–598), Nurr1 (uniprot entry: hNURR1-P43354, residues 360–598), and NOR1 (isoform alpha; uniprot entry: hNOR1-Q92570-1, residues 393–626) were constructed by integrating cDNA fragments obtained from PCR amplification using natural cDNA (Nur77: GenBank entry: BC016147.1, purchased as I.M.A.G.E. cDNA clone from Source BioScience, Nottingham, UK; Nurr1: GenBank entry: BC009288.2, purchased as I.M.A.G.E. cDNA clone from Source BioScience) or the pcDNA3.1 plasmid OHu22293D (NOR1; GenScript, USA; NCBI ref. NM_173200.2) as template between the BamHI cleavage site of the pFA-CMV vector (Stratagene, La Jolla, CA, USA) and an afore inserted KpnI cleavage site. Frame and sequence of the fusion plasmids were verified by sequencing. The Gal4-fusion receptor plasmids used for selectivity profiling were pFA-CMV-hPPAR α -LBD, pFA-CMV-hPPAR γ -LBD, pFA-CMV-hPPAR δ -LBD, pFA-CMV-hRXR α -LBD, and pFA-CMV-hRAR α -LBD coding for the hinge region and ligand-binding domain of the canonical isoform of the respective nuclear receptor have been reported previously^{27–29}. pFR-Luc (Stratagene) was used as reporter plasmid and pRL-SV40 (Promega, Madison, WI, USA) for normalization of transfection efficiency and test compound toxicity. The Gal4-VP16¹² expressed from plasmid pECE-SV40-Gal4-VP16³⁰ (Addgene, entry 71728, Watertown, MA, USA) was used as ligand-independent transcriptional inducer for control experiments. The reporter plasmid pFR-Luc (Stratagene) used for the Gal4-hybrid assays contains a section between 176 to 83 base pairs upstream of the start codon of the firefly CDS that encompasses five copies of the Gal4 response element. To enable transactivation assays based on full-length NRs, this section was replaced with the human Nurr1 response elements DR5 (pFR-Luc-DR5; TGATAGGTTACCCGAAAGGTC A), NBRE NL3 (pFR-Luc-NBRE; TGA-TATCGAAAACAAAAGGTC A), or NurRE (from proopiomelanocortin (POMC); pFR-Luc-NurRE; TGATATTTACCTCCAATGCC A), respectively. The human nuclear receptors Nurr1 (pcDNA3.1-hNurr1-NE; #102363, Addgene, Cambridge, MA, USA) and, for DR5, RXR α (pSG5-hRXR³¹) were overexpressed. *Assay procedure:* HEK293T cells (German Collection of Microorganisms and Cell Cultures (DSMZ), Braunschweig, Germany) were grown in DMEM high glucose, supplemented with 10% FCS, sodium pyruvate (1 mM), penicillin (100 U/mL), and streptomycin (100 μ g/mL) at 37 °C and 5% CO₂. The day before transfection, HEK293T cells were seeded in 96-well plates (3 \times 10⁴ cells/well). Before transfection, medium was changed to Opti-MEM without supplements. Transient transfection was performed using Lipofectamine LTX reagent (Invitrogen, Carlsbad, CA, USA) according to the manufacturer's protocol with the corresponding plasmid mixture. For Gal4-hybrid assays, the plasmid mixtures comprised the respective Gal4-fusion nuclear receptor plasmid (pFA-CMV-NR-LBD), pFR-Luc, and pRL-SV40. For assays on full-length human Nurr1, the plasmid mixtures were pcDNA3.1-hNurr1-NE/pFR-Luc-NBRE/pRL-SV40 (NBRE), pcDNA3.1-hNurr1-NE/pFR-Luc-NurRE/pRL-SV40 (NurRE), and pcDNA3.1-hNurr1-NE/pSG5-RXR/pFR-Luc-DR5/pRL-SV40 (DR5). Five hours after transfection, medium was changed to Opti-MEM supplemented with penicillin (100 U/mL) and streptomycin (100 μ g/mL), now additionally containing 0.1% DMSO and the respective test compound or 0.1% DMSO alone as untreated control. Each concentration was tested in duplicates and each experiment was performed independently at least three times. Following overnight (12–14 h) incubation with the test compounds, cells were assayed for luciferase activity using Dual-Glo[™] Luciferase Assay System (Promega) according to the manufacturer's protocol. Luminescence was measured with a Spark 10 M luminometer (Tecan Group Ltd., Männedorf, Switzerland). Normalization of transfection efficiency and cell growth was done by division of firefly luciferase data by renilla luciferase data and multiplying the value by 1000 resulting in relative light units (RLU). Fold activation was obtained by dividing the mean RLU of a test compound at a respective concentration by the mean RLU of untreated control. Max. relative activation refers to fold reporter activation of a test compound divided by the fold activation of the respective reference agonist (PPAR α : GW7647; PPAR γ : pioglitazone/rosiglitazone²⁹; PPAR δ : L165,041; RXR α : bexarotene; RAR α : tretinoin; all at a concentration of 1 μ M; Nurr1: amodiaquine (100 μ M)). All hybrid assays were validated with the above mentioned reference agonists which yielded EC₅₀ values in agreement with the literature.

Production of recombinant RXR α and Nurr1 fusion proteins. The coding sequence for RXR α LBD and Nurr1 LBD was codon optimized for *E. coli* and purchased from Geneart (Regensburg, Germany), respectively. For expression of fusion proteins with N-terminal green fluorescent protein (GFP), an expression construct based on pET29b was prepared. For this, the entire section between the original NdeI site and the forth position following the His-Tag coding sequence of pET29b was replaced, hence, essentially leaving only the vector backbone unmodified. The section was replaced by a sequence encoding a restriction site for NcoI (overlapping with the start codon) and an open reading frame for Met-Gly-[His₁₀-Tag]-Asp-Tyr-Asp-Ile-Pro-Thr-Thr-[TEV site]-superfolder GFP³² followed by restriction sites for BamHI (in frame) and XhoI. The sequences coding for the LBDs of RXR α (uniprot entry: P19793-1, residues 226–462) or Nurr1 (uniprot entry: P43354-1, residues 364–598) each followed by a stop codon were then

introduced in frame between the afore inserted restriction sites for BamHI and XhoI.

For generation of biotinylated Nurr1 LBD, the pMal vector system (New England Biolabs, NEB, Ipswich, MA, USA) was used. In pMal-c2E, the section between the sequence encoding 10x Asparagine (Asn₁₀) and the SalI restriction site was replaced with a sequence encoding Leu-Gly-Ile-Glu-Leu-Val-[His₈-Tag]-Asp-Tyr-Asp-Ile-Pro-Gly-Thr-Leu-[TEV site] followed by an Avi-Tag and restriction sites for BamHI and XhoI. The sequence encoding Nurr1 (aa 364–598) followed by two stop codons was cloned in frame between these restriction sites. From this construct, a fusion protein is expressed with N-terminal maltose-binding protein (MBP) followed by an Asn₁₀ linker, a His₈-Tag, a cleavage site for TEV protease, an Avi-Tag, and the Nurr1 LBD with unmodified C-terminus.

For expression, *E. coli* T7 express cells (NEB) were co-transformed with pGro7 (TAKARA Bio Inc., Kusatsu, Japan) and one of the Nurr1 (pMal or pET) or RXR α (pET) expression constructs and selected overnight at 37 °C on LB (Luria Broth) agar containing 34 μ g/ml chloramphenicol and either 100 μ g/ml ampicillin (for pMal) or 35 μ g/ml kanamycin (for pET). Culture in liquid LB was inoculated and grown at 37 °C with constant shaking at 180 rpm until optical density at 600 nm (OD₆₀₀) reached 0.7. At this time point, expression of the chaperone GroEL/ES from pGro7 was induced with 1 g/L L(+)-Arabinose and the temperature was reduced to 20 °C. At OD₆₀₀ = 1 expression of the target protein was induced by addition of 0.5 mM IPTG. After 12–16 h, cells were harvested by centrifugation and resuspended in buffer A (400 mM NaCl, 20 mM NaP_i, pH 7.8, 10% (w/v) Glycerol, and 20 mM β -mercaptoethanol). Cells were kept on ice and disrupted in presence of 1 mM ATP, DNase I, RNase A, 20 mM MgSO₄, and EDTA-free cOmplete™ protease inhibitor cocktail (F. Hoffmann-La Roche AG, Basel, Switzerland) by addition of lysozyme and 10 passages through an Invensys APV-1000 homogenizer (APV Systems, Silkeborg, Denmark). Cell debris was removed by centrifugation at 16,500 \times g for 20 min at 4 °C.

Purification was achieved by immobilized metal chromatography (IMAC) using columns packed with Ni Sepharose 6 Fast Flow resin on an AKTApurifier FPLC system (GE Healthcare, Chicago, IL, USA). After washing with buffer supplemented with 50 mM imidazole the protein was eluted with 300 mM imidazole. Afterward, GFP fusion proteins were processed with His tagged TEV protease overnight while imidazole content was reduced to 10 mM by dialysis against buffer A in order to allow for reverse IMAC. The flow through was concentrated and applied to size exclusion chromatography using a 16/60 Superdex200™ column equilibrated and run in HTRF assay buffer [25 mM HEPES pH 7.5, 150 mM KF, 10% (w/v) glycerol, 5 mM DTT]. Following the initial IMAC purification step, the MBP fusion protein for generation of biotin-labeled Nurr1 LBD was processed with MBP-tagged TEV protease during overnight dialysis against buffer A. Afterward, uncleaved fusion protein, free MBP-Tag, and TEV protease were removed by passing through a gravity flow column packed with Amylose High Flow resin (NEB). The flow through was then supplemented with 0.5 mM biotin, 0.5 mM ATP, 5 mM MgCl₂, and *E. coli* biotin ligase BirA at a molar ratio of ~1:10 for enzymatic conjugation of biotin to the lysine residue in the avitag. After overnight incubation at 4 °C, the solution was subjected to a column packed with 5 ml monomeric avidin UltraLink™ resin (Pierce Biotechnology Inc., Rockford, IL, USA). Unlabeled protein and BirA were removed by washing for 10 column volumes with buffer A before biotin-labeled Nurr1 LBD was eluted using buffer A supplemented with 2 mM biotin. The product was then concentrated and subjected to size exclusion chromatography using a 10/30 Superdex75™ column equilibrated and run in HTRF assay buffer.

Nurr1 co-regulator recruitment assays. Recruitment of co-regulator peptides to the Nurr1 LBD was studied in a homogeneous time-resolved fluorescence resonance energy transfer (HT-FRET) assay system. Terbium cryptate as streptavidin conjugate (Tb-SA; Cisbio Bioassays, Codolet, France) was used as FRET donor for stable coupling to biotinylated recombinant Nurr1-LBD protein. Twenty-nine co-regulator peptides fused to fluorescein as FRET acceptor were purchased from ThermoFisher Scientific (Life Technologies GmbH, Darmstadt, Germany). Assay solutions were prepared in HTRF assay buffer supplemented with 0.1% (w/v) CHAPS and contained recombinant biotinylated Nurr1 LBD (final concentration 3 nM), Tb-SA (3 nM) and the respective fluorescein-labeled co-regulator peptide (100 nM) as well as 1% DMSO with test compounds at 100 μ M or DMSO alone as negative control. All HTRF experiments were carried out in 384 well format using white flat bottom polystyrol microtiter plates (Greiner Bio-One, Frickenhausen, Germany). After 2 h incubation at RT, fluorescence intensities (FI) after excitation at 340 nm were recorded at 520 nm for fluorescein acceptor fluorescence and 620 nm for Tb-SA donor fluorescence on a SPARK plate reader (Tecan Group Ltd.). FI520nm was divided by FI620nm and multiplied with 10,000 to give a dimensionless HTRF signal. Dose–response experiments with varying concentrations of the test compounds amodiaquine, chloroquine, meclofenamic acid, piroxicam, and oxapropin were conducted in the same manner and setting. The co-regulator peptides in this experiment were the following: steroid receptor co-activator (SRC) 1-1, Fluorescein-KYSQTSHKLVQLLTTTAEQQL-OH; SRC 1-2, Fluorescein-LTARHKILHRLLEQEGSPSD-OH; SRC 1-3, Fluorescein-ESKDHQLLRYLLDK-DEKDL-OH; SRC 1-4, Fluorescein-GPQTPQAQKSLQLLQTE-OH; SRC 2-1, Fluorescein-DSKGQTKLLQLLTTKSDQM-OH; SRC 2-2, Fluorescein-LKEKH KILHRLLEQSSSPV-OH; SRC 2-3, Fluorescein-KKKNALLRYLLDKDDTKD-

OH; SRC 3-1, Fluorescein-ESKGHKKLLQLLTCSSDDR-OH; SRC 3-2, Fluorescein-LQEKHRLHKLQNGNSPA-OH; SRC 3-3, Fluorescein-KKENNALLR YLLDRDDPSD-OH; nuclear receptor co-repressor (NCOR) ID1, Fluorescein-RTHRLITLADHICQIITQDFARN-OH; NCOR ID2, Fluorescein-DPASNLGLE DIIRKALMGSFDDK-OH; silencing mediator for retinoid and thyroid hormone receptor (SMRT) ID1, Fluorescein-GHQRVVTLAQHISEVITQDYTRH-OH; SMRT ID2, Fluorescein-HASTNMGLEAIRKALMGKYDQW-OH; CREB-binding protein 1 (CBP-1), Fluorescein-AASKHKQSELLRGGSGSS-OH; C33, Fluorescein-HVEMHPLLMLGMLMESQWGA-OH; D11-FXXLF, Fluorescein-VEGSSRFMQLFMANDLLT-OH; D22, Fluorescein-LPYEGSLLKLLRAPVEEV-OH; EAB1, Fluorescein-SSNHQSSRLIELLSR-OH; EA2, Fluorescein-SSKGV LWRMLAEPVSR-OH; androgen receptor-associated protein 70 (ARA70), Fluorescein-SRETSEKFKLLFQSYNVND-OH; N-terminal sequence of androgen receptor (AR N-term), Fluorescein-SKTYRGAFQNLQFQSVREVI-OH; peroxisome proliferator-activated receptor gamma co-activator 1-alpha (PGC1a), Fluorescein-EAEEPSSLLKLLAPANTQ-OH; nuclear receptor co-activator 6 (NCoA6, also termed PRIPRAP250), Fluorescein-VTLTSPLLVNLQSDISAG-OH, nuclear receptor interacting protein 1 (NRI1, also termed RIP140, interaction motif L6), Fluorescein-SHQKVTLQLLGHKNEEN-OH; RIP140L8, Fluorescein-SFSKNGLLSRLRQNDQSY-OH; TB3, Fluorescein-SSVASREWWVRELSR-OH; thyroid hormone receptor-associated protein (TRAP) TRAP220/DRIP-1, Fluorescein-KVSQNPILTSLQLITGNGG-OH; TRAP220/DRIP-2, Fluorescein-NTKNHPMLMNLKDNPAQD-OH.

Nurr1-RXR heterodimerization. Strength and modulation of the formation of the heterodimer composed of the LBDs of Nurr1 and RXR α was investigated by titration of GFP-RXR α LBD against a fixed concentration of Nurr1 LBD. Assay solutions were prepared in HTRF assay buffer supplemented with 0.1% (w/v) CHAPS as well as 1% DMSO with test compounds at 100 μ M or DMSO alone as negative control. The FRET donor complex formed from biotinylated Nurr1 LBD (final concentration 0.375 nM) and Tb-SA (0.75 nM) was kept constant while the concentration of GFP-RXR α LBD was varied starting with 4 μ M as the highest concentration and titrated with a dilution factor of 0.7. Free GFP was added to keep the total GFP content stable at 4 μ M throughout the entire series in order to suppress artefacts from changes in degree of diffusion enhanced FRET. Samples were equilibrated at RT for 2 h before FI520 and FI620 were recorded after excitation at 340 nm, and the HTRF signal was calculated as described above.

Nurr1 homodimerization. Nurr1 homodimerization was studied by the same strategy using GFP-Nurr1 LBD instead of GFP-RXR α LBD. Since affinity observed for Nurr1 homodimer formation was higher, the maximum concentration for GFP-Nurr1 LBD and the total GFP concentration was reduced to 500 nM.

Nurr1-NCoR-1 interaction. The Nurr1–NCoR-1 interaction was studied by titrating GFP-Nurr1 LBD against biotinylated NCoR-1 copeptide (18 nM) and Tb-SA (12 nM) in presence of a fixed concentration (100 μ M, in assay buffer containing 1% DMSO) of the respective ligand or 1% DMSO. To maintain a constant GFP concentration, free GFP protein was added to the dilution series. The experiments were performed in HTRF assay buffer (150 mM KF, 25 mM HEPES pH 7.5 (KOH), 5% (w/v) Glycerol, supplemented with 0.1% (w/v) CHAPS and 5 mM DTT) with 1% DMSO in an assay volume of 20 μ l. After 1 h incubation at RT, fluorescence intensities after excitation at 340 nm were recorded at 520 nm for GFP acceptor fluorescence and 620 nm for Tb-SA donor fluorescence and the HTRF signal was calculated as described above.

Computational methods. *General:* Calculations were conducted in Molecular Operating Environment (MOE, version 2018.0101, Chemical Computing Group Inc., Montreal, QC, Canada) using default settings for each tool/function unless stated otherwise. *Crystal structure analysis:* Alignment of the Nurr1 LBD in apo state (PDB: 1OVL¹), bound to prostaglandin A1 (PDB: 5Y41⁷) and to dopamine metabolite DHI (PDB: 6DDA⁹) was conducted using MOE sequence editor. The subunits B were used in all cases. The proposed binding region for amodiaquine type ligands was highlighted according to annotated amino acids from NMR perturbation experiments and mutational studies⁶. Distances of the salt bridge between Lys590 to Glu440 were measured in angstrom (Å) in MOE from nitrogen (NH₃⁺) of Lys590 to oxygen (O⁻) of Glu440. Data shown are the mean \pm SD corresponding to the different subunits of the X-ray structures.

Statistics. Calculations and graphical analysis of experimental data was conducted using GraphPad Prism version 7.00 for Windows (GraphPad Software, La Jolla, CA, USA) and Microsoft Excel 2016 (Microsoft Corporation, Redmond, WA, USA). All cellular experiments were performed with at least three independent biological repeats ($n \geq 3$), each in duplicates. The cell-free experiments were performed with three technical replicates ($N = 3$), whereas the cofactor screen was performed with four technical replicates ($N = 4$). All dose–response curves were calculated in GraphPad Prism using a nonlinear regression with variable slope ([Agonist] or [Inhibitor] vs. response; four parameters). Statistical significance was evaluated by two-tailed student's *t*-test (two samples, unequal variance; calculated in Excel) with $n \geq 4$. Results were considered statistically significant with

p values < 0.05; significance levels are denoted as **p* < 0.05, ***p* < 0.01, ****p* < 0.001. Boxplots were generated in GraphPad Prism and show: center line, median; box limits, upper and lower quartiles; whiskers, min/max; *n* ≥ 4.

Reporting summary. Further information on research design is available in the Nature Research Reporting Summary linked to this article.

Data availability

The datasets generated and analyzed during the current study are available from the corresponding author on reasonable request.

Received: 24 December 2019; Accepted: 5 June 2020;

Published online: 03 July 2020

References

- Wang, Z. et al. Structure and function of Nurr1 identifies a class of ligand-independent nuclear receptors. *Nature* **423**, 555–560 (2003).
- Benoit, G. et al. International union of pharmacology. LXVI. Orphan nuclear receptors. *Pharmacol. Rev.* **58**, 798–836 (2006).
- Decressac, M., Volakakis, N., Björklund, A. & Perlmann, T. NURR1 in Parkinson disease—from pathogenesis to therapeutic potential. *Nat. Rev. Neurol.* **9**, 629–636 (2013).
- de Vera, I. M. S. et al. Identification of a binding site for unsaturated fatty acids in the orphan nuclear receptor Nurr1. *ACS Chem. Biol.* **11**, 1795–1799 (2016).
- de Vera, I. M. S. et al. Defining a canonical ligand-binding pocket in the orphan nuclear receptor Nurr1. *Structure* **27**, 66–77.e5 (2018).
- Kim, C.-H. et al. Nuclear receptor Nurr1 agonists enhance its dual functions and improve behavioral deficits in an animal model of Parkinson's disease. *Proc. Natl Acad. Sci. USA* **112**, 8756–8761 (2015).
- Rajan, S. et al. PGE1 and PGA1 bind to Nurr1 and activate its transcriptional function. *Nat. Chem. Biol.* <https://doi.org/10.1038/s41589-020-0553-6> (2020).
- Rajan, S., Toh, H. T., Lim, K. H. & Yoon, H. S. Structure of Nurr1 bound to cyclopentenone prostaglandin A2 and its mechanism of action in ameliorating dopaminergic neurodegeneration in *Drosophila*. *PDB ID 5YD6*, <https://doi.org/10.2210/PDB5YD6/PDB> (2019).
- Bruning, J. M. et al. Covalent modification and regulation of the nuclear receptor Nurr1 by a dopamine metabolite. *Cell Chem. Biol.* **26**, 1–12 (2019).
- McFedries, A. K. *Characterization of Protein-Metabolite and Protein-Substrate Interactions of Disease Genes*. (Harvard University, 2014).
- Hintermann, S. et al. Identification of a series of highly potent activators of the Nurr1 signaling pathway. *Bioorg. Med. Chem. Lett.* **17**, 193–196 (2007).
- Sadowski, I., Ma, J., Triezenberg, S. & Ptashne, M. GAL4-VP16 is an unusually potent transcriptional activator. *Nature* **335**, 563–564 (1988).
- Proschak, E., Heitel, P., Kalinowsky, L. & Merk, D. Opportunities and challenges for fatty acid mimetics in drug discovery. *J. Med. Chem.* **60**, 5235–5266 (2017).
- Kramer, J. S. et al. Discovery of the first in vivo active inhibitors of the soluble epoxide hydrolase phosphatase domain. *J. Med. Chem.* **62**, 8443–8460 (2019).
- Perlmann, T. & Jansson, L. A novel pathway for vitamin A signaling mediated by RXR heterodimerization with NGFI-B and NURR1. *Genes Dev.* **9**, 769–782 (1995).
- Codina, A. et al. Identification of a novel co-regulator interaction surface on the ligand binding domain of Nurr1 using NMR footprinting. *J. Biol. Chem.* **279**, 53338–53345 (2004).
- Chang, C. et al. Dissection of the LXXLL nuclear receptor-coactivator interaction motif using combinatorial peptide libraries: discovery of peptide antagonists of estrogen receptors α and β . *Mol. Cell. Biol.* **19**, 8226–8239 (1999).
- Viola, G. et al. Photophysical properties and photobiological behavior of amodiaquine, primaquine and chloroquine. *Photochem. Photobiol.* **83**, 1415–1427 (2007).
- Pan, T. et al. Nurr1 deficiency predisposes to lactacystin-induced dopaminergic neuron injury in vitro and in vivo. *Brain Res.* **1222**, 222–229 (2008).
- Liu, W., Gao, Y. & Chang, N. Nurr1 overexpression exerts neuroprotective and anti-inflammatory roles via down-regulating CCL2 expression in both in vivo and in vitro Parkinson's disease models. *Biochem. Biophys. Res. Commun.* **482**, 1312–1319 (2017).
- Moon, M. et al. Correlation between orphan nuclear receptor Nurr1 expression and amyloid deposition in 5XFAD mice, an animal model of Alzheimer's disease. *J. Neurochem.* **132**, 254–262 (2015).
- Moon, M. et al. Nurr1 (NR4A2) regulates Alzheimer's disease-related pathogenesis and cognitive function in the 5XFAD mouse model. *Aging Cell* **18**, e12866 (2019).
- Satoh, J. et al. Microarray analysis identifies an aberrant expression of apoptosis and DNA damage-regulatory genes in multiple sclerosis. *Neurobiol. Dis.* **18**, 537–550 (2005).
- Montarolo, F., Perga, S., Martire, S. & Bertolotto, A. Nurr1 reduction influences the onset of chronic EAE in mice. *Inflamm. Res.* **64**, 841–844 (2015).
- Montarolo, F. et al. Effects of isoxazolo-pyridinone 7e, a potent activator of the Nurr1 signaling pathway, on experimental autoimmune encephalomyelitis in mice. *PLoS ONE* **9**, e108791 (2014).
- Jiang, L. et al. Structural basis of binding of homodimers of the nuclear receptor NR4A2 to selective Nur-responsive DNA elements. *J. Biol. Chem.* <https://doi.org/10.1074/jbc.RA119.010730> (2019).
- Rau, O. et al. Carnosic acid and carnosol, phenolic diterpene compounds of the labiate herbs rosemary and sage, are activators of the human peroxisome proliferator-activated receptor gamma. *Planta Med.* **72**, 881–887 (2006).
- Flesch, D. et al. Non-acidic farnesoid X receptor modulators. *J. Med. Chem.* **60**, 7199–7205 (2017).
- Pollinger, J. et al. Tuning nuclear receptor selectivity of Wy14,643 towards selective retinoid X receptor modulation. *J. Med. Chem.* **62**, 2112–2126 (2019).
- Budzyński, M. A., Puustinen, M. C., Joutsen, J. & Sistonen, L. Uncoupling stress-inducible phosphorylation of heat shock factor 1 from its activation. *Mol. Cell. Biol.* **35**, 2530–2540 (2015).
- Merk, D. et al. Extending the structure-activity relationship of anthranilic acid derivatives as farnesoid x receptor modulators: Development of a highly potent partial farnesoid x receptor agonist. *J. Med. Chem.* **57**, 8035–8055 (2014).
- Pédélecq, J. D., Cabantous, S., Tran, T., Terwilliger, T. C. & Waldo, G. S. Engineering and characterization of a superfolder green fluorescent protein. *Nat. Biotechnol.* **24**, 79–88 (2006).

Acknowledgements

D.M. is grateful for support by the Aventis Foundation. This work was supported by the research funding program LOEWE of the State of Hessen, Research Center for Translational Medicine and Pharmacology TMP.

Author contributions

S.W., W.K., J.H. and D.M. performed the experiments. S.W. and D.M. analyzed the Nurr1 LBD structures. X.N., A.C. and S.K. generated recombinant Nurr1 LBD protein. J.H. cloned the NR4A receptor and full-length reporter constructs. D.M. designed and supervised the study. S.W. and D.M. analyzed the data, prepared the figures, and wrote the paper.

Competing interests

The authors declare no competing interests.

Additional information

Supplementary information is available for this paper at <https://doi.org/10.1038/s42004-020-0331-0>.

Correspondence and requests for materials should be addressed to D.M.

Reprints and permission information is available at <http://www.nature.com/reprints>

Publisher's note Springer Nature remains neutral with regard to jurisdictional claims in published maps and institutional affiliations.



Open Access This article is licensed under a Creative Commons Attribution 4.0 International License, which permits use, sharing, adaptation, distribution and reproduction in any medium or format, as long as you give appropriate credit to the original author(s) and the source, provide a link to the Creative Commons license, and indicate if changes were made. The images or other third party material in this article are included in the article's Creative Commons license, unless indicated otherwise in a credit line to the material. If material is not included in the article's Creative Commons license and your intended use is not permitted by statutory regulation or exceeds the permitted use, you will need to obtain permission directly from the copyright holder. To view a copy of this license, visit <http://creativecommons.org/licenses/by/4.0/>.

© The Author(s) 2020

The orphan nuclear receptor Nurr1 is responsive to non-steroidal anti-inflammatory drugs

Sabine Willems¹, Whitney Kilu¹, Xiaomin Ni^{1,2}, Apirat Chaikwad^{1,2}, Stefan Knapp^{1,2}, Jan Heering³, Daniel Merk¹

¹ Institute of Pharmaceutical Chemistry, Goethe University Frankfurt, Max-von-Laue-Str. 9, 60438 Frankfurt, Germany

² Structural Genomics Consortium, BMLS, Goethe-University Frankfurt, 60438 Frankfurt, Germany

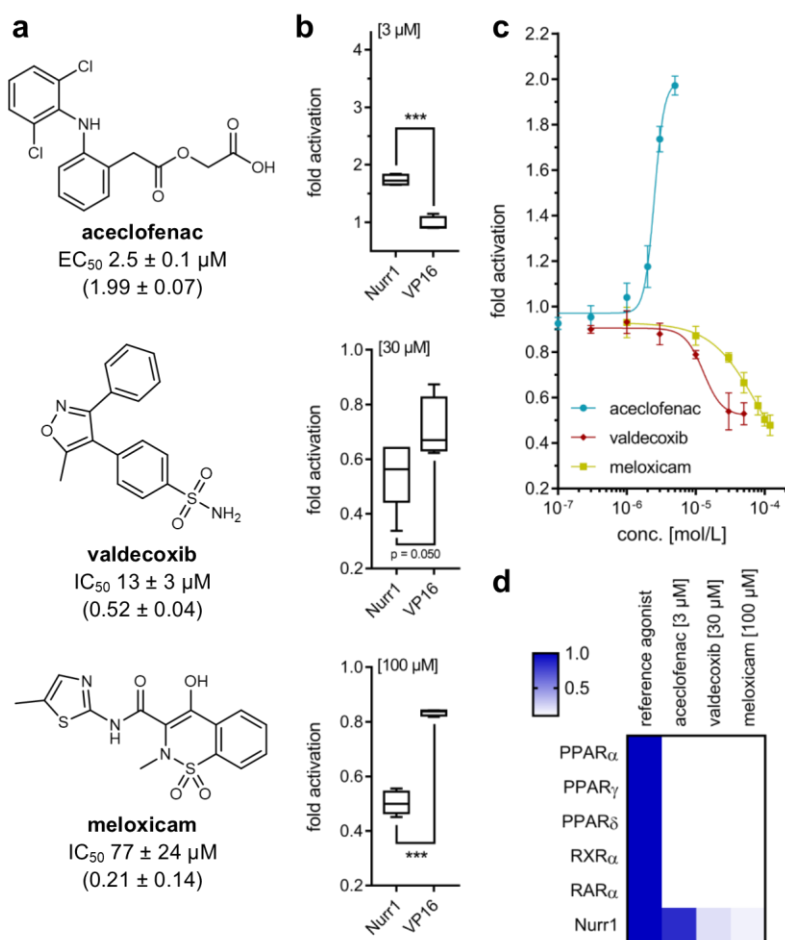
³ Fraunhofer Institute for Molecular Biology and Applied Ecology IME, Branch for Translational Medicine and Pharmacology TMP, Theodor-Stern-Kai 7, 60596 Frankfurt, Germany

- Supplementary Information -

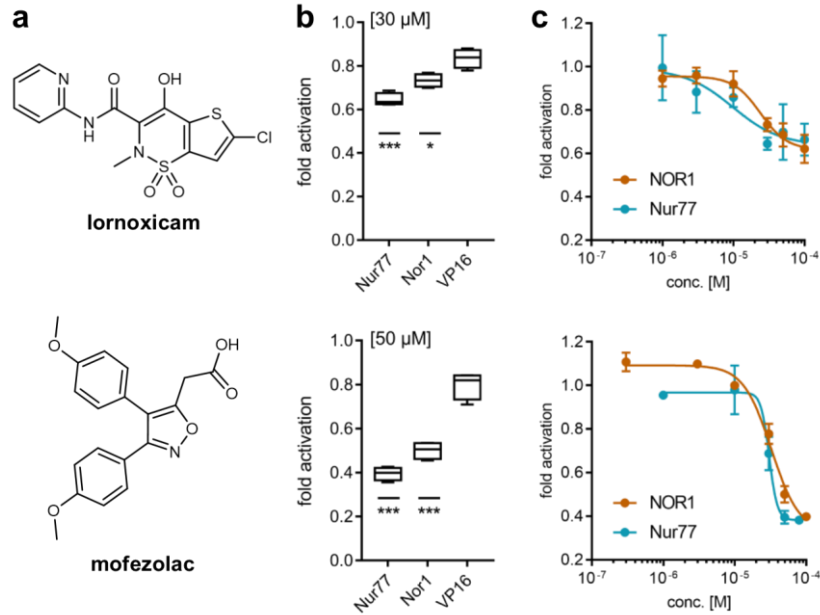
Table of contents

Supplementary Figures and Tables	2
Supplementary References	5

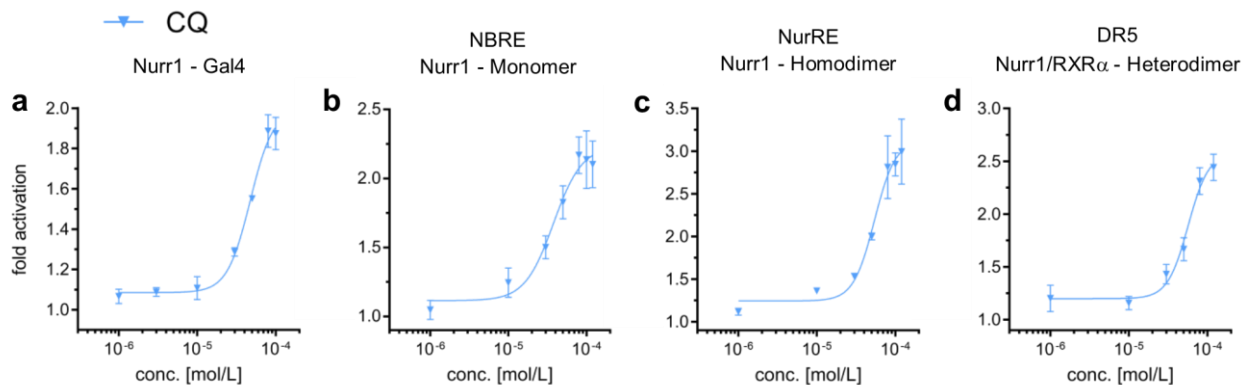
Supplementary Figures and Tables



Supplementary Figure 1. Bidirectional modulation of Nurr1 activity by drug approved COX inhibitors. (a) Molecular structures and activities of Nurr1 modulators aceclofenac, valdecoxib and meloxicam. EC_{50} and IC_{50} values were determined in the Gal4-Nurr1 hybrid reporter gene assay and are the mean \pm SD; $n \geq 3$. (b) Control experiments employing a Gal4-VP16 hybrid receptor confirmed Nurr1 mediated activity of aceclofenac, valdecoxib and oxaprozin. Boxplots show: center line, median; box limits, upper and lower quartiles; whiskers, min/max; $n \geq 4$. *** $p < 0.001$. (c) Gal4-hybrid reporter gene assay demonstrated Nurr1 activation by aceclofenac as well as inverse Nurr1 agonism for valdecoxib and meloxicam. Results are mean \pm S.E.M.; $n \geq 3$. (d) Selectivity profile of Nurr1 modulators over lipid activated transcription factors. Heatmap shows mean rel. activation which refers to reference agonists at 1 μM for PPARs (α : GW7647; γ : rosiglitazone; δ : L165,041), RXR α (bexaroten), RAR α (tretinoin) and 100 μM for Nurr1 (AQ); $n \geq 4$.



Supplementary Figure 2. Inverse agonists of related NR4A receptors Nur77 and NOR1 not affecting Nurr1 activity. (a) Molecular structures of NR4A receptor modulators lornoxicam and mofezolac. (b) Control experiments employing a Gal4-VP16 hybrid receptor confirmed Nur77 and NOR1 mediated activity of lornoxicam and mofezolac. Boxplots show: center line, median; box limits, upper and lower quartiles; whiskers, min/max; $n \geq 4$. * $p < 0.05$, ** $p < 0.01$ *** $p < 0.001$. (c) Dose-response curves demonstrate dose-dependent inverse Nur77 and NOR1 agonism. Data are mean \pm SD, $n \geq 3$.



Supplementary Figure 3. Cellular profiling of Nurr1 modulator chloroquine (CQ). Data shown here are identical with Fig. 3a-d for CQ in the manuscript but y-axis scaling has been adapted here to depict the CQ dose-response. The Nurr1 activation efficacy of CQ is markedly lower compared to AQ. (a) Gal4-hybrid reporter gene assay demonstrated Nurr1 activation by CQ. (b-d) Nurr1 full-length reporter gene assays with the human Nurr1 response elements NBRE (Nurr1 monomer, b), NurRE (Nurr1 homodimer, c), and DR5 (Nurr1:RXR heterodimer, d) confirmed agonism of CQ. All cellular experiments were performed in transiently transfected HEK293T cells. Results are the mean \pm S.E.M.; $n \geq 3$.

Supplementary Table 1. Activity of NSAIDs on NR4A nuclear receptors Nur77 (NR4A1), Nurr1 (NR4A2) and NOR1 (NR4A3) determined in uniform Gal4-hybrid reporter gene assays in transiently transfected HEK293T cells. Activity was verified using Gal4-VP16^{1,2} as control and only compounds with statistically significant ($p < 0.05$) activity on the respective NR4A receptor versus VP16 control are reported as active. EC₅₀/IC₅₀ values are reported in [μ M]. Values in parentheses are min./max. activation compared to 0.1% DMSO serving as vehicle. Data are the mean \pm SD, $n \geq 3$.

	Nur77	Nurr1	NOR1
meclofenamic acid	EC ₅₀ 3.9 \pm 0.7 (3.3 \pm 0.4)	EC ₅₀ 4.7 \pm 0.1 (3.52 \pm 0.05)	EC ₅₀ 7.9 \pm 0.8 (5.5 \pm 0.6)
meloxicam	IC ₅₀ 73 \pm 2 (0.23 \pm 0.02)	IC ₅₀ 77 \pm 24 (0.2 \pm 0.1)	IC ₅₀ 84 \pm 17 (0.1 \pm 0.1)
lornoxicam	IC ₅₀ 9.4 \pm 6.3 (0.63 \pm 0.09)	-	IC ₅₀ 24 \pm 3 (0.62 \pm 0.02)
aceclofenac	-	EC ₅₀ 2.5 \pm 0.1 (1.99 \pm 0.07)	-
mofezolac	IC ₅₀ 30 \pm 1 (0.38 \pm 0.02)	-	IC ₅₀ 33 \pm 5 (0.32 \pm 0.10)
oxaprozin	IC ₅₀ 16 \pm 5 (0.2 \pm 0.1)	IC ₅₀ 40 \pm 6 (0.26 \pm 0.08)	IC ₅₀ 22 \pm 4 (\geq 0.00)
valdecoxib	-	IC ₅₀ 13 \pm 3 (0.52 \pm 0.04)	-
parecoxib	IC ₅₀ 23.7 \pm 0.2 (0.1 \pm 0.0)	IC ₅₀ 13.4 \pm 0.3 (0.48 \pm 0.01)	IC ₅₀ 25 \pm 4 (0.22 \pm 0.05)

Supplementary References

1. Sadowski, I., Ma, J., Triezenberg, S. & Ptashne, M. GAL4-VP16 is an unusually potent transcriptional activator. *Nature* **335**, 563–564 (1988).
2. Budzyński, M. A., Puustinen, M. C., Joutsen, J. & Sistonen, L. Uncoupling Stress-Inducible Phosphorylation of Heat Shock Factor 1 from Its Activation. *Mol. Cell. Biol.* **35**, 2530–2540 (2015).

16.5 Fragment-like Chloroquinolineamines Activate the Orphan Nuclear Receptor Nurr1 and Elucidate Activation Mechanisms

Willems, S.; Ohrndorf, J.; Kilu, W.; Heering, J.; Merk, D. Fragment-like Chloroquinolineamines Activate the Orphan Nuclear Receptor Nurr1 and Elucidate Activation Mechanisms. *J. Med. Chem.* **2021**, *64* (5), 2659–2668.

Reprinted with permission from Willems, S.; Ohrndorf, J.; Kilu, W.; Heering, J.; Merk, D. *J. Med. Chem.* **2021**, *64* (5), 2659–2668. Copyright (2021) American Chemical Society.

Fragment-like Chloroquinolineamines Activate the Orphan Nuclear Receptor Nurr1 and Elucidate Activation Mechanisms

Sabine Willems, Julia Ohrndorf, Whitney Kilu, Jan Heering, and Daniel Merk*

Cite This: *J. Med. Chem.* 2021, 64, 2659–2668

Read Online

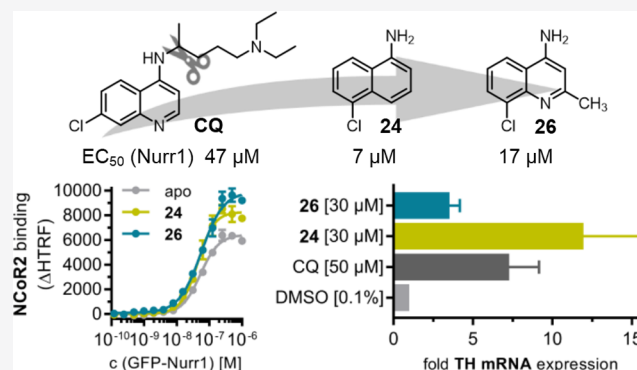
ACCESS |

Metrics & More

Article Recommendations

Supporting Information

ABSTRACT: The ligand-activated transcription factor nuclear receptor related-1 (Nurr1) exhibits great potential for neurodegenerative disease treatment, but potent Nurr1 modulators to further probe and validate the nuclear receptor as a therapeutic target are lacking. We have systematically studied the structure–activity relationship of the 4-amino-7-chloroquinoline scaffold contained in Nurr1 activators amodiaquine and chloroquine and discovered fragment-like analogues that activated Nurr1 in several cellular settings. The most active descendants promoted the transcriptional activity of Nurr1 on human response elements as monomer, homodimer, and heterodimer and markedly enhanced Nurr1-dependent gene expression in human astrocytes. As a tool to elucidate mechanisms involving in Nurr1 activation, these Nurr1 agonists induced robust recruitment of NCoR1 and NCoR2 co-regulators to the Nurr1 ligand binding domain and promoted Nurr1 dimerization. These findings provide important insights in Nurr1 regulation. The fragment-sized Nurr1 agonists are appealing starting points for medicinal chemistry and valuable early Nurr1 agonist tools for pharmacology and chemical biology.



INTRODUCTION

The ligand-sensing transcription factor nuclear receptor related-1 (Nurr1, NR4A2)¹ is an orphan nuclear receptor with neuroprotective properties. Nurr1 is found in several neuronal cells with particularly high expression in dopaminergic neurons.² It regulates the expression of various genes in dopamine metabolism and transport, which turned out to be crucial for the protection and survival of dopaminergic neurons.² Altered expression of Nurr1 in patients of Parkinson's Disease (PD) and the observation that neuronal Nurr1 knockout in mice causes a phenotype resembling PD further point to high therapeutic potential of Nurr1 modulation in PD and other neurodegenerative pathologies.^{2,3} The prostaglandins PGA1 and PGE1 were recently discovered as endogenous Nurr1 ligands with intermediate micromolar potency and neuroprotective effects.⁴ However, the lack of potent Nurr1 modulators as tools hinders further evaluation and validation of Nurr1 as a therapeutic target.

Amodiaquine (AQ, 1), chloroquine (CQ, 2), and glafenine (3) have been reported as first-in-class activators of Nurr1³ with micromolar activity (Table 1). These compounds importantly demonstrate that Nurr1 can be activated with small molecules. However, their limited potency and their effects on various other proteins and signaling pathways^{5–13} render them insufficient as tools for pharmacology and chemical biology. Optimized Nurr1 activators are required to

study the role of the orphan nuclear receptor in health and disease.

Munoz-Tello et al.¹³ have recently demonstrated that among the putative Nurr1 modulators reported in the literature, only AQ (1), CQ (2), and cytosporone B act as direct ligands of the nuclear receptor to control its transcriptional activity. Moreover, this recent study confirms previous observations that AQ (1) and CQ (2) likely target the canonical ligand binding site of the Nurr1 ligand binding domain (LBD)³ in contrast to PGA1 and PGE1, which bind to a noncanonical site between helices H5, H11, and H12.⁴ These important findings¹³ make the AQ/CQ chemotype of Nurr1 modulators an attractive starting point for the development of Nurr1 targeting tool compounds.

Using 1–3 as the starting matter, we have assessed the structure–activity relationship (SAR) of this AQ chemotype of Nurr1 ligands by a rapid fragment-based strategy. We have discovered that the 4-amino-7-chloroquinoline (4) scaffold alone is sufficient for Nurr1 activation despite low potency. By

Received: October 19, 2020

Published: February 25, 2021



Table 1. SAR of Side-Chain Motifs in the AQ/CQ Chemotype. Biological Activity of 1–10 on Nurr1 In Vitro^a

ID	R	Nurr1	
		Activity type	EC ₅₀ (max. fold act.)
1 (AQ)		Agonist	36±4 μM (3.6±0.1)
2 (CQ)		Agonist	47±5 μM (2.0±0.1)
3		inactive (10 μM) ^b	
4	-H	Agonist	259±70 μM (2.5±0.4)
5		Agonist	116±4 μM (3.1±0.2)
6		inactive (30 μM) ^b	
7		Inverse agonist	IC ₅₀ =132±1 μM
8		Agonist	1.8±0.3 μM (1.47±0.03)
9		inactive (30 μM) ^b	
10		inactive (10 μM) ^b	

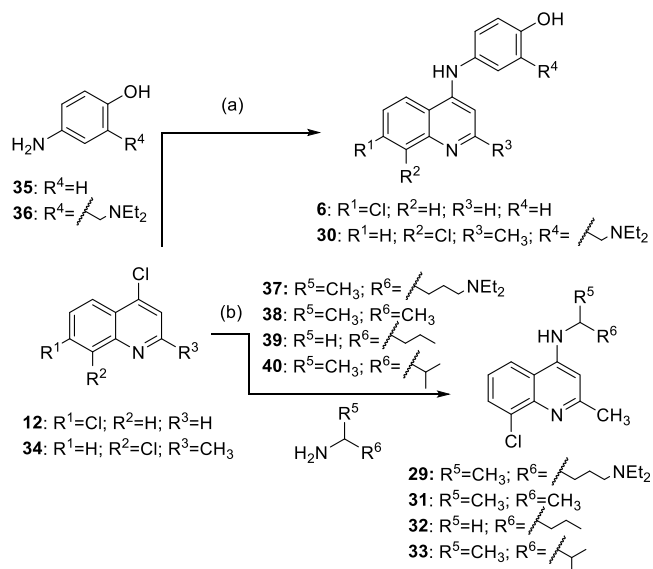
^aActivity was determined in a Gal4-Nurr1 hybrid reporter gene assay. EC₅₀ and IC₅₀ values are the mean ± SD; *n* ≥ 3. Max. fold activation refers to fold reporter activity compared to DMSO (0.1%) treated cells. ^bInactive: no significant effect on reporter activity (≥1.5-fold activation or compared to Gal4-VP16 at the highest nontoxic concentration as indicated).

systematically varying its substitution pattern, we discovered potent, fragment-like Nurr1 agonists (**24** and **26**), which activated Nurr1 in cellular and cell-free settings. **26** evolves as a valuable chemical tool to probe molecular mechanisms of Nurr1 activation. In contrast to AQ and CQ, whose tool compound applicability is hindered by nonspecific effects on transcriptional activity,¹³ **26** overcomes this limitation. Using **26** for functional studies, we observed robust recruitment of the nuclear receptor co-regulators NCoR1 and NCoR2 to Nurr1 by **26** and a promoting effect on Nurr1 homodimerization, which provide improved understanding of molecular Nurr1 activation mechanisms.

RESULTS AND DISCUSSION

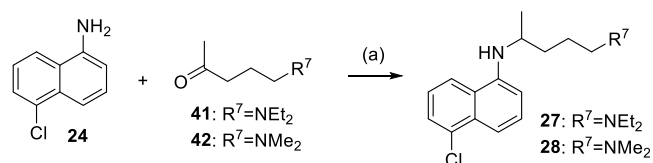
Chemistry. Nurr1 modulators **4–33** were synthesized according to Schemes 1 and 2 or commercially available. **6** and **29–33** were prepared from the respective 4-chloroquinolines **12** and **34** and the respective amines **35–40** by nucleophilic aromatic substitution according to a previously reported procedure to **6**¹⁴ with suitable adaptations (Scheme 1). **27** and **28** were generated by reductive amination from 5-

Scheme 1. Synthesis of 6 and 29–33^a



^aReagents and conditions: (a) KI, EtOH, 2 N HCl, 90 °C, 14–20 h; (b) EtOH, μw, 140 °C, 36–48 h.

Scheme 2. Synthesis of 27 and 28^a



^aReagents and conditions: (a) HOAc, DCE, room temperature, 30 min; then NaB(OAc)₃H, DCE, 50 °C, 24 h.

chloronaphthalen-1-amine (**24**) and the respective ketones **41** and **42** (Scheme 2).

Biological Evaluation. A cellular hybrid reporter gene assay in HEK293 cells served as a primary test system to determine Nurr1 modulation by **1–33**. This assay is based on a hybrid receptor construct composed of the human Nurr1 LBD and the Gal4 DNA binding domain from yeast. A Gal4-sensitive firefly luciferase construct served as the reporter gene, and constitutively expressed renilla luciferase (SV40 promoter) was used to normalize for transfection efficiency and to monitor test compound toxicity. In agreement with the constitutively active nature of Nurr1,¹ the chimeric Gal4-Nurr1 receptor displays strong intrinsic transcriptional inducer activity also in the absence of a ligand. As a control experiment, all tested compounds were assessed for unspecific effects on reporter activity in an analogous setting with the potent transcriptional inducer Gal4-VP16¹⁵ replacing Gal4-Nurr1 (Figure S1). By providing insights into the type of activity (agonist or inverse agonist), potency, and efficacy of the tested compounds, this hybrid reporter gene assay appeared as the most suitable primary test system, especially since knowledge on Nurr1-interacting co-regulators and their response to ligands as the basis for cell-free recruitment assays is still limited.¹⁶

For further insights into cellular Nurr1 modulation in more physiological settings, selected compounds were profiled for activation of full-length human Nurr1 as the monomer, homodimer, or RXR-heterodimer. For this, firefly reporter

constructs comprising a single repeat of the respective human response elements of monomeric Nurr1 (NBRE), the Nurr1 homodimer (NurRE), or the RXR-Nurr1 heterodimer (DRS) in front of the reporter gene were used. Nurr1 and, in the case of DRS, also RXR α were overexpressed using CMV promoter-dependent expression constructs. As for the hybrid Gal4-Nurr1 assay, constitutively expressed renilla luciferase served for normalization purposes. In addition, effects of selected compounds on Nurr1-regulated gene expression were evaluated in Nurr1 expressing¹⁷ T98G glioblastoma cells on the mRNA level by quantitative real-time polymerase chain reaction (qRT-PCR).

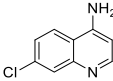
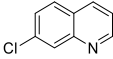
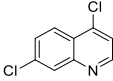
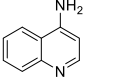
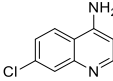
Nurr1 modulation was also studied in cell-free, homogeneous time-resolved fluorescence resonance energy transfer (HTRF)-based settings using Tb³⁺-cryptate-labeled co-regulator peptides derived from NCoR1 and NCoR2 as FRET donors and recombinant, GFP-labeled Nurr1 LBD protein as the FRET acceptor.

Structure–Activity Relationship. All three reported Nurr1 activators AQ (1), CQ (2), and glafenine (3) share an identical 4-amino-7-chloroquinoline scaffold prompting the hypothesis that this shared structural feature strongly contributes to their biological activity on Nurr1. To preliminarily test this assumption, we determined the Nurr1 modulatory activity of a small series of further 4-amino-7-chloroquinoline derivatives (4–10, Table 1).

AQ (1) and CQ (2) activated Gal4-Nurr1 with intermediate micromolar EC₅₀ values of 36 ± 4 μM (3.6 ± 0.1 max. fold activation) and 47 ± 5 μM (2.0 ± 0.1 max. fold activation), respectively, which agreed with their reported activities³ and validated our in vitro test system. Glafenine (3) turned out to be too toxic to be reasonably characterized in the cellular setting. The minimal shared structure 4-amino-7-chloroquinoline (4) of AQ (1) and CQ (2) was indeed sufficient to activate Nurr1 despite lower potency in a high micromolar range. AQ analogue 5 lacking the phenolic hydroxyl group retained reduced Nurr1 agonistic potency, too, while removal of the diethylaminomethyl motif (6) resulted in full loss of activity. Replacement of the basic side chain of AQ (1) and CQ (2) by a butyric acid motif of similar size in 7 produced an inverse agonist that markedly reduced the transcriptional activity of Nurr1. A small lipophilic isopentyl side chain residue (8) recovered Nurr1 agonism with a remarkable 1.8 μM EC₅₀ value but low activation efficacy. The bulkier 4-methylcyclohexyl- (9) and benzyl- (10) derivatives failed to modulate Nurr1 activity. These preliminary SAR observations indicate that the side chain motif contributes to Nurr1 modulation but characterize the 4-amino-7-chloroquinoline (4) as the key structural feature for Nurr1 modulation. Intrigued by the observation that the fragment-sized structure 4 was sufficient to activate Nurr1, we studied the SAR of the isolated chloroquinoline-amine motif individually.

First, we evaluated the individual contributions of structural features of 4 to Nurr1 activation by their systematic removal (Table 2). 7-Chloroquinoline (11) lacking the 4-amino group revealed inverse Nurr1 agonism with moderate repressor efficacy, while 4,7-dichloroquinoline (12) was inactive pointing to an important contribution of the amino group to Nurr1 activation. 4-Aminoquinoline (13) lacking the 7-chlorine substituent was inactive, too, indicating the chlorine as another important feature for Nurr1 agonism. Introduction of an additional methyl group in the 2-position of the 4-amino-7-

Table 2. Contribution of Chlorine and Amine Residues in the Chloroquinolineamine Scaffold. Biological Activity of 11–14 on Nurr1 In Vitro^a

ID	structure	Nurr1	
		Activity type	EC ₅₀ (max. fold act.)
4		Agonist	259±70 μM (2.5±0.4)
11		Inverse agonist	IC ₅₀ =89±14 μM
12		inactive (300 μM) ^b	
13		inactive (300 μM) ^b	
14		Agonist	33±5 μM (2.3±0.2)

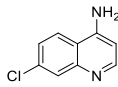
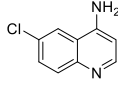
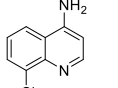
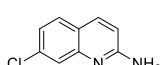
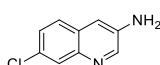
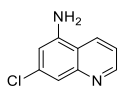
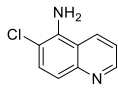
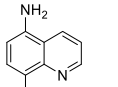
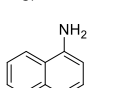
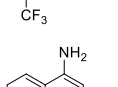
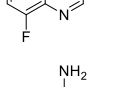
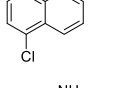
^aActivity was determined in a Gal4-Nurr1 hybrid reporter gene assay. EC₅₀ and IC₅₀ values are the mean ± SD; n ≥ 3. Max. fold activation refers to fold reporter activity compared to DMSO (0.1%) treated cells. ^bInactive: no significant effect on reporter activity (≥1.5-fold activation or compared to Gal4-VP16 at the highest nontoxic concentration as indicated).

chloroquinoline (14) was accompanied with a remarkable gain in potency by almost a factor of 10 compared to 4.

We then systematically varied the regiochemistry of the essential chlorine and amine substituents (Table 3). Shifting the chlorine atom from the 7- (4) to the 6- (15) or 8-position (16) strongly promoted potency on Nurr1, with 8-chloro-4-aminoquinoline (16) as the most favored isomer. For the amine substituent, agonism on Nurr1 was lost when the amino group was moved from the 4-position in 4 to the 2- (17) or 3-position (18), while shifting the amine to the benzoid ring in the 5-position (19) was favored by Nurr1. However, this structural modification turned out to be incompatible with the favored 6- (15) or 8-position (16) of the chlorine substituent since 6-chloro-5-aminoquinoline (20) and 8-chloro-5-aminoquinoline (21) were inactive. When we replaced the 8-chlorine substituent of the preferred chloroquinolineamine isomer 16 by a bulkier trifluoromethyl group (22) or by a smaller fluorine atom (23), we observed a drastic loss in potency, suggesting that the chlorine atom was highly favored in this position. Eventually, we also addressed the contribution of the quinoline nitrogen atom in the favored regioisomer 16 whose removal in naphthalene 24 was favored and promoted potency by a factor of 5, whereas shifting the nitrogen by one position to isoquinoline 25 resulted in inactivity.

The in vitro activities of 11–25 demonstrated the presence and regiochemistry of the amine and chlorine substituents as crucial contributing factors for potency on Nurr1. Additionally, we observed an increase in potency for a methyl group in the 2-position. Combination of this favorable methyl substituent (14) with a preferred regiochemistry of the chlorine and amine substituents (16) in 26 further enhanced potency to a low micromolar EC₅₀ value (Table 4).

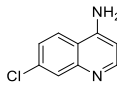
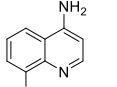
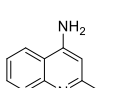
Table 3. SAR and Biological Activity of Chloroquinoline-Amine Regioisomers 15–25 on Nurr1 In Vitro^a

ID	structure	Nurr1	
		Activity type	EC ₅₀ (max. fold act.)
4		Agonist	259±70 μM (2.5±0.4)
15		Agonist	117±24 μM (2.8±0.3)
16		Agonist	49±5 μM (2.6±0.1)
17		inactive (100 μM) ^b	
18		inactive (300 μM) ^b	
19		Agonist	19±4 μM (3.4±0.3)
20		inactive (100 μM) ^b	
21		inactive (100 μM) ^b	
22		inactive (300 μM) ^b	
23		inactive (300 μM) ^b	
24		Agonist	7.3±0.5 μM (5.3±0.2)
25		inactive (200 μM) ^b	

^aActivity was determined in a Gal4-Nurr1 hybrid reporter gene assay. EC₅₀ values are the mean ± SD; n ≥ 3. Max. fold activation refers to fold reporter activity compared to DMSO (0.1%)-treated cells. ^bInactive: no significant effect on reporter activity (≥1.5-fold activation or compared to Gal4-VP16 at the highest nontoxic concentration as indicated).

Our systematic SAR analysis of 4 and analogues as Nurr1 agonists rendered 24 and 26 as the most favorable derivatives. With EC₅₀ values of 7 and 17 μM, respectively, both fragment-like molecules 24 and 26 possess slightly higher potencies on Nurr1 than the template drugs AQ (1) and CQ (2) while

Table 4. Fused SAR in the Chloroquinolineamine Fragment. Biological Activity of 14, 16, and 26 on Nurr1 In Vitro^a

ID	structure	Nurr1	
		Activity type	EC ₅₀ (max. fold act.)
14		Agonist	33±5 μM (2.3±0.2)
16		Agonist	49±5 μM (2.6±0.1)
26		Agonist	17±6 μM (1.71±0.11)

^aActivity was determined in a Gal4-Nurr1 hybrid reporter gene assay. EC₅₀ values are the mean ± SD; n ≥ 3. Max. fold activation refers to fold reporter activity compared to DMSO (0.1%)-treated cells.

comprising markedly lower molecular weights. Accordingly, 24 and 26 are superior in terms of ligand efficiency (LE), lipophilic ligand efficiency (LLE), and size-independent ligand efficiency (SILE)¹⁸ compared to AQ (1) and CQ (2), which were employed as leads (Table 5).

Table 5. Efficiency Metrics of Nurr1 Agonists^a

ID	EC ₅₀ (Nurr1)	LE	LLE ^b	SILE
1	36 ± 4 μM	0.24	-0.39	1.7
2	47 ± 5 μM	0.27	-0.95	1.7
24	7.3 ± 0.5 μM	0.59	1.85	2.4
26	17 ± 6 μM	0.50	1.83	2.2

^aMetrics were calculated as described in ref 18. ^blogP for LLE calculations was retrieved from the ALOGPS 2.1 resource.¹⁹

In an attempt to recombine 24 and 26 with the substituents of the template drugs, we prepared and characterized the respective CQ analogues (Table 6). Compound 27 resulting from fusion of CQ (2) and fragment 24 was active but too toxic for full dose–response characterization on Gal4-Nurr1. Its potency was inferior to fragment 24 but might be a minor improvement over CQ (2). To exclude steric hindrance as a reason for the surprisingly low potency of 27, we studied its smaller dimethyl analogue 28, which was inactive up to 10 μM and toxic at higher concentrations. The fusion of 26 and 2 in 29 was nontoxic but inactive on Gal4-Nurr1 up to high 100 μM concentration. Despite the undesirable nonspecific activities of AQ (1),^{5–10,20,21} we also fused 26 with the AQ side chain, but the resulting compound 30 was inactive, too. These results suggest that recombination of the optimized fragment with the AQ (1) or CQ (2) side chains was not a constructive strategy to achieve further optimization.

The early SAR analysis had also revealed a branched lipophilic side chain (8) as favored for Nurr1 activation. Hence, we additionally probed fusion of this isopentyl motif and related small lipophilic groups with the optimized chloroquinoline fragment 26 (31–33, Table 6). All three derivatives comprising an isopropyl (31), *n*-butyl (32), or isopentyl (33) substituent activated Nurr1 with micromolar

Table 6. Biological Activity of Fused Structures 27–33 on Nurr1 In Vitro^a

ID	structure	Nurr1	
		Activity type	EC ₅₀ (max. fold act.)
27		Agonist	EC ₅₀ n.d., (1.46-fold act. at 20 μM, toxic above)
28		inactive (10 μM) ^b , toxic above	
29		inactive (100 μM) ^b	
30		inactive (100 μM) ^b	
31		Agonist	31±5 μM (2.0±0.2)
32		Agonist	12±1 μM (2.4±0.2)
33		Agonist	17±3 μM (2.3±0.3)

^aActivity was determined in a Gal4-Nurr1 hybrid reporter gene assay. EC₅₀ values are the mean ± SD; n ≥ 3. Max. fold activation refers to fold reporter activity compared to DMSO (0.1%)-treated cells. ^bInactive: no significant effect on reporter activity (≥1.5-fold activation or compared to Gal4-VP16 at the highest nontoxic concentration as indicated).

potencies, but neither modification provided an improvement in potency compared to the fragment **26**. Together, the weak Nurr1 modulatory activities of the fused derivatives **27–33**, hence, indicate that the SAR of the chloroquinoline core and the side chain motif is not additive and that systematic efforts are needed for further optimization.

While compound **24** evolved as the most potent Nurr1 agonist in this study, it also exhibited nonspecific effects on the control gene (renilla luciferase) in our reporter gene assays (Figures S2a and S3). Its efficacy in Nurr1 activation may therefore be overestimated. Control experiments on Gal4-VP16 (Figure S1) and a pronounced increase in Nurr1-induced reporter activity demonstrate, however, that **24**

activates Nurr1 despite nonspecific effects. Of note, the previously reported Nurr1 agonists CQ (**2**) and especially AQ (**1**) cause opposite nonspecific effects on control gene activity (Figure S2a), indicating nonspecific transcriptional activation as already observed by Munoz-Tello et al.¹³ Compound **26**, in contrast, did not affect renilla activity (Figure S2a) and VP16-dependent transcriptional activity (Figure S1), suggesting it as an improved Nurr1 agonist tool with reduced nonspecific effects.

Based on these considerations, **26** evolved as the most attractive fragment descendant of AQ (**1**) and CQ (**2**) for further studies on Nurr1 agonist characteristics. In addition, fragment **24** presents as an attractive starting point for further optimization despite nonspecific activity that will require attention (Figure S2). Hence, we studied the effects of **24** and **26** on Nurr1 activity in more physiological settings involving the full-length human nuclear receptor (Figure 1a and 1b;

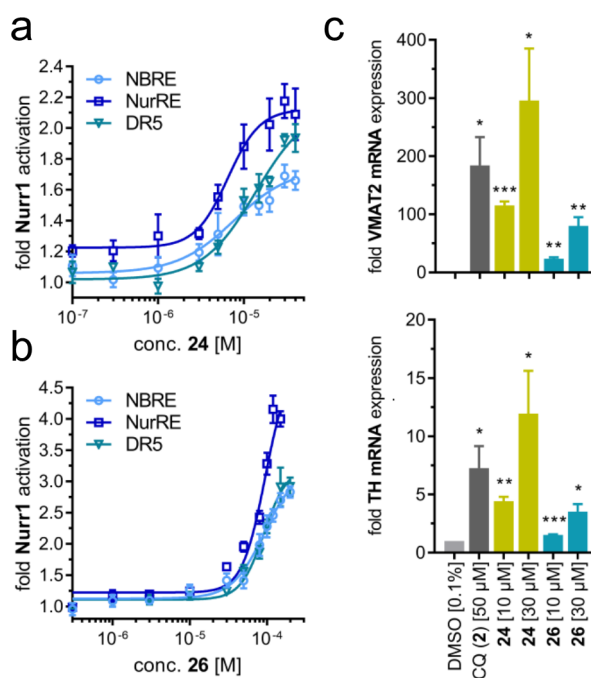


Figure 1. Nurr1 agonism of **24** and **26** in cellular settings. (a, b) Nurr1 agonist activity of (a) **24** and (b) **26** on full-length human Nurr1 as the monomer (NBRE), homodimer (NurRE), and RXR-heterodimer (DR5). Data are the mean ± S.E.M.; n ≥ 3. Individual curves are shown in Figure S4, and corresponding EC₅₀ values are listed in Table S1. (c) Effects of **24** and **26** on mRNA expression of vesicular monoamine transporter 2 (VMAT2) and tyrosine hydroxylase (TH) in human astrocytes (T98G). CQ (**2**) for comparison. Nurr1 agonists **24** and **26** strongly promoted Nurr1-regulated VMAT2 and TH expression in a dose-dependent manner. Data are the mean ± S.E.M.; n = 4. mRNA levels were determined by qRT-PCR and analyzed by the 2^{-ΔΔCt} method. * p < 0.05, ** p < 0.01, *** p < 0.001 vs. DMSO control (t-test).

Figure S4). Both compounds activated the Nurr1 monomer, homodimer, and RXR-heterodimer on the human Nurr1 response elements NBRE, NurRE, and DR5. In line with the hybrid reporter gene assay data (Figure S5), **24** revealed higher potency compared to **26** and CQ (**2**),¹⁶ while **26** activated the human Nurr1 response elements with higher efficacy. To confirm Nurr1 modulation also in an orthogonal native cellular setting, we determined the effects of **24** and **26** on Nurr1-

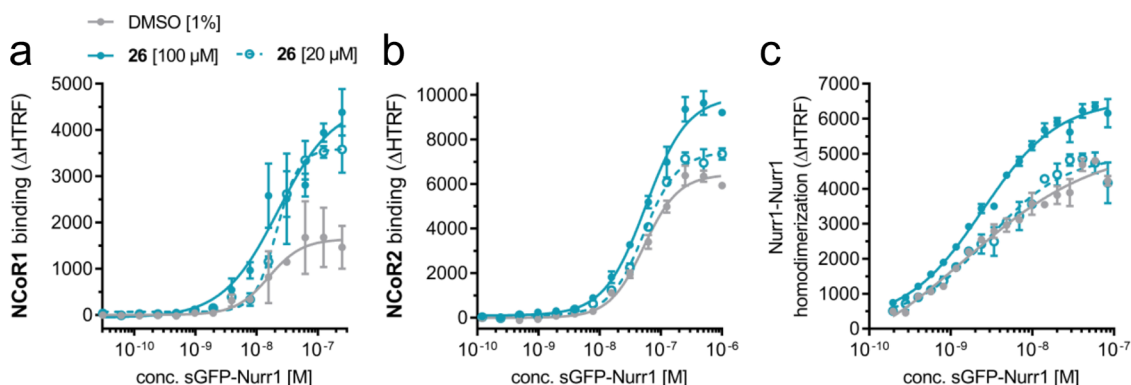


Figure 2. Effects of Nurr1 agonist **26** (20 and 100 μM) on co-regulator recruitment to the Nurr1 LBD in homogeneous time-resolved fluorescence resonance energy transfer (HTRF) assays. (a) Recruitment of Tb^{3+} -cryptate-labeled NCoR1 to the sGFP-labeled Nurr1 LBD. (b) Recruitment of Tb^{3+} -cryptate-labeled NCoR2 to the sGFP-labeled Nurr1 LBD. (c) Homodimerization between the Tb^{3+} -cryptate-labeled and sGFP-labeled Nurr1 LBD. Data are the mean \pm SD; $N = 3$. Compound **24** exhibits comparable effects (Figure S6).

regulated gene expression in Nurr1 expressing¹⁷ human astrocytes (T98G) on the mRNA level (Figure 1c). Both **24** and **26** caused a marked induction of vesicular monoamine transporter 2 (VMAT2; SLC18A2) and tyrosine hydroxylase (TH) in a dose-dependent fashion. These results demonstrate Nurr1 activation by **24** and **26** in various cellular settings, and hence, fully characterize the fragments **24** and **26** as Nurr1 agonists useful as lead compounds for medicinal chemistry and as early tools to study Nurr1 biology.

The chloroquinoline **26** comprises a consistent Nurr1 agonist profile in multiple orthogonal cellular settings including hybrid and full-length Nurr1 reporter gene assays and gene expression studies in native cells. In addition, the compound is characterized by reduced nonspecific effects compared to AQ (**1**) and CQ (**2**) and thus seemed suitable as a tool to study regulatory interactions involving in Nurr1 activation in HTRF-based systems. Using inverse Nurr1 agonists, we have previously discovered a ligand-sensitive interaction of Nurr1 with the nuclear receptor co-repressors NCoR1 and NCoR2.¹⁶ However, the previously available Nurr1 agonists AQ (**1**) and CQ (**2**) exhibited very weak (CQ) or no (AQ) effects at all on the binding of these co-regulators to Nurr1.¹⁶ In addition, their nonspecific transcriptional effects put the applicability of AQ (**1**) and CQ (**2**) as tools into question. The regulatory contributions of the bona fide co-repressors NCoR1 and NCoR2 to Nurr1 activation, thus, remained elusive. Initial experiments (not shown) suggested enhanced recruitment of NCoR1 and NCoR2 upon binding of **26** to the Nurr1 LBD, which aligned with our previous finding that these co-regulators are displaced from Nurr1 by inverse agonists. To avoid any photophysical effects of **26** in studying co-regulator recruitment to Nurr1, we determined NCoR1 and NCoR2 binding by titrating the GFP-labeled Nurr1 LBD in the presence of a fixed concentration of **26** and a fixed concentration of the FRET donor-labeled co-regulator peptide. The FRET acceptor concentration was also kept constant throughout the titration by adding respective amounts of free GFP. This setting ensured that any photophysical effects of **26** were constant over the full curve and that an increase in the HTRF signal only resulted from binding of the labeled co-regulator to the labeled Nurr1 LBD. Using this assay setup, we observed a dose-dependent increase in NCoR1 and NCoR2 recruitment to the Nurr1 LBD in the presence of **26** (20 and 100 μM , Figure 2a and 2b) or **24** (100 μM , Figure S6). In line with the previously discovered co-regulator displacement by

inverse agonists, these results indicate involvement of NCoR1 and NCoR2 binding in Nurr1 activation. This is further supported by the fact that Nurr1 acts as a constitutive transcriptional activator and markedly recruits NCoR1 and NCoR2 also in the apo state (Figure 2a and 2b, DMSO). In addition to effects on NCoR1 and NCoR2 recruitment, we have previously observed a ligand-sensitive dimerization of the Nurr1 LBD,¹⁶ wherein inverse Nurr1 agonists strongly counteracted Nurr1 homodimer formation. In line with this, the Nurr1 activators **24** and **26** enhanced Nurr1 homodimerization (Figure 2c; Figure S6) as another factor likely involving in Nurr1 activation. This observation aligns with the higher agonist efficacy of **26** on the human Nurr1 homodimer response element NurRE (Figure 1b). Hence, the Nurr1 agonist **26** as a tool in HTRF settings revealed increased recruitment of NCoR1 and NCoR2 to the Nurr1 LBD as well as enhanced Nurr1 homodimerization as contributing factors of Nurr1 activation.

CONCLUSIONS

The available collection of direct Nurr1 modulating small molecules is scarce, limiting further efforts to validate Nurr1 as a drug target. Munoz-Tello et al.¹³ have demonstrated that the majority of the putative Nurr1 ligands does not directly interact with the nuclear receptor and thereby characterized the AQ/CQ chemotype as the most suitable starting point for further tool compound development. They have also shown that despite directly activating Nurr1, AQ and CQ have nonspecific effects on transcriptional activity, limiting their applicability as tools to study Nurr1. This aligns with several previously reported activities of the antimalarials^{5–13} and with our observation of elevated control gene transcription upon AQ and CQ treatment.

By fragmentation of the AQ/CQ chemotype of Nurr1 activators and systematic SAR elucidation of the fragment-sized chloroquinoline scaffold, we discovered **24** and **26** as novel Nurr1 agonists. Despite providing only moderately increased potency compared to AQ and CQ, these compounds have remarkably lower size and molecular weight, which make them attractive lead compounds for further expansion and optimization by medicinal chemistry. In addition, while **24** also exhibited nonspecific (potentially cytotoxic) effects on transcriptional activity, **26** had no such activity. Thereby, **26** overcomes one limitation of AQ and CQ as Nurr1 ligands, and

hence, is a valuable early Nurrl agonist tool to study the receptor's molecular and cellular function. Using **26** for extended functional studies, we confirmed the hypothesis that the inverse Nurrl agonist responsive¹⁶ co-regulators NCoR1 and NCoR2 are robustly recruited to Nurrl in the presence of agonists, which together with strengthened Nurrl homodimerization upon binding of **26** provides insights in the activation mechanism of Nurrl.

EXPERIMENTAL SECTION

Chemistry. *General.* All chemicals and solvents for synthesis were obtained from commercial sources in reagent grade and used without further purification. TLC was performed using TLC plates (silica gel 60 F254, 0.2 mm, Merck or Alugram Xtra Sil G/UV 0.2 mm, Macherey-Nagel) with detection under UV light (254 and 366 nm). Preparative column chromatography was performed using Silicagel 60 (Macherey-Nagel) and solvents of technical grade. Reactions with air- or moisture-sensitive compounds were carried out under an argon atmosphere and in anhydrous solvents. NMR spectra were recorded on Bruker AV 500 and AV 600 spectrometers (Bruker Corporation, Billerica, MA, USA). Chemical shifts (δ) are reported in ppm relative to TMS and coupling constants (J) in Hz. Multiplicity of signals is indicated as s for singlet, d for doublet, t for triplet, q for quartet, and m for multiplet. High-resolution mass spectra were recorded on a MALDI LTQ ORBITRAP XL instrument (Thermo Fisher Scientific) or on a Bruker maXis ESI-Qq-TOF-MS instrument (Bruker). Compound purity was analyzed using a Varian ProStar HPLC (SpectraLab Scientific Inc., Markham, ON, Canada) equipped with a MultoHigh100 Phenyl-5 μ 240 + 4 mm column (CS-Chromatographie Service GmbH, Langerwehe, Germany) using a gradient (H₂O/MeOH 80:20 + 0.1% formic acid isocratic for 5 min to MeOH + 0.1% formic acid after additional 45 min and MeOH + 0.1% formic acid for additional 10 min) at a flow rate of 1 mL/min and UV detection at 245 and 280 nm. All final compounds for biological evaluation had a purity >95% according to the AUC at 245 and 280 nm UV detection. Final compounds from commercial sources were obtained from Sigma Aldrich, Enamine, TCI, Fluorochem, abcr, Apollo Scientific or Life Chemicals and had a purity >95% according to the supplier's certificate.

4-((7-Chloroquinolin-4-yl)amino)phenol (**6**). 4,7-Dichloroquinoline (**12**, 0.99 g, 5.0 mmol, 1.0 equiv), 4-aminophenol (**35**, 0.60 g, 5.5 mmol, 1.1 equiv), and a catalytic amount of potassium iodide were dissolved in ethanol (EtOH, 20 mL), aqueous hydrochloric acid (1.0 mL, 2 N) was added dropwise, and the mixture was stirred under reflux for 14 h. After cooling to room temperature, the crude product was filtered off and washed with EtOH to obtain **6** as a yellow solid in 98% yield. ¹H NMR (500 MHz, DMSO-*d*₆): δ = 10.99 (s, 1H), 9.94 (s, 1H), 8.80 (d, J = 9.1 Hz, 1H), 8.45 (d, J = 7.1 Hz, 1H), 8.14 (d, J = 2.0 Hz, 1H), 7.84 (dd, J = 9.1, 2.1 Hz, 1H), 7.30–7.19 (m, 2H), 7.00–6.93 (m, 2H), 6.62 (d, J = 7.0 Hz, 1H). ¹³C NMR (126 MHz, DMSO-*d*₆): δ = 157.09, 155.43, 143.10, 139.02, 138.31, 127.69, 127.23, 127.19 (2C), 125.98, 119.19, 116.49 (2C), 115.66, 99.99. HRMS (MALDI): m/z calculated 271.06327 for C₁₃H₁₂ClN₂O, found 271.06403 ([M + H]⁺).

N⁴-(5-Chloronaphthalen-1-yl)-N¹,N¹-diethylpentane-1,4-diamine (**27**). 5-Chloronaphthalen-1-amine (**24**, 89 mg, 0.50 mmol, 1.0 equiv) and 5-(diethylamino)pentan-2-one (**41**, 73 μ L, 0.55 mmol, 1.1 equiv) were dissolved in 1,2-dichloroethane (10 mL), molecular sieves (4 Å) were added, and the mixture was stirred at room temperature for 2 h. Then, acetic acid (0.75 mL) was added, and the mixture was stirred at 50 °C for another 2 h. NaB(OAc)₃H (0.32 g, 1.5 mmol, 3.0 equiv) was then added, and the mixture was stirred at 50 °C for 24 h. After quenching with aqueous sodium hydroxide solution (100 mL, 1 M), phases were separated, and the aqueous layer was extracted twice with EtOAc (2x 100 mL). The combined organic layers were dried over Na₂SO₄, and solvents were removed under reduced pressure. The crude product was purified by column chromatography in hexane/EtOAc (10:1) + 2% triethylamine to obtain **27** as a brown oil in 45% yield. ¹H NMR (500 MHz, acetone-*d*₆): δ = 8.14 (dt, J = 8.6, 1.0 Hz,

1H), 7.56 (dd, J = 7.4, 1.0 Hz, 1H), 7.51–7.40 (m, 2H), 7.32 (dd, J = 8.6, 7.3 Hz, 1H), 6.74 (dt, J = 7.3, 1.0 Hz, 1H), 5.43 (s, 1H), 3.80–3.71 (m, 1H), 2.54–2.45 (m, 6H), 1.86–1.78 (m, 1H), 1.69–1.58 (m, 3H), 1.30 (d, J = 6.3 Hz, 3H), 0.98 (t, J = 7.1 Hz, 6H). ¹³C NMR (126 MHz, acetone-*d*₆): δ = 144.93, 132.72, 132.44, 129.17, 126.86, 125.65, 124.43, 121.54, 111.98, 105.72, 53.51, 49.24, 47.55 (2C), 35.01, 24.70, 20.63, 12.12 (2C). HRMS (ESI⁺): m/z calculated 320.1973 for C₁₉H₂₈ClN₂, found 320.1982 ([M + H]⁺).

N⁴-(5-Chloronaphthalen-1-yl)-N¹,N¹-dimethylpentane-1,4-diamine (**28**). 5-Chloronaphthalen-1-amine (**24**, 44 mg, 0.25 mmol, 1.0 equiv) and 5-(dimethylamino)pentan-2-one (**42**, 50 mg, 0.33 mmol, 1.3 equiv) were dissolved in 1,2-dichloroethane (10 mL), molecular sieves (4 Å) were added, and the mixture was stirred at room temperature for 2 h. Then, acetic acid (0.75 mL) was added, and the mixture was stirred at 50 °C for another 2 h. NaB(OAc)₃H (0.16 g, 0.75 mmol, 3.0 equiv) was then added, and the mixture was stirred at 50 °C for 24 h. After quenching with aqueous sodium hydroxide solution (50 mL, 1 M), phases were separated, and the aqueous layer was extracted twice with EtOAc (2x 25 mL). The combined organic layers were dried over Na₂SO₄, and solvents were removed under reduced pressure. The crude product was purified by column chromatography with hexane/EtOAc (1:1) and acetone/toluene (20:1) + 2% triethylamine to obtain **28** as a pale brown solid in 25% yield. ¹H NMR (500 MHz, acetone-*d*₆): δ = 8.16 (dt, J = 8.6, 0.9 Hz, 1H), 7.56 (dd, J = 7.4, 1.0 Hz, 1H), 7.51–7.41 (m, 2H), 7.33 (dd, J = 8.6, 7.4 Hz, 1H), 6.73 (dt, J = 7.2, 1.1 Hz, 1H), 3.79–3.73 (m, 1H), 2.50 (t, J = 7.0 Hz, 2H), 2.31 (s, 6H), 1.90–1.61 (m, 4H), 1.30 (d, J = 6.3 Hz, 3H). ¹³C NMR (126 MHz, acetone-*d*₆): δ = 144.93, 132.71, 132.39, 129.17, 126.88, 125.68, 124.46, 121.67, 111.98, 105.63, 59.56, 49.15, 44.76 (2C), 34.70, 24.32, 20.76. HRMS (ESI⁺): m/z calculated 291.1628 for C₁₇H₂₄ClN₂, found 291.1626 ([M + H]⁺).

N⁴-(8-Chloro-2-methylquinolin-4-yl)-N¹,N¹-diethylpentane-1,4-diamine (**29**). 4,8-Dichloro-2-methylquinoline (**34**, 106 mg, 0.5 mmol, 1.0 equiv) and N¹,N¹-diethylpentane-1,4-diamine (**37**, 0.12 mL, 0.6 mmol, 1.2 equiv) were dissolved in EtOH (6 mL). The mixture was stirred under microwave irradiation at 140 °C for 36 h. After cooling to room temperature, the solvent was removed under vacuum. The crude product was purified by column chromatography using a gradient of hexane/EtOAc (5:1) + 2% triethylamine to hexane/EtOAc (1:1) + 2% triethylamine to obtain **29** as a pale yellow solid in 54% yield. ¹H NMR (600 MHz, deuterium oxide): δ = 7.90 (d, J = 8.5 Hz, 1H), 7.75 (d, J = 7.7 Hz, 1H), 7.30 (t, J = 8.0 Hz, 1H), 6.58 (s, 1H), 3.90–3.82 (m, 1H), 3.17 (q, J = 7.2 Hz, 4H), 2.96–2.91 (m, 2H), 2.49 (s, 3H), 1.23 (d, J = 6.3 Hz, 3H), 1.15 (t, J = 7.3 Hz, 6H), 1.06–1.01 (m, 4H). ¹³C NMR (126 MHz, DMSO-*d*₆): δ = 160.90, 150.68, 144.75, 131.99, 130.01, 123.74, 121.57, 119.50, 99.90, 52.34, 49.22, 48.27 (2C), 33.93, 25.84, 23.08, 20.47, 11.44 (2C). HRMS (ESI⁺): m/z calculated 334.2050 for C₁₉H₂₉ClN₃, found 334.2055 ([M + H]⁺).

4-((8-Chloro-2-methylquinolin-4-yl)amino)-2-((diethylamino)-methyl)phenol (**30**). 4,8-Dichloro-2-methylquinoline (**34**, 0.21 g, 1.0 mmol, 1.0 equiv), 4-amino-2-((diethylamino)methyl)phenol dihydrochloride (**36**, 293 mg, 1.1 mmol, 1.1 equiv), and a catalytic amount of potassium iodide were dissolved in EtOH (30 mL), aqueous hydrochloric acid (0.2 mL, 2 N) was added dropwise, and the mixture was stirred under reflux for 20 h. After cooling to room temperature, the mixture was filtered, and the filtrate was concentrated under reduced pressure. The crude product was washed with cold EtOH to obtain **30** as a yellow solid in 51% yield. ¹H NMR (500 MHz, deuterium oxide): δ = 8.18 (dd, J = 8.6, 1.2 Hz, 1H), 7.99 (dd, J = 7.7, 1.2 Hz, 1H), 7.60 (t, 1H), 7.46–7.41 (m, 2H), 7.19–7.14 (m, 1H), 6.67 (s, 1H), 4.37 (s, 2H), 3.30 (dq, J = 10.1, 7.2 Hz, 4H), 2.62 (s, 3H), 1.38 (t, J = 7.3 Hz, 6H). ¹³C NMR (126 MHz, Deuterium Oxide): δ = 156.20, 156.16, 155.95, 135.40, 134.52, 130.28, 129.90, 129.18, 127.36, 124.08, 121.94, 118.78, 117.82, 117.66, 101.72, 52.20, 48.36 (2C), 20.68, 8.83 (2C). HRMS (MALDI): m/z calculated 370.16807 for C₂₁H₂₅ClN₃O, found 370.16737 ([M + H]⁺).

8-Chloro-*N*-isopropyl-2-methylquinolin-4-amine (**31**). 4,8-Dichloro-2-methylquinoline (**34**, 0.11 g, 0.50 mmol, 1.0 equiv) and propan-2-amine (**38**, 51 μ L, 0.60 mmol, 1.2 equiv) were dissolved in EtOH (6.0 mL), and the mixture was stirred for 36 h at 140 °C under microwave irradiation. The solvent was evaporated in vacuum, aqueous sodium hydroxide solution (20 mL) and ethyl acetate (20 mL) were added, phases were separated, and the aqueous layer was extracted two times with ethyl acetate (2x 20 mL). The combined organic layers were dried over Na₂SO₄, and the solvent was evaporated in vacuum. The crude product was purified by column chromatography (hexane/ethyl acetate 5:1 + 2% NEt₃ and hexane/ethyl acetate 1:1 + 2% NEt₃) to obtain the title compound as a yellow oil (15 mg, 13%). ¹H NMR (500 MHz, Acetone-*d*₆): δ = 8.05 (dd, *J* = 8.5, 1.3 Hz, 1H), 7.70 (dd, *J* = 7.4, 1.3 Hz, 1H), 7.29–7.22 (m, 1H), 6.54 (s, 1H), 6.14 (d, *J* = 6.9 Hz, 1H), 4.01–3.90 (m, 1H), 2.54 (s, 3H), 1.34 (d, *J* = 6.4 Hz, 6H). ¹³C NMR (126 MHz, acetone-*d*₆): δ = 160.73, 150.50, 145.82, 133.84, 129.73, 123.57, 120.86, 120.12, 100.33, 44.81, 25.92, 22.31 (2C). HRMS (MALDI): *m/z* calculated 235.09965 for C₁₃H₁₆ClN₂, found 235.10002 ([M + H]⁺).

N-Butyl-8-chloro-2-methylquinolin-4-amine (**32**). 4,8-Dichloro-2-methylquinoline (**34**, 0.11 g, 0.50 mmol, 1.0 equiv) and butan-1-amine (**39**, 73 mg, 1.0 mmol, 2.0 equiv) were dissolved in EtOH (6.0 mL), and the mixture was stirred for 48 h at 140 °C under microwave irradiation. The solvent was evaporated in vacuum, and the crude product was purified by column chromatography (hexane/ethyl acetate 5:1 + 2% NEt₃) to obtain the title compound as a yellow oil (30 mg, 24%). ¹H NMR (500 MHz, CDCl₃): δ = 7.71–7.64 (m, 2H), 7.20 (t, *J* = 8.0 Hz, 1H), 6.26 (s, 1H), 3.27–3.22 (m, 2H), 2.62 (s, 3H), 1.72–1.65 (m, 2H), 1.48–1.40 (m, 2H), 0.94 (t, *J* = 7.4 Hz, 3H). ¹³C NMR (126 MHz, CDCl₃): δ = 159.86, 150.46, 129.63, 123.57, 118.83, 118.61, 99.63, 43.18, 30.92, 25.76, 20.34, 13.85. HRMS (MALDI): *m/z* calculated 249.11530 for C₁₄H₁₈ClN₂, found 249.11583 ([M + H]⁺).

8-Chloro-2-methyl-*N*-(3-methylbutan-2-yl)quinolin-4-amine (**33**). 4,8-Dichloro-2-methylquinoline (**34**, 0.11 g, 0.50 mmol, 1.0 equiv) and 3-methylbutan-2-amine (**40**, 87 mg, 1.0 mmol, 2.0 equiv) were dissolved in EtOH (6.0 mL), and the mixture was stirred for 48 h at 140 °C under microwave irradiation. The solvent was evaporated in vacuum, aqueous sodium hydroxide solution (20 mL) and ethyl acetate (20 mL) were added, phases were separated, and the aqueous layer was extracted two times with ethyl acetate (2x 20 mL). The combined organic layers were dried over Na₂SO₄, and the solvent was evaporated in vacuum. The crude product was purified by column chromatography (hexane/ethyl acetate 5:1 + 2% NEt₃ and hexane/ethyl acetate 1:1 + 2% NEt₃) to obtain the title compound as a green oil (6 mg, 4%). ¹H NMR (500 MHz, MeOD): δ = 8.08 (dd, *J* = 8.5, 1.2 Hz, 1H), 7.70 (dd, *J* = 7.5, 1.2 Hz, 1H), 7.31–7.26 (m, 1H), 6.49 (s, 1H), 3.57 (quint, *J* = 6.7 Hz, 1H), 2.53 (s, 3H), 1.95–1.84 (m, *J* = 6.8, 1H), 1.19 (d, *J* = 6.6, 3H), 0.94–0.91 (m, 6H). ¹³C NMR (126 MHz, MeOD): δ = 159.03, 152.19, 130.57, 123.81, 120.37, 118.63, 99.28, 54.29, 32.47, 22.35, 18.62, 17.36, 15.44. HRMS (MALDI): *m/z* calculated 263.13095 for C₁₅H₂₀ClN₂, found 263.13157 ([M + H]⁺).

Hybrid Gal4-Nurr1 Reporter Gene Assay. *Plasmids.* The Gal4-fusion receptor plasmid pFA-CMV-hNURR1-LBD¹⁶ coding for the hinge region and LBD of the canonical isoform of human Nurr1 has been reported previously. The Gal4-VP16¹⁵ fusion protein expressed from plasmid pECE-SV40-Gal4-VP16²² (Addgene, entry 71728, Watertown, MA, USA) served as a ligand-independent transcriptional inducer for control experiments. pFR-Luc (Stratagene, La Jolla, CA, USA) was used as a reporter plasmid and pRL-SV40 (Promega, Madison, WI, USA) for normalization of transfection efficiency and test compound toxicity. *Assay procedure.* HEK293T cells were grown in DMEM high glucose, supplemented with 10% fetal calf serum (FCS), sodium pyruvate (1 mM), penicillin (100 U/mL), and streptomycin (100 μ g/mL) at 37 °C and 5% CO₂. The day before transfection, HEK293T cells were seeded in 96-well plates (3 × 10⁴ cells/well). The medium was changed to Opti-MEM without supplements right before transfection. Transient transfection was performed using the Lipofectamine LTX reagent (Invitrogen, Carlsbad, CA, USA) according to the manufacturer's protocol with

pFR-Luc (Stratagene), pRL-SV40 (Promega), and the corresponding Gal4-fusion nuclear receptor plasmid pFA-CMV-hNR-LBD. Five hours after transfection, the medium was changed to Opti-MEM supplemented with penicillin (100 U/mL) and streptomycin (100 μ g/mL), now additionally containing 0.1% DMSO and the respective test compound or 0.1% DMSO alone as untreated control. Each concentration was tested in duplicates, and each experiment was performed independently at least three times. The Gal4-VP16 control experiments were carried out in duplicates as well, with at least four independent repeats. Following overnight (12–14 h) incubation with the test compounds, the cells were assayed for luciferase activity using the Dual-GloTM Luciferase Assay System (Promega) according to the manufacturer's protocol. Luminescence was measured with a Spark 10 M luminometer (Tecan Group AG, Männedorf, Switzerland). Normalization of transfection efficiency and cell growth were done by division of firefly luciferase data by renilla luciferase data and multiplying the value by 1000 resulting in relative light units (RLU). Fold activation was obtained by dividing the mean RLU of a test compound at a respective concentration by the mean RLU of untreated control. The hybrid assay was validated with amodiaquine and chloroquine as reference agonists, which yielded EC₅₀ values in agreement with the literature. For dose–response curve fitting and calculation of EC₅₀/IC₅₀ values, the equations “[Agonist]/[Inhibitor] vs. response – variable slope (four parameters)” were performed with mean fold activations \pm SD using GraphPad Prism (version 7.00, GraphPad Software, La Jolla, CA, USA).

Full-Length Nurr1 Reporter Gene Assays. *Plasmids:* The reporter plasmids pFR-Luc-NBRE,¹⁶ pFR-Luc-NurRE,¹⁶ and pFR-Luc-DR5¹⁶ each containing one copy of the respective human Nurr1 response element NBRE N13 (TGATATCGAAAACAAAGGTCA), NurRE (from POMC; TGATATTTACCTCCAATGCCA), or DR5 (TGATAGGTTACCGAAAGGTCA) were described previously. The full length human nuclear receptor Nurr1 (pcDNA3.1-hNurr1-NE; Addgene, entry 102363) and, for DR5, RXR α (pSG5-hRXR²³) were overexpressed. pFL-SV40 (Promega) was used for normalization of transfection efficacy and evaluation of compound toxicity. *Assay procedure:* HEK293T cells were grown in DMEM high glucose, supplemented with 10% FCS, sodium pyruvate (1 mM), penicillin (100 U/mL), and streptomycin (100 μ g/mL) at 37 °C and 5% CO₂. The day before transfection, HEK293T cells were seeded in 96-well plates (3 × 10⁴ cells/well). The medium was changed to Opti-MEM without supplements right before transfection. Transient transfection was performed using the Lipofectamine LTX reagent (Invitrogen) according to the manufacturer's protocol with pFR-Luc-NBRE,¹⁶ pFR-Luc-NurRE¹⁶ or pFR-Luc-DR5,¹⁶ pRL-SV40 (Promega), the human full length receptor plasmid pcDNA3.1-hNurr1-NE, and, for DR5, also pSG5-hRXR²³. Five hours after transfection, the medium was changed to Opti-MEM supplemented with penicillin (100 U/mL) and streptomycin (100 μ g/mL), now additionally containing 0.1% DMSO and the respective test compound or 0.1% DMSO alone as untreated control. For full dose–response characterization, each concentration was tested in duplicates and each experiment was performed independently at least three times. Following overnight (12–14 h) incubation with the test compounds, the cells were assayed for luciferase activity using a Dual-GloTM Luciferase Assay System (Promega) according to the manufacturer's protocol. Luminescence was measured with a Spark 10 M luminometer (Tecan Group AG). Normalization of transfection efficiency and cell growth were done by division of firefly luciferase data by renilla luciferase data and multiplying the value by 1000 resulting in RLU. Fold activation was obtained by dividing the mean RLU of a test compound at a respective concentration by the mean RLU of untreated control. The full length Nurr1 reporter gene assays were validated with amodiaquine and chloroquine as reference agonists.

Nurr1 Co-Regulator Recruitment Assays. Interaction of co-regulator peptides to the Nurr1-LBD was studied in a homogeneous time-resolved fluorescence resonance energy transfer (HT-FRET) assay system. Terbium cryptate as streptavidin conjugate (Tb-SA; Cisbio Bioassays, Codolet, France) was used as FRET donor for stable coupling to biotinylated co-regulator peptides NCoR1 or

NCoR2. As FRET acceptor, recombinant Nurr1-LBD protein¹⁶ fused to sGFP was used, which has been reported previously. GFP-Nurr1-LBD was titrated against biotinylated NCoR1 (1 nM) or NCoR2 (18 nM) copeptide and Tb-SA (2 or 12 nM, respectively) in the presence of a fixed concentration (20 or 100 μ M, in assay buffer containing 1% DMSO) of the respective ligand or 1% DMSO. To maintain a constant GFP concentration, free GFP protein was added to the dilution series. The experiments were performed in HTRF assay buffer (150 mM KF, 25 mM HEPES pH 7.5 (KOH), 5% (w/v) Glycerol, supplemented with 0.1% (w/v) CHAPS and 5 mM DTT) with 1% DMSO in an assay volume of 20 μ L. All HTRF experiments were carried out in a 384-well format using white flat bottom polystyrol microtiter plates (Greiner Bio-One, Frickenhausen, Germany), and each concentration was tested in technical triplicates. After 1 h incubation at room temperature, fluorescence intensities after excitation at 340 nm were recorded at 520 nm for GFP acceptor fluorescence and 620 nm for Tb-SA donor fluorescence on a SPARK plate reader (Tecan Group Ltd.). FI520nm was divided by FI620nm and multiplied with 10,000 to give a dimensionless HTRF signal. Δ HTRFs were calculated as differences between each individual HTRF value and the corresponding untreated control (1% DMSO) of the same dissolution series. For the dose–response curve fitting, the equation “[Agonist] vs. response – variable slope (four parameters)” was performed with three replicate values of Δ HTRF using GraphPad Prism (version 7.00, GraphPad Software). The co-regulator peptides were purchased from Eurogentec (Seraing, Belgium), and sequences were the following: nuclear receptor co-repressor 1 (NCoR1) nuclear receptor-interaction domain 1 (ID1), Biotin-GMGQVPRTHRLI-TLADHICQIITQDFARN-COOH; and NCoR2 ID2, Biotin-SQAV-HEASTNMGLEAIIRKALMGKYDQW-COOH.

Nurr1 Homodimerization Assay. Modulation of Nurr1 LBD homodimerization was studied in an HT-FRET assay setup using the biotinylated recombinant Nurr1 LBD¹⁶ and GFP-Nurr1 LBD. Assay solutions were prepared in HTRF assay buffer supplemented with 0.1% (w/v) CHAPS and 5 mM DTT as well as 1% DMSO with test compounds **24** (100 μ M) and **26** (20 or 100 μ M) or DMSO alone as negative control. The biotinylated Nurr1 LBD (0.375 nM) and Tb-SA (0.75 nM) served as the FRET donor complex, which was kept constant, while the GFP-coupled protein as the FRET acceptor was varied in concentration. Titration of the GFP-Nurr1 LBD started at 500 nM, and each concentration was tested in technical triplicates. Accordingly, free GFP was added to keep the total GFP content stable throughout the entire series in order to suppress artifacts from changes in the degree of diffusion-enhanced FRET. The samples were equilibrated at room temperature for 2 h before FI520nm and FI620nm were recorded after excitation at 340 nm, and the HTRF signal, Δ HTRF, and dose–response curves were calculated as described above.

Quantification of Nurr1-Regulated mRNA Expression in T98G Cells by qRT-PCR. T98G cells were grown in 6-well plates (2.5×10^5 cells/well) in DMEM high glucose, supplemented with 10% FCS, sodium pyruvate (1 mM), penicillin (100 U/mL), and streptomycin (100 μ g/mL) at 37 °C and 5% CO₂. Before incubation with test compounds, the medium was changed to DMEM supplemented with 1% charcoal-stripped FCS, sodium pyruvate (1 mM), penicillin (100 U/mL), and streptomycin (100 μ g/mL) for 24 h. For gene expression analysis, the cells were incubated with **2** (50 μ M), **24** (10 or 30 μ M), **26** (10 or 30 μ M), or 0.1% DMSO as untreated control for 8 h. The cells were then harvested and directly used for RNA extraction. Total RNA (3 μ g) was extracted from T98G cells by the E.Z.N.A. Total RNA Kit I (R6834–02, Omega Bio-Tek, Inc., Norcross, GA). RNA was reverse-transcribed into cDNA using the High-Capacity RNA-to-cDNA Kit (4387406, Thermo Fischer Scientific, Inc.) according to the manufacturer’s protocol. Nurr1 target gene expression was evaluated by qRT-PCR analysis with a StepOnePlus System (Life Technologies, Carlsbad, CA) using Power SYBR Green (Life Technologies; 12.5 μ L/well). Each sample was set up in duplicates and repeated in four independent experiments. The expression was quantified by the comparative 2^{– $\Delta\Delta$ Ct} method, and glyceraldehyde 3-phosphate dehydrogenase

(GAPDH) served as the reference gene. Primer sequences for Nurr1 target genes vesicular monoamine transporter 2 (VMAT2) and tyrosine hydroxylase (TH) were obtained from OriGene (OriGene Technologies Inc., Rockville, MD, USA). The following PCR primers were used: hGAPDH: 5'-ATA TGA TTC CAC CCA TGG CA (fw), 5'-GAT GAT GAC CCT TTT GGC TC (rev), hVMAT2: 5'-GCT ATG CCT TCC TGC TGA TTG C (fw), 5'-CCA AGG CGA TTC CCA TGA CGT T (rev), and hTH: 5'-GCT GGA CAA GTG TCA TCA CCT G (fw), and 5'-CCT GTA CTG GAA GGC GAT CTC A (rev).

■ ASSOCIATED CONTENT

Supporting Information

The Supporting Information is available free of charge at <https://pubs.acs.org/doi/10.1021/acs.jmedchem.0c01779>.

Control experiments; nonspecific effects and cytotoxicity; raw luminescence data; effects of Nurr1 agonist **24**; summarized cellular Nurr1 modulatory activities; and WST-1 toxicity assay (PDF)

HPLC traces of compounds synthesized in this study (PDF)

Molecular formula strings with structures and activity data (csv)

■ AUTHOR INFORMATION

Corresponding Author

Daniel Merk – Institute of Pharmaceutical Chemistry, Goethe University, D-60438 Frankfurt, Germany; orcid.org/0000-0002-5359-8128; Email: merk@pharmchem.uni-frankfurt.de

Authors

Sabine Willems – Institute of Pharmaceutical Chemistry, Goethe University, D-60438 Frankfurt, Germany

Julia Ohrndorf – Institute of Pharmaceutical Chemistry, Goethe University, D-60438 Frankfurt, Germany

Whitney Kilu – Institute of Pharmaceutical Chemistry, Goethe University, D-60438 Frankfurt, Germany

Jan Heering – Fraunhofer Institute for Translational Medicine and Pharmacology ITMP, D-60596 Frankfurt am Main, Germany

Complete contact information is available at: <https://pubs.acs.org/doi/10.1021/acs.jmedchem.0c01779>

Author Contributions

All authors have given approval to the final version of the manuscript.

Notes

The authors declare no competing financial interest.

■ ACKNOWLEDGMENTS

This research was financially supported by the Aventis Foundation (Life Science Bridge Award to D.M.) and the LOEWE center Translational Medicine and Pharmacology (TMP). Gal4-VP16 was a gift from Lea Sistonen (Addgene plasmid # 71728 ; <http://n2t.net/addgene:71728> ; RRID:Addgene_71728). pcDNA3.1-hNurr1-NE was a gift from Shu Leong Ho (Addgene plasmid # 102363 ; <http://n2t.net/addgene:102363> ; RRID:Addgene_102363).

■ ABBREVIATIONS

AQ, amodiaquine; CQ, chloroquine; DR5, direct repeats spaced by five nucleotides; FRET, fluorescence resonance

energy transfer; GFP, green fluorescent protein; HTRF, homogeneous time-resolved fluorescence resonance energy transfer; LBD, ligand binding domain; LE, ligand efficiency; LLE, lipophilic ligand efficiency; NBRE, NGFI-B response element; NCoR1, nuclear receptor co-repressor 1; NCoR2, nuclear receptor co-repressor 2; Nurr1, nuclear receptor related 1; NurRE, Nur-response element; PD, Parkinson's Disease; qRT-PCR, quantitative real-time polymerase chain reaction; SAR, structure–activity relationship; SILE, size-independent ligand efficiency; TH, tyrosine hydroxylase; VMAT2, vesicular monoamine transporter 2; VP16, Herpes simplex virus protein vmw65

REFERENCES

- (1) Wang, Z.; Benoit, G.; Liu, J.; Prasad, S.; Aarnisalo, P.; Liu, X.; Xu, H.; Walker, N. P.; Perlmann, T. Structure and Function of Nurr1 Identifies a Class of Ligand-Independent Nuclear Receptors. *Nature* **2003**, *423*, 555–560.
- (2) Decressac, M.; Volakakis, N.; Björklund, A.; Perlmann, T. NURR1 in Parkinson Disease—From Pathogenesis to Therapeutic Potential. *Nat. Rev. Neurol.* **2013**, *9*, 629–636.
- (3) Kim, C.-H.; Han, B.-S.; Moon, J.; Kim, D.-J.; Shin, J.; Rajan, S.; Nguyen, Q. T.; Sohn, M.; Kim, W.-G.; Han, M.; Jeong, I.; Kim, K.-S.; Lee, E.-H.; Tu, Y.; Naffin-Olivos, J. L.; Park, C.-H.; Ringe, D.; Yoon, H. S.; Petsko, G. A.; Kim, K.-S. Nuclear Receptor Nurr1 Agonists Enhance Its Dual Functions and Improve Behavioral Deficits in an Animal Model of Parkinson's Disease. *Proc. Natl. Acad. Sci.* **2015**, *112*, 8756–8761.
- (4) Rajan, S.; Jang, Y.; Kim, C. H.; Kim, W.; Toh, H. T.; Jeon, J.; Song, B.; Serra, A.; Lescar, J.; Yoo, J. Y.; Beldar, S.; Ye, H.; Kang, C.; Liu, X. W.; Feitosa, M.; Kim, Y.; Hwang, D.; Goh, G.; Lim, K. L.; Park, H. M.; Lee, C. H.; Oh, S. F.; Petsko, G. A.; Yoon, H. S.; Kim, K.-S. PGE1 and PGA1 Bind to Nurr1 and Activate Its Transcriptional Function. *Nat. Chem. Biol.* **2020**, *16*, 876–886.
- (5) De Bruyn, T.; Van Westen, G. J. P.; IJzerman, A. P.; Stieger, B.; De Witte, P.; Augustijns, P. F.; Annaert, P. P. Structure-Based Identification of Oatp1b1/3 Inhibitors. *Mol. Pharmacol.* **2013**, *83*, 1257–1267.
- (6) Lee, S. G.; Alpert, T. D.; Jez, J. M. Crystal Structure of Phosphoethanolamine Methyltransferase from *Plasmodium falciparum* in Complex with Amodiaquine. *Bioorganic Med. Chem. Lett.* **2012**, *22*, 4990–4993.
- (7) Ren, S.; Zeng, J.; Mei, Y.; Zhang, J. Z. H.; Yan, S. F.; Fei, J.; Chen, L. Discovery and Characterization of Novel, Potent, and Selective Cytochrome P450 2J2 Inhibitors. *Drug Metab. Dispos.* **2012**, *41*, 60–71.
- (8) O'Neill, P. M.; Park, B. K.; Shone, A. E.; Maggs, J. L.; Roberts, P.; Stocks, P. A.; Biagini, G. A.; Bray, P. G.; Gibbons, P.; Berry, N.; Winstanley, P. A.; Mukhtar, A.; Bonar-Law, R.; Hindley, S.; Bambal, R. B.; Davis, C. B.; Bates, M.; Hart, T. K.; Gresham, S. L.; Lawrence, R. M.; Brigandi, R. A.; Gomez-delas-Heras, F. M.; Gargallo, D. V.; Ward, S. A. Candidate Selection and Preclinical Evaluation of N-Tert-Butyl Isoquine (GSK369796), an Affordable and Effective 4-Aminoquinoline Antimalarial for the 21st Century. *J. Med. Chem.* **2009**, *52*, 1408–1415.
- (9) Kim, T. H.; Kim, H. K.; Hwang, E. S. Novel Anti-adipogenic Activity of Anti-malarial Amodiaquine Through Suppression of PPAR γ Activity. *Arch. Pharmacol. Res.* **2017**, *40*, 1336–1343.
- (10) Tang, Y.; Wu, Q.; Beland, F. A.; Chen, S.; Fang, J. L. Apoptosis Contributes to the Cytotoxicity Induced by Amodiaquine and Its Major Metabolite N-Desethylamodiaquine in Hepatic Cells. *Toxicol. Vitro.* **2020**, *62*, No. 104669.
- (11) Gordon, D. E.; Jang, G. M.; Bouhaddou, M.; Xu, J.; Obernier, K.; White, K. M.; O'Meara, M. J.; Rezelj, V. V.; Guo, J. Z.; Swaney, D. L.; Tummino, T. A.; Hüttenhain, R.; Kaake, R. M.; Richards, A. L.; Tutuncuoglu, B.; Foussard, H.; Batra, J.; Haas, K.; Modak, M.; Kim, M.; Haas, P.; Polacco, B. J.; Braberg, H.; Fabius, J. M.; Eckhardt, M.; Souheray, M.; Bennett, M. J.; Cakir, M.; McGregor, M. J.; Li, Q.; Meyer, B.; Roesch, F.; Vallet, T.; Mac Kain, A.; Miorin, L.; Moreno, E.; Naing, Z. Z. C.; Zhou, Y.; Peng, S.; Shi, Y.; Zhang, Z.; Shen, W.; Kirby, I. T.; Melynyk, J. E.; Chorba, J. S.; Lou, K.; Dai, S. A.; Barrio-Hernandez, I.; Memon, D.; Hernandez-Armenta, C.; Lyu, J.; Mathy, C. J. P.; Perica, T.; Pilla, K. B.; Ganesan, S. J.; Saltzberg, D. J.; Rakesh, R.; Liu, X.; Rosenthal, S. B.; Calviello, L.; Venkataramanan, S.; Liboy-Lugo, J.; Lin, Y.; Huang, X. P.; Liu, Y.; Wankowicz, S. A.; Bohn, M.; Safari, M.; Ugur, F. S.; Koh, C.; Savar, N. S.; Tran, Q. D.; Shengjuler, D.; Fletcher, S. J.; O'Neal, M. C.; Cai, Y.; Chang, J. C. J.; Broadhurst, D. J.; Klippsten, S.; Sharp, P. P.; Wenzell, N. A.; Kuzuoglu-Ozturk, D.; Wang, H. Y.; Trenker, R.; Young, J. M.; Caverio, D. A.; Hiatt, J.; Roth, T. L.; Rathore, U.; Subramanian, A.; Noack, J.; Hubert, M.; Stroud, R. M.; Frankel, A. D.; Rosenberg, O. S.; Verba, K. A.; Agard, D. A.; Ott, M.; Emerman, M.; Jura, N.; von Zastrow, M.; Verdine, E.; Ashworth, A.; Schwartz, O.; d'Enfert, C.; Mukherjee, S.; Jacobson, M.; Malik, H. S.; Fujimori, D. G.; Ideker, T.; Craik, C. S.; Floor, S. N.; Fraser, J. S.; Gross, J. D.; Sali, A.; Roth, B. L.; Ruggiero, D.; Taunton, J.; Kortemme, T.; Beltrao, P.; Vignuzzi, M.; Garcia-Sastre, A.; Shokat, K. M.; Shoichet, B. K.; Krogan, N. J. A SARS-CoV-2 Protein Interaction Map Reveals Targets for Drug Repurposing. *Nature* **2020**, *583*, 459–468.
- (12) Nolan, K. A.; Caraher, M. C.; Humphries, M. P.; Bettley, H. A. A.; Bryce, R. A.; Stratford, I. J. In Silico Identification and Biochemical Evaluation of Novel Inhibitors of NRH:Quinone Oxidoreductase 2 (NQO2). *Bioorganic Med. Chem. Lett.* **2010**, *20*, 7331–7336.
- (13) Munoz-Tello, P.; Lin, H.; Khan, P.; De Vera, I. M. S.; Kamenecka, T. M.; Kojetin, D. J. Assessment of NR4A Ligands That Directly Bind and Modulate the Orphan Nuclear Receptor Nurr1. *J. Med. Chem.* **2020**, *63*, 15639–15654.
- (14) Apelt, J.; Ligneau, X.; Pertz, H. H.; Arrang, J.; Ganellin, C. R.; Schwartz, J.-C.; Schunack, W.; Stark, H. Development of a New Class of Nonimidazole Histamine H₃ Receptor Ligands with Combined Inhibitory Histamine N-Methyltransferase Activity. *J. Med. Chem.* **2002**, *45*, 1128–1141.
- (15) Sadowski, L.; Ma, J.; Triezenberg, S.; Ptashne, M. GAL4-VP16 Is an Unusually Potent Transcriptional Activator. *Nature* **1988**, *335*, 563–564.
- (16) Willems, S.; Kilu, W.; Ni, X.; Chaikuad, A.; Knapp, S.; Heering, J.; Merk, D. The Orphan Nuclear Receptor Nurr1 Is Responsive to Non-steroidal Anti-inflammatory Drugs. *Commun. Chem.* **2020**, *3*, 85.
- (17) Karki, K.; Li, X.; Jin, U. H.; Mohankumar, K.; Zarei, M.; Michelhaugh, S. K.; Mittal, S.; Tjalkens, R.; Safe, S. Nuclear Receptor 4A2 (NR4A2) Is a Druggable Target for Glioblastomas. *J. Neurooncol.* **2020**, *146*, 25–39.
- (18) Hopkins, A. L.; Keserü, G. M.; Leeson, P. D.; Rees, D. C.; Reynolds, C. H. The Role of Ligand Efficiency Metrics in Drug Discovery. *Nat. Rev. Drug Discov.* **2014**, *13*, 105–121.
- (19) Tetko, I. V.; Tanchuk, V. Y. Application of Associative Neural Networks for Prediction of Lipophilicity in ALOGPS 2.1 Program. *J. Chem. Inf. Comput. Sci.* **2002**, *42*, 1136–1145.
- (20) Niu, Y. R.; Wei, B.; Chen, B.; Xu, L. H.; Jing, X.; Peng, C. L.; Ma, T. Z. Amodiaquine-Induced Reproductive Toxicity in Adult Male Rats. *Mol. Reprod. Dev.* **2016**, *83*, 174–182.
- (21) Bernuau, J.; Larrey, D.; Campillo, B.; Degott, C.; Verdier, F.; Rueff, B.; Pessayre, D.; Benhamou, J. P. Amodiaquine-Induced Fulminant Hepatitis. *J. Hepatol.* **1988**, *6*, 109–112.
- (22) Budzyński, M. A.; Puustinen, M. C.; Joutsen, J.; Sistonen, L. Uncoupling Stress-Inducible Phosphorylation of Heat Shock Factor 1 from Its Activation. *Mol. Cell. Biol.* **2015**, *35*, 2530–2540.
- (23) Merk, D.; Lamers, C.; Ahmad, K.; Carrasco Gomez, R.; Schneider, G.; Steinhilber, D.; Schubert-Zsilavecz, M. Extending the Structure-Activity Relationship of Anthranilic Acid Derivatives as Farnesoid x Receptor Modulators: Development of a Highly Potent Partial Farnesoid X Receptor Agonist. *J. Med. Chem.* **2014**, *57*, 8035–8055.

Fragment-like chloroquinolineamines activate the orphan nuclear receptor Nurr1 and elucidate activation mechanisms

Sabine Willems¹, Julia Ohrndorf¹, Whitney Kilu¹, Jan Heering², Daniel Merk^{1*}

¹ Institute of Pharmaceutical Chemistry, Goethe University Frankfurt, Max-von-Laue-Str. 9, 60438 Frankfurt, Germany

² Fraunhofer Institute for Translational Medicine and Pharmacology ITMP, Theodor-Stern-Kai 7, 60596 Frankfurt, Germany

- Supporting Information -

Table of contents

Supporting Figures and Tables	S2
Supporting Methods	S6

Supplementary Figures and Tables

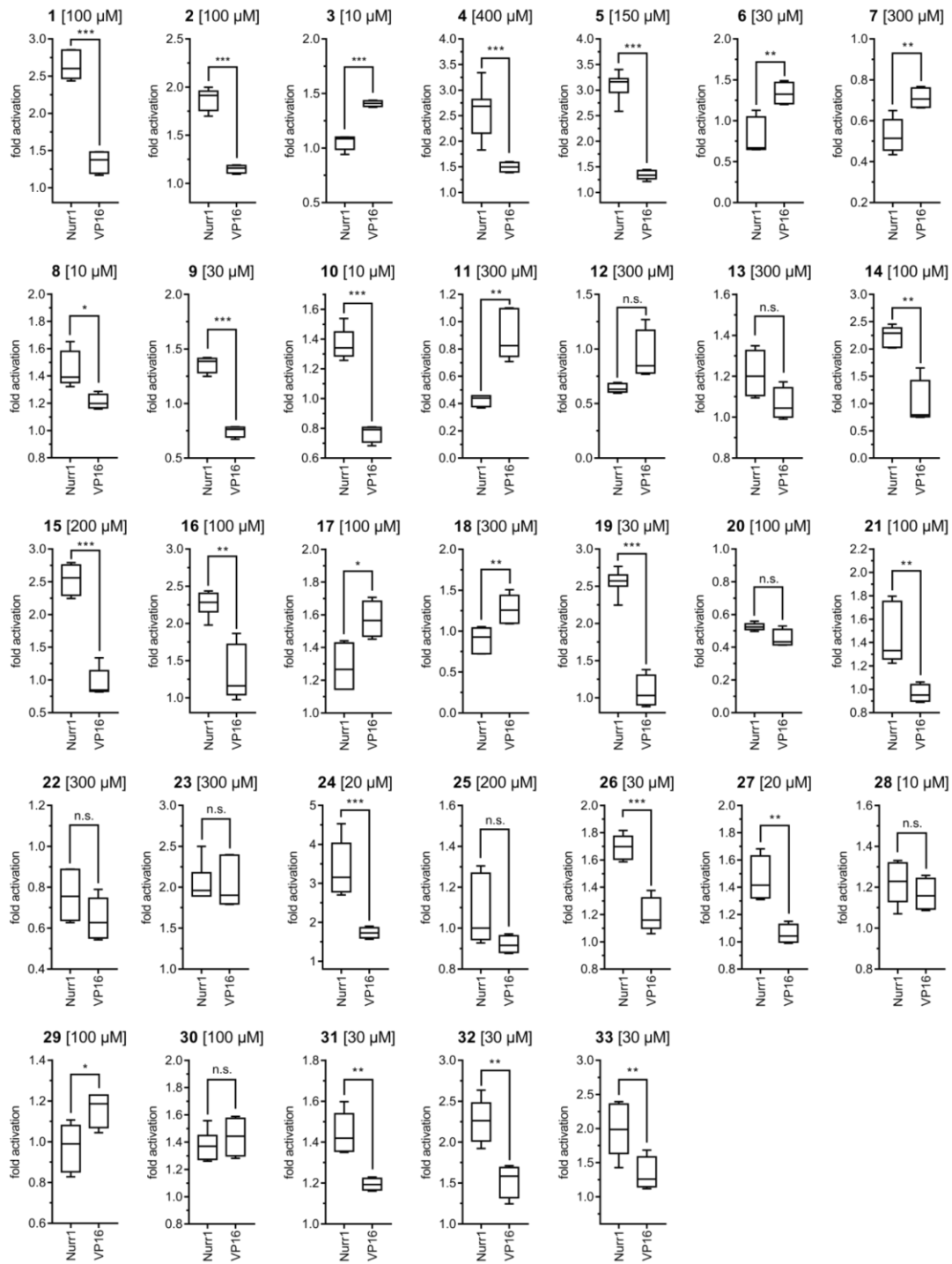


Figure S1. Control experiments employing a Gal4-VP16 hybrid receptor were performed for all tested compounds to confirm or refute Gal4-Nurr1 mediated activity in the cellular hybrid reporter gene assay. Boxplots show: center line, median; box limits, upper and lower quartiles; whiskers, min/max; $n \geq 4$. * $p < 0.05$, ** $p < 0.01$ *** $p < 0.001$ (t-test).

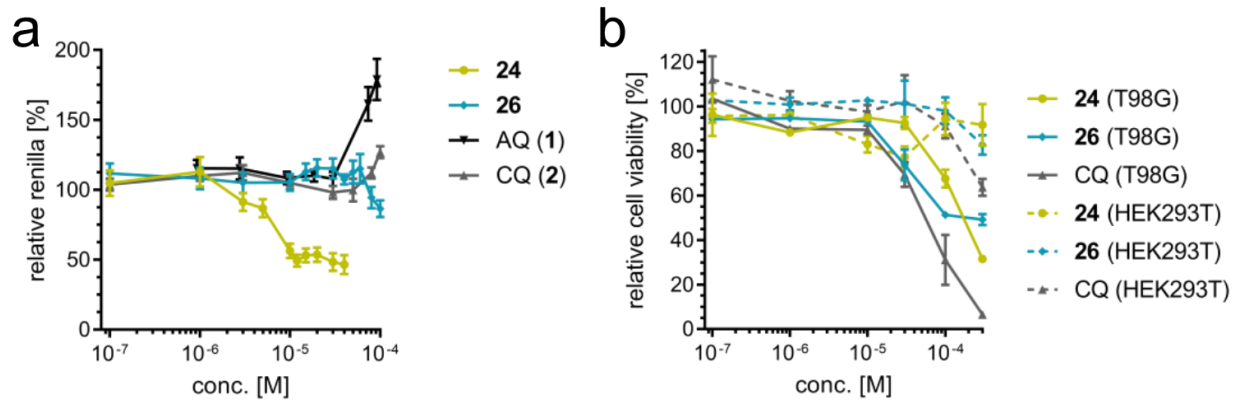


Figure S2. Nonspecific effects and cytotoxicity of Nurr1 agonists. (a) Relative renilla luminescence from cellular Gal4 hybrid reporter gene assay in HEK293T cells compared to DMSO 0.1% control reveals pronounced non-specific effects on transcriptional activity for AQ and **24**. Data are the mean \pm SEM; $n \geq 3$. (b) Treatment of human astrocytes (T98G) and HEK293T cells with increasing concentrations of **24** and **26** revealed no cytotoxicity up to 300 μ M in HEK293T cells and increasing toxicity from 100 μ M in astrocytes. Cell viability was determined by a WST-1 assay. CQ (**2**) is shown for comparison. Data are the mean \pm SEM; $n \geq 3$.

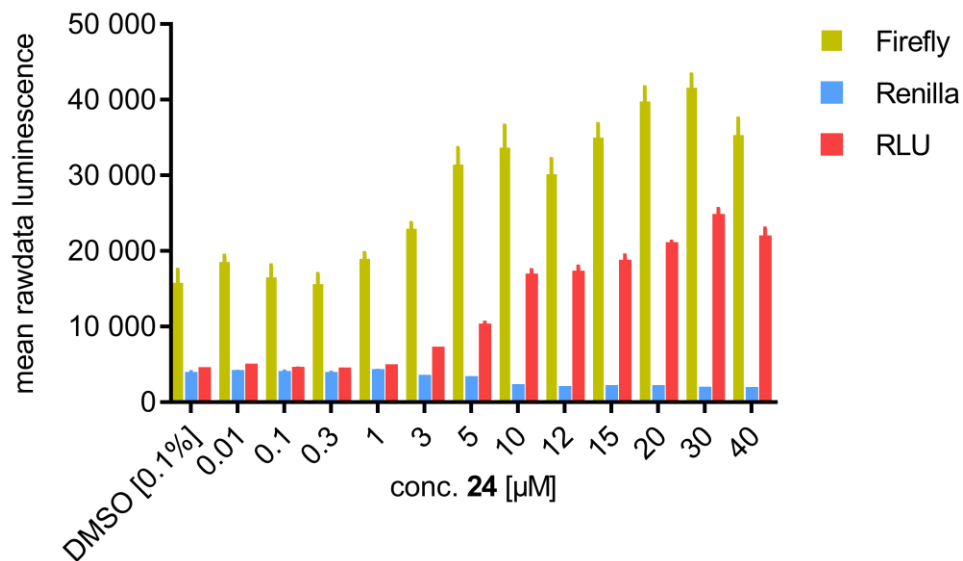


Figure S3. Raw luminescence data for **24** from the cellular Gal4-Nurr1 hybrid reporter gene assay. Relative light units (RLU) were obtained by division of firefly luciferase data by renilla luciferase data and multiplying the value by 1000. Although a pronounced increase in firefly activity shows Gal4-Nurr1 activation by **24**, its Nurr1 activation efficacy is overestimated as a result of decreasing renilla activity. Data are the mean \pm SEM; $n \geq 4$.

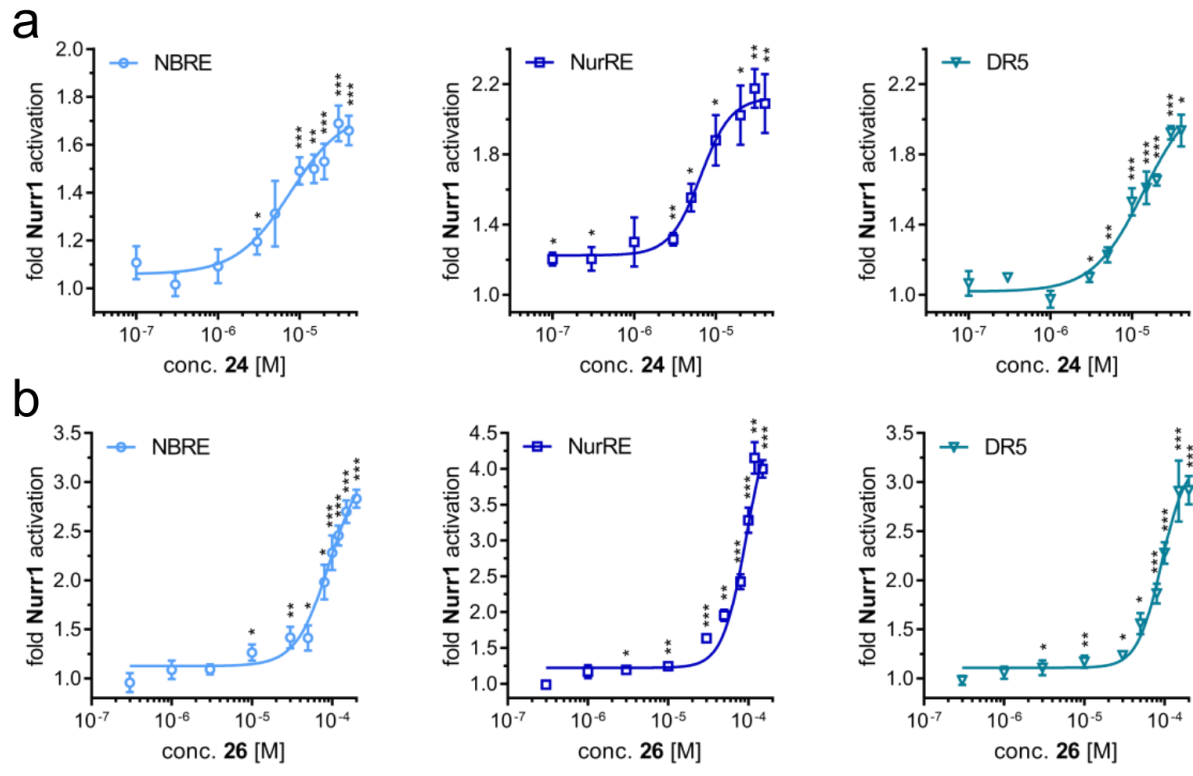


Figure S4. Activity of **24** (a) and **26** (b) in cellular full length Nurr1 reporter gene assays employing the human Nurr1 response elements NBRE (monomer), NurRE (homodimer) and DR5 (heterodimer with RXR α) to govern reporter gene expression. Data are the mean \pm SEM, $n \geq 3$. Statistical significance is indicated compared to DMSO 0.1% control, * $p < 0.05$, ** $p < 0.01$ *** $p < 0.001$ (t-test).

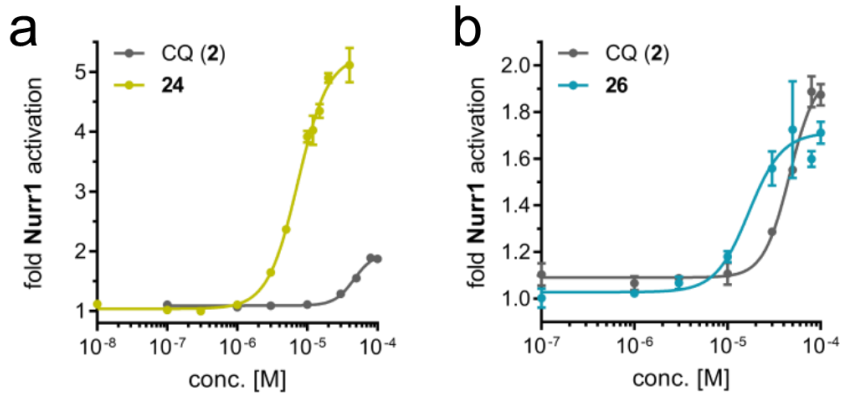


Figure S5. Activity of **24** (a) and **26** (b) in the cellular Gal4-Nurr1 hybrid reporter gene assay. CQ (**2**) is shown for comparison. Data are the mean \pm SEM; $n \geq 3$.

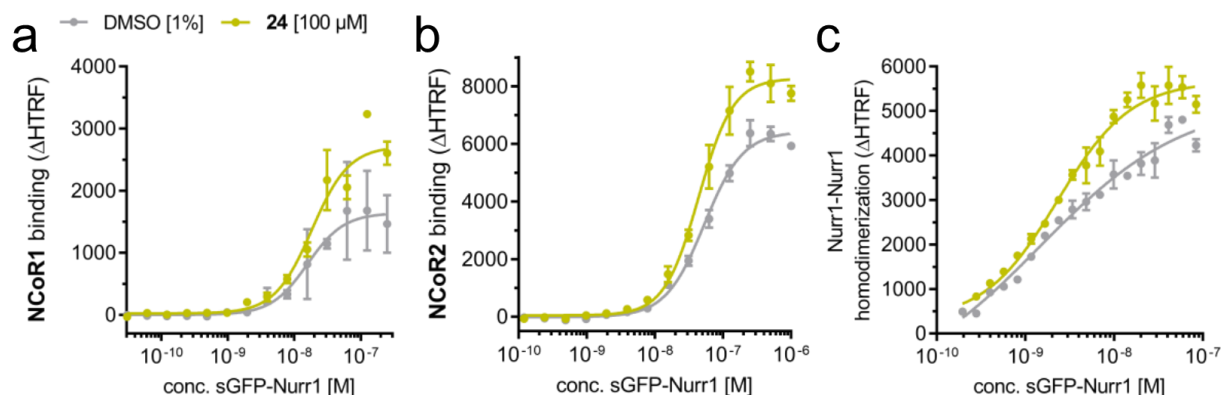


Figure S6. Effects of Nurr1 agonist **24** on co-factor binding to the Nurr1 LBD and on Nurr1 homodimerization in homogenous time-resolved fluorescence resonance energy transfer (HTRF) assays. (a) NCoR1 interaction with the Nurr1 LBD. (b) NCoR2 interaction with the Nurr1 LBD. (c) Nurr1-Nurr1 homodimerization. Data are the mean \pm SD; N = 3.

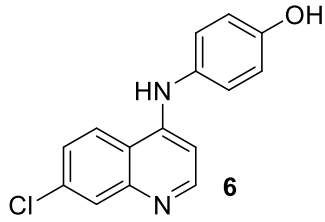
Table S1. Summarized cellular Nurr1 modulatory activities of fragments **24** and **26**. The Gal4-Nurr1 hybrid reporter gene assay and full length Nurr1 reporter gene assays under control of the NBRE (monomer), NurRE (homodimer) and DR5 (heterodimer with RXR α) response elements were performed in transiently transfected HEK293T cells. Values in parentheses are max. activation compared to 0.1% DMSO serving as vehicle. Data are the mean \pm SD, $n \geq 3$. Hill slopes calculated from non-linear fit ([Agonist] vs. response -- Variable slope (four parameters)).

	24	26
Gal4-Nurr1	EC ₅₀ 7.3 \pm 0.5 μ M (5.28 \pm 0.15 fold act.) hillslope 2.00 \pm 0.19	EC ₅₀ 17 \pm 6 μ M (1.71 \pm 0.11 fold act.) hillslope 2.42 \pm 1.31
NBRE: Nurr1 monomer	EC ₅₀ 7.7 \pm 3.3 μ M (1.74 \pm 0.16 fold act.) hillslope 1.31 \pm 0.75	EC ₅₀ 92 \pm 21 μ M (3.23 \pm 0.44 fold act.) hillslope 2.09 \pm 0.71
NurRE: Nurr1 homodimer	EC ₅₀ 6.5 \pm 1.6 μ M (2.12 \pm 0.10 fold act.) hillslope 2.31 \pm 1.21	EC ₅₀ 95 \pm 15 μ M (4.92 \pm 0.73 fold act.) hillslope 2.90 \pm 0.85
DR5: Nurr1:RXR α heterodimer	EC ₅₀ 14 \pm 5 μ M (2.15 \pm 0.29 fold act.) hillslope 1.41 \pm 0.50	EC ₅₀ 92 \pm 18 μ M (3.24 \pm 0.44 fold act.) hillslope 2.86 \pm 1.29

Supplementary Methods

WST-1 Toxicity Assay

WST-1 assay (Roche Diagnostics International AG, Rotkreuz, Switzerland) was performed according to the manufacturer's protocol. In brief, T98G cells and HEK293T cells were seeded in DMEM high glucose, supplemented with sodium pyruvate (1 mM), penicillin (100 U/mL), streptomycin (100 µg/mL), and 10% FCS in 96-well plates at a density of 3×10^4 cells/well, respectively. After 24 h, the medium was changed to DMEM high glucose, supplemented with penicillin (100 U/mL), streptomycin (100 µg/mL), and 1% charcoal stripped FCS additionally containing 0.1% DMSO and the test compound **2**, **24** or **26** (final concentrations 0.1 µM, 1 µM, 10 µM, 30 µM, 100 µM, and 300 µM) or 0.1% DMSO alone as negative control. After 24 h, WST reagent (Roche Diagnostics International AG) was added to each well according to the manufacturer's instructions. After 45 min incubation, absorption (450 nm/reference, 620 nm) was determined with a Spark 10M luminometer (Tecan Group AG, Männedorf, Switzerland). Each experiment was repeated at least three times in duplicates.



Analyzed Date and Time: 12/20/2018
 02:20 PM
 Processed Date and Time: 12/20/2018
 03:04 PM

Reported Date and Time: 12/20/2018
 03:05:38 PM

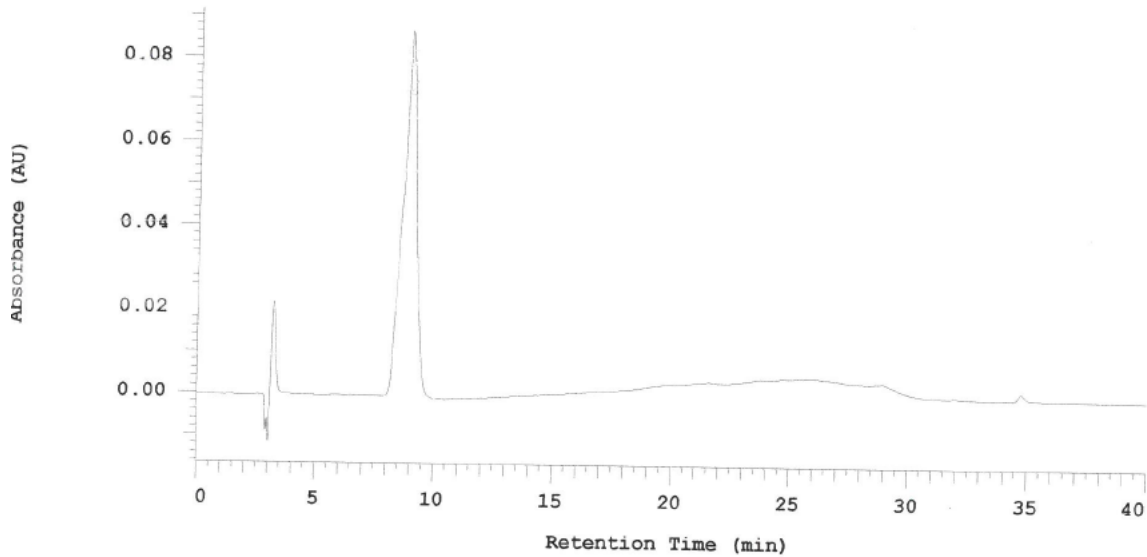
Sample Name: SW15

Processing Method: Reinheit
 Application(data): Reinheit

Vial Number: 15
 Volume: 50.0 ul

Sample Description:

Chrom Type: Fixed WL Chromatogram, 254 nm



ump 1: 5160

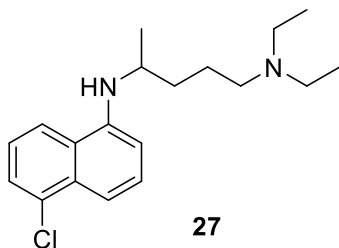
Pump 1 Solvent A: MeOH

Pump 1 Solvent C: MeOH

Pump 1 Solvent B: Wasser

Pump 1 Solvent D: MeOH

No.	RT	Area	Area %	Height
1	8.927	1716010	100.000	43647
		1716010	100.000	43647



Analyzed Date and Time: 11/27/2019
 01:12 PM
 Processed Date and Time: 11/27/2019
 02:04 PM

Reported Date and Time: 11/27/2019
 02:04:10 PM

Sample Name: JO12

Processing Method: Reinheit

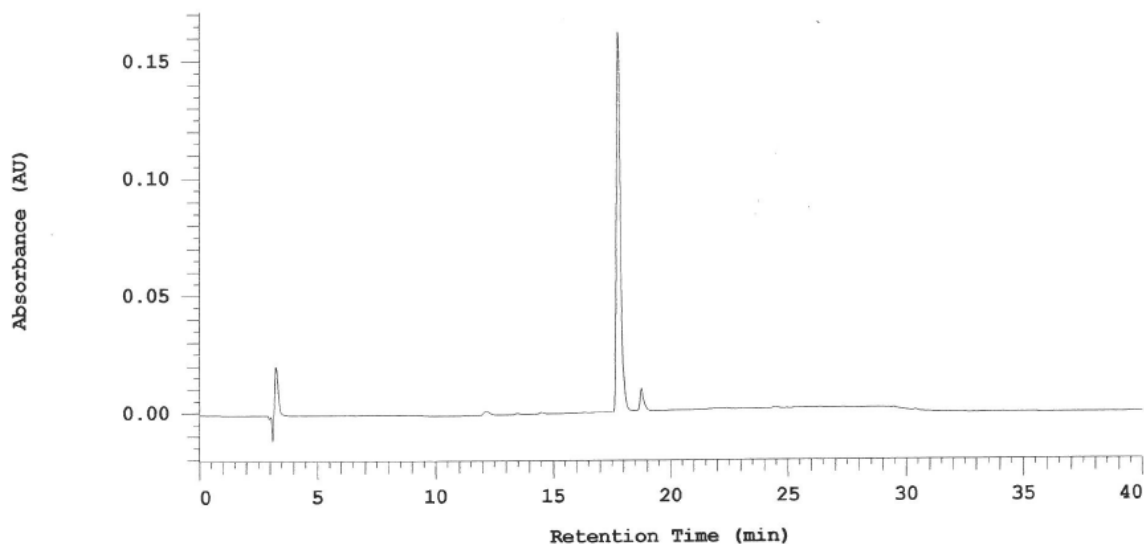
Application(data): Reinheit

Vial Number: 3

Volume: 50.0 ul

Sample Description:

Chrom Type: Fixed WL Chromatogram, 254 nm



Pump 1: 5160

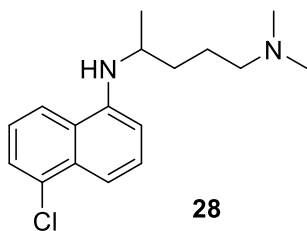
Pump 1 Solvent A: MeOH

Pump 1 Solvent B: Wasser

Pump 1 Solvent C: MeOH

Pump 1 Solvent D: MeOH

No.	RT	Area	Area %	Height
1	17.753	941729	95.148	81100
2	18.747	48022	4.852	4691
		989751	100.000	85791



Analyzed Date and Time: 10/10/2019
 12:56 PM
 Processed Date and Time: 09/22/2020
 03:13 PM

Reported Date and Time: 09/22/2020
 03:13:45 PM

Sample Name: JO11

Processing Method: Reinheit

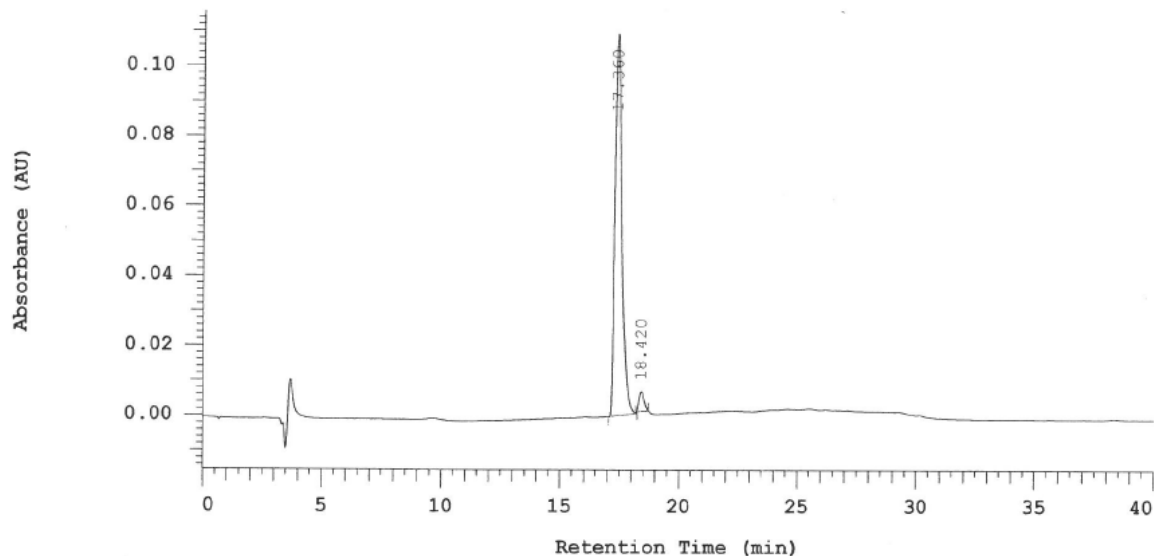
Application(data): Reinheit

Vial Number: 20

Volume: 50.0 ul

Sample Description:

Chrom Type: Fixed WL Chromatogram, 254 nm



Pump 1: 5160

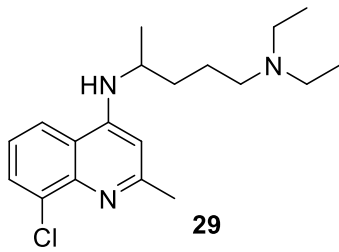
Pump 1 Solvent A: MeOH

Pump 1 Solvent B: Wasser

Pump 1 Solvent C: MeOH

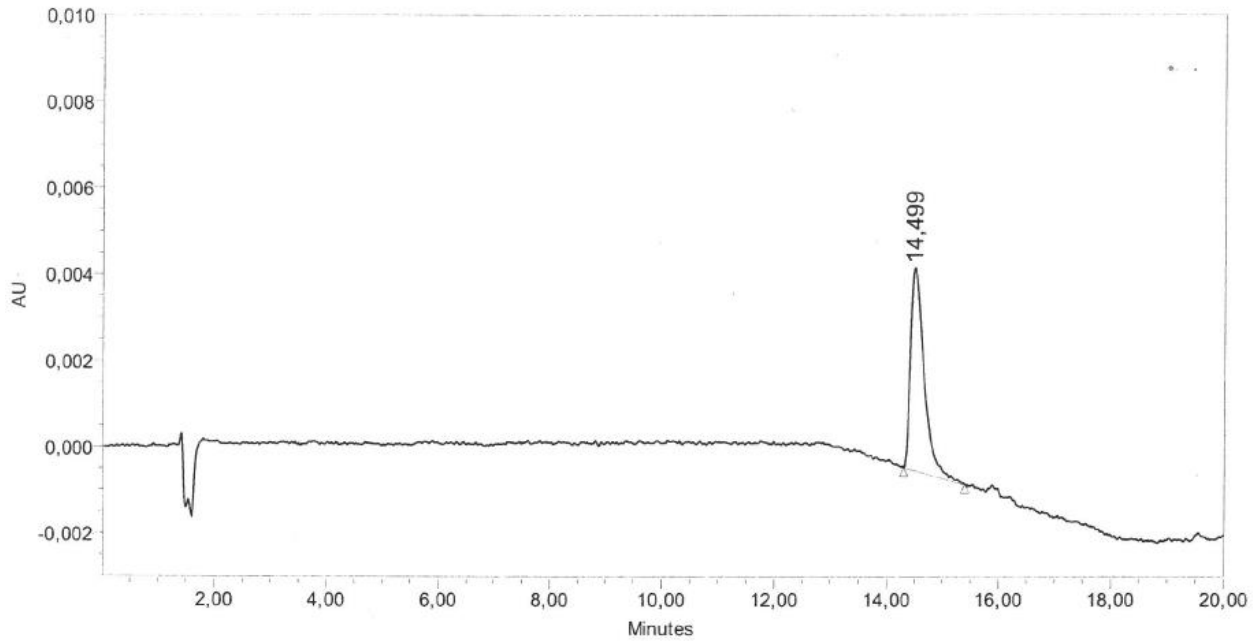
Pump 1 Solvent D: MeOH

No.	RT	Area	Area %	Height
1	17.360	1068111	96.331	54677
2	18.420	40680	3.669	2799
		1108791	100.000	57476

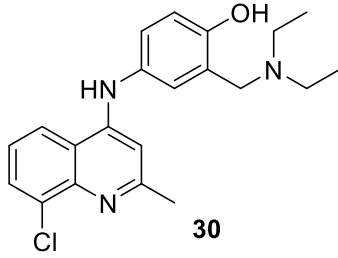


SAMPLE INFORMATION

Sample Name:	JO24_15/85_20µg/mL in H2O_G	Acquired By:	System
Sample Type:	Standard	Sample Set Name:	
Vial:	53	Acq. Method Set:	EP6
Injection #:	1	Processing Method:	EP6
Injection Volume:	50,00 ul	Channel Name:	2487Channel 1
Run Time:	20,0 Minutes	Proc. Chnl. Descr.:	254
Date Acquired: 04.09.2020 14:10:54 CEST			
Date Processed: 07.09.2020 10:29:26 CEST			

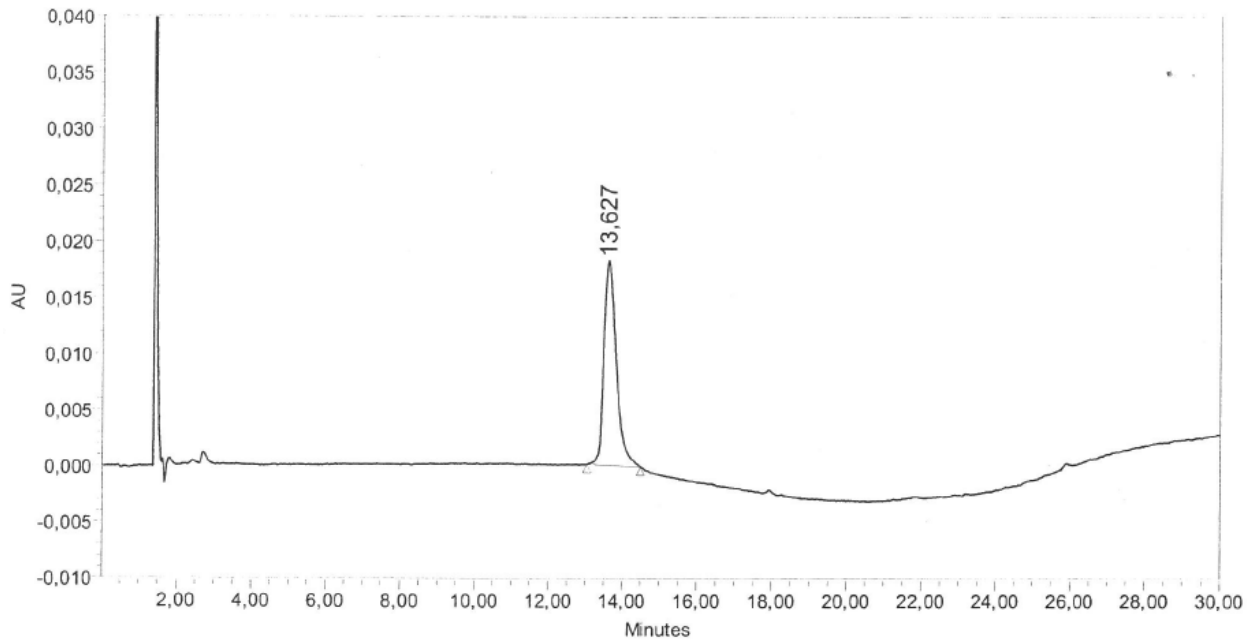


	RT	Area	% Area	Height
1	14,499	79752	100,00	4721

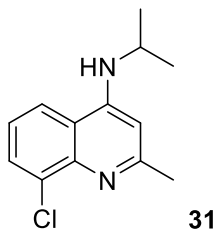


SAMPLE INFORMATION

Sample Name:	JO23_H2O	Acquired By:	System
Sample Type:	Standard	Sample Set Name:	
Vial:	2	Acq. Method Set:	EP6
Injection #:	2	Processing Method:	EP6
Injection Volume:	50,00 ul	Channel Name:	2487Channel 1
Run Time:	30,0 Minutes	Proc. Chnl. Descr.:	254
Date Acquired: 26.08.2020 14:46:38 CEST			
Date Processed: 31.08.2020 10:37:28 CEST			



	RT	Area	% Area	Height
1	13,627	424642	100,00	18222



Analyzed Date and Time: 01/19/2021
 12:31 PM
 Processed Date and Time: 01/19/2021
 04:49 PM

Reported Date and Time: 01/19/2021
 04:49:14 PM

Sample Name: JO34

Processing Method: Reinheit

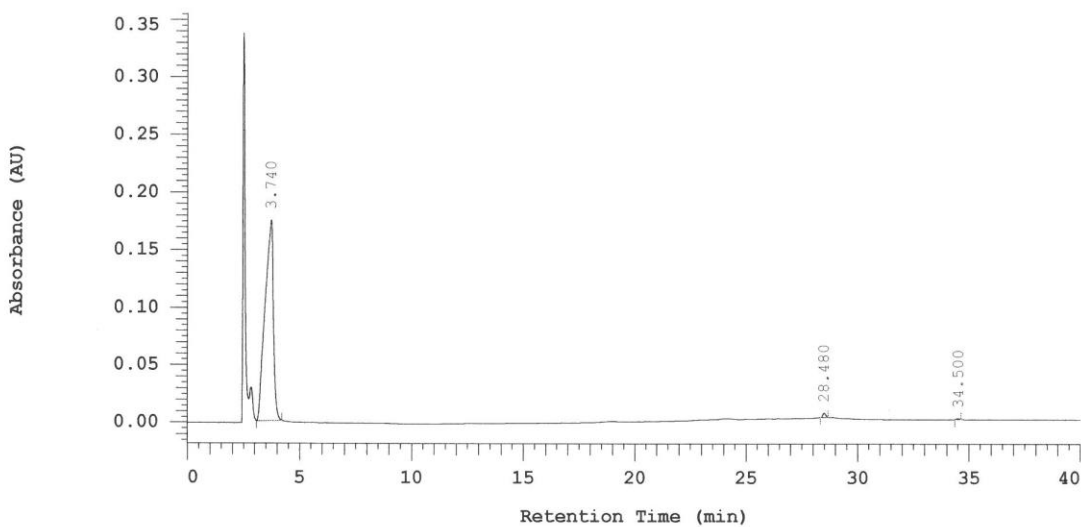
Application(data): Reinheit

Sample Description:

Vial Number: 9

Volume: 50.0 ul

Chrom Type: Fixed WL Chromatogram, 254 nm



Pump 1: 5160

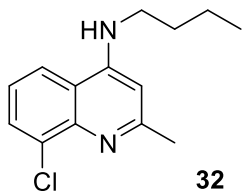
Pump 1 Solvent A: MeOH

Pump 1 Solvent C: MeOH

Pump 1 Solvent B: Wasser

Pump 1 Solvent D: MeOH

No.	RT	Area	Area %	Height
1	3.740	2227751	99.153	87083
2	28.480	15591	0.694	1818
3	34.500	3428	0.153	368
		2246770	100.000	89269



Analyzed Date and Time: 12/16/2020
 01:17 PM
 Processed Date and Time: 12/16/2020
 02:17 PM

Reported Date and Time: 12/16/2020
 02:17:50 PM

Sample Name: JO38_b

Processing Method: Reinheit

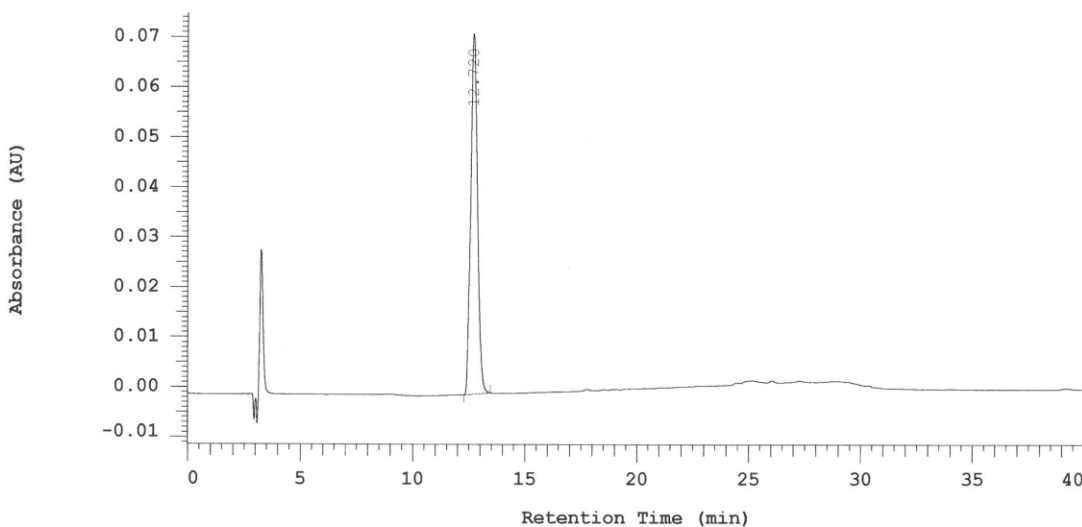
Application(data): Reinheit

Vial Number: 12

Volume: 50.0 ul

Sample Description:

Chrom Type: Fixed WL Chromatogram, 254 nm



Pump 1: 5160

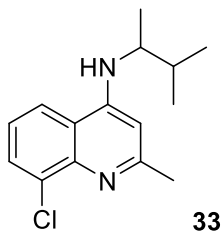
Pump 1 Solvent A: MeOH

Pump 1 Solvent B: Wasser

Pump 1 Solvent C: MeOH

Pump 1 Solvent D: MeOH

No.	RT	Area	Area %	Height
1	12.720	736093	100.000	36032
		736093	100.000	36032



Analyzed Date and Time: 01/06/2021
 11:05 AM
 Processed Date and Time: 01/06/2021
 11:49 AM

Reported Date and Time: 01/06/2021
 11:49:21 AM

Sample Name: JO37

Processing Method: Reinheit

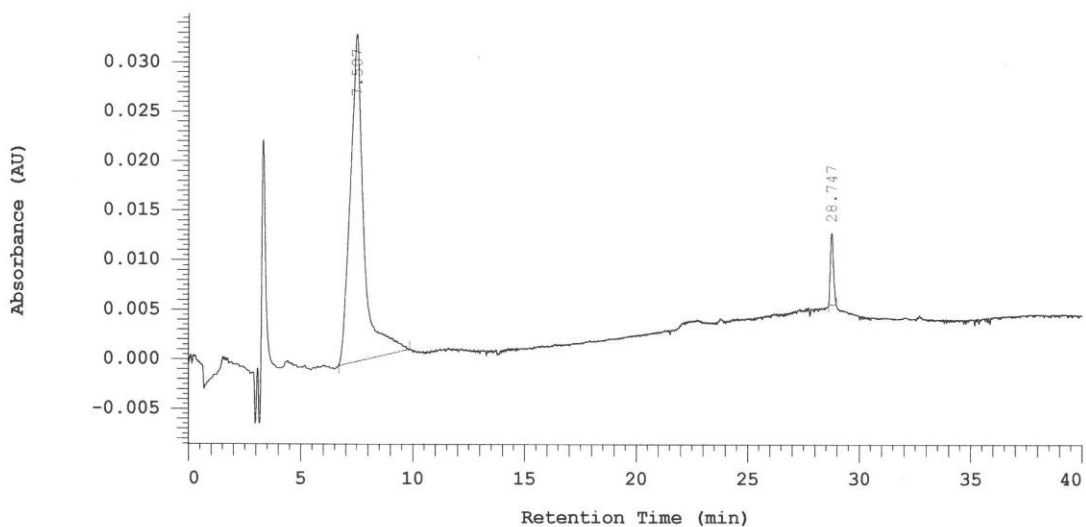
Application(data): Reinheit

Vial Number: 25

Volume: 50.0 ul

Sample Description:

Chrom Type: Fixed WL Chromatogram, 254 nm



Pump 1: 5160

Pump 1 Solvent A: MeOH

Pump 1 Solvent C: MeOH

Pump 1 Solvent B: Wasser

Pump 1 Solvent D: MeOH

No.	RT	Area	Area %	Height
1	7.507	685819	95.309	16523
2	28.747	33752	4.691	3608
		719571	100.000	20131

16.6 Development and profiling of inverse agonist tools for the neuroprotective transcription factor Nurr1

Zaienne, D.[‡]; **Willems, S.[‡]**; Schierle, S.; Heering, J.; Merk, D. Development and profiling of inverse agonist tools for the neuroprotective transcription factor Nurr1. *J. Med. Chem.* **2021**, 64 (20), 15126-15140.

[‡] *Hier liegt eine geteilte Erstautorenschaft zwischen D. Z. und S. W. vor.*

Reprinted with permission from Zaienne, D.[‡]; Willems, S.[‡]; Schierle, S.; Heering, J.; Merk, D. Development and profiling of inverse agonist tools for the neuroprotective transcription factor Nurr1. *J. Med. Chem.* **2021**, 64 (20), 15126-15140. Copyright (2021) American Chemical Society.

Development and Profiling of Inverse Agonist Tools for the Neuroprotective Transcription Factor Nurr1

Daniel Zaienne,^{||} Sabine Willems,^{||} Simone Schierle, Jan Heering, and Daniel Merk*Cite This: *J. Med. Chem.* 2021, 64, 15126–15140

Read Online

ACCESS |



Metrics & More

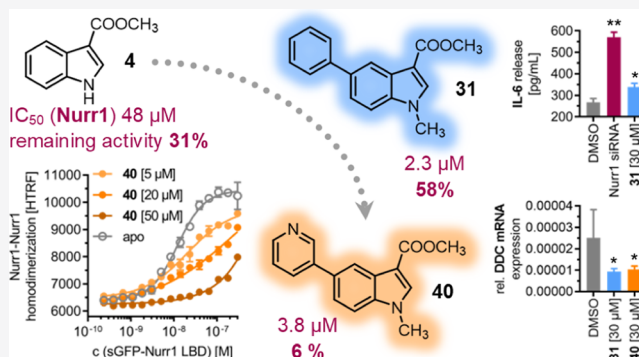


Article Recommendations



Supporting Information

ABSTRACT: The ligand-sensing transcription factor nuclear receptor related 1 (Nurr1) evolves as an appealing target to treat neurodegenerative diseases. Despite its therapeutic potential observed in various rodent models, potent modulators for Nurr1 are lacking as pharmacological tools. Here, we report the structure–activity relationship and systematic optimization of indole-based inverse Nurr1 agonists. Optimized analogues decreased the receptor’s intrinsic transcriptional activity by up to more than 90% and revealed preference for inhibiting Nurr1 monomer activity. In orthogonal cell-free settings, we detected displacement of NCoRs and disruption of the Nurr1 homodimer as molecular modes of action. The inverse Nurr1 agonists reduced the expression of Nurr1-regulated genes in T98G cells, and treatment with an inverse Nurr1 agonist mimicked the effect of Nurr1 silencing on interleukin-6 release from LPS-stimulated human astrocytes. The indole-based inverse Nurr1 agonists valuably extend the toolbox of Nurr1 modulators to further probe the role of Nurr1 in neuroinflammation, cancer, and beyond.



INTRODUCTION

Nuclear receptor related 1 (Nurr1) is a ligand-activated transcription factor belonging to the nuclear receptor protein family.¹ Nurr1 expression is high in the central nervous system where the receptor is mainly found in (dopaminergic) neurons.² Several lines of evidence point to a critical role of Nurr1 in neurodegeneration and neuroinflammation. Altered Nurr1 expression levels have been detected in Parkinson’s disease (PD),³ Alzheimer’s disease (AD),^{4,5} and multiple sclerosis (MS).⁶ Similarly, Nurr1 expression was diminished in AD (SXFAD)⁴ and PD (MPTP)³ rodent models. Moreover, knock-out of Nurr1 in dopaminergic neurons in mice produced a phenotype resembling progressive PD,² and heterozygous Nurr1 knockout mice developed experimental autoimmune encephalomyelitis (EAE) faster than wild-type mice.⁷ Pharmacological Nurr1 modulation, hence, may hold remarkable therapeutic potential in neurodegenerative diseases.^{4–6,8,9} Experimental validation of Nurr1 as a therapeutic target is, however, hindered by the lack of Nurr1 modulators as tool compounds.

Nurr1 displays high ligand-independent transcriptional inducer activity and likely lacks the canonical ligand binding site of nuclear receptors.^{1,10,11} A number of small molecules have been reported as Nurr1 ligands, but a recent systematic analysis by Munoz-Tello et al.¹² revealed also indirect effects for several Nurr1 modulators. The antimalarial amodiaquine (AQ, 1),¹³ certain fatty acid metabolites,^{10,14} the dopamine metabolite 5,6-dihydroxyindole (DHI)¹⁵ and analogues,¹⁶ and

AQ-fragments¹⁷ act as direct Nurr1 activators. Additionally, we have discovered several nonsteroidal anti-inflammatory drugs¹⁸ such as 2 and 3 as direct Nurr1 modulators (Chart 1). However, 1–3 mainly target other macromolecules and signaling pathways^{19–22} than Nurr1 with higher potency and can only serve as early tools for functional studies on Nurr1. Novel Nurr1 ligands are hence needed to probe the therapeutic potential of Nurr1 in neurodegeneration and other pathologies. Importantly, while the moderately potent Nurr1 agonist AQ (1) has been successfully used to probe Nurr1 activation in vivo,^{5,13,23,24} no potent inverse Nurr1 agonist that blocks the nuclear receptor’s high basal activity is available to date.

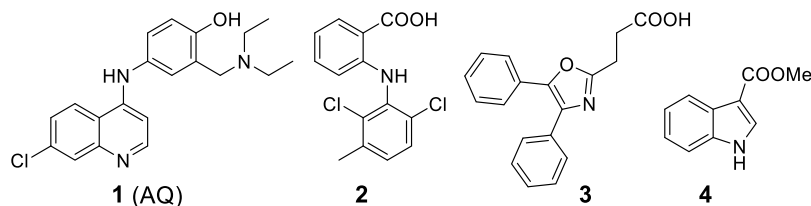
In an in vitro fragment screening campaign to identify chemical starting matter for Nurr1 ligand development, we have discovered the indole derivative 4 as a weak repressor of Nurr1 activity (IC₅₀ 48 μM). Using 4 as a lead, we have systematically elucidated the structure–activity relationship (SAR) of this new Nurr1 ligand chemotype with analogues 5–42 to obtain the efficient inverse Nurr1 agonists 31 and 40,

Received: June 15, 2021

Published: October 11, 2021



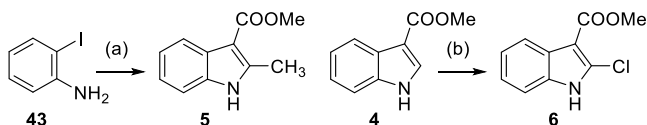
Chart 1. Known Nurr1 ligands 1–3 and screening hit 4.



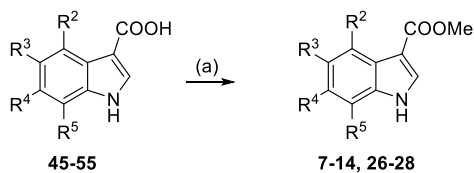
which decreased residual Nurr1 activity by up to 90%. Cell-free assays indicated disruption of the Nurr1 homodimer as well as NCoR displacement from Nurr1 as modes of action, and the inverse agonists revealed a preference for Nurr1 monomer inhibition on the NBRE response element. In human T98G astrocytes, the inverse Nurr1 agonist **31** exacerbated the neuroinflammatory response to LPS in a similar fashion as Nurr1 knockdown. Compounds **31** and **40** hence emerge as valuable new tools to study the mechanisms and biology of Nurr1.

RESULTS AND DISCUSSION

Compounds **5–19** and **22–42** were prepared according to Schemes 1–7. Compounds **20** and **21** were commercially

Scheme 1. Synthesis of **5** and **6**^a

^aReagents and conditions: (a) methyl acetoacetate (**44**), Cu₂O, Cs₂CO₃, DMSO/H₂O (3:1), 100 °C, 6 h, 51%; (b) NCS, DMF, 75 °C, 2 h, 27%.

Scheme 2. Synthesis of **7–14** and **26–28**^a

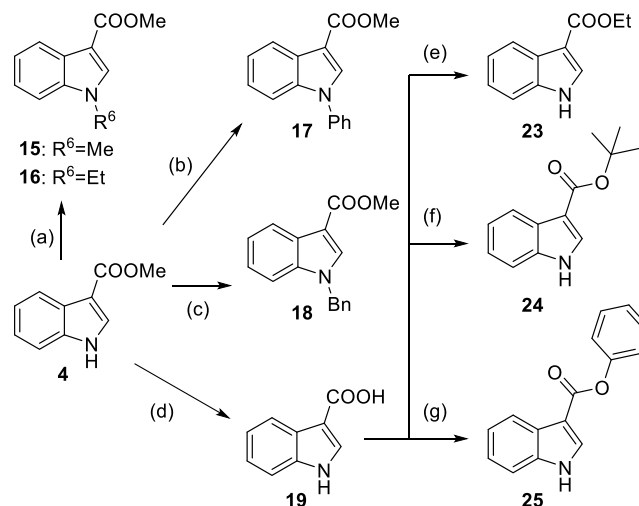
- | | |
|---|--|
| 45 , 7 : R ² =Me, R ³ =R ⁴ =R ⁵ =H | 51 , 13 : R ⁵ =Me, R ² =R ³ =R ⁴ =H |
| 46 , 8 : R ² =Cl, R ³ =R ⁴ =R ⁵ =H | 52 , 14 : R ⁵ =Cl, R ² =R ³ =R ⁴ =H |
| 47 , 9 : R ³ =Me, R ² =R ⁴ =R ⁵ =H | 53 , 26 : R ³ =OMe, R ² =R ⁴ =R ⁵ =H |
| 48 , 10 : R ³ =Cl, R ² =R ⁴ =R ⁵ =H | 54 , 27 : R ⁵ =OMe, R ² =R ³ =R ⁴ =H |
| 49 , 11 : R ⁴ =Me, R ² =R ³ =R ⁵ =H | 55 , 28 : R ³ =Br, R ² =R ⁴ =R ⁵ =H |
| 50 , 12 : R ⁴ =Cl, R ² =R ³ =R ⁵ =H | |

^aReagents and conditions: (a) methanol, H₂SO₄, 70–80 °C, 5–23 h, 6–89%.

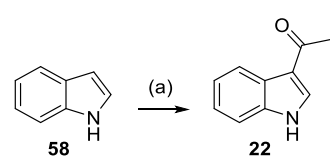
available. 2-Methylindole-3-carboxylic acid methyl ester (**5**) was obtained by treating 2-iodoaniline (**43**) with methyl acetoacetate (**44**) in the presence of Cu₂O. The 2-chloroindole analogue **6** was synthesized by treating **4** with NCS (Scheme 1).

Further analogues of **4** with methyl, chloro, methoxy, or bromo substituents on the ring system (**7–14** and **26–28**) were obtained by esterification of the respective free indole-3-carboxylic acids **45–55** (Scheme 2).

N-substituted derivatives **15–18** were prepared from **4** using dimethyl (for **15**) or diethyl sulfate (for **16**) and base, iodobenzene (**56**) and CuI (for **17**), or benzyl bromide (**57**)

Scheme 3. Synthesis of **15–19** and **23–25**^a

^aReagents and conditions: (a) dimethyl sulfate or diethyl sulfate, NaOH, DMF, 130 °C, 4–5 h, 17–35%; (b) iodobenzene (**56**), CuI, Cs₂CO₃, DMF, 120 °C, 24 h, 3%; (c) benzyl bromide (**57**), NaH, DMF, rt, 3.5 h, 59%; (d) KOH, H₂O, 65 °C, overnight, 87%; (e) ethanol, H₂SO₄, 80 °C, 5 h, 23%; (f) oxalyl chloride, CH₂Cl₂, DMF, rt, 3 h, then *t*-BuOH, KOtBu, rt, 2 h, 60%; (g) SOCl₂, phenol, CH₂Cl₂, DMF, reflux, 7.5 d, 4%.

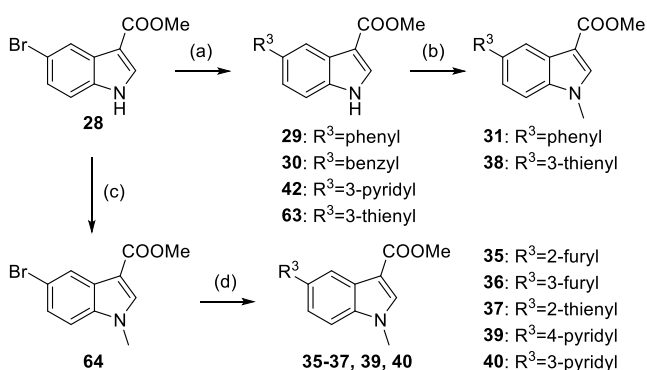
Scheme 4. Synthesis of **22**^a

^aReagents and conditions: (a) Et₂AlCl, CH₂Cl₂, 0 °C, 45 min, then propionyl chloride (**59**), 0 °C, 3 h, 11%.

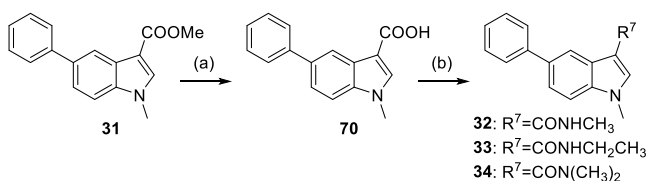
and base (for **18**). The free indole-3-carboxylic acid (**19**) was obtained by alkaline hydrolysis of **4** and then served for the preparation of esters **23–25** (Scheme 3).

For the synthesis of ethyl ketone **22**, indole (**58**) was treated with Et₂AlCl followed by propionyl chloride (**59**, Scheme 4).

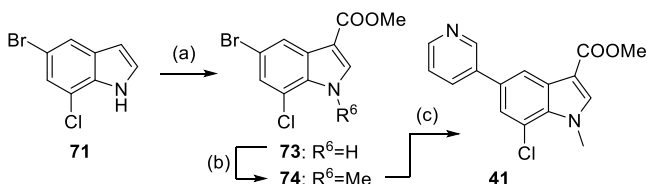
5-Phenyl (**29**)- and 5-benzyl (**30**)-substituted indole-3-carboxylic acid methyl esters were obtained from the 5-bromoindole **28** by Suzuki coupling with boronic acids **60** and **61**, respectively (Scheme 5). Treatment of **29** with dimethyl sulfate afforded the *N*-methyl analogue **31**. The 3-thienyl derivative **38** was synthesized following the same strategy by Suzuki coupling of **28** with boronic acid **62** to **63** followed by methylation with dimethyl sulfate. Further 5-aryl-substituted indole-3-carboxylic acid methyl esters **35–37** and **39** and **40** were prepared by a more economic inverted strategy. For this, **28** was first *N*-methylated with iodomethane to **64**, which was

Scheme 5. Synthesis of 29–31, 35–40, and 42^a

^aReagents and conditions: (a) boronic acid **60–62**, Pd(PPh₃)₄, Na₂CO₃, 1,4-dioxane/H₂O (4:1), reflux, 14–72 h, 2–84%; (b) dimethyl sulfate, NaOH, DMF, 130 °C, 16–24 h, 7%; (c) NaH, DMF, CH₃I, 0 °C to rt, 4 h, 87%; (d) boronic acid **65–69**, Pd(PPh₃)₄, Na₂CO₃, 1,4-dioxane/H₂O (4:1), reflux, 16–72 h, 49–93%.

Scheme 6. Synthesis of 32–34^a

^aReagents and conditions: (a) LiOH, H₂O/THF, 90 °C, 28 h, 78%; (b) methylamine, ethylamine, or dimethylamine, EDC·HCl, 4-DMAP, THF, DMF, reflux, 16–24 h, 27–75%.

Scheme 7. Synthesis of 41^a

^aReagents and conditions: (a) trichloroacetyl chloride (**72**), pyridine, CH₂Cl₂, 48 °C, 14 h, then KOH, MeOH, rt, 21 h, 50%; (b) CH₃I, NaH, DMF, 0 °C, 6 h, 65%; (c) 3-pyridylboronic acid (**69**), Pd(PPh₃)₄, Na₂CO₃, dioxane/H₂O (4:1), reflux, 16 h, 40%.

then used for Suzuki coupling with boronic acids **65–69** to obtain **35–37** and **39–40**.

Amide analogues **32–34** of **31** were prepared by hydrolysis of **31** to the free carboxylic acid **70**, which was then treated with methylamine, ethylamine, or dimethylamine, respectively, in the presence of EDC·HCl and 4-DMAP (Scheme 6).

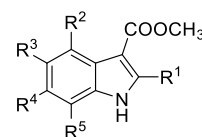
The tetrasubstituted indole **41** was prepared according to Scheme 7 from 5-bromo-7-chloroindole (**71**), which was first treated with trichloroacetyl chloride (**72**) followed by methanol and base to introduce the 3-carboxylic acid methyl ester in **73**. Methylation with iodomethane afforded **74**, which was reacted with boronic acid **69** under Suzuki conditions to obtain **41**.

Nurr1 modulation by **4–42** was determined in a cellular (HEK293T) hybrid reporter gene assay based on the human Nurr1 ligand binding domain (LBD) fused to the DNA binding domain of the yeast protein Gal4 with a Gal4-

responsive firefly luciferase serving as a reporter gene. To normalize for transfection efficiency and to monitor test compound toxicity, a constitutively expressed renilla luciferase was cotransfected. In this assay, Nurr1 displays high transcriptional inducer activity in the absence of a ligand. Known Nurr1 activators AQ (**1**) and meclofenamic acid (MFA, **2**) were used to validate the test system and to continuously monitor assay performance.

The fragment-like indole-3-carboxylic acid methyl ester (**4**) was discovered as a weak inverse Nurr1 agonist in a systematic screening for Nurr1 modulators. It presented as an attractive starting point for systematic structural optimization toward inverse Nurr1 agonists since its low molecular weight allowed for marked expansion. To identify suitable positions for derivatization of the scaffold, we commenced our SAR elucidation by probing every free position of the indole skeleton of **4** for toleration of a methyl and chlorine substituent (**5–14**, Table 1). Substitution in the 2-position was tolerated

Table 1. Systematic Evaluation of Substituents on the Indole Skeleton^a

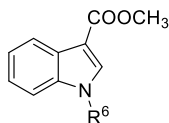


ID	R ¹	R ²	R ³	R ⁴	R ⁵	Nurr1 IC ₅₀ [μM] (remaining act.)
4	H	H	H	H	H	48 ± 11 (0.31 ± 0.08)
5	CH ₃	H	H	H	H	53 ± 20 (0.29 ± 0.18)
6	Cl	H	H	H	H	34 ± 10 (0.39 ± 0.09)
7	H	CH ₃	H	H	H	Inactive
8	H	Cl	H	H	H	55 ± 7 (0.72 ± 0.03)
9	H	H	CH ₃	H	H	20 ± 4 (0.61 ± 0.03)
10	H	H	Cl	H	H	24 ± 5 (0.18 ± 0.06)
11	H	H	H	CH ₃	H	57 ± 7 (0.49 ± 0.05)
12	H	H	H	Cl	H	8.9 ± 0.1 (0.73 ± 0.01)
13	H	H	H	H	CH ₃	35 ± 6 (0.46 ± 0.07)
14	H	H	H	H	Cl	19 ± 9 (0.30 ± 0.15)

^aInverse agonist activity of **4–14** on Nurr1 was determined in a cellular Gal4 hybrid reporter gene assay. Data are the mean ± S.E.M., n ≥ 3. Remaining activity refers to 0.1% DMSO-treated cells.

for both the methyl group (**5**) and the chlorine atom (**6**) with little effect on potency but slight preference for chlorine. Substituents in the 4-position (**7** and **8**) were not favored. In the 5-position, a methyl group (**9**) and a chlorine substituent (**10**) promoted potency, but in the case of **9**, the lower IC₅₀ value was accompanied by a marked drop in Nurr1 repression efficacy. The 6-position tolerated a methyl substituent (**11**) and favored a chlorine atom (**12**), but both substitutions diminished repressor efficacy, as well. In the 7-position, a methyl substituent (**13**) was tolerated, and a chlorine atom (**14**) enhanced potency without loss in efficacy.

We also evaluated substituents on the indole nitrogen (**15–18**, Table 2) and observed a twofold improvement in inverse agonist potency for *N*-methyl analogue **15**. Extension to *N*-ethyl (**16**) decreased potency and efficacy, suggesting that further chain elongation was not constructive. Phenyl derivative **17** lost inverse agonistic potency but even promoted Nurr1 activity, and benzyl derivative **18** was inactive. Based on these preliminary SAR data, the 5- (**9** and **10**) and 7- (**13** and

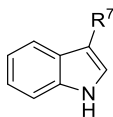
Table 2. Evaluation of Indole *N*-Substituents^a

ID	R ⁶	Nurr1 IC ₅₀ [μM] (remaining act.)
4	H	48 ± 11 (0.31 ± 0.08)
15	CH ₃	21 ± 2 (0.31 ± 0.04)
16	CH ₂ -CH ₃	31 ± 2 (0.73 ± 0.02)
17	Ph	agonist, EC ₅₀ 81 ± 3 μM (1.9 ± 0.1-fold act.)
18	Bn	inactive

^aInverse agonist activity of **15**–**18** on Nurr1 was determined in a cellular Gal4 hybrid reporter gene assay. Compound **4** is shown for comparison. Data are the mean ± S.E.M., *n* ≥ 3. Remaining activity refers to 0.1% DMSO-treated cells.

14) positions appeared as the most favored for structural expansion, and an *N*-methyl moiety (**15**) seemed worth preserving in optimized compounds.

Subsequently, we studied the SAR of the ester moiety (**19**–**25**, Table 3). The free carboxylate **19**, the aldehyde **20**, and the

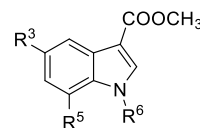
Table 3. Evaluation of the Ester Motif^a

ID	R ⁷	Nurr1 IC ₅₀ [μM] (remaining act.)
4	-COOCH ₃	48 ± 11 (0.31 ± 0.08)
19	-COOH	inactive
20	-CHO	inactive
21	-COCH ₃	inactive
22	-COCH ₂ CH ₃	inactive
23	-COOCH ₂ CH ₃	inactive
24	-COO <i>t</i> Bu	inactive
25	-COOPh	agonist, EC ₅₀ 11 ± 1 μM (1.93 ± 0.02-fold act.)

^aInverse agonist activity of **19**–**25** on Nurr1 was determined in a cellular Gal4 hybrid reporter gene assay. Compound **4** is shown for comparison. Data are the mean ± S.E.M., *n* ≥ 3. Remaining activity refers to 0.1% DMSO-treated cells.

ketones **21** and **22** were inactive on Nurr1, indicating that the ester was essential. Alternative aliphatic esters (ethyl (**23**) and *tert*-butyl (**24**)) were, however, neither tolerated, and the phenyl ester analogue **25** even exhibited Nurr1 agonistic activity. Such a shift from inverse agonism to agonism had already occurred in *N*-phenyl derivative **17**, suggesting an important role of phenyl modification in causing agonist activity. Flexible alignment of **25** with AQ (Figure S1) indeed demonstrated high structural similarity of both Nurr1 agonists and revealed superposition of the phenyl ester motif in **25** with the phenyl amine of AQ. Since this phenyl residue also distinguishes AQ from chloroquine,^{12,13,18} which is a considerably less-efficient Nurr1 agonist, it likely contributes key interactions with Nurr1 that promote activation.

Following up on the promising results for 5- and 7-derivatizations on the indole skeleton, we systematically probed further substituents in these positions (**26**–**31**, Table 4). Introduction of a 5-methoxy group (**26**) conserved the favorable inverse agonistic potency of **9** and **10**, while a 7-methoxy substituent (**27**) disrupted activity, indicating more

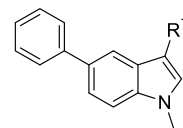
Table 4. Focused Evaluation of Substituents in the Favored Indole 5- and 7-positions^a

ID	R ³	R ⁵	R ⁶	Nurr1 IC ₅₀ [μM] (remaining act.)
9	CH ₃	H	H	20 ± 4 (0.61 ± 0.03)
10	Cl	H	H	24 ± 5 (0.18 ± 0.06)
26	OCH ₃	H	H	23 ± 3 (0.28 ± 0.04)
13	H	CH ₃	H	35 ± 6 (0.46 ± 0.07)
14	H	Cl	H	19 ± 9 (0.30 ± 0.15)
27	H	OCH ₃	H	inactive
28	Br	H	H	15 ± 3 (0.16 ± 0.07)
29	Ph	H	H	2.5 ± 0.5 (0.56 ± 0.02)
30	Bn	H	H	inactive
15	H	H	CH ₃	21 ± 2 (0.31 ± 0.04)
31	Ph	H	CH ₃	2.3 ± 0.7 (0.58 ± 0.04)

^aInverse agonist activity of **26**–**31** on Nurr1 was determined in a cellular Gal4 hybrid reporter gene assay. Compounds **9**, **10**, and **13**–**15** are shown for comparison. Data are the mean ± S.E.M., *n* ≥ 3. Remaining activity refers to 0.1% DMSO-treated cells.

potential for further modifications in the 5-position. A 5-bromine substituent (**28**) slightly enhanced potency, while a 5-phenyl residue (**29**) had a pronounced effect and generated the first inverse Nurr1 agonist with low micromolar potency. The benzyl analogue **30** was inactive, suggesting that the rigid and linear geometry of the biaryl structure in **29** was essential. Introduction of the favored *N*-methyl substituent of **15** in **31** did not further enhance potency.

In another attempt to replace the potentially labile methyl ester motif, we used the optimized analogue **31** to probe the potential of amide groups in the 3-position (Table 5). The methylamide analogue **32**, however, showed a 10-fold loss in potency, and larger *N*-substituents (ethyl, **33**; isopropyl, **34**) led to inactive compounds.

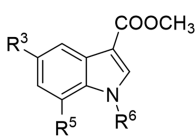
Table 5. Replacement of the Ester Motif in **31** by Amides^a

ID	R ⁷	Nurr1 IC ₅₀ [μM] (remaining act.)
31	-COOCH ₃	2.3 ± 0.7 (0.58 ± 0.07)
32	-CONHCH ₃	14 ± 3 (0.08 ± 0.05)
33	-CONHCH ₂ CH ₃	Inactive
34	-CON(CH ₃) ₂	>30 μM ^b

^aInverse agonist activity of **32**–**34** on Nurr1 was determined in a cellular Gal4 hybrid reporter gene assay. Compound **31** is shown for comparison. Data are the mean ± S.E.M., *n* ≥ 3. Remaining activity refers to 0.1% DMSO-treated cells. ^bA precise IC₅₀ value could not be determined due to toxicity.

Subsequently, we probed the SAR of the favored 5-aryl substituent (**35**–**40**, Table 6) by replacing the phenyl moiety through furyl (**35** and **36**), thiophenyl (**37** and **38**) and pyridyl (**39** and **40**) heterocycles. Introduction of furan (**35** and **36**) was well tolerated and markedly enhanced efficacy regarding Nurr1 repression despite a slight loss in potency for the 3-furyl

Table 6. Evaluation of Heterocycles as Substituents in the Indole 5-Position^a



ID	R ³	R ⁵	R ⁶	Nurr1 IC ₅₀ [μM] (remaining act.)
31		-H	-CH ₃	2.3±0.7 (0.58±0.04)
35		-H	-CH ₃	1.5±0.5 (0.36±0.06)
36		-H	-CH ₃	8±2 (0.01±0.01)
37		-H	-CH ₃	4±1 (0.39±0.05)
38		-H	-CH ₃	2.5±0.7 (0.53±0.04)
39		-H	-CH ₃	9±4 (0.1±0.2)
40		-H	-CH ₃	3.8±0.6 (0.06±0.05)
41		-Cl	-CH ₃	11±1 (0.17±0.05)
42		-H	-H	5±1 (0.14±0.07)

^aInverse agonist activity of 35–42 on Nurr1 was determined in a cellular Gal4 hybrid reporter gene assay. Compound 31 is shown for comparison. Data are the mean ± S.E.M., *n* ≥ 3. Remaining activity refers to 0.1% DMSO-treated cells.

analogue 36. The same held true for the thiophene analogues 37 and 38, which both had similar potency as phenyl derivative 31 and slightly higher Nurr1 repression efficacy. Among the pyridine analogues 39 and 40, 3-pyridyl derivative 40 comprised a favorable profile with an IC₅₀ value of 3.8 μM and high Nurr1 repression efficacy with as low as 6% remaining Nurr1 activity. The 4-pyridyl derivative 39 was less active.

In an attempt to fuse all favored modifications on the indole skeleton, we eventually combined the 7-chlorine substituent (14), the *N*-methyl residue (15), and the 3-pyridyl motif in 5-position (40) in one molecule (41), which was a potent and efficient inverse Nurr1 agonist but failed to outmatch 31 and 40. As *N*-methylation had not markedly enhanced potency in the case of 31 (vs 29), we also probed the corresponding free indole analogue 42 lacking the *N*-methyl substituent of 40. Despite only minor differences, 42 was slightly less active on Nurr1 than 40 in terms of the IC₅₀ value and repression efficacy, however, indicating that the *N*-methyl group was favored in this case.

Our SAR evaluation (summarized in Figure 1) revealed aryl substituents in the 5-position of the indole scaffold as highly favored modification to gain inverse Nurr1 agonistic potency. Therein, 3-pyridyl and 3-furyl motifs were also preferred in

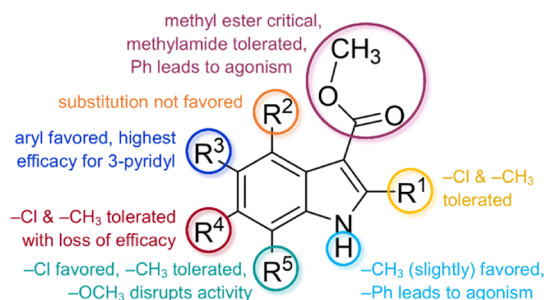


Figure 1. SAR summary of indole-based inverse Nurr1 agonists.

terms of Nurr1 repression efficacy, potentially suggesting a polar contact of the heteroatom in this region. The mechanistic basis of differing inverse Nurr1 agonist efficacy remains to be elucidated but likely resembles other nuclear receptors where differential shifts in coregulator recruitment and dimerization equilibria result in distinct levels of activation or repression.^{25–29} In addition to the 5-substituent, we identified structural optimization potential for modifications in 1- and 7-positions but with lower impact. Interestingly, a phenyl ester or *N*-phenyl substituent inverted the activity to agonism, potentially allowing optimization of the chemotype to Nurr1 activators, too. For the envisioned use as an inverse agonist tool, the trisubstituted indole derivatives 31 (5-phenyl) and 40 (5-pyridin-3-yl) evolved as the most active compounds of this series and were hence selected for further in vitro profiling and for mechanistic evaluation of inverse Nurr1 agonism.

For preliminary insights into the potential binding site of the indole-based inverse agonists on Nurr1, we performed cross-titration experiments with 40 and the reference Nurr1 agonist AQ (Figure 2). The presence of AQ (100 μM) shifted the

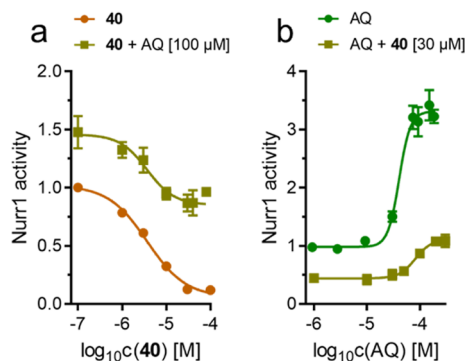


Figure 2. Cross-titration experiments in the Gal4-Nurr1 assay with 40 and AQ suggested no competitive behavior but different binding sites. (a) Dose–response curve of 40 in the absence and presence of AQ (100 μM). (b) Dose–response curve of AQ in the absence and presence of 40 (30 μM). Data are the mean ± S.E.M. reporter activation vs 0.1% DMSO; *n* ≥ 3.

dose–response curve of 40 upward (to higher Nurr1 activity, Figure 2a) but did not alter the IC₅₀ value (3.8 μM vs 3.7 μM) of the inverse agonist, suggesting no competitive binding with AQ. Congruently, titration of AQ in the presence of 40 (30 μM) resulted in a marked downward shift of the dose–response curve without a relevant change in the EC₅₀ (41 μM vs 82 μM) of AQ (Figure 2b). Hence, while the agonists 17 and 25 potentially address the AQ binding site, the indole-based inverse Nurr1 agonists likely bind to a different site than the AQ-type agonists. Their structural similarity with recently

reported DHI analogues may point to binding in the epitope of DHI between helices 4/5, 11 and 12.¹⁶

To obtain mechanistic insights into the mode of action of the indole-based inverse Nurr1 agonists, we studied how **40** modulated Nurr1 on the molecular level in homogeneous time-resolved fluorescence resonance energy transfer (HTRF)-based settings. Nuclear receptor coregulator fragment–biotin conjugates coupled to Tb³⁺-cryptate-labeled streptavidin (Tb-SA) served as FRET donor with the GFP-labeled Nurr1 LBD as FRET acceptor. For dimerization experiments, biotin Nurr1 LBD coupled to Tb-SA was used as the FRET donor together with GFP-labeled Nurr1 or RXR α LBD as the FRET acceptor. We have previously observed ligand-sensitive interactions of Nurr1 with NCoR1 and NCoR2^{17,18} and hence probed whether **40** would affect NCoR recruitment to Nurr1 (Figure 3a,b). Indeed, **40** efficiently displaced both coregulators from

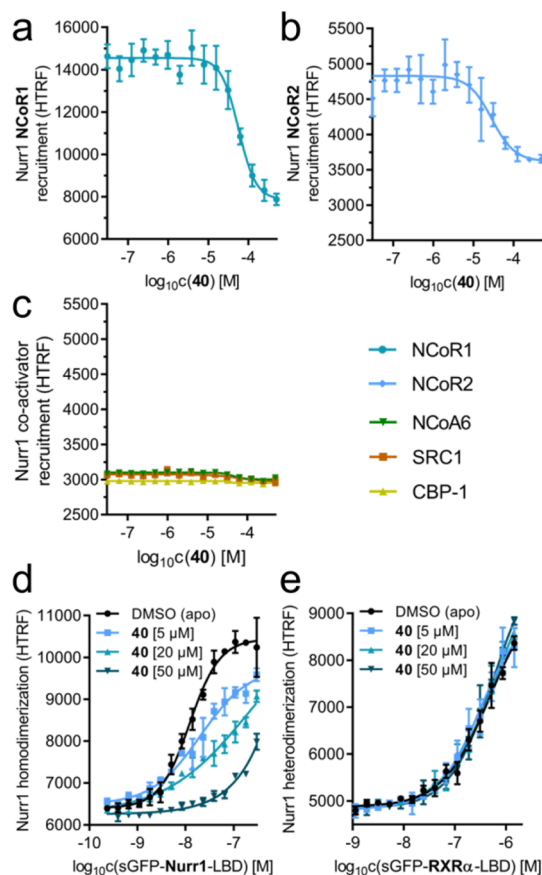


Figure 3. Effects of inverse Nurr1 agonist **40** on Nurr1 coregulator interactions and dimerization. (a–c) **40** displaced NCoR1 (a) and NCoR2 (b) from Nurr1 but had no effect on the binding of NCoA6, SRC1, and CBP-1 (c) to Nurr1. Data are mean \pm SD HTRF, $N = 4$. (d,e) **40** efficiently blocked Nurr1 homodimerization (d) in a dose-dependent fashion, while no effect on Nurr1-RXR α heterodimer formation (e) was observable. Data are mean \pm SD HTRF, $N = 3$.

the Nurr1 LBD with intermediate micromolar IC₅₀ values (NCoR1: 57 μ M, NCoR2: 29 μ M), which aligns with our previous observations on NCoR release from Nurr1 upon inverse agonist binding.¹⁸ In contrast, no effect of **40** on binding of the coactivators NCoA6, SRC1, and CBP-1 to Nurr1 was observable (Figure 3c).

In addition to coregulator recruitment, nuclear receptor activity is critically modulated by monomer–oligomer

equilibria, and we have previously found pronounced homodimerization of Nurr1, which has also turned out to be responsive to ligands.^{17,18} The inverse Nurr1 agonist **40** antagonized homodimerization of Nurr1 in a dose-dependent fashion (Figure 3d). Heterodimerization of Nurr1 with RXR α was not affected by **40** (Figure 3e). Hence, modulation of the homodimerization state of Nurr1 and NCoR displacement evolve as major mechanistic contributions to inverse Nurr1 agonism.

Next, we evaluated the effects of **31** and **40** on human full-length Nurr1 in cellular settings. Dose–response characterization of **31** and **40** in reporter gene assays for the human Nurr1 response elements NBRE (monomer), NurRE (homodimer), and DR5 (RXR-heterodimer) interestingly revealed a preference for the Nurr1 monomer (Table 7). Both inverse

Table 7. Activities of **31** and **40** on Human Response Elements for Full-Length Nurr1

	NBRE (monomer)	NurRE (homodimer)	DR5 (heterodimer)
31	IC ₅₀ = 5 \pm 3 μ M	inactive	inactive
40	IC ₅₀ = 10 \pm 4 μ M	inactive	inactive

agonists counteracted Nurr1 activity on the monomer response element NBRE but were inactive up to 50 μ M on NurRE and DR5, which aligns with their effect on Nurr1 in the HTRF-based assays.

Further in vitro profiling of **31** and **40** showed no pronounced cytotoxicity in a WST-1 assay in T98G cells or HEK293T cells (Figure 4a). Compound **31** was nontoxic up to a high 100 μ M concentration, while **40** exhibited slight antiproliferative effects above 30 μ M. Selectivity profiling of **31** and **40** on nuclear receptors (Figure 4b) revealed preference

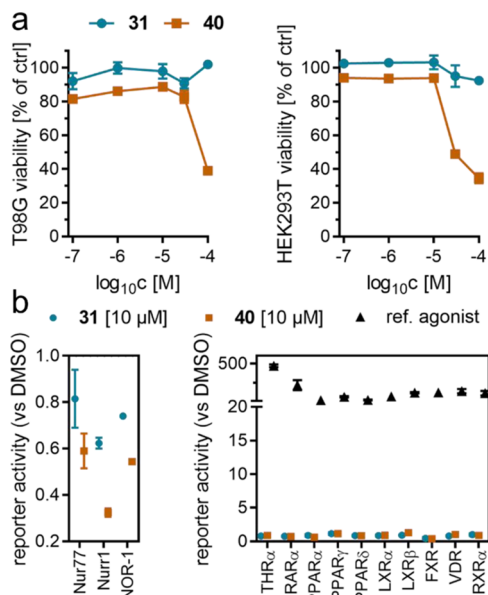


Figure 4. In vitro characterization of inverse Nurr1 agonists. (a) Compound **31** was nontoxic in a WST-1 assay in T98G and HEK293T cells up to 100 μ M. Compound **40** exhibited slight antiproliferative effects \geq 30 μ M. (b) Compounds **31** and **40** revealed preference for Nurr1 in the NR4A family and did not affect the activity of other nuclear receptors. All assays were performed in the Gal4-format. Data are the mean \pm S.E.M. relative reporter activity vs 0.1% DMSO; $n = 3$.

over the related NR4A receptors Nur77 and NOR-1, which was stronger for **40**. Both inverse Nurr1 agonists showed no effect on nuclear receptor activity outside the NR4A subfamily. Moreover, target prediction by the similarity ensemble approach (SEA)³⁰ revealed no relevant similarity of **31** to the ligands of any target (max. Tanimoto coefficient (Tc) < 0.5 for all targets) and only moderate similarity of **40** to CYP11B2 ligands (Tc 0.54, *E* value 2.255×10^{-65}). Hence, both compounds appear suitable as early tools for cellular studies on Nurr1.

To validate inverse Nurr1 agonism of **31** and **40** in a native setting, we evaluated their effects on Nurr1-regulated gene expression in Nurr1-expressing human astrocytes (T98G) on the mRNA level by quantitative real-time polymerase chain reaction (qRT-PCR, Figure 5a). Compound **31** caused a

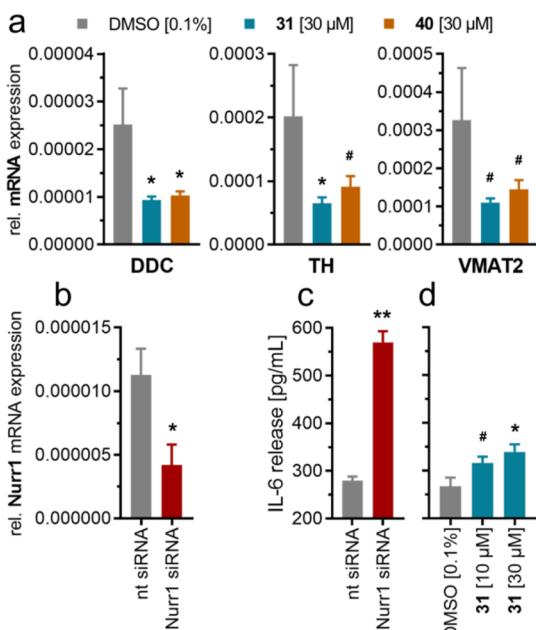


Figure 5. Biological effects of inverse Nurr1 agonists **31** and **40**. (a) Compounds **31** and **40** affected Nurr1-regulated mRNA expression of DOPA decarboxylase (DDC), tyrosine hydroxylase (TH), and vesicular monoamine transporter 2 (VMAT2). Data are mean \pm S.E.M. relative mRNA expression as determined by the $2^{-\Delta\Delta Ct}$ method with GAPDH as a reference gene. $n = 4$. (b) siRNA-mediated silencing of Nurr1 in T98G astrocytes. Data are mean \pm S.E.M. relative Nurr1 mRNA expression as determined by the $2^{-\Delta\Delta Ct}$ method with GAPDH as a reference gene; $n = 8$. (c) LPS-treated ($1 \mu\text{g/mL}$) human glioblastoma cells (T98G) released considerable amounts of interleukin-6 (IL-6), which was remarkably enhanced by siRNA-mediated Nurr1 knockdown, suggesting reverse Nurr1 involvement in this inflammatory response. Data are the mean \pm S.E.M. IL-6 levels; $n = 3$. (d) Similarly, the inverse Nurr1 agonist **31** significantly promoted IL-6 release from LPS-treated T98G cells. Data are the mean \pm S.E.M. IL-6 levels; $n = 4$. # $p < 0.1$, * $p < 0.05$, ** $p < 0.01$ (*t*-test).

pronounced downregulation of the Nurr1-regulated genes DOPA decarboxylase (DDC), tyrosine hydroxylase (TH), and vesicular monoamine transporter 2 (VMAT2). Compound **40** diminished the expression of Nurr1-regulated genes too but also affected the reference gene glyceraldehyde 3-phosphate dehydrogenase (GAPDH), further suggesting toxic effects. Hence, despite the higher efficacy of **40** in the Gal4-Nurr1 assay, **31** evolved as a better suitable tool compound for cellular studies.

Eventually, we aimed to probe Nurr1-mediated biological effects of the inverse agonists in a native cellular setting and evaluated how inverse Nurr1 agonism would affect the inflammatory response of T98G cells to lipopolysaccharide (LPS) treatment. To exclude any toxic effects, the inverse agonist **31** was used for these experiments. T98G cells produce remarkable amounts of interleukin-6 (IL-6) upon LPS treatment. When we silenced Nurr1 by RNAi (Figure 5b), we detected a pronounced increase in IL-6 release (Figure 5c), confirming involvement of Nurr1 in inflammatory signaling in T98G cells. When LPS-stimulated T98G cells were treated with the inverse Nurr1 agonist **31**, IL-6 release was also significantly enhanced, despite weaker efficacy compared to silencing (Figure 5d).

CONCLUSIONS

Several lines of evidence point to a remarkable potential of Nurr1 as a therapeutic target in neurodegeneration^{4–6,8} and cancer.^{31,32} Potent Nurr1 modulators enabling pharmacological control of Nurr1 are lacking but required for target validation studies. Since Nurr1 has a pronounced constitutive activity, inverse agonists are needed as tools to probe the effects of reduced Nurr1 activity.

Using a weak inverse agonist from an *in vitro* screening for Nurr1 modulators as a lead compound, we have developed inverse Nurr1 agonists with a trisubstituted indole skeleton. Nurr1 modulation by these compounds has been confirmed in several orthogonal cellular and cell-free settings. Therein, we observed displacement of NCoRs from Nurr1 and disruption of the Nurr1 homodimer as mechanistic contributions to inverse Nurr1 agonism, while no effect on Nurr1-RXR heterodimerization was detectable. Cellular studies involving full-length human Nurr1 and reporter constructs for all three human Nurr1 response elements (NBRE, NurRE, and DR5)¹⁸ revealed a functional preference for the Nurr1 monomer too. This is in contrast to oxaprozin (**3**) and parecoxib, which we have previously identified as weak inverse Nurr1 agonists on all Nurr1 response elements.¹⁸ Gene expression studies in human astrocytes (T98G) confirmed effects of the indole-based inverse Nurr1 agonists **31** and **40** on Nurr1 activity in a cellular setting and hence cellular target engagement. As **40** also exhibited cytotoxic effects, **31** evolves as the most suitable inverse Nurr1 agonist tool compound. Treatment of LPS-stimulated human astrocytes with the inverse Nurr1 agonist **31** indicated importance of Nurr1 in the protection against inflammatory stimulation. Like siRNA-mediated Nurr1 knockdown, **31** increased the LPS-induced IL-6 release by astrocytes, further confirming a critical role of Nurr1 in neuroinflammation and validating **31** as a valuable inverse Nurr1 agonist tool.

EXPERIMENTAL SECTION

Chemistry. General. All used chemicals were purchased from commercial sources (Alfa Aesar, Sigma-Aldrich, TCI, abcr, Chempur, and Fluorochem), at least 95% pure, and used without further purification. Test compound **4** was obtained from abcr, test compounds **20** and **21** were acquired from Alfa Aesar. All reactions were carried out under an argon atmosphere in oven-dried glassware and in absolute solvents purchased from Sigma-Aldrich. Solvents used for compound purification by column chromatography (*n*-hexane and ethyl acetate) were of technical grade and used without further purification. Deuterated solvents DMSO-*d*₆ and acetone-*d*₆ used for NMR spectroscopy were purchased and used without further drying. Thin-layer chromatography (TLC) was performed on silica (particle

size of 60 μm)-coated aluminum plates with a UV254 fluorescence indicator from Macherey-Nagel. Purification by column chromatography was carried out using silica gel from Sigma-Aldrich. For preparative HPLC purification, a Shimadzu Preparative LC-20A Prominence (Shimadzu, Kyoto, Japan) was used with the following settings: Column: Luna (10 μ C18 (2) 100 \AA ; 250 \times 21.2 mm; Phenomenex, Torrance, CA, USA). NMR spectra were recorded on Bruker AV300, AV400, and AV500 spectrometers (Bruker Corporation, Billerica, MA, USA). Chemical shift values (δ) are reported in ppm, and coupling constants (J) are shown in Hertz (Hz). Signal multiplicities are abbreviated as s for singlet, d for doublet, t for triplet, q for quartet, and m for multiplet. ESI mass spectra were recorded on a VG Platform II device (Thermo Fisher Scientific, Waltham, MA, USA), and high-resolution mass spectra were obtained on an LTQ Orbitrap XL device (Thermo Fisher Scientific). Purity of all final products was analyzed by HPLC on a Varian ProStar HPLC instrument from SpectraLab Scientific Inc. equipped with a MultiHigh 100 Phenyl-5 μ , 240 + 4 mm column at a flow rate of 1 mL per minute and UV-detection (254 and 280 nm). Only compounds having $\geq 95\%$ purity (AUC at 254 and 280 nm) were used for biological testing.

General Procedures. General Procedure (a) for Esterifications (7–14). The respective carboxylic acid, 45–52, was dissolved in methanol (20 mL), and H_2SO_4 (conc., 1 mL) was added. The solution was stirred at 80 $^\circ\text{C}$ for 5 h. After cooling to room temperature, the resulting solution was neutralized with diluted NaOH solution. The solvent was removed under reduced pressure. The resulting residue was dissolved in EtOAc (20 mL) and washed with H_2O (10 mL). The organic layer was dried (Na_2SO_4), filtered, and concentrated. Further purification was performed by column chromatography (*n*-hexane/EtOAc 2:1).

General Procedure (b) for Esterifications (26 and 27). The respective carboxylic acid 53 or 54 was dissolved in methanol (20 mL), and H_2SO_4 (conc., 1 mL) was added. The solution was stirred at 70 $^\circ\text{C}$ for 23 h. After cooling to room temperature, the resulting solution was neutralized with diluted NaOH solution, and the solvents were evaporated under reduced pressure. The resulting residue was dissolved in EtOAc (20 mL) and washed with H_2O (10 mL). The organic layer was dried (Na_2SO_4), filtered, and concentrated. Further purification was performed by column chromatography (*n*-hexane/EtOAc 2:1).

General Procedure (c) for Suzuki Couplings (35–37 and 39). Compound 64 (1.00 equiv), the respective boronic acid (1.20 equiv), $\text{Pd}(\text{PPh}_3)_4$ (0.05 equiv), and Na_2CO_3 (3.00 equiv) were dissolved in 1,4-dioxane/ H_2O (15 mL, 4:1). The solution was stirred under reflux for 16 h. After cooling to room temperature, the catalyst was removed by filtration over celite, and EtOAc (30 mL) was added to the filtrate, which was washed with H_2O (3 \times 10 mL). The organic layer was dried (Na_2SO_4), filtered, and concentrated. Further purification was performed by column chromatography (*n*-hexane/EtOAc 3:1).

2-Methyl-1H-indole-3-carboxylic Acid Methyl Ester (5). A solution of 2-iodoaniline (43, 200 mg, 0.91 mmol, 1.00 equiv), methyl acetoacetate (44, 128 mg, 1.09 mmol, 1.20 equiv), Cu_2O (13.0 mg, 0.09 mmol, 10 mol %), and Cs_2CO_3 (298 mg, 0.91 mmol, 1.00 equiv) in DMSO/ H_2O (4 mL, 3:1) was stirred at 100 $^\circ\text{C}$ for 6 h. After cooling to room temperature, EtOAc (20 mL) was added, and the solution was washed with saturated NaCl solution (10 mL) and H_2O (10 mL). The organic layer was dried (Na_2SO_4), filtered, and concentrated. Further purification was performed by column chromatography (*n*-hexane/EtOAc 3:1) to yield 5 as a brown solid (88 mg, 51%). ^1H NMR (500 MHz, DMSO- d_6): δ 11.82 (s, 1H), 7.91–7.90 (m, 1H), 7.37–7.33 (m, 1H), 7.14–7.09 (m, 2H), 3.80 (s, 3H), 2.65 (s, 3H). ^{13}C NMR (126 MHz, DMSO- d_6): δ 165.52, 144.66, 134.77, 126.76, 121.65, 120.91, 120.33, 111.20, 102.56, 50.43, 13.73. MS (ESI $^+$): m/z calcd for $\text{C}_{11}\text{H}_{12}\text{NO}_2$, 190.08; found, 190.12 ($[\text{M} + \text{H}]^+$). HRMS (MALDI): m/z calcd for $\text{C}_{11}\text{H}_{12}\text{NO}_2$, 190.08626; found, 190.08631 ($[\text{M} + \text{H}]^+$).

2-Chloro-1H-indole-3-carboxylic Acid Methyl Ester (6). A solution of NCS (153 mg, 1.14 mmol, 1.00 equiv) in DMF (5 mL) was added to a solution of methyl 1H-indole-3-carboxylate (4, 200 mg, 1.14 mmol, 1.00 equiv) in DMF (5 mL) at room temperature.

The reaction mixture was stirred at 75 $^\circ\text{C}$ for 2 h. After cooling to room temperature, the solvent was evaporated under reduced pressure, and H_2O (10 mL) was slowly added. The solution was extracted with EtOAc (3 \times 20 mL), and the combined organic layers were washed with H_2O (10 mL) and a saturated NaCl solution (10 mL), dried (Na_2SO_4), filtered, and concentrated. Further purification was performed by column chromatography (*n*-hexane/EtOAc 3:1) to yield 6 as a colorless solid (65 mg, 27%). ^1H NMR (500 MHz, DMSO- d_6): δ 12.81 (s, 1H), 7.96–7.94 (m, 1H), 7.40–7.38 (m, 1H), 7.25–7.18 (m, 2H), 3.84 (s, 3H). ^{13}C NMR (126 MHz, DMSO- d_6): δ 163.46, 134.14, 129.92, 125.72, 123.02, 121.83, 120.49, 111.46, 102.31, 50.95. MS (ESI $^+$): m/z calcd for $\text{C}_{10}\text{H}_9\text{ClNO}_2$, 210.02; found, 210.11 ($[\text{M} + \text{H}]^+$). HRMS (MALDI): m/z calcd for $\text{C}_{10}\text{H}_9\text{ClNO}_2$, 210.03163; found, 210.03174 ($[\text{M} + \text{H}]^+$).

4-Methyl-1H-indole-3-carboxylic Acid Methyl Ester (7). Preparation was according to general procedure (a) using 45 (200 mg, 1.14 mmol, 1.00 equiv) to yield 7 as a brown solid (13 mg, 6%). ^1H NMR (500 MHz, acetone- d_6): δ 10.90 (s, 1H), 8.04 (d, $J = 3.0$ Hz, 1H), 7.32 (d, $J = 8.1$ Hz, 1H), 7.10–7.07 (m, 1H), 6.94 (d, $J = 7.2$ Hz, 1H), 3.78 (s, 3H), 2.82 (s, 3H). ^{13}C NMR (126 MHz, acetone- d_6): δ 165.50, 138.42, 133.70, 133.53, 132.36, 124.18, 123.63, 110.63, 110.58, 51.00, 22.64. MS (ESI $^+$): m/z calcd for $\text{C}_{11}\text{H}_{12}\text{NO}_2$, 190.08; found, 190.06 ($[\text{M} + \text{H}]^+$). HRMS (MALDI): m/z calcd for $\text{C}_{11}\text{H}_{12}\text{NO}_2$, 189.07843; found, 189.07818 (M^+).

4-Chloro-1H-indole-3-carboxylic Acid Methyl Ester (8). Preparation was according to general procedure (a) using 46 (200 mg, 1.02 mmol, 1.00 equiv) to yield 8 as a brown solid (38 mg, 18%). ^1H NMR (500 MHz, DMSO- d_6): δ 12.17 (s, 1H), 8.12 (s, 1H), 7.48–7.43 (m, 1H), 7.21–7.16 (m, 2H), 3.76 (s, 3H). ^{13}C NMR (126 MHz, DMSO- d_6): δ 163.49, 138.38, 134.19, 124.89, 123.30, 122.74, 122.42, 111.54, 106.85, 50.91. MS (ESI $^+$): m/z calcd for $\text{C}_{10}\text{H}_8\text{ClNO}_2$, 210.02; found, 210.00 ($[\text{M} + \text{H}]^+$). HRMS (MALDI): m/z calcd for $\text{C}_{10}\text{H}_8\text{ClNO}_2$, 209.02381; found, 209.02348 (M^+).

5-Methyl-1H-indole-3-carboxylic Acid Methyl Ester (9). Preparation was according to general procedure (a) using 47 (200 mg, 1.14 mmol, 1.00 equiv) to yield 9 as a brown solid (68 mg, 32%). ^1H NMR (500 MHz, DMSO- d_6): δ 11.80 (s, 1H), 8.01 (d, $J = 3.0$ Hz, 1H), 7.79 (s, 1H), 7.35 (d, $J = 8.3$ Hz, 1H), 7.02 (dd, $J = 8.3$ Hz, 1.4 Hz, 1H), 3.79 (s, 3H), 2.41 (s, 3H). ^{13}C NMR (126 MHz, DMSO- d_6): δ 164.85, 134.71, 132.40, 130.03, 125.91, 123.93, 120.08, 112.02, 105.83, 50.59, 21.36. MS (ESI $^+$): m/z calcd for $\text{C}_{11}\text{H}_{12}\text{NO}_2$, 190.08; found, 190.09 ($[\text{M} + \text{H}]^+$). HRMS (MALDI): m/z calcd for $\text{C}_{11}\text{H}_{12}\text{NO}_2$, 190.08626; found, 190.08610 ($[\text{M} + \text{H}]^+$).

5-Chloro-1H-indole-3-carboxylic Acid Methyl Ester (10). Preparation was according to general procedure (a) using 48 (200 mg, 1.02 mmol, 1.00 equiv) to yield 10 as a brown solid (88 mg, 41%). ^1H NMR (500 MHz, DMSO- d_6): δ 12.12 (s, 1H), 8.16 (d, $J = 3.0$ Hz, 1H), 7.96 (d, $J = 2.0$ Hz, 1H), 7.50 (d, $J = 8.6$ Hz, 1H), 7.22 (dd, $J = 8.6$ Hz, 1H), 3.81 (s, 3H). ^{13}C NMR (126 MHz, DMSO- d_6): δ 164.42, 134.89, 133.95, 126.78, 126.08, 122.49, 119.51, 114.08, 106.13, 50.84. MS (ESI $^-$): m/z calcd for $\text{C}_{10}\text{H}_7\text{ClNO}_2$, 208.02; found, 207.98 ($[\text{M} - \text{H}]^-$). HRMS (MALDI): m/z calcd for $\text{C}_{10}\text{H}_9\text{ClNO}_2$, 210.03163; found, 210.03136 ($[\text{M} + \text{H}]^+$).

6-Methyl-1H-indole-3-carboxylic Acid Methyl Ester (11). Preparation was according to general procedure (a) using 49 (200 mg, 1.14 mmol, 1.00 equiv) to yield 11 as a brown solid (120 mg, 56%). ^1H NMR (500 MHz, DMSO- d_6): δ 11.77 (s, 1H), 7.99 (d, $J = 2.9$ Hz, 1H), 7.85 (d, $J = 8.1$ Hz, 1H), 7.26 (s, 1H), 7.01 (d, $J = 8.1$ Hz, 1H), 3.78 (s, 3H), 2.40 (s, 3H). ^{13}C NMR (126 MHz, DMSO- d_6): δ 164.88, 136.82, 131.90, 131.65, 123.53, 123.03, 120.15, 112.12, 106.25, 50.65, 21.30. MS (ESI $^+$): m/z calcd for $\text{C}_{11}\text{H}_{12}\text{NO}_2$, 190.08; found, 190.08 ($[\text{M} + \text{H}]^+$). HRMS (MALDI): m/z calcd for $\text{C}_{11}\text{H}_{12}\text{NO}_2$, 190.08626; found, 190.08600 ($[\text{M} + \text{H}]^+$).

6-Chloro-1H-indole-3-carboxylic Acid Methyl Ester (12). Preparation was according to general procedure (a) using 50 (200 mg, 1.02 mmol, 1.00 equiv) to yield 12 as an orange solid (167 mg, 78%). ^1H NMR (500 MHz, DMSO- d_6): δ 12.03 (s, 1H), 8.13 (d, $J = 2.9$ Hz, 1H), 7.97 (d, $J = 8.5$ Hz, 1H), 7.53 (d, $J = 1.8$ Hz, 1H), 7.21 (dd, $J = 8.5$ Hz, 1H), 3.80 (s, 3H). ^{13}C NMR (126 MHz, DMSO- d_6): δ 164.45, 136.79, 133.49, 127.05, 124.40, 121.75, 121.66, 112.07,

106.55, 50.83. MS (ESI⁻): *m/z* calcd for C₁₀H₇ClNO₂, 208.02; found, 207.98 ([M - H]⁻). HRMS (MALDI): *m/z* calcd for C₁₀H₉ClNO₂, 210.03163; found, 210.03181 ([M + H]⁺).

7-Methyl-1H-indole-3-carboxylic Acid Methyl Ester (13). Preparation was according to general procedure (a) using **51** (200 mg, 1.14 mmol, 1.00 equiv) to yield **13** as a colorless solid (135 mg, 63%). ¹H NMR (500 MHz, DMSO-*d*₆): δ 11.95 (s, 1H), 8.06 (d, *J* = 3.0 Hz, 1H), 7.83 (d, *J* = 7.9 Hz, 1H), 7.10–7.07 (m, 1H), 7.00 (d, *J* = 7.1 Hz, 1H), 3.80 (s, 3H), 2.49 (s, 3H). ¹³C NMR (126 MHz, DMSO-*d*₆): δ 164.85, 135.88, 132.06, 125.45, 122.93, 121.69, 121.47, 118.01, 106.71, 50.64, 16.69. MS (ESI⁺): *m/z* calcd for C₁₁H₁₂NO₂, 190.08; found, 190.07 ([M + H]⁺). HRMS (MALDI): *m/z* calcd for C₁₁H₁₂NO₂, 190.08626; found, 190.08588 ([M + H]⁺).

7-Chloro-1H-indole-3-carboxylic Acid Methyl Ester (14). Preparation was according to general procedure (a) using **52** (200 mg, 1.02 mmol, 1.00 equiv) to yield **14** as an orange solid (190 mg, 89%). ¹H NMR (500 MHz, DMSO-*d*₆): δ 12.37 (s, 1H), 8.11 (d, *J* = 2.6 Hz, 1H), 7.97 (d, *J* = 7.9 Hz, 1H), 7.30 (d, *J* = 7.6 Hz, 1H), 7.19 (t, *J* = 7.8 Hz, 1H), 3.82 (s, 3H). ¹³C NMR (126 MHz, DMSO-*d*₆): δ 164.36, 133.30, 133.29, 127.54, 122.42, 122.07, 119.48, 116.70, 107.64, 50.90. MS (ESI⁺): *m/z* calcd for C₁₀H₉ClNO₂, 210.02; found, 210.00 ([M + H]⁺). HRMS (MALDI): *m/z* calcd for C₁₀H₉ClNO₂, 210.03163; found, 210.03179 ([M + H]⁺).

1-Methylindole-3-carboxylic Acid Methyl Ester (15). A solution of **4** (200 mg, 1.14 mmol, 1.00 equiv), dimethyl sulfate (0.33 mL, 3.43 mmol, 3.00 equiv), and NaOH (100 mg, 2.50 mmol, 2.20 equiv) in DMF (7 mL) was stirred at 130 °C for 4 h. After cooling to 0 °C, cold H₂O (40 mL) was added; the precipitate was filtered off, and the crude product was purified by column chromatography (*n*-hexane/EtOAc 3:1) to yield **15** as a colorless solid (76 mg, 35%). ¹H NMR (500 MHz, DMSO-*d*₆): δ 8.13 (s, 1H), 8.00 (d, *J* = 7.5 Hz, 1H), 7.54 (d, *J* = 8.0 Hz, 1H), 7.29–7.21 (m, 2H), 3.86 (s, 3H), 3.80 (s, 3H). ¹³C NMR (126 MHz, DMSO-*d*₆): δ 164.47, 136.97, 136.21, 126.03, 122.42, 121.58, 120.55, 110.81, 105.09, 50.68, 33.07. MS (ESI⁺): *m/z* calcd for C₁₁H₁₂NO₂, 190.08; found, 190.13 ([M + H]⁺). HRMS (MALDI): *m/z* calcd for C₁₁H₁₂NO₂, 190.08626; found, 190.08631 ([M + H]⁺).

1-Ethylindole-3-carboxylic Acid Methyl Ester (16). A solution of **4** (200 mg, 1.14 mmol, 1.00 equiv), diethyl sulfate (0.45 mL, 3.43 mmol, 3.00 equiv), and NaOH (100 mg, 2.50 mmol, 2.20 equiv) in DMF (7 mL) was stirred at 130 °C for 5 h. After cooling to room temperature, the solvent was evaporated under reduced pressure, and the resulting residue was dissolved in EtOAc (20 mL) and washed with H₂O (10 mL). The organic layer was dried (Na₂SO₄), filtered, and concentrated. Further purification was performed by column chromatography (*n*-hexane/EtOAc 3:1) to yield **16** as a colorless solid (34 mg, 17%). ¹H NMR (500 MHz, acetone-*d*₆): δ 8.13–8.11 (m, 1H), 8.02 (s, 1H), 7.54 (d, *J* = 8.1 Hz, 1H), 7.28–7.20 (m, 2H), 4.34 (q, *J* = 7.3 Hz, 2H), 3.83 (s, 3H), 1.49 (t, *J* = 7.3 Hz, 3H). ¹³C NMR (126 MHz, acetone-*d*₆): δ 165.45, 137.28, 134.83, 127.81, 123.28, 122.28, 122.10, 111.19, 107.24, 50.85, 42.13, 15.58. MS (ESI⁺): *m/z* calcd for C₁₂H₁₄NO₂, 204.09; found, 204.07 ([M + H]⁺). HRMS (MALDI): *m/z* calcd for C₁₂H₁₄NO₂, 204.10191; found, 204.10184 ([M + H]⁺).

1-Phenylindole-3-carboxylic Acid Methyl Ester (17). A solution of **4** (200 mg, 1.14 mmol, 1.00 equiv), iodobenzene (**56**, 166 mg, 0.82 mmol, 1.00 equiv), CuI (31.0 mg, 0.16 mmol, 20 mol %), and Cs₂CO₃ (532 mg, 1.63 mmol, 2.00 equiv) in DMF (7 mL) was stirred at 120 °C for 24 h. After cooling to room temperature, H₂O was added (10 mL), and the solution was extracted with EtOAc (3 × 20 mL). The combined organic layers were dried (Na₂SO₄), filtered, and concentrated. Further purification was performed by column chromatography (*n*-hexane/EtOAc 2:1) to yield **17** as a colorless solid (6 mg, 3%). ¹H NMR (500 MHz, acetone-*d*₆): δ 8.24–8.20 (m, 1H), 8.16 (s, 1H), 7.69–7.64 (m, 4H), 7.56–7.51 (m, 2H), 7.33–7.29 (m, 2H), 3.88 (s, 3H). ¹³C NMR (126 MHz, acetone-*d*₆): δ 165.35, 139.31, 137.54, 134.99, 130.82, 128.77, 127.97, 125.75, 124.32, 123.17, 122.35, 111.91, 109.61, 51.18. MS (ESI⁺): *m/z* calcd for C₁₆H₁₄NO₂, 252.09; found, 252.13 ([M + H]⁺). HRMS

(MALDI): *m/z* calcd for C₁₆H₁₄NO₂, 252.10191; found, 252.10212 ([M + H]⁺).

1-Benzylindole-3-carboxylic Acid Methyl Ester (18). DMF (7 mL) was added to **4** (200 mg, 1.14 mmol, 1.00 equiv) and NaH (60.0 mg, 2.51 mmol, 1.10 equiv) at 0 °C. Benzyl bromide (**57**, 0.35 mL, 2.97 mmol, 1.30 equiv) was added dropwise at 0 °C, and the reaction mixture was stirred at room temperature for 3.5 h. H₂O was then added (10 mL), and the solution was extracted with EtOAc (3 × 20 mL). The combined organic layers were dried (Na₂SO₄), filtered, and concentrated. Further purification was performed by column chromatography (*n*-hexane/EtOAc 5:1) to yield **18** as a colorless solid (355 mg, 59%). ¹H NMR (500 MHz, DMSO-*d*₆): δ 8.32 (s, 1H), 8.04–8.00 (m, 1H), 7.57–7.53 (m, 1H), 7.34–7.19 (m, 7H), 5.51 (s, 2H), 3.81 (s, 3H). ¹³C NMR (126 MHz, DMSO-*d*₆): δ 164.88, 137.53, 136.67, 136.07, 129.14, 128.15, 127.77, 126.74, 123.05, 122.15, 121.17, 111.76, 106.26, 51.21, 50.04. MS (ESI⁺): *m/z* calcd for C₁₇H₁₆NO₂, 266.11; found, 266.08 ([M + H]⁺). HRMS (MALDI): *m/z* calcd for C₁₇H₁₆NO₂, 265.10973; found, 265.11066 (M⁺).

1H-Indole-3-carboxylic Acid (19). KOH (97.0 mg, 1.71 mmol, 1.50 equiv) was dissolved in H₂O (40 mL), **4** (200 mg, 1.14 mmol, 1.00 equiv) was added, and the solution was stirred at 65 °C overnight. After cooling to room temperature, aqueous hydrochloric acid was added to obtain a pH of 3. The precipitated solid was filtered off and washed with H₂O to yield **19** as a colorless solid (161 mg, 87%). ¹H NMR (500 MHz, DMSO-*d*₆): δ 11.92 (s, 1H), 11.81 (s, 1H), 8.03–7.99 (m, 2H), 7.46 (d, *J* = 7.4 Hz, 1H), 7.20–7.13 (m, 2H). ¹³C NMR (126 MHz, DMSO-*d*₆): δ 165.98, 136.45, 132.32, 126.03, 122.16, 121.00, 120.60, 112.23, 107.37. MS (ESI⁺): *m/z* calcd for C₉H₈NO₂, 162.05; found, 162.06 ([M + H]⁺). HRMS (MALDI): *m/z* calcd for C₉H₇NO₂, 161.04713; found, 161.04713 (M⁺).

1H-Indole-3-propan-1-one (22). Et₂AlCl (309 mg, 2.56 mmol, 1.50 equiv) was added to a solution of **58** (200 mg, 1.71 mmol, 1.00 equiv) in CH₂Cl₂ (10 mL) at 0 °C. The reaction mixture was stirred for 45 min at 0 °C. Propionyl chloride (**59**, 0.30 mL, 3.41 mmol, 2.00 equiv) was added at 0 °C, and the reaction mixture was stirred for 3 h. Saturated NaHCO₃ solution (5 mL) and H₂O (10 mL) were then added, and the mixture was extracted with EtOAc (3 × 20 mL). The combined organic layers were dried (Na₂SO₄), filtered, and concentrated. Further purification was performed by column chromatography (*n*-hexane/EtOAc 3:1) to yield **22** as a colorless solid (32 mg, 11%). ¹H NMR (500 MHz, DMSO-*d*₆): δ 11.87 (s, 1H), 8.30 (s, 1H), 8.20–8.18 (m, 1H), 7.46–7.45 (m, 1H), 7.21–7.15 (m, 2H), 2.87 (q, *J* = 7.4 Hz, 2H), 1.11 (t, *J* = 7.4 Hz, 3H). ¹³C NMR (126 MHz, DMSO-*d*₆): δ 196.32, 137.06, 133.98, 125.87, 123.09, 122.02, 121.79, 116.44, 112.49, 32.30, 9.58. MS (ESI⁺): *m/z* calcd for C₁₁H₁₂NO, 174.08; found, 174.10 ([M + H]⁺). HRMS (MALDI): *m/z* calcd for C₁₁H₁₂NO, 174.09134; found, 174.09139 ([M + H]⁺).

1H-Indole-3-carboxylic Acid Ethyl Ester (23). H₂SO₄ (conc., 1 mL) was added to a solution of **19** (200 mg, 1.24 mmol, 1.00 equiv) in ethanol (20 mL). The solution was stirred at 80 °C for 5 h. After cooling to room temperature, the solution was neutralized with diluted NaOH solution, and the solvents were evaporated under reduced pressure. The resulting residue was dissolved in EtOAc (20 mL) and washed with H₂O (10 mL). The organic layer was dried (Na₂SO₄), filtered, and concentrated. Further purification was performed by column chromatography (*n*-hexane/EtOAc 3:1) to yield **23** as a brown solid (65 mg, 23%). ¹H NMR (500 MHz, DMSO-*d*₆): δ 11.91 (s, 1H), 8.06 (d, *J* = 3.0 Hz, 1H), 8.00–7.99 (m, 1H), 7.48–7.46 (m, 1H), 7.21–7.16 (m, 2H), 4.28 (q, *J* = 7.1 Hz, 2H), 1.33 (t, *J* = 7.1 Hz, 3H). ¹³C NMR (126 MHz, DMSO-*d*₆): δ 164.40, 136.38, 132.40, 125.62, 122.33, 121.22, 120.47, 112.34, 106.61, 58.97, 14.52. MS (ESI⁺): *m/z* calcd for C₁₁H₁₂NO₂, 190.08; found, 190.05 ([M + H]⁺). HRMS (MALDI): *m/z* calcd for C₁₁H₁₂NO₂, 190.08626; found, 190.08603 ([M + H]⁺).

1H-Indole-3-carboxylic tert Butyl Ester (24). To a suspension of **19** (200 mg, 1.24 mmol, 1.00 equiv) and 10 mL of CH₂Cl₂, oxalyl chloride (0.32 mL, 3.72 mmol, 3.00 equiv) and DMF (3 drops) were added. The solution was stirred at room temperature for 3 h,

whereupon the solvent was evaporated under reduced pressure. *t*-BuOH (3 mL) and KOtBu (226 mg, 2.02 mmol, 1.60 equiv) were added to the residue. The reaction mixture was stirred at room temperature for 2 h. Et₂O (10 mL) was then added, and the solution was washed with saturated NH₄Cl solution (10 mL) and saturated NaCl solution (10 mL). The organic layer was dried (Na₂SO₄), filtered, and concentrated. Further purification was performed by column chromatography (*n*-hexane/EtOAc 3:1) to yield **24** as a yellow solid (161 mg, 60%). ¹H NMR (500 MHz, DMSO-*d*₆): δ 11.82 (s, 1H), 7.97–7.96 (m, 2H), 7.47–7.45 (m, 1H), 7.19–7.14 (m, 2H), 1.56 (s, 9H). ¹³C NMR (126 MHz, DMSO-*d*₆): δ 164.47, 136.83, 132.65, 126.01, 122.61, 121.48, 120.98, 112.70, 108.67, 79.28, 28.71. MS (ESI⁻): *m/z* calcd for C₁₃H₁₄NO₂, 216.11; found, 216.03 ([M - H]⁻). HRMS (MALDI): *m/z* calcd for C₁₃H₁₆NO₂, 218.11309; found, 218.11257 ([M + H]⁺).

1H-Indole-3 Carboxylic Acid phenyl Ester (25). To a solution of **19** (200 mg, 1.24 mmol, 1.00 equiv) in CH₂Cl₂ (20 mL) and DMF (4 mL), SOCl₂ (0.34 mL, 4.66 mmol, 3.00 equiv) and phenol (138 mg, 1.47 mmol, 0.95 equiv) were added. The solution was stirred under reflux for 16 h. Subsequently, the same amount of phenol was added, and the solution was stirred for additional 7 days under the same conditions. After cooling to room temperature, the solvents were evaporated under reduced pressure, and the resulting residue was dissolved in EtOAc (20 mL) and washed with saturated NaHCO₃ solution (10 mL). The organic layer was dried (Na₂SO₄), filtered, and concentrated. Further purification was performed by column chromatography (*n*-hexane/EtOAc 2:1) to yield **25** as a colorless solid (13 mg, 4%). ¹H NMR (500 MHz, acetone-*d*₆): δ 11.20 (s, 1H), 8.27 (s, 1H), 8.19–8.14 (m, 1H), 7.60–7.56 (m, 1H), 7.48–7.44 (m, 2H), 7.29–7.23 (m, 5H). ¹³C NMR (126 MHz, acetone-*d*₆): δ 162.6, 151.38, 136.87, 133.02, 129.22, 126.33, 125.18, 122.85, 122.17, 121.68, 120.85, 112.27, 106.72. MS (ESI⁺): *m/z* calcd for C₁₅H₁₁NaNO₂, 260.08; found, 260.96 ([M + Na]⁺). HRMS (MALDI): *m/z* calcd for C₁₅H₁₂NO₂, 238.08626; found, 238.08649 ([M + H]⁺).

5-Methoxy-1H-indole-3-carboxylic Acid Methyl Ester (26). Preparation was according to general procedure (b) using **53** (200 mg, 1.05 mmol, 1.00 equiv) to yield **26** as a brown solid (106 mg, 51%). ¹H NMR (500 MHz, DMSO-*d*₆): δ 11.79 (s, 1H), 8.00 (d, *J* = 2.5 Hz, 1H), 7.47 (d, *J* = 2.5 Hz, 1H), 7.37 (d, *J* = 8.8 Hz, 1H), 6.84 (dd, *J* = 8.8 Hz, 1H), 3.79 (s, 3H), 3.78 (s, 3H). ¹³C NMR (126 MHz, DMSO-*d*₆): δ 165.27, 155.43, 132.95, 131.71, 126.93, 113.56, 112.83, 106.42, 102.53, 55.71, 51.02. MS (ESI⁺): *m/z* calcd for C₁₁H₁₂NO₃, 206.07; found, 206.11 ([M + H]⁺). HRMS (MALDI): *m/z* calcd for C₁₁H₁₂NO₃, 206.08117; found, 206.08138 ([M + H]⁺).

7-Methoxy-1H-indole-3-carboxylic Acid Methyl Ester (27). Preparation was according to general procedure (b) using **54** (200 mg, 1.05 mmol, 1.00 equiv) to yield **27** as a colorless solid (154 mg, 74%). ¹H NMR (500 MHz, DMSO-*d*₆): δ 12.09 (s, 1H), 7.90 (d, *J* = 3.1 Hz, 1H), 7.57 (d, *J* = 8.0 Hz, 1H), 7.10 (t, *J* = 7.9 Hz, 1H), 6.77 (d, *J* = 7.5 Hz, 1H), 3.93 (s, 3H), 3.79 (s, 3H). ¹³C NMR (126 MHz, DMSO-*d*₆): δ 164.77, 146.40, 131.51, 127.20, 126.42, 122.03, 113.00, 106.94, 102.93, 55.29, 50.66. MS (ESI⁺): *m/z* calcd for C₁₁H₁₂NO₃, 206.07; found, 206.05 ([M + H]⁺). HRMS (MALDI): *m/z* calcd for C₁₁H₁₁NO₃, 205.07334; found, 205.07424 (M⁺).

5-Bromo-1H-indole-3-carboxylic Acid Methyl Ester (28). H₂SO₄ (conc., 1 mL) was added to a solution of **55** (800 mg, 3.33 mmol, 1.00 equiv) in methanol (20 mL). The solution was stirred at 70 °C for 26 h. After cooling to room temperature, the resulting solution was neutralized with diluted NaOH solution, and the solvents were evaporated under reduced pressure. The resulting residue was dissolved in EtOAc (20 mL) and washed with H₂O (10 mL). The organic layer was dried (Na₂SO₄), filtered, and concentrated. Further purification was performed by column chromatography (*n*-hexane/EtOAc 2:1) to yield **28** as a colorless solid (735 mg, 87%). ¹H NMR (500 MHz, DMSO-*d*₆): δ 12.12 (s, 1H), 8.14 (s, 1H), 8.11 (d, *J* = 1.9 Hz, 1H), 7.46 (d, *J* = 8.6 Hz, 1H), 7.33 (dd, *J* = 8.6 Hz, 1H), 3.81 (s, 3H). ¹³C NMR (126 MHz, DMSO-*d*₆): δ 164.40, 135.13, 133.76, 127.38, 125.03, 122.53, 114.49, 114.12, 106.02, 50.85. MS (ESI⁻): *m/z* calcd for C₁₀H₇BrNO₂, 251.97; found, 251.89 ([M - H]⁻). HRMS

(MALDI): *m/z* calcd for C₁₀H₈BrNO₂, 252.97329; found, 252.97360 (M⁺).

5-Phenyl-1H-indole-3-carboxylic Acid Methyl Ester (29). Compound **28** (200 mg, 0.79 mmol, 1.00 equiv), phenylboronic acid (**60**, 115 mg, 0.95 mmol, 1.20 equiv), Pd(PPh₃)₄ (46.0 mg, 0.04 mmol, 0.05 equiv), and Na₂CO₃ (250 mg, 2.36 mmol, 3.00 equiv) were dissolved in 1,4-dioxane/H₂O (15 mL, 4:1). The solution was stirred under reflux for 24 h. After cooling to room temperature, the catalyst was removed by filtration over celite, and EtOAc (30 mL) was added to the filtrate, which was washed with H₂O (3 × 10 mL). The organic layer was dried (Na₂SO₄), filtered, and concentrated. The crude product was purified by column chromatography (*n*-hexane/EtOAc 2:1) to yield **29** as a colorless solid (164 mg, 84%). ¹H NMR (500 MHz, DMSO-*d*₆): δ 12.00 (s, 1H), 8.23 (d, *J* = 1.5 Hz, 1H), 8.12 (d, *J* = 2.9 Hz, 1H), 7.69–7.63 (m, 2H), 7.57 (d, *J* = 8.4 Hz, 1H), 7.51–7.46 (m, 3H), 7.35–7.32 (m, 1H), 3.83 (s, 3H). ¹³C NMR (126 MHz, DMSO-*d*₆): δ 164.77, 141.51, 135.96, 133.95, 133.20, 128.92, 126.90, 126.69, 126.26, 121.89, 118.44, 112.84, 106.64, 50.73. MS (ESI⁺): *m/z* calcd for C₁₆H₁₄NO₂, 252.09; found, 252.09 ([M + H]⁺). HRMS (MALDI): *m/z* calcd for C₁₆H₁₃NO₂, 251.09408; found, 251.09511 (M⁺).

5-Benzyl-1H-indole-3-carboxylic Acid Methyl Ester (30). Compound **28** (160 mg, 0.63 mmol, 1.00 equiv), benzylboronic acid (**61**, 103 mg, 0.76 mmol, 1.20 equiv), Pd(PPh₃)₄ (72.0 mg, 0.06 mmol, 0.10 equiv), and Na₂CO₃ (200 mg, 1.89 mmol, 3.00 equiv) were dissolved in 1,4-dioxane/H₂O (15 mL, 4:1). The solution was stirred under reflux for 72 h. After cooling to room temperature, the catalyst was removed by filtration over celite, and EtOAc (30 mL) was added to the filtrate, which was washed with H₂O (3 × 10 mL). The organic layer was dried (Na₂SO₄), filtered, and concentrated. The crude product was purified by preparative HPLC (acetonitrile/H₂O 50:50; flow rate: 21 mL/min) to yield **30** as a colorless solid (3.5 mg, 2%). ¹H NMR (500 MHz, acetone-*d*₆): δ 10.91 (s, 1H), 8.02 (s, 1H), 7.99 (d, *J* = 3.0 Hz, 1H), 7.50–7.39 (m, 1H), 7.34–7.23 (m, 4H), 7.19–7.14 (m, 1H), 7.10–7.08 (m, 1H), 4.09 (s, 2H), 3.81 (s, 3H). ¹³C NMR (126 MHz, acetone-*d*₆): δ 165.71, 143.32, 135.40, 132.77, 130.49, 129.61, 129.15, 127.39, 126.61, 124.89, 121.71, 112.86, 52.28, 50.84, 42.76. MS (ESI⁺): *m/z* calcd for C₁₇H₁₆NO₂, 266.11; found, 266.09 ([M + H]⁺). HRMS (MALDI): *m/z* calcd for C₁₇H₁₆NO₂, 266.11756; found, 266.11770 ([M + H]⁺).

5-Phenyl-1-methylindole-3-carboxylic Acid Methyl Ester (31). Dimethyl sulfate (0.23 mL, 2.39 mmol, 3.00 equiv) was added dropwise to a solution of **29** (200 mg, 0.78 mmol, 1.00 equiv) and NaOH (100 mg, 2.50 mmol, 2.20 equiv) in DMF (7 mL). The reaction mixture was stirred at 130 °C for 16 h. After cooling to room temperature, the solvent was evaporated under reduced pressure, and the resulting residue was dissolved in EtOAc (20 mL) and washed with H₂O (10 mL). The organic layer was dried (Na₂SO₄), filtered, and concentrated. Further purification was performed by column chromatography (*n*-hexane/EtOAc 3:1) to yield **31** as a colorless solid (15 mg, 7%). ¹H NMR (500 MHz, acetone-*d*₆): δ 8.38 (s, 1H), 8.00 (s, 1H), 7.72–7.68 (m, 2H), 7.58 (s, 2H), 7.49–7.46 (m, 2H), 7.35–7.32 (m, 1H), 3.96 (s, 3H), 3.85 (s, 3H). ¹³C NMR (126 MHz, acetone-*d*₆): δ 165.41, 142.99, 137.89, 137.08, 135.79, 129.65, 128.18, 128.04, 127.50, 122.95, 120.20, 111.61, 107.38, 50.93, 33.66. MS (ESI⁺): *m/z* calcd for C₁₇H₁₆NO₂, 266.11; found, 266.10 ([M + H]⁺). HRMS (MALDI): *m/z* calcd for C₁₇H₁₆NO₂, 266.11756; found, 266.11601 ([M + H]⁺).

N-Methyl-1-methyl-5-phenylindole-3-carboxamide (32). Methylamine (83.5 μL, 0.17 mmol, 1.20 equiv) was dissolved in THF (15 mL) and added to **70** (35.0 mg, 0.14 mmol, 1.00 equiv), EDC-HCl (32.0 mg, 0.17 mmol, 1.20 equiv), and 4-DMAP (1.90 mg, 0.01 mmol, 0.10 equiv), and DMF (3 mL) was added. The solution was stirred under reflux for 20 h. After cooling to room temperature, EtOAc (30 mL) was added, and the organic layer was washed with H₂O (4 × 10 mL). The organic layer was dried over Na₂SO₄, filtered, and concentrated. The crude product was purified by column chromatography (EtOAc) to yield **32** as a colorless solid (10 mg, 27%). ¹H NMR (500 MHz, acetone-*d*₆): δ 8.52 (q, *J* = 0.8 Hz, 1H), 7.85 (s, 1H), 7.70–7.68 (m, 2H), 7.55–7.50 (m, 2H), 7.47–7.43 (m,

2H), 7.33–7.30 (m, 1H), 7.20 (s, 1H), 3.89 (s, 3H), 2.90 (d, $J = 4.7$ Hz, 3H). ^{13}C NMR (126 MHz, acetone- d_6): δ 165.85, 143.24, 137.73, 134.87, 132.67, 129.57, 128.12, 128.03, 127.27, 122.49, 120.56, 112.11, 111.12, 33.43, 26.09. MS (ESI $^+$): m/z calcd for $\text{C}_{17}\text{H}_{17}\text{N}_2\text{O}$, 265.13; found, 265.14 ([$\text{M} + \text{H}$] $^+$). HRMS (MALDI): m/z calcd for $\text{C}_{17}\text{H}_{17}\text{NO}_2$, 265.13354; found, 265.13372 ([$\text{M} + \text{H}$] $^+$).

***N*-Ethyl-1-methyl-5-phenylindole-3-carboxamide (33).** Ethylamine (83.5 μL , 0.17 mmol, 1.20 equiv) was dissolved in THF (6 mL) and added to a solution of **70** (35.0 mg, 0.14 mmol, 1.00 equiv), EDC-HCl (32.0 mg, 0.17 mmol, 1.20 equiv), and 4-DMAP (1.90 mg, 0.01 mmol, 0.10 equiv) in THF (6 mL). The solution was stirred under reflux for 24 h. After cooling to room temperature, EtOAc (30 mL) was added, and the organic layer was washed with H_2O (3×10 mL). The organic layer was dried over Na_2SO_4 , filtered, and concentrated. The crude product was purified by column chromatography (EtOAc) to yield **33** as a colorless solid (23 mg, 60%). ^1H NMR (500 MHz, acetone- d_6): δ 8.53–8.52 (m, 1H), 7.86 (s, 1H), 7.71–7.68 (m, 2H), 7.55–7.50 (m, 2H), 7.47–7.43 (m, 2H), 7.33–7.30 (m, 1H), 7.24 (s, 1H), 3.90 (s, 3H), 3.45–3.40 (m, 2H), 1.19 (t, 3H). ^{13}C NMR (126 MHz, acetone- d_6): δ 165.17, 143.26, 137.73, 134.83, 132.57, 129.57, 128.28, 128.02, 127.27, 122.48, 120.69, 112.16, 111.09, 34.48, 33.43, 15.63. MS (ESI $^+$): m/z calcd for $\text{C}_{18}\text{H}_{19}\text{N}_2\text{O}$, 279.14; found, 279.16 ([$\text{M} + \text{H}$] $^+$). HRMS (MALDI): m/z calcd for $\text{C}_{18}\text{H}_{19}\text{N}_2\text{O}$, 279.14919; found, 279.14945 ([$\text{M} + \text{H}$] $^+$).

***N*-Dimethyl-1-methyl-5-phenylindole-3-carboxamide (34).** Dimethylamine (83.5 μL , 0.17 mmol, 1.20 equiv) was dissolved in THF (6 mL) and added to a solution of **70** (35.0 mg, 0.14 mmol, 1.00 equiv), EDC-HCl (32.0 mg, 0.17 mmol, 1.20 equiv), and 4-DMAP (1.90 mg, 0.01 mmol, 0.10 equiv) in THF (6 mL). The solution was stirred under reflux for 16 h. After cooling to room temperature, EtOAc (30 mL) was added, and the organic layer was washed with H_2O (3×10 mL). The organic layer was dried over Na_2SO_4 , filtered, and concentrated. The crude product was purified by column chromatography (EtOAc) to yield **34** as a colorless solid (29 mg, 75%). ^1H NMR (500 MHz, acetone- d_6): δ 8.21–8.20 (m, 1H), 7.69–7.67 (m, 2H), 7.66 (s, 1H), 7.55–7.50 (m, 2H), 7.46–7.43 (m, 2H), 7.33–7.29 (m, 1H), 3.91 (s, 3H), 3.16 (s, 6H). ^{13}C NMR (126 MHz, acetone- d_6): δ 166.94, 143.22, 137.12, 134.55, 132.92, 129.58, 129.09, 127.97, 127.25, 122.48, 120.67, 111.26, 111.00, 33.28. MS (ESI $^+$): m/z calcd for $\text{C}_{18}\text{H}_{19}\text{N}_2\text{O}$, 279.14; found, 279.16 ([$\text{M} + \text{H}$] $^+$). HRMS (MALDI): m/z calcd for $\text{C}_{18}\text{H}_{19}\text{N}_2\text{O}$, 279.14919; found, 279.15047 ([$\text{M} + \text{H}$] $^+$).

***5*-(Furan-2-yl)-1-methylindole-3-carboxylic Acid Methyl Ester (35).** Preparation was according to general procedure (c) using **64** (100 mg, 0.37 mmol, 1.00 equiv), 2-furylboronic acid (**65**, 63.0 mg, 0.56 mmol, 1.50 equiv), $\text{Pd}(\text{PPh}_3)_4$ (22.0 mg, 0.02 mmol, 0.05 equiv), and Na_2CO_3 (119 mg, 1.12 mmol, 3.00 equiv) to yield **35** as a brown solid (87 mg, 92%). ^1H NMR (500 MHz, acetone- d_6): δ 8.32–8.31 (m, 1H), 8.14 (s, 1H), 7.74–7.73 (m, 1H), 7.66–7.64 (m, 1H), 7.60–7.58 (m, 1H), 6.88–6.87 (m, 1H), 6.59–6.58 (m, 1H), 3.87 (s, 3H), 3.83 (s, 3H). ^{13}C NMR (126 MHz, acetone- d_6): δ 164.33, 154.03, 142.28, 136.93, 136.37, 126.26, 124.45, 119.00, 115.26, 111.99, 111.44, 105.47, 104.52, 50.74, 33.17. MS (ESI $^+$): m/z calcd for $\text{C}_{15}\text{H}_{14}\text{NO}_3$, 256.27; found, 256.08 ([$\text{M} + \text{H}$] $^+$). HRMS (MALDI): m/z calcd for $\text{C}_{15}\text{H}_{13}\text{NO}_3$, 255.08899; found, 255.08943 (M^*).

***5*-(Furan-3-yl)-1-methylindole-3-carboxylic Acid Methyl Ester (36).** Preparation was according to general procedure (c) using **64** (86.0 mg, 0.32 mmol, 1.00 equiv), 3-furylboronic acid (**66**, 54.0 mg, 0.48 mmol, 1.50 equiv), $\text{Pd}(\text{PPh}_3)_4$ (19.0 mg, 0.02 mmol, 0.05 equiv), and Na_2CO_3 (102 mg, 0.96 mmol, 3.00 equiv) to yield **36** as a yellow solid (40 mg, 49%). ^1H NMR (500 MHz, acetone- d_6): δ 8.31–8.30 (m, 1H), 8.00–7.99 (m, 1H), 7.95 (s, 1H), 7.64 (t, $J = 1.7$ Hz, 1H), 7.55–7.49 (m, 2H), 6.92 (q, $J = 0.9$ Hz, 1H), 3.93 (s, 3H), 3.85 (s, 3H). ^{13}C NMR (126 MHz, acetone- d_6): δ 165.40, 144.74, 139.21, 137.60, 136.87, 128.21, 128.11, 127.05, 121.93, 118.86, 111.61, 109.91, 107.16, 50.91, 33.61. MS (ESI $^+$): m/z calcd for $\text{C}_{15}\text{H}_{14}\text{NO}_3$, 256.09; found, 256.17 ([$\text{M} + \text{H}$] $^+$). HRMS (MALDI): m/z calcd for $\text{C}_{15}\text{H}_{13}\text{NO}_3$, 255.08899; found, 255.08924 (M^*).

***5*-(Thiophen-2-yl)-1-methylindole-3-carboxylic Acid Methyl Ester (37).** Preparation was according to general procedure (c) using **64** (100 mg, 0.37 mmol, 1.00 equiv), 2-thiopheneboronic acid (**67**, 72.0 mg, 0.56 mmol, 1.50 equiv), $\text{Pd}(\text{PPh}_3)_4$ (22.0 mg, 0.02 mmol, 0.05 equiv), and Na_2CO_3 (119 mg, 1.12 mmol, 3.00 equiv) to yield **37** as a yellow solid (80 mg, 79%). ^1H NMR (500 MHz, DMSO- d_6): δ 8.24–8.23 (m, 1H), 8.14 (s, 1H), 7.62–7.57 (m, 2H), 7.49 (dd, $J = 5.1, 1.1$ Hz, 1H), 7.45 (dd, $J = 3.6, 1.1$ Hz, 1H), 7.14–7.12 (m, 1H), 3.87 (s, 3H), 3.82 (s, 3H). ^{13}C NMR (126 MHz, DMSO- d_6): δ 164.56, 144.78, 137.23, 136.77, 128.68, 127.98, 126.76, 124.99, 123.08, 120.98, 117.43, 111.80, 105.54, 51.00, 33.42. MS (ESI $^+$): m/z calcd for $\text{C}_{15}\text{H}_{14}\text{NO}_2\text{S}$, 272.33; found, 272.07 ([$\text{M} + \text{H}$] $^+$). HRMS (MALDI): m/z calcd for $\text{C}_{15}\text{H}_{13}\text{NO}_2\text{S}$, 271.06615; found, 271.06654 (M^*).

***5*-(Thiophen-3-yl)-1-methylindole-3-carboxylic Acid Methyl Ester (38).** Dimethyl sulfate (0.19 mL, 2.04 mmol, 3.00 equiv) was added dropwise to a solution of **63** (175 mg, 0.68 mmol, 1.00 equiv) and NaOH (41.0 mg, 1.02 mmol, 1.50 equiv) in DMF (7 mL). The reaction mixture was stirred at 130 °C for 24 h. After cooling to room temperature, the solvent was evaporated under reduced pressure, and the resulting residue was dissolved in EtOAc (20 mL) and washed with H_2O (10 mL). The organic layer was dried (Na_2SO_4), filtered, and concentrated. Further purification was performed by column chromatography (*n*-hexane/EtOAc 3:1) to yield **38** as a yellow solid (12 mg, 7%). ^1H NMR (400 MHz, acetone- d_6): δ 8.41–8.40 (m, 1H), 7.97 (s, 1H), 7.68–7.63 (m, 2H), 7.56–7.52 (m, 3H), 3.95 (s, 3H), 3.85 (s, 3H). ^{13}C NMR (101 MHz, acetone- d_6): δ 165.42, 144.10, 137.72, 137.02, 132.63, 130.71, 128.13, 127.43, 127.12, 122.52, 120.22, 119.49, 111.59, 50.92, 33.64. MS (ESI $^+$): m/z calcd for $\text{C}_{15}\text{H}_{14}\text{NO}_2\text{S}$, 272.07; found, 272.17 ([$\text{M} + \text{H}$] $^+$). HRMS (MALDI): m/z calcd for $\text{C}_{15}\text{H}_{14}\text{NO}_2\text{S}$, 272.07398; found, 272.07297 ([$\text{M} + \text{H}$] $^+$).

***5*-(Pyridin-4-yl)-1-methylindole-3-carboxylic Acid Methyl Ester (39).** Preparation was according to general procedure (c) using **64** (90.0 mg, 0.34 mmol, 1.00 equiv), 4-pyridylboronic acid (**68**, 62.0 mg, 0.50 mmol, 1.50 equiv), $\text{Pd}(\text{PPh}_3)_4$ (19.0 mg, 0.02 mmol, 0.05 equiv), and Na_2CO_3 (107 mg, 1.01 mmol, 3.00 equiv) to yield **39** as a colorless solid (44 mg, 49%). ^1H NMR (400 MHz, acetone- d_6): δ 8.63 (m, 2H), 8.50–8.49 (m, 1H), 8.03 (s, 1H), 7.70–7.68 (m, 3H), 7.65–7.63 (m, 1H), 3.98 (s, 3H), 3.86 (s, 3H). ^{13}C NMR (101 MHz, acetone- d_6): δ 165.29, 151.15, 149.68, 138.77, 137.55, 132.53, 128.21, 122.52, 122.40, 120.48, 112.06, 107.68, 51.04, 33.72. MS (ESI $^+$): m/z calcd for $\text{C}_{16}\text{H}_{15}\text{N}_2\text{O}_2$, 267.11; found, 267.12 ([$\text{M} + \text{H}$] $^+$). HRMS (MALDI): m/z calcd for $\text{C}_{16}\text{H}_{15}\text{N}_2\text{O}_2$, 267.11280; found, 267.11347 ([$\text{M} + \text{H}$] $^+$).

***5*-(Pyridin-3-yl)-1-methylindole-3-carboxylic Acid Methyl Ester (40).** Compound **64** (100 mg, 0.37 mmol, 1.00 equiv), 3-pyridylboronic acid (**69**, 69.0 mg, 0.56 mmol, 1.50 equiv), $\text{Pd}(\text{PPh}_3)_4$ (22.0 mg, 0.02 mmol, 0.05 equiv), and Na_2CO_3 (119 mg, 1.12 mmol, 3.00 equiv) were dissolved in 1,4-dioxane/ H_2O (15 mL, 4:1). The solution was stirred under reflux for 16 h. After cooling to room temperature, the catalyst was removed by filtration over celite, and EtOAc (30 mL) was added to the filtrate, which was washed with H_2O (10 mL). The organic layer was dried (Na_2SO_4), filtered, and concentrated. The crude product was purified by column chromatography (EtOAc) to yield **40** as a colorless solid (92 mg, 93%). ^1H NMR (500 MHz, DMSO- d_6): δ 8.89–8.88 (m, 1H), 8.56 (dd, $J = 4.7, 1.6$ Hz, 1H), 8.26 (d, $J = 1.5$ Hz, 1H), 8.19 (s, 1H), 8.09–8.06 (m, 1H), 7.69–7.68 (m, 1H), 7.63–7.61 (m, 1H), 7.51–7.48 (m, 1H), 3.90 (s, 3H), 3.83 (s, 3H). ^{13}C NMR (126 MHz, DMSO- d_6): δ 164.41, 147.90, 147.81, 137.14, 136.91, 136.71, 134.32, 130.96, 126.66, 123.93, 121.83, 118.86, 111.72, 105.57, 50.81, 33.24. MS (ESI $^+$): m/z calcd for $\text{C}_{16}\text{H}_{15}\text{N}_2\text{O}_2$, 267.30; found, 267.12 ([$\text{M} + \text{H}$] $^+$). HRMS (MALDI): m/z calcd for $\text{C}_{16}\text{H}_{15}\text{N}_2\text{O}_2$, 267.11280; found, 267.11384 ([$\text{M} + \text{H}$] $^+$).

***7*-Chloro-1-methyl-5-(pyridin-3-yl)-1H-indole-3-carboxylic Acid Methyl Ester (41).** Compound **74** (50.0 mg, 0.17 mmol, 1.00 equiv), 3-pyridylboronic acid (**69**, 31.0 mg, 0.25 mmol, 1.50 equiv), $\text{Pd}(\text{PPh}_3)_4$ (10.0 mg, 8.25 μmol , 0.05 equiv), and Na_2CO_3 (53.0 mg, 0.50 mmol, 3.00 equiv) were dissolved in 1,4-dioxane/ H_2O (15 mL,

4:1). The solution was stirred under reflux for 18 h. After cooling to room temperature, the catalyst was removed by filtration over celite, and EtOAc (30 mL) was added to the filtrate, which was washed with H₂O (3 × 10 mL). The organic layer was dried (Na₂SO₄), filtered, and concentrated. The crude product was purified by column chromatography (EtOAc) to yield **41** as a colorless solid (20 mg, 40%). ¹H NMR (500 MHz, CDCl₃): δ 8.91 (s, 1H), 8.60 (d, *J* = 4.3 Hz, 1H), 8.32 (d, *J* = 1.6 Hz, 1H), 8.00–7.98 (m, 1H), 7.74 (s, 1H), 7.44–7.41 (m, 2H), 4.20 (s, 3H), 3.91 (s, 3H). ¹³C NMR (126 MHz, CDCl₃): δ 164.77, 147.73, 147.58, 138.48, 136.63, 135.46, 132.46, 130.29, 123.97, 123.53, 119.18, 118.35, 107.49, 51.34, 37.80. MS (ESI⁺): *m/z* calcd for C₁₆H₁₄ClN₂O₂, 301.07; found, 301.05 ([*M* + *H*]⁺). HRMS (MALDI): *m/z* calcd for C₁₆H₁₄ClN₂O₂, 301.07383; found, 301.07314 ([*M* + *H*]⁺).

5-(Pyridin-3-yl)-1H-indole-3-carboxylic Acid Methyl Ester (42). Compound **28** (200 mg, 0.79 mmol, 1.00 equiv), 3-pyridylboronic acid (**69**, 145 mg, 1.18 mmol, 1.50 equiv), Pd(PPh₃)₄ (45.5 mg, 0.04 mmol, 0.05 equiv), and Na₂CO₃ (250 mg, 2.36 mmol, 3.00 equiv) were dissolved in 1,4-dioxane/H₂O (15 mL, 4:1). The solution was stirred under reflux for 14 h. After cooling to room temperature, the catalyst was removed by filtration over celite, and EtOAc (30 mL) was added to the filtrate, which was washed with H₂O (10 mL). The organic layer was dried (Na₂SO₄), filtered, and concentrated. The crude product was purified by column chromatography (EtOAc) to yield **42** as a colorless solid (129 mg, 65%). ¹H NMR (500 MHz, DMSO-*d*₆): δ 12.06 (s, 1H), 8.89–8.88 (m, 1H), 8.55 (dd, *J* = 4.7, 1.6 Hz, 1H), 8.26 (d, *J* = 1.7 Hz, 1H), 8.15 (d, *J* = 2.9 Hz, 1H), 8.07–8.05 (m, 1H), 7.62–7.60 (m, 1H), 7.56–7.54 (m, 1H), 7.50–7.48 (m, 1H), 3.83 (s, 3H). ¹³C NMR (126 MHz, DMSO-*d*₆): δ 164.68, 147.78, 147.77, 136.88, 136.27, 134.23, 133.43, 130.64, 126.30, 123.87, 121.82, 118.76, 113.14, 106.74, 50.74. MS (ESI⁺): *m/z* calcd for C₁₅H₁₃N₂O₂, 253.09; found, 253.17 ([*M* + *H*]⁺). HRMS (MALDI): *m/z* calcd for C₁₅H₁₃N₂O₂, 253.09715; found, 253.09729 ([*M* + *H*]⁺).

5-(Thiophen-3-yl)-1H-indole-3-carboxylic Acid Methyl Ester (63). Compound **28** (230 mg, 0.91 mmol, 1.00 equiv), 3-thiopheneboronic acid (**62**, 174 mg, 1.36 mmol, 1.50 equiv), Pd(PPh₃)₄ (52.0 mg, 0.05 mmol, 0.05 equiv), and Na₂CO₃ (288 mg, 2.72 mmol, 3.00 equiv) were dissolved in 1,4-dioxane/H₂O (15 mL, 4:1). The solution was stirred under reflux for 20 h. After cooling to room temperature, the catalyst was removed by filtration over celite, and EtOAc (30 mL) was added to the filtrate, which was washed with H₂O (3 × 10 mL). The organic layer was dried (Na₂SO₄), filtered, and concentrated. The crude product was purified by column chromatography (*n*-hexane/EtOAc 2:1) to yield **63** as a yellow solid (178 mg, 76%). ¹H NMR (400 MHz, DMSO-*d*₆): δ 11.95 (s, 1H), 8.26–8.25 (m, 1H), 8.09 (d, *J* = 3.0 Hz, 1H), 7.75–7.74 (m, 1H), 7.64–7.62 (m, 1H), 7.58–7.50 (m, 3H), 3.83 (s, 3H). ¹³C NMR (101 MHz, DMSO-*d*₆): δ 164.76, 142.62, 135.72, 133.07, 128.99, 126.92, 126.43, 126.15, 121.53, 119.67, 117.71, 112.77, 106.60, 50.71. MS (ESI⁺): *m/z* calcd for C₁₄H₁₂NO₂S, 258.05; found, 258.17 ([*M* + *H*]⁺).

5-Bromo-1-methylindole-3-carboxylic Acid Methyl Ester (64). DMF (8 mL) was added to **28** (1.00 g, 3.94 mmol, 1.00 equiv) and NaH (189 mg, 7.87 mmol, 2.00 equiv) at 0 °C. The reaction mixture was stirred for 30 min. Methyl iodide (0.74 mL, 11.8 mmol, 3.00 equiv) was added dropwise at 0 °C, and the reaction mixture was stirred at room temperature for 4 h. H₂O was then added (20 mL), and the solution was extracted with EtOAc (3 × 20 mL). The combined organic layers were dried (Na₂SO₄), filtered, and concentrated. Further purification was performed by column chromatography (*n*-hexane/EtOAc 3:1) to yield **64** as a colorless solid (913 mg, 87%). ¹H NMR (300 MHz, acetone-*d*₆): δ 8.24 (d, *J* = 1.70 Hz, 1H), 8.00 (s, 1H), 7.49–7.37 (m, 2H), 3.94 (s, 3H), 3.84 (s, 3H). ¹³C NMR (75 MHz, acetone-*d*₆): δ 165.04, 137.61, 137.07, 129.20, 126.08, 124.27, 115.66, 113.22, 106.71, 51.07, 33.77. MS (ESI⁺): *m/z* calcd for C₁₁H₁₀BrNaNO₂, 289.99; found, 290.00 ([*M* + Na]⁺).

1-Methyl-5-phenylindole-3-carboxylic Acid (70). Compound **31** (90.0 mg, 0.34 mmol, 1.00 equiv) and LiOH (142 mg, 3.39 mmol, 10.0 equiv) were dissolved in a mixture of H₂O/THF (20 mL/14

mL). The solution was stirred at 90 °C for 28 h. After cooling to room temperature, the solution was washed with DCM (3 × 20 mL), and the aqueous layer was acidified with HCl solution (10%). The resulting suspension was extracted with EtOAc (3 × 20 mL), and the combined organic layers were dried (Na₂SO₄), filtered, and concentrated. The crude product was purified by column chromatography (EtOAc) to yield **70** as a colorless solid (66 mg, 78%). ¹H NMR (500 MHz, DMSO-*d*₆): δ 12.01 (s, 1H), 8.26–8.25 (m, 1H), 8.07 (s, 1H), 7.68–7.60 (m, 3H), 7.57–7.53 (m, 1H), 7.50–7.45 (m, 2H), 7.37–7.31 (m, 1H), 3.88 (s, 3H). ¹³C NMR (126 MHz, DMSO-*d*₆): δ 165.57, 141.37, 136.78, 136.63, 133.89, 128.90, 126.97, 126.88, 126.69, 121.57, 118.72, 111.16, 106.48, 33.09. MS (ESI⁺): *m/z* calcd for C₁₆H₁₄NO₂, 252.09; found, 252.12 ([*M* + *H*]⁺).

5-Bromo-7-chloro-1H-indole-3-carboxylic Acid Methyl Ester (73). Trichloroacetyl chloride (**72**, 0.39 mL, 3.47 mmol, 4.00 equiv) was added to a solution of **71** (200 mg, 0.87 mmol, 1.00 equiv) in DCM (10 mL). Pyridine (0.28 mL, 3.47 mmol, 4.00 equiv) was added dropwise, and the solution was stirred at 48 °C for 14 h. After cooling to room temperature, the solution was poured into ice water, which was then extracted with DCM (3 × 20 mL). The combined organic layers were dried (Na₂SO₄), filtered, and concentrated, resulting in a brown solid. The crude product was used without any purification. The crude product (477 mg, 1.27 mmol, 1.00 equiv) and KOH (92.0 mg, 1.65 mmol, 1.10 equiv) were dissolved in MeOH (15 mL). The solution was stirred at room temperature for 21 h. H₂O (7 mL) and aqueous hydrochloric acid (1N) were added to obtain a pH of 6. The solution was extracted with EtOAc (3 × 20 mL), and the combined organic layers were dried (Na₂SO₄), filtered, and concentrated. The crude product was purified by column chromatography (*n*-hexane/EtOAc 3:1) to yield **73** as a yellow solid (125 mg, 50%). ¹H NMR (500 MHz, acetone-*d*₆): δ 11.48 (s, 1H), 8.22–8.21 (m, 1H), 8.13 (d, *J* = 3.0 Hz, 1H), 7.46 (d, *J* = 1.7 Hz, 1H), 3.87 (s, 3H). ¹³C NMR (126 MHz, acetone-*d*₆): δ 164.88, 134.52, 133.58, 129.83, 125.40, 123.30, 118.91, 114.90, 109.45, 51.36. MS (ESI⁺): *m/z* calcd for C₁₀H₈BrClNO₂, 287.93; found, 287.93 ([*M* + *H*]⁺).

5-Bromo-7-chloro-1-methyl-1H-indole-3-carboxylic Acid Methyl Ester (74). Compound **73** (125 mg, 0.43 mmol, 1.00 equiv) and NaH (21.0 mg, 0.87 mmol, 2.00 equiv) were dissolved in DMF (10 mL) and cooled to 0 °C. Methyl iodide (81.0 μL, 1.30 mmol, 3.00 equiv) was added dropwise at 0 °C, and the reaction was stirred at room temperature for 6 h. H₂O was then added (20 mL), and the solution was extracted with EtOAc (3 × 20 mL). The combined organic layers were dried (Na₂SO₄), filtered, and concentrated. Further purification was performed by column chromatography (*n*-hexane/EtOAc 3:1) to yield **74** as a colorless solid (85 mg, 65%). ¹H NMR (500 MHz, acetone-*d*₆): δ 8.19 (d, *J* = 1.8 Hz, 1H), 7.99 (s, 1H), 7.36 (d, *J* = 1.8 Hz, 1H), 4.22 (s, 3H), 3.85 (s, 3H). ¹³C NMR (126 MHz, acetone-*d*₆): δ 164.52, 140.16, 132.37, 131.74, 126.84, 123.45, 119.18, 114.84, 106.87, 51.28, 37.84. MS (ESI⁺): *m/z* calcd for C₁₁H₉BrClNaNO₂, 323.95; found, 323.99 ([*M* + Na]⁺).

In Vitro Assays. Hybrid Reporter Gene Assays. Reporter gene assays were performed in the 96-well format in HEK293T cells as reported previously using the Gal4-fusion receptor plasmids pFA-CMV-hTHRα-LBD,³³ pFA-CMV-hRARα-LBD,³⁴ pFA-CMV-hPPARα-LBD,³⁵ pFA-CMV-hPPARγ-LBD,³⁵ pFA-CMV-hPPARδ-LBD,³⁵ pFA-CMV-hLXRα-LBD,³⁶ pFA-CMV-hLXRβ-LBD,³⁶ pFA-CMV-hFXR-LBD,³⁷ pFA-CMV-hVDR-LBD,³⁴ pFA-CMV-hRXRα-LBD,³⁴ pFA-CMV-hNur77-LBD,¹⁸ pFA-CMV-hNurr1-LBD,¹⁸ and pFA-CMV-hNOR1-LBD,¹⁸ which code for the hinge region and LBD of the canonical isoform of the respective human nuclear receptor. The Gal4-VP16³⁸ fusion protein (pECE-SV40-Gal4-VP16,³⁹ Addgene, entry 71728, Watertown, MA, USA) was employed as a ligand-independent transcriptional inducer for control experiments. pFR-Luc (Stratagene, La Jolla, CA, USA) served as a reporter plasmid, and pRL-SV40 (Promega, Madison, WI, USA) was used for normalization of transfection efficiency and test compound toxicity. Transient transfection was achieved with the Lipofectamine LTX reagent (Invitrogen, Carlsbad, CA, USA). The test compound solutions were prepared in Opti-MEM supplemented with penicillin (100 U/mL), streptomycin (100 μg/mL), and 0.1% DMSO. Each concentration

was tested in duplicates, and each experiment was performed independently at least three times. Luminescence was measured with a Spark 10 M luminometer (Tecan Group AG, Männedorf, Switzerland); firefly luciferase data were divided by renilla luciferase data and multiplied by 1000 to obtain relative light units (RLU). Fold activation was obtained by dividing the mean RLU of a test compound at a respective concentration by the mean RLU of untreated control and used for dose–response curve fitting with the equations “[inhibitor]/[agonist] vs response – variable slope (four parameters)” in GraphPad Prism (version 7.00, GraphPad software, La Jolla, CA, USA).

Full-Length Nurr1 Reporter Gene Assays. The reporter gene assays to observe modulation of full-length human Nurr1 were performed as described previously with the reporter plasmids pFR-Luc-NBRE,¹⁸ pFR-Luc-NurRE,¹⁸ and pFRLuc-DRS,¹⁸ each containing one copy of the respective human Nurr1 response element NBRE N13, NurRE, or DRS. Full-length human Nurr1 was expressed from pcDNA3.1-hNurr1-NE, Addgene, (entry 102363); RXR α (for DRS) was expressed from pSG5-hRXR.⁴⁰ The assay procedure, luminescence measurement, and data analysis were performed as described for the hybrid reporter gene assays.

HTRF Assays. Effects of **40** on the coregulator (NCoR1, NCoR2, NCoA6, SRC1, and CBP-1) interaction and dimerization (Nurr1 and RXR α) of the Nurr1-LBD were studied in homogeneous time-resolved fluorescence resonance energy-transfer assay systems. Terbium cryptate as a streptavidin conjugate (Tb-SA; Cisbio Bioassays, Codolet, France) served as a FRET donor and was coupled to a biotinylated Nurr1-LBD protein (produced as described previously¹⁸) or coregulator peptides (obtained from Eurogentec, Seraing, Belgium; NCoR1: biotin-GMGQVPRTHRLITLADHIC-QIITQDFARN; NCoR2: biotin-SQAVQEHAHNMGLEAIIR-KALMGKYDQW; NCoA6: biotin-VNKDVTLSPLVNLQSDI-SAGH; SRC1: biotin-CPSSHSLSLTERHKILHRLQLQEGSPS; and CBP-1: biotin-NLVPDAASKHKQLSELLRGGSGS). Recombinant sGFP-Nurr1-LBD or sGFP-RXR α -LBD (produced as described previously¹⁸) were used as FRET acceptors. All experiments were performed in white flat-bottom polystyrol 384 well microtiter plates (Greiner Bio-One, Frickenhausen, Germany) in HTRF assay buffer (150 mM KF, 25 mM HEPES pH 7.5 (KOH), 10% (w/v) Glycerol, 5 mM DTT) supplemented with 0.1% (w/v) CHAPS and 1% DMSO. The assay solutions contained biotinylated coregulator peptides (final concentration 12 nM), Tb-SA (12 nM), and sGFP-Nurr1-LBD (100 nM) for coregulator recruitment or biotinylated Nurr1-LBD (final concentration 0.6 nM), Tb-SA (1.2 nM), and sGFP-Nurr1-LBD (at varying concentrations up to 300 nM) or sGFP-RXR α -LBD (at varying concentrations up to 4000 nM) for dimerization experiments. The test compound **40** was used at varying concentrations. Free sGFP was added in the Nurr1 dimerization assays to keep the total sGFP content stable (300 or 4000 nM) and to suppress artifacts from changes in the degree of diffusion-enhanced FRET. Samples were set up in four technical replicates for coregulator peptide recruitment and in three technical replicates for dimerization assays. After 2 h of incubation at RT, fluorescence intensities (FI) after excitation at 340 nm were recorded at 520 nm for sGFP FRET acceptor fluorescence and 620 nm for Tb-SA FRET donor fluorescence on a SPARK plate reader (Tecan Group AG). FI_{520nm} was divided by FI_{620nm} and multiplied with 10,000 to give a dimensionless HTRF signal.

WST-1 Toxicity Assay. WST-1 assay (Roche Diagnostics International AG, Rotkreuz, Switzerland) was performed in HEK293T cells and T98G cells according to the manufacturer's protocol. The cells were grown and seeded in Dulbecco's modified Eagle medium (DMEM) high glucose, supplemented with sodium pyruvate (1 mM), penicillin (100 U/mL), streptomycin (100 μ g/mL), and 10% FCS in 96-well plates at a density of 3×10^4 cells/well. After 24 h, cells were incubated with the test compound **31** or **40** (final concentrations 0.1, 1, 10, 30, and 100 μ M) in DMEM high glucose, supplemented with penicillin (100 U/mL), streptomycin (100 μ g/mL), 1% charcoal stripped FCS, and 0.1% DMSO. After 24 h of incubation, WST reagent was added to each well, and absorbance (450 nm/reference, 620 nm) was determined with a Spark 10M luminometer (Tecan

Group AG) after 45 min. Each experiment was repeated four times in duplicates.

Nurr1 Knockdown in T98G cells. T98G cells were grown in DMEM high glucose, supplemented with 10% FCS, sodium pyruvate (1 mM), penicillin (100 U/mL), and streptomycin (100 μ g/mL) at 37 °C and 5% CO₂. A period of 24 h before transfection, T98G cells were seeded in 12-well plates (1×10^5 cells/well). The medium was changed to reduced serum medium containing DMEM high glucose supplemented with 1% charcoal-stripped FCS, sodium pyruvate (1 mM), penicillin (100 U/mL), and streptomycin (100 μ g/mL) right before transfection. Knockdown was mediated by transient transfection using the RNAiMAX reagent (Invitrogen) according to the manufacturer's protocol with 30 nM Nurr1-targeting esiRNA (Cat# EHU008731) or nontargeting control siRNA (Cat# SIC001, both from Sigma-Aldrich). A period of 24 h after transfection, the cells were harvested and directly used for RNA extraction or used for quantification of IL-6 release (as described below). A total of 2 μ g of total RNA was extracted from T98G cells using the E.Z.N.A. total RNA kit I (R6834-02, Omega Bio-Tek, Inc., Norcross, GA). RNA was reverse-transcribed into cDNA using the high-capacity RNA-to-cDNA kit (4387406, Thermo Fischer Scientific Inc., Waltham, MA, USA) according to the manufacturer's protocol. Nurr1 knockdown efficiency was evaluated by quantitative real-time PCR analysis with a StepOnePlus system (Life Technologies, Carlsbad, CA) using Power SYBR Green (Life Technologies; 12.5 μ L/well). Each sample was set up in duplicate and repeated in eight independent experiments. The expression was quantified by the comparative $2^{-\Delta\Delta Ct}$ method, and glyceraldehyde 3-phosphate dehydrogenase (GAPDH) served as the reference gene. Primer sequences for the human Nurr1 gene were obtained from OriGene (OriGene Technologies Inc., Rockville, MD, USA). The following PCR primers were used: hGAPDH: 5'-ATA TGA TTC CAC CCA TGG CA (fw), 5'-GAT GAT GAC CCT TTT GGC TC (rev), hNurr1: 5'-AAA CTG CCC AGT GGA CAA GCG T (fw), and 5'-GCT CTT CGG TTT CGA GGG CAA A (rev).

Quantification of IL-6 Release in T98G cells. T98G cells were grown in 12-well plates (1×10^5 cells/well) or 24-well plates (5×10^4 cells/well) in DMEM high glucose, supplemented with 10% FCS, sodium pyruvate (1 mM), penicillin (100 U/mL), and streptomycin (100 μ g/mL) at 37 °C and 5% CO₂ for 24 h. Before incubation with LPS and test compound **31**, the medium was changed to DMEM supplemented with 1% charcoal-stripped FCS, sodium pyruvate (1 mM), penicillin (100 U/mL), and streptomycin (100 μ g/mL) for 12 h, or Nurr1 knockdown was performed by transient transfection for 24 h as outlined above. The cells were then treated with LPS (1 μ g/mL) to induce inflammation and simultaneously incubated with **31** and 0.1% DMSO or 0.1% DMSO alone as an untreated control. Each sample was repeated independently at least three times. Following overnight (24 h) incubation, 100 μ L of the respective supernatants was collected and assayed for IL-6 using the human IL-6 ELISA kit (Cat# KHC0061, Thermo Fisher Scientific, Inc.) according to the manufacturer's protocol. Absorbance at 450 nm was measured with a Spark 10 M luminometer (Tecan Group AG).

Quantification of Nurr1-Regulated mRNA Expression in T98G cells by qRT-PCR. Nurr1-regulated gene expression in T98G cells was performed as described previously¹⁷ with the test compounds **31** (30 μ M) and **40** (30 μ M). Cells were incubated with test compounds for 8 h, and mRNA was extracted, processed, and quantified as described for the knockdown experiments. The expression levels were quantified by the $2^{-\Delta\Delta Ct}$ method with glyceraldehyde 3-phosphate dehydrogenase (GAPDH) as the reference gene. The following primers were used: hGAPDH: 5'-ATA TGA TTC CAC CCA TGG CA (fw), 5'-GAT GAT GAC CCT TTT GGC TC (rev), hVMAT2: 5'-GCT ATG CCT TCC TGC TGA TTG C (fw), 5'-CCA AGG CGA TTC CCA TGA CGT T (rev); hTH: 5'-GCT GGA CAA GTG TCA CCA CCT G (fw), 5'-CCT GTA CTG GAA GGC GAT CTC A (rev); hDDC: 5'-GGA CCA CAA CAT GCT GCT CCT T (fw), and 5'-CTC CAC TCC ATT CAG AAG GTG C (rev).

Computational Methods. Flexible Alignment. Calculations were conducted in Molecular Operating Environment (MOE, version

2020.09, Chemical Computing Group Inc. Montreal, QC, Canada) using default settings for each tool/function unless stated otherwise. Amber10:EHT was used as the default force field. For *flexible alignment*, the molecular structures of amodiaquine and **25** were prepared using the MOE Wash tool: protonation state dominant at pH 7; coordinates rebuilt in 3D; and preserved existing chirality. Alignment of the two compounds was performed using the MOE flexible alignment tool. A total of 9 out of 10 conformations of **25** aligned with the amodiaquine scaffold and were superposed.

Target Prediction. The similarity ensemble approach (SEA)³⁰ server at <https://sea.bkslab.org/> was used for target prediction of **31** and **40**. Only predictions with a Tanimoto coefficient of ≥ 0.5 and expectancy (*E*) value of $\leq 1 \times 10^{-50}$ were considered.

■ ASSOCIATED CONTENT

Supporting Information

The Supporting Information is available free of charge at <https://pubs.acs.org/doi/10.1021/acs.jmedchem.1c01077>.

Figure S1 and chromatographic purity data for **4–42** (PDF)

Molecular structures of **4–42** and associated activity data (CSV)

■ AUTHOR INFORMATION

Corresponding Author

Daniel Merk – Institute of Pharmaceutical Chemistry, Goethe University Frankfurt, D-60438 Frankfurt, Germany; Department of Pharmacy, Ludwig-Maximilians-Universität München, D-81377 Munich, Germany; orcid.org/0000-0002-5359-8128; Phone: +49 69 79829327; Email: merk@pharmchem.uni-frankfurt.de

Authors

Daniel Zaienne – Institute of Pharmaceutical Chemistry, Goethe University Frankfurt, D-60438 Frankfurt, Germany

Sabine Willems – Institute of Pharmaceutical Chemistry, Goethe University Frankfurt, D-60438 Frankfurt, Germany; orcid.org/0000-0002-9755-3394

Simone Schierle – Institute of Pharmaceutical Chemistry, Goethe University Frankfurt, D-60438 Frankfurt, Germany

Jan Heering – Fraunhofer Institute for Translational Medicine and Pharmacology ITMP, D-60596 Frankfurt, Germany; orcid.org/0000-0002-4922-1993

Complete contact information is available at: <https://pubs.acs.org/doi/10.1021/acs.jmedchem.1c01077>

Author Contributions

^{||}D.Z. and S.W. contributed equally to this study.

Notes

The authors declare no competing financial interest.

■ ACKNOWLEDGMENTS

D.M. is grateful for financial support by the Aventis Foundation. Gal4-VP16 was a gift from Lea Sistonen (Addgene plasmid #71728). pcDNA3.1-hNurr1-NE was a gift from Shu Leong Ho (Addgene plasmid #102363).

■ ABBREVIATIONS

AD, Alzheimer's disease; AQ, amodiaquine; CBP-1, CREB-binding protein coactivator motif 1; DDC, DOPA decarboxylase; DR5, Nurr1-RXR heterodimer response element; EAE, experimental autoimmune encephalomyelitis; FRET, fluorescence resonance energy transfer; FXR, farnesoid X receptor;

HTRF, homogeneous time-resolved fluorescence resonance energy transfer; IL-6, interleukin-6; LBD, ligand binding domain; LPS, lipopolysaccharide; LXR, liver X receptor; MPTP, 1-methyl-4-phenyl-1,2,3,6-tetrahydropyridine; MS, multiple sclerosis; NBRE, Nurr1 monomer response element; NCoA, nuclear receptor coactivator; NCoR, nuclear receptor corepressor; Nurr1, Nuclear receptor related 1; NurRE, Nurr1 homodimer response element; PD, Parkinson's disease; PPAR, peroxisome proliferator-activated receptor; RNAi, RNA interference; RAR, retinoic acid receptor; RXR, retinoid X receptor; SAR, structure–activity relationship; siRNA, small interfering RNA; SRC1, steroid receptor co-activator 1; Tb-SA, terbium cryptate coupled to streptavidin; TH, tyrosine hydroxylase; THR, thyroid hormone receptor; VDR, vitamin D receptor; VMAT2, vesicular monoamine transporter 2

■ REFERENCES

- (1) Wang, Z.; Benoit, G.; Liu, J.; Prasad, S.; Aarnisalo, P.; Liu, X.; Xu, H.; Walker, N. P. C.; Perlmann, T. Structure and Function of Nurr1 Identifies a Class of Ligand-Independent Nuclear Receptors. *Nature* **2003**, *423*, 555–560.
- (2) Decressac, M.; Volakakis, N.; Björklund, A.; Perlmann, T. NURR1 in Parkinson Disease - From Pathogenesis to Therapeutic Potential. *Nat. Rev. Neurol.* **2013**, *9*, 629–636.
- (3) Liu, W.; Gao, Y.; Chang, N. Nurr1 Overexpression Exerts Neuroprotective and Anti-Inflammatory Roles via down-Regulating CCL2 Expression in Both in Vivo and in Vitro Parkinson's Disease Models. *Biochem. Biophys. Res. Commun.* **2017**, *482*, 1312–1319.
- (4) Moon, M.; Jeong, I.; Kim, C.-H.; Kim, J.; Lee, P. K. J.; Mook-Jung, I.; Leblanc, P.; Kim, K.-S. Correlation between Orphan Nuclear Receptor Nurr1 Expression and Amyloid Deposition in 5XFAD Mice, an Animal Model of Alzheimer's Disease. *J. Neurochem.* **2015**, *132*, 254–262.
- (5) Moon, M.; Jung, E. S.; Jeon, S. G.; Cha, M.-Y.; Jang, Y.; Kim, W.; Lopes, C.; Mook-Jung, I.; Kim, K.-S. Nurr1 (NR4A2) Regulates Alzheimer's Disease-Related Pathogenesis and Cognitive Function in the 5XFAD Mouse Model. *Aging Cell* **2019**, *18*, No. e12866.
- (6) Satoh, J.-i.; Nakanishi, M.; Koike, F.; Miyake, S.; Yamamoto, T.; Kawai, M.; Kikuchi, S.; Nomura, K.; Yokoyama, K.; Ota, K.; Kanda, T.; Fukazawa, T.; Yamamura, T. Microarray Analysis Identifies an Aberrant Expression of Apoptosis and DNA Damage-Regulatory Genes in Multiple Sclerosis. *Neurobiol. Dis.* **2005**, *18*, 537–550.
- (7) Montarolo, F.; Perga, S.; Martire, S.; Bertolotto, A. Nurr1 Reduction Influences the Onset of Chronic EAE in Mice. *Inflammation Res.* **2015**, *64*, 841–844.
- (8) Jakaria, M.; Haque, M. E.; Cho, D.-Y.; Azam, S.; Kim, I.-S.; Choi, D.-K. Molecular Insights into NR4A2(Nurr1): An Emerging Target for Neuroprotective Therapy Against Neuroinflammation and Neuronal Cell Death. *Mol. Neurobiol.* **2019**, *56*, 5799–5814.
- (9) Willems, S.; Zaienne, D.; Merk, D. Targeting Nuclear Receptors in Neurodegeneration and Neuroinflammation. *J. Med. Chem.* **2021**, *64*, 9592–9638.
- (10) de Vera, I. M. S.; Giri, P. K.; Munoz-Tello, P.; Brust, R.; Fuhrmann, J.; Matta-Camacho, E.; Shang, J.; Campbell, S.; Wilson, H. D.; Granados, J.; Gardner, W. J.; Creamer, T. P.; Solt, L. A.; Kojetin, D. J. Identification of a Binding Site for Unsaturated Fatty Acids in the Orphan Nuclear Receptor Nurr1. *ACS Chem. Biol.* **2016**, *11*, 1795–1799.
- (11) de Vera, I. M. S.; Munoz-Tello, P.; Zheng, J.; Dharmarajan, V.; Marciano, D. P.; Matta-Camacho, E.; Giri, P. K.; Shang, J.; Hughes, T. S.; Rance, M.; Griffin, P. R.; Kojetin, D. J. Defining a Canonical Ligand-Binding Pocket in the Orphan Nuclear Receptor Nurr1. *Structure* **2019**, *27*, 66.
- (12) Munoz-Tello, P.; Lin, H.; Khan, P.; De Vera, I. M. S.; Kamenecka, T. M.; Kojetin, D. J. Assessment of NR4A Ligands That Directly Bind and Modulate the Orphan Nuclear Receptor Nurr1. *J. Med. Chem.* **2020**, *63*, 15639.

- (13) Kim, C.-H.; Han, B.-S.; Moon, J.; Kim, D.-J.; Shin, J.; Rajan, S.; Nguyen, Q. T.; Sohn, M.; Kim, W.-G.; Han, M.; Jeong, I.; Kim, K.-S.; Lee, E.-H.; Tu, Y.; Naffin-Olivos, J. L.; Park, C.-H.; Ringe, D.; Yoon, H. S.; Petsko, G. A.; Kim, K.-S. Nuclear Receptor Nurr1 Agonists Enhance Its Dual Functions and Improve Behavioral Deficits in an Animal Model of Parkinson's Disease. *Proc. Natl. Acad. Sci. U.S.A.* **2015**, *112*, 8756–8761.
- (14) Rajan, S.; Jang, Y.; Kim, C.-H.; Kim, W.; Toh, H. T.; Jeon, J.; Song, B.; Serra, A.; Lescar, J.; Yoo, J. Y.; Beldar, S.; Ye, H.; Kang, C.; Liu, X.-W.; Feitosa, M.; Kim, Y.; Hwang, D.; Goh, G.; Lim, K.-L.; Park, H. M.; Lee, C. H.; Oh, S. F.; Petsko, G. A.; Yoon, H. S.; Kim, K.-S. PGE1 and PGA1 Bind to Nurr1 and Activate Its Transcriptional Function. *Nat. Chem. Biol.* **2020**, *16*, 876–886.
- (15) Bruning, J. M.; Wang, Y.; Oltrabella, F.; Tian, B.; Kholodar, S. A.; Liu, H.; Bhattacharya, P.; Guo, S.; Holton, J. M.; Fletterick, R. J.; Jacobson, M. P.; England, P. M. Covalent Modification and Regulation of the Nuclear Receptor Nurr1 by a Dopamine Metabolite. *Cell Chem. Biol.* **2019**, *26*, 674–685.
- (16) Kholodar, S. A.; Lang, G.; Cortopassi, W. A.; Iizuka, Y.; Brah, H. S.; Jacobson, M. P.; England, P. M. Analogs of the Dopamine Metabolite 5,6-Dihydroxyindole Bind Directly to and Activate the Nuclear Receptor Nurr1. *ACS Chem. Biol.* **2021**, *16*, 1159–1163.
- (17) Willems, S.; Ohrndorf, J.; Kilu, W.; Heering, J.; Merk, D. Fragment-like Chloroquinolineamines Activate the Orphan Nuclear Receptor Nurr1 and Elucidate Activation Mechanisms. *J. Med. Chem.* **2021**, *64*, 2659–2668.
- (18) Willems, S.; Kilu, W.; Ni, X.; Chaikuad, A.; Knapp, S.; Heering, J.; Merk, D. The Orphan Nuclear Receptor Nurr1 Is Responsive to Non-Steroidal Anti-Inflammatory Drugs. *Commun. Chem.* **2020**, *3*, 85.
- (19) De Bruyn, T.; Van Westen, G. J. P.; IJzerman, A. P.; Stieger, B.; De Witte, P.; Augustijns, P. F.; Annaert, P. P. Structure-Based Identification of Oatp1b1/3 Inhibitors. *Mol. Pharmacol.* **2013**, *83*, 1257–1267.
- (20) Ren, S.; Zeng, J.; Mei, Y.; Zhang, J. Z. H.; Yan, S. F.; Fei, J.; Chen, L. Discovery and Characterization of Novel, Potent, and Selective Cytochrome P450 2J2 Inhibitors. *Drug Metab. Dispos.* **2013**, *41*, 60–71.
- (21) Tang, Y.; Wu, Q.; Beland, F. A.; Chen, S.; Fang, J.-L. Apoptosis Contributes to the Cytotoxicity Induced by Amodiaquine and Its Major Metabolite N-Desethylamodiaquine in Hepatic Cells. *Toxicol. Vitro* **2020**, *62*, 104669.
- (22) Schierle, S.; Chaikuad, A.; Lillich, F. F.; Ni, X.; Woltersdorf, S.; Schallmayer, E.; Renelt, B.; Ronchetti, R.; Knapp, S.; Proschak, E.; Merk, D. Oxaprozin Analogues as Selective RXR Agonists with Superior Properties and Pharmacokinetics. *J. Med. Chem.* **2021**, *64*, 5123–5136.
- (23) Kambey, P. A.; Chengcheng, M.; Xiaoxiao, G.; Abdulrahman, A. A.; Kanwore, K.; Nadeem, I.; Jiao, W.; Gao, D. The Orphan Nuclear Receptor Nurr1 Agonist Amodiaquine Mediates Neuroprotective Effects in 6-OHDA Parkinson's Disease Animal Model by Enhancing the Phosphorylation of P38 Mitogen-Activated Kinase but Not PI3K/AKT Signaling Pathway. *Metab. Brain Dis.* **2021**, *36*, 609–625.
- (24) Kinoshita, K.; Matsumoto, K.; Kurauchi, Y.; Hisatsune, A.; Seki, T.; Katsuki, H. A Nurr1 Agonist Amodiaquine Attenuates Inflammatory Events and Neurological Deficits in a Mouse Model of Intracerebral Hemorrhage. *J. Neuroimmunol.* **2019**, *330*, 48–54.
- (25) Merk, D.; Sreeramulu, S.; Kudlinzki, D.; Saxena, K.; Linhard, V.; Gande, S. L.; Hiller, F.; Lamers, C.; Nilsson, E.; Aagaard, A.; Wissler, L.; Dekker, N.; Bamberg, K.; Schubert-Zsilavecz, M.; Schwalbe, H. Molecular Tuning of Farnesoid X Receptor Partial Agonism. *Nat. Commun.* **2019**, *10*, 2915.
- (26) De Bosscher, K.; Desmet, S. J.; Clarisse, D.; Estébanez-Perpiña, E.; Brunsveld, L. Nuclear Receptor Crosstalk — Defining the Mechanisms for Therapeutic Innovation. *Nat. Rev. Endocrinol.* **2020**, *16*, 363–377.
- (27) Rastinejad, F.; Huang, P.; Chandra, V.; Khorasanizadeh, S. Understanding Nuclear Receptor Form and Function Using Structural Biology. *J. Mol. Endocrinol.* **2013**, *51*, T1–T21.
- (28) de Vries, R. M. J. M.; Meijer, F. A.; Doveston, R. G.; Leijten-Van de Gevel, I. A.; Brunsveld, L. Cooperativity between the Orthosteric and Allosteric Ligand Binding Sites of ROR γ t. *Proc. Natl. Acad. Sci. U.S.A.* **2021**, *118*, No. e2021287118.
- (29) Marcotte, D. J.; Liu, Y.; Little, K.; Jones, J. H.; Powell, N. A.; Wildes, C. P.; Silvian, L. F.; Chodaparambil, J. V. Structural Determinant for Inducing ROR γ Specific Inverse Agonism Triggered by a Synthetic Benzoxazinone Ligand. *BMC Struct. Biol.* **2016**, *16*, 7.
- (30) Keiser, M. J.; Roth, B. L.; Armbruster, B. N.; Ernsberger, P.; Irwin, J. J.; Shoichet, B. K. Relating Protein Pharmacology by Ligand Chemistry. *Nat. Biotechnol.* **2007**, *25*, 197–206.
- (31) Safe, S.; Jin, U.-H.; Hedrick, E.; Reeder, A.; Lee, S.-O. Minireview: Role of Orphan Nuclear Receptors in Cancer and Potential as Drug Targets. *Mol. Endocrinol.* **2014**, *28*, 157–172.
- (32) Safe, S.; Karki, K. The Paradoxical Roles of Orphan Nuclear Receptor 4A (NR4A) in Cancer. *Mol. Cancer Res.* **2021**, *19*, 180–191.
- (33) Gellrich, L.; Heitel, P.; Heering, J.; Kilu, W.; Pollinger, J.; Goebel, T.; Kahnt, A.; Arifi, S.; Pogoda, W.; Paulke, A.; Steinhilber, D.; Proschak, E.; Wurglics, M.; Schubert-Zsilavecz, M.; Chaikuad, A.; Knapp, S.; Bischoff, I.; Fürst, R.; Merk, D. L-Thyroxin and the Nonclassical Thyroid Hormone TETRAC Are Potent Activators of PPAR γ . *J. Med. Chem.* **2020**, *63*, 6727–6740.
- (34) Flesch, D.; Cheung, S.-Y.; Schmidt, J.; Gabler, M.; Heitel, P.; Kramer, J.; Kaiser, A.; Hartmann, M.; Lindner, M.; Lüddens-Dämgen, K.; Heering, J.; Lamers, C.; Lüddens, H.; Wurglics, M.; Proschak, E.; Schubert-Zsilavecz, M.; Merk, D. Non-Acidic Farnesoid X Receptor Modulators. *J. Med. Chem.* **2017**, *60*, 7199–7205.
- (35) Rau, O.; Wurglics, M.; Paulke, A.; Zitzkowski, J.; Meindl, N.; Bock, A.; Dingermann, T.; Abdel-Tawab, M.; Schubert-Zsilavecz, M. Carnosic Acid and Carnosol, Phenolic Diterpene Compounds of the Labiate Herbs Rosemary and Sage, Are Activators of the Human Peroxisome Proliferator-Activated Receptor Gamma. *Planta Med.* **2006**, *72*, 881–887.
- (36) Heitel, P.; Achenbach, J.; Moser, D.; Proschak, E.; Merk, D. DrugBank Screening Revealed Alitretinoin and Bexarotene as Liver X Receptor Modulators. *Bioorg. Med. Chem. Lett.* **2017**, *27*, 1193–1198.
- (37) Schmidt, J.; Klingler, F.-M.; Proschak, E.; Steinhilber, D.; Schubert-Zsilavecz, M.; Merk, D. NSAIDs Ibuprofen, Indometacin, and Diclofenac Do Not Interact with Farnesoid X Receptor. *Sci. Rep.* **2015**, *5*, 14782.
- (38) Sadowski, I.; Ma, J.; Triezenberg, S.; Ptashne, M. GAL4-VP16 Is an Unusually Potent Transcriptional Activator. *Nature* **1988**, *335*, 563–564.
- (39) Budzyński, M. A.; Puustinen, M. C.; Joutsen, J.; Sistonen, L. Uncoupling Stress-Inducible Phosphorylation of Heat Shock Factor 1 from Its Activation. *Mol. Cell. Biol.* **2015**, *35*, 2530–2540.
- (40) Seuter, S.; Väisänen, S.; Rådmark, O.; Carlberg, C.; Steinhilber, D. Functional Characterization of Vitamin D Responding Regions in the Human 5-Lipoxygenase Gene. *Biochim. Biophys. Acta, Mol. Cell Biol. Lipids* **2007**, *1771*, 864–872.

- Supporting Information -

Development and profiling of inverse agonist tools for the neuroprotective transcription factor Nurr1

Daniel Zaienne^{1‡}, Sabine Willems^{1‡}, Simone Schierle¹, Jan Heering², Daniel Merk^{1,3*}

¹ Institute of Pharmaceutical Chemistry, Goethe University Frankfurt, D-60438 Frankfurt, Germany

² Fraunhofer Institute for Translational Medicine and Pharmacology ITMP, D-60596 Frankfurt, Germany

³ Department of Pharmacy, Ludwig-Maximilians-Universität München, D-81377 Munich, Germany

* merk@pharmchem.uni-frankfurt.de

Table of Contents

Supplementary Figures	S2
HPLC traces of 4-42	S3

Supplementary Figures

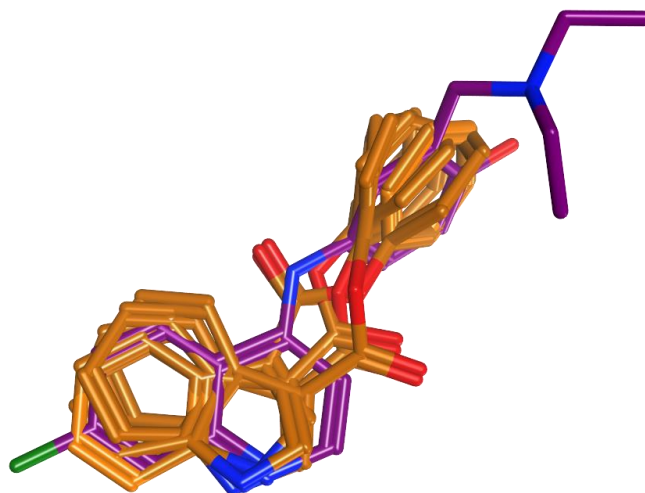
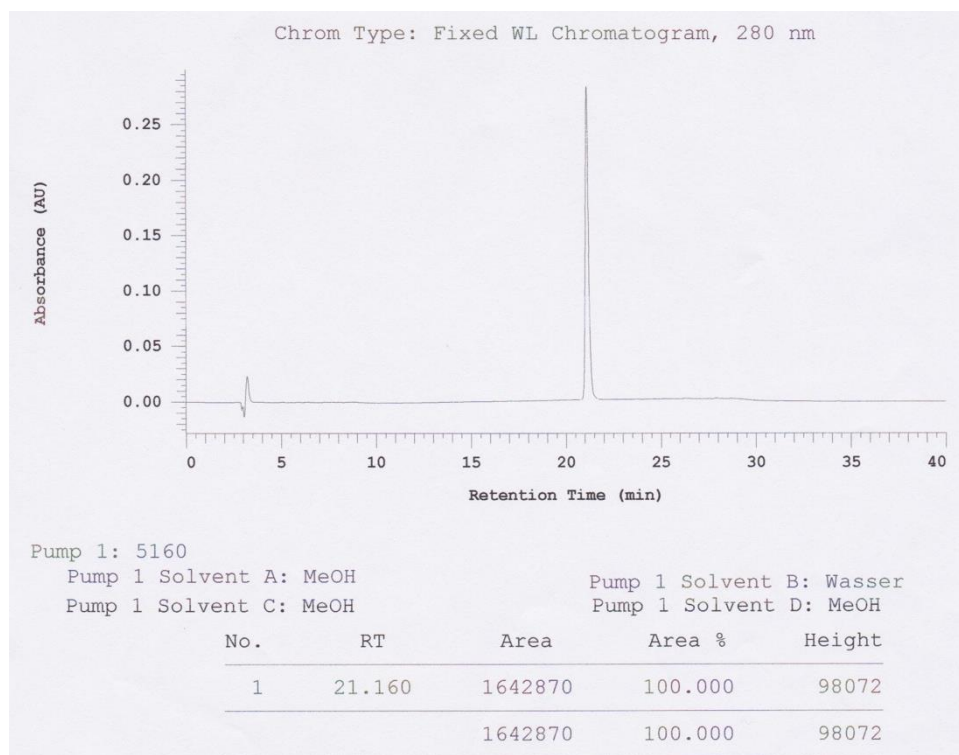
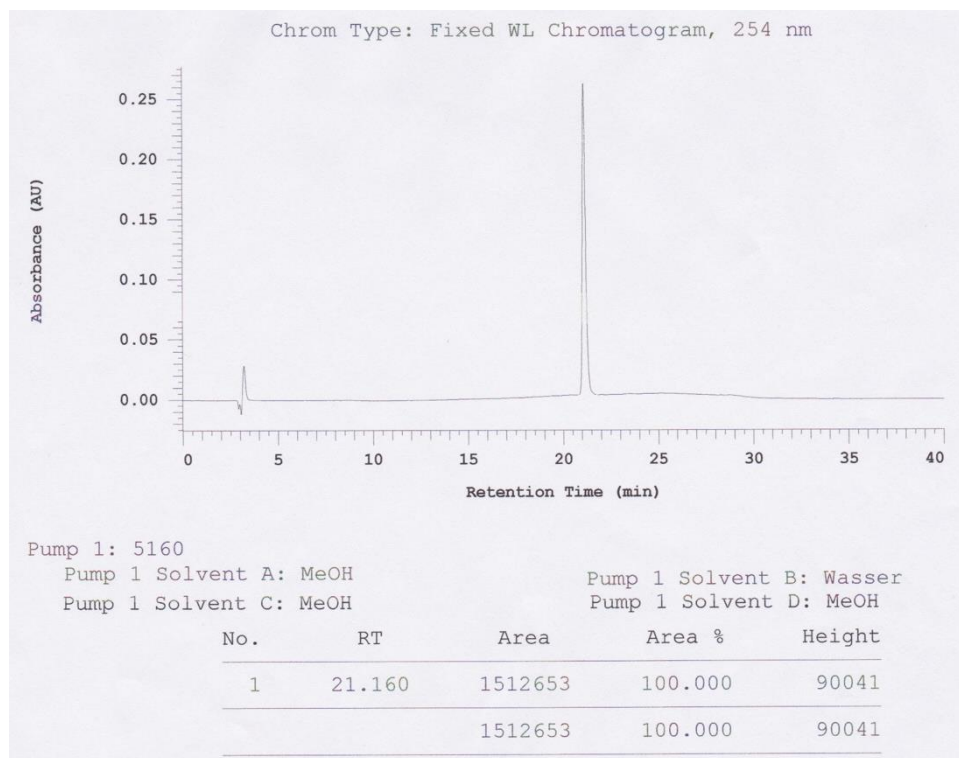


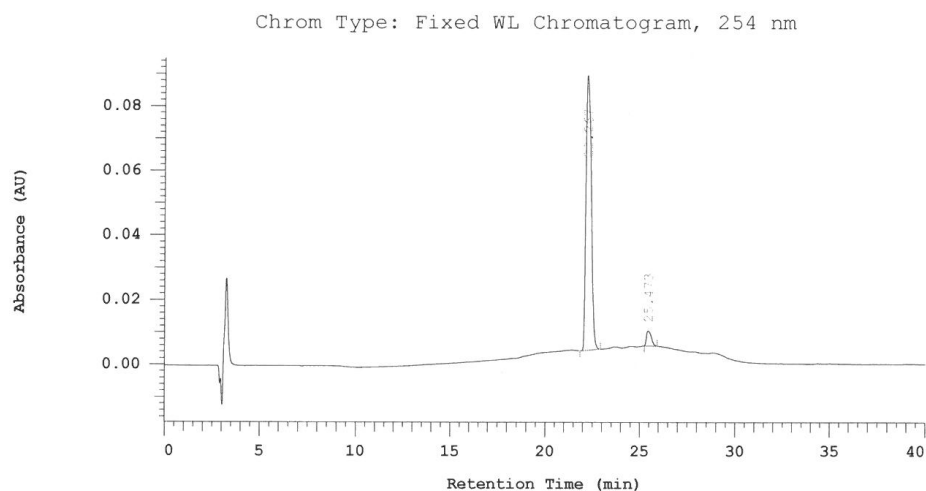
Figure S1. Flexible alignment (MOE) of Nurr1 agonists **25** and AQ reveals structural similarity with superposition of phenyl ester (**25**) and phenyl amine (AQ).

HPLC traces of 4-42

2-Methyl-1*H*-indole-3-carboxylic acid methyl ester (5):



2-Chloro-1*H*-indole-3-carboxylic acid methyl ester (**6**):



Pump 1: 5160

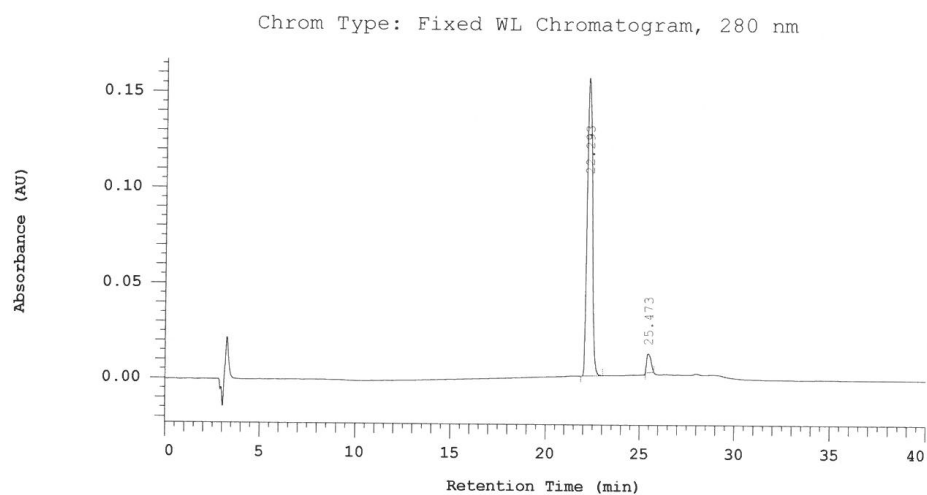
Pump 1 Solvent A: MeOH

Pump 1 Solvent B: Wasser

Pump 1 Solvent C: MeOH

Pump 1 Solvent D: MeOH

No.	RT	Area	Area %	Height
1	22.267	810083	95.244	39340
2	25.473	40450	4.756	2249
		850533	100.000	41589



Pump 1: 5160

Pump 1 Solvent A: MeOH

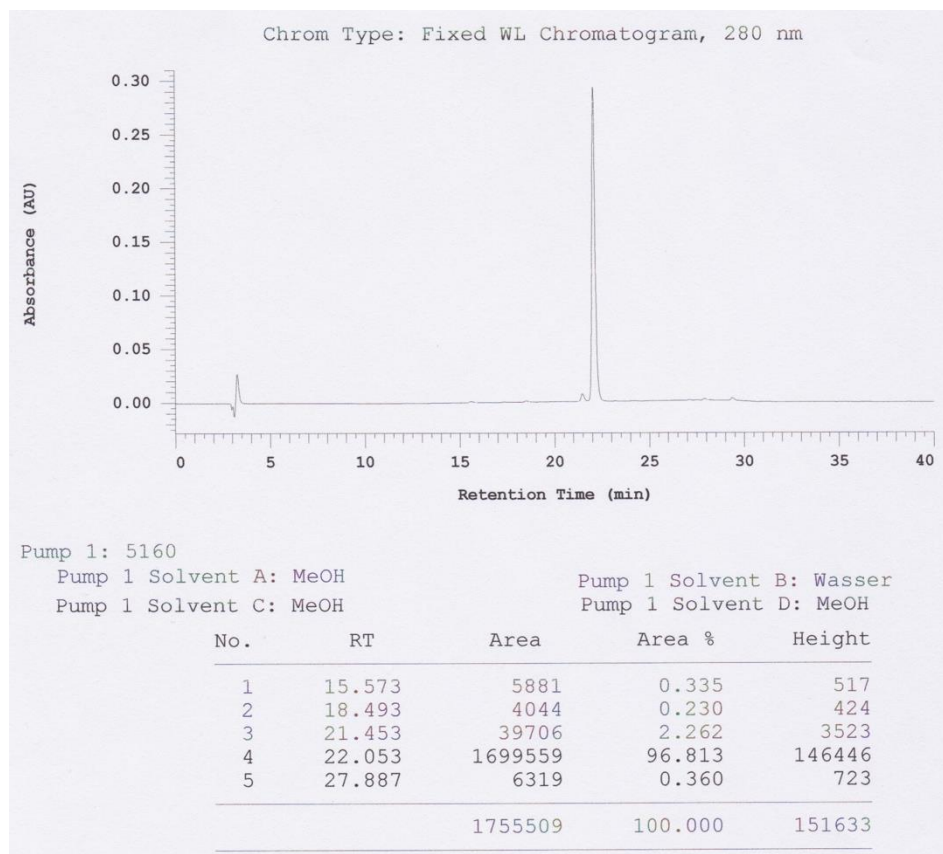
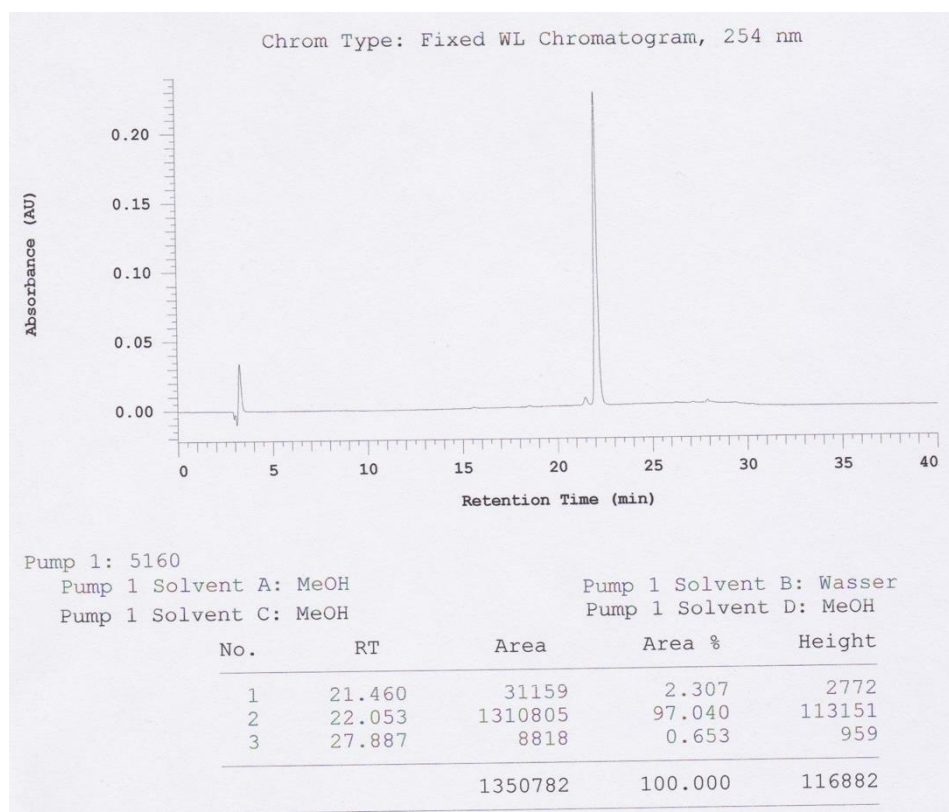
Pump 1 Solvent B: Wasser

Pump 1 Solvent C: MeOH

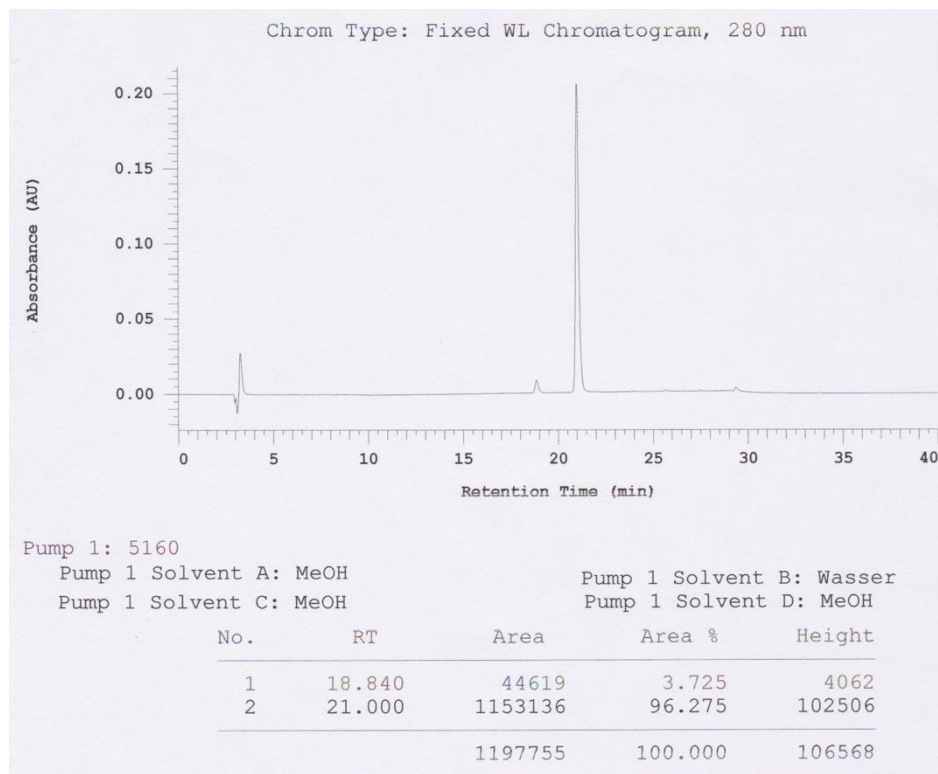
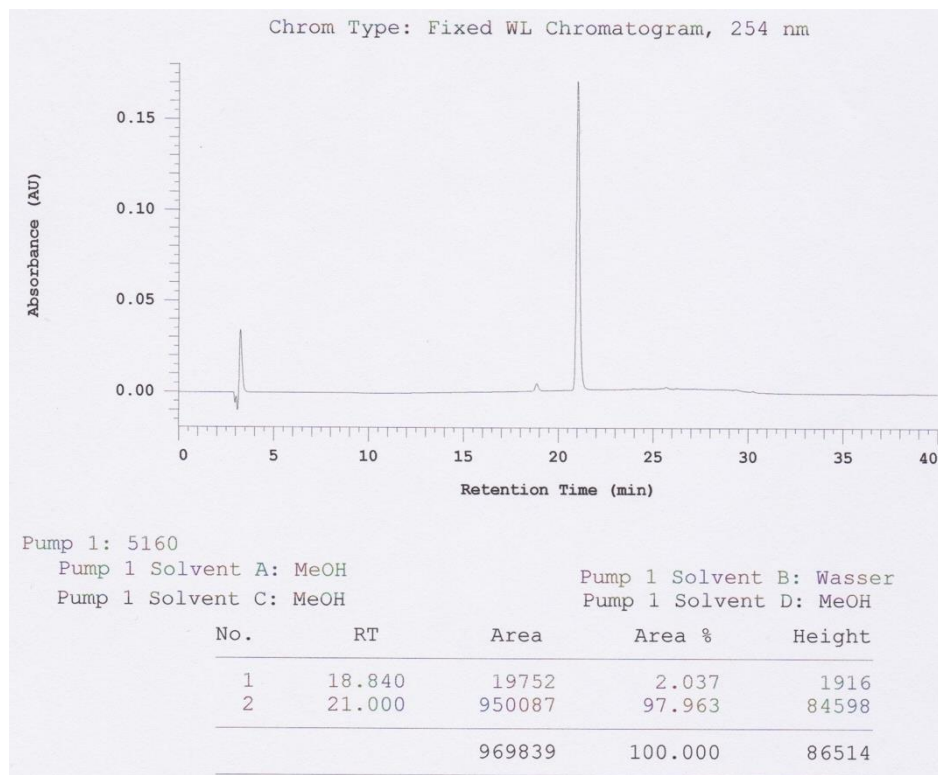
Pump 1 Solvent D: MeOH

No.	RT	Area	Area %	Height
1	22.293	1489299	95.109	68869
2	25.473	76591	4.891	4740
		1565890	100.000	73609

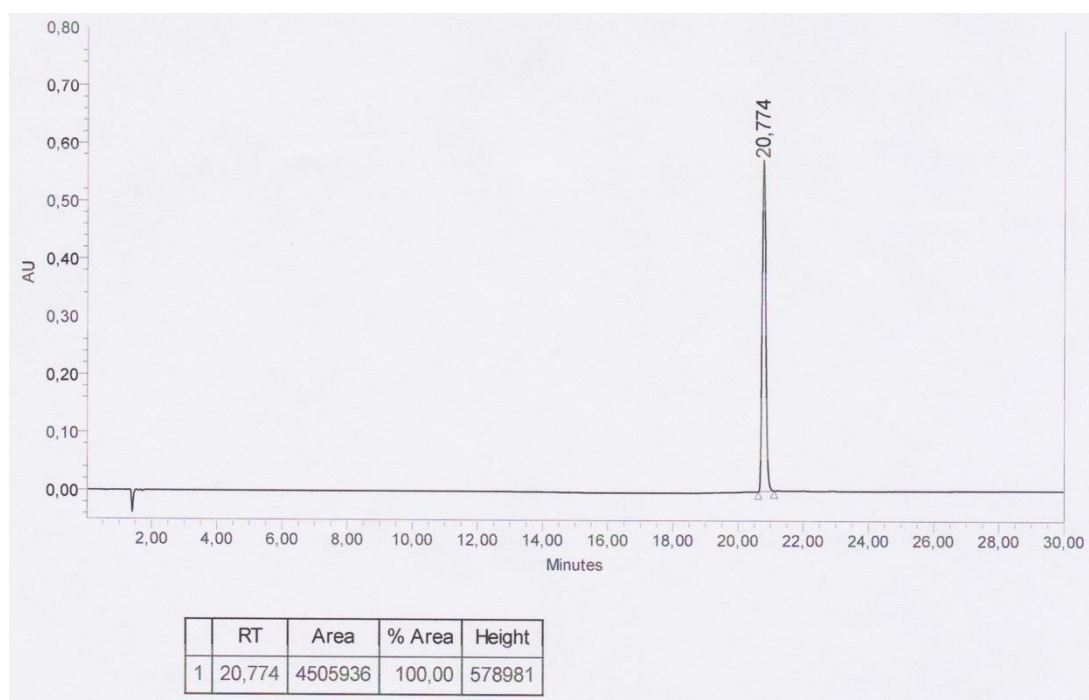
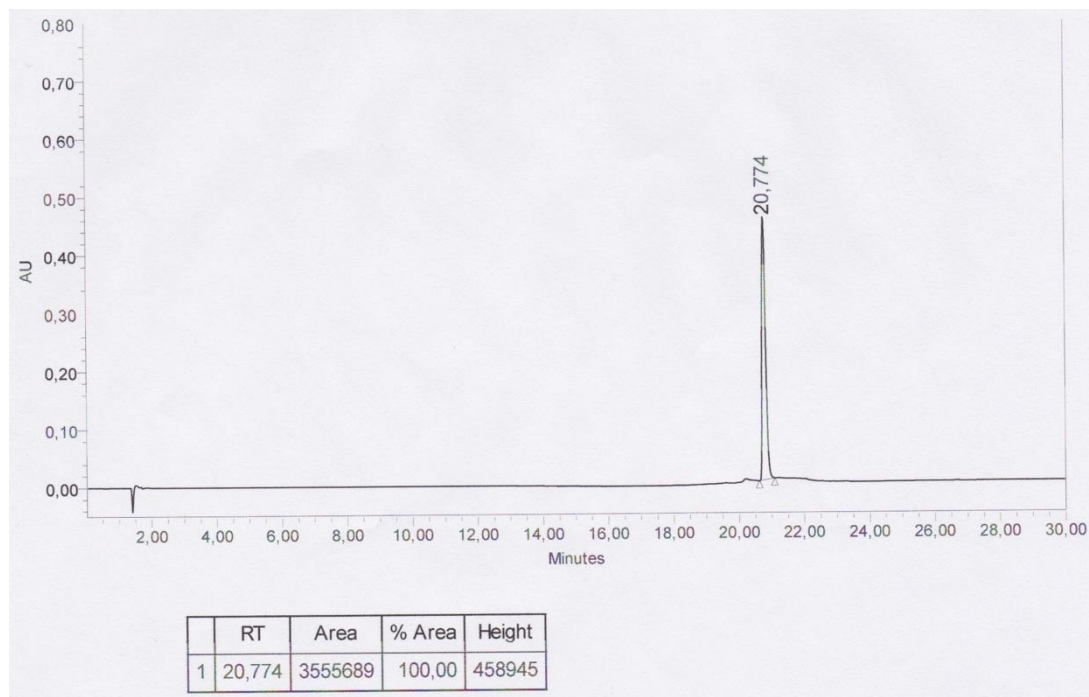
4-Methyl-1*H*-indole-3-carboxylic acid methyl ester (**7**):



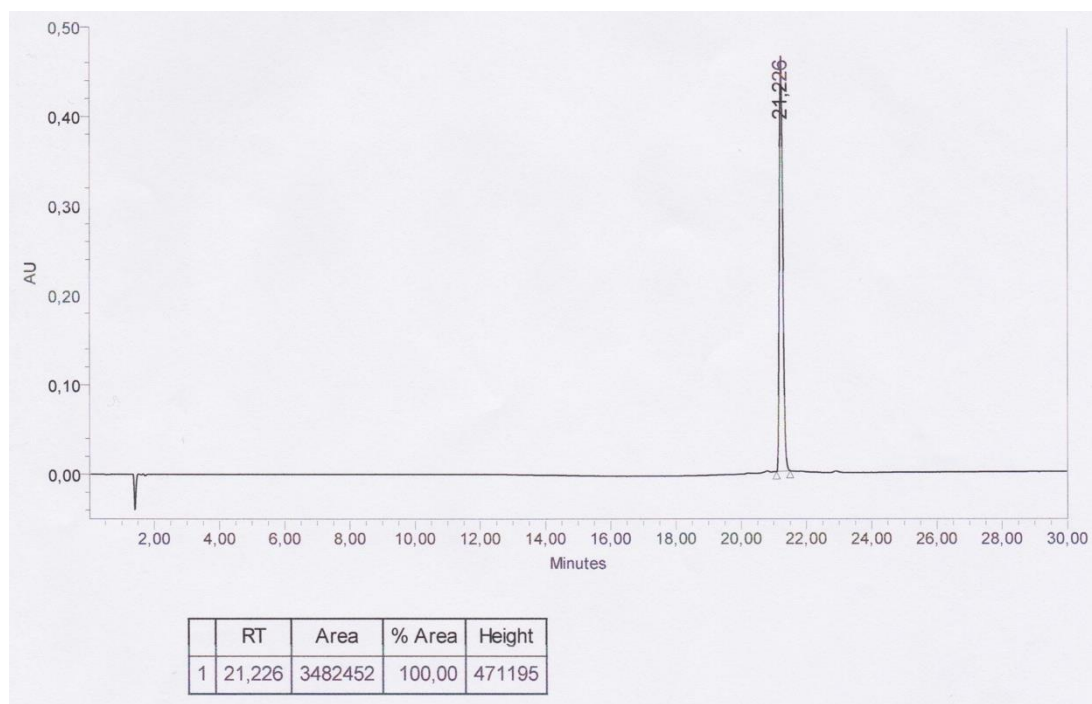
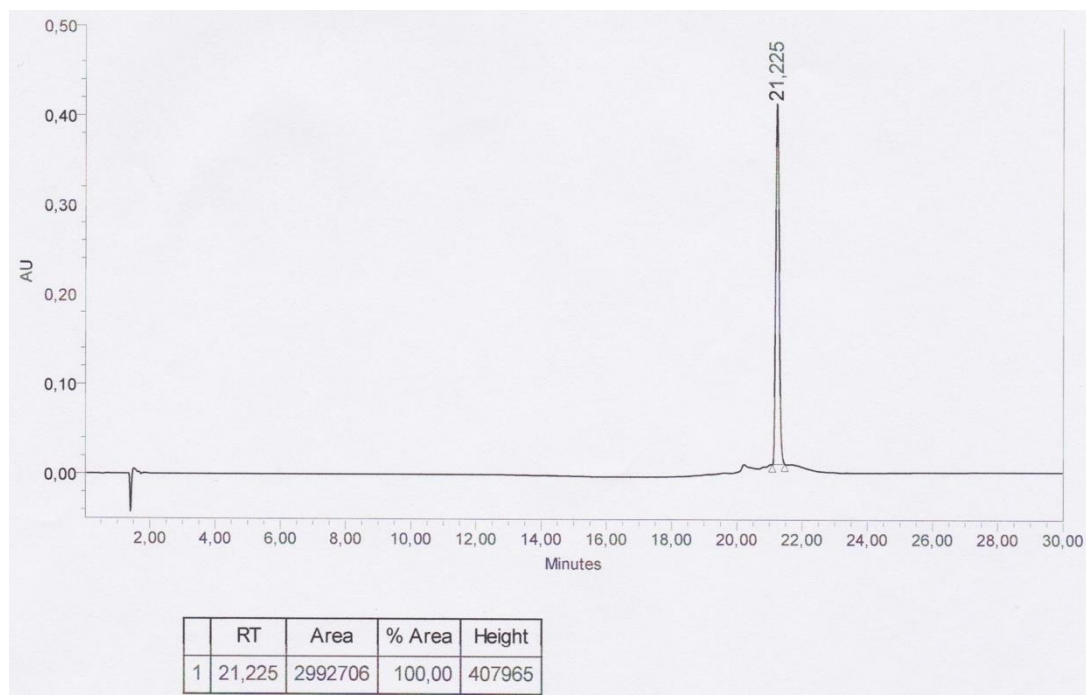
4-Chloro-1*H*-indole-3-carboxylic acid methyl ester (**8**):



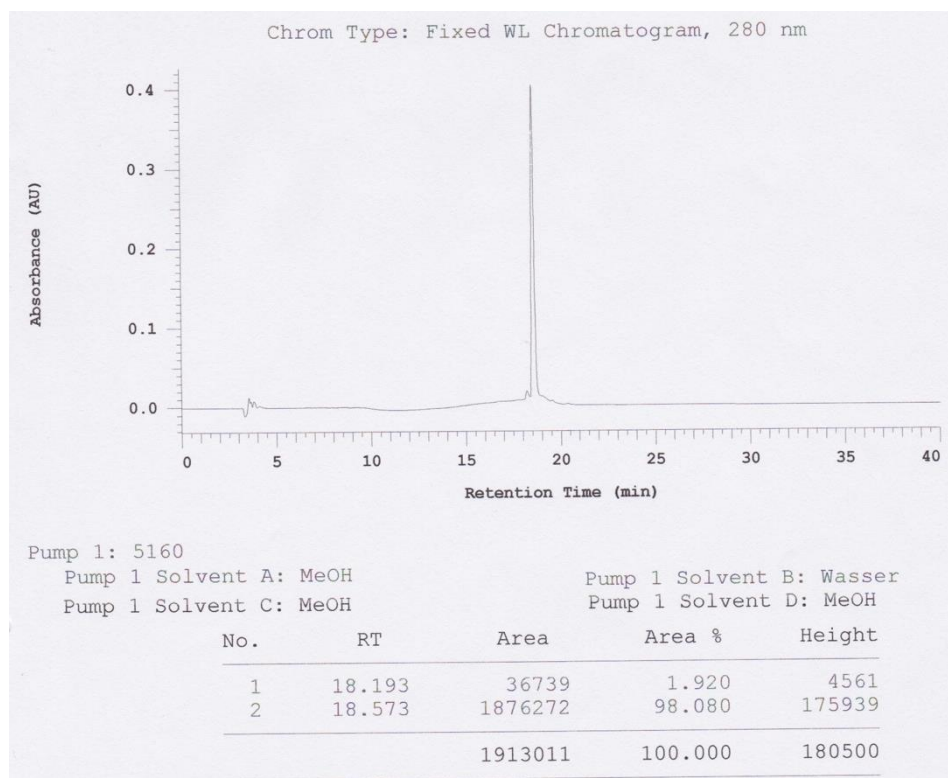
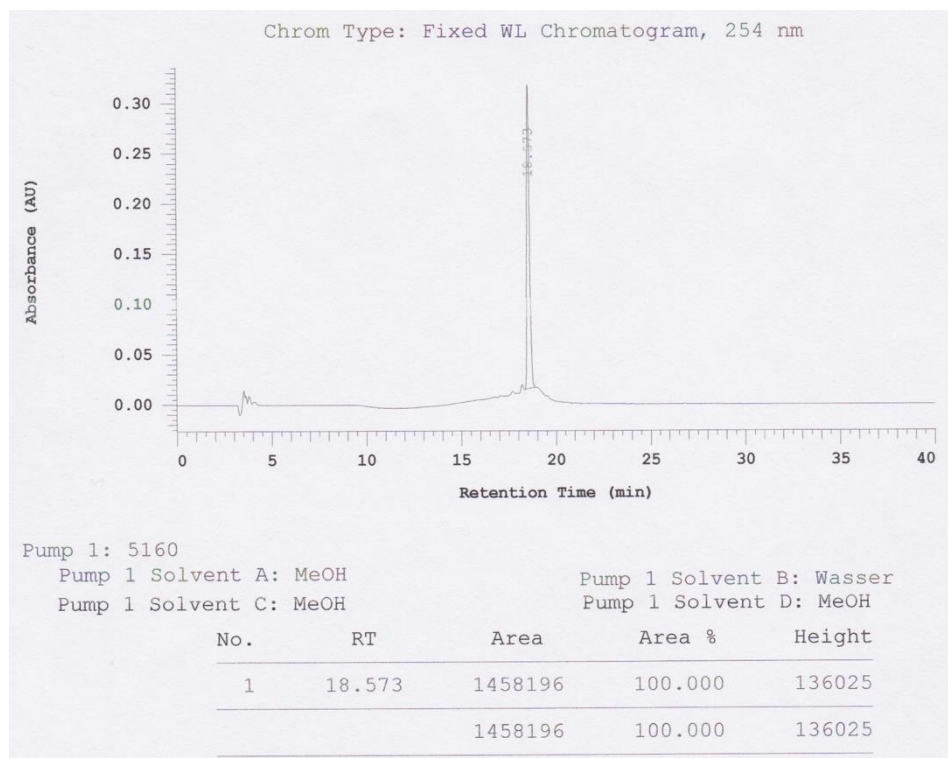
5-Methyl-1*H*-indole-3-carboxylic acid methyl ester (**9**):



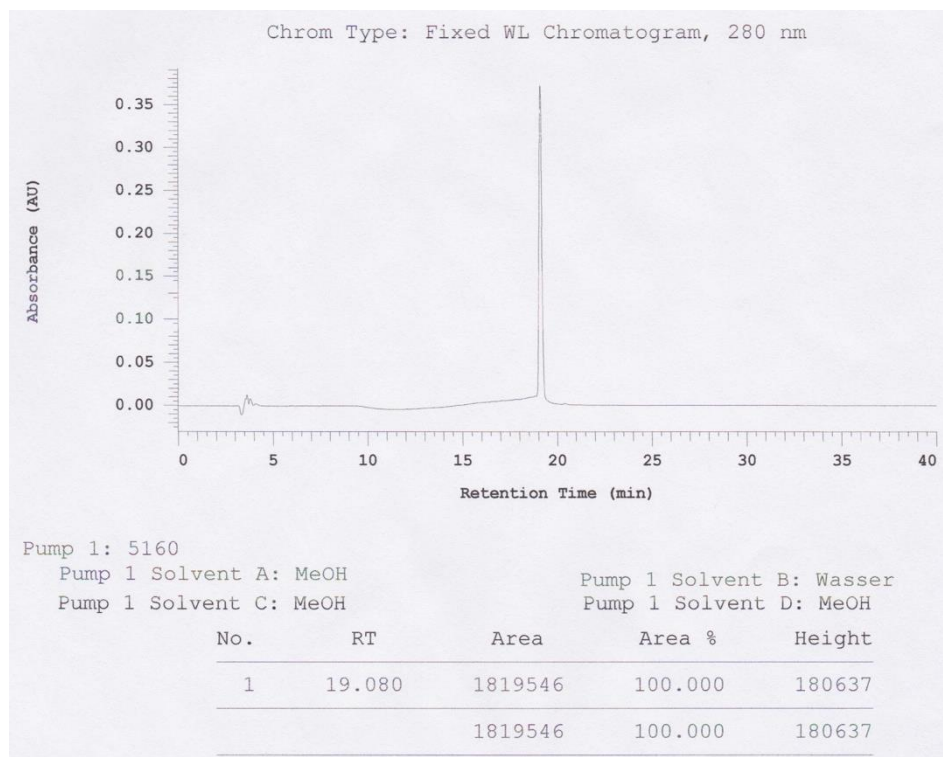
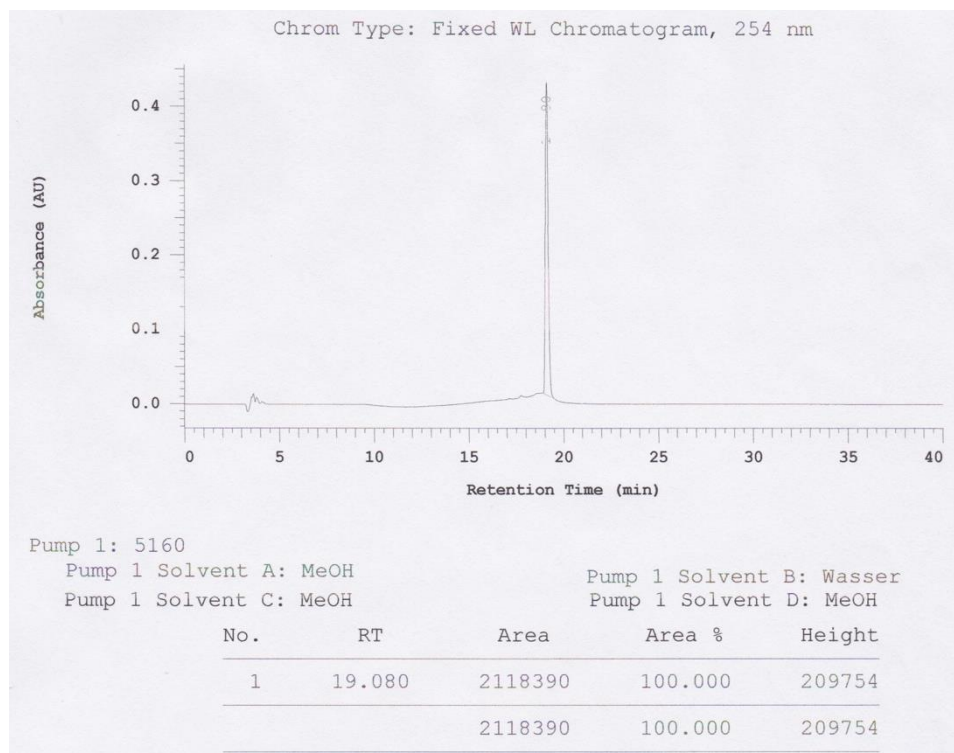
5-Chloro-1*H*-indole-3-carboxylic acid methyl ester (**10**):



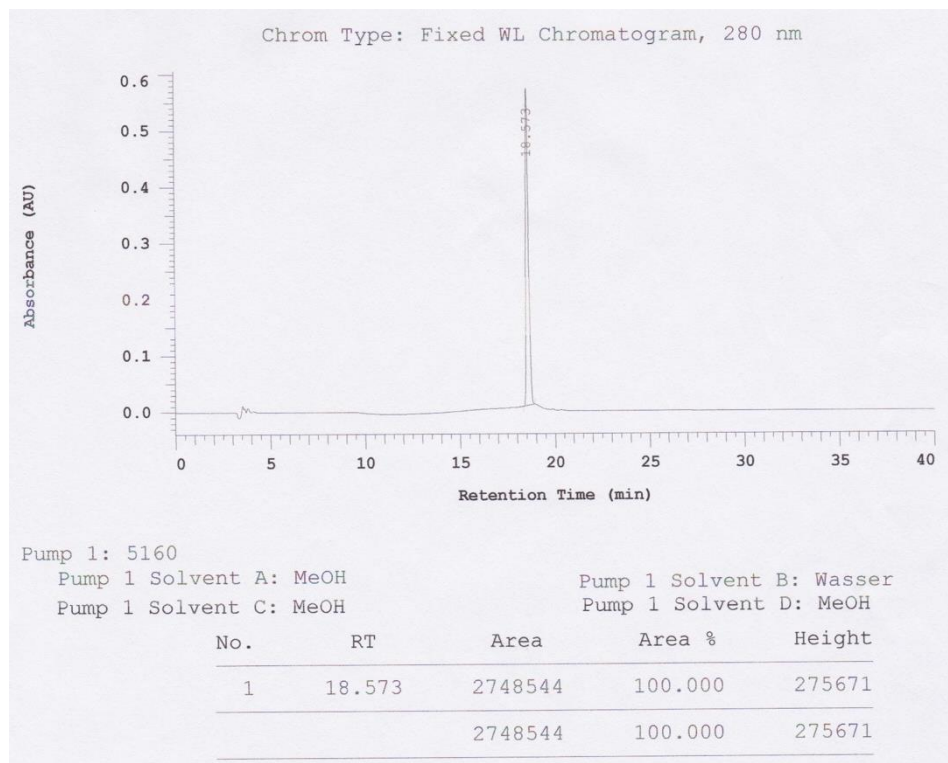
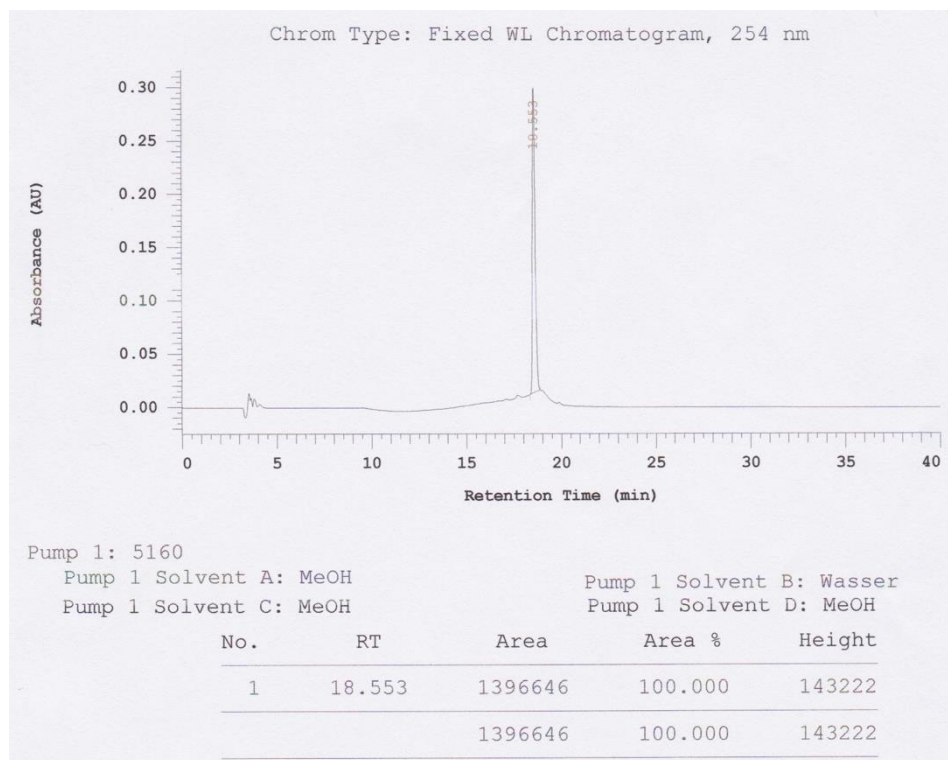
6-Methyl-1*H*-indole-3-carboxylic acid methyl ester (**11**):



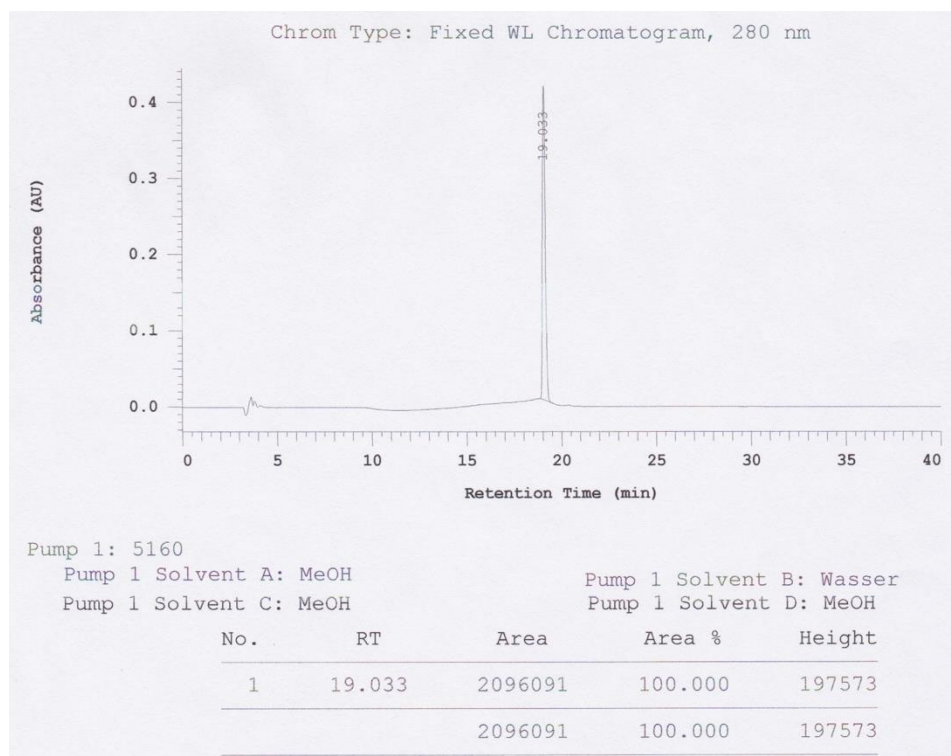
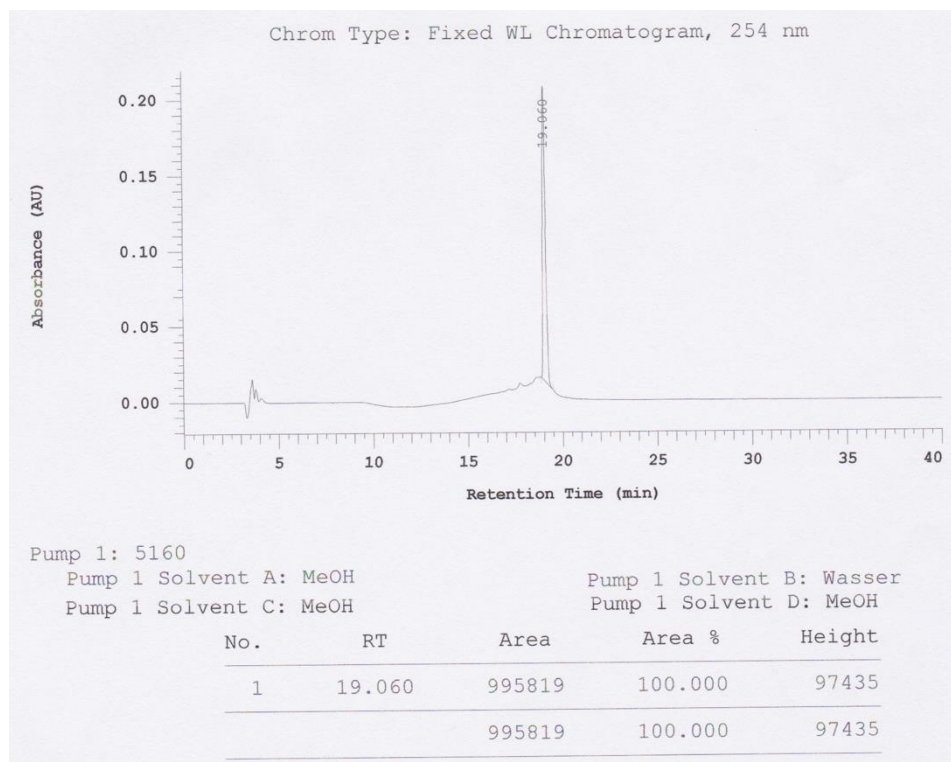
6-Chloro-1*H*-indole-3-carboxylic acid methyl ester (**12**):



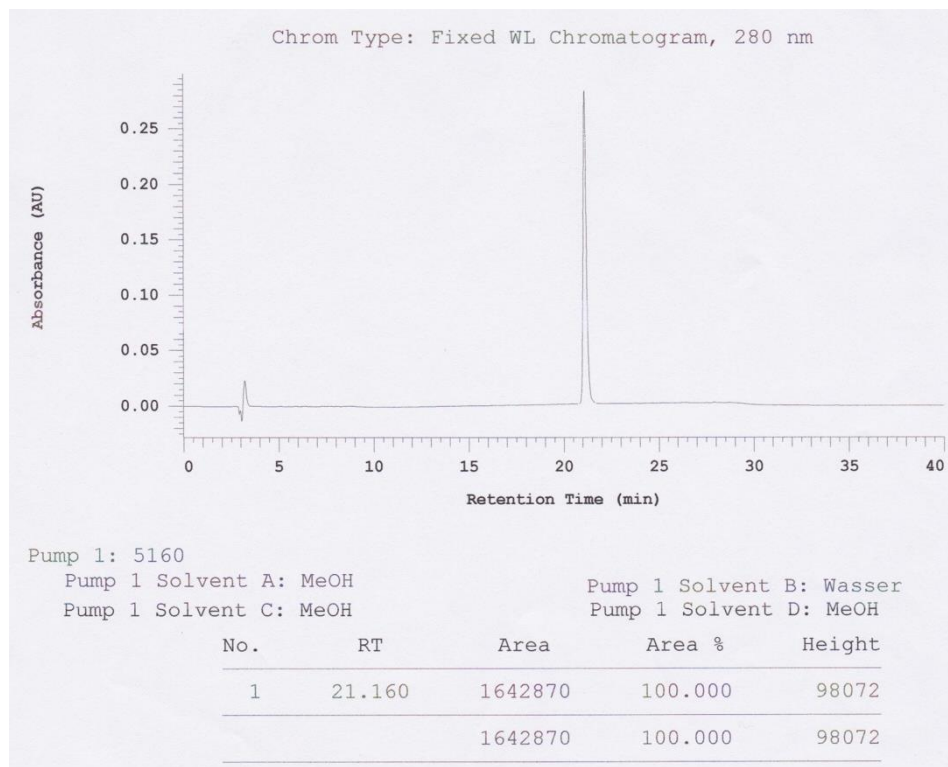
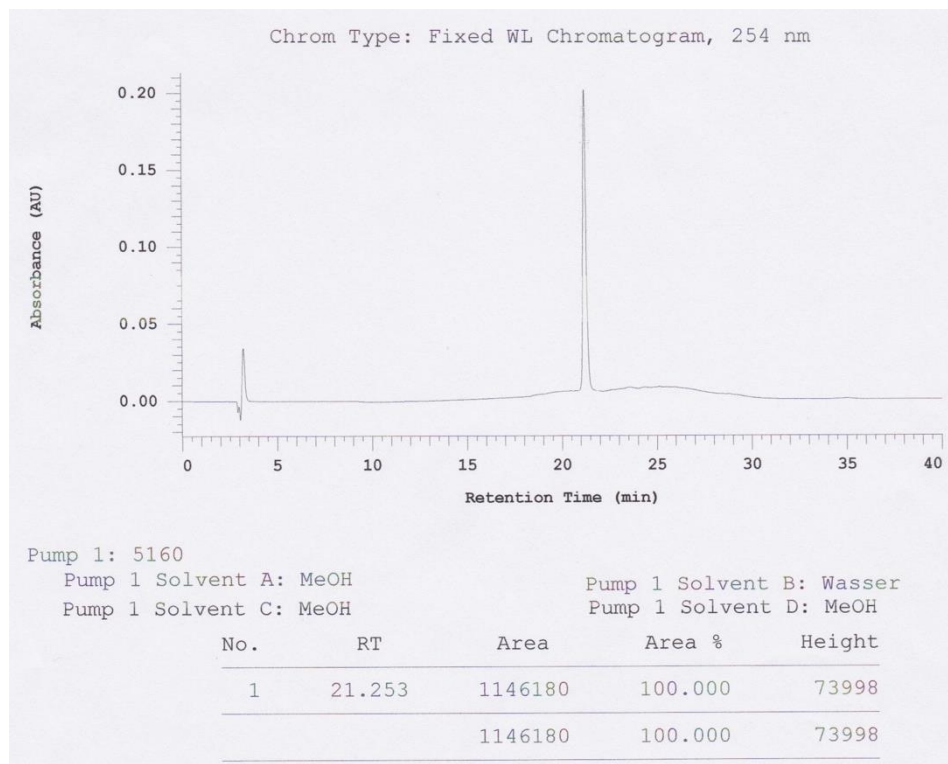
7-Methyl-1*H*-indole-3-carboxylic acid methyl ester (**13**):



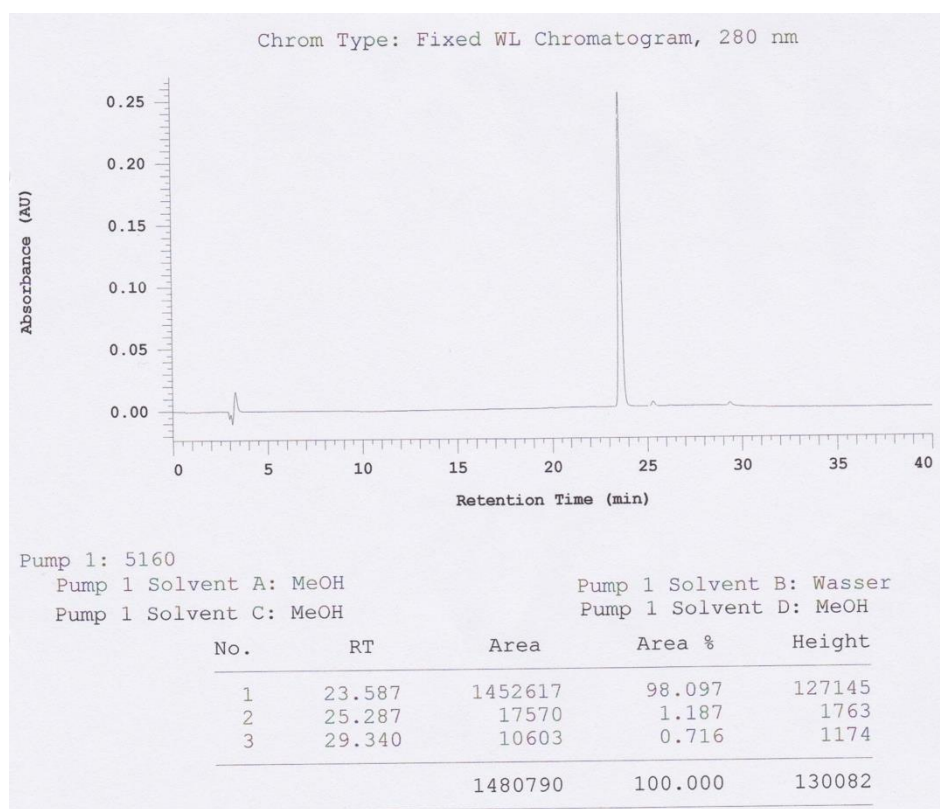
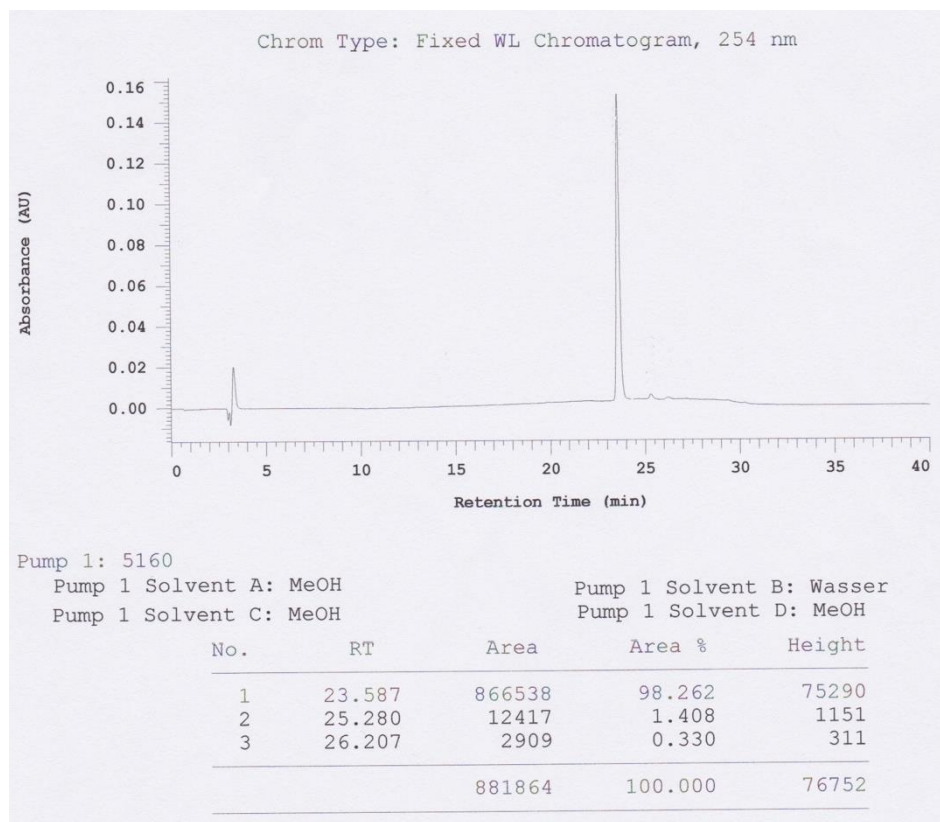
7-Chloro-1*H*-indole-3-carboxylic acid methyl ester (**14**):



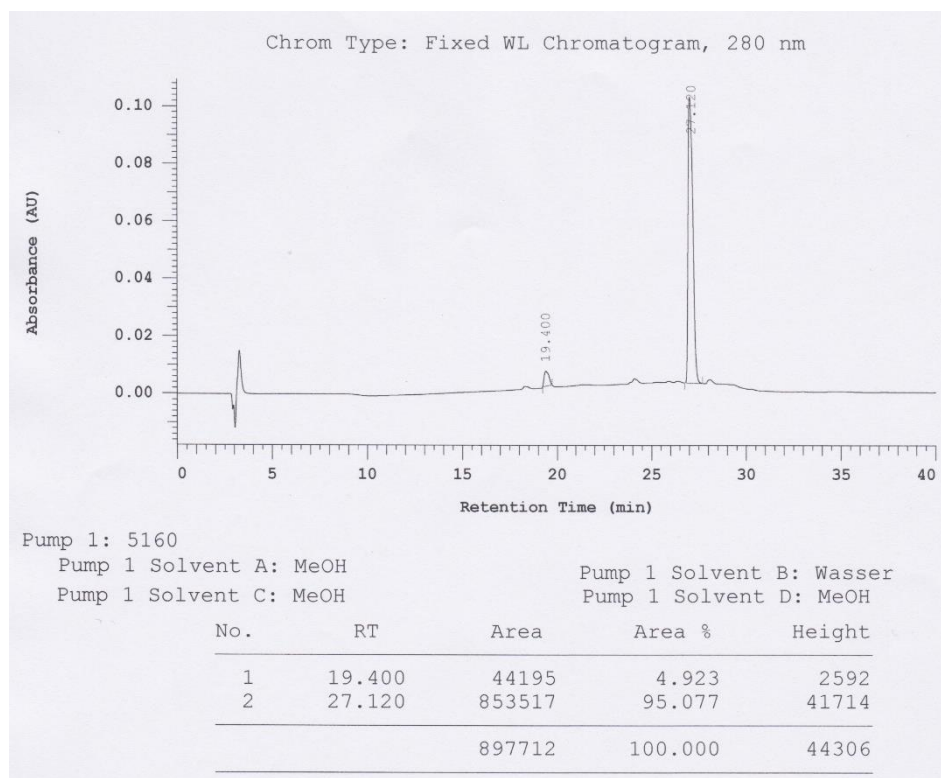
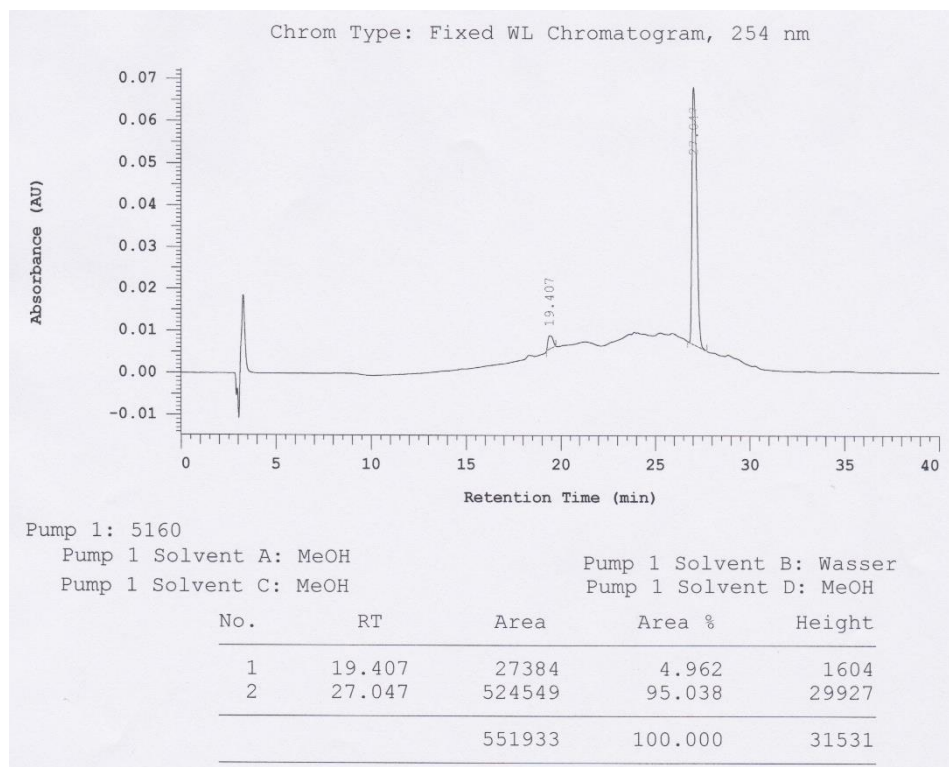
1-Methylindole-3-carboxylic acid methyl ester (**15**):



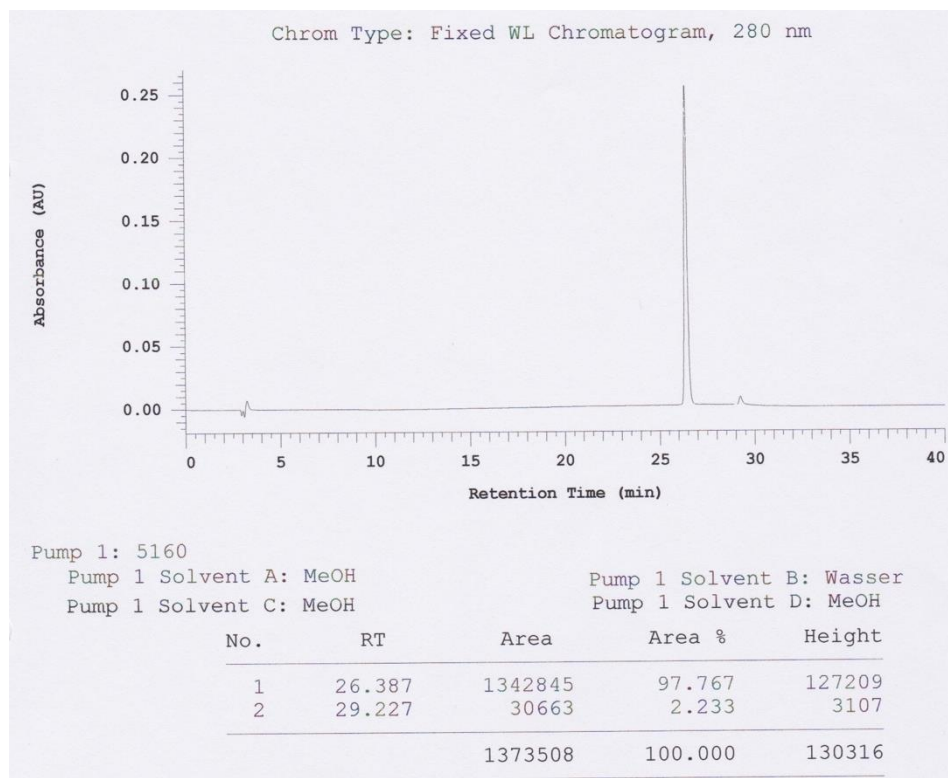
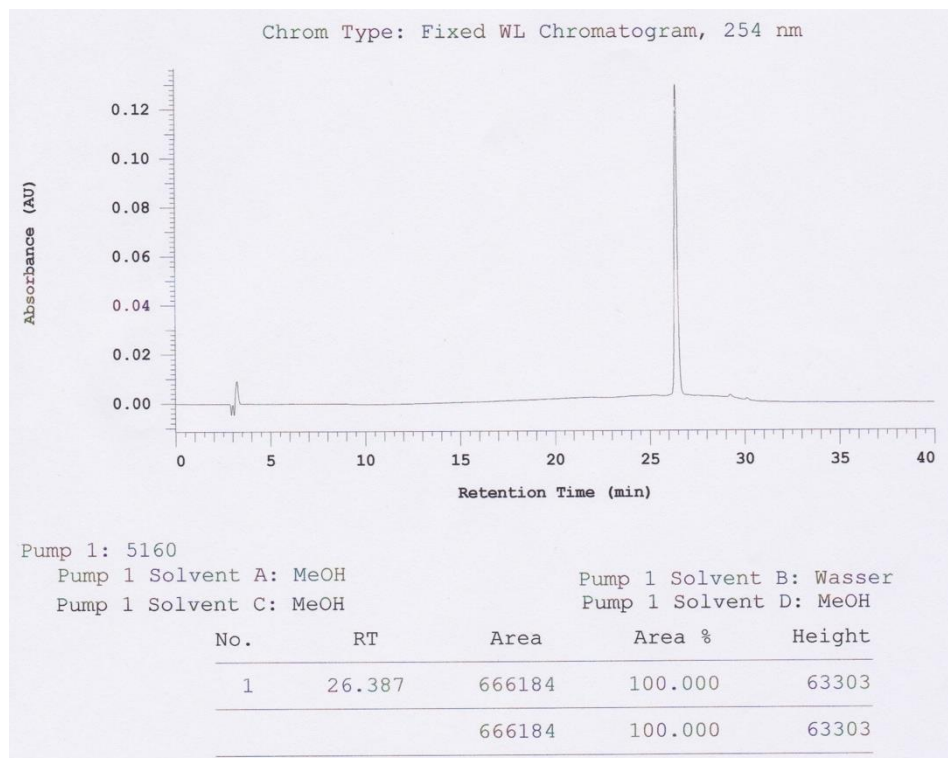
1-Ethylindole-3-carboxylic acid methyl ester (**16**):



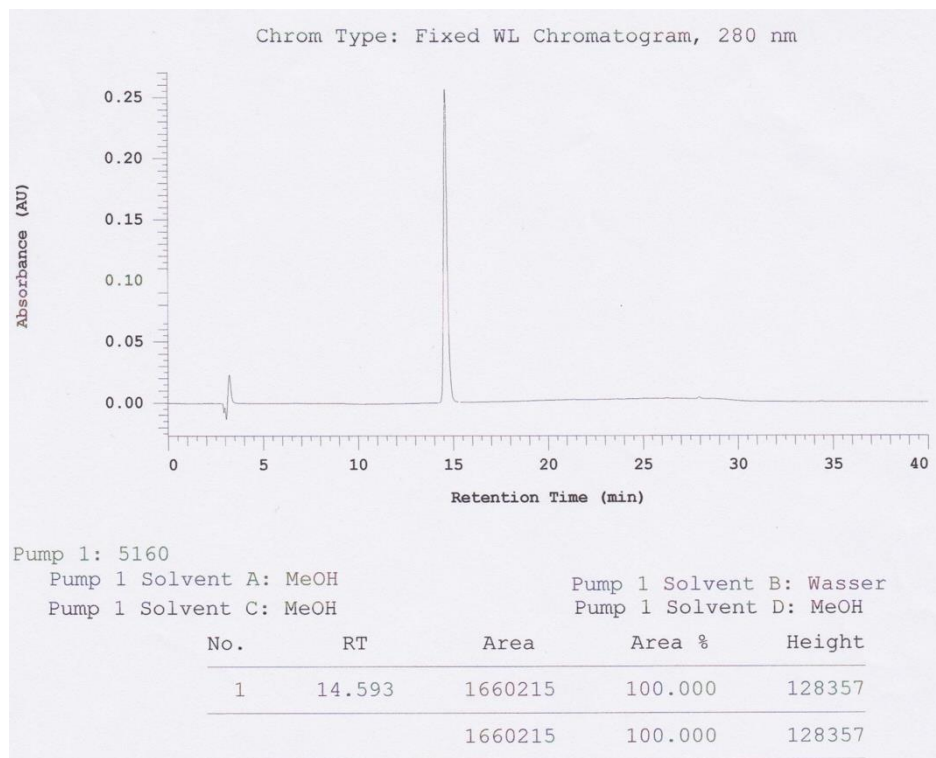
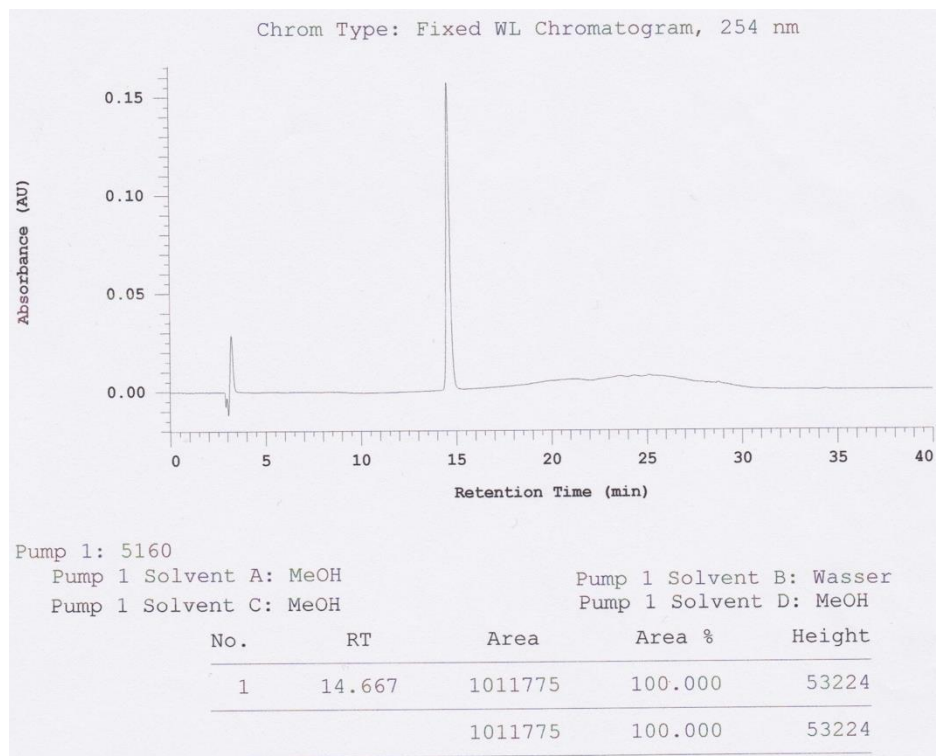
1-Phenylindole-3-carboxylic acid methyl ester (**17**):



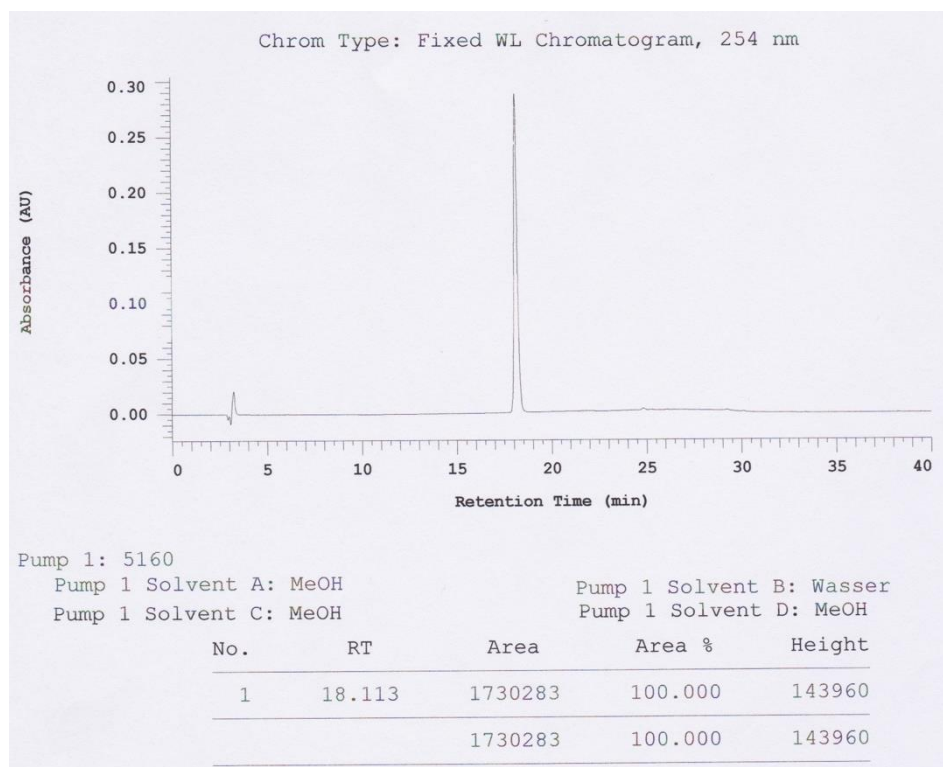
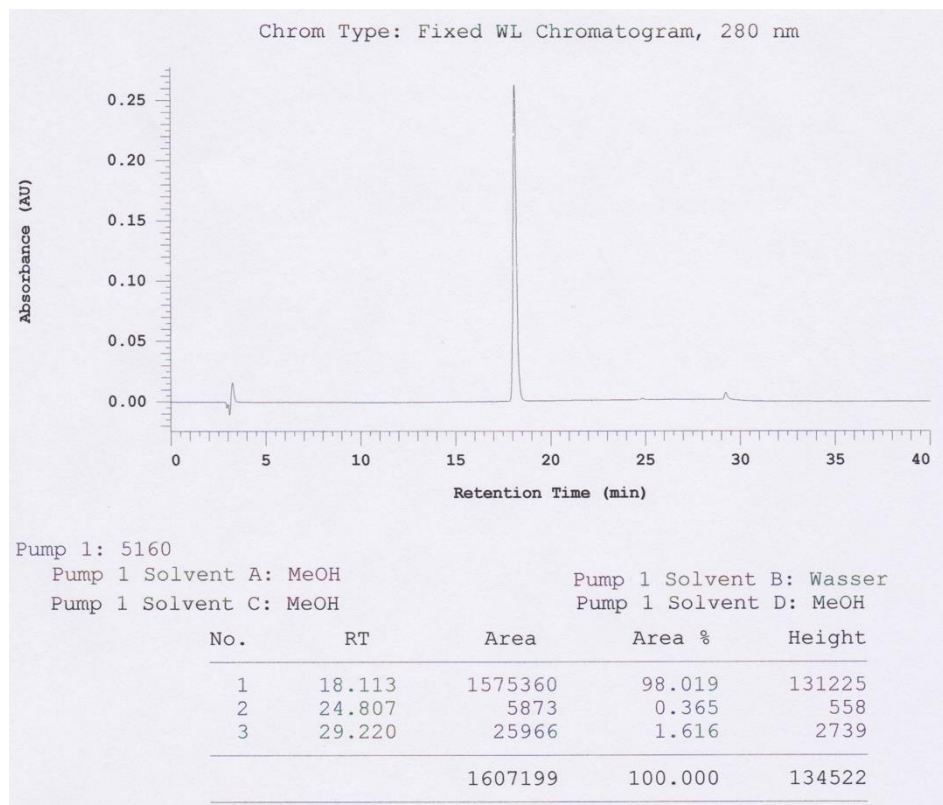
1-Benzylindole-3-carboxylic acid methyl ester (**18**):



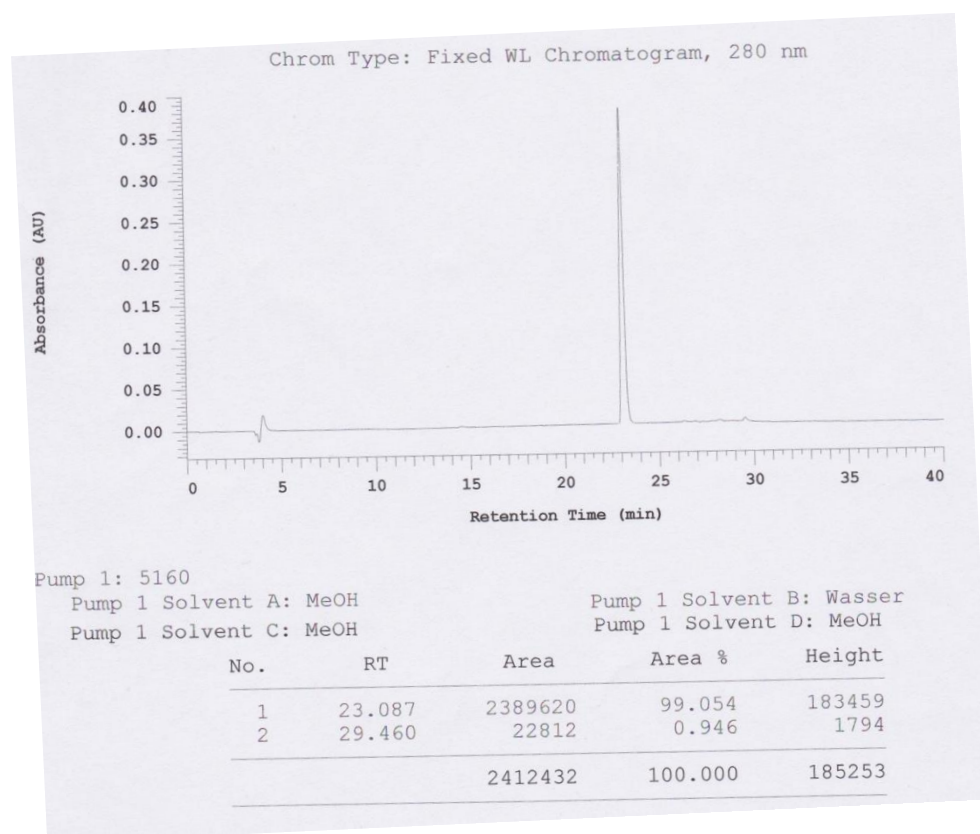
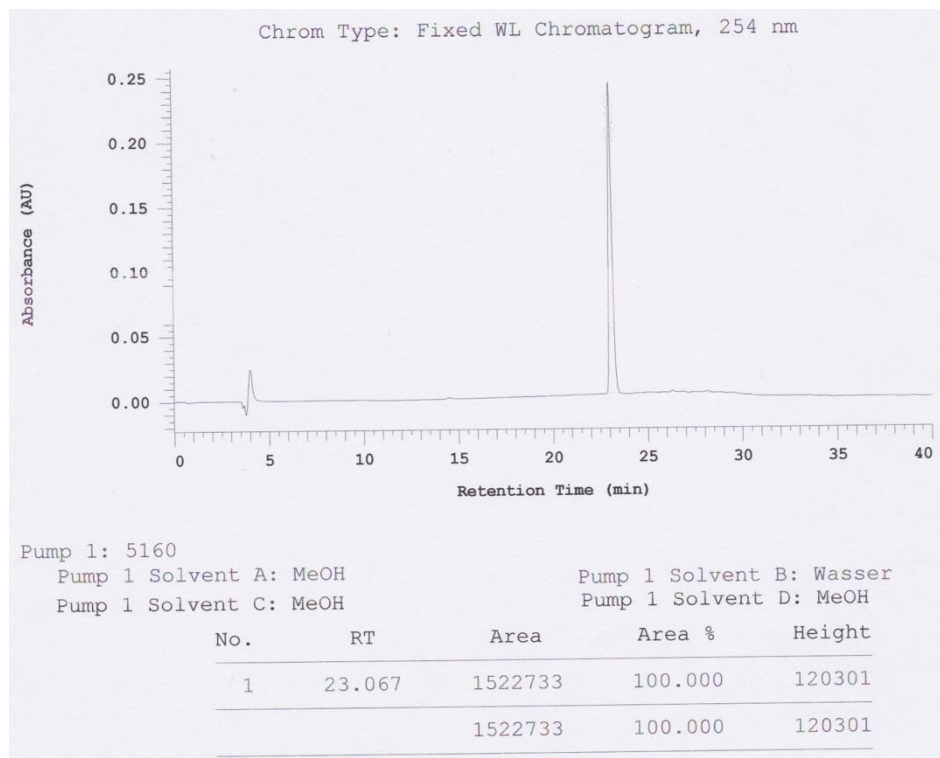
1*H*-Indole-3-carboxylic acid (**19**):



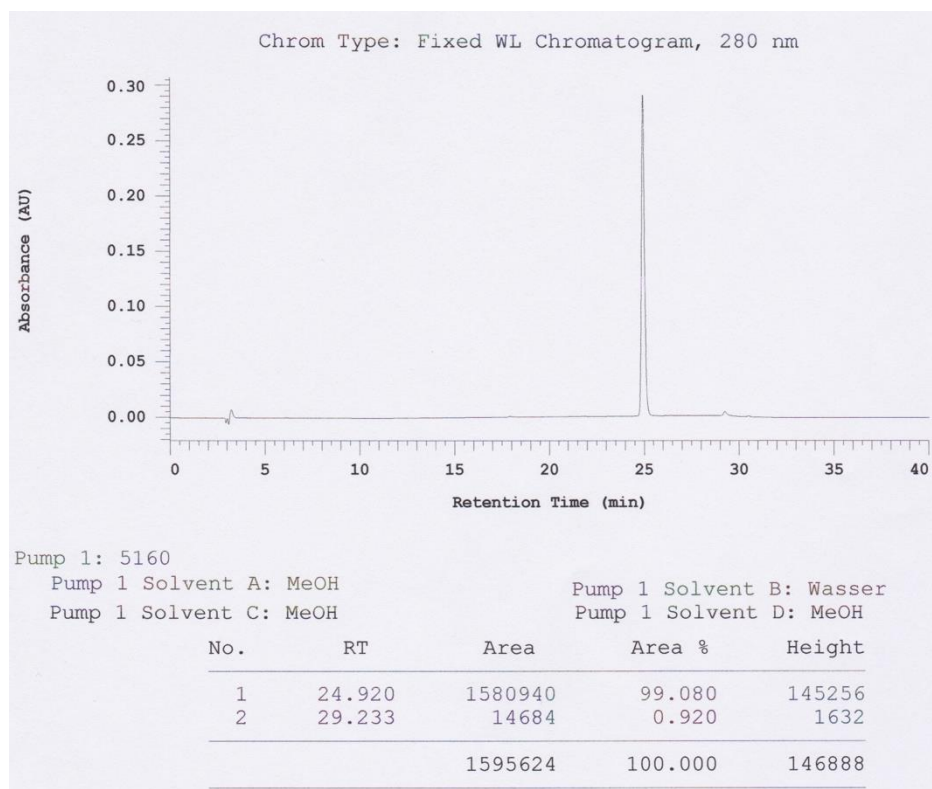
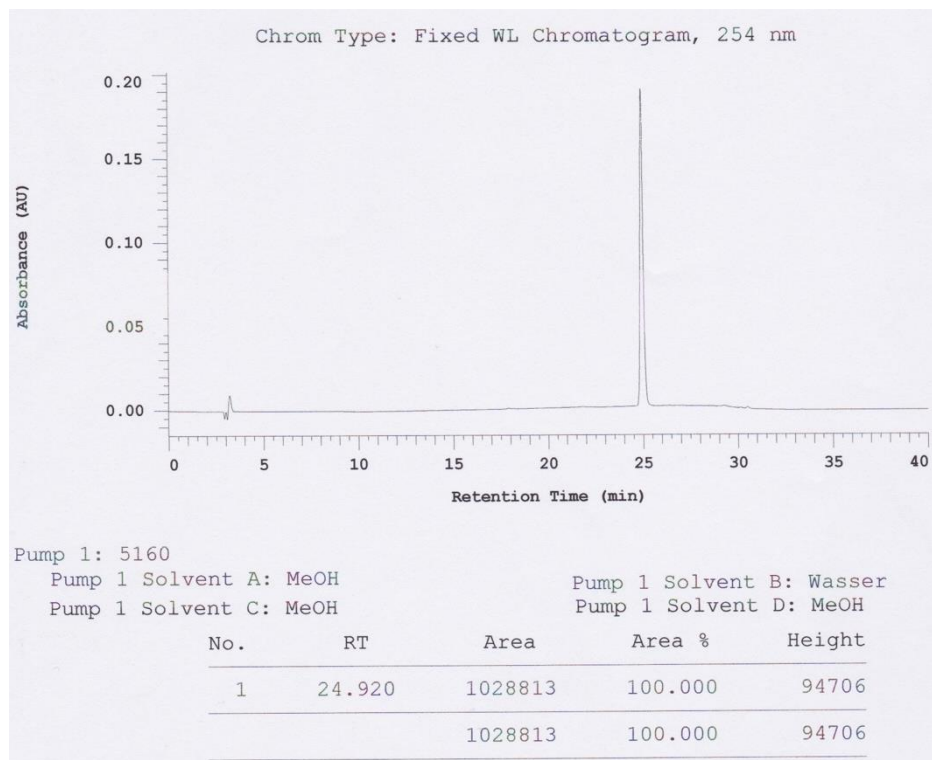
1*H*-Indole-3-propan-1-one (**22**):



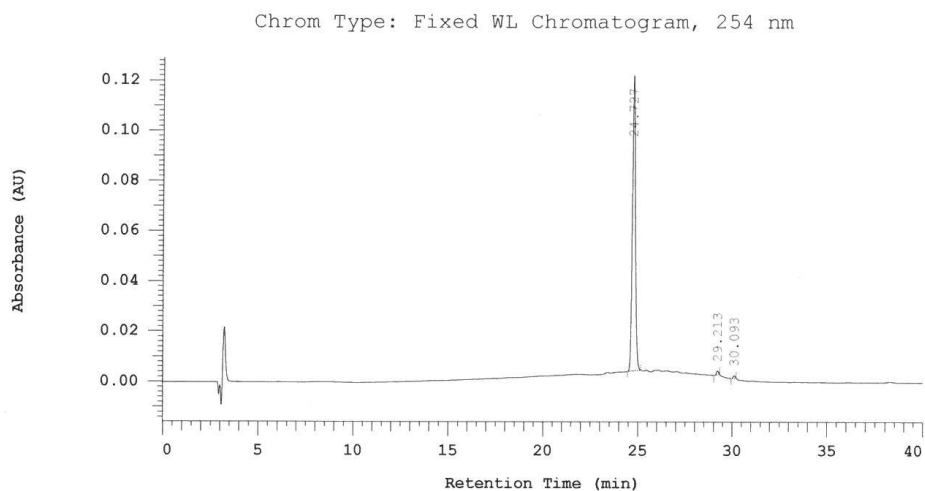
1*H*-Indole-3-carboxylic acid ethyl ester (**23**):



1*H*-Indole-3-carboxylic *tert* butyl ester (**24**):



1*H*-Indole-3 carboxylic acid phenyl ester (**25**):



Pump 1: 5160

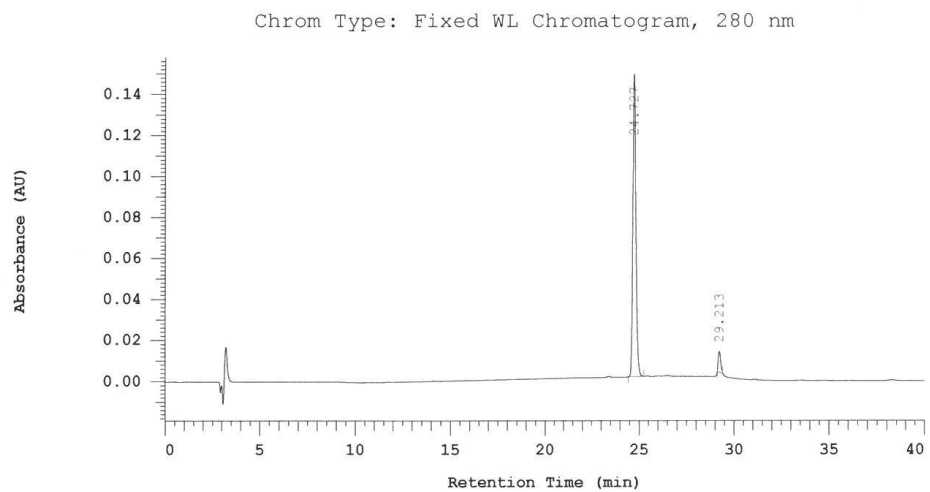
Pump 1 Solvent A: MeOH

Pump 1 Solvent B: Wasser

Pump 1 Solvent C: MeOH

Pump 1 Solvent D: MeOH

No.	RT	Area	Area %	Height
1	24.727	633365	98.620	58842
2	29.213	5053	0.787	701
3	30.093	3812	0.594	499
		642230	100.000	60042



Pump 1: 5160

Pump 1 Solvent A: MeOH

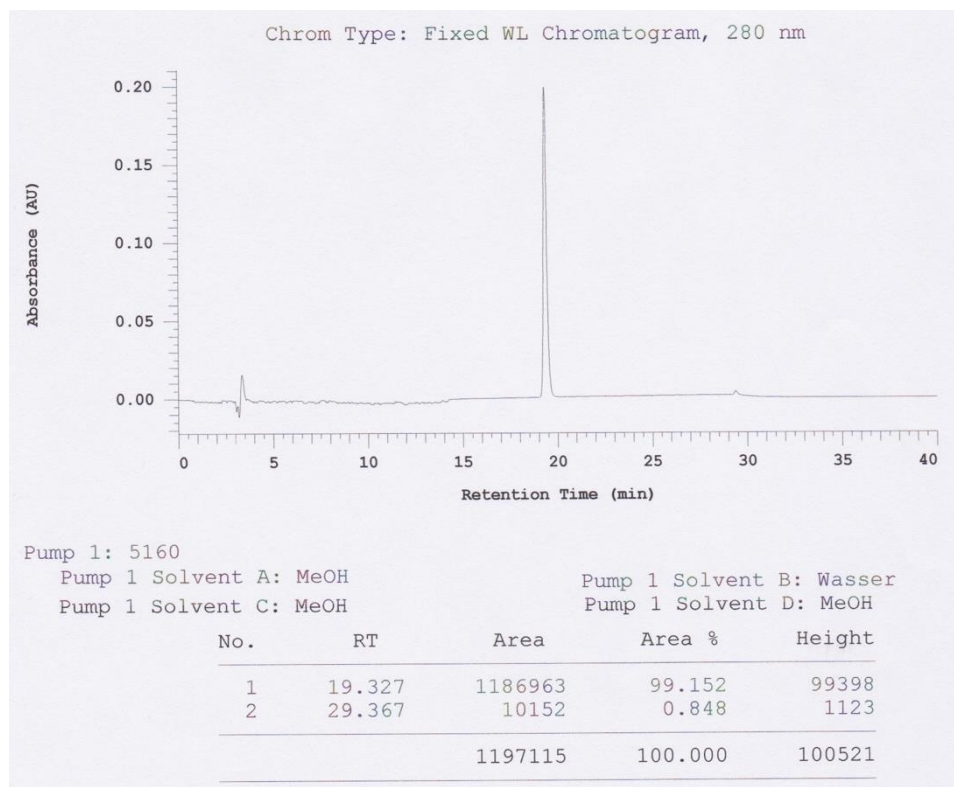
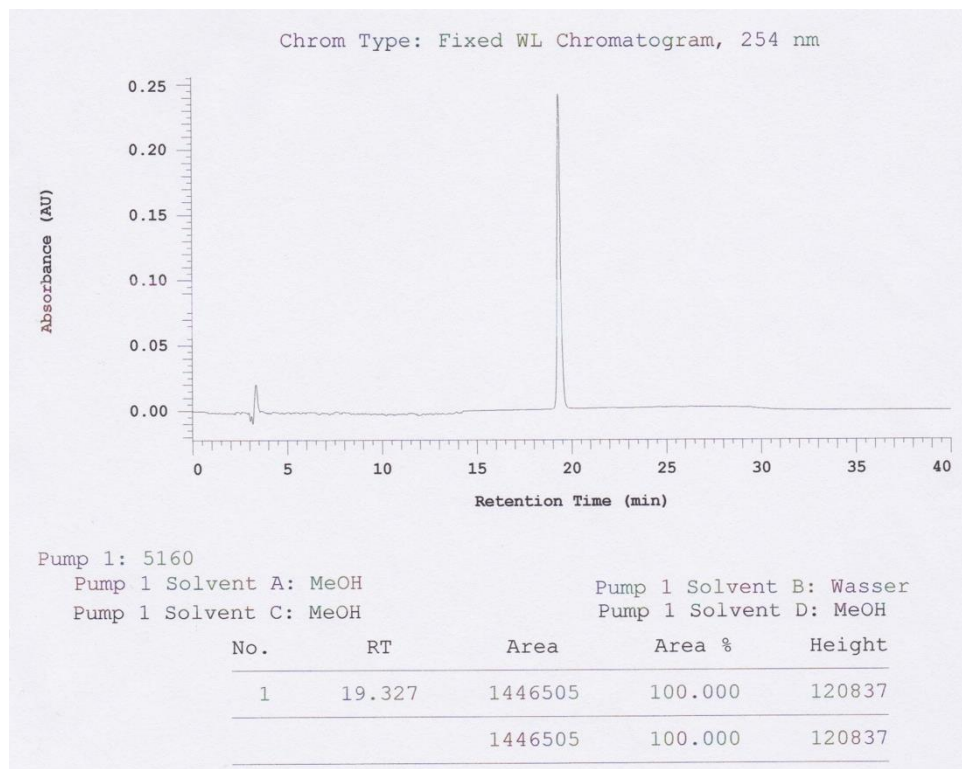
Pump 1 Solvent B: Wasser

Pump 1 Solvent C: MeOH

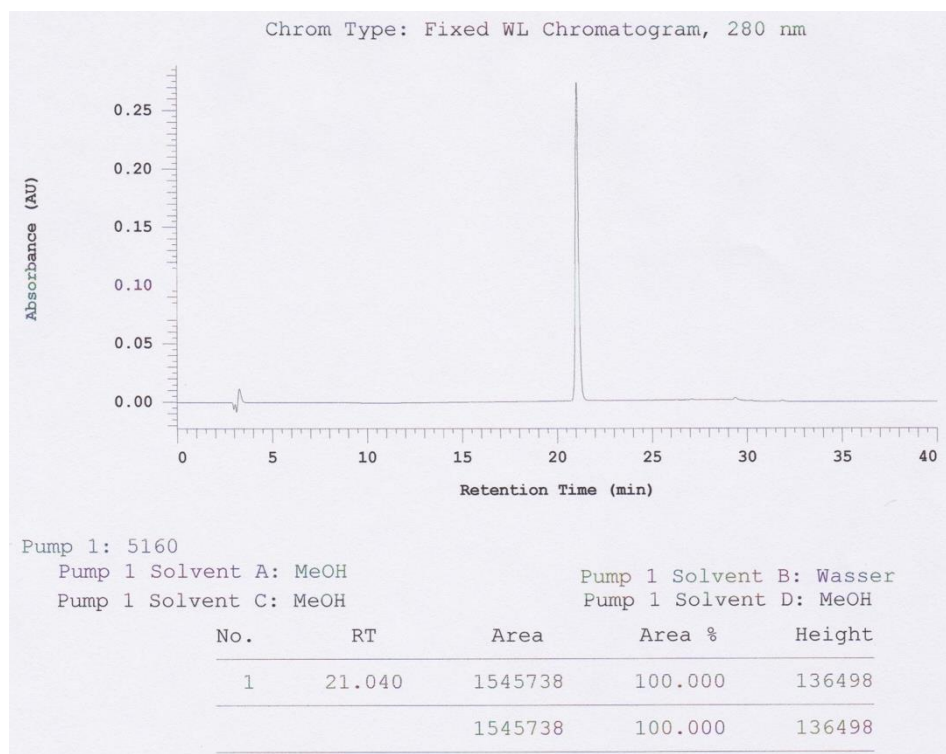
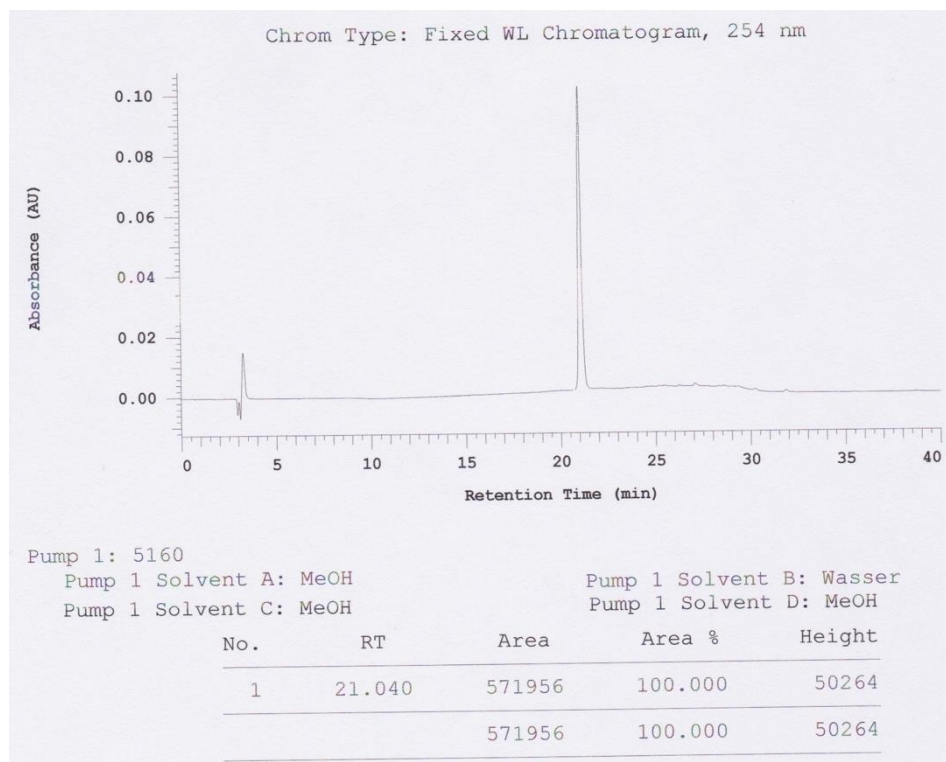
Pump 1 Solvent D: MeOH

No.	RT	Area	Area %	Height
1	24.727	796102	95.008	73749
2	29.213	41828	4.992	4985
		837930	100.000	78734

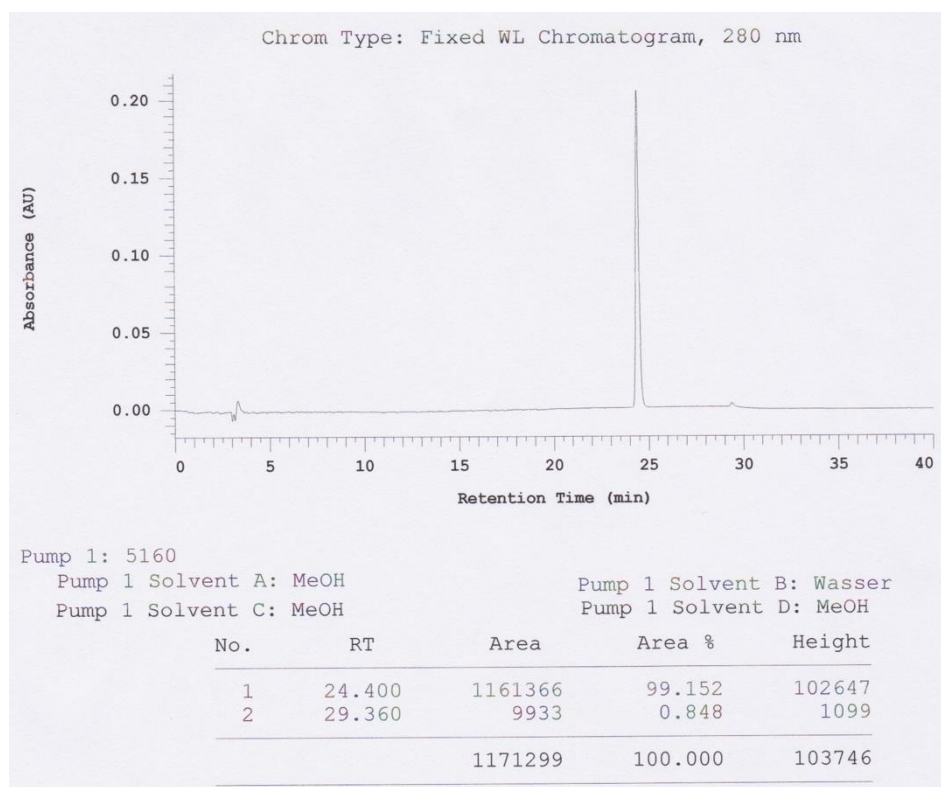
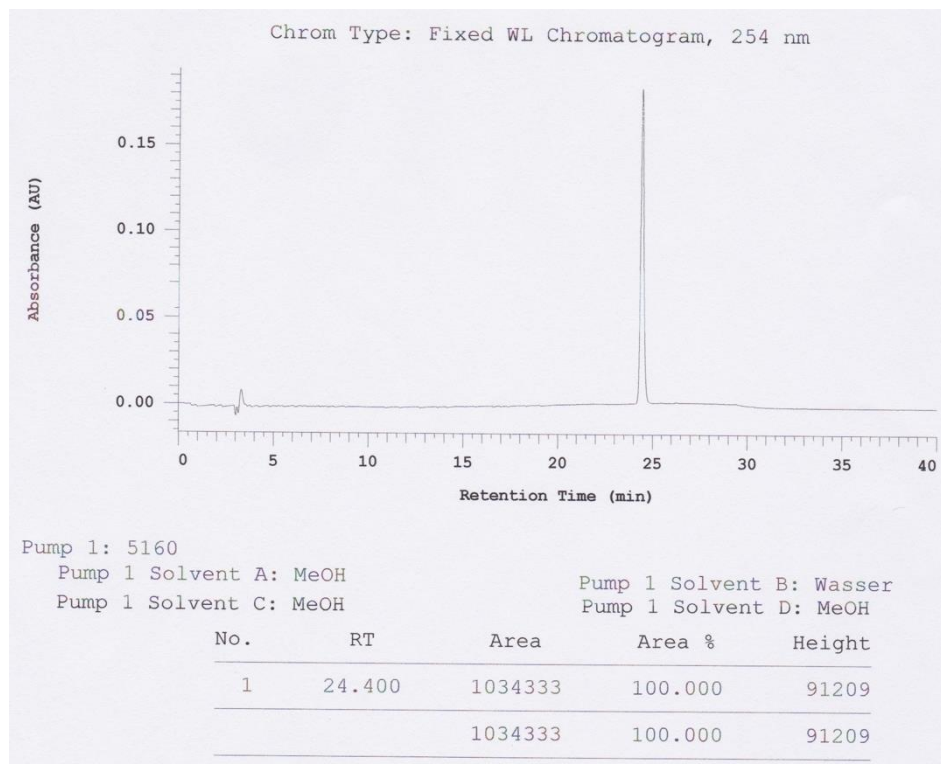
5-Methoxy-1*H*-indole-3-carboxylic acid methyl ester (**26**):



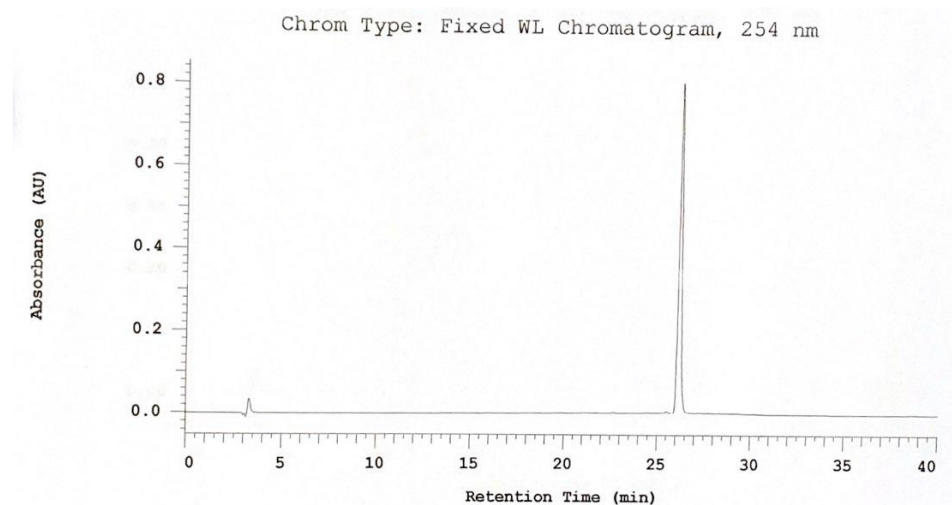
7-Methoxy-1*H*-indole-3-carboxylic acid methyl ester (**27**):



5-Bromo-1*H*-indole-3-carboxylic acid methyl ester (**28**):



5-Phenyl-1*H*-indole-3-carboxylic acid methyl ester (**29**):



Pump 1: 5160

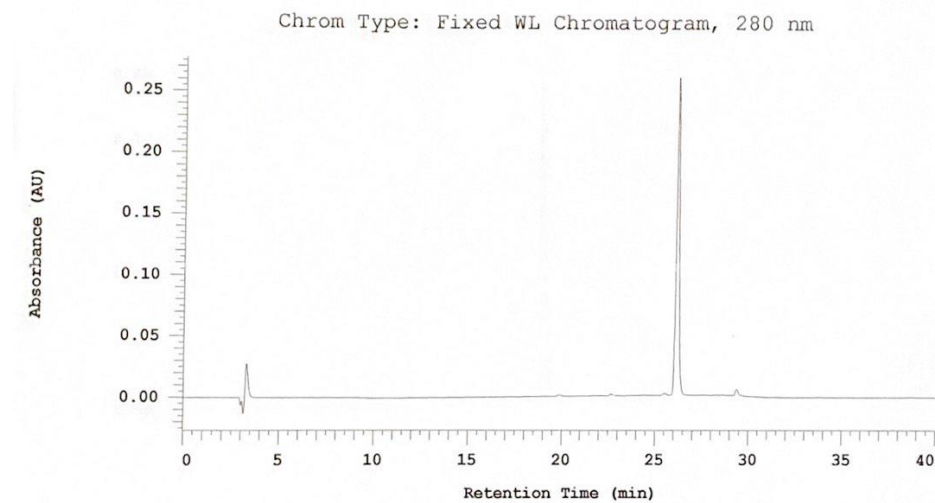
Pump 1 Solvent A: MeOH

Pump 1 Solvent B: Wasser

Pump 1 Solvent C: MeOH

Pump 1 Solvent D: MeOH

No.	RT	Area	Area %	Height
1	25.493	16369	0.377	1502
2	26.113	4321096	99.623	403279
		4337465	100.000	404781



Pump 1: 5160

Pump 1 Solvent A: MeOH

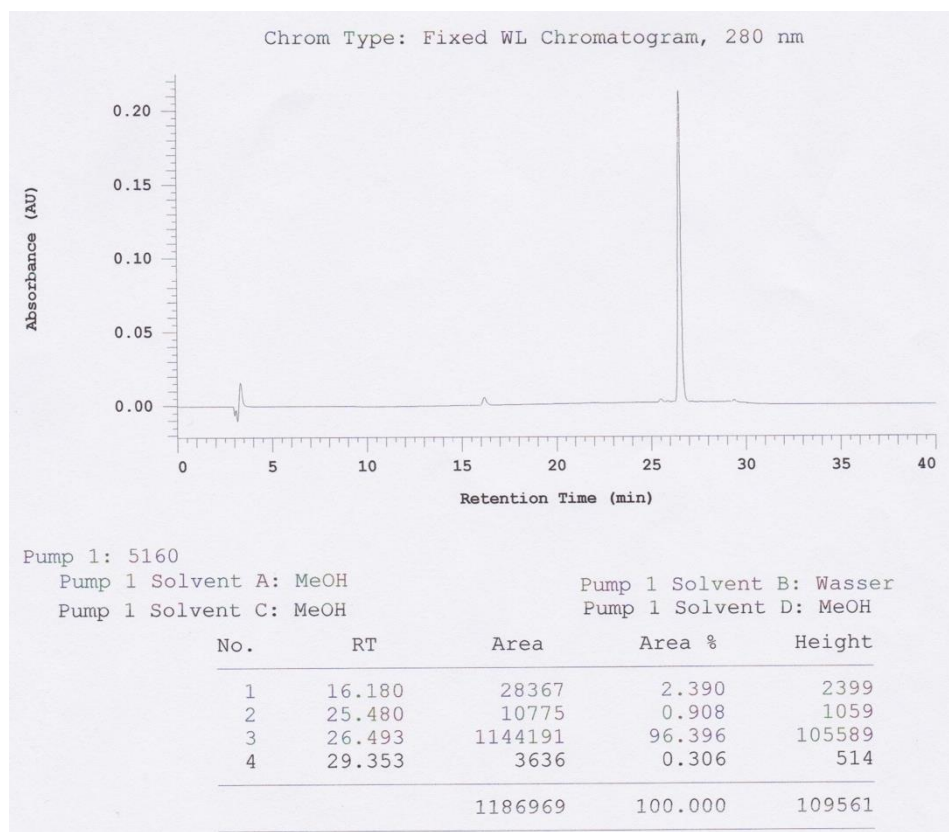
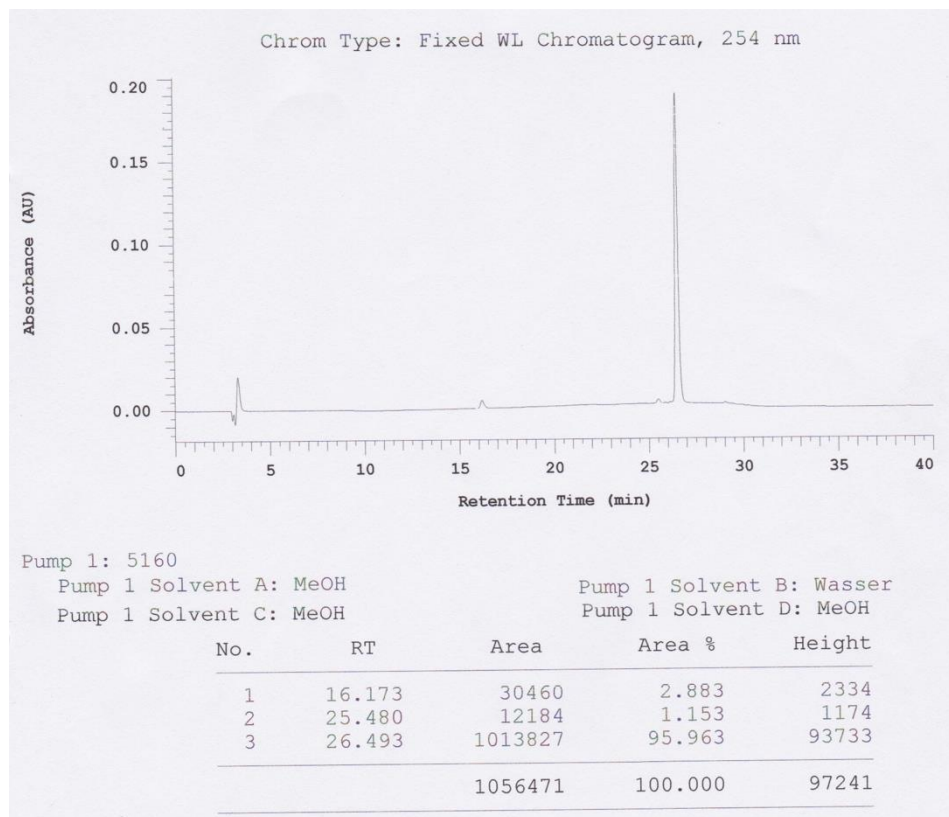
Pump 1 Solvent B: Wasser

Pump 1 Solvent C: MeOH

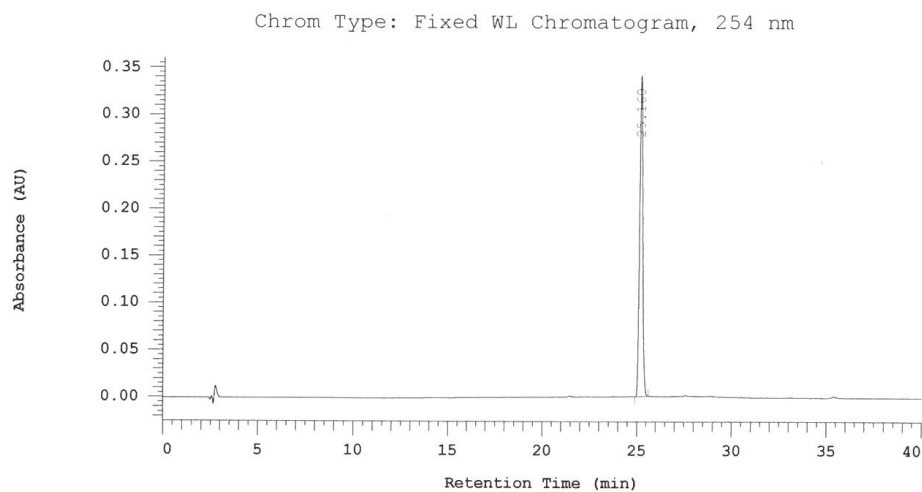
Pump 1 Solvent D: MeOH

No.	RT	Area	Area %	Height
1	22.647	5437	0.390	580
2	25.493	5605	0.402	663
3	26.113	1383479	99.208	130264
		1394521	100.000	131507

5-Benzyl-1*H*-indole-3-carboxylic acid methyl ester (**30**):



5-Phenyl-1-methylindole-3-carboxylic acid methyl ester (**31**):



Pump 1: 5160

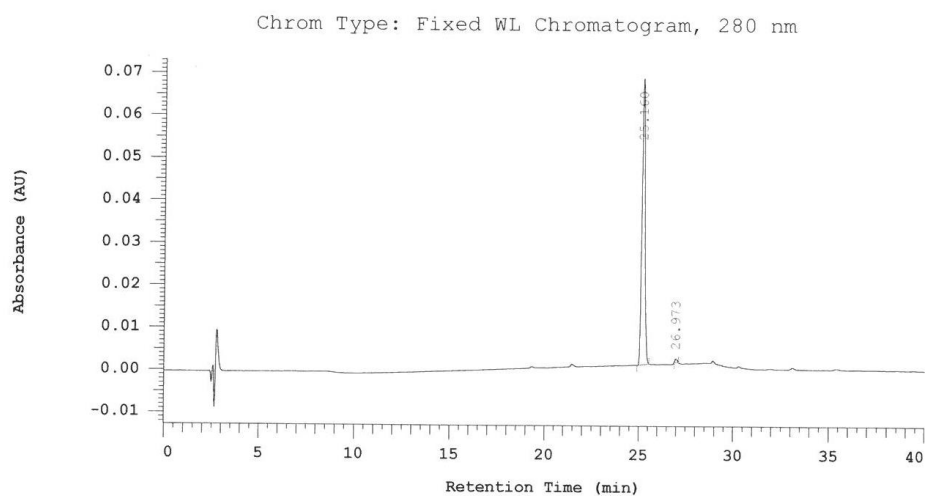
Pump 1 Solvent A: MeOH

Pump 1 Solvent B: Wasser

Pump 1 Solvent C: MeOH

Pump 1 Solvent D: MeOH

No.	RT	Area	Area %	Height
1	25.160	1919342	100.000	170134
		1919342	100.000	170134



Pump 1: 5160

Pump 1 Solvent A: MeOH

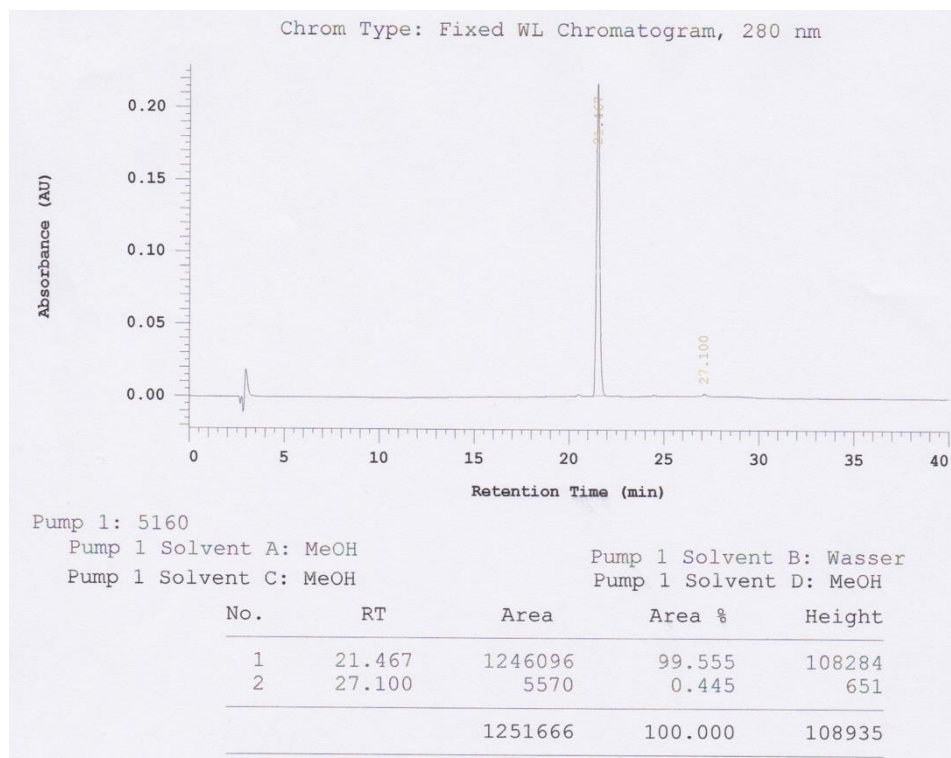
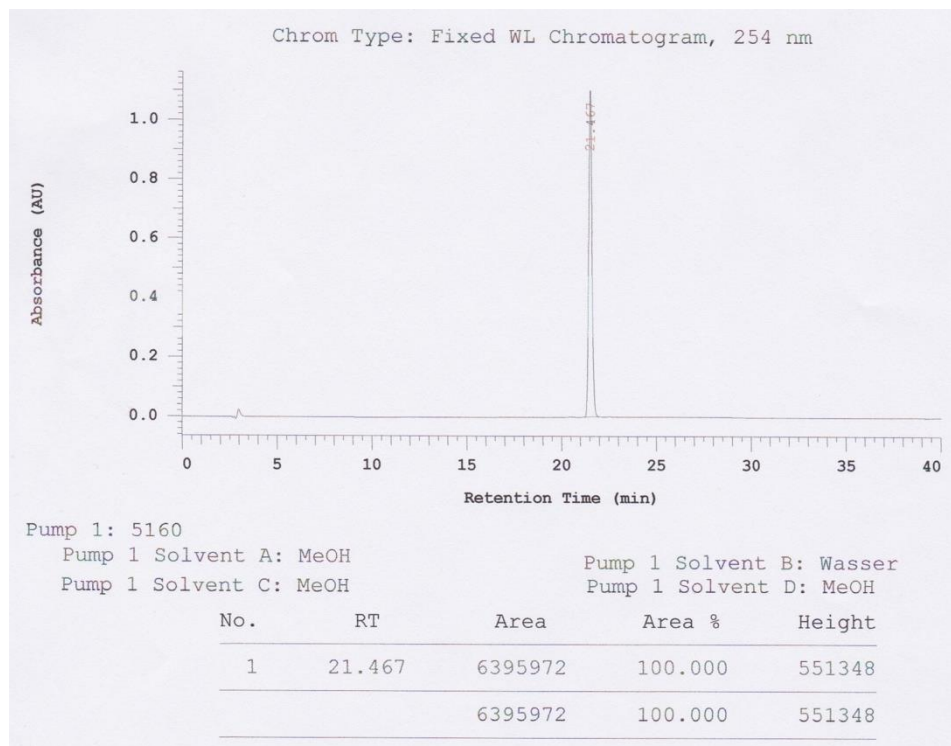
Pump 1 Solvent B: Wasser

Pump 1 Solvent C: MeOH

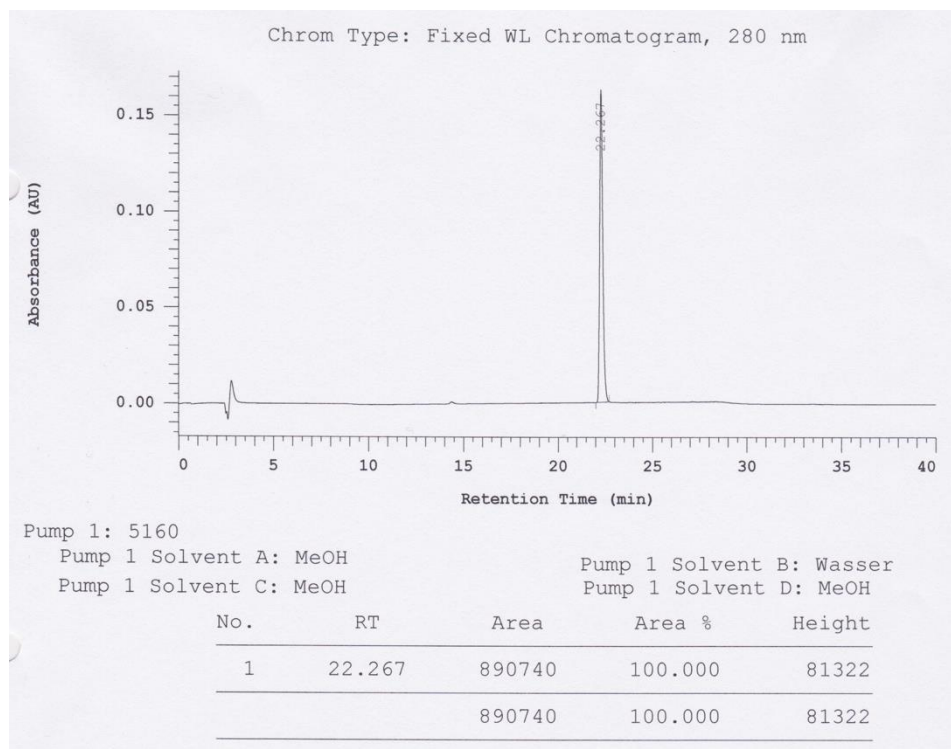
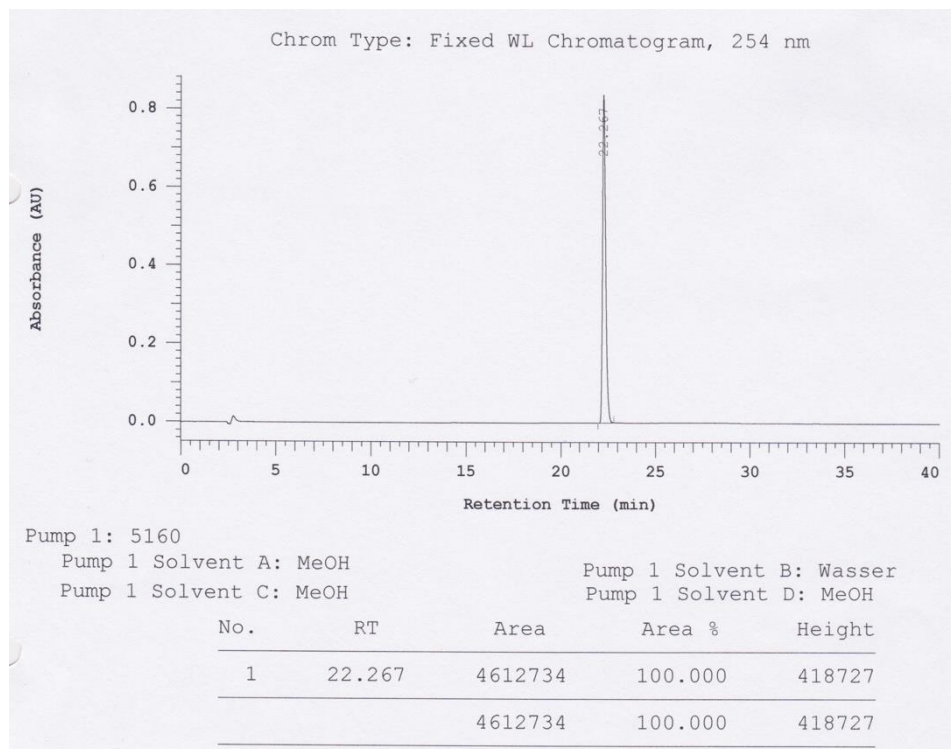
Pump 1 Solvent D: MeOH

No.	RT	Area	Area %	Height
1	25.160	378207	99.104	33665
2	26.973	3418	0.896	428
		381625	100.000	34093

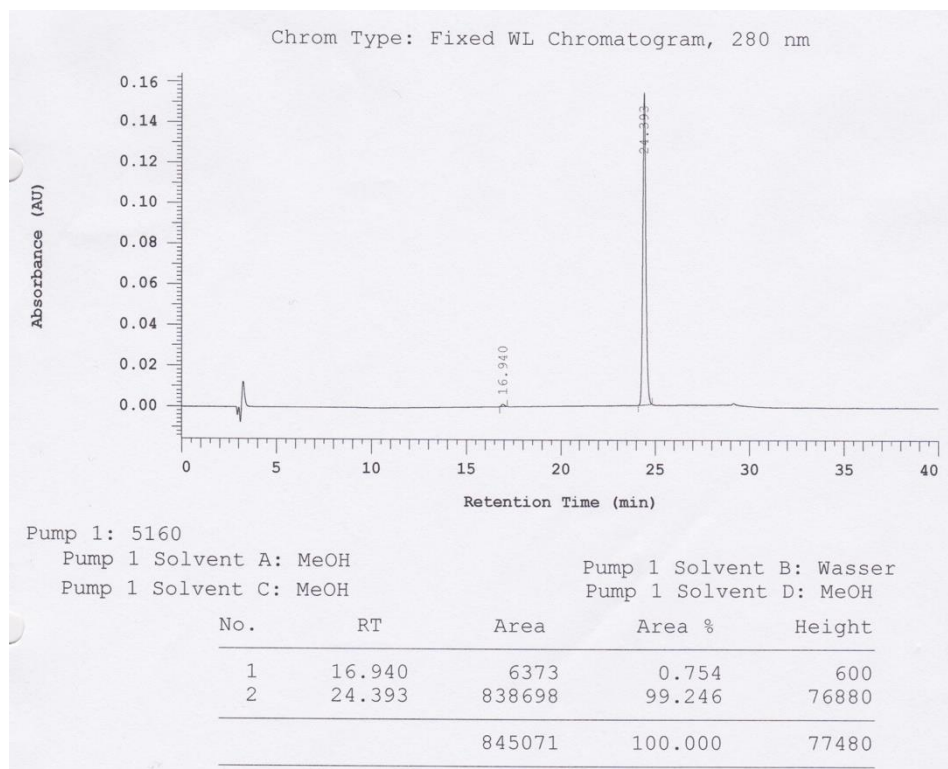
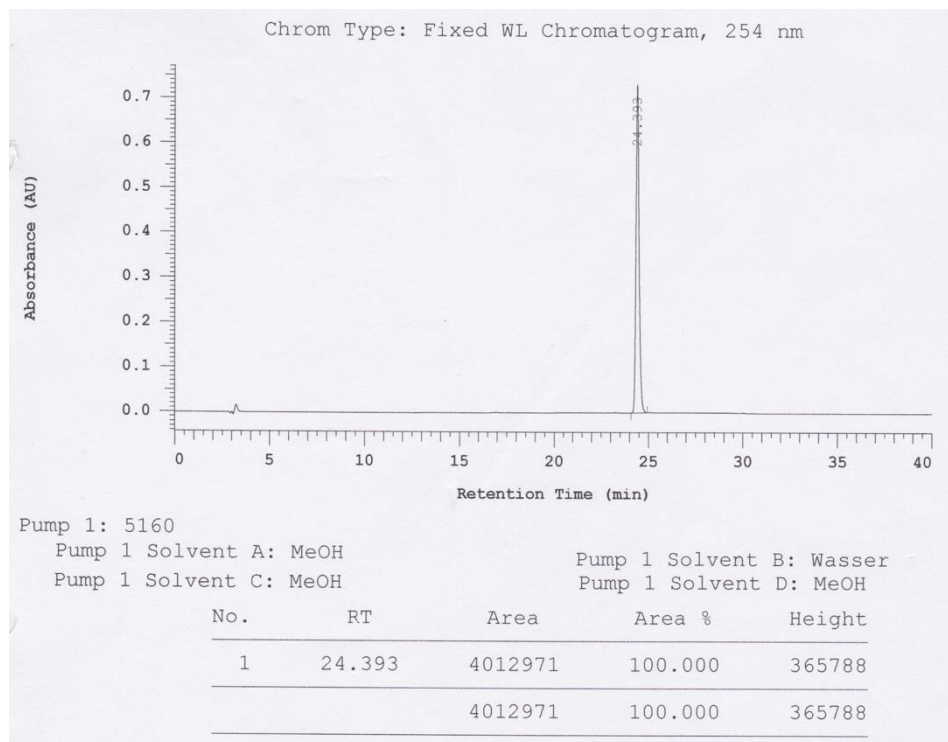
N-methyl-1-methyl-5-phenylindole-3-carboxamide (**32**):



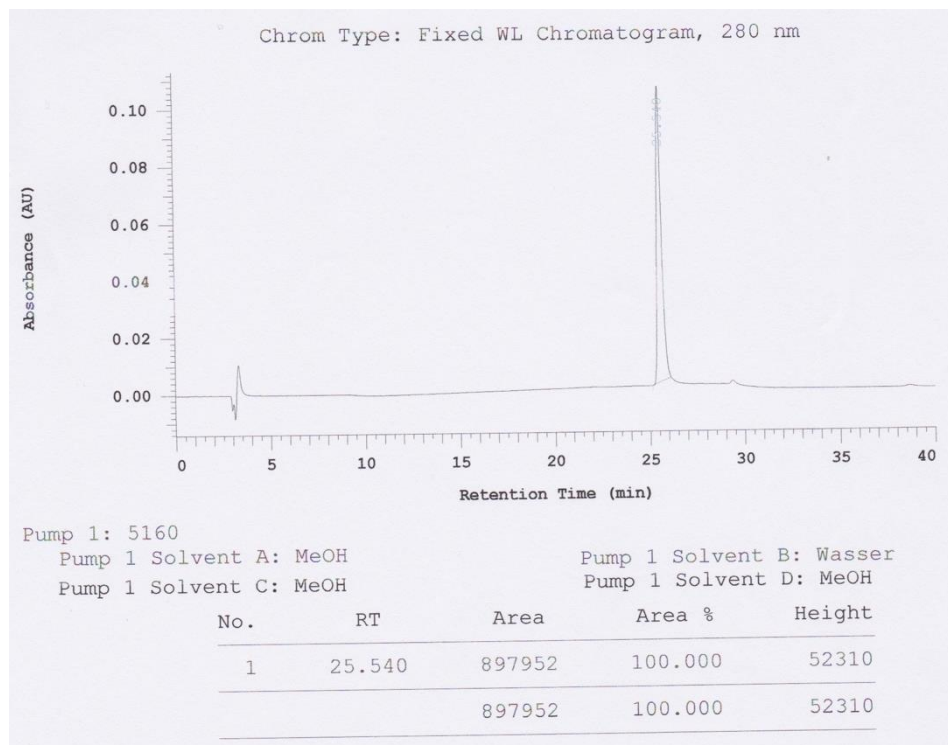
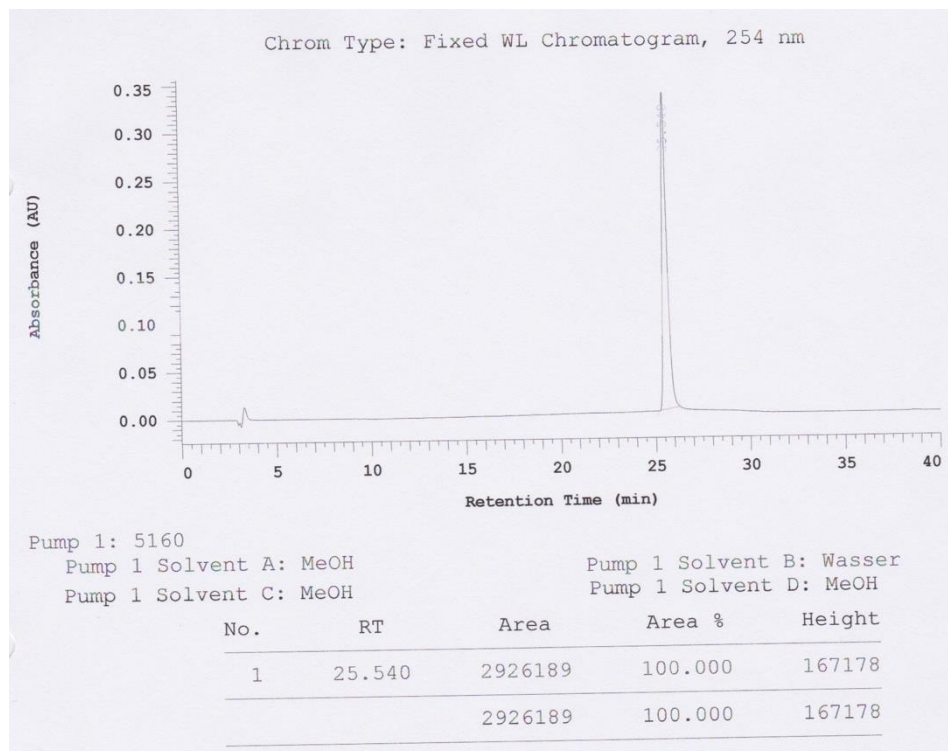
N-ethyl-1-methyl-5-phenylindole-3-carboxamide (**33**):



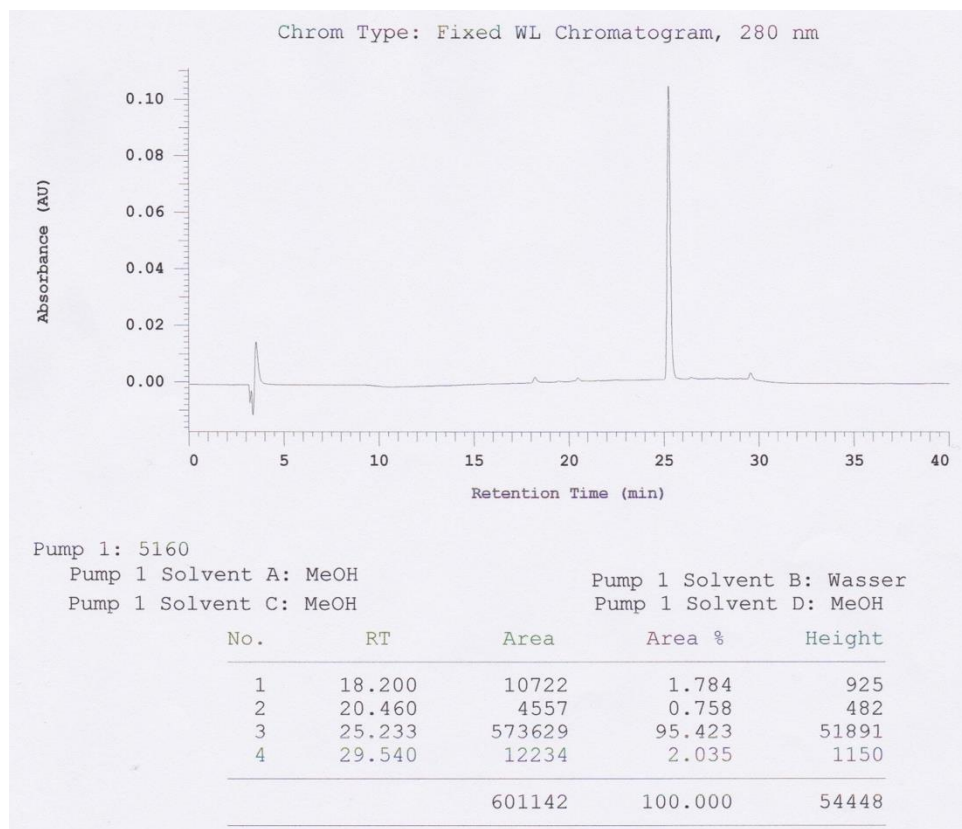
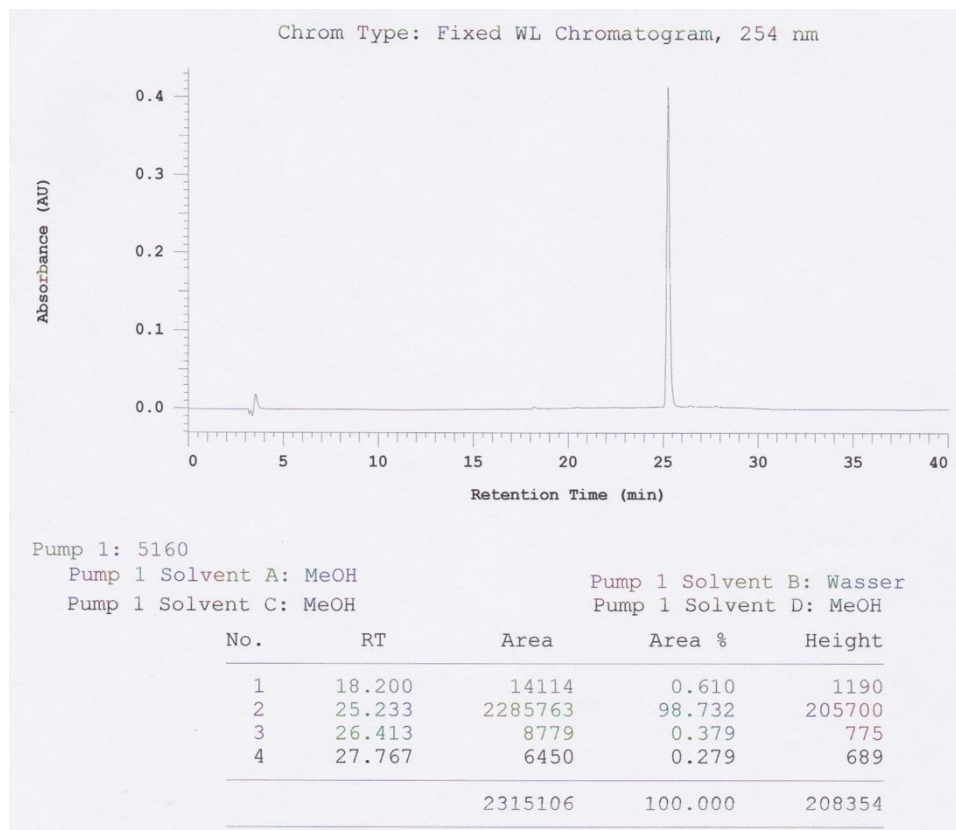
N-dimethyl-1-methyl-5-phenylindole-3-carboxamide (34):



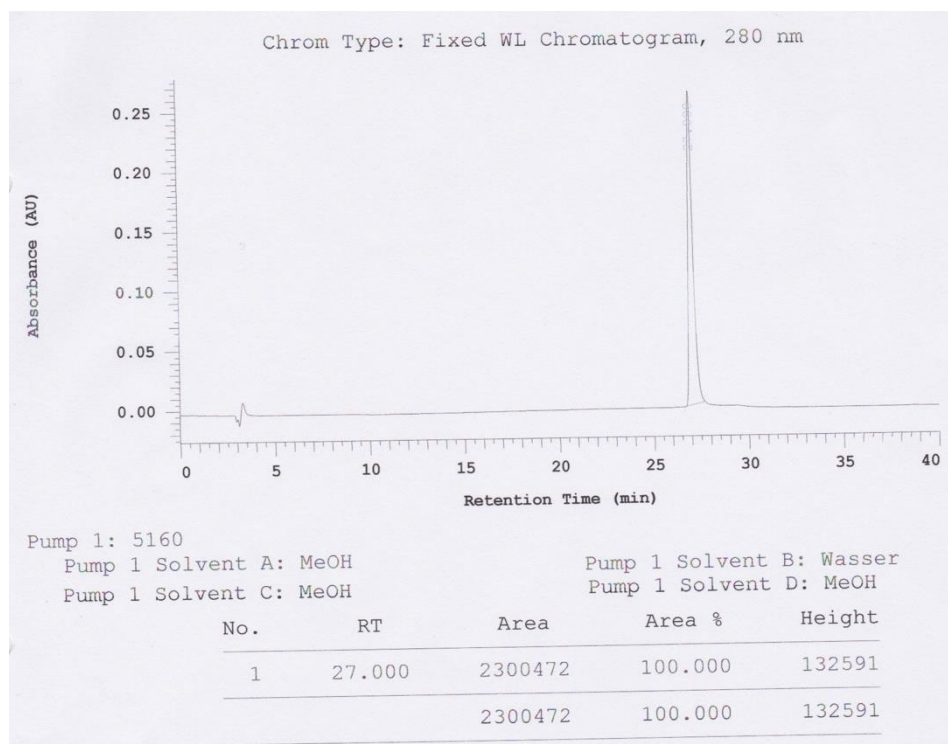
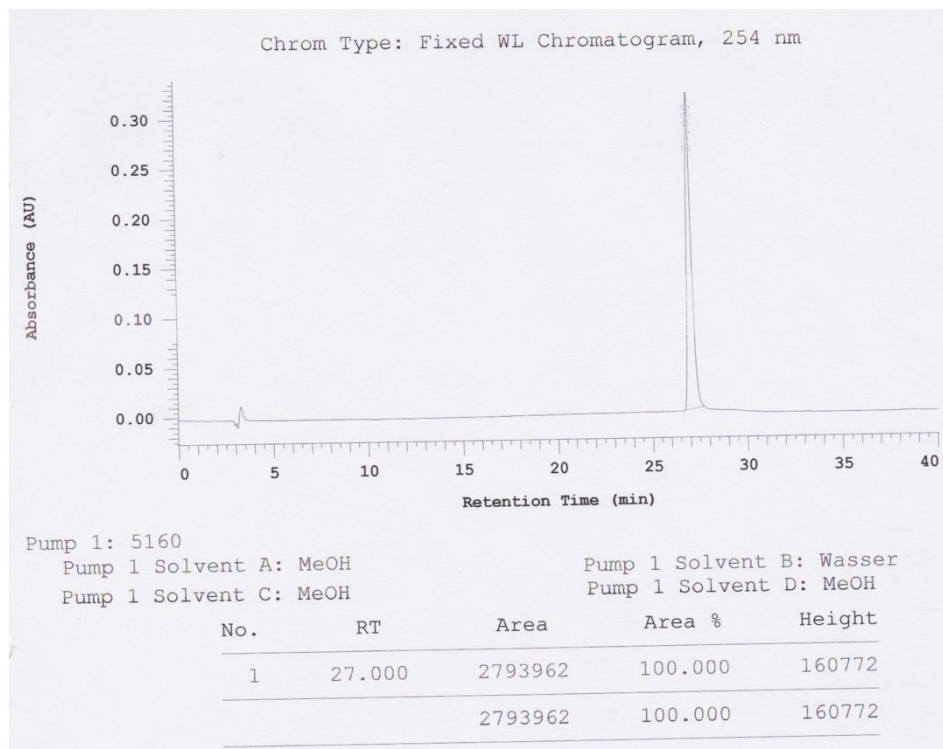
5-(Furan-2-yl)-1-methylindole-3-carboxylic acid methyl ester (**35**):



5-(Furan-3-yl)-1-methylindole-3-carboxylic acid methyl ester (**36**):

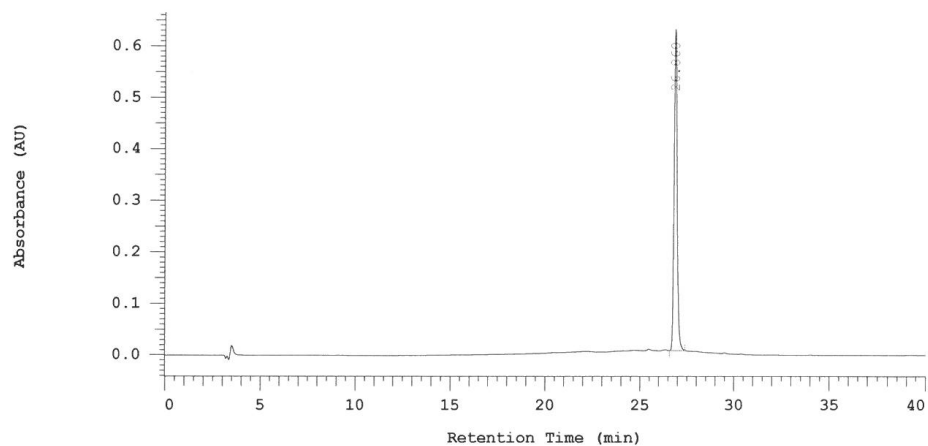


5-(Thiophen-2-yl)-1-methylindole-3-carboxylic acid methyl ester (**37**):



5-(Thiophen-3-yl)-1-methylindole-3-carboxylic acid methyl ester (**38**):

Chrom Type: Fixed WL Chromatogram, 254 nm



Pump 1: 5160

Pump 1 Solvent A: MeOH

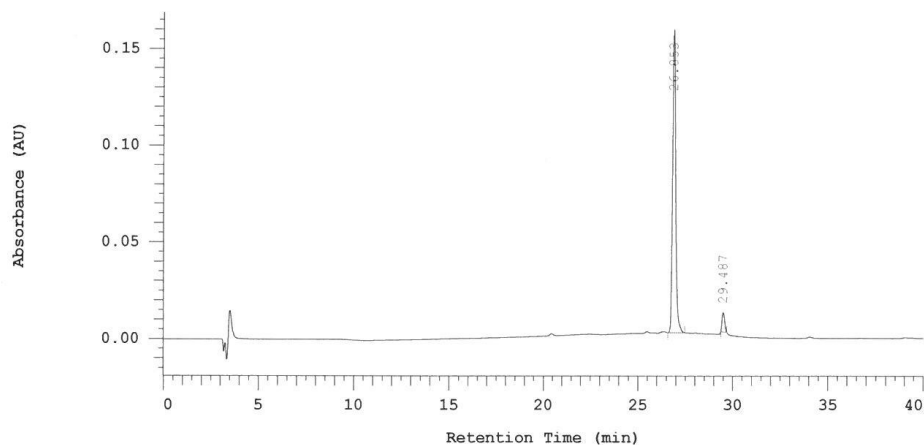
Pump 1 Solvent B: Wasser

Pump 1 Solvent C: MeOH

Pump 1 Solvent D: MeOH

No.	RT	Area	Area %	Height
1	26.860	3446143	100.000	311366
		3446143	100.000	311366

Chrom Type: Fixed WL Chromatogram, 280 nm



Pump 1: 5160

Pump 1 Solvent A: MeOH

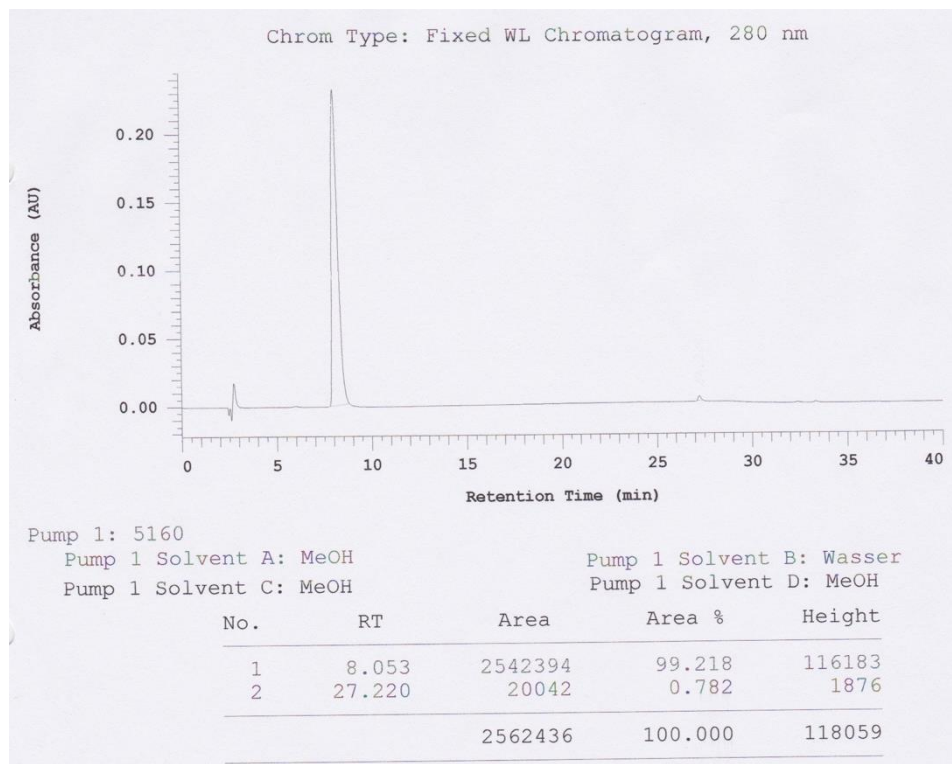
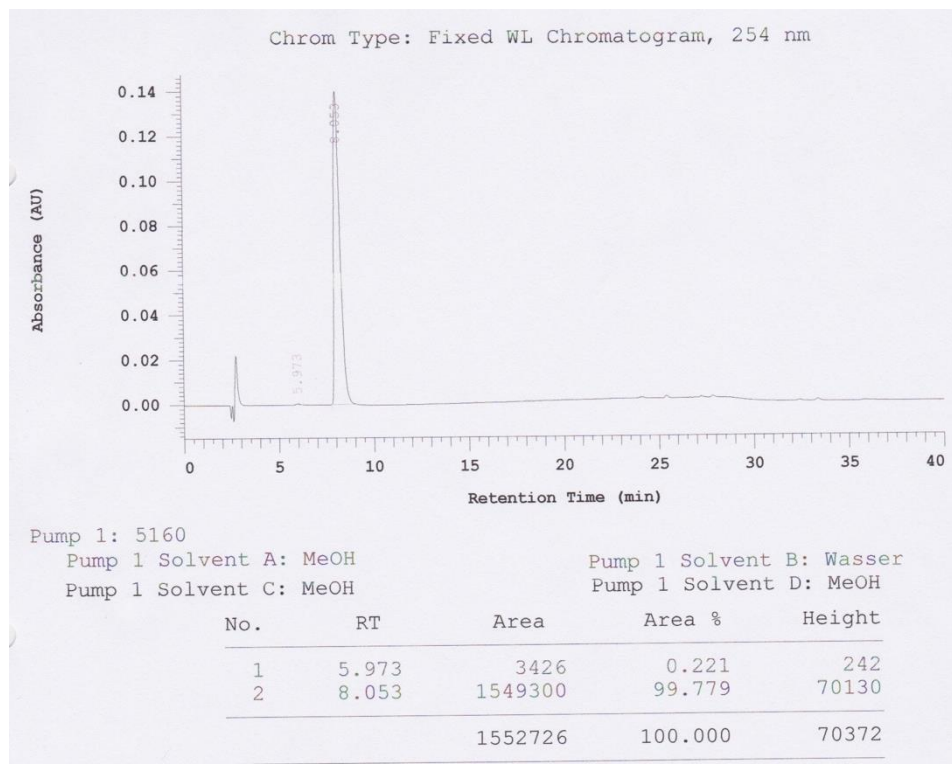
Pump 1 Solvent B: Wasser

Pump 1 Solvent C: MeOH

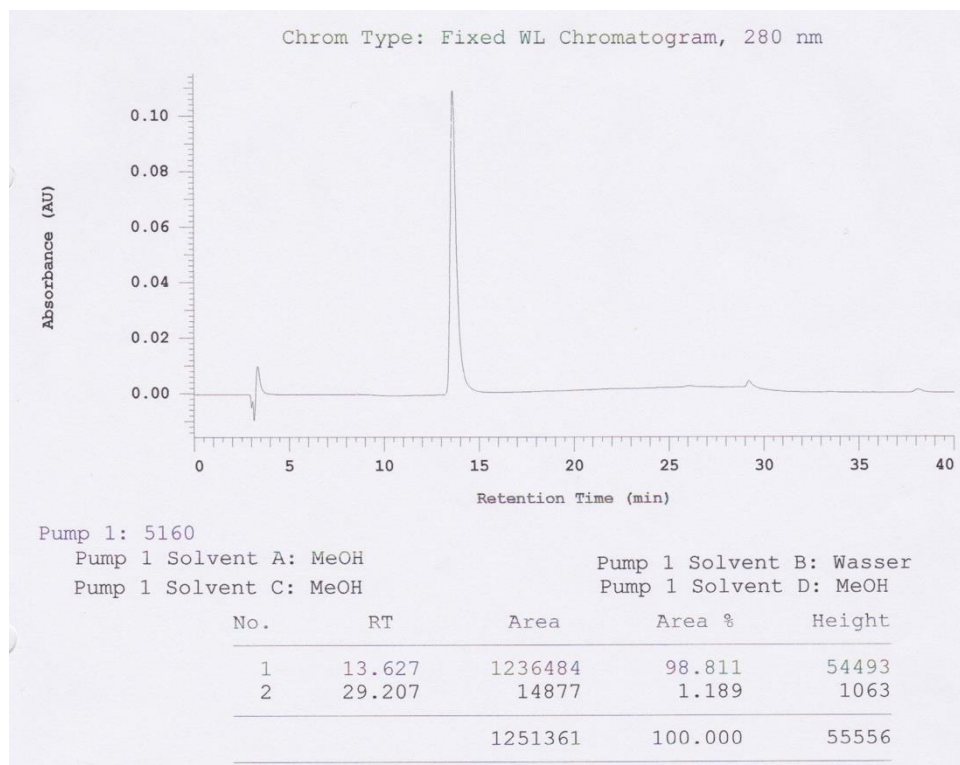
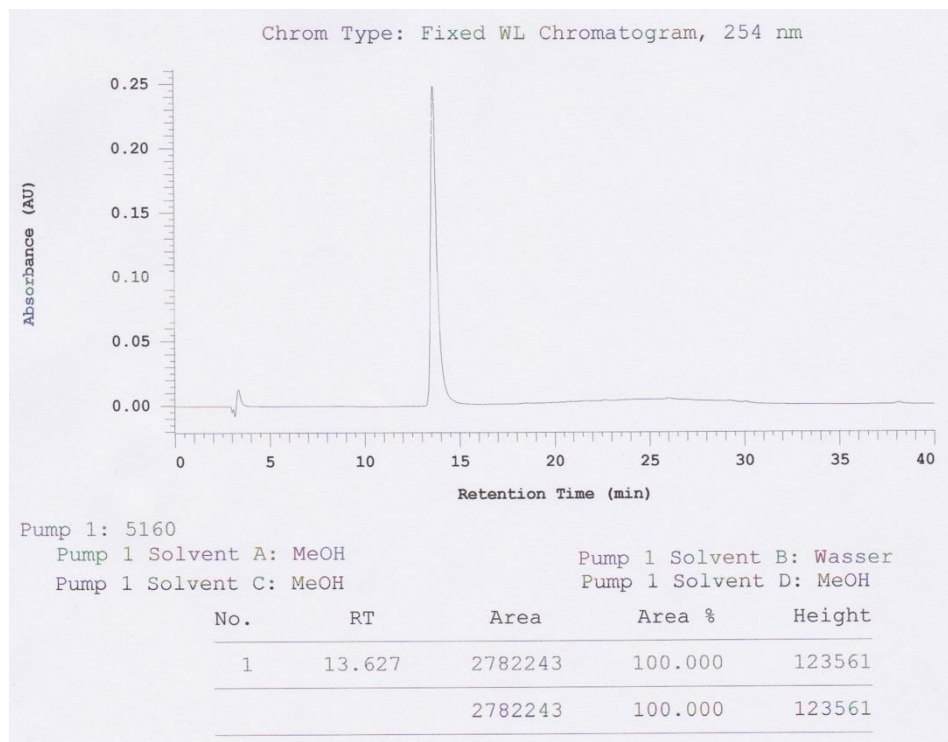
Pump 1 Solvent D: MeOH

No.	RT	Area	Area %	Height
1	26.853	877309	95.069	78358
2	29.487	45503	4.931	4979
		922812	100.000	83337

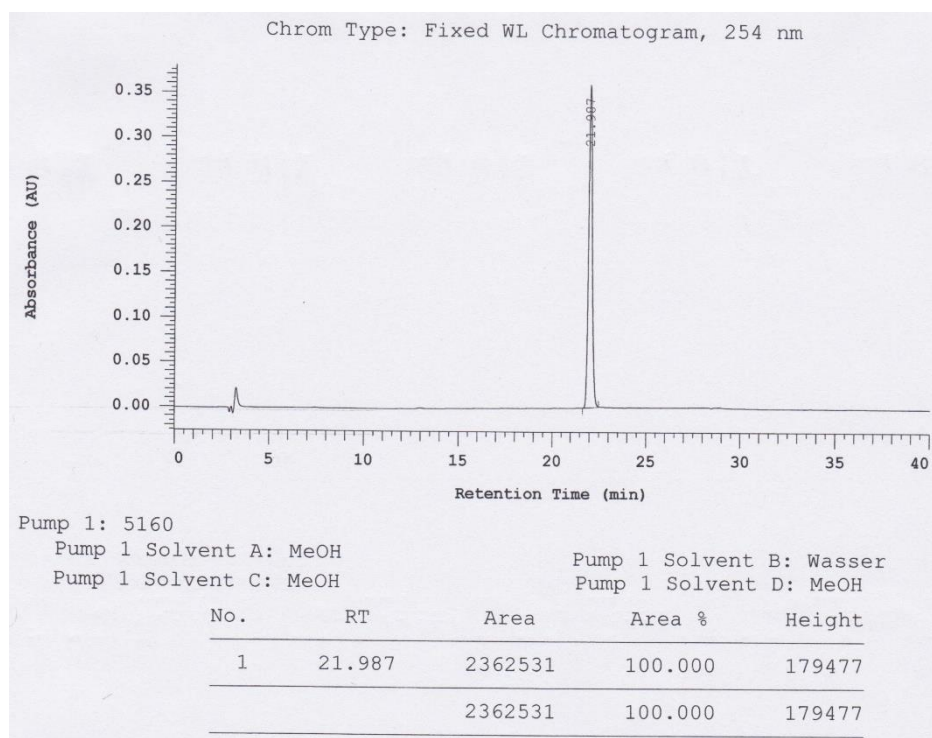
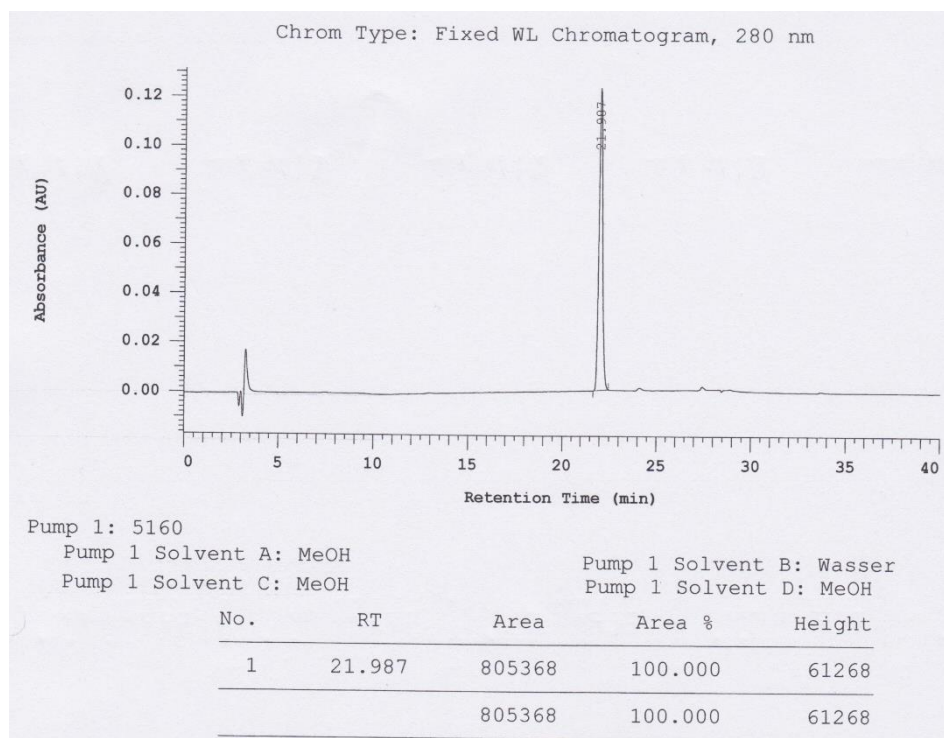
5-(Pyridin-4-yl)-1-methylindole-3-carboxylic acid methyl ester (**39**):



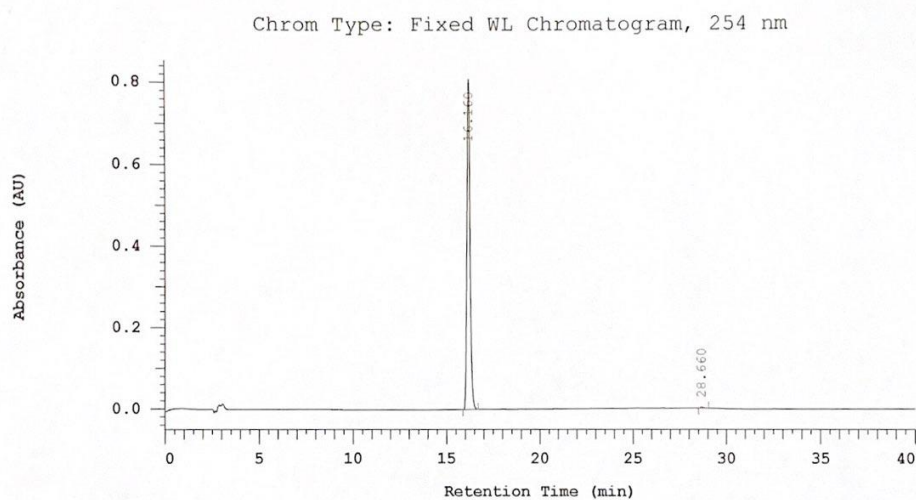
5-(Pyridin-3-yl)-1-methylindole-3-carboxylic acid methyl ester (**40**):



7-Chloro-1-methyl-5(pyridin-3-yl)-1H-indole-3-carboxylic acid methyl ester (**41**):



5-(Pyridin-3-yl)-1*H*-indole-3-carboxylic acid methyl ester (**42**):



Pump 1: 5160

Pump 1 Solvent A: MeOH

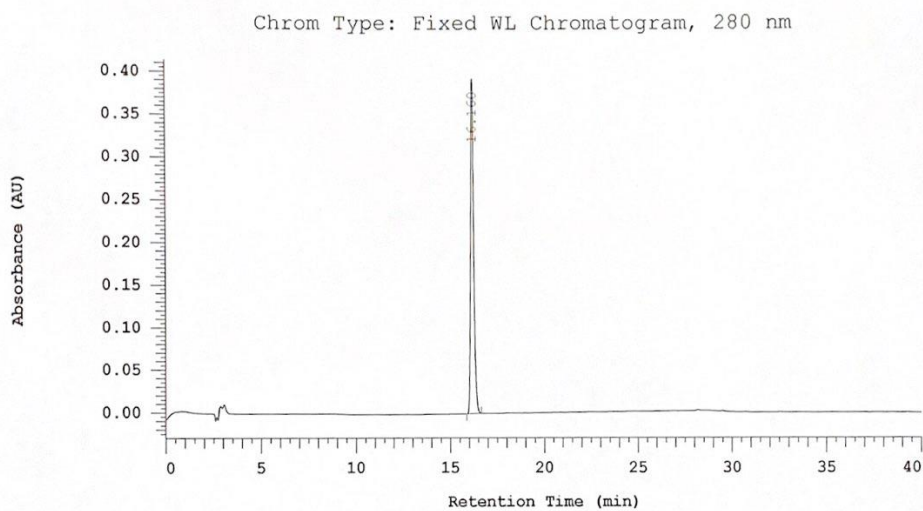
Pump 1 Solvent C: MeOH

Pump 1 Solvent B: Wasser

Pump 1 Solvent D: MeOH

No.	RT	Area	Area %	Height
1	16.160	4536785	99.705	406272
2	28.660	13424	0.295	1316
		4550209	100.000	407588

Peak rejection level: 0



Pump 1: 5160

Pump 1 Solvent A: MeOH

Pump 1 Solvent C: MeOH

Pump 1 Solvent B: Wasser

Pump 1 Solvent D: MeOH

No.	RT	Area	Area %	Height
1	16.160	2198212	100.000	197051
		2198212	100.000	197051

Peak rejection level: 0

16.7 Nurr1 modulation mediates neuroprotective effects of statins

Willems, S.; Kilu, W.; Faudone, G.; Heering, J.; Merk, D. Nurr1 modulation mediates neuroprotective effects of statins. *bioRxiv* **2021**, 2021.09.15.460433.

Dieser Artikel ist lizenziert durch eine Creative Commons Attribution 4.0 International License. Eine Kopie dieser Lizenz ist unter <http://creativecommons.org/licenses/by/4.0/> verfügbar. Es wurden keine Änderungen vorgenommen.

Nurr1 modulation mediates neuroprotective effects of statins

Sabine Willems¹, Whitney Kilu¹, Giuseppe Faudone¹, Jan Heering², Daniel Merk^{1,3,4,*}

¹ Goethe University Frankfurt, Institute of Pharmaceutical Chemistry, Max-von-Laue-Str. 9, D-60438 Frankfurt, Germany

² Fraunhofer Institute for Translational Medicine and Pharmacology ITMP, Theodor-Stern-Kai 7, 60596 Frankfurt, Germany

³ LMU Munich, Department of Pharmacy, Butenandtstr. 5-13, 81377 Munich, Germany

⁴ Lead contact

* Correspondence: merk@pharmchem.uni-frankfurt.de (D.M.)

Abstract. The ligand-sensing transcription factor Nurr1 emerges as a promising therapeutic target for neurodegenerative pathologies but Nurr1 ligands for functional studies and therapeutic validation are lacking. Here we report pronounced Nurr1 modulation by statins for which clinically relevant neuroprotective effects have been demonstrated. Several statins directly affected Nurr1 activity in cellular and cell-free settings with low micromolar to sub-micromolar potencies. Simvastatin exhibited anti-inflammatory effects in astrocytes which were abrogated by Nurr1 knockdown. Differential gene expression analysis in native and Nurr1 silenced cells revealed strong proinflammatory effects of Nurr1 knockdown while simvastatin treatment induced several neuroprotective mechanisms via Nurr1, for example, in energy utilization and reduced apoptosis. These findings suggest Nurr1 involvement in the well-documented but mechanistically elusive neuroprotection by statins.

Keywords. Nuclear receptor related-1, NR4A2, neurodegeneration, Parkinson's Disease, Alzheimer's Disease, multiple sclerosis, neuroinflammation, simvastatin, fluvastatin

Introduction

The ligand-activated transcription factor nuclear receptor related-1 (Nurr1, NR4A2)(Wang et al., 2003) is a constitutively active orphan nuclear receptor. It is considered as neuroprotective transcriptional regulator and ascribed high therapeutic potential in neurodegenerative diseases. Nurr1 is expressed in several neuronal cell populations with highest levels in dopaminergic neurons and thought to protect neurons against injury(Decressac et al., 2013). Neuronal Nurr1 knockout in mice produced a phenotype resembling Parkinson's Disease (PD)(Decressac et al., 2013; Kim et al., 2015) and in the neurotoxin MPTP induced model of PD in rodents, Nurr1 was downregulated resulting in neuroinflammation and enhanced apoptosis of neuronal cells(Liu et al., 2017) while Nurr1 overexpression in the same model reduced motor impairment and spatial learning deficits(Liu et al., 2017). In experimental autoimmune encephalomyelitis (EAE), heterozygous Nurr1 knockout mice developed the disease faster than wild-type mice(Montarolo et al., 2015), while enhanced Nurr1 signaling reduced incidence and severity of EAE(Montarolo et al., 2014). Neuronal Nurr1 expression was also significantly downregulated in models of Alzheimer's Disease (AD) in an age-dependent fashion(Moon et al., 2015, 2019) and the transcription factor was shown to protect against AD-related pathology including A β accumulation, neuronal loss and microglial activation in vivo(Moon et al., 2019). In line with these observations from rodent models, altered Nurr1 expression has been detected in human PD, AD and multiple sclerosis (MS) patients(Liu et al., 2017; Moon et al., 2015, 2019; Satoh et al., 2005) further highlighting the great neuroprotective potential of Nurr1(Jakaria et al., 2019) which may hence be a very attractive therapeutic target to treat neurodegenerative pathologies.

Despite this therapeutic promise, knowledge on Nurr1 function and ligands is still scarce. A few weak Nurr1 modulators have been discovered(Bruning et al., 2019; Kim et al., 2015; Munoz-Tello et al., 2020; Rajan et al., 2020; de Vera et al., 2019; Willems et al., 2020, 2021) such as the prostaglandins A1 and E1 as potential endogenous ligands(Rajan et al., 2020). The antimalarials amodiaquine (AQ) and chloroquine (CQ) have served as early Nurr1 agonist tools to evaluate Nurr1 activation in neurodegeneration(Kim et al., 2015, 2016; Moon et al., 2019). Therapeutic validation of Nurr1 in neurodegenerative pathologies and beyond, however, requires potent and selective Nurr1 modulators. Aiming to close this gap and expand the sparse collection of Nurr1 ligand scaffolds, we have screened a drug fragment library for Nurr1 modulation in a cellular setting resulting in the discovery of statins as potent Nurr1 modulators. Intrigued by this finding and reports on clinically relevant effects of this drug class in neurodegeneration(Carroll and Wyse, 2017; Chataway et al., 2014; Torrandell-Haro et al., 2020), we have evaluated the potential involvement of Nurr1 in the neuroprotective actions of statins. Differential gene expression experiments in native and Nurr1-silenced astrocytes demonstrated several Nurr1 mediated neuroprotective mechanisms of simvastatin indicating important contributions of Nurr1 modulation in the pharmacological effects of simvastatin and related drugs in neurodegeneration.

Results

Fragment screening reveals structurally diverse Nurr1 ligands. As rapid approach to discover Nurr1 ligands, we have screened a commercially available collection of 480 drug fragments (see Supplementary Figure 1 for details) for Nurr1 modulation in a cellular Gal4-Nurr1 hybrid reporter gene assay at a single concentration of 100 μ M. Fragments affecting reporter activity ≥ 1.5 -fold (Nurr1 activation) or ≤ 0.6 -fold (Nurr1 repression) were considered for further evaluation (Figure 1 and Supplementary Figure 2A). Curation for toxicity and PAINS structures, and control experiments for non-specific effects on reporter activity (using Gal4-VP16(Budzyński et al., 2015; Sadowski et al., 1988)) resulted in a collection of seven Nurr1 ligand fragments with no privileged scaffold for further characterization. Four fragments promoted Nurr1 activity and three fragments acted as inverse Nurr1 agonists (Supplementary Figure 2). 3-(4-Fluorophenyl)indole emerged as most active Nurr1 activator fragment (EC_{50} 8.2 μ M, 2.1-fold eff.). It is contained in the widely used cholesterol-lowering drug fluvastatin which was an even more potent Nurr1 agonist (EC_{50} 1.8 μ M, 2.2-fold eff.). Following this remarkable finding, we tested all seven marketed statins (fluvastatin, lovastatin, simvastatin, pravastatin, atorvastatin, rosuvastatin, pitavastatin) for Nurr1 modulatory activity and observed Nurr1 agonism for all seven drugs except pravastatin (Figure 1B) but with differing potencies. Lovastatin and simvastatin demonstrated similar potencies as fluvastatin while rosuvastatin was less active. Atorvastatin weakly activated Nurr1 (1.4-fold eff.) with sub-micromolar potency (EC_{50} 0.78 μ M) and

pitavastatin evolved as the most potent Nurr1 agonist amongst statins (EC_{50} 0.12 μ M, 1.7-fold eff.). Interestingly, statins share structural features with the known Nurr1 agonists AQ and CQ as illustrated by multiple alignment (Figure 1C) but exhibit remarkably higher potencies (up to 400-fold) on Nurr1 (Figure 1D).

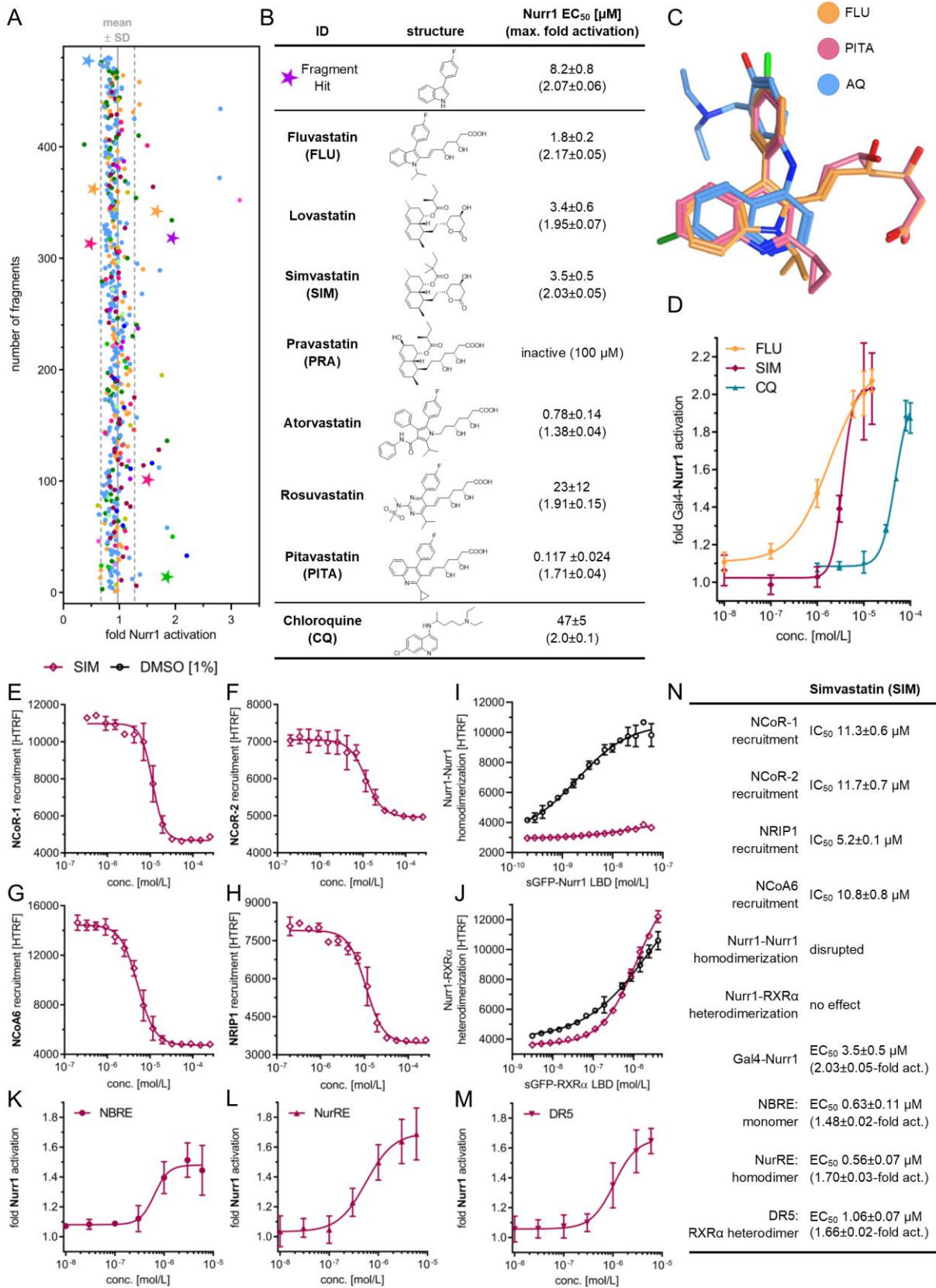


Figure 1. Discovery of statins as Nurr1 modulators and their profiling. (A) Primary fragment screening results. Nurr1 modulatory activity of the entire drug fragment library in a Gal4 reporter gene assay. Data are the mean reporter activity vs. 0.4% DMSO at 100 μ M; n=2. Different

colors represent different graph frameworks (see also Supplementary Figure 1). Compounds marked with a star relate to the fragment hits validated in control experiments on Gal4-VP16. Gray lines represent mean \pm SD of the entire screening. (B) Nurr1 modulatory activity of the fragment screening hit and of the statin class of drugs (vs. 0.1% DMSO) in a Gal4 hybrid Nurr1 reporter gene assay. Data are the mean \pm S.E.M.; n \geq 3. (C) Multiple alignment of fluvastatin (FLU), pitavastatin, and AQ reveals common structural features with overlap of the indole and quinoline scaffolds as well as the phenyl substituents. (D) Dose-response curves of simvastatin (SIM) and FLU determined in a Gal4-Nurr1 hybrid reporter gene assay. Chloroquine (CQ) for comparison. Data are the mean \pm S.E.M., n \geq 3. (E-J) Effects of SIM on co-regulator interactions and dimerization of Nurr1 in HTRF assays. SIM displaced NCoR-1 (E), NCoR-2 (F), NCoA6 (G) and NRIP1 (H) from the Nurr1 LBD and SIM (30 μ M) decreased homodimerization of Nurr1 (I) without affecting Nurr1-RXR α heterodimerization (J). Data are the mean \pm SD; N=3. (K-M) Profiling of SIM in human full-length Nurr1 reporter gene assays for the Nurr1 response elements NBRE (K, Nurr1 monomer), NurRE (L, Nurr1 homodimer), DR5 (M, Nurr1-RXR α heterodimer). Data are the mean \pm S.E.M., n \geq 3. (N) Summarized activities of Nurr1 modulator SIM in cell-free and cellular experiments.

Statins modulate Nurr1 activity in cellular and cell-free settings. To further characterize the intriguing Nurr1 agonism of statins, we selected fluvastatin (highest Nurr1 agonist efficacy) and simvastatin (most widely used statin) as representative compounds. Additionally, simvastatin lacks a chromophore and was best suited for homogenous time-resolved fluorescence resonance energy transfer (HTRF) based assays. To obtain mechanistic insights in Nurr1 modulation by statins, we evaluated modulation of Nurr1 interactions with co-regulators by statins in cell-free HTRF based systems. We have previously discovered ligand-sensitive interaction of Nurr1 with nuclear receptor co-repressors (NCoR) 1 and 2, nuclear receptor interacting protein 1 (NRIP1) and nuclear receptor co-activator 6 (NCoA6)(Willems et al., 2020). Fluvastatin and simvastatin caused a concentration dependent displacement of all four co-regulators (Figure 1E-H, Supplementary Figure 3). Moreover, since Nurr1 can act as monomer, homodimer and RXR-heterodimer on different DNA response elements, its activity also depends on its dimerization state(Jiang et al., 2019; Willems et al., 2020). Fluvastatin and simvastatin did not alter heterodimerization of Nurr1 with RXR α but robustly inhibited Nurr1 homodimerization (Figure 1I,J, Supplementary Figure 3). The HTRF assays revealed higher potency of simvastatin compared to fluvastatin prompting us to perform further experiments with simvastatin. Next, we characterized the ability of simvastatin to modulate full-length human Nurr1 on the human monomer (NGFI-B response element, NBRE), homodimer (Nur-response element, NurRE), and heterodimer (direct repeat 5, DR5) response elements(Jiang et al., 2019). Simvastatin activated the full-length human Nurr1 on all three response elements with low micromolar to sub-micromolar potencies (Figure 1K-N). Despite disrupting Nurr1 homodimerization, simvastatin also activated the homodimer response element NurRE. As NurRE naturally also contains a Nurr1 monomer binding site(Maira et al., 1999; Willems et al., 2020), this finding is not surprising, however. A selectivity screen over lipid sensing nuclear receptors revealed no other activities of simvastatin and fluvastatin (Supplementary Figure 3G).

Statins block the inflammatory response of astrocytes. To probe the relevance of Nurr1 modulation by statins in neuroinflammation, we studied the effects of simvastatin and fluvastatin on interleukin-6 (IL-6) release by Nurr1 expressing human astrocytes (T98G) in response to LPS treatment. Pravastatin, which does not activate Nurr1, was used as negative control. Simvastatin and fluvastatin markedly diminished LPS-induced IL-6 release while pravastatin had no effect suggesting Nurr1 involvement (Figure 2A). Silencing of Nurr1 by RNAi in T98G cells (Figure 2B) remarkably increased IL-6 production and abrogated the effect of simvastatin on IL-6 levels (Figure 2C) further supporting Nurr1 mediated activity of the statins.

Nurr1 knockdown alters neuroinflammatory signaling in vitro. The pronounced effect of Nurr1 knockdown on IL-6 levels aligned with the transcription factor's important role in neuroprotection and -inflammation. To obtain insights in its neuroprotective mechanisms in astrocytes, we studied differential gene expression of T98G cells treated with Nurr1 siRNA or non-targeting (nt) siRNA in presence or absence of LPS (Figure 2D-H). siRNA mediated Nurr1 knockdown altered the expression of almost 8000 genes in both untreated and LPS-treated T98G cells but with pronounced differences of almost 2000 genes differentially affected by Nurr1 knockdown in presence or absence of LPS (Figure 2F). Silencing of Nurr1 strongly increased expression of multiple cytokines (interferons, C-C and C-X-C chemokines), cytokine receptors, TNF superfamily genes (e.g., CD40), and members of JAK-STAT signaling (STAT1, STAT2) even in absence of LPS stimulation (Figure 2H) indicating that diminished Nurr1 activity is sufficient to induce neuroinflammation. Still, LPS treatment caused upregulation of additional cytokines (CCL13, CCL20) in Nurr1 silenced cells. Pathway analysis of altered gene expression levels additionally revealed strong

effects of Nurr1 silencing on genes involved in PD and AD, oxidative phosphorylation, apoptosis, and p53 signaling (Figure 2G).

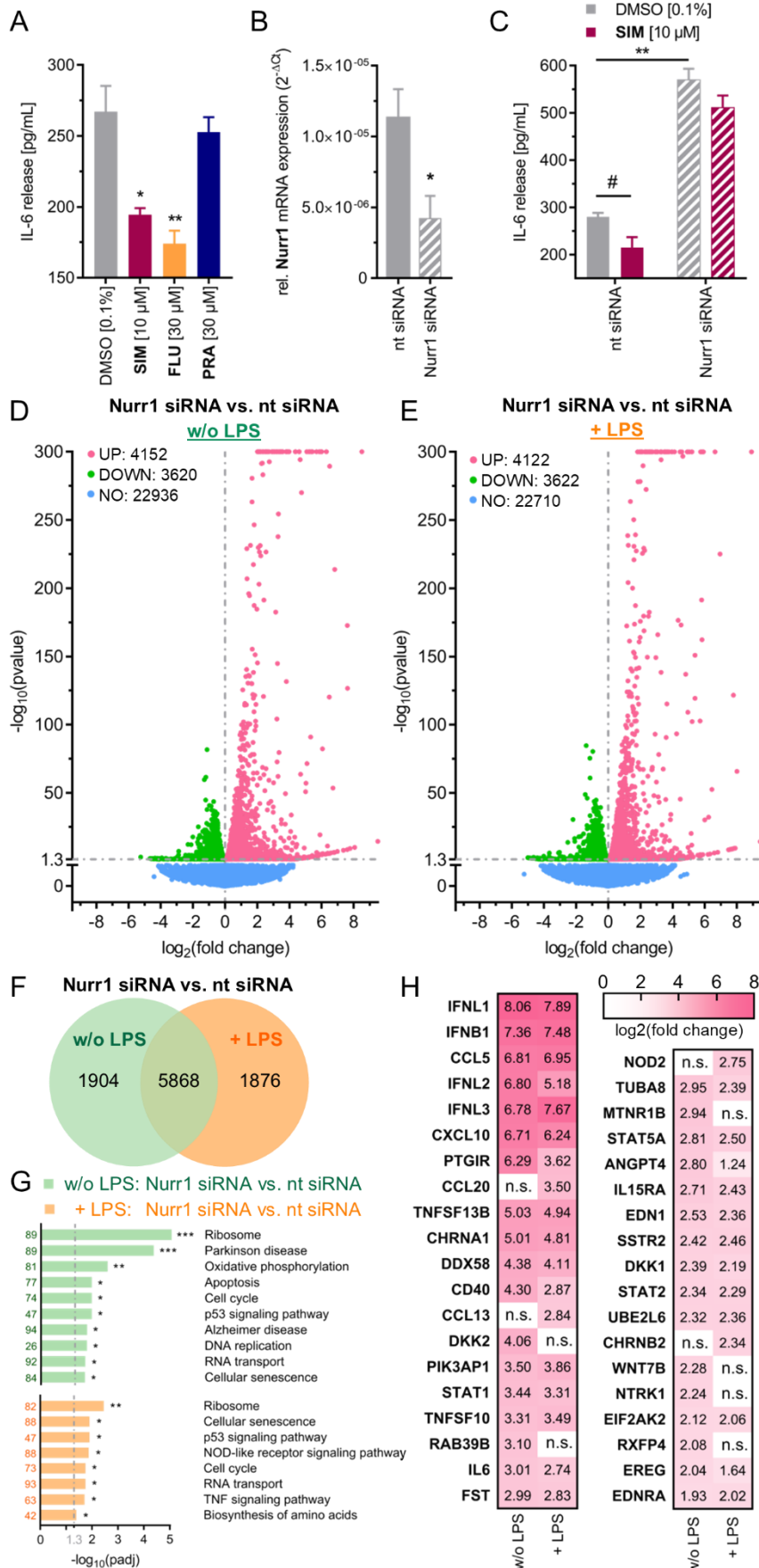


Figure 2. Nurr1 is involved in neuroinflammatory signaling. (A) The Nurr1 agonists SIM and FLU significantly countered interleukin-6 (IL-6) release from LPS-treated (1 µg/mL) T98G cells, whereas pravastatin (PRA), as negative control, did not affect IL-6 release. Data are the mean±S.E.M., n=4, # p < 0.1, * p < 0.05, ** p < 0.01 (t-test). (B) Nurr1 knockdown efficiency as determined by Nurr1 mRNA levels (qRT-PCR, 2^{-ΔCt} method with GAPDH as reference gene). Data are the mean±S.E.M., n=8, * p < 0.05 vs. non-targeting (nt) control siRNA (t-test). (C) LPS-treated T98G cells released considerable amounts of IL-6 which was further enhanced by siRNA-mediated Nurr1 knockdown suggesting reverse Nurr1 involvement in this inflammatory response. The Nurr1 agonist SIM ameliorated the inflammatory response of T98G cells in a Nurr1 dependent manner. Data are the mean±S.E.M., n=3, # p < 0.1, ** p < 0.01 (t-test). (D & E) Differential gene expression in T98G cells treated with nt or Nurr1 siRNA in absence (D) or presence (E) of LPS. Volcano plots show log₂fold change in gene expression level (x axis) versus statistical significance level (-log₁₀(p value); y axis). (F) Co-expression Venn diagram for differential gene expression in Nurr1 silenced cells versus nt siRNA for +/- LPS treated cells. (G) KEGG pathway enrichment analysis illustrates involvement of Nurr1 in signaling pathways related to neurodegenerative diseases and neuroinflammation. Bar plot shows statistical significance level (-log₁₀(padj)) of regulated KEGG pathways, numbers refer to the count of differentially expressed genes related to the pathway. n=3, * p < 0.05, ** p < 0.01, *** p < 0.001. (H) Differentially expressed genes with log₂fold change > |2| associated with neurodegenerative diseases (PD, AD, neurodegeneration) or neuroinflammatory signaling (TNF, NFκB, WNT, TGFβ, JAK-STAT, PI3K-Akt, apoptosis, neuroactive interaction) according to KEGG are listed with their respective log₂fold change values for Nurr1 silencing compared to nt siRNA control in absence or presence of LPS. n.s. – not significant.

Simvastatin exhibits neuroprotective effects via Nurr1. As simvastatin had exhibited potential neuroprotective effects in LPS-treated astrocytes and significantly decreased IL-6 release, we evaluated its effect on gene expression in presence or absence of Nurr1. We treated astrocytes (T98G) with nt siRNA or Nurr1 siRNA and with DMSO or Simvastatin, stimulated the cells with LPS and determined differential gene expression (Figure 3). Compared to DMSO, simvastatin treatment had a pronounced effect on gene expression in both groups (nt and Nurr1 siRNA, Figure 3A,B). The expression levels of 1322 genes were affected by simvastatin treatment in both groups (Figure 3C) indicating that also other pathways were involved. 1389 genes were selectively affected by simvastatin (vs. DMSO) in nt siRNA treated cells but not altered upon simvastatin treatment of Nurr1 silenced cells (Figure 3B,C). Pathway analysis of nt siRNA vs. Nurr1 siRNA treated cells demonstrated Nurr1 mediated effects of simvastatin on genes related to PD, AD, apoptosis, p53 signaling, cell cycle and oxidative phosphorylation (Figure 3D). 109 genes revealed a strong response to simvastatin only in presence of Nurr1 with > |0.5| log₂fold change (Table 1). Closer inspection of these Nurr1 mediated simvastatin effects revealed several neuroprotective effects including pronounced induction of hexokinase 3 (HK3), the E3-ubiquitin ligases RING finger protein RNF43 and RNF222, and notch4 as well as downregulation of gasdermin C (Figure 3E). HK3 is the rate-limiting enzyme of glucose utilization and its induction by simvastatin may importantly contribute to neuroprotective effects. Energy metabolism is critical for neuronal health and function, and altered glucose utilization in brain has been linked to neurodegenerative diseases, particularly to AD(Cisternas et al., 2016; Haenig et al., 2020; Winkler et al., 2015). Additionally, HK3 has been associated with cytoprotective effects against oxidative stress, increased ATP levels and enhanced mitochondrial biogenesis(Wyatt et al., 2010). RNF43 is considered as an anti-apoptotic regulator(Shinada et al., 2011), as a Wnt antagonist(Zhong et al., 2021) and to be involved in DNA repair(Lerksuthirat et al., 2020) suggesting its upregulation as another neuroprotective contribution. Moreover, despite incomplete understanding of notch in neurodegeneration(Ables et al., 2011), decreased notch signaling has been detected in AD(Alberi et al., 2013; Moehmann et al., 2002) indicating a potential benefit of notch induction by simvastatin. Gasdermin C is a membrane pore-forming protein and a key mediator of inflammation and cell death(Broz et al., 2020; Feng et al., 2018; Rogers et al., 2019). Gasdermin pores permeabilize cell membranes and damage mitochondria to release cytochrome C leading to inflammasome activation and enhanced apoptosis(Broz et al., 2020; Feng et al., 2018; Rogers et al., 2019). The pronounced Nurr1 mediated downregulation of gasdermin C by simvastatin potentially emerges as a key neuroprotective effect preventing inflammation, apoptosis and neuronal cell death. In addition, marked Nurr1 mediated effects of simvastatin on neurotransmitter receptors and transporters as well as on inflammatory genes were evident from the comparison of nt siRNA and Nurr1 siRNA treated cells. Simvastatin downregulated metabotropic glutamate receptor 4 (GRM4), GABA receptor A3 (GABRA3) and the neuropeptide PEN receptor GPR83 while no neurotransmitter or neuropeptide receptor was induced. Simvastatin treatment also diminished expression of the GABA transporter SLC6A12 and several ion channels (KCNA7, KCNB1, TRPV2). Nurr1 mediated effects of simvastatin on genes involved in inflammation included induction of NFκB inhibitor alpha (NFKBIA) and intercellular adhesion molecule 1 (ICAM1), and downregulation of arachidonate 12 lipoxygenase (ALOX12) and IL-31 receptor (IL31RA). Cyclooxygenase 2 (COX-

2, PTGS2) was upregulated suggesting that Nurr1 activation did not fully block LPS effects. Overall, differential gene expression analysis demonstrated distinguished Nurr1 mediated neuroprotective effects of simvastatin with anti-apoptotic, metabolic and anti-inflammatory contributions.

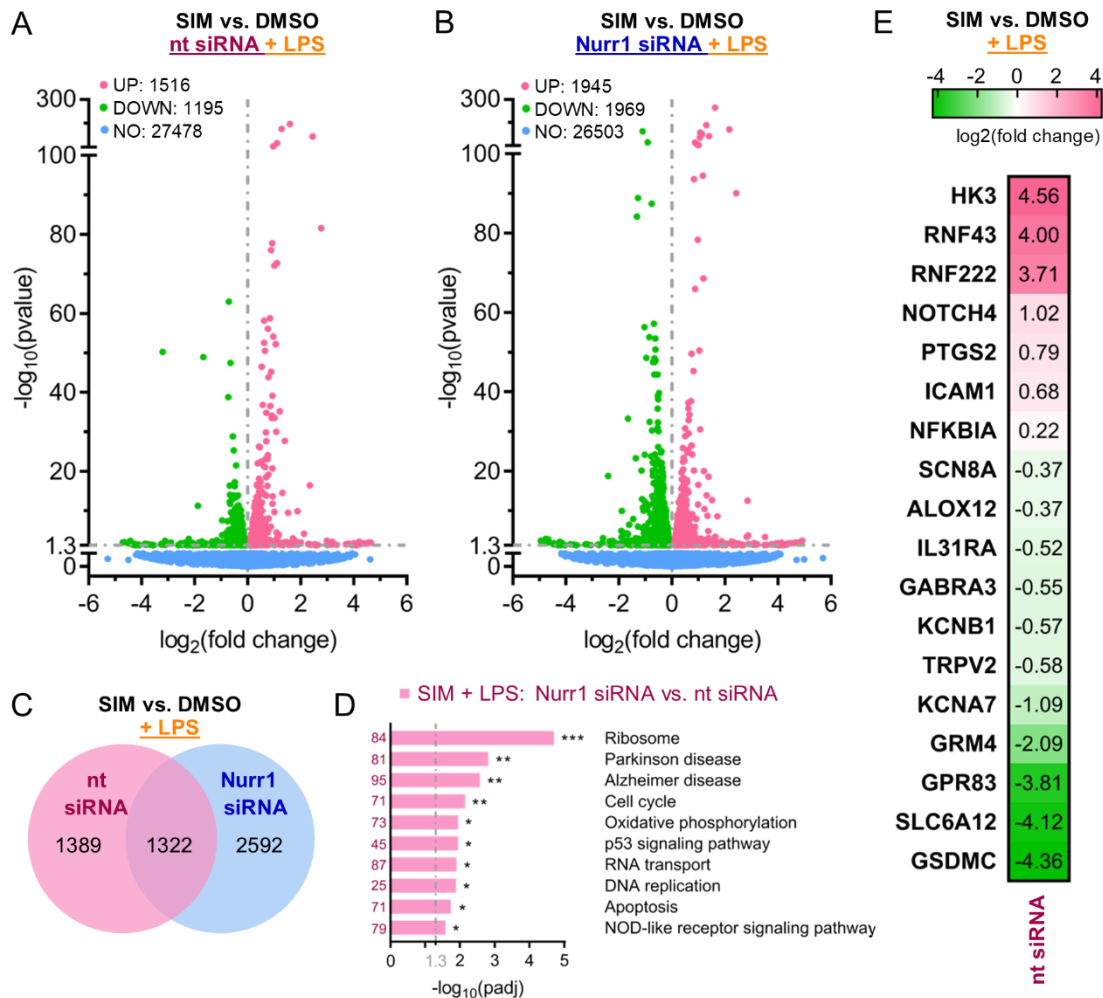


Figure 3. Simvastatin affected gene expression of LPS-treated human astrocytes (T98G) in a Nurr1 dependent manner. (A & B) Differentially expressed genes for SIM (10 μ M) versus DMSO in LPS-stimulated T98G cells treated with nt siRNA (A) or Nurr1 siRNA (B). Volcano plots show log₂fold change in gene expression level (x axis) versus statistical significance level (-log₁₀(p value); y axis), n=3. (C) Co-expression Venn diagram shows effects of SIM vs. DMSO in LPS-stimulated T98G cells treated with nt siRNA (magenta) or Nurr1 siRNA (blue). (D) KEGG pathway enrichment analysis illustrates involvement of Nurr1 activation by SIM in signaling pathways related to neurodegeneration and neuroinflammation. Bar plot shows statistical significance level (-log₁₀(padj)) of regulated KEGG pathways, numbers refer to the count of differentially expressed genes related to the pathway. n=3, * p < 0.05, ** p < 0.01, *** p < 0.001. (E) Genes regulated by SIM (vs. DMSO) in LPS stimulated nt siRNA treated cells whose expression was unaffected in Nurr1 siRNA treated cells. Only selected genes related to neuroprotection and neuroinflammation are shown, further regulated genes in Table 1. Heatmap shows log₂fold change in gene expression.

Table 1. Effects of Simvastatin on differential gene expression in LPS-stimulated T98G cells. Only protein coding genes with log₂fold change > |0.5| that were selectively altered by Simvastatin in nt siRNA treated cells but not altered in Nurr1 silenced cells are shown.

Gene name	Gene description	log ₂ (fold change)	-log ₁₀ (p value)
HK3	hexokinase 3	4.559	2.002
GJB5	gap junction protein beta 5	4.250	1.605
C3orf67	chromosome 3 open reading frame 67	4.242	2.106
LRRD1	leucine rich repeats and death domain containing 1	4.195	2.135
CLEC18A	C-type lectin domain family 18 member A	4.083	1.379
CFHR1	complement factor H related 1	4.083	1.439

KLHL35	kelch like family member 35	4.080	1.397
COL9A2	collagen type IX alpha 2 chain	4.070	1.368
RNF43	ring finger protein 43	4.004	1.785
RNF222	ring finger protein 222	3.708	1.545
C16orf46	chromosome 16 open reading frame 46	3.367	1.431
MUC15	mucin 15, cell surface associated	2.549	1.302
RCAN2	regulator of calcineurin 2	1.823	2.312
ATP10B	ATPase phospholipid transporting 10B (putative)	1.761	1.744
DNAJB13	DnaJ heat shock protein family (Hsp40) member B13	1.752	1.835
C11orf96	chromosome 11 open reading frame 96	1.704	3.066
PHOSPHO1	phosphoethanolamine/phosphocholine phosphatase	1.339	1.303
SNAI3	snail family transcriptional repressor 3	1.124	3.420
TMEM216	transmembrane protein 216	1.116	2.046
NOTCH4	notch 4	1.020	1.821
EPS8L1	EPS8 like 1	1.019	1.896
C19orf73	chromosome 19 open reading frame 73	0.842	1.828
AKAP12	A-kinase anchoring protein 12	0.837	1.637
XKRX	XK related X-linked	0.831	2.609
CCDC151	coiled-coil domain containing 151	0.816	1.625
PTGS2	prostaglandin-endoperoxide synthase 2	0.789	8.047
FKBP1B	FK506 binding protein 1B	0.781	1.336
DNAAF3	dynein axonemal assembly factor 3	0.778	2.180
INHBE	inhibin subunit beta E	0.771	1.551
CPEB3	cytoplasmic polyadenylation element binding protein 3	0.749	1.484
HSD11B1	hydroxysteroid 11-beta dehydrogenase 1	0.738	1.525
CD7	CD7 molecule	0.713	2.130
SLC2A5	solute carrier family 2 member 5	0.688	1.390
C4A	complement C4A (Rodgers blood group)	0.685	1.540
ABCA3	ATP binding cassette subfamily A member 3	0.680	1.863
ICAM1	intercellular adhesion molecule 1	0.675	4.838
STBD1	starch binding domain 1	0.640	1.932
EN2	engrailed homeobox 2	0.638	3.077
SWSAP1	SWIM-type zinc finger 7 associated protein 1	0.632	1.534
CDKN2D	cyclin dependent kinase inhibitor 2D	0.631	6.371
ATP6V0C	ATPase H ⁺ transporting V0 subunit c	0.618	2.651
TMPRSS6	transmembrane serine protease 6	0.610	1.352
PAK6	p21 (RAC1) activated kinase 6	0.602	1.844
TUBB2A	tubulin beta 2A class IIa	0.600	6.127
SERPINE1	serpin family E member 1	0.599	4.268
MT1X	metallothionein 1X	0.547	4.060
TRNP1	TMF1-regulated nuclear protein 1	0.542	2.065
ETV4	ETS variant 4	0.538	12.089
SEMA6A	semaphorin 6A	0.512	1.731
CBLN2	cerebellin 2 precursor	-0.502	2.847
DENND2A	DENN domain containing 2A	-0.506	1.386
KIAA0319	KIAA0319	-0.515	1.774
TLN2	talin 2	-0.516	4.222
IL31RA	interleukin 31 receptor A	-0.517	3.058
LEAP2	liver enriched antimicrobial peptide 2	-0.526	1.638
LDLRAD4	low density lipoprotein receptor class A domain containing 4	-0.529	1.761
S100A1	S100 calcium binding protein A1	-0.539	1.517
GABRA3	gamma-aminobutyric acid type A receptor alpha3 subunit	-0.555	2.330
GATA2	GATA binding protein 2	-0.559	1.589
KCNB1	potassium voltage-gated channel subfamily B member 1	-0.571	3.349
TRPV2	transient receptor potential cation channel subfamily V member 2	-0.580	1.503
PSG4	pregnancy specific beta-1-glycoprotein 4	-0.588	1.799
NPIP9	nuclear pore complex interacting protein family member B9	-0.616	1.306
ZNF835	zinc finger protein 835	-0.617	1.418
ANKRD23	ankyrin repeat domain 23	-0.640	1.324
ZNF10	zinc finger protein 10	-0.641	2.733
CKMT2	creatine kinase, mitochondrial 2	-0.729	1.788

TNXB	tenascin XB	-0.741	1.565
MYH3	myosin heavy chain 3	-0.772	1.930
FGF14	fibroblast growth factor 14	-0.789	1.989
COX16	cytochrome c oxidase assembly factor COX16	-0.808	1.951
PI15	peptidase inhibitor 15	-0.811	2.124
TSTD3	thiosulfate sulfurtransferase like domain containing 3	-0.832	1.303
AKAP5	A-kinase anchoring protein 5	-0.847	1.468
SLC16A14	solute carrier family 16 member 14	-0.855	1.412
FHOD3	formin homology 2 domain containing 3	-0.860	1.560
AC009336.2	homeobox D4	-0.918	1.433
CDRT15	CMT1A duplicated region transcript 15	-1.043	1.479
KCNA7	potassium voltage-gated channel subfamily A member 7	-1.093	1.686
TYRP1	tyrosinase related protein 1	-1.165	2.589
FBXO24	F-box protein 24	-1.201	1.965
DNAH7	dynein axonemal heavy chain 7	-1.204	1.679
CPA5	carboxypeptidase A5	-1.210	1.618
MARCH4	membrane associated ring-CH-type finger 4	-1.219	1.886
SLC35G6	solute carrier family 35 member G6	-1.249	1.402
C3orf80	chromosome 3 open reading frame 80	-1.420	1.404
PROSER2	proline and serine rich 2	-1.728	2.285
PDE6B	phosphodiesterase 6B	-1.752	1.471
METTL7B	methyltransferase like 7B	-1.838	1.388
BEGAIN	brain enriched guanylate kinase associated	-1.841	2.021
GRM4	glutamate metabotropic receptor 4	-2.086	1.341
RAB11FIP1	RAB11 family interacting protein 1	-2.102	1.743
APELA	apelin receptor early endogenous ligand	-2.210	1.466
DEF6	DEF6, guanine nucleotide exchange factor	-2.264	2.100
NANOS3	nanos C2HC-type zinc finger 3	-2.471	1.420
MYBPC1	myosin binding protein C, slow type	-2.520	1.808
ACSL6	acyl-CoA synthetase long chain family member 6	-2.891	1.999
ANKRD65	ankyrin repeat domain 65	-3.200	1.496
GPR83	G protein-coupled receptor 83	-3.808	1.638
DEGS2	delta 4-desaturase, sphingolipid 2	-3.882	1.673
SLC6A12	solute carrier family 6 member 12	-4.119	1.445
VSTM5	V-set and transmembrane domain containing 5	-4.238	1.512
HORMAD1	HORMA domain containing 1	-4.282	1.606
GSDMC	gasdermin C	-4.357	1.454
SLC35F1	solute carrier family 35 member F1	-4.426	2.395
EBF3	early B cell factor 3	-4.531	1.889
HS6ST2	heparan sulfate 6-O-sulfotransferase 2	-4.656	2.089
ZNF366	zinc finger protein 366	-4.718	2.046
TBC1D3B	TBC1 domain family member 3B	-7.221	2.770

Discussion

Several lines of evidence point to an important role and great therapeutic potential of the ligand sensing transcription factor Nurr1 in AD, PD and MS but pharmacological validation and exploitation of Nurr1 as therapeutic target is pending. In an attempt to rapidly expand the knowledge on Nurr1 ligand scaffolds, we have screened a drug fragment collection for Nurr1 modulation and discovered remarkable Nurr1 agonism of statins. Simvastatin activated the human Nurr1 on all its three human response elements with low micromolar to sub-micromolar potency and comprehensive mechanistic characterization revealed displacement of NCoR-1, NCoR-2, NRIP1 and NCoA6 from the Nurr1 LBD, and decreased Nurr1 homodimerization as key contributions to statin dependent Nurr1 activation.

The unprecedented molecular activity of the widely used drug class of statins on Nurr1 intriguingly aligns with several reports on neuroprotective effects of statins and suggests a potential involvement of Nurr1. Indeed, simvastatin counteracted inflammation in Nurr1 expressing astrocytes while this effect was lost in cells silenced for Nurr1 confirming relevance of Nurr1 activation by statins in neuronal cells. To capture neuronal effects of Nurr1

modulation by statins, we studied differential gene expression in Nurr1 expressing and silenced astrocytes upon simvastatin treatment. These experiments interestingly revealed strong pro-inflammatory effects of Nurr1 knockdown with strongly increased expression of multiple cytokines. Even more intriguing, our results demonstrate Nurr1 mediated neuroprotective effects of simvastatin including, for example, enhanced glucose utilization, altered notch signaling and several anti-apoptotic mechanisms that were not significantly affected in Nurr1 silenced cells. Of note, simvastatin (and other statins) crosses the blood-brain-barrier (Johnson-Anuna et al., 2005) supporting a potential clinical relevance of Nurr1 activation in the CNS by statins. Hence, our findings suggest that Nurr1 activation – together with other confirmed mechanisms (Ghosh et al., 2009; Huang et al., 2017; van der Most et al., 2009; Xu et al., 2013; Yan et al., 2020) – is involved in the neuroprotective effects of statins.

Protective and therapeutic effects of statin treatment in neurodegenerative diseases have been reported by several studies (Carroll and Wyse, 2017; Chataway et al., 2014; Torrandell-Haro et al., 2020). Particularly the use of simvastatin has been correlated with a suppression of proinflammatory molecules and microglial activation, inhibition of oxidative stress and attenuation of alpha-synuclein aggregation (Carroll and Wyse, 2017). Important clinical evidence for therapeutic potential of statins was described by Wahner et al. who found protective effects for all statins except pravastatin against PD (Wahner et al., 2008) which is particularly notable since pravastatin as only statin also failed to activate Nurr1. Observations on promising therapeutic potential in neurodegenerative diseases have evoked interventional clinical trials to reveal efficacy of simvastatin treatment in AD, PD and MS. While the PD-STAT (Carroll et al., 2019) trial could not confirm that simvastatin slows PD progression (Leigh, 2020), impressive results on efficacy of simvastatin in secondary progressive MS have been reported from the MS-STAT phase 2 trial (Chan et al., 2017; Chataway et al., 2014). Daily simvastatin treatment over two years significantly reduced brain atrophy compared to placebo and improved frontal lobe function and physical quality-of-life. The study concluded that its results support phase 3 testing but also noted that the mode-of-action for the observed neuroprotective effects of simvastatin in MS remains to be established. While HMG-CoA reductase inhibition and improved cholesterol balance undoubtedly contribute to neuroprotective statin effects, there are also cholesterol-independent activities the biochemical mechanisms of which remained elusive. Here, Nurr1 activation by statins evolves as a potentially critical mechanistic aspect in neuroprotective statin actions.

Experimental Procedures

Chemicals and compounds. All compounds tested in this study were obtained from commercial vendors (Prestwick Chemical Libraries, Illkirch, France; TCI Chemicals Deutschland GmbH, Eschborn, Germany; Sigma Aldrich, St. Louis, MO, U.S.A.; Alfa Aesar, Ward Hill, MA, U.S.A.; abcr GmbH, Karlsruhe, Germany; Cayman Chemical, Ann Arbor, MI, U.S.A.; Fluorochem Ltd., Glossop, United Kingdom; Oxchem Corp., Wood Dale, IL, U.S.A.).

Hybrid reporter gene assays. *Plasmids:* The Gal4-fusion receptor plasmids pFA-CMV-hNURR1-LBD, pFA-CMV-hPPAR α -LBD, pFA-CMV-hPPAR γ -LBD, pFA-CMV-hPPAR δ -LBD, pFA-CMV-hRAR α -LBD and pFA-CMV-hRXR α -LBD coding for the hinge region and LBD of the canonical isoform of the respective human nuclear receptor have been reported previously (Willems et al., 2020). The Gal4-VP16 (Sadowski et al., 1988) fusion protein expressed from plasmid pECE-SV40-Gal4-VP16 (Budzyński et al., 2015) (Addgene, entry 71728, Watertown, MA, USA) served as ligand-independent transcriptional inducer for control experiments. pFR-Luc (Stratagene, La Jolla, CA, USA) was used as reporter plasmid and pRL-SV40 (Promega, Madison, WI, USA) for normalization of transfection efficiency and test compound toxicity. *Assay procedure:* HEK293T cells were grown in DMEM high glucose, supplemented with 10% fetal calf serum (FCS), sodium pyruvate (1 mM), penicillin (100 U/mL) and streptomycin (100 μ g/mL) at 37 °C and 5% CO₂. The day before transfection, HEK293T cells were seeded in 96-well plates (3 \times 10⁴ cells/well). Medium was changed to Opti-MEM without supplements right before transfection. Transient transfection was performed using Lipofectamine LTX reagent (Invitrogen, Carlsbad, CA, USA) according to the manufacturer's protocol with pFR-Luc (Stratagene), pRL-SV40 (Promega) and the corresponding Gal4-fusion nuclear receptor plasmid pFA-CMV-hNR-LBD. 5 h after transfection, medium was changed to Opti-MEM supplemented with penicillin (100 U/mL) and streptomycin (100 μ g/mL), now additionally containing 0.1% DMSO and the respective test compound or 0.1% DMSO alone as untreated control. For the primary screen, each

concentration was tested as single point measurements and each experiment was performed independently two times with 0.4% DMSO, respectively. For full dose-response characterization, each concentration was tested in duplicates and each experiment was performed independently at least three times. The Gal4-VP16 control experiment was carried out in duplicates as well, with at least four independent repeats. Following overnight (12-14 h) incubation with the test compounds, cells were assayed for luciferase activity using Dual-Glo™ Luciferase Assay System (Promega) according to the manufacturer's protocol. Luminescence was measured with a Spark 10M luminometer (Tecan Group AG, Männedorf, Switzerland). Normalization of transfection efficiency and cell growth was done by division of firefly luciferase data by renilla luciferase data and multiplying the value by 1000 resulting in relative light units (RLU). Fold activation was obtained by dividing the mean RLU of a test compound at a respective concentration by the mean RLU of untreated control. Max. relative activation refers to fold reporter activation of a test compound divided by the fold activation of the respective reference agonist (PPAR α : GW7647; PPAR γ : rosiglitazone; PPAR δ : L165,041; RXR α : bexarotene; RAR α : tretinoin; all at a concentration of 1 μ M; Nurr1: amodiaquine (100 μ M)). All hybrid assays were validated with the above mentioned reference agonists which yielded EC₅₀ values in agreement with the literature. For dose-response curve fitting and calculation of EC₅₀/IC₅₀ values, the equations "[Agonist]/[Inhibitor] vs. response – Variable slope (four parameters)" were performed with mean fold activations \pm S.E.M. using GraphPad Prism (version 7.00, GraphPad Software, La Jolla, CA, USA).

Reporter gene assays involving full-length human Nurr1. *Plasmids:* The reporter plasmids pFR-Luc-NBRE(Willems et al., 2020), pFR-Luc-NurRE(Willems et al., 2020) and pFR-Luc-DR5(Willems et al., 2020) each containing one copy of the respective human Nurr1 response element NBRE N13 (TGATATCGAAAACAAAAGGTCA), NurRE (from POMC; TGATATTTACCTCCAAATGCCA) or DR5 (TGATAGGTTCCACCGAAAAGGTCA), were described previously. The full length human nuclear receptor Nurr1 (pcDNA3.1-hNurr1-NE; Addgene, entry 102363) and, for DR5, RXR α (pSG5-hRXR) were overexpressed. pFL-SV40 (Promega) was used for normalization of transfection efficacy and evaluation of compound toxicity. *Assay procedure:* HEK293T cells were grown in DMEM high glucose, supplemented with 10% FCS, sodium pyruvate (1 mM), penicillin (100 U/mL) and streptomycin (100 μ g/mL) at 37 °C and 5% CO₂. The day before transfection, HEK293T cells were seeded in 96-well plates (3 \times 10⁴ cells/well). Medium was changed to Opti-MEM without supplements right before transfection. Transient transfection was performed using Lipofectamine LTX reagent (Invitrogen) according to the manufacturer's protocol with pFR-Luc-NBRE(Willems et al., 2020), pFR-Luc-NurRE(Willems et al., 2020) or pFR-Luc-DR5(Willems et al., 2020), pRL-SV40 (Promega), the human full length receptor plasmid pcDNA3.1-hNurr1-NE, and, for DR5, also pSG5-hRXR. 5 h after transfection, medium was changed to Opti-MEM supplemented with penicillin (100 U/mL) and streptomycin (100 μ g/mL), now additionally containing 0.1% DMSO and the respective test compound or 0.1% DMSO alone as untreated control. For full dose-response characterization, each concentration was tested in duplicates and each experiment was performed independently at least three times. Following overnight (12-14 h) incubation with the test compounds, cells were assayed for luciferase activity using Dual-Glo™ Luciferase Assay System (Promega) according to the manufacturer's protocol. Luminescence was measured with a Spark 10M luminometer (Tecan Group AG). Normalization of transfection efficiency and cell growth was done by division of firefly luciferase data by renilla luciferase data and multiplying the value by 1000 resulting in relative light units (RLU). Fold activation was obtained by dividing the mean RLU of a test compound at a respective concentration by the mean RLU of untreated control. The full length Nurr1 reporter gene assays were validated with amodiaquine and chloroquine as reference agonists. For dose-response curve fitting and calculation of EC₅₀ values, the equation "[Agonist] vs. response – Variable slope (four parameters)" was performed with mean fold activations \pm S.E.M. using GraphPad Prism (version 7.00, GraphPad Software).

Nurr1 co-regulator recruitment assays. Recruitment of co-regulator peptides to the Nurr1-LBD was studied in a homogeneous time-resolved fluorescence resonance energy transfer (HT-FRET) assay system. Terbium cryptate as streptavidin conjugate (Tb-SA; Cisbio Bioassays, Codolet, France) was used as FRET donor for stable coupling to biotinylated recombinant Nurr1-LBD protein(Willems et al., 2020) which has been reported previously. Four co-regulator peptides fused to fluorescein as FRET acceptor were purchased from ThermoFisher Scientific (Life Technologies GmbH, Darmstadt, Germany). Assay solutions were prepared in HTRF assay buffer (25 mM HEPES pH 7.5, 150 mM KF, 5% (w/v) glycerol, 5 mM DTT) supplemented with 0.1% (w/v) CHAPS and contained

recombinant biotinylated Nurr1-LBD (3 nM), Tb-SA (3 nM) and the respective fluorescein-labeled co-regulator peptide (100 nM) as well as 1% DMSO with varying concentrations of the test compounds simvastatin or fluvastatin, or DMSO alone as negative control. All HTRF experiments were carried out in 384 well format using white flat bottom polystyrol microtiter plates (Greiner Bio-One, Frickenhausen, Germany). All samples were set up in triplicates. After 2 h incubation at RT, fluorescence intensities (FI) after excitation at 340 nm were recorded at 520 nm for fluorescein acceptor fluorescence and 620 nm for Tb-SA donor fluorescence on a SPARK plate reader (Tecan Group AG). FI520nm was divided by FI620nm and multiplied with 10,000 to give a dimensionless HTRF signal. The co-regulator peptides in this experiment were the following: nuclear receptor co-repressor (NCoR) 1, fluorescein-RTHRLITLADHICQIITQDFARN-OH; NCoR-2, fluorescein-HASTNMGLEAIIRKALMGKYDQW-OH; nuclear receptor co-activator 6 (NCoA6) fluorescein-VTLTSPLLVNLLQSDISAG-OH; nuclear receptor interacting protein 1 (NRIP1), fluorescein-SHQKVTLQLLGHKNEEN-OH. For dose-response curve fitting and calculation of IC₅₀ values, the equation “[Inhibitor] vs. response – Variable slope (four parameters)” was performed with mean fold activations ± SD using GraphPad Prism (version 7.00, GraphPad Software).

Nurr1 dimerization assays. Modulation of Nurr1 LBD homodimerization and heterodimerization with RXRα LBD were studied in HT-FRET assay setups using biotinylated recombinant Nurr1-LBD(Willems et al., 2020) and GFP-Nurr1 LBD(Willems et al., 2020) or GFP-RXRα LBD(Willems et al., 2020), respectively. Assay solutions were prepared in HTRF assay buffer supplemented with 0.1% (w/v) CHAPS as well as 1% DMSO with test compounds at 30 μM or DMSO alone as negative control. The biotinylated Nurr1 LBD (0.375 nM) and Tb-SA (0.75 nM) served as FRET donor complex which was kept constant while the GFP-coupled protein as FRET acceptor was varied in concentration. Since affinity of both Nurr1 dimer formations differ, titration of GFP-Nurr1 LBD started at 500 nM and, for GFP-RXRα LBD, at 4 μM, respectively. Accordingly, free GFP was added to keep the total GFP content stable throughout the entire series in order to suppress artefacts from changes in degree of diffusion enhanced FRET. All samples were set up in triplicates and equilibrated at RT for 2 h before FI520 and FI620 were recorded after excitation at 340 nm, and the HTRF signal was calculated as described above.

Nurr1 knockdown in T98G cells. T98G cells (ATCC® CRL1690™) were grown in DMEM high glucose, supplemented with 10% FCS, sodium pyruvate (1 mM), penicillin (100 U/mL), and streptomycin (100 μg/mL) at 37°C and 5% CO₂. 24 h before transfection, T98G cells were seeded in 12-well plates (1 × 10⁵ cells/well). The medium was changed to reduced serum medium containing DMEM high glucose supplemented with 1% charcoal-stripped FCS, sodium pyruvate (1 mM), penicillin (100 U/mL), and streptomycin (100 μg/mL) right before transfection. Knockdown was mediated by transient transfection using the RNAiMAX reagent (Invitrogen) according to the manufacturer’s protocol with 30 nM of Nurr1 targeting esiRNA (Cat# EHU008731) or non-targeting control siRNA (Cat# SIC001, both Sigma Aldrich). 24 h after transfection, the cells were rather harvested and directly used for RNA extraction or used for further experiments. 2 μg of total RNA were extracted from T98G cells by the E.Z.N.A. Total RNA Kit I (R6834-02, Omega Bio-Tek, Inc., Norcross, GA). RNA was reverse-transcribed into cDNA using the High-Capacity RNA-to-cDNA Kit (4387406, Thermo Fischer Scientific Inc., Waltham, MA, USA) according to the manufacturer’s protocol. Nurr1 knockdown efficiency was evaluated by quantitative real-time PCR (qRT-PCR) analysis with a StepOnePlus System (Life Technologies, Carlsbad, CA) using Power SYBR Green (Life Technologies; 12.5 μL/well). Each sample was set up in duplicates and repeated in eight independent experiments. The expression was quantified by the comparative 2^{-ΔCt} method and glyceraldehyde 3-phosphate dehydrogenase (GAPDH) served as the reference gene. Primer sequences for the human Nurr1 gene were obtained from OriGene (OriGene Technologies Inc., Rockville, MD, USA). The following PCR primers were used: hGAPDH: 5'-ATA TGA TTC CAC CCA TGG CA (fw), 5'-GAT GAT GAC CCT TTT GGC TC (rev), hNurr1: 5'-AAA CTG CCC AGT GGA CAA GCG T (fw), 5'-GCT CTT CGG TTT CGA GGG CAA A (rev).

Quantification of IL-6 Release in T98G cells. T98G (ATCC® CRL1690™) cells were grown in 12-well plates (1 × 10⁵ cells/well) for knockdown experiments or 24-well plates (5 × 10⁴ cells/well) in DMEM high glucose, supplemented with 10% FCS, sodium pyruvate (1 mM), penicillin (100 U/mL), and streptomycin (100 μg/mL) at 37 °C and 5% CO₂ for 24 h. Before incubation with LPS and test compounds, the medium was changed to DMEM supplemented with 1% charcoal-stripped FCS, sodium pyruvate (1 mM), penicillin (100 U/mL), and streptomycin (100 μg/mL) for 12 h, or Nurr1 knockdown was performed by transient transfection for 24 h as outlined above. The cells were then treated with LPS (1 μg/mL) to induce inflammation and simultaneously incubated with simvastatin

(10 μ M), fluvastatin (30 μ M) or pravastatin (30 μ M), and 0.1% DMSO, or 0.1 % DMSO alone as untreated control. Each sample was repeated independently at least three times. Following overnight (12 h for knockdown or 24 h) incubation, 100 μ L of the respective supernatants were collected and assayed for IL-6 using the Human IL-6 ELISA Kit (Cat# KHC0061, Thermo Fisher Scientific, Inc.) according to the manufacturer's protocol. Absorbance at 450 nm was measured with a Spark 10 M luminometer (Tecan Group AG).

Differential gene expression analysis. *Sample preparation.* T98G cells (ATCC® CRL1690™) were cultured in DMEM, high glucose supplemented with 10% fetal calf serum (FCS), sodium pyruvate (1 mM), penicillin (100 U/mL), and streptomycin (100 μ g/mL) at 37 °C and 5% CO₂ and seeded in 12-well plates (1 \times 10⁵ cells/well) for gene expression analysis. 24 h after seeding, medium was changed to reduced serum medium containing DMEM high glucose supplemented with 1% charcoal-stripped FCS, sodium pyruvate (1 mM), penicillin (100 U/mL), and streptomycin (100 μ g/mL) right before transfection. Knockdown was mediated by transient transfection using the RNAiMAX reagent (Invitrogen) according to the manufacturer's protocol with 30 nM of Nurr1 targeting esiRNA (Cat# EHU008731) or non-targeting control siRNA (Cat# SIC001, both Sigma Aldrich). After further 24 h, medium was changed again to reduced serum medium supplemented as described above now additionally containing 0.1% DMSO and the test compound simvastatin (10 μ M) or 0.1% DMSO alone as control. Additionally, LPS (1 μ g/mL) was added simultaneously to induce inflammation in one treatment arm. Each condition was set up in three independent biological repeats (n=3). After 12 h incubation, cells were harvested, washed twice with cold phosphate buffered saline (PBS) and then directly used for RNA extraction by the E.Z.N.A.® Total RNA Kit I (R6834-02, Omega Bio-Tek Inc., Norcross, GA, USA). *mRNA sequencing.* A total amount of 1 μ g RNA per sample was used as input material for the RNA sample preparations. Sequencing libraries were generated using NEBNext® Ultra™ RNA Library Prep Kit for Illumina® (New England Biolabs (NEB), Ipswich, MA, U.S.A.) following manufacturer's recommendations and index codes were added to attribute sequences to each sample. Briefly, mRNA was purified from total RNA using poly-T oligo-attached magnetic beads. Fragmentation was carried out using divalent cations under elevated temperature in NEBNext First Strand Synthesis Reaction Buffer (5X). First strand cDNA was synthesized using random hexamer primer and M-MuLV Reverse Transcriptase (RNase H-). Second strand cDNA synthesis was subsequently performed using DNA Polymerase I and RNase H. Remaining overhangs were converted into blunt ends via exonuclease/polymerase activities. After adenylation of 3' ends of DNA fragments, NEBNext Adaptor with hairpin loop structure were ligated to prepare for hybridization. In order to select cDNA fragments of preferentially 150~200 bp in length, the library fragments were purified with AMPure XP system (Beckman Coulter, Beverly, USA). Then 3 μ L USER Enzyme (NEB, USA) was used with size-selected, adaptor ligated cDNA at 37 °C for 15 min followed by 5 min at 95°C before PCR. Then PCR was performed with Phusion High-Fidelity DNA polymerase, Universal PCR primers and Index (X) Primer. At last, PCR products were purified (AMPure XP system) and library quality was assessed on the Agilent Bioanalyzer 2100 system. The clustering of the index-coded samples was performed on a cBot Cluster Generation System using PE Cluster Kit cBot-HS (Illumina) according to the manufacturer's instructions. After cluster generation, the library preparations were sequenced on an Illumina NovaSeq 6000 platform and paired-end reads were generated. *Data analysis.* Raw data (raw reads) of FASTQ format were firstly processed through fastp(Chen et al., 2018). In this step, clean data (clean reads) were obtained by removing reads containing adapter and poly-N sequences and reads with low quality from raw data. At the same time, Q20, Q30 and GC content of the clean data were calculated. All the downstream analyses were based on the clean data with high quality. Downstream analysis was performed using a combination of programs including STAR(Dobin et al., 2013), HTseq(Anders et al., 2015), Cufflink(Trapnell et al., 2012) and wrapped scripts. Alignments were parsed using TopHat program(Trapnell et al., 2012) and differential expressions were determined through DESeq2(Love et al., 2014). KEGG enrichment analysis was implemented by the ClusterProfiler. Reference genome and gene model annotation files were downloaded from genome website browser (NCBI/UCSC/Ensembl) directly. Indexes of the reference genome were built using STAR and paired-end clean reads were aligned to the reference genome using STAR (v2.5). STAR used the method of Maximal Mappable Prefix (MMP) which can generate a precise mapping result for junction reads. HTSeq v0.6.1 was used to count the read numbers mapped of each gene. Reads per kilobase of exon model per million mapped reads (RPKM, considering the effect of sequencing depth and gene length for the reads count at the same time) of each gene was calculated based on the length of the gene and reads count mapped to this gene. Differential expression analysis between two conditions/groups (three biological repeats per condition) was performed using the DESeq2

R package (2_1.6.3). DESeq2 provides statistical routines for determining differential expression in digital gene expression data using a model based on the negative binomial distribution. The resulting p-values were adjusted using the Benjamini and Hochberg's approach for controlling the False Discovery Rate (FDR). Genes with an adjusted P-value <0.05 found by DESeq2 were assigned as differentially expressed. Venn diagrams were prepared using the function `vennDiagram` in R based on the gene list for different group. We used `clusterProfiler` R package (Yu et al., 2012) to test the statistical enrichment of differential expression of genes in KEGG pathways using the KEGG database resource (<http://www.genome.jp/kegg/>) (Kanehisa et al., 2017). Correlations between individual samples were determined using the `cor.test` function in R with options set `alternative = "greater"` and `method = "Spearman"`. To identify the correlation between differences, different samples were clustered by expression level RPKM using hierarchical clustering distance method with the function `heatmap`, SOM (Self-organization mapping) and `kmeans` using silhouette coefficient to adapt the optimal classification with default parameter in R.

Data and code availability

Differential gene expression data are available at ArrayExpress with the accession code E-MTAB-10624.

Declaration of Interest

The authors declare no competing financial interests.

Acknowledgements

D.M. is grateful for support by the Aventis Foundation. This work was supported by the research funding program LOEWE of the State of Hessen, Research Center for Translational Medicine and Pharmacology TMP.

Abbreviations

AD, Alzheimer's Disease; DR5, direct repeats spaced by 5 nucleotides; AQ, amodiaquine; EAE, experimental autoimmune encephalomyelitis; GFP, green fluorescent protein; HBA, number of hydrogen-bond acceptor; HBD, number of hydrogen-bond donor; HTRF, homogenous time-resolved fluorescence resonance energy transfer; KEGG, Kyoto encyclopedia of genes and genomes; LBD, ligand binding domain; MPTP, 1-Methyl-4-phenyl-1,2,3,6-tetrahydropyridin; MS, multiple sclerosis; NBRE, NGFI-B response element; NCoA6, nuclear receptor co-activator 6; NCoR-1, nuclear receptor co-repressor 1; NCoR-2, nuclear receptor co-repressor 2; NR, nuclear receptor; NRIP1, nuclear receptor interacting protein 1; NSAIDs, non-steroidal anti-inflammatory drugs; Nurr1, nuclear receptor related 1; NurRE, Nur-response element; PAINS, pan assay interference compounds; PD, Parkinson's Disease; POMC, pro-opiomelanocortin; PPAR, peroxisome proliferator-activated receptor; qRT-PCR, quantitative real-time polymerase chain reaction; RAR, retinoic acid receptor; RT, room temperature; RXR, retinoid X receptor; SD, standard deviation; S.E.M., standard error of the mean; TPSA, topological polar surface area; TR-FRET, time-resolved fluorescence resonance energy transfer.

Supplementary Information

Figure S1. Characteristics of the fragment library and primary screening results.

Figure S2. Follow up of the primary drug fragment screen for Nurr1 modulation.

Figure S3. Effects of fluvastatin (FLU) on co-regulator interactions and dimerization of Nurr1.

Supplementary Methods: Computational Methods.

References

- Ables, J.L., Breunig, J.J., Eisch, A.J., and Rakic, P. (2011). Not(ch) just development: Notch signalling in the adult brain. *Nat. Rev. Neurosci.* *12*, 269–283.
- Alberi, L., Hoey, S.E., Brai, E., Scotti, A.L., and Marathe, S. (2013). Notch signaling in the brain: In good and bad times. *Ageing Res. Rev.* *12*, 801–814.
- Anders, S., Pyl, P.T., and Huber, W. (2015). HTSeq—a Python framework to work with high-throughput sequencing data. *Bioinformatics* *31*, 166–169.
- Broz, P., Pelegrín, P., and Shao, F. (2020). The gasdermins, a protein family executing cell death and inflammation. *Nat. Rev. Immunol.* *20*, 143–157.
- Bruning, J.M., Wang, Y., Oltrabella, F., Tian, B., Kholodar, S.A., Liu, H., Bhattacharya, P., Guo, S., Holton, J.M., Fletterick, R.J., et al. (2019). Covalent Modification and Regulation of the Nuclear Receptor Nurr1 by a Dopamine Metabolite. *Cell Chem. Biol.* *26*, 674–685.e6.
- Budzyński, M.A., Puustinen, M.C., Joutsen, J., and Sistonen, L. (2015). Uncoupling Stress-Inducible Phosphorylation of Heat Shock Factor 1 from Its Activation. *Mol. Cell. Biol.* *35*, 2530–2540.
- Carroll, C.B., and Wyse, R.K.H. (2017). Simvastatin as a Potential Disease-Modifying Therapy for Patients with Parkinson's Disease: Rationale for Clinical Trial, and Current Progress. *J. Parkinsons. Dis.* *7*, 545–568.
- Carroll, C.B., Webb, D., Stevens, K.N., Vickery, J., Eyre, V., Ball, S., Wyse, R., Webber, M., Foggo, A., Zajicek, J., et al. (2019). Simvastatin as a neuroprotective treatment for Parkinson's disease (PD STAT): Protocol for a double-blind, randomised, placebo-controlled futility study. *BMJ Open* *9*, e029740.
- Chan, D., Binks, S., Nicholas, J.M., Frost, C., Cardoso, M.J., Ourselin, S., Wilkie, D., Nicholas, R., and Chataway, J. (2017). Effect of high-dose simvastatin on cognitive, neuropsychiatric, and health-related quality-of-life measures in secondary progressive multiple sclerosis: secondary analyses from the MS-STAT randomised, placebo-controlled trial. *Lancet Neurol.* *16*, 591–600.
- Chataway, J., Schuerer, N., Alsanousi, A., Chan, D., MacManus, D., Hunter, K., Anderson, V., Bangham, C.R.M., Clegg, S., Nielsen, C., et al. (2014). Effect of high-dose simvastatin on brain atrophy and disability in secondary progressive multiple sclerosis (MS-STAT): A randomised, placebo-controlled, phase 2 trial. *Lancet* *383*, 2213–2221.
- Chen, S., Zhou, Y., Chen, Y., and Gu, J. (2018). fastp: an ultra-fast all-in-one FASTQ preprocessor. *Bioinformatics* *34*, i884–i890.
- Cisternas, P., Salazar, P., Silva-Álvarez, C., Barros, L.F., and Inestrosa, N.C. (2016). Activation of Wnt signaling in cortical neurons enhances glucose utilization through glycolysis. *J. Biol. Chem.* *291*, 25950–25964.
- Decressac, M., Volakakis, N., Björklund, A., and Perlmann, T. (2013). NURR1 in Parkinson disease - From pathogenesis to therapeutic potential. *Nat. Rev. Neurosci.* *9*, 629–636.
- Dobin, A., Davis, C.A., Schlesinger, F., Drenkow, J., Zaleski, C., Jha, S., Batut, P., Chaisson, M., and Gingeras, T.R. (2013). STAR: ultrafast universal RNA-seq aligner. *Bioinformatics* *29*, 15–21.
- Feng, S., Fox, D., and Man, S.M. (2018). Mechanisms of Gasdermin Family Members in Inflammasome Signaling and Cell Death. *J. Mol. Biol.* *430*, 3068–3080.
- Ghosh, A., Roy, A., Matras, J., Brahmachari, S., Gendelman, H.E., and Pahan, K. (2009). Simvastatin inhibits the activation of p21ras and prevents the loss of dopaminergic neurons in a mouse model of Parkinson's disease. *J. Neurosci.* *29*, 13543–13556.
- Haenig, C., Atias, N., Taylor, A.K., Mazza, A., Schaefer, M.H., Russ, J., Riechers, S.P., Jain, S., Coughlin, M., Fontaine, J.F., et al. (2020). Interactome Mapping Provides a Network of Neurodegenerative Disease Proteins and Uncovers Widespread Protein Aggregation in Affected Brains. *Cell Rep.* *32*, 108050.
- Huang, W., Li, Z., Zhao, L., and Zhao, W. (2017). Simvastatin ameliorate memory deficits and inflammation in clinical and mouse model of Alzheimer's disease via modulating the expression of miR-106b. *Biomed. Pharmacother.* *92*, 46–57.
- Jakaria, M., Haque, M.E., Cho, D.-Y., Azam, S., Kim, I.-S., and Choi, D.-K. (2019). Molecular Insights into NR4A2(Nurr1): an Emerging Target for Neuroprotective Therapy Against Neuroinflammation and Neuronal Cell Death. *Mol. Neurobiol.* *56*, 5799–5814.

- Jiang, L., Dai, S., Li, J., Liang, X., Qu, L., Chen, X., Guo, M., Chen, Z., Chen, L., Wei, H., et al. (2019). Structural basis of binding of homodimers of the nuclear receptor NR4A2 to selective Nur-responsive DNA elements. *J. Biol. Chem.* *294*, 19795–19803.
- Johnson-Anuna, L.N., Eckert, G.P., Keller, J.H., Igbavboa, U., Franke, C., Fechner, T., Schubert-Zsilavecz, M., Karas, M., Müller, W.E., and Wood, W.G. (2005). Chronic administration of statins alters multiple gene expression patterns in mouse cerebral cortex. *J. Pharmacol. Exp. Ther.* *312*, 786–793.
- Kanehisa, M., Furumichi, M., Tanabe, M., Sato, Y., and Morishima, K. (2017). KEGG: New perspectives on genomes, pathways, diseases and drugs. *Nucleic Acids Res.* *45*, D353–D361.
- Kim, C.-H., Han, B.-S., Moon, J., Kim, D.-J., Shin, J., Rajan, S., Nguyen, Q.T., Sohn, M., Kim, W.-G., Han, M., et al. (2015). Nuclear receptor Nurr1 agonists enhance its dual functions and improve behavioral deficits in an animal model of Parkinson's disease. *Proc. Natl. Acad. Sci.* *112*, 8756–8761.
- Kim, J. il, Jeon, S.G., Kim, K.A., Kim, Y.J., Song, E.J., Choi, J., Ahn, K.J., Kim, C.J., Chung, H.Y., Moon, M., et al. (2016). The pharmacological stimulation of Nurr1 improves cognitive functions via enhancement of adult hippocampal neurogenesis. *Stem Cell Res.* *17*, 534–543.
- Leigh, T. (2020). Parkinson's drug trial gives definitive answer on possible statin treatment - University of Plymouth.
- Lersuthirat, T., Wikiniyadhanee, R., Stitchantrakul, W., Chitphuk, S., Stansook, N., Pipatpanyanugoon, N., Jirawatnotai, S., and Dejsuphong, D. (2020). A DNA repair player, ring finger protein 43, relieves etoposide-induced topoisomerase II poisoning. *Genes to Cells* *25*, 718–729.
- Liu, W., Gao, Y., and Chang, N. (2017). Nurr1 overexpression exerts neuroprotective and anti-inflammatory roles via down-regulating CCL2 expression in both in vivo and in vitro Parkinson's disease models. *Biochem. Biophys. Res. Commun.* *482*, 1312–1319.
- Love, M.I., Huber, W., and Anders, S. (2014). Moderated estimation of fold change and dispersion for RNA-seq data with DESeq2. *Genome Biol.* *15*, 550.
- Maira, M., Martens, C., Philips, A., and Drouin, J. (1999). Heterodimerization between Members of the Nur Subfamily of Orphan Nuclear Receptors as a Novel Mechanism for Gene Activation. *Mol. Cell. Biol.* *19*, 7549–7557.
- Moehlmann, T., Winkler, E., Xia, X., Edbauer, D., Murrell, J., Capell, A., Kaether, C., Zheng, H., Ghetti, B., Haass, C., et al. (2002). Presenilin-1 mutations of leucine 166 equally affect the generation of the Notch and APP intracellular domains independent of their effect on A β 42 production. *Proc. Natl. Acad. Sci.* *99*, 8025–8030.
- Montarolo, F., Raffaele, C., Perga, S., Martire, S., Finardi, A., Furlan, R., Hintermann, S., and Bertolotto, A. (2014). Effects of Isoxazolo-Pyridinone 7e, a Potent Activator of the Nurr1 Signaling Pathway, on Experimental Autoimmune Encephalomyelitis in Mice. *PLoS One* *9*, e108791.
- Montarolo, F., Perga, S., Martire, S., and Bertolotto, A. (2015). Nurr1 reduction influences the onset of chronic EAE in mice. *Inflamm. Res.* *64*, 841–844.
- Moon, M., Jeong, I., Kim, C.-H., Kim, J., Lee, P.K.J., Mook-Jung, I., Leblanc, P., and Kim, K.-S. (2015). Correlation between orphan nuclear receptor Nurr1 expression and amyloid deposition in 5XFAD mice, an animal model of Alzheimer's disease. *J. Neurochem.* *132*, 254–262.
- Moon, M., Jung, E.S., Jeon, S.G., Cha, M.-Y., Jang, Y., Kim, W., Lopes, C., Mook-Jung, I., and Kim, K.-S. (2019). Nurr1 (NR4A2) regulates Alzheimer's disease-related pathogenesis and cognitive function in the 5XFAD mouse model. *Aging Cell* *18*, e12866.
- van der Most, P.J., Dolga, A.M., Nijholt, I.M., Luiten, P.G.M., and Eisel, U.L.M. (2009). Statins: Mechanisms of neuroprotection. *Prog. Neurobiol.* *88*, 64–75.
- Munoz-Tello, P., Lin, H., Khan, P., de Vera, I.M.S., Kamenecka, T.M., and Kojetin, D.J. (2020). Assessment of NR4A Ligands That Directly Bind and Modulate the Orphan Nuclear Receptor Nurr1. *J. Med. Chem.* *63*, 15639–15654.
- Rajan, S., Jang, Y., Kim, C.-H., Kim, W., Toh, H.T., Jeon, J., Song, B., Serra, A., Lescar, J., Yoo, J.Y., et al. (2020). PGE1 and PGA1 bind to Nurr1 and activate its transcriptional function. *Nat. Chem. Biol.* *16*, 876–886.
- Rogers, C., Erkes, D.A., Nardone, A., Aplin, A.E., Fernandes-Alnemri, T., and Alnemri, E.S. (2019). Gasdermin pores permeabilize mitochondria to augment caspase-3 activation during apoptosis and inflammasome activation. *Nat. Commun.* *10*, 1689.

- Sadowski, I., Ma, J., Triezenberg, S., and Ptashne, M. (1988). GAL4-VP16 is an unusually potent transcriptional activator. *Nature* 335, 563–564.
- Satoh, J., Nakanishi, M., Koike, F., Miyake, S., Yamamoto, T., Kawai, M., Kikuchi, S., Nomura, K., Yokoyama, K., Ota, K., et al. (2005). Microarray analysis identifies an aberrant expression of apoptosis and DNA damage-regulatory genes in multiple sclerosis. *Neurobiol. Dis.* 18, 537–550.
- Shinada, K., Tsukiyama, T., Sho, T., Okumura, F., Asaka, M., and Hatakeyama, S. (2011). RNF43 interacts with NEDL1 and regulates p53-mediated transcription. *Biochem. Biophys. Res. Commun.* 404, 143–147.
- Torrandell-Haro, G., Branigan, G.L., Vitali, F., Geifman, N., Zissimopoulos, J.M., and Brinton, R.D. (2020). Statin therapy and risk of Alzheimer’s and age-related neurodegenerative diseases. *Alzheimer’s Dement. Transl. Res. Clin. Interv.* 6, e12108.
- Trapnell, C., Roberts, A., Goff, L., Pertea, G., Kim, D., Kelley, D.R., Pimentel, H., Salzberg, S.L., Rinn, J.L., and Pachter, L. (2012). Differential gene and transcript expression analysis of RNA-seq experiments with TopHat and Cufflinks. *Nat. Protoc.* 7, 562–578.
- de Vera, I.M.S., Munoz-Tello, P., Zheng, J., Dharmarajan, V., Marciano, D.P., Matta-Camacho, E., Giri, P.K., Shang, J., Hughes, T.S., Rance, M., et al. (2019). Defining a Canonical Ligand-Binding Pocket in the Orphan Nuclear Receptor Nurr1. *Structure* 27, 66-77.e5.
- Wahner, A.D., Bronstein, J.M., Bordelon, Y.M., and Ritz, B. (2008). Statin use and the risk of Parkinson disease. *Neurology* 70, 1418–1422.
- Wang, Z., Benoit, G., Liu, J., Prasad, S., Aarnisalo, P., Liu, X., Xu, H., Walker, N.P.C., and Perlmann, T. (2003). Structure and function of Nurr1 identifies a class of ligand-independent nuclear receptors. *Nature* 423, 555–560.
- Willems, S., Kilu, W., Ni, X., Chaikuad, A., Knapp, S., Heering, J., and Merk, D. (2020). The orphan nuclear receptor Nurr1 is responsive to non-steroidal anti-inflammatory drugs. *Commun. Chem.* 3, 85.
- Willems, S., Ohrndorf, J., Kilu, W., Heering, J., and Merk, D. (2021). Fragment-like Chloroquinolineamines Activate the Orphan Nuclear Receptor Nurr1 and Elucidate Activation Mechanisms. *J. Med. Chem.* 64, 2659–2668.
- Winkler, E.A., Nishida, Y., Sagare, A.P., Rege, S. V., Bell, R.D., Perlmutter, D., Sengillo, J.D., Hillman, S., Kong, P., Nelson, A.R., et al. (2015). GLUT1 reductions exacerbate Alzheimer’s disease vasculo-neuronal dysfunction and degeneration. *Nat. Neurosci.* 18, 521–530.
- Wyatt, E., Wu, R., Rabeh, W., Park, H.-W., Ghanefar, M., and Ardehali, H. (2010). Regulation and Cytoprotective Role of Hexokinase III. *PLoS One* 5, e13823.
- Xu, Y.-Q., Long, L., Yan, J.-Q., Wei, L., Pan, M.-Q., Gao, H.-M., Zhou, P., Liu, M., Zhu, C.S., Tang, B.S., et al. (2013). Simvastatin induces neuroprotection in 6-OHDA-Lesioned PC12 via the PI3K/AKT/Caspase 3 pathway and anti-inflammatory responses. *CNS Neurosci. Ther.* 19, 170–177.
- Yan, J., Liu, A., Fan, H., Qiao, L., Wu, J., Shen, M., Lai, X., and Huang, J. (2020). Simvastatin Improves Behavioral Disorders and Hippocampal Inflammatory Reaction by NMDA-Mediated Anti-inflammatory Function in MPTP-Treated Mice. *Cell. Mol. Neurobiol.* 40, 1155–1164.
- Yu, G., Wang, L.G., Han, Y., and He, Q.Y. (2012). ClusterProfiler: An R package for comparing biological themes among gene clusters. *Omi. A J. Integr. Biol.* 16, 284–287.
- Zhong, Z.A., Michalski, M.N., Stevens, P.D., Sall, E.A., and Williams, B.O. (2021). Regulation of Wnt Receptor Activity: Implications for Therapeutic Development in Colon Cancer. *J. Biol. Chem.* 296, 100782.

Nurr1 modulation mediates neuroprotective effects of statins

Sabine Willems¹, Whitney Kilu¹, Giuseppe Faudone¹, Jan Heering², Daniel Merk^{1,3}

¹ Institute of Pharmaceutical Chemistry, Goethe University Frankfurt, Max-von-Laue-Str. 9, 60438 Frankfurt, Germany

² Fraunhofer Institute for Translational Medicine and Pharmacology ITMP, Theodor-Stern-Kai 7, 60596 Frankfurt, Germany

³ LMU Munich, Department of Pharmacy, Butenandtstr. 5-13, 81377 Munich, Germany

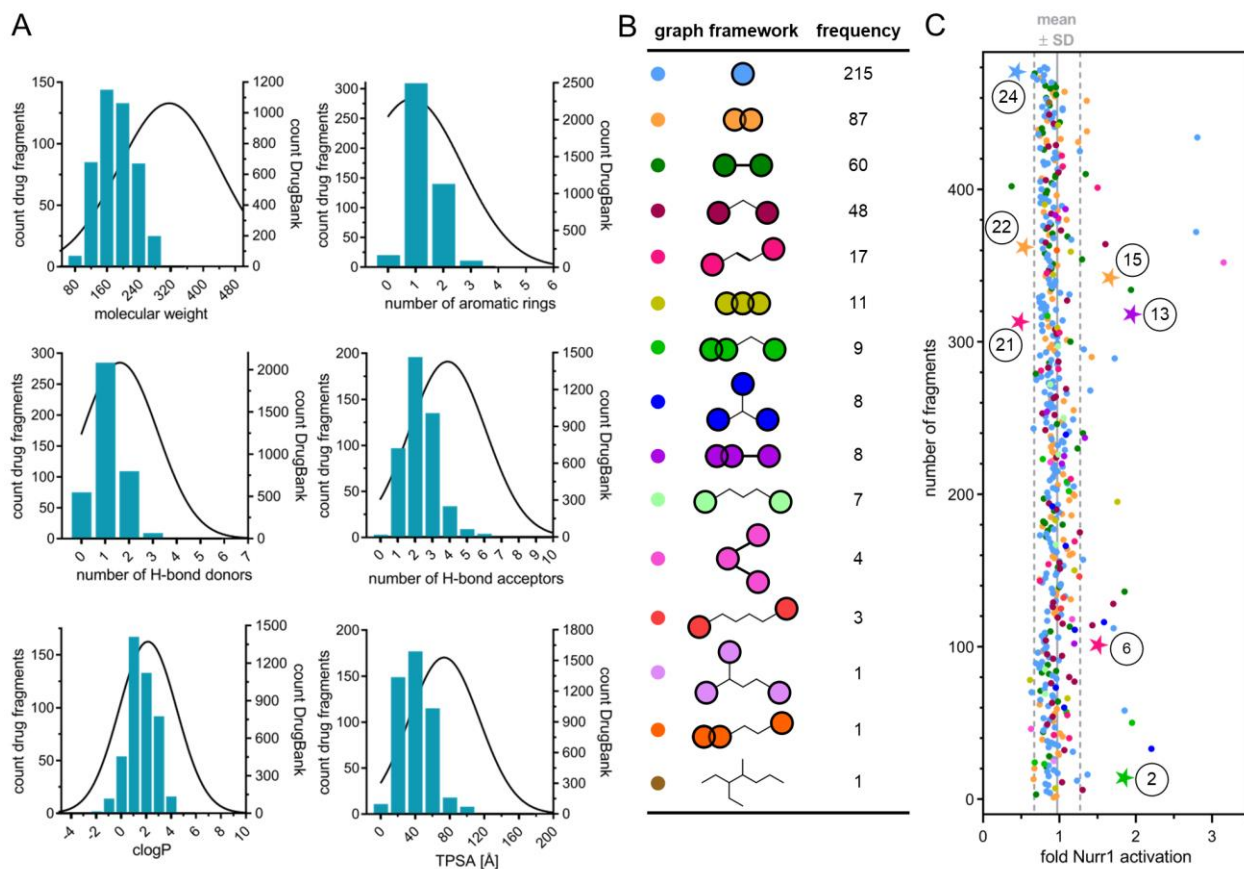
- Supplementary Information -

Table of contents

Supplementary Figures 2

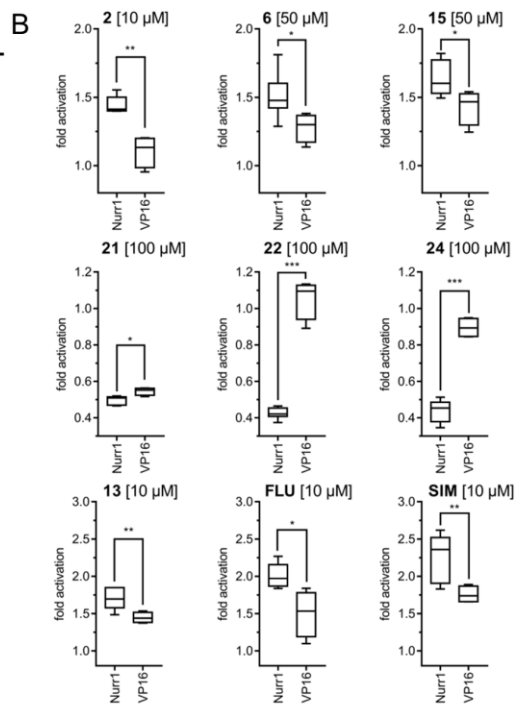
Supplementary Methods 6

Supplementary Figures



Supplementary Figure 1. (A) Feature distributions of the drug fragment library (N=480) in comparison with the DrugBank database (N=7946). Bars are plotted on the left y-axis for Prestwick drug fragments. Gaussian distributions of DrugBank compounds (MW \leq 500) are plotted on the right y-axis. (B) Representations of the different graph frameworks contained in the drug fragment library and their frequencies. (C) Nurr1 modulatory activity of the drug fragment library in a Gal4 hybrid Nurr1 reporter gene assay. Results from primary screen are the mean reporter activity vs. 0.4% DMSO; n=2. Fragments affecting reporter activity \geq 1.5-fold (Nurr1 activation, 1-20) or \leq 0.6-fold (Nurr1 repression, 21-24) were considered for further evaluation as primary screening hits. Labeled compounds marked with a star relate to the fragment hits validated in control experiments on Gal4-VP16. Different colors refer to different graph frameworks (from B). Gray lines represent mean \pm SD of the entire screening.

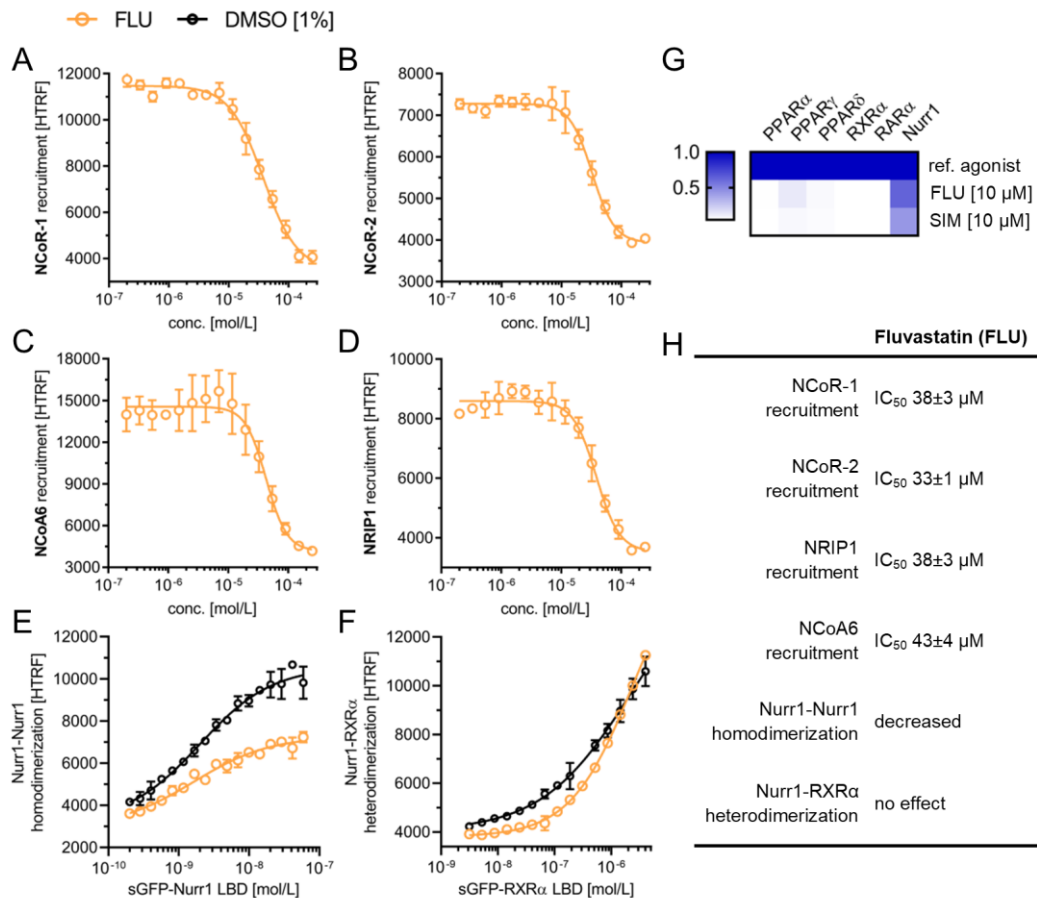
A	fragment hit	structure	primary screen (reporter act. at 100 μ M)	Nurr1 modulation
	1		4.16 \pm 5.23	toxic in primary screen
	2		1.85 \pm 0.04	EC ₅₀ 7.2 \pm 1.1 (1.68 \pm 0.07 max. act.)
	3		2.21 \pm 0.83	inactive (50 μ M) toxic (\geq 100 μ M)
	4		1.95 \pm 0.33	inactive (50 μ M) toxic (\geq 100 μ M)
	5		1.85 \pm 0.31	inactive (30 μ M) toxic (\geq 50 μ M)
	6		1.51 \pm 0.36	EC ₅₀ 16 \pm 1 (1.50 \pm 0.02 max. act.)
	7		1.71 \pm 0.07	inactive (50 μ M) toxic (\geq 100 μ M)
	8		1.59 \pm 0.29	inactive (30 μ M) toxic (\geq 50 μ M)
	9		1.71 \pm 0.02	toxic in primary screen
	10		1.86 \pm 0.43	inactive (30 μ M) toxic (\geq 100 μ M)
	11		1.76 \pm 0.10	inactive(50 μ M) toxic (\geq 100 μ M)
	12		1.73 \pm 0.35	toxic in primary screen
	13		1.95 \pm 1.44	EC ₅₀ 8.2 \pm 0.8 (2.07 \pm 0.06 max. act.)
	14		1.94 \pm 0.24	inactive (10 μ M) toxic (\geq 30 μ M)
	15		1.66 \pm 0.33	EC ₅₀ 22 \pm 2 (1.62 \pm 0.02 max. act.)
	16		3.15 \pm 0.79	inactive (10 μ M) toxic (\geq 30 μ M)
	17		1.60 \pm 0.23	inactive(10 μ M) toxic (\geq 30 μ M)
	18		2.79 \pm 0.00	toxic in primary screen
	19		1.50 \pm 0.05	inactive (100 μ M)
	20		2.81 \pm 0.32	toxic in primary screen
	21		0.48 \pm 0.05	IC ₅₀ 35 \pm 3 (0.48 \pm 0.03 rem. act.)
	22		0.54 \pm 0.06	IC ₅₀ 48 \pm 11 (0.31 \pm 0.08 rem. act.)
	23		0.38 \pm 0.02	inactive (30 μ M) toxic (\geq 50 μ M)
	24		0.44 \pm 0.03	IC ₅₀ 36 \pm 9 (0.31 \pm 0.08 rem. act.)



C

drug INN (related fragment)	structure	Nurr1 modulation
Astemizole (from 2)		inactive (10 μ M) toxic (\geq 30 μ M)
Mizolastine (from 2)		inactive (30 μ M) toxic (\geq 100 μ M)
Chlorpyramine (from 6)		inactive (100 μ M)
Mirtazapine (from 6)		inactive (100 μ M)
Procateterol (from 15)		inactive (100 μ M)
Chloroxine (from 15)		toxic (\geq 10 μ M)
Sulfadoxine (from 21)		IC ₅₀ 47 \pm 18 μ M (0.57 \pm 0.10 rem. act.)
Sulfodimethoxine (from 21)		IC ₅₀ 14 \pm 6 μ M (0.38 \pm 0.11 rem. act.)
Dolasetron (from 22)		inactive (100 μ M)
Ondansetron (from 22)		inactive (100 μ M)
Cisapride (from 24)		inactive (100 μ M)
Metoclopramide (from 24)		inactive (100 μ M)

Supplementary Figure 2. Follow up of the primary drug fragment screen for Nurr1 modulation. (A) 24 primary screening hits further considered and their Nurr1 modulatory activity in a Gal4-Nurr1 hybrid reporter gene assay. Reporter activity in primary screen is mean±SD reporter activity, n=2. Nurr1 modulation: only activities validated against Gal4-VP16 are reported. EC₅₀ or IC₅₀ values are mean±S.E.M.; n≥3. Maximum activation or remaining activity refers to the maximum reporter activation or repression efficacy compared to DMSO (0.1%) treated cells. Toxic false positive hits from the initial screen were not further investigated. (B) Control experiments employing a Gal4-VP16 hybrid receptor were performed to confirm or refute Gal4-Nurr1 mediated activity in the cellular hybrid reporter gene assay. Boxplots show: center line, median; box limits, upper and lower quartiles; whiskers, min/max; n ≥ 4. * p < 0.05, ** p < 0.01 *** p < 0.001 (t-test). (C) Nurr1 modulatory activity of fragment derived drugs on Nurr1 in a Gal4-Nurr1 hybrid reporter gene assay. Structural extensions compared to the underlying fragments are shown in blue. Only statins and the antibiotics sulfadoxine and sulfadimethoxine retained the Nurr1 modulatory activity of their fragment precursors **13** and **21** (see also Figure 1B). IC₅₀ values are mean±S.E.M.; n≥3.



Supplementary Figure 3. Effects of fluvastatin (FLU) on co-regulator interactions and dimerization of Nurr1. (A-D) Fluvastatin displaced NCoR-1 (A), NCoR-2 (B), NCoA6 (C) and NRIP1 (D) from the Nurr1 LBD. (E, F) Fluvastatin decreased homodimerization of Nurr1 (E) without affecting Nurr1-RXR α heterodimerization (F). Data are the mean \pm SD; N=3. (G) Selectivity profiles of FLU and SIM at 10 μ M on related lipid-activated transcription factors in Gal4 hybrid reporter gene assays. Heatmap shows mean relative activation compared to reference agonists at 1 μ M for PPARs (α : GW7647; γ : rosiglitazone; δ : L165,041), RXR α (bexarotene), RAR α (tretinoin) and 100 μ M for Nurr1 (amodiaquine); n \geq 2. (H) Summarized cell-free Nurr1 modulatory activities of FLU.

Supplementary Methods

Computational Methods. *General:* Calculations were conducted in KNIME (version 3.7.2, KNIME AG, Zurich, Switzerland) and Molecular Operating Environment (MOE, version 2018.0101, Chemical Computing Group Inc. Montreal, QC, Canada) using default settings for each tool/function unless stated otherwise. Amber10:EHT was used as default force field for all calculations. *Library processing:* Analysis of the drug fragment library from Prestwick (Prestwick Chemical, Illkirch, France) was performed in KNIME using the provided SMILES strings compared to the DrugBank database (all drug structures in SDF Format, version 5.1.1, released on 2018-07-03). The RDKit extension nodes (version 4.0.1.v202002121354) were used to filter for PAINS structures and calculate features (MW, clogP, number of H-bond donors/acceptors and rotatable bonds, aromatic rings, TPSA). For hits from the primary screen, a search for parent and related drugs was performed via molecule substructure and murcko scaffold (both RDKit nodes) compared to the DrugBank database (version 5.1.1). Graph based frameworks were extracted with the MOE KNIME extension node murcko frameworks ignoring small terminal rings of size 3 or 4. Rings of size 5 to 7 atoms as well as annealed rings, bicyclo and spiro compounds of equal ring count were assigned to the same groups. Geometry in terms of linker attachment points and connectivity was ignored, only the linker length was considered. *Multiple alignment:* Molecular structures of amodiaquine, fluvastatin and pitavastatin were prepared using MOE Wash tool: protonation state dominant at pH 7; coordinates rebuild 3D; preserved existing chirality. Multiple alignment of these three compounds was performed using default settings from MOE flexible alignment tool.

16.8 Targeting nuclear receptors in neurodegeneration and neuroinflammation

Willems, S.[‡]; Zaienne, D.[‡]; Merk, D. Targeting nuclear receptors in neurodegeneration and neuroinflammation. *J. Med. Chem.* **2021**, *64* (14), 9592–9638.

[‡] *Hier liegt eine geteilte Erstautorenschaft zwischen S. W. und D. Z. vor.*

Reprinted with permission from Willems, S.[‡]; Zaienne, D.[‡]; Merk, D. *J. Med. Chem.* **2021**, *64* (14), 9592–9638. Copyright (2021) American Chemical Society.

Targeting Nuclear Receptors in Neurodegeneration and Neuroinflammation

Sabine Willems,[#] Daniel Zaienne,[#] and Daniel Merk*



Cite This: *J. Med. Chem.* 2021, 64, 9592–9638



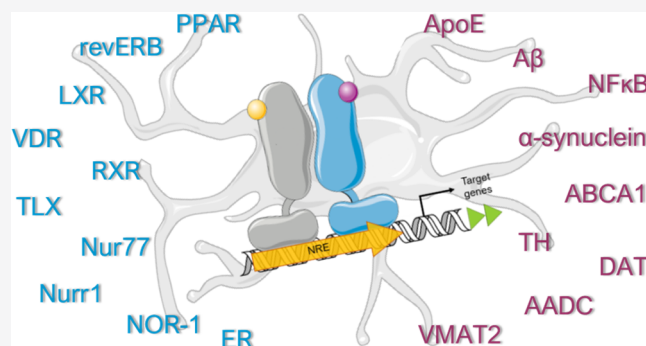
Read Online

ACCESS |

Metrics & More

Article Recommendations

ABSTRACT: Nuclear receptors, also known as ligand-activated transcription factors, regulate gene expression upon ligand signals and present as attractive therapeutic targets especially in chronic diseases. Despite the therapeutic relevance of some nuclear receptors in various pathologies, their potential in neurodegeneration and neuroinflammation is insufficiently established. This perspective gathers preclinical and clinical data for a potential role of individual nuclear receptors as future targets in Alzheimer's disease, Parkinson's disease, and multiple sclerosis, and concomitantly evaluates the level of medicinal chemistry targeting these proteins. Considerable evidence suggests the high promise of ligand-activated transcription factors to counteract neurodegenerative diseases with a particularly high potential of several orphan nuclear receptors. However, potent tools are lacking for orphan receptors, and limited central nervous system exposure or insufficient selectivity also compromises the suitability of well-studied nuclear receptor ligands for functional studies. Medicinal chemistry efforts are needed to develop dedicated high-quality tool compounds for the therapeutic validation of nuclear receptors in neurodegenerative pathologies.



1. INTRODUCTION

Diseases associated with a loss of neuronal function such as Alzheimer's disease (AD), Parkinson's disease (PD), and multiple sclerosis (MS) have a high and constantly growing global prevalence.^{1,2} They span a wide spectrum of diseases leading to cognitive decline and/or disability affecting more than 40 million people in the world.^{1,2} Neurodegenerative diseases are severe health burdens that massively affect quality of life and globally pressure healthcare systems and economics. In contrast to several other severe pathologies such as cancer or chronic inflammation, for which pharmacological treatment has significantly improved in the recent past, most neurodegenerative diseases lack efficient therapeutic interventions. The multifaceted neurodegenerative pathologies arise from different etiologies and disease mechanisms but still share certain common characteristics such as neuronal degeneration, loss of neuronal function, involvement of neuroinflammation, and in many cases the abnormal neuronal disposal of certain proteins.

Dementia including AD has a global prevalence of 5–7% in people above the age of 60 years^{1,3} with 36 million patients in 2010 and an alarming estimated number of 115 million patients in 2050.¹ Despite these enormous numbers, current options for dementia treatment are almost negligible. For example, acetylcholinesterase inhibitors and memantine show only limited symptomatic effects^{4,5} in early disease stages, and

efficacy of ginkgo biloba could not be demonstrated, yet.⁶ So far, no therapeutic intervention is available which counteracts underlying disease mechanisms.⁷ Tau directed agents are immature,⁸ and amyloid-β (Aβ) targeting therapies have failed in clinical development.⁹ As a consequence of several recent drawbacks, research on pharmacological agents for dementia treatment has significantly decreased.¹⁰ Improved understanding of the complex underlying pathomechanisms¹¹ and the search for new molecular targets to counteract AD and other forms of dementia are hence imperative. Therein, particularly regenerative strategies are urgently needed.¹⁰

PD, which mainly arises from degeneration of dopaminergic neurons in the substantia nigra due to deposition of α-synuclein and other toxic factors,¹² has an estimated prevalence of 1.0% in people above the age of 60.¹³ Its pathology and disease mechanisms are better defined than in AD, and therapeutic options, which include, for example, dopaminergic agents, monoamine oxidase inhibitors, catechol-*O*-methyl

Received: February 1, 2021

Published: July 12, 2021



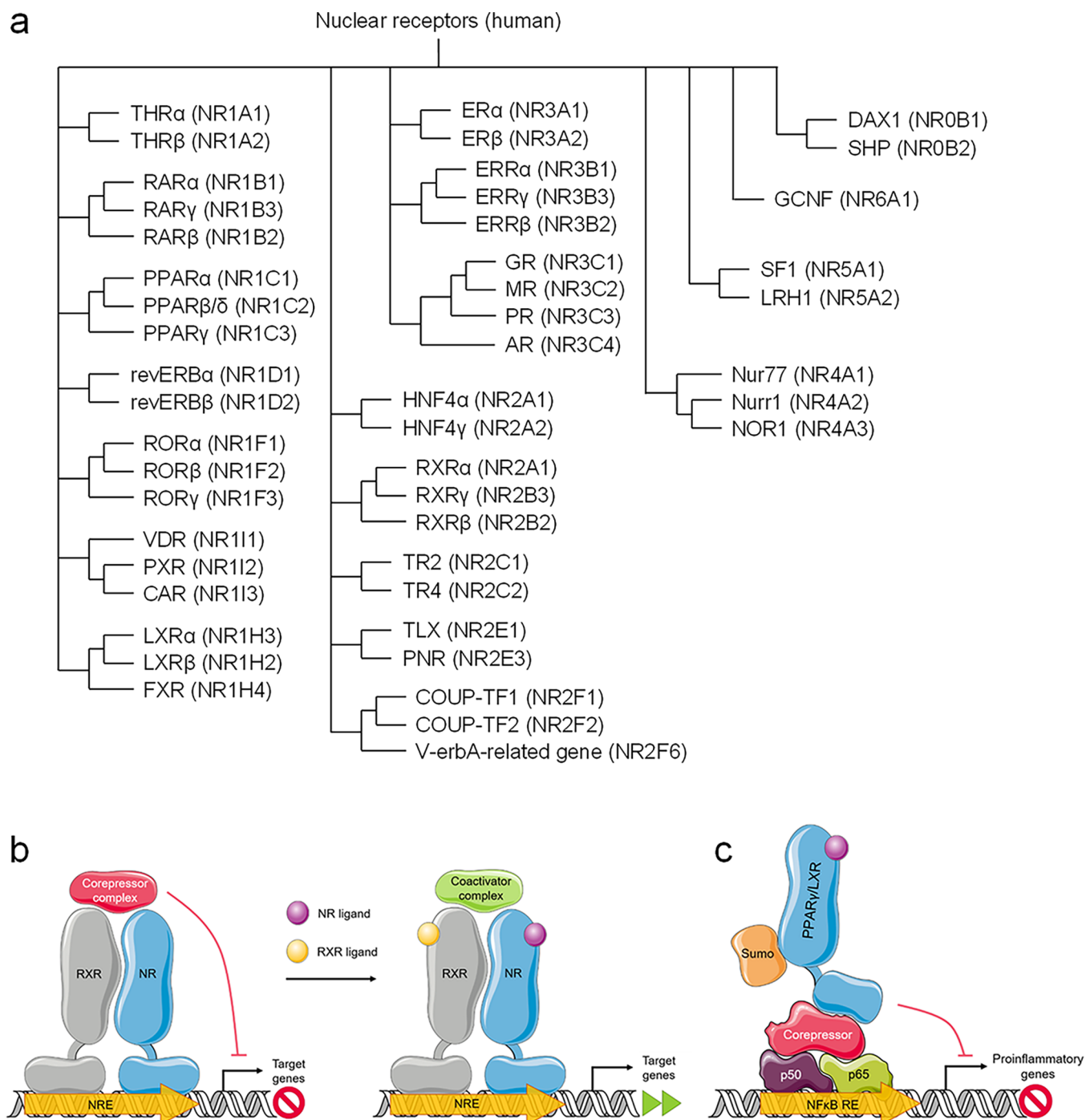


Figure 1. Nuclear receptors. (a) Overview over the nuclear receptor superfamily comprising 48 members in human.³⁰ (b) Basic mechanism of genomic nuclear receptor function. NRs of the NR1 family like LXRs and PPARs bind to their specific NRE within the promoter region of their target genes as obligate heterodimers with RXR. In the absence of ligand binding, these heterodimers associate with corepressor complexes, which results in repression of transcription. Conformational changes of the complex occur upon ligand binding, which involves displacement of the corepressor complex and subsequent coactivator recruitment, resulting in the transcription of target genes. (c) Exemplified indirect genomic action of nuclear receptors. For example, NFκB-regulated pro-inflammatory genes are differently controlled by NRs. Monomers such as PPARγ or LXR can undergo SUMOylation upon ligand binding and recruit corepressors to inhibit gene expression via NFκB (p50 and p65 subunits) interaction with its response elements.

transferase inhibitors, NMDA antagonists, and anticholinergics,¹⁴ are somewhat more effective. Still, available therapeutic interventions for PD only address disease symptoms without affecting the underlying causes as well, and research on disease-modifying interventions that delay progression or even provide a cure was characterized by several recent failures, too.¹⁵

Hence, new strategies to reverse the disease are urgently needed in PD.

MS is the most prevalent disabling disease in younger people and affects approximately 3 million people in the world.¹⁶ An autoimmune destruction of neuronal myelin sheaths and constant neuroinflammation are the central factors in MS

leading to progressive neuronal damage. The treatment of MS has markedly evolved over the last decades¹⁷ allowing a significantly slowed progression with modern therapeutic interventions in several cases.^{16,17} However, the multiple available MS treatment options target the immune system to counteract inflammatory processes and consequently prevent neuronal destruction.¹⁸ Despite the remarkable progress achieved by the new MS medications, therapeutic interventions to reverse MS are urgently required.¹⁸

Several lines of evidence present certain nuclear receptors as potential molecular targets to treat neurodegenerative diseases. As ligand-sensing transcriptional regulators, nuclear receptors control metabolic homeostasis and have multiple cell-protective functions against toxic metabolites. Hence, a potential neuroprotective role of these transcription factors is obvious. Moreover, nuclear receptors are involved in the control of cell proliferation, differentiation, and survival, suggesting their modulation also as potential avenue to regenerative approaches. Putative strategies for regenerative treatment in neurodegenerative diseases may target neuronal protection and repair mechanisms. Therapeutic strategies which are able to promote neuronal regeneration, restore neuronal integrity, and counteract neuroinflammation would hold enormous potential for numerous diseases associated with neurodegeneration. Although the adult human brain is one of the organs with the lowest regenerative ability, neurogenesis occurs throughout life from neural stem cells (NSCs),¹⁹ and knockout studies have already revealed certain growth factors and their downstream signaling pathways, transcriptional regulators, and epigenetic proteins as important mediators in neuroregeneration.¹⁹ Putative novel therapeutic approaches to neurodegenerative diseases might target these regulatory proteins to modulate survival, proliferation, differentiation, or migration of NSCs. In addition to NSCs, which may open a general avenue to regenerative effects, other neuronal cell types hold regenerative potential in the various pathologies. Oligodendrocytes (OLs), for example, play a key role in myelination, and considerable efforts have been spent on identifying mechanisms that promote remyelination by OLs in MS.¹⁸ This perspective gathers preclinical and clinical evidence for the potential of nuclear receptors²⁰ as future molecular targets in the treatment of neurodegenerative pathologies and focuses on the current stage of medicinal chemistry to target these transcriptional regulators as new avenues for a cure in neurodegenerative diseases.

2. NUCLEAR RECEPTORS AND NEURODEGENERATION

The protein family of nuclear receptors (NRs) in humans comprises 48 members (Figure 1a) that act as ligand-sensing transcription factors and regulate gene expression profiles upon changes in ligand concentrations.²¹ As their key function, NRs translate stimuli by signal molecules—e.g., hormones or lipid mediators—into enhanced or decreased expression of certain sets of genes. However, the cellular functions of NRs are multifaceted (Figure 1b,c) and include direct and indirect genomic effects, for example, by interacting with other transcription factors (tethering, transrepression, Figure 1c), as well as nongenomic activities. The complex roles and network of NRs involve multiple regulatory mechanisms (reviewed in, e.g., refs 22–25) such as ligand-dependent and -independent regulation, post-translational modifications (phosphorylation and SUMOylation) which can be activating

or inhibiting, ligand effects on subcellular localization, NR monomer–dimer–oligomer equilibria, and a network of coregulators that are recruited or released upon ligand binding.²⁶ Most NRs share a typical common architecture of an N-terminal ligand-independent activation function 1 (AF-1) followed by the DNA binding domain (DBD) and a C-terminal ligand binding domain (LBD), the latter of which recognizes the ligand and undergoes conformational changes upon ligand binding.^{27,28} These changes often affect the structure and position of the so-called ligand-dependent activation function 2 (AF-2), which is located in the C-terminal helix (H12) of the LBD. Ligand chemotype recognition varies remarkably between different NRs, enabling selective NR modulation by small molecule ligands and rendering NRs as attractive targets for a pharmacological modulation of gene expression.^{21,26} About half of the NR family is well studied and has pharmacological relevance. Endogenous ligands of these receptors are known, and several potent and selective small molecule modulators are available to determine their roles in health and disease. For other NRs, available knowledge on ligands, biochemical function, and interaction networks as well as pathological relevance is limited, and for several so-called orphan NRs,²⁹ endogenous ligands remain elusive. Some nuclear receptors are considered as potentially attractive pharmacological targets in the context of neurodegeneration based on varying levels of evidence. In the following, we summarize findings pointing to an involvement of individual NRs in neurodegeneration, neuroprotection, and neuroinflammation, and discuss the potential and limitations of their available ligands.

2.1. Peroxisome Proliferator-Activated Receptors (PPAR, NR1C)

2.1.1. Overview. The three peroxisome proliferator-activated receptors PPAR α , PPAR γ , and PPAR δ (also termed PPAR β) are cellular lipid sensors and considered as master regulators of lipid and glucose homeostasis.³¹ While the PPARs are differentially expressed in peripheral tissues with PPAR α as the major hepatic isoform, PPAR γ in adipose tissue and immune cells, and ubiquitous expression of PPAR δ , all three subtypes are found in the brain with the highest levels in neurons.³² PPARs are activated by various nutritional and endogenous lipids such as polyunsaturated fatty acids, vitamin E metabolites, and fatty acid mimetic molecules.^{31,33–35} The PPAR α and PPAR γ isoforms have a long history as drug targets in metabolic diseases (PPAR α : hyperlipidemia, PPAR γ : type 2 diabetes), but relevance of fibrates (PPAR α agonists), glitazones (PPAR γ agonists) and glitazars (dual PPAR α/γ agonists) for these indications has declined.^{31,36} Preclinical evidence ascribes all three PPARs therapeutic potential in a number of neurodegenerative pathologies, and interest of drug discovery and pharmacology in the PPARs remains high.

2.1.2. PPARs in Alzheimer's Disease. In AD, evidence for therapeutic potential is mainly available for PPAR γ activation. Observational studies in patients receiving antidiabetic medication point to a protective role of PPAR γ activation.^{37–39} In several large cohorts, treatment with the PPAR γ agonist pioglitazone (**1**) decreased the risk of developing dementia.^{37–39} Additionally, some nonsteroidal anti-inflammatory drugs (NSAIDs) were found to reduce the risk for AD, which might be associated with the PPAR γ agonistic component of these drugs.^{2,40} The therapeutic potential of PPAR activation in AD-related pathologies is rationalized by PPAR-mediated reduction of A β and tau burden, anti-inflammatory activities, and protective effects on mitochondria.^{2,41} Numerous

preclinical studies have observed beneficial effects in AD-related models. For example, PPAR γ activation caused upregulation of insulin-degrading enzyme in primary neurons from rats and AD model mice, a protease which is also able to degrade A β .^{42,43} Additionally, PPAR γ activity was found to decrease expression of β -secretase, which cleaves amyloid precursor protein (APP) to produce A β .^{43–45} PPAR γ activation with pioglitazone (1) in rats,⁴⁶ in double transgenic APP/PS1 mice,⁴⁷ and in triple transgenic AD mice⁴⁸ reduced A β levels in the central nervous system (CNS) and improved energy homeostasis, whereas the irreversible PPAR γ antagonist GW9662 (2) caused the opposite effect.⁴⁹ Congruently, several studies^{50,51} report reduced memory deficits in APP/PS1 mice upon pioglitazone (1) treatment, while intraventricular administration of the PPAR γ antagonist GW9662 (2) caused motor dysfunction.⁴⁹ In APP/PS1 mice, pioglitazone (1) was also remarkably effective in clearing A β , decreasing neuroinflammation, and improving cognitive function when administered in a short-term fashion after disease onset.⁵² Similar improvements of cognitive deficits upon pioglitazone (1) treatment were observed in double transgenic mice expressing mutant human APP and a constitutively active form of transforming growth factor- β 1 (TGF- β 1) but without effects on A β burden.⁵³ In rats receiving an intracerebroventricular A β injection to establish an AD model, pioglitazone (1) improved cognitive function, reduced neuroinflammation, and reversed oxidative mitochondrial damage.⁵⁴ PPAR γ antagonist treatment counteracted the beneficial effects of pioglitazone (1). Pioglitazone (1) was also found to improve synaptic function in APP/PS1 mice in a pathway involving cyclin-dependent kinase 5 (cdk5).⁵¹ Moreover, pioglitazone (1) and troglitazone reduced tau protein levels and tau aggregation in cellular models and in primary neurons, while GW9662 (2) reversed these effects.^{55,56} Accordingly, four months of treatment with pioglitazone (1) and rosiglitazone (3) attenuated tau hyperphosphorylation in triple transgenic AD mice.⁴⁸

Despite the mostly promising preclinical observations, late-stage clinical trials with the PPAR γ agonist rosiglitazone (3) failed to reveal a clinical benefit in the treatment of mild-to-moderate AD.^{57,58} Meta-analyses of the reported small and larger clinical trials on pioglitazone (1) and rosiglitazone (3) in AD came to the conclusion that based on the available data rosiglitazone (3) has no benefit in mild-to-moderate AD, while pioglitazone (1) might have some efficacy.^{59,60}

2.1.3. PPARs in Parkinson's Disease. Protective effects of PPAR activation in PD have also been reported from numerous preclinical models with a focus on the PPAR γ agonistic thiazolidinediones. In the 1-methyl-4-phenyl-1,2,3,6-tetrahydropyridine (MPTP)-induced mouse model of PD, pioglitazone (1) prevented microglial activation and loss of dopaminergic neurons,⁶¹ restored tyrosine hydroxylase (TH) levels,⁶¹ and improved motor impairments.⁶² A potential involvement of monoamine oxidase B inhibition⁶² in these effects of pioglitazone (1) is speculated. Rosiglitazone (3) exhibited anti-inflammatory effects in MPTP-induced PD in mice, too, and reverted microglial activation as well as pro-inflammatory cytokine levels.⁶³ Pioglitazone (1) was even examined in MPTP-induced PD in rhesus monkeys, where it also normalized TH levels and other CNS markers of PD. Concomitantly, pioglitazone (1) administration (5 mg/kg p.o. daily) caused a marked improvement in several behavioral tests compared to placebo-treated animals including performance in

fine motor skills.⁶⁴ Even in a rare and severe model of late-stage PD in mice induced by mitochondrial complex IV defects in dopaminergic neurons, which is characterized by extensive loss of dopaminergic neurons and strong motor deficits, pioglitazone (1) exhibited improvements in motor impairment and neuroinflammation.⁶⁵

In addition to the glitazones, neuroprotective and anti-neuroinflammatory effects in the rodent MPTP model were also observed upon treatment with the non-thiazolidinedione PPAR γ (partial) agonists MDG548^{66,67} or LSN862,⁶⁸ which further corroborates involvement of PPAR γ modulation in therapeutic effects. Moreover, treatment of lipopolysaccharide (LPS)-stimulated primary mouse microglia with MDG548 revealed increased phagocytic activity as another potential mechanism of PPAR-mediated beneficial effects in neurodegenerative diseases.⁶⁷

Similar to PPAR γ agonists, the PPAR α agonist fenofibrate, the structurally related PPAR δ agonists GW0742 (4) and GWS01516 (5), and the dual PPAR α/γ agonist MHY908 ameliorated MPTP-induced PD in mice with cognitive and locomotor improvements, reduced TH levels, decreased neuroinflammation, and less neuronal damage in several studies.^{69–74} In line with this, PPAR δ antagonist (GSK0660) treatment worsened the toxicity of 1-methyl-4-phenylpyridinium iodide (MPP⁺) on neuronal cells in vitro, while the agonist GW0742 (4) reversed this effect.⁷² Neuron-specific knockout of PPAR γ and/or PPAR δ in the MPTP-induced model of PD did, however, not result in more severe neuronal damage, potentially suggesting that PPAR in other cell types is important for the protective effects observed with PPAR agonists.⁷⁵ In the less common rotenone-induced rat model of PD, which has a strong endoplasmic reticulum stress component, intracerebroventricular infusion of PPAR δ agonist GWS01516 (5) improved locomotor activity, decreased endoplasmic reticulum stress, reduced neuronal apoptosis, and counteracted the loss of dopaminergic neurons.⁷⁶

PPAR ligands were also examined in the 6-hydroxy dopamine (6-OHDA)-induced rodent model of PD. Pioglitazone (1) decreased mortality, ameliorated microglial activation and reduced NF κ B activity, enhanced neuronal survival, and improved locomotor deficits in 6-OHDA treated rats.^{77,78} Similarly, intraperitoneal administration of rosiglitazone (3) to 6-OHDA rats restored TH levels, prevented microglial activation, and decreased pro-inflammatory markers such as cyclooxygenase-2 (COX-2) and tumor necrosis factor α (TNF α) in the CNS.⁷⁹ Since the beneficial effects of rosiglitazone (3) were strengthened when the drug was administered before disease induction, a potential involvement of decreased COX-2 activity in the neuroprotective effects is speculated.⁷⁹ In an extended 6-OHDA rat model with concomitant chronic levodopa administration, rosiglitazone (3) was also found to attenuate levodopa-induced dyskinesia.⁸⁰

A recent in vitro study provided a link between PPARs and Nurr1 (see section 2.7.2) activity.⁸¹ A PPAR response element is located in the promoter region of the neuroprotective transcription factor Nurr1, and the PPAR α agonist gemfibrozil enhanced Nurr1 expression in wild-type but not in PPAR α knockout dopaminergic neurons and mice.

In line with the promising neuroprotective activities of PPAR γ agonists in preclinical models of PD, a retrospective study has revealed protective effects of glitazone⁸² intake. Incidence of PD was reduced in patients receiving a thiazolidinedione as antidiabetic medication compared to

other antidiabetic drugs. Previous thiazolidinedione use was not protective,⁸² and no protective effect was observed for fibrate use.⁸³

2.1.4. PPARs in Multiple Sclerosis. In MS patients, a significant upregulation of PPAR γ has been detected in cerebrospinal fluid (CSF).⁸⁴ PPAR γ levels additionally correlated with the number of immune cells and IgG index in CSF as neuroinflammatory markers.⁸⁴ PPAR α , PPAR δ , and the key PPAR coactivator PGC-1 α were below the detection limit and hence not considered as elevated.⁸⁵ A recent study⁸⁶ reported strong downregulation of PPAR γ but not PPAR α or LXR α/β in macrophages derived from MS patients compared to healthy controls. Moreover, treatment of macrophages from healthy donors with the MS-associated pro-inflammatory cytokines interferon γ (IFN γ) and interleukin-1 β (IL-1 β) resulted in a similar downregulation of PPAR γ .

In line with these findings, considerable preclinical evidence for the therapeutic potential of PPAR agonism in MS has accumulated and mainly suggests the PPAR γ subtype as a promising target. Multiple studies have demonstrated that PPAR γ activation by pioglitazone (**1**)^{87–89} or 15-deoxy-delta(12,14)-prostaglandin J(2) (15d-PGJ2)⁹⁰ treatment ameliorates experimental autoimmune encephalomyelitis (EAE), and, expectedly, dual treatment with 15d-PGJ2 and RXR agonist 9-cis retinoid acid (9-cis RA, **43**) achieved enhanced efficacy.⁹¹ Mechanistically, these effects of PPAR γ activation are hypothesized to involve protective effects on mitochondria, enhanced OL differentiation, anti-inflammatory effects on phagocytic macrophages and microglia, and modulation of T cell differentiation.

In cellular setting, pioglitazone (**1**) or docosahexaenoic acid (**45**) activated PPAR γ in oligodendrocyte progenitor cells (OPCs) to promote their maturation. The effect was blocked by the PPAR γ antagonist GW9662 (**2**). PPAR γ activation also counteracted the TNF α -induced arrest of OPCs in a pathway putatively involving phosphorylation of extracellular signal kinases (ERKs).⁹² Moreover, PPAR γ agonists were found to protect OLs against inflammatory damage to mitochondria.⁹³ Inflammatory stimuli with TNF α cause enhanced superoxide production by mitochondria and decreased membrane potential. Pioglitazone (**1**) counteracted these effects and promoted PGC-1 α expression, which increases the biogenesis of mitochondria.

Treatment of primary mouse microglia with PPAR γ agonists (15d-PGJ2, pioglitazone (**1**), rosiglitazone (**3**), ciglitazone) prevented LPS- or cytokine-induced NO production, IL-1 β release, and IL-6 release.⁹⁴ Similar effects were observed in primary mouse astrocyte cultures⁹⁴ and in primary rat Schwann cells.⁹⁵ A recent study demonstrated the importance of the PPAR γ -regulated fatty acid translocase CD36 in clearance of myelin debris by phagocytes and suppression of neuroinflammation.⁹⁶ Through enhanced CD36-mediated myelin uptake, phagocytic macrophages and microglia adopted a less inflammatory phenotype. Inhibition of CD36 promoted neuroinflammation in EAE. In line with this, Wouters et al.⁸⁶ detected increased PPAR γ signaling in macrophages upon myelin phagocytosis—potentially induced by fatty acids contained in myelin debris—which was blocked by GW9662 (**2**). PPAR γ expression was not altered by myelin uptake. Vice versa, the PPAR γ antagonist GW9662 (**2**) did not affect myelin phagocytosis but disturbed intracellular lipid processing.

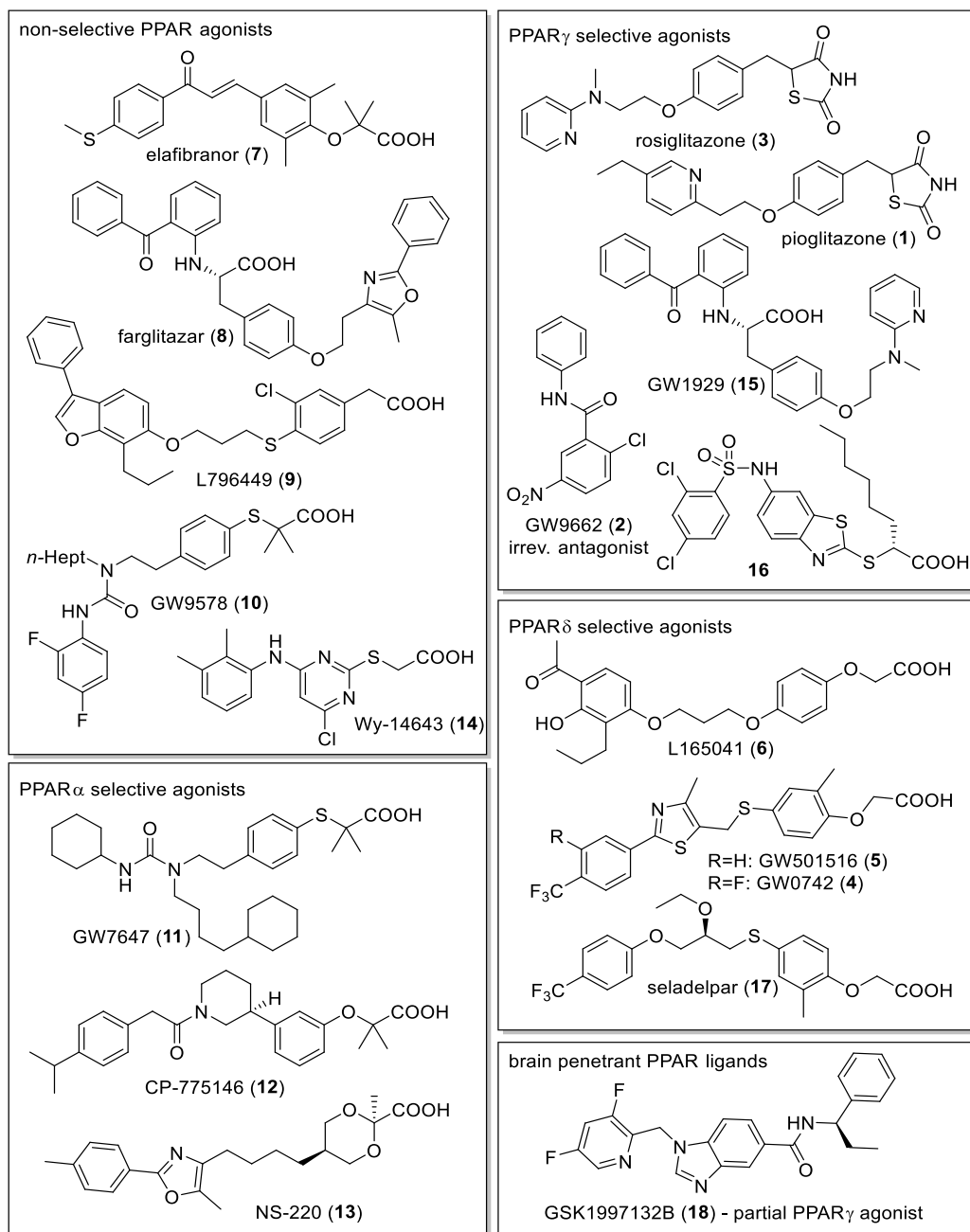
In T cells, PPAR γ activation was found to act as a negative regulator of differentiation to Th17 cells in a pathway involving

TGF- β , IL-6, and ROR γ t.⁸⁸ The PPAR γ agonists pioglitazone (**1**), ciglitazone, and GW347845 reduced proliferation and pro-inflammatory cytokine secretion in a T cell line (Jurkat) and in phytohemagglutinin (PHA)-stimulated peripheral blood mononuclear cells (PBMCs) derived from 21 MS patients and 12 healthy donors.⁹⁷ In EAE, pioglitazone (**1**) treatment selectively reduced Th17 but not Th1 differentiation.⁸⁸ Th17 cell differentiation was also reduced by treatment with an endogenous PPAR γ activator (13s-HODE).⁸⁸ T cell-specific PPAR γ knockout had the opposite effect, strongly enhanced Th17 cell differentiation, and caused an earlier disease onset in EAE.⁸⁸ Notably, pioglitazone (**1**) treatment of T cells from healthy donors or MS patients also reduced the number of IL-17 producing T cells formed upon TGF- β /IL-21 stimulation.⁸⁸ PPAR γ is hence speculated to regulate autoimmunity in the CNS by controlling T cell differentiation.⁸⁸

Some studies also point to a potential of PPAR δ in MS. Treatment with the PPAR δ agonist GW0742 (**4**)⁹⁸ had therapeutic efficacy in EAE, and PPAR δ -deficient mice displayed prolonged disease duration in EAE with compromised remission and recovery.⁹⁹ Therein, PPAR δ knockout animals revealed elevated IFN γ and IL-17 levels in the brain and alterations in T cell populations. In an in vitro model of demyelination and neuroinflammation using embryonal rat neuronal cells and antibodies against myelin oligodendrocyte glycoprotein (MOG), PPAR δ agonist GW501516 (**5**) exhibited anti-inflammatory effects but failed to counteract demyelination-induced changes in gene expression.¹⁰⁰ In MOGp35-55-induced EAE in mice, PPAR δ activation (with GW501516 (**5**) or L165041 (**6**)) counteracted IFN γ and IL-17 production by T cells and lowered levels of other pro-inflammatory cytokines in the CNS.¹⁰¹ PPAR δ activation is therefore speculated to have anti-inflammatory effects in MS and might be involved in remission and recovery of MS-associated pathology. In line with this, treatment of human OLs or primary mouse OLs with the nonselective PPAR agonist gemfibrozil promoted differentiation and enhanced expression of myelin-related genes.^{102,103} In primary mouse OLs, the effect was lost in cultures from PPAR δ -deficient animals but not in cells lacking PPAR α .¹⁰²

On the basis of accumulating evidence for the therapeutic potential of PPAR γ activation in MS, pioglitazone (**1**) was studied in some small clinical trials. In a one-year, placebo-controlled trial, pioglitazone (**1**) use was safe in relapsing remitting MS.¹⁰⁴ The study discovered a reduction in gray matter atrophy and a tendency to decreased lesion burden, while no improvement in the expanded disability status scale was observed.¹⁰⁴ Another small study suggested that pioglitazone (**1**) treatment may reduce lesion development in relapsing remitting MS.¹⁰⁵ In a cohort study¹⁰⁶ with MS patients also affected by the metabolic syndrome, treatment with either of the antidiabetic drugs metformin and pioglitazone (**1**) over 6 months resulted in a decreased number of lesions compared to untreated patients. Both drugs also had anti-inflammatory effects as observed by lower cytokine secretion. This limited evidence for therapeutic efficacy of pioglitazone (**1**) in MS is encouraging, but larger and longer trials would be needed to demonstrate a clinical benefit. Moreover, it may be doubted whether poorly CNS available pioglitazone (**1**) is a good choice in this indication since PPAR γ activation in the brain appears to mediate the desired anti-inflammatory and neuroprotective effects.

Scheme 1. Selected PPAR Ligands Used in Studies on Neurodegeneration or with Preferable Tool Compound Characteristics



2.1.5. PPAR Ligands. In the past, the PPARs have been in the focus of drug discovery for their involvement in metabolic balance and their potential as drug targets for highly prevalent metabolic diseases.³⁶ Extensive efforts were made to develop various types of PPAR ligands (Scheme 1). Numerous subtype selective and nonselective ligands target one, two, or all three PPARs. Elafibranor (7)¹⁰⁷ activates PPAR α and PPAR δ , farglitazar (8)^{108–110} is an example of a potent dual PPAR α/γ agonist, L796449 (9)¹¹¹ is a dual PPAR γ/δ agonist, and GW9578 (10)¹¹² is a balanced pan-PPAR agonist. Achieving subtype selectivity among the PPARs is not trivial, but several potent subtype selective agonists have been developed. GW7647 (11),¹¹² CP-775146 (12),¹¹³ and NS-220 (13, also termed LS-191458)¹¹⁴ are potent and selective PPAR α agonists. In past studies, Wy-14643 (14)¹¹⁵ was used as

PPAR α agonist but later found to activate PPAR γ ¹¹⁶ and RXRs¹¹⁷ as well. For PPAR γ , the drug approved thiazolidinediones rosiglitazone (3)¹¹⁸ and pioglitazone (1),¹¹⁹ GW1929 (15),¹²⁰ and 16¹²¹ comprise high potency and strong subtype selectivity. In addition, the covalent, irreversible PPAR γ antagonist GW9662 (2)¹²² is a very valuable tool to study PPAR γ biology. L165041 (6),¹¹¹ GW501516 (5),^{123,124} GW0742 (4),¹²⁴ and seladelpar (17)¹²⁵ are the most selective PPAR δ activators with high potency. Since the majority of PPAR agonists comprise acidic, fatty acid mimetic structures,³⁴ their CNS availability is limited, however. Several preclinical studies have hence applied the PPAR agonists via intracerebroventricular infusion.⁷⁴ Pioglitazone (1), the most widely used PPAR γ agonist in studies and trials on neurodegenerative diseases, presents poor CNS availability mainly

due to P-glycoprotein (P-gp) efflux.¹²⁶ GSK1997132B (**18**)¹²⁷ has been specifically developed as a brain-penetrant (partial) PPAR γ agonist.

2.1.6. Conclusion. Overall, activation of PPAR, especially the PPAR γ subtype, has been found to exhibit attractive effects in multiple in vitro and in vivo models of neurodegenerative diseases (summarized in Table 1), but translation toward

Table 1. Summarized Observations on PPARs in Neurodegeneration

PPAR α (= NR1C1), PPAR δ (= NR1C2; also known as PPAR β , NUC1, and FAAR), and PPAR γ (= NR1C3)	
PPARs in AD	Pioglitazone (1) use reduced AD risk in cohort studies. ^{37–39} PPAR γ activation induces insulin-degrading enzyme which can degrade A β . ^{42,43} PPAR γ activation downregulates β -secretase which cleaves APP to produce A β . ^{43–45} PPAR γ activation decreased memory deficits ^{50,51} and reduced A β ^{46–48} and tau ⁴⁸ levels in rodent models of AD.
PPARs in PD	PPAR activation prevented microglial activation and loss of dopaminergic neurons, restored tyrosine hydroxylase (TH) levels, and improved motor impairments in rodent models of PD (PPAR α , ^{69–74} PPAR γ , ^{61–65,77–80} PPAR δ ^{69–74}). Incidence of PD was reduced in patients receiving pioglitazone (1) as an antidiabetic medication. ⁸² Fibrate use had no such effect. ⁸³
PPARs in MS	PPAR γ but not PPAR α and PPAR δ was found upregulated in CSF of MS patients. ^{84,85} PPAR γ but not PPAR α and LXR was found downregulated in macrophages from MS patients. ⁸⁶ PPAR γ activation ameliorated EAE. ^{87–90} PPAR δ activation ameliorated EAE, ⁹⁸ and PPAR δ knockout compromised recovery from EAE. ⁹⁹ PPAR γ activation reduced inflammatory response of PBMCs from healthy donors and MS patients. ⁹⁷ PPAR γ activation prevented arrest of OPCs ⁹² and protected OLs against inflammatory damage. ⁹³ PPAR γ activation induced CD36 to enhance myelin debris clearance. ⁹⁶ Pioglitazone (1) treatment reduced number of lesions and gray matter atrophy in MS patients. ^{104–106}

therapeutic efficacy in humans is lacking. This may be due to a merely protective rather than therapeutic role of PPAR agonism, which aligns with observations that the use of pioglitazone (**1**) as an antidiabetic medication reduced AD risk and PD incidence. It may also be speculated that the glitazones, which were used in the majority of preclinical studies on neurodegeneration but have poor CNS bioavailability, exhibited most of their effects through peripheral rather than CNS activity. PPAR ligands specifically designed for blood–brain barrier (BBB) penetration are needed to further validate PPAR activation as a therapeutic approach in neurodegeneration. Additionally, the beneficial effects observed with glitazones require confirmation with other PPAR agonist scaffolds to exclude involvement of other, non-PPAR-mediated mechanisms.

2.2. RevERB (NR1D). **2.2.1. Overview.** Recent data also point to a potential involvement of the transcriptional repressors reverse ERB (revERB α , NR1D1; revERB β , NR1D2) in neurodegenerative pathologies.^{128,129} These proteins participate in the circadian clock as repressors and are considered as counterparts/antagonists of the retinoic acid receptor related orphan receptors (RORs).^{129,130} RevERB α is encoded by the opposite DNA strand of the thyroid hormone receptor α (THR α , also termed ERBA oncogene) explaining

the unusual name of the nuclear receptor.^{129,131} RevERBs act mainly as monomers and lack the typical C-terminal AF-2 of NRs providing a first hint to their transcriptional repressor activity.^{132,133} Accordingly, revERBs strongly recruit corepressors such as NCoR, resulting in chromatin condensation and gene repression.¹³⁴ Expression of revERBs varies in a circadian fashion.^{135,136}

2.2.2. RevERB in Neuroinflammation. A number of preclinical studies have revealed promising effects of revERB modulation in neuroinflammation and neurodegeneration, but the reported observations are also controversial. In vitro, effects of treatment with the revERB agonist SR9011 (**19**) were analyzed in primary microglia from neonatal rats.¹³⁷ The compound diminished pro-inflammatory cytokine release upon TNF α treatment and decreased phagocytic activity. Mitochondrial activity and ATP generation as well as expression of genes involved in carbohydrate metabolism were also reduced. Guo et al.¹³⁸ found beneficial effects of pharmacological revERB α activation with GSK4112 (**20**) and SR9011 (**19**), which dose-dependently counteracted LPS-induced microglial activation in the murine microglial cell line BV2, in primary mouse microglia, and in mice. The observed anti-inflammatory effects of revERB α activation involved NF κ B-dependent pathways and a decreased release of pro-inflammatory cytokines.

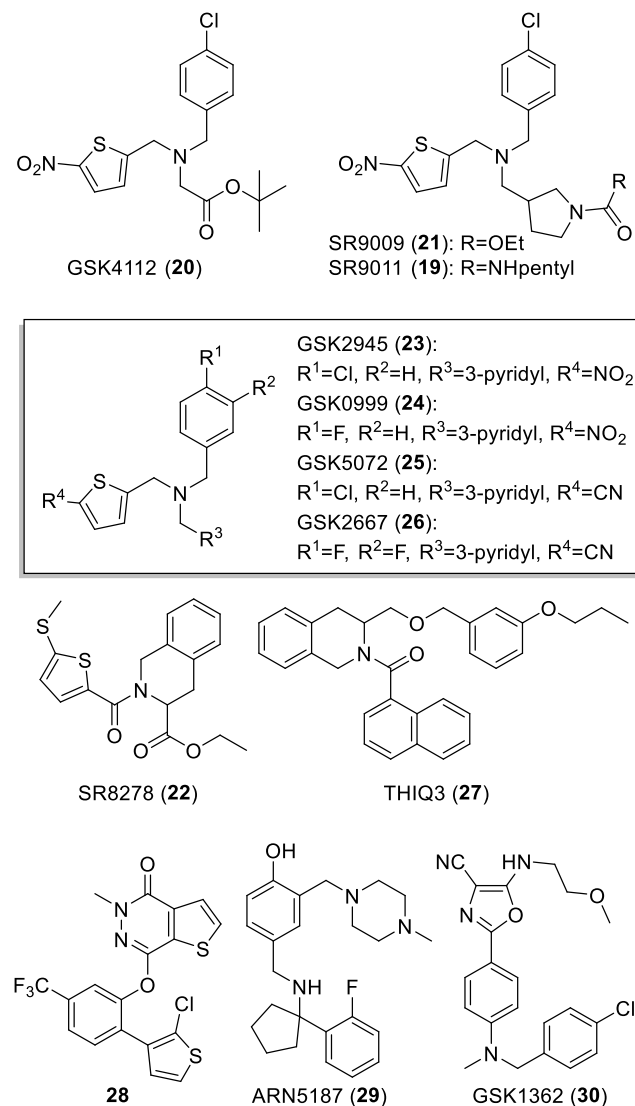
2.2.3. RevERB in Alzheimer's Disease. Similarly, the revERB activator SR9009 (**21**) counteracted cognitive dysfunction and decreased cortical A β levels in the SAMP8 mouse model of AD.¹³⁹ Additionally, revERB activation enhanced the number of synapses and upregulated marker proteins of synaptic health, which are decreased in the disease model. In line with these findings, Griffin et al.¹⁴⁰ showed that revERB α knockout enhanced microglial activation in vivo with spontaneous inflammation in the hippocampus, and revERB α knockout mice revealed a markedly increased neuroinflammatory reaction to LPS. As in other studies, these effects were linked to altered NF κ B signaling. In vitro, cultured revERB α -deficient primary microglia exhibited a pro-inflammatory phenotype, and a coculture model revealed increased neuronal death for revERB α -deficient microglia. Somewhat contradictory to these encouraging observations for pharmacological revERB activation, Lee et al.¹⁴¹ discovered beneficial effects in neurodegeneration upon inhibition of revERB activity. RevERB knockdown or inhibition with the antagonist SR8278 (**22**) in the 5XFAD model of AD in mice enhanced A β uptake by microglial cells and decreased size and number of A β plaques.

2.2.4. RevERB in Multiple Sclerosis. Chang et al.¹³⁰ probed the role of revERB in EAE and observed anti-inflammatory activity of the transcription factor in Th17 cells. RevERB antagonized ROR γ t, which regulates expression of IL-17 to drive inflammation. RevERB overexpression or treatment with revERB activator SR9009 (**21**) remarkably ameliorated EAE in mice and suppressed disease progression. At the same time, Chang et al. also observed milder EAE in revERB-deficient mice, however, which appeared to be due to disturbed T cell differentiation to Th17 cells. Hence, despite being promising, the findings on revERB modulation in neurodegenerative and neuroinflammatory pathologies are inconsistent.

2.2.5. RevERB Ligands. In the recent decade, considerable knowledge on revERB ligands has been obtained (summarized in a recent review¹²⁸). Heme was found as a natural revERB ligand¹⁴² and constitutes the first endogenous nuclear receptor ligand which is not a hormone, steroid, or lipid. Medicinal chemistry has provided a number of revERB modulators as

useful tool compounds (Scheme 2). GSK4112 (20) is the prototype of the most widely used revERB agonists, and

Scheme 2. RevERB Modulators



several descendants (19, 21–26) of this chemotype with enhanced potency and improved properties were developed.^{128,129} Within this series, GSK2945 (23) provides the most preferable profile with high revERB agonist activity (EC₅₀ 0.05 μM), sufficient selectivity, and a pharmacokinetic profile suitable for in vivo studies.¹⁴³ In addition, two further revERB agonist chemotypes have been described,^{144,145} exemplified by 27 and 28, which are highly active examples of each series with sub-micromolar potencies. Development of revERB antagonists was not as successful as for agonists. SR8278 (22) with an IC₅₀ value of 0.47 μM is the most potent tool to date.^{128,129,146} Two further weak revERB antagonist scaffolds (29, 30)^{147,148} have been recently described and provide a solid basis for the development of improved tools to study revERB biology.

2.2.6. Conclusion. Despite some promising observations (summarized in Table 2), available data on revERB in neurodegeneration are limited and contradictory since beneficial effects were observed for both knockout/inhibition and overexpression/activation. Consistent understanding of

Table 2. Summarized Observations on revERB in Neurodegeneration

RevERBα (= NR1D1; also known as EAR1) and revERBβ (= NR1D2; also known as EAR1β, BD73, RVR, and HZF-2)	
RevERB in neuroinflammation	RevERBα knockout in mice enhanced microglial activation and neuroinflammatory reaction to LPS. ¹⁴⁰ RevERB activation counteracted microglial activation ¹³⁸ and pro-inflammatory cytokine release. ¹³⁷
RevERB in AD	RevERB knockout or inhibition enhanced microglial Aβ uptake and decreased the size and number of Aβ plaques in 5XFAD mice. ¹⁴¹ RevERB activation decreased cognitive dysfunction and cortical Aβ levels in a rodent AD model. ¹³⁹
RevERB in MS	RevERB knockout caused milder EAE. ¹³⁰ RevERB overexpression or activation ameliorated EAE and suppressed disease progression. ¹³⁰

the transcription factor's role in neurodegeneration is lacking, and further research is required to validate revERB as a therapeutic target. Additional and improved tool compounds to study pharmacological revERB modulation will be needed since the revERB activators GSK4112 (20), SR9009 (21), and SR9011 (19) that were used in most experiments share a common chemotype and are likely to share common off-targets. Accordingly, a recent report¹⁴⁹ suggests revERB-independent effects of SR9009 (21). Validation of revERB would strongly benefit from a set of structurally diverse modulator scaffolds to exclude off-target effects in a chemogenomic fashion. RevERB modulator development should also consider the CNS as attractive site of action and provide BBB penetration data. In addition, the majority of studies on revERB in neurodegeneration have been conducted without important control experiments such as revERB knockdown to validate revERB-mediated effects. Future studies would profit from considering the unclear specificity of revERB ligands and a design comprising control experiments to demonstrate involvement of revERB modulation in therapeutic effects.

2.3. Liver X receptors (LXRs). **2.3.1. Overview.** The liver X receptors (LXRs)¹⁵⁰ act as key regulators of cholesterol homeostasis and as such control, for example, the expression of the cholesterol transporters ATP-binding cassette transporter A1 (ABCA1) and ABCG1 as well as the apolipoproteins ApoE and ApoC. Additionally, LXR activation exhibits anti-inflammatory effects. The receptors are endogenously activated by oxysterols (oxidized cholesterol derivatives) such as 24(S),25-epoxycholesterol and 24(S)-hydroxycholesterol, the latter of which is also found in the brain with high abundance and hence also termed cerebesterol.^{151,152} The two LXR subtypes (LXRα, NR1H2; LXRβ, NR1H3)¹⁵⁰ are structurally conserved but differ in their expression patterns. LXRα is found at high levels in liver, intestine, adipose tissue, and macrophages, while LXRβ is ubiquitously expressed. The therapeutic potential of LXR modulation in neurodegeneration is mainly attributed to three general mechanisms, the regulation of (CNS-)cholesterol homeostasis, anti-inflammatory effects, and involvement in Aβ elimination in AD.^{152–155}

2.3.2. LXR, Cholesterol, and Neuronal Health. Approximately one-fourth of the body's cholesterol content is found in the CNS where it is a key component of myelin sheaths and neuronal cell membranes illustrating the importance of cholesterol homeostasis in the brain.^{156–158} Most of the CNS cholesterol content arises from de novo synthesis—mostly by astrocytes—which as cholesterol transport and

degradation is tightly regulated by LXRs.^{152,159} LXR agonists were found to promote the cholesterol supply from astrocytes to neurons via induction of the cholesterol transporters ABCA1 and ABCG1 mediating cholesterol efflux and via upregulation of ApoE for cholesterol transport to neurons.^{159,160} LXR activity hence appears crucial for neuronal health, and several knockout studies support this hypothesis. While LXR α knockout mainly impairs peripheral cholesterol homeostasis,¹⁶¹ LXR β -deficient mice at seven months of age developed neuronal lipid accumulation, degeneration of motor neurons, and axonal atrophy resulting in an amyotrophic lateral sclerosis-like phenotype.^{162,163} Double knockout of both LXR subtypes in mice led to impairment in spatial learning and motor coordination which was associated with thinner myelin sheaths in the cerebellum.¹⁶⁴ Expression levels of the myelin components myelin basic protein and proteolipid protein as well as ABCA1 were decreased in these animals.¹⁶⁴ Knockout of LXR β also caused neurodegeneration of the optic nerve and in retinal ganglia, and was associated with increased deposition of A β in ganglion cells, while LXR α -deficient mice did not show such characteristics.¹⁶⁵

2.3.3. LXR in Alzheimer's Disease. Most efforts in studying LXRs in neurodegeneration focused on aspects of AD. Anti-inflammatory effects of LXR activation were found to be beneficial in several in vitro and in vivo studies related to AD. Both LXRs are found in microglial cells.¹⁶⁶ Treatment of primary microglia from wild-type mice with A β causes an inflammatory response with upregulation of, for example, RANTES, TNF α , IL-1 β , COX-2, and inducible NO-synthase (iNOS). In primary mouse microglia, LXR agonist (T0901317 (31)) treatment diminished A β -stimulated expression of these pro-inflammatory genes including COX-2 and iNOS, and counteracted NF κ B activation.^{166,167} Primary microglia from LXR knockout mice displayed diminished ABCA1 expression but similar basal levels of pro-inflammatory genes. Upon A β treatment, however, the inflammatory response of LXR knockout microglia was stronger than for wild-type glia.¹⁶⁶ LXR activity, therefore, seems to counteract neuroinflammatory responses to A β .

In addition to LXR-mediated anti-inflammatory effects, a potential relevance of LXR in AD is rationalized by the observation that ApoE associates with A β plaques and that the ApoE epsilon-4 (ApoE- ϵ 4) allele is strongly associated with an increased risk for AD.¹⁶⁸ With levels as high as 5% of extracellular soluble protein, ApoE is highly abundant in the brain.¹⁶⁸ It is secreted mainly by astrocytes and serves for cholesterol transport in the CNS.^{168–170} Early in vitro and in vivo studies^{171–173} on effects of LXR on ApoE, ABCA1, and A β levels have reported conflicting observations. While these studies agree that LXR activation causes ABCA1 upregulation, Fukumoto et al.¹⁷¹ observed increased secretion of A β upon LXR activation, whereas later reports detected decreased cellular A β secretion¹⁷² and production¹⁷³ upon LXR agonist (T0901317 (31)) treatment.

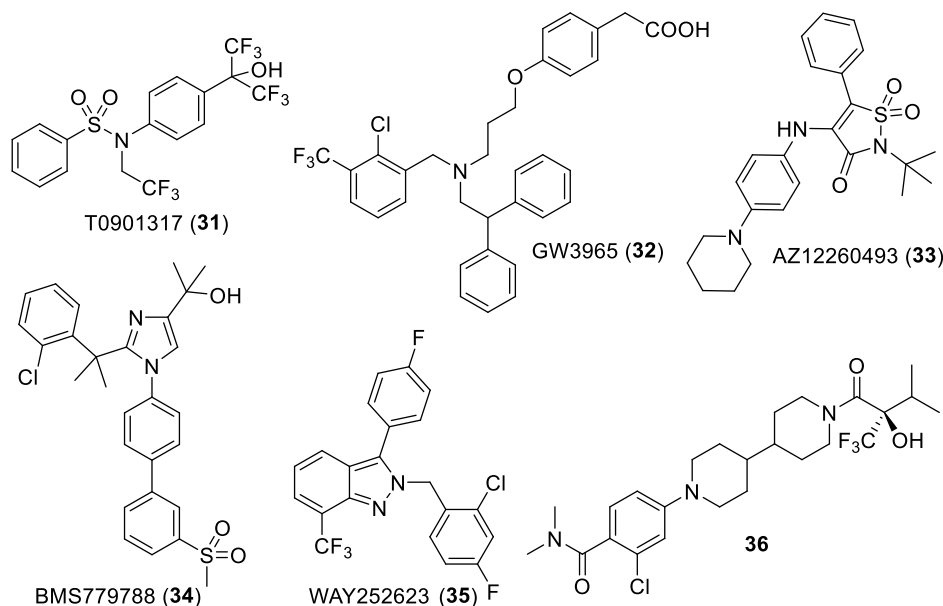
In transgenic APP23 mice with neuronal expression of a disease-associated APP, a high-fat/high-cholesterol diet was found to exacerbate the disease as observed by a higher A β load and impaired spatial learning and memory function. LXR agonist treatment (T0901317 (31)) counteracted these effects of a high-fat/high-cholesterol diet,¹⁷⁴ suggesting an involvement of lipid/cholesterol homeostasis in LXR-mediated effects on A β load and cognitive function.

LXR activation with T0901317 (31) in double transgenic APP/PS1 mice expressing human APP with disease-associated mutations and presenilin 1 (PS1) decreased membrane cholesterol levels in the CNS.¹⁷⁵ APP levels were not affected by LXR agonist treatment, but LXR activation reduced β -secretase expression and activity resulting in lower A β levels. A connection between membrane cholesterol levels and β -secretase activity was deduced from in vitro experiments in which membrane cholesterol depletion in primary mouse neuronal cells with β -methyl cyclodextrin reduced β -secretase activity. LXR agonist treatment diminished membrane cholesterol levels and β -secretase activity in primary mouse neuronal cells, as well, and this effect was abrogated by ABCA1 inhibition with glyburide. In contrast to these observations, silencing of LXR β in primary rat neurons expectedly decreased expression of ABCA1 but also lowered cholesterol levels.¹⁷⁶ Concomitantly, HMG-CoA reductase expression and secretion of A β were reduced.

Genetic knockout of either LXR subtype in transgenic APP/PS1 mice increased A β plaque burden and plaque size with a stronger effect of LXR α knockout.¹⁶⁶ In line with this, treatment of LXR wild-type transgenic APP/PS1 mice with the LXR agonist T0901317 (31) decreased A β levels and deposition¹⁶⁷ and reduced microglial activation as well as pro-inflammatory cytokine levels in the CNS. Pharmacological LXR activation furthermore increased the number of cholinergic neurons in the transgenic animals compared to vehicle treatment and improved spatial learning as observed by a maze test. In a related in vivo study using double transgenic APP/PS1 mice, long-term pharmacological LXR activation with T0901317 (31) failed to reduce A β plaques but improved memory function in object recognition and object location tests.¹⁷⁷ In a triple transgenic mouse model of AD (3xTgAD, also involving Tau pathology), treatment with the LXR agonist GW3965 (32) increased expression of ABCA1 and ApoE in the CNS.¹⁷⁸ Interestingly, higher ApoE expression upon LXR agonist treatment was mainly found in neurons. Additionally, GW3965 (32) treatment enhanced expression of neural stem cell and proliferation markers. LXR agonist-treated transgenic mice demonstrated significantly improved performance in learning tasks compared to vehicle-treated animals. No effects of LXR agonist treatment on A β load were detected, however. These results suggest other mechanisms of LXR activation mediating cognitive improvements in AD. A recent in vitro study¹⁷⁹ on hippocampal neurons suggested that oligomeric A β alters expression levels of synaptic proteins and the number of synaptic contacts. Treatment with the LXR agonist GW3965 (32) prevented synaptic changes, increased the expression of neuronal survival genes, decreased caspase activity, and promoted the number of synaptic contacts. The not fully consistent effects of T0901317 (31) and GW3965 (32) in AD-related studies might at least partly arise from different selectivity profiles since T0901317 (31) also modulates RORs.¹⁸⁰

2.3.4. LXR and Parkinson's Disease. While the therapeutic potential of LXR modulation in AD has been extensively evaluated, few studies have focused on LXR in PD, but there are observations supporting a role of LXR also in this pathology. In addition to the general anti-neuroinflammatory effects of LXR (2.3.2), the MPTP-induced model of PD has revealed stronger damage of dopaminergic neurons in the substantia nigra and enhanced microglial activation in LXR β ^{-/-} mice compared to wild-type littermates.¹⁸¹

Scheme 3. Selected LXR Ligands



2.3.5. LXR and Multiple Sclerosis. As is obvious from the role of LXR in (neuro)inflammatory processes, LXR modulation also holds promise for MS treatment, and several *in vitro* and *in vivo* studies support this assumption. In wild-type mice, treatment with the LXR agonist T0901317 (31) promoted expression of the myelin components myelin basic protein and proteolipid protein, while its effects were lost in LXR double knockout animals suggesting LXR involvement in the regulation of these important neural proteins.¹⁶⁴ Similar observations were made in primary cerebellar cultures.¹⁶⁴ LXR signaling was also found to be important to regulate cholesterol homeostasis in OLs which mediate remyelination.¹⁸² T0901317 (31) treatment of OLs enhanced LXR-regulated gene expression and cholesterol efflux.¹⁸² Overall, these results point to a therapeutic potential of LXR in MS but may be compromised by the limited selectivity of LXR agonist T0901317 (31), which is also an inverse ROR agonist.¹⁸⁰ A recent study¹⁸³ has provided further evidence for a therapeutic role of LXR in MS and indicates the importance of LXR signaling for a pro-inflammatory to anti-inflammatory switch of microglia in MS lesions which is needed for repair. After demyelination, myelin and cell debris have to be cleared by phagocytosis requiring a pro-inflammatory response before repair mechanisms are initiated in an anti-inflammatory phase.¹⁸³ LXR signaling appears to be important in this switch and to provide cholesterol for remyelination.¹⁸³ In line with this, levels of the LXR ligand 27-hydroxycholesterol, LXR activity, and LXR-regulated gene expression were induced in human macrophages after myelin phagocytosis *in vitro*.¹⁸⁴ Autopsies from active human MS lesions confirmed increased LXR signaling and upregulation of ABCA1 and ApoE.¹⁸⁴ Moreover, LXR has been suggested to involve in T cell differentiation to Th17 cells which are key cellular factors of MS pathology.¹⁸⁵ LXR knockout in EAE mice resulted in enhanced Th17 cell differentiation, whereas the LXR activators T0901317 (31) and GW3965 (32) decreased Th17 cell differentiation.¹⁸⁵ In line with this, IL-17 secretion was reduced in wild-type mice upon LXR agonist treatment.¹⁸⁵ *In vitro*, T0901317 (31) and GW3965 (32) dose-dependently inhibited Th17 cell differentiation which was also observed

upon overexpression of either LXR α or LXR β . T cells from mice with LXR α , LXR β , or dual knockout revealed the opposite effect.¹⁸⁵

2.3.6. LXR Ligands. Several potent LXR ligands have been developed as valuable tools and experimental drugs (Scheme 3). The most widely used LXR reference agonists T0901317 (31)¹⁸⁶ and GW3965 (32)¹⁸⁷ activate both LXR subtypes with similar potencies. Activation of brain LXR has been demonstrated for both compounds in animal models, e.g., by increased expression of LXR-regulated genes in the CNS.^{171,173,178} T0901317 (31) also is an inverse ROR agonist,¹⁸⁰ which potentially affects outcomes of *in vivo* studies. AZ12260493 (33) is another agonist of both LXRs, while BMS779788 (34)¹⁸⁸ and WAY252623 (also termed LXR623, 35)¹⁸⁹ exhibit a slight LXR β preference. Development of LXR ligands with a pronounced subtype selectivity has been hindered by the high similarity of LXR α and LXR β providing a remaining challenge for future LXR ligand design. The functionally selective LXR β agonist 36¹⁹⁰ presents as a successful example to overcome the lack of subtype selectivity. It exhibits markedly higher LXR β activation efficacy (104%) compared to the LXR α subtype (31%) and was developed for the potential treatment of AD-related pathologies based on the hypothesis that LXR β preference might avoid hepatic side effects but exhibit full therapeutic efficacy in the brain. 36 was brain-penetrant in mice and rhesus monkeys and increased CNS levels of ABCA1 and ApoE. As hypothesized, no adverse effects on liver triglycerides were observed upon treatment with 36 in either species. In Tg2576 mice overproducing A β peptides, 36 caused a reduction of A β levels in the brain and improved locomotor activity. In rhesus monkeys, 36 induced a 3-fold increase in brain ApoE levels, while a related compound with high P-gp efflux ratio did not alter ApoE indicating that the effect of 36 was mediated by brain LXR activation. 36, therefore, appears as very promising tool to study LXR β activation in neurodegeneration with reduced adverse effects of hepatic LXR α agonism.

2.3.7. Conclusion. As a key regulator of cholesterol homeostasis and anti-inflammatory transcription factor, LXR has attracted attention as a potential target in AD and MS

(Table 3). Anti-inflammatory effects in microglia have been demonstrated for LXR activation, and a role in AD is

Table 3. Summarized Observations on LXRs in Neurodegeneration

LXR α (= NR1H3; also known as RLD-1) and LXR β (= NR1H2; also known as UNR, NER, and RIP15)	
LXRs in AD	LXR activation ameliorated and LXR knockout enhanced the inflammatory response of microglia to A β . ^{166,167} LXR knockout in transgenic AD mice increased A β plaque burden and plaque size. ¹⁶⁶ Observations regarding effects of LXR activation on A β levels are inconsistent. ^{167,171–173} Long-term LXR agonist treatment improved cognitive function in transgenic AD mice. ¹⁷⁷
LXRs in PD	LXR β knockout in MPTP-induced PD enhanced microglial activation and dopaminergic neuron damage. ¹⁸¹
LXRs in MS	LXR activation promoted expression of myelin components (myelin basic protein, proteolipid protein). ¹⁶⁴ LXR signaling was found to be important in regulating cholesterol homeostasis in (myelinating) OLS ¹⁸² and to provide cholesterol for remyelination. ¹⁸³ In EAE, LXR knockout enhanced and LXR agonist treatment decreased Th17 cell differentiation. ¹⁸⁵

rationalized by the LXR-dependent regulation of ApoE expression, although some observations on LXR in AD models are controversial. LXR agonist tools with sufficient BBB penetration are available, and several studies support the potential of pharmacological LXR activation in AD and MS treatment. Some promising observations, especially regarding anti-inflammatory effects, are compromised by the use of the LXR agonist **31** as tool, which also has considerable potency as an inverse ROR agonist. Among the two LXR isoforms, LXR β activation has shown greater therapeutic potential in neurodegeneration and less adverse hepatic effects, but fully subtype selective LXR agonists to exploit this potential are lacking, and novel LXR modulators are needed. The functionally selective and brain penetrant LXR β agonist **36** is a promising example of a next-generation tool to capture the effects of LXR β activation in the CNS.

2.4. Vitamin D Receptor (VDR). **2.4.1. Overview.** The vitamin D receptor (VDR, NR1I1) is a cellular sensor for vitamin D with 1 α ,25-dihydroxyvitamin D3 (1,25(OH)₂D3) as the main endogenous ligand.¹⁵⁰ It binds the DR3 response element as a heterodimer with RXR. VDR is essentially involved in the regulation of vitamin D and calcium

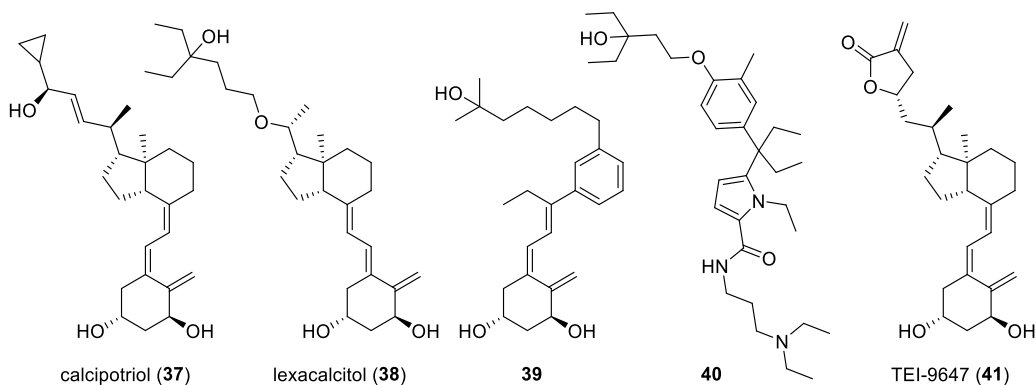
homeostasis by controlling expression of crucial enzymes for vitamin D biosynthesis and degradation.¹⁵⁰

2.4.2. VDR in Neurodegenerative Diseases. The importance of calcium homeostasis in the neuronal system for Ca²⁺ signaling provides a link between VDR, neuronal function, and neurodegeneration.¹⁹¹ Additionally, VDR has been ascribed a cell-protective role against toxic metabolites^{150,192,193} that might contribute to neuroprotective effects. In the brain, VDR is expressed in neurons and glial cells,¹⁹⁴ and VDR knockout in mice caused motor impairment without affecting cognitive function.¹⁹⁵

In recent years, a number of reports on VDR-mediated beneficial effects in neurodegenerative diseases have accumulated. Most notably, VDR genetic polymorphisms in humans were correlated with AD or PD, among which one single-nucleotide polymorphism (SNP) showed correlation with both diseases,^{196–198} suggesting VDR as a potential susceptibility gene. Genetic polymorphisms of VDR were also found in MS patients.¹⁹⁹ Evidence for the importance of sufficient vitamin D levels in AD, PD, and MS also results from epidemiological and clinical studies.^{199–204} In PD, vitamin D supplementation appears beneficial,^{200,202} and a correlation between vitamin D deficiency and AD is proposed²⁰¹ as epidemiological studies have revealed high prevalence of hypovitaminosis D²⁰¹ in AD patient populations. Moreover, prospective studies involving samples of up to 7 million individuals found a correlation between high vitamin D levels and decreased MS risk.^{203,205} Altered expression of AD-associated VDR-regulated genes was detected in the brains of mice with hypovitaminosis D,²⁰⁶ suggesting that low vitamin D levels affect gene expression in the brain.

In vitro, a protective potential of VDR signaling in neuronal cell populations including astrocytes as brain immune cells has been demonstrated in several studies.^{207–210} Moreover, it has been proposed that A β formed in AD suppresses VDR expression, while administration of vitamin D counteracted this effect.²¹¹ Vitamin D was also found to inhibit LPS-induced astrocyte activation in vitro and in rats,²¹⁰ suggesting an anti-neuroinflammatory potential. In line with this, in vivo studies have reported therapeutic effects of vitamin D and analogues in EAE.²¹² In the context of PD, diminished VDR expression was detected in the 6-OHDA-induced and the preformed fibril (PFF) injection rodent models of PD.²¹³ The reduced VDR activity resulted in decreased P-gp levels, which is thought to be important for clearance of intracerebral α -synuclein load in

Scheme 4. Potent and Selective VDR Ligands (Agonists 37–40; Antagonist 41) from the Literature^{214–217} as Potential Tools for Functional Studies in Neurodegeneration



PD.²¹³ Treatment with 1,25(OH)₂D₃ counteracted these effects and restored VDR and P-gp activity.²¹³

2.4.3. VDR Ligands. Despite promising preliminary data, the potential of VDR as a therapeutic target for neurodegenerative diseases remains to be validated. Several potent (up to subnanomolar EC₅₀ and K_d values) and selective VDR modulators (37–41, Scheme 4) including vitamin D analogues and nonsteroidal compounds are available.²¹⁴ They can serve for further functional in vivo studies in the context of neurodegeneration. Adverse effects on calcium homeostasis may, of course, limit a long-term therapeutic VDR modulation in neurodegenerative diseases, but extensive efforts in medicinal chemistry²¹⁴ have provided potent VDR modulators with low calcemic effects in vivo (e.g., 39) that might overcome this obstacle.

2.4.4. Conclusion. Disease-associated SNPs of VDR and the correlation between vitamin D levels and incidence of neurodegenerative diseases provide the strongest evidence for a potential involvement of VDR in neurodegeneration (summarized in Table 4), and motor impairment observed

Table 4. Summarized Observations on VDR in Neurodegeneration

VDR (= NR1H1)	
VDR in AD	Genetic polymorphisms of VDR were correlated with AD. ¹⁹⁶ High prevalence of hypovitaminosis D in AD patients. ²⁰¹ Low vitamin D levels altered expression of AD-associated genes in mice. ²⁰⁶
VDR in PD	Genetic polymorphisms of VDR were correlated with PD. ^{197,198} Beneficial effects of vitamin D supplementation. ^{200,202} VDR expression was diminished in 6-OHDA-induced PD. ²¹³ VDR knockout in mice caused motor impairment without affecting cognitive function. ¹⁹⁵
VDR in MS	Genetic polymorphisms of VDR were correlated with MS. ¹⁹⁹ High vitamin D levels correlated with lower MS risk. ^{203,205} VDR activation inhibited LPS-induced astrocyte activation in vitro and in rats. ²¹⁰ VDR activation ameliorated EAE. ²¹²

in VDR knockout animals further supports this assumption. However, mechanistic understanding of VDR involvement in neurodegenerative diseases is incomplete, and studies on effects of pharmacological VDR modulation in this context are limited despite the availability of multiple potent and selective VDR modulators. Although involvement of brain VDR in the observed effects, for example, regarding anti-neuroinflammatory activity has been demonstrated, contributions of peripheral VDR activation remain to be evaluated, and adverse effects of systemic VDR activation must be considered.

2.5. Retinoid X Receptors (RXR). **2.5.1. Overview.** RXR belongs to the second subfamily of nuclear receptors and has the typical NR structure. It exists in three subtypes which are encoded by independent genes²¹⁸ but still exhibit very high structural similarity, especially in the LBD. The amino acids, which are responsible for the formation of the ligand binding site, are identical in all three subtypes.^{219–221} A key feature of RXR is that it acts as a universal heterodimer partner for many other NRs.²¹ These heterodimers are distinguished between permissive (e.g., PPAR/RXR, FXR/RXR and LXR/RXR) and nonpermissive heterodimers (e.g., RAR/RXR)²¹ (Figure 2). Nonpermissive heterodimers can only be activated by ligands of the heterodimer partner and not by an RXR agonist alone.²¹ In contrast, permissive heterodimers can be activated by

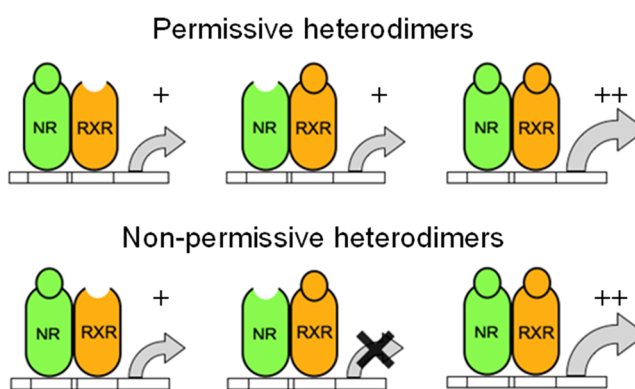


Figure 2. Role of RXR in NR heterodimers. Permissive heterodimers respond to RXR ligands and to ligands of the heterodimer partner. The presence of ligands for both partners causes synergistic activation. Nonpermissive heterodimers can only be activated by ligands of the heterodimer partner.²¹

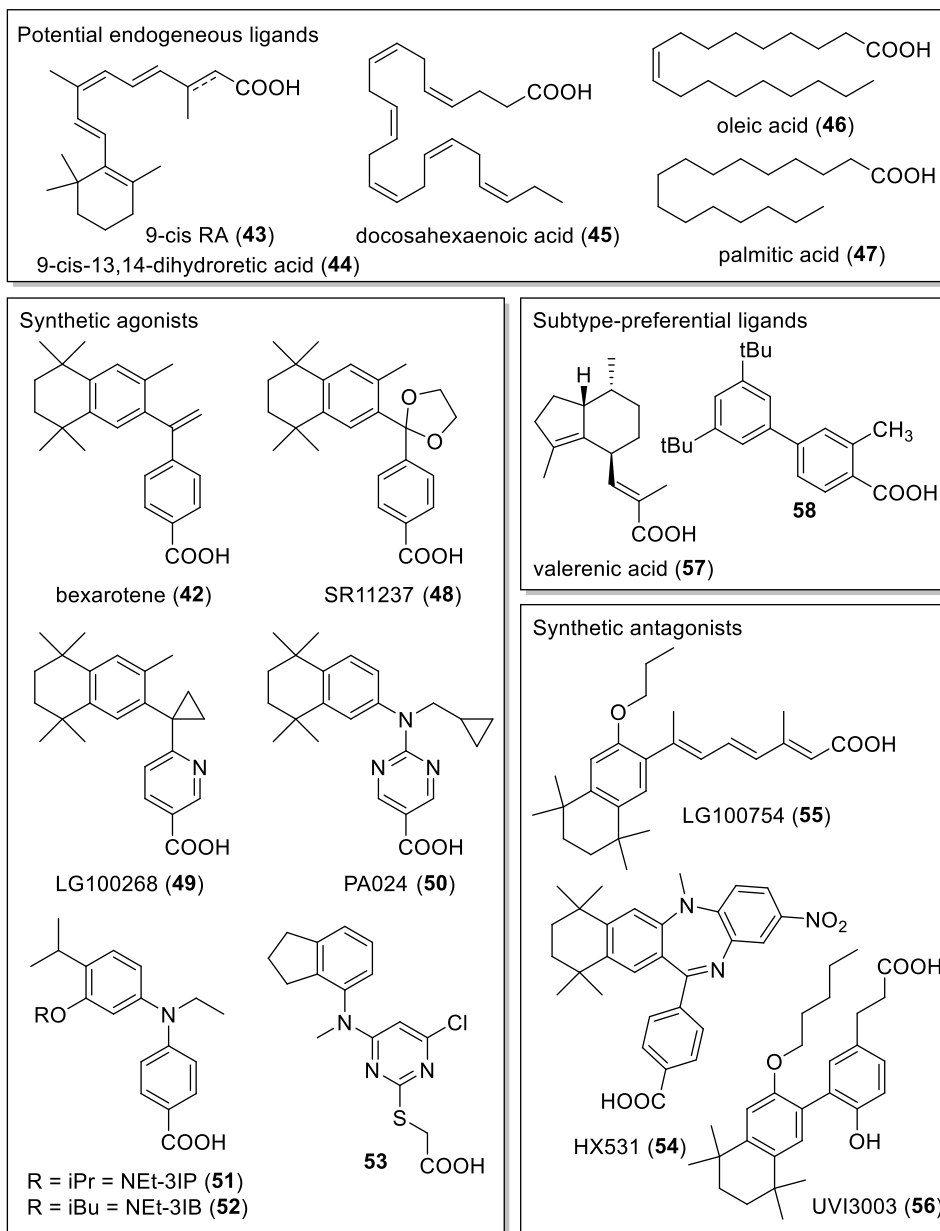
ligands of RXR and by ligands of the heterodimer partner, and are synergistically activated in the presence of ligands for both partners.²¹

Owing to this important role in the NR network, at least one subtype of RXR is expressed in every cell that has a nucleus,^{218,222} but the subtype distribution differs. In mice, RXR α was found distributed over the whole body but with particularly high expression in the liver, spleen, epidermis, and kidney.^{218,223} For RXR β , no explicit expression pattern could be observed, resulting in the assumption that this subtype is almost ubiquitous.^{218,223} Regarding neurodegenerative diseases, it is important to mention that, in contrast to the other two subtypes, higher CNS localization was observed for RXR γ . Additionally, this subtype is found in heart muscles, adrenal glands, and muscle cells.^{218,223} Within the CNS, there is no distinct distribution. RXR γ is expressed in the striatum, parts of the amygdala, the spinal cord, and in the hypothalamus.^{224,225} A particularly high expression was found in basal ganglia, and an association with motor function and addiction has been suggested.²²⁶ Especially noteworthy is the high expression of RXR γ in glial cells,²²⁶ as these cells are involved in pathophysiological processes in neurodegenerative diseases.^{227,228}

Because of its crucial involvement in numerous (patho-)physiological processes as a universal NR heterodimer partner, the pharmacological potential of RXR may be very high. In addition to the established role of RXR activation in the field of cancer therapy,²²² the role of RXR in neurodegenerative diseases has been intensively studied in recent years. Therein, RXR involves in neuroprotective, neuro-inflammatory, and regenerative processes regulated by its heterodimers.²²⁹ Especially for the treatment of AD, MS, and PD, RXR is evolving as an attractive target.

2.5.2. RXR in Alzheimer's Disease. One of the major risk factors for the development of AD is ApoE, especially the ApoE- ϵ 4 variant.^{230–234} Together with the ABCA1, ApoE regulates the lipid and cholesterol transport in the CNS.²³⁵ ABCA1 mediates the cellular efflux of phospholipids and cholesterol toward ApoE.²³⁶ It has been proposed that ApoE inadequately equipped with lipids and cholesterol affects the accumulation and transport of A β .^{235,237,238} Both the ApoE and the ABCA1 genes are under transcriptional control of the PPAR γ /RXR- and LXR/RXR-heterodimers.²³⁰ For this reason, an RXR agonist could exhibit a dual effect through the

Scheme 5. Selected RXR Ligands



simultaneous activation of both heterodimers, since both heterodimers are permissive.²³

Therapeutic effects of RXR agonists have been observed in common preclinical models of AD. In APP/PS1 mice, acute treatment with bexarotene (42) caused a removal of diffuse and compact A β plaques in the cortex and hippocampus, elevated levels of ApoE, ABCA1, and ABCG1, reduced soluble and insoluble A β levels, counteracted cognitive and behavioral deficits and restored cognition and memory.²³⁹ The bexarotene (42)-treated APP/PS1 mice also showed an improved hippocampal function, and in total, the A β plaques were reduced by 75%.²³⁹ This acute and chronic efficacy of RXR activation with bexarotene (42) in AD in both early and late stages presents as a very attractive and promising therapeutic strategy. However, four independent groups, despite also observing therapeutic effects, failed to reproduce these findings thoroughly.^{240–243}

The effects of bexarotene (42) in AD have also been investigated in two small clinical studies. A phase 1 trial with 12 patients receiving either 450 mg/day bexarotene (42) or placebo reported that only a very small proportion of bexarotene (42) enters the CNS. Bexarotene (42) treatment only slightly elevated ApoE levels in CSF and had no effect on the synthesis, clearance, or total levels of A β in CSF.²⁴⁴ In a small, double-blind, placebo-controlled phase 2 trial, 20 patients with AD were randomized to receive 300 mg/day of bexarotene (42) or placebo for 4 weeks.²⁴⁵ No difference regarding composite or regional A β burden was observed between bexarotene (42) and placebo when all patients were included in the analysis.²⁴⁵ However, ApoE- ϵ 4 noncarriers showed reduced A β burden in all measured cortical regions after bexarotene (42) treatment compared to placebo.²⁴⁵ In addition, an observed correlation between reduced cortical A β and an increasing serum level of A β _{1–42} potentially indicates an excretion of soluble A β forms from brain to blood.²⁴⁵ This

short-term trial was not powered to detect cognitive changes, however.²⁴⁵

2.5.3. RXR in Parkinson's Disease. Similar to AD, involvement of RXR in PD is connected with permissive RXR heterodimer formation. In the case of PD, the permissive RXR/Nurr1 heterodimer is most relevant due to the key role of Nurr1 in PD (see section 2.7.2).^{2,246}

2.5.4. RXR in Multiple Sclerosis. An involvement of RXR in MS is evident from the fact that its expression is elevated upon CNS damage.²⁴⁷ An increased expression of RXR γ in OPCs, which develop into adult OLs and are responsible for the formation of the myelin layer, has been detected in MS lesions.²²⁷ OLs can repair damage to myelin sheaths caused by MS-associated autoimmune inflammation to a certain extent and thus may have regenerative potential.²²⁷ The increased RXR γ expression was observed both in rats with toxin-induced central demyelination and post mortem in human tissue samples.²²⁷ Moreover, RXR γ knockout mice displayed significantly less differentiated OLs in lesions after toxin-induced demyelination compared to wild-type animals.²²⁷

A second possible mechanism of RXR involvement in MS²⁴⁸ refers to the fact that myelin fragments resulting from demyelization inhibit OPC differentiation.^{249,250} Removal of these fragments represents an important step in the regeneration of CNS damage. Macrophage-specific RXR α knockout mice exhibited reduced myelin phagocytosis capacity after induced demyelination and delayed OPC differentiation,²⁴⁸ suggesting involvement of RXR in this process together with its heterodimer partners PPAR and LXR (see sections 2.1 and 2.3). Moreover, an interesting reversal of functional defects in myelin phagocytosis by MS monocytes upon bexarotene (42) treatment was observed in patient-derived monocyte samples.²⁴⁸

The effect of RXR activation in MS was examined in several preclinical models. In vitro, 9-cis RA (43) exhibited anti-inflammatory effects on microglia and astrocytes by inhibiting the production of pro-inflammatory cytokines, such as TNF α and IL-1 β .²⁵¹ RXR activation hence counteracted neuroinflammation and might intervene in the acute phase of the disease. Furthermore, 9-cis RA (43) promoted the differentiation of OPCs ex vivo and enhanced myelin basic protein production.²²⁷ In focal toxin-induced demyelination in aged rats, 9-cis RA (43) enhanced expression of myelin basic protein mRNA in lesions and accelerated remyelination.²²⁷ In addition to 9-cis RA (43) and bexarotene (42), the second-generation rexinoid IRX4204 (90, see section 2.7.2.6) has been studied in several preclinical models of MS. It alleviated the symptoms of EAE in mice and supported the differentiation of OPCs from mouse brains to OLs.²⁵² In focal toxin (ethidium bromide) induced demyelination in rats (one-year-old), IRX4204 (90) treatment caused an increase in CNS remyelination,²⁵² and in a mouse model of nonimmune-mediated demyelination, IRX4204 (90) exhibited neuroprotective activity by directly affecting demyelinated axons.²⁵²

2.5.5. RXR Ligands. As outlined above, RXR has a central role in the network of NRs as a heterodimer partner. From this unique characteristic, a potential involvement of RXR in multiple regulatory systems can be inferred since the majority of RXR heterodimers is permissive, meaning that they can be activated by RXR agonists.²⁵³ In addition, ligand-dependent allosteric modulation between the heterodimer partners is discussed.²⁶ The resulting therapeutic potential of RXR modulation in multiple indications has stimulated considerable

efforts in RXR ligand development. In addition to the high similarity of the three RXR isoform LBDs,²²¹ the RXR ligand binding sites are very lipophilic and provide little potential for polar ligand–protein interactions.^{221,222} Consequently, the majority of RXR ligands are exceptionally lipophilic.

Very early on, metabolites of vitamin A were suspected as natural RXR ligands, and based on this, 9-cis RA (43, Scheme 5) was identified as a high-affinity ligand.^{107,254} Reported EC₅₀ values for 9-cis RA (43) vary depending on the test system between 1.7 and 200 nM for all RXR subtypes.^{222,254–258} Because of its low endogenous levels, the physiological relevance of 9-cis RA (43) is controversially discussed, however. Exogenous 9-cis RA (43) has therapeutic relevance (as alitretinoin) to treat chronic hand eczema and skin lesions in connection with Kaposi's sarcoma^{259,260} and is studied for the treatment of atopic dermatitis and psoriasis.²⁶¹ 9-Cis-13,14-dihydroretinoic acid (44), another metabolite of vitamin A, activates RXR as well and was detected in mice at relevant levels.^{262,263} In addition, several fatty acids were discovered as potential endogenous RXR ligands including docosahexaenoic acid (DHA, 45), oleic acid (46), palmitic acid (47), and stearic acid.^{221,222,256,264,265} The potency of these fatty acids on RXR is limited (micromolar range), however, and despite considerable concentrations found in plasma and even the brain, a physiological relevance remains to be demonstrated.

The first potent synthetic RXR agonists were based on the structure of 9-cis RA (43), which conforms well to the L-shaped ligand binding pocket of RXR. The most prominent synthetic RXR agonist is bexarotene (42) is the only synthetic RXR ligand that has received drug approval to date. It is used as a second-line therapy in the treatment of cutaneous T cell lymphoma.^{222,266,267} Bexarotene (42) is a pan-RXR agonist with similar potency on all three subtypes (EC₅₀: RXR α : 33 nM, RXR β : 24 nM, RXR γ : 25 nM)²⁶⁸ and comprises nonfavorable physicochemical properties¹¹⁷ with exceptionally high lipophilicity (logP 6.9), low solubility, and poor pharmacokinetics.^{117,269,270} In addition, bexarotene (42) is associated with risks/adverse effects²⁷¹ such as severe disturbances in lipid homeostasis (elevated triglyceride and cholesterol levels), leukopenia, hypothyroidism, and an increased risk of acute pancreatitis. From bexarotene (42), several other rexinoids were developed such as SR11237 (48, EC₅₀: RXR α : 29 nM, RXR β : 98 nM, RXR γ : 232 nM),²⁷² LG100268 (49, EC₅₀: 3–4 nM),²⁷³ PA024 (50, EC₅₀: RXR α : 3 nM, RXR β : 24 nM, RXR γ : 8 nM),²⁷² NET-3IP (51, EC₅₀: RXR α : 32 nM, RXR β : 36 nM, RXR γ : 376 nM),²⁷⁴ and NET-3IB (52, EC₅₀: RXR α : 0.58 nM, RXR β : 23 nM, RXR γ : 3 nM).²⁷⁴ Derived from the unselective PPAR agonist Wy14-643 (14),²⁷⁵ the RXR agonist 53¹¹⁷ has been developed as a potent next-generation RXR ligand with strong selectivity, superior physicochemical properties, and improved pharmacokinetics. RXR antagonists were obtained from rexinoid scaffolds by introduction of bulky side chains.^{276,277} Representative RXR antagonists useful as tool compounds are HX531 (54, IC₅₀: RXR α : 1 μ M), LG100754 (55, IC₅₀: RXR α : 16 nM), and UVI3003 (56, IC₅₀: RXR α : 0.24 μ M).²⁷⁶

Progress has recently been made in subtype selective targeting of RXR. The natural product valerenic acid (57) was discovered as an RXR β agonist with functional preference. In addition to a lower EC₅₀ value for RXR β activation (EC₅₀: RXR α : 27 μ M, RXR β : 5.2 μ M, RXR γ : 43 μ M) valerenic acid (57) exhibits remarkably higher efficacy on the RXR β subtype (fold activation: RXR α : 9-fold, RXR β : 69-fold, RXR γ : 4-

fold).²⁷⁸ Moreover, computational de novo design²⁷⁹ has yielded biphenyl-based RXR modulators, which could be tuned in their subtype-preference profile as exemplified by the RXR β preferential compound **58**.²⁸⁰ Together, these results demonstrate that RXR subtype selectivity can be achieved despite their high LBD similarity.²²¹

2.5.6. Conclusion. Because of its ability to act as a universal heterodimer partner for multiple other NRs, RXR is involved in various aspects of neurodegenerative diseases (summarized in Table 5) and has been intensively studied for this role in

Table 5. Summarized Observations on RXR in Neurodegeneration

RXR α (= NR2B1), RXR β (= NR2B2; also known as H-2RIIBP and RCoR-1) and RXR γ (= NR2B3)	
RXR in AD	In APP/PS1 mice, bexarotene (42) treatment (3, 7, or 14 days) reduced A β levels and caused removal of A β plaques, elevated ApoE, ABCA1, and ABCG1 levels, restored cognition and memory function, and improved hippocampal function. ²³⁹ In human patients, bexarotene (42) treatment slightly elevated ApoE levels in CSF but had no effect on synthesis, clearance, or total levels of A β . ApoE- ϵ 4 noncarriers showed reduced A β burden. ^{244,245}
RXR in MS	RXR γ -knockout mice had less differentiated OLs in lesions after toxin-induced demyelination. ²²⁷ RXR α -knockout mice exhibited reduced myelin phagocytosis after demyelination and delayed OPC differentiation. ²⁴⁸ Bexarotene (42) reversed functional defects of MS patient monocytes in myelin phagocytosis. ²⁴⁸ 9-cis RA (43) exhibited anti-inflammatory effects on microglia and astrocytes by inhibiting the production of pro-inflammatory cytokines, such as TNF α and IL-1 β . ²⁵¹ 9-cis RA (43) and IRX4204 (90) caused CNS remyelination in young and aged rats after toxin-induced demyelination. ^{227,252} IRX4204 (90) alleviated symptoms of EAE in mice and promoted differentiation of OPC. ²⁵²
RXR in PD	See permissive RXR/Nurr1-heterodimer.

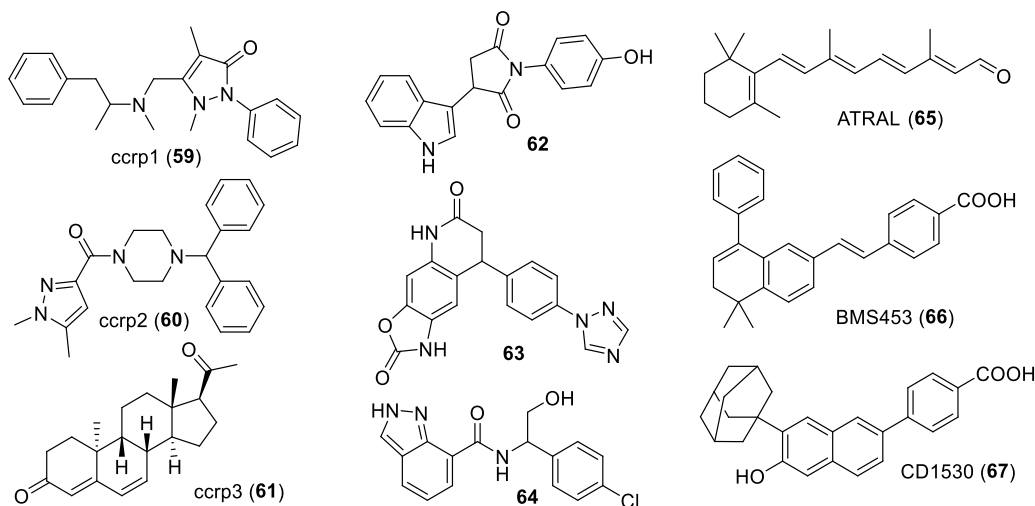
recent years. Despite some controversial reports, therapeutic effects of pharmacological RXR activation in many preclinical models support a promising therapeutic potential of RXR especially in AD and MS. Most remarkably, pharmacological RXR activation reduced A β plaques in cortex and hippocampus of AD mice, promoted remyelination in mouse models of MS, and reversed functional defects of MS monocytes in myelin phagocytosis. However, available RXR agonists such as bexarotene (**42**), 9-cis RA (**43**), or IRX4204 (**90**), though exhibiting remarkable potency, have several limitations. BBB penetration was found to be very low for bexarotene (**42**) and is likely poor for the other structurally related rexinoids due to their common carboxylic acid group. The low CNS bioavailability of the RXR agonist tools used in the preclinical studies might raise the question of whether the attractive effects were actually mediated by RXR activation in the brain. However, several studies have included knockout or antagonist control experiments, suggesting that RXR in the CNS is at least in part involved in the therapeutic activities. Moreover, the involvement of the universal heterodimer partner RXR in multiple nuclear receptor signaling systems and the associated adverse effects that were, for example, observed with bexarotene (**42**), demand the development of subtype selective RXR modulators. The recent discovery of valerenic acid (**57**) as a selective RXR β agonist²⁷⁸ demonstrates that this selectivity can be achieved despite remarkable similarity of the three RXR isoforms.²²¹ Hence, a lot of further research is needed to enable subtype selective RXR activation in the brain

and to capture the full potential of RXR modulation in neurodegenerative diseases.

2.6. Tailless Homologue (TLX, NR2E1). **2.6.1. Overview.** The orphan NR TLX (NR2E1) is one of the least studied and most elusive nuclear receptors. It is considered a master regulator of neural stem cell (NSC) maintenance²⁸¹ and is evolutionarily conserved in vertebrates and invertebrates. TLX was found to exhibit an essential role in embryonal brain development, and high TLX expression in adults was detected exclusively in quiescent and rapidly dividing NSCs in neurogenic regions as well as in retinal progenitor cells.^{282–285}

Mechanistically, TLX appears to differ from other nuclear receptors in a number of aspects. In line with its role in maintaining NSCs in a proliferating state and the underlying suppression of pten and p21, TLX was found to act mostly as a negative regulator of gene expression. It binds to the NR response element sequence AAGTCA as a monomer with high affinity²⁸⁶ and according to current knowledge differs also in its corepressor recruitment profile from most other NRs as it strongly binds atrophin, lysine-specific histone demethylase 1A (LSD-1), and histone deacetylases to inhibit gene expression.^{286–291} Structurally, TLX comprises the typical architecture of NRs despite a shorter LBD that lacks the first two of 12 helices which are present in most NRs.²⁸⁶ Early modeling approaches suggested that TLX may possess a ligand binding pocket within the LBD,^{286,292} but evidence from a cocrystal structure supporting this assumption is lacking. A TLX apo structure revealed the terminal α helix H12 of TLX bound at the canonical coactivator binding site of nuclear receptors indicating an autorepression.²⁹³ This autorepressed state resembles other NRs with repressor activity such as the TLX-related photoreceptor-specific nuclear receptor (PNR, NR2E3)²⁹⁴ and the dosage-sensitive sex-reversal adrenal hypoplasia congenital critical region on the X chromosome gene 1 (Dax-1, NR0B1).²⁹⁵ The putative ligand binding site of TLX is mostly blocked by bulky hydrophobic residues in the apo structure.^{291,293} Molecular dynamics and subsequent mutagenesis studies have suggested a potential binding site (for rexinoids) inside the TLX LBD close to the interface of helices H3 and H11.²⁹¹ This site has a higher solvent exposure than the ligand binding pockets of common NRs and is not present in the apo structure but requires conformational changes of H11 or H3 depending on the ligand type.^{291,293}

2.6.2. TLX in Neurodegeneration. Despite limited knowledge on TLX and the lack of TLX modulator tools for functional studies, there is preliminary evidence for a great potential of TLX in neurodegenerative diseases. In the brain, TLX regulates the maintenance of NSC populations and neurogenesis.^{281,290} It governs behavior and activation of NSCs²⁸¹ through directly controlling the expression of the tumor suppressor pten and the cyclin-dependent kinase inhibitor p21, thereby enabling re-entry in the cell cycle.^{281,284,286} Accordingly, the putative TLX activator oleic acid (**46**) was recently shown to induce NSC mitosis and neurogenesis in mice.²⁹⁶ Thus, maintaining NSCs in the brain in a proliferating, self-renewing state and preventing their differentiation appear to be key roles of TLX.^{281,282,297–299} NSCs are found in at least two main regions of the adult (human) brain, the subgranular zone of the dentate gyrus and the subventricular zone of the lateral ventricle, from where NSCs initiate the formation of new neurons.^{281,282,300} TLX appears to be a key regulator of this process by maintaining a balance between proliferating NSCs and differentiated

Scheme 6. TLX Ligands Reported in the Literature^{291,292,315}

neurons.^{281,282,300} The absence of TLX, accordingly, caused an entire loss of neurogenesis.³⁰¹ A number of knockout studies in rodents have revealed promising links of TLX to neurological and neurodegenerative diseases. TLX knockout led to limbic defects, hyperactivity, and violent behavior in adult mice.^{281,302,303} Concomitantly, active neurogenic regions in the brains of these mice showed severe deficits.^{281,304} NSCs from TLX knockout mice were unable to proliferate and self-renew, while an ectopic expression of TLX efficiently rescued this ability.^{281,282} A brain-specific TLX overexpression in mice led to improved learning capacity and memory function.³⁰⁵

These observations from *in vitro* and *in vivo* studies together draw a picture of TLX as a crucially important regulator of neuronal health and neuro-regeneration, and demonstrate an involvement of the orphan NR in spatial learning and cognitive functions during adolescence and adulthood.^{281,306–308} Moreover, TLX mutations in humans are linked to microcephaly and mental diseases such as bipolar disorders and schizophrenia.^{281,309} A recent study observed a correlation between schizophrenia risk and certain TLX haplotypes that were predicted to affect the expression rate of TLX,³¹⁰ ascribing the orphan NR also a key role in mental health. Overall, compelling evidence points to a great therapeutic potential of targeting TLX in neurodegeneration and neurological diseases.

In addition to its involvement in neuronal and retinal function, TLX has been associated with glioblastoma development, the most common and a highly aggressive brain tumor.^{311–313} The orphan NR was found overexpressed in tumor stem cells of glioblastoma,³¹² while TLX knockdown decreased tumor progression and enhanced survival in a xenograft tumor model in mice.³¹⁴ TLX modulators, therefore, might hold strong potential in this context as well. However, there is no evidence that ectopic TLX overexpression in animal models promotes cancer development,²⁹¹ which is an important aspect for pharmacological targeting of TLX in neurodegeneration.

2.6.3. TLX Ligands and Modulators. A number of studies have demonstrated that TLX activity can be modulated by small molecule ligands, and a few TLX modulators with mostly weak potency (micromolar range) have been described^{286,291,292,315} (Scheme 6). Benod et al.²⁹² were the first to report small molecule modulators of TLX from a

medium-throughput screening campaign. By differential scanning fluorimetry with the recombinant TLX LBD protein, they identified 190 primary hits from a library of 20 000 compounds. Three compounds (famprofazone, ccrp1 (59); ccrp2 (60); dydrogesterone, ccrp3 (61)) showed activity on TLX in an orthogonal cellular reporter gene assay. In another study,³¹⁵ the activity of famprofazone (59) and ccrp2 (60) (ccrp3 (61) was not tested) could not be reproduced, however. Dueva et al.³¹⁵ applied a computational approach to TLX ligand discovery and reported 62–64 as TLX modulators in a cellular setting. Orthogonal validation of these compounds as TLX ligands is pending, however, and they comprise PAINS suspect elements. Retinoids (ligands of the nuclear retinoic acid receptors, RARs) have recently been proposed to act as TLX modulators, too. *In vitro*, certain natural (all-trans retinal, ATRAL (65)) and synthetic (BMS453 (66); CD1530 (67)) compounds showed TLX activation or inverse agonism with potencies ranging approximately between 0.2 μM and 2 μM .²⁹¹ Retinoid efficacy in TLX activation (~ 5 -fold, BMS453 (66)) and repression (~ 4 -fold, ATRAL (65)) was limited, however. NMR experiments were employed to orthogonally validate a direct interaction between TLX and the retinoids, which revealed chemical shift perturbations and line broadening.²⁹¹ Another recent study²⁹⁶ has discovered oleic acid (46) as a putative endogenous TLX ligand that is capable of switching TLX activity from transcriptional repression to cell cycle activation and was shown to be present in human NSCs.

2.6.4. Conclusion. Despite a very limited understanding of TLX, the essential regulator of NSC homeostasis holds remarkable promise in neurodegenerative diseases (summarized in Table 6). However, owing to the lack of TLX modulators as tools, functional understanding of TLX is incomplete, and insights in its (patho-)physiological role stem only from knockout experiments. Current evidence of TLX mutations disrupting neurogenesis and knockout causing abnormal brain development and behavioral deficits points to a high potential of targeting TLX for regenerative approaches in neurodegeneration. Therein, the exclusive expression of TLX in certain brain regions may suggest few adverse effects of TLX modulation since no other tissues would be affected. However, the known TLX ligand space is very limited and somewhat controversial. Biochemical and biophysical charac-

Table 6. Summarized Observations on TLX in Neurodegeneration

TLX (= NR2E1; also known as TLL and XTLL)	
TLX in neurodegeneration	TLX mutations in human were associated with microcephaly and mental diseases. ^{281,309}
	TLX regulates the maintenance of NSCs and neurogenesis. ^{281,290}
	TLX maintains a balance between proliferating NSCs and differentiated neurons. ^{281,282,300}
	TLX knockout led to defects in neurogenesis, limbic defects, hyperactivity, and violent behavior in adult mice. ^{281,302,303}
	Brain-specific TLX overexpression improved learning capacity and memory function. ³⁰⁵

terization of most putative TLX modulators is not comprehensive. Broad reproduction of their activities in various settings and orthogonal validation is pending. Despite preliminary data, binding sites and the molecular mode-of-action remain elusive for TLX. With their limited potency, efficacy, and selectivity, and their unclear modes of action, the available TLX ligands are insufficient for pharmacological evaluation and validation of the orphan NR. More potent, selective, and broadly profiled TLX agonists and inverse agonists are required as pharmacological tools for target validation. The development of potent TLX ligands as highly profiled tools for functional studies on TLX is imperative.

2.7. NR4A Receptors. **2.7.1. Nur77 (NR4A1).** **2.7.1.1. Overview.** As the first member of the NR4A subfamily of NRs, Nur77 was originally identified as nerve growth factor-induced clone B (NGFI-B)³¹⁶ and is an orphan nuclear receptor since no endogenous ligands are known so far. Nur77 was thought to be a ligand-independent transcription factor due to its closed and tightly packed conformation of the LBD in which the canonical ligand binding pocket is occupied by bulky hydrophobic amino acids that are conserved among the three NR4A subfamily members.³¹⁷ The resulting autoactivated conformation (Figure 3c) renders Nur77 (and the related NR4A receptors Nurr1 and NOR-1) as a constitutively active transcriptional inducer with high transcriptional activity in the absence of a ligand. Nur77 can act in three forms, as a monomer on NGFI-B response elements (NBRE), as a homodimer on Nur response elements (NurRE), which were first detected in the promoter region of the proopiomelanocortin (POMC)³¹⁸ gene, or as a heterodimer with an RXR on DR5 response elements.^{319–321} Nur77 is widely expressed in several tissues including the pituitary gland, adrenal gland, thyroid, liver, testis, ovary, thymus, muscle, lung, and prostate²⁹ but also in the nervous system with the highest levels in the cerebral cortex and hippocampus.³²² In contrast to Nurr1, it is highly expressed in target areas of dopaminergic neurons such as the striatum, nucleus accumbens, and prefrontal cortex. Interestingly, Nur77 mRNA was not found in the prenatal CNS but only in the adult brain.³²³ The functions of Nur77 are manifold and appear to be tissue specific. In metabolic diseases like diabetes, it seems to participate in the regulation of blood glucose levels since genetic deletion of Nur77 in mice increased insulin resistance.^{324,325} Also several inflammatory conditions such as asthma,³²⁶ atherosclerosis,^{327,328} arthritis,³²⁹ and sepsis³³⁰ are linked to Nur77 activity. Additionally, Nur77 is overexpressed in multiple solid tumors and plays a pro-oncogenic role in cancer (reviewed in Beard et al.³³¹). Moreover, Nur77 was shown to induce apoptosis by targeting mitochondria, whereby

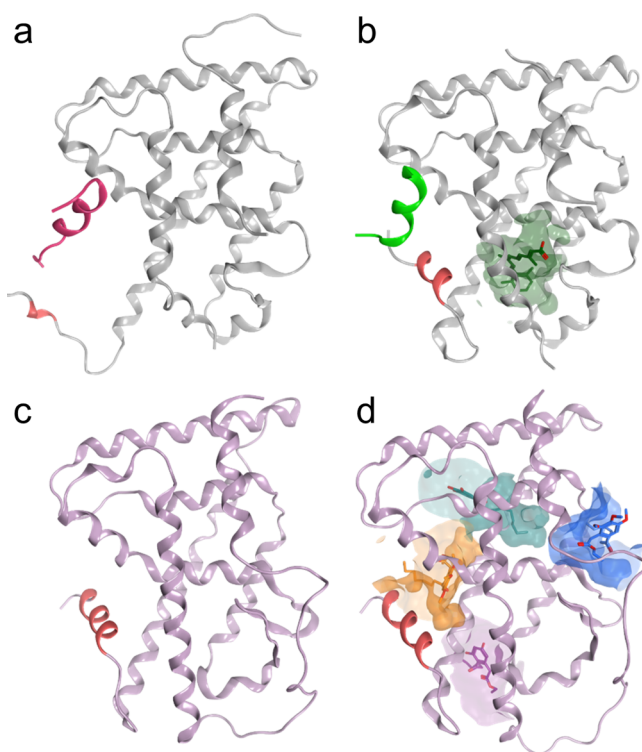


Figure 3. Comparison of the crystal structures of “classical” nuclear receptors (RXR α) and NR4A receptors (Nur77). (a) The apo structure of the RXR α LBD (pdb 3R29) in complex with the corepressor peptide SMRT (magenta) reveals the NR in its inactive state in which the C-terminal α -helix (H12, colored red) comprises the AF-2 in an unordered conformation. (b) The ligand-activated state of RXR α (pdb 3OAP) shows the NR cocrystallized with its endogenous ligand 9-cis RA (43) and the coactivator peptide TIF2 (neon green) with H12 in its active conformation. (c) The apo structure of the Nur77 LBD (pdb 3V3E) reveals the NR in an autoactivated state with H12 coordinated to the LBD core without a bound ligand. (d) Ligand-activated cocrystal structure (pdb 6KZ5) of the Nur77 LBD in complex with agonist Csn-B (68, purple) superimposed with ligand binding pockets and their respective ligands from other Nur77 cocrystal structures revealing other binding sites with high solvent exposure. Csn-B (68, purple) is bound at the dimeric interface, THPN (71, teal, pdb 4JGV) is protruding toward a sub-pocket between H5 and H7, and TMPA (69, blue and orange, pdb 3V3Q) is bound to two different sites. Site A (orange) is located at the interaction site of H12, which resembles the binding pockets identified for covalently bound Nurr1 ligands DHI (83) and PGA1 (80), while site B (blue) constitutes a cavity on the surface close to helices 1, 5, and 8. Alignment and superposition of the structures were performed in MOE 2020.09.

it translocates from the nucleus to the cytoplasm in an RXR α regulated fashion,^{332,333} suggesting that Nur77 also exhibits activities via non-transcriptional mechanisms.

2.7.1.2. Nur77 in Parkinson’s Disease. Growing evidence, mainly from PD models, ascribes Nur77 a role in neurodegenerative diseases. Although Nur77 knockout mice³³⁴ and rats³³⁵ exhibited only a mild phenotype, they tended to have higher basal locomotor activity. In line with this, a SNP in the Nur77 gene was found to be strongly associated with tardive dyskinesias in a cohort of schizophrenic patients.³³⁶ Several studies further investigated the role of Nur77 in drug-induced dyskinesias and PD models with somewhat controversial results. Still, all studies demonstrate involvement of Nur77 in aberrant dopamine-related behavior.

Full Nur77 knockout in mice displayed beneficial effects on dopamine neuron function.³³⁴ Moreover, the regulation of the neuropeptides enkephalin and neurotensin was shown to be Nur77 dependent in the context of dopamine denervation in 6-OHDA-lesioned mice;³³⁷ however, they remain to be validated as direct Nur77 target genes.^{337,338} In two MPTP animal models, Nur77 was downregulated,^{339,340} and Nur77 knockout resulted in a sensitization to dopaminergic cell death following MPTP treatment.³⁴⁰ In drug-induced dyskinesia, induction of Nur77 by administration of RXR agonist DHA (45) following levodopa treatment ameliorated symptoms.³³⁹ The latter was proven with DHA (45) administration in Nur77 knockout mice,³⁴¹ which failed to counteract haloperidol-induced dyskinesia pointing toward a potential involvement of the Nur77-RXR heterodimer.

The findings of Rouillard et al.³³⁵ and Wei et al.³⁴² are hence controversial: Although Nur77 expression is almost negligible in substantia nigra and the ventral tegmental area, rapid upregulation of Nur77 in substantia nigra and midbrain was observed in a 6-OHDA-induced rat PD model with concomitant downregulation of Nurr1 and TH in midbrain.³³⁵ Moreover, Nur77 deficiency decreased dopaminergic neuronal loss in two different rodent PD models.³³⁵ Accordingly, Nur77 protein expression was rapidly upregulated upon 6-OHDA treatment in vitro, and Nurr1 protein expression decreased over time, supporting a contradirectional coupling of these two receptors in the context of neurodegeneration.^{342,343} The NMDA receptor antagonist memantine and lentiviral Nur77 knockdown reversed these effects, prevented neurodegeneration by inhibiting Nur77 translocation to the cytosol, and promoted neuroprotection via post-translational modifications of Nurr1.³⁴²

Contributions of Nur77 to neuroinflammation in the context of PD are more consistent. In microglia, Nur77 expression was reduced upon microglial activation by LPS treatment in vitro and in vivo.³⁴⁴ Silencing of Nur77 enhanced inflammatory responses and overexpression or activation of Nur77 with the agonist cytosporone B (Csn-B, 68) suppressed pro-inflammatory responses.³⁴⁴ These anti-inflammatory effects were shown to involve Nur77-mediated inhibition of I κ B- α phosphorylation and NF κ B repression.³⁴⁵ Additionally, anti-inflammatory and antioxidant stress effects of Nur77 activity were demonstrated with Csn-B (68) counteracting MPP⁺-induced inflammation in vitro,³⁴⁵ and with C-DIMS, a Nur77 and Nurr1 activating compound, diminishing NF κ B activity in MPTP/TNF/IFN-treated astrocytes.³⁴³ Of note, Popichak et al. detected compensatory expression of Nur77 and Nurr1 in astrocytes by knocking down either nuclear receptor by RNA interference (RNAi), whereas NOR-1 expression was not affected.³⁴³ Therein, the anti-inflammatory effect of C-DIMS increased upon Nur77 knockdown, pointing rather toward Nurr1-mediated effects. Double knockdown of both receptors fully prevented the anti-inflammatory activity of C-DIMS. However, direct binding of C-DIMS to either receptor is only supported by molecular docking studies.

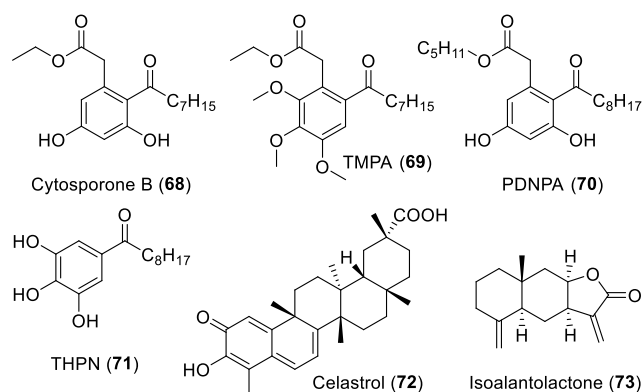
2.7.1.3. Nur77 in Multiple Sclerosis. In the context of MS, Nur77 is expressed during early T cell activation and acts as a key regulator of T cell immunometabolism, which controls the development of aberrant pro-inflammatory T cell responses and autoimmunity.³⁴⁶ Nur77 deficiency led to enhanced T cell proliferation, and Nur77 knockout in EAE in mice caused earlier disease onset and significantly increased the clinical EAE score.³⁴⁶ Based on Nur77's role as a negative regulator of

microglial activation, the Nur77 agonist Csn-B (68) was studied in EAE in mice. Treatment with 68 markedly ameliorated disease progression in wild-type mice but not in Nur77 knockout animals and protected from demyelination.³⁴⁷ As Nur77 restricts T cell activation and T cell-mediated CNS autoimmunity, and acts as regulator of metabolic genes in activated T cells, selective Nur77 agonists may emerge as a new approach to counteract T cell-mediated autoimmune diseases like MS.

2.7.1.4. Nur77 in Alzheimer's Disease. In AD, there is little evidence for an involvement of Nur77 to date. Expression of alpha 1-antichymotrypsin/serpinA3, a member of the serine protease inhibitor family, was found to be induced by Nur77 as it contains a Nur77 monomer response element in its promoter region.³⁴⁸ It is involved in acute phase and inflammatory responses but is also known to contribute to the development of AD as it interacts with A β peptide and turned out to be a major component of A β plaques. Moreover, RXR α and Nur77 were found to translocate from the nucleus to the mitochondria in neurons after A β and H₂O₂ treatment which resulted in apoptosis.³⁴⁹ Accordingly, treatment with the RXR agonist 9-cis RA (43) reduced apoptosis by blocking the translocation in vitro and in vivo and enhanced B-cell lymphoma 2 (Bcl-2) protein expression.

2.7.1.5. Nur77 Ligands. Although Nur77 is an orphan nuclear receptor, several studies have reported Nur77 modulating small molecules (Scheme 7). Growing evidence

Scheme 7. Nur77 Ligands Reported in the Literature^{325,330,350,354,356,357}



from crystal structures supports the assumption of a blocked canonical ligand binding pocket since all known Nur77 ligands to date bind to noncanonical sites on the surface of the LBD (Figure 3d). Among them, the agonist cytosporone B (Csn-B, 68), a natural product, was the first compound shown to directly bind to the Nur77 LBD³⁵⁰ by glutathione S-transferase-pull-down, circular dichroism (CD) spectroscopy, surface plasmon resonance (SPR) binding kinetics, and mutagenesis studies. Two different reporter gene assays in BGC-823 cells, a human gastric cancer cell line, confirmed transactivation of Gal4-Nur77-full-length (fl) (EC₅₀ 0.278 nM) and Gal4-Nur77-LBD (EC₅₀ 0.115 nM) constructs. No response was observed with Gal4-Nur77-DBD and Gal4-Nur77-Y453A mutant constructs supporting a direct interaction with the Nur77 LBD. In addition to Nur77, binding of Csn-B (68) to the related receptor Nurr1 was observed in NMR perturbation studies, but Nurr1 transactivation by Csn-B (68) was weak.^{350,351} Csn-B (68) was also evaluated in vivo

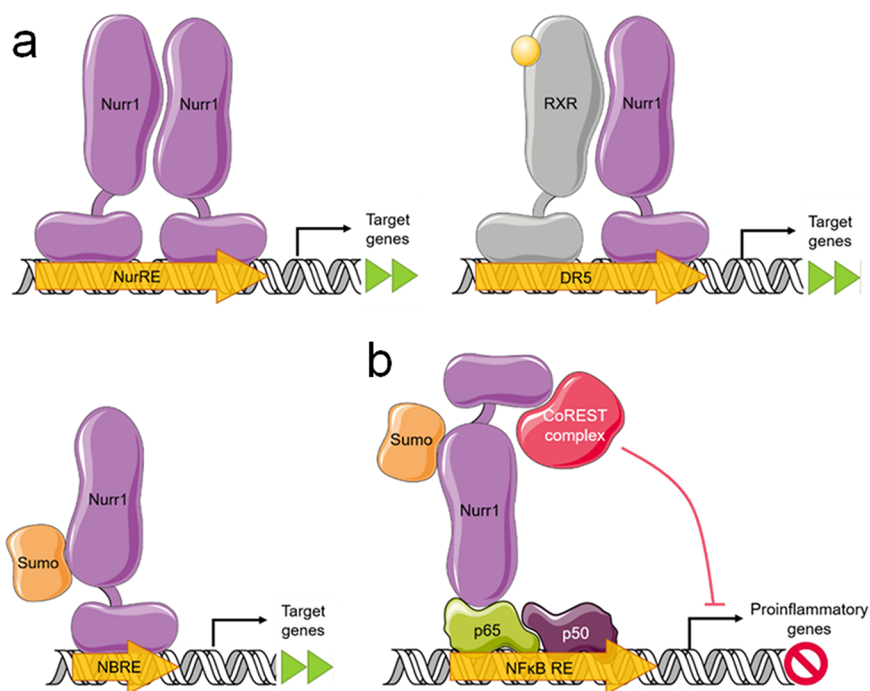


Figure 4. NR4A receptor mechanisms of action. (a) The constitutively active NR4A receptors (Nur77, Nur1, and NOR-1) can directly bind to specific response elements as a homodimer, as a heterodimer with RXR (only Nur77 and Nur1), or as a monomer. Sumoylation of the respective NR causes monomerization, and these monomers activate NBRE. NR4A homodimers bind to NurRE, while NR4A:RXR heterodimers bind to DR5 response elements. (b) Additionally, Nur1 monomers directly interact with p65 on the NFκB RE upon sumoylation and recruit the CoREST corepressor complex, which results in suppression of NFκB-regulated pro-inflammatory genes. Abbreviations: CoREST, REST corepressor; DR5, direct repeat spaced by five nucleotides; NBRE, NGFI-B responsive element; NFκB, nuclear factor-κB; NOR-1, neuron derived orphan receptor 1; NurRE, Nur response element; Nur1, nuclear receptor related-1 protein; RXR, retinoid X receptor.

where it increased blood glucose levels and induced gluconeogenic genes in wild-type animals but not in Nur77^{-/-} knockout mice. Additionally, Nur77-induced apoptosis by targeted translocation from nucleus to cytoplasm was observed upon treatment of BGC-823 cells with Csn-B (68). Many further studies^{352,353} focused on the anticancer activity of Csn-B (68), and systematic structure–activity relationship (SAR) studies on the Csn-B (68) scaffold were conducted which identified the alkyl ester function as a key pharmacophore feature for Nur77 transactivation.³⁵² Recently, a cocrystal structure (pdb 6KZ5) of Nur77 in complex with Csn-B (68) revealed an unusual pocket at the dimer interface between two LBD molecules³⁵³ (Figure 3d, purple site).

Following the discovery of Csn-B (68) as a direct Nur77 agonist, several derivatives were developed and intensively studied for their modes of action. Effects in the field of metabolic diseases were further investigated in vitro and in vivo with ethyl 2-[2,3,4-trimethoxy-6-(1-octanoyl)phenyl]acetate (TMPA, 69),³²⁵ a neutral antagonist derived from Csn-B (68) with no effect in a Nur77 reporter gene assay. A cocrystal structure (pdb 3V3Q) demonstrated direct binding to two different sites on the surface of the Nur77 LBD. Site A is located between helices 4, 11, and 12 (Figure 3d, orange site), while site B constitutes a cavity on the surface close to helices 1, 5, and 8 (Figure 3d, blue site).

A potential anti-inflammatory compound was developed with the Csn-B (68) derivative *n*-pentyl 2-[3,5-dihydroxy-2-(1-nonanoyl)phenyl]acetate (PDNPA, 70),³³⁰ a competitive inhibitor of the Nur77–p38α interaction via binding to Nur77. The compound prevented phosphorylation of Nur77 and but conserved the ability of Nur77 to inhibit NFκB activity

by direct interaction with the NFκB subunit p65 (Figure 4b). Despite also binding to the Nur1- and NOR-1-LBDs, PDNPA (70) antagonized an NFκB reporter gene assay in a RAW264.7 murine macrophage cell line only in a Nur77-dependent fashion with an IC₅₀ value of 1.6 μM. Ligand binding of PDNPA (70) to Nur77 was confirmed by a cocrystal structure (pdb 4RZG), which revealed binding to site A like TMPA (69), between helices 4, 11 and 12, but PDNPA (70) and TMPA (69) differed in their in vitro and in vivo activities.

Another Csn-B (68) derivative with anticancer activity is 1-(3,4,5-trihydroxyphenyl)nonan-1-one (THPN, 71).³⁵⁴ A cocrystal structure (pdb 4JGV) revealed binding to the Nur77 LBD surface between helices 5, 7, 8, 9, and 10 (Figure 3d, teal site), where also the close analogue 1-(3,5-dimethoxyphenyl)-decan-1-one (DPDO, pdb 4KZI) bound but without protruding toward the subpocket between helices 5 and 7. THPN (71) induced a mitochondrial signaling pathway toward autophagic cell death and was, hence, characterized in cell viability tests in several melanoma and non-melanoma cancer cell lines, in binding studies and in knockdown experiments, while Nur77 transactivation has not been studied. A small SAR evaluation with six THPN (71) derivatives differing in chain length and hydroxyl group substitution pattern revealed a correlation between LBD binding affinity and potency, and resulted in an optimized descendant with C9 instead of C8.³⁵⁵

The pentacyclic triterpene celastrol (72) was discovered in a screening of anti-inflammatory natural products in an SPR assay for Nur77 binding where it exhibited a K_d value of 0.29 μM.³⁵⁶ Binding was confirmed by CD and HPLC analysis, and celastrol (72) reduced transcriptional activity of Nur77 in a

reporter gene assay at 0.5 μM in HEK293T cells. Mechanistic investigation revealed enhanced Nur77 mitochondrial translocation to inhibit inflammation via autophagy by direct interaction with a LxxLL motif of TNF receptor-associated factor 2 (TRAF2). Molecular docking studies suggested a similar binding site for celastrol (72) as shown for THPN (71). Isoalantolactone (73) was derived from a natural-product-based small molecule library screen as another Nur77-modulating compound.³⁵⁷ Two different reporter gene assays in human pancreatic MiaPaCa2 cells and murine 3T3-L1 preadipocytes revealed inverse Nur77 agonism of isoalantolactone (73). By additionally activating AMPK α , the compound exhibited a dual mechanism which collectively inhibited adipogenesis in vitro and in vivo. However, direct interaction of isoalantolactone (73) with Nur77 and its binding site remain elusive.

Early findings on potential endogenous Nur77 ligands were reported by Vinayavekhin et al.³⁵⁸ who discovered unsaturated fatty acids, namely, arachidonic acid and DHA (45), as Nur77 binders in a metabolomics approach from brain and testes samples. Evidence for binding was reported from an 8-anilino-1-naphthalenesulfonic acid (ANS) displacement assay and from CD experiments with the His₆-Nur77 LBD. Prostaglandin A2 (PGA2, 92)³⁵⁹ was later identified as another potential endogenous agonist for Nur77, and addition of biotinylated PGA2 (92) to recombinant Nur77 protein revealed binding with a K_d value of 2.05 μM according to Western blot analysis and an SPR assay. Covalent interaction of PGA2 (92) with Cys566 was postulated based on covalent molecular docking and molecular dynamic simulation based on the observation that only PGs with an endocyclic C β electrophile bound to Nur77. A full-length Nur77 reporter gene assay with a NurRE response element in human bronchial epithelial NHBE cells revealed dose-dependent activity with up to 15-fold Nur77 transactivation at 10 μM PGA2 (92). In line with this, we have recently discovered NSAIDs as Nur77 and NOR-1 modulators with meclofenamic acid (85) acting as Nur77 agonist, and meloxicam, lornoxicam, mofezolac, oxaprozin (83), and parecoxib (84) as inverse Nur77 agonists in a Gal4-Nur77 hybrid reporter gene assay in HEK293T cells.³⁶⁰ In addition, amodiaquine (AQ, 75) and chloroquine (CQ, 76), initially characterized as Nurr1 modulators, revealed Nur77 and NOR-1 agonism in the same setting. These findings of similar ligand activities on Nur77, Nurr1, and NOR-1 suggest that obtaining selective ligands for the individual NR4A receptors will be challenging.

The antimetabolite 6-mercaptopurine (6-MP, 91), a well-known anticancer agent, was extensively studied as a Nurr1³⁶¹ and NOR-1³⁶² agonist and found to modulate the receptors through the AF-1 region. Nur77 activation by 6-MP (91) is hence thought to follow a similar mechanism. 6-MP (91) strongly activated Nur77 in a full-length reporter gene assay using a homodimer responsive reporter construct in C2C12 murine myoblast cells.³⁶² However, this activity was accompanied by an induction of Nur77 and other NR4A protein levels suggesting nonspecific effects of 6-MP (91).³⁶³ Fangchinoline,³⁶⁴ a bisbenzyltetrahydroisoquinoline alkaloid from *Stephania tetrandra*, modulated Nur77 through the N-terminal region, too, and inhibited Nur77 transactivation in MiaPaCa-2 cells. The natural product exhibited anticancer activity in part via inducing Nur77-dependent pro-apoptotic pathways, whereas no translocation from the nucleus occurred.

Nur77 modulation by the compound series of 1,1-bis(3'-indolyl)-1-(p-phenyl)methane (C-DIM) and analogues is controversial.^{365–367} Activating (DIM-C-pPhOCH₃, C-DIMS)³⁶⁷ and inhibiting (DIM-C-pPhOH, C-DIM8)³⁶⁶ compounds have been reported from this series and were investigated in various types of cancer cell lines. The compounds exhibited Nur77-independent apoptosis induction, kinase induction, and endoplasmic reticulum stress activation, but conclusive evidence for direct modulation of NR4A receptors is missing. The authors of C-DIM characterization as putative NR4A ligands conclude that the modulating activity on Nur77 may be due to indirect activation or deactivation rather than ligand binding.³⁶⁷ Despite some evidence for direct binding from pull-down assays and CD spectroscopy, no IC₅₀ or EC₅₀ values for C-DIM and analogues are available, and their effects vary significantly depending on the cell context.³⁶⁵ Effects of C-DIM and analogues reported from animal models are hence difficult to interpret and cannot be related to a clear mode-of-action.

Three further compounds have been reported in the context of Nur77 which do not directly bind to or interact with Nur77 but affect its activity by other mechanisms. 1,3,7-Trihydroxy-2,4-diprenylxanthone (CCE9)³⁶⁸ and the anticancer agent cisplatin³⁶⁹ were found to induce Nur77 protein expression, which may have similar effects as Nur77 activation owing to the high constitutive transcriptional activity of Nur77. Z-ligustilide,³⁷⁰ a phthalide compound from *Radix Angelica sinensis*, is characterized as an autophagy inhibitor that restored Nur77 from selective degradation by autophagy, thereby enabling Nur77–Ku80 interaction which suppressed double-strand break repair. As a consequence, cell sensitivity to tamoxifen was enhanced in an autophagy-associated fashion.

2.7.1.6. Conclusion. The orphan nuclear receptor Nur77 is an emerging target in several indications including neurodegenerative diseases (summarized in Table 7). Despite ubiquitous expression as well as pleiotropic and nontranscriptional effects, a role of Nur77 in neuroinflammation and dopamine neurotransmission is well described. Validation of Nur77 as a therapeutic target will require multiple further studies, however, which are hindered by the lack of high-quality tool compounds. The unclear mode-of-action, lacking proof for direct interaction, and poor selectivity of C-DIM-based Nur77 modulators compromises the significance of several studies on Nur77 in neurodegeneration. Selective Nur77 agonists and inverse agonists with confirmed direct binding are needed for a deeper understanding of Nur77 in neurodegeneration. Future studies should also further analyze the nongenomic effects involving translocation of Nur77 and whether this pathway can be selectively modulated with ligands.

2.7.2. Nurr1 (NR4A2).
2.7.2.1. Overview. The orphan nuclear receptor related 1 (Nurr1) is the second member of the NR4A subfamily and was initially considered as a ligand-independent transcription factor. The first crystal structure (pdb 1OVL) of the NR4A family in 2003 revealed Nurr1 in apo form in an autoactivated conformation and lacking a canonical ligand binding site due to tightly packed bulky hydrophobic residues within the LBD core³¹⁷ (compare Figure 3c). Moreover, structural analysis identified a hydrophobic coregulator interaction surface between helices 11 and 12 distinct from the canonical nuclear receptor coactivator interaction site, which in turn is a highly polar area in the Nurr1 LBD.^{371,372} These early findings indicated different

Table 7. Summarized Observations on Nur77 in Neurodegeneration

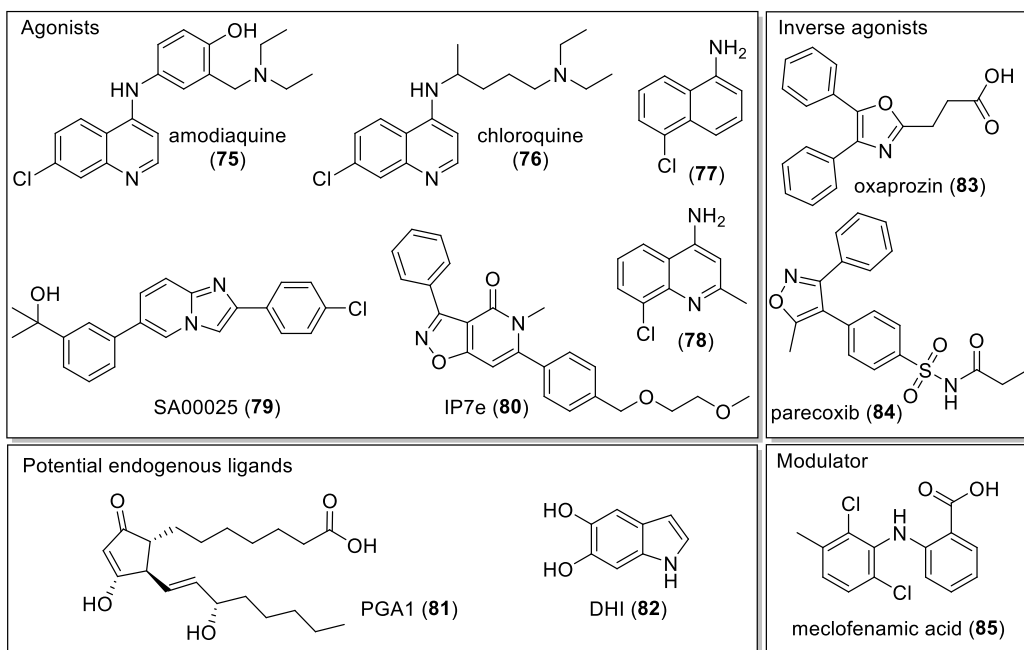
Nur77 (= NR4A1; also known as NGFI-B, TR3, NAK-1, and N10)	
Nur77 in AD	Alpha 1-antichymotrypsin/serpinA3 is involved in AD development and Nur77 regulated. ³⁴⁸ Translocation of Nur77-RXR to mitochondria in neurons upon A β /H ₂ O ₂ treatment results in apoptosis. ³⁴⁹ Activation with the RXR agonist 9-RA (43) prevented translocation, reduced apoptosis, and enhanced Bcl-2 expression in vitro and in vivo. ³⁴⁹
Nur77 in PD	Nur77 knockout slightly enhanced basal locomotor activity in mice and rats. ^{334,335} Nur77 knockout in mice: TH \uparrow , dopamine metabolite DOPAC \uparrow , COMT \downarrow . ³³⁴ Nur77 knockout in the MPTP PD model had conflicting results: sensitization to dopaminergic cell death ³⁴⁰ and decreased dopaminergic neuronal loss after perturbation. ³³⁵ Nur77 knockout in the 6-OHDA PD model decreased dopaminergic neuronal loss in rats. ³³⁵ Nur77 was downregulated in MPTP in monkeys and in the nigrostriatal region of mice. ^{339,340} 6-OHDA treatment induced Nur77 expression in vitro ³⁴² and in vivo. ³³⁵ Nur77 was counter-regulated. Microglial activation by LPS treatment reduced Nur77 expression in vitro and in vivo (MPTP model). ³⁴⁴ Nur77 activation (Csn-B (68) or C-DIMS) suppressed NF κ B activity in BV2 microglia and counteracted inflammation in vitro. ^{343–345}
Nur77 in MS	Nur77 knockout enhanced T cells activation and T cell-mediated CNS autoimmunity in vitro and in vivo. ³⁴⁶ Nur77 knockout in EAE caused earlier disease onset and increased EAE score/severity. ³⁴⁶ Nur77 activation (Csn-B (68)) ameliorated EAE progression and protected from demyelination in wild-type mice but not in Nur77 knockout animals. ³⁴⁷

regulatory mechanisms and a potentially different coregulatory network for Nurr1. In line with this, we observed ligand-dependent displacement of four coregulator peptides by inverse Nurr1 agonists, namely, NCoR-1 and SMRT, considered as corepressors, the coactivator NCoA6 and the coregulator NRIP1.³⁶⁰ Additionally, the SUMO-E3 ligase PIAS γ is known as a potent repressor of Nurr1 transactivation.³⁷³ Like its relative Nur77 (see section 2.7.1), Nurr1 can act as a monomer (on the NBRE), a homodimer (on the NurRE), and a heterodimer with RXR (on the DRS) on different response elements^{319–321} (Figure 4a). Nurr1 is the most extensively studied NR4A member in the context of neurodegenerative diseases. It is mainly expressed in the central nervous system with particularly high abundance in mesencephalic dopaminergic neurons of the ventral tegmental area and substantia nigra pars compacta, and the paraventricular thalamic nuclei.³²² As a key regulator in dopaminergic neuron development and maintenance, Nurr1 is expressed in the midbrain from early prenatal state to adulthood.³⁷⁴ Nurr1 regulates genes that are essential factors in dopamine neurotransmission such as tyrosine hydroxylase (TH), dopamine transporter (DAT), vesicular monoamine transporter 2 (VMAT2), and aromatic L-amino acid decarboxylase (AADC).^{374–377} Various Nurr1-regulated genes were discovered in dopaminergic neurons including Dlk1, Ptpu, and Klhl1,³⁷⁸ the GTP cyclohydrolase,³⁷⁹ vasoactive intestinal peptide (VIP),³⁸⁰ receptor tyrosine kinase Ret³⁸¹ critical in neurotrophic factor signaling, and topoisomerase II β ,³⁸² but also osteopontin, osteocalcin, and neuropilin²⁹ are Nurr1-dependent. Although Nurr1 is considered as a contributing factor in attention-deficit hyperactivity disorder,³⁸³ inflammatory arthritis,³⁸⁴ metabolic disease, and cancer (reviewed in ref 385), emerging evidence ascribes Nurr1 a particularly

important role in the pathogenesis of neurodegenerative diseases and presents as a very promising drug target especially in PD.

2.7.2.2. Nurr1 in Parkinson's Disease. The key regulatory role of Nurr1 in dopaminergic neuron development became apparent in knockout studies, as homozygous Nurr1 knockout mice exhibited a complete loss of ventral mesencephalic dopaminergic neurons, altered gene expression in the dorsal motor nucleus of the brainstem, respiratory dysfunction, and notable hypoactivity, and died within two days after birth.^{29,374} Moreover, a number of Nurr1 SNPs were found in patients with familial PD.^{29,386} Most notably, the polymorphism rs35479735 located in intron 6 of the Nurr1 gene, which may affect the splicing process, strongly correlates with an increased risk of sporadic and familial PD.³⁸⁷ Post-mortem analysis of PD patients revealed a significant decrease of Nurr1 expression in nigral neurons containing α -synuclein inclusions, which correlated with loss of TH⁺ neurons.³⁸⁸ Accordingly, diminished levels of Nurr1 were also found in nigral dopaminergic rat neurons caused by elevated α -synuclein levels³⁸⁹ and in MPTP-treated mice.³⁹⁰ In contrast, Nurr1 overexpression protected dopaminergic neurons against several toxic insults in vitro and in vivo, which was apparent from upregulation of neuroprotective genes and increased neuronal survival.^{389–392} Moreover, transplantation of mesenchymal stem cells with lentiviral Nurr1 overexpression in 6-OHDA-treated rats increased the number of TH⁺ neurons, lowered microglial activation, and reduced expression of inflammatory mediators in the substantia nigra.³⁹³ In microglia and astrocytes, Nurr1 acted as a negative regulator of NF κ B-regulated inflammatory genes by stabilizing the CoREST corepressor complex at p65/p50 cis-acting promoter elements³⁹⁴ (Figure 4b) and thereby limited the production of neurotoxic mediators like TNF α , IL-1 β , and iNOS in the substantia nigra of LPS-injected mice. In contrast, interaction of Nurr1 and coactivator Foxa2 in midbrain dopaminergic neurons was found to diminish the Nurr1–CoREST interaction and to induce dopamine phenotype gene expression.³⁹⁵

Despite the early assumption that Nurr1 is ligand independent, the antimalarial amodiaquine (AQ, 75) was discovered as an activator of Nurr1 and enhanced the expression of Nurr1-regulated genes (TH, DAT, VMAT2, AADC) in rat NSCs. Moreover, AQ (75) suppressed pro-inflammatory cytokine release after LPS treatment in primary rat microglia and improved behavioral deficits in 6-OHDA-lesioned rats.³⁹⁶ In addition to AQ (75), the prostaglandins A1 (PGA1, 81) and E1³⁹⁷ as well as the dopamine metabolite 5,6-dihydroxyindole (DHI, 82)³⁹⁸ were identified as potential endogenous Nurr1 activators. PGA1 (81) and PGE1 exhibited neuroprotective effects in a primary midbrain dopaminergic neuron-glia coculture derived from rat embryos treated with MPTP or LPS, induced dopaminergic gene expression in MN9D cells in a Nurr1-dependent manner, and attenuated motor deficits in MPTP-induced PD in mice.³⁹⁷ DHI (82) significantly increased mRNA expression of Nurr1-regulated genes (TH, VMAT2, and DAT) in wild-type zebrafish larvae.³⁹⁸ The synthetic Nurr1 agonists SA00025 (79)³⁹⁹ and IP7e (80)⁴⁰⁰ also exhibited neuroprotective and anti-inflammatory effects in different rodent PD models. However, Nurr1 levels in the brain were also increased upon treatment with IP7e (80)⁴⁰⁰ pointing to other mechanisms than direct Nurr1 activation.

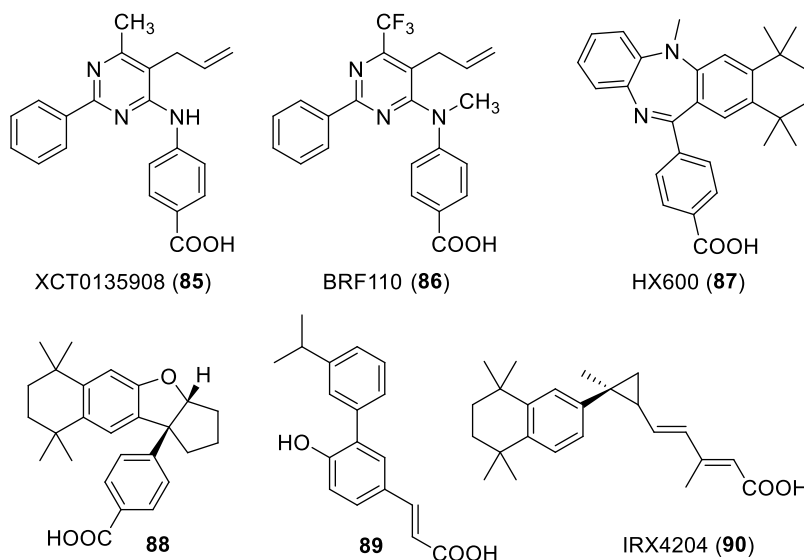
Scheme 8. Nurr1 Modulators Reported in the Literature^{360,396–398,418,422}

Exploration of Nurr1–RXR heterodimer-specific RXR agonists has further validated Nurr1 activation as a valuable approach to counteract neuroinflammation and PD in vitro and in vivo. XTC0139508 (85),⁴⁰¹ its descendant BRF110 (86),⁴⁰² and IRX4204 (90)⁴⁰³ were intensively studied in vitro for their neuroprotective effects in various neuronal cell cultures and induced Nurr1-regulated genes. Additionally, BRF110 (86)⁴⁰² and IRX4204 (90)⁴⁰³ improved motor function and reduced dopaminergic neuron loss in 6-OHDA and MPTP rodent models. HX600 (87) exhibited neuroprotective effects, too, by lowering levels of pro-inflammatory mediators in LPS-stimulated primary mouse microglia and by reducing ischemic neuronal damage and impaired motor function in an ischemic stroke model in mice.⁴⁰⁴

2.7.2.3. Nurr1 in Alzheimer's Disease. Beyond Nurr1's overall neuroprotective and anti-neuroinflammatory activity, its role in AD remains to be studied in detail (recently reviewed in ref 405). A number of studies indicates involvement of Nurr1 dysregulation as a contributing factor in the pathogenesis of AD. Two in vitro models of AD using A β _{1–42} fibril-treated cells observed downregulation of Nurr1 protein and mRNA levels in primary rat neurons and in a neuronally differentiated human mesenchymal cell line.⁴⁰⁶ In addition, Nurr1 mRNA levels in the hippocampus were reduced in mutant APP transgenic mice as a model of early memory loss in AD.⁴⁰⁷ Most notably, post-mortem analysis of AD patients revealed a significant decrease of Nurr1 expression in nigral neurons containing neurofibrillary tangles, which correlated with a loss of TH⁺ neurons.³⁸⁸ In line with this, 5XFAD mice displayed Nurr1 coexpression with A β accumulation in the subiculum and frontal cortex at early stages, and an age-dependent loss of Nurr1-expressing cells in later stages.⁴⁰⁸ Nurr1 knockdown by stereotactic Nurr1-shRNA injection in the subiculum amplified AD pathology in 5XFAD mice, whereas Nurr1 overexpression and Nurr1 activation with the agonist AQ (75) ameliorated AD symptoms with reduced A β accumulation, less neurodegeneration, and improved cognitive function.⁴⁰⁹

2.7.2.4. Nurr1 in Multiple Sclerosis. Studies on Nurr1 involvement in the context of MS reported contradictory findings. The Nurr1 activator IP7e (80) caused protective effects in EAE in mice by inhibiting NF κ B-mediated inflammation in early disease stage.⁴¹⁰ Accordingly, heterozygous Nurr1 knockout mice exhibited an early EAE disease onset with elevated inflammatory infiltrates in the spinal cord.⁴¹¹ In contrast, systemic RNAi-mediated Nurr1 knockdown in mice attenuated EAE, which was referred to a potential role of Nurr1 in Th17 cell differentiation via regulation of IL-21 and IL-23R expression.⁴¹² The Nurr1 agonist chloroquine (CQ, 76) activated Treg cell differentiation from naïve murine T cells in a Nurr1-dependent manner and significantly suppressed the progression of inflammatory bowel disease, another autoimmune disease, in a dextran sulfate sodium (DSS)-induced mouse model.⁴¹³

2.7.2.5. Nurr1 Ligands and Modulators. Although Nurr1 is considered as an orphan nuclear receptor and lacking a classical ligand-binding site, recent findings of potential endogenous ligands, evidence from cocrystal structures, and mechanistic studies revealed Nurr1 as a promising drug target. In 2015, Kim et al.³⁹⁶ demonstrated that Nurr1 can be directly modulated via its LBD by small molecules and discovered the two antimalarial drugs AQ (75) and CQ (76) as Nurr1 ligands in a drug screening in a full-length Nurr1 reporter gene assay using a monomer responsive reporter construct in human neuroblastoma SK-N-BE(2)C cells (Scheme 8). Both compounds were shown to interact directly with the LBD by NMR perturbation experiments and mutagenesis studies located the interaction site close to the canonical ligand-binding pocket, which was recently confirmed by Munoz-Tello et al.³⁵¹ In addition, we have recently discovered the two AQ-derived fragment-sized Nurr1 agonists 77 and 78 which provided new insights in the activation mechanism of Nurr1 by causing recruitment of NCoR-1 and SMRT upon agonist binding.⁴¹⁴ Another noncanonical binding pocket within the Nurr1 LBD was first discovered for the dopamine metabolite DHI (82) which covalently bound to Cys566 in a Nurr1 cocrystal

Scheme 9. Nurr1-RXR Heterodimer-Specific RXR Agonists Reported in the Literature^{402,403,435,436,438,439}

structure (pdb 6DDA) and thereby induced a pocket between helices 4, 11, and 12 involving outward movement of helix 12³⁹⁸ (compare Figure 3d, orange site). In vitro, DHI (82) stimulated Nurr1 activity in a Gal4-Nurr1 hybrid reporter gene assay in human choriocarcinoma JGE3 cells by 1.6-fold at 100 μ M.

First evidence for a potential endogenous Nurr1 ligand was reported for the unsaturated fatty acid DHA (45).⁴¹⁵ Solution NMR spectroscopy mapped the putative ligand-binding pocket close to the AQ binding site and recruitment of a PIAS γ peptide was found enhanced by DHA (45) binding. Two full-length reporter gene assays using a monomer responsive reporter construct in HEK293T cells and murine dopaminergic MN9D cells showed dose-dependent repression of Nurr1 activity by \sim 25% at 50 μ M DHA (45). Further structural analysis by NMR experiments, deuterium uptake mass spectrometry, and molecular dynamic simulations suggested that the putative canonical ligand-binding pocket is able to expand from its collapsed conformation to harbor the unsaturated fatty acid.^{416,417} Rajan et al. added two prostaglandins, namely, PGA1 (81) and PGE1, to the collection of Nurr1's endogenous ligands³⁹⁷ and found covalent binding of PGA1 (81) to Cys566 (pdb 5Y41) comparable to the ligand-binding pocket induced by DHI (82) with an even stronger 21° shift of helix 12. PGA1 (81) and PGE1 induced Nurr1 transactivation in two different reporter gene assays, Gal4-Nurr1 and full-length Nurr1, performed in murine dopaminergic MN9D cells and N27-A rat dopaminergic neurons with estimated EC₅₀ values of 5 μ M and 3 μ M. In line with this, we recently discovered several NSAIDs as Nurr1 modulators.³⁶⁰ Among them, the first-in-class inverse Nurr1 agonists oxaprozin (83) and parecoxib (84) counteracted intrinsic Nurr1 activity in four different reporter gene assay settings in HEK293T cells. Meclofenamic acid (85, Gal4-Nurr1 EC₅₀ 4.7 μ M) evolved as a Nurr1 modulator with differential activity on different Nurr1 response elements. The NSAIDs also affected the coregulator interaction profile of Nurr1 with NCoR-1, SMRT, NCoA6, and NRIP as well as the receptor's dimerization equilibrium in HTRF-based assays. Moreover, NSAIDs and AQ-type ligands exhibited simultaneous Nurr1 modulation with additive effects pointing to the

existence of two independent binding sites within the Nurr1 LBD.

In addition to these few orthogonally validated direct Nurr1 modulators, further compounds were reported to affect Nurr1 activity for which confirmation of direct interaction is lacking. The imidazopyridine SA00025 (79)⁴¹⁸ has been reported as a potent and selective Nurr1 agonist based on two luciferase reporter gene assays (Gal4-Nurr1fl (EC₅₀ 218 nM)⁴¹⁸ and monomer responsive reporter construct (EC₅₀ 0.7 nM)⁴¹⁹). The compound has favorable ADMET and pharmacokinetic properties^{418,420} except for a hErg liability (IC₅₀ 1.5 μ M) and was found to reach the brain of rats after oral administration where it significantly induced Nurr1-regulated gene expression in the substantia nigra after seven days of daily dosing.³⁹⁹ Direct binding to Nurr1 was studied for several compounds of the SA00025 (79) series by SPR,⁴¹⁹ but the reported data are incomplete, and a direct Nurr1 binding of the lead compound SR24237⁴¹⁸ could not be confirmed.³⁵¹

A benzimidazole-based combinatorial approach to Nurr1 modulators has reported SR10098⁴²¹ as one of three hits, and Nurr1 agonists with isoxazolopyridinone scaffold were derived from a high-throughput screening (HTS) campaign⁴²² with subsequent SAR studies. Both series reached low nanomolar potencies in a reporter gene assay in stably Nurr1-expressing MN9D cells. Among these compounds, IP7e (80, EC₅₀ 3.9 nM) showed brain bioavailability in mice⁴²² and was applied to the EAE⁴¹⁰ and a PD⁴⁰⁰ mouse model. Data from a recent NMR structural footprinting analysis puts a direct binding of SR10098, IP7e (80), and analogue SR10658 to the Nurr1 LBD into question, however.³⁵¹

As stated for Nur77 (see section 2.7.1), C-DIM derivatives were also extensively studied as Nurr1 modulators with contradictory results in pancreatic⁴²³ and bladder cancer⁴²⁴ cells, neuronal cells,^{425–427} and glioblastoma cells.⁴²⁸ Multiple anti-inflammatory and neuroprotective effects were also reported from PD mouse models.^{425,427,429} Mechanistic evaluation of NR4A modulation by C-DIM derivatives using various hybrid receptor constructs in reporter gene assays demonstrated that the NH₂-terminal domain was sufficient for transactivation.⁴²³ Through N-terminal Nurr1 modulation, C-DIM derivatives may hence exhibit direct effects on Nurr1 for

Table 8. Summarized Observations on Nurr1 in Neurodegeneration

Nurr1 (= NR4A2; also known as NOT, TINUR, and HZF-3)	
Nurr1 in AD	Nurr1 expression in nigral neurons was found diminished in AD patients. ³⁸⁸ Nurr1 mRNA levels in the hippocampus were decreased in APP transgenic mice. ⁴⁰⁷ Nurr1 was coexpressed with A β accumulation in the subiculum and frontal cortex in early-stage 5XFAD mice. ⁴⁰⁸ 5XFAD mice lose Nurr1 expressing cells in an age-dependent fashion. ⁴⁰⁸ shRNA-mediated Nurr1 knockdown in the subiculum worsened AD pathology in 5XFAD mice. ⁴⁰⁹ Nurr1 overexpression or activation (AQ (78)) improved AD symptoms (A β ↓, neurodegeneration ↓, cognitive function ↑) in 5XFAD mice. ⁴⁰⁹
Nurr1 in PD	Nurr1 knockout caused loss of dopaminergic neuron development and respiratory dysfunction and is lethal. ^{29,374} Nurr1 expression in nigral neurons was found decreased in PD patients and in rodent models of PD. ^{388–390} Diminished Nurr1 levels correlated with high α -synuclein levels and loss of TH ⁺ neurons. ^{388–390} Nurr1 overexpression protected neurons against toxic insults of α -synuclein in vitro and in rodent PD models. ^{389–393} Nurr1 agonists upregulated neuroprotective and dopaminergic genes in vitro and in vivo. ^{396–398,403,414} Nurr1 agonists decreased expression of pro-inflammatory cytokines in vitro. ^{396,397,404} Nurr1 agonists and heterodimer-specific Nurr1-RXR agonists exhibited neuroprotective effects and improved symptoms in 6-OHDA-induced PD in mice and rats ^{396,399,401–403} and attenuated motor deficits in MPTP-treated mice. ^{397,402}
Nurr1 in MS	Heterozygous Nurr1 knockout caused early EAE onset and enhanced inflammatory infiltrates in the spinal cord. ⁴¹¹ Systemic Nurr1 knockdown attenuated EAE via diminished Th17 cell differentiation. ⁴¹² Nurr1 activator IP7e (80) had protective effects in EAE by decreasing NF κ B activity. ⁴¹⁰

example in NF κ B transrepression⁴²⁹ (Figure 4b), but altered Nurr1 protein levels⁴²⁶ and indirect mechanisms rather than direct Nurr1 transactivation via its LBD appear to dominate the effects.³⁵¹

In addition, the antimetabolite 6-MP (91) was identified as a Nurr1 activator from an HTS utilizing a full-length reporter gene assay under the control of the homodimer responsive element in CV1 cells.³⁶¹ Closer evaluation of Nurr1³⁶¹ and NOR-1³⁶² modulation suggested a noncanonical mechanism of nuclear receptor activation through the N-terminal AF-1 domain not involving interaction with the LBD.

A number of other compounds, mostly chemotherapeutic agents, such as camptothecin,⁴³⁰ the metabolite 7-ethyl-10-hydroxy-camptothecin of irinotecan, and KU0171309⁴³¹ (from HTS) were found to inhibit Nurr1 transactivation. Apart from KU0171309 whose mode of Nurr1 modulation remains elusive, these agents were found to suppress Nurr1 activity via inhibition of the EGFR cascade. Furthermore, neuroprotective agents have been discovered which do not directly modulate Nurr1 activity but were shown to induce Nurr1 expression in vitro and in vivo. Among them were the anti-PD drug pramipexol,⁴³² for which Nurr1 upregulation was proposed to be mediated via the dopamine D₃ receptor, the phosphodiesterase-3 inhibitor cilostazol,⁴³³ and moracenin D,⁴³⁴ a flavonoid extracted from *Mori Cortex radialis*.

2.7.2.6. Nurr1-RXR Heterodimer-Specific RXR Ligands. As discussed above, Nurr1 can act as a permissive heterodimer with RXR opening another avenue to Nurr1 modulation via heterodimer activation with RXR agonists. Owing to the multitude of RXR heterodimers and associated effects, heterodimer preferential activity is very desirable in this context. Hence, a number of Nurr1-RXR heterodimer-specific RXR ligands (Scheme 9) have been reported which were shown to promote Nurr1 activity or enhance its function in PD models (outlined above). The aminopyrimidine derivative XCT0135908 (XCT, 85)⁴³⁵ selectively induced luciferase activity dependent on a Gal4-Nurr1-RXR α heterodimer in CV-1 cells. Its activity was blocked by the RXR antagonist LG1208. However, XCT (85) has low plasma stability and poor brain exposure after intraperitoneal administration, and even intracerebroventricular injection failed to show in vivo activity as the expression of Nurr1 regulated genes in midbrain such as TH was not changed.⁴⁰² BRF110 (86),⁴⁰² a close

analogue of XCT (85), activated a full-length Nurr1-RXR α reporter gene assay utilizing a heterodimer responsive reporter construct in the human dopaminergic neuroblastoma cell line SH-SY5Y with an EC₅₀ value of ~0.9 μ M. Its binding to RXR α is only supported by molecular docking studies, but lentiviral knockdown of Nurr1 demonstrated involvement of Nurr1 in heterodimer activation. Pharmacokinetic properties of BRF110 (86) after intraperitoneal administration in mice were improved compared to 85 with CNS bioavailability and a moderate half-life of 1.5 h in plasma and brain. The dibenzodiazepine RXR ligand HX600 (87) was also found to selectively activate Nurr1- and Nur77-RXR heterodimers in several cellular settings.^{436,437} The chiral dihydrobenzofuran 88⁴³⁸ was designed as a full RXR agonist from a series of conformationally constrained RXR ligands with a slight (3-fold) preference for the Nurr1-RXR heterodimer (pEC₅₀ 7.9, 111% efficacy) compared to the RXR homodimer (pEC₅₀ 7.6, 85% efficacy) in a bioluminescence resonance energy transfer (BRET) assay. Cocrystal structure analysis of RXR α in complex with dihydrobenzofuran 88 and the TIF2 coactivator peptide (pdb 5EC9) confirmed orthosteric binding to RXR and a typical agonist conformation. The synthetic honokiol derivative 89 with a biaryl scaffold demonstrated a greater 25-fold selectivity for the Nurr1-RXR α heterodimer (pEC₅₀ 9.1, 129% efficacy) compared to the RXR α homodimer (pEC₅₀ 7.7, 291% efficacy) determined in a BRET assay.⁴³⁹ The respective cocrystal structure analysis indicated that compact ligands, allowing movement of helix 7 and 11, favor RXR α heterodimerization with Nurr1 (pdb 5MKU), whereas ligands with substituents in the 2' position on the biaryl scaffold induced pocket expansion with helix 12 movement, resulting in lower binding affinity or antagonistic behavior (pdb 5MKJ) and promoting RXR α homodimerization.

The RXR ligand IRX4204 (90) has been studied most extensively in the context of neurodegeneration. Profiling of IRX4204 (90) demonstrated potent induction of Nurr1-dependent transcriptional activity (EC₅₀ < 1 nM) in COS7 cells transfected with full-length Nurr1 and RXR α constructs and, surprisingly, a monomer responsive (NBRE) reporter construct.⁴⁰³ Pharmacokinetic parameters (determined in rats) of IRX4204 (90) were favorable with bioavailability in the brain at reasonable concentrations (11.5 \pm 2.9 nM) after oral administration of IRX4204 (90), which was sufficient to

induce Nurr1-regulated gene expression in the substantia nigra. In addition to IRX4204 (90), also the most widely used RXR agonist bexarotene (42) was found to favor the Nurr1-RXR heterodimer (pEC_{50} 8.3) over the RXR homodimer (pEC_{50} 7.5) in a BRET assay in HEK293T cells.⁴⁴⁰ In vivo experiments demonstrated that bexarotene (42) upregulated Nurr1-dependent genes DAT and VMAT2, rescued dopaminergic neuronal loss, and reversed behavioral deficits in 6-OHDA-lesioned rats. However, the neuroprotective effects of bexarotene (42) cannot be ascribed to Nurr1-mediated effects alone as the LXR-RXR and PPAR-RXR heterodimers are also effectively activated by bexarotene (42). Volakakis et al.³⁹¹ observed no effect of bexarotene (42) on dopamine neuron loss and motor impairment in 6-OHDA-injected rats but found bexarotene (42) able to restore disrupted Ret expression and neurotrophic GDNF signaling.

2.7.2.7. Conclusion. Nurr1 is an emerging drug target being extensively studied in the context of neurodegenerative diseases (summarized in Table 8) in which it holds enormous potential as a key regulator of dopaminergic neuron function. However, the available Nurr1 modulator tools are of insufficient quality to fully explore the potential of Nurr1 modulation, and the limited quality of (putative) Nurr1 modulators used in preclinical studies weakens the significance of these experiments. More potent, more selective, and particularly better characterized tools are needed for pharmacological validation of Nurr1 in neurodegeneration and other pathologies. Pending further validation of Nurr1 as a therapeutic target, potent and selective Nurr1 agonists may hold remarkable potential as a disease-modifying approach especially in PD.

2.7.3. NOR-1 (NR4A3). **2.7.3.1. Overview.** The neuron derived orphan receptor 1 (NOR-1, NR4A3) is a very poorly studied NR, whose developmental and physiological functions remain widely elusive.⁴⁴¹ As third member of the NR4A subfamily, it shares many characteristics of the other two members of this family, with the exception that NOR-1 appears not to form heterodimers with RXR in contrast to Nurr1 and Nur77³⁸⁵ (compare Figure 4a). Similar as for Nur77 and Nurr1, structural analysis of NOR-1 suggested that the receptor lacks an accessible ligand binding pocket. NOR-1 adopts a self-activated conformation in the absence of a ligand to be constitutively active (compare Figure 3c). Its transcriptional activity hence primarily depends on the expression level.⁴⁴² NOR-1 mRNA is expressed in many rodent tissues. A notably high abundance was observed in the developing rat brain, whereas NOR-1 levels in the adult brain were lower.⁴⁴³ NOR-1 is mainly expressed in the cerebral neocortex, hippocampus, amygdala, cerebellum, and dopaminergic areas, for example, striatum, nucleus accumbens, olfactory tubercle, and prefrontal and cingulate cortices.^{443,444} In contrast, NOR-1 mRNA levels in dopaminergic neurons of the midbrain are low.⁴⁴³ Additionally, NOR-1 is present in the neuronal cytoplasm throughout the brain and spinal cord.⁴⁴³ Although one study has reported NOR-1 knockout as embryolethal,^{385,445} most knowledge on the therapeutic potential of the orphan receptor results from knockout studies.

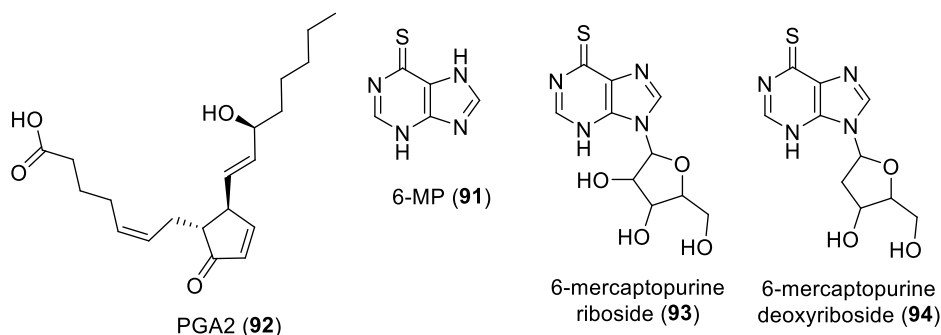
2.7.3.2. NOR-1 and Neurodegeneration. According to the scarce available knowledge, NOR-1 is involved in inflammation, vascular biology, immunity, and lipid and glucose metabolism, suggesting that dysregulation of NOR-1 could lead to diseases such as obesity, diabetes, cardiovascular disease, and cancer.⁴⁴² In addition, some preliminary evidence

indicates that NOR-1 might be involved in the pathogenesis of neurodegenerative diseases. NOR-1 was found to play an important role during development of the CNS by mediating neuronal differentiation and maintaining neuronal plasticity in the adult CNS.⁴⁴¹ In mice, NOR-1 knockout led to impaired axonal growth in the hippocampus, postnatal neuronal cell death, and a compact pyramidal cell layer of Ammon's horn was not formed at CA1 and CA3 in NOR-1^{-/-} mice.⁴⁴¹ This suggests a specific role for NOR-1 in the survival of CA1 pyramidal cells.⁴⁴¹ In addition, an increased liability to limbic seizures as well as a compromised axonal guidance in the dentate gyrus and in the mossy fibers were observed in NOR-1 knockout mice.⁴⁴³ Further important evidence for an involvement of NOR-1 in neurodegenerative diseases evolves from its accumulation in Lewy bodies of patients with PD and dementia with Lewy bodies (DLB), and in glial and neuronal cytoplasmic inclusions in multiple system atrophy (MSA).⁴⁴³ Moreover, NOR-1 induced the anti-apoptotic protein cIAP2 in neuronal cells under oxidative stress, hypoxia, and ischemia⁴⁴⁶ and was upregulated by the transcription factor cAMP response element binding protein (CREB) which is considered as an important factor for neuronal survival and neuroprotection.³⁹² CREB-regulated expression of NOR-1 and the other NR4A receptors was detected in neuronal cells, raising the assumption that the NR4A family receptors function as mediators of CREB-induced neuroprotection and neuronal survival.^{392,446}

2.7.3.3. NOR-1 Ligands and Modulators. NOR-1 is classified as an orphan nuclear receptor, and no potent ligand for NOR-1 has been discovered so far. Two NOR-1-activating compounds have been reported in the literature, the anti-inflammatory and antineoplastic drug 6-MP (91)³⁶² and the eicosanoid prostaglandin A2 (PGA2, 92).⁴⁴⁷ PGA2 (92) was shown to bind to the NOR-1 LBD and to activate NOR-1-dependent gene transcription at 10 μ M concentration.⁴⁴⁷ PGA2 (92) activated the full-length NOR-1 in the presence and absence of RXR α , indicating that RXR α was not necessary for its activity, which agrees with the assumed monomeric activity of NOR-1.⁴⁴⁷ Furthermore, it was shown that a NOR-1 mutant lacking the LBD was not activated by PGA2 (92).⁴⁴⁷ The effect exerted by PGA2 (92) on NOR-1 is rather weak, however. In contrast to PGA2 (92), which likely activates NOR-1 through its LBD, 6-MP (91) required the N-terminal AF-1 domain for NOR-1 activation.³⁶² More specifically, the region between amino acid residues 1 and 150 mediated the NOR-1 activation by 6-MP (91).³⁶² In a Gal4-NOR-1-AF-1-assay, 6-MP (91) achieved a strong 113-fold NOR-1 activation at 50 μ M in proliferating murine C2C12 myoblasts.³⁶² The 6-MP analogues 6-mercaptopurine riboside (93) and 6-mercaptopurine deoxyriboside (94) also activated the N-terminal NOR-1 region.³⁶²

2.7.3.4. Conclusion. NOR-1 is a very poorly studied orphan nuclear receptor, and little is known about its therapeutic potential (summarized in Table 9). Knockout studies provide preliminary evidence that NOR-1 is involved in neuronal cell survival and might therefore be an attractive target in neurodegenerative diseases. Particularly, the observed accumulation of NOR-1 in Lewy bodies of PD patients and in neuronal cytoplasmic inclusions in MSA as well as its function as a mediator of CREB-induced neuroprotection support this assumption. However, only observations on decreased NOR-1 activity (knockout) are available so far since potent and selective NOR-1 activators are lacking. NOR-1 agonist and

Scheme 10. NOR-1 Activating Compounds



inverse agonist tools are urgently required to capture the orphan receptor's potential in neurodegenerative diseases.

Table 9. Summarized Observations on NOR-1 in Neurodegeneration

NOR-1 (= NR4A3; also known as TEC, MINOR, and CHN)	
NOR-1 in neurodegeneration	NOR-1 knockout in mice ⁴⁴¹ impaired axonal growth in hippocampus, caused postnatal neuronal cell death, and compromised axonal guidance in dentate gyrus and mossy fibers. NOR-1 expression is enhanced by the stress-induced transcription factor CREB, which is an important factor for neuronal survival and neuroprotection. ^{392,446}

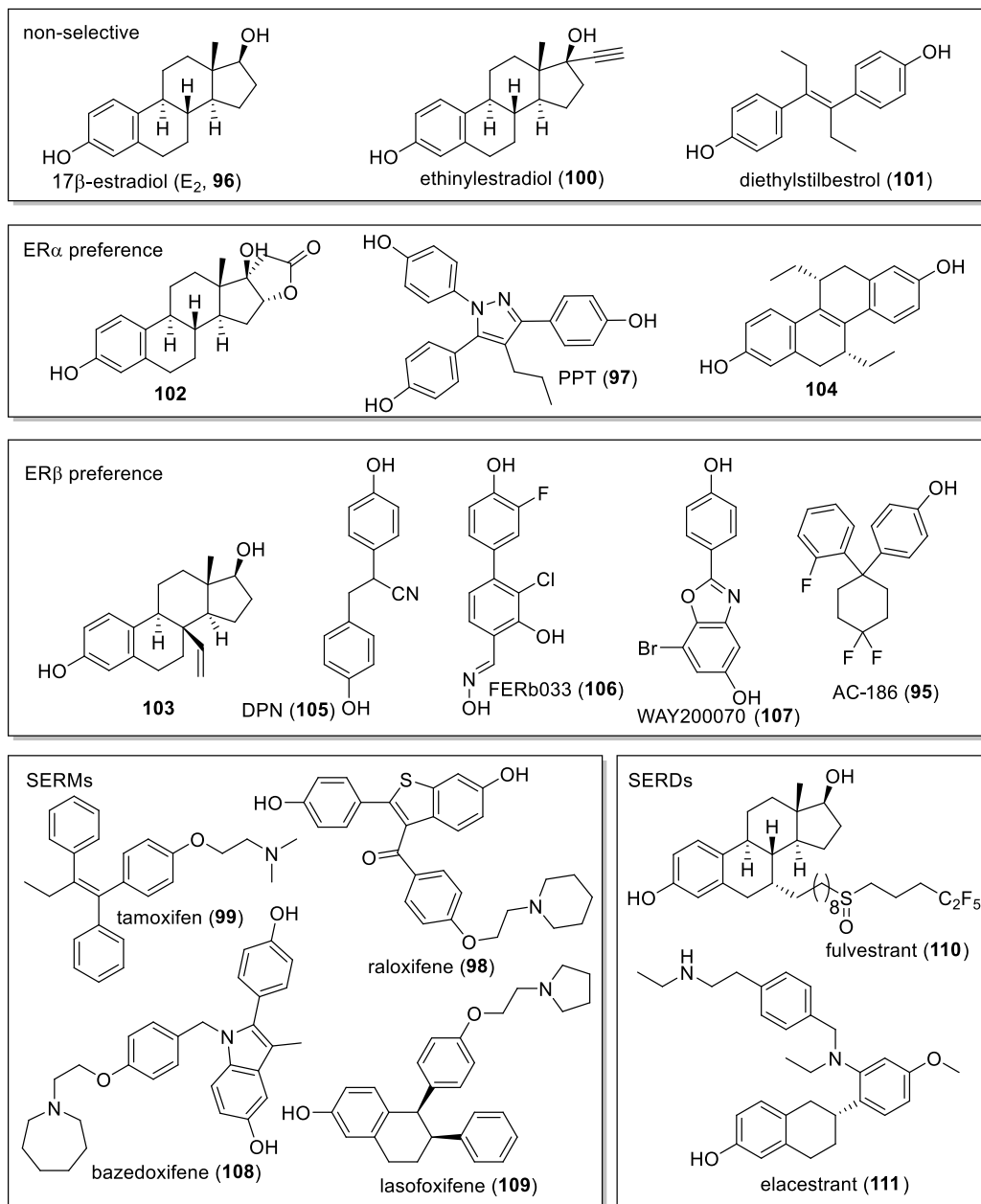
2.8. Estrogen receptors (ER, NR3A). 2.8.1. Overview.

Estrogen receptors (ER)^{448–450} comprise two subtypes ER α and ER β (ER α , NR3A1; ER β , NR3A2), which together with the G protein coupled estrogen receptor GPER mediate the effects of estrogens and estrogenic compounds. Although estrogens are primarily female hormones, ERs are crucial transcription factors not only in females but have relevance also in males as illustrated by the infertility of male ER α knockout mice.^{449–451} With ER agonists as part of contraceptives and ER antagonists as well as the selective ER modulators (SERMs) as anticancer drugs, ERs have considerable relevance as drug targets.^{448,449} ERs are found in female reproductive organs, as well as in bone, brain, liver, colon, skin, and salivary gland with different subtype distributions.^{448,449} Although ER α and ER β share high structural similarity, selective targeting has been achieved with synthetic ligands.^{448,449} As steroid receptors, ERs act as homodimers on their response element ERE (GGTCAnnnTGACC) but also exhibit other mechanisms of activity including indirect interaction with the DNA via binding to other transcription factors (“tethering”) as well as rapid nongenomic effects.^{448–450} The fact that several neurodegenerative and neuroinflammatory diseases (e.g., MS, AD) have a higher incidence in women^{452,453} may suggest an involvement of sexual hormones in their pathogenesis and point to a potential role of ERs as pharmacological targets in neurodegeneration. Mainly based on epidemiological observations, postmenopausal decline in estrogen levels is hypothesized as a potential link to higher prevalence of AD in women.^{452,454} Additionally, evidence for an association between ER variants and AD has been reported.⁴⁵⁵ ER modulation, therefore, is considered as promising therapeutic strategy particularly in age-related neurodegenerative diseases.⁴⁵⁴

2.8.2. ER in Alzheimer's Disease. The mechanisms by which estrogens contribute neuroprotective, anti-neuroinflammatory, and anti-neurodegenerative effects are multifaceted. In vitro, estrogens protected cultured neurons against several toxic insults including oxidative stress, excitotoxicity, and A β -mediated toxicity.^{456–461} These effects were shown to be at least in part dependent on ER activation^{459,462,463} and to involve ER-mediated induction of Bcl-2 proteins⁴⁶⁴ that promote cell survival. Neuroprotective effects were individually demonstrated for both ER subtypes. In cultured rat cortical neurons, selective ER β activation was sufficient for neuroprotective effects against A β ,⁴⁶⁵ while in SH-SY5Y neuroblastoma cells, ER α activation protected against A β toxicity also in the absence of ER β .⁴⁶⁶ Estrogens also exhibited neuroprotective effects in several rodent models of neurotoxicity,^{459,467–470} which could be linked to ER activation.⁴⁵⁹ While some observations point to a more prominent role of ER α in neuroprotection,^{471,472} activation of both ER subtypes exhibited similar neuroprotective effects in several studies, and their individual contributions have not been elucidated.^{473–475} The signaling pathways of ER α - and ER β -mediated neuroprotection seem to differ,^{454,466,472,473,476–478} however, suggesting potentially additive effects for activation of both isoforms. Additionally, extranuclear mechanisms of ERs have been reported to involve in neuroprotection⁴⁷⁹ among which mitochondrial activities of ER β seem to be of particular importance.⁴⁸⁰ Estrogens were also found to decrease A β formation and to promote its clearance in several studies,^{481–487} whereas estrogen deficiency in the brain enhanced plaque formation in a transgenic AD mouse model.⁴⁸⁸ Estrogen effects on A β levels likely involve ER-mediated upregulation of degrading enzymes (insulin-degrading enzyme and neprilysin),^{454,489} but experimental observations also indicate participation of rapid, nongenomic mechanisms.^{481–486} A recent in vitro study⁴⁹⁰ has shown that ER β activation with diethylpropionitrile or ER β overexpression can promote autophagy of extracellular A β , while ER β silencing had the opposite effect.

2.8.3. ER in Parkinson's Disease. In the context of PD, which in contrast to AD and MS has a higher prevalence in men,⁴⁹¹ effects of estrogen use are controversial,^{492–495} and clinical trials^{496,497} have failed to demonstrate pronounced therapeutic efficacy of estrogens despite the broad evidence for neuroprotective activity of ER activation in other pathologies. Preclinical studies observed sex differences in estrogen effects in rodent PD models and varying efficacy depending on the treatment start, suggesting that the response to estrogens in the brain is lost over time and that estrogen therapy may have

Scheme 11. ER Ligands



protective effects only when applied during early menopause.⁴⁹⁵ Alterations in brain ER levels might hence affect treatment outcomes.⁴⁹⁵ Use of ER agonists or SERMs in most rodent PD models was not associated with therapeutic effects,^{495,498–500} and only few studies have reported beneficial activities of ER modulation in PD. In 6-OHDA-induced disease in rats, AC-186 (**95**), a selective ER β agonist counteracted the loss of dopaminergic neurons in the substantia nigra, cognitive impairment, and motor deficits.⁵⁰¹ Interestingly, AC-186 (**95**) was superior to 17 β -estradiol (**96**), suggesting an advantage of ER β selectivity, and the beneficial effects were only present in male animals. Baraka et al.⁵⁰⁰ applied different types of ER ligands to 6-OHDA-induced PD in rats. They report therapeutic effects as determined by behavioral observations and biochemical parameters for 17 β -estradiol (**96**), the selective ER α agonists propylpyrazoletriol (PPT, **97**), and the SERM raloxifene (**98**), while the ER β

selective agonist diarylpropionitrile (DPN, **105**) and tamoxifen (**99**) were not active. Overall, strong evidence for ERs as promising targets for PD is lacking.

2.8.4. ER in Neuroinflammation and Multiple Sclerosis. Estrogens also exhibit pronounced anti-neuroinflammatory activity which is mainly attributed to their effects on astrocytes and microglial cells.^{453,502–505} ER agonists suppressed the release of pro-inflammatory cytokines after LPS stimulation from primary human astrocyte cultures⁵⁰⁶ and inhibited LPS-induced astrocyte activation in rats.⁵⁰⁷ Effects of estrogens and ER agonists have hence been broadly studied in the context of MS. Estrogen treatment was effective in several studies in the EAE model of MS in mice^{508–511} and downregulated pro-inflammatory cytokine production.⁵⁰⁹ Therein, also treatment after disease onset was sufficient to reduce severity.⁵¹² Tiwari-Woodruff et al.⁴⁷⁶ observed differences of ER α and ER β activation in EAE. ER α agonist treatment reduced severity of

the disease from onset on, while ER β agonist treatment had no effect in the early disease stage. At a later stage, ER β activation caused a pronounced protective effect, however, as observed by faster recovery. ER β knockout abolished this effect. ER α agonist treatment modulated cytokine levels toward an anti-inflammatory profile, suggesting a systemic immune-modulatory effect, whereas ER β agonist treatment did not alter cytokine levels compared to vehicle. Both types of selective ER ligands reduced demyelination and axonal loss. Overall, these observations suggest beneficial effects of ER signaling for both subtypes^{511,513} in neurodegeneration with a stronger anti-neuroinflammatory component for ER α and more pronounced neuroprotective activity for ER β . The promising observations on estrogen actions in MS have also led to a number of clinical trials^{514–517} to study estrogen treatment in female MS patients, which reported some beneficial effects but were not fully consistent. Circulating estrogen levels were found to inversely correlate with the number of active lesions and relapses. Estrogen treatment reduced the size of lesions and the annual number of relapses.

2.8.5. ER Ligands. Regarding medicinal chemistry, ERs are among the most well-studied NRs and the first NRs for which selective modulation has been broadly established with the selective estrogen receptor modulators (SERMs). Estrogens as the endogenous ER ligands are highly active on both isoforms and also have pharmacological relevance as drugs, but their use is limited by severe adverse effects including elevated risk for breast and endometrial cancer, thromboembolisms, and strokes.^{518,519} The ligand binding domains of ER α and ER β display only 59% sequence identity, which would suggest large differences. The ligand binding sites, however, differ in only two lipophilic residues (ER α : Leu384 and Met421 vs ER β : Met336 and Ile373). In addition to these minor changes, differences in pocket shape and volume provide access to subtype preferential ligands. Advanced structural understanding of ERs and their modulation by ligands has been obtained from extensive cocrystal structure analysis and mechanistic studies,^{520–523} which draw specific pharmacophore models and allow the design of subtype preferential modulators exhibiting agonism or antagonism on the ERs.⁵¹⁹ The two ER subtypes also differ in their expression patterns throughout the body which enables tissue selective ER modulation and can improve safety.^{449,524} Because of their reduced systemic adverse effects, selective ER β agonists might hold potential in neurodegenerative diseases. As outlined above, ER β activation revealed protective effects in EAE models and against A β toxicity suggesting beneficial effects in MS and AD, respectively. However, both ERs are expressed in the CNS and are involved in anti-neuroinflammatory or anti-neurodegenerative effects. ER α activation exhibited stronger therapeutic effects in EAE, and several studies suggest different mechanisms for ER α - and ER β -mediated effects in the CNS. ER subtype preferential ligands and SERMs might, therefore, not be sufficient to establish safe and effective ER modulators for therapeutic application in neurodegenerative diseases.

The large available collection of small molecule ER ligands comprises steroidal and nonsteroidal compounds and agonists, antagonists, and modulators (Scheme 11). The medicinal chemistry of ER ligands has been extensively summarized in several reviews.^{519,525,526} The most active natural estrogen 17 β -estradiol (**96**) and its derivative ethinylestradiol (**100**) as well as diethylstilbestrol (**101**) are widely used nonselective agonists for ER α and ER β . Subtype preferential steroidal ER

ligands were developed from estradiol by introduction of a γ -lactone over ring D (**102**, ER α preference) and a vinyl substituent in 8 β -position (**103**, ER β preference).⁵¹⁹ Medicinal chemistry efforts have also yielded several chemotypes of nonsteroidal subtype preferential ER agonists such as propylpyrazoletriol (**97**, PPT, ER α preference),⁵²⁷ the rigid stilbene analogue **104** (ER α preference),⁵²⁸ diarylpropionitrile (**105**, DPN, ER β preference),⁵²⁹ FERb033 (**106**, ER β preference),⁵³⁰ prinaberel and its descendant WAY200070 (**107**, ER β preference),⁵³¹ and AC-186 (**95**, ER β preference).⁵⁰¹ Activity in the CNS has been demonstrated for example for ER β agonist DPN (**105**) in EAE⁴⁷⁶ and for ER β agonist AC-186 (**95**) in 6-OHDA-induced PD in rats,⁵⁰¹ suggesting them as preferable tools to further probe ERs in neurodegeneration. A key innovation in targeting ERs were the SERMs^{532,533} tamoxifen (**99**), raloxifene (**98**),^{527,534} bazedoxifene (**108**), and lasofoxifene (**109**),⁵³⁵ which exhibit specific activity profiles on the ER subtypes in different tissues. Owing to the bulky residues added to the ER ligand pharmacophore, SERMs antagonize ER activity by preventing the binding of the activation function in helix H12 to the core of the ER LBD. In the resulting antagonist conformation, the ER LBD exhibits a different coregulator recruitment profile with a preference for corepressor binding.^{532,533} Therein, ER modulation by SERMs varies in different tissues, which is rationalized by differential coregulator equipment of different cell types and tissues. They act as ER antagonists in breast tissue, as partial agonists in bone, and activity in endometrium varies depending on the SERM.^{532,533} Brain penetration and activation of ER signaling in the CNS were recently demonstrated⁵³⁶ for the SERM bazedoxifene (**108**), which could hence serve as an attractive tool to further probe ER modulation in neurodegeneration. Following the SERMs as ER modulatory drugs, the antiestrogen fulvestrant (**110**)⁵³⁷ acting as a selective estrogen receptor degrader (SERD) has introduced another strategy to inhibit ER activity, and several further SERDs have been developed⁵³³ of which elacestrant (**111**)⁵³⁸ was found to cross the blood–brain barrier⁵³⁹ suggesting it as a potential tool to study inhibition of ER signaling in the CNS.

2.8.6. Conclusion. While evidence for a role of ER in PD is rather weak, the higher incidence of AD and MS in women and observations from multiple preclinical studies indicate a therapeutic potential of ER modulation in these neurodegenerative pathologies (summarized in Table 10). However, clinical trials have mostly failed to translate the beneficial effects from animal models to patients so far. Varying levels of circulating hormones in the patient cohorts might be an important factor for these failures and suggest that certain patient subgroups might benefit from ER modulation in neurodegeneration. The multitude of estrogen activities and potential adverse effects of ER activation must be considered as a potential limiting factor for ER agonist use in neurodegeneration. Selective targeting of ER in the brain might be an avenue to overcome such obstacles, but whether ER activation in the CNS is sufficient for the beneficial effects in neurodegeneration or whether peripheral effects are contributing remains elusive.

3. SUMMARY AND PERSPECTIVES

The NR superfamily with its 48 ligand-activated transcription factors in human presents as a very attractive panel of potential therapeutic targets. Owing to the pronounced and durable effects that modulation of NRs exhibits on gene expression and

Table 10. Summarized Observations on ER in Neurodegeneration

ER α (= NR3A1; also known as ESR1) and ER β (= NR3A2; also known as ESR2 and Erb)	
ER in AD	AD prevalence is higher in women than in men. ⁴⁵²
	ER activation protected against oxidative stress, excitotoxicity, and A β -mediated toxicity in cultured neurons ^{459,462,463} and in rodent models of neurotoxicity. ^{459,467–470}
	ER activation decreased A β formation and promoted its clearance in vivo. ^{481–487}
	Estrogen deficiency in the brain enhanced plaque formation in transgenic AD mice. ⁴⁸⁸
ER in PD	PD prevalence is higher in men than in women. ⁴⁹¹
	No therapeutic benefit of ER activation in clinical trials. ^{496,497}
	ER β activation counteracted loss of dopaminergic neurons, cognitive impairment, and motor deficits in 6-OHDA induced PD in rats. ⁵⁰¹
ER in MS	MS prevalence is higher in women than in men. ⁴⁵³
	ER activation suppressed the inflammatory response of astrocytes in vitro ⁵⁰⁶ and in vivo. ⁵⁰⁷
	ER activation ameliorated EAE and downregulated pro-inflammatory cytokine release. ^{508–511}
	ER α activation reduced EAE severity from onset on; ER β activation improved recovery from EAE at a later stage. ⁴⁷⁶
	Clinical trials on ER activation in female MS patients reported some beneficial but inconsistent outcomes. ^{514–517}

hence on cellular phenotypes, it appears particularly suitable in the treatment of chronic diseases. Accordingly, NR ligands are used as drugs in cancer treatment (e.g., RXR, ER, androgen receptor), as potent anti-inflammatory agents (e.g., glucocorticoid receptor), and to counteract metabolic imbalance (e.g., PPAR, farnesoid X receptor). Neurodegenerative diseases such as AD, PD, and MS are chronic pathologies and closely linked to chronic inflammation or metabolic imbalance, suggesting a high potential of NR modulation in these diseases, too. Although early evidence for therapeutic effects of NR modulation in neurodegeneration dates back several decades, a major breakthrough has not been achieved, yet, and no NR ligand is used as a drug in such indications. However, preclinical research on NRs as therapeutic targets in neurodegeneration is constantly increasing, and cumulative evidence from pilot clinical trials and cohort studies on polymorphisms or altered NR expression in patients strongly supports the high potential of several NRs as future anti-neurodegenerative and anti-neuroinflammatory targets. The level of evidence for such therapeutic potential, naturally, varies for the different NRs, and most studies in the field have been performed for well-studied proteins such as PPAR and RXR. Nevertheless, recent findings particularly highlight also the orphan receptors Nurr1 and TLX, which are predominantly found in the brain as very promising targets for neurodegenerative disease treatment.

Despite very encouraging preclinical observations and evidence from human patients for the therapeutic potential of several NRs in neurodegeneration, pharmacological validation of these findings is often an obstacle and remains widely incomplete. This is mostly due to a lack of (custom) tool compounds with suitable properties to provide unambiguous data supporting observations from knockout studies or genetic overexpression. Especially the most promising targets such as the orphan receptors Nurr1 and TLX are poorly studied in terms of pharmacological control since potent modulators are not available. It is hence imperative to strengthen ligand discovery and tool compound development efforts for these NRs with the potentially greatest therapeutic promise in neurodegeneration. In addition, the mode-of-action

or selectivity of several available tools that have already been used in preclinical models of neurodegeneration is questionable, especially for LXR, revERB, and NR4A receptors, which compromises the significance of studies based on these compounds. Achieving strong selectivity within the protein family may be challenging for some NR ligands, especially within NR families (such as NR4A) but is a key aspect for their proper applicability as pharmacological tools. For example, some evidence points to different roles of LXR subtypes and ER subtypes in the CNS, and recent observations suggest that the NR4A receptors Nur77 and Nurr1 may even have counteracting roles in neuroprotection and neurodegeneration. Such scenarios might also hold true for other closely related NRs, which highlights the importance of selectivity for tool compounds in this context. Some preclinical observations made with nonselective or poorly characterized tools hence cannot be clearly interpreted. Therefore, dedicated (custom) tool compounds to probe the potential of NRs in neurodegeneration are urgently required and must fulfill key criteria such as selectivity and clear mode-of-action but also sufficient BBB penetration.

Another open question often is the desired site/tissue of action for NR modulators to obtain therapeutic effects in neurodegeneration. The RXR agonist bexarotene (42), for example, exhibited some attractive therapeutic effects in vivo, but pharmacokinetic analysis demonstrated very limited CNS exposure suggesting involvement of systemic anti-inflammatory or metabolic effects. For certain widely expressed NRs (RXR, PPAR, LXR, VDR), specific brain targeting may hence not be necessary but should still be studied with suitable CNS penetrant tools to decipher systemic contributions and brain-directed effects of their therapeutic activities. In some cases (e.g., ER, PPAR, LXR), systemic effects might even be the dominant mode-of-action leading to improvements in neurodegenerative pathologies. Therein, adverse effects of systemic actions must also be considered when a long-term modulation of a NR is desired for anti-neurodegenerative activity. In contrast, less distributed NRs with a particularly high abundance in the brain (e.g., Nurr1) or even almost exclusive expression in the brain (e.g., TLX) will require ligands that are able to reach sufficient CNS concentrations which presents as an additional challenge to medicinal chemistry but has, for example, been achieved with dedicated brain-penetrant PPAR agonists. The dominant expression of these NRs in the brain on the other hand might be predictive of lower adverse effects upon their therapeutic modulation since systemic on-target effects are reduced. This may suggest potentially greater safety and hence a greater therapeutic potential for these orphan NRs as targets to treat neurodegeneration.

In summary, ligand-activated transcription factors present as highly attractive molecular targets to counteract neurodegenerative pathologies and thereby hold great promise to address high unmet medical needs in severe health burdens. Despite very promising findings for various nuclear receptors in preclinical models of neurodegeneration, we lack high-quality tool compounds to validate nuclear receptor modulation as a therapeutic strategy. Medicinal chemistry efforts must provide potent, selective, and brain-penetrant pharmacological tools especially for insufficiently studied orphan nuclear receptors to capture the full therapeutic potential of these proteins in neurodegeneration and beyond.

AUTHOR INFORMATION

Corresponding Author

Daniel Merk – Institute of Pharmaceutical Chemistry, Goethe University Frankfurt, 60438 Frankfurt, Germany;
orcid.org/0000-0002-5359-8128; Email: merk@pharmchem.uni-frankfurt.de

Authors

Sabine Willems – Institute of Pharmaceutical Chemistry, Goethe University Frankfurt, 60438 Frankfurt, Germany
Daniel Zaienne – Institute of Pharmaceutical Chemistry, Goethe University Frankfurt, 60438 Frankfurt, Germany

Complete contact information is available at:

<https://pubs.acs.org/10.1021/acs.jmedchem.1c00186>

Author Contributions

#S.W. and D.Z. contributed equally to this work.

Notes

The authors declare no competing financial interest.

Biographies

Sabine Willems studied Pharmacy at Goethe University Frankfurt between 2012 and 2016 and received her license as a pharmacist in 2017. Currently, she is a Ph.D. student in Medicinal Chemistry at the Institute of Pharmaceutical Chemistry at the Goethe University focusing on the development and characterization of (orphan) nuclear receptor ligands.

Daniel Zaienne obtained Bachelor and Master of Science degrees in Chemistry from Goethe University Frankfurt in 2017 and in 2019, respectively. He then joined the Institute of Pharmaceutical Chemistry at Goethe University Frankfurt as a Ph.D. student, where he currently focuses on the synthesis and characterization of nuclear receptor ligands.

Daniel Merk graduated in Pharmaceutical Sciences and Pharmacy from LMU Munich in 2011 and obtained his Ph.D. in Pharmaceutical and Medicinal Chemistry from Goethe University Frankfurt in 2015. He was a Junior Group Leader in Pharmaceutical Chemistry at Goethe University Frankfurt and Postdoctoral ETH Fellowship Scholar at the Institute of Pharmaceutical Sciences of the Swiss Federal Institute of Technology (ETH) Zurich before he finished his Habilitation in Pharmaceutical Chemistry at Goethe University Frankfurt in 2019. Since then, he has been Independent Group Leader in Pharmaceutical Chemistry at Goethe University Frankfurt focusing on the Medicinal Chemistry and Pharmacology of nuclear receptors and their ligands. Recently, he joined LMU Munich as Chair of Pharmaceutical and Medicinal Chemistry.

ABBREVIATIONS

6-MP, 6-mercaptopurine; 6-OHDA, 6-hydroxy dopamine; 9-cis RA, 9-cis retinoic acid; AADC, aromatic L-amino acid decarboxylase; ABC, ATP-binding cassette transporter; AD, Alzheimer's disease; ADMET, absorption, distribution, metabolism, excretion, and toxicity; AF, activation function; APP, amyloid precursor protein; ATP, adenosine triphosphate; A β , amyloid- β ; Bcl-2, B-cell lymphoma 2; BBB, blood–brain barrier; BRET, bioluminescence resonance energy transfer; CD, circular dichroism; C-DIM, 1,1-bis(3'-indolyl)-1-(p-substituted phenyl)-methane derivatives; CNS, central nervous system; CoREST, REST corepressor; COX, cyclooxygenase; CREB, cAMP response element binding protein; CSF, cerebrospinal fluid; DAT, dopamine transporter; DBD, DNA binding domain; DHA, docosahexaenoic acid; DR3/5, direct

repeats spaced by 3/5 nucleotides; EAE, experimental autoimmune encephalomyelitis; EGFR, epidermal growth factor receptor; ER, estrogen receptor; fl, full length; GDNF, glial cell-derived neurotrophic factor; HTS, high-throughput screening; IFN, interferon; IL, interleukin; iNOS, inducible NO-synthase; I κ B α , inhibitor of NF- κ B; LBD, ligand binding domain; LPS, lipopolysaccharide; LXR, liver X receptor; MOG, myelin oligodendrocyte glycoprotein; MPP⁺, 1-methyl-4-phenylpyridinium; MPTP, 1-methyl-4-phenyl-1,2,3,6-tetrahydropyridine; MS, multiple sclerosis; NBRE, NGFI-B responsive element; NCoR, nuclear receptor corepressor; NF κ B, nuclear factor- κ B; NGFI-B, nerve growth factor-induced clone B; NMDA, N-methyl-D-aspartate; NOR-1, neuron derived orphan receptor 1; NR, nuclear receptor; NRE, nuclear receptor response element; NRIP, nuclear receptor-interacting protein; NSAIDs, nonsteroidal anti-inflammatory drugs; NSC, neural stem cell; Nurr1, nuclear receptor related-1 protein; NurRE, Nur response element; OL, oligodendrocyte; OPC, oligodendrocyte progenitor cells; PAINS, pan-assay interference compounds; PBMC, peripheral blood mononuclear cell; PD, Parkinson's disease; PG, prostaglandin; P-gp, P-glycoprotein; PHA, phytohemagglutinin; PIAS γ , protein inhibitor of activated STAT protein gamma; POMC, proopiomelanocortin; PPAR, peroxisome proliferator-activated receptor; PS1, presenilin 1; RE, response element; Ret, receptor tyrosine kinase Ret; RevERB, reverse ERB; RNAi, RNA interference; ROR, retinoic acid receptor related orphan receptors; RXR, retinoid X receptor; SAR, structure–activity relationship; SERM, selective estrogen receptor modulator; SMRT, silencing mediator for retinoid or thyroid hormone receptors; SNP, single-nucleotide polymorphism; SPR, surface plasmon resonance; TGF, transforming growth factor; Th, T helper cell; TH, tyrosine hydroxylase; THR, thyroid hormone receptor; TLX, tailless homologue; TNF α , tumor necrosis factor α ; Treg, regulatory T cell; VDR, vitamin D receptor; VMAT2, vesicular monoamine transporter 2

REFERENCES

- (1) Prince, M.; Bryce, R.; Albanese, E.; Wimo, A.; Ribeiro, W.; Ferri, C. P. The Global Prevalence of Dementia: A Systematic Review and Metaanalysis. *Alzheimer's Dementia* **2013**, *9* (1), 63–75.e2.
- (2) Moutinho, M.; Codocedo, J. F.; Puntambekar, S. S.; Landreth, G. E. Nuclear Receptors as Therapeutic Targets for Neurodegenerative Diseases: Lost in Translation. *Annu. Rev. Pharmacol. Toxicol.* **2019**, *59*, 237–261.
- (3) Abroha, I.; Rimland, J. M.; Trotta, F. M.; Dell'Aquila, G.; Cruz-Jentoft, A.; Petrovic, M.; Gudmundsson, A.; Soiza, R.; O'Mahony, D.; Guaita, A.; Cherubini, A. Systematic Review of Systematic Reviews of Non-Pharmacological Interventions to Treat Behavioural Disturbances in Older Patients with Dementia. The SENATOR-OnTop Series. *BMJ. Open* **2017**, *7*, e012759.
- (4) Schmidt, R.; Hofer, E.; Bouwman, F. H.; Buerger, K.; Cordonnier, C.; Fladby, T.; Galimberti, D.; Georges, J.; Heneka, M. T.; Hort, J.; Laczó, J.; Molinuevo, J. L.; O'Brien, J. T.; Religa, D.; Scheltens, P.; Schott, J. M.; Sorbi, S. EFNS-ENS/EAN Guideline on Concomitant Use of Cholinesterase Inhibitors and Memantine in Moderate to Severe Alzheimer's Disease. *Eur. J. Neurol.* **2015**, *22* (6), 889–898.
- (5) McShane, R.; Areosa Sastre, A.; Minakaran, N. Memantine for Dementia. *Cochrane Database Syst. Rev.* **2006**, No. 2. DOI: 10.1002/14651858.CD003154.pub5
- (6) Birks, J.; Grimley Evans, J. Ginkgo Biloba for Cognitive Impairment and Dementia. *Cochrane Database Syst. Rev.* **2009**, No. 1. DOI: 10.1002/14651858.CD003120.pub3

- (7) Masters, C. L.; Bateman, R.; Blennow, K.; Rowe, C. C.; Sperling, R. A.; Cummings, J. L. Alzheimer's Disease. *Nat. Rev. Dis. Prim.* **2015**, *1* (1), 15056.
- (8) Congdon, E. E.; Sigurdsson, E. M. Tau-Targeting Therapies for Alzheimer Disease. *Nat. Rev. Neurol.* **2018**, *14* (7), 399–415.
- (9) Panza, F.; Lozupone, M.; Logroscino, G.; Imbimbo, B. P. A Critical Appraisal of Amyloid- β -Targeting Therapies for Alzheimer Disease. *Nat. Rev. Neurol.* **2019**, *15* (2), 73–88.
- (10) Uliassi, E.; Gandini, A.; Perone, R. C.; Bolognesi, M. L. Neuroregeneration versus Neurodegeneration: Toward a Paradigm Shift in Alzheimer's Disease Drug Discovery. *Future Med. Chem.* **2017**, *9* (10), 995–1013.
- (11) Wang, J.; Gu, B. J.; Masters, C. L.; Wang, Y.-J. A Systemic View of Alzheimer Disease — Insights from Amyloid- β Metabolism beyond the Brain. *Nat. Rev. Neurol.* **2017**, *13* (10), 612–623.
- (12) Elkouzi, A.; Vedam-Mai, V.; Eisinger, R. S.; Okun, M. S. Emerging Therapies in Parkinson Disease — Repurposed Drugs and New Approaches. *Nat. Rev. Neurol.* **2019**, *15* (4), 204–223.
- (13) de Lau, L. M. L.; Breteler, M. M. B. Epidemiology of Parkinson's Disease. *Lancet Neurol.* **2006**, *5* (6), 525–535.
- (14) Parkinson's Disease in Adults. *NICE Guidelines*, 2017, NG71.
- (15) Deuschl, G.; de Bie, R. M. A. New Therapeutic Developments for Parkinson Disease. *Nat. Rev. Neurol.* **2019**, *15* (2), 68–69.
- (16) Doshi, A.; Chataway, J. Multiple Sclerosis, a Treatable Disease. *Clin. Med. (Northfield, Ill.)* **2016**, *16* (6), s53–s59.
- (17) Tintore, M.; Vidal-Jordana, A.; Sastre-Garriga, J. Treatment of Multiple Sclerosis — Success from Bench to Bedside. *Nat. Rev. Neurol.* **2019**, *15* (1), 53–58.
- (18) Stangel, M.; Kuhlmann, T.; Matthews, P. M.; Kilpatrick, T. J. Achievements and Obstacles of Remyelinating Therapies in Multiple Sclerosis. *Nat. Rev. Neurol.* **2017**, *13* (12), 742–754.
- (19) Zhao, C.; Deng, W.; Gage, F. H. Mechanisms and Functional Implications of Adult Neurogenesis. *Cell* **2008**, *132* (4), 645–660.
- (20) Germain, P.; Staels, B.; Dacquet, C.; Spedding, M.; Laudet, V. Overview of Nomenclature of Nuclear Receptors. *Pharmacol. Rev.* **2006**, *58* (4), 685–704.
- (21) Aranda, A.; Pascual, A. Nuclear Hormone Receptors and Gene Expression. *Physiol. Rev.* **2001**, *81* (3), 1269–1304.
- (22) De Bosscher, K.; Desmet, S. J.; Clarisse, D.; Estébanez-Perpiña, E.; Brunsveld, L. Nuclear Receptor Crosstalk — Defining the Mechanisms for Therapeutic Innovation. *Nat. Rev. Endocrinol.* **2020**, *16* (7), 363–377.
- (23) Evans, R. M.; Mangelsdorf, D. J. Nuclear Receptors, RXR, and the Big Bang. *Cell* **2014**, *157*, 255–266.
- (24) Rastinejad, F.; Huang, P.; Chandra, V.; Khorasanizadeh, S. Understanding Nuclear Receptor Form and Function Using Structural Biology. *J. Mol. Endocrinol.* **2013**, *51* (3), T1–T21.
- (25) Negishi, M.; Kobayashi, K.; Sakuma, T.; Sueyoshi, T. Nuclear Receptor Phosphorylation in Xenobiotic Signal Transduction. *J. Biol. Chem.* **2020**, *295* (45), 15210–15225.
- (26) Rastinejad, F.; Ollendorff, V.; Polikarpov, I. Nuclear Receptor Full-Length Architectures: Confronting Myth and Illusion with High Resolution. *Trends Biochem. Sci.* **2015**, *40* (1), 16–24.
- (27) Weikum, E. R.; Liu, X.; Ortlund, E. A. The Nuclear Receptor Superfamily: A Structural Perspective. *Protein Sci.* **2018**, *27*, 1876–1892.
- (28) Bain, D. L.; Heneghan, A. F.; Connaghan-Jones, K. D.; Miura, M. T. Nuclear Receptor Structure: Implications for Function. *Annu. Rev. Physiol.* **2007**, *69* (1), 201–220.
- (29) Benoit, G.; Cooney, A.; Giguere, V.; Ingraham, H.; Lazar, M.; Muscat, G.; Perlmann, T.; Renaud, J.-P.; Schwabe, J.; Sladek, F.; Tsai, M.-J.; Laudet, V. International Union of Pharmacology. LXVI. Orphan Nuclear Receptors. *Pharmacol. Rev.* **2006**, *58* (4), 798–836.
- (30) Robinson-Rechavi, M.; Garcia, H. E.; Garcia, H. E.; Laudet, V. The Nuclear Receptor Superfamily. *J. Cell Sci.* **2003**, *116* (4), 585–586.
- (31) Michalik, L.; Auwerx, J.; Berger, J. P.; Chatterjee, V. K.; Glass, C. K.; Gonzalez, F. J.; Grimaldi, P. A.; Kadowaki, T.; Lazar, M. A.; O'Rahilly, S.; Palmer, C. N. A.; Plutzky, J.; Reddy, J. K.; Spiegelman, B. M.; Staels, B.; Wahli, W. International Union of Pharmacology. LXI. Peroxisome Proliferator-Activated Receptors. *Pharmacol. Rev.* **2006**, *58* (4), 726–741.
- (32) Warden, A.; Truitt, J.; Merriman, M.; Ponomareva, O.; Jameson, K.; Ferguson, L. B.; Mayfield, R. D.; Harris, R. A. Localization of PPAR Isotypes in the Adult Mouse and Human Brain. *Sci. Rep.* **2016**, *6*, 27681 DOI: 10.1038/srep27618.
- (33) Gellrich, L.; Heitel, P.; Heering, J.; Kilu, W.; Pollinger, J.; Goebel, T.; Kahnt, A.; Arifi, S.; Pogoda, W.; Paulke, A.; Steinhilber, D.; Proschak, E.; Wurglics, M.; Schubert-Zsilavecz, M.; Chaikuad, A.; Knapp, S.; Bischoff, L.; Fürst, R.; Merk, D. L-Thyroxin and the Nonclassical Thyroid Hormone TETRAC Are Potent Activators of PPAR γ . *J. Med. Chem.* **2020**, *63* (13), 6727–6740.
- (34) Proschak, E.; Heitel, P.; Kalinowsky, L.; Merk, D. Opportunities and Challenges for Fatty Acid Mimetics in Drug Discovery. *J. Med. Chem.* **2017**, *60* (13), 5235–5266.
- (35) Wahli, W.; Michalik, L. PPARs at the Crossroads of Lipid Signaling and Inflammation. *Trends Endocrinol. Metab.* **2012**, *23*, 351–363.
- (36) Lamers, C.; Schubert-Zsilavecz, M.; Merk, D. Therapeutic Modulators of Peroxisome Proliferator-Activated Receptors (PPAR): A Patent Review (2008–Present). *Expert Opin. Ther. Pat.* **2012**, *22* (7), 803–841.
- (37) Lu, C.-H.; Yang, C.-Y.; Li, C.-Y.; Hsieh, C.; Ou, H.-T. Lower Risk of Dementia with Pioglitazone, Compared with Other Second-Line Treatments, in Metformin-Based Dual Therapy: A Population-Based Longitudinal Study. *Diabetologia* **2018**, *61* (3), 562–573.
- (38) Heneka, M. T.; Fink, A.; Doblhammer, G. Effect of Pioglitazone Medication on the Incidence of Dementia. *Ann. Neurol.* **2015**, *78* (2), 284–294.
- (39) Chou, P.-S.; Ho, B.-L.; Yang, Y.-H. Effects of Pioglitazone on the Incidence of Dementia in Patients with Diabetes. *J. Diabetes Complications* **2017**, *31* (6), 1053–1057.
- (40) Kummer, M. P.; Heneka, M. T. PPARs in Alzheimer's Disease. *PPAR Res.* **2008**, *2008*, 403896.
- (41) Heneka, M. T.; Reyes-Irisarri, E.; Hull, M.; Kummer, M. P. Impact and Therapeutic Potential of PPARs in Alzheimers Disease. *Curr. Neuropharmacol.* **2011**, *9* (4), 643–650.
- (42) Du, J.; Zhang, L.; Liu, S.; Zhang, C.; Huang, X.; Li, J.; Zhao, N.; Wang, Z. PPAR γ Transcriptionally Regulates the Expression of Insulin-Degrading Enzyme in Primary Neurons. *Biochem. Biophys. Res. Commun.* **2009**, *383* (4), 485–490.
- (43) Quan, Q.; Qian, Y.; Li, X.; Li, M. Pioglitazone Reduces β Amyloid Levels via Inhibition of PPAR γ Phosphorylation in a Neuronal Model of Alzheimer's Disease. *Front. Aging Neurosci.* **2019**, *11*, 178.
- (44) Sastre, M.; Dewachter, I.; Rossner, S.; Bogdanovic, N.; Rosen, E.; Borghgraef, P.; Evert, B. O.; Dumitrescu-Ozimek, L.; Thal, D. R.; Landreth, G.; Walter, J.; Klockgether, T.; Van Leuven, F.; Heneka, M. T. Nonsteroidal Anti-Inflammatory Drugs Repress β -Secretase Gene Promoter Activity by the Activation of PPAR γ . *Proc. Natl. Acad. Sci. U. S. A.* **2006**, *103* (2), 443–448.
- (45) Sastre, M.; Dewachter, I.; Landreth, G. E.; Willson, T. M.; Klockgether, T.; Van Leuven, F.; Heneka, M. T. Nonsteroidal Anti-Inflammatory Drugs and Peroxisome Proliferator-Activated Receptor- γ Agonists Modulate Immunostimulated Processing of Amyloid Precursor Protein through Regulation of β -Secretase. *J. Neurosci.* **2003**, *23* (30), 9796–9804.
- (46) Yang, S.; Chen, Z.; Cao, M.; Li, R.; Wang, Z.; Zhang, M. Pioglitazone Ameliorates A β 42 Deposition in Rats with Diet-Induced Insulin Resistance Associated with AKT/GSK3 β Activation. *Mol. Med. Rep.* **2017**, *15* (5), 2588–2594.
- (47) Chang, K. L.; Wong, L. R.; Pee, H. N.; Yang, S.; Ho, P. C. L. Reverting Metabolic Dysfunction in Cortex and Cerebellum of APP/PS1 Mice, a Model for Alzheimer's Disease by Pioglitazone, a Peroxisome Proliferator-Activated Receptor Gamma (PPAR γ) Agonist. *Mol. Neurobiol.* **2019**, *56* (11), 7267–7283.
- (48) Yu, Y.; Li, X.; Blanchard, J.; Li, Y.; Iqbal, K.; Liu, F.; Gong, C.-X. Insulin Sensitizers Improve Learning and Attenuate Tau Hyper-

phosphorylation and Neuroinflammation in 3xTg-AD Mice. *J. Neural Transm.* **2015**, *122* (4), 593–606.

(49) Du, J.; Sun, B.; Chen, K.; Fan, L.; Wang, Z. Antagonist of Peroxisome Proliferator-Activated Receptor γ Induces Cerebellar Amyloid- β Levels and Motor Dysfunction in APP/PS1 Transgenic Mice. *Biochem. Biophys. Res. Commun.* **2009**, *384* (3), 357–361.

(50) Fernandez-Martos, C. M.; Atkinson, R. A. K.; Chuah, M. I.; King, A. E.; Vickers, J. C. Combination Treatment with Leptin and Pioglitazone in a Mouse Model of Alzheimer's Disease. *Alzheimer's Dement. Transl. Res. Clin. Interv.* **2017**, *3* (1), 92–106.

(51) Chen, J.; Li, S.; Sun, W.; Li, J. Anti-Diabetes Drug Pioglitazone Ameliorates Synaptic Defects in AD Transgenic Mice by Inhibiting Cyclin-Dependent Kinase5 Activity. *PLoS One* **2015**, *10*, No. e0123864.

(52) Mandrekar-Colucci, S.; Karlo, J. C.; Landreth, G. E. Mechanisms Underlying the Rapid Peroxisome Proliferator-Activated Receptor- γ -Mediated Amyloid Clearance and Reversal of Cognitive Deficits in a Murine Model of Alzheimer's Disease. *J. Neurosci.* **2012**, *32* (30), 10117–10128.

(53) Papadopoulos, P.; Rosa-Neto, P.; Rochford, J.; Hamel, E. Pioglitazone Improves Reversal Learning and Exerts Mixed Cerebrovascular Effects in a Mouse Model of Alzheimer's Disease with Combined Amyloid- β and Cerebrovascular Pathology. *PLoS One* **2013**, *8* (7), e68612.

(54) Prakash, A.; Kumar, A. Role of Nuclear Receptor on Regulation of BDNF and Neuroinflammation in Hippocampus of β -Amyloid Animal Model of Alzheimer's Disease. *Neurotoxic. Res.* **2014**, *25* (5), 335–347.

(55) Hamano, T.; Shirafuji, N.; Makino, C.; Yen, S.-H.; Kanaan, N. M.; Ueno, A.; Suzuki, J.; Ikawa, M.; Matsunaga, A.; Yamamura, O.; Kuriyama, M.; Nakamoto, Y. Pioglitazone Prevents Tau Oligomerization. *Biochem. Biophys. Res. Commun.* **2016**, *478* (3), 1035–1042.

(56) Cho, D.-H.; Lee, E. J.; Kwon, K. J.; Shin, C. Y.; Song, K.-H.; Park, J.-H.; Jo, I.; Han, S.-H. Troglitazone, a Thiazolidinedione, Decreases Tau Phosphorylation through the Inhibition of Cyclin-Dependent Kinase 5 Activity in SH-SY5Y Neuroblastoma Cells and Primary Neurons. *J. Neurochem.* **2013**, *126* (5), 685–695.

(57) Harrington, C.; Sawchak, S.; Chiang, C.; Davies, J.; Donovan, C.; Saunders, A. M.; Irizarry, M.; Jeter, B.; Zvartau-Hind, M.; H. van Dyck, C.; Gold, M. Rosiglitazone Does Not Improve Cognition or Global Function When Used as Adjunctive Therapy to AChE Inhibitors in Mild-to-Moderate Alzheimer's Disease: Two Phase 3 Studies. *Curr. Alzheimer Res.* **2011**, *8* (5), 592–606.

(58) Gold, M.; Alderton, C.; Zvartau-Hind, M.; Egginton, S.; Saunders, A. M.; Irizarry, M.; Craft, S.; Landreth, G.; Linnamägi, Ü.; Sawchak, S. Rosiglitazone Monotherapy in Mild-to-Moderate Alzheimer's Disease: Results from a Randomized, Double-Blind, Placebo-Controlled Phase III Study. *Dementia Geriatr. Cognit. Disord.* **2010**, *30* (2), 131–146.

(59) Cheng, H.; Shang, Y.; Jiang, L.; Shi, T.-L.; Wang, L. The Peroxisome Proliferators Activated Receptor-Gamma Agonists as Therapeutics for the Treatment of Alzheimer's Disease and Mild-to-Moderate Alzheimer's Disease: A Meta-Analysis. *Int. J. Neurosci.* **2016**, *126* (4), 299–307.

(60) Liu, J.; Wang, L.; Jia, J. Peroxisome Proliferator-Activated Receptor-Gamma Agonists for Alzheimer's Disease and Amnesic Mild Cognitive Impairment: A Systematic Review and Meta-Analysis. *Drugs Aging* **2015**, *32* (1), 57–65.

(61) Breidert, T.; Callebert, J.; Heneka, M. T.; Landreth, G.; Launay, J. M.; Hirsch, E. C. Protective Action of the Peroxisome Proliferator-Activated Receptor- γ Agonist Pioglitazone in a Mouse Model of Parkinson's Disease. *J. Neurochem.* **2002**, *82* (3), 615–624.

(62) Quinn, L. P.; Crook, B.; Hows, M. E.; Videon-Hart, M.; Chapman, H.; Upton, N.; Medhurst, A. D.; Virley, D. J. The PPAR γ Agonist Pioglitazone Is Effective in the MPTP Mouse Model of Parkinson's Disease through Inhibition of Monoamine Oxidase B. *Br. J. Pharmacol.* **2008**, *154* (1), 226–233.

(63) Pisantu, A.; Lecca, D.; Mulas, G.; Wardas, J.; Simbula, G.; Spiga, S.; Carta, A. R. Dynamic Changes in Pro-and Anti-Inflammatory

Cytokines in Microglia after PPAR- γ Agonist Neuroprotective Treatment in the MPTPp Mouse Model of Progressive Parkinson's Disease. *Neurobiol. Dis.* **2014**, *71*, 280–291.

(64) Swanson, C. R.; Joers, V.; Bondarenko, V.; Brunner, K.; Simmons, H. A.; Ziegler, T. E.; Kemnitz, J. W.; Johnson, J. A.; Emborg, M. E. The PPAR- γ Agonist Pioglitazone Modulates Inflammation and Induces Neuroprotection in Parkinsonian Monkeys. *J. Neuroinflammation* **2011**, *8*, 91.

(65) Pinto, M.; Nissanka, N.; Peralta, S.; Brambilla, R.; Diaz, F.; Moraes, C. T. Pioglitazone Ameliorates the Phenotype of a Novel Parkinson's Disease Mouse Model by Reducing Neuroinflammation. *Mol. Neurodegener.* **2016**, *11*, 25.

(66) Lecca, D.; Nevin, D. K.; Mulas, G.; Casu, M. A.; Diana, A.; Rossi, D.; Sacchetti, G.; Carta, A. R. Neuroprotective and Anti-Inflammatory Properties of a Novel Non-Thiazolidinedione PPAR γ Agonist in Vitro and in MPTP-Treated Mice. *Neuroscience* **2015**, *302*, 23–35.

(67) Lecca, D.; Janda, E.; Mulas, G.; Diana, A.; Martino, C.; Angius, F.; Spolitu, S.; Casu, M. A.; Simbula, G.; Boi, L.; Batetta, B.; Spiga, S.; Carta, A. R. Boosting Phagocytosis and Anti-Inflammatory Phenotype in Microglia Mediates Neuroprotection by PPAR γ Agonist MDG548 in Parkinson's Disease Models. *Br. J. Pharmacol.* **2018**, *175* (16), 3298–3314.

(68) Swanson, C. R.; Du, E.; Johnson, D. A.; Johnson, J. A.; Emborg, M. E. Neuroprotective Properties of a Novel Non-Thiazolidinedione Partial PPAR- γ Agonist against MPTP. *PPAR Res.* **2013**, *2013*, No. 582809.

(69) Das, N. R.; Gangwal, R. P.; Damre, M. V.; Sangamwar, A. T.; Sharma, S. S. A PPAR- β/δ Agonist Is Neuroprotective and Decreases Cognitive Impairment in a Rodent Model of Parkinson's Disease. *Curr. Neurovasc. Res.* **2014**, *11* (2), 114–124.

(70) Uppalapati, D.; Das, N. R.; Gangwal, R. P.; Damre, M. V.; Sangamwar, A. T.; Sharma, S. S. Neuroprotective Potential of Peroxisome Proliferator Activated Receptor- α Agonist in Cognitive Impairment in Parkinson's Disease: Behavioral, Biochemical, and PBPK Profile. *PPAR Res.* **2014**, *2014*, 753587.

(71) Barbiero, J. K.; Santiago, R.; Tonin, F. S.; Boschen, S.; Da Silva, L. M.; De Paula Werner, M. F.; Da Cunha, C.; Lima, M. M. S.; Vital, M. A. B. F. PPAR- α Agonist Fenofibrate Protects against the Damaging Effects of MPTP in a Rat Model of Parkinson's Disease. *Prog. Neuro-Psychopharmacol. Biol. Psychiatry* **2014**, *53*, 35–44.

(72) Martin, H. L.; Mounsey, R. B.; Sathe, K.; Mustafa, S.; Nelson, M. C.; Evans, R. M.; Teismann, P. A Peroxisome Proliferator-Activated Receptor- δ Agonist Provides Neuroprotection in the 1-Methyl-4-Phenyl-1,2,3,6-Tetrahydropyridine Model of Parkinson's Disease. *Neuroscience* **2013**, *240*, 191–203.

(73) Lee, Y.; Cho, J.-H.; Lee, S.; Lee, W.; Chang, S.-C.; Chung, H. Y.; Moon, H. R.; Lee, J. Neuroprotective Effects of MHY908, a PPAR α/γ Dual Agonist, in a MPTP-Induced Parkinson's Disease Model. *Brain Res.* **2019**, *1704*, 47–58.

(74) Chen, L.; Xue, L.; Zheng, J.; Tian, X.; Zhang, Y.; Tong, Q. PPAR β/δ Agonist Alleviates NLRP3 Inflammasome-Mediated Neuroinflammation in the MPTP Mouse Model of Parkinson's Disease. *Behav. Brain Res.* **2019**, *356*, 483–489.

(75) Mounsey, R. B.; Martin, H. L.; Nelson, M. C.; Evans, R. M.; Teismann, P. The Effect of Neuronal Conditional Knock-out of Peroxisome Proliferator-Activated Receptors in the MPTP Mouse Model of Parkinson's Disease. *Neuroscience* **2015**, *300*, 576–584.

(76) Tong, Q.; Wu, L.; Gao, Q.; Ou, Z.; Zhu, D.; Zhang, Y. PPAR β/δ Agonist Provides Neuroprotection by Suppression of IRE1 α -Caspase-12-Mediated Endoplasmic Reticulum Stress Pathway in the Rotenone Rat Model of Parkinson's Disease. *Mol. Neurobiol.* **2016**, *53* (8), 3822–3831.

(77) Bonato, J. M.; Bassani, T. B.; Milani, H.; Vital, M. A. B. F.; de Oliveira, R. M. W. Pioglitazone Reduces Mortality, Prevents Depressive-like Behavior, and Impacts Hippocampal Neurogenesis in the 6-OHDA Model of Parkinson's Disease in Rats. *Exp. Neurol.* **2018**, *300*, 188–200.

- (78) Machado, M. M. F.; Bassani, T. B.; C oppola-Segovia, V.; Moura, E. L. R.; Zanata, S. M.; Andreatini, R.; Vital, M. A. B. F. PPAR- γ Agonist Pioglitazone Reduces Microglial Proliferation and NF- κ B Activation in the Substantia Nigra in the 6-Hydroxydopamine Model of Parkinson's Disease. *Pharmacol. Rep.* **2019**, *71* (4), 556–564.
- (79) Lee, E. Y.; Lee, J. E.; Park, J. H.; Shin, I. C.; Koh, H. C. Rosiglitazone, a PPAR- γ Agonist, Protects against Striatal Dopaminergic Neurodegeneration Induced by 6-OHDA Lesions in the Substantia Nigra of Rats. *Toxicol. Lett.* **2012**, *213* (3), 332–344.
- (80) Martinez, A. A.; Morgese, M. G.; Pisanu, A.; Macheda, T.; Paquette, M. A.; Seillier, A.; Cassano, T.; Carta, A. R.; Giuffrida, A. Activation of PPAR Gamma Receptors Reduces Levodopa-Induced Dyskinesias in 6-OHDA-Lesioned Rats. *Neurobiol. Dis.* **2015**, *74*, 295–304.
- (81) Gottschalk, C. G.; Roy, A.; Jana, M.; Kundu, M.; Pahan, K. Activation of Peroxisome Proliferator-Activated Receptor- α Increases the Expression of Nuclear Receptor Related 1 Protein (Nurr1) in Dopaminergic Neurons. *Mol. Neurobiol.* **2019**, *56* (11), 7872–7887.
- (82) Brauer, R.; Bhaskaran, K.; Chaturvedi, N.; Dexter, D. T.; Smeeth, L.; Douglas, I. Glitazone Treatment and Incidence of Parkinson's Disease among People with Diabetes: A Retrospective Cohort Study. *PLoS Med.* **2015**, *12* (7), e1001854.
- (83) Mutez, E.; Duhamel, A.; Defebvre, L.; Bordet, R.; Dest ee, A.; Kreisler, A. Lipid-Lowering Drugs Are Associated with Delayed Onset and Slower Course of Parkinson's Disease. *Pharmacol. Res.* **2009**, *60* (1), 41–45.
- (84) Szalardy, L.; Zadori, D.; Tanczos, E.; Simu, M.; Bencsik, K.; Vecsei, L.; Klivenyi, P. Elevated Levels of PPAR-Gamma in the Cerebrospinal Fluid of Patients with Multiple Sclerosis. *Neurosci. Lett.* **2013**, *554*, 131–134.
- (85) Szalardy, L.; Zadori, D.; Bencsik, K.; Vecsei, L.; Klivenyi, P. Unlike PPARgamma, Neither Other PPARs nor PGC-1alpha Is Elevated in the Cerebrospinal Fluid of Patients with Multiple Sclerosis. *Neurosci. Lett.* **2017**, *651*, 128–133.
- (86) Wouters, E.; Grajchen, E.; Jorissen, W.; Dierckx, T.; Wetzels, S.; Loix, M.; Tulleners, M. P.; Staels, B.; Stinissen, P.; Haidar, M.; Bogie, J. F. J.; Hendriks, J. J. A. Altered PPAR γ Expression Promotes Myelin-Induced Foam Cell Formation in Macrophages in Multiple Sclerosis. *Int. J. Mol. Sci.* **2020**, *21* (23), 9329.
- (87) Feinstein, D. L.; Galea, E.; Gavriluk, V.; Brosnan, C. F.; Whitacre, C. C.; Dumitrescu-Ozimek, L.; Landreth, G. E.; Pershadsingh, H. A.; Weinberg, G.; Heneka, M. T. Peroxisome Proliferator-Activated Receptor- γ Agonists Prevent Experimental Autoimmune Encephalomyelitis. *Ann. Neurol.* **2002**, *51* (6), 694–702.
- (88) Klotz, L.; Burgdorf, S.; Dani, I.; Saijo, K.; Flossdorf, J.; Hucke, S.; Alferink, J.; Novak, N.; Beyer, M.; Mayer, G.; Langhans, B.; Klockgether, T.; Waisman, A.; Eberl, G.; Schultze, J.; Famulok, M.; Kolanus, W.; Glass, C.; Kurts, C.; Knolle, P. The Nuclear Receptor PPAR γ Selectively Inhibits Th17 Differentiation in a T Cell–Intrinsic Fashion and Suppresses CNS Autoimmunity. *J. Exp. Med.* **2009**, *206* (10), 2079–2089.
- (89) Chedrawe, M. A. J.; Holman, S. P.; Lampport, A.-C.; Akay, T.; Robertson, G. S. Pioglitazone Is Superior to Quetiapine, Clozapine and Tamoxifen at Alleviating Experimental Autoimmune Encephalomyelitis in Mice. *J. Neuroimmunol.* **2018**, *321*, 72–82.
- (90) Diab, A.; Deng, C.; Smith, J. D.; Hussain, R. Z.; Phanavanh, B.; Lovett-Racke, A. E.; Drew, P. D.; Racke, M. K. Peroxisome Proliferator-Activated Receptor- γ Agonist 15-Deoxy- Δ 12,14,14-Prostaglandin J2 Ameliorates Experimental Autoimmune Encephalomyelitis. *J. Immunol.* **2002**, *168* (5), 2508–2515.
- (91) Diab, A.; Hussain, R. Z.; Lovett-Racke, A. E.; Chavis, J. A.; Drew, P. D.; Racke, M. K. Ligands for the Peroxisome Proliferator-Activated Receptor- γ and the Retinoid X Receptor Exert Additive Anti-Inflammatory Effects on Experimental Autoimmune Encephalomyelitis. *J. Neuroimmunol.* **2004**, *148* (1–2), 116–126.
- (92) Bernardo, A.; Giammarco, M. L.; De Nuccio, C.; Ajmone-Cat, M. A.; Visentin, S.; De Simone, R.; Minghetti, L. Docosahexaenoic Acid Promotes Oligodendrocyte Differentiation via PPAR- γ Signalling and Prevents Tumor Necrosis Factor- α -Dependent Maturation Arrest. *Biochim. Biophys. Acta, Mol. Cell Biol. Lipids* **2017**, *1862* (9), 1013–1023.
- (93) De Nuccio, C.; Bernardo, A.; Cruciani, C.; De Simone, R.; Visentin, S.; Minghetti, L. Peroxisome Proliferator Activated Receptor- γ Agonists Protect Oligodendrocyte Progenitors against Tumor Necrosis Factor-Alpha-Induced Damage: Effects on Mitochondrial Functions and Differentiation. *Exp. Neurol.* **2015**, *271*, 506–514.
- (94) Storer, P. D.; Xu, J.; Chavis, J.; Drew, P. D. Peroxisome Proliferator-Activated Receptor-Gamma Agonists Inhibit the Activation of Microglia and Astrocytes: Implications for Multiple Sclerosis. *J. Neuroimmunol.* **2005**, *161* (1–2), 113–122.
- (95) Zhang, F.; Liu, F.; Yan, M.; Ji, H.; Hu, L.; Li, X.; Qian, J.; He, X.; Zhang, L.; Shen, A.; Cheng, C. Peroxisome Proliferator-Activated Receptor- γ Agonists Suppress INOS Expression Induced by LPS in Rat Primary Schwann Cells. *J. Neuroimmunol.* **2010**, *218* (1–2), 36–47.
- (96) Grajchen, E.; Wouters, E.; Van De Haterd, B.; Haidar, M.; Hardonni re, K.; Dierckx, T.; Van Broeckhoven, J.; Erens, C.; Hendrix, S.; Kerdine-R mer, S.; Hendriks, J. J. A.; Bogie, J. F. J. CD36-Mediated Uptake of Myelin Debris by Macrophages and Microglia Reduces Neuroinflammation. *J. Neuroinflammation* **2020**, *17*, 224.
- (97) Schmidt, S.; Moric, E.; Schmidt, M.; Sastre, M.; Feinstein, D. L.; Heneka, M. T. Anti-Inflammatory and Antiproliferative Actions of PPAR- γ Agonists on T Lymphocytes Derived from MS Patients. *J. Leukocyte Biol.* **2004**, *75* (3), 478–485.
- (98) Polak, P. E.; Kalinin, S.; Dello Russo, C.; Gavriluk, V.; Sharp, A.; Peters, J. M.; Richardson, J.; Willson, T. M.; Weinberg, G.; Feinstein, D. L. Protective Effects of a Peroxisome Proliferator-Activated Receptor- β/δ Agonist in Experimental Autoimmune Encephalomyelitis. *J. Neuroimmunol.* **2005**, *168* (1–2), 65–75.
- (99) Kanakasabai, S.; Walline, C. C.; Chakraborty, S.; Bright, J. J. PPAR δ Deficient Mice Develop Elevated Th1/Th17 Responses and Prolonged Experimental Autoimmune Encephalomyelitis. *Brain Res.* **2011**, *1376*, 101–112.
- (100) Defaux, A.; Zurich, M. G.; Braissant, O.; Honegger, P.; Monnet-Tschudi, F. Effects of the PPAR- β Agonist GW501516 in an in Vitro Model of Brain Inflammation and Antibody-Induced Demyelination. *J. Neuroinflammation* **2009**, *6*, 15.
- (101) Kanakasabai, S.; Chearwae, W.; Walline, C. C.; Iams, W.; Adams, S. M.; Bright, J. J. Peroxisome Proliferator-Activated Receptor δ Agonists Inhibit T Helper Type 1 (Th1) and Th17 Responses in Experimental Allergic Encephalomyelitis. *Immunology* **2010**, *130* (4), 572–588.
- (102) Jana, M.; Mondal, S.; Gonzalez, F. J.; Pahan, K. Gemfibrozil, a Lipid-Lowering Drug, Increases Myelin Genes in Human Oligodendrocytes via Peroxisome Proliferator-Activated Receptor- β . *J. Biol. Chem.* **2012**, *287* (41), 34134–34148.
- (103) Sakuma, S.; Endo, T.; Kanda, T.; Nakamura, H.; Yamasaki, S.; Yamakawa, T. Synthesis of a Novel Human PPAR δ Selective Agonist and Its Stimulatory Effect on Oligodendrocyte Differentiation. *Bioorg. Med. Chem. Lett.* **2011**, *21* (1), 240–244.
- (104) Kaiser, C. C.; Shukla, D. K.; Stebbins, G. T.; Skias, D. D.; Jeffery, D. R.; Stefoski, D.; Katsamakis, G.; Feinstein, D. L. A Pilot Test of Pioglitazone as an Add-on in Patients with Relapsing Remitting Multiple Sclerosis. *J. Neuroimmunol.* **2009**, *211* (1–2), 124–130.
- (105) Shukla, D. K.; Kaiser, C. C.; Stebbins, G. T.; Feinstein, D. L. Effects of Pioglitazone on Diffusion Tensor Imaging Indices in Multiple Sclerosis Patients. *Neurosci. Lett.* **2010**, *472* (3), 153–156.
- (106) Negrotto, L.; Farez, M. F.; Correale, J. Immunologic Effects of Metformin and Pioglitazone Treatment on Metabolic Syndrome and Multiple Sclerosis. *JAMA Neurol.* **2016**, *73* (5), 520–528.
- (107) Ratzu, V.; Harrison, S. A.; Francque, S.; Bedossa, P.; Leherter, P.; Serfaty, L.; Romero-Gomez, M.; Boursier, J.; Abdelmalek, M.; Caldwell, S.; Drenth, J.; Anstee, Q. M.; Hum, D.; Hanf, R.; Roudot, A.; Megnien, S.; Staels, B.; Sanyal, A.; et al. Elafibranor, an Agonist of

the Peroxisome Proliferator-Activated Receptor- α and - δ , Induces Resolution of Nonalcoholic Steatohepatitis Without Fibrosis Worsening. *Gastroenterology* **2016**, *150* (5), 1147–1159.

(108) Henke, B. R.; Blanchard, S. G.; Brackeen, M. F.; Brown, K. K.; Cobb, J. E.; Collins, J. L.; Harrington, W. W.; Hashim, M. A.; Hull-Ryde, E. A.; Kaldor, I.; Kliewer, S. A.; Lake, D. H.; Leesnitzer, L. M.; Lehmann, J. M.; Lenhard, J. M.; Orband-Miller, L. A.; Miller, J. F.; Mook, R. A.; Noble, S. A.; Oliver, W.; Parks, D. J.; Plunket, K. D.; Szewczyk, J. R.; Willson, T. M. N-(2-Benzoylphenyl)-L-Tyrosine PPAR γ Agonists. 1. Discovery of a Novel Series of Potent Antihyperglycemic and Antihyperlipidemic Agents. *J. Med. Chem.* **1998**, *41* (25), 5020–5036.

(109) Cobb, J. E.; Blanchard, S. G.; Boswell, E. G.; Brown, K. K.; Charifson, P. S.; Cooper, J. P.; Collins, J. L.; Dezube, M.; Henke, B. R.; Hull-Ryde, E. A.; Lake, D. H.; Lenhard, J. M.; Oliver, W.; Oplinger, J.; Pentti, M.; Parks, D. J.; Plunket, K. D.; Tong, W.-Q. N-(2-Benzoylphenyl)-L-Tyrosine PPAR γ Agonists. 3. Structure-Activity Relationship and Optimization of the N-Aryl Substituent. *J. Med. Chem.* **1998**, *41* (25), 5055–5069.

(110) Collins, J. L.; Blanchard, S. G.; Boswell, G. E.; Charifson, P. S.; Cobb, J. E.; Henke, B. R.; Hull-Ryde, E. A.; Kazmierski, W. M.; Lake, D. H.; Leesnitzer, L. M.; Lehmann, J.; Lenhard, J. M.; Orband-Miller, L. A.; Gray-Nunez, Y.; Parks, D. J.; Plunkett, K. D.; Tong, W.-Q. N-(2-Benzoylphenyl)-L-Tyrosine PPAR γ Agonists. 2. Structure-Activity Relationship and Optimization of the Phenyl Alkyl Ether Moiety. *J. Med. Chem.* **1998**, *41* (25), 5037–5054.

(111) Berger, J.; Leibowitz, M. D.; Doebber, T. W.; Elbrecht, A.; Zhang, B.; Zhou, G.; Biswas, C.; Cullinan, C. A.; Hayes, N. S.; Li, Y.; Tanen, M.; Ventre, J.; Wu, M. S.; Berger, G. D.; Mosley, R.; Marquis, R.; Santini, C.; Sahoo, S. P.; Tolman, R. L.; Smith, R. G.; Miller, D. E. Novel Peroxisome Proliferator-Activated Receptor (PPAR) γ and PPAR δ Ligands Produce Distinct Biological Effects. *J. Biol. Chem.* **1999**, *274* (10), 6718–6725.

(112) Brown, P. J.; Stuart, L. W.; Hurley, K. P.; Lewis, M. C.; Winegar, D. A.; Wilson, J. G.; Wilkison, W. O.; Ittoop, O. R.; Willson, T. M. Identification of a Subtype Selective Human PPAR α Agonist through Parallel-Array Synthesis. *Bioorg. Med. Chem. Lett.* **2001**, *11* (9), 1225–1227.

(113) Kane, C. D.; Stevens, K. A.; Fischer, J. E.; Haghpassand, M.; Royer, L. J.; Aldinger, C.; Landschulz, K. T.; Zagouras, P.; Bagley, S. W.; Hada, W.; Dullea, R.; Hayward, C. M.; Francone, O. L. Molecular Characterization of Novel and Selective Peroxisome Proliferator-Activated Receptor α Agonists with Robust Hypolipidemic Activity in Vivo. *Mol. Pharmacol.* **2009**, *75* (2), 296–306.

(114) Kuwabara, K.; Murakami, K.; Todo, M.; Aoki, T.; Asaki, T.; Murai, M.; Yano, J. A Novel Selective Peroxisome Proliferator-Activated Receptor α Agonist, 2-Methyl-c-5-[4-[5-Methyl-2-(4-Methylphenyl)-4-Oxazolyl]Butyl]-1, 3-Dioxane-r-2-Carboxylic Acid (NS-220), Potently Decreases Plasma Triglyceride and Glucose Levels and Modifies Lipopr. *J. Pharmacol. Exp. Ther.* **2004**, *309* (3), 970–977.

(115) Santilli, A. A.; Scotese, A. C.; Tomarelli, R. M. A Potent Antihypercholesterolemic Agent: [4-Chloro-6-(2,3-Xylidino)-2-Pyrimidinylthio]Acetic Acid (Wy-14643). *Experientia* **1974**, *30* (10), 1110–1111.

(116) Willson, T. M.; Brown, P. J.; Sternbach, D. D.; Henke, B. R. The PPARs: From Orphan Receptors to Drug Discovery. *J. Med. Chem.* **2000**, *43*, 527–550.

(117) Pollinger, J.; Gellrich, L.; Schierle, S.; Kilu, W.; Schmidt, J.; Kalinowsky, L.; Ohrndorf, J.; Kaiser, A.; Heering, J.; Proschak, E.; Merk, D. Tuning Nuclear Receptor Selectivity of Wy14,643 towards Selective Retinoid X Receptor Modulation. *J. Med. Chem.* **2019**, *62* (4), 2112–2126.

(118) Willson, T. M.; Cobb, J. E.; Cowan, D. J.; Wiethe, R. W.; Correa, I. D.; Prakash, S. R.; Beck, K. D.; Moore, L. B.; Kliewer, S. A.; Lehmann, J. M. The Structure-Activity Relationship between Peroxisome Proliferator-Activated Receptor γ Agonism and the Antihyperglycemic Activity of Thiazolidinediones. *J. Med. Chem.* **1996**, *39* (3), 665–668.

(119) Lehmann, J. M.; Moore, L. B.; Smith-Oliver, T. A.; Wilkison, W. O.; Willson, T. M.; Kliewer, S. A. An Antidiabetic Thiazolidinedione Is a High Affinity Ligand for Peroxisome Proliferator-Activated Receptor γ (PPAR γ). *J. Biol. Chem.* **1995**, *270* (22), 12953–12956.

(120) Brown, K. K.; Henke, B. R.; Blanchard, S. G.; Cobb, J. E.; Mook, R.; Kaldor, I.; Kliewer, S. A.; Lehmann, J. M.; Lenhard, J. M.; Harrington, W. W.; Novak, P. J.; Faison, W.; Binz, J. G.; Hashim, M. A.; Oliver, W. O.; Brown, H. R.; Parks, D. J.; Plunket, K. D.; Tong, W. Q.; Menius, J. A.; Adkison, K.; Noble, S. A.; Willson, T. M. A Novel N-Aryl Tyrosine Activator of Peroxisome Proliferator-Activated Receptor- γ Reverses the Diabetic Phenotype of the Zucker Diabetic Fatty Rat. *Diabetes* **1999**, *48* (7), 1415–1424.

(121) Hanke, T.; Cheung, S.-Y.; Kilu, W.; Heering, J.; Ni, X.; Planz, V.; Schierle, S.; Faudone, G.; Friedrich, M.; Wanior, M.; Werz, O.; Windbergs, M.; Proschak, E.; Schubert-Zsilavecz, M.; Chaikuad, A.; Knapp, S.; Merk, D. A Selective Modulator of Peroxisome Proliferator-Activated Receptor γ with an Unprecedented Binding Mode. *J. Med. Chem.* **2020**, *63* (9), 4555–4561.

(122) Leesnitzer, L. M.; Parks, D. J.; Bledsoe, R. K.; Cobb, J. E.; Collins, J. L.; Consler, T. G.; Davis, R. G.; Hull-Ryde, E. A.; Lenhard, J. M.; Patel, L.; Plunket, K. D.; Shenk, J. L.; Stimmel, J. B.; Therapontos, C.; Willson, T. M.; Blanchard, S. G. Functional Consequences of Cysteine Modification in the Ligand Binding Sites of Peroxisome Proliferator Activated Receptors by GW9662. *Biochemistry* **2002**, *41* (21), 6640–6650.

(123) Oliver, W. R.; Shenk, J. L.; Snaith, M. R.; Russell, C. S.; Plunket, K. D.; Bodkin, N. L.; Lewis, M. C.; Winegar, D. A.; Sznajdman, M. L.; Lambert, M. H.; Xu, H. E.; Sternbach, D. D.; Kliewer, S. A.; Hansen, B. C.; Willson, T. M. A Selective Peroxisome Proliferator-Activated Receptor δ Agonist Promotes Reverse Cholesterol Transport. *Proc. Natl. Acad. Sci. U. S. A.* **2001**, *98* (9), 5306–5311.

(124) Sznajdman, M. L.; Haffner, C. D.; Maloney, P. R.; Fivush, A.; Chao, E.; Goreham, D.; Sierra, M. L.; LeGrumelec, C.; Xu, H. E.; Montana, V. G.; Lambert, M. H.; Willson, T. M.; Oliver, W. R.; Sternbach, D. D. Novel Selective Small Molecule Agonists for Peroxisome Proliferator-Activated Receptor δ (PPAR δ) - Synthesis and Biological Activity. *Bioorg. Med. Chem. Lett.* **2003**, *13* (9), 1517–1521.

(125) Zhang, R.; Wang, A.; DeAngelis, A.; Pelton, P.; Xu, J.; Zhu, P.; Zhou, L.; Demarest, K.; Murray, W. V.; Kuo, G.-H. Discovery of Para-Alkylthiophenoxyacetic Acids as a Novel Series of Potent and Selective PPAR δ Agonists. *Bioorg. Med. Chem. Lett.* **2007**, *17* (14), 3855–3859.

(126) Chang, K. L.; Pee, H. N.; Yang, S.; Ho, P. C. Influence of Drug Transporters and Stereoselectivity on the Brain Penetration of Pioglitazone as a Potential Medicine against Alzheimer's Disease. *Sci. Rep.* **2015**, *5*, 9000.

(127) Sime, M.; Allan, A. C.; Chapman, P.; Fieldhouse, C.; Giblin, G. M. P.; Healy, M. P.; Lambert, M. H.; Leesnitzer, L. M.; Lewis, A.; Merrihew, R. V.; Rutter, R. A.; Sasse, R.; Shearer, B. G.; Willson, T. M.; Xu, R. X.; Virley, D. J. Discovery of GSK1997132B a Novel Centrally Penetrant Benzimidazole PPAR γ Partial Agonist. *Bioorg. Med. Chem. Lett.* **2011**, *21* (18), 5568–5572.

(128) Uriz-Huarte, A.; Date, A.; Ang, H.; Ali, S.; Brady, H. J. M.; Fuchter, M. J. The Transcriptional Repressor REV-ERB as a Novel Target for Disease. *Bioorg. Med. Chem. Lett.* **2020**, *30* (17), 127395.

(129) Kojetin, D. J.; Burris, T. P. REV-ERB and ROR Nuclear Receptors as Drug Targets. *Nat. Rev. Drug Discovery* **2014**, *13* (3), 197–216.

(130) Chang, C.; Loo, C.-S.; Zhao, X.; Solt, L. A.; Liang, Y.; Bapat, S. P.; Cho, H.; Kamenecka, T. M.; Leblanc, M.; Atkins, A. R.; Yu, R. T.; Downes, M.; Burris, T. P.; Evans, R. M.; Zheng, Y. The Nuclear Receptor REV-ERB α Modulates Th17 Cell-Mediated Autoimmune Disease. *Proc. Natl. Acad. Sci. U. S. A.* **2019**, *116* (37), 18528–18536.

(131) Lazar, M. A.; Hodin, R. A.; Darling, D. S.; Chin, W. W. A Novel Member of the Thyroid/Steroid Hormone Receptor Family Is

Encoded by the Opposite Strand of the Rat c-ErbA Alpha Transcriptional Unit. *Mol. Cell. Biol.* **1989**, *9* (3), 1128–1136.

(132) Forman, B. M.; Chen, J.; Blumberg, B.; Kliewer, S. A.; Henshaw, R.; Ong, E. S.; Evans, R. M. Cross-Talk among ROR Alpha 1 and the Rev-Erb Family of Orphan Nuclear Receptors. *Mol. Endocrinol.* **1994**, *8* (9), 1253–1261.

(133) Dumas, B.; Harding, H. P.; Choi, H. S.; Lehmann, K. A.; Chung, M.; Lazar, M. A.; Moore, D. D. A New Orphan Member of the Nuclear Hormone Receptor Superfamily Closely Related to Rev-Erb. *Mol. Endocrinol.* **1994**, *8* (8), 996–1005.

(134) Yin, L.; Lazar, M. A. The Orphan Nuclear Receptor Rev-Erb α Recruits the N-CoR/Histone Deacetylase 3 Corepressor to Regulate the Circadian Bmal1 Gene. *Mol. Endocrinol.* **2005**, *19* (6), 1452–1459.

(135) Torra, I. P.; Tsubulsky, V.; Delaunay, F.; Saladin, R.; Laudet, V.; Fruchart, J.-C.; Kosykh, V.; Staels, B. Circadian and Glucocorticoid Regulation of Rev-Erb α Expression in Liver. *Endocrinology* **2000**, *141* (10), 3799–3806.

(136) Balsalobre, A.; Damiola, F.; Schibler, U. A Serum Shock Induces Circadian Gene Expression in Mammalian Tissue Culture Cells. *Cell* **1998**, *93* (6), 929–937.

(137) Wolff, S. E. C.; Wang, X.-L.; Jiao, H.; Sun, J.; Kalsbeek, A.; Yi, C.-X.; Gao, Y. The Effect of Rev-Erb α Agonist SR9011 on the Immune Response and Cell Metabolism of Microglia. *Front. Immunol.* **2020**, *11*, 550145.

(138) Guo, D.; Zhu, Y.; Sun, H.; Xu, X.; Zhang, S.; Hao, Z.; Wang, G.; Mu, C.; Ren, H. Pharmacological Activation of REV-ERB α Represses LPS-Induced Microglial Activation through the NF-KB Pathway. *Acta Pharmacol. Sin.* **2019**, *40* (1), 26–34.

(139) Roby, D. A.; Ruiz, F.; Kermath, B. A.; Voorhees, J. R.; Niehoff, M.; Zhang, J.; Morley, J. E.; Musiek, E. S.; Farr, S. A.; Burris, T. P. Pharmacological Activation of the Nuclear Receptor REV-ERB Reverses Cognitive Deficits and Reduces Amyloid- β Burden in a Mouse Model of Alzheimer's Disease. *PLoS One* **2019**, *14* (4), e0215004.

(140) Griffin, P.; Dimitry, J. M.; Sheehan, P. W.; Lananna, B. V.; Guo, C.; Robinette, M. L.; Hayes, M. E.; Cedeño, M. R.; Nadarajah, C. J.; Ezerskiy, L. A.; Colonna, M.; Zhang, J.; Bauer, A. Q.; Burris, T. P.; Musiek, E. S. Circadian Clock Protein Rev-Erb α Regulates Neuroinflammation. *Proc. Natl. Acad. Sci. U. S. A.* **2019**, *116* (11), 5102–5107.

(141) Lee, J.; Kim, D. E.; Griffin, P.; Sheehan, P. W.; Kim, D.-H.; Musiek, E. S.; Yoon, S.-Y. Inhibition of REV-ERBs Stimulates Microglial Amyloid-Beta Clearance and Reduces Amyloid Plaque Deposition in the 5XFAD Mouse Model of Alzheimer's Disease. *Aging Cell* **2020**, *19* (2), e13078.

(142) Raghuram, S.; Stayrook, K. R.; Huang, P.; Rogers, P. M.; Nosie, A. K.; McClure, D. B.; Burris, L. L.; Khorasanizadeh, S.; Burris, T. P.; Rastinejad, F. Identification of Heme as the Ligand for the Orphan Nuclear Receptors REV-ERB α and REV-ERB β . *Nat. Struct. Mol. Biol.* **2007**, *14* (12), 1207–1213.

(143) Trump, R. P.; Bresciani, S.; Cooper, A. W. J.; Tellam, J. P.; Wojno, J.; Blakley, J.; Orband-Miller, L. A.; Kashatus, J. A.; Boudjelal, M.; Dawson, H. C.; Loudon, A.; Ray, D.; Grant, D.; Farrow, S. N.; Willson, T. M.; Tomkinson, N. C. O. Optimized Chemical Probes for REV-ERB α . *J. Med. Chem.* **2013**, *56* (11), 4729–4737.

(144) Noel, R.; Song, X.; Shin, Y.; Banerjee, S.; Kojetin, D.; Lin, L.; Ruiz, C. H.; Cameron, M. D.; Burris, T. P.; Kamenecka, T. M. Synthesis and SAR of Tetrahydroisoquinolines as Rev-Erb α Agonists. *Bioorg. Med. Chem. Lett.* **2012**, *22* (11), 3739–3742.

(145) Westermaier, Y.; Ruiz-Carmona, S.; Theret, I.; Perron-Sierra, F.; Poissonnet, G.; Dacquet, C.; Boutin, J. A.; Ducrot, P.; Barril, X. Binding Mode Prediction and MD/MMPBSA-Based Free Energy Ranking for Agonists of REV-ERB α /NCoR. *J. Comput.-Aided Mol. Des.* **2017**, *31* (8), 755–775.

(146) Kojetin, D.; Wang, Y.; Kamenecka, T. M.; Burris, T. P. Identification of SR8278, a Synthetic Antagonist of the Nuclear Heme Receptor REV-ERB. *ACS Chem. Biol.* **2011**, *6* (2), 131–134.

(147) De Mei, C.; Ercolani, L.; Parodi, C.; Veronesi, M.; Vecchio, C. L.; Bottegoni, G.; Torrente, E.; Scarpelli, R.; Marotta, R.; Ruffili, R.; Mattioli, M.; Reggiani, A.; Wade, M.; Grimaldi, B. Dual Inhibition of REV-ERB β and Autophagy as a Novel Pharmacological Approach to Induce Cytotoxicity in Cancer Cells. *Oncogene* **2015**, *34* (20), 2597–2608.

(148) Torrente, E.; Parodi, C.; Ercolani, L.; De Mei, C.; Ferrari, A.; Scarpelli, R.; Grimaldi, B. Synthesis and in Vitro Anticancer Activity of the First Class of Dual Inhibitors of REV-ERB β and Autophagy. *J. Med. Chem.* **2015**, *58* (15), 5900–5915.

(149) Dierickx, P.; Emmett, M. J.; Jiang, C.; Uehara, K.; Liu, M.; Adlanmerini, M.; Lazar, M. A. SR9009 Has REV-ERB-Independent Effects on Cell Proliferation and Metabolism. *Proc. Natl. Acad. Sci. U. S. A.* **2019**, *116* (25), 12147–12152.

(150) Moore, D. D.; Kato, S.; Xie, W.; Mangelsdorf, D. J.; Schmidt, D. R.; Xiao, R.; Kliewer, S. A. International Union of Pharmacology. LXII. The NR1H and NR1I Receptors: Constitutive Androstane Receptor, Pregnane X Receptor, Farnesoid X Receptor α , Farnesoid X Receptor β , Liver X Receptor α , Liver X Receptor β , and Vitamin D Receptor. *Pharmacol. Rev.* **2006**, *58* (4), 742–759.

(151) Viennois, E.; Mouzat, K.; Dufour, J.; Morel, L.; Lobaccaro, J.-M.; Baron, S. Selective Liver X Receptor Modulators (SLiMs): What Use in Human Health? *Mol. Cell. Endocrinol.* **2012**, *351* (2), 129–141.

(152) Mouzat, K.; Chudinova, A.; Polge, A.; Kantar, J.; Camu, W.; Raoul, C.; Lumbroso, S. Regulation of Brain Cholesterol: What Role Do Liver X Receptors Play in Neurodegenerative Diseases? *Int. J. Mol. Sci.* **2019**, *20* (16), 3858.

(153) Hong, C.; Tontonoz, P. Liver X Receptors in Lipid Metabolism: Opportunities for Drug Discovery. *Nature Reviews Drug Discovery* **2014**, *13*, 433–444.

(154) Sodhi, R. K.; Singh, N. Liver X Receptors: Emerging Therapeutic Targets for Alzheimer's Disease. *Pharmacol Res.* **2013**, *72*, 45–51.

(155) Moutinho, M.; Landreth, G. E. Therapeutic Potential of Nuclear Receptor Agonists in Alzheimer's Disease. *J. Lipid Res.* **2017**, *58* (10), 1937–1949.

(156) Björkhem, I.; Meaney, S. Brain Cholesterol: Long Secret Life behind a Barrier. *Arterioscler., Thromb., Vasc. Biol.* **2004**, *24* (5), 806–815.

(157) Hussain, G.; Wang, J.; Rasul, A.; Anwar, H.; Imran, A.; Qasim, M.; Zafar, S.; Kamran, S. K. S.; Razaq, A.; Aziz, N.; Ahmad, W.; Shabbir, A.; Iqbal, J.; Baig, S. M.; Sun, T. Role of Cholesterol and Sphingolipids in Brain Development and Neurological Diseases. *Lipids in Health and Disease* **2019**, *18*, 26.

(158) Mauch, D. H.; Nägler, K.; Schumacher, S.; Göritz, C.; Müller, E.-C.; Otto, A.; Pfrieger, F. W. CNS Synaptogenesis Promoted by Glia-Derived Cholesterol. *Science* **2001**, *294* (5545), 1354–1357.

(159) Zhang, J.; Liu, Q. Cholesterol Metabolism and Homeostasis in the Brain. *Protein Cell* **2015**, *6* (4), 254–264.

(160) Abildayeva, K.; Jansen, P. J.; Hirsch-Reinshagen, V.; Bloks, V. W.; Bakker, A. H. F.; Ramaekers, F. C. S.; De Vente, J.; Groen, A. K.; Wellington, C. L.; Kuipers, F.; Mulder, M. 24(S)-Hydroxycholesterol Participates in a Liver X Receptor-Controlled Pathway in Astrocytes That Regulates Apolipoprotein E-Mediated Cholesterol Efflux. *J. Biol. Chem.* **2006**, *281* (18), 12799–12808.

(161) Peet, D. J.; Turley, S. D.; Ma, W.; Janowski, B. A.; Lobaccaro, J. M. A.; Hammer, R. E.; Mangelsdorf, D. J. Cholesterol and Bile Acid Metabolism Are Impaired in Mice Lacking the Nuclear Oxysterol Receptor LXR α . *Cell* **1998**, *93* (5), 693–704.

(162) Andersson, S.; Gustafsson, N.; Warner, M.; Gustafsson, J.-Å. Inactivation of Liver X Receptor β Leads to Adult-Onset Motor Neuron Degeneration in Male Mice. *Proc. Natl. Acad. Sci. U. S. A.* **2005**, *102* (10), 3857–3862.

(163) Bigini, P.; Steffensen, K. R.; Ferrario, A.; Diomedea, L.; Ferrara, G.; Barbera, S.; Salzano, S.; Fumagalli, E.; Ghezzi, P.; Mennini, T.; Gustafsson, J.-Å. Neuropathologic and Biochemical Changes During Disease Progression in Liver X Receptor β $^{-/-}$ Mice, A Model of Adult Neuron Disease. *J. Neuropathol. Exp. Neurol.* **2010**, *69* (6), 593–605.

- (164) Meffre, D.; Shackelford, G.; Hichor, M.; Gorgievski, V.; Tzavara, E. T.; Trousson, A.; Ghomari, A. M.; Deboux, C.; Oumesmar, B. N.; Liere, P.; Schumacher, M.; Baulieu, E.-E.; Charbonnier, F.; Grenier, J.; Massaad, C. Liver X Receptors Alpha and Beta Promote Myelination and Remyelination in the Cerebellum. *Proc. Natl. Acad. Sci. U. S. A.* **2015**, *112* (24), 7587–7592.
- (165) Song, X.-Y.; Wu, W.-F.; Gabbi, C.; Dai, Y.-B.; So, M.; Chaurasiya, S. P.; Wang, L.; Warner, M.; Gustafsson, J. Å. Retinal and Optic Nerve Degeneration in Liver X Receptor β Knockout Mice. *Proc. Natl. Acad. Sci. U. S. A.* **2019**, *116* (33), 16507–16512.
- (166) Zelcer, N.; Khanlou, N.; Clare, R.; Jiang, Q.; Reed-Geaghan, E. G.; Landreth, G. E.; Vinters, H. V.; Tontonoz, P. Attenuation of Neuroinflammation and Alzheimer's Disease Pathology by Liver x Receptors. *Proc. Natl. Acad. Sci. U. S. A.* **2007**, *104* (25), 10601–10606.
- (167) Cui, W.; Sun, Y.; Wang, Z.; Xu, C.; Peng, Y.; Li, R. Liver X Receptor Activation Attenuates Inflammatory Response and Protects Cholinergic Neurons in APP/PS1 Transgenic Mice. *Neuroscience* **2012**, *210*, 200–210.
- (168) Strittmatter, W. J.; Saunders, A. M.; Schmechel, D.; Pericak-Vance, M.; Englund, J.; Salvesen, G. S.; Roses, A. D. Apolipoprotein E: High-Avidity Binding to β -Amyloid and Increased Frequency of Type 4 Allele in Late-Onset Familial Alzheimer Disease. *Proc. Natl. Acad. Sci. U. S. A.* **1993**, *90* (5), 1977–1981.
- (169) Pitas, R. E.; Boyles, J. K.; Lee, S. H.; Foss, D.; Mahley, R. W. Astrocytes Synthesize Apolipoprotein E and Metabolize Apolipoprotein E-Containing Lipoproteins. *Biochim. Biophys. Acta, Lipids Lipid Metab.* **1987**, *917* (1), 148–161.
- (170) Ignatius, M. J.; Gebicke-Harter, P. J.; Skene, J. H.; Schilling, J. W.; Weisgraber, K. H.; Mahley, R. W.; Shooter, E. M. Expression of Apolipoprotein E during Nerve Degeneration and Regeneration. *Proc. Natl. Acad. Sci. U. S. A.* **1986**, *83* (4), 1125–1129.
- (171) Fukumoto, H.; Deng, A.; Irizarry, M. C.; Fitzgerald, M. L.; Rebeck, G. W. Induction of the Cholesterol Transporter ABCA1 in Central Nervous System Cells by Liver X Receptor Agonists Increases Secreted $A\beta$ Levels. *J. Biol. Chem.* **2002**, *277* (50), 48508–48513.
- (172) Sun, Y.; Yao, J.; Kim, T.-W.; Tall, A. R. Expression of Liver X Receptor Target Genes Decreases Cellular Amyloid β Peptide Secretion. *J. Biol. Chem.* **2003**, *278* (30), 27688–27694.
- (173) Koldamova, R. P.; Lefterov, I. M.; Staufenbiel, M.; Wolfe, D.; Huang, S.; Glorioso, J. C.; Walter, M.; Roth, M. G.; Lazo, J. S. The Liver X Receptor Ligand T0901317 Decreases Amyloid β Production in Vitro and in a Mouse Model of Alzheimer's Disease. *J. Biol. Chem.* **2005**, *280* (6), 4079–4088.
- (174) Fitz, N. F.; Cronican, A.; Pham, T.; Fogg, A.; Fauq, A. H.; Chapman, R.; Lefterov, I.; Koldamova, R. Liver X Receptor Agonist Treatment Ameliorates Amyloid Pathology and Memory Deficits Caused by High-Fat Diet in APP23 Mice. *J. Neurosci.* **2010**, *30* (20), 6862–6872.
- (175) Cui, W.; Sun, Y.; Wang, Z.; Xu, C.; Xu, L.; Wang, F.; Chen, Z.; Peng, Y.; Li, R. Activation of Liver x Receptor Decreases BACE1 Expression and Activity by Reducing Membrane Cholesterol Levels. *Neurochem. Res.* **2011**, *36* (10), 1910–1921.
- (176) Wang, Q.; Wang, S.; Shi, Y.; Yao, M.; Hou, L.; Jiang, L. Reduction of Liver X Receptor β Expression in Primary Rat Neurons by Antisense Oligodeoxynucleotides Decreases Secreted Amyloid β Levels. *Neurosci. Lett.* **2014**, *561*, 146–150.
- (177) Vanmierlo, T.; Rutten, K.; Dederen, J.; Bloks, V. W.; van Vark-van der Zee, L. C.; Kuipers, F.; Kiliaan, A.; Blokland, A.; Sijbrands, E. J. G.; Steinbusch, H.; Prickaerts, J.; Lütjohann, D.; Mulder, M. Liver X Receptor Activation Restores Memory in Aged AD Mice without Reducing Amyloid. *Neurobiol. Aging* **2011**, *32* (7), 1262–1272.
- (178) Sandoval-Hernández, A. G.; Buitrago, L.; Moreno, H.; Cardona-Gómez, G. P.; Arboleda, G. Role of Liver X Receptor in AD Pathophysiology. *PLoS One* **2015**, *10* (12), e0145467.
- (179) Báez-Becerra, C.; Filipello, F.; Sandoval-Hernández, A.; Arboleda, H.; Arboleda, G. Liver X Receptor Agonist GW3965 Regulates Synaptic Function upon Amyloid Beta Exposure in Hippocampal Neurons. *Neurotoxic. Res.* **2018**, *33* (4), 569–579.
- (180) Kumar, N.; Solt, L. A.; Conkright, J. J.; Wang, Y.; Istrate, M. A.; Busby, S. A.; Garcia-Ordóñez, R. D.; Burris, T. P.; Griffin, P. R. The Benzenesulfoamide T0901317 [N-(2,2,2-Trifluoroethyl)-N-[4-[2,2,2-Trifluoro-1-Hydroxy-1-(Trifluoromethyl)Ethyl]Phenyl]-Benzenesulfonamide] Is a Novel Retinoic Acid Receptor-Related Orphan Receptor- α/γ Inverse Agonist. *Mol. Pharmacol.* **2010**, *77* (2), 228–236.
- (181) Dai, Y.-B.; Tan, X.-J.; Wu, W.-F.; Warner, M.; Gustafsson, J.-Å. Liver X Receptor β Protects Dopaminergic Neurons in a Mouse Model of Parkinson Disease. *Proc. Natl. Acad. Sci. U. S. A.* **2012**, *109* (32), 13112–13117.
- (182) Nelissen, K.; Mulder, M.; Smets, I.; Timmermans, S.; Smeets, K.; Ameloot, M.; Hendriks, J. J. A. Liver X Receptors Regulate Cholesterol Homeostasis in Oligodendrocytes. *J. Neurosci. Res.* **2012**, *90* (1), 60–71.
- (183) Berghoff, S. A.; Spieth, L.; Sun, T.; Hosang, L.; Schlaphoff, L.; Depp, C.; Düking, T.; Winchenbach, J.; Neuber, J.; Ewers, D.; Scholz, P.; van der Meer, F.; Cantuti-Castelvetri, L.; Sasmita, A. O.; Meschkat, M.; Ruhwedel, T.; Möbius, W.; Sankowski, R.; Prinz, M.; Huitinga, I.; Sereda, M. W.; Odoardi, F.; Ischebeck, T.; Simons, M.; Stadelmann-Nessler, C.; Edgar, J. M.; Nave, K.-A.; Saher, G. Microglia Facilitate Repair of Demyelinated Lesions via Post-Squalene Sterol Synthesis. *Nat. Neurosci.* **2021**, *24* (1), 47–60.
- (184) Maillieux, J.; Vanmierlo, T.; Bogie, J. F. J.; Wouters, E.; Lütjohann, D.; Hendriks, J. J. A.; van Horssen, J. Active Liver X Receptor Signaling in Phagocytes in Multiple Sclerosis Lesions. *Mult. Scler. J.* **2018**, *24* (3), 279–289.
- (185) Cui, G.; Qin, X.; Wu, L.; Zhang, Y.; Sheng, X.; Yu, Q.; Sheng, H.; Xi, B.; Zhang, J. Z.; Zang, Y. Q. Liver X Receptor (LXR) Mediates Negative Regulation of Mouse and Human Th17 Differentiation. *J. Clin. Invest.* **2011**, *121* (2), 658–670.
- (186) Schultz, J. R.; Tu, H.; Luk, A.; Repa, J. J.; Medina, J. C.; Li, L.; Schwendner, S.; Wang, S.; Thoolen, M.; Mangelsdorf, D. J.; Lustig, K. D.; Shan, B. Role of LXRs in Control of Lipogenesis. *Genes Dev.* **2000**, *14* (22), 2831–2838.
- (187) Collins, J. L.; Fivush, A. M.; Watson, M. A.; Galardi, C. M.; Lewis, M. C.; Moore, L. B.; Parks, D. J.; Wilson, J. G.; Tippin, T. K.; Binz, J. G.; Plunket, K. D.; Morgan, D. G.; Beaudet, E. J.; Whitney, K. D.; Klierer, S. A.; Willson, T. M. Identification of a Nonsteroidal Liver X Receptor Agonist through Parallel Array Synthesis of Tertiary Amines. *J. Med. Chem.* **2002**, *45* (10), 1963–1966.
- (188) Kirchgessner, T. G.; Martin, R.; Sleph, P.; Grimm, D.; Liu, X.; Lupisella, J.; Smalley, J.; Narayanan, R.; Xie, Y.; Ostrowski, J.; Cantor, G. H.; Mohan, R.; Kick, E. Pharmacological Characterization of a Novel Liver X Receptor Agonist with Partial LXR α Activity and a Favorable Window in Nonhuman Primates. *J. Pharmacol. Exp. Ther.* **2015**, *352* (2), 305–314.
- (189) Wrobel, J.; Steffan, R.; Bowen, S. M.; Magolda, R.; Matelan, E.; Unwalla, R.; Basso, M.; Clerin, V.; Gardell, S. J.; Nambi, P.; Quinet, E.; Reminick, J. I.; Vlasuk, G. P.; Wang, S.; Feingold, I.; Huselton, C.; Bonn, T.; Farnegardh, M.; Hansson, T.; Nilsson, A. G.; Wilhelmsson, A.; Zamaratski, E.; Evans, M. J. Indazole-Based Liver X Receptor (LXR) Modulators with Maintained Atherosclerotic Lesion Reduction Activity but Diminished Stimulation of Hepatic Triglyceride Synthesis. *J. Med. Chem.* **2008**, *51* (22), 7161–7168.
- (190) Stachel, S. J.; Zerbinatti, C.; Rudd, M. T.; Cosden, M.; Suon, S.; Nanda, K. K.; Wessner, K.; Dimuzio, J.; Maxwell, J.; Wu, Z.; Uslander, J. M.; Michener, M. S.; Szczerba, P.; Brnardic, E.; Rada, V.; Kim, Y.; Meissner, R.; Wuelfing, P.; Yuan, Y.; Ballard, J.; Holahan, M.; Klein, D. J.; Lu, J.; Fradera, X.; Parthasarathy, G.; Uebele, V. N.; Chen, Z.; Li, Y.; Li, J.; Cooke, A. J.; Bennett, D. J.; Bilodeau, M. T.; Renger, J. Identification and in Vivo Evaluation of Liver X Receptor β -Selective Agonists for the Potential Treatment of Alzheimer's Disease. *J. Med. Chem.* **2016**, *59* (7), 3489–3498.
- (191) Gezen-Ak, D.; Dursun, E. Molecular Basis of Vitamin D Action in Neurodegeneration: The Story of a Team Perspective. *Hormones* **2019**, *18* (3), 17–21.
- (192) Makishima, M.; Lu, T. T.; Xie, W.; Whitfield, G. K.; Domoto, H.; Evans, R. M.; Haussler, M. R.; Mangelsdorf, D. J. Vitamin D

Receptor as an Intestinal Bile Acid Sensor. *Science* **2002**, *296* (5571), 1313–1316.

(193) Yao, B.; He, J.; Yin, X.; Shi, Y.; Wan, J.; Tian, Z. The Protective Effect of Lithocholic Acid on the Intestinal Epithelial Barrier Is Mediated by the Vitamin D Receptor via a SIRT1/Nrf2 and NF-KB Dependent Mechanism in Caco-2 Cells. *Toxicol. Lett.* **2019**, *316*, 109–118.

(194) Eyles, D. W.; Smith, S.; Kinobe, R.; Hewison, M.; McGrath, J. J. Distribution of the Vitamin D Receptor and 1 α -Hydroxylase in Human Brain. *J. Chem. Neuroanat.* **2005**, *29* (1), 21–30.

(195) Burne, T. H. J.; McGrath, J. J.; Eyles, D. W.; Mackay-Sim, A. Behavioural Characterization of Vitamin D Receptor Knockout Mice. *Behav. Brain Res.* **2005**, *157* (2), 299–308.

(196) Beecham, G. W.; Martin, E. R.; Li, Y. J.; Slifer, M. A.; Gilbert, J. R.; Haines, J. L.; Pericak-Vance, M. A. Genome-Wide Association Study Implicates a Chromosome 12 Risk Locus for Late-Onset Alzheimer Disease. *Am. J. Hum. Genet.* **2009**, *84* (1), 35–43.

(197) Butler, M. W.; Burt, A.; Edwards, T. L.; Zuchner, S.; Scott, W. K.; Martin, E. R.; Vance, J. M.; Wang, L. Vitamin D Receptor Gene as a Candidate Gene for Parkinson Disease. *Ann. Hum. Genet.* **2011**, *75* (2), 201–210.

(198) Kim, J.-S.; Kim, Y.-I.; Song, C.; Yoon, I.; Park, J.-W.; Choi, Y.-B.; Kim, H.-T.; Lee, K.-S. Association of Vitamin D Receptor Gene Polymorphism and Parkinson's Disease in Koreans. *J. Korean Med. Sci.* **2005**, *20* (3), 495–498.

(199) Niino, M.; Miyazaki, Y. Genetic Polymorphisms Related to Vitamin D and the Therapeutic Potential of Vitamin D in Multiple Sclerosis. *Can. J. Physiol. Pharmacol.* **2015**, *93* (5), 319–325.

(200) Vinh quốc Luong, K.; Thi Hoàng Nguyễn, L. Vitamin D and Parkinson's Disease. *J. Neurosci Res.* **2012**, *90*, 2227–2236.

(201) Banerjee, A.; Khemka, V. K.; Ganguly, A.; Roy, D.; Ganguly, U.; Chakrabarti, S. Vitamin D and Alzheimer's Disease: Neuro-cognition to Therapeutics. *Int. J. Alzheimer's Dis.* **2015**, *2015*, 192747.

(202) Luong, K.; Nguyen, L. Role of Vitamin D in Parkinson's Disease. *ISRN Neurol.* **2012**, *2012*, No. 134289.

(203) Munger, K. L.; Levin, L. I.; Hollis, B. W.; Howard, N. S.; Ascherio, A. Serum 25-Hydroxyvitamin D Levels and Risk of Multiple Sclerosis. *J. Am. Med. Assoc.* **2006**, *296* (23), 2832–2838.

(204) Moretti, R.; Morelli, M. E.; Caruso, P. Vitamin D in Neurological Diseases: A Rationale for a Pathogenic Impact. *Int. J. Mol. Sci.* **2018**, *19* (8), 2245.

(205) Salzer, J.; Hallmans, G.; Nyström, M.; Stenlund, H.; Wadell, G.; Sundström, P. Vitamin D as a Protective Factor in Multiple Sclerosis. *Neurology* **2012**, *79* (21), 2140–2145.

(206) Grimm, M. O. W.; Lauer, A. A.; Grösgen, S.; Thiel, A.; Lehmann, J.; Winkler, J.; Janitschke, D.; Herr, C.; Beisswenger, C.; Bals, R.; Grimm, H. S.; Hartmann, T. Profiling of Alzheimer's Disease Related Genes in Mild to Moderate Vitamin D Hypovitaminosis. *J. Nutr. Biochem.* **2019**, *67*, 123–137.

(207) Uberti, F.; Morsanuto, V.; Bardelli, C.; Molinari, C. Protective Effects of 1 α ,25-Dihydroxyvitamin D3 on Cultured Neural Cells Exposed to Catalytic Iron. *Physiol. Rep.* **2016**, *4* (11), e12769.

(208) Ibi, M.; Sawada, H.; Nakanishi, M.; Kume, T.; Katsuki, H.; Kaneko, S.; Shimohama, S.; Akaike, A. Protective Effects of 1 α ,25-(OH)₂D₃ against the Neurotoxicity of Glutamate and Reactive Oxygen Species in Mesencephalic Culture. *Neuropharmacology* **2001**, *40* (6), 761–771.

(209) Zhang, D.; Li, M.; Dong, Y.; Zhang, X.; Liu, X.; Chen, Z.; Zhu, Y.; Wang, H.; Liu, X.; Zhu, J.; Shen, Y.; Korner, H.; Ying, S.; Fang, S.; Shen, Y. 1 α ,25-Dihydroxyvitamin D3 up-Regulates IL-34 Expression in SH-SY5Y Neural Cells. *Innate Immun.* **2017**, *23* (7), 584–591.

(210) Jiao, K.-P.; Li, S.-M.; Lv, W.-Y.; Jv, M.-L.; He, H.-Y. Vitamin D3 Repressed Astrocyte Activation Following Lipopolysaccharide Stimulation in Vitro and in Neonatal Rats. *NeuroReport* **2017**, *28* (9), 492–497.

(211) Dursun, E.; Gezen-Ak, D.; Yilmazer, S. A Novel Perspective for Alzheimer's Disease: Vitamin D Receptor Suppression by Amyloid- β and Preventing the Amyloid- β Induced Alterations by

Vitamin D in Cortical Neurons. *Journal of Alzheimer's Disease* **2011**, *23* (2), 207–219.

(212) Niino, M. Vitamin D and Its Immunoregulatory Role in Multiple Sclerosis. *Drugs Today (Barc)* **2010**, *46* (4), 279–290.

(213) Kim, H.; Shin, J.-Y.; Lee, Y.-S.; Yun, S. P.; Maeng, H.-J.; Lee, Y. Brain Endothelial P-Glycoprotein Level Is Reduced in Parkinson's Disease via a Vitamin D Receptor-Dependent Pathway. *Int. J. Mol. Sci.* **2020**, *21* (22), 8538.

(214) Maestro, M. A.; Molnár, F.; Carlberg, C. Vitamin D and Its Synthetic Analogs. *J. Med. Chem.* **2019**, *62* (15), 6854–6875.

(215) Bishop, J. E.; Collins, E. D.; Okamura, W. H.; Norman, A. W. Profile of Ligand Specificity of the Vitamin D Binding Protein for 1 α ,25-dihydroxyvitamin D3 and Its Analogs. *J. Bone Miner. Res.* **1994**, *9* (8), 1277–1288.

(216) Saito, N.; Matsunaga, T.; Saito, H.; Anzai, M.; Takenouchi, K.; Miura, D.; Namekawa, J.; Ishizuka, S.; Kittaka, A. Further Synthetic and Biological Studies on Vitamin D Hormone Antagonists Based on C24-Alkylation and C2 α -Functionalization of 25-Dehydro-1 α -Hydroxyvitamin D3–26,23-Lactones. *J. Med. Chem.* **2006**, *49* (24), 7063–7075.

(217) Wiberg, K.; Ljunghall, S.; Binderup, L.; Ljunggren, Ö. Studies on Two New Vitamin D Analogs, EB 1089 and KH 1060: Effects on Bone Resorption and Osteoclast Recruitment in Vitro. *Bone* **1995**, *17* (4), 391–395.

(218) Germain, P.; Chambon, P.; Eichele, G.; Evans, R. M.; Lazar, M. A.; Leid, M.; De Lera, A. R.; Lotan, R.; Mangelsdorf, D. J.; Gronemeyer, H. International Union of Pharmacology. LXIII. Retinoid X Receptors. *Pharmacol. Rev.* **2006**, *58* (4), 760–772.

(219) de Lera, A. R.; Bourguet, W.; Altucci, L.; Gronemeyer, H. Design of Selective Nuclear Receptor Modulators: RAR and RXR as a Case Study. *Nat. Rev. Drug Discovery* **2007**, *6* (10), 811–820.

(220) Dominguez, M.; Alvarez, S.; de Lera, A. R. Natural and Structure-Based RXR Ligand Scaffolds and Their Functions. *Curr. Top. Med. Chem.* **2017**, *17* (6), 631–662.

(221) Chaikwad, A.; Pollinger, J.; Rühl, M.; Ni, X.; Kilu, W.; Heering, J.; Merk, D. Comprehensive Set of Tertiary Complex Structures and Palmitic Acid Binding Provide Molecular Insights into Ligand Design for RXR Isoforms. *Int. J. Mol. Sci.* **2020**, *21* (22), 8457.

(222) Schierle, S.; Merk, D. Therapeutic Modulation of Retinoid X Receptors - SAR and Therapeutic Potential of RXR Ligands and Recent Patents. *Expert Opin. Ther. Pat.* **2019**, *29* (8), 605–621.

(223) Egea, P. F.; Mitschler, A.; Moras, D. Molecular Recognition of Agonist Ligands by RXRs. *Mol. Endocrinol.* **2002**, *16* (5), 987–997.

(224) Zetterstrom, R. H.; Lindqvist, E.; De Urquiza, A. M.; Tomac, A.; Eriksson, U.; Perlmann, T.; Olson, L. Role of Retinoids in the CNS: Differential Expression of Retinoid Binding Proteins and Receptors and Evidence for Presence of Retinoic Acid. *Eur. J. Neurosci.* **1999**, *11* (2), 407–416.

(225) Ferré, S.; Fredholm, B. B.; Morelli, M.; Popoli, P.; Fuxe, K. Adenosine – Dopamine Receptor – Receptor Interactions as an Integrative Mechanism in the Basal Ganglia. *Trends Neurosci.* **1997**, *20* (10), 482–487.

(226) Moreno, S.; Farioli-Vecchioli, S.; Cerù, M. P. Immunolocalization of Peroxisome Proliferator-Activated Receptors and Retinoid X Receptors in the Adult Rat CNS. *Neuroscience* **2004**, *123* (1), 131–145.

(227) Huang, J. K.; Jarjour, A. A.; Nait Oumesmar, B.; Kerninon, C.; Williams, A.; Krezel, W.; Kagechika, H.; Bauer, J.; Zhao, C.; Baron-Van Evercooren, A.; Chambon, P.; Ffrench-Constant, C.; Franklin, R. J. M. Retinoid X Receptor Gamma Signaling Accelerates CNS Remyelination. *Nat. Neurosci.* **2011**, *14* (1), 45–53.

(228) Hanafy, K. A.; Sloane, J. A. Regulation of Remyelination in Multiple Sclerosis. *FEBS Lett.* **2011**, *585* (23), 3821–3828.

(229) Vaz, B.; de Lera, A. R. Advances in Drug Design with RXR Modulators. *Expert Opin. Drug Discovery* **2012**, *7* (11), 1003–1016.

(230) Koster, K. P.; Smith, C.; Valencia-Olvera, A. C.; Thatcher, G. R. J.; Tai, L. M.; LaDu, M. J. Retinoids as Therapeutics for Alzheimer's Disease: Role of APOE. *Curr. Top. Med. Chem.* **2017**, *17* (6), 708–720.

- (231) Corder, E. H.; Saunders, A. M.; Strittmatter, W. J.; Schmechel, D. E.; Gaskell, P. C.; Small, G. W.; Roses, A. D.; Haines, J. L.; Pericak-Vance, M. A. Gene Dose of Apolipoprotein E Type 4 Allele and the Risk of Alzheimer's Disease in Late Onset Families. *Science* **1993**, *261* (5123), 921–923.
- (232) Cosentino, S.; Scarmeas, N.; Helzner, E.; Glymour, M. M.; Brandt, J.; Albert, M.; Blacker, D.; Stern, Y. APOE Epsilon 4 Allele Predicts Faster Cognitive Decline in Mild Alzheimer Disease. *Neurology* **2008**, *70* (19), 1842–1849.
- (233) Khachaturian, A. S.; Corcoran, C. D.; Mayer, L. S.; Zandi, P. P.; Breitner, J. C. S. Apolipoprotein E Epsilon4 Count Affects Age at Onset of Alzheimer Disease, but Not Lifetime Susceptibility: The Cache County Study. *Arch. Gen. Psychiatry* **2004**, *61* (5), 518–524.
- (234) Mandrekar-Colucci, S.; Landreth, G. E. Nuclear Receptors as Therapeutic Targets for Alzheimer's Disease. *Expert Opin. Ther. Targets* **2011**, *15* (9), 1085–1097.
- (235) Koldamova, R.; Fitz, N. F.; Lefterov, I. ATP-Binding Cassette Transporter A1: From Metabolism to Neurodegeneration. *Neurobiol. Dis.* **2014**, *72A*, 13–21.
- (236) Oram, J. F.; Vaughan, A. M. ATP-Binding Cassette Cholesterol Transporters and Cardiovascular Disease. *Circ. Res.* **2006**, *99* (10), 1031–1043.
- (237) Tai, L. M.; Mehra, S.; Shete, V.; Estus, S.; Rebeck, G. W.; Bu, G.; Ladu, M. J. Soluble ApoE/A β Complex: Mechanism and Therapeutic Target for APOE4-Induced AD Risk. *Mol. Neurodegener.* **2014**, *9*, 2.
- (238) Yu, C.; Youmans, K. L.; Ladu, M. J. Proposed Mechanism for Lipoprotein Remodelling in the Brain. *Biochim. Biophys. Acta, Mol. Cell Biol. Lipids* **2010**, *1801* (8), 819–823.
- (239) Cramer, P. E.; Cirrito, J. R.; Wesson, D. W.; Lee, C. Y. D.; Karlo, J. C.; Zinn, A. E.; Casali, B. T.; Restivo, J. L.; Goebel, W. D.; James, M. J.; Brunden, K. R.; Wilson, D. A.; Landreth, G. E. ApoE-Directed Therapeutics Rapidly Clear β -Amyloid and Reverse Deficits in AD Mouse Models. *Science* **2012**, *335* (6075), 1503–1506.
- (240) Fitz, N. F.; Cronican, A. A.; Lefterov, I.; Koldamova, R. Comment on "ApoE-Directed Therapeutics Rapidly Clear β -Amyloid and Reverse Deficits in AD Mouse Models. *Science* **2013**, *340* (6135), 924–c.
- (241) Price, A. R.; Xu, G.; Siemienski, Z. B.; Smithson, L. A.; Borchelt, D. R.; Golde, T. E.; Felsenstein, K. M. Comment on "ApoE-Directed Therapeutics Rapidly Clear β -Amyloid and Reverse Deficits in AD Mouse Models. *Science* **2013**, *340* (6135), 924–d.
- (242) Tesseur, I.; Lo, A. C.; Roberfroid, A.; Dietvorst, S.; Van Broeck, B.; Borgers, M.; Gijssen, H.; Moechars, D.; Mercken, M.; Kemp, J.; D'Hooge, R.; De Strooper, B. Comment on "ApoE-Directed Therapeutics Rapidly Clear β -Amyloid and Reverse Deficits in AD Mouse Models. *Science* **2013**, *340* (6135), 924–e.
- (243) Veeraraghavalu, K.; Zhang, C.; Miller, S.; Hefendehl, J. K.; Rajapaksha, T. W.; Ulrich, J.; Jucker, M.; Holtzman, D. M.; Tanzi, R. E.; Vassar, R.; Sisodia, S. S. Comment on "ApoE-Directed Therapeutics Rapidly Clear β -Amyloid and Reverse Deficits in AD Mouse Models. *Science* **2013**, *340* (6135), 924–f.
- (244) Ghosal, K.; Haag, M.; Verghese, P. B.; West, T.; Veenstra, T.; Braunstein, J. B.; Bateman, R. J.; Holtzman, D. M.; Landreth, G. E. A Randomized Controlled Study to Evaluate the Effect of Bexarotene on Amyloid- β and Apolipoprotein E Metabolism in Healthy Subjects. *Alzheimer's Dement. Transl. Res. Clin. Interv.* **2016**, *2* (2), 110–120.
- (245) Cummings, J. L.; Zhong, K.; Kinney, J. W.; Heaney, C.; Moll-Tudla, J.; Joshi, A.; Pontecorvo, M.; Devous, M.; Tang, A.; Bena, J. Double-Blind, Placebo-Controlled, Proof-of-Concept Trial of Bexarotene in Moderate Alzheimer's Disease. *Alzheimer's Res. Ther.* **2016**, *8* (4), 4.
- (246) Lammi, J.; Perlmann, T.; Aarnisalo, P. Corepressor Interaction Differentiates the Permissive and Non-Permissive Retinoid X Receptor Heterodimers. *Arch. Biochem. Biophys.* **2008**, *472* (2), 105–114.
- (247) Schrage, K.; Koopmans, G.; Joosten, E. A. J.; Mey, J. Macrophages and Neurons Are Targets of Retinoic Acid Signaling after Spinal Cord Contusion Injury. *Eur. J. Neurosci.* **2006**, *23* (2), 285–295.
- (248) Natrajan, M. S.; de la Fuente, A. G.; Crawford, A. H.; Linehan, E.; Nuñez, V.; Johnson, K. R.; Wu, T.; Fitzgerald, D. C.; Ricote, M.; Bielekova, B.; Franklin, R. J. M. Retinoid X Receptor Activation Reverses Age-Related Deficiencies in Myelin Debris Phagocytosis and Remyelination. *Brain* **2015**, *138* (12), 3581–3597.
- (249) Baer, A. S.; Syed, Y. A.; Kang, S. U.; Mitteregger, D.; Vig, R.; Ffrench-Constant, C.; Franklin, R. J. M.; Altmann, F.; Lubec, G.; Kotter, M. R. Myelin-Mediated Inhibition of Oligodendrocyte Precursor Differentiation Can Be Overcome by Pharmacological Modulation of Fyn-RhoA and Protein Kinase C Signalling. *Brain* **2009**, *132* (2), 465–481.
- (250) Kotter, M. R.; Zhao, C.; van Rooijen, N.; Franklin, R. J. M. Macrophage-Depletion Induced Impairment of Experimental CNS Remyelination Is Associated with a Reduced Oligodendrocyte Progenitor Cell Response and Altered Growth Factor Expression. *Neurobiol. Dis.* **2005**, *18* (1), 166–175.
- (251) Xu, J.; Drew, P. D. 9-Cis-Retinoic Acid Suppresses Inflammatory Responses of Microglia and Astrocytes. *J. Neuroimmunol.* **2006**, *171* (1–2), 135–144.
- (252) Chandraratna, R. A.; Sanders, M. E. WO2017/075607 Treatment of Nervous System Disorders Using Combinations of RXR Agonists and Thyroid Hormones, IO Ther. INC, 2017.
- (253) Volle, D. H. Nuclear Receptors as Pharmacological Targets, Where Are We Now? *Cell. Mol. Life Sci.* **2016**, *73* (10), 3777–3780.
- (254) Levin, A. A.; Sturzenbecker, L. J.; Kazmer, S.; Bosakowski, T.; Huselton, C.; Allenby, G.; Speck, J.; Kratzeisen, C.; Rosenberger, M.; Lovey, A.; Grippo, J. F. 9-Cis Retinoic Acid Stereoisomer Binds and Activates the Nuclear Receptor RXR Alpha. *Nature* **1992**, *355* (6358), 359–361.
- (255) Goldstein, J. T.; Dobrzyn, A.; Clagett-Dame, M.; Pike, J. W.; Deluca, H. F. Isolation and Characterization of Unsaturated Fatty Acids as Natural Ligands for the Retinoid-X Receptor. *Arch. Biochem. Biophys.* **2003**, *420* (1), 185–193.
- (256) Fitzgerald, P.; Teng, M.; Chandraratna, R. A. S.; Heyman, A.; Allegretto, A. Retinoic Acid Receptor α Expression Correlates with Retinoid-Induced Growth Inhibition of Human Breast Cancer Cells Regardless of Estrogen Receptor Status. *Cancer Res.* **1997**, *57* (13), 2642–2650.
- (257) Vuligonda, V.; Thacher, S. M.; Chandraratna, R. A. Enantioselective Syntheses of Potent Retinoid X Receptor Ligands: Differential Biological Activities of Individual Antipodes. *J. Med. Chem.* **2001**, *44* (14), 2298–2303.
- (258) Boehm, M. F.; McClurg, M. R.; Pathirana, C.; Mangelsdorf, D.; White, S. K.; Hebert, J.; Winn, D.; Goldman, M. E.; Heyman, R. A. Synthesis of High Specific Activity [3 H]-9-Cis-Retinoic Acid and Its Application for Identifying Retinoids with Unusual Binding Properties. *J. Med. Chem.* **1994**, *37* (3), 408–414.
- (259) Blair, H. A.; Scott, L. J. Alitretinoin: A Review in Severe Chronic Hand Eczema. *Drugs* **2016**, *76* (13), 1271–1279.
- (260) Cheer, S. M.; Foster, R. H. Alitretinoin. *Am. J. Clin. Dermatol.* **2000**, *1* (5), 307–314.
- (261) Son, J. H.; Park, S. Y.; Cho, Y. S.; Byun, Y. S.; Chung, B. Y.; Cho, H. J.; Kim, H. O.; Park, C. W. Two Cases of Successful Treatment of Refractory Chronic Inflammatory Skin Disease, Atopic Dermatitis and Psoriasis with Oral Alitretinoin. *Ann. Dermatol.* **2017**, *29* (4), S03–S06.
- (262) Rühl, R.; Krzyzosiak, A.; Niewiadomska-Cimicka, A.; Rochel, N.; Szeles, L.; Vaz, B.; Wietrzyk-Schindler, M.; Álvarez, S.; Szklenar, M.; Nagy, L.; de Lera, A. R.; Krezel, W. 9-Cis-13,14-Dihydroretinoic Acid Is an Endogenous Retinoid Acting as RXR Ligand in Mice. *PLoS Genet.* **2015**, *11* (6), e1005213.
- (263) de Lera, A.; Krezel, W.; Rühl, R. An Endogenous Mammalian Retinoid X Receptor Ligand, at Last! *ChemMedChem* **2016**, *11* (10), 1027–1037.
- (264) Neuringer, M.; Anderson, G. J.; Connor, W. E. The Essentiality of N-3 Fatty Acids for the Development and Function of the Retina and Brain. *Annu. Rev. Nutr.* **1988**, *8*, 517–541.

- (265) Bourguet, W.; Vivat, V.; Wurtz, J.-M.; Chambon, P.; Gronemeyer, H.; Moras, D. Crystal Structure of a Heterodimeric Complex of RAR and RXR Ligand-Binding Domains. *Mol. Cell* **2000**, *5* (2), 289–298.
- (266) Heald, P.; Mehlmauer, M.; Martin, A. G.; Crowley, C. A.; Yocum, R. C.; Reich, S. D. Topical Bexarotene Therapy for Patients with Refractory or Persistent Early-Stage Cutaneous T-Cell Lymphoma: Results of the Phase III Clinical Trial. *J. Am. Acad. Dermatol.* **2003**, *49* (5), 801–815.
- (267) Wong, S. F. Oral Bexarotene in the Treatment of Cutaneous T-Cell Lymphoma. *Ann. Pharmacother.* **2001**, *35* (9), 1056–1065.
- (268) Boehm, M. F.; Zhang, L.; Badea, B. A.; White, S. K.; Mais, D. E.; Berger, E.; Suto, C. M.; Goldman, M. E.; Heyman, R. A. Synthesis and Structure-Activity Relationships of Novel Retinoid X Receptor-Selective Retinoids. *J. Med. Chem.* **1994**, *37* (18), 2930–2941.
- (269) Howell, S. R.; Shirley, M. A.; Grese, T. A.; Neel, D. A.; Wells, K. E.; Ulm, E. H. Bexarotene Metabolism in Rat, Dog, and Human, Synthesis of Oxidative Metabolites, and in Vitro Activity at Retinoid Receptors. *Drug Metab. Dispos.* **2001**, *29* (7), 990–998.
- (270) Wang, Y.; Rong, J.; Zhang, J.; Liu, Y.; Meng, X.; Guo, H.; Liu, H.; Chen, L. Morphology, *in Vivo* Distribution and Antitumor Activity of Bexarotene Nanocrystals in Lung Cancer. *Drug Dev. Ind. Pharm.* **2017**, *43* (1), 132–141.
- (271) Lowenthal, J.; Hull, S. C.; Pearson, S. D. The Ethics of Early Evidence - Preparing for a Possible Breakthrough in Alzheimer's Disease. *N. Engl. J. Med.* **2012**, *367* (6), 488–490.
- (272) Takamatsu, K.; Takano, A.; Yakushiji, N.; Morishita, K.; Matsuura, N.; Makishima, M.; Ali, H. I.; Akaho, E.; Tai, A.; Sasaki, K.; Kakuta, H. Reduction of Lipophilicity at the Lipophilic Domain of RXR Agonists Enables Production of Subtype Preference: RXR α -Preferential Agonist Possessing a Sulfonamide Moiety. *ChemMedChem* **2008**, *3* (3), 454–460.
- (273) Boehm, M. F.; Zhang, L.; Zhi, L.; McClurg, M. R.; Berger, E.; Wagoner, M.; Mais, D. E.; Suto, C. M.; Davies, P. J. A.; Heyman, R. A.; Nadzan, A. M. Design and Synthesis of Potent Retinoid X Receptor Selective Ligands That Induce Apoptosis in Leukemia Cells. *J. Med. Chem.* **1995**, *38* (16), 3146–3155.
- (274) Takamatsu, K.; Takano, A.; Yakushiji, N.; Morohashi, K.; Morishita, K.; Matsuura, N.; Makishima, M.; Tai, A.; Sasaki, K.; Kakuta, H. The First Potent Subtype-Selective Retinoid X Receptor (RXR) Agonist Possessing a 3-Isopropoxy-4-isopropylphenylamino Moiety, NET-3IP (RXR α /B-dual Agonist). *ChemMedChem* **2008**, *3* (5), 780–787.
- (275) Pollinger, J.; Merk, D. Therapeutic Applications of the Versatile Fatty Acid Mimetic WY14643. *Expert Opin. Ther. Pat.* **2017**, *27* (4), 517–525.
- (276) Watanabe, M.; Kakuta, H. Retinoid X Receptor Antagonists. *Int. J. Mol. Sci.* **2018**, *19* (8), No. 2354.
- (277) Nakayama, M.; Yamada, S.; Ohsawa, F.; Ohta, Y.; Kawata, K.; Makishima, M.; Kakuta, H. Discovery of a Potent Retinoid X Receptor Antagonist Structurally Closely Related to RXR Agonist NET-3IB. *ACS Med. Chem. Lett.* **2011**, *2* (12), 896–900.
- (278) Merk, D.; Grisoni, F.; Friedrich, L.; Gelzinyte, E.; Schneider, G. Computer-Assisted Discovery of Retinoid X Receptor Modulating Natural Products and Isofunctional Mimetics. *J. Med. Chem.* **2018**, *61* (12), 5442–5447.
- (279) Merk, D.; Grisoni, F.; Friedrich, L.; Gelzinyte, E.; Schneider, G. Scaffold Hopping from Synthetic RXR Modulators by Virtual Screening and de Novo Design. *MedChemComm* **2018**, *9*, 1289–1292.
- (280) Pollinger, J.; Schierle, S.; Gellrich, L.; Ohrndorf, J.; Kaiser, A.; Heitel, P.; Chaikuad, A.; Knapp, S.; Merk, D. A Novel Biphenyl-Based Chemotype of Retinoid X Receptor Ligands Enables Subtype and Heterodimer Preferences. *ACS Med. Chem. Lett.* **2019**, *10* (9), 1346–1352.
- (281) Islam, M. M.; Zhang, C.-L. TLX: A Master Regulator for Neural Stem Cell Maintenance and Neurogenesis. *Biochim. Biophys. Acta, Gene Regul. Mech.* **2015**, *1849* (2), 210–216.
- (282) Shi, Y.; Lie, D. C.; Taupin, P.; Nakashima, K.; Ray, J.; Yu, R. T.; Gage, F. H.; Evans, R. M. Expression and Function of Orphan Nuclear Receptor TLX in Adult Neural Stem Cells. *Nature* **2004**, *427* (6969), 78–83.
- (283) Miyawaki, T.; Uemura, A.; Dezawa, M.; Yu, R. T.; Ide, C.; Nishikawa, S.; Honda, Y.; Tanabe, Y.; Tanabe, T. Tlx, an Orphan Nuclear Receptor, Regulates Cell Numbers and Astrocyte Development in the Developing Retina. *J. Neurosci.* **2004**, *24* (37), 8124–8134.
- (284) Monaghan, A. P.; Grau, E.; Bock, D.; Schütz, G. The Mouse Homolog of the Orphan Nuclear Receptor Tailless Is Expressed in the Developing Forebrain. *Development* **1995**, *121* (3), 839–853.
- (285) Li, S.; Sun, G.; Murai, K.; Ye, P.; Shi, Y. Characterization of TLX Expression in Neural Stem Cells and Progenitor Cells in Adult Brains. *PLoS One* **2012**, *7* (8), e43324.
- (286) Benod, C.; Villagomez, R.; Webb, P. TLX: An Elusive Receptor. *J. Steroid Biochem. Mol. Biol.* **2016**, *157*, 41–47.
- (287) Yokoyama, A.; Takezawa, S.; Schule, R.; Kitagawa, H.; Kato, S. Transrepressive Function of TLX Requires the Histone Demethylase LSD1. *Mol. Cell. Biol.* **2008**, *28* (12), 3995–4003.
- (288) Zhang, C.-L.; Zou, Y.; Yu, R. T.; Gage, F. H.; Evans, R. M. Nuclear Receptor TLX Prevents Retinal Dystrophy and Recruits the Corepressor Atrophin1. *Genes Dev.* **2006**, *20* (10), 1308–1320.
- (289) Estruch, S. B.; Buzón, V.; Carbó, L. R.; Schorova, L.; Lüders, J.; Estébanez-Perpiñá, E. The Oncoprotein BCL11A Binds to Orphan Nuclear Receptor TLX and Potentiates Its Transrepressive Function. *PLoS One* **2012**, *7* (6), e37963.
- (290) Sun, G.; Yu, R. T.; Evans, R. M.; Shi, Y. Orphan Nuclear Receptor TLX Recruits Histone Deacetylases to Repress Transcription and Regulate Neural Stem Cell Proliferation. *Proc. Natl. Acad. Sci. U. S. A.* **2007**, *104* (39), 15282–15287.
- (291) Griffett, K.; Bedia-Diaz, G.; Hegazy, L.; de Vera, I. M. S.; Wanninayake, U. S.; Billon, C.; Koelblen, T.; Wilhelm, M. L.; Burris, T. P. The Orphan Nuclear Receptor TLX Is a Receptor for Synthetic and Natural Retinoids. *Cell Chem. Biol.* **2020**, *27* (10), 1272–1284.
- (292) Benod, C.; Villagomez, R.; Filgueira, C. S.; Hwang, P. K.; Leonard, P. G.; Poncet-Montange, G.; Rajagopalan, S.; Fletterick, R. J.; Gustafsson, J.-Å.; Webb, P. The Human Orphan Nuclear Receptor Tailless (TLX, NR2E1) Is Druggable. *PLoS One* **2014**, *9* (6), e99440.
- (293) Zhi, X.; Zhou, X. E.; He, Y.; Searose-Xu, K.; Zhang, C.-L.; Tsai, C.-C.; Melcher, K.; Xu, H. E. Structural Basis for Corepressor Assembly by the Orphan Nuclear Receptor TLX. *Genes Dev.* **2015**, *29* (4), 440–450.
- (294) Tan, M. H. E.; Zhou, X. E.; Soon, F.-F.; Li, X.; Li, J.; Yong, E.-L.; Melcher, K.; Xu, H. E. The Crystal Structure of the Orphan Nuclear Receptor NR2E3/PNR Ligand Binding Domain Reveals a Dimeric Auto-Repressed Conformation. *PLoS One* **2013**, *8* (9), e74359.
- (295) Sablin, E. P.; Woods, A.; Krylova, I. N.; Hwang, P.; Ingraham, H. A.; Fletterick, R. J. The Structure of Corepressor Dax-1 Bound to Its Target Nuclear Receptor LRH-1. *Proc. Natl. Acad. Sci. U. S. A.* **2008**, *105* (47), 18390–18395.
- (296) Kandel, P.; Semerci, F.; Bajic, A.; Baluya, D.; Ma, L.; Chen, K.; Cao, A.; Phongmekhin, T.; Matinyan, N.; Choi, W.; Jiménez-Panizo, A.; Chamakuri, S.; Raji, I. O.; Chang, L.; Fuentes-Prior, P.; MacKenzie, K. R.; Benn, C. L.; Estébanez-Perpiñá, E.; Venken, K.; Moore, D. D.; Young, D. W.; Maletic-Savatic, M. Oleic Acid Triggers Hippocampal Neurogenesis by Binding to TLX/NR2E1. *bioRxiv* **2020**, 2020.10.28.359810.
- (297) Niu, W.; Zou, Y.; Shen, C.; Zhang, C.-L. Activation of Postnatal Neural Stem Cells Requires Nuclear Receptor TLX. *J. Neurosci.* **2011**, *31* (39), 13816–13828.
- (298) Roy, K.; Kuznicki, K.; Wu, Q.; Sun, Z.; Bock, D.; Schutz, G.; Vranich, N.; Monaghan, A. P. The Tlx Gene Regulates the Timing of Neurogenesis in the Cortex. *J. Neurosci.* **2004**, *24* (38), 8333–8345.
- (299) Shi, Y.; Sun, G.; Zhao, C.; Stewart, R. Neural Stem Cell Self-Renewal. *Crit. Rev. Oncol. Hematol.* **2008**, *65* (1), 43–53.
- (300) Elmi, M.; Matsumoto, Y.; Zeng, Z.; Lakshminarasimhan, P.; Yang, W.; Uemura, A.; Nishikawa, S.; Moshiri, A.; Tajima, N.; Agren,

H.; Funa, K. TLX Activates MASH1 for Induction of Neuronal Lineage Commitment of Adult Hippocampal Neuroprogenitors. *Mol. Cell. Neurosci.* **2010**, *45* (2), 121–131.

(301) Liu, H.-K.; Belz, T.; Bock, D.; Takacs, A.; Wu, H.; Lichter, P.; Chai, M.; Schütz, G. The Nuclear Receptor Tailless Is Required for Neurogenesis in the Adult Subventricular Zone. *Genes Dev.* **2008**, *22* (18), 2473–2478.

(302) Monaghan, A. P.; Bock, D.; Gass, P.; Schwger, A.; Wolfer, D. P.; Lipp, H.-P.; Schütz, G. Defective Limbic System in Mice Lacking the Tailless Gene. *Nature* **1997**, *390* (6659), 515–517.

(303) Yu, R. T.; Chiang, M.-Y.; Tanabe, T.; Kobayashi, M.; Yasuda, K.; Evans, R. M.; Umesono, K. The Orphan Nuclear Receptor Tlx Regulates Pax2 and Is Essential for Vision. *Proc. Natl. Acad. Sci. U. S. A.* **2000**, *97* (6), 2621–2625.

(304) Juárez, P.; Valdovinos, M. G.; May, M. E.; Lloyd, B. P.; Couppis, M. H.; Kennedy, C. H. Serotonin2A/C Receptors Mediate the Aggressive Phenotype of TLX Gene Knockout Mice. *Behav. Brain Res.* **2013**, *256*, 354–361.

(305) Murai, K.; Qu, Q.; Sun, G.; Ye, P.; Li, W.; Asulime, G.; Sun, E.; Tsai, G. E.; Shi, Y. Nuclear Receptor TLX Stimulates Hippocampal Neurogenesis and Enhances Learning and Memory in a Transgenic Mouse Model. *Proc. Natl. Acad. Sci. U. S. A.* **2014**, *111* (25), 9115–9120.

(306) O'Leary, J. D.; Kozareva, D. A.; Hueston, C. M.; O'Leary, O. F.; Cryan, J. F.; Nolan, Y. M. The Nuclear Receptor Tlx Regulates Motor, Cognitive and Anxiety-Related Behaviours during Adolescence and Adulthood. *Behav. Brain Res.* **2016**, *306*, 36–47.

(307) Kozareva, D. A.; O'Leary, O. F.; Cryan, J. F.; Nolan, Y. M. Deletion of TLX and Social Isolation Impairs Exercise-Induced Neurogenesis in the Adolescent Hippocampus. *Hippocampus* **2018**, *28* (1), 3–11.

(308) O'Leary, J. D.; O'Leary, O. F.; Cryan, J. F.; Nolan, Y. M. Regulation of Behaviour by the Nuclear Receptor TLX. *Genes, Brain Behav.* **2018**, *17* (3), e12357.

(309) Kumar, R. A.; McGhee, K. A.; Leach, S.; Bonaguro, R.; Maclean, A.; Aguirre-Hernandez, R.; Abrahams, B. S.; Coccaro, E. F.; Hodgins, S.; Turecki, G.; Condon, A.; Muir, W. J.; Brooks-Wilson, A. R.; Blackwood, D. H.; Simpson, E. M. Initial Association of NR2E1 with Bipolar Disorder and Identification of Candidate Mutations in Bipolar Disorder, Schizophrenia, and Aggression through Resequencing. *Am. J. Med. Genet., Part B* **2008**, *147B* (6), 880–889.

(310) Wang, Y. Y.; Hsu, S. H.; Tsai, H. Y.; Cheng, M. C. Genetic Analysis of the NR2E1 Gene as a Candidate Gene of Schizophrenia. *Psychiatry Res.* **2020**, *293*, 113386.

(311) Liu, H. K.; Wang, Y.; Belz, T.; Bock, D.; Takacs, A.; Radlwimmer, B.; Barbus, S.; Reifenberger, G.; Lichter, P.; Schütz, G. The Nuclear Receptor Tailless Induces Long-Term Neural Stem Cell Expansion and Brain Tumor Initiation. *Genes Dev.* **2010**, *24* (7), 683–695.

(312) Park, H.-J.; Kim, J.-K.; Jeon, H.-M.; Oh, S.-Y.; Kim, S.-H.; Park, M.-J.; Soeda, A.; Nam, D.-H.; Kim, H. The Neural Stem Cell Fate Determinant TLX Promotes Tumorigenesis and Genesis of Cells Resembling Glioma Stem Cells. *Mol. Cells* **2010**, *30* (5), 403–408.

(313) Louis, D. N.; Ohgaki, H.; Wiestler, O. D.; Cavenee, W. K.; Burger, P. C.; Jouvet, A.; Scheithauer, B. W.; Kleihues, P. The 2007 WHO Classification of Tumours of the Central Nervous System. *Acta Neuropathologica* **2007**, *114*, 97–109.

(314) Cui, Q.; Yang, S.; Ye, P.; Tian, E.; Sun, G.; Zhou, J.; Sun, G.; Liu, X.; Chen, C.; Murai, K.; Zhao, C.; Azizian, K. T.; Yang, L.; Warden, C.; Wu, X.; D'Apuzzo, M.; Brown, C.; Badie, B.; Peng, L.; Riggs, A. D.; Rossi, J. J.; Shi, Y. Downregulation of TLX Induces TET3 Expression and Inhibits Glioblastoma Stem Cell Self-Renewal and Tumorigenesis. *Nat. Commun.* **2016**, *7*, 10637.

(315) Dueva, E.; Singh, K.; Kalyta, A.; LeBlanc, E.; Rennie, P. S.; Cherkasov, A. Computer-Aided Discovery of Small Molecule Inhibitors of Transcriptional Activity of TLX (NR2E1) Nuclear Receptor. *Molecules* **2018**, *23* (11), 2967.

(316) Milbrandt, J. Nerve Growth Factor Induces a Gene Homologous to the Glucocorticoid Receptor Gene. *Neuron* **1988**, *1* (3), 183–188.

(317) Wang, Z.; Benoit, G.; Liu, J.; Prasad, S.; Aarnisalo, P.; Liu, X.; Xu, H.; Walker, N. P. C.; Perlmann, T. Structure and Function of Nurr1 Identifies a Class of Ligand-Independent Nuclear Receptors. *Nature* **2003**, *423* (6939), 555–560.

(318) Murphy, E. P.; Conneely, O. M. Neuroendocrine Regulation of the Hypothalamic Pituitary Adrenal Axis by the Nurr1/Nur77 Subfamily of Nuclear Receptors. *Mol. Endocrinol.* **1997**, *11* (1), 39–47.

(319) Paulsen, R. E.; Granås, K.; Johnsen, H.; Rolseth, V.; Sterri, S. Three Related Brain Nuclear Receptors, NGFI-B, Nurr1, and NOR-1, as Transcriptional Activators. *J. Mol. Neurosci.* **1995**, *6* (4), 249–255.

(320) Maira, M.; Martens, C.; Philips, A.; Drouin, J. Heterodimerization between Members of the Nur Subfamily of Orphan Nuclear Receptors as a Novel Mechanism for Gene Activation. *Mol. Cell. Biol.* **1999**, *19* (11), 7549–7557.

(321) Perlmann, T.; Jansson, L. A Novel Pathway for Vitamin A Signaling Mediated by RXR Heterodimerization with NGFI-B and NURR1. *Genes Dev.* **1995**, *9* (7), 769–782.

(322) Xiao, Q.; Castillo, S. O.; Nikodem, V. M. Distribution of Messenger RNAs for the Orphan Nuclear Receptors NURR1 and NUR77 (NGFI-B) in Adult Rat Brain Using in Situ Hybridization. *Neuroscience* **1996**, *75* (1), 221–230.

(323) Zetterström, R. H.; Williams, R.; Perlmann, T.; Olson, L. Cellular Expression of the Immediate Early Transcription Factors Nurr1 and NGFI-B Suggests a Gene Regulatory Role in Several Brain Regions Including the Nigrostriatal Dopamine System. *Mol. Brain Res.* **1996**, *41* (1–2), 111–120.

(324) Chao, L. C.; Wroblewski, K.; Zhang, Z.; Pei, L.; Vergnes, L.; Ilkayeva, O. R.; Ding, S. Y.; Reue, K.; Watt, M. J.; Newgard, C. B.; Pilch, P. F.; Hevener, A. L.; Tontonoz, P. Insulin Resistance and Altered Systemic Glucose Metabolism in Mice Lacking Nur77. *Diabetes* **2009**, *58* (12), 2788–2796.

(325) Zhan, Y.; Chen, Y.; Zhang, Q.; Zhuang, J.; Tian, M.; Chen, H.; Zhang, L.; Zhang, H.; He, J.; Wang, W.; Wu, R.; Wang, Y.; Shi, C.; Yang, K.; Li, A.; Xin, Y.; Li, T. Y.; Yang, J. Y.; Zheng, Z.; Yu, C.; Lin, S.-C.; Chang, C.; Huang, P.; Lin, T.; Wu, Q. The Orphan Nuclear Receptor Nur77 Regulates LKB1 Localization and Activates AMPK. *Nat. Chem. Biol.* **2012**, *8* (11), 897–904.

(326) Kurakula, K.; Vos, M.; Logiantara, A.; Roelofs, J. J.; Nieuwenhuis, M. A.; Koppelman, G. H.; Postma, D. S.; van Rij, L. S.; de Vries, C. J. M. Nuclear Receptor Nur77 Attenuates Airway Inflammation in Mice by Suppressing NF- κ B Activity in Lung Epithelial Cells. *J. Immunol.* **2015**, *195* (4), 1388–1398.

(327) Hamers, A. A. J.; Vos, M.; Rassam, F.; Marinkovic, G.; Kurakula, K.; van Gorp, P. J.; de Winther, M. P. J.; Gijbels, M. J. J.; de Waard, V.; de Vries, C. J. M. Bone Marrow-Specific Deficiency of Nuclear Receptor Nur77 Enhances Atherosclerosis. *Circ. Res.* **2012**, *110* (3), 428–438.

(328) Hanna, R. N.; Shaked, I.; Hubbeling, H. G.; Punt, J. A.; Wu, R.; Herrley, E.; Zaugg, C.; Pei, H.; Geissmann, F.; Ley, K.; Hedrick, C. C. NR4A1 (Nur77) Deletion Polarizes Macrophages Toward an Inflammatory Phenotype and Increases Atherosclerosis. *Circ. Res.* **2012**, *110* (3), 416–427.

(329) De Silva, S.; Han, S.; Zhang, X.; Huston, D. P.; Winoto, A.; Zheng, B. Reduction of the Incidence and Severity of Collagen-Induced Arthritis by Constitutive Nur77 Expression in the T Cell Lineage. *Arthritis Rheum.* **2005**, *52* (1), 333–338.

(330) Li, L.; Liu, Y.; Chen, H.; Li, F.; Wu, J.; Zhang, H.; He, J.; Xing, Y.; Chen, Y.; Wang, W.; Tian, X.; Li, A.; Zhang, Q.; Huang, P.; Han, J.; Lin, T.; Wu, Q. Impeding the Interaction between Nur77 and P38 Reduces LPS-Induced Inflammation. *Nat. Chem. Biol.* **2015**, *11* (5), 339–346.

(331) Beard, J. A.; Tenga, A.; Chen, T. The Interplay of NR4A Receptors and the Oncogene-Tumor Suppressor Networks in Cancer. *Cell. Signalling* **2015**, *27* (2), 257–266.

- (332) Li, H.; Kolluri, S. K.; Gu, J.; Dawson, M. I.; Cao, X.; Hobbs, P. D.; Lin, B.; Chen, G.; Lu, J.; Lin, F.; Xie, Z.; Fontana, J. A.; Reed, J. C.; Zhang, X. Cytochrome c Release and Apoptosis Induced by Mitochondrial Targeting of Nuclear Orphan Receptor TR3. *Science* **2000**, *289* (5482), 1159–1164.
- (333) Cao, X.; Liu, W.; Lin, F.; Li, H.; Kolluri, S. K.; Lin, B.; Han, Y.; Dawson, M. I.; Zhang, X. Retinoid X Receptor Regulates Nur77/Thyroid Hormone Receptor 3-Dependent Apoptosis by Modulating Its Nuclear Export and Mitochondrial Targeting. *Mol. Cell. Biol.* **2004**, *24* (22), 9705–9725.
- (334) Gilbert, F.; Morissette, M.; St-Hilaire, M.; Paquet, B.; Rouillard, C.; Di Paolo, T.; Lévesque, D. Nur77 Gene Knockout Alters Dopamine Neuron Biochemical Activity and Dopamine Turnover. *Biol. Psychiatry* **2006**, *60* (6), 538–547.
- (335) Rouillard, C.; Baillargeon, J.; Paquet, B.; St-Hilaire, M.; Maheux, J.; Lévesque, C.; Darlix, N.; Majeur, S.; Lévesque, D. Genetic Disruption of the Nuclear Receptor Nur77 (Nr4a1) in Rat Reduces Dopamine Cell Loss and L-Dopa-Induced Dyskinesia in Experimental Parkinson's Disease. *Exp. Neurol.* **2018**, *304*, 143–153.
- (336) Novak, G.; Gallo, A.; Zai, C. C.; Meltzer, H. Y.; Lieberman, J. A.; Potkin, S. G.; Voineskos, A. N.; Remington, G.; Kennedy, J. L.; Levesque, D.; Le Foll, B. Association of the Orphan Nuclear Receptor NR4A1 with Tardive Dyskinesia. *Psychiatr. Genet.* **2010**, *20* (1), 39–43.
- (337) St-Hilaire, M.; Bourhis, E.; Lévesque, D.; Rouillard, C. Impaired Behavioural and Molecular Adaptations to Dopamine Denervation and Repeated L-DOPA Treatment in Nur77-Knockout Mice. *Eur. J. Neurosci.* **2006**, *24* (3), 795–805.
- (338) Éthier, I.; Beaudry, G.; St-Hilaire, M.; Milbrandt, J.; Rouillard, C.; Lévesque, D. The Transcription Factor NGFI-B (Nur77) and Retinoids Play a Critical Role in Acute Neuroleptic-Induced Extrapyramidal Effect and Striatal Neuropeptide Gene Expression. *Neuropsychopharmacology* **2004**, *29* (2), 335–346.
- (339) Mahmoudi, S.; Samadi, P.; Gilbert, F.; Ouattara, B.; Morissette, M.; Grégoire, L.; Rouillard, C.; Di Paolo, T.; Lévesque, D. Nur77 mRNA Levels and L-Dopa-Induced Dyskinesias in MPTP Monkeys Treated with Docosahexaenoic Acid. *Neurobiol. Dis.* **2009**, *36* (1), 213–222.
- (340) Mount, M. P.; Zhang, Y.; Amini, M.; Callaghan, S.; Kulczycki, J.; Mao, Z.; Slack, R. S.; Anisman, H.; Park, D. S. Perturbation of Transcription Factor Nur77 Expression Mediated by Myocyte Enhancer Factor 2D (MEF2D) Regulates Dopaminergic Neuron Loss in Response to 1-Methyl-4-Phenyl-1,2,3,6-Tetrahydropyridine (MPTP). *J. Biol. Chem.* **2013**, *288* (20), 14362–14371.
- (341) Éthier, I.; Kagechika, H.; Shudo, K.; Rouillard, C.; Lévesque, D. Docosahexaenoic Acid Reduces Haloperidol-Induced Dyskinesias in Mice: Involvement of Nur77 and Retinoid Receptors. *Biol. Psychiatry* **2004**, *56* (7), 522–526.
- (342) Wei, X.; Gao, H.; Zou, J.; Liu, X.; Chen, D.; Liao, J.; Xu, Y.; Ma, L.; Tang, B.; Zhang, Z.; Cai, X.; Jin, K.; Xia, Y.; Wang, Q. Contradirectional Coupling of Nur77 and Nurr1 in Neurodegeneration: A Novel Mechanism for Memantine-Induced Anti-Inflammation and Anti-Mitochondrial Impairment. *Mol. Neurobiol.* **2016**, *53* (9), 5876–5892.
- (343) Popichak, K. A.; Hammond, S. L.; Moreno, J. A.; Afzali, M. F.; Backos, D. S.; Slayden, R. D.; Safe, S.; Tjalkens, R. B. Compensatory Expression of Nur77 and NURR1 Regulates NF- κ B-Dependent Inflammatory Signaling in Astrocytes. *Mol. Pharmacol.* **2018**, *94* (4), 1174–1186.
- (344) Liu, T.-Y.; Yang, X.-Y.; Zheng, L.-T.; Wang, G.-H.; Zhen, X.-C. Activation of Nur77 in Microglia Attenuates Proinflammatory Mediators Production and Protects Dopaminergic Neurons from Inflammation-Induced Cell Death. *J. Neurochem.* **2017**, *140* (4), 589–604.
- (345) Yan, J.; Huang, J.; Wu, J.; Fan, H.; Liu, A.; Qiao, L.; Shen, M.; Lai, X. Nur77 Attenuates Inflammatory Responses and Oxidative Stress by Inhibiting Phosphorylated I κ B- α in Parkinson's Disease Cell Model. *Aging* **2020**, *12* (9), 8107–8119.
- (346) Liebmann, M.; Hucke, S.; Koch, K.; Eschborn, M.; Ghelman, J.; Chasan, A. I.; Glander, S.; Schädlich, M.; Kuhlencord, M.; Daber, N. M.; Eveslage, M.; Beyer, M.; Dietrich, M.; Albrecht, P.; Stoll, M.; Busch, K. B.; Wiendl, H.; Roth, J.; Kuhlmann, T.; Klotz, L. Nur77 Serves as a Molecular Brake of the Metabolic Switch during T Cell Activation to Restrict Autoimmunity. *Proc. Natl. Acad. Sci. U. S. A.* **2018**, *115* (34), E8017–E8026.
- (347) Rothe, T.; Ipseiz, N.; Faas, M.; Lang, S.; Perez-Branguli, F.; Metzger, D.; Ichinose, H.; Winner, B.; Schett, G.; Krönke, G. The Nuclear Receptor Nr4a1 Acts as a Microglia Rheostat and Serves as a Therapeutic Target in Autoimmune-Driven Central Nervous System Inflammation. *J. Immunol.* **2017**, *198* (10), 3878–3885.
- (348) Zhao, Y.; Liu, Y.; Zheng, D. Alpha 1-Antichymotrypsin/Serpina3 Is a Novel Target of Orphan Nuclear Receptor Nur77. *FEBS J.* **2008**, *275* (5), 1025–1038.
- (349) Wang, L.; Zheng, Y.; Gao, X.; Liu, Y.; You, X. Retinoid X Receptor Ligand Regulates RXR α /Nur77-Dependent Apoptosis via Modulating Its Nuclear Export and Mitochondrial Targeting. *Int. J. Clin. Exp. Pathol.* **2017**, *10* (11), 10770–10780.
- (350) Zhan, Y.; Du, X.; Chen, H.; Liu, J.; Zhao, B.; Huang, D.; Li, G.; Xu, Q.; Zhang, M.; Weimer, B. C.; Chen, D.; Cheng, Z.; Zhang, L.; Li, Q.; Li, S.; Zheng, Z.; Song, S.; Huang, Y.; Ye, Z.; Su, W.; Lin, S.-C.; Shen, Y.; Wu, Q. Cytosporone B Is an Agonist for Nuclear Orphan Receptor Nur77. *Nat. Chem. Biol.* **2008**, *4* (9), 548–556.
- (351) Munoz-Tello, P.; Lin, H.; Khan, P.; De Vera, I. M. S.; Kamenecka, T. M.; Kojetin, D. J. Assessment of NR4A Ligands That Directly Bind and Modulate the Orphan Nuclear Receptor Nurr1. *J. Med. Chem.* **2020**, *63* (24), 15639–15654.
- (352) Liu, J.-J.; Zeng, H.-N.; Zhang, L.-R.; Zhan, Y.-Y.; Chen, Y.; Wang, Y.; Wang, J.; Xiang, S.-H.; Liu, W.-J.; Wang, W.-J.; Chen, H.-Z.; Shen, Y.-M.; Su, W.-J.; Huang, P.-Q.; Zhang, H.-K.; Wu, Q. A Unique Pharmacophore for Activation of the Nuclear Orphan Receptor Nur77 In Vivo and In Vitro. *Cancer Res.* **2010**, *70* (9), 3628–3637.
- (353) Yang, P.-B.; Hou, P.-P.; Liu, F.-Y.; Hong, W.-B.; Chen, H.-Z.; Sun, X.-Y.; Li, P.; Zhang, Y.; Ju, C.-Y.; Luo, L.-J.; Wu, S.-F.; Zhou, J.-X.; Wang, Z.-J.; He, J.-P.; Li, L.; Zhao, T.-J.; Deng, X.; Lin, T.; Wu, Q. Blocking PPAR γ Interaction Facilitates Nur77 Interdiction of Fatty Acid Uptake and Suppresses Breast Cancer Progression. *Proc. Natl. Acad. Sci. U. S. A.* **2020**, *117* (44), 27412–27422.
- (354) Wang, W.; Wang, Y.; Chen, H.; Xing, Y.; Li, F.; Zhang, Q.; Zhou, B.; Zhang, H.; Zhang, J.; Bian, X.; Li, L.; Liu, Y.; Zhao, B.; Chen, Y.; Wu, R.; Li, A.; Yao, L.; Chen, P.; Zhang, Y.; Tian, X.; Beermann, F.; Wu, M.; Han, J.; Huang, P.; Lin, T.; Wu, Q. Orphan Nuclear Receptor TR3 Acts in Autophagic Cell Death via Mitochondrial Signaling Pathway. *Nat. Chem. Biol.* **2014**, *10* (2), 133–140.
- (355) Wang, W.; Wang, Y.; Hou, P.-P.; Li, F.-W.; Zhou, B.; Chen, H.-Z.; Bian, X.-L.; Cai, Q.-X.; Xing, Y.-Z.; He, J.-P.; Zhang, H.; Huang, P.-Q.; Lin, T.; Wu, Q. Induction of Autophagic Death in Cancer Cells by Agonizing TR3 and Attenuating Akt2 Activity. *Chem. Biol.* **2015**, *22* (8), 1040–1051.
- (356) Hu, M.; Luo, Q.; Alitongbieke, G.; Chong, S.; Xu, C.; Xie, L.; Chen, X.; Zhang, D.; Zhou, Y.; Wang, Z.; Ye, X.; Cai, L.; Zhang, F.; Chen, H.; Jiang, F.; Fang, H.; Yang, S.; Liu, J.; Diaz-Meco, M. T.; Su, Y.; Zhou, H.; Moscat, J.; Lin, X.; Zhang, X.-K. Celastrol-Induced Nur77 Interaction with TRAF2 Alleviates Inflammation by Promoting Mitochondrial Ubiquitination and Autophagy. *Mol. Cell* **2017**, *66* (1), 141–153.
- (357) Jung, Y.-S.; Lee, H.-S.; Cho, H.-R.; Kim, K.-J.; Kim, J.-H.; Safe, S.; Lee, S.-O. Dual Targeting of Nur77 and AMPK α by Isoalantolactone Inhibits Adipogenesis In Vitro and Decreases Body Fat Mass in Vivo. *Int. J. Obes.* **2019**, *43* (5), 952–962.
- (358) Vinayavekhin, N.; Saghatelian, A. Discovery of a Protein-Metabolite Interaction between Unsaturated Fatty Acids and the Nuclear Receptor Nur77 Using a Metabolomics Approach. *J. Am. Chem. Soc.* **2011**, *133* (43), 17168–17171.
- (359) Lakshmi, S. P.; Reddy, A. T.; Banno, A.; Reddy, R. C. Molecular, Chemical, and Structural Characterization of Prostaglan-

din A2 as a Novel Agonist for Nur77. *Biochem. J.* **2019**, *476* (19), 2757–2767.

(360) Willems, S.; Kilu, W.; Ni, X.; Chaikuad, A.; Knapp, S.; Heering, J.; Merk, D. The Orphan Nuclear Receptor Nurr1 Is Responsive to Non-Steroidal Anti-Inflammatory Drugs. *Commun. Chem.* **2020**, *3* (1), 85.

(361) Ordentlich, P.; Yan, Y.; Zhou, S.; Heyman, R. A. Identification of the Antineoplastic Agent 6-Mercaptopurine as an Activator of the Orphan Nuclear Hormone Receptor Nurr1. *J. Biol. Chem.* **2003**, *278* (27), 24791–24799.

(362) Wansa, K. D. S. A.; Harris, J. M.; Yan, G.; Ordentlich, P.; Muscat, G. E. O. The AF-1 Domain of the Orphan Nuclear Receptor NOR-1 Mediates Trans-Activation, Coactivator Recruitment, and Activation by the Purine Anti-Metabolite 6-Mercaptopurine. *J. Biol. Chem.* **2003**, *278* (27), 24776–24790.

(363) Yoo, Y. G.; Na, T. Y.; Yang, W. K.; Kim, H. J.; Lee, I. K.; Kong, G.; Chung, J. H.; Lee, M. O. 6-Mercaptopurine, an Activator of Nur77, Enhances Transcriptional Activity of HIF-1 α Resulting in New Vessel Formation. *Oncogene* **2007**, *26* (26), 3823–3834.

(364) Lee, H.-S.; Safe, S.; Lee, S.-O. Inactivation of the Orphan Nuclear Receptor NR4A1 Contributes to Apoptosis Induction by Fangchinoline in Pancreatic Cancer Cells. *Toxicol. Appl. Pharmacol.* **2017**, *332*, 32–39.

(365) Lee, S.-O.; Li, X.; Hedrick, E.; Jin, U.-H.; Tjalkens, R. B.; Backos, D. S.; Li, L.; Zhang, Y.; Wu, Q.; Safe, S. Diindolylmethane Analogs Bind NR4A1 and Are NR4A1 Antagonists in Colon Cancer Cells. *Mol. Endocrinol.* **2014**, *28* (10), 1729–1739.

(366) Lee, S. O.; Abdelrahim, M.; Yoon, K.; Chintharlapalli, S.; Papineni, S.; Kim, K.; Wang, H.; Safe, S. Inactivation of the Orphan Nuclear Receptor TR3/Nur77 Inhibits Pancreatic Cancer Cell and Tumor Growth. *Cancer Res.* **2010**, *70* (17), 6824–6836.

(367) Yoon, K.; Lee, S.-O.; Cho, S.-D.; Kim, K.; Khan, S.; Safe, S. Activation of Nuclear TR3 (NR4A1) by a Diindolylmethane Analog Induces Apoptosis and Proapoptotic Genes in Pancreatic Cancer Cells and Tumors. *Carcinogenesis* **2011**, *32* (6), 836–842.

(368) Liu, J.; Wang, G.-H.; Duan, Y.-H.; Dai, Y.; Bao, Y.; Hu, M.; Zhou, Y.-Q.; Li, M.; Jiang, F.; Zhou, H.; Yao, X.-S.; Zhang, X.-K. Modulation of the Nur77-Bcl-2 Apoptotic Pathway by P38 α MAPK. *Oncotarget* **2017**, *8* (41), 69731–69745.

(369) Yao, L.-M.; He, J.-P.; Chen, H.-Z.; Wang, Y.; Wang, W.-J.; Wu, R.; Yu, C.-D.; Wu, Q. Orphan Receptor TR3 Participates in Cisplatin-Induced Apoptosis via Chk2 Phosphorylation to Repress Intestinal Tumorigenesis. *Carcinogenesis* **2012**, *33* (2), 301–311.

(370) Qi, H.; Jiang, Z.; Wang, C.; Yang, Y.; Li, L.; He, H.; Yu, Z. Sensitization of Tamoxifen-Resistant Breast Cancer Cells by Z-Ligustilide through Inhibiting Autophagy and Accumulating DNA Damages. *Oncotarget* **2017**, *8* (17), 29300–29317.

(371) Codina, A.; Benoit, G.; Gooch, J. T.; Neuhaus, D.; Perlmann, T.; Schwabe, J. W. R. Identification of a Novel Co-Regulator Interaction Surface on the Ligand Binding Domain of Nurr1 Using NMR Footprinting. *J. Biol. Chem.* **2004**, *279* (51), 53338–53345.

(372) Volakakis, N.; Malewicz, M.; Kadkhodai, B.; Perlmann, T.; Benoit, G. Characterization of the Nurr1 Ligand-Binding Domain Co-Activator Interaction Surface. *J. Mol. Endocrinol.* **2006**, *37* (2), 317–326.

(373) Galleguillos, D.; Vecchiola, A.; Fuentealba, J. A.; Ojeda, V.; Alvarez, K.; Gómez, A.; Andrés, M. E. PIAS γ Represses the Transcriptional Activation Induced by the Nuclear Receptor Nurr1. *J. Biol. Chem.* **2004**, *279* (3), 2005–2011.

(374) Zetterström, R. H.; Solomin, L.; Jansson, L.; Hoffer, B. J.; Olson, L.; Perlmann, T. Dopamine Neuron Agenesis in Nurr1-Deficient Mice. *Science* **1997**, *276* (5310), 248–250.

(375) Wallén, Å.; Zetterström, R. H.; Solomin, L.; Arvidsson, M.; Olson, L.; Perlmann, T. Fate of Mesencephalic AHD2-Expressing Dopamine Progenitor Cells in Nurr1 Mutant Mice. *Exp. Cell Res.* **1999**, *253* (2), 737–746.

(376) Smits, S. M.; Ponnio, T.; Conneely, O. M.; Burbach, J. P. H.; Smidt, M. P. Involvement of Nurr1 in Specifying the Neuro-

transmitter Identity of Ventral Midbrain Dopaminergic Neurons. *Eur. J. Neurosci.* **2003**, *18* (7), 1731–1738.

(377) Hermanson, E.; Joseph, B.; Castro, D.; Lindqvist, E.; Aarnisalo, P.; Wallén, Å.; Benoit, G.; Hengerer, B.; Olson, L.; Perlmann, T. Nurr1 Regulates Dopamine Synthesis and Storage in MN9D Dopamine Cells. *Exp. Cell Res.* **2003**, *288* (2), 324–334.

(378) Jacobs, F. M. J.; van der Linden, A. J. A.; Wang, Y.; von Oerthel, L.; Sul, H. S.; Burbach, J. P. H.; Smidt, M. P. Identification of Dlk1, Ptpru and Khlh1 as Novel Nurr1 Target Genes in Meso-Diencephalic Dopamine Neurons. *Development* **2009**, *136* (14), 2363–2373.

(379) Gil, M.; McKinney, C.; Lee, M. K.; Eells, J. B.; Phyllaier, M. A.; Nikodem, V. M. Regulation of GTP Cyclohydrolase I Expression by Orphan Receptor Nurr1 in Cell Culture and in Vivo. *J. Neurochem.* **2007**, *101* (1), 142–150.

(380) Luo, Y.; Henricksen, L. A.; Giuliano, R. E.; Prifti, L.; Callahan, L. M.; Federoff, H. J. VIP Is a Transcriptional Target of Nurr1 in Dopaminergic Cells. *Exp. Neurol.* **2007**, *203* (1), 221–232.

(381) Wallén, Å.; Castro, D. S.; Zetterström, R. H.; Karlén, M.; Olson, L.; Ericson, J.; Perlmann, T. Orphan Nuclear Receptor Nurr1 Is Essential for Ret Expression in Midbrain Dopamine Neurons and in the Brain Stem. *Mol. Cell. Neurosci.* **2001**, *18* (6), 649–663.

(382) Heng, X.; Jin, G.; Zhang, X.; Yang, D.; Zhu, M.; Fu, S.; Li, X.; Le, W. Nurr1 Regulates Top II β and Functions in Axon Genesis of Mesencephalic Dopaminergic Neurons. *Mol. Neurodegener.* **2012**, *7* (1), 4.

(383) Montarolo, F.; Martire, S.; Perga, S.; Spadaro, M.; Brescia, I.; Allegra, S.; De Francia, S.; Bertolotto, A. NURR1 Deficiency Is Associated to ADHD-like Phenotypes in Mice. *Transl. Psychiatry* **2019**, *9* (1), 207.

(384) McCoy, J. M.; Walkenhorst, D. E.; McCauley, K. S.; Elaasar, H.; Everett, J. R.; Mix, K. S. Orphan Nuclear Receptor NR4A2 Induces Transcription of the Immunomodulatory Peptide Hormone Prolactin. *J. Inflammation* **2015**, *12*, 13.

(385) Safe, S.; Jin, U. H.; Morpurgo, B.; Abudayyeh, A.; Singh, M.; Tjalkens, R. B. Nuclear Receptor 4A (NR4A) Family - Orphans No More. *J. Steroid Biochem. Mol. Biol.* **2016**, *157*, 48–60.

(386) Decressac, M.; Volakakis, N.; Björklund, A.; Perlmann, T. NURR1 in Parkinson Disease - From Pathogenesis to Therapeutic Potential. *Nat. Rev. Neurol.* **2013**, *9* (11), 629–636.

(387) Liu, H.; Liu, H.; Li, T.; Cui, J.; Fu, Y.; Ren, J.; Sun, X.; Jiang, P.; Yu, S.; Li, C. NR4A2 Genetic Variation and Parkinson's Disease: Evidence from a Systematic Review and Meta-Analysis. *Neurosci. Lett.* **2017**, *650*, 25–32.

(388) Chu, Y.; Le, W.; Kompoliti, K.; Jankovic, J.; Mufson, E. J.; Kordower, J. H. Nurr1 in Parkinson's Disease and Related Disorders. *J. Comp. Neurol.* **2006**, *494* (3), 495–514.

(389) Decressac, M.; Kadkhodaei, B.; Mattsson, B.; Laguna, A.; Perlmann, T.; Björklund, A. α -Synuclein-Induced down-Regulation of Nurr1 Disrupts GDNF Signaling in Nigral Dopamine Neurons. *Sci. Transl. Med.* **2012**, *4* (163), 163ra156.

(390) Liu, W.; Gao, Y.; Chang, N. Nurr1 Overexpression Exerts Neuroprotective and Anti-Inflammatory Roles via down-Regulating CCL2 Expression in Both in Vivo and in Vitro Parkinson's Disease Models. *Biochem. Biophys. Res. Commun.* **2017**, *482* (4), 1312–1319.

(391) Volakakis, N.; Tiklova, K.; Decressac, M.; Papathanou, M.; Mattsson, B.; Gillberg, L.; Nobre, A.; Björklund, A.; Perlmann, T. Nurr1 and Retinoid X Receptor Ligands Stimulate Ret Signaling in Dopamine Neurons and Can Alleviate α -Synuclein Disrupted Gene Expression. *J. Neurosci.* **2015**, *35* (42), 14370–14385.

(392) Volakakis, N.; Kadkhodaei, B.; Joodmardi, E.; Wallis, K.; Panman, L.; Silvaggi, J.; Spiegelman, B. M.; Perlmann, T. NR4A Orphan Nuclear Receptors as Mediators of CREB-Dependent Neuroprotection. *Proc. Natl. Acad. Sci. U. S. A.* **2010**, *107* (27), 12317–12322.

(393) Wang, X.; Zhuang, W.; Fu, W.; Wang, X.; Lv, E.; Li, F.; Zhou, S.; Rausch, W.-D.; Wang, X. The Lentiviral-Mediated Nurr1 Genetic Engineering Mesenchymal Stem Cells Protect Dopaminergic Neurons

in a Rat Model of Parkinson's Disease. *Am. J. Transl. Res.* **2018**, *10* (6), 1583–1599.

(394) Saijo, K.; Winner, B.; Carson, C. T.; Collier, J. G.; Boyer, L.; Rosenfeld, M. G.; Gage, F. H.; Glass, C. K. A Nurr1/CoREST Pathway in Microglia and Astrocytes Protects Dopaminergic Neurons from Inflammation-Induced Death. *Cell* **2009**, *137* (1), 47–59.

(395) Yi, S.-H.; He, X.-B.; Rhee, Y.-H.; Park, C.-H.; Takizawa, T.; Nakashima, K.; Lee, S.-H. Foxa2 Acts as a Co-Activator Potentiating Expression of the Nurr1-Induced DA Phenotype via Epigenetic Regulation. *Development* **2014**, *141* (4), 761–772.

(396) Kim, C.-H.; Han, B.-S.; Moon, J.; Kim, D.-J.; Shin, J.; Rajan, S.; Nguyen, Q. T.; Sohn, M.; Kim, W.-G.; Han, M.; Jeong, I.; Kim, K.-S.; Lee, E.-H.; Tu, Y.; Naffin-Olivos, J. L.; Park, C.-H.; Ringe, D.; Yoon, H. S.; Petsko, G. A.; Kim, K.-S. Nuclear Receptor Nurr1 Agonists Enhance Its Dual Functions and Improve Behavioral Deficits in an Animal Model of Parkinson's Disease. *Proc. Natl. Acad. Sci. U. S. A.* **2015**, *112* (28), 8756–8761.

(397) Rajan, S.; Jang, Y.; Kim, C.-H.; Kim, W.; Toh, H. T.; Jeon, J.; Song, B.; Serra, A.; Lescar, J.; Yoo, J. Y.; Beldar, S.; Ye, H.; Kang, C.; Liu, X.-W.; Feitosa, M.; Kim, Y.; Hwang, D.; Goh, G.; Lim, K.-L.; Park, H. M.; Lee, C. H.; Oh, S. F.; Petsko, G. A.; Yoon, H. S.; Kim, K.-S. PGE1 and PGA1 Bind to Nurr1 and Activate Its Transcriptional Function. *Nat. Chem. Biol.* **2020**, *16*, 876–886.

(398) Bruning, J. M.; Wang, Y.; Oltrabella, F.; Tian, B.; Kholodar, S. A.; Liu, H.; Bhattacharya, P.; Guo, S.; Holton, J. M.; Fletterick, R. J.; Jacobson, M. P.; England, P. M. Covalent Modification and Regulation of the Nuclear Receptor Nurr1 by a Dopamine Metabolite. *Cell Chem. Biol.* **2019**, *26* (5), 674–685.

(399) Smith, G. A.; Rocha, E. M.; Rooney, T.; Barneoud, P.; McLean, J. R.; Beagan, J.; Osborn, T.; Coimbra, M.; Luo, Y.; Hallett, P. J.; Isacson, O. A Nurr1 Agonist Causes Neuroprotection in a Parkinson's Disease Lesion Model Primed with the Toll-Like Receptor 3 DsRNA Inflammatory Stimulant Poly(I:C). *PLoS One* **2015**, *10* (3), e0121072.

(400) Zhang, Z.; Li, X.; Xie, W.; Tuo, H.; Hintermann, S.; Jankovic, J.; Le, W. Anti-Parkinsonian Effects of Nurr1 Activator in Ubiquitin-Proteasome System Impairment Induced Animal Model of Parkinson's Disease. *CNS Neurol. Disord.: Drug Targets* **2012**, *11* (6), 768–773.

(401) Friling, S.; Bergsland, M.; Kjellander, S. Activation of Retinoid X Receptor Increases Dopamine Cell Survival in Models for Parkinson's Disease. *BMC Neurosci.* **2009**, *10*, 146.

(402) Spathis, A. D.; Asvos, X.; Ziavra, D.; Karampelas, T.; Topouzis, S.; Cournia, Z.; Qing, X.; Alexakos, P.; Smits, L. M.; Dalla, C.; Rideout, H. J.; Schwamborn, J. C.; Tamvakopoulos, C.; Fokas, D.; Vassilatis, D. K. Nurr1:RXR α Heterodimer Activation as Monotherapy for Parkinson's Disease. *Proc. Natl. Acad. Sci. U. S. A.* **2017**, *114* (15), 3999–4004.

(403) Wang, J.; Bi, W.; Zhao, W.; Varghese, M.; Koch, R. J.; Walker, R. H.; Chandraratna, R. A.; Sanders, M. E.; Janesick, A.; Blumberg, B.; Ward, L.; Ho, L.; Pasinetti, G. M. Selective Brain Penetrable Nurr1 Transactivator for Treating Parkinson's Disease. *Oncotarget* **2016**, *7* (7), 7469–7479.

(404) Loppi, S.; Kolosowska, N.; Kärkkäinen, O.; Korhonen, P.; Huuskonen, M.; Grubman, A.; Dhungana, H.; Wojciechowski, S.; Pomeschik, Y.; Giordano, M.; Kagechika, H.; White, A.; Auriola, S.; Koistinaho, J.; Landreth, G.; Hanhineva, K.; Kanninen, K.; Malm, T. HX600, a Synthetic Agonist for RXR-Nurr1 Heterodimer Complex, Prevents Ischemia-Induced Neuronal Damage. *Brain, Behav., Immun.* **2018**, *73*, 670–681.

(405) Jeon, S. G.; Yoo, A.; Chun, D. W.; Hong, S. B.; Chung, H.; Kim, J.-I.; Moon, M. The Critical Role of Nurr1 as a Mediator and Therapeutic Target in Alzheimer's Disease-Related Pathogenesis. *Aging Dis.* **2020**, *11* (3), 705–724.

(406) Terzioglu-Usak, S.; Negis, Y.; Karabulut, D. S.; Zaim, M.; Isik, S. Cellular Model of Alzheimer's Disease: A β 1–42 Peptide Induces Amyloid Deposition and a Decrease in Topo Isomerase II β and Nurr1 Expression. *Curr. Alzheimer Res.* **2017**, *14* (6), 636–644.

(407) Parra-Damas, A.; Valero, J.; Chen, M.; España, J.; Martín, E.; Ferrer, I.; Rodríguez-Alvarez, J.; Saura, C. A. Crct1 Activates a Transcriptional Program Deregulated at Early Alzheimer's Disease-Related Stages. *J. Neurosci.* **2014**, *34* (17), 5776–5787.

(408) Moon, M.; Jeong, I.; Kim, C.-H.; Kim, J.; Lee, P. K. J.; Mook-Jung, I.; Leblanc, P.; Kim, K.-S. Correlation between Orphan Nuclear Receptor Nurr1 Expression and Amyloid Deposition in 5XFAD Mice, an Animal Model of Alzheimer's Disease. *J. Neurochem.* **2015**, *132* (2), 254–262.

(409) Moon, M.; Jung, E. S.; Jeon, S. G.; Cha, M.-Y.; Jang, Y.; Kim, W.; Lopes, C.; Mook-Jung, I.; Kim, K.-S. Nurr1 (NR4A2) Regulates Alzheimer's Disease-Related Pathogenesis and Cognitive Function in the 5XFAD Mouse Model. *Aging Cell* **2019**, *18* (1), e12866.

(410) Montarolo, F.; Raffaele, C.; Perga, S.; Martire, S.; Finardi, A.; Furlan, R.; Hintermann, S.; Bertolotto, A. Effects of Isoxazolo-Pyridinone 7e, a Potent Activator of the Nurr1 Signaling Pathway, on Experimental Autoimmune Encephalomyelitis in Mice. *PLoS One* **2014**, *9* (9), e108791.

(411) Montarolo, F.; Perga, S.; Martire, S.; Bertolotto, A. Nurr1 Reduction Influences the Onset of Chronic EAE in Mice. *Inflammation Res.* **2015**, *64* (11), 841–844.

(412) Raveney, B. J. E.; Oki, S.; Yamamura, T. Nuclear Receptor NR4A2 Orchestrates Th17 Cell-Mediated Autoimmune Inflammation via IL-21 Signalling. *PLoS One* **2013**, *8* (2), e56595.

(413) Park, T.-Y.; Jang, Y.; Kim, W.; Shin, J.; Toh, H. T.; Kim, C.-H.; Yoon, H. S.; Leblanc, P.; Kim, K.-S. Chloroquine Modulates Inflammatory Autoimmune Responses through Nurr1 in Autoimmune Diseases. *Sci. Rep.* **2019**, *9*, 15559.

(414) Willems, S.; Ohrndorf, J.; Kilu, W.; Heering, J.; Merk, D. Fragment-like Chloroquinolineamines Activate the Orphan Nuclear Receptor Nurr1 and Elucidate Activation Mechanisms. *J. Med. Chem.* **2021**, *64* (5), 2659–2668.

(415) de Vera, I. M. S.; Giri, P. K.; Munoz-Tello, P.; Brust, R.; Fuhrmann, J.; Matta-Camacho, E.; Shang, J.; Campbell, S.; Wilson, H. D.; Granados, J.; Gardner, W. J. J.; Creamer, T. P.; Solt, L. A.; Kojetin, D. J. Identification of a Binding Site for Unsaturated Fatty Acids in the Orphan Nuclear Receptor Nurr1. *ACS Chem. Biol.* **2016**, *11* (7), 1795–1799.

(416) de Vera, I. M. S.; Munoz-Tello, P.; Zheng, J.; Dharmarajan, V.; Marciano, D. P.; Matta-Camacho, E.; Giri, P. K.; Shang, J.; Hughes, T. S.; Rance, M.; Griffin, P. R.; Kojetin, D. J. Defining a Canonical Ligand-Binding Pocket in the Orphan Nuclear Receptor Nurr1. *Structure* **2019**, *27* (1), 66–77.

(417) Windshügel, B. Structural Insights into Ligand-Binding Pocket Formation in Nurr1 by Molecular Dynamics Simulations. *J. Biomol. Struct. Dyn.* **2019**, *37* (17), 4651–4657.

(418) Lesuisse, D.; Malanda, A.; Peyronel, J. F.; Evanno, Y.; Lardenois, P.; De-Peretti, D.; Abécassis, P.-Y.; Barnéoud, P.; Brunel, P.; Burgevin, M.-C.; Cegarra, C.; Auger, F.; Dommergue, A.; Lafon, C.; Even, L.; Tsi, J.; Luc, T. P. H.; Almario, A.; Olivier, A.; Castel, M.-N.; Taupin, V.; Rooney, T.; Vigé, X. Development of a Novel NURR1/NOT Agonist from Hit to Lead and Candidate for the Potential Treatment of Parkinson's Disease. *Bioorg. Med. Chem. Lett.* **2019**, *29* (7), 929–932.

(419) Almario Garcia, A.; Lardenois, P.; Olivier, A. Derivatives of 2-Aryl-6-Phenyl-Imidazo [1, 2- α]Pyridines, Their Preparation and Their Therapeutic Use. WO2008/034974A1. Sanofi-Aventis, 2008.

(420) Malanda, A.; Abécassis, P.-Y.; Barnéoud, P.; Brunel, P.; Taupin, V.; Vigé, X.; Lesuisse, D. Data on Synthesis, ADME and Pharmacological Properties and Early Safety Pharmacology Evaluation of a Series of Novel NURR1/NOT Agonist Potentially Useful for the Treatment of Parkinson's Disease. *Data Br.* **2019**, *27*, 104057.

(421) Dubois, C.; Hengerer, B.; Mattes, H. Identification of a Potent Agonist of the Orphan Nuclear Receptor Nurr1. *ChemMedChem* **2006**, *1* (9), 955–958.

(422) Hintermann, S.; Chiesi, M.; von Krosigk, U.; Mathé, D.; Felber, R.; Hengerer, B. Identification of a Series of Highly Potent Activators of the Nurr1 Signaling Pathway. *Bioorg. Med. Chem. Lett.* **2007**, *17* (1), 193–196.

- (423) Li, X.; Lee, S.-O.; Safe, S. Structure-Dependent Activation of NR4A2 (Nurr1) by 1,1-Bis(3'-Indolyl)-1-(Aromatic)Methane Analogs in Pancreatic Cancer Cells. *Biochem. Pharmacol.* **2012**, *83* (10), 1445–1455.
- (424) Inamoto, T.; Papineni, S.; Chintharlapalli, S.; Cho, S. D.; Safe, S.; Kamat, A. M. 1,1-Bis(3'-Indolyl)-1-(p-Chlorophenyl)Methane Activates the Orphan Nuclear Receptor Nurr1 and Inhibits Bladder Cancer Growth. *Mol. Cancer Ther.* **2008**, *7* (12), 3825–3833.
- (425) De Miranda, B. R.; Popichak, K. A.; Hammond, S. L.; Miller, J. A.; Safe, S.; Tjalkens, R. B. Novel Para-Phenyl Substituted Diindolylmethanes Protect against MPTP Neurotoxicity and Suppress Glial Activation in a Mouse Model of Parkinson's Disease. *Toxicol. Sci.* **2015**, *143* (2), 360–373.
- (426) Hammond, S. L.; Safe, S.; Tjalkens, R. B. A Novel Synthetic Activator of Nurr1 Induces Dopaminergic Gene Expression and Protects against 6-Hydroxydopamine Neurotoxicity in Vitro. *Neurosci. Lett.* **2015**, *607*, 83–89.
- (427) Hammond, S. L.; Tjalkens, R. B.; Safe, S.; Richman, E. H.; Backos, D. S.; Li, X.; Hunt, L. G.; Chong, E.; Popichak, K. A.; Damale, P. The Nurr1 Ligand, 1,1-Bis(3'-Indolyl)-1-(p-Chlorophenyl)-Methane, Modulates Glial Reactivity and Is Neuroprotective in MPTP-Induced Parkinsonism. *J. Pharmacol. Exp. Ther.* **2018**, *365* (3), 636–651.
- (428) Karki, K.; Li, X.; Jin, U.-H.; Mohankumar, K.; Zarei, M.; Michelhaugh, S. K.; Mittal, S.; Tjalkens, R.; Safe, S. Nuclear Receptor 4A2 (NR4A2) Is a Druggable Target for Glioblastomas. *J. Neuro-Oncol.* **2020**, *146* (1), 25–39.
- (429) De Miranda, B. R.; Miller, J. A.; Hansen, R. J.; Lunghofer, P. J.; Safe, S.; Gustafson, D. L.; Colagiovanni, D.; Tjalkens, R. B. Neuroprotective Efficacy and Pharmacokinetic Behavior of Novel Anti-Inflammatory Para-Phenyl Substituted Diindolylmethanes in a Mouse Model of Parkinson's Disease. *J. Pharmacol. Exp. Ther.* **2013**, *345* (1), 125–138.
- (430) Hibino, S.; Chikuma, S.; Kondo, T.; Ito, M.; Nakatsukasa, H.; Omata-Mise, S.; Yoshimura, A. Inhibition of Nr4a Receptors Enhances Antitumor Immunity by Breaking Treg-Mediated Immune Tolerance. *Cancer Res.* **2018**, *78* (11), 3027–3040.
- (431) Komiya, T.; Yamamoto, S.; Roy, A.; McDonald, P.; Perez, R. P. Drug Screening to Target Nuclear Orphan Receptor NR4A2 for Cancer Therapeutics. *Transl. Lung Cancer Res.* **2017**, *6* (5), 600–610.
- (432) Pan, T.; Xie, W.; Jankovic, J.; Le, W. Biological Effects of Pramipexole on Dopaminergic Neuron-Associated Genes: Relevance to Neuroprotection. *Neurosci. Lett.* **2005**, *377* (2), 106–109.
- (433) Hedy, S. A.; Safar, M. M.; Bahgat, A. K. Cilostazol Mediated Nurr1 and Autophagy Enhancement: Neuroprotective Activity in Rat Rotenone PD Model. *Mol. Neurobiol.* **2018**, *55* (9), 7579–7587.
- (434) Ham, A.; Lee, H. J.; Hong, S. S.; Lee, D.; Mar, W. Moracenin D from Mori Cortex Radicis Protects SH-SY5Y Cells against Dopamine-Induced Cell Death by Regulating Nurr1 and α -Synuclein Expression. *Phytother. Res.* **2012**, *26* (4), 620–624.
- (435) Wallén-Mackenzie, Å.; De Urquiza, A. M.; Petersson, S.; Rodriguez, F. J.; Friling, S.; Wagner, J.; Ordentlich, P.; Lengqvist, J.; Heyman, R. A.; Arenas, E.; Perlmann, T. Nurr1-RXR Heterodimers Mediate RXR Ligand-Induced Signaling in Neuronal Cells. *Genes Dev.* **2003**, *17* (24), 3036–3047.
- (436) Morita, K.; Kawana, K.; Sodeyama, M.; Shimomura, I.; Kagechika, H.; Makishima, M. Selective Allosteric Ligand Activation of the Retinoid X Receptor Heterodimers of NGFI-B and Nurr1. *Biochem. Pharmacol.* **2005**, *71* (1–2), 98–107.
- (437) Ishizawa, M.; Kagechika, H.; Makishima, M. NR4A Nuclear Receptors Mediate Carnitine Palmitoyltransferase 1A Gene Expression by the Rexinoid HX600. *Biochem. Biophys. Res. Commun.* **2012**, *418* (4), 780–785.
- (438) Sundén, H.; Schäfer, A.; Scheepstra, M.; Leysen, S.; Malo, M.; Ma, J.-N.; Burstein, E. S.; Ottmann, C.; Brunsveld, L.; Olsson, R. Chiral Dihydrobenzofuran Acids Show Potent Retinoid X Receptor-Nuclear Receptor Related 1 Protein Dimer Activation. *J. Med. Chem.* **2016**, *59* (3), 1232–1238.
- (439) Scheepstra, M.; Andrei, S. A.; de Vries, R. M. J. M.; Meijer, F. A.; Ma, J.-N.; Burstein, E. S.; Olsson, R.; Ottmann, C.; Milroy, L.-G.; Brunsveld, L. Ligand Dependent Switch from RXR Homo- to RXR-NURR1 Heterodimerization. *ACS Chem. Neurosci.* **2017**, *8* (9), 2065–2077.
- (440) McFarland, K.; Spalding, T. A.; Hubbard, D.; Ma, J.-N.; Olsson, R.; Burstein, E. S. Low Dose Bexarotene Treatment Rescues Dopamine Neurons and Restores Behavioral Function in Models of Parkinson's Disease. *ACS Chem. Neurosci.* **2013**, *4* (11), 1430–1438.
- (441) Pönniö, T.; Conneely, O. M. Nor-1 Regulates Hippocampal Axon Guidance, Pyramidal Cell Survival, and Seizure Susceptibility. *Mol. Cell. Biol.* **2004**, *24* (20), 9070–9078.
- (442) Ferrán, B.; Martí-Pàmies, I.; Alonso, J.; Rodríguez-calvo, R.; Aguiló, S.; Vidal, F.; Rodríguez, C.; Martínez-gonzález, J. The Nuclear Receptor NOR-1 Regulates the Small Muscle Protein, X-Linked (SMPX) and Myotube Differentiation. *Sci. Rep.* **2016**, *6*, 25944.
- (443) Kon, T.; Miki, Y.; Tanji, K.; Mori, F.; Tomiyama, M.; Toyoshima, Y.; Kakita, A.; Takahashi, H.; Utsumi, J.; Sasaki, H.; Wakabayashi, K. Localization of Nuclear Receptor Subfamily 4, Group A, Member 3 (NR4A3) in Lewy Body Disease and Multiple System Atrophy. *Neuropathology* **2015**, *35* (6), 503–509.
- (444) Maheux, J.; Ethier, I.; Rouillard, C.; Levesque, D. Induction Patterns of Transcription Factors of the Nur Family (Nurr1, Nur77, and Nor -1) by Typical and Atypical Antipsychotics in the Mouse Brain: Implication for Their Mechanism of Action. *J. Pharmacol. Exp. Ther.* **2005**, *313* (1), 460–473.
- (445) DeYoung, R. A.; Baker, J. C.; Cado, D.; Winoto, A. The Orphan Steroid Receptor Nur77 Family Member Nor-1 Is Essential for Early Mouse Embryogenesis. *J. Biol. Chem.* **2003**, *278* (47), 47104–47109.
- (446) Chio, C.-C.; Wei, L.; Chen, T. G.; Lin, C.-M.; Shieh, J.-P.; Yeh, P.-S.; Chen, R.-M. Neuron-Derived Orphan Receptor 1 Transduces Survival Signals in Neuronal Cells in Response to Hypoxia-Induced Apoptotic Insults. *J. Neurosurg.* **2016**, *124* (6), 1654–1664.
- (447) Kagaya, S.; Ohkura, N.; Tsukada, T.; Miyagawa, M.; Sugita, Y.; Tsujimoto, G.; Matsumoto, K.; Saito, H.; Hashida, R. Prostaglandin A 2 Acts as a Transactivator for NOR1 (NR4A3) within the Nuclear Receptor Superfamily. *Biol. Pharm. Bull.* **2005**, *28* (9), 1603–1607.
- (448) Eyster, K. M. The Estrogen Receptors: An Overview from Different Perspectives. In *Methods in Molecular Biology*; Humana Press Inc., 2016; Vol. 1366, pp 1–10.
- (449) Dahlman-Wright, K.; Cavailles, V.; Fuqua, S. A.; Jordan, V. C.; Katzenellenbogen, J. A.; Korach, K. S.; Maggi, A.; Muramatsu, M.; Parker, M. G.; Gustafsson, J.-Å. International Union of Pharmacology. LXIV. Estrogen Receptors. *Pharmacol. Rev.* **2006**, *58* (4), 773–781.
- (450) Hewitt, S. C.; Korach, K. S. Estrogen Receptors: New Directions in the New Millennium. *Endocr. Rev.* **2018**, *39* (5), 664–675.
- (451) Dupont, S.; Krust, A.; Gansmuller, A.; Dierich, A.; Chambon, P.; Mark, M. Effect of Single and Compound Knockouts of Estrogen Receptors Alpha (ERalpha) and Beta (ERbeta) on Mouse Reproductive Phenotypes. *Development* **2000**, *127* (19), 4277–4291.
- (452) Lan, Y.-L.; Zhao, J.; Li, S. Update on the Neuroprotective Effect of Estrogen Receptor Alpha Against Alzheimer's Disease. *J. Alzheimer's Dis.* **2015**, *43* (4), 1137–1148.
- (453) Chakrabarti, M.; Haque, A.; Banik, N. L.; Nagarkatti, P.; Nagarkatti, M.; Ray, S. K. Estrogen Receptor Agonists for Attenuation of Neuroinflammation and Neurodegeneration. *Brain Res. Bull.* **2014**, *109*, 22–31.
- (454) Pike, C. J.; Carroll, J. C.; Rosario, E. R.; Barron, A. M. Protective Actions of Sex Steroid Hormones in Alzheimer's Disease. *Frontiers in Neuroendocrinology* **2009**, *30* (2), 239–258.
- (455) Boada, M.; Antunez, C.; López-Arrieta, J.; Caruz, A.; Moreno-Rey, C.; Ramírez-Lorca, R.; Morón, F. J.; Hernández, I.; Mauleón, A.; Rosende-Roca, M.; Martínez-Lage, P.; Marín, J.; Tárraga, L.; Alegret, M.; Pedrajas, J. R.; Urda, N.; Royo, J. L.; Saez, M. E.; Gayán, J.; González-Pérez, A.; Real, L. M.; Ruiz, A.; Galán, J. J. Estrogen

Receptor Alpha Gene Variants Are Associated with Alzheimer's Disease. *Neurobiol. Aging* **2012**, *33* (1), 198.e15–198.e24.

(456) Goodman, Y.; Bruce, A. J.; Cheng, B.; Mattson, M. P. Estrogens Attenuate and Corticosterone Exacerbates Excitotoxicity, Oxidative Injury, and Amyloid β -Peptide Toxicity in Hippocampal Neurons. *J. Neurochem.* **1996**, *66* (5), 1836–1844.

(457) Green, P. S.; Gridley, K. E.; Simpkins, J. W. Estradiol Protects against β -Amyloid (25–35)-Induced Toxicity in SK-N-SH Human Neuroblastoma Cells. *Neurosci. Lett.* **1996**, *218* (3), 165–168.

(458) Behl, C.; Widmann, M.; Trapp, T.; Holsboer, F. 17- β Estradiol Protects Neurons from Oxidative Stress-Induced Cell Death in Vitro. *Biochem. Biophys. Res. Commun.* **1995**, *216* (2), 473–482.

(459) Singer, C. A.; Rogers, K. L.; Strickland, T. M.; Dorsa, D. M. Estrogen Protects Primary Cortical Neurons from Glutamate Toxicity. *Neurosci. Lett.* **1996**, *212* (1), 13–16.

(460) Zhang, Q.-G.; Raz, L.; Wang, R.; Han, D.; De Sevilla, L.; Yang, F.; Vadlamudi, R. K.; Brann, D. W. Estrogen Attenuates Ischemic Oxidative Damage Via an Estrogen Receptor α -Mediated Inhibition of NADPH Oxidase Activation. *J. Neurosci.* **2009**, *29* (44), 13823–13836.

(461) Spampinato, S. F.; Molinaro, G.; Merlo, S.; Iacovelli, L.; Caraci, F.; Battaglia, G.; Nicoletti, F.; Bruno, V.; Sortino, M. A. Estrogen Receptors and Type 1 Metabotropic Glutamate Receptors Are Interdependent in Protecting Cortical Neurons against β -Amyloid Toxicity. *Mol. Pharmacol.* **2012**, *81* (1), 12–20.

(462) Pike, C. J. Estrogen Modulates Neuronal Bcl-XL Expression and β -Amyloid-Induced Apoptosis: Relevance to Alzheimer's Disease. *J. Neurochem.* **1999**, *72* (4), 1552–1563.

(463) Yao, M.; Nguyen, T.-V. V.; Pike, C. J. Estrogen Regulates Bcl-w and Bim Expression: Role in Protection against β -Amyloid Peptide-Induced Neuronal Death. *J. Neurosci.* **2007**, *27* (6), 1422–1433.

(464) Zhao, L.; Wu, T.-W.; Brinton, R. D. Estrogen Receptor Subtypes Alpha and Beta Contribute to Neuroprotection and Increased Bcl-2 Expression in Primary Hippocampal Neurons. *Brain Res.* **2004**, *1010* (1–2), 22–34.

(465) Suwanna, N.; Thangnipon, W.; Soi-ampornkul, R. Neuroprotective Effects of Diarylpropionitrile against β -Amyloid Peptide-Induced Neurotoxicity in Rat Cultured Cortical Neurons. *Neurosci. Lett.* **2014**, *578*, 44–49.

(466) Mateos, L.; Persson, T.; Kathozi, S.; Gil-Bea, F. J.; Cedazo-Minguez, A. Estrogen Protects against Amyloid- β Toxicity by Estrogen Receptor α -Mediated Inhibition of Daxx Translocation. *Neurosci. Lett.* **2012**, *506* (2), 245–250.

(467) Witty, C. F.; Gardella, L. P.; Perez, M. C.; Daniel, J. M. Short-Term Estradiol Administration in Aging Ovariectomized Rats Provides Lasting Benefits for Memory and the Hippocampus: A Role for Insulin-like Growth Factor-I. *Endocrinology* **2013**, *154* (2), 842–852.

(468) Azcoitia, I.; Sierra, A.; Garcia-Segura, L. M. Neuroprotective Effects of Estradiol in the Adult Rat Hippocampus: Interaction with Insulin-like Growth Factor-I Signalling. *J. Neurosci. Res.* **1999**, *58* (6), 815–822.

(469) Rosario, E. R.; Ramsden, M.; Pike, C. J. Progestins Inhibit the Neuroprotective Effects of Estrogen in Rat Hippocampus. *Brain Res.* **2006**, *1099* (1), 206–210.

(470) Carroll, J. C.; Rosario, E. R.; Pike, C. J. Progesterone Blocks Estrogen Neuroprotection from Kainate in Middle-Aged Female Rats. *Neurosci. Lett.* **2008**, *445* (3), 229–232.

(471) Kim, H.; Bang, O. Y.; Jung, M. W.; Ha, S. D.; Hong, H. S.; Huh, K.; Kim, S. U.; Mook-Jung, I. Neuroprotective Effects of Estrogen against Beta-Amyloid Toxicity Are Mediated by Estrogen Receptors in Cultured Neuronal Cells. *Neurosci. Lett.* **2001**, *302* (1), 58–62.

(472) Benvenuti, S.; Luciani, P.; Vannelli, G. B.; Gelmini, S.; Franceschi, E.; Serio, M.; Peri, A. Estrogen and Selective Estrogen Receptor Modulators Exert Neuroprotective Effects and Stimulate the Expression of Selective Alzheimer's Disease Indicator-1, a Recently Discovered Antiapoptotic Gene, in Human Neuroblast Long-Term Cell Cultures. *J. Clin. Endocrinol. Metab.* **2005**, *90* (3), 1775–1782.

(473) Mize, A. L.; Young, L. J.; Alper, R. H. Uncoupling of 5-HT_{1A} Receptors in the Brain by Estrogens: Regional Variations in Antagonism by ICI 182,780. *Neuropharmacology* **2003**, *44* (5), 584–591.

(474) Cordey, M.; Pike, C. J. Neuroprotective Properties of Selective Estrogen Receptor Agonists in Cultured Neurons. *Brain Res.* **2005**, *1045* (1–2), 217–223.

(475) Fitzpatrick, J. L.; Mize, A. L.; Wade, C. B.; Harris, J. A.; Shapiro, R. A.; Dorsa, D. M. Estrogen-Mediated Neuroprotection against β -Amyloid Toxicity Requires Expression of Estrogen Receptor α or β and Activation of the MAPK Pathway. *J. Neurochem.* **2002**, *82* (3), 674–682.

(476) Tiwari-Woodruff, S.; Morales, L. B. J.; Lee, R.; Voskuhl, R. R. Differential Neuroprotective and Antiinflammatory Effects of Estrogen Receptor (ER) α and ER β Ligand Treatment. *Proc. Natl. Acad. Sci. U. S. A.* **2007**, *104* (37), 14813–14818.

(477) Bourque, M.; Dluzen, D. E.; Di Paolo, T. Signaling Pathways Mediating the Neuroprotective Effects of Sex Steroids and SERMs in Parkinson's Disease. *Front. Neuroendocrinol.* **2012**, *33* (2), 169–178.

(478) Zhao, L.; Brinton, R. D. Estrogen Receptor α and β Differentially Regulate Intracellular Ca²⁺ Dynamics Leading to ERK Phosphorylation and Estrogen Neuroprotection in Hippocampal Neurons. *Brain Res.* **2007**, *1172*, 48–59.

(479) Yang, L.-C.; Zhang, Q.-G.; Zhou, C.-F.; Yang, F.; Zhang, Y.-D.; Wang, R.-M.; Brann, D. W. Extracellular Estrogen Receptors Mediate the Neuroprotective Effects of Estrogen in the Rat Hippocampus. *PLoS One* **2010**, *5* (5), e9851.

(480) Long, J.; He, P.; Shen, Y.; Li, R. New Evidence of Mitochondria Dysfunction in the Female Alzheimer's Disease Brain: Deficiency of Estrogen Receptor- β . *J. Alzheimer's Dis.* **2012**, *30* (3), 545–558.

(481) Xu, H.; Gouras, G. K.; Greenfield, J. P.; Vincent, B.; Naslund, J.; Mazarrelli, L.; Fried, G.; Jovanovic, J. N.; Seeger, M.; Relkin, N. R.; Liao, F.; Checler, F.; Buxbaum, J. D.; Chait, B. T.; Thinakaran, G.; Sisodia, S. S.; Wang, R.; Greengard, P.; Gandy, S. Estrogen Reduces Neuronal Generation of Alzheimer β -Amyloid Peptides. *Nat. Med.* **1998**, *4* (4), 447–451.

(482) Watters, J. J.; Campbell, J. S.; Cunningham, M. J.; Krebs, E. G.; Dorsa, D. M. Rapid Membrane Effects of Steroids in Neuroblastoma Cells: Effects of Estrogen on Mitogen Activated Protein Kinase Signalling Cascade and c-Fos Immediate Early Gene Transcription. *Endocrinology* **1997**, *138* (9), 4030–4033.

(483) Manthey, D.; Heck, S.; Engert, S.; Behl, C. Estrogen Induces a Rapid Secretion of Amyloid β Precursor Protein via the Mitogen-Activated Protein Kinase Pathway. *Eur. J. Biochem.* **2001**, *268* (15), 4285–4291.

(484) Li, R.; Shen, Y.; Yang, L.-B.; Lue, L.-F.; Finch, C.; Rogers, J. Estrogen Enhances Uptake of Amyloid β -Protein by Microglia Derived from the Human Cortex. *J. Neurochem.* **2000**, *75* (4), 1447–1454.

(485) Harris-White, M. E.; Chu, T.; Miller, S. A.; Simmons, M.; Teter, B.; Nash, D.; Cole, G. M.; Frautschy, S. A. Estrogen (E₂) and Glucocorticoid (Gc) Effects on Microglia and A β Clearance in Vitro and in Vivo. *Neurochem. Int.* **2001**, *39* (5–6), 435–448.

(486) Bruce-Keller, A. J.; Keeling, J. L.; Keller, J. N.; Huang, F. F.; Camandola, S.; Mattson, M. P. Antiinflammatory Effects of Estrogen on Microglial Activation. *Endocrinology* **2000**, *141* (10), 3646–3656.

(487) George, S.; Petit, G. H.; Gouras, G. K.; Brundin, P.; Olsson, R. Nonsteroidal Selective Androgen Receptor Modulators and Selective Estrogen Receptor β Agonists Moderate Cognitive Deficits and Amyloid- β Levels in a Mouse Model of Alzheimer's Disease. *ACS Chem. Neurosci.* **2013**, *4* (12), 1537–1548.

(488) Yue, X.; Lu, M.; Lancaster, T.; Cao, P.; Honda, S. I.; Staufenbiel, M.; Harada, N.; Zhong, Z.; Shen, Y.; Li, R. Brain Estrogen Deficiency Accelerates A β Plaque Formation in an Alzheimer's Disease Animal Model. *Proc. Natl. Acad. Sci. U. S. A.* **2005**, *102* (52), 19198–19203.

- (489) Tanzi, R. E.; Moir, R. D.; Wagner, S. L. Clearance of Alzheimer's A β Peptide: The Many Roads to Perdition. *Neuron* **2004**, *43*, 605–608.
- (490) Wei, Y.; Zhou, J.; Wu, J.; Huang, J. ER β Promotes A β Degradation via the Modulation of Autophagy. *Cell Death Dis.* **2019**, *10* (8), 565.
- (491) Hayes, M. T. Parkinson's Disease and Parkinsonism. *American Journal of Medicine* **2019**, *132* (7), 802–807.
- (492) Popat, R. A.; Van Den Eeden, S. K.; Tanner, C. M.; McGuire, V.; Bernstein, A. L.; Bloch, D. A.; Leimpeter, A.; Nelson, L. M. Effect of Reproductive Factors and Postmenopausal Hormone Use on the Risk of Parkinson Disease. *Neurology* **2005**, *65* (3), 383–390.
- (493) Wang, P.; Li, J.; Qiu, S.; Wen, H.; Du, J. Hormone Replacement Therapy and Parkinson's Disease Risk in Women: A Meta-Analysis of 14 Observational Studies. *Neuropsychiatr. Dis. Treat.* **2015**, *11*, 59–66.
- (494) Currie, L. J.; Harrison, M. B.; Trugman, J. M.; Bennett, J. P.; Wooten, G. F. Postmenopausal Estrogen Use Affects Risk for Parkinson Disease. *Arch. Neurol.* **2004**, *61* (6), 886–888.
- (495) Bourque, M.; Morissette, M.; Di Paolo, T. Repurposing Sex Steroids and Related Drugs as Potential Treatment for Parkinson's Disease. *Neuropharmacology* **2019**, *147*, 37–54.
- (496) Blanchet, P. J.; Fang, J.; Hyland, K.; Arnold, L. A.; Mouradian, M. M.; Chase, T. N. Short-Term Effects of High-Dose 17 β -Estradiol in Postmenopausal PD Patients: A Crossover Study. *Neurology* **1999**, *53* (1), 91–95.
- (497) Strijks, E.; Kremer, J. A. M.; Horstink, M. W. I. M. Effects of Female Sex Steroids on Parkinson's Disease in Postmenopausal Women. *Clin. Neuropharmacol.* **1999**, *22* (2), 93–97.
- (498) Dluzen, D. E.; McDermott, J. L.; Anderson, L. I. Tamoxifen Eliminates Estrogen's Neuroprotective Effect upon MPTP-Induced Neurotoxicity of the Nigrostriatal Dopaminergic System. *Neurotoxic. Res.* **2001**, *3* (3), 291–300.
- (499) Morissette, M.; Sweidi, S. Al; Callier, S.; Di Paolo, T. Estrogen and SERM Neuroprotection in Animal Models of Parkinson's Disease. *Mol. Cell. Endocrinol.* **2008**, *290* (1–2), 60–69.
- (500) Baraka, A. M.; Korish, A. A.; Soliman, G. A.; Kamal, H. The Possible Role of Estrogen and Selective Estrogen Receptor Modulators in a Rat Model of Parkinson's Disease. *Life Sci.* **2011**, *88* (19–20), 879–885.
- (501) McFarland, K.; Price, D. L.; Davis, C. N.; Ma, J.-N.; Bonhaus, D. W.; Burstein, E. S.; Olsson, R. AC-186, a Selective Nonsteroidal Estrogen Receptor β Agonist, Shows Gender Specific Neuroprotection in a Parkinson's Disease Rat Model. *ACS Chem. Neurosci.* **2013**, *4* (9), 1249–1255.
- (502) Sierra, A.; Gottfried-Blackmore, A.; Milner, T. A.; McEwen, B. S.; Bulloch, K. Steroid Hormone Receptor Expression and Function in Microglia. *Glia* **2008**, *56* (6), 659–674.
- (503) Barreto, G.; Santos-Galindo, M.; Diz-Chaves, Y.; Pernía, O.; Carrero, P.; Azcoitia, I.; Garcia-Segura, L. M. Selective Estrogen Receptor Modulators Decrease Reactive Astroglia in the Injured Brain: Effects of Aging and Prolonged Depletion of Ovarian Hormones. *Endocrinology* **2009**, *150* (11), 5010–5015.
- (504) Maglione, A.; Rolla, S.; De Mercanti, S. F.; Cutrupi, S.; Clerico, M. The Adaptive Immune System in Multiple Sclerosis: An Estrogen-Mediated Point of View. *Cells* **2019**, *8* (10), 1280.
- (505) Villa, A.; Vegeto, E.; Poletti, A.; Maggi, A. Estrogens, Neuroinflammation, and Neurodegeneration. *Endocrine Reviews* **2016**, *37* (4), 372–402.
- (506) Lewis, D. K.; Johnson, A. B.; Stohlgren, S.; Harms, A.; Sohrabji, F. Effects of Estrogen Receptor Agonists on Regulation of the Inflammatory Response in Astrocytes from Young Adult and Middle-Aged Female Rats. *J. Neuroimmunol.* **2008**, *195* (1–2), 47–59.
- (507) Vegeto, E.; Belcredito, S.; Etteri, S.; Ghisletti, S.; Brusadelli, A.; Meda, C.; Krust, A.; Dupont, S.; Ciana, P.; Chambon, P.; Maggi, A. Estrogen Receptor- α Mediates the Brain Antiinflammatory Activity of Estradiol. *Proc. Natl. Acad. Sci. U. S. A.* **2003**, *100* (16), 9614–9619.
- (508) Bebo, B. F.; Fyfe-Johnson, A.; Adlard, K.; Beam, A. G.; Vandenbark, A. A.; Offner, H. Low-Dose Estrogen Therapy Ameliorates Experimental Autoimmune Encephalomyelitis in Two Different Inbred Mouse Strains. *J. Immunol.* **2001**, *166* (3), 2080–2089.
- (509) Ito, A.; Bebo, B. F.; Matejuk, A.; Zamora, A.; Silverman, M.; Fyfe-Johnson, A.; Offner, H. Estrogen Treatment Down-Regulates TNF- α Production and Reduces the Severity of Experimental Autoimmune Encephalomyelitis in Cytokine Knockout Mice. *J. Immunol.* **2001**, *167* (1), 542–552.
- (510) Liu, H. Y.; Buenafe, A. C.; Matejuk, A.; Ito, A.; Zamora, A.; Dwyer, J.; Vandenbark, A. A.; Offner, H. Estrogen Inhibition of EAE Involves Effects on Dendritic Cell Function. *J. Neurosci. Res.* **2002**, *70* (2), 238–248.
- (511) Spence, R. D.; Hamby, M. E.; Umeda, E.; Itoh, N.; Du, S.; Wisdom, A. J.; Cao, Y.; Bondar, G.; Lam, J.; Ao, Y.; Sandoval, F.; Suriany, S.; Sofroniew, M. V.; Voskuhl, R. R. Neuroprotection Mediated through Estrogen Receptor- α in Astrocytes. *Proc. Natl. Acad. Sci. U. S. A.* **2011**, *108* (21), 8867–8872.
- (512) Kim, S.; Liva, S. M.; Dalal, M. A.; Verity, M. A.; Voskuhl, R. R. Estriol Ameliorates Autoimmune Demyelinating Disease: Implications for Multiple Sclerosis. *Neurology* **1999**, *52* (6), 1230–1238.
- (513) Spence, R. D.; Wisdom, A. J.; Cao, Y.; Hill, H. M.; Mongerson, C. R. L.; Stapornkul, B.; Itoh, N.; Sofroniew, M. V.; Voskuhl, R. R. Estrogen Mediates Neuroprotection and Anti-Inflammatory Effects during EAE through ER α Signaling on Astrocytes but Not through ER β Signaling on Astrocytes or Neurons. *J. Neurosci.* **2013**, *33* (26), 10924–10933.
- (514) Sicotte, N. L.; Liva, S. M.; Klutch, R.; Pfeiffer, P.; Bouvier, S.; Odesa, S.; Wu, T. C. J.; Voskuhl, R. R. Treatment of Multiple Sclerosis with the Pregnancy Hormone Estriol. *Ann. Neurol.* **2002**, *52* (4), 421–428.
- (515) Vukusic, S.; Ionescu, I.; El-Etr, M.; Schumacher, M.; Baulieu, E. E.; Cornu, C.; Confavreux, C. The Prevention of Post-Partum Relapses with Progesterin and Estradiol in Multiple Sclerosis (POPART/MUS) Trial: Rationale, Objectives and State of Advancement. *J. Neurol. Sci.* **2009**, *286* (1–2), 114–118.
- (516) Pozzilli, C.; De Giglio, L.; Barletta, V. T.; Marinelli, F.; De Angelis, F.; Gallo, V.; Pagano, V. A.; Marini, S.; Piattella, M. C.; Tomassini, V.; Pantano, P. Oral Contraceptives Combined with Interferon b in Multiple Sclerosis. *Neurol. Neuroimmunol. Neuro-Inflammation* **2015**, *2* (4), e120.
- (517) Voskuhl, R. R.; Wang, H. J.; Wu, T. C. J.; Sicotte, N. L.; Nakamura, K.; Kurth, F.; Itoh, N.; Bardens, J.; Bernard, J. T.; Corboy, J. R.; Cross, A. H.; Dhib-Jalbut, S.; Ford, C. C.; Frohman, E. M.; Giesser, B.; Jacobs, D.; Kasper, L. H.; Lynch, S.; Parry, G.; Racke, M. K.; Reider, A. T.; Rose, J.; Wingerchuk, D. M.; MacKenzie-Graham, A. J.; Arnold, D. L.; Tseng, C. H.; Elashoff, R. Estriol Combined with Glatiramer Acetate for Women with Relapsing-Remitting Multiple Sclerosis: A Randomised, Placebo-Controlled, Phase 2 Trial. *Lancet Neurol.* **2016**, *15* (1), 35–46.
- (518) Rossouw, J. E.; Anderson, G. L.; Prentice, R. L.; LaCroix, A. Z.; Kooperberg, C.; Stefanick, M. L.; Jackson, R. D.; Beresford, S. A. A.; Howard, B. V.; Johnson, K. C.; Kotchen, J. M.; Ockene, J. Risks and Benefits of Estrogen plus Progesterin in Healthy Postmenopausal Women: Principal Results from the Women's Health Initiative Randomized Controlled Trial. *JAMA, J. Am. Med. Assoc.* **2002**, *288* (3), 321–333.
- (519) Paterni, I.; Granchi, C.; Katzenellenbogen, J. A.; Minutolo, F. Estrogen Receptors Alpha (ER α) and Beta (ER β): Subtype-Selective Ligands and Clinical Potential. *Steroids* **2014**, *90*, 13–29.
- (520) Brzozowski, A. M.; Pike, A. C. W.; Dauter, Z.; Hubbard, R. E.; Bonn, T.; Engström, O.; Öhman, L.; Greene, G. L.; Gustafsson, J.-Å.; Carlquist, M. Molecular Basis of Agonism and Antagonism in the Oestrogen Receptor. *Nature* **1997**, *389* (6652), 753–758.
- (521) Pike, A. C. W.; Brzozowski, A. M.; Hubbard, R. E.; Bonn, T.; Thorsell, A.-G.; Engström, O.; Ljunggren, J.; Gustafsson, J.-Å.; Carlquist, M. Structure of the Ligand-Binding Domain of Oestrogen

Receptor Beta in the Presence of a Partial Agonist and a Full Antagonist. *EMBO J.* **1999**, *18* (17), 4608–4618.

(522) Shiau, A. K.; Barstad, D.; Radek, J. T.; Meyers, M. J.; Nettles, K. W.; Katzenellenbogen, B. S.; Katzenellenbogen, J. A.; Agard, D. A.; Greene, G. L. Structural Characterization of a Subtype-Selective Ligand Reveals a Novel Mode of Estrogen Receptor Antagonism. *Nat. Struct. Biol.* **2002**, *9* (5), 359–364.

(523) Levenson, A. S.; Craig Jordan, V. The Key to the Antiestrogenic Mechanism of Raloxifene Is Amino Acid 351 (Aspartate) in the Estrogen Receptor. *Cancer Res.* **1998**, *58* (9), 1872–1875.

(524) Heldring, N.; Pike, A.; Andersson, S.; Matthews, J.; Cheng, G.; Hartman, J.; Tujague, M.; Ström, A.; Treuter, E.; Warner, M.; Gustafsson, J.-Å. Estrogen Receptors: How Do They Signal and What Are Their Targets. *Physiol. Rev.* **2007**, *87* (3), 905–931.

(525) Nilsson, S.; Koehler, K. F.; Gustafsson, J.-Å. Development of Subtype-Selective Oestrogen Receptor-Based Therapeutics. *Nat. Rev. Drug Discovery* **2011**, *10* (10), 778–792.

(526) Jordan, V. C. Antiestrogens and Selective Estrogen Receptor Modulators as Multifunctional Medicines. 1. Receptor Interactions. *J. Med. Chem.* **2003**, *46*, 883–908.

(527) Stauffer, S. R.; Coletta, C. J.; Tedesco, R.; Nishiguchi, G.; Carlson, K.; Sun, J.; Katzenellenbogen, B. S.; Katzenellenbogen, J. A. Pyrazole Ligands: Structure - Affinity/Activity Relationships and Estrogen Receptor- α -Selective Agonists. *J. Med. Chem.* **2000**, *43* (26), 4934–4947.

(528) Meyers, M. J.; Sun, J.; Carlson, K. E.; Katzenellenbogen, B. S.; Katzenellenbogen, J. A. Estrogen Receptor Subtype-Selective Ligands: Asymmetric Synthesis and Biological Evaluation of Cis- and Trans-5,11-Dialkyl-5,6,11,12-Tetrahydrochrysenes. *J. Med. Chem.* **1999**, *42* (13), 2456–2468.

(529) Meyers, M. J.; Sun, J.; Carlson, K. E.; Marriner, G. A.; Katzenellenbogen, B. S.; Katzenellenbogen, J. A. Estrogen Receptor- β Potency-Selective Ligands: Structure-Activity Relationship Studies of Diarylpropionitriles and Their Acetylene and Polar Analogues. *J. Med. Chem.* **2001**, *44* (24), 4230–4251.

(530) Minutolo, F.; Bertini, S.; Granchi, C.; Marchitello, T.; Prota, G.; Rapposelli, S.; Tuccinardi, T.; Martinelli, A.; Gunther, J. R.; Carlson, K. E.; Katzenellenbogen, J. A.; Macchia, M. Structural Evolutions of Salicylaldoximes as Selective Agonists for Estrogen Receptor β . *J. Med. Chem.* **2009**, *52* (3), 858–867.

(531) Malamas, M. S.; Manas, E. S.; McDevitt, R. E.; Gunawan, I.; Xu, Z. B.; Collini, M. D.; Miller, C. P.; Dinh, T.; Henderson, R. A.; Keith, J. C.; Harris, H. A. Design and Synthesis of Aryl Diphenolic Azoles as Potent and Selective Estrogen Receptor- β Ligands. *J. Med. Chem.* **2004**, *47* (21), 5021–5040.

(532) Komm, B. S.; Mirkin, S. An Overview of Current and Emerging SERMs. *J. Steroid Biochem. Mol. Biol.* **2014**, *143*, 207–222.

(533) Patel, H. K.; Bihani, T. Selective Estrogen Receptor Modulators (SERMs) and Selective Estrogen Receptor Degraders (SERDs) in Cancer Treatment. *Pharmacol. Ther.* **2018**, *186*, 1–24.

(534) Henke, B. R.; Drewry, D. H.; Jones, S. A.; Stewart, E. L.; Weaver, S. L.; Wiethe, R. W. 2-Amino-4,6-Diarylpyridines as Novel Ligands for the Estrogen Receptor. *Bioorg. Med. Chem. Lett.* **2001**, *11* (14), 1939–1942.

(535) Renaud, J.; Bischoff, S. F.; Buhl, T.; Floersheim, P.; Fournier, B.; Geiser, M.; Halleux, C.; Kallen, J.; Keller, H.; Ramage, P. Selective Estrogen Receptor Modulators with Conformationally Restricted Side Chains. Synthesis and Structure-Activity Relationship of ER α -Selective Tetrahydroisoquinoline Ligands. *J. Med. Chem.* **2005**, *48* (2), 364–379.

(536) Hill, R. A.; Kouremenos, K.; Tull, D.; Maggi, A.; Schroeder, A.; Gibbons, A.; Kulkarni, J.; Sundram, S.; Du, X. Bazedoxifene – a Promising Brain Active SERM That Crosses the Blood Brain Barrier and Enhances Spatial Memory. *Psychoneuroendocrinology* **2020**, *121*, 104830.

(537) Wakeling, A. E.; Dukes, M.; Bowler, J. A Potent Specific Pure Antiestrogen with Clinical Potential. *Cancer Res.* **1991**, *51* (15), 3867–3873.

(538) Garner, F.; Shomali, M.; Paquin, D.; Lyttle, C. R.; Hattersley, G. RAD1901: A Novel, Orally Bioavailable Selective Estrogen Receptor Degradator That Demonstrates Antitumor Activity in Breast Cancer Xenograft Models. *Anti-Cancer Drugs* **2015**, *26* (9), 948–956.

(539) Conlan, M. G.; de Vries, E. F. J.; Glaudemans, A.; Wang, Y.; Troy, S. Pharmacokinetic and Pharmacodynamic Studies of Elacestrant, A Novel Oral Selective Estrogen Receptor Degradator, in Healthy Post-Menopausal Women. *Eur. J. Drug Metab. Pharmacokinet.* **2020**, *45* (5), 675–689.